The Phylogeny of Basal Coelurosaurian Theropods (Archosauria: Dinosauria) and Patterns of Morphological Evolution during the Dinosaur-Bird Transition

Stephen L. Brusatte

Submitted in partial fulfillment of the
requirements for the degree of
Doctor of Philosophy
in the Graduate School of Arts and Sciences

COLUMBIA UNIVERSITY

2013

ABSTRACT

The Phylogeny of Basal Coelurosaurian Theropods (Archosauria: Dinosauria) and patterns of Morphological Evolution during the Dinosaur-Bird Transition

Stephen L. Brusatte

Theropod dinosaurs are an iconic and familiar group of extinct species that include predators such as *Tyrannosaurus* and *Velociraptor*, as well as an array of other Mesozoic taxa. Carnivorous theropods are the evolutionary ancestors of birds, and the evolutionary transition between theropods and birds is a textbook example of a major evolutionary transformation in the history of life. Despite a flurry of research on early birds and their dinosaurian relatives, however, several questions still remain. First, the anatomy of some major theropod groups has yet to be described in detail. Second, there is little consensus on the phylogenetic relationships of the basal members of a theropod subgroup called Coelurosauria: the clade of birds and their closest relatives (defined as all taxa closer to birds than to *Allosaurus*). Third, there has been little synthetic work on large-scale macroevolutionary patterns during theropod evolution. This dissertation includes three chapters that touches on these three major issues.

Chapter 1 is a detailed description of the Late Cretaceous tyrannosaurid theropod *Alioramus altai*, based on its holotype specimen from the Tsaagan Khuushu locality in the Maastrichtian Nemegt Formation of Mongolia. This monographic description provides further evidence that *Alioramus* is an unusual long-snouted, gracile, and slender-limbed taxon with an unpredecented degree of cranial ornamentation among tyrannosaurids and an extremely

pneumatized skeleton. Anatomical comparisons indicate that the long skull of *Alioramus* is an autapomorphic feature that is proportionally longer (relative to femur length) than in any other known tyrannosaurid specimen, including juveniles, and that *Alioramus* is morphologically distinctive relative to similarly-sized individuals of the contemporary and sympatric *Tarbosaurus*. The coexistence of the long-snouted *Alioramus* and robust and deep-snouted *Tarbosaurus*, which are found together at the Tsaagan Khuushu locality, demonstrate that multiple large tyrannosaurids were able to live in sympatry, likely because of niche partitioning due to differences in craniofacial morphology and functional behavior.

Chapter 2 presents a comprehensive new phylogenetic analysis of coelurosaurian theropods, which is an updated version (and thus the latest iteration) of the long-standing Theropod Working Group (TWiG) analysis. The new analysis incoroporates a wealth of new taxa and character data into the TWiG matrix for the first time, most of which is relevant to basal (non-maniraptoran) coelurosaurs such as tyrannosauroids and ornithomimosaurs, which had previously been the subject of only cursory character and taxon sampling in TWiG studies. The full dataset was analyzed under parsimony, and the resulting phylogeny includes several well supported relationships and agrees with previous analyses in many aspects. As a result, it is argued that a consensus view of basal coelurosaurian relationships has emerged, including: 1) the monophyly of major subclades such as Tyrannosauroidea, Compsognathidae, and Ornithomimosauria; 2) the position of the singleton genera *Bicentenaria*, *Zuolong*, and *Tugulusaurus* near the base of Coelurosauria; 3) the placement of Tyrannosauroidea as the most basal major coelurosaurian subclade; 4) the inclusion of *Guanlong*, *Dilong*, and *Proceratosaurus* within Tyrannosauroidea; 5) the existence of a derived maniraptoran clade that includes alvarezsauroids, therizinosauroids, oviraptorosaurs, and paravians to the exclusion of

ornithomimosaurs and tyrannosauroids. Remaining areas of uncertainty include the phylogenetic position of Compsognathidae and the singleton genus *Ornitholestes*, and relationships at the base of the Ornithomimosauria + Maniraptora clade and Maniraptora itself. The phylogeny indicates that much of the early history of Coelurosauria has yet to be sampled in the fossil record, that coelurosaurs originated at small body size, and that the evolution of the iconic *Tyrannosaurus*-like bauplan occurred only towards the end of the Cretaceous.

Chapter 3 presents a geometric morphometric analysis that is used to study broad patterns in theropod skull shape variation and compare the distribution of taxa in cranial morphospace (form) to both phylogeny and quantitative metrics of biting behaviour (function). The analysis finds that theropod skulls primarily differ in relative anteroposterior length and snout depth and to a lesser extent in orbit size and depth of the cheek region, and that oviraptorosaurs deviate most strongly from the "typical" and ancestral theropod morphologies. Noncarnivorous taxa generally fall out in distinct regions of morphospace and exhibit greater overall disparity than carnivorous taxa, whereas large-bodied carnivores independently converge on the same region of morphospace. The distribution of taxa in morphospace is strongly correlated with phylogeny but only weakly correlated with functional biting behaviour. These results imply that phylogeny, not biting function, was the major determinant of theropod skull shape.

TABLE OF CONTENTS

LIST OF ILLUSTRATIONS

ACKNOWLEDGEMENTS

It's been quite a ride doing science at the American Museum of Natural History and Columbia University for the past four and a half years, and there are many people that I need to thank for advice, assistance, guidance, help, and friendship during my time working on this thesis.

First and foremost, I am deeply grateful to my advisor, Mark Norell, who has been a trusted mentor, collaborator, and friend during my time in New York. None of this project would have been possible without Mark—not without the Theropod Working Group that he established at the AMNH over a decade ago, not without the reams of specimens that he has collected in Mongolia, not without the unparalleled group of researchers that he has cultivated at the AMNH (which now form a large collaborative community), not without the funding he provided and helped me secure, and certainly not without the many fun times from Billy's to Bucharest and everywhere in between. Along with Mark, my other committee members at the AMNH (John Flynn) and Columbia (Paul Olsen) have provided valuable help and support. Although I am not officially an RGGS graduate student at the American Museum, John and his staff have made me feel most welcome in the museum and have the given me the opportunity to integrate within two graduate schools. Paul gave me two great opportunities to assist him with his wonderful Dinosaurs and the History of Life course at Columbia, and has also kept me grounded in the Triassic while I worked on a thesis that was largely Cretaceous dinosaur-centric. I also thank my other committee members, Nick Christie-Blick at Columbia and my external member Pete Makovicky from the Field Museum, especiall for stepping in relatively late in the game to make sure this thesis was finished on time.

There is no place in the world quite like the AMNH. Everyone in the field of paleontology is envious of the museum's world-leading collections, but my favorite part of working here was getting a chance to work with and become friends with a wonderfully diverse group of students and fellow scientists. My fellow paleontology graduate students have been a constant source of inspiration: Amy Balanoff, Jianye Chen, Andres Giallombardo, Eugenia Gold, Shaena Montanari, Sterling Nesbitt, Rui Pei, Michelle Spauling, Kaori Tsukui, Aki Watanabe, Abby West, and Hongyu Yi. So have a number of postdocs who have become good friends and colleagues: Rob Beck, Gabe Bever, Jonah Choiniere, Christian Kammerer, Fernando Perini, Alan Pradel, and Albert Prieto-Marquez. I must also acknowledge the incredible community of RGGS students at the museum, and especially those guinea pig students who inaugurated the RGGS program in the fall of 2008 when I began my work at Columbia: Zach Baldwin, Bryan Falk, Antonia Florio, Sebastian Kvist. The curators at the AMNH set the standard for creativity and productivity that I hope to emulate during my career: Denton Ebel, Jin Meng, Mike Novacek, Susan Perkins, Mark Siddall, Ward Wheeler. I would be daft, indeed, to even think about forgetting to acknowledge the large support staff at the AMNH and Columbia who have ensured that the bureaucracy always flowed smoothly, my stipend checks arrived on time, and that I had keys to my office and collections: Maria Dickson, Judy Galkin, Jorge Galvez, Taylor Johnson, Adam Kashuba, Mia Leo, Anna Manuel, Carol Mountain, Sally Odland. And in the same vein, I could have done nothing without Mick Ellison. Mick is a good friend, a trusted sidekick, and probably the best all-around artist (photography, illustration, painting, digital art, you name it) that I have ever known. His photos are used liberally in this dissertation and have been the bright spots in several of my papers. So many projects would have been impossible without him, and in particular, I will always be grateful for the 300+ photos that Mick took for

our *Alioramus* project. In addition to Mick, the alarmingly-talented Frank Ippolito and Jason Brougham have helped with several projects, and they're also good company over a beer. And the same goes for the collections and preparation staff at the AMNH: Carl Mehling, Ruth O'Leary, Alana Gishlick, Amy Davidson, Justy Alicea, and Anna Balcarcel. And thanks also to Mary Knight in the publications office for all of her help.

Probably the best part of doing science is the opportunity to travel and work with a global community of creative researchers. I would like to thank my many collaborators on projects over the years, who have always inspired me and have taken me in research directions unimaginable: Carol Abraczinskas, Marco Andrade, Brian Andres, Brian Beatty, Mark Bell, Roger Benson, Mike Benton, Robert Bronowicz, Richard Butler, Thomas Carr, Matt Carrano, Dan Chure, Zoltan Csiki, Phil Currie, Julia Desojo, Phil Donoghue, Jerzy Dzik, Gareth Dyke, Greg Erickson, Martin Ezcurra, Christian Foth, Dave Gower, Will Harcourt-Smith, Mike Henderson, Christophe Hendrickx, Tom Holtz, Dave Hone, John Hutchinson, Steve Hutt, Randy Irmis, Dwight Jennison, Dan Ksepka, Mike LaBarbera, Max Langer, Jeff Liston, Graeme Lloyd, Mark Loewen Octavio Mateus, Josh Mathews, Ralph Molnar, Tetsuto Miyashita, Darren Naish, Grzegorz Niedźwiedzki, Chris Organ, Dan Peppe, Emily Rayfield, Mike Reich, Marcello Ruta, Manabu Sakamoto, Jonas Satkunas, Rainer Schoch, Ross Secord, Paul Sereno, Akiko Shinya, Nate Smith, Lorna Steel, Seb Steyer, Tomasz Sulej, Corwin Sullivan, Piotr Szrek, Radu Totoianu, Emanuel Tschopp, Alan Turner, Matyas Vremir, Steve Wang, Mark Webster, Anne Weil, Jessica Whiteside, Scott Williams, Tom Williamson, Mark Young, Zhao Xijin, and Xu Xing.

I visited a number of collections to collect data for this thesis project, and I think the curators that helped arrange my visits, granted access to specimens, and provided hospitality during my trips: Ronan Allain, Sebastian Apesteguia, Ruben Barbieri, Jeff Bartlett, Bernard

Battail, Magdalena Borsuk-Bialynicka, Dan Brinkman, Angela Buscalioni, Premji Carabajal, Sandra Chapman, Karen Cloward, Rodolfo Coria, Ted Daeschler, Ross Elgin, Dino Frey, Jacques Gauthier, Mike Getty, Steve Hutt, Randy Irmis, Paul Jeffrey, Martina Kolbl-Ebert, Alejandro Kramarz, Jesús Marguán-Lobón, Clark Miles, Cliff Miles, Fernando Novas, Oliver Rauhut, Jose Sanz, Paul Sereno, Tomasz Sulej, Pino Volkl, Xu Xing, and Zhao Xijin.

My PhD research was funded primarily by an NSF Graduate Research Fellowship, as well as a research fellowship at the American Museum of Natural History. This dissertation work was funded by an NSF Doctoral Dissertation Improvement Grant (DEB 1110357) as well as a Columbia University Graduate School of Arts and Sciences Travel Fellowship, a Malcolm McKenna Graduate Student Research Award at Columbia University, and an M.A. Fritz Travel Grant from the Royal Ontario Museum.

In closing, I will thank the most important people in my life. First and foremost, my lovely and understanding wife Anne, who moved to New York with me (a long way from England) so that I could do fulfill my dream of doing a PhD at the American Museum of Natural History. I will always deeply appreciate that and do hope that I can repay the gift soon, immigration foibles pending. My parents Jim and Roxanne Brusatte always supported whatever my interest of the week was as a child, and when my passions focused in on paleontology as a teenager they were always there to buy me that book I wanted, or visit a museum on a family vacation, or let me use the car to look for fossils. My brothers, Mike and Chris, put up with it. And to my relatives, my inlaws, my friends and neighbors back in Ottawa, Illinois, thank you to you all as well. To anyone I have forgotten, my deepest apologies. And to all: May the hinges o frien'ship ne'er rust, nor the wings o love lose a feather!

INTRODUCTION

Theropod dinosaurs—the major group of mostly predatory forms such as *Tyrannosaurus* and *Velociraptor*—are among the most familiar and iconic organisms in earth history. Not only are these species charismatic to the general public, but they also hold a critical significance in the history of life for one simple reason: theropod dinosaurs are the evolutionary ancestors of birds. In fact, to phrase it more properly, birds are actually living theropods.

The evolution of birds from theropod dinosaurs was one of the great evolutionary transitions in the history of life. This transition has emerged as a textbook example—something of a "model system"—for understanding the origins of major clades, body plans, and ecological behaviors, thanks to a rapidly expanding fossil record of early birds and their closest dinosaurian relatives (the coelurosaurian theropods: the group defined as all theropods more closely related to birds than to *Allosaurus*). This influx of new discoveries includes theropod dinosaurs covered with bona fide feathery integument (e.g., Chen et al. 1998; Norell and Xu 2005; Xu and Guo 2009), theropods with stereotypical "avian" features such as wishbones and a wrist that can fold against the body (e.g., Nesbitt et al. 2009; Sullivan et al. 2010), and theropods preserved in the characteristic sleeping and egg-brooding postures of living birds (e.g., Norell et al. 1995; Xu and Norell 2004). Furthermore, more than 50 new species of early birds and close coelurosaurian relatives have come to light over the past two decades, largely from the exceptionally-preserved Early Cretaceous Jehol Group of northeastern China (e.g., Chen et al. 1998; Ji et al. 1998; Zhou et al. 2003; Norell and Xu 2005).

These discoveries, as well as other important new fossils from South America, Europe, and North America, have been the subject of extensive phylogenetic research. As a result, the genealogy of birds and their very closest coelurosaurian cousins—taxa such as the sickle-clawed dromaeosaurids and the mostly crested and toothless oviraptorosaurs—is understood in fine detail, although of course some debates still remain (e.g., Turner et al. 2007a, 2012; Senter 2007; Choiniere et al. 2010a, 2012; Csiki et al. 2010). This provides a phylogenetic context for understanding major macroevolutionary changes and trends during the evolution of birds and powered flight, a great asset that is not available when studying many other major transitions in the history of life. For instance, studying the origin of animals, insects, or tetrapods is made difficult by a patchy fossil record and a less complete phylogenetic framework, making it tricky to pinpoint when major anatomical changes occurred and understand more general patterns and rates of character change. The theropod-bird transition, therefore, provides a remarkable opportunity to study a classic evolutionary transformation in meticulous detail.

The recent explosion of new fossil discoveries, incorporated into ever-expanding phylogenetic datasets, has provided several general revelations about the evolution of birds. Birds evolved from theropod dinosaurs, many supposedly quintessential avian characters such as feathers and wishbones originated in non-flying theropods, and familiar theropods such as *Velociraptor* and *Deinonychus* are some of the closest relatives to birds (see review in Padian and Chiappe 1998). However, despite the flurry of research on birds and their dinosaurian relatives, several questions and problems still remain. First, many important theropod taxa are still poorly described in the literature and the anatomy of some major theropod groups has yet to be studied in detail, which hinders the development of large anatomical datasets needed to reconstruct phylogeny and study patterns of evolution. Second, and following from this issue,

there is little consensus on the phylogenetic relationships of the most basal coelurosaurian theropods, impeding our ability to reconstruct a complete, species-level genealogy of birds and their closest dinosaurian forbearers. Third, there has been little synthetic work on large-scale macroevolutionary patterns during theropod evolution, both over the course of 150+ million years of Mesozoic theropod history and across the theropod-bird transition.

This dissertation touches on these three major issues. The first chapter is a detailed anatomical description of *Alioramus altai*, a new species of long-snouted and gracile theropod closely related to *Tyrannosaurus* that my colleagues and I named during the first year of my graduate work at Columbia-AMNH (Brusatte et al. 2009a). Despite their tremendous popularity with the public and their frequent use as "exemplar taxa" for paleobiological studies, tyrannosauroids are relatively poorly described in the paleontological anatomical literature. More specifically, detailed descriptions of tyrannosauroid postcranial skeletons are almost nonexistent. The first chapter, therefore, aims to comprehensively describe a well preserved and relatively complete tyrannosauroid specimen, and establish anatomical data that can be useful for future phylogenetic and evolutionary studies. Indeed, a revision of tyrannosauroid phylogeny stemmed from this descriptive project (Brusatte et al. 2010a; see below). This chapter was recently published in the *Bulletin of the American Museum of Natural History* (Brusatte et al. 2012a).

The second chapter is a comprehensive species-level phylogeny of coelurosaurian theropods. It is the latest iteration of the decade-long Theropod Working Group project at the American Museum of Natural History, led by Mark Norell, which continuously incorporates new character and taxon data into an ever-growing phylogeny of coelurosaurs. Previous TWiG analyses have focused heavily on birds and their closest relatives, whereas more basal

coelurosaurs such as tyrannosauroids, ornithomimosaurs, and compsognathids have been represented by limited taxa and characters. This portion of my dissertation seeks to rectify this issue by combining the most recent TWiG dataset (presented by Turner et al. 2012) with a wealth of new data relvant to basal coelurosaurs, some of which is compiled from the literature but most of which was established as part of this dissertation project. These new data include characters and character scores relevant to tyrannosauroid ingroup phylogeny that were published by Brusatte et al. (2010a) in *Science*. The new phylogeny presented here allows for a more stringent test of coelurosaurian relationships, especially the phylogeny of the oldest and earliest diverging members of the clade. It establishes a more robust framework for understanding the origin of birds and their closest relatives and patterns of morphological evolution associated with the Mesozoic radiation of theropods and the theropod-bird transition.

The third chapter is a macroevolutionary study that uses specimen-level anatomical information and a phylogenetic context to quantify major trends in theropod morphological evolution during the Mesozoic. It is a geometric morphometric analysis that examines differences in cranial shape among theropods, looks at progressive changes in theropod cranial shape on the line to birds, and tests whether phylogeny or feeding style (function) was a more important determinant of major trends in theropod skull evolution. This chapter was recently published in the *Journal of Evolutionary Biology* (Brusatte et al. 2012b).

Taken together, these chapters on anatomy, phylogeny, and macroevolution present new data that help to better understand the morphology of basal coelurosaurian theropods, the genealogy of birds and their closest relatives, and fundamental patterns of evolution during the Mesozoic history of theropod dinosaurs. Each chapter is presented separately, with tables and figures relevant to that chapter following the text of the chapter in question. All references,

however, are pooled together at the end of this dissertation. Three appendices are also presented at the end of the dissertation, two of which are relevant to Chapter 2 (phylogeny) and one of which pertains to Chapter 3 (macroevolution).

ABBREVIATIONS

The following abbreviations for museum collections are used in this work:

AMNH FARB	Fossil Amphibian, Reptile, and Bird Collections, American Museum of Natural History, New York, USA
ANSP	Academy of Natural Sciences, Philadelphia, Pennsylvania, USA
BHI	Black Hills Institute of Geological Research, Hill City, South Dakota, USA
BMR	Burpee Museum of Natural History, Rockford, Illinois, USA
BSP	Bayerische Staatssammlung für Paläontologie und Geologie, Munich, Germany
BYU	Brigham Young University Museum, Provo, Utah, USA
CEUM	College of Eastern Utah Prehistoric Museum, Price, Utah, USA
CM	Carnegie Museum of Natural History, Pittsburgh, Pennsylvania, USA
CMN	Canadian Museum of Nature, Ottawa, Ontario, Canada
CMNH	Cleveland Museum of Natural History, Cleveland, Ohio, USA
EME	Transylvanian Museum Society, Cluj-Napoca, Romania
FDRC	Fossil Research and Development Center, Gansu Bureau of Geology and Mineral Resources Exploration, Lanzhou, People's Republic of China

HMN Humboldt Museum für Naturkunde, Berlin, Germany

JME Jura Museum, Eichstatt, Germany

IGM Institute of Geology, Ulaan Baatar, Mongolia

IVPP Institute of Vertebrate Paleontology and Paleoanthropology, Beijing, People's Republic of China

LACM Los Angeles County Museum, Los Angeles, California, USA

LH Museo de Cuenca, Cuenca, Spain (housed at Unidad de Paleontologiá, Universidad Autonomá de Madrid, Spain)

LH PV Long Hao Institute of Geology and Paleontology, Hohhot, People's Republic of China

LVP (FGGUB) Paleontology Collection, Faculty of Geology and Geophysics, University of Bucharest, Bucharest, Romania

MCF Museo Municipal Carmen Funes, Plaza Huincul, Argentina

MIWG Museum of Isle of Wight Geology (Dinosaur Isle, Isle of Wight Museum Services, IWCMS), Sandown, England, United Kingdom

MML MML Collection of Museo Argentino de Ciencias Naturales, Buenos Aires, Argentina

MNHN Muséum National d'Histoire Naturelle, Paris, France

MOR Museum of the Rockies, Bozeman, Montana, USA

MPC Mongolian Paleontological Center, Ulaan Baatar, Mongolia

MPCA Museo Carlos Ameghino, Cipolletti, Argentina

NGMC National Geological Museum of China, Beijing, China

NHM The Natural History Museum, London, England, United Kingdom

NMC	National Museums of Canada (Canadian Museum of Nature—CMN), Ottawa, Ontario, Canada
NMMNH	New Mexico Museum of Natural History and Science, Albuquerque, New Mexico, USA
OUMNH	Oxford University Museum of Natural History, Oxford, England, United Kingdom
PIN	Paleontological Institute, Moscow, Russia
RMM	Red Mountain Museum, McWane Center, Birmingham, Alabama, USA
ROM	Royal Ontario Museum Toronto, Ontario, Canada
RTMP	Royal Tyrrell Museum of Palaeontology, Drumheller, Alberta, Canada
SMNK	Staatliches Museum für Naturkunde, Karlsruhe, Germany
TPII	Thanksgiving Point Institute, Lehi, Utah, USA
UALVP	University of Alberta Laboratory for Vertebrate Paleontology, Edmonton, Canada
UMNH	University of Utah Museum of Natural History, Salt Lake City, Utah, USA
UUVP	University of Utah Vertebrate Paleontology Collection, UMNH (see above)
YPM	Yale Peabody Museum, New Haven, Connecticut, USA
ZPAL	Instytut Paleobiologii PAN, Warsaw, Poland

CHAPTER 1:

THE OSTEOLOGY OF *ALIORAMUS*, A GRACILE AND LONG-SNOUTED TYRANNOSAURID (DINOSAURIA: THEROPODA) FROM THE LATE CRETACEOUS OF MONGOLIA

PREFACE NOTE: This chapter was published as Brusatte et al. (2012a). This publication was a collaboration between me, Thomas Carr, and Mark Norell. The great majority of this paper was my original work, including most of the descriptions, comparisons, and the construction of the figures (which include photographs taken by Mick Ellison under my direction). I wrote and formatted the manuscript. Carr contributed comparative information for other tyrannosaurid species (e.g., *Albertosaurus*, *Gorgosaurus*, *Tyrannosaurus*), helped clarify the descriptions, contributed information on tyrannosaurid ontogeny and ontogenetically-related differences between *Alioramus altai* and *Alioramus remotus*, and edited the manuscript thoroughly. He largely wrote three sections in the discussion of the original paper ("Discrete character changes during tyrannosaurid ontogeny"; "Cephalic ornamentation of *Alioramus*"; "Evolutionary development of the long, low skull of *Alioramus*"). Because these are largely his work and not mine, they are not included in this thesis. Norell led the team that discovered the specimen, helped clarify descriptions, and edited the manuscript thoroughly.

INTRODUCTION

The Late Cretaceous tyrannosaurid *Alioramus* has long been one of the most puzzling and poorly understood large carnivorous theropod dinosaurs. Kurzanov (1976) established this

genus, and named the type species *A. remotus*, based on a series of fragmentary cranial bones and limited postcranial material from the Late Cretaceous of Mongolia. The specimen was collected at the Nogon Tsav locality in Bayankhnongor Aimag and is now housed in the the Paleontological Institute in Moscow, Russia (PIN 3141/1). Kurzanov (1976) recognized numerous similarities shared between *Alioramus* and tyrannosaurids such as *Tyrannosaurus* and *Tarbosaurus*, and formally assigned the new genus to this iconic group of colossal predatory dinosaurs. Later authors accepted the tyrannosaurid affinities of the *Alioramus* type specimen and noted that it was smaller and more gracile than other tyrannosaurids, likely due its immaturity (e.g., Currie, 2003a; Hurum and Sabath, 2003). However, subsequent authors disagreed on whether it represented a new taxon or was a juvenile of *Tarbosaurus* (e.g., Currie, 2003a), and if a valid taxon, whether it could be referred to the Tyrannosauridae proper (sensu Sereno et al., 2005) or represented a more basal taxon on the tyrannosauroid stem (Holtz, 2001, 2004; Currie et al., 2003; Hurum and Sabath, 2003).

The discovery of a well preserved and substantially complete *Alioramus* skeleton at the Tsaagan Khuushu locality in the Maastrichtian Nemegt Formation of Mongolia has clarified these riddles (fig. 1). Brusatte et al. (2009a) described this specimen, which was discovered by Julia Clarke and collected during the 2001 American Museum-Mongolian Academy of Sciences expedition, as a new species of *Alioramus*, *A. altai*. The specimen was recovered within in a tan sandstone lens sandwiched between two indurated shelves of more coarse sandstone (fig. 2). Some of the skeleton was destroyed by erosion previous to reovery and thousands of fragments were exposed downslope. Preliminary excavation showed that while some of the skeleton was missing, most of the cranial elements were present, although disarticulated (fig. 2). Further excavation during the 2001 expedition revealed that these cranial elements were exquisitely

preserved (fig. 3), oftentimes retaining detailed surface texture and thin flanges of bone less than a few millimeters in thickness. The specimen was collected in four blocks and prepared by Amy Davidson (and others under her direction) in the AMNH preperation laboratory.

This specimen is critical because it is only the second fossil of *Alioramus* that has been reported (although others are known to exist via the illicit commercial trade) and offers a great improvement on the fragmentary, poorly-preserved, and often difficult to access *A. remotus* type specimen. In a brief report, Brusatte et al. (2009a) described this specimen as belonging to an immature individual that was substantially different in morphology and body proportions than similarly-aged members of other tyrannosaurid species, notably the contemporary *Tarbosaurus*, a taxon that also found at Tsaagan Khushu. Most importantly, *Alioramus* is smaller (approximately half the body mass) and more gracile than other tyrannosaurids, and possesses a long snout and numerous cranial horns (figs. 1, 4). Nonetheless, phylogenetic analyses in the short description and a subsequent publication (Brusatte et al., 2010a) show that, despite its divergent morphology, *Alioramus* is nested within the tyrannosaurid clade and is more closely related to *Tarbosaurus* and *Tyrannosaurus* than to taxa such as *Albertosaurus* and *Gorgosaurus*.

Here we present an exhaustive description of the skeletal osteology of the *A. altai* type specimen (IGM 100/1844), expanding on the short initial report of Brusatte et al. (2009a). Surprisingly, such monographs have rarely been undertaken for individual tyrannosaurid taxa, despite the iconic status of this clade, the rich fossil record of the group, and the popularity of tyrannosaurids as exemplary research models in paleobiology. Most existing tyrannosaurid monographs were completed long before the advent of phylogenetic systematics (e.g., Osborn, 1912; Lambe, 1917; Parks, 1928; Russell, 1970; Maleev, 1974) or have focused specifically on the most famous tyrannosaurid of all, *Tyrannosaurus rex* (Molnar, 1991; Brochu, 2003). Other

taxa, such as *Albertosaurus*, *Gorgosaurus*, and *Tarbosaurus*, have been revised recently but have not been the subject of exhaustive and well-illustrated descriptions (e.g., Carr, 1999, 2010; Currie, 2003a; Hurum and Sabath, 2003). Furthermore, most of these descriptions have focused on the skull, and only limited information on tyrannosaurid postcrania, especially the axial skeleton, is available in the modern literature.

In this monograph, we provide a thorough, bone-by-bone description of the skull (excluding the braincase, whose most salient features were described by Bever et al. [2011] and which will be fully described in a separate publication), axial skeleton, and appendicular skeleton of the *Alioramus altai* type specimen. Such a detailed description is made possible by the fine preservation and disarticulated nature of most of the skeleton, especially the skull. Following from our observations and descriptions, we present wide-ranging comparisons between *Alioramus* and other tyrannosauroids, running the gamut from basal taxa such as *Dilong*, *Guanlong*, and *Eotyrannus* to more derived tyrannosaurids. These comparisons are based extensively on first-hand specimen observations of basal tyrannosauroids (SLB, MAN, TDC) and tyrannosaurids (TDC, SLB). The comparative aspect of this project was used as a foundation for the tyrannosauroid phylogenetic analysis of Brusatte et al. (2010a), which was able to combine these new observations and information from newly discovered taxa to greatly expand taxonomic and character sampling relative to previous studies. This monograph is, in many ways, a companion to the phylogeneic analysis of Brusatte et al. (2010a). Many characters used in the analysis, which could only merit cursory description in the phylogeny paper, are explained more fully here. Aside from providing a robust phylogeny, the comparative phylogenetic study also illuminates patterns of character transition over the 100-million-year evolutionary history of

these quintessential dinosaurian predators, elucidating the major changes as small, nimble basal taxa developed into some of the most colossal terrestrial predators to ever live.

SYSTEMATIC PALEONTOLOGY

Theropoda Marsh, 1881a

Tetanurae Gauthier, 1986

Coelurosauria Huene, 1914

Tyrannosauroidea Osborn, 1905

Tyrannosauridae Osborn, 1905 (sensu Sereno et al., 2005)

Tyrannosaurinae Osborn, 1905 (sensu Currie et al., 2003)

Alioramus Kurzanov, 1976

Alioramus altai Brusatte et al., 2009

Holotype: IGM 100/1844. Substantially complete skeleton found associated and belonging to a single individual, including a nearly complete and disarticulated skull; the cervical series; dorsal, sacral, and caudal vertebrae; cervical and dorsal ribs; chevrons; right ilium; left and right ischium; left and right femur; right crus, tarsus, and metatarsus; various metatarsals and pedal phalanges. Completely unknown are many of the dorsal, sacral, and caudal vertebrae; shoulder girdle and forelimbs; the pubes; regions of the hindlimbs; and some pedal phalanges (fig. 1).

Type Locality: Maastrichtian Nemegt Formation, collected at Tsaggan Khushuu (originally called Tsagaan Uul), Mongolia (fig. 2).

Preparation Details of the Holotype: The specimen (IGM 100/1844) was prepared primarily by Amy Davidson at the American Museum of Natural History, and preparation records are held in the AMNH Division of Paleontology database. Some techniques for preparation and curation that were used on the specimen are described in three published abstracts (Davidson et al., 2006; Davidson, 2008, 2009). The specimen was consolidated with Butvar® B-76 (Monsanto Company), a terpolymer of vinyl butyral, vinyl alcohol, and vinyl acetate monomers. Joins were made with Paraloid® B-72 (Rohm and Haas Company), an ethyl methacrylate and methyl acrylate copolymer. The specimen is very brittle and archival supports for all the skull elements were made out of

Ethafoam® polyethylene foam, polyester batting and Tyvek® Soft Structure polyethylene fabric.

Diagnosis: A tyrannosauroid theropod possessing the following autapomorphies: an accessory pneumatic fenestra posterodorsal to the promaxillary fenestra; large and elongate maxillary fenestra (length:depth ratio of 1.9); a conical and dorsally extending cornual process (horn) on the lacrimal*; a laterally projecting horn on the jugal; a thick ridge on the dorsal surface of the ectopterygoid; a palatine pneumatic recess that extends posteriorly beyond the posterior margin of the vomeropterygoid process; 20 dentary alveoli; an anteroposteriorly long anterior mylohyoid foramen of the splenial; a thin epipophysis on the atlantal neurapophysis that terminates as a sharp point; a pneumatic pocket on the anterior surface of the cervical transverse processes; an external pneumatic foramen on the dorsal ribs; a posterior margin of iliac postacetabular process projecting posterodorsally*. Asterisks denote autapomorphies recognized here for the first time, whereas characters without an asterisk were recognized by Brusatte et al. (2009a).

Two characters considered autapomorphies of *A. altai* by Brusatte et al. (2009a) are now known to be more widely distributed in tyrannosaurids, and therefore not unique to *A. altai*. A palatine pneumatic recess that extends posteriorly beyond the posterior margin of the vomeropterygoid process is also present in *Daspletosaurus* (MOR 1130). An anterodorsally inclined midline ridge on the lateral surface of the ilium is also present in some, but not all, specimens of *Daspletosaurus* (CMN 8506), *Gorgosaurus* (CMN 2120), and *Tyrannosaurus* (BMR 2002.4.1); it is likely that the orientation of the ridge is individually variabile in many tyrannosaurid taxa, and therefore of little diagnostic value.

DESCRIPTION

General Skull: In general, the skull of *Alioramus altai* is long and low in comparison to other tyrannosaurids (fig. 4; cranial measurements in Table 1). The longirostrine skull shape is mostly a function of elongated snout bones anterior to the orbit, including the maxilla, nasal, jugal, lacrimal, and dentary. These bones, as well as the circumorbital and circumtemporal bones, are gracile compared to other tyrannosaurids. The skull is heavily ornamented, with eight discrete "horns" on each side (lacrimal, postorbital, jugal cornual process, autapomorphic jugal lateral horn) and three prominent rugosities on the midline of the nasal.

Kurzanov (1976) originally noted the long, gracile nature of certain cranial bones in his description of *Alioramus remotus*. However, Currie (2003a:221) did not consider the longirostrine skull shape as a distinctive feature of the genus, instead stating that the "skull is low because of the small size of the specimen, and the 'greatly elongated jaws' are typical for all tyrannosaurid individuals of this size." Currie (2003a) was correct that smaller and more

immature tyrannosaurids have proportionally longer skulls than larger and more mature individuals, a pattern borne out by discrete character analysis (Carr 1999) and allometric growth curves (Currie 2003b). However, the type specimen of *A*. *remotus* is comprised almost entirely of the skull, with only a few postcranial fragments. This is problematic because long bones such as the femur and tibia are standard proxies for body size (e.g., Christiansen and Farina 2004), and their absence in *A*. *remotus* prevents an accurate estimate of its body size. Thus, the hypothesis that the *A. remotus* skull is typical for tyrannosaurids of its size cannot be rigorously tested.

Fortunately, the *A*. *altai* holotype includes a nearly complete skull and a complete femur. When skull length and femur length are plotted with those of other tyrannosaurids assessed by Currie (2003b), *Alioramus* falls above the regression line for other taxa. In other words, *Alioramus* has a longer skull than other tyrannosaurids of similar femoral length, and thus similar body size (fig. 5). Currie's (2003a) hypothesis that ontogenetic scaling, not taxonomic differentiation, explains the longirostrine skull of *Alioramus* is therefore falsified. The long skull of *Alioramus* is a diagnostic feature of the genus and it is a unique morphology that sets it apart from close tyrannosaurid relatives.

Maxilla: Both left and right maxillae are known, each of which is essentially complete (figs. 6-9). The left is well preserved and undistorted (figs. 6, 8-9), whereas the right bone is slightly crushed dorsoventrally (fig. 7). The maxilla is long and low, and more closely resembles the proportions of juvenile tyrannosauroid maxillae (e.g., Carr, 1999: fig. 2) than the deeper and shorter maxillae of large, adult tyrannosaurids such as *Tyrannosaurus* (Osborn, 1912: fig. 1), *Tarbosaurus* (Hurum and Sabath, 2003: fig. 4), *Daspletosaurus* (Russell, 1970: fig. 1), and *Gorgosaurus* (Currie, 2003a: fig. 2), as well as adults of the basal tyrannosauroid *Bistahieversor*

(Carr and Williamson, 2010: fig. 1). However, the maxilla of *A. altai* is especially elongate, even compared to those of juveniles (Table 2). The *A. altai* maxilla is most similar in proportions to that of *Applachiosaurus* (Table 2; Carr et al., 2005), and appears generally similar to the reconstructed maxilla of *Alioramus remotus* (Kurzanov, 1976: fig. 1). However, the maxilla of *A. remotus* is broken dorsally and incomplete (as described by Kurzanov, 1976: fig. 4), precluding exact comparison.

The maxilla is comprised of two main processes: the main body ventrally and the ascending ramus dorsally, which diverge to form the anterior margin of the antorbital fenestra. There is no distinct anterior ramus, as the anterior margin of the maxilla, where the main body meets the ascending ramus, is smoothly confluent and not marked by a convex step. This is a characteristic of tyrannosauroids in general, but an anterior ramus set off by a convex step is present in the basal tyrannosauroids *Guanlong* (Xu et al., 2006: fig 2), *Proceratosaurus* (Rauhut et al., 2010: fig. 2), and *Sinotyrannus* (Ji et al., 2009: fig. 1). A small anterior ramus appears to be present in *Dilong* (Xu et al., 2004: fig 1), but this is an artifact of breakage (IVPP V14343).

The anterior margin of the *A. altai* maxilla extends at a low posterodorsal angle and is only slightly convex, in contrast to the relatively steep posterodorsal angle and strongly convex and rounded margins of most tyrannosaurids (e.g., Brochu, 2003: fig. 2; Currie, 2003a: fig. 2; Hurum and Sabath, 2003: fig. 4; Carr et al., 2005: fig. 5), including juveniles (Carr, 1999: fig. 2; Currie and Dong, 2001a: fig. 1) (Table 3). The ventral margin along the tooth row is approximately straight in *A. altai*. Although there is a region of slight convexity along alveoli 1-6, this contrasts with the strongly convex profile of the entire ventral margin in most tyrannosaurids, including both adults (e.g., Osborn, 1912: fig. 1; Hurum and Sabath, 2003: fig. 4) and juveniles (e.g., Carr, 1999: figs. 2, 5, 6; Currie and Dong, 2001a: fig. 1). The condition in

Alioramus remotus (Kurzanov, 1976: fig. 4) and *Raptorex* (Sereno et al., 2009) are similar to that in *A. altai*.

The main body of the maxilla is shallow (Table 2), and in medial view crypts for replacement teeth extend, at most, approximately 40 mm above the tooth row. Once again, this differs from the deeper main bodies of adult tyrannosaurids, which are expanded dorsoventrally to accommodate extremely long tooth roots and replacement teeth (e.g., Osborn, 1912: fig. 1; Hurum and Sabath, 2003: fig. 4). *Applachiosaurus* (Carr et al., 2005: fig. 5), *Alioramus remotus* (Kurzanov, 1976: fig. 4), and some juvenile tyrannosaurids (Carr, 1999: figs. 2, 5, 6; Currie and Dong, 2001a: fig. 1) have shallower main bodies similar to the condition in *A. altai.* In *A. altai* the main body tapers in depth posteriorly below the antorbital fenestra; it begins as a 50 mm deep process at the anterior margin of the fenestra and reduces to a depth of only eight mm at its posterior tip. A similar degree of posterior tapering of the maxilla is generally present in tyrannosaurids, including both adults and juveniles (e.g., Carr, 1999: fig. 2; Brochu, 2003: fig. 2; Currie, 2003a: fig. 18).

The premaxilla articulated with the maxilla anteriorly, along the ventral region of the sloping anterior margin of the maxilla. The strong posterodorsal orientation of the anterior margin, along with its straight profile, results in a sharp point at the anteroventral corner of the maxilla where the anterior and ventral margins meet. A sharp point is also seen in *Alioramus remotus* (Kurzanov, 1976: fig. 4), but differs from the more rounded anteroventral corners of most tyrannosaurids, including adults and juveniles (e.g., Carr, 1999: figs. 1, 5, 6; Currie, 2003a: fig. 2; Hurum and Sabath, 2003: fig. 4; Carr et al., 2005: fig. 5). Thus, in *A. altai*, the premaxillary articulation slopes strongly posterodorsally, following the straight anterior margin of the maxilla, when seen in lateral view. This contact is oriented much more dorsoventrally in

most other tyrannosaurids (e.g., Carr, 1999: fig. 5; Currie and Dong, 2001a: fig. 1; Brochu, 2003: fig. 2; Hurum and Sabath, 2003: fig. 4).

The premaxillary articulation is complex. As seen in anterior and dorsal views, there is a deep notch between the main body of the maxilla laterally and the anteromedial process medially, which would have received the palatal process of the premaxilla. This notch is 20 mm long anteroposteriorly and is surrounded by several small rugosities and foramina, suggesting that the premaxilla-maxilla contact was immobile. Lateral to the notch, and visible in anterior and lateral views, is an anterolaterally facing surface pierced by two large foramina. The anterior edge of this surface is marked by a notch, which is the maxillary contribution to the small subnarial foramen, which would have opened between the premaxilla and maxilla in life (fig. 6, snf). The subnarial foramen is always small in tyrannosaurids and not always visible in lateral view (e.g., Carr, 1999: fig. 6; Currie, 2003a: fig. 2; Hurum and Sabath, 2003: fig. 1). The anterolaterally facing surface is indented somewhat from the lateral surface of the main body, and represents the extension of the narial fossa onto the maxilla. Dorsal to this fossa is a smooth groove, which is located on the anterior margin of the maxillary ascending ramus and faces dorsally and anteriorly, which would have articulated with the subnarial process of the premaxilla. This groove is not visible in lateral view, as it is concealed by a sharp lip of bone. Posteriorly, this groove becomes confluent with another groove, which articulated with the nasal. Thus, the maxilla would not have contributed to the floor of the external naris, as is the case in derived tyrannosauroids generally (e.g., Brochu, 2003: fig. 2; Currie, 2003a: fig. 18; Hurum and Sabath, 2003: fig. 1).

The nasal articulates with the maxilla along a groove, described above, that extends along the anterior margin of the ascending ramus. This groove faces anteriorly and dorsally, and

extends for 115 mm posteriorly from the point where it joins the groove for the subnarial process of the premaxilla. This nasal groove is widest anteriorly, where it meets the groove for the premaxilla, and then narrows in width posteriorly before terminating at a narrow point, where it is bounded laterally and medially by very thin and sharp ridges. The nasal articulation is a smooth suture, and is not reinforced with a complex series of interlocking rugosities as in adult *Daspletosaurus*, *Tyrannosaurus* and *Tarbosaurus* (Carr, 1999; Hurum and Sabath, 2003), as well as the more basal tyrannosauroid *Bistahieversor* (Carr, 2004). Juvenile *Tarbosaurus* also possesses a smooth suture (Tsuihiji et al., 2011), suggesting that this morphology is present in *A. altai* because of the young age of the specimen.

The lacrimal articulates with the posterior end of the maxillary ascending ramus, which is bifurcated to "accept a slender anterior process of the lacrimal" (Brochu 2003:21). This condition is seen in other derived tyrannosauroids. Medially, the posterior end of the ascending ramus is marked by a long indentation, which extends nearly to the anterior margin of the antorbital fenestra and is covered with a fine series of anteroposteriorly-trending lineations (fig. 6, lac). This shallowly depressed region would have received the medial process of the lacrimal. Anteriorly, this depression continues as a thin groove paralleling the anterior margin of the ascending ramus, which is located approximately 5 mm ventral to the dorsal margin of the ramus. This groove clearly was not an articular surface, and it may have supported cartilage or soft tissues associated with the paranasal sinus.

The jugal articulates with the posterior end of the main body of the maxilla, below the posteroventral corner of the antorbital fenestra (figs. 6, 8, jug). This articulation takes the form of a scarf joint, with the jugal laterally overlapping the tapering posterior end of the maxilla. Ventrally, the jugal rested within a deep and narrow, dorsally-facing groove on the maxilla,

which strengthened the contact. This groove is confluent anteriorly with the smooth internal antorbital fossa. The maxilla-jugal contact is further strengthened by a small subsidiary process of the maxilla, which rises dorsally to contact the anterior margin of the jugal (figs. 6, 8, bif). This small process, which is partially broken in both maxillae, results in a "bifurcation" of the jugal articular surface, a characteristic feature of tyrannosaurids (Currie, 2003a) and more basal taxa (e.g., *Dilong*: IVPP V14243). The ventral, plate-like expansion of the lacrimal does not appear to contact the maxilla in this region, but the two bones would have closely approached each other.

The lateral surface of the main body of the maxilla is slightly rugose. This rugosity is best developed in the region anterior to the antorbital fossa, which is sculptured with striations, small grooves, and knobs of bone that produce a rough texture. This condition is also seen in juvenile *Tyrannosaurus* (BMR 2002.4.1, CMNH 7541). However, these rugosities are not as developed as the deeper, more prominent, and generally dorsoventrally-trending grooves and ridges present on other tyrannosaurids, especially adult *Daspletosaurus* (CMN 8506), *Tarbosaurus* (ZPAL MgD-I/4; Hurum and Sabath, 2003: fig. 4) and *Tyrannosaurus* (AMNH FARB 5027).

Two primary rows of foramina piece the main body in *A. altai*: an alveolar row that parallels the ventral margin (fig. 6, afr) and a circumfenestral row that surrounds the antorbital fossa (fig. 6, cfr). Both rows are common features of tyrannosaurids (Brochu, 2003; Currie, 2003a). The alveolar row consists of a series of small (2-3 mm diameter) but distinctive foramina, which are located immediately dorsal to the tooth row and are not set into a single groove. The row is approximately parallel to the tooth row but rises (elevates dorsally) as it continues posteriorly; it is approximately two millimeters dorsal to the tooth row anteriorly, but

ascends to five mm at its posterior termination. Anteriorly there are two or three foramina per alveolus, but posteriorly there is approximately one per tooth position. This pattern is also seen in other derived tyrannosauroids (e.g., *Bistahieversor*, *Gorgosaurus*, *Daspletosaurus*, *Tarbosaurus*, *Tyrannosaurus*). The circumfenestral row begins above alveolus 5 and generally follows the ventral margin of the antorbital fossa. These foramina are smaller than those of the alveolar row (1-2 mm diameter). Posteriorly the two principal rows merge at the level of alveolus 15 on the left maxilla and 13 on the right bone, and the last foramen continues posteriorly as a groove that does not breach the ventral margin of the maxilla (fig. 6, gr) (see Carr, 1999).

The antorbital fossa is extensive and occupies much of the lateral surface of the maxilla. It is especially long anteroposteriorly, extending 118 mm anteriorly from the anterior margin of the antorbital fenestra, and is also present ventral to the fenestra across the entire length of the main body of the maxilla. This is similar to the condition in *Appalachiosaurus* (RMM 6670; Carr et al., 2005), juvenile tyrannosaurids (Carr, 1999; Carr and Williamson, 2004), and basal tyrannosauroids (e.g., *Dilong*: IVPP V14243), but contrasts with the morphology of large adult tyrannosaurids (most notably *Tyrannosaurus* and *Tarbosaurus*) in which there is little lateral exposure of the fossa below the fenestra. Instead, in large specimens of these taxa the ventral margin of the fenestra abuts the roughened lateral surface of the main body (Brochu, 2003: fig. 2; Hurum and Sabath, 2003: fig. 4). *Alioramus remotus* appears to have little or no ventral fossa (Kurzanov, 1976: fig. 4), but the holotype maxilla is clearly broken. *Albertosaurus*, *Gorgosaurus*, *Daspletosaurus*, *Raptorex*, and juvenile *Bistahieversor* have what may be an intermediate condition, in which there is a low and narrow extension of the fossa ventral to the fenestra (Currie, 2003a: figs. 2, 6, 18; Sereno et al., 2009: fig. 1; Carr and Williamson, 2010: fig. 1).

Anteriorly, the antorbital fossa is demarcated by a distinct ridge. This ridge, which marks the contact between the lateral and medial laminae of the ascending ramus (see Witmer 1997), continues dorsally but gradually pinches out so that the two laminae become confluent, and the entire lateral surface of the posterior region of the ascending ramus is smoothly excavated by the fossa. However, it is clear that the fossa does not continue dorsally onto the nasal, but abruptly terminates at the dorsal margin of the ascending ramus (the subcutaneous surface of the ascending ramus and the lacrimal intervene between the antorbital fossa and the nasal). Ventrally the antorbital fossa is bordered by a swollen and rugose rim (fig. 6, rim). This rim is most rugose anteriorly and becomes smoother posteriorly, where it gradually thins into a sharp ridge that becomes confluent with the ventral groove for the jugal articulation. This ventral swelling is more pronounced on the right maxilla, as are the circumfenestral foramina that parallel it ventrally. In general, the swelling is typical of small juvenile tyrannosaurids (Carr, 1999). The anteroventral margin of the antorbital fossa is not delineated by a distinctive, sharp rim of bone as in *Dilong* (Xu et al., 2004: fig. 1), *Guanlong* (Xu et al., 2006: fig. 2), and other basal coelurosaurs (e.g., *Huaxiagnathus*: Hwang et al., 2004; *Juravenator*: Gohlich and Chiappe, 2006).

The maxillary antorbital fossa contains two principal accessory antorbital openings: an anterior promaxillary fenestra and a more posterior and larger maxillary fenestra (fig. 6, pmf, mf) (Witmer 1997). These openings are present in all tyrannosauroids, as well as tetanuran theropods in general. The promaxillary fenestra is a dorsoventrally tall oval, with a long axis oriented slightly anteroventrally-posterodorsally. On the better preserved left maxilla it is 17 mm tall dorsoventrally and 8 mm wide mediolaterally. The fenestra is slightly visible in lateral view, but faces mostly anteriorly and trends anteriorly into the body of the maxilla, into what appears to be

the promaxillary recess (Witmer, 1997), directly above the anteromedial process. A 27-mm-long, laterally smooth, region of the antorbital fossa separates the promaxillary fenestra from the maxillary fenestra.

The maxillary fenestra is an enormous, anteroposteriorly elongate oval, measuring 57 mm long by 30 mm deep on the better preserved left maxilla. Such extreme elongation of the fenestra is not seen in other tyrannosaurids, which have more circular fenestrae (Table 4), although the basal tyrannosauroid *Dilong* has a much more elongate opening (Table 4; Xu et al., 2004). The maxillary fenestra and antorbital fenestra are separated by a 25-mm-long strut of bone, the interfenestral pillar. The pillar is generally hourglass shaped, with a broadly concave posterior margin and a sharper, V-shaped anterior margin.

The maxillary fenestra does not approach the anterodorsal corner of the antorbital fossa (i.e., lie along the anterior margin of the fossa) as in *Daspletosaurus*, *Tyrannosaurus*, and *Tarbosaurus* (Carr et al., 2005). Instead, the condition in *A. altai* is more similar to that in adult *Albertosaurus*, *Appalachiosaurus*, *Bistahieversor*, and *Gorgosaurus*, and juveniles of *Daspletosaurus*, *Tarbosaurus*, and *Tyrannosaurus* (Carr, 1999; Currie, 2003a; Carr et al., 2005; Tsuihiji et al., 2011), in which a smooth region of fossa separates the maxillary fenestra from the anterodorsal corner of the fossa. Similarly, the maxillary fenestra of *A. altai* is also separated from the ventral margin of the antorbital fossa by a deep (14 mm) strip of bone. Once again, this differs from the condition in adult *Daspletosaurus* (Russell, 1970: fig. 1; Carr, 1999: fig. 1), *Tarbosaurus* (Hurum and Sabath, 2003: fig. 4), and *Tyrannosaurus* (Osborn, 1912: fig. 1; Brochu, 2003: fig. 2), in which the fenestra closely approaches or abuts the ventral margin of the fossa. The location of the fenestra in *A. altai* is similar to that in *Appalachiosaurus*, *Albertosaurus*, *Bistahieversor* (Carr and Williamson, 2010), *Gorgosaurus*, and juvenile

tyrannosaurines (Carr, 1999: fig. 6; Currie and Dong, 2001a: fig. 1; Tsuihiji et al., 2011), where it is located more centrally within the antorbital fossa, and thus separated from the ventral edge of the fossa by a deep margin. *Dilong* has a unique condition: the anterior end of the maxillary fenestra lies against the anterior margin of the antorbital fossa as in tyrannosaurines, but the ventral margin is located far dorsal to the ventral edge of the fossa (IVPP V14243; Xu et al., 2004: fig 1). *Raptorex* also has an unusual condition in which the maxillary fenestra approaches the anterodorsal corner and the ventral margin of the antorbital fossa, but is separated from both by a relatively constant width of smooth fossa (Sereno et al., 2009). Compared to the condition in *Raptorex*, the maxillary fenestra is proportionally smaller, and therefore the separation between the fenestra and the margins of the antorbital fossa is larger, in similarly-sized juvenile *Tarbosaurus* (Tsuihiji, et al., 2011).

The maxillary fenestra is open medially (i.e., pierces the antorbital fossa) on the right maxilla, but on the better-preserved left maxilla the fenestra is enclosed medially by a thin wall of bone (figs. 6, 9, mbw). This wall was surely present on the right side as well, but has been mostly lost to erosion. The wall is also entirely preserved in a specimen of cf. *Daspletosaurus* (TMP 97.12.223) and partly in a subadult *Gorgosaurus* (ROM 1247), but is otherwise difficult to observe in most other tyrannosaurid specimens due to erosion. It is clearly present in many other derived tyrannosauroid specimens (e.g., *Bistahieversor*, *Gorgosaurus*, *Daspletosaurus*, *Tyrannosaurus*), but usually all that remains of it are its broken edges surrounding the maxillary antrum and promaxillary sinus (Witmer, 1997; Brochu, 2003). In *A. altai*, however, the morphology of the wall can be described with certainty, as the sheet of bone is well preserved nearly in its entirety and clearly extends across the maxillary antrum and promaxillary sinus medially.

In *A. altai*, it is clear that the medial wall is confluent with the dorsal surface of the medial maxillary shelf (= palatal process of Brochu 2003 and other authors), as the two structures are continuous with each other. The wall attaches to the dorsolateral surface of the maxillary shelf; the floor of the shelf is visible because of small regions of damage in the medial wall, and is clearly perforated by several openings that represent the dorsal tips of the tooth replacement crypts. In *A. altai* and all other tyrannosauroids for which the wall is well-preserved, a large perforation occurs ahead of the posterodorsal corner of the maxillary antrum above the epiantral recess.

The medial wall encloses the promaxillary sinus and the maxillary antrum (fig. 9, mant) (Witmer, 1997), the latter of which is anteroposteriorly long, in accord with the greatly enlarged maxillary fenestra. The antrum opens laterally via the maxillary fenestra and posteriorly through a large posterior anteromaxillary fenestra. This ovoid foramen, which measures 26 mm deep by 20 mm wide, opens posteriorly into a deep trough of bone: the internal antorbital fossa. Dorsally, the margin of the maxillary antrum on the medial surface is only slightly anteroventrally oriented, intermediate between the horizontal condition of *Albertosaurus* and the strongly sloping orientation of *Daspletosaurus* (Carr, 1999). However, the maxillary fenestra reaches the dorsal margin of the antrum as in *Daspletosaurus* (and *Tyrannosaurus*), and it does not terminate at midheight of the antrum as in *Albertosaurus* (Carr, 1999), *Raptorex* (LH PV18), and *Appalachiosaurus* (RMM 6670; Carr et al., 2005).

On the medial surface of the maxilla, posterodorsal to the maxillary antrum, is a second recess, the epiantral recess (figs. 6, 9, epi) (Witmer 1997; Brochu 2003). The relationship between these two recesses is clearly visible in the right maxilla, where the medial wall is broken. The epiantral recess is a separate cavity, and judging from the better preserved left

maxilla, it was enclosed medially by its own web of bone. This web is not complete, but remnants of it are present along the posterior and ventral margins of the recess. Furthermore, a thin ridge dorsal to the recess probably represents the dorsal extent of the web. The epiantral recess opens dorsally through a large opening in the medial wall, and ventrally it appears to communicate with the maxillary antrum internally, indicated by the presence of several invaginations in the dorsal wall of the maxillary antrum along the contact with the ventral margin of the epiantral recess. In other completely prepared tyrannosaurid specimens that are well-preserved or have been CT scanned, the epiantral recess communicates with the maxillary antrum (e.g., *Albertosaurus*: TMP 99.50.140; *Gorgosaurus*: ROM 1247; *Daspletosaurus*: CMN 8506; *Raptorex*: LH PV18; *Tyrannosaurus*: BHI 3033). The epiantral recess is not expressed on the lateral surface of the maxilla as either a foramen or depression.

In *A. altai* there are two additional pneumatic depressions on the lateral surface of the antorbital fossa. First, there is an accessory depression immediately posterodorsal to the promaxillary fenestra (figs. 6, 8, acd). This opening is more pronounced on the right maxilla, where it takes the form of a deep and circular pit (diameter 10 mm), which is separated from the larger promaxillary fenestra by a distinct strut. This accessory opening is not so distinctive on the left maxilla, but a homologous structure is clearly present as a shallow fossa separated from the promaxillary fenestra by the same strut. Although pneumaticity can sometimes be randomly variable (see, for instance, Witmer, 1997 and Brochu, 2003), we consider this accessory fossa to be an autapomorphy of *A. altai* because it is present on both sides of the skull and is not observed in other tyrannosauroids.

Second, there is a shallow, elongate fossa dorsal to the maxillary fenestra, paralleling and undercutting the posterodorsally-trending rim of the antorbital fossa on the ascending ramus (fig.

6, acf). This fossa is more prominent on the right maxilla, where it is exaggerated by dorsoventral crushing. However, a shallow indentation is also present on the left maxilla. This fossa is similar in shape and position to a shallow, ovoid depression in *Dilong* (IVPP V14243), *Raptorex* (LH PV18; Sereno et al., 2009), and a subadult specimen of *Tarbosaurus* (Tsuihiji et al., 2011). It is located in the same region as a structure referred to as the excavatio pneumatica by Witmer (1997), but its shape and prominence differ from the more discrete, circular or pocket-like excavations on the ascending ramus in more basal theropods such as *Acrocanthosaurus* (Eddy, 2008; Eddy and Clarke, 2011), *Ceratosaurus* (Witmer, 1997), *Eocarcharia* (Sereno and Brusatte, 2008), and *Sinraptor* (Currie and Zhao, 1993).

On the medial surface of the maxilla, the interdental plates are unfused and in many cases they are separated from each other by gaps (fig. 6, idp). They are generally rectangular anteriorly, but become triangular posteriorly, and their surfaces are covered in a series of prominent anteroposteriorly trending striations. The size of the plates corresponds to the size of the alveoli (Table 5): the plates are small anteriorly, increase in size, then decrease in size posterior to alveolus 6. The plates are not as dorsoventrally high relative to their lengths as in large tyrannosaurids (Currie, 2003a), in concert with the shallower maxillary main body of *A. altai*. Along the entire tooth row the lateral parapet of the maxilla, comprised of the main body, is located further ventrally than the medial parapet, formed from the interdental plates. The difference becomes strongly pronounced posteriorly, as the plates are reduced to small triangles of bone located approximately 5 mm dorsal to the lateral parapet. This condition is also seen in other derived tyrannosauroids (e.g., *Albertosaurus*: TMP 99.50.120; *Gorgosaurus*: ROM 1247); *Daspletosaurus*: CMN 8506; *Raptorex*: PH LV18; *Tyrannosaurus*: CM 9380).

Immediately dorsal to the interdental plates is the groove for the dental lamina (fig. 6, gdl), which is sharp and demarcates a strong step between the plates and the main body of the maxilla dorsally. Above the first five alveoli, and their interdental plates, is a series of deep pits on the medial surface of the main body, below the anteromedial process. These likely accommodated the large anterior dentary teeth when the jaws were closed (Currie, 2003a), as is the case in many archosaurs, including some living crocodilians. However, these pits are limited to the anterior end of the maxilla, and do not continue posteriorly for much of the tooth row as they do in *Albertosaurus* (Currie, 2003a), *Gorgosaurus* (TMP 94.12.602), and *Tyrannosaurus* (RSM 2523.8). There are some slight depressions posteriorly in *A. altai*, but these are not discrete and rugose pits but rather shallow concavities between the tooth replacement crypts. On the right maxilla there is a series of pronounced circular pits above alveoli 12-14, but these are extremely subtle on the left bone; the deep pits, therefore, may be pathological, or an artifact of crushing, on the right maxilla.

At the anterior end of the medial surface, dorsal to the five deep pits, is an elongate anteromedial process (figs. 6, 9, amp), which extends from the level of the second and third alveoli posteriorly to the level of the sixth alveolus. This is equivalent to the so-called "secondary palate" of tyrannosaurids; this structure, however, is homologous to the primary palate of tetrapods and not to the true secondary palate of derived synapsids. Tyrannosaurids and some other theropods (e.g., dromaeosaurids) display the primitive tetrapod condition of a largely bony and enclosed primary palate, whose internal openings are reduced in size due to the expansion of medial shelves from the maxillae and the palatines.

In *A. altai*, the anteromedial process is approximately parallel to the tooth row posteriorly, but anteriorly it sweeps strongly ventrally at the level of alveolus 3. Four deep

grooves excavate the anteromedial process, which are separated by paper-thin ridges of bone. The most dorsal groove faces mostly dorsally, whereas the ventral three face mostly medially. Dorsal to the dorsalmost groove is a very small and smooth anterior concavity which likely would have articulated with a small process of the premaxilla, dorsomedial to the long notch in the maxilla (described above) which represents a hiatus between the joint surface for the premaxilla and the anteromedial process. The four grooves would have interlocked with those grooves on the opposing maxilla (and perhaps also slightly with the vomer), a contact that evidently was stable, as indicated by the complexity and mediolateral depth of this joint. The anteromedial process does not protrude anteriorly ahead of the main body of the maxilla.

The four grooves on the anteromedial process gradually pinch out posteriorly, and gradually the process itself becomes confluent with a robust medial shelf (the palatal shelf of many authors) (fig. 6, mms). For most of the length of the maxilla the palatal shelf is located approximately 15 mm dorsal to the groove for the dental lamina. The shelf is distinct and strongly extends medially to overhang the remainder of the medial surface of the maxilla at the spot where it (the shelf) merges with the anteromedial process. Posterior to this point the shelf becomes smooth and flattens out, such that there is essentially no overhang in the region ventral to the midpoint of the maxillary antrum. However, the shelf becomes robust again as it continues posteriorly below the posterior antromaxillary foramen, before gradually pinching out and essentially disappearing posterior to the final alveolus. From this point posteriorly the shelf continues as a very thin crest above the joint surface for the jugal, above which is the flattened joint surface for the palatine (fig. 6, pal).

The palatine articulation is long, extending from the level of alveolus 10 to approximately 20 mm posterior to alveolus 17. It increases in depth as it extends anteriorly, and faces mostly

medially, although it sweeps slightly dorsally above alveolus 13. In contrast to other tyrannosauroids the palatine joint surface is flat throughout and is indistinct anteriorly and ventrally. The joint surface is a concave groove in *Albertosaurus* (TMP 99.50.140), *Daspletosaurus* (TMP 2001.36.1), *Gorgosaurus* (TMP 94.12.602), *Raptorex* (PH LV18), and in juveniles (BMR 2002.4.1) and adults (CM 9380) of *Tyrannosaurus*. The joint surface is distinct, but it is dorsoventrally deep and flat in mature *Daspletosaurus* (CMN 8506). In *A. altai*, the internal antorbital fossa is located dorsal to the palatal articulation (fig. 6, iaof). The maxilla forms the lateral and ventral margins of the internal fossa, whereas the palatine forms its medial margin. The internal fossa projects farther ventrally than the external (lateral) exposure of the antorbital fossa.

In dorsal view, with the anterior portion of the tooth row held straight parasagittally for reference, both the ascending process and posterior part of the main body (= jugal ramus) curve laterally. This curvature is strongly pronounced, and it almost certainly is not an artifact of crushing or deformation since it is present on both left and right maxillae. Such curvature is a common feature of tyrannosaurids (e.g., Osborn, 1912: fig. 1; Carr, 1999: fig. 5; Currie, 2003a: fig. 2; Hurum and Sabath, 2003: fig. 1).

Both maxillae contain 17 alveoli (figs. 6, 7). The first two alveoli are small: the first is tiny and incisiform, and the second is among the smallest in the tooth row and much smaller than the third alveolus (Table 5). The alveoli increase in size, with an abrupt jump in size between alveoli 2 and 3, until alveolus 5, which is the largest in the tooth row. From this point posteriorly the alveoli decrease in size, eventually ending with a small and nearly circular alveolus. The largest alveolus is also at the fifth opening in *Raptorex* (PH LV18). The largest position is variable in *Gorgosaurus*, as it is at the fifth (AMNH FARB 5342) or sixth (CMN 2120) socket.

The seventh tooth is the largest in *Appalachiosaurus* (RMM 6670; Carr et al., 2005). The largest tooth is positioned posteriorly in *Daspletosaurus* (AMNH FARB 5346, CMN 8506), at the eighth socket. This is also seen in small juvenile *Tyrannosaurus* (LACM 28471), whereas it is in a progressively anterior position in subadult (BMR 20024.1) and adult (LACM 23833) specimens of *Tyrannosaurus*, at the sixth and third socket, respectively. A similar anterior position is seen in adult *Tarbosaurus* (PIN 551-3), in which the fourth tooth is the largest.

Maxillary tooth counts are variable in derived tyrannosauroids: there are 11-12 alveoli in adult *Tyrannosaurus* (Osborn, 1912; Brochu, 2003), 14 in some juvenile *Tyrannosaurus* (Carr, 1999), 12-13 in *Tarbosaurus* (Hurum and Sabath, 2003), 13-15 in *Albertosaurus* and *Gorgosaurus* (Currie, 2003a) , 13-17 in *Daspletosaurus* (Currie 2003a), 15 in *Appalachiosaurus* (Carr et al., 2005), 12 in *Teratophoneus* (Carr et al., 2011), and 16 in *Alioramus remotus* (Kurzanov, 1976). Although tooth count is variable in some taxa, the significant feature is that *A. altai* has more alveoli than nearly all other tyrannosaurid specimens.

Nasal: The left and right nasals are fused into a single vaulted element, which is well preserved, nearly complete, and uncrushed (figs. 10-11). Fused and vaulted nasals are a characteristic feature of tyrannosauroids (Holtz, 2001; Snively et al., 2006) and presumably developed early in ontogeny, as they are present in the smallest and youngest known specimens (Carr, 1999; Carr and Williamson, 2004), as well as early in tyrannosauroid evolutionary history. Indeed, there are no known examples of unfused tyrannosaurid nasals, regardless of size or ontogeny, and even very basal tyrannosauroids (e.g., *Dilong*: Xu et al., 2004; *Eotyrannus*: Hutt et al., 2001; *Guanlong*: Xu et al., 2006) possess fused nasals. It has been suggested that nasal fusion helped

increase skull strength and was an important adaptation for "puncture pull" feeding and bone-crushing in tyrannosaurids (Rayfield, 2004; Snively et al., 2006).

In *A. altai* the nasals are firmly fused, but regions of the internasal suture are visible (fig. 10, ons). In dorsal view, the suture is open anteriorly, where it extends from between the premaxillary processes to the level of the posterior end of the external naris. Posteriorly, the suture is open as an elongate (90 mm long), thin cleft in the flat, plate-like region that articulated with the frontals and lacrimals. In ventral view the suture is broadly visible as a raised rim of bone with a narrow and shallow median depression, which extends for the entire length of the nasal.

The nasals are elongate, and are widest immediately at the posterior margin of the external naris, as in *Tyrannosaurus* (Brochu, 2003) and most other tyrannosaurid specimens. In contrast, the greast width of bone is posterior to the naris in the holotype of *Daspletosaurus* (CMN 8506) and in some specimens of *Gorgosaurus* (TCM 2001.89.1). From this point the nasals decrease in width posteriorly, are constricted to a minimum width near their midpoint, and then expand again posteriorly. This shape is generally similar to that in other derived tyrannosaurids, although there are some subtle differences that may have phylogenetic utility (see Brusatte et al., 2010a). This morphology is also present in *Alioramus remotus*, judging from the description of Kurzanov (1976:95; "posteriorly they become wider and flatter") and photos of the holotype (P.J. Currie, pers comm.). The basal tyrannosauroid *Dilong* has a unique condition, which is probably primitive because it is also present in outgroup taxa, in which the nasals gradually expand posteriorly, without a midpoint constriction (IVPP V14243; Xu et al., 2004: fig 1). Additionally, although the nasals of *Dilong* are fused, they are not vaulted, thickened, and rugose like those of *Eotyrannus* and tyrannosaurids.

The nasals are vaulted anteriorly, but flatten out and become thin and plate-like posteriorly. The posterior end of this region is broken in *A. altai*, but only a few millimeters are likely missing. The posterior, plate-like region is nearly flat (only ever so slightly concave), not distinctly concave as in *Eotyrannus* (MIWG 1997.550), and there are no elaborate crests on the nasals as in *Dilong* and *Guanlong* (Xu et al., 2004, 2006). The nasal is excluded from the antorbital fossa by the maxilla and lacrimal; instead, the fossa stops immediately ventral to the nasal on the maxilla (see above), and the fossa does not "reach" the nasal as described by (Carr, 1999) in some juvenile tyrannosaurid specimens. Similarly, there is no external evidence of nasal pneumaticity as in basal tyrannosauroids (e.g., *Dilong*, *Eotyrannus*, *Guanlong*), allosauroids, and some other basal theropods (Brusatte et al., 2010b; Li et al., 2010).

Anteriorly each nasal divides into two processes: a subnarial process that articulates with the ascending ramus of the maxilla and floors the external naris (fig. 10, snp), and a premaxillary process that contacts the ascending nasal process of the premaxilla and forms the ceiling of the external naris (fig. 10, pmp). The premaxillary processes are long, measuring 65 mm in length, and widely separated on the midline. Wide separation is also present in *Daspletosaurus* (CMN 8506), Tarbosaurus (ZPAL MgD−I/4), and *Tyrannosaurus* (BHI 4100), but in *Albertosaurus* and *Gorgosaurus* the processes are narrowly separated (ROM 1247) or are tightly apposed to each other (TMP 86.64.1). In *A. altai*, however, each individual premaxillary process is not split anteriorly into separate prongs to clasp the premaxilla, as is present in *Albertosaurus* and *Gorgosaurus*, and possibly other tyrannosaurids (Currie, 2003a).

The subnarial processes are shorter, measuring only 42 mm in length, thinner, and more delicate than the premaxillary processes. In dorsal view they are located lateral to the premaxillary processes, meaning that the external naris would have been widely exposed

dorsally. This condition is also seen in *Gorgosaurus* (ROM 1247), *Albertosaurus* (TMP 86.64.1), and some specimens of *Tyrannosaurus* (BHI 3033), but in contrast, the subnarial process is nearly beneath the premaxillary process in *Daspletosaurus* (CMN 8506) and other specimens of *Tyrannosaurus* (CM 79057). The subnarial processes are finger-like projections: they keep a relatively constant width before slightly tapering to a blunt anterior end. This blunt tip does not appear to have an articular surface for the maxillary process of the premaxilla, suggesting that the two processes may have been separated, thus allowing the maxilla to contribute to the floor of the external naris. However, the articular surfaces on the maxilla for the premaxilla and nasal are confluent (see above), indicating that they must have touched slightly, or that there was an unossified gap filled with cartilage. Both the premaxillary and subnarial processes are smooth, and there is no distinct fossa dorsal, ventral, or posterior to the external naris. Such a fossa is present in some adult specimens of *Tyrannosaurus* (MOR 555).

The articulation for the maxilla continues posteriorly from the subnarial process, and takes the form of a deep groove on both the lateral and ventral margin of the main body of the nasal (fig. 10, max). The orientation of the maxilla-nasal articulation changes along the great length of this contact. Anteriorly, the subnarial process sits directly on top of the maxilla, so that the articular surface on the nasal faces ventrally; the joint surface in this region is largely convex, having the form of a low ridge that fits into the groove on the maxilla. Immediately posterior to the external naris, where the subnarial process joins the main body of the nasal, the articulation twists so that the articular groove faces almost equally ventrally and laterally. Further posteriorly the groove deepens and faces almost entirely ventrally, until the midpoint of the nasal. Here, the dorsal rim of the groove sweeps dorsally and exposes the articular groove broadly in lateral view. In this region the contact is no longer a groove, as the medial margin of the groove extends

ventrally to form a deep plate (10 mm deep) extensively exposed in lateral view. This plate is nearly flat and articulated with the lacrimal (fig. 10, lac).

Dorsal to the laterally-facing articular plate for the lacrimal is a secondary groove (fig. 10, sgr). This structure is not a continuation of the deep groove anterior to the plate, but instead emerges from the posterodorsal region of the plate itself. This accessory groove faces laterally and slightly ventrally, and would have given extra strength to the lacrimal articulation. Posteriorly, both the plate and the secondary groove taper in depth, as the nasal itself thins and flattens to overlap the anterior margin of the frontal. Posterior breakage obscures details of the frontal articulation, but an articular surface for the prefrontal is visible at the very posterior end of the nasal (fig. 10, prf). This contact takes the form of a shallow (3 mm deep), smooth, and flat surface that faces entirely laterally, is supported ventrally by a ridge, and is confluent with the more anterior articulation for the lacrimal. The form of this contact suggests that the nasal-prefrontal articulation was weak.

The nasal does not send a "short ventrolateral process that projects (onto) the lacrimal" laterally (Brochu, 2003:16). This subsidiary process is present in *Albertosaurus* (TMP 86.64.1), *Bistahieversor* (Carr and Williamson, 2010), *Gorgosaurus* (Carr, 1999), juvenile *Daspletosaurus* (Currie, 2003a: fig. 18A), and *Tyrannosaurus* (Brochu, 2003: fig. 2; Carr and Williamson, 2004: fig. 9; Snively et al., 2006: fig. 4A), in which it projects ventrolaterally from the main body of the nasal to cover part of the lacrimal laterally. As in *A. altai*, this process is absent in *Tarbosaurus* (ZPAL MgD−I/4), and is very short (CMN 8506) or absent (TMP 85.65.1) in adult *Daspletosaurus*. The process appears to be absent in *Raptorex*, although the bone is incomplete and damaged (Sereno et al., 2009).

The external surface of the nasal has a complex texture, which varies across the length of the bone. The region between the subnarial processes and the midpoint of the main body is extremely rugose, as it is covered with an array of swollen protuberances, foramina, and neurovascular canals. This rugose region is located anterior to the antorbital fenestra. In most other tyrannosaurids (but see Brochu, 2003) the rugosities extend further posteriorly, and are located dorsal to the antorbital fenestra. Specifically, the coarse region starts over the anterior third to quarter of the fenestra in *Albertosaurus* (TMP 85.98.1). There is variation in *Gorgosaurus*, as the coarse region intensifies either above the anterior half to quarter of the fenestra (AMNH FARB 5664, AMNH FARB 5336, UALVP 10), or ahead of it (TMP 95.36.500). In *Daspletosaurus* juveniles (TMP 94.143.1) and adults (FMNH PR308) the rugosities intensify over the anterior half of the fenestra, whereas in some adults (CMN 8506, MOR 590) this region occurs ahead of the level of the fenestra. In *Tarbosaurus* adults, the coarse region either intensifies above the anterior quarter of the antorbital fenestra (ZPAL MgD-I/4), or ahead of it (PIN 551-3). Finally, in *Tyrannosaurus* the rugosity intensifies over the anterior half (SDSM 12047) or quarter (AMNH FARB 5027, CMNH 7541, LACM 23844, MOR 008) of the fenestra, or ahead of it (BHI 3033). Without a complete maxilla, the pattern in *A. remotus* is unclear, although the increased number of rugosities suggests that the coarsest extended posteriorly above the fenestra. The presence of rugosities above the fenestra in subadults of *Daspletosaurus* (TMP 94.143.1), *Gorgosaurus* (AMNH FARB 5664), and *Tyrannosaurus* (CMNH 7541) suggests that the rugosities shifted anteriorly with maturity, whereas the opposite pattern occurred in *Alioramus*, if the ontogenetic trend for the genus can be accurately deduced from the holotypes of the two species (which are both immature individuals).

Much of the texture on *A. altai* appears to be random, but three general rugosities ("bumps") are apparent (figs. 10-11, rug). Although these are not as discrete as the six bumps that are seen on the holotype of *Alioramus remotus*, which is regarded as an autapomorphy of that species (Kurzanov, 1976; Holtz, 2004), they still form localized, coherent structures, which may have supported small keratin hornlets or mounds. In *A. altai* the middle protuberance is the longest (but shortest dorsoventrally), the most posterior one is the smallest, and the tall anterior bump forms the most discrete, well-defined mound. The three excrescences are separated by smoother concave areas, which more than anything serve to define the individual structures. Poor preservation and genuine difficulty in making sense of complicated rugose patterns hampers identification and description of similar protuberances in other taxa. Clearly, the mounds of *Alioramus remotus* are the most discrete structures yet described for a tyrannosaurid. However, Carr et al. (2005) consider *Appalachiosaurus*, *Daspletosaurus*, *Gorgosaurus*, and *Tarbosaurus* to also possess discrete, but low, bumps. Indeed, some very large specimens of *Tarbosaurus* (e.g., ZPAL MgD−I/4) do exhibit small mounds on the midline that are larger than surrounding rugosities, although these are not as discrete as the structures in *A. remotus* and *A. altai*. *Tyrannosaurus*, on the other hand, is described as possessing an irregular array of rugosities (Osborn, 1912; Brochu, 2003; Carr et al., 2005).

As in other derived tyrannosaurids, foramina are common on the nasal of *A. altai*, and they are concentrated anteriorly (fig. 10, for). Many of the larger foramina have anterodorsally curving neurovascular canals that trend towards the external naris. Most of the anterior foramina are organized into two principal rows (lateral and medial) that extend anteroposteriorly along the length of the nasal. The lateral row is positioned immediately above the ventral margin of the nasal and faces mostly laterally (although it is slightly visible in dorsal view), whereas the medial

row is visible only in dorsal view. Immediately posterior to the midpoint of the nasal, the two rows of foramina converge into a single row, and here the foramina are larger (~5 mm diameter) and often more distinctive than those present anteriorly. These foramina extend ventrally through the nasal and pierce the ventral surface of the bone. The first foramina in the divided anterior series are located immediately posterior to the external naris, and the last foramen in the conjoined posterior series is positioned approximately 100 mm anterior to the posterior end of the nasal. A similar arrangement of foramina is present in *Appalachiosaurus* (Carr et al., 2005), *Albertosaurus* and *Daspletosaurus* (Currie, 2003a), but fewer foramina comprise the rows in *Tarbosaurus* and *Tyrannosaurus* (Hurum and Sabath, 2003). In ventral view it is clear that the foramina are most concentrated under the rugose region, suggesting that they are related to blood supply for a keratinous covering. Possibly, they could be associated with the upper nasal artery, as suggested by Kurzanov (1976).

The posterior end of the nasals is broken, but the shape of the joint surfaces on the frontals can be of help in inferring the morphology of the posterior nasals. As in other tyrannosaurids, the posterior margin of the nasals is divided into a pair of processes that overlap the frontals. The medial processes were short, triangular, and diverged from each other. This is unlike the condition in *Albertosaurus* and *Gorgosaurus*, in which the medial processes lie parallel to each other (e.g., Carr, 1999). The lateral processes were wider and longer than the medial processes, and a wide notch on the frontal separates them from each other. This condition is also seen in *Gorgosaurus* (CMN 2120), *Tyrannosaurus* (CM 79057), and in juvenile *Daspletosaurus* (TMP 94.143.1), whereas the medial processes are as long as or longer than the lateral processes in *Albertosaurus* (TMP 81.10.1) and adult *Daspletosaurus* (CMN 8506). Furthermore, the frontal articular surface indicates that there was no tongue-like process of the

conjoined nasals, which sits in a midline groove on the dorsal surface of the frontals in some tyrannosaurids (Carr, 1999; Currie, 2003a). A tongue-like process is also absent in juvenile *Tyrannosaurus* (CMNH 7541).

Lacrimal: Both left and right lacrimals are preserved (figs. 12-14). The left bone is more complete and better preserved (figs. 12, 14), whereas the right element is crushed dorsoventrally and broken ventrally (fig. 13). The lacrimal is the shape of the number "7", due to elongate anterior and ventral rami which meet at an acute angle. This is also the case in some tyrannosaurids, including adult *Daspletosaurus*, *Tarbosaurus*, and *Tyrannosaurus* (Osborn, 1912; Molnar, 1991; Carr, 1999; Brochu, 2003; Carr and Williamson, 2010). On the contrary, most theropods, including the tyrannosauroids *Albertosaurus*, *Appalachiosaurus*, *Bistahieversor* and *Gorgosaurus*, *Raptorex*, and juvenile *Tarbosaurus*, *Tyrannosaurus*, and *Daspletosaurus* have lacrimals shaped like an inverted "L," due to sub-perpendicular rami (Currie, 2003a; Carr et al., 2005; Sereno et al., 2009; Carr and Williamson, 2010; Tsuihiji et al., 2011). The divergence of the anterior and ventral rami defines the posterior and dorsal margins of the antorbital fenestra, and portions of each ramus are covered by the smooth surface of the antorbital fossa. In addition to the two principal rami, a third process, a small posterior ramus that projects medially and posteriorly to articulate with the frontal and prefrontal, is also present (fig. 12, pr). The divergence of the ventral and posterior rami defines the anterior and dorsal margin of the orbit.

The ventral ramus is best thought of as two laminae of bone: a medial lamina and a lateral lamina (fig. 12, ml, ll). The two are separated anteriorly by a deep cleft, which faces anteriorly and is the posterior extent of the antorbital fossa (fig. 12, cle). This cleft tapers ventrally and ends at the point where the two laminae can be said to merge. This condition,

where the cleft may be deep or shallow, is present in other tyrannosauroids (e.g., *Albertosaurus*, *Bistahieversor*, *Daspletosaurus*, *Gorgosaurus*, *Raptorex*, *Tyrannosaurus*). Ventral to the point where the laminae meet, the antorbital fossa smoothly excavates the lateral surface of the merged region (fig. 12, aof). The fossa is very shallowly excavated here, and ventrally it is continuous with a narrow region of the fossa that extends onto the jugal. The better preserved left lacrimal is pierced by a small foramen in the anterodorsal region of the lacrimal antorbital fossa (fig. 12A, for). This opening is also present, and opens anteriorly, in *Albertosaurus* (CMN 5601) and *Raptorex* (LH PV18); in adult *Daspletosaurus* (CMN 8506) and *Tyrannosaurus* (CM 9380) this foramen opens onto the medial surface of the bone. In *A. altai*, the lateral lamina projects further anteriorly than the medial lamina, obscuring the cleft between them in lateral view. Instead, in lateral view, the lateral lamina is seen as an overhanging flange that projects slightly into the antorbital fenestra and thus slightly covers the posterior margin of the fenestra. This lamina is convex anteriorly where it projects into the fenestra, but concave posteriorly, where it forms the anterior margin of the orbit. The anterior margin of the region where the two laminae are merged (the "rostroventral lamina" of Carr, 1999) is slightly concave, a characteristic of juvenile *Albertosaurus* (Carr, 1999) and *Tyrannosaurus* (Carr and Williamson, 2004), but not adults.

The anterior ramus is elongate, and is also comprised of two distinct laminae of bone: a lateral lamina, which is dorsally placed (fig. 12, all), and a medial lamina, which is placed ventrally (fig. 12, aml). This condition is also present in other tyrannosauroids (e.g., *Albertosaurus*, *Bistahieversor*, *Daspletosaurus*, *Gorgosaurus*, *Raptorex*, *Tyrannosaurus*). The anterior ramus in *A. altai* is especially long, which can be quantified by taking the ratio of the lengths of the anterior and ventral rami (Table 6). This ratio indicates that the anterior ramus of *A. altai* is longer, relative to the ventral ramus, than in other tyrannosaurids such as

Daspletosaurus and *Tyrannosaurus*. As discussed below, in *A*. *altai* the lateral surface of the medial (= ventral) lamina of the anterior ramus is excavated by several pneumatic foramina. The lateral lamina is poorly developed, as is the case in juvenile *Albertosaurus* and *Tyrannosaurus* (Carr, 1999). In contrast, adults of these genera develop an extensive lateral lamina that expands ventrally to cover the medial lamina laterally, thus also concealing much of the lacrimal pneumaticity in lateral view, as well as the antorbital fossa on the anterior ramus. In *A*. *altai* the anterior ramus is forked anteriorly into lateral and medial processes (fig. 12, lpr, mpr; terminology from Carr, 1999), as is also the case in other tyrannosauroids (e.g., *Albertosaurus*, *Bistahieversor*, *Daspletosaurus*, *Gorgosaurus*, *Raptorex*, *Tyrannosaurus*). The two processes are elongate and nearly equal in size and length in *A*. *altai*, a characteristic of larger and more mature *Albertosaurus* (Carr, 1999).

Much of the lacrimal is heavily rugose. The entire lateral surface of the lateral lamina of the ventral ramus is rugose, and this mottled texture is especially concentrated anteriorly, most prominently in the region adjacent to the posterodorsal corner of the antorbital fenestra. The entire anterior margin of the lateral lamina is slightly raised relative to the posterior margin of the ramus, and it is covered with a series of fine, arcuate, roughly anteroposteriorly trending striations, which are more strongly developed on the right lacrimal. Posterior to this roughened area the ventral ramus is concave, with a shallow and slightly rugose fossa, which is part of a broader orbital fossa that is also present on other circumorbital bones (fig. 12, orbfos). Ahead of this fossa, a low strut extends ventrally along the anterodorsal edge of the ventral ramus for a short distance—this strut represents the division between the raised anterior region of the bone and the depressed orbital fossa. Extending across the entire lateral lamina, and crossing both the upturned anterior margin and the posterior fossa, are several elongate, arcuate grooves, which are

especially prominent ventrally (fig. 12, str). In contrast, the anterior ramus is only slightly rugose dorsally, and the triangular portion of the lacrimal visible on the skull roof is almost completely smooth. The posterior ramus is covered with a fine series of lineations and rugosities on its lateral surface, but is smooth dorsally. This contrasts with the heavily roughened texture of the posterior ramus in many other tyrannosaurids, most prominently *Tyrannosaurus* (Osborn, 1912; Molnar, 1991; Brochu, 2003).

The most prominent rugose feature on the lacrimal is a roughened, pyramidal tubercle (the cornual process) located on the dorsal margin of the bone immediately above where the anterior and ventral margins meet (figs. 12, 14, cor). This structure is better preserved on the left bone, where it is a discrete, nearly conical projection that is best described as a small "hornlet." It is bordered ventrally by a series of ovoid excresences (bone papillae; fig. 14, ovo) that are visible in lateral view, and dorsally it is roughened by a series of small tubercles and pits. Also visible on the dorsal surface of the lacrimal is a series of four foramina medial to the hornlet (fig. 12C, for), whose position and relative size are nearly identical on both left and right bones. These are likely associated with blood vessels that innervated a keratinous sheath that covered the hornlet in life (Hieronymus et al., 2009). Fine preservation on the left lacrimal shows that at least the middle two foramina, which are the two largest on the left element, extend into the bone and emerge inside the pneumatic recess immediately posterodorsal to the antorbital fenestra (see below).

The hornlet of *A. altai* is equivalent to the cornual process of Carr (1999), a common feature of tyrannosaurids whose shape, size, and position vary both taxonomically and ontogenetically. Several features of the cornual process of *A. altai* can be compared with the hornlet morphology of other tyrannosaurids. First, the hornlet of *A. altai* is a single, discrete

structure that clearly stands out from the remainder of the dorsal margin of the lacrimal. This is a rare condition in adult tyrannosaurids. Mature *Albertosaurus*, *Bistahieversor*, *Gorgosaurus*, *Daspletosaurus*, and *Teratophoneus* also have discrete hornlets, but these are larger, anteroposteriorly broader, more prominent, extend farther dorsally, and gradually slope to occupy much of the dorsal margin of the lacrimal (Currie, 2003a: figs. 2, 7; Carr et al., 2011). Discrete hornlets are not present in adult *Tarbosaurus* and *Tyrannosaurus*, but rather the entire dorsal margin of the lacrimal is inflated (Brochu, 2003: fig. 2; Currie, 2003a, Hurum and Sabath, 2003: figs. 6, 7). A similar condition is present in *Appalachiosaurus*, which does not possess a discrete hornlet, but rather a convex ridge that extends across the dorsal surface (Carr et al., 2005: figs. 4, 5), as well as *Bistahieversor* (Carr and Williamson, 2010), *Eotyrannus* (MIWG 1997.550) and *Xiongguanlong* (Li et al., 2010). However, small, discrete, pyramidal hornlets are a common feature of juveniles, and are present in *Albertosaurus* (TMP 2001.45.74), *Gorgosaurus* (Carr, 1999: fig. 3), *Daspletosaurus* (TMP 94.143.1), *Tarbosaurus* (Maleev, 1974: fig. 55; Carpenter, 1992: fig. 2; Tsuihiji et al., 2011: fig. 8E,F), and *Tyrannosaurus* (BMR 2002.4.1). Thus, Currie (2003:200) suggests that the cornual process becomes "wider, more massive, and less pronounced in large individuals."

Additionally, other aspects of the cornual process vary in tyrannosaurids. In *A. altai* the hornlet is located directly dorsal to the ventral ramus, and posterior to the lacrimal pneumatic recess. The apex of the process is located anterior to the ventral ramus, and above or anterior to the pneumatic recess, in *Albertosaurus* (CMN 5601; Currie, 2003a: fig. 7), *Appalachiosaurus* (Carr et al., 2005: figs. 4, 5), *Bistahieversor* (Carr and Williamson, 2010), subadult *Gorgosaurus* (Currie, 2003a: fig. 2), juvenile *Daspletosaurus* (TMP 94.143.1), and juvenile *Tyrannosaurus* (BMR 2002.4.1). However, it is positioned dorsal to the ventral ramus and pneumatic recess in

Tarbosaurus (Hurum and Sabath, 2003: fig. 6), *Tyrannosaurus* (Hurum and Sabath, 2003: fig. 6), most specimens of adult *Daspletosaurus* (e.g., CMN 8506; Carr, 1999: fig. 3F; Carr and Williamson, 2004: fig. 10; Carr et al. 2005), *Teratophoneus* (Carr et al., 2011), and adult specimens of *Gorgosaurus* (CMN 2120). The cornual process of juvenile *Tarbosaurus* (Maleev, 1974: fig. 55) is more similar in position to that of *A. altai*, and is located above the ventral ramus.

The hornlet of *A. altai* is marked by a single apex and projects straight dorsally. This condition is also seen in *Teratophoneus* (Carr et al., 2011), but contrasts with the condition in juveniles of *Albertosaurus* (TMP 2001.45.74), *Gorgosaurus* (TMP 86.144.1), and *Daspletosaurus* (TMP 94.143.1), in which the hornlet is comprised of multiple (usually two or three) apices and trends anterodorsally (Carr, 1999: fig. 3). The hornlet of *A. altai* is also slightly eave-like: it overhangs the lateral margin of the lacrimal, but only very marginally. This condition is also present in juveniles of *Gorgosaurus* (TMP 86.144.1) and other tyrannosaurids; in adults of *Daspletosaurus* (CMN 8506), *Tarbosaurus* (PIN 551-3), and *Tyrannosaurus* (CM 9380) the prominent eave seen in subadults of the same genera is obliterated by internal inflation of the bone. In *A. altai*, the overhang of the eave appears superficially greater on the right lacrimal, but this is an artifact of postmortem crushing. Compared to the well-described growth series of *Gorgosaurus*, the overhang of *A. altai* appears intermediate between the pronounced eave-like hornlets of adults and the barely overhanging projections of juveniles (Carr, 1999). In *A. altai* the overhang continues posteriorly onto the posterior ramus of the lacrimal as a shallow shelf, which continues to slightly overhang the lateral surface. Here the hornlet is not heavily swollen or pneumatized, as in adult *Tarbosaurus* (Hurum and Sabath 2003), *Tyrannosaurus*

(Osborn, 1912; Molnar, 1991; Brochu, 2003), and *Daspletosaurus* (Carr, 1999; Carr and Williamson, 2004).

We here consider the discrete conical shape of the hornlet in *A. altai* as autapomorphic among tyrannosauroids. In *A. altai*, the hornlet arises abruptly from the dorsal surface of the bone, making it unusually distinct relative to the rest of the dorsal margin. In contrast, the horn grades posteriorly into the dorsal surface of the bone in other tyrannosauroids, including subadults of *Albertosaurus* (TMP 2001.45.74), *Daspletosaurus* (TMP 94.143.1), and *Gorgosaurus* (ROM 1247), in which the horn is not inflated and the anterior margin of the horn arises abruptly from the dorsal ramus.

Unfortunately, the status of much of this variation cannot be assessed in *Alioramus remotus* based on published sources (Kurzanov, 1976). Although this taxon is reconstructed as possessing a lacrimal with a small, discrete hornlet above the ventral ramus (Kurzanov, 1976: fig. 1), the actual fossil material is insufficient to determine any of these features, as the anterior ramus of the lacrimal is missing (Kurzanov, 1976: fig. 5).

The lacrimal of *A. altai* is extensively pneumatized. Both the lateral surface of the anterior ramus (the medial lamina) and the anterior surface of the ventral ramus (between the lateral and medial lamina) are deeply pocketed by several pneumatic foramina and fossae. In *A. altai* there are three principal pneumatic openings: the primary pneumatic recess (figs. 12, 14, lrec; "lacrimal recess" sensu Witmer [1997]) and two accessory fossae ahead of it, a proximal fossa and a distal fossa (figs. 12, 14, apo). There are two vertical septa that separate these openings: one between the pneumatic recess and the proximal fossa, and another that separates the proximal and distal fossae. This pattern is also seen in adult *Gorgosaurus* (TMP 96.12.151), adult *Daspletosaurus* (CMN 8506) and in juvenile *Tyrannosaurus* (BMR 2002.4.1). In

progressively mature *Tyrannosaurus*, the proximal fossa is obliterated by inflation, whereas the distal fossa remains open (CM 9380). In contrast, only the pneumatic recess and the proximal fossa are present in *Raptorex*, juvenile (TMP 86.144.1) and subadult (ROM 1247) *Gorgosaurus*, and juvenile *Daspletosaurus* (TMP 94.143.1). Both conditions (the primary recess plus either one or two accessory recesses), however, are seen in *Albertosaurus* (TMP 99.50.57, TMP 810.10.1).

In *A. altai*, the primary pneumatic recess is immediately dorsal to the posterodorsal corner of the antorbital fenestra, and is present in the region where the anterior and ventral rami join. This is a large chamber, 32 mm long anteroposteriorly and 16 mm deep at its posterior margin on the better preserved left lacrimal. Internally it is a single recess, whose anterior region is partly divided internally by an arcuate ridge that thins as it extends posterodorsally (figs. 12, 14, air). The internal surface of the lacrimal recess is uneven, and many fossae and pockets extend in a seemingly random pattern. One such pocket extends deeply into the bone medially, and nearly pieces the medial sutural surface for the nasal. Another pocket projects ventrally and may communicate with recesses in the anterior portion of the ventral ramus. Matrix obscures details of any possible connection in *A. altai*, but the two recesses do not communicate in *Tyrannosaurus* (Brochu, 2003). In general, the primary recess of *A. altai* is enormous, and much larger in comparison to the size of the lacrimal than in all known growth stages of *Appalachiosaurus*, *Daspletosaurus*, and *Tyrannosaurus* (Carr et al., 2005). However, a similarly proportioned large recess is seen in all stages of *Gorgosaurus* ontogeny (Carr, 1999; Carr et al., 2005).

The two additional pneumatic excavations, the proximal and distal fossae, are located on the anterior ramus of the lacrimal, anterior to the primary recess (figs. 12, 14, apo). These

structures are often referred to as "accessory pneumatic openings" (e.g., Currie, 2003a). In the *A. altai* holotype these accessory fossae are deformed by crushing, but their general form and position are apparent. The right lacrimal has a long proximal fossa, which extends from the primary recess anteriorly as a shallow groove, and terminates anteriorly in an ovoid foramen that penetrates the bone surface. Ahead of this is the distal fossa, which is smaller and more deeply excavated than the proximal fossa; its posterior end is penetrated by a foramen. On the left lacrimal the distal fossa is larger recess (17 mm long anteroposteriorly, 7 mm tall dorsoventrally), more discrete, and more deeply excavated than on the right bone. On both sides, narrow septa separate the pneumatic recess from the proximal fossa (less than 9 mm wide) and the proximal fossa from the distal fossa (less than 4 mm wide).

The primary, proximal, and distal pneumatic openings are a common feature of tyrannosaurids (see above), but *Tarbosaurus* appears to possess an unusual morphology. Currie (2003:202) stated that *Tarbosaurus* "does not have accessory openings" at any point throughout ontogeny, but distally located pneumatic foramina are clearly present in some specimens (e.g., Carr and Williamson, 2004: fig. 10). It is true, however, that these pneumatopores are generally smaller than the accessory recesses of other tyrannosaurids, and are not associated with the large pneumatic fossae or grooves characteristic of *A. altai* and other taxa. Juvenile *Tarbosaurus* appears to have a more traditional tyrannosaurid morphology in which the three openings are clearly present and discrete (Tsuihiji et al., 2011). *Tarbosaurus*, therefore, appears to have underwent an ontogenetic transformation in which the proximal and distal accessory fossae of juveniles are obliterated, or greatly reduced in size, during the transition to adulthood.

The second region of extreme pneumaticity is located on the anterior surface of the ventral ramus, between the lateral and medial laminae. As with the pneumaticity on the anterior

ramus, details of ventral ramus pneumaticity differ in detail on the left and right lacrimals. However, both bones are excavated by a dorsoventrally elongate, ovoid pocket that extends deeply posteriorly into the ventral ramus at the posterodorsal corner of the antorbital fenestra (fig. 12, antpp). An anteriorly-facing opening is also present in *Albertosaurus* (Carr, 2010). A similarly positioned, but medially-opening and much larger, pneumatic foramen is present in subadult and adult *Daspletosaurus* (CMN 8506), adult *Tarbosaurus* (ZPAL MgD-I/4) and *Tyrannosaurus* (CM 9380). This opening is absent, however, in juveniles of *Tyrannosaurus* (TMP 94.143.1, BMR 2002.4.1), which instead possess a small neurovascular foramen in this region.

In *A. altai*, this pneumatic opening is immediately ventral to the primary recess on the anterior ramus, but is separated from it by a prominent strut. This opening is likely associated with the lacrimal canal, and appears to be continuous with a foramen that pierces the medial surface of the lacrimal to open posteriorly. Ventral to the lacrimal canal are several discrete fossae (fig. 12, antpf), some of which lead posteriorly into foramina. On the right bone there is one small foramen, located ventral to the lacrimal canal and clearly distinct from it, that opens onto the medial surface. This pneumaticity is better developed on the left lacrimal, where a larger number of ventral fossae are present. Here, a large fossa is situated below the canal, followed by another fossa is situated below it. The second (most ventral) fossa contains its own subsidiary and ventrally positioned fossa.

The lacrimal articulates with several bones on the skull roof. In medial view several articulations are visible on the anterior ramus. Anteriorly there are two long grooves, one on the lateral process and one on the medial processes of the forked anterior end of the lacrimal (see above). The groove on the lateral process, which is the more dorsally positioned of the two

grooves, articulates with the nasal (fig. 14, nas). It is shallow dorsoventrally in its anterior region, where it also faces medially. As this groove continues posteriorly it deepens, but then sweeps medially, becomes shallower, and faces nearly equally medially and dorsally. This region articulates with the posterior region of the nasal, where a plate-like portion expands ventrally to back the lacrimal medially (see above).

The groove on the medial process (fig. 14, max) is of a similar depth to the dorsal groove, and the two extend to approximately the same level anteriorly. This groove begins as a dorsoventrally deep, nearly flat, medially-facing structure, but posteriorly it thins in depth and continues into a deeply inset socket. The ventral groove articulates with the maxilla, but is only one of two articular contacts between the two bones. As described above, the ascending ramus of the maxilla bifurcates into two prongs posteriorly: a dorsal one which is overlapped by the lacrimal (thus articulating with the ventral groove on the medial surface of the medial process of the lacrimal) and a ventral one that slightly overlapped the anteroventral corner of the anterior ramus of the lacrimal laterally. This second maxillary contact site (fig. 12, secmax) is an elongate, triangular indentation on the lateral surface of the anterior ramus of the lacrimal, which is coarsened by anteroposteriorly oriented striations and demarcated dorsally by a ridge.

An identical bifurcated, medially-and-laterally interlocking articulation between the maxilla and lacrimal is also seen in *Appalachiosaurus* (Carr et al., 2005: fig. 4), *Albertosaurus* (TMP 86.64.1), *Gorgosaurus* (ROM 1247), *Daspletosaurus* (CMN 8506), *Tarbosaurus* (Hurum and Sabath, 2003: fig. 6), and *Tyrannosaurus* (AMNH FARB 5027). Hurum and Sabath (2003:171) describe *Alioramus remotus* as possessing the same condition, citing Kurzanov's (1976: fig. 1) reconstruction as evidence. However, details of the lacrimal-maxilla contact are unclear in this figure, and the preserved fossil material (Kurzanov, 1976: fig. 4) lacks the contact

zone between these two bones. Similarly, Hurum and Sabath (2003:171) describe *Tyrannosaurus* as possessing a simplified articulation in which contact between the maxilla and lacrimal is "limited to a shallow groove in the anteroventral part (of the lacrimal)." *Tyrannosaurus*, however, also clearly possesses medial and lateral articular surfaces on the anterior ramus of the lacrimal (CM 9380; Hurum and Sabath, 2003: fig. 7), nearly identical to those of *A. altai*.

Posterior to the articulation with the maxilla and the nasal, the lacrimal contacts the prefrontal medially for a short region (fig. 12, prf). Posteriorly, the prefrontal contact sweeps ventrally and then anteriorly to follow the posterior margin of the medial surface of the ventral ramus of the lacrimal. Above where the prefrontal articulation twists anteroventrally there is a small, peg-like projection from the medial surface of the posterior ramus of the lacrimal (fig. 12, fro). This fits into a socket on the frontal and represents the sole contact between these two bones. There is a small contact surface on the dorsal surface of the posterior ramus, where a small projection of the frontal (the dorsal portion of the aforementioned socket) would have overlapped the lacrimal. This articular surface is located at the posteriormost tip of the lacrimal, and there is no evidence for further contact with the postorbital, as occurs in some large tyrannosaurids (Currie, 2003a).

The lacrimal also contacted the jugal ventrally along two distinct suture zones. First, the ventral region of the ventral ramus was overlapped by the jugal laterally (fig. 12, jug sut). This condition is seen in all derived tyrannosauroids (*Albertosaurus*, *Bistahieversor*, *Daspletosaurus*, *Gorgosaurus*, *Raptorex*, *Tarbosaurus*, *Teratophoneus*, *Tyrannosaurus*). The ventral-most 20 millimeters of the ramus is roughened for this contact, and here the bone is especially thin and plate-like. In lateral view, when the bones are in articulation, this contact would project as a nearly straight, smooth suture. Additionally, a small portion of the lacrimal laterally overlapped

the jugal to strengthen contact between the bones. This secondary articulation is marked by a second sutural surface on the lacrimal: a step-like notch on the posteroventral corner of the medial surface of the ventral ramus (fig. 12, jug not). This notch clearly fit on top of and slightly laterally overlapped the small, mound-like process of the jugal anterior to the orbit (see below). A nearly identical subsidiary articulation is seen in other tyrannosaurids (e.g., Currie, 2003a: fig. 23). However, the jugal-lacrimal articulation of *A. altai* may be unique. The plate-like ventral region of the lacrimal is extensive: it is both dorsoventrally and anteroposteriorly expanded relative to those preserved in other tyrannosaurids (e.g., Carr, 1999: fig. 3; Hurum and Sabath, 2003: figs. 6, 7). However, this thin region is easily eroded, and it is possible that the abbreviated contact surface seen in other tyrannosaurid specimens would have been larger in life and more similar to the condition in the well-preserved *A. altai* lacrimal.

In medial view, there is a prominent ridge on the anterior margin of the ventral ramus, which gives the lacrimal somewhat of a "T" shape in cross section (fig. 12, ridge). This ridge, the orbitonasal ridge of Carr et al. (2005), separated the orbit and antorbital cavities, and may have also strengthened the lacrimal (Currie, 2003a). The ridge in *A. altai* is narrow anteroposteriorly on the left, but it is wide on the right side. In comparison with other derived tyrannosauroids, the narrow condition is present in *Raptorex* (LH PV18, a juvenile specimen), juvenile *Gorgosaurus* (TMP 86.144.1), subadult *Albertosaurus* (TMP 200045.26), and juvenile *Tyrannosaurus* (BMR 2002.4.1). In contrast, the ridge is wide in adult *Gorgosaurus* (96.12.151), adult *Albertosaurus* (TMP 81.10.1), juvenile (TMP 94.143.1) and adult (CMN 8506) *Daspletosaurus*, and adult *Tyrannosaurus* (CM 9380). The asymmetrical condition seen in *A. altai* is consistent with the hypothesis that the holotype was a subadult at death, and died during the stage at which the ridge was becoming wider.

Jugal: Only the left jugal is known, but it is essentially complete and exceptionally well preserved (figs. 15-16). The jugal is divided into three principal processes: an anterior ramus that contacts the lacrimal and maxilla, a dorsal ramus that meets the postorbital, and a posterior ramus that is overlapped by the quadratojugal. Only the anterior tip of the anterior ramus and the posterior ends of the forked posterior ramus are missing.

The lateral surface of the jugal is generally smooth, especially compared to the rougher texture of most of the maxilla, lacrimal, and nasal. There is a region of mottled bone texture, comprised mostly of slightly raised lineations, along the ventral margin of the anterior ramus and immediately underneath the orbit. The most striking ornamental feature of the jugal is a greatly expanded and rugose knob of bone that projects laterally, immediately ventral to the posterior margin of the orbit (figs. 15-16, jh). This tubercle, best referred to as a jugal "hornlet," projects approximately 10 mm laterally from the surface of the jugal. This hornlet is not present in any other tyrannosauroid specimen, with the possible exception of *A. remotus* (see below). In *A. altai*, it is a single process, but is sculpted by deep grooves that define several ovoid tubercles of bone (bony papillae). Ventral to the hornlet is a large foramen, on the lateral surface of the cornual process (see below). There are additional foramina anterior and posterior to this, and the three form an arc with equal spacing between them (fig. 15A, for). There is also a fourth foramen located posterodorsal to the posterior-most foramen of the arc. It is likely that these foramina are associated with blood vessels that innervated a keratin sheath that surrounded the hornlet in life.

No other tyrannosauroids possess a discrete, laterally projecting hornlet on the jugal. The region beneath the orbit is commonly rugose in tyrannosaurids (e.g., Osborn, 1912: fig. 1; Brochu, 2003: fig. 2; Currie, 2003a: fig. 6; Hurum and Sabath, 2003: fig. 12), but it never

develops into a conical structure like that seen in *A. altai*. The situation in *Alioramus remotus* is unclear: Kurzanov (1976: fig. 1) reconstructs this taxon as lacking clear jugal rugosity, but describes a "tubercled surface…for a possible horny covering" in this region (Kurzanov, 1976:98). Tyrannosauroids in general are also characterized by an additional, and clearly different, rugose structure underneath the orbit. This is the "cornual process" of Carr (1999): a convex projection on the ventral margin of the jugal beneath the posteroventral corner of the orbit. This process is also present in *A. altai*, and is distinct in lateral view (i.e., projects far ventrally as a discrete convexity) and mediolaterally thickened (fig. 15, cor). The prominence of the cornual process is similar to that in adult *Bistahieversor* and *Albertosaurus*, juvenile and adult *Gorgosaurus* (Carr, 1999) and juvenile, but not adult, *Tyrannosaurus* (Carr and Williamson, 2004). The process is low and indistinct in adult *Tyrannosaurus* and in juveniles of *Bistahieversor* (NMMNH P-25049) and *Daspletosaurus* (TMP 94.143.1). On the other hand, it is most prominent among tyrannosauroids (and much larger and more prominent than in *A. altai*) in adult *Daspletosaurus* (CMN 8506).

The orbital margin on the jugal is smoothly concave. The jugal contributes widely to the floor of the orbit, and forms its entire ventral margin. This contrasts with the case in some specimens of *Tyrannosaurus*, in which the jugal makes only a very slight contribution to the orbital floor, due to the extensive ventral ramus of the postorbital (Brochu, 2003: fig. 2). The morphology of *A. altai*, in which the postorbital approaches the ventral floor of the orbit, is also seen in most other derived tyrannosauroids (Carr, 1999). In contrast, the postorbital stops far above the ventral margin of the orbit in adult *Daspletosaurus*, *Tarbosaurus*, and *Tyrannosaurus* (e.g., Currie, 2003a; Hurum and Sabath, 2003).

As in other adult tyrannosauroids, the jugal is highly pneumatic in *A. altai*. Most prominently, there is a greatly enlarged pneumatic recess on the lateral surface of the anterior ramus, in the posteroventral corner of the antorbital fossa and immediately posteroventral to the point where the jugal makes a small contribution to the antorbital fenestra. Two clear divisions of this recess are present (figs. 15-16, app, ppp). First, the entire posteroventral region of the jugal antorbital fossa is deeply embayed, as this recess continues deep into the jugal posteriorly and medially (into the "main internal chamber", see below) (figs. 15-16, ppp). Second, a smaller anterior fossa leads into a smaller pocket, which extends into the region of the jugal between the bifurcated processes for the maxilla (figs. 15-16, app). Ventral to the anterior embayment is a circular hole with smooth margins, which pierces the jugal medially. The porous and remodeled surface of this embayment suggests that it is a pathologic feature. In the holotype of *A. altai* there clearly was some absorption of the posterior margin of the recess, which exposes the pneumatic fossa broadly in lateral view. This is rare in juvenile *Albertosaurus*, but common in adults, and is also present in large specimens of *Daspletosaurus* and *Tyrannosaurus* (Carr, 1999).

The pneumatic recess of *A. altai* is larger and more complex than those of other tyrannosaurids, which often only possess the posterior embayment and not an additional anterior pocket (e.g., Currie, 2003a: figs. 6, 23; Hurum and Sabath, 2003: fig. 12). In other specimens that possess an anterior pocket, this feature is usually small, and there is no broad fossa between it and the posterior embayment (e.g., Hurum and Sabath, 2003: fig. 7). The posterior pocket of *A. altai* is very similar to that described in *Gorgosaurus* by Currie (2003); it is teardrop shaped in anterior view, with a wider ventral margin, and its long axis is oriented at an angle of about 45 degrees from the ventral margin of the skull (see also Carr, 1999: fig. 3; Currie, 2003a: fig. 6). By contrast, the pneumatic recesses of *Daspletosaurus*, *Tarbosaurus*, and *Tyrannosaurus* are

generally smaller and oriented either horizontally or vertically (e.g., Osborn, 1912: fig. 1; Russell, 1970: fig. 1; Carr, 1999: fig. 1; Brochu, 2003: fig. 2; Currie, 2003a: fig. 23; Hurum and Sabath, 2003: figs. 7, 12). Furthermore, the recess of *Tarbosaurus* is also generally more circular than that of *A. altai* (ZPAL MgD-I/4, MgD-I/38; Hurum and Sabath, 2003: fig. 12). This condition is also seen in some specimens of *Daspletosaurus* (CMN 8506) and in *Tyrannosaurus* (AMNH FARB 5027).

Interestingly, the lateral surface of the jugal is not visibly inflated by the pneumatic recess, but rather is flat. A similar morphology is present in juveniles of *Bistshievesor* and *Gorgosaurus*. Lateral inflation is a clear, one-to-one correlate of jugal pneumaticity in basal tetanuran theropods (e.g., Brusatte et al., 2010b), and is also seen in large tyrannosaurids, where the inflated jugals are often described as "cheeks" (e.g., Brochu, 2003; *Tarbosaurus*: ZPAL MgD−I/3). In *Daspletosaurus* (TMP 94.143.1) and *Tyrannosaurus* (CMNH 7541), inflation is already present in juveniles. In *A. altai*, the medial surface of the jugal is slightly inflated, and is pierced by two large foramina that lead into the jugal recess (fig. 15B, for). The anterior foramen is smaller and leads into the anterior pocket of the recess. The larger, posterior foramen evidently continues into the main internal chamber of the sinus. This "main chamber" is continuous with the posterior pocket of the external recess, but matrix obscures internal details of the extent and form of this cavity. There are some additional small foramina on the lateral and medial surfaces more posteriorly, but these do not appear to lead into the main internal chamber. There are no distinctive posterior pneumatic openings immediately anterior to the posterior ramus, as in some specimens of *Tyrannosaurus* (Hurum and Sabath, 2003: fig. 7).

The jugal contacts the maxilla along two surfaces. First, there is a narrow and deep groove on the ventral surface of the anterior ramus (figs. 15-16, vmax). This groove would have

fit on top of, and deeply interlocked with, the tapering main body of the maxilla below the antorbital fenestra. Additionally, the anterodorsal corner of the anterior ramus of the jugal has a much shorter groove, which faces dorsally and laterally (figs. 15-16, dmax). This would have articulated with the subsidiary fork of the maxilla, which rises dorsally from the posterior end of the maxillary main body to strengthen the connection between the two bones. This complex joint surface for the maxilla can be seen in all derived tyrannosauroids. In *A. altai*, the anterior tip of the lateral lamina of the anterior ramus (i.e., that portion lateral to the dorsally and laterally-facing groove) is bifurcated, resulting in a small subsidiary process that would have strengthened the articulation with the maxilla (figs. 15-16, sub). This subtle process is probably easily broken in specimens, but is present on well-preserved jugals of juvenile (CMNH 7541) and adult (AMNH FARB 5027) *Tyrannosaurus*.

The jugal contacts the lacrimal immediately anterior to the orbit. Much of the ventral ramus of the lacrimal was overlapped laterally by the jugal, but a small region of the posteroventral corner of the lacrimal laterally overlapped a small dorsal convexity on the jugal immediately in front of the orbit. This convex bulge, the "anterior ascending process" of Brochu (2003) is only a small projection (fig. 15, aap), whereas it is much larger in *Tyrannosaurus* (Brochu 2003: fig. 2). Furthermore, in *Albertosaurus*, *Gorgosaurus*, *Daspletosaurus*, *Tyrannosaurus* and *Tarbosaurus* (Currie 2003a; Hurum and Sabath, 2003: fig. 7) the lateral surface of the projection is marked by an indented cleft, where the overlapping lacrimal would have fit into the jugal. An interlocking articulation is also seen in *A. altai*, as described above, although the lateral surface of the jugal anterior ascending process is not as deeply excavated as in *Tarbosaurus* and *Tyrannosaurus*.

The dorsal ramus of the jugal meets the postorbital along an extensive contact (fig. 15, porb), where together they form the posterior margin of the orbit. Almost the entire anterior edge of the dorsal ramus of the jugal participates in this articulation (the lower quarter of the ramus does not articulate with the postorbital and comprises the orbital margin). The entire postorbital contact zone is demarcated posteriorly by a pronounced ridge (fig. 15, rid). Ventrally, the postorbital joint surface faces equally anteriorly and laterally. Above this region it is separated by a thin ridge that extends from ventromedial to dorsolateral (fig. 15, trid), which separates the surface into separate anteriorly and laterally facing portions. The contact faces fully anterorly anterior (medial) to the thin ridge and laterally posterior to the ridge. Dorsally, after the thin ridge meets the pronounced ridge at an inflection point (fig. 15, ip), the postorbital contact faces solely anteriorly. In anterior view the postorbital joint surface is generally concave above and below the thin ridge; it is most deeply concave above the ridge.

Although the jugal-postorbital articulation changes in orientation across its length, the entire contact is an overlapping scarf joint, and it is not reinforced by any interlocking rugosities. The prominent ridge, however, extends along the posterior margin of the contact and would have helped to stabilize the articulation between the jugal and postorbital (fig. 15, rid). The shape and orientation of the scarf joint is similar to that in *Albertosaurus* (Currie, 2003a: fig. 6), *Gorgosaurus* (TMP 86.144.1), and juvenile *Daspletosaurus* (Currie, 2003a: fig. 23), but differs from the condition in adult *Daspletosaurus* (CMN 8506), *Tarbosaurus* and *Tyrannosaurus* (Hurum and Sabath, 2003: figs. 6, 12), in which the contact is broader and faces strongly laterally across its entire length. The holotype of *Raptorex*, which belongs to a young individual, exhibits an unusual condition in which the joint surface faces entirely anteriorly across its entire length.

In *A. altai* there is a slight concavity at the ventral end of the postorbital articulation, where the ventral tip of the postorbital would sit (fig. 15, tc). This concavity is demarcated anteriorly by a slight, pointed projection (fig. 15, p). A similar morphology characterizes juvenile *Albertosaurus* and *Gorgosaurus* (Carr, 1999: fig. 3; Currie, 2003a: fig. 2), as well as all growth stages of *Tarbosaurus* (Hurum and Sabath, 2003: fig. 12), *Tyrannosaurus* (Hurum and Sabath, 2003: fig. 12), and *Daspletosaurus* (Carr, 1999: fig. 3; Currie, 2003a: fig. 23). However, in larger albertosaurines the anterior projection develops into a larger, more pronounced, and strongly rugose shelf (Currie, 2003a: fig. 6).

The dorsal process of the jugal is narrow anteroposteriorly, and the most salient feature on its lateral surface is the prominent ridge that braces the postorbital articulation (fig. 15, rid). Posterior to the ridge the lateral surface of the process is smooth, as is the case in *Albertosaurus*, *Bistahieversor*, *Gorgosaurus*, *Teratophoneus*, and juvenile tyrannosaurines. By contrast, this surface is excavated by a broad concavity in large subadult and adult tyrannosaurines (*Daspletosaurus*, *Tarbosaurus*, *Tyrannosaurus*: Currie, 2003a). Finally, the posterior margin of the dorsal ramus is straight to slightly convex, similar to the condition in *Bistahieversor* (NMMNH P-27469), juvenile *Gorgosaurus* (Carr, 1999: fig. 3), and all growth stages of *Tarbosaurus* and *Tyrannosaurus* (Hurum and Sabath, 2003; Carr and Williamson, 2004). In contrast, this margin is strongly convex in adult *Albertosaurus* (Carr, 1999; Currie, 2003a: fig. 6) and juvenile (Currie, 2003a: fig. 23), but not subadult or adult (Carr, 1999: fig. 3), specimens of *Daspletosaurus*.

The quadratojugal overlapped the posterior ramus of the jugal (fig. 15, qj), which is forked into dorsal and ventral prongs (fig. 15, dp, vp). This condition is seen in all derived tyrannosauroids (*Bistahieversor* and tyrannosaurids). Both prongs are broken posteriorly,

preventing accurate measurements of their length and relative posterior extents. The tapering anterior ramus of the quadratojugal would have fit in between the prongs, and broadly overlapped the dorsal margin of the ventral prong. The joint surface on the ventral process is supported posteriorly by a prominent ridge. The dorsal prong, on the other hand, marginally overlapped the dorsal edge of the anterior process of the quadratojugal.

The jugal articulates with the palatine and ectopterygoid medially. These palatal bones contact the jugal along a flat region on the ventral margin of the anterior ramus, which is continuous with the flat palatine articulation on the maxilla. The ectopterygoid broadly contacts the jugal anterodorsal to the cornual process (fig. 15, ect). The posteriorly-projecting jugal process of the palatine may have also made contact on the medial surface of the anterior ramus (fig. 15, pal?), but exact details are difficult to discern.

Postorbital: Both left and right postorbitals are preserved (figs. 17-19). The left is preserved as a disarticulated, single element, which is essentially complete and very well preserved (figs. 17-18). The right postorbital is appressed to the squamosal in articulation, but is missing approximately half of the ventral process (fig. 19). The postorbital is T-shaped as in most theropods, with anterior, posterior, and ventral processes. Together, the anterior and posterior processes form a "dorsal bar," which roofed much of the orbit anteriorly and lateral temporal fenestra posteriorly.

The lateral surface of the postorbital is rugose in some areas. The most prominent rugosities are present on the ventral margin of the anterior ramus, in the region that roofed the posterodorsal corner of the orbit. Here, a coarse and swollen ridge overhangs the corner of the orbit, which is visible as a small flange in lateral view (figs. 17-18, cor). This ridge is covered by

fine grooves, which demarcate individual ovoid tubercles of bone (bony papillae) oriented roughly perpendicular to the trend of the ridge itself. Immediately posterodorsal to the ridge is a smooth fossa.

The rugose ridge is homologous to the cornual process of tyrannosaurids (Carr, 1999; Currie, 2003a). This process is absent in basal tyrannosauroids such as *Dilong* (Xu et al., 2004), *Guanlong* (Xu et al., 2006), *Xiongguanlong* (Li et al., 2010), and *Raptorex* (Sereno et al., 2009). In contrast, all tyrannosaurids, as well as *Bistahieversor*, have a rugose swelling above the posterodorsal corner of the orbit, but in most other genera it is larger and more swollen, and is oftentimes expanded into a convex bulge referred to as a "horn" (e.g., Currie, 2003a:205). This condition is present in *Albertosaurus* (Currie, 2003a: fig. 8), *Bistahieversor* (Carr and Williamson, 2010), juvenile *Daspletosaurus* (Russell, 1970: fig. 1; Carr, 1999: fig. 3P), *Gorgosaurus* (Currie, 2003a: fig. 2), and is especially well developed in *Tarbosaurus* and *Tyrannosaurus* (Hurum and Sabath, 2003: fig. 11). The greastest development of the horn is seen in adult *Daspletosaurus* (CMN 8506). A robust and rugose cornual process is also present in juvenile *Tarbosaurus* individuals slightly larger than the holotype of *Alioramus altai* (ZPAL MgD-I/29; ZPAL MgD-I/175).

Currie (2003a) and Currie et al. (2003) describe a taxonomic difference in the shape and extent of the "horn" in tyrannosaurids, but the ridge-like and unswollen cornual process of *A. altai* does not seem to exhibit either the "rounded" or "C-shaped" condition of albertosaurines and tyrannosaurines, respectively. The morphology of the process in *A. altai* seems to most closely approximate the condition in juvenile *Daspletosaurus* (TMP 94.143.1), in which the cornual process is a low coarse ridge along the margin of the orbital fenestra. Currie (2003a) also notes that the process is larger, more prominent, and more rugose in adults. The condition in

Alioramus remotus also seems similar to that in *A. altai*, judging by the figures (Kurzanov, 1976: fig. 4) and description of Kurzanov (1976:97), who notes that the postorbital is unexpanded "without any clearly expressed outgrowths."

The lateral surface of the remainder of the anterior process and the entire posterior process is smooth and generally flat. However, the lateral surface of the ventral ramus is scoured by several fine, centimeter-scale, arcuate lineations that are dorsally convex (fig. 17, lin). The lineations are more discrete and prominent dorsally, whereas the texture is more randomly mottled ventrally. These have been described as a feature of juvenile *Gorgosaurus*, which eventually transition into a rougher and more random bone texture in adults (Carr, 1999). Less discrete lineations are also present in larger and mature tyrannosaurids (e.g., Currie, 2003a: figs. 2, 8).

The ventral process is tongue-shaped, as it only slightly tapers ventrally and terminates in a rounded margin. Compared to the condition in derived tyrannosaurid adults, this process is narrow and gracile in *A. altai* (Osborn, 1912: fig. 1; Brochu, 2003: fig. 2; Hurum and Sabath, 2003: figs. 8, 11). The ventral process does not reach the floor of the orbit, but ends approximately 20 mm above it. The process also does not curve strongly anteriorly and protrude into the orbit as a "suborbital process" (Chure, 2000). This condition seen in *A. altai* is also present in juveniles of *Gorgosaurus* (TMP 86.144.1), *Daspletosaurus* (TMP 94.143.1), and *Tyrannosaurus* (CMNH 7541). In contrast, the orbits of many tyrannosaurids are keyhole shaped due to an expansive subocular flange (e.g., Osborn, 1912: pl. 1; Brochu, 2003: fig. 1; Hurum and Sabath, 2003: fig. 1; Sampson and Loewen, 2005; Urban and Lamanna, 2006). In these taxa the ventral process not only curves anteriorly into the orbit, but also expands in width as it extends ventrally. Brochu (2003:27) describes the flange as present in *Tarbosaurus* and *Tyrannosaurus*,

with an "incipient" condition in *Daspletosaurus*. Carr (1999) and Brochu (2003) also consider the flange as absent in *Albertosaurus* and *Gorgosaurus*, but it is present in large individuals (Currie, 2003a: fig. 8). Clearly, the size and shape of the flange is ontogenetically controlled, as it is absent in juvenile albertosaurines and tyrannosaurines (Carr, 1999: fig. 6). Similarly, it is absent in *Alioramus remotus* (Kurzanov, 1976: fig. 4), as well as *Dilong* and *Guanlong* (Xu et al., 2004, 2006). An incipient version of the flange, however, is present in juvenile *Tarbosaurus* individuals slightly larger than the holotype of *Alioramus altai* (ZPAL MgD-I/29; ZPAL MgD-I/175).

The medial surface of the postorbital is excavated by a pronounced concave fossa where the anterior, posterior, and ventral processes meet (fig. 17B, fos); this fossa is present in all other derived tyrannosauroids. The anterior rim of this fossa is formed from a ridge extending ventrally from the laterosphenoid contact (figs. 17-18, lat; see below). The dorsal surface of the postorbital is smooth, as the rugose cornual process does not extend dorsally (see above). When seen in lateral view the dorsal margin is sinuous; it is gently concave anteriorly and convex posteriorly. A small portion of the dorsal surface of the anterior ramus is smoothed by the supratemporal fossa (fig. 17, stfossa), but this is neither extensive nor deep.

As in other derived tyrannosauroids, the postorbital has an extensive and bipartite contact with the frontal medially. This articulation is divided into two surfaces: an elongate contact that is oriented parasagitally and faces medially and ventrally (figs. 17-18, froph), and a more anteriorly positioned convex, bulbous surface that faces entirely medially and is oriented obliquely (anterolaterally) when seen in dorsal view (figs. 17-18, froab). Currie et al. (2003: character 14) consider the differentiation of a "horizontal" posterior region and an anterior "vertical" region of the frontal suture as a synapomorphy of albertosaurines. However, not only

is this differentiation present in *A. altai*, but also in basal tyrannosauroids such as *Bistahieversor* and other tyrannosaurines (e.g., *Daspletosaurus*: CMN 8506; *Tarbosaurus*: ZPAL MgD-I/3; *Teratophoneus*: BYU 8120/9396; *Tyrannosaurus*: BHI 3033). In these other taxa, as well as *Albertosaurus* (Currie, 2003a: fig. 8), the entire frontal articulation is much deeper dorsoventrally than in *A. altai*.

Both the anterior and posterior regions of the differentiated frontal articulation made contact with the frontal only. There is no sign of a discrete, anteriorly facing articular surface for the lacrimal, as is sometimes seen in large tyrannosaurids (Currie, 2003a). However, the bulbuous anterior articular surface would have approached the lacrimal, and there was only narrow separation between the two bones. Here, a short margin on the frontal formed the dorsal rim of the orbit.

Two additional articular contacts are present on the medial surface of the postorbital. First, there is a posteromedially facing, concave notch that would have received the head of the laterosphenoid (figs. 17-18, lat). This notch flattens ventrally and continues as a flat and rectangular contact surface. A rim of bone separates this notch dorsally from a second articular surface: a small, triangular region that would have narrowly contacted the parietal (figs. 17-18, par). This articulation also takes the form of an inset notch, no more than seven millimeters at its widest point, and lies between the contact for the laterosphenoid and the posterior, horizontal articulation for the frontal. The parietal articulation faces strongly dorsally, and is located at the dorsal tip of a ridge that separates the joint surfaces for the frontal and laterosphenoid. A similar, small articulation with the parietal is also present in other derived tyrannosauroids (e.g., *Bistahieversor*: NMMNH P-25049; *Tarbosaurus*: Hurum and Sabath, 2003; *Tyrannosaurus*: Brochu, 2003).

The thin and tapering posterior process of the postorbital laterally overlapped the forked anterior ramus of the squamosal (fig. 17, squ). This process, which is gracile in *A. altai*, is deep in adult tyrannosaurines (Carr and Williamson, 2004). Details of this articulation are well preserved and visible on the conjoined right postorbital and squamosal (fig. 19). The posterior process of the postorbital tapers in depth and thins in mediolateral width as it extends posteriorly. Its tip is rather blunt and somewhat triangular. On the medial surface of the posterior process are two grooves for the dorsal and ventral prongs of the anterior ramus of the squamosal (fig. 17, squ). The ventral groove is much larger and deeper, and it faces almost entirely medially, reflecting the larger size of the ventral prong. Dorsally this groove is demarcated by a strongly overhanging but thin rim (fig. 17, rid). The dorsal groove is much smaller and shallower, and it faces strongly dorsally, but also medially.

Finally, the ventral process of the postorbital overlaps the anterior end of the jugal across an elongate scarf joint (fig. 17, jug). The contact surface on the postorbital faces posteromedially, and subtly changes orientation in concert with the shape of the dorsal process of the jugal, as described above. The articulation was overlapping across its entire length, and there is no inset articular surface on the postorbital as is the case in some theropods (e.g., megalosauroids: Sereno et al., 1996).

Squamosal: Both left and right squamosals are known, and each is well preserved and nearly complete (figs. 19-20). The left bone is slightly compressed mediolaterally and is missing the posterior tip of the posterior process (fig. 20), whereas the right element is missing the posterior process and much of the ventral process (fig. 19). The squamosal is comprised of four principal processes: an anterior process, ventral process, posterior process, and medial process. The first

three are visible in lateral view, giving the squamosal a triradiate appearance. However, because the posterior process is small (and broken in these specimens), the squamosal appears somewhat C-shaped in lateral view. With the skull bones articulated, the anterior process trends anterodorsally as is typical of most theropods, and the ventral process projects ventrally and anteriorly.

The anterior process is dorsoventrally deep, and its lateral surface is excavated by a pronounced notch, which was overlapped by the posterior ramus of the postorbital (fig. 20, post). Anteriorly the notch separates into two prongs, which extend to the same level anteriorly (fig. 19, apr). The dorsal prong is long and thin, and would have been widely exposed in lateral view when the squamosal and postorbital were articulated. This prong sits on top of the posterior process of the postorbital. In contrast, the ventral prong is not widely visible in lateral view when the bones are articulated, but rather is extensively covered by the postorbital. However, when the squamosal is disarticulated it can be seen that the ventral prong is long and deep, and is much more extensive than the narrow region that is exposed laterally. The ventral prong lacks a discrete, ventrally projecting, sheet-like process anteriorly as in *Tyrannosaurus* (Brochu, 2003: fig. 24B). Additionally, the ventral prong of *A. altai* is smoothly arched, and there are no inflections as in some specimens of *Tyrannosaurus*, which display two concave regions separated by a point (FMNH PR2081; Brochu, 2003: fig. 24B). This condition in FMNH PR2081, however, may be an artifact of crushing.

The ventral process projects anteroventrally, and is oriented at approximately 45 degrees relative to the anterior process (when the anterior process is held horizontally for reference). When the squamosal is viewed in articulation with the surrounding bones, the long axis of the ventral process projects roughly anteroposteriorly, as in other tyrannosaurids (Carr and

Williamson, 2010: character 111). It becomes mediolaterally thinner and expands in anteroposterior length as it continues ventrally, where it meets the quadratojugal at an elongate contact (fig. 20, qj). The quadratojugal overlapped the squamosal here, and the dorsal extent of the contact is marked by a thick ridge, which trends nearly horizontally, on the ventral process of the squamosal (fig. 20, qjr). The region of the squamosal overlapped by the quadratojugal is extremely thin and plate-like (less than one millimeter thick mediolaterally). Because this process extends anteroventrally, it would have joined with the quadratojugal to project into the lateral temporal fenestra, as is the case in tyrannosaurids generally. In *A. altai* this projection would have nearly bisected the fenestra, but it falls 25 millimeters short of doing so. In contrast, the squamosal and quadratojugal of *Gorgosaurus* (Currie, 2003: fig. 2) and *Tyrannosaurus* bisect the fenestra more completely (Osborn, 1912: pl. 1), and in some cases has been described as making contact with the postorbital anteriorly to completely separate the fenestra into dorsal and ventral partitions (Brochu, 2003).

The posterior process is broken distally on both specimens but is better preserved on the left squamosal (fig. 20, ppr). It evidently was short and thinned distally, and did not end in a swelling or expansion.

The lateral surface of the squamosal is generally unornamented. There is a slight lateral ridge oriented approximately parallel with the trend of the anterior process, which is most prominent immediately posterior to the postorbital groove and becomes less prominent anteriorly (fig. 20, rid). This structure is more pronounced on the left squamosal. A similar feature is seen in *Tarbosaurus* (Hurum and Sabath, 2003: fig. 9; ZPAL MgD−I/4) and *Tyrannosaurus* (Brochu, 2003: fig. 24B), where it is very thick, rugose, and projects dorsally from the skull roof as a horn-like ridge. The more pronounced morphology of this ridge in large tyrannosaurids may be

related to an increased attachment area for the mandibular depressor musculature (Brochu, 2003). In *A. altai*, the lateral surface is additionally excavated by a smooth, arcuate concavity immediately posterodorsal to the margin of the lateral temporal fenestra, in the region where the anterior and ventral processes meet (fig. 20, ltfos). This is part of the lateral temporal fossa, which surrounds the fenestra on regions of the squamosal, quadratojugal, postorbital, and jugal. The fossa is also present in other tyrannosaurids, and is deeper and more prominent in larger taxa (e.g., *Tarbosaurus*: ZPAL MgD−I/4).

The squamosal is arched dorsally, as a web of bone connects the anterior and medial processes. This is best seen in dorsal view (fig. 19, web). The medial process is a small, finger-like projection that trends anteriorly (figs. 19-20, mpr), almost parallel to the anterior process. It thins in both mediolateral thickness and dorsoventral depth as it extends anteriorly. This process forms the posteromedial corner of the supratemporal fenestra. Immediately posterior to the medial process, and facing dorsally and strongly medially, is a wide and deep groove for articulation with the paroccipital process (figs. 19-20, pop). This groove is most visible in medial view, but can also be seen in dorsal view. Separated from the groove, and ventral to it, is a medially and slightly ventrally facing articular surface for the parietal, which is only visible in medial view (figs. 19-20, par). The anterior half of this joint surface overlaps the prootic.

In medial view, a web of bone extends posteriorly and ventrally from the medial process. This web joins an anterodorsally trending and thickened ridge that begins at the anterior margin of the posterior process. Posterior to the ridge is the deeply excavated fossa for the quadrate head (figs. 19-20, qh). The fossa faces entirely medially and posteriorly, and none of it is visible in lateral view. It is teardrop shaped, tapers in width ventrally, and is oriented approximately 45 degrees relative to the horizontal. The region where the web of bone meets the anteroventrally

trending ridge is expanded medially into a small, convex tab that is visible in dorsal view (figs. 19-20, tab). This tab would have braced the head of the quadrate, as the smooth quadrate articular surface extends onto its ventral surface. Thus, articulation of the quadrate here suggests that there may have been a wide range of motion between the two bones.

Ventrally the squamosal is extensively hollowed by a pneumatic recess, which is a deep, circular opening in the uncrushed right squamosal (fig. 20, sqr). This recess is small in *Teratophoneus* (Carr et al., 2011) and large in *Daspletosaurus* (CMN 8506), *Tarbosaurus*, and in *Tyrannosaurus* (CM 9380). The recess is extremely small, and possibly absent, in at least one specimen of *Gorgosaurus* (TMP 86.144.1). The anterior margin of the recess is approximately level with the point where the medial process emerges, which is also the most posterior extent of the articulation with the postorbital. The anterior wall of the recess is penetrated with four small, circular depressions; the most medial of these appears to continue into the bone anteriorly. A similar condition is clearly seen in one specimen of *Tyrannosaurus* (RSM 2523.8), in which two extra openings penetrate the bone at the anteromedial corner of the recess. Posteriorly, the squamosal recess is extremely deep. It continues past the level of the articular surface for the quadrate head and into the interior of the posterior process. Here, it appears to end posteriorly as a blind pocket. On the right squamosal there is a thin ridge that partially divides the posterior pocket from the more anterior part of the recess. There appears to be one or two foramina on the dorsal region of the articular surface for the quadrate head, on the medial surface of the squamosal, which trend anteriorly into the squamosal recess.

The squamosal recess of *A. altai* is enormous, reaching the relative size that is seen in *Tyrannosaurus* (e.g., MOR 555). It excavates the entire ventral margin of the squamosal, and appears to be relatively larger than the recesses of *Tarbosaurus* (ZPAL MgD−I/4). The anterior,

posterior, medial, and lateral margins of the recess are well defined, but not the posterolateral margin (right side) or the anterolateral margin (left side), as is the case in adult tyrannosaurids (Currie, 2003a), and quite unlike the more poorly defined margins of juvenile *Daspletosaurus* (Currie, 2003a: fig. 25D). It is likely that this recess housed an air sac affiliated with the paratympanic system (Currie, 2003a).

Quadratojugal: Both left and right quadratojugals are present. The right bone is essentially complete and is missing only the anterior tip of the anterior process (fig. 21), whereas the left is heavily broken. This bone is L-shaped in lateral view, and comprised of a large dorsal process and a smaller anterior process, as well as a short posterior tab at the posteroventral corner.

The dorsal process expands dorsally to overlap the squamosal laterally and the quadrate medially. The dorsal expansion is plate-like and very thin (less than one millimeter thick at its center). The lateral surface of the entire dorsal process is excavated by a broad fossa (fig. 21, fos), which is demarcated anteriorly by a strong ridge (fig. 21, arim). The fossa is more pronounced on the left quadratojugal, and is smooth, as is the entire lateral surface of the bone. Both the anterior and posterior margins of the dorsal process are concave (except on the right side where the posterior margin is essentially straight), giving this part of the quadratojugal an hourglass shape in lateral view. A similar condition is present in other tyrannosaurids, and is often used as a character in phylogenetic analyses (e.g., Sereno et al., 2009; Carr and Williamson, 2010; Li et al., 2010). *Daspletosaurus* juveniles, however, exhibit a unique morphology in which the margins are relatively straight and the dorsal process does not expand greatly as it extends dorsally (Currie, 2004: fig. 24).

A. altai lacks a notch on the anterodorsal margin of the lateral surface of the dorsal process; the notch is characteristic of *Tyrannosaurus* (Carr and Williamson, 2004: fig. 12). Instead, the anterior ridge demarcating the lateral fossa gradually thins out and becomes confluent with the anterior surface. This ridge extends dorsally to the dorsal edge of the bone, as in *Daspletosaurus*, *Tarbosaurus*, and *Tyrannosaurus*, but unlike in other tyrannosauroids in which the ridge terminates further ventrally (Carr and Williamson, 2010: character 117). Finally, the anterodorsal margin of the bone is unusual among tyrannosaurids in that it extends anteroventrally for a great distance (fig. 21, adm). This condition is also present in juvenile *Tyrannosaurus* (BMR 2002.4.1), but is unlike the morphology seen in most other taxa, where the anterodorsal margin is short and extends at a low angle.

In medial view, the posterior margin of the dorsal process develops into a posterior tab (fig. 21, dptab), which curves medially to clasp an elongate, anteroventrally trending ridge on the quadrate shaft, which is positioned immediately below, and separated from, the head of the quadrate (see below). Here, the quadratojugal wraps around the posterolateral surface of the quadrate shaft, as described by Currie (2003a).

The anterior process is finger-like, and thins in depth anteriorly where it overlaps the posteror process of the jugal. The medial surface of the anterior ramus is flattened for this articulation (fig. 21, jug). Furthermore, the dorsal margin of the anterior process is excavated by a sharp groove, demarcated by paper-thin edges, upon which rested the dorsal prong of the jugal posterior process (fig. 21, djug). This would have made a slightly interlocking contact, thus strengthening the articulation between these two bones. The groove faces primarily dorsally, but also slightly laterally, and becomes narrower as it tapers anteriorly.

Although the anterior tip of the quadratojugal is missing, the contact surface on the jugal suggests that the anterior ramus projected anterior to the lateral temporal fenestra as in most tyrannosaurids. Brochu (2003) described the quadratojugal of *Albertosaurus* and *Tarbosaurus* as terminating posterior to the fenestra, but specimens of both of these genera show the more normal, anteriorly-extensive process of tyrannosaurids (Carr, 1999: fig. 5; Hurum and Sabath, 2003: fig. 1). However, there does appear to be some variation in the anterior extent of the anterior process among different genera (see Discussion). The more proper distinction is between processes that only project slightly in front of the fenestra versus those that extend far anteriorly (Holtz, 2004). Among tyrannosaurids, only *Tyrannosaurus* (Osborn, 1912: pl. 1) and possibly *Daspletosaurus* have the second condition, which is probably derived (Holtz, 2004).

In *A. altai* the anterior ramus tapers anteriorly into a rounded tip as in *Albertosaurus*, *Bistahieversor* (Carr and Williamson, 2010), *Gorgosaurus*, (Currie, 2003a), *Raptorex* (Sereno et al., 2009), and *Xiongguanlong* (Li et al., 2010). In contrast, the anterior process of *Daspletosaurus* (Russell, 1970: fig. 1; Carr, 1999: fig. 1), *Tarbosaurus* (Hurum and Sabath, 2003: fig. 9), and *Tyrannosaurus* (Osborn, 1912: pl. 1; Brochu, 2003: fig. 2) ends in a deep, spatulate, notched, or square-shaped termination (Currie et al., 2003); the process was almost certainly notched in *Teratophoneus* as well (Carr et al., 2011). In contrast, the anterior processes of *Dilong*, *Guanlong*, and *Proceratosaurus* taper into a fine point (Xu et al., 2004, 2006; Rauhut et al., 2010). The lateral surface of the anterior process is smooth, and lacks any rugosities or clear muscle attachment scars, such as those present in *Tyrannosaurus* (Brochu, 2003).

Finally, there is a small posterior tab that wraps around the posteroventral corner of the quadratojugal (fig. 21, pptab). This morphology is present in other tyrannosaurids, as well as the more basal taxon *Xiongguanlong* (Li et al., 2010), but is absent in *Dilong*, *Guanlong*,

Proceratosaurus, and most basal coelurosaurian outgroups, in which the posterior tab faces strongly laterally and does not wrap around the quadrate posteriorly. In *Alioramus altai*, this tab is cup-like, as it is deeply concave medially to clasp the quadratojugal flange on the posteroventral corner of the quadrate (see below). The posterior tab is actually comprised of two separate small processes: a main process that descends ventrally as a convex bulb and covers the quadrate laterally (fig. 21, pptab), and a secondary process that wraps around the posterior end of the lateral quadrate condyle as a small, subsidiary tab (fig. 21, subtab). The depth of the notch that separates these processes is variable between each side of *A. altai* and in other tyrannosaurids.

Immediately above this smaller tab, the posterior surface of the dorsal ramus is deeply excavated by a smooth, crescent-shaped fossa (fig. 21, qffos). In *Alioramus altai* the fossa is demarcated laterally by the posterior edge of the quadratojugal, which curves medially as it continues posteriorly, thus cupping the fossa in posterior view. This morphology is present in *Xiongguanlong* and tyrannosaurids, but not more basal tyrannosauroids and other coelurosaurian taxa (Li et al. 2010). The crescentic fossa surrounds the quadrate foramen, which is a teardrop shaped opening (26 mm deep, 9 mm wide at its midpoint) that is nearly equally shared by the quadrate and quadratojugal. The quadratojugal forms the entire lateral margin, whereas the quadrate forms the dorsal, ventral, and medial margins. This is also the case in other tyrannosaurids, including *Alioramus remotus* (Kurzanov, 1976: fig. 6). In *Dilong* (IVPP V14243), however, the foramen is located entirely within the quadrate.

Quadrate: A nearly complete left quadrate is preserved (figs. 22-24), along with a nearly complete right element that is missing only the ventral condyles. Like most theropods, the

quadrate is comprised of a shaft, which links the ventral articular condyles and the dorsal head, as well as a long, deep, and anteriorly projecting flange.

On the lateral surface, there is a large flange on the lateral condyle, which articulates with the medial side of the posteroventral corner of the quadratojugal. This quadratojugal flange is comprised of two separate articular surfaces. The ventral surface is a larger, circular, mostly laterally facing surface that is convex dorsally and concave ventrally (figs. 22-23, vsqjf). The dorsal surface is a smaller, convex, rectangular region that faces almost equally laterally and posteriorly (figs. 22-23, dsqjf). These surfaces correspond to the two separate flanges of the quadratojugal articulation described above. Dorsal to these articulations is the smooth surface for the quadrate foramen (figs. 22-24, qf). The foramen is only visible in anterior posterior views, but the smooth surface is widely visible as a 25 millimeter tall notch when the disarticulated quadrate is seen in lateral view.

Posterodorsal to the quadrate foramen lies another articular surface for the quadratojugal. Here, the posterodorsal region of the quadratojugal dorsal process cupped the quadrate laterally and posteriorly, as described above. Thus, there are two distinct articular surfaces on the quadrate here: a laterally facing surface (fig. 22, qjlat) and one that faces slightly laterally but primarily posteriorly (fig. 22, qjpost). The lateral contact surface is hourglass shaped: there are dorsal and ventral triangular regions, each excavated by a deep groove laterally, but they are constricted where they meet. The second, posteriorly facing articulation is broader and forms a single continuous surface. It is ovoid, slightly concave dorsally and convex ventrally, and is not scored by deep articular grooves (as the lateral articular surface is). In posterior view, the long axis of this surface trends ventrolaterally-dorsomedially. A wide ridge divides the posterior surface from the lateral articulation dorsally, and continues ventrally until ending at the midline

constriction of the hourglass-shaped lateral surface (fig. 22, rid). Because of this architecture, the ventral triangle of the lateral articulation is widely visible in posterior view (although it only faces laterally), whereas the dorsal triangle is concealed by the ridge. In lateral view the ventral triangle projects slightly ventral to the dorsal margin of the quadrate foramen, forming a small notch in the posterodorsal corner of the foramen (fig. 22, not).

The quadrate flange (pterygoid flange of some authors) is large and prominent in lateral view, but is a sheet-like structure only three millimeters thick mediolaterally at its midpoint. It is gently convex laterally and strongly concave medially (fig. 22B, fos), where it was possibly excavated by an air sac that abutted the medial surface (Currie, 2003a). Additionally, a shallow fossa is present on the lateral surface immediately anterior to the point where the flange and shaft meet (fig. 22A, fos). This is located directly in front of the lateral, hourglass-shaped articulation for the quadratojugal, and is present on both left and right quadrates. The dorsal margin of the quadrate flange, which extends anteroventrally from the head, is slightly concave, but nearly straight. The ventral margin, which terminates ventrally between the condyles, is strongly concave. Anteriorly, the flange is slightly thickened, and the anterior margin curves slightly laterally. In medial view a robust ridge forms the posterior margin of the flange, and links the anteromedial corner of the medial quadrate condyle with the head dorsally (fig. 22, posrid). The quadrate flange articulates with the pterygoid and epipterygoid. The former bone contacts the medial surface of the flange. Slight striations on the edges around the medial concavity mark this overlapping contact, which evidently was quite weak.

The head of the quadrate is convex and spherical, with a diameter of 15 millimeters (figs. 22-23, h). It is thickened relative to the remainder of the shaft, and is smooth dorsally for articulation with the squamosal. On both the left and right quadrates the head has a poorly

defined trochlear surface, with a parasagitally (anteroposteriorly) oriented trough. The medial surface of the head makes contact with the exoccipital-opisthotic of the braincase, a characteristic feature of birds which therefore developed long before the genesis of birds or avian flight.

The quadrate condyles, which articulate with the articular and surangular of the lower jaw, are large (figs. 22-23, lc, mc). In ventral view the conjoined condyles are rectangular, with a mediolateral width of 45 millimeters and an anteroposterior length of 20 millimeters at the point where the two condyles join. The medial margin of the medial condyle is slightly longer than the lateral margin of the lateral condyle, which tapers to a rounded point where it meets the quadratojugal flange laterally. There is a single, ventrally facing trochlear surface between the condyles, which trends anteromedially (figs. 23-24, vtr). Much of this smooth surface is located on the medial condyle, and only the medial margin of this condyle did not participate in the trochlea. Instead, this margin is upturned and rugose. In contrast, the lateral condyle is only slightly smoothed for the trochlear surface, and the lateral margin is convex and prominent. Despite the dominance of the trochlear surface on the medial condyle, the two condyles are approximately equal in size.

A large pneumatic opening lies immediately dorsal to the medial condyle (figs. 22-23, qrec). This opening, the quadrate recess, is visible in anterior view, and extends ventrally and medially from the pterygoid flange. Its long axis trends medioventrally, and it takes the shape of an arcuate teardrop, with the concave margin facing medially and slightly dorsally. The quadrate recess is bound medially by a web of bone linking the quadrate flange to the medial margin of the medial condyle (fig. 22, medrid). Laterally, it is bound by a web that extends ventrally from the quadrate flange above the medial condyle in anterior view. The recess tapers to a smooth

point dorsally, whereas it is wide ventrally, and a smooth fossa extends from it ventrally and medially. Quadrate pneumaticity is characteristic of tyrannosaurids, and the shape and position of the external foramen of the recess of *A. altai* is generally identical to that in other taxa (Brochu, 2003: fig. 25; Currie, 2003a: figs. 10, 28), including *Dilong* (IVPP V14243). However, *Guanlong* (IVPP 14531) and *Proceratosaurus* (Rauhut et al., 2010) lack pneumatic quadrates, as do most outgroup taxa. Quadrate pneumaticity is present in some ornithomimosaurs, but pneumatic foramina leading into the internal recess are located on the posterior surface of the quadrate (e.g., Makovicky and Norell, 1998; Kobayashi and Lu, 2003).

Internal details of the recess are visible in both quadrates, and are especially clear in the better preserved left bone (fig. 23C). Here, the recess is divided internally into three separate chambers by two struts that trend mediolaterally. The ventral chamber is the largest, and it is divided further into several small pockets that may continue deep into the bone. It is likely that some of these penetrate into the body of the medial condyle, which may have housed a discrete condylar recess, like that described for *Tyrannosaurus* (Brochu, 2003) and is also clearly present in *Bistahieversor* (NMMNH P-25049). The middle chamber of *A. altai* appears to extend medially and laterally to hollow the region of the quadrate immediately anterior to the quadrate foramen. This hollow region may have extended further into the body of the flange itself, as in *Tyrannosaurus*, to form a recess termed the "quadrate recess" by Brochu (2003). Note here that the term quadrate recess is used to refer to the deep, externally visible pneumatic opening itself. Finally, the small dorsal chamber inflates the base of the quadrate flange. All three chambers of the quadrate recess in *A. altai* communicate within the body of the quadrate (i.e., the struts of bone dividing them are internal). Whether the communication is internal or external is variable in single specimens of *Tyrannosaurus* (Brochu, 2003), but internal communication is seen on both

quadrates of *A. altai*. Finally, there is no sign that the quadrate recess joined the squamosal recess dorsally, via a large foramen near the quadrate head, as Molnar (1991) observed in one specimen of *Tyrannosaurus*.

Palatine: Nearly complete left and right palatines are preserved (figs. 25-28). The palatine is tetraradiate, and comprised of four distinct processes. The maxillary process projects anteriorly to articulate with the maxilla, whereas the jugal process extends posteriorly to articulate with the jugal and the lacrimal. In lateral view, a vomeropterygoid process arises between the maxillary and jugal processes to project dorsally to articulate with the vomer, pterygoid, and opposite palatine. Finally, the medial process projects posteriorly and medially to contact the pterygoid. In dorsal view, the jugal and medial processes diverge from each other to partly enclose the suborbital fenestra. All four processes converge at a "waisted region" near the midpoint of the bone.

The maxillary process is 90 millimeters long and is oriented approximately parasagittally when in articulation with the maxilla (fig. 25, maxp). The process tapers in depth anteriorly, beginning with a depth of 27 mm where it emerges from the waisted region and terminating anteriorly at a depth of four millimeters. The latter measure is likely an overestimate, because the anterior tip of the process is broken in both specimens. The dorsal margin of the process is gently concave, whereas the ventral margin is convex posteriorly, but becomes concave anteriorly. This anterior concavity occurs as the dorsal margin of the process twists laterally to slightly wrap around the dorsal margin of the maxilla for a short region (fig. 25, max). Because of this, the "lateral surface" of the maxillary process faces fully laterally posteriorly, but then faces strongly ventrally and only slightly laterally anteriorly as it twists around the maxilla.

The medial surface of the maxillary process is smoothly convex, but the lateral surface is concave. Most of this concavity is a non-articular fossa: the palatine contribution to the internal antorbital fossa (fig. 25, 28, iaof). This fossa is triangular and tapers anteriorly, and is similar in size and shape to that in other tyrannosaurids (e.g., Currie, 2003a: figs. 11, 29). It is clearly a continuation of the internal antorbital fossa on the maxilla, and although it communicates with the palatine pneumatic recess posteriorly (see below), it is not a second discrete pneumatic foramen. Secondary pneumatopores have been described in some tyrannosaurids (Carr, 1999; Currie, 2003a: fig. 29), and such a feature is clearly visible in some specimens of *Tarbosaurus* (Hurum and Sabath, 2003: fig. 13; ZPAL MgD-I/4) and *Daspletosaurus* (Currie, 2003a: fig. 29). It is likely that the internal antorbital fossa between the maxilla and palatine housed a pneumatic air sac, perhaps a diverticulum emanating from the primary antorbital air sac that led into the palatine internal recess (Witmer, 1997; Currie, 2003a).

Ventral to the antorbital fossa region, and separated from it by a sharp rim (fig. 25, rim), is a long groove that marks the palatine articulation for the maxilla (figs. 25, 28, max). The groove is deeply inset into the bone, the "slot-like" condition described by Carr et al. (2005). This morphology is present in other tyrannosaurids, but not the more basal taxon *Appalachiosaurus*, which has a flatter maxillary contact that is not demarcated dorsally by a sharp rim (RMM 6670; Carr et al., 2005). In *Alioramus altai*, the rim extends anteriorly as a continuation of the ventral margin of the jugal process (see below), and is located only approximately five millimeters above the ventral margin of the maxillary process. Thus, the maxilla-palatine articulation is shallow in depth. The rim is sharp posteriorly, where it strongly overhangs the maxillary articulation, but dissipates as it continues anteriorly, gradually curving dorsally before merging with the lateral surface of the palatine (fig. 25, rim). The maxilla

articulation faces completely laterally anteriorly, but twists so that it faces laterally and ventrally posteriorly, below the strongly overhanging rim. Further posteriorly, this articulation continues as a shallow, ventrally-facing groove on the ventral margin of the jugal process (fig. 25E, max; see below).

The jugal process, sometimes referred to as the "jugal-lacrimal process" (Hurum and Sabath 2003) or the "dorsolateral process" (Carr et al. 2005), projects posteriorly and slightly laterally, in concert with the lateral expansion of the cheek region relative to the snout (fig. 25, jugp). This process is rectangular, and is longer anteroposteriorly (60 mm) than deep (25 mm). It is thin and sheet like, and is less than one millimeter thick mediolaterally at its posterior end. Articular surfaces for the maxilla, jugal, and lacrimal are present on the jugal process. In *A. altai*, the jugal process is divided into a subordinate dorsal and ventral process, a condition that is seen in other tyrannosaurids such as *Daspletosaurus* (TMP 2001.36.1). The dorsal process is displaced such that it overlaps the dorsal margin of the ventral process posteriorly on both sides (the separation is denoted as "for" in figures 25 and 28). The dorsal process is significantly deeper than the ventral process, and a groove extends onto the lateral surface ahead of where the processes join.

The ventral surface of the jugal process is thin, but it is marked by an anteroposteriorly elongate and sharp groove across its entire length (fig. 25E, maxgr). This groove expands in mediolateral width anteriorly and merges with the laterally-facing maxillary articulation on the maxillary process, as described above. The anterior part of this groove clearly sits on top of the tapering main body of the maxilla, but posteriorly it juts laterally and appears to have rested on the dorsal surface of the anterior process of the jugal (i.e., within the dorsally and laterally-facing groove at the anterodorsal corner of the jugal anterior ramus, where the maxilla also contacted).

However, the articulation between these three bones (as well as the lacrimal) is difficult to trace in this region, and it is possible that the groove on the ventral surface of the jugal process of the palatine did not contact the jugal and only sat on the maxilla.

The palatine-maxilla articulation is reinforced by the anterior end of the jugal process, which projects ventrally as a convexity that braces the maxilla laterally, at the posterior end of the internal antorbital fossa (figs. 25, 28, cb). This was evidently a weak contact, as there is no clear joint surface on the maxilla for the convex brace. This brace is present in *Albertosaurus* (Currie, 2003a: fig. 11, "maxillary contact") and *Daspletosaurus* (CMN 8506; Carr et al., 2005: fig. 11), but not *Appalachiosaurus* (Carr et al., 2005: fig. 9E). It is also present in *Tarbosaurus* (ZPAL MgD-I/4), but not obvious in published figures (Hurum and Sabath, 2003: fig. 13), as well as *Tyrannosaurus* (Carr et al., 2005: fig. 11). However, unlike in *A. altai*, the brace in *Tarbosaurus* and *Tyrannosaurus* projects far laterally, and in lateral view is not seen to project ventrally beyond the remainder of the palatine. Although a similar feature is present in *Sinraptor* (Currie and Zhao, 1993: fig. 9), the brace is also absent in many other theropods, such as *Acrocanthosaurus* (Harris, 1998: fig. 4; Eddy, 2008), *Allosaurus* (Madsen, 1976: pl. 10A), and *Majungasaurus* (Sampson and Witmer, 2007: fig. 20). Instead, in these taxa the jugal process is located at the same level as, or dorsal to, the maxilla process in lateral view, and the groove for the maxilla on the palatine is always entirely laterally facing. In *A. altai*, in contrast, the jugal process is located far ventral to the maxillary process, and the groove for the maxilla on the jugal process is therefore concealed in lateral view. Again, this differs from *Tarbosaurus* and *Tyrannosaurus*, in which the two processes are at the same approximate level in lateral view (ZPAL MgD-I/4; BHI 3033).

The lateral surface of the jugal process would have articulated with the medial surface of the jugal and lacrimal. The dorsal limit of the lacrimal articular facet is marked by a sharp rim, which trends anteroventrally from the dorsal margin of the jugal process (figs. 25, 28, jlrim). The region posterior to the rim, which covers most of the lateral surface of the process, would have articulated almost entirely with the lacrimal, except for a small surface ventrally that apparently contacted the medial surface of the anterior process of the jugal (although sutures are difficult to trace in this region, see above). The rim is located anteriorly on the jugal process, allowing the lacrimal to closely approach the external opening of the palatine recess. This condition is also seen in other tyrannosaurids, including *Albertosaurus* (CMN 5601), *Daspletosaurus* (CMN 8506, *Tarbosaurus* (ZPAL MgD-I/4), and *Tyrannosaurus* (BHI 3033), but deviates from the more posteriorly located rim in *Appalachiosaurus*, which results in wide separation between the lacrimal and palatine recess (RMM 6670; Carr et al., 2005).

The medial process, also referred to as the "pterygoid process" (Brochu, 2003; Hurum and Sabath, 2003), projects posteromedially from the waisted central region of the palatine (fig. 25, medp). In dorsal view the medial and jugal processes are seen to diverge approximately equally medially and laterally, and their separation marks the anterior and much of the lateral and medial borders of the suborbital fenestra (fig. 25, suborb; not the palatine fenestra as it is often referred to, see below). Also in dorsal view, the anterior and lateral/medial margins of the fenestra on the two processes are smoothly concave and excavated by a fossa (fig. 25C, fos), likely for the insertion of jaw musculature (Witmer, 1997). The fossa is more extensive on the medial process, as this process is much longer than the jugal process. Anteriorly, where the jugal and medial processes meet, there are two separate pits, one on each process (fig. 25, pit). The pit on the jugal process is larger and deeper in both left and right palatines. These pits may be

pneumatic and related to the palatine recess, as described in the allosauroid *Neovenator* (Brusatte et al., 2008). However, the pits are absent in *Tarbosaurus* (ZPAL MgD-I/4), which has a much more pneumatic palatine (i.e., a larger and more extensive palatine recess) than *Alioramus altai*. It is possible, therefore, that they are artifacts of damage in *A. altai* rather than pneumatic structures, although their presence in other theropods (*Neovenator*) suggests that they are a genuine feature.

The medal process is 82 millimeters long. Its base is 15 mm deep dorsoventrally, where it diverges from the waisted region, then narrows to a height of 12 mm before expanding out to 16 mm and then narrowing again to a spatulate point distally. The lateral surface of the process is concave for the muscular fossa, but the medial margin is convex, and strengthened by a ridge ventrally (fig. 25, mrid), which is especially thick and prominent anteriorly where the process diverges from the waisted region. The ridge thins out posteriorly, and the end of the process becomes extremely thin (less than one mm thick medioventrally at its posterior margin). The flattened region of the medial surface of the posterior part of the process contacts the pterygoid (fig. 25, pter), and this articulation is marked by several anteroposteriorly oriented striations, as well as a low ridge that braces its anterior end. Finally, a striated swelling is present on the ventral surface of the process.

The fourth and final principal process of the palatine, the vomeropterygoid process, projects dorsally and somewhat anteriorly (fig. 25, vptp). This ramus is also referred to as the "ascending process" (Brochu, 2003), "vomerine process" (Currie, 2003a), or "dorsomedial process" (Currie, 2003a). It is 31 millimeters tall dorsoventrally, begins with an anteroposterior length of 29 mm where it diverges from the central waisted region, and fans out dorsally as it expands to a length of 80 mm at its tip. In lateral view it can be seen that the process has separate

anterior and posterior projections (fig. 25, ap, pp). The posterior projection is small and blunt, and barely separated as a discrete projection (it is only 5 mm long anteroposteriorly). On the other hand, the anterior projection, also referred to as the "choanal process" (Carr et al., 2005), is extremely elongated (47 mm long). It is triangular, with a sharply tapering anterior point, and thins out to less than one mm in mediolateral width anteriorly, where it is delicate and plate-like.

The lateral surface of the vomeropterygoid process is gently convex, but the medial surface exhibits three distinct sutural surfaces. First, there is an anteroposteriorly elongate contact comprising nearly the entire ventral margin of the anterior projection, which would have articulated with the vomer (figs. 25, 28, vom). This surface is slightly convex as in *Appalachiosaurus*, not sinuous as in *Albertosaurus* and *Daspletosaurus* (Carr et al., 2005), or flat as in *Tarbosaurus* (ZPAL MgD-I/4). Second, there is a large contact that comprises most of the medial surface of the entire process, which is slightly concave on the right palatine and slightly convex on the left. These are the contact surfaces for the anterior process of the pterygoid (figs. 25, 28, appter). Dorsal to this contact, and flat on both palatines, is another articulation which covers most of the dorsal margin of the vomeropterygoid process. This surface faces dorsomedially, and contacts the opposing palatine (figs. 25, 28, pal). Thus, the palatine would have covered the anterior end of the pterygoid in lateral view in this region, which is visible laterally through the antorbital fenestra.

The vomeropterygoid process of *A. altai* shows similarities with and differences from those of other tyrannosaurids. The great anteroposterior expansion of the dorsal region of the process of *A. altai* and other tyrannosaurids is not seen in *Tarbosaurus* and *Tyrannosaurus*, which instead have vomeropterygoid processes that are rectangular, with only slight anterior and posterior projections dorsally (Brochu, 2003; Hurum and Sabath, 2003: fig. 13). The process

does expand dorsally in *Albertosaurus* and *Daspletosaurus*, but in these taxa it does not taper to a sharp anterior point as in *A. altai* (Currie, 2003a). The general morphology of the vomeropterygoid process of *A. altai* is similar to that of *Appalachiosaurus*, which expands dorsally and has a discrete and elongate anterior projection that tapers to a point (Carr et al., 2005: fig. 9E). However, there is no obvious foramen at the posteroventral corner of the base of the vomeropterygoid process medially as there is in *Appalachiosaurus* (RMM 6670; Carr et al., 2005) or a deep fossa in this region as in *Daspletosaurus* (CMN 8506).

The anteroposteriorly expanded dorsal region of the vomeropterygoid process is often called the "palatine process" (e.g., Brochu, 2003). There is no pronounced tuberosity, possibly for the insertion of the ventral pterygoideus muscle, on the ventral surface of the process, as described in one specimen of *Tyrannosaurus* (Brochu, 2003). There are, however, low swellings on *A. altai* that may be homologous muscle attachment sites. The lateral surface of this region is generally smooth, not rugose and covered with Sharpey's fibers (possibly for muscle attachment) as in *Tyrannosaurus* (Brochu, 2003).

The palatine of *A. altai* is extremely pneumatic. The anterior end of the jugal process, above the convex maxillary brace, is excavated by a large and deep pneumatic foramen, which is roughly circular in both left and right palatines (figs. 25, 28, palrec). On the left palatine the recess is 17 millimeters in diameter, and it excavates nearly the entire depth of the jugal process. The pneumatic foramen opens into a large pneumatic space that extends dorsally and posteromedially into the bone. The anterior region of the medial process is moderately inflated, based on its external "swollen" morphology. Similarly, most of the vomeropterygoid process appears to be inflated as well, especially the "neck" region ventral to the dorsal expansion of the process.

Anterior to the pneumatic opening is the triangular, non articular internal antorbital fossa on the lateral surface of the maxillary process. This fossa is separated from the pneumatic foramen by a pillar, which is slightly thicker (anteroposteriorly longer) on the right palatine (fig. 25, pil). Immediately anterior to the pillar is the posterior region of the fossa, which is deeply embayed, and in the left palatine is divided into two pockets (a smaller circular one anteriorly and a larger posterior depression) by a dorsally extending ridge. These are much shallower on the right side. There appears to be a foramen connecting the pneumatic foramen with the fossa internally in the left palatine, but unremovable matrix obscures this region in the right bone. There is no clear evidence that the pits on the jugal and medial processes, at the anterior end of the mucular fossa (described above), lead into the recess, but their smooth surfaces suggest they may be from a pneumatic source.

Palatine pneumaticity is typical of tyrannosaurids (e.g., Molnar, 1991; Brochu, 2003; Currie, 2003a; Hurum and Sabath, 2003). In *A. altai* the pneumatic recess extends posteriorly far beyond the posterior margin of the vomeropterygoid process. This condition was described as an autapomorphy of *A. altai* by Brusatte et al. (2009a), but is also seen in at least one specimen *Daspletosaurus* (MOR 1130). This morphology is not present, however, in other tyrannosauroids (e.g., *Appalachiosaurus*: Carr et al., 2005: fig. 9E; *Albertosaurus*: Currie, 2003a: fig. 11; some speciems of *Daspletosaurus*: Currie, 2003a: fig. 29; *Gorgosaurus*: Carr et al., 2005; *Tarbosaurus*: Hurum and Sabath, 2003: fig. 13; *Tyrannosaurus*: Carr et al., 2005), in which the recess is either located entirely anteriorly or level with the posterior margin of the vomeropterygoid process, and centered directly below the process itself, or extends only slightly posterior to the process. The condition in *A. altai* and *Daspletosaurus* (MOR 1130), therefore, is more similar to the morphology of some other large theropods than to the morphology of other

tyrannosauroids (e.g., *Acrocanthosaurus*: Harris, 1998: fig. 4; *Sinraptor*: Currie and Zhao, 1993: fig. 9). Furthermore, the pneumatic foramen of *A. altai* is relatively not as large as in some *Albertosaurus* specimens (Currie, 2003a: fig. 11), and the region medial to the pneumatic foramen is not greatly inflated as in large specimens of *Daspletosaurus*, *Tarbosaurus*, and *Tyrannosaurus* (Currie, 2003a).

Anteriorly, the divergent maxillary and vomeroptergygoid processes demarcate an elongate, ovoid internal choana (figs. 25, 28, cho), which faces almost entirely laterally as in many theropods. The ovoid shape is also seen in *Albertosaurus* (Currie, 2003a: fig. 11), *Appalachiosaurus* (Carr et al., 2005: fig. 9E), *Daspletosaurus* (Currie, 2003a: fig. 29), *Gorgosaurus* (Carr et al., 2005: fig. 11), *Raptorex* (Sereno et al., 2009: fig. 1), and *Proceratosaurus* (Rauhut et al., 2010: fig. 12), as well as theropods more generally (e.g., Madsen, 1976; Ji et al., 2003; Peyer, 2006). In contrast, the choana is more circular in *Tarbosaurus*, as shown by the more broadly concave anterior margin of the vomeropterygoid process (Hurum and Sabath, 2003: fig. 13).

The suborbital fenestra, located between the jugal and medial processes and facing almost entirely dorsally, is large and ovoid as in *Appalachiosaurus* (Carr et al., 2005: fig. 9F), *Daspletosaurus* (Currie, 2003a: fig. 29), and *Albertosaurus* and *Gorgosaurus* (Carr et al., 2005: fig. 11). In contrast, it is larger and more circular in *Tarbosaurus* (Hurum and Sabath, 2003: fig. 13) and apparently *Tyrannosaurus* (Osborn, 1912: fig. 5); in these taxa the anterior margin of the fenestra on the palatine is wide and nearly semicircular in outline, not narrow and ovoid in outline as in *A. altai*.

In addition to the internal choana and suborbital fenestra, a third palatal fenestra is present, between the vomeroptergoid process, medial process, and pterygoid. This fenestra, visible in lateral view, is the palatine fenestra, and is described below (figs. 25, 28, palfen).

Pterygoid: Only two fragments of the right pterygoid are known (fig. 29). The more complete piece preserves the anterior palatine process, much of the posterior palatine process, and part of the ectopterygoid process (fig. 29A-B). Additionally, there is a second smaller piece that preserves much of quadrate flange at the posterior end of the bone (fig. 29C-D). The two fragments are not continuous with each other, although only a small missing region separates them. In the following description, we use the term "lateral surface" to refer to the surface of the pterygoid which faced dorsolaterally in life, and "medial surface" to denote the opposing, ventromedially-facing surface.

The larger preserved fragment is 245 millimeters long anteroposteriorly. The elongate anterior region of the pterygoid, often called the "vomeropalatine ramus" (e.g., Eddy, 2008), is here divided into two discrete processes, both for articulation with different parts of the palatine. The anterior palatine process (fig. 29, app), also referred to as the "vomerine process" (Molnar, 1991; Brochu, 2003) or the "anterodorsal ramus" (Currie, 2003a), articulates with the dorsally-projecting vomeropterygoid process of the palatine. It is shaped like an elongate spade, and is 110 mm long anteroposteriorly, 30 mm deep dorsoventrally at its midlength, and anteriorly tapers to a rounded point. This process, like most of the pterygoid, is incredibly thin: it is only 1.5 mm thick mediolaterally at its midpoint. Unfortunately, the process is slightly crushed, with the anterior region pushed laterally relative to the posterior region. Matrix also covers most of the anterior region of the process laterally, obscuring details of the articular contact with the

palatine. The right palatine has a slightly concave articular surface, so it is possible that the region of the pterygoid obscured by matrix was mildly convex to fit this contact. The ventral margin of the medial surface of the anterior palatine process would have contacted the vomer, as it is continuous with the vomer facet on the medial surface of the vomeropterygoid ramus of the palatine. A thin neck connects the anterior palatine process to the main body of the pterygoid. The second process of the vomeropalatine ramus, the posterior palatine process (fig. 29, ppp), articulated with the medial process of the palatine. It is broken distally (=anteriorly), but its base is preserved.

The anterior and posterior palatine processes are joined by a thin bar dorsally, which is eight millimeters deep dorsoventrally at its midpoint (fig. 29, bar). In *Albertosaurus* (Currie, 2003a: fig. 13) and *Tyrannosaurus* (BHI 3033) the bar is much thicker, and thus the anterior process is less expanded relative to the neck. The bar forms the medial margin of the palatine fenestra (see below). It is supported laterally by a thickened ridge extending from the dorsal margin of the posterior palatine process onto the posterior part of the lateral surface of the anterior palatine process (fig. 29, rid), where it gradually thins and merges with the lateral surface of the bone. The ridge is narrow in *A. altai*, whereas it is wide in *Tyrannosaurus* (BHI 3033). In *A. altai*, the ridge trends anterodorsally and twists as it continues onto the anterior process; it begins posteriorly as a sheet that faces ventrally but transitions to a ridge that faces laterally. Below the ridge on the anterior palatine process, and especially prominent posteriorly where the ridge faces ventrally, is a smooth triangular fossa for muscle attachment (fig. 29, trifos). In concert with the orientation of the ridge, the fossa faces entirely ventrally posteriorly, but twists such that it comes to face laterally anteriorly. Above the ridge there is a groove, which is especially prominent as a distinct structure for 25 mm anterior to the ridge (fig. 29, gr). The

ventral margin of the groove is distinct from the rim anteriorly, but posteriorly the two structures merge. Apparently this was not an articular surface, and may have been a muscle attachment surface or housed cartilage in life.

Posterior to the vomeropalatine ramus is a small prong, broken distally, which projects laterally, anteriorly, and ventrally to contact the ectopterygoid (fig. 29, ecp). The dorsal surface of the ectopterygoid process is strengthend by a robust ridge laterally, which would have reinforced contact with the ectopterygoid. Many other details of the ectopterygoid articulation are not visible due to the distal breakage of the process. However, based on the shape of the articulation on the ectopterygoid, it is clear that proximally (=medially) near the base of the process, the pterygoid contacts the ventral surface of the posteromedial corner of the ectopterygoid. Anteriorly, the articular flange on the pterygoid curves dorsally to overlap the dorsal surface of the ectopterygoid. On the ectopterygoid there are separate ventral and dorsal surfaces that reflect this complex contact; these surfaces on the ectopterygoid are separated by a ridge laterally but smoothly confluent with each other medially. Finally, the articulation between the pterygoid and ectopterygoid shows that the latter bone did not contact the palatine. When the ectopterygoid articulates with the pterygoid, the ectopterygoid does not approach the posterior end of the medial process of the palatine. Therefore, the ectopterygoid and palatine certainly did not make contact with each other.

The ectopterygoid process and posterior palatine process are joined by a thick bar, which is rectangular and 23 mm deep dorsoventrally. This is the “palatal plate” region of the pterygoid (fig. 29, pp; terminology from Molnar [1991]), and links the vomeropalatine ramus anteriorly with the ectopterygoid ramus and expanding quadrate flange posteriorly. The lateral surface of the palatal plate, as well as the posterior palatine process itself, is deeply concave with a smooth

fossa, likely for muscle attachment (fig. 29B, fos). The center of this fossa is very thin mediolaterally (only about 1 mm), but the dorsal and ventral rims are thick and both slightly curve laterally. The fossa is deepest posteriorly, immediately anterior to where the ectopterygoid process diverges, and becomes less distinct and shallower anteriorly. In medial view, the palatal plate is strongly convex posteriorly, in concert with the concave lateral fossa, but anteriorly becomes markedly concave, as a separate smooth fossa surrounds the posterior margin of the palatine fenestra (fig. 29A, fos).

In dorsal view, crushing makes it difficult to determine the orientation of the pterygoid, but it is apparent that the bone diverts laterally posterior to the anterior palatine process. This lateral diversion formed the lateral border of the interpterygoid vacuity, an elongate opening between the opposing pterygoids. Thus, the two pterygoids did not contact each other on the midline posteriorly, nor anteriorly where they were separated by the vomer (Russell, 1970; Currie, 2003a).

The separation between the anterior and posterior palatine processes defines the medial margin of a palatal opening (fig. 29, palfen), which deserves further comment and clarification. This opening is the palatine fenestra, and is often referred to as the "accessory fenestra (e.g., Currie, 2003a) or the "palatopterygoid fenestra" (e.g., Hurum and Sabath, 2003). Its medial margin is formed by the neck between the anterior and posterior palatine processes of the pterygoid, whereas its lateral margin is defined by the diverging medial and vomeropterygoid processes of the palatine. Thus, this opening is between the articulated palatine and pterygoid. It is visible both in lateral and ventral views, but faces more laterally than ventrally.

The identification of this fenestra is inconsistent in the literature. Aside from the multiple names applied to this opening, it is often confused with the suborbital fenestra. Specifically, the

fenestra that is often labeled as the "palatine fenestra" or "palatopterygoid fenestra" is in fact the suborbital fenestra (e.g., Madsen, 1976: pl. 2; Harris, 1998: fig. 4; Brusatte et al., 2008: fig. 7). Properly, the suborbital fenestra is a separate palatal opening, which is located lateral to the palatine fenestra and opens dorsoventrally, and is thus obscured in lateral view. The medial margin of the suborbital fenestra is formed by the articulated medial process of the palatine and posterior palatine process of the pterygoid, as well as the "palatal plate" region of the pterygoid. The lateral border of the suborbital fenestra is formed by the jugal ramus of the palatine and by the jugal itself, whereas the anterior margin is defined by the diverging jugal and medial process of the palatine and the posterior margin by the ectopterygoid.

In *A. altai* the palatine fenestra is large and sub-triangular, as in *Albertosaurus* (Currie, 2003a: fig. 13) and *Daspletosaurus* (Russell, 1970: fig. 9; Currie, 2003a: fig. 29). In adult *Tarbosaurus* the fenestra is also triangular, but it is much smaller in relative size (Hurum and Sabath, 2003:180), whereas it is relatively large in juveniles (Maleev, 1974: fig. 9), with similar proportions to *A. altai*. Large, adult *Tyrannosaurus* exhibits a novel condition in which the fenestra is nearly completely closed, due to the widening of the anterior palatine process of the pterygoid and the medial expansion of the palatine (Osborn, 1912: fig. 5; Molnar, 1991; Carr, 1999; Currie, 2003a). In other words, in *Tyrannosaurus* the pterygoid and palatine broadly articulate in the region where the two are separated by the fenestra in *A. altai* and other tyrannosaurids.

The presence and morphology of the palatine fenestra is variable in theropods. Madsen (1976: pl. 2) does not figure a palatine fenestra in *Allosaurus*. Instead, the palatine and pterygoid make broad contact and are not separated from each other to form a fenestra. The anterior region of the pterygoid has a single, elongate articular surface for the palatine, not the separate anterior

and posterior projections that define the posteromedial corner of the palatine fenestra in other taxa (Madsen, 1976: pl. 10I). An identical condition is present in *Sinraptor* (Currie and Zhao, 1993: figs. 3, 9). *Acrocanthosaurus* is reconstructed as possessing a small, slit-like fenestra between the palatine and pterygoid, but the anterior process of the pterygoid is clearly lacking a subdivision of anterior and posterior processes (Eddy, 2008: fig. 1.17, 1.19, 1.21). Here, the diverging vomeropterygoid and medial processes of the palatine demarcate a small fenestra, but it is backed medially by the single, elongate anterior ramus of the pterygoid. This condition is seen in the reconstruction of the skull in palatal view: the small fenestra is not visible because it is closed medially and ventrally by the pterygoid. Thus, it is likely that a similar condition characterizes *Allosaurus* and *Sinraptor*, but it has yet to be clearly figured.

The well-preserved skull of *Majungasaurus* is reconstructed as possessing a unique condition, in which there is a small triangular opening in the region of the palatine fenestra of tyrannosaurids, but this is apparently open medially (or closed by the vomer; Sampson and Witmer, 2007: fig. 1). In other words, there is no medial margin of the fenestra formed by the pterygoid, as the anterior process of the pterygoid only makes contact with the medial process of the palatine and does not extend anteriorly to also contact the vomeropterygoid process. The condition in most theropods is difficult to describe, due to incompletely preserved and poorly figured palates. A well illustrated revision of theropod palatal anatomy is clearly needed to clarify structural homologies, as current interpretation is largely reliant on reconstructions instead of images of actual specimens.

The second fragment of the right pterygoid is 78 mm in maximum dimension (an oblique measurement extending antroventrally, in parallel with the ridge separating the quadrate and epipterygoid articular surfaces. Anteriorly this fragment is shallow, as it is constricted to a depth

of 17 mm near where it would have approached the ectopterygoid contact if this pierce were in articulation with the remainder of the right pterygoid. Posteriorly the fragment expands in dorsoventral depth as it gives rise to the quadrate flange, which is 55 mm in maximum depth as preserved. In general, the shape of this portion of the pterygoid is similar to that in other derived tyrannosauroids for which pterygoids are known (*Albertosaurus*: Currie, 2003a; *Appalachiosaurus*: Carr et al., 2005; *Gorgosaurus*: Currie, 2003a; *Tarbosaurus*: Hurum and Sabath, 2003; *Tyrannosaurus*: Molnar, 1991; Brochu, 2003).

The quadrate flange is a thin, curved sheet of bone that is convex laterally and concave medially (i.e., its lateral surface curves posteromedially). The most salient feature of the lateral surface is an oblique ridge (fig. 29, qfrid), which trends anteroventrally and separates discrete fossae for articulation with the anterior flange of the quadrate and epipterygoid (fig. 29, epi, quad). The quadrate articulation is located posteroventral to the ridge and the epipterygoid contact surface is positioned anterodorsally. The anterior margin of the epipterygoid contact surface is delineated by a raised rim, which continues anteroventrally as a sharp ridge on the lateral surface of the pterygoid (fig. 29, qfrim). This ridge terminates against the anterior edge of the fragment, and ventral to it is a smooth fossa likely for muscle attachment (fig. 29D, fos). The medial surface of the quadrate flange is generally smooth and depressed, and a subtle ridge separates it into anterior and posterior fossae, likely for muscle attachment (fig. 29C, fos). Anteriorly, at the anterior end of the fragment, the base of a medially-projecting process is preserved (fig. 29, basi). This would have articulated with the basipterygoid process of the braincase in life. In dorsal view, this project is seen to project strongly medialy and also slightly posteriorly, such that it is separated from the quadrate flange by an acute angle.

Ectopterygoid: The right ectopterygoid is well preserved (fig. 30). It is hook shaped as is typical of theropods, and is comprised of two main regions: a main body which contacts the pterygoid and a jugal process that curves laterally to contact the jugal.

The jugal process curves strongly laterally as it extends anteriorly (fig. 30, jpr). Its lateral surface is flattened for articulation with the medial surface of the jugal (fig. 30, jug). This surface is complex in shape: the dorsal margin is slightly concave at the midpoint, whereas the ventral margin is nearly straight and slopes strongly anteroventrally, terminating at a small but sharp point that projects ventrally. This is also seen in other tyrannosauroids (e.g., *Albertosaurus*, *Bistahieversor*, *Gorgosaurus*, *Daspletosaurus*, *Tyrannosaurus*). The region of this surface overlapped by the jugal is covered with a series of fine striations that are generally oriented anteroposteriorly to anterodorsally-posteroventrally. The ventral projection may contact the maxilla, as suggested by Currie (2003a), but it is difficult to be certain. The jugal process is ovoid in cross section posteriorly where it diverges from the main body of the ectopterygoid. It thins as it continues anteriorly and curves laterally, such that the jugal articular surface is thin (2 mm thick) and plate like at its distal end.

The main body of the ectopterygoid, the "broad plate" of Currie (2003a:213), is triangular. It expands in width posteriorly, and gives rise to medial and lateral projections at its posterior corners (fig. 30, lc, mc). The medial projection, the "pterygoid ramus" of Brochu (2003), articulates with the pterygoid across a plate-like contact, and distally expands into a small peg that would have fit into a socket on the pterygoid (fig. 30, pterpeg; Currie 2003a). The lateral projection is oriented posteriorly and ventrally, and in lateral view is seen to terminate in a triangular corner that would have protruded below the ventral margin of the skull, as described

by Currie (2003) and present in other tyrannosaurids (e.g., *Tarbosaurus*: ZPAL MgD-I/3, MgD-I/4).

The lateral projection defines the anterolateral corner of a large pneumatic foramen, which is widely visible in ventral view (fig. 30, ectorec). This is often referred to as the ectopterygoid recess or the "siphonial opening" (Brochu 2003:29). The pneumatic foramen is sub-triangular in shape, with an equilateral measure of 15 millimeters. Posteriorly it is bound by a slight lip (fig. 30, lip), which continues anteriorly from the posterior margin of the ectopterygoid to overhang the pneumatic foramen and separate it from the subtemporal fenestra (i.e., the floor of the lateral temporal fenestra). Because this lip is thin, the pneumatic foramen essentially abuts the posterior margin of the ectopterygoid. More robust lips are present in *Daspletosaurus* (Currie, 2003a: fig. 32; Carr et al., 2005: fig. 10), *Tarbosaurus* (Hurum and Sabath, 2003: fig. 14; Carr et al., 2005: fig. 10; ZPAL MgD−I/3), and *Tyrannosaurus* (Brochu, 2003: fig. 4; Carr et al., 2005: fig. 10). In contrast, the surface adjacent to the pneumatic foramen is flat, and smoothly grades into the lateral temporal fenestra, in several other tyrannosauroids, including: *Albertosaurus* (Currie, 2003a: fig. 12; Carr et al., 2005: fig. 10), *Appalachisaurus* (Carr et al., 2005: fig. 9), *Gorgosaurus* (Currie, 2003a: fig. 2; Carr et al., 2005: fig. 10), *Guanlong* (IVPP V14531), and apparently *Xiongguanlong* (Li et al., 2010:fig. 1C).

The pneumatic foramen continues deep into the ectopterygoid anteriorly, rendering most of the main body hollow. The recess does not visually extend into the jugal process. However, the base of the process does appear to be inflated based on external morphology (as is true of all tyrannosaurids: Brusatte et al., 2010a), although it is not as greatly "swollen" as in adult *Daspletosaurus*, *Tyrannosaurus* (Carr, 1999) and *Tarbosaurus* (ZPAL MgD−I/3). The recess

clearly does extend anteromedially into the medial projection of the main body, as this region is excavated internally by a deep pocket.

In *A. altai* there is a single pneumatic foramen, not two of them as in some specimens of *Daspletosaurus* (Carr et al., 2005: fig. 10), *Gorgosaurus* (Carr et al., 2005: fig. 10), and *Tyrannosaurus* (Brochu, 2003). This single opening is shaped like a broad triangle, most similar to the condition in *Daspletosaurus* (Currie, 2003a: fig. 32; Carr et al., 2005: fig. 10). In contrast, the pneumatic foramen is thin and slit-like in *Albertosaurus* (Currie, 2003a: fig. 12), *Appalachiosaurus* (Carr et al., 2005: figs. 9, 10), *Gorgosaurus* (Currie, 2003a: fig. 2; Carr et al., 2005: fig. 10), and and *Guanlong* (IVPP V14531), and is a large, elongate oval in *Tarbosaurus* (Hurum and Sabath, 2003: fig. 14; ZPAL MgD−I/3) and *Tyrannosaurus* (Brochu, 2003: fig. 4; Carr et al., 2005: fig. 10). On the ventral surface of the ectopterygoid, anterolateral to the pneumatic foramen, is an elongate fossa that is bound laterally by a ventrally projecting lip on the lateral margin of the main body. This lip is the same region of the ectopterygoid lateral projection that projects below the skull, described above.

Posteromedial to the pneumatic foramen the main body of the ectopterygoid thins and flattens, and there is a thin, striated surface for articulation with the pterygoid (fig. 30, ptervent). Here, the pterygoid wrapped around the ectopterygoid in a complex articulation, described above. The lateral surface of the main body, which formed the medial margin of the subtemporal fenestra (floor of the lateral temporal fenestra), is convex and scoured by several anteroposterior striations (fig. 30, lsmb). However, no bone seems to have articulated here (contra Currie, 2003a), and this may have been a muscle attachment site (Carr, 1999). In *A. altai* this surface faces entirely laterally as in juvenile *Albertosaurus* and *Guanlong* (IVPP V14351), not ventrally as in *Daspletosaurus* and *Tyrannosaurus* (Carr, 1999: fig. 4C,D).

The dorsal surface of the main body is excavated by two fossae: a large triangular region laterally (fig. 30, foslat), which is partially exaggerated by crushing, and an anteroposteriorly elongate and deeper fossa medially (fig. 30, fosmed). The two are separated by a thick, anteroposteriorly trending ridge (fig. 30, rid) that terminates posteriorly as the small peg for articulation with the pterygoid, described above. A laterally trending foramen in the medial fossa projects deeply into the bone, indicating that this excavation likely communicated with the ectopterygoid recess. The thick ridge is autapomorphic of *A. altai*, as it is either absent or present as a much less prominent crest in *Albertosaurus* (Currie, 2003a: fig. 12), *Daspletosaurus* (Currie, 2003a: fig. 32), *Guanlong* (IVPP V14531) *Tarbosaurus* (ZPAL MgD-I/3, MgD-I/4; Hurum and Sabath, 2003: fig. 14), and *Tyrannosaurus* (TMP 81.6.1). It is possible, however, that the strength of the ridge in the holotype of *A. altai* (and therefore the depth of the fossae that it separates) may be exaggerated by crushing. Additional discoveries may reveal that the morphology of this region, especially the shape and strength of the ridge, is little different from the condition in other tyrannosaurids.

Epipterygoid: Both left and right epipterygoids are present, both of which are nearly complete and exquisitely preserved (fig. 31). These palatal bones, which are rarely preserved and poorly known among theropods, are roughly triangular in shape. They are perhaps better described as "teardrop shaped," as the anterior margin is generally convex, the posterior margin is strongly concave, and the bone tapers to a point dorsally.

The anterior margin is broadly convex, but slightly sinuous in detail. It is convex ventrally, then becomes slightly concave dorsally, and then for the last 12 mm dorsally it is extensively concave as an inset notch (fig. 31, not). Posterior to the notch is a ridge on the lateral

surface, which begins at the dorsal tip of the bone as a rugose point, trends anteroventrally, and then gradually merges with the lateral surface (fig. 31, latrid). This ridge is not confluent with the posterior margin of the epipterygoid. Dorally, the tapered and thickened point of the epipterygoid would have articulated with the laterosphenoid (fig. 31, lat), as described in other tyrannosaurids (Molnar 1991; Brochu 2003).

The lateral surface of the epipterygoid is deeply concave ventrally, where it is excavated by a smooth fossa and extremely thin (less than 1 mm thick mediolaterally) (fig. 31, fos). The medial surface is generally flat, and ventrally the bone surface is roughened where it articulates with the quadrate process of the pterygoid (fig. 31, pter). On both specimens there is a small notch on the anterior margin of the medial surface, approximately 10 mm from the ventral end of the bone, which would have reinforced the articulation (fig. 31, pternot). Dorsal to the pterygoid articulation a ridge extends along the posterior margin of the medial surface, which thins out ventrally (fig. 31, medrid).

The epipterygoid is also teardrop shaped in *Bistahieversor* (NMMNH P-27469), *Daspletosaurus* (FMNH PR308), and *Tyrannosaurus* (Brochu, 2003). *Bistahieversor* and *Tyrannosaurus* also possess the pronounced lateral fossa and the posteriorly backswept dorsal tip (a result of the convex anterior margin sweeping posteriorly as it continues dorsally) (Brochu, 2003). However, in this taxon there is a much thicker ridge forming the posterior rim of the lateral fossa, which projects anteriorly and dorsally (Brochu, 2003: fig. 27). The epipterygoid of *A. altai* is very similar to that of *Alioramus remotus* (Kurzanov, 1976: fig. 7), but the bone in *A. altai* appears to have a more prominent ridge along the anterior margin. Similarly, the *A. altai* epipterygoid is very similar to a specimen of juvenile *Daspletosaurus* figured by Currie (2003: fig. 31). However, the latter specimen appears to have a thicker rim demarcating the lateral fossa

anteriorly, as well as a more rugose medial articular surface for the pterygoid, with pronounced anterior and posterior rims. Morevoer, in *A. altai* there is no sign of any ventral forking into anterior and posterior processes as reported in *Daspletosaurus* (Currie, 2003a) and appears to be present, although could conceivably represent a break, in *A. remotus* (Kurzanov, 1976: fig. 7). *Tyrannosaurus* is variable in this character, as its epipterygoid is sometimes forked (BHI 3033, which appears to be genuine, but could be an artifact of breakage) or paddle shaped (BMR 2002.4.1). Instead, in *A. altai*, both left and right epipterygoids are smoothly convex ventrally, and although there may be broken bone surfaces, the ventral margins of each bone are nearly identical in shape. In *A. altai* the lateral fossa does not continue to the ventral margin, but it is separated from it by a change in slope. In *Daspletosaurus*, however, the fossa continues to the ventral margin of the epipterygoid.

The shape of the epipterygoid in *A. altai* and tyrannosaurids in general is similar to that of other theropods for which this bone is known. In *Ceratosaurus* (Madsen and Welles, 2000: pl. 5) the epipterygoid is also a thin and triangular bone with a lateral fossa and a tapering dorsal point, although this bone is more triangular than teardrop shaped (due to a long, straight ventral base) and there is less recurvature of the anterior margin, which is straight instead of convex. The epipterygoid of *Allosaurus* is much different in morphology (Madsen, 1976: pl. 10): it is trapezoidal in shape and its dorsal end does not taper to a tip, but is rather quite elongated compared to the condition in tyrannosaurids and *Ceratosaurus*. The anterior margin resembles that of *A. altai*, and is much more recurved than that of *Ceratosaurus*, and the dorsal end is thick. However, a deep lateral fossa is absent. The basal tetanuran *Monolophosaurus* has an epipterygoid that is generally triangular in shape, but poor preservation presents adequate

description, such that we (SLB pers. obs; Brusatte et al., 2010b) was unable to confirm the shape of this bone in the holotype as it was reconstructed in a figure by Zhao and Currie (1993: fig. 1).

Dentary: A well preserved and essentially complete left dentary is known (figs. 32-33), as well as a nearly complete right bone that is missing the anterior tip and is broken posteriorly at the level of the surangular articulation. The dentary is slender compared to those of other tyrannosaurids, and is more comparable in proportions to the dentaries of juvenile albertosaurines (Table 7), and perhaps some specimens of very small, juvenile *Tarbosaurus* (Currie and Dong, 2001a). The general outline of the dentary is similar to the condition in other tyrannosaurids: it is slightly expanded anteriorly (39 mm deep at the third alveolus), faintly shallows across its midregion (35 mm deep at the ninth alveolus), and then deepens posteriorly such that it is tall and plate-like at the level of the surangular articulation (73 mm deep).

The dentary is mediolaterally thick along the tooth row (20 mm anteriorly) but posteriorly it thins into a plate-like region, with a thickness of less than 2 mm. The lateral surface under the tooth row is convex and the medial surface is flat, giving the dentary a D-shaped cross section like in other tyrannosauroids. In lateral view, the ventral margin of the dentary is gently sinuous below the tooth row (gently convex anteriorly, gently concave posteriorly), but behind the tooth row it diverges ventrally as the dentary expands to articulate with the surangular and angular. Anteriorly the ventral margin meets the anterior margin at a point ventral to the level of the fourth and fifth alveoli. This point, which has been referred to as the "chin" (Carr et al., 2005), does not project ventrally as a discrete, offset projection (the projection is present in carcharodontosaurids: Brusatte and Sereno, 2007, 2008), but rather is only a low convexity that braced the dentary symphysis medially (see below). There is great variation in the position of

this point in derived tyrannosauroids: it is below the second alveolus in *Raptorex* (LH PV18); between the second and third alveoli in adult *Tyrannosaurus* (RSM 2523.8); below the third alveolus in *Gorgosaurus* (ROM 1247), *Daspletosaurus* (CMN 8506) and subadult *Tyrannosaurus* (CM 79057); and below the fourth alveolus in *Gorgosaurus* (ROM 1247), *Daspletosaurus* (MOR 533S), juvenile (BMR 2002.4.1) and adult *Tyrannosaurus* (CM 9380).

In *A. altai*, the anterior margin of the dentary is slightly convex and trends strongly anterodorsally-posteroventrally. The dorsal margin of the dentary is concave across the entire length of the bone. In contrast, the dorsal margin is usually convex along the first several alveoli in other derived tyrannosauroids, including *Raptorex* (PV LH18), *Bistahievesor* (NMMNH P-27469), *Gorgosaurus* (CMN 2120), *Daspletosaurus* (MOR 590), *Tarbosaurus* (PIN 551-3), and *Tyrannosaurus* (AMNH FARB 5027).

The lateral surface of the dentary is gently rugose, and exhibits clear anteroposteriorly oriented bone fibers along the entire length of the bone. Several neurovascular foramina pierce the bone, and these are especially concentrated anteriorly, ventral to the tooth row, and immediately above the ventral margin of the dentary. There are two primary rows of foramina: an alveolar and a ventral row. The alveolar row is located directly ventral to the alveolar margin (fig. 32, alvr). Anteriorly, below the first three alveoli, this row closely parallels the alveolar margin, and it is located only four millimeters below it. However, beginning at the fourth alveolus the row curves ventrally, such that, by the level of the sixth alveolus, it is 15 mm below the tooth row. There are approximately two foramina per alveolus anteriorly, each of which is large and has a diameter of ~3 mm, but posteriorly the foramina become shallower, longer, and more widely spaced, such that there is approximately one per alveolus. Posterior to alveolus 14 the foramina are replaced by a shallow groove (fig. 32, alvgr), which arches dorsally and

eventually merges with the notch for the surangular, and continues onto the lateral surface of the suranglar as a groove that terminates at the anterior surangular foramen. However, as the dentary itself deepens in this region, the groove does not approach the dorsal margin of the bone even though it curves dorsally. Instead, it ends 11 mm ventral to the dorsal margin of the dentary at its posterior end. The downward curvature and dorsally concave profile of the alveolar groove is seen in all tyrannosaurids, including juveniles (Carr and Williamson, 2004: fig. 5), as well as the basal tyrannosauroids *Dilong*, *Guanlong* (Xu et al., 2004, 2006), and *Eotyrannus* (MIWG 1997.550).

The second major row of foramina, the ventral row, parallels the anterior and ventral margins of the dentary, and is continuous along the change in orientation between the two margins (fig. 32, ventr). A similar ventral row is present in other tyrannosaurids (e.g., Brochu, 2003; Currie, 2003a), as well as basal tyrannosauroids such as *Proceratosaurus* (NHM R 4860) and *Raptorex* (Sereno et al., 2009). It is not apparent in specimens of *Dilong* and *Guanlong*, but its absence is likely a result of poor preservation (IVPP V14243, V14532). In *Alioramus altai*, the first foramen in this row, located at the anterodorsal tip of the dentary, is large (3 mm in diameter) and deep, and opens mostly anteriorly into a distinct triangular fossa. Subsequent foramina are also large, deep, closely spaced, and distinctive along the anterior margin. However, after the transition to the ventral margin the foramina are smaller, less distinct, longer, and more widely spaced. This row continues until a point immediately posterior to the final alveolus, where there is a shallow, 22 mm long, ovoid fossa (fig. 32, fvfor). The ventral row is never set into a groove, whereas the alveolar row is inset into a shallow trough posterior to the fifth alveolus. The region between the alveolar and ventral rows is textured with several random foramina anteriorly, but these generally are not present posterior to the fourth alveolus.

On the medial surface, the sharp groove for the dental lamina separates the interdental plates dorsally from the remainder of the dentary ventrally (fig. 32, gdl). A pronounced step separates these regions, but in life the interdental plates were covered medially by the ossified supradentary/coronoid, so that the medial surface of the lower jaw was approximately flat. The interdental plates are small, triangular, and unfused to each other, and their medial surfaces are covered with a series of small pits and thin, anteroposteriorly trending striations (fig. 32, idp). The groove for the dental lamina curves dorsally as it extends anteriorly, giving the entire groove a dorsally concave profile in medial view. At its anterior point the groove reaches the anterodorsal corner of the dentary. As a result, the first three interdental plates are small and nearly entirely concealed in medial view. Instead, these alveoli are nearly entirely covered medially by the main body of the dentary and not the interdental plates.

The symphysis for the opposing dentary is long and flat, and was probably weak in life (fig. 32, sym). It is much more rugose and beveled in *Daspletosaurus* (CMN 8506), *Tarbosaurus* (Hurum and Sabath, 2003), and *Tyrannosaurus* (Brochu, 2003). The opposing dentaries contacted each other beneath the first five alveoli, and the articular surface terminates at the level of the anterior Meckelian foramen. There is a slightly raised region on the medial surface of the ventral "point" ("chin") where the anterior and ventral margins meet (fig. 32, ab). Similar convexities, which project ventrally and are also visible in lateral view, are present in tyrannosaurids in general (e.g., Brochu, 2003: fig. 40; Currie, 2003a: fig. 33; Carr et al., 2005: fig. 12) as well as many other theropods (e.g., Brusatte et al., 2008). This feature reaches an extreme in carcharodontosaurids, in which it is expanded into a bulge that braced and reinforced the dentary symphysis (Brusatte and Sereno, 2007). Despite being approximately equal in body size to some carcharodontosaurids, tyrannosaurids do not possess an enlarged bulge, only the

slight "chin," although this structure probably still served to brace the symphysis. A discrete "chin" is not present in *Eotyrannus* (Hutt et al., 2001: fig. 3) and cannot be assessed in *Guanlong* (Xu et al., 2006) and *Proceratosaurus* (Rauhut et al., 2010) due to poor preservation. A subtle "chin" may be present in *Dilong* (IVPP V14243), based on the outline of the dentary in lateral view, but the morphology of the medial dentary cannot be assessed in this specimen. In *A. altai* the symphysis is further strengthened by a thin and sinuous rim, which trends anterodorsally from the ventral margin of the brace (fig. 32, rim).

Immediately posterior to the brace is the anterior Meckelian foramen (fig. 32, amf). Surface erosion makes it difficult to determine if there was a single or double set of openings. The left bone shows signs of what may be a separate opening. Here, a small flake, of what appears to be broken bone, projects into the foramen, which partially divides it into two openings. While apparently broken in the left dentary, the same projection of bone is also present on the less well preserved right dentary, but it is located anterior to the foramen and thus does not divide it into two openings. Therefore, it is unclear if there is a separate foramen anterior to the projection. A divided foramen is absent from other derived tyrannosauroids. The entire foramen region, whether one or two openings, is 11 mm long anteroposteriorly and 3.5 mm deep dorsoventrally in the left dentary. This region is located ventral to the septum between alveoli five and six, the same general position as in *Tyrannosaurus* (Brochu, 2003, Carr and Williamson, 2004).

The anterior Meckelian foramen is located at the anterior terminus of the Meckelian groove, which is deeply inset laterally into the main body of the dentary (fig. 32, mg). The groove is inset most deeply below the 10^{th} alveolus, where it is only 10 mm in dorsoventral height but protrudes laterally more than 5 mm into the dentary. Anteriorly and posteriorly to this

region the groove expands in dorsoventral height but becomes less inset. Posteriorly it expands into the Meckelian fossa (fig. 32, mf), which is large, triangular, and extends to the posterior end of the dentary and continues onto the medial surface of the surangular and angular. It is here where the dentary is especially thin and plate-like. The fossa is positioned lateral to the Meckelian groove, resulting in a distinct step where the two structures meet, at the level of alveolus 17 (fig. 32, step). Here, a deep pocket leads from the fossa anteriorly and projects internally into the body of the dentary, extending lateral to the Meckelian groove. It is unclear how far this opening continues anteriorly, but it is present as a deep, matrix-filled pocket in both bones. Ventral to the pocket, and confluent with the ventral margin of the fossa itself, is a deeply inset notch (fig. 32, spnot). This structure slopes anteromedially, and thus smoothly connects the fossa and the groove without a distinct step. It is present on both bones and received a peg from the splenial (see below). Dorsally, the lappet of the main body of the dentary above the Meckelian groove continues posteriorly, where it overhangs the fossa before becoming part of the medial articulation for the surangular (fig. 32, lap). Because of this, a thin, but deep, region of the fossa continues dorsally, between the lappet and the lateral wall of the dentary.

The dentary contacts several postdentary bones of the lower jaw, including the surangular and angular, as well as the splenial and supradentary/coronoid. The surangular contacts the posterodorsal corner of the dentary. This articulation is complex, and the two bones extensively interlocked here, as is the case in theropods in general (e.g., Madsen, 1976; Currie and Zhao, 1993). The posterodorsal corner of the lateral surface projects posterodorsally as a tongue-like protrusion (fig. 32, surl; the intermandibular process of Currie and Zhao [1993] and Carr [1999]), which ventrally defines a notch (fig. 32, surnot). Below this is another process, which extends posterodorsally from the medial surface of the dentary (fig. 32, surm). The dorsal projection is

flat medially, where it overlapped the anterodorsal region of the surangular. The ventral process has a long, sharp ridge on its lateral surface, which trends posterodorsally, parallel to the long axis of the process itself. The surangular contact would have continued ventrally and posteriorly along the dorsal margin of the flat, plate-like region of the dentary. There likely was a gap between the denatary and surangular here. This was first noted by Osborn (1912) and referred to as the "hinge gap" by Brochu (2003). Thus, aside from the interlocking processes dorsally, the contact between the dentary and surangular was quite loose and flat.

The angular overlapped the medial surface of the dentary ventrally. Immediately below the external mandibular fenestra, the tapering anterior process of the angular contacts the medial surface of the posteroventral region of the dentary. However, this was apparently a loose contact, as no clear articular surface on the dentary is present. Additionally, the ventral margin of the splenial abuts the raised ventral rim of the Meckelian fossa on the medial surface of the dentary (fig. 32, spl). This articular surface faces entirely dorsally and medially, and thus the splenial would not have been visible in lateral view like it is in some basal theropods (e.g., *Monolophosaurus*: Zhao and Currie, 1993, Brusatte et al., 2010b) and derived maniraptorans (e.g., Barsbold and Osmólska, 1999; Norell et al., 2006). The articulation for the splenial is smooth and shallow, not deep and rugose as in adult *Tyrannosaurus* (Brochu, 2003), where the articulation was presumably immobile. This joint surface is relatively smooth in juvenile *Tyrannosaurus* (BMR 2002.4.1), and it has been hypothesized to become coarse with maturity in tyrannosaurids (Carr, 1999). Finally, the supradentary/coronoid rested upon the groove for the dental lamina and covered the interdental plates medially across the entire length of the tooth row, except apparently the first three alveoli. This articulation continued posterior to the tooth

row, as shown by a smoothly concave articular surface on the dentary across the 36 mm margin that separates the last alveolus from the interlocking contact for the surangular (fig. 32, sdc).

The posterior margin of the dentary is concave to form the smoothly rounded anterior margin of the external mandibular fenestra (fig. 32, emf). A similar condition is present in other tyrannosaurids (e.g., Brochu, 2003: fig. 40; Currie, 2003a: fig. 2). The fenestra is small in *A. altai*: it is 22 mm deep dorsoventrally at its midpoint and ~55 mm long anteroposteriorly. The entire anterior margin of the fenestra is formed by the dentary, and a small prong of the dentary forms approximately one third of the dorsal margin. This process, which extends posterodorsally, marks the posterior limit of the dentary-surangular articulation. It is also seen in many other tyrannosaurid skulls (e.g., Osborn, 1912; Maleev, 1974; Brochu, 2003; Currie, 2003a), but is fragile and may often not be preserved in some specimens. Yet, in one well preserved specimen, it appears to be truly absent (*Gorgosaurus*: ROM 1247, Carr, 1999: fig. 5).

In dorsal view the tooth row is slightly sinuous. Anteriorly it is shallowly concave laterally, but posterior to alveolus 12 it is laterally convex. There are 20 alveoli in the left bone (Table 5), and 17 are preserved in the right bone, which is broken anteriorly. The first alveolus is tiny, and trends anteromedially relative to the remainder of the alveoli, which are oriented approximately anteroposteriorly. The second alveolus is also quite small, and the first two alveoli are nearly circular, in contrast to the rectangular shape of the remaining alveoli. This condition is seen in other tyrannosaurids (e.g., ROM 1247). These alveoli are most properly described as "figure 8" shaped, as they are pinched medially. This pinching is most pronounced on the medial wall of the alveolus, and is simply formed by the gap between separate interdental plates where a new replacement tooth is erupting. The replacement teeth are positioned lingual to the erupted teeth, as in most basal theropods (Norell and Hwang, 2004). The largest alveoli are in positions

4-6, and posteriorly they gradually become shorter anteroposteriorly and thinner mediolaterally (Table 5). The last two alveoli are extremely reduced; the final alveolus is nearly circular and is the second smallest in the entire tooth row (only the first alveolus is smaller).

The labial wall of the alveoli, comprised of the main body of the dentary laterally, extends much farther dorsally than the lingual (medial) wall, formed by the interdental plates. Thus, the alveoli and crowns of the replacement teeth are widely visible in medial view. The groove for the dental lamina is visible both medially and dorsally (fig. 32, gdl). Such wide dorsal exposure is seen in other tyrannosaurids, but it is a rare feature among theropods. It is also present in megalosauroids (Benson et al., 2008) and may be associated with the presence of an ossified supradentary/coronoid. However, the presence of an ossified supradentary element is not a predictor of a dorsally-exposed groove, as *Allosaurus* (Madsen, 1976) possesses the former but not the latter. In dorsal view, the anterior region of the dentary is oriented approximately anteroposteriorly (deviating slightly laterally), and does not curve strongly medially to meet the opposing dentary as in large allosauroids (Brusatte and Sereno, 2007, 2008). Thus, the anterior end of the lower jaw was narrow, not wide and "U-shaped" in dorsal view (Brusatte and Sereno, 2008).

The high number of 20 alveoli in *A. altai* is autapomorphic among tyrannosaurids. *Tyrannosaurus* usually possesses 12-17 dentary alveoli depending on growth stage (e.g., BMR P2002.4.1; LACM 23844; Osborn, 1912; Molnar, 1991; Brochu, 2003), and other taxa variably possess 14-16 (see discussion in Brochu, 2003). Additionally, the second alveolus is proportionally much larger in *Tarbosaurus* (ZPAL uncatalogued) and *Tyrannosaurus* (Osborn, 1912: fig. 1; Brochu, 2003: fig. 40), whereas it is extremely small in *A. altai*. However, the

relative pattern of alveoli size, with alveoli 4-6 the largest in the tooth row, is the same across these taxa.

Surangular: Both left and right surangulars are present (figs. 34-36). The left bone is slightly more complete than the right, which is broken ventrally and crushed dorsoventrally. The left bone is also damaged ventrally, but when it is put into articulation with the dentary it is apparent that only a small region is missing. In overall proportions, the surangular of *A. altai* is longer and less deep than those of large, adult tyrannosaurids (e.g., Hurum and Currie, 2000). For example, the depth:length ratio of the bone in *Gorgosaurus* (UALVP 10) is 0.4, whereas the ratio in *A. altai* is 0.22 (with depth taken at the level of the surangular foramen).

The lateral surface of the surangular is generally smooth. Nearly the entire bone is plate-like and no greater than 1.5 millimeters in mediolateral thickness; this is due to the excavation of the medial surface by the Meckelian fossa. However, the dorsal margin of the surangular is robust and thick mediolaterally. Anteriorly, this thick dorsal margin ends in a notched articulation for the dentary (fig. 34, dennot). The notch separates dorsal and ventral processes; the dorsal process was overlapped by the dentary, whereas the ventral process covered the dentary. These processes interlocked with corresponding prongs on the dentary, described above, to strengthen the contact between the two bones. The dentary-surangular articulation interrupts the primary neurovascular groove on the dentary, but the groove continues posteriorly onto the surangular (fig. 34, ngr), where it ends in an elongate anterior surangular foramen, 80 mm behind the dentary articulation (fig. 34, asf). This dorsolaterally-facing foramen is an anteroposteriorly long oval, six millimeters long by two mm deep.

The dentary articulation is also expressed on the medial surface of the surangular; the supradentary/coronoid also articulated in this region, and the three bones meet in a complex geometry here. Separate articulations for the supradentary/coronoid and dentary are present on the surangular (fig. 34B, sdc, dengr). The supradentary element fits inside a long (76 mm), triangular notch, which faces completely medially (fig. 34B, sdc). The anterior margin of the notch is the anterior margin of the surangular itself. The notch is deepest dorsoventrally at its anterior margin, and thins in depth but becomes more deeply inset into the surangular as it continues posteriorly. The supradentary element is expanded into the triangular "coronoid region" here (see below). However, when in articulation, the notch on the surangular is too deeply inset to tightly articulate with the flattened coronoid. Therefore, the plate-like coronoid would have sat medially upon this notch, leaving space in between the two bones. Thus, there may have been cartilage or membraneous tissue in this region in life, and therefore the articulation between the coronoid and surangular may have been looser than often considered (Hurum and Currie, 2000; Hurum and Sabath, 2003).

Ventral to the coronoid notch is a separate, smaller articular surface for reception of the dentary (fig. 34B, dengr). This surface is approximately four millimeters deep and is no more than 20 mm long anteroposteriorly. It is flat and faces medially and ventrally. This surface articulated with the lateral surface of the ventral articular process of the dentary (see above). The dentary prong has a long, thin ridge on its lateral surface, which would have abutted the suranglar and strengthened the contact between the bones. The surangular does not contact the prearticular or splenial at or near this articulation, even though these bones approach the dentary and surangular in this region. A nearly identical arrangement is seen in *Tarbosaurus* (Hurum and Currie, 2000: fig. 1) and *Tyrannosaurus* (Brochu, 2003: fig. 40).

Ventrally, the surangular and dentary continued their articulation across a loose contact, and there possibly was a gap between the two bones for most of this margin (see above). However, the surangular clearly overlapped the dentary at least at the dorsal region of this contact (fig. 34, denol), as is usually reconstructed for tyrannosaurids (e.g., Carr, 1999: figs. 5, 6). In contrast, Hurum and Sabath (2003:183) described the dentary of *Tarbosaurus* as overlapping the surangular in this region, but the material they describe appears to be too broken to determine details of this contact (Hurum and Sabath, 2003: fig. 19). Nevertheless, other specimens (ZPAL MgD−I/4) indicate that *Tarbosaurus* has the usual tyrannosaurid condition of the surangular overlapping the dentary. In *A. altai* the ventral margin of the surangular is slightly convex across its contact with the dentary. Breakage makes it difficult to describe the surangular border of the external mandibular fenestra, but the ventral margin of the surangular would have formed most of the dorsal margin of this opening.

Posterior to the external mandibular fenestra, the angular laterally overlapped the surangular. This articulation is expressed as a flat surface on the surangular, which is coarsened by elongate striations and delimited dorsally by a slight rim (fig. 34, ang). This surface nearly abuts the enlarged surangular foramen (see below) and is separated from it by only five millimeters. In other tyrannosaurids this separation is wider (e.g., Brochu, 2003: fig. 40; Currie, 2003a: figs. 14, 36). For example, these structures are separated from each other by 10 mm in slightly larger individuals of *Tyrannosaurus* (BMR 2002.4.1) and *Gorgosaurus* (12.5 mm: ROM 1247), and the separation is twice this in subadult *Tyrannosaurus* (MOR 1125).

The articular would have covered nearly the entire posterior end of the medial surface of the surangular (the “retroarticular region” of the surangular). Neither articular is preserved, but the surangular contact surface gives details of the shape and size of the articular (fig. 34, art).

First, the articular was clearly unfused to the surangular. In contrast, the entire medial surface of the surangular is smoothly embayed for articulation with the articular, and this contact zone is not rugose or reinforced by any interlocking pegs and sockets, except for some posterodorsally trending ridges and grooves behind the glenoid fossa. The ventral margin of the retroarticular region is excavated by a flat, medially facing groove, which anteriorly is overhung by a ridge of bone that gradually dissipates posteriorly (fig. 34, preart). This groove received the prearticular, and the surangular and prearticular would have formed a concave "cup" to enclose the articular. The anterior surface of this cup is formed by a process that extends medially from the surangular (fig. 34, mhp; the "hook like process" of Currie [2003]). In posterior view this process is triangular in shape, with a roughened and concave ventral region and a smoother, convex dorsal margin. Along with contacting the articular, this medioventral margin of the hook articulates with the prearticular. The medial process also forms the posterior wall of the Meckelian fossa (fig. 34, mf).

The surangular foramen is enormous (fig. 34, sfor). This is the case in tyrannosaurids in general (e.g., Holtz, 2001, 2004; Currie et al., 2003), as well as more basal taxa such as *Dryptosaurus* (ANSP 9995), *Eotyrannus* (MIWG 1997.550), and *Raptorex* (Sereno et al., 2009), but the foramen is tiny or entirely absent in *Dilong*, *Guanlong*, and *Proceratosaurus* (Xu et al., 2004, 2006; Rauhut et al., 2010). In the undeformed left surangular the foramen is nearly circular, with a diameter of 30 millimeters, which is more than 10% of the length of the entire bone. In adult *Gorgosaurus* this ratio is similar (9% in UALVP 10).

Immediately posterodorsal to the surangular foramen, and located within the same fossa, is a deep pocket that extends posteriorly and medially into the surangular (figs. 34-35, pp). In the better preserved left bone it is clear that this pocket is penetrated by three separate foramina at its

deepest point. A similar condition is present in *Tyrannosaurus* (Brochu, 2003), for which CT scans show that the pocket extends into an interior recess of the articular (the "articular antrum"). Unfortunately, in *A. altai*, erosion medially makes it difficult to identify any foramina piercing the surangular that may connect this pneumatic pocket to the articular recess. Unlike in *Alioramus altai*, *Tyrannosaurus* has only a single channel between the pocket and the recess, and there are no signs of multiple internal foramina (Brochu, 2003: fig. 44). Shallow pockets, much less inset than those in *Alioramus altai* and *Tyrannosaurus*, are present in *Bistahieversor* (NMMNH P-27469), *Gorgosaurus* (ROM 1247), and *Tarbosaurus* (ZPAL MgD−I/4), as well as *Raptorex*. However, they are absent in the basal taxa *Dilong* (IVPP V14243), *Guanlong* (IVPP V14531), and *Proceratosaurus* (NHM R 4860). The fossa is absent entirely in juvenile *Tarbosaurus* individuals approximately the same size as the *Alioramus altai* holotype (ZPAL MgD-I/31).

Dorsally, the surangular foramen is overhung by a robust lateral surangular shelf, which is most prominent above the foramen (fig. 34, lss). Here, it laterally overhangs the lateral surface of the surangular by approximately 10 millimeters. The shelf gradually becomes less prominent anteriorly, and merges with the lateral surface of the bone approximately 40 mm anterior to the foramen. Thus, the shelf is not pendant anteriorly as in some theropods (e.g., Holtz et al., 2004). The shelf ends posteriorly above the posterodorsal corner of the foramen, where it becomes confluent with the anterior margin of the glenoid. Near its posterior termination, the shelf is penetrated by a small (10 mm long anteroposteriorly) yet deep triangular fossa that faces laterally and dorsally (figs. 34-36, trifos). This fossa is also clearly present in *Tyrannosaurus* (Brochu, 2003: fig. 40) and other derived tyrannosauroids (e.g., *Albertosaurus*: CMN 5600; *Daspletosaurus*: FMNH PR308; *Gorgosaurus*: ROM 1247). The shelf itself projects entirely

laterally (the "horizontal" condition of Carr and Williamson, 2004) and does not curve laterally and ventrally to partially obscure the surangular foramen in lateral view, as in large *Tyrannosaurus* (Carr and Williamson, 2004), as well as *Daspletosaurus* (Holtz, 2001) and *Tarbosaurus* (Holtz, 2001; ZPAL MgD−I/4). However, *Raptorex* (LH PV18), *Gorgosaurus* (ROM 1247), juvenile *Tarbosaurus* (ZPAL MgD-I/31), and subadult *Tyrannosaurus* (AMNH FARB 5029) have a horizontal shelf that does not obscure the foramen, as in *Alioramus altai*.

Dorsal to the shelf is a smooth and elongate fossa for the external jaw adductor muscles (figs. 34, 36, addfos) (Currie, 2003a). This is the "dorsomedial flange" of (Carr 1999), and it faces mostly dorsally and only slightly laterally in *A. altai*. The fossa is bound laterally by the shelf and medially by the slightly everted dorsomedial margin of the surangular (the "coronoid process"), and it is not pierced by a large foramen as has been described in at least one specimen of *Tyrannosaurus* (Brochu, 2003). This region is described as a flat or slightly convex "facet," with several distinct planes, in *Tyrannosaurus* by Molnar (1991). Here, however, it is a single smooth surface. Brochu (2003: fig. 40) figures a similar condition in *Tyrannosaurus*, but this surface faces almost completely laterally, whereas in *A. altai* it is oriented primarily dorsally. Thus, when the surangulars of *Tyrannosaurus* and *A. altai* are compared in lateral view, it appears as if the surangular shelf of *Tyrannosaurus* is located much further ventrally, and that the surangular of *Tyrannosaurus* is much deeper (the "expanded" condition). This morphology is also seen in *Tarbosaurus* (ZPAL MgD−I/4), including juveniles (ZPAL MgD-I/31), and the basal tyrannosauroid *Dilong* (IVPP V14243). An unexpanded condition, where the muscle fossa is oriented primarily dorsally as in *A. altai*, is present in *Alioramus remotus* (Kurzanov, 1976: fig. 8), whereas an intermediate condition is seen in *Albertosaurus* and *Daspletosaurus* (Currie, 2003a: figs. 14, 36).

The surangular forms the lateral region of the mandibular glenoid fossa (figs. 34, 36, gl), although the articular would have formed most of this joint surface. In lateral view the surangular glenoid is expressed as a deep concavity, bounded anteriorly and posteriorly by dorsally-extended processes. The anterior process is the posterior-most point of the lateral surangular shelf, and it bounds the above-described triangular fossa posteriorly. This projection also separates the glenoid from the elongate jaw muscle fossa. In dorsal view, the surangular glenoid is crescent shaped, and is 12 mm wide mediolaterally at its midpoint and 16 mm long anteroposteriorly. A thin ridge separates the smooth glenoid surface from a shallow, laterally facing fossa on the lateral surface of the suranglar, positioned immediately ventral to the glenoid concavity (figs. 34-36, ngf). This fossa is described in *Tyrannosaurus* as an accessory "non-glenoid fossa" (Brochu, 2003:45), and is also present in all derived tyrannosauroids, including *Tarbosaurus* (ZPAL MgD-I/31). In these taxa, however, the fossa is much more rugose than in *A. altai*; this may reflect the young ontogenetic stage of *A. altai* because this surface is known to become larger and more rugose as an individual matures (Carr, 1999). Finally, in lateral view, there is a separate small dorsal projection posterior to the glenoid. This continues as a ridge on the medial surface, where it strengthened the contact with the articular (fig. 34, artrid). This feature is also present in other derived tyrannosauroids, including *Tarbosaurus* (ZPAL MgD-I/31), and the possible tyrannosauroid *Bagaraatan*, in which the region between the glenoid and this smaller projection is identified as a "cleft" (Osmólska, 1996: fig. 3).

On the medial surface of the surangular, the dorsal margin overhangs the smooth surface for the Meckelian fossa as a deep, ventrally extending rim. The robust dorsal margin begins anteriorly as the complex articulation with the dentary and supradentary, which is slightly thickened but does not strongly overhang the medial surface. Posteriorly, the articular region

gradually becomes more prominent and transitions into the medial shelf (fig. 34, ms), which is most prominent at its midpoint, where it is 16 mm wide mediolaterally. More posteriorly, however, the dorsal margin becomes less shelf-like, as the underlying Meckelian fossa becomes shallower in the region of the surangular foramen.

The retroarticular region of the surangular includes a retroarticular process proper, which is the shape of an equilateral triangle with vertices of 30 millimeters (figs. 34, 36, rap). It is short as in tyrannosauroids in general. The short condition is often used as a character in phylogenetic analyses (e.g., Holtz, 2001), and character statements usually refer to the retroarticular process of the articular. Although the articular is not preserved in *A. altai*, the size and shape of its retroarticular process can be inferred from the closely-matching surface on the surangular. Here, the posterior margin of the process is straight and slopes posteroventrally, and is not concave as in juvenile *Gorgosaurus* (Carr, 1999) nor oriented primarily dorsoventrally as in larger tyrannosaurids, including *Daspletosaurus* (Carr, 1999: fig. 1), *Gorgosaurus* (Carr, 1999: fig. 5; Currie, 2003a: fig. 2), *Tarbosaurus* (Hurum and Sabath, 2003: fig. 19), and *Tyrannosaurus* (Brochu, 2003: fig. 40). Some specimens of juvenile *Tarbosaurus* have a unique condition in which the posterior margin thins to a point (Currie and Dong, 2001a: fig. 1), whereas others have a morphology similar to *Alioramus altai* (ZPAL MgD-I/31). Furthermore, the posterior margin is vertical and the entire process is rectangular in *Dilong* (IVPP V14243). In general, the retroarticular process of *A. altai* is most similar to that of *Alioramus remotus* (Kurzanov, 1976: figs. 1, 8).

Angular: Only the right angular is preserved, but it is virtually complete and only slightly broken anteriorly and posteriorly (fig. 37). This bone is comprised of two processes: a shallow

anterior process that forms the ventral margin of the external mandibular fenestra and is overlapped laterally by the dentary (fig. 37, apr), and a deep posterior plate that overlaps the surangular (fig. 37, pp). The anterior process is thick in mediolateral width (5 mm) but the posterior plate is remarkably thin (less than 1 mm) where it contacts the surangular. The angular has a maximum depth of 41 mm at the anterior corner of its contact with the surangular, is 21 mm deep underneath the midpoint of the external mandibular fenesra, and then tapers to a depth of 7 mm at the anterior edge of the anterior process. However, as this edge is broken, the angular was longer and likely tapered even further anteriorly.

The angular has a convex lateral surface. This surface is generally smooth but some regions are covered with fine striations; these are especially prevalent posteriorly, on the plate-like region that overlapped the surangular, where they trend anteroventrally. The joint surface for the dentary is a concave depression on the lateral surface of the angular directly below the external mandibular fenestra (fig. 37, den), which is bordered ventrally by a slightly raised rim (fig. 37, rid); this joint surface extends to the anterior tip of the angular. Hurum and Sabath (2003:185) consider a "vertical ridge" on the lateral surface of the angular of *Tarbosaurus* as an autapomorphic structure, which probably braced the dentary articulation. However, a vertical ridge is absent from PIN 551-3, a skull of an adult *Tarbosaurus*, in which the joint surface is indistinct and not braced by a vertical ridge. The condition in this specimen is more similar to the condition seen in other derived tyrannosauroids (including *A. altai*), where there clearly is a distinct overlap surface that is delimited by a rim that trends anterodorsally-posteroventrally. This rim may be homologous to the "vertical ridge" noted by Hurum and Sabath (2003) in some specimens of *Tarbosaurus*, but the polymorphic condition in *Tarbosaurus* suggests that the morphology of the dentary-angular articular surface is highly variable.

The dorsal margin of the angular is concave where it forms the ventral edge of the external mandibular fenestra (fig. 37, emf). This margin is smooth anteriorly, but the posterior portion is raised into a series of small rugosities. A similar series of protuberances is present in *Tyrannosaurus* (Brochu, 2003: fig. 40A), but these are more pronounced than the corresponding texture in *A. altai*. The dorsal margin of the expanded posterior plate of the angular is broken, but judging by the articular surface on the suranglar it appears as if this edge was roughly straight. The ventral border of the angular is broadly convex, and there are no prominent rugosities as reported in *Tyrannosaurus* (Brochu, 2003). Moreover, the anterior process is not "flexed" dorsally relative to the posterior plate as in some tyrannosaurines (*Daspletosaurus*: Carr, 1999: fig. 4I; *Tyrannosaurus*: Carr, 1999: fig. 8E).

The medial surface of the angular is concave. This concavity is deepest below the external mandibular fenestra, where there is a smoothly inset fossa (fig. 37, fos). Posterior to this, the medial surface is scoured by numerous ridges and grooves, most of which trend anteroventrally, but some of which are arcuate in shape. These mark the region where the angular laterally overlaps the surangular (fig. 37, sur).

The prearticular and splenial also contact the ventral margin of the angular medially. The splenial articulation is located anterior to the prearticular contact surface. It is clear that the splenial contacted the anteriormost 85 mm of the angular, along the region where the angular was overlapped by the dentary. The first 44 mm of the splenial articulation occupies the narrow ventral surface of the angular, and is entirely ventrally facing (fig. 37, splv). However, posterior to this point the final 41 mm of the contact is present as a separate region: a wide (10 mm wide at its midpoint) and concave facet that faces ventrally and slightly medially (fig. 37, splm). The two articular surfaces are not continuous. However, across the length of the entire articulation the

angular sits on top of the splenial dorsally. Thus, if there was no dentary (which covers both the splenial and angular laterally) in articulation, the splenial would be visible laterally here as a narrow band.

Posterior to the splenial articulation the ventral margin of the angular remains mediolaterally expanded to contact the prearticular. This articulation also changes in orientation, albeit gradually, and the contact zone does not divide into separate surfaces. Anteriorly the articulation faces dorsally (fig. 37, pdors), then gradually medially (fig. 37, pvent), and then fully ventrally (fig. 37, pmed). The ventrally-facing part of this contact becomes narrow posteriorly, and the prearticular continues to contact the angular until nearly the posterior tip of the angular. Here, the prearticular expands and projects medially to meet the surangular and articular, leaving a narrow gap between itself and the angular. Some of this region may have been filled by the surangular, as in other tyrannosauroids (e.g., *Bistahieversor*: NMMNH P-27469), or a thin band of cartilage. There is no secondary "accessory" ridge on the angular for contact with the prearticular, nor is there a separate contact surface on the prearticular for such a ridge. This architecture has been described as a jaw-strengthening feature in *Tarbosaurus* (Hurum and Currie, 2000; Hurum and Sabath, 2003).

Prearticular: A complete right prearticular is preserved (figs. 38-39). The prearticular is a long and curved bar of bone, which expands anteriorly into a thin, spade-shaped plate (fig. 38, apr) and posteriorly into a medially convex cup that embraces the articular (fig. 38, ppr). This bone is shallowest dorsoventrally at its midpoint, where it is only 14 mm deep, whereas the anterior process is 31 mm deep at its midpoint. However, the prearticular is thickest mediolaterally where it is shallowest dorsoventrally: it is 10 mm thick at its midpoint (the dorsoventrally shortest

region), but thins to less than 1 mm both anteriorly and posteriorly (which are both dorsoventrally expanded relative to the midpoint).

The shape of the prearticular in tyrannosaurids changes with ontogeny (Carr, 1999). The holotype of *A. altai* has the condition seen in juveniles, in which the bone is shallow, the dorsal and ventral margins of the posterior process are parallel, and the ridge on the dorsal edge of the bone is short and is limited posteriorly. Also, the anterior process is straplike, in contrast to the deep paddle-like condition seen in adult *Daspletosaurus* (CMN 8506) and *Tyrannosaurus* (AMNH FARB 5027).

In *A. altai*, the medial surface of the prearticular is generally convex and smooth, especially along the thin bar linking the anterior and posterior processes. This bar is referred to as the "central segment" by Molnar (1991) and the "body" of the prearticular by Hurum and Sabath (2003). Here the prearticular forms the floor of the Meckelian fossa (fig. 38, mf).

The dorsal margin of the bar and the posterior process is smoothly concave, where it forms the ventral and posterior border of the Meckelian fossa and fenestra. In contrast, the dorsal margin of the anterior process has two nearly straight regions separated by an inflection point (fig. 38, ip). Posteriorly to this point the margin trends strongly anterodorsally, whereas anteriorly it is nearly horizontally oriented. The ventral margin of the bar and posterior process is smoothly convex, without the rugosities described in *Tyrannosaurus* (Brochu 2003), whereas that of the anterior process is more complicated. Posteriorly there is a smooth, 15 mm long concave notch (fig. 38, not), which contacted the splenial where this bone extends below the angular. Anterior to this notch the ventral edge develops into a convex lobe (fig. 38, cl), but then straightens out further anteriorly in the region of the internal mandibular fenestra.

The dorsal and ventral margins of the anterior process are not parallel as reconstructed for *Tyrannosaurus* (Brochu, 2003: fig. 44), but rather converge towards each other as the process tapers to an anterior point. This is also unlike the condition in other *Tyrannosaurus* specimens, in which the anterior process deepens anteriorly (Osborn, 1912; Molnar, 1991: pl. 14). However, the shape of the anterior process in *A. altai* is identical to that illustrated in *Tarbosaurus* (Hurum and Sabath, 2003: fig. 19). On the posterior process, there is no pronounced fossa on the medial surface of the ventral region, as Molnar (1991) described in *Tyrannosaurus*, possibly as an attachment site for branchiomandibularis musculature.

Laterally the prearticular contacts several bones. First, the dorsal margin of the anterior process of the prearticular meets the anteroventral margin of the coronoid along an extensive butt joint (fig. 38, sdc), as in *Tarbosaurus* and *Tyrannosaurus* (Hurum and Currie, 2000: figs. 1, 2; Brochu, 2003: fig. 43). The tip of the prearticular may slightly overlap the coronoid medially, but there are no clear articular surfaces on either bone marking this articulation. The medial surface of the prearticular was likely overlapped by the splenial here, as indicated by a shallow and narrow facet along its lower margin (fig. 38, spl), and by a similar facet on the complementary surface of the splenial. This condition is also seen in *Tarbosaurus* and *Tyrannosaurus* (Hurum and Currie, 2000; Brochu, 2003; Hurum and Sabath, 2003).

The ventral margin of the prearticular bar contacts the angular along a broad suture. The orientation of this contact, which twists along its length, is described above. Most of this joint surface is a lateroventrally facing groove, which is 55 mm long anteroposteriorly and 15 mm deep dorsoventrally at its midpoint (figs. 38-39, anggr). In lateral view, the dorsal margin of the groove extends as a thin flange laterally and slightly dorsally (fig. 38, fl), as seen in *Albertosaurus* (Currie 2003a: fig. 16). Anteriorly, the articular groove is bisected by an

anteroposteriorly trending ridge (fig. 38, rid) that separates the smooth articular surface from the coarser medial half of the joint surface that faces ventrally. This part of the joint surface, which is less than 5 mm wide mediolaterally, extends for 30 mm anteriorly, until it terminates at the notch for the splenial (fig. 38, not). There is no sign of a second accessory articulation between the angular and prearticular, as described in *Tarbosaurus* (Hurum and Currie, 2000), nor are there a series of ridges that have been described as "strengthining" the articulation of these bones in *Tarbosaurus* and *Tyrannosaurus* (Hurum and Currie, 2000; ZPAL D-I/34). However, the articular groove for the angular is much wider mediolaterally than in other theropods with well described prearticulars (e.g., Madsen, 1976: pl. 7F; Sampson and Witmer, 2007: fig. 31).

Posterior to the angular groove, and separated from it by a 15 mm nonarticular margin (fig. 38, nam), is a thick and rugose region scoured by several posterodorsally oriented lineations (fig. 38, surv). This is the anterior region of the contact for the ventral margin of the retroarticular region of the surangular. This contact is long and extends for 75 mm to the posterior tip of the prearticular. Thus, the surangular and prearticular extend to the same level posteriorly. Anteriorly the contact surface on the prearticular faces strongly laterally, but it decreases in depth posteriorly. This surface becomes more deeply inset posteriorly, and gradually twists onto the ventral surface of the bone.

The prearticular also contacts the surangular at a second contact surface dorsally (fig. 38, surd). This articulation is located on the dorsal margin of the lateral surface of the posterior process of the prearticular. It is a long (25 mm), shallow (5 mm deep), laterally facing, and slightly concave surface that contacts the medially-projecting "hook like" process of the surangular. There is no fusion here between the articular, angular prearticular, and surangular

like there is in large individuals of *Tarbosaurus* (Hurum and Currie, 2000; Hurum and Sabath, 2003).

Between the dorsal and ventral contacts with the surangular is a deep, triangular concavity (fig. 38, artcup). This laterally-facing surface is slightly rugose and scoured by small lineations. It embraced the articular medially, forming the second half of the articular "cup" that is laterally defined by the retroarticular region of the surangular. Anteriorly, this deep fossa continues as a dorsoventrally shallow but deeply excavated groove (figs. 38-39, gr), which follows the curving contours of the prearticular bar as it continues anteriorly. It eventually merges smoothly with the lateral surface of the prearticular at the posterior base of the anterior process. The ventral margin of this groove is formed by the laterally projecting ridge that forms the dorsal margin of the angular contact (figs. 38-39, fl), whereas the dorsal margin is demarcated by a sharp rim. The groove is clearly nonarticular and properly forms the ventral floor of the Meckelian fossa. This is a typical feature of theropods (e.g., Madsen, 1976: pl. 7F; Sampson and Witmer, 2007: fig. 31) and may have held membraneous tissue or cartilage associated with the Meckelian fossa, which persists into adulthood as isolated regions of cartilage in some living tetrapods (e.g., Rodríguez-Vázquez, et al. 1997).

Splenial: The right splenial is nearly complete and well preserved (fig. 40). The splenial is a thick, plate-like bone that covers most of the Meckelian fossa of the dentary medially. It is somewhat triangular in shape and comprised of three processes: a thin anterior process (fig. 40, apr), a dorsal flange (fig. 40, df), and a posterior process (fig. 40, ppr). The anterior process is finger-like, tapers anteriorly, and covers much of the Meckelian groove of the dentary medially. It is 65 mm long but broken anteriorly, making it difficult to determine how far the bone

extended. The posterior process is elongate (107 mm long) and trends posteroventrally in concert with the posterior deepening of the lower jaw. This process tapers in depth, beginning with a dorsoventral height of 35 mm and terminating at a depth of 7 mm. Between the anterior and posterior process is the dorsal flange, which medially covers much of the dentary dorsal to the Meckelian groove, as well as the coronoid.

Although often described as a thin sheet, the splenial is quite thick. It is especially robust ventrally, where it is 10 mm thick mediolaterally where it contacts the dentary and angular. However, the much thinner dorsal flange is also somewhat robust: it is 3 mm thick, about three times thicker than the dentary that it covers medially. The medial surface of the splenial is generally convex and smooth, whereas the lateral surface is excavated by the Meckelian fossa.

The splenial is pierced by a large anterior mylohyoid foramen (fig. 40, amf), which is the shape of an anteroposteriorly elongate oval with a nearly horizontal (anteroposterior) long axis. It is 30 mm long anteroposteriorly and 7 mm deep at its midpoint. On the medial surface of the splenial, the foramen is bordered anteriorly and especially posteriorly by a smooth fossa (fig. 40, fos); the fossa is most deeply inset anteriorly, but is more anteroposteriorly elongate posteriorly. When the mandible articulated, the foramen is positioned below dentary alveoli 18-20 and it extends posteriorly beyond the rooth row.

The shape, size, and orientation of the foramen are unique in *A. altai*. First, the foramen is greatly elongated anteroposteriorly compared with its depth. In most tyrannosaurids, in contrast, the foramen is more circular (Table 8). Second, the nearly horizontal inclination of the foramen in *A. altai* contrasts with the more anteroventral-posterodorsal orientation in many other tyrannosaurids (e.g., Brochu, 2003: fig. 40; Currie, 2003a: fig. 34; Hurum and Sabath, 2003: fig. 19). A nearly horizontal foramen is present in juvenile *Tarbosarus* (Currie and Dong, 2001a: fig.

1), but it is not nearly as long and shallow as that of *A. altai*. Additionally, Kurzanov (1976:102) describes the foramen of *Alioramus remotus* as "horizontally extended," but a figure was not provided. The foramen of *A. altai* is most similar to that of *Applachiosaurus*, which is elongate and only slightly anteroventrally oriented (Carr et al., 2005: fig. 12). However, the foramen in *Appalachiosaurus* is much deeper than that of *A. altai*, and has a nearly identical anteroventral orientation as the foramen of *Daspletosaurus* (Currie, 2003a: fig. 34), not a nearly horizontal inclination.

The anterior mylohyoid foramen of *A. altai* is completely enclosed by the splenial. It essentially parallels the ventral margin of the bone, due to its horizontal orientation, and is only separated from the ventral edge of the bone by a thin bar that is 5 mm deep. In *Tarbosaurus* there is sometimes only a very thin margin between the foramen and the ventral edge of the splenial (Hurum and Sabath, 2003: fig. 20). In some *Tarbosaurus* specimens the foramen appears to breach the ventral margin of the bone (Maleev, 1974: fig. 19), although this may be an artifact of breakage (Hurum and Sabath, 2003:185). Specimens of *Daspletosaurus* (Currie, 2003a: fig. 34) and juvenile *Tarbosaurus* (Currie and Dong, 2001a: fig. 1) also possess foramina that breach the ventral margin, and it has been suggested that the foramen may be open in juveniles but becomes enclosed later in ontogeny (Currie and Dong, 2001a).

The ventral margin of the splenial, which is comprised of the ventral margins of the anterior and posterior processes, is smoothly concave. The anterior margin of the bone is notched between the anterior and dorsal processes (fig. 40, not). There is some broken bone in this area but the notch is likely a real feature. It is also present in *Albertosaurus* (CMN 5601), *Daspletosaurus* (CMN 8506), *Gorgosaurus* (ROM 1247), and *Tyrannosaurus* (Brochu, 2003: fig. 40), where it overlaps the region of the dentary between the Meckelian groove and

interdental plates. Anterior to the notch the dorsal margin of the anterior process is slightly concave, whereas that of the dorsal flange is basically straight and extends posterodorsally across the supradentary/coronoid (fig. 40, sdc), following the trend of the posterior expansion of the dentary.

The posterior margin of the splenial trends anterodorsally-to-posteroventrally. It is marked by a concave notch, which separates the dorsal and posterior processes (fig. 40, not). The posterior process is squared off posteriorly and ends in a straight edge that is oriented posteroventrally. A straight margin is also seen in *Tarbosaurus* (Hurum and Sabath, 2003: fig. 20) and *Tyrannosaurus* (Brochu, 2003: fig. 40), but in those genera the orientation of the edge is much closer to vertical than in *A. altai*. Similarly, the notch separating the posterior and dorsal processes is also present in *Tarbosaurus*, *Tyrannosaurus*, and *Appalachiosaurus*, but is a much broader concavity in these taxa. This is apparently due to an anterodorsal rotation of the dorsal flange (=clockwise when the right splenial is seen in lateral view), which results in a more open notch and also a deeper splenial. In other words, the dorsal flange of other tyrannosaurids is dorsoventrally taller, and also has a long axis that trends more steeply anteroventrally than that in *A. altai*, in which the axis is closer to horizontal. The relative rotation of the flange is seen by comparing the splenial of *A. altai* with those of other tyrannosaurids (Hurum and Currie, 2000; Brochu, 2003; Hurum and Sabath, 2003; Carr et al., 2005). The condition in *A. altai* is likely autapomorphic, as outgroup taxa have a more similar morphology to other tyrannosaurids (e.g., Currie, 1995; Kobayashi and Barsbold, 2004).

There is no sign of a small, dorsally projecting finger of bone within the anterior margin notch as has been described in on specimen of *Tyrannosaurus* (Brochu, 2003: fig. 42), although this likely reflects damage in that specimen. Additionally, in *A. altai*, there is no articulation at

this notch, but rather empty space between the splenial and prearticular, which do not contact in this region (see above). The lack of contact between these bones is suggested by two lines of evidence. First, as described above, they do not approach each other when the mandible is articulated. Second, there is no groove on the posterior margin of the medial surface of the dorsal ramus where the prearticular overlapped, as is clearly visible in other tyrannosaurids (e.g., *Tarbosaurus*: Hurum and Sabath, 2003: fig. 20). Many authors consider the notch as the anterior and ventral margin of the Meckelian fenestra (=internal mandibular fenestra; e.g., Brochu, 2003; Carr et al., 2005), but more properly this margin is formed by the prearticular (see, for instance, Hurum and Currie [2000: figs. 1, 2]; Hurum and Sabath [2003: fig. 19]).

The splenial articulates with the dentary laterally, and all three processes of the splenial make contact with this bone. The articulation is most extensive on the anterior process, the entirety of which covers the Meckelian groove of the dentary (fig. 40, den), and the dorsal flange, which covers the medial surface of the dentary dorsal to the Meckelian groove. On the lateral surface of the dorsal flange there is an anteroposteriorly elongate shelf, approximately 20 mm below the dorsal margin, that marks the articulation between the splenial and dentary bar (fig. 40, densh).

Contact between the posterior process of the splenial and the dentary was limited. The process may have made slight contact with the dentary along the lateral surface of its ventral margin, but this was short, because posterior to the mylohyoid foramen the surangular and dentary diverge from each other and the angular fits between them. Interestingly, the lateral surface of the ventral region of the splenial is thick and smooth on the posterior process (fig. 40, thick), even though the dentary and splenial diverge and clearly do not contact each other broadly here. If this condition is real, and not an artifact of distortion, it supports Brochu's

(2003) contention that there was a ligamentous connection, but not direct articulation, between the two bones in this region. In contrast, Hurum and Sabath (2003:185) note that the "ventral edge of the splenial (in *Tarbosaurus*) is thicker than the rest of the bone and in close contact with the ventral bar of bone in the posterior part of the dentary." It is possible that they have mistaken the thick ventral edge of the splenial as evidence for a direct and close contact with the dentary, but the condition in the aforementioned specimens of *A. altai* and *Tyrannosaurus* (if there is no distortion in either specimen) shows that the first condition is not evidence for the latter interpretation. However, more basal theropods (e.g., *Baryonyx*: Charig and Milner, 1997; *Majungasaurus*: Sampson & Witmer, 2007) do have a tighter articulation between the posterior region of the splenial and the dentary, which is reinforced with a series of interlocking ridges and grooves.

Immediately anterior to the mylohyoid foramen the articulation with the dentary is strengthened by a peg and socket articulation (fig. 40, peg). Here, a laterally and slightly ventrally projecting ridge from the lateral surface of the splenial fits into a deep groove on the dentary, at the floor of the Meckelian fossa (as described above). This contact is 20 mm long anteroposteriorly. Posteriorly there is a small notch in the ventral margin of the groove on the dentary, which matches a ventrally projecting nubbin of bone on the splenial, although fine details on the splenial are obscured here due to breakage.

A peg and groove articulation is also present in *Tyrannosaurus* (Brochu, 2003:43), but the groove in the dentary is described as "ventral to the Meckelian fossa." However, Brochu (2002:fig. 41) figures the groove as occupying the anteroventral margin of the fossa itself, identical to the condition in *A. altai*. A nearly identical peg and groove are also present in *Daspletosaurus* (Currie, 2003a: fig. 34) and *Gorgosaurus* (ROM 1247). Brochu (2003:42)

considered the contact between the splenial and dentary to be "ligamentous" in *Tyrannosaurus* because of the smooth, elongate nonarticular surface described above. However, the peg and groove articulation would have strengthened the dentary-splenial contact anteriorly, and the two bones would have strongly interlocked in spite of the long nonarticular region. In *A. altai*, however, there are no signs of any additional interlocking contacts between the dentary and splenial in the region of the peg and socket, as have been described in large specimens of *Gorgosaurus* (Currie, 2003a) and *Daspletosaurus* (Carr, 1999:507) as "arcuate, interleaving ridges that fit into corresponding slots in the dentary."

The splenial also contacts the supradentary/coronoid element laterally (fig. 40, sdc). The lateral surface of the dorsal region of the dorsal flange overlapped the supradentary medially, beginning immediately posterior to the dentary tooth row. This contact is preserved as a 40 mm long groove on the lateral surface of the dorsal process, immediately posterior to the notch between the anterior and dorsal processes described above. The groove parallels the dorsal margin of the splenial, faces dorsally anteriorly, but deepens posteriorly and twists to face directly laterally. Posterior to the groove the splenial would have still contacted the supradentary, but here there was a simple overlapping contact that left no clear articular surface on either bone. Of the two conditions figured and discussed by Hurum and Sabath (2003: fig. 20), the supradentary contact on the splenial of *A. altai* is more similar to that of *Tyrannosaurus*. In these taxa the groove expands in dorsoventral depth posteriorly and is shallow, whereas in *Tarbosaurus* the groove keeps a relatively constant depth across its length and thus appears to "abruptly" rise from the anterior margin of the splenial, at the notch between the anterior and dorsal processes (Hurum and Sabath, 2003:185).

The splenial of *A. altai* is proportionally longer and shallower than those of other tyrannosaurids (see above discussion of the "rotated" dorsal flange). In fact, the splenial of *A. altai* is similar in shape and proportions to that of the basal tetanuran *Monolophosaurus* (Zhao and Currie, 1993: fig. 2). In *A. altai* and *Monolophosaurus* the splenial is elongate anteroposteriorly and short dorsoventrally, and the long axis of the dorsal process is oriented at a low angle extending anteroventrally-to-posterodorsally. In contrast, the long axis of the dorsal flange is much steeper in other tyrannosaurids, resulting in a more dorsoventrally expanded splenial. However, there are some differences between the splenials of *A. altai* and *Monolophosaurus*. In the latter taxon the notch between the dorsal and posterior processes is better defined, the anterior mylohyoid foramen breaches the ventral margin of the bone, and the splenial has limited lateral exposure between the dentary and the angular (as in basal theropods and dinosaurs in general: Sereno and Novas, 1993).

The splenial of *A. altai* is also similar to that of *Allosaurus* (Madsen, 1976) in both general proportions and the shape of the notches between the anterior and dorsal, and posterior and dorsal, processes. However, in *Allosaurus* the mylohyoid foramen breaches the ventral margin of the splenial, the anterior process is much shorter, and the dorsal process terminates in a blunt, rounded margin that is unlike the straight margin in *A. altai* and tyrannosaurids in general. Finally, the splenial of *A. altai* is very different from the deeper, more triangular splenial of *Majungasaurus* (Sampson and Witmer, 2007), in which the posterior process is very short and the anterior process is short and divided into two prongs. A similar morphology is apparently present in *Ceratosaurus* (Madsen and Welles, 2000) and *Baryonyx* (Charig and Milner, 1997). Compared to basal theropods, the anterior mylohyoid foramen is much larger in *A. altai* and other tyrannosauroids.

Supradentary/Coronoid: A flat, elongate bone extends across most of the dorsal region of the medial surface of the mandible (fig. 41). This bone is often referred to as the supradentary/coronoid element (Brochu, 2003; Currie, 2003a; Hurum and Sabath, 2003), and we follow this terminology here. Individual coronoids and supradentaries have been described as separate ossifications in some dinosaurs (see review in Brochu, 2003), but in *A. altai* they form a single structure, as in tyrannosaurids in general (e.g., *Daspletosaurus*: FMNH PR308; *Tyrannosaurus*: FMNH PR2081) and other theropods with well preserved lower jaws (e.g., *Monolophosaurus*: Zhao and Currie, 1993). Although Osborn (1912:22) suggested that this element "may be an outgrowth of the splenial," it is clearly a separate ossification (or series of ossifications) in *A. altai* and other tyrannosaurids.

In *A. altai* and other theropods, this bone is clearly comprised of two regions: a shallow and elongate supradentary portion that covers the interdental plates medially (fig. 41, sd), and a smaller, triangular coronoid region that articulates with the anterodorsal margin of the surangular, posterior to the intramandibular joint (fig. 41, cor). These regions are indistinguishably fused to each other, identical to the condition in other well preserved tyrannosaurid specimens (Brochu, 2003; Currie, 2003a).

Only the right supradentary/coronoid is preserved in *A. altai*, but it is essentially complete, and measures 380 mm long anteroposteriorly. It is broken slightly anteriorly, in the region of alveoli 1-3; this missing region overlapped the anterior portion of the right dentary that is also eroded. Based on comparison to the more complete left dentary, it is likely that approximately 30 mm of the supradentary/coronoid is missing. Thus, the element would have been approximately 410 mm long in life.

The supradentary/coronoid of *A. altai* is extremely thin, shallow, and long. It is 6 mm deep dorsoventrally at its broken anterior margin, then expands in depth to 11 mm at the level of alveolus 6, keeps a relatively constant depth until the region of alveolus 13, then steadily decreases to 6 mm at the level of the last alveolus. Here the bone deepens again, to 9 mm in depth, as it covers the depressed region of the dentary immediately posterior to the alveolar row. From this point it tapers again to a depth of 5 mm before expanding into the triangular coronoid, which achieves a maximum depth of 20 mm and a mediolateral thickness of 1.5 mm.

The dorsal margin of the supradentary/coronoid is gently concave along the entire supradentary region, where it medially covers the tooth row. Posterior to the tooth row the dorsal margin is convex where the bone overlaps the dentary behind the tooth row (fig. 41, deno) and extends across the interlocking dentary-surangular articulation. Posterior to this convexity the dorsal margin of the triangular coronoid region is gently concave, as is also the case in other tyrannosaurids (e.g., Osborn, 1912: fig. 18; Brochu, 2003: fig. 40; Hurum and Sabath, 2003: fig. 20). However, although concave, the dorsal margin of the triangle is much straighter than in *Tyrannosaurus*, in which the dorsal edge is described as "boomerang shaped" (Brochu, 2003: 43).

The ventral margin of the supradentary/coronoid is mostly convex, but becomes concave posteriorly at the level of the dentary-surangular articulation. This concavity continues posteriorly and terminates at the ventral, rounded point of the coronoid triangle. The point of the triangle separates the anterior concavity, which forms the anteroventral edge of the coronoid, from another, more posterior concave region, which forms the posteroventral margin of the bone. The anteroventral margin of the triangle contacts the prearticular across an elongate butt joint, but it is not thickened or rugose. Thus, the two bones simply butted against each other as thin

plates. The entire ventral margin of the coronoid is broken in many places, but it is smooth in those areas that are well preserved. It lacks any rugosities or pits, which have been described in *Tyrannosaurus* (Brochu, 2003:43, fig. 40). Moreover, on the ventral margin of the elongate supradentary region there is no separate ventral process as is sometimes present in *Tyrannosaurus*, in which it fits into the anterior notch between the anterior and dorsal processes of the splenial (Brochu, 2003: fig. 40B).

The medial surface of the supradentary/coronoid is flat to slightly convex. It is generally smooth, and matches the texture of the dorsal bar of the dentary (the region above the Meckelian groove), which it sits upon and joins to form a continuous, flat medial surface of the mandible. Behind the tooth row, the medial surface is excavated by a smooth fossa in the region where the supradentary flares upwards as it covers the dentary-surangular articulation (fig. 41, fos). This fossa faces medially and slightly dorsally. The medial surface of the coronoid region is flat, not rugose as in *Tyrannosaurus* (Brochu, 2003: fig. 40). Moreover, there are no signs of any foramina piercing the supradentary/coronoid as in *Tyrannosaurus* (Brochu, 2003: fig. 41).

The lateral surface of the supradentary/coronoid has a "wavy," undulating texture, which is also present in other tyrannosaurids (e.g., Hurum and Sabath, 2003: fig. 20). This is the result of discrete and alternating convexities and concavities; the convexities form the medial wall of the alveoli above the interdental plates and the concavities fit against the septa that separate the alveoli. Both the concavities and the convexities are more pronounced dorsally, where they played a greater role in forming the medial wall of the alveoli above the interdental plates. Thus, when the mandible is observed in dorsal view, the supradentary/coronoid, and not the interdental plates, is seen to form the main component of the medial wall of the tooth row.

In cross section the supradentary/coronoid is ovoid. The bone widens posteriorly: it is plate-like anteriorly, with a mediolateral thickness of 1 mm, and achieves a maximum thickness of 3 mm in the region covering the posteriormost three dentary teeth, which are among the smallest in the jaw. Behind this point it thins again into the coronoid plate. The lateral surface is more convex than the medial surface, making the bone somewhat of a D-shaped oval in cross section. The coronoid triangle region is extremely flat and thin for its entire length, and is not thickened in certain areas as in *Tyrannosaurus* (Brochu, 2003).

The supradentary/coronoid is overlapped medially by the splenial, immediately posterior to the tooth row. Here the supradentary/coronoid is concave medially, and in dorsal view it can be seen that this region fits against a lateral concavity of the splenial. This is the "bottleneck" region between the dentary, splenial, and supradentary/coronoid described by Brochu (2003:44). A nearly identical concavity on the supradentary/coronoid is seen in *Daspletosaurus* (Currie, 2003a: fig. 35), but this contact surface is longer in the basal theropod *Majungasaurus* (Sampson and Witmer, 2007: fig. 27).

The coronoid region laterally contacts the surangular. As discussed above, there is a deep, triangular facet in the medial surface of the anterodorsal corner of the surangular, but although this facet matches the shape of the coronoid it is far too deep for the two to fit together strongly.

The supradentary/coronoid of *Tyrannosaurus* is much deeper anteriorly than the corresponding bone in *A. altai*. Furthermore, the ventral margin of the anterior portion of the supradentary region is highly convex in *Tyrannosaurus*, whereas it is only slightly convex in *A. altai* (Osborn, 1912: fig. 18; Brochu, 2003: fig. 40). These differences are associated with the larger, deeper interdental plates of *Tyrannosaurus*, which form an arcuate arcade, and thus necessitate a deeper and more ventrally convex supradentary to cover them. In other words, the

supradentary of *Tyrannosaurus* is "U shaped" (Brochu, 2003:43). An identical morphology is seen in adult *Tarbosaurus* (Hurum and Currie, 2000: fig. 1), in which it is described as a "stretched crescent" with a "ventral edge (that is) more curved than the dorsal edge" (Hurum and Sabath, 2003:185). The condition in *A. altai* is more similar to that seen in basal theropods (*Allosaurus*: Madsen, 1976: p. 9C; *Majungasaurus*: Sampson and Witmer, 2007: fig. 27; *Monolophosaurus*: Zhao and Currie, 1993: fig. 2), in which the supradentary region is a "strip of bone" (Hurum and Sabath, 2003:185). A "strip-like" condition is also seen in juvenile *Tarbosaurus* (Currie and Dong, 2001a: fig. 1) and *Daspletosaurus* (Currie, 2003a: fig. 35). Moreover, in *A. altai*, *Daspletosaurus*, and basal theropods there is no notch on the dorsal margin between the supradentary and coronoid regions. This notch is present in *Tarbosaurus* and *Tyrannosaurus* (Hurum and Sabath, 2003: fig. 20).

Hyoid: Two hyoid bones were found with the specimen (fig. 42). These bones are sinuous in outline and nearly equal in size, with the more complete one measuring approximately 200 mm along its curved surface. The shaft is smooth and each end is slightly expanded and rugose; one end is marked by a small, flattened, lineated surface where additional components of the hyoid apparatus (perhaps cartilaginous) would have articulated. The hyoid of *A. altai* is similar to those of other tyrannosauroids in general shape, degree of curvature, and proportions (*Gorgosaurus*: AMNH FARB 564; *Proceratosaurus*: Rauhut et al., 2010; juvenile *Tyrannosaurus*: Gilmore, 1946). Hyoid bones are unknown, or undescribed, for other tyrannosauroids. Similar hyoids are also present in other basal coelurosaurs (e.g., *Pelecanimimus*: Perez-Moreno et al., 1994; *Sinornithomimus*: Kobayashi and Lu, 2003) and more basal theropods (e.g., *Coelophysis*:

Colbert, 1989; *Syntarsus*: Rowe, 1989; *Zupaysaurus*: Ezcurra, 2007), indicating that hyoid morphology is conservative among theropod dinosaurs.

Dentition: Several erupted teeth are preserved in situ in the maxillae and dentaries, and several disarticulated lateral teeth were found associated with the cranial bones (figs. 43-44). Unfortunately, no premaxillary teeth (nor premaxillae) are known. All lateral teeth are transversely narrow, recurved, and serrated, similar to those of most other theropods, including basal tyrannosauroids (e.g., Xu et al., 2004, 2006). Teeth from the middle of the maxillary and dentary tooth rows are approximately 2.5-3.5 times longer mesiodistally than thick labiolingually (Table 5). In contrast, the equivalent teeth of other tyrannosaurids are relatively thicker (the "incrassate" condition). *Albertosaurus*, *Daspletosaurus*, and *Gorgosaurus* have teeth that are approximately 1.67 times longer than thick (Currie 2003a), whereas *Tarbosaurus* and *Tyrannosaurus* have even more robust teeth that are nearly as thick as long (Brochu, 2003; Hurum and Sabath, 2003; Brusatte et al., 2010a). *Alioramus*, therefore, is anomalous among tyrannosaurids in possessing thin teeth, more reminiscent of the basal tyrannosauroid condition. However, the teeth of *Albertosaurus* and *Tyrannosaurus* are known to increase in thickness during ontogeny (Carr, 1999; Carr and Williamson, 2004), so it is unclear whether the thin teeth of the *A. altai* holotype are truly aberrant or simply reflect its young age, or both.

The maxillary teeth are best preserved on the left maxilla, which houses a nearly complete series. The first two preserved teeth are somewhat incisiform, as they are thinner mesiodistally than the teeth that follow. The largest teeth (i.e., those that are longest mesiodistally) lie immediately posterior to the incisform anterior teeth, and further posteriorly the teeth become smaller and more strongly recurved posteriorly. The denticles are chisel-

shaped, unilobate, and continuous over the apex of the tooth. Those on the distal carina extend closer to the tooth base than those on the mesial carina, but the denticles of both carinae are approximately the same size on all teeth (15 denticles/5 mm on the mesial carina and 14/5 mm on the distal carina of the fifth tooth, which is the best preserved exemplar; measurements taken at middle of carina). The carinae are not symmetrically placed on the anterior incisiform teeth, but rather the mesial carina is deflected lingually and the distal carina labially. The mesial carina migrates to the center of the mesial surface of the tooth on the crowns at the center of the tooth row, but the distal carina remains in a labial postion. Far posteriorly, on the final six preserved teeth, the distal carina is centered, and thus the two carinae are symmetrical.

Interdenticular sulci (sensu Smith, 2007; 'blood grooves' of Currie et al., 1990) are present between the denticles of both carinae, extend a short distance onto the labial surfaces of the tooth, and are essentially horizontal (but with a subtle inclination towards the tooth base). Subtle, band-like enamel wrinkles are present on the labial and lingual tooth surfaces, which extend between the mesial and distal carinae as apically concave curves of equal relief over their mesiodistal length. These are widespread among tetanuran theropods, including tyrannosaurids (Brusatte et al., 2007). Where the tooth roots are exposed, the labial and lingual surfaces are depressed, giving the impression of a groove. Such grooves were recently mistaken as adaptations for a venomous delivery system in a dromaeosaurid (Gong et al., 2010), but are widespread among theropods and almost uniformly present whenever a tooth root is exposed (Gianechini et al., 2011).

The dentary teeth are extremely similar to the maxillary teeth in overall morphology and size (Table 5). Their denticles are also continuous over the apex, the distal carina extends further basally than the mesial carina, and subtle enamel wrinkles and grooves on the exposed roots are

present. The individual denticles are approximately the same size as in the maxillary teeth, although the discrepancy between the mesial (16/5 mm) and distal (14/5 mm) denticles on the best exemplar tooth (that in alveolus 7) is slightly more marked. Furthermore, the denticles slightly decrease in size toward the tooth base and apex, more so than in the maxillary teeth.

Cervical Vertebrae General: Nearly the entire cervical column is preserved in *A. altai*. The atlas is represented by the intercentrum and both neurapophyses (fig. 45), the axis is well preserved (fig. 46), and nine postaxial cervicals are represented (figs. 47-54). Only the odontoid and axial intercentrum are missing. Measurements for all cervicals are given in table 9.

Atlas: The atlas intercentrum is a small, crescentic element that is wider mediolaterally (40 mm) than tall dorsoventrally (20 mm at the midpoint) (fig. 45A-B). The anterior surface is strongly concave to articulate with the occipital condyle (fig. 45A, oc). In anterior view this surface is reniform in shape, with a concavity at the midpoint of the dorsal margin that would have received the odontoid (atlantal centrum) (fig. 45, od). The concave surface for the condyle faces both anteriorly and dorsally: in dorsal view the ventral margin of the intercentrum is seen to extend forward as a lip of bone, which would have underlain the occipital condyle and strengthened the articulation (fig. 45, lip).

The dorsolateral corners of the intercentrum are raised into small pedicels to articulate with the neurapophyses (fig. 45, np). The articular surfaces are eroded but clearly face dorsally and laterally. The dorsal margin of the intercentrum is smooth for articulation with the odontoid, and the ventral surface is smooth as well. On the right side the ventral surface is pierced by a circular foramen (1.5 mm diameter), and the broken margin of a similar foramen appears to be

present on the left side. The foramen is surrounded by a broad but shallow fossa, which is bordered anteriorly by a slight bulge. This bulge represents part of the anterior margin of the ventral surface, which is swollen and placed further ventrally relative to the posterior region. The posterior surface of the intercentrum is eroded but appears to have been slightly convex to articulate with the axial intercentrum. The left side is excavated by a circular concavity which appears to be a real surface, but this is not present on the right side. It may represent an attachment surface for the axial intercentrum (fig. 45, axic).

The shape of the intercentrum is similar to that in *Guanlong* (IVPP V14531), *Tarbosaurus* (Maleev, 1974: fig. 21) and *Tyrannosaurus* (Brochu, 2003: fig. 47), as well as other theropods (e.g., *Ceratosaurus*: Madsen and Welles, 2000: pl. 14D; *Dilophosaurus*: Welles, 1984: fig. 8; *Orkoraptor*: Novas et al., 2008: fig. 5; *Sinraptor*: Currie and Zhao, 1993: fig. 12; *Torvosaurus*: Britt, 1991: fig. 7C). Thus, this element appears to be conservative across theropod phylogeny.

Both left and right neurapophyses are present (fig. 45C-E). The right element is well preserved and uncrushed, but the left bone is crushed anteroposteriorly. This crushing has flattened the anterior surface, which is curved in life, thus making the left element appear larger than it was in life. The neurapophysis is triradiate. The ventral base is a pedicle for articulation with the atlas intercentrum and occipital condyle (fig. 45, vpr). Dorsally the neurapophysis bifurcates into two additional processes: a spike-like epipophysis laterally (fig. 45, epi) and a thin medial process (fig. 45, mpr) (terminology from O'Connor 2007).

The articular surface on the ventral pedicle is well preserved. It is teardrop shaped, with a 25 mm long axis and a 10 mm perpendicular axis. Two separate articular surfaces are visible, one for the atlas intercentrum laterally (fig. 45, atic) and the other for the occipital condyle

medially (fig. 45C, E, oc). The former contact is larger, more circular, and faces ventrally and medially when the atlantal elements are in articulation, whereas the contact surface for the occipital condyle is more ovoid and faces mostly anteriorly and slightly medially. These two surfaces are divided by a subtle ridge (fig. 45, arid). The pedicle itself continues dorsolaterally for a short distance before giving rise to the two additional processes.

The laterally placed epipophysis is a long, thin, spike-like process placed lateral to the postzygapophyseal facet (fig. 45, epi). A ridge continues from the lateral margin of the epipophysis onto the anterior surface of the neurapophysis pedicle, where it thins out (fig. 45, rid). The medial process is a thin, anteriorly convex, curved plate (fig. 45, mpr). The margin connecting the epipophysis and medial process is complex in shape: there are two concave regions, separated by a midline bulge when seen in dorsal view (fig. 45, bul). This bulge represents the posterior extent of the postzygapophysis (fig. 45, posz). The concave region between the epipophysis and postzygapophysis is thicker and more robust than the region between the zygapophysis and the medial process. This former region is marked by a posterodorsally facing fossa, which is thin and elongate (fig. 45, fos).

The lateral surface of the neurapophysis is generally smooth, especially the plate-like medial process. However, there are some ventromedially trending lineations on the lateral side of the pedicle (fig. 45, lin). Medially the pedicle is gently concave, and its lateral margin is raised as a rim (fig. 45, rim). The dorsal margin of the neurapophysis, or that region between the epipophysis and the medial process, overhangs the pedicle as a web of bone. At the midpoint of this web lies the postzygapophysis, which is a flat and ovoid (12 mm anteroposteriorly by 10 mm mediolaterally) articular surface, which faces almost entirely ventrally and only slightly laterally (fig. 45, posz). It is possible that the left and right medial processes (the “tecta” of Brochu 2003)

met at the midline medial to the postzygapophysis, as has been described in *Tyrannosaurus*, but they were clearly not fused and there is no obvious articular surface on either process.

The neurapophyses of *A. altai* are similar to those described in *Tarbosaurus* (Maleev, 1974: fig. 21) and *Tyrannosaurus* (Brochu, 2003: fig. 47). However, the epipophysis of *A. altai* is a thin spike that ends at a point, whereas those of *Tarbosaurus* and *Tyrannosaurus* are larger, blunter processes that terminate in a rounded knob. The epipophysis also is thicker and ends in a knob in other theropods (e.g., *Allosaurus*: Madsen, 1976: pl. 11I, J; *Sinraptor*: Currie and Zhao, 1993: fig. 12D; *Torvosaurus*: Britt, 1991: fig. 7C). In the abelisaurid *Majungasaurus* the epipophysis ends in a point as in *A. altai*, but its base is much thicker (O'Connor, 2007: fig. 5). Thus, a thin, spike-like epipophysis that ends at a sharp point is considered an autapomorphy of *A. altai* among theropods. However, as few theropod neurapophyses are known, this character may have a wider distribution.

One further difference is notable: the neurapophysis of *Tarbosaurus* (Maleev, 1974: fig. 21) is best described as having four processes, as there is an additional projection that trends medially from the ventromedial corner of the pedicle. This is not present in *A. altai* or *Tyrannosaurus* (Brochu, 2003), as well as most other theropods (*Allosaurus*, *Sinraptor*, *Torvosaurus*). However, a small process is present in this region in *Majungasaurus*, and referred to as the "uncinate process" by O'Connor (2007).

Left and right neurapophyses are appressed to the axis on the holotype skull block of *Dilong* (IVPP V14243). They are triangular, with no obvious processes, and thus are simpler in form than those of *A. altai* and other tyrannosaurids. Because outgroup taxa also possess several processes on the neuropophysis (e.g., Madsen, 1976; Norell et al., 2006; Peyer, 2006), the simple triangular morphology is likely an autapomorphy of *Dilong*.

Axis: Only the axial centrum and neural arch are known, but these elements are well preserved (together they are herein referred to as the "axis") (fig. 46). The axis is crushed, however, and the centrum is rotated somewhat to the left relative to the neural arch. Fragments of the odontoid and axial intercentrum appear to be appressed to the anterior articular surface of the axis, poor presevation dissallows any other observations.The centrum and neural arch appear to be fused and no suture is clearly visible. However, this could be an artifact of erosion, and the postmortem rotation of the two elements relative to each other suggests that their line of fusion may have been weak or partially opened.

The centrum is short anteroposteriorly but still longer than the height of either articular surface (Table 9). This is usually the case in theropods generally (e.g., *Garudimimus*: Kobayashi and Barsbold, 2004: fig. 6), as well as *Dilong* (IVPP V14243) and juvenile *Tarbosaurus* (Currie and Dong, 2001a). However, in *Daspletosaurus* (AMNH FARB 5468), adult *Tarbosaurus* (Maleev, 1974: fig. 21), and *Tyrannosaurus* (Brochu, 2003) the axis is extremely short anteroposteriorly. In *A. altai* the two articular faces extend to the same level ventrally, unlike the morphology of the postaxial cervicals in which the anterior articular face is offset dorsally. This is also seen in *Daspletosaurus*, *Dilong*, *Tarbosaurus* and *Tyrannosaurus* (Maleev, 1974, Brochu, 2003).

The lateral surface of the centrum is mostly eroded on both sides, but on the right side it is clearly penetrated by a pneumatic foramen (pleurocoel) (fig. 46, pf). This opening is ovoid, with a six mm long axis, and is located slightly anterior to the midpoint of the centrum. It is a single structure, not bifurcated as is sometimes the case in *Tyrannosaurus* (Brochu, 2003), and is not surrounded by a broad fossa. In contrast, the pneumatic foramen in *Tyrannosaurus* is usually

centered within a deep fossa and is more dorsal in position, as it is located immediately posterior to the diapophysis and at or near the neurocentral suture (Brochu, 2003: fig. 71A). The *Tyrannosaurus* condition is also seen in adult *Tarbosaurus* (e.g., ZPAL MgD/I-09). In juvenile *Tarbosaurus* the foramina are more circular (as is also the case in *Daspletosaurus*: AMNH FARB 5468) and the number of pneumatic foramina is variable on the left and right sides of single elements (Currie and Dong, 2001a). However, the foramina of *Daspletosaurus* and juvenile *Tarbosaurus* are located further ventrally in a position similar to that in *A. altai*. The axial pneumatic foramen of *A. altai* is different in morphology than those of the postaxial cervicals: it is more ovoid and less slit like, and is located further posteriorly near midlength of the centrum instead of immediately posterior to the parapophysis.

The ventral surface of the centrum is marked by a strong keel extending across the entire length of the element (fig. 46, vk). *Daspletosaurus* (AMNH FARB 5468), *Dilong* (IVPP V14243), and juvenile *Tarbosaurus* (Currie and Dong 2001a) lack a keel, but this structure is present in many basal theropods, although often variable within groups (e.g., Brusatte and Sereno, 2008). A keel is also present in *Tarbosaurus* (ZPAL MgD/I-09) and *Tyrannosaurus* (Brochu, 2003). Details of the anterior articular face cannot be observed due to erosion and the appressed fragments of the odontoid and intercentrum. However, the posterior surface is widely visible and is strongly concave. It is deeper dorsoventrally than wide mediolaterally, as is also the case in *Daspletosaurus* (AMNH FARB 5468), *Dilong* (IVPP V14243), *Tyrannosaurus* (Brochu, 2003: fig. 49A), and juvenile *Tarbosaurus* (Currie and Dong, 2001a: fig 2C). The parapophysis is not well preserved on either side of the centrum.

The neural arch is nearly complete. In lateral view the neural spine is triangular, with a vertical posterior margin and an anterior edge that slopes strongly anteroventrally-

posterodorsally. The anterior surface of the spine is marked by a prominent ridge (fig. 46, arid), which extends from the dorsal tip of the spine ventrally to the rim overhanging the neural canal (fig. 46, ncrim). The ridge is likely for the attachment of splenius capitis musculature (Brochu, 2003), and also defines smooth surfaces on both sides of the neural arch. Additionally, weak ridges extend ventrally and medially from the lateral edges of the dorsal margin of the neural spine (fig. 46, lrid), dividing each lateral fossa into two regions. These regions are barely distinguishable, but on the left side the lateral region is apparently excavated by a deep fossa. This fossa is not present on the right side, and its presence on the left side is likely an artifact of crushing. The regions lateral to the central ridge, which face primarily dorsally but also laterally, are smooth externally. In contrast, in *Tyrannosaurus* and *Tarbosaurus* they are deeply excavated by a discrete pneumatic recess, termed the lateral axial pneumatic chamber (Brochu, 2003: figs. 48, 50, 51; ZPAL MgD-I/09). Some pneumaticity appears to be present in *Daspletosaurus* (AMNH FARB 5468), but poor preservation obscures additional details. The axial neural spines of *Dilong* (IVPP V14243), *Raptorex* (LH PV18), and *Xiongguanlong* (FRDC-GS JB16-2-1) show no external signs of pneumaticity, nor do outgroup taxa (e.g., Madsen, 1976; Norell et al., 2006).

Dorsally the neural spine is somewhat thickened, but it is not as rugose as in *Daspletosaurus* (AMNH FARB 5468), *Tarbosaurus* (ZPAL MgD-I/09), or *Tyrannosaurus* (Brochu 2003: figs. 50, 51). In anterior view the dorsal region of the spine is seen to extend mediolaterally into a "crown" region (fig. 46, cr). On both lateral sides of the crown are rounded projections that extend dorsally and laterally (fig. 46, lp). The margin between these projections is a smooth, concave surface, and there is no third projection on the midline (aside from perhaps a very subtle bulge). Only two projections are present in *Raptorex* (Sereno et al., 2009) and

Xiongguanlong (FRDC-GS JB16-2-1), whereas three projections are present in *Daspletosaurus* (AMNH FARB 5468) and *Dilong* (IVPP V14243). *Tyrannosaurus* exhibits a subtle midline projection, but this is extremely small in comparison to the lateral processes (Brochu, 2003). Thus, the condition in *Tyrannosaurus* is more similar to that of *A. altai* than that of *Daspletosaurus*. In *A. altai* the left projection is broken, but it appears to have been positioned slightly lower than the right process. This is opposite the condition described in one specimen of *Tyrannosaurus*, which was ascribed to crushing, and differs from the more symmetrical arrangement found in most other theropods (Brochu, 2003). Thus, it is likely that this is an artifact of crushing and erosion.

The prezygapophysis is best preserved on the right side (fig. 46, prez). Here, it is present simply as a circular, flat surface at the anteroventral corner of the neural arch. It faces laterally and dorsally, and is not set off on a pedicle. Although the anteroventral corner of the prezygapophysis is broken, it appears to have a more circular shape than the atlantal postzygapophysis.

Immediately posterior to the prezygapophysis is a small, spherical mound-like structure representing the diapophysis (fig. 46, diap). The two are separated by a short (3.5 mm long anteroposteriorly) concave notch. The articular surface of the diapophysis is abraded and eroded, but appears to have been a simple convex bulge, and may have been nonarticular as described in *Tyrannosaurus* (Brochu, 2003). A similar reduced diapophysis is also present in *Daspletosaurus* (AMNH FARB 5468), *Dilong* (IVPP V14243), *Raptorex* (Sereno et al., 2009), juvenile (Currie and Dong, 2001a) and adult (ZPAL MgD-I/09) *Tarbosaurus*, and *Xiongguanlong* (FRDC-GS JB16-2-1).

No clear laminae link the diapophysis and the centrum ventrally. However, a robust lamina sweeps dorsally and posteriorly from the diapophysis to join the postzygapophysis. This strut, the postzygapodiapophyseal lamina, is a broad, sweeping concave edge in anterior view (fig. 46, pzdl). Ventral to the lamina and posterodorsal to the diapophysis is a deep and elongate fossa (fig. 46, sdf). This has been termed the supradiapohyseal fossa by Brochu (2003) and is also present in other tyrannosaurids. It has a similar form in *Daspletosaurus* (AMNH FARB 5468), but in *Tyrannosaurus* the fossa is deeper and more triangular (Brochu, 2003: fig. 51) and in *Dilong* it is triangular but shallow (IVPP V14243). At its dorsal termination, immediately underneath the postzygapophysis, the fossa is separated from an elongate, ovoid foramen that faces primarily posteriorly (fig. 46B, for). This foramen is absent in *Daspletosaurus* (AMNH FARB 5468) and does not appear to be present in *Tyrannosaurus* (Brochu, 2003); it may be an autapomorphy of *A. altai*.

Both postzygapophyses are present (fig. 46, posz), but the left process is obscured by a fragment of the prezygapophysis of the third cervical that remains preserved in articulation (fig. 46, pre3c). The right postzygapophysis, however, is well preserved. Its articular surface is flat, circular, and faces mostly ventrally, but also posteriorly and laterally. In posterior view an intrapostzygapophyseal lamina sweeps ventrally to join a corresponding lamina from the left side (fig. 46, ipdl). Ventral to these laminae is the neural canal, whose size and shape are difficult to describe because of poor preservation, and dorsally is a deep postspinal fossa that continues dorsally up the posterior margin of the neural spine (fig. 46, posf). The entire posterior surface of the neural spine is excavated by the fossa, which is deepest ventrally and becomes less inset dorsally. There is an ovoid bulge at approximately midheight of the fossa (fig. 46, islt). This is likely a tuberosity for the interspinous ligaments, which is more circular and placed further

ventrally in *Tyrannosaurus* (Brochu, 2003: fig. 49A). Ventral to the postspinal fossa there is no hyposphene, as is also the case in *Tyrannosaurus* (Brochu, 2003). In anterior view the region between the neural spine and postzygapophysis, defined by the spinoepipophyseal lamina (Wilson 1999) is a broad, concave edge.

A triangular, peg-like, and robust epipophysis projects dorsally and posteriorly from the dorsal surface of the postzygapophysis (fig. 46, epi). This structure is also prominent in the anterior cervicals but is reduced to a low mound in more posterior cervicals. However, the axial epipophysis of *A. altai* is a small and discrete structure when compared to many other theropods. It is nowhere near as large, robust, and rugose as the axial epipophyses of *Daspletosaurus* (AMNH FARB 5468) and *Tyrannosaurus* (Brochu 2003), which extend far past the postzygapophyses as broad flanges. The latter condition is typical of many basal theropods (e.g., *Acrocanthosaurus*: Harris, 1998; *Allosaurus*: Madsen, 1976; *Baryonyx*: Charig and Milner, 1997; *Ceratosaurus*: Madsen and Welles, 2000; *Majungasaurus*: O'Connor, 2007; *Mapusaurus*: Coria and Currie, 2006; *Sinraptor*: Currie and Zhao, 1993). The basal tyrannosauroids *Eotyrannus* (MIWG 1997.550), *Raptorex* (Sereno et al., 2009), and *Xiongguanlong* (FRDC-GS JB16-2-1) exhibit a similar morphology to *Alioramus altai*, as does the ornithomimosaur *Garudimimus* (Kobayashi and Barsbold, 2005: fig. 6A). *Dilong* also exhibits a similar morphology to *A. altai* and other basal tyrannosauroids, but has a somewhat unique condition in which the epipophysis is reduced to a convex bulb that does not extend past the postzygapophysis posteriorly (IVPP V14243).

Postaxial Cervical Vertebrae: The entire postaxial cervical column is known, although some vertebrae are better preserved than others. Ten cervical vertebrae, including the atlas and axis,

are generally well preserved, and eroded fragments suggest that an 11th cervical was also present (figs. 47-54).

The distinction between cervical, cervicodorsal, and dorsal vertebrae is arbitrary (Brochu, 2003; Brusatte et al., 2008), and different authors have utilized different systems of numbering. However, in *A. altai* these 11 vertebrae clearly share a morphology that is different from not only the three preserved dorsal vertebrae (see below), but also the dorsals of other tyrannosaurids (e.g., Osborn, 1916) and theropods in general (e.g., Brusatte et al., 2008). For instance, all postaxial cervicals are opisthocoelous, have an anterior face that is dorsally offset relative to the posterior face, and possess parapophysis restricted to the centrum. Unfortunately, the dorsal column is not well preserved, so it is impossible to determine if any of the posterior "cervicals" are actually anterior dorsals with transitional morphology, as is often present in theropods (e.g., Brusatte et al., 2008). Thus, all 11 elements are described here as cervicals. It is possible that the neck of *A. altai* was elongate, with additional vertebrae compared to other tyrannosaurids, but such a conclusion is premature and currently unsupportable.

Ten primary cervicals (eight postaxial cervicals) are complete enough to describe and place relative to each other in a numbered cervical series. The fragmentary final cervical is too poorly preserved to describe, but it appears to have an anteroposteriorly short centrum and is most likely an anterior cervical. This element is not discussed further, and since it is unclear where it fits in the series, the remaining vertebrae are described consecutively as cervicals 3-10 (figs. 47-54). This numbering is based on the increasingly greater separation of the diapophyses and parapophyses posteriorly across the column, as described by Brochu (2003) for *Tyrannosaurus*. A gradual separation, caused by the progressive lateral rotation of the transverse process relative to the centrum along the neck, is clearly present in the cervicals of *A. altai*.

In all cervicals of *A. altai* the neural arch and centrum are fused, and where visible the suture between them is completely closed (i.e., the arch and centrum are connected by a continuous surface of bone along their entire contact, but a gutter still marks where the plane of contact once was). The centra are more elongate than in other mature or near-mature tyrannosaurids, in which the anteroposterior length of the centrum is subequal to the depth of the anterior and posterior faces (Holtz, 2004). However, elongate centra are also present in juvenile *Tarbosaurus* (Currie and Dong, 2001a), as well as the basal tyrannosauroids *Dilong* (IVPP V14243), *Eotyrannus* (MIWG 1997.550), *Guanlong* (IVPP V14531), *Raptorex* (Sereno et al., 2009), *Stokesosaurus* (Benson, 2008), and *Xiongguanlong* (Li et al., 2010. The anterior centra are the shortest of the series, and centrum length peaks around the middle of the neck and then decreases posteriorly (Table 9).

The centra are opisthocoelous, with a flat to slightly convex anterior articular surface and a shallowly concave posterior surface. The degree of opisthocoely is subtle compared to the condition in other theropod groups, as is characteristic of tyrannosaurids (Brochu, 2003, Benson, 2008), and in general the degree of opisthocoely decreases posteriorly along the neck, such that the tenth centrum is nearly amphiplatyan. The anterior articular surface is raised relative to the posterior surface as in dinosaurs generally (Benton, 2004; Brusatte et al., 2010c), but unlike the condition in some other large-bodied theropods (e.g., carcharodontosaurids: Sereno et al., 1996; Brusatte and Sereno, 2007). The offset of the anterior face is greatest anteriorly and decreases posteriorly (i.e., is progressively less offset in more posterior cervicals) as in other tyrannosauroids such as *Tyrannosaurus* (Brochu, 2003: fig. 50) and *Guanlong* (IVPP V14531).

The centra are generally well preserved. The parapophyses are located at the anteroventral corner of the lateral surface and project slightly ventrally relative to the centrum

itself in all cervicals but the last two, where they are located at midheight of the anterior articular surface (figs. 47-54, para). Where well preserved the parapophyses are slightly concave and rugose, and are not laterally set off on pedicles. The parapophyses are small and ovoid in the anterior cervicals and become larger and teardrop shaped posteriorly, before becoming small and ovoid again in the posterior cervicals. This is unlike the condition in *Tyrannosaurus*, in which the posterior parapophyses are the largest in the neck (Brochu, 2003: figs. 50, 51).

The lateral surface of the centrum is smooth and is excavated by a deep pneumatic foramen ("pleurocoel") immediately posterodorsal to the parapophysis (figs. 47-54, pf). The foramen is anteroposteriorly elongate and slit-like in all cervicals and is never surrounded by a broad, shallow pneumatic fossa. A fossa appears to be present on the left side of the fourth cervical but this is probably an artifact of crushing. The foramen appears to be nothing more than a thin slit in the fifth and sixth cervicals, but this also may be an artifact of dorsoventral crushing (figs. 49-50). This pneumatic opening is undeformed in the seventh cervical (fig. 51), where it is oval-shaped and longer anteroposteriorly on the right side (21 mm vs. 15 mm on the left). It is also well preserved in the eighth cervical, where it is dorsoventrally deeper, more circular in shape, and less slit-like (fig. 52). Only a single foramen is present in each element and none exhibits a bifurcation like is sometimes present in *Tyrannosaurus* (Brochu, 2003). The foramina of *A. altai* are more ovoid in shape than those of other tyrannosauroids, which are proportionally larger and more circular (*Dilong*: Xu et al., 2004: fig. 1g and IVPP V14243; *Guanlong*: IVPP V14531; *Stokesosaurus*: Benson, 2008: fig. 2; juvenile *Tarbosaurus*: Currie and Dong, 2001a: fig. 3). Additionally, the foramina of *Stokesosaurus* are set within a shallow fossa (Benson, 2008) and those of *Guanlong* (IVPP V14531) are confluent with a posterior fossa that stretches across the lateral surface of the centrum, neither of which is present in *A. altai*.

The ventral surface of the centrum is smooth and nearly flat on cervicals 3-8, with no sign of a midline ridge or groove on any of the cervicals (figs. 47-52). However, a subtle keel is present anteriorly on the ninth cervical (fig. 53) and a sharper, more distinctive keel is present across the entire ventral surface of the tenth cervical (fig. 54, keel). Keels are also present in the posterior cervicals of juvenile *Tarbosaurus* (Currie and Dong, 2001a; IVPP V4878). The base of a hypapophysis appears to be present on the ventral surface anteriorly in the fourth cervical, but this has been completely eroded. There are clearly no pronounced hypaophyses on cervicals five-nine, although the rim of the anterior surface does project somewhat ventrally relative to the remainder of the ventral surface. However, a prominent hypapophyis is present at the anterior terminus of the ventral keel of the tenth cervical (fig. 54, hypa). Hypapophyses are present in the anterior cervicals of *Tyrannosaurus*, but not in all vertebrae posterior to cervical five (Brochu, 2003). In the vicinity of the articular surfaces the ventral surface becomes rounded and rugose. The roughened texture appears to be more pronounced posteriorly, but surface erosion makes comparisons uncertain.

Portions of the neural arch are present on all cervicals and especially well preserved in the more posterior elements (figs. 47-54). However, only the base of the neural spine is present on each vertebra. Based on the shape of the base, the spine was anteroposteriorly longer than mediolaterally wide in the fourth cervical, elongate and extremely thin in the fifth and sixth cervicals, and nearly square shaped in the seventh to tenth cervicals. The neural canal is circular in the fourth cervical, but is heart shaped and nearly equal in size in most of the posterior cervicals. Here it tapers to a rounded point ventrally, where it is constricted by the neural arch pedicles that nearly meet on the midline to cut off the centrum from participating in the neural canal. The dorsal margin is wide and marked by a small U-shaped cleft, defined by converging

laminae (the intrapre- and postzygapophyseal laminae of Wilson [1999]) that extend medially from the anteromedial margin of each zygapophysis. The cleft is especially prominent in anterior view in cervical seven (fig. 51, iprdl).

The prezygapophyses are large flanges that reach past the centrum anteriorly (figs. 47-54, prez). They are widely placed relative to the midline of the vertebra, such that their lateral edges extend past the lateral edge of the centrum by approximately 15 mm. The articular surfaces become smaller and more circular posteriorly until cervical eight, at which point they become larger and more ovoid. The long axis of the articular surface is oriented anterolaterally in all cervicals but the tenth; here the long axis trends mediolaterally. The articular surfaces are flat in *A. altai* as in most other tyrannosauroids (Brochu, 2003; AMNH FARB 5468; IVPP V14531; IVPP V4878, contra Currie and Dong, 2001a), but they are convex in *Stokesosaurus* (Benson, 2008) and many other coleurosaurs (Rauhut, 2003a).

The articular surfaces are often described as "dorsally oriented" (e.g., Holtz, 2004:121) in tyrannosaurids, which differs from the more anteriorly oriented facets in many other coelurosaurs. However, in *A. altai* and other tyrannosaurids (e.g., AMNH FARB 5468, IVPP V4878) the articular surfaces, although facing primary dorsally, actually face slightly medially and anteriorly. In particular, the prezygapophyses of the fourth cervical face strongly anteriorly (fig. 48). In *A. altai* the articular surfaces progressively face more dorsally as they continue posteriorly, such that they are oriented nearly entirely dorsally in the seventh cervical. This is probably associated with the progressive reduction of the offset of the anterior articular surface relative to the posterior surface across the neck. However, posterior to the seventh cervical the flanges progressively become oriented more medially, such that the articular surfaces of the tenth cervical face more strongly medially than dorsally.

A wide neck of bone connects the articular surface of the prezygapophysis, which is offset relative to the neck itself, to the base of the neural spine. This is the spinoprezygapophyseal lamina (figs. 47-54, sprel), and it becomes thinner, sharper, and shaped more like a proper lamina (rather than a wide neck) as it continues medially and dorsally from each prezygapophysis. The left and right laminae demarcate the anterolateral edges of the prespinal fossa, a large midline fossa located above the neural canal (figs. 47-54, pref). It is unknown whether the fossa dorsally continues up the anterior surface of the neural spine, but the preserved region is large and ovoid. It becomes larger and deeper dorsoventrally posteriorly across the cervicals. The fossa is defined ventrally by the intraprezygapophyseal laminae (see above) (figs. 47-54, iprdl). These form a thin web of bone that projects far anteriorly in cervical six, thus giving the fossa an elongate floor and making it widely visible in dorsal view (fig. 50). This condition is not present in the seventh cervical, or any other cervicals, but it often may be obscured by matrix and erosion.

In anterior view, an additional thin lamina continues medially and ventrally from the anteromedial corner of the prezygapophysis (figs. 51-52, accl). It essentially parallels the intraprezygapophyseal lamina, but the two are separated by 15 mm. The accessory lamina is strongest on the seventh and eighth cervicals, and does not appear to be present as a discrete structure on the fourth, fifth, and sixth cervicals. In the seventh and eighth cervicals it serves to define two additional shallow fossae: one dorsomedial to the lamina and the second ventrolateral to it (figs. 51-52, dmf, vlf). The ventrolateral fossa is larger and ovoid, and is pierced by an ovoid foramen (2-3 mm long axis). Both fossae end abruptly against the medial edge of the neural arch pedicels, which define the lateral margins of the neural canal.

The prezygapophysis and the diapophysis are linked by a prezygapodiapophyseal lamina (figs. 47-54, predl). This strut forms the lateral margin of a deep, anteriorly-facing pneumatic pocket on the anterior surface of the transverse process, which is visible on each cervical (figs. 47-54, atvpfos). This excavation is a true pocket in most cervicals, but in the tenth cervical it is expressed as a fossa that does not appear to deeply penetrate into the bone. This excavation is not present in other tyrannosaurids (e.g., Maleev, 1974, Brochu, 2003, IVPP V4878), and is considered autapomorphic of *A. altai*. A small, subsidiary pocket or fossa is present medioventral to the main excavation. Furthermore, there are rugose regions extending laterally and ventrally on the proximal part of the prezygapophysis neck. These structures are described as hypantra by Brochu (2003), but it is not clear that they formed articular structures in *A. altai*.

The postzygapophyses are generally poorly preserved (figs. 47-54, posz). The bases of the postzygapophyses are present in all cervicals but complete pairs are only known from the eighth and ninth cervical. Additionally, the left postzygapophysis of the third cervical and the right process of the sixth cervical are also preserved. The articular surface is flat and ovoid in shape, with a posterolaterally oriented long axis. The long axis of the postzygapophysis of the eighth cervical, however, is more mediolaterally oriented, in concert with the mediolateral prezygapophysis of the tenth cervical. The articular surface faces primarily ventrally and only slightly laterally, but it is difficult to identify clear trends along the neck because of the scarcity of preserved postzygapophyses.

In dorsal view the postzygapophysis blends smoothly into a neck of bone linking it to the neural spine: the spinopostzygapophyseal lamina (figs. 47-54, sposl). This differs from the morphology of the prezygapophyses, which expand relative to the spinoprezygapophyseal lamina and thus form discrete, tab-like structures. The dorsal surface of the postzygapophysis is

mostly flat, but the medial margin is raised as a slight lip, which represents the posterior base of the spinopostzygapophyseal lamina. Furthermore, the midpoint of the lateral margin is marked by an epipophysis (figs. 47-54, epi), which is confluent anteriorly with a thick lamina that extends anteriorly in a parasagittal plane and terminates at the prezygapophysis (the epipophyseal-prezygapophyseal lamina of Wilson [1999]). The epipophysis is a pronounced, peg-like process on the third cervical, but is reduced to a low, mound-like bulge posteriorly (on the sixth, eighth, and ninth cervicals). The epipophyseal-prezygapophyseal lamina (figs. 47-54, epl) is most prounounced on the sixth cervical, and appears to be absent or highly modified in the eighth and ninth cervicals.

Also in dorsal view, the postzygapophyses are widely placed relative to the midline and extend slightly lateral to the prezygapophyses. The region of the neural arch between the pre- and postzygapophysis is excavated by a shallow triangular fossa, which is widely visible in dorsal view (figs. 47-54, dorsfos). The fossa faces dorsally and laterally and terminates at the broken surface of the base of the neural spine, suggesting that it may have continued dorsally up the lateral surface of the spine. The anterior and posterior margins of the fossa are formed by the respective spinozygapophyseal laminae and the ventral margin is formed by the epipophyseal-prezygapophyseal lamina.

The postzygapophysis and diapophysis are connected by a lamina, the postzygapodiapophyseal lamina (figs. 47-54, posdl) (Wilson 1999). This lamina, along with the prezygapopdiapophyseal lamina, defines a separate smooth fossa on the dorsal surface of the transverse process (figs. 47-54, dtvpfos). This excavation is located ventral to the triangular fossa defined above, and is the smaller of the two excavations. The dorsal border of the ventral fossa, and the region that separates it from the more dorsal fossa, is the epipophyseal-prezygapophyseal

lamina. This fossa is most visible on the sixth cervical (fig. 50), is not present on the fourth cervical (since the transverse process is small and not laterally oriented), and is small on the eighth and ninth vertebrae.

On the posterior surface of the cervicals there is a postspinal fossa medial to the postzygapophysis (figs. 47-54, posf) and an infrapostzygapophyseal fossa on the posterior surface of the neural arch pedicels. This latter fossa is circular, deeper than the corresponding infraprezygapophyseal fossa on the anterior surface of the vertebra, and is not subdivided into seprate regions as is the infraprezygapophyseal fossa of the seventh and eighth cervicals (see above). The fossa is penetrated by a pneumatic foramen on the right side of the sixth and ninth cervicals, but foramina are not visible on either side on the well preserved eighth cervical.

The diapophyses are located at the lateral end of a short transverse process, whose inclination changes across the three cervicals as described above (figs. 47-54, diap, tvp). The diapophysis itself is a convex surface that is ovoid to nearly circular in shape, although erosion makes it difficult to identify trends in size and shape across the vertebrae. There are no separate, discrete laminae linking the diapophysis with the parapophysis or centrum anteriorly. However, there is a thick lamina that connects the diapophysis and the centrum posteriorly. This strut, the posterior centrodiapophyseal lamina (Wilson 1999), extends from the posteroventral corner of the diapophysis to the posterodorsal corner of the centrum (figs. 47-54, pcdl). It is present and robust across the entire cervical series.

The posterior centrodiapophyseal lamina is web-like and strongly overhangs a deep, triangular fossa on the lateral surface of the neural arch and centrum (figs. 47-54, pcdlfv). This opening has been referred to as “the pneumatic fossa” in *Tyrannosaurus* (Brochu, 2003:63), but is only one of several pneumatic features on the cervicals of *A. altai*. It is present in other

tyrannosaurids, but is often smaller and shallower (e.g., *Daspletosaurus*: AMNH FARB 5468), usually in concert with a much reduced posterior centrodiapophyseal lamina. Although the lamina of *A*. *altai* is extremely pronounced for a tyrannosaurid, the more general pattern in tyrannosauroid phylogeny is that tyrannosaurids (e.g., *Alioramus*; *Daspletosaurus*; *Tarbosaurus*: Maleev, 1974: fig. 22; *Tyrannosaurus*: Brochu, 2003: fig. 50-51) have thick and laterally-offset lamina, compared to the shorter and weaker structures in basal taxa such as *Dilong* (IVPP V14243), *Eotyrannus* (MIWG 1997.550), *Guanlong* (IVPP V14531), and *Xiongguanlong* (FRDC-GS JB16-2-1). A pneumatic fossa in the same region is figured as a small, more discrete, ovoid excavation in juvenile *Tarbosaurus* (Currie and Dong, 2001a: fig. 3F; IVPP V4878). In *A*. *altai* and juvenile *Tarbosaurus* the fossa is separated from the "pleurocoel" (pneumatic foramen) by a thin osseous web, and the two are distinctive structures. The fossa progressively becomes more widely visible in lateral view in the more posterior cervicals of *A. altai*, corresponding with the dorsally-rotated transverse processes. It is small and not widely visible laterally in the fourth cervical, as it is mostly obscured by the ventrally oriented transverse process.

The fossa is best preserved as a deep, undistorted excavation in the seventh cervical (fig. 51). Here, it is triangular and divisible into three regions. The most ventral region faces entirely laterally and is ovoid, with a posteroventrally oriented long axis. It is located entirely on the centrum and terminates dorsally against the suture with the neural arch. Dorsal to the suture the fossa is divided into two pockets that trend deep into the neural arch dorsally. These are divided by a thin but sharp lamina that extends posterolaterally. The possibility of further laminae is suggested by several thin lineations, which may represent the broken bases of bony struts, which parallel the sharp primary lamina. The same general structure is seen on the well preserved left and right sides of the eighth cervical (fig. 52), but the fossa in the ninth and tenth cervicals is

shallower, with the latter fossa assuming an ovoid shape (figs. 53-54). The discrete pneumatic fossa of juvenile *Tarbosaurus*, described above, corresponds in form and position to one of these dorsal pockets; additional pockets are not present (IVPP V4878; Currie and Dong, 2001a: fig. 3F).

Posterodorsal to the deep fossa is a second highly pneumatic region of the cervical, located on the dorsally and laterally facing surface of the web of bone connecting the diapophysis and centrum (posterior centrodiapophyseal lamina) (figs. 47-54, pcdlfd). This excavation is demarcated ventrally by the posterior centrodiapophyseal lamina, posteriorly by the centropostzygopophyseal lamina, and anteriorly by a raised lamina that projects medially and sightly posterior from the diapophysis and onto the postzygapophysis. This pneumatic fossa is present on all cervicals and is deep across the entire neck. It is best preserved in the seventh cervical, where it is triangular in shape and extends to the anterior margin of the postzygapophysis articular surface (fig. 51). The fossa is deep and divisible into two main regions by a sharp and thin lamina that extends posterodorsally. The anterodorsal pocket is slit-like and more elongate dorsoventrally, whereas the posteroventral one is a shorter triangle. Both pockets appear to penetrate far medially into the neural arch. Pneumaticity in this region is absent in most other tyrannosauroids (*Daspletosaurus*: AMNH FARB 5468; *Dilong*: Xu et al., 2004: fig. 1g and IVPP V14243; *Gorgosaurus*: AMNH FARB 5458, 5664, Lambe, 1917: fig. 14; *Guanlong*: IVPP V14531; *Tarbosaurus*: Maleev, 1974: fig. 22; *Tyrannosaurus*: Brochu, 2003), but is present in juvenile *Tarbosaurus* (IVPP V4878; Currie and Dong 2001a: figs. 3B, C).

Overall, pneumaticity in the cervicals is well developed, and is present on multiple regions of the centrum and neural arch. Pneumatic features include the “pleurocoel” (pneumatic foramen), the deep fossa on the centrum and neural arch below the diapophysis, the fossa on the

neural arch on the web of bone linking the diapophysis and centrum, the autapomorphic deep pocket on the anterior surface of the transverse process, and foramina on the anterior and posterior surfaces of the neural arch pedicels. This degree of pneumaticity is extreme compared to all other tyrannosaurids (e.g., Brochu 2003), but is most similar to the highly pneumatic cervicals of juvenile *Tarbosaurus* (IVPP V4878; Currie and Dong, 2001a).

Dorsal Vertebrae: Parts of three dorsal vertebrae are present (figs. 55-58; measurements in Table 9). These are here referred to with the letters A-C, denoting their sequential location in the dorsal column. The first dorsal, dorsal A, is represented only by the right lateral half of the vertebra, minus the neural arch (fig. 55). This is clearly an anterior dorsal: the transverse process is swung far dorsally, there are distinct and large anterior and posterior centrodiapophyseal laminae, and the parapophysis is shared between the centrum and neural arch, each of which occurs in the anterior dorsals of *Tyrannosaurus* (Brochu, 2003). Dorsal B is a fragmentary piece of the anterior part of the left lateral half of the neural arch, with a small flake of the anterodorsal corner of the centrum (fig. 56). The final dorsal, dorsal C, is essentially complete (figs. 57-58). It is clearly more posterior than dorsal A and likely more so than dorsal B, judging by its slightly thinner anterior centrodiapophyseal lamina. The broken surfaces of these fragments display an internal honeycombed texture, as has also been described for *Tyrannosaurus* (Brochu, 2003).

The centrum and neural arch are fused in all three dorsal vertebrae (i.e., the arch and centrum are firmly joined together), but their interdigitating suture is visible in each specimen. In dorsal A the suture bisects the parapophysis, but in the two more posterior dorsals the suture runs immediately beneath the parapophysis. The centrum is longer anteroposteriorly than deep dorsoventrally, as in the basal tyrannosauroids *Guanlong* (IVPP V14531) and *Stokesosaurus*

(Benson, 2008) and some dorsals of juvenile *Tarbosaurus* (Currie and Dong, 2001a), but unlike the deeper dorsals in derived tyrannosaurids (e.g., *Daspletosaurus*: AMNH FARB 5468; *Tarbosaurus*: Maleev, 1974; *Tyrannosaurus*: Brochu, 2003).

Parts of the anterior and posterior centrum faces are preserved in both dorsals A and C and are weakly amphicoelous. In dorsal C it is clear that the anterior face is more deeply concave than the posterior face, which is nearly flat. The same appears to be true in dorsal A, but only a small region of the posterior surface is preserved. The two faces extend to essentially the same level ventrally in dorsal A, whereas the anterior face projects slightly ventral to the posterior face in dorsal C. The ventral surface of the centrum of dorsal A appears to be marked by a very weak keel, along which the vertebra has broken. The presence of a hypapophysis cannot be determined. The ventral surface of dorsal C is smooth, and a hypapophysis is clearly absent. The dorsal surface of the centrum, which forms the floor of the neural canal, is marked by an anteroposteriorly elongate ridge, which is strongest at the midpoint, in dorsal C. This structure is not preserved in dorsal A, but it may have been obliterated by poor preservation.

Laterally both centra are penetrated by a large, ovoid pneumatic foramen ("pleurocoel") (figs. 55, 57-58, pf). The presence of a pleurocoel in dorsal C indicates that these structures continued throughout the dorsal series, as in derived tyrannosaurids (Rauhut, 2003a) but not basal tyrannosauroids and other coelurosaur groups (Benson, 2008). In dorsal A the pneumatic foramen is 15 mm long anteroposteriorly and 10 mm deep dorsoventrally, and is closer to the anterior face of the centrum than the posterior face. It is subdivided into two pockets by a thin, sharp lamina that projects anteroventrally. Of these pockets, the anterior depression is the larger. The foramen is surrounded by a broad and shallow pneumatic fossa that continues as a shallow indentation up to the posterior margin of the parapophysis. In dorsal C there is a single undivided

pneumatic foramen on each side. On the right side, the uncrushed foramen is 18 mm long by 6 mm deep, and is surrounded by a slight fossa around its margins.

The parapophysis is nearly equally shared between the centrum and neural arch in dorsal A, but is located entirely on the anteroventral corner of the neural arch in dorsals B and C (figs. 55-57, para). This structure is largest and most distinctive on dorsal A, where it is a shallowly concave surface that is slightly offset from the centrum and the arch. It is crescent shaped, measuring 30 mm deep dorsoventrally by 15 mm long anteroposteriorly at its midpoint. The dorsal half of the parapophysis—that region located on the neural arch—is expanded anteriorly and curves laterally, such that it is visible as a laterally projecting flange in anterior view like has been described in the dorsals of *Tyrannosaurus* (Brochu, 2003). The parapophysis of dorsal B is ovoid (20 mm deep by 12 mm long), whereas it is teardrop shaped (21 mm deep by 10 mm long) on dorsal C. On the latter dorsal the parapophysis is slightly concave and rugose, and is only visible slightly in anterior view.

The left prezygapophyses is preserved on dorsals B and C (figs. 56-57, prez). On dorsal B the articular surface is a flat, circular (19 mm diameter) facet that faces strongly dorsally and slightly anteriorly and medially. Erosion has removed the articular facet on dorsal C but based on the trend of the break it appears as if the prezygapophysis faced strongly medially and dorsally. Both prezygapophyses are placed slightly anterior to the anterior surface of the centrum, as well as slightly lateral to the centrum. A thin, elongate, and web-like lamina links the prezygapophysis to the diapophysis (the prezygapodiapophyseal lamina) (fig. 57, predl), and a thinner lamina connects the prezygapophysis and neural spine (the spinoprezygapophyseal lamina) (fig. 57, sprel). On the better preserved dorsal C the two prezygapophyses are separated on the midline by an 11 mm wide gap, the hypantrum (fig. 57, hypa). Additionally, underneath

the prezygapophyses are deep, anteriorly facing fossae. These do not bear clear pneumatopores as have been reported in *Tyrannosaurus* (Brochu, 2003).

Both postzygapophyses are well preserved on dorsal C and the right postzygapophysis is present on dorsal A (figs. 55, 57, posz). The facet on dorsal A is flat, ovoid (27 mm by 19 mm), and faces almost equally laterally and ventrally. Those of dorsal C are similar in size and shape (25 mm by 16 mm oval), but face almost entirely ventrally and only slightly laterally. In addition, although the facets of dorsal C are flat, they are surrounded by a thin rim that gives the impression that they are slightly concave. This rim is not present on dorsal A but may have been eroded away. The postzygapophysis of dorsal A is positioned slightly posterior to the posterior surface of the centrum, whereas those of dorsal C project approximately 4 mm past the centrum posteriorly. In both vertebrae the postzygapophyses terminate medial to the lateral edges of the centrum, are connected to the diapophysis by a thin lamina (the postzygapodiapophyseal lamina; fig. 57, posdl), and join the neural spine via a thin lamina (the spinopostzygapophyseal lamina; fis. 57, sposl). In dorsal C the postzygapophyses are positioned 20 mm higher than the prezygapophyses, an "offset" condition previously considered an autapomorphy of *Stokesosaurus langhami* (Benson, 2008).

On the better preserved dorsal C there is a pronounced hyposphene between the postzygapophyses, which is 17 mm deep dorsoventrally by 14 mm wide mediolaterally (fig. 57, hypo). The hyposphene is formed by thin laminae that continue ventrally from the ventromedial corner of the postzygapophyses. These laminae are sinuous and between them is a broad, posteriorly-facing, posteriorly concave surface. Ventral to the hyposphene, but only present on the left side, is a deep, ovoid (8 by 6 mm) fossa that appears to lead into a foramen (fig. 57, pfos). This structure is not present on other tyrannosaurids (e.g., *Daspletosaurus*: AMNH FARB

5468) and thus may be an autapomorphy of *A. altai*. However, it is also possible that this feature represents nothing more than random (asymmetrical) pneumaticity; indeed, it is absent on the right side, and this region is instead occupied by the stout, convex neck that links the hyposphene to the centrum below. Pneumatopores have been described in this general region in *Tyrannosaurus* but these face laterally on the postzygapophyseal neck (Brochu, 2003), not posteriorly as in *A. altai*.

Parts of the transverse processes are present in all three dorsal fragments (figs. 55-57, tvp). In dorsal A the transverse process projects strongly dorsally and only slightly laterally, such that it appears strongly upturned in anterior and posterior views. It does not project at all posteriorly. In contrast, the transverse processes of dorsals B and C project nearly equally laterally and dorsally and are also posteriorly backswept. The posterior margin of the process is broken on dorsal A, precluding measurement of its exact shape. It is clear, however, that the process thickens as it continues laterally, eventually terminating at the diapophysis (figs. 55-57, diap). This articular structure is a large, teardrop shaped (29 mm anteroposteriorly by 17 mm dorsoventrally), slightly convex surface that faces laterally and dorsally. On dorsal C the left transverse process is 41 mm long at its base and quickly tapers to 28 mm long, a dimension that it keeps for the next 27 mm of its lateral extent before terminating at the diapophysis. Here the diapophysis is a very small, triangular (17 mm long by 8 mm deep) structure that faces laterally. The dorsal surface of the transverse process is smooth and flat, but there is a small, shallow, dorsally and laterally facing fossa in the region where the neural spine and transverse process meet.

Ventrally the diapophysis connects to the centrum via separate anterior and posterior centrodiapophyseal laminae (figs. 55-57, acdl, pcdl) (Wilson 1999). Brochu (2003) refers to

these struts as the "centrodiapophyseal lamina" and the "ventral lamina of the transverse process," respectively, although his figures use the label "centrodiapophyseal lamina" for the structure that he refers to as the "ventral lamina" in the text. In any case, these two laminae in tyrannosaurids such as *Tyrannosaurus* and *A. altai* correspond to the anterior and posterior centrodiapophyseal laminae of Wilson (1999), and will be referred to as such here.

Both the anterior and posterior centrodiapophyseal laminae are prominent and elongate in dorsal A (fig. 55). The posterior lamina is much thicker (5 mm vs. 0.5 mm), and the two diverge ventrally at nearly the same angle, with the anterior lamina projecting anteroventrally and the posterior lamina trending posteroventrally. The two laminae join approximately 40 mm from the distal end of the transverse process and continue as a single enlarged lamina that eventually merges with the diapophysis. This single lamina is thick: it is 10 mm long anteroposteriorly at its base and expands to 17 mm long where it meets the diapophysis. In between the anterior and posterior centrodiapophyseal laminae there is a deep, triangular infradiapophyseal fossa (fig. 55, idf). Posterior to the posterior lamina is a large and deep infrapostzygapophyseal fossa, which faces strongly laterally and also posteriorly (fig. 55, ipof). Anterior to the anterior lamina is a small infraprezygapophyseal fossa; its anterior region is broken, but it clearly faced laterally and anteriorly (fig. 55, iprf). The infraprezygapophyseal and infrapostzygapophyseal fossae both continue up the anterior and posterior surfaces of the transverse process, respectively, and distally they are separated by the single, thick midline lamina. Of the three fossae the infrapostzygapophyseal fossa is the largest and the infraprezygapophyseal fossa the smallest.

The morphology of the laminae is markedly different in dorsal B. Here, a single large and thick lamina (7 mm thickness) trends down the midpoint of the lateroventrally facing surface of the transverse process. This structure is the posterior centrodiapophyseal lamina, which is much

larger, longer, thicker, and more pronounced than the anterior centrodiapophyseal lamina, which is present as a thin and sinuous ridge 21 mm anterior to the posterior lamina. This ridge bisects a deep, triangular fossa between the posterior lamina and the prezygapodiapophyseal lamina. This deep depression, which is inset nearly 30 mm into the vertebrae relative to the lateral surface of the centrum, is a conjoined infraprezygapophyseal and infradiapophyseal fossa (fig. 56, idf + iprf). The entire fossa faces laterally, as it is concealed dorsally and anteriorly by the strongly overhanging, web-like prezygapodiapophyseal lamina.

The condition in dorsal C is similar to that in dorsal B (fig. 57). There is a stout posterior centrodiapophyseal lamina that links the diapophysis with the centrum. This lamina is 8 mm thick at its midpoint, and thickens both dorsally and ventrally where it meets the diapophysis and centrum, respectively. There is a greatly reduced anterior centrodiapophyseal lamina (10 mm long, 1 mm thick), which again is located within a deep, funnel-like fossa that represents a merged infradiapophyseal and infraprezygapophyseal fossa. The anterior and posterior centrodiapophyseal laminae clearly do not meet, as the anterior lamina trends strongly anteroventrally and the posterior lamina is nearly straight dorsoventrally in lateral view. Posterior to the posterior lamina is a deep infrapostzygapophyseal fossa, which is barely visible in lateral view but extensive in posterior view, where it deeply excavates the posterior surface of the transverse process medial and ventral to the postzygapophyses (fig. 57, ipof). This excavation is deeper than in other tyrannosaurids (*Daspletosaurus*: AMNH FARB 5468; *Tyrannosaurus*: Brochu, 2003). Additionally, on the left side of dorsal C there is a stout lamina (5 mm thick) that trends dorsomedially (fig. 57, acclam), separating the posterior surface of the infrapostzygapophyseal fossa into two regions, a small and shallow laterodorsal region and a deep and larger medioventral pocket. This lamina is not present on the right side and appears to

be genuinely absent. Accessory laminae such as this one are described in *Stokesosaurus*, but in this taxon several laminae are present within each fossa (Benson, 2008). These laminae are absent in *Daspletosaurus* (AMNH FARB 5468) and *Tyrannosaurus* (Brochu, 2003), and the single stout lamina may be an autapomorphy of *A. altai*.

The neural spine is incompletely preserved in all dorsal vertebrae. The base of the spine is present in dorsal B and a more extensive part of the spine is preserved in dorsal C. Here the neural spine is 30 mm long anteroposteriorly at its base and eroded dorsally. It is placed posteriorly on the centrum, inset relative to the anterior face of the centrum but level with the posterior face. Its lateral surfaces are smooth, and in anterior and posterior view there are prominent pre- and postspinal fossae, respectively (fig. 57, pref, posf). Both are deepest ventrally but continue dorsally up the neural spine. Unfortunately, poor preservation makes it difficult to determine how far up the spine each fossa continued. The postspinal fossa faces posteriorly only but the prespinal fossa faces dorsally at its ventral base and the anteriorly on the surface of the spine itself. There are some rugosities for ligaments in both fossae, and although erosion precludes an exact comparison, these do not appear to be as strongly developed as those of adult *Gorgosaurus* (Lambe, 1917), *Daspletosaurus* (AMNH FARB 5468), or *Tyrannosaurus* (Brochu, 2003).

Sacral Vertebrae: Portions of four sacral vertebrae are preserved in articulation with the right ilium (see below; figs. 66-67; measurements in Table 9). Thus, the left lateral surfaces of the sacrals are broadly visible, but fine details of their articulation with the ilium are not observable. Based on comparisons with other tyrannosaurids (Osborn, 1906, 1916; Parks, 1917; Lambe, 1928; Maleev, 1974; Brochu, 2003) it is likely that five sacrals were present in *A. altai*, and the

preserved elements correspond closely to the morphology and position of sacrals 2-5 in other taxa. Of these, sacrals 3-5 are nearly complete, although badly weathered in many areas, whereas sacral 2 is only represented by a small portion of the neural spine fused to sacral 3.

Nearly complete centra are preserved for sacrals 3-5. These are coossified, but individual spool-shaped elements are visible. This is common for tyrannosaurids (e.g., Osborn, 1906, 1916; Lambe, 1917; Parks, 1928; Brochu, 2003), as well as *Guanlong* (IVPP V14531) and *Stokesosaurus* (Benson, 2008). In *A. altai* the centra increase in anteroposterior length posteriorly, and the fifth centrum is approximately 20% longer than the fourth (Table 9). This is also the case in *Tyrannosaurus* (Brochu, 2003), but the centra show a posterior decrease in length in *Stokesosaurus* (Benson, 2008) and are of approximately constant length in *Guanlong* (IVPP V14531).

The exposed left lateral surfaces of the centra are mostly eroded, but the few well preserved regions exhibit a smooth texture. The right lateral surfaces are better preserved and visible broadly below the ilium. These surfaces are also smooth, and there are no signs of "pleurocoels" (pneumatic fossae or foramina), which have been described in other tyrannosaurids (Osborn, 1906, 1916; Brochu, 2003). However, as these excavations are most prominent in anterior sacrals (Osborn, 1906, 1916), which are not preserved in *A. altai*, their presence cannot be ruled out. Additionally, clear intervertebral foramina between the neural arch and centrum are not visible, although there is an eroded cavity on the third sacral, immediately anterior to the fourth sacral rib articulation, that likely represents one of these structures. Indeed, a foramen is placed in this postion in *Stokesosaurus* (Benson, 2008: fig. 4C). Furthermore, there are no distinct laminae connecting the centra with the diapophyses or parapophyses.

Articular surfaces of the centra are generally not visible, and only the posterior surface of the fifth sacral is exposed. Although its left lateral surface is slightly eroded it is apparent that the posterior articular surface is deeper (67 mm) than wide (47 mm). Unfortunately, surface details are not preserved due to erosion, but it was clearly flat or slightly concave, as in other tyrannosaurids (e.g., Brochu, 2003). Articulated centra indicate that the posterior articular surface is deeper than the anterior surface, as it extends slightly further ventrally. This is especially evident in the fifth sacral, in which the posterior face continues approximately 10 mm ventral to the anterior surface, a condition present in other tyrannosauroid taxa (Osborn, 1906, 1916; Lambe, 1917; Brochu, 2003; Benson, 2008). The ventral margin of the centrum between the articular surfaces is concave, thus constricting the centrum at its midpoint, as seen in lateral view.

The region of the lateral and ventral surfaces immediately adjacent to the articular faces is scoured by a series of fine, anteroposteriorly trending striations in all areas that are well preserved. The ventral surfaces of all three centra are smooth and rounded, without any keels or grooves.

The centrum is fused (firmly joined) to the neural arch in all three well preserved sacrals. On the right side of the fifth centrum there is a visible but closed interdigitating suture where the two meet. The neural arch of this vertebra is the best preserved of the sacrum. Here, the neural canal is ovoid, with a dorsoventral depth of 14 mm and a mediolateral width of 11 mm, between the arch and centrum. Both postzygapophyses are visible in posterior view, and the better preserved right structure appears as a tongue shaped processes when seen in ventral view (fig. 67, posz). Its long axis trends posterolaterally and the smooth articular surface faces mostly ventrally but also slightly laterally. The left postzygapophysis appears to give rise to a separate

flange of bone projecting straight posteriorly, but this is poorly preserved and may be an artifact of breakage, or perhaps a flake of bone from the prezygapophysis of the first caudal. Unfortunately, the corresponding region on the right postzygapophysis is broken.

Ventrally the postzygapophyses give rise to a hyposphene, which is largely covered by matrix (fig. 67, hypo). This accessory articular structure is comprised of individual sheets that extend ventrally and slightly laterally from each postzygapophysis. Between these sheets is a deep midline cleft, which expands in width ventrally due to the slight lateral projection of the left and right sheets. Dorsally the postzygapophyses are connected to the neural spine via a thin and sharp spinopostzygapophyseal lamina, which begins at the posterolateral corner of the postzygapophysis and trends medially and dorsally (fig. 67, sposl). The left and right laminae enclose a deep postspinal fossa on the posterior surface of the neural spine, which expands slightly in mediolateral width dorsally (fig. 67, posf). The fossa appears to be continuous with the hyposphene cleft ventrally. In posterior view there appears to be a thin lamina linking the right postzygapophysis with the diapophysis, but this region is covered by unremovable matrix.

Little can be said about the prezygapophyses. These structures are only visible in lateral view, and they appear to be fused to the postzygapophyses, forming a single elongate structure. The zone of fusion is difficult to interpret due to erosion, but seems to be marked by a raised area, and in some cases a thin line that may represent an open suture. However, these structures may easily be surface cracks. If the site of fusion is interpreted correctly here, then the prezygapophyses extend to approximately the level of the midpoint of the preceding centrum. This is similar to the condition in other tyrannosaurids, in which the zygapophyses fuse at a similar position (Osborn, 1906, 1917; Brochu, 2003). One further detail is visible in *A. altai*: the base of the prezygapophysis of the fifth sacral shows that there was a prespinal fossa between

separate spinoprezygapophyseal laminae, which linked the prezygapophysis and neural spine on each side of the vertebra.

The neural spines are large (fig. 66). They are invariably deeper dorsoventrally than the centrum and expand in anteroposterior length as they extend dorsally, resulting in a "fan shaped" morphology typical of tyrannosaurids (Osborn, 1906, 1916; Brochu, 2003). The expansion is greatest in the third sacral, where the dorsal margin of the spine is approximately double its narrowest length, whereas in the fifth sacral it is only 15% greater. Sacral neural spine morphology is difficult to observe in many basal coelurosaurs, as the sacrum is often obscured by the ilium. However, the neural spines are fan shaped in the compsognathid *Mirischia* (Naish et al., 2004: fig. 1), but are not in *Compsognathus* (Peyer, 2006).

The lateral surfaces of the spines are generally smooth but in places are covered in fine striations. The spines are thin: the third sacral spine is 6 mm thick at its dorsal margin, and the fifth spine is only 2 mm thick. However, the posterior margin of the fifth spine is greatly expanded (15 mm thick) and rugose, to accompany the deep postspinal fossa (see above).

The neural spines are fused into a single apron, as is characteristic of tyrannosaurids (Osborn, 1906, 1917; Lambe, 1917; Brochu, 2003), as well as *Guanlong* (IVPP V14531). Fusion is limited between the posterior neural spines: spines 3 and 4 and 4 and 5 only make brief contact at their dorsal tips, and surface breakage makes it difficult to determine whether this contact was even fused. However, fusion between spines 2 and 3 is much more extensive, as they are clearly fused (confluent as a single apron) for 70 mm ventral to the dorsal margins of the spines. A small triangular fenestra is located below the fused region, between the spines and the zygapophyses; this fenestra is 32 mm long anteroposteriorly at its base and 26 mm deep dorsoventrally (fig. 66,

tfen). Fenestrae are also present between spines 3 and 4 and 4 and 5, but these are much larger and deeper due to the less extensive contact between the individual spines.

Fenestrae like these are sometimes considered to be a diagnostic characteristic of abelisaurids (Wilson et al., 2003, Sereno and Brusatte, 2008). However, in abelisaurids like *Majungasaurus* (O'Connor, 2007: figs. 13, 14) the fenestrae are located between the transverse processes and are positioned at the same level of the zygapophyses, clearly more ventrally placed than the fenestrae in *A. altai*. More dorsally placed fenestrae similar to those described here are also present in some basal tetanurans (e.g., *Giganotosaurus*, *Lourinahnosaurus*, *Megalosaurus*: R. B. J. Benson, pers comm.) and other tyrannosaurids (e.g., Osborn, 1906, 1917; Brochu, 2003). However, in these tyrannosaurids the fusion between spines is more extensive, resulting in smaller fenestrae than in *A. altai*. Brochu (2003) suggests that spine fusion, and thus fenestra size, may be ontogenetically controlled, with more mature specimens exhibiting greater fusion. *Guanlong* (IVPP V14531) does not possess any fenestrae, but rather a completely fused sacral neural arch apron.

Parts of the transverse processes are preserved in sacrals 3-5 (fig. 66, tvp). Because of the close contact between the ilia and sacrum, in which the ilia nearly contact the fused sacral apron (see below), the transverse processes are nearly parasagittal in orientation. The transverse process of sacral 4 is the best preserved of the sacrum, and is a gracile (thin and narrow) projection that extends dorsally and only slightly laterally. It expands in anteroposterior length as it extends dorsally and terminates in a rounded, wing like expansion. Ventrally the transverse process is connected to the sacral rib attachment scar by a thick neck of bone, which is as wide as the base of the transverse process itself. This is supported by a thin and sharp lamina extending from the lateral surface of the transverse process ventrally onto the dorsal surface of the scar.

The lamina is best preserved on sacral 3, in which it extends far laterally as a web that separates anterior and posterior fossae (fig. 66, lam). The anterior fossa is dorsoventrally elongate, very deep, and faces mostly anteriorly. A similar feature was described in *Tyrannosaurus* by Brochu (2003), who considered it possibly pneumatic in origin. The posterior fossa of *A. altai* is shallower, triangular, and faces almost entirely laterally.

Only limited details of the sacral ribs are observable. The lone well preserved, nearly complete, and visible rib is the left fifth sacral rib (fig. 66, sr5). However, attachment scars for the third and fourth sacral ribs are visible on the exposed left lateral side of the sacrum (fig. 66, sr3, sr4). Each of these ribs rises from a single vertebra, and neither the fifth rib nor the third or fourth scars bridge two vertebrae as in many basal theropods (e.g., *Allosaurus*: Madsen, 1976; *Condorraptor*: Rauhut, 2005; *Neovenator*: Brusatte et al., 2008); the basal theropod condition is also seen in the basal tyrannosauroids *Stokesosaurus* (Benson, 2008) and *Guanlong* (IVPP V14531). Ribs limited to a single vertebra are present in other tyrannosaurids (Osborn, 1906, 1916; Brochu, 2003). The fifth sacral rib is located entirely on the neural arch and does not breach the neurocentral suture, but the positions of the third and fourth scars are unclear due to poor preservation. However, it appears as if part of the fourth scar does occur on the centrum, which is not the case in *Tyrannosaurus* (Osborn, 1906). In fact, the condition in *Tyrannosaurus* and *Tarbosaurus* (Maleev, 1974), in which the rib scars are restricted to the neural arch and positioned far dorsally, differs from the morphology of theropods in general, in which the scars are located partially or entirely on the centrum and thus positioned further ventrally (e.g., Madsen, 1976). In *A. altai* all three vertebrae exhibit a clear separation between the sacral rib or scar and the transverse process. This separation is greatest in sacral five, where it is filled with matrix.

Based on the size of the scars it is likely that the fifth rib was the largest of the sacral series as in other tyrannosaurids (*Gorgosaurus*: Lambe, 1917; *Tyrannosaurus*: Osborn, 1906, 1916, Brochu, 2003), but unlike *Stokesosaurus*, in which the fourth rib is largest (Benson, 2008). In *A. altai* the fifth rib is roughly triangular in shape, with an anteroventrally oriented long axis that measures over 90 mm (this is an underestimate due to breakage). The rib is thin and expands in anteroposterior length as it extends anteriorly. Its lateral surface is generally smooth—and much smoother than the rugose texture of *Tyrannosaurus* (Osborn, 1906, 1916; Brochu, 2003)—and would have rested against the medial flange of the postacetabular process (i.e., the brevis shelf, see below). This was a broad contact, as shown by the articulated right rib, which is partially visible in ventral view. The contact does not extend to the very end of the ilium posteriorly, as is shown by the broken right side of the ilium. Here, the medial flange is broken right where the sacral rib articulation ends but the lateral flange continues for another 75 mm posteriorly. As the lateral and medial flanges both extend to the same point posteriorly in other tyrannosaurids, it is likely that approximately 75 mm of the medial flange is missing posterior to the end of the sacral rib contact.

Only small portions of the fourth sacral rib are present but its scar is visible. This scar is comprised of two main portions (fig. 66, sr4dor, sr4ven). The primary region is anteroposteriorly elongate and hourglass shaped (47 mm long anteroposteriorly by 20 mm deep dorsoventrally at its constricted point) (fig. 66, sr4ven). It terminates anteriorly at the level of the anterior articular surface of the centrum, and is slightly more than half of the length of the centrum itself. A secondary long, thin flange extends dorsally from the posterodorsal corner of the hourglass (fig. 66, sr4dor) to link the primary scar with the transverse process (fig. 66, tvp). It is here where a small part of the rib itself appears to be preserved. Brochu (2003) describes a third region of the

scar in *Tyrannosaurus*, which is positioned dorsal to the thin secondary flange and resembles a teardrop. This is not preserved in *A. altai* due to erosion, but it may have been present. Overall, the fourth rib scar of *A. altai* is similar to *Tyrannosaurus* in position and size but differs slightly in shape, as in the latter taxon it is more ovoid and the thin dorsal flange is located at the midpoint of the primary bulge, not its posterodorsal corner (Osborn, 1906, 1916; Brochu, 2003).

The scar is all that remains of the third sacral rib (fig. 66, sr3). This is a triangular feature, 50 mm long anteroposteriorly at its base and 37 mm tall dorsoventrally at its midpoint. It lacks a distinct, secondary dorsal flange that connects the primary scar to the transverse process, as in the fourth rib scar. *Tyrannosaurus* also lacks this flange (Brochu 2003), and in both taxa the connection between the two structures is comprised of the web-like lateral lamina of the transverse process described above.

Caudal Vertebrae: Two anterior caudals were found in articulation, and are referred to as caudals A (the more proximal caudal) and B (the more distal specimen) (figs. 59-60). A third caudal, referred to as caudal C, is from the posterior part of the tail and is described separately below (fig. 61). Measurements for all three caudals are given in Table 9.

In the two anterior caudals, the neural arch and centrum are fused (firmly joined together) but their interdigitating suture is partially open and clearly visible. This is also the case in the anterior caudals of adult *Tyrannosaurus* (Brochu, 2003), as well as other tyrannosaurlids that appear to be juveniles or subadults (*Applachiosaurus*, *Tarbosaurus*: Carr et al., 2005; *Bistahieversor*: NMMNH P-25049). The identification of the two vertebrae as anterior caudals is based on several criteria: the centra are slightly longer than tall, the neurocentral suture is visible, the transverse processes are backswept in dorsal view, and a hyposphene is present, all of which

are features of the anterior caudals of *Tyrannosaurus* (Brochu, 2003) and tyrannosaurids in general.

Both anterior caudals are amphicoelous, but damage makes it impossible to determine if either face was more strongly conave than the other. The centra are longer anteroposteriorly than the dorsoventral depth of either articular surface. Caudal A is longer than caudal B but has shallower articular surfaces. The lateral surfaces of the centra are smooth and lack pneumatic excavations. The ventral surfaces are crushed and eroded but apparently lack a midline keel or groove. Regions of the centra adjacent to the articular surfaces are marked by short anteroposterior lineations in all well preserved regions; these are especially prominent on the right lateral surface of the anterior face of caudal B (fig. 60, lin). The posterior articular surface extends slightly ventral relative to the anterior surface and would have articulated with a chevron. Clear chevron articular surfaces, however, are not preserved because of erosion.

The neural arch is present on both specimens but is broken in many areas. The neural spine is also present on both caudals, and is a robust rectangular process that is longer anteroposteriorly than wide transversely. The length of the spine is approximately half of the centrum length, and it projects past the posterior margin of the centrum as in the anterior and middle caudals of *Tyrannosaurus* (Brochu, 2003: fig. 60). In *A. altai* the spine does not project straight vertically, but rather curves posteriorly as it continues dorsally, thus giving it a backswept appearance. The lateral surfaces of the spine are smooth and excavated by a shallow, dorsoventrally elongate fossa along their entire heights (figs. 59-60, fos). This fossa is defined laterally by the laminae that link the zygapophyses and the neural spine, the spinozygopophyseal laminae of Wilson (1999) (figs. 59-60, sposl, sprel).

In anterior and posterior view the spinozygopophyseal laminae also define anterior and posterior fossae, the pre- and postspinal fossae (Wilson 1999), that extend dorsally up the entire preserved length of the neural spine (figs. 59-60, posf, pref). Both fossae are widest mediolaterally ventrally between the zygapophyses and taper dorsally, such that they reach a constant thickness along the height of the entire neural spine proper. The surfaces of these fossae are not well preserved, but in *Tyrannosaurus* (Brochu, 2003: fig. 59) and other tyrannosaurids they are often rugose for spinal ligament attachment. Thickening of the bounding laminae dorsally suggests that some rugosity was present in *A. altai*.

The dorsal regions of the neural spines are not well preserved, but caudal A has a small fragment of bone representing part of a dorsal expansion (fig. 59, de), as is also present in the anterior caudals of *Tyrannosaurus* (Brochu 2003: figs. 59, 60) and *Tarbosaurus* (PIN 551-2), where the expansion is dorsoventrally deeper than the condition seen in *A. altai*.. However, in *A. altai* the broken surface of the expansion is anteroposteriorly elongate and thin mediolaterally, suggesting that the expansion was mostly in the parasagittal plane. In contrast, in *Tyrannosaurus* (Brochu, 2003), *Tarbosaurus* (PIN 551-2), and other tyrannosaurids (e.g., *Daspletosaurus*: AMNH FARB 5468; *Gorgosaurus*: AMNH FARB 5434, 5664) the dorsal end of the neural spine is expanded both anteroposteriorly and mediolaterally.

The transverse processes are thin flanges that prjoject straight horizontally, perpendicular to the neural spine (figs. 59-60, tvp). They are located approximately 25 mm dorsal to the neurocentral suture, and extend both laterally and posteriorly, such that they have a backswept appearance in dorsal view. The transverse process of caudal A is more backswept than that of caudal B, in concert with the progressive straightening of the processes posteriorly along the caudal column in other tyrannosaurids (Brochu, 2003: fig. 61). The tip of the transverse process

is expanded relative to the remainder of the flange, and appears as a spatulate expansion (figs. 59-60, se), as is also the case in many anterior and middle caudals of *Bistahieversor* (NMMNH P-25049), *Tarbosaurus* (PIN 551-2), and *Tyrannosaurus* (Brochu, 2003: fig. 61). The expansion is gradual as in *Bistahieversor* (NMMNH P-25049), *Tarbosaurus* (PIN 551-2), and *Tyrannosaurus* (Brochu, 2003:fig. 61) and not abrupt as in *Appalachiosaurus* (Carr et al., 2005: fig. 14).

Ventrally, anteroposteriorly broad but indistinct ridges extend anteroventrally and posteroventrally from the transverse process onto the body of the vertebra (figs. 59-60, acdl, pcdl). They do not reach the centrum, but terminate on the deep region of the neural arch immediately dorsal to the neurocentral suture but below the transverse process. These are the remnants of the anterior and posterior centrodiapophyseal laminae (Wilson, 1999), which are generally indistinct and sometimes absent in the caudal vertebrae of theropods (Benson, 2008).

In dorsal view, the region where the transverse process and neural spine meet is excavated by a deep, triangular depression (figs. 59-60, td). This is best preserved on the right side of caudal B (fig. 60E). This fossa is present as a much broader and shallower depression in *Bagaraatan* (Osmólska, 1996: fig. 6D), and is present as a smaller, shallower, and less distinct excavation in some tyrannosaurids (e.g., *Gorgosaurus*: AMNH FARB 5664). However, other taxa preserve no trace of a fossa whatsoever (e.g., *Gorgosaurus*: AMNH FARB 5434; *Daspletosaurus*: AMNH FARB 5468), and this feature may be individually or ontogenetically variable judging by its variable presence in *Gorgosaurus*.

Only the right prezygapophysis of caudal B is preserved (fig. 60, prez). It extends slightly anterior to the centrum but is not placed laterally, as are the prezygapophyses of the cervical vertebrae (see above). This condition is also seen in other tyrannosaurids, including *Tarbosaurus*

(PIN 551-2) and *Tyrannosaurus* (Brochu, 2003:fig. 61). In lateral view the prezygapophysis is oriented anteriorly and slightly dorsally as in most theropods, not nearly vertically as in *Bagaraatan* (Osmólska, 1996). In *A. altai* the articular surface is ovoid, longer anteroposteriorly (21 mm) than wide mediolaterally (15 mm). This surface faces mostly dorsally but also slightly medially. Erosion ventral to the prezygapophysis precludes observation of a hypantrum, as well as the neural canal. However, it is apparent that there is a deep, smooth channel between the zygapophyses that faces dorsally and merges with the prespinal fossa on the anterior surface of the neural spine.

A thick spinoprezygapophyseal lamina links the prezygapophysis to the neural spine and a stout lamina bridges the prezygapophysis to the centrum ventrally. Two separate laminae connect the prezygapophysis to the transverse process: one extends from the anterolateral corner of the articular surface of the prezygapophysis and the second, more ventral lamina extends from the base of the zygapophysis. In lateral view these laminae are widely spaced anteriorly but converge posteriorly to merge at the base of the transverse process. Where they are separated they define a deep triangular fossa that faces laterally (fig. 60, pretf). A similar structure has been described, and sometimes bears pneumatic foramina, in *Tyrannosaurus* (Brochu, 2003). It is also present in *Tarbosaurus* (PIN 551-2, ZPAL MgD-I/226) and *Daspletosaurus* (AMNH FARB 5468), but not in *Gorgosaurus* (AMNH FARB 5434, 5458, 5664). Anteroventral to the fossa is a small, bulbous knob on the lateral surface of the thick neck that links the prezygapophysis to the remainder of the neural arch (fig. 60, kn). This is also seen in *Tarbosaurus* (PIN 551-2), and may be more widely distributed among the poorly described caudal vertebrae of many tyrannosaurids.

The right postzygapophysis is preserved on both caudals (figs. 59-60, posz). The left postzygapophysis of caudal A is also present, but is obscured due to an appressed fragment of

the prezygapophysis of caudal B. The postzygapophyses extend far posterior to the centrum, in concert with the posteriorly placed neural spine, but do not extend laterally past the centrum. This is also seen in *Tarbosaurus* (PIN 551-2) and *Tyrannosaurus* (Brochu, 2003:fig. 60). The articular surfaces are flat, ovoid, and face mostly ventrally but slightly laterally.

A thin spinopostzygapophyseal lamina connects the postzygapophysis to the neural spine. A pair of thin laminae links the base of the postzygapophysis to the transverse process, as is the case with the prezygapophyses. These also define a triangular fossa between them, except that this depression faces entirely posteriorly and is located underneath the postzygapophyses (figs. 59-60, posfos). The differing orientation of the pre- and postzygapophyseal fossae is related to the backswept transverse processes: the region between the process and the prezygapophysis is widely exposed laterally, whereas that between the process and the postzygapophysis is not. These fossae are not equivalent to the infrapre- and postzygapophyseal fossae that are common in the dorsal vertebrae of theropods, which are partially defined by the anterior and posterior centrodiapophyseal laminae (Wilson, 1999). In *A. altai* these laminae are reduced, but present, and they clearly do not demarcate the triangular fossa between the zygapophyses and transverse process.

The region ventral to the postzygapophyses is not well preserved in caudal A, but in caudal B the base of a small hyposphene is visible (figs. 59-60, hypo). This structure is not as large and stout as the hyposphenes of *Bagaraatan*, which resemble rectangular sheets (Osmólska, 1996: fig. 6C). Immediately ventral to the hyposphene the neural canal is visible. It is ovoid, 16 mm deep dorsoventrally and 10 mm wide mediolaterally, and the centrum participates in its ventral margin.

The single distal caudal (caudal C) is very different in morphology from the two anterior caudals (fig. 61). Comparison with the well described caudal series of *Tyrannosaurus* suggests that this vertebra falls somewhere within the range of caudals 21-25 (Brochu, 2003: fig. 60). The centrum and neural arch are fused, and unlike in the anterior caudals, there is no sign of the neurocentral suture. This is also seen in other tyrannosaurids, including *Daspletosaurus* (CMN 8506), *Tarbosaurus* (PIN 551-2), and *Tyrannosaurus* (RSM 2523.8).

The centrum is smooth laterally, lacking any pneumatic features, and does not possess a ventral ridge or groove. However, the ventral surface is posteriorly excavated by a triangular notch for articulation with a chevron (fig. 61, ch). The centrum is elongate, both articular faces are concave, and the anterior face is more ovoid than the nearly circular posterior face. Both faces extend to the same level ventrally. The neural canal is oval shaped, and measures 8 mm dorsoventrally by 5 mm mediolaterally.

The neural arch is complete and well preserved. There is no transverse process, and hence no anterior and posterior centrodiapophyseal laminae linking the neural arch and the centrum. The prezygapophyses are elongate flanges that extend 20 mm anterior to the anterior face of the centrum (fig. 61, prez). Neither they nor the postzygapophyses are placed lateral to the centrum. The prezygapophyseal articular surface is only a small region on the medial surface of the zygapophysis: it is flat, ovoid with an anteroventral-posterodorsal long axis, and faces strongly medially and only slightly dorsally. The entire prezygapophysis is somewhat hook shaped in lateral view: the anterior tip is rounded and slightly recurved ventrally, whereas the ventral margin of the process is marked by a convex bulge at midlength (fig. 61, bul). This bulge, which represents the anteroventral corner of the articular surface proper, is also present in *Tarbosaurus* (PIN 551-2) and *Tyrannosaurus* (Brochu, 2003: fig. 60), but it is not seen in *Albertosaurus*

(AMNH FARB 5226) or *Daspletosaurus* (AMNH FARB 5468). This character may have phylogenetic significance, but the absence of the bulge may also be an artifact of breakage in some specimens and thus is difficult to score in a phylogenetic analysis. A hypantrum is absent, consistent with the lack of these structures on more posterior caudal vertebrae in *Tyrannosaurus* (Brochu, 2003).

The postzygapophyses are small flanges offset on small pedicles from the posterior margin of the neural spine (fig. 61, posz). This condition is also seen in other tyrannosaurids, including *Tarbosaurus* (PIN 553-2) and *Tyrannosaurus* (Brochu, 2003:fig. 60). The articular surface is flat and faces mostly laterally and slightly ventrally, as is also the case in the aforementioned tyrannosaurids. This surface is ovoid in shape, with a dorsoventral long axis. Posterodorsal to the articular surface proper is a small, convex bulge that projects posteriorly from the zygapophysis as a nonarticular flange (fig. 61, naf). The flange is also present in other tyrannosaurids (*Albertosaurus*: AMNH FARB 5226; *Daspletosaurus* 5468; *Tyrannosaurus*: Brochu, 2003). Well preserved and articulated specimens of *Albertosaurus* (AMNH FARB 5226) clearly show that the flange is nonarticular, and that distally along the tail it develops into a long, spike like projection that trends anteroposteriorly medial to the articulating prezygapophyses. However, some specimens of *Daspletosaurus* (AMNH FARB 5468) show that the flange may appear to be continuous with the articular surface, and thus an articular structure, when the caudals are highly eroded. There is no hyposphene ventral to the postzygapophyses.

The pre- and postzygapophyses are linked to each other via a thin lamina that is a broad, sweeping, concave ridge when seen in lateral view (fig. 61, lam). This condition is also seen in *Tarbosaurus* (PIN 551-2) and *Tyrannosaurus* (Brochu, 2003:fig. 60). The neural spine is short but elongate: it is shorter dorsoventrally than the height of either articular face but is

approximately ¾ of the anteroposterior length of the centrum. The lateral surfaces of the spine are smooth and excavated by a broad fossa, defined anteriorly and posteriorly by raised rims. These rims are the spinoprezygapophyseal laminae, which also define pre- and postspinal fossae on the anterior and posterior surfaces of the neural spine, respectively (fig. 61, pref, posf). The prespinal fossa is exposed widely in anterior view, in concert with the vertical anterior margin of the spine. In contrast, the postspinal fossa faces equally posteriorly and ventrally, corresponding to the strongly sloped posterior margin of the spine. This condition is also seen in other tyrannosaurids, including *Tarbosaurus* (PIN 553-2) and *Tyrannosaurus* (Brochu, 2003:fig. 60). The dorsal margin of the spine is concave in lateral view. It is very thin mediolaterally (less than 1 mm) across most of its length, but anteriorly and posteriorly the spine is thickened and rugose.

Cervical Ribs: Eight ribs are known from across the neck and the anterior part of the trunk (fig. 62). They are described together here, due to the transitional nature between the neck and the trunk discussed above. These range in size and shape from small, thin splints to larger, most robust elements that resemble the dorsal ribs. None of the ribs were found in articulation, and so they cannot be numbered with confidence, but they can be arranged in a progressive series based on size and shape. Notably, as the ribs progress along the column posteriorly in *Tyrannosaurus* (Brochu, 2003) the shaft becomes thicker and longer, the proximal end becomes deeper, the proximal end and shaft are separated more abruptly, and the capitulum and tuberculum become more widely separated. The same criteria are used to assign the ribs of *A. altai* to a progressive series (A-H) (numbered as such in fig. 62). Note that these ribs come from both sides of the neck.

The anterior cervical ribs (A-E) are extremely thin and splint-like, and their shafts would have nearly paralleled the neck in life. The ribs are divided into two main regions: the proximal end that contains the tuberculum and capitulum and the distal shaft. The capitulum is much larger than the tuberculum, corresponding to the large parapophyses and small diapophyses of the anterior cervicals (see above) (fig. 62, cap, tub). The capitulum is nearly circular and gets larger posteriorly. The articular surface is hummocky, and where well preserved, is seen to give rise to a pyramidal peg near its midpoint (fig. 62, peg). This peg would have fit into a corresponding socket in the parapophysis, strengthening the articulation. The tuberculum is an ovoid, flat facet, and is oriented at an angle relative to the capitulum. With the ribs in articulation the capitulum faces strongly medially and slightly ventrally, whereas the tuberculum faces primarily dorsally and somewhat medially.

The capitulum and tuberculum are separated by a deep notch, which becomes more deeply excavated and extends further distally in the more posterior anterior cervical ribs (fig. 62, not). In rib D the notch is penetrated by a small, ovoid pneumatopore, whereas in the larger rib E the notch is extremely deep and separated from a smaller, more slit-like pneumatopore on the medial surface of the proximal end (fig. 62, pf). Pneumatopores are not visible on the proximal ends of ribs B and C, and rib A is missing its proximal region. Medial pneumatic foramina are also seen in subadult *Tyrannosaurus* (BMR P2002.4.1).

The lateral surface of the proximal region projects as a thin flange anterior to the capitulum (fig. 62, cp). This is referred to as the "cranial process" by Brochu (2003). Where best preserved, in rib D, the flange appears as a thin, triangular plate that is smooth laterally. However, medially it is penetrated by a deep pneumatopore immediately anterodorsal to the

capitulum. This pneumatic pocket is not visible in any other cervical ribs, but may be damaged by erosion.

The proximal end grades smoothly into the shaft, but this transition becomes more abrupt posteriorly across the neck. The shaft tapers disally into a thin point, which is broken in most specimens. The shaft cross section is ovoid proximally and becomes thin and plate-like distally, except in rib E where it is circular distally. The lateral and medial surfaces of the shaft are generally smooth, but rib E is excavated laterally by an elongate fossa on the ventral margin of the proximal region right where it begins to grade into the shaft. A similar, but smaller, fossa is also present in rib D, and may represent a muscle attachment site.

A right rib (rib F) has a different morphology than the anterior cervical ribs, and appears to represent a rib from the posterior part of the neck. It closely corresponds with the 9th and 10th cervical ribs of *Tyrannosaurus*, figured by Brochu (2003: fig. 62). This rib is shorter in overall length than ribs B-E, which is not the case in *Tyrannosaurus*, in which the posterior ribs are longer than the anterior ones (Brochu, 2003). However, like the posterior cervical ribs of *Tyrannosaurus*, this rib has a much more extensive proximal region and a more abrupt transition between the proximal region and the shaft when compared to the anterior cervical ribs.

In rib F the capitulum and tuberculum are nearly equal in size (fig. 62). The capitulum has a smoothly convex, ovoid articular surface. It is smaller than the capitulum of the more anterior rib E, which is different from the condition in *Tyrannosaurus* in which the capitula (and the corresponding parapophyses) become larger across the neck (Brochu, 2003). The tuberculum has a nearly circular and flat articular surface and is widely separated from the capitulum. These two structures are linked by a thin web of bone that is excavated medially by a deep fossa. There appears to be a pneumatopore penetrating into the rib in the dorsal part of the fossa, but the

medial surface is damaged here by erosion. The fossa continues distally onto the shaft but gradually becomes less distinct before fading entirely.

On the lateral surface, the proximal region gives rise to a discrete, rectangular flange that projects anteriorly immediately above the parapophysis (when the rib is in articulation). This is in the same position as the cranial process of more anterior cervicals, although it differs in morphology (fig. 62F, cp). Most notably, this cranial process is more discrete than those of the anterior cervicals, and is rectangular instead of triangular. Additionally, the flange and the capitulum are more widely separated in rib F. In this rib the ventral margin of the flange is confluent with the ventral margin of the shaft distally, whereas the dorsal margin grades smoothly into a convex region of bone on the lateral surface that connects to the tuberculum. Ventral and anterior to the flange the proximal region is smoothly excavated by two distinct fossae, which are separated by the neck of bone that links the flange to the lateral surface. A separate, smaller flange may project laterally immediately lateral to the tuberculum: a flake of bone protrudes here, but it has been damaged by erosion.

The transition between the proximal region and shaft in rib F is more abrupt than in anterior cervicals. The shaft is smooth laterally and medially. It is thin in cross section proximally but becomes rounded distally before tapering to a point. There is a slight fossa along much of the ventral margin of the lateral surface, which may be homologous to the costal groove of the dorsal ribs (see below).

The final two ribs, G and H, belong to the transitional vertebrae between the neck and trunk. Based on comparison to *Tyrannosaurus* (Brochu, 2003) it is likely that rib G belongs to the final cervical and rib H to one of the first dorsals.

In rib G the proximal end is expansive, the shaft is long and thick and does not taper strongly distally, the medial surface of the shaft is deeply concave, and the lateral surface is excavated by a distinct fossa, all of which are seen in the dorsal ribs (see below). However, like the cervical ribs, the shaft has a sinuous outline, instead of the broadly curved profile of the dorsal ribs, and would have nearly paralleled the vertebral column when in articulation. The capitulum is completely preserved; it is set off on a distinct neck and has a teardrop shaped, somewhat trochlear articular surface. The base of the tuberculum is present, and the two structures are separated by a smooth, concave arc. The lateral and medial surfaces of the proximal region are generally flat and smooth with no apparent pneumaticity. The ventral margin of the lateral surface of the proximal region is thick, and on the shaft there is a shallow fossa along the ventral margin laterally. This latter fossa is bordered dorsally by an ovoid, upraised muscle attachment scar slightly proximal to midlength of the rib. The shaft is crescentric in cross section proximally, due to the deep medial fossa, but tapers distally to a circular shape.

The final rib, rib H, is likely a dorsal rib but is described here since it falls into the transitional zone between the neck and trunk ribs. Only the shaft is preserved, but it is broadly convex and bow-like as in the dorsal ribs, not sinuous in ouline as is characteristic of the cervical ribs. Additionally, the shaft is longer and more robust than any of the cervical rib shafts, and it does not taper distally to a thin point. The shaft is very similar in overall morphology to a complete dorsal rib described below.

Dorsal Ribs: A single left dorsal rib is present, which is well preserved and nearly complete (figs. 63-64). The rib can be readily divided into two main regions: a proximal portion including the tuberculum and the capitulum, and the distal shaft. The proximal region is well preserved,

with only the articular surfaces of the capitulum and tuberculum suffering minor abrasion. The shaft is broken distally, but the small cross section of the broken surface suggests that only a small part is missing.

The rib is 355 millimeters long, measured as a straight line from the proximal region to the distal broken end. However, the rib is strongly curved, which would have resulted in a wide, barrel-shaped chest. Taking into account the curvature the length of the rib is approximately 500 mm. We describe the rib as it would have articulated in life, and all directional descriptions (medial, dorsal, etc.) are relative to this orientation. In life the tuberculum and capitulum would have been oriented relative to each other in an oblique plane (closer to vertical than horizontal), with the capitulum (which articulates with the parapophysis) located slightly medioventral to the tuberculum (which articulates with the diapophysis). Articulated in this way, the distal end of the shaft would have reached slightly ventral to the capitulum when seen in anterior or posterior view.

The capitulum is nearly complete but the articular surface for the parapophysis is slightly eroded (figs. 63-64, cap). However, it is clear that the capitulum expanded at this contact, and preserved surfaces here are rugose. The tuberculum is a small, discrete projection that is triangular in anterior view, with rugose lateral and medial surfaces (figs. 63-64, tub). The base of the process is thin, but it expands in thickness proximally to articulate with the diapophysis. This articular surface is teardrop shaped, with a thin anterior edge and a more bulbous posterior region.

An elongate neck of bone connects the capitulum with the tuberculum. This neck, which can also be described as web-like, is 100 mm long and 3.5 mm thick anteroposteriorly at its medial margin. The shape of the neck is indicative of the position of the rib in the dorsal series.

The medial margin—that surface linking the capitulum and tuberculum—is slightly concave to flat for most of its length. It is not a deeply concave "notch," as is characteristic of the anterior dorsal ribs of *Tyrannosaurus* (Brochu, 2003). In *Tyrannosaurus* the medial margin becomes flatter posteriorly, and based on the well-described dorsal series of FMNH PR2081 it is likely that the rib of *A. altai* comes from the middle or posterior part of the trunk.

Additionally, *A. altai* shows a unique feature not present in other tyrannosaurids. Although the medial margin of the proximal neck is nearly flat for most of its length, there is a separate, discrete, and deeper concave emargination immediately adjacent to the tuberculum (figs. 63, 64, con). This is not an artifact of breakage, as the margin is comprised of smooth, original bone surface. This region is normally rugose, or simply undifferentiated from the more ventral part of the medial margin, in other tyrannosaurids (*Albertosaurus*: AMNH FARB 5428; *Daspletosaurus*: AMNH FARB 5438; *Gorgosaurus*: AMNH FARB 5432; *Tarbosaurus*: Maleev, 1974: fig. 30; *Tyrannosaurus*: Brochu, 2003: fig. 76). A similar feature does appear to be present in the non-tyrannosaurid tyrannosauroid *Bistahieversor* (NMMNH P-27469), however.

On the lateral surface of the proximal neck, approximately 10 mm ventral to the tuberculum, is a small pneumatic foramen (figs. 63-64, pf). This opening is oval shaped, 7 mm by 4 mm, with a long axis that nearly parallels the long axis of the neck itself. External pneumatic foramina are unknown in other tyrannosaurids (e.g., AMNH FARB 5428, 5432, 5438; ZPAL D-I/3; Currie and Dong, 2001a; Brochu, 2003), but they are present in an array of basal theropods (e.g., *Carnotaurus*: Bonaparte et al., 1990; *Ceratosaurus*: Madsen and Welles, 2000; *Dubreuillosaurus*: Allain, 2005; *Monolophosaurus*: Zhao and Currie, 1993; *Sinraptor*: Currie and Zhao, 1993). Thus, the presence of a pneumatopore is an autapomorphy of *A. altai* among tyrannosaurids.

In *A. altai* the pneumatic foramen leads anteriorly into a smooth, elongate, and shallow fossa that excavates nearly the entire lateral surface of the neck (figs. 63-64, fos). However, the foramen is bordered dorsally and laterally by raised regions of bone. The medial surface of the neck is flat and heavily striated with lineations that trend along the long axis of the neck itself. Near the midpoint of the neck is a single, thickened ridge that stands out from the remainder of the lineations (fig. 63, rid).

The shaft tapers as it extends laterally and ventrally. It begins with a dorsoventral depth of 29 mm and an anteroposterior thickness of 16 mm at the proximal point where it arises from the neck, but terminates at a 7 by 3 mm broken surface. This surface is teardrop shaped, due to a thicker anterior region and a thinner posterior edge.

Much of the lateral surface of the shaft is covered by a smooth fossa (the costal groove of Brochu [2003]), which is especially prominent and deep proximally (fig. 63, cg). This groove is separated from the pneumatic fossa on the neck by a raised region of bone that extends straight ventrally from the lateral border of the pneumatopore. The costal groove is demarcated dorsally by a robust rim, which like the groove is prominent proximally but tapers distally. In contrast, the groove terminates smoothly against the ventral margin of the shaft. However, the ventral margin of the fossa is marked by a sharp and rugose ridge approximately 50 mm distal to where the shaft arises from the neck. This ridge is short, and only extends for 17 mm, but is bordered laterally and medially by a series of fine striations. This is likely a muscle attachment site.

The medial surface of the shaft is smooth and strongly concave. The dorsal margin of the shaft is developed into a strong lip that overhangs the medial surface. This lip is especially prominent proximally but thins out distally, such that the medial surface is simply flat at the

midlength of the shaft. Further distally the medial surface gives rise to a second, thin ridge of bone on the dorsal margin.

Chevron: One well preserved chevron is known (fig. 65). This element likely belongs to the posterior part of the tail, based on comparison to the well described chevron series of *Tyrannosaurus* (Brochu, 2003). The chevron of *A. altai* is essentially L-shaped in lateral view, and comprised of three main processes: a shaft that is nearly vertical when the chevron is in articulation (fig. 65, sh), an elongate posterior process ventrally (fig. 65, pp), and a small and knob-like anterior process ventrally (fig. 65, ap).

The lateral surface of the shaft is smooth but convex lateral ridges follow the long axis of both the anterior and posterior processes. These ridges are bordered dorsally and especially ventrally by thin lineations on the lateral surface. Ventral to the ridges the chevron is very thin, eventually terminating in a broad edge that is less than 0.5 mm thick mediolaterally. The ventral margin of the posterior process is gently convex, as is the ventral margin of the anterior process, but there is a concave notch ventrally where the two processes meet. This is also the case in *Daspletosaurus* (CMN 8506) and *Tyrannosaurus* (Brochu, 2003: fig. 68Q). The anterior process of *A. altai* terminates in a slightly expanded and rugose bulbous knob, whereas the posterior process is broken at its posterior end but appears to terminate in a thin plate.

In dorsal view both sides (rami) of the chevron meet above the haemal canal to articulate with two adjoining caudal vertebrae. The articular facet occupies the posterior half of the dorsal surface of the shaft, is trochlear, and expands laterally relative to the shaft on each side (fig. 65, af). This condition is also seen in other tyrannosaurids, including *Daspletosaurus* (CMN 8506) and *Tyrannosaurus* (Brochu, 2003:fig. 69). This surface is ovoid in shape, with a 25 mm

mediolateral axis and a 10 mm anteroposterior axis at its midpoint. The trochlear surface is gently divided into separate anterior and posterior articular surfaces, which are separated by a transverse ridge. These surfaces mark the articulations with separate (adjacent) caudals. The posterior articular surface is much larger and faces mostly dorsally and slightly posteriorly, whereas the smaller anterior region is much shorter anteroposteriorly and faces anteriorly and dorsally.

The posterior margin of the articular trochlea is smoothly convex and the anterior margin is concave. Anterior to this concavity each side of the chevron shaft gives rise to an anterior prong, which together define the haemal canal (fig. 65, apr). This condition is also seen in *Daspletosaurus* (CMN 8506) and *Tyrannosaurus* (Brochu, 2003:fig. 69). These prongs are robust dorsally and taper ventrally into thin, sheet-like ridges that continue onto the dorsal surface of the anterior process. Dorsally, at the anterodorsal corner of the anterior prong, there is a small, ovoid facet that faces laterally and slightly anteriorly (fig. 65, ovf). Its function is unclear.

The haemal canal is ovoid, 11 mm dorsoventrally deep by 5 mm mediolaterally wide at its midpoint (fig. 65, hc). It is approximately the same shape in both anterior and posterior view, which is true of only some chevrons of *Tyrannosaurus* (Brochu, 2003). A smooth fossa extends ventrally from the canal on both the anterior and posterior surfaces of the shaft (fig. 65, fos). The edges of the anterior fossa are defined by the sheet-like anterior prongs as they taper ventrally. Posteriorly, the fossa is demarcated by a separate set of lineations that extend ventrally from the trochlear surface. At midheight of the shaft these thin sheets are marked by triangular flanges, which project straight posteriorly (fig. 65, tf). This condition is also seen in *Daspletosaurus* (CMN 8506) and *Tyrannosaurus* (Brochu, 2003:fig. 68), except in these taxa the flanges are

positioned well above the midheight of the shaft. Furthermore, the posterior fossa is excavated by two ovoid pockets, one on top of the other, immediately ventral to the haemal canal (fig. 65, poc). The dorsal pocket is the larger of the two, and these may be pneumatic features.

Ilium: Only the right ilium is preserved and it lies against the sacral vertebrae, concealing details of its medial surface (figs. 66-68; measurements in Table 10). The ilium is well preserved and complete posterior to the pubic peduncle but is missing the entire preacetabular process and most of the pubic peduncle. The preserved portion of the ilium is 380 mm long anteroposteriorly and the blade is 160 mm deep dorsoventrally above the acetabulum. The blade is thin: it is 7 mm thick mediolaterally at the posterior end of the postacetabular process, but only 2 mm thick anteriorly where it is broken. In lateral view, the neural spines of sacral vertebrae 3-5 extend into view above the dorsal margin of the ilium.

The lateral surface of the ilium is well preserved although fine surface details such as muscle attachment striations are generally not visible (figs. 66, 68). The most distinctive feature on this surface is a robust ridge that extends dorsally and somewhat anteriorly above the acetabulum (fig. 66, arid). This ridge is present in many theropods but is especially prominent and discrete in tyrannosauroids, and thus is often considered a synapomorphy of this group (e.g., Holtz, 2001, 2004; see also Benson, 2009). However, the form of the ridge differs in tyrannosauroid taxa. For instance, the ridge trends nearly straight dorsoventrally (with the iliac blade held horizontal for reference) in most tyrannosauroids (*Albertosaurus*: Parks, 1928: fig. 10; *Aviatyrannus*: Rauhut, 2003b: fig. 1; *Dilong*: IVPP 14243; *Gorgosaurus*: AMNH FARB 5664, Lambe, 1917: fig. 38; *Guanlong*: IVPP V14531, Xu et al., 2006: fig. 2; *Tarbosaurus*: ZPAL MgD-I/204; *Tyrannosaurus*: AMNH FARB 5027, Osborn, 1916, Brochu, 2003: fig. 90) and is

oriented posterodorsally in *Stokesosaurus* (Madsen, 1974: fig. 1; Benson, 2008: figs. 8, 9) and *Eotyrannus* (MIWG 1997.550). An anterodorsal orientation, like that present in *A. altai*, is also present in some, but not all, specimens of *Daspletosaurus* (CMN 8506), *Gorgosaurus* (CMN 2120), and *Tyrannosaurus* (BMR 2002.4.1), and therefore is not an autapomorphy of *A. altai* as it was originally considered (Brusatte et al., 2009).

In *A. altai* the ridge begins immediately dorsal to the midpoint of the acetabulum as a robust structure, 33 mm in anteroposterior length, that is strongly offset from the lateral surface of the ilium. The ridge becomes less offset and thinner as it continues dorsally, and ceases to be recognized as a discrete structure approximately 40 mm below the dorsal margin of the ilium. The ridge also terminates proximally in other tyrannosaurids (*Daspletosaurus*: CMN 8506; *Gorgosaurus*: AMNH FARB 5664, Lambe, 1917: fig. 38; *Tarbosaurus*: ZPAL MgD-I/204; *Tyrannosaurus*: AMNH FARB 5027, Osborn, 1916, Brochu, 2003) and in the basal taxon *Dilong* (IVPP V14243). In contrast, it extends farther distally (dorsally) in most basal tyrannosauroids, such as *Aviatyrannus* (Rauhut, 2003b: fig. 1), *Guanlong* (Xu et al., 2006: fig. 2), and *Stokesosaurus clevelandi* (Madsen, 1974: fig. 1; not *S. langhami*, which has a ridge that terminates ventrally: Benson, 2008: figs. 8, 9).

Two accessory swellings are also present on the lateral surface of the iliac blade in *A. altai* (fig. 66, antrid, postrid) These structures have been described in other tyrannosauroids, but are often difficult to observe unless the lateral surface is very well preserved (Benson 2008). Anterior to the primary median ridge is an accessory ridge, which takes the form of a narrow bulge that is much less robust and offset than the median ridge (fig. 66, antrid). This anterior ridge projects slightly more anteriorly than the primary ridge, and thus the two are separated by an acute angle. They radiate outwards from the dorsal margin of the acetabulum but breakge

obscures whether they contacted here. At their midpoints the primary and anterior ridges are separated by 22 mm. Additionally, approximately 65 mm posterior to the primary ridge, is a slightly offset swelling that is only visible under horizontal, raking light (fig. 66, postrid). This ridge is in a similar position to a more discrete structure described in *Bagaraatan* (Osmólska, 1996).

The lateral surface is shallowly concave immediately anterior and posterior to the primary median ridge. The posterior concavity is deeper, and is bounded ventrally by an additional robust ridge comprised of the thickened ventral margin of the postacetabular process (fig. 66, ventrid). The dorsal margin of this ridge curves dorsally as it continues posteriorly, and thus the fossa that it defines is triangular. This condition is also seen in other tyrannosaurids, including *Daspletosaurus* (CMN 8506), *Tarbosaurus* (PIN 551-2), and *Tyrannosaurus* (AMNH 5027). This fossa is bisected by the posterior accessory swelling described above. Based on the muscle reconstructions for *Tyrannosaurus* by Carrano and Hutchinson (2002: fig. 9D), it is likely that two muscles (the M. iliofibularis, anteriorly, and M. flexor tibialis externus, posteriorly) attached to this fossa, separated by the accessory swelling. Additionally, it is likely that two other muscles (the M. iliofemoralis externus and M. iliotrochantericus caudalis) attached to the anterior fossa, anterior to the median primary ridge. Whether these were separated by the anterior accessory swelling is difficult to assess. Carrano and Hutchinson (2002: fig. 9D) reconstruct the separation of these muscles to be positioned much further anteriorly than the accessory ridge in *A. altai*, in a region of the preacetabular process that is not preserved here. If the anterior accessory ridge of *A. altai* did separate these muscles, then the iliofemoralis attachment site between the primary and accessory ridges was very small. Alternatively, the anterior accessory ridge may have separated two heads of the M. iliofemoralis externus.

The acetabulum is 105 mm in anteroposterior diameter, between the pubic and ischial peduncles. Much of the supracetabular crest is broken, but it clearly originated on the posterior portion of the lateral surface of the pubic peduncle (fig. 66, sac). Here, the crest begins as a thin ridge that projects entirely laterally, but as it curves dorsally it begins to slightly overhang the anterodorsal region of the acetabulum. More posteriorly the surface of the crest is eroded and broken, but it appears as if it faced more laterally and did not strongly overhang the acetabulum here. The overhanging morphology of the crest in the anterodorsal region of the acetabulum is minimal and similar to that in other (e.g., *Daspletosaurus*: CMN 8506; *Tarbosaurus*: PIN 551-2; *Tyrannosaurus*: Brochu, 2003: fig. 90), as well as *Raptorex* (Sereno et al., 2009) and *Xiongguanlong* (FRDC-GS JB16-2-1). It differs from the hood-like morphology of the crest in more basal theropods, in which the entire structure curves ventrally to roof the acetabulum both dorsally and laterally (e.g., Carrano, 2007: fig. 4; Zhao et al., 2010: fig. 7). This primitive morphology is also present in *Guanlong* (IVPP V14531), and *Dilong* (IVPP V14243) and *Stokesosaurus* (OUMNH J.3311-20, 21) also have crests that extensively overhang the acetabulum laterally. In dorsal or ventral view the supracetabular crest of *A. altai* is straight as in most tyrannosauroids, not semicircular as in *Guanlong* (IVPP V14531, contra Benson, 2008), *Aviatyrannus* (Rauhut, 2003b: fig. 1A) and *Stokesosaurus* (Madsen, 1974: fig. 1B, Benson, 2008: fig. 8D). The shape of the crest in dorsal view is probably correlated with its lateral extent, as semicircular crests are only seen in those taxa with laterally extensive crests. Additionally, in lateral view, the crest is separated from the thickened ventral margin of the postacetabular process by a notch as is typical of tetanurans.

All but the base of the pubic peduncle is missing, and thus little of its morphology is visible (fig. 66, pp). Anterodorsal to the pubic peduncle, and immediately anterodorsal to the

acetabulum, there is a triangular fossa on the lateral surface of the ilium (fig. 66, cupfos). This is the cuppedicus fossa, a feature of tyrannosaurids and other tetanurans, that likely was an attachment site for the M. iliofemoralis internus (Hutchinson 2001; Carrano and Hutchinson 2002). The fossa is delimited dorsally by a swollen region, which appears to be a posterior continuation of the ventral margin of the preacetabular process, judging by the condition in better preserved tyrannosaurid specimens (e.g., Brochu, 2003: fig 92). The medial ridge bounding the fossa internally, which is strong in tyrannosaurids and sometimes considered a diagnostic feature of the group (Holtz, 2001), is not widely visible, although its base is seen in cross section at the broken anterior margin of the ilium.

The ischial peduncle is well preserved but slightly eroded ventrally (fig. 66, ip). It is 38 mm wide mediolaterally by 27 mm long anterposteriorly at its midpoint. The lateral surface of the peduncle is swollen and robust, but not nearly as much so as the iliac peduncle of the ischium. The ischial peduncle makes a wide contribution to the antitrochanter (fig. 66, anti); this contribution is clearly more extensive than in basal taxa such as *Guanlong* and *Stokesosaurus*, but not as pronounced as in large tyrannosaurids such as *Tarbosaurus* (PIN 551-2) and *Tyrannosaurus* (Brochu, 2003:figs. 90-91), in which the iliac contribution to the antitrochanter takes the form of an extensive flange that is deeply inset from the remainder of the ischial peduncle (e.g., Holtz, 2001; Sereno et al., 2009).

Ventrally the peduncle tapers to a blunt peg (fig. 66, peg) that would have fit into the funnel-shaped socket in the iliac peduncle of the ischium (see above). The peg has not been described in other tyrannosaurids, and is often difficult to assess due to breakage or articulation of pelvic elements. A reduced version of the peg seems to be present in *Aviatyrannus* (Rauhut, 2003b: fig. 1) and *Stokesosaurus* (Madsen, 1974: fig. 1C; Benson, 2008: fig. 8), but this structure

is clearly not present in *Tyrannosaurus* (Brochu, 2003). A large specimen of *Tarbosaurus* (ZPAL MgD-I/38) has a funnel-like iliac peduncle on the ischium, but it is unclear whether this funnel received a discrete peg-like projection from the ischial peduncle or simply the highly convex and conical pecuncle itself. A discrete peg is also present in some ornithomimosaurs (e.g., *Gallimimus*: ZPAL MgD-I/3).

In *A. altai* the ischial peduncle is a small process, similar in size and shape to those of other tyrannosaurids. Although much of the pubic peduncle is broken, it appears as if the dorsal bases of the pubic and ischial peduncles (where they arise from the main body of the ilium) were approximately the same anteroposterior length. This is also true of other tyrannosaurids (e.g., Lambe, 1917; Parks, 1928; Maleev, 1974; Brochu, 2003), but not more basal taxa such as *Guanlong* (IVPP V14531), *Raptorex* (Sereno et al., 2009), and *Stokesosaurus* (Benson, 2008), in which the ischial peduncle is much smaller than the pubic peduncle. This latter condition is normal for tetanuran theropods (e.g., Holtz et al., 2001; Benson, 2008; Benson et al., 2010a; Benson, 2010), indicating that the tyrannosaurid morphology is a reversal to the primitive theropod condition in which both peduncles are similarly sized.

A large and deep brevis fossa excavates the ventral surface of the postacetabular process of the ilium (figs. 66-67, bf). The fossa is broad mediolaterally and gradually expands in width posteriorly. It begins anteriorly at a rounded margin that is excavated by an ovoid foramen (8 mm long axis) that faces laterally. Posterior to the foramen the fossa abruptly expands to 27 mm in width and continues to widen until reaching a width of 63 mm at its broken posterior margin. A narrow brevis fossa that does not widen posteriorly is often regarded as a synapomorphy of tetanurans (Holtz, 2000; Hutchinson, 2001; Rauhut, 2003a, but see Brusatte et al., 2008) and is present in most coelurosaurs (Rauhut, 2003a). In contrast, a fossa that expands posteriorly is

present in basal theropods such as coelophysoids and *Ceratosaurus*, as well as some basal tetanurans (Brusatte et al., 2008). However, a few basal coelurosaurs possess the latter condition, including: *A. altai*, *Aviatyrannus* (Rauhut, 2003b), *Dilong* (IVPP 14243), *Guanlong* (IVPP V14531), *Stokesosaurus* (OUMNH J.3311-20-21), and *Bagaraatan* (Osmólska, 1996).

The brevis fossa is demarcated by separate lateral and medial flanges of the postacetabular process. The lateral flange is slightly thicker and more robust at its base than the medial flange (=brevis shelf) and both flanges become thin and rise dorsally as they continue posteriorly. The brevis fossa is visible in lateral view anteriorly but is concealed posteriorly by the overhanging lateral lamina, which extends farther ventrally than the medial lamina in this region of the ilium (fig. 66, ll). The fossa is entirely concealed in lateral view in some basal tyrannosauroids (*Aviatyrannus*: Rauhut, 2003b; *Stokesosaurus*: Madsen, 1974, Benson, 2008), but its anterior portion is visible laterally in *Dilong* (IVPP 14243), *Guanlong* (Xu et al., 2006; IVPP V14531), tyrannosaurids, and most theropods in general (Benson, 2008). However, compared to other derived tyrannosaurids, the laterally exposed portion of the brevis fossa is short in *A. altai*, as it terminates at the anterior end of the fifth sacral vertebra. In other tyrannosaurids, the ofssa reaches the posterior end of the sacral series (*Daspletosaurus*: CMN 8506; *Tarbosaurus*: PIN 551-2; *Tyrannosaurus*: AMNH 5037). Furthermore, in *A. altai*, *Dilong*, *Gorgosaurus* (Lambe 1917), *Guanlong*, and *Raptorex* (Sereno et al., 2009) the ventral margin of the region of the medial flange visible laterally is straight to slightly convex, but does not form a discrete convex lobe-like flange that is offset from the remainder of the medial flange as in some tyrannosaurids (e.g., *Albertosaurus*: Parks, 1928: fig. 10; *Daspletosaurus*: CMN 8506; *Tarbosaurus*: Maleev, 1974: fig. 38; *Tyrannosaurus*: AMNH FARB 5027).

The dorsal margin of the preserved iliac blade describes a smoothly rounded, dorsally convex arc for most of its length. Posterior to the level of the ischial peduncle the dorsal margin straightens out and the convex and straight regions are separated by an inflection point. Such a profile is present in other tyrannosaurids (e.g., *Gorgosaurus*: Lambe, 1917: fig. 16; *Tarbosaurus*: Maleev, 1974: fig. 38; *Tyrannosaurus*: Brochu, 2003: fig. 92), whereas the entire dorsal margin of the ilium is smoothly rounded in more basal taxa (e.g., *Aviatyrannus*: Rauhut, 2003b: fig. 1; *Guanlong*: Xu et al., 2006: fig. 1; *Stokesosaurus*: Madsen, 1974: fig. 1, Benson, 2008: fig. 9). In *A. altai* the posterior margin of the postacetabular process is slightly rounded but essentially squared off and does not taper to a point. This is also characteristic of tyrannosaurids (e.g., *Albertosaurus*: Parks, 1928: fig. 10; *Tyrannosaurus*: Brochu, 2003: figs. 90-92), whereas the ilia of more basal taxa taper posteriorly (*Aviatyrannus*, *Bagaraatan*: Osmólska, 1996; *Dilong*: Xu et al., 2004: fig. 1k, *Guanlong*, *Stokesosaurus*). The non-tyrannosaurids *Raptorex* and *Xiongguanlong* also possess the squared-off condition (Sereno et al., 2009; LH PV18). Furthermore, the orientation of the posterior margin of the ilium is unique in *A. altai*, as it extends posterodorsally. This is in contrast to the condition seen in other tyrannosaurids, where it extends anterodorsally (*Daspletosaurus*: CMN 8506; *Tyrannosaurus*: FMNH PR2081).

Details of the medial surface are not visible, but in dorsal view it is evident that the opposing ilia would have been inclined medially, thus leaving little room between the ilium and sacral neural spines (fig. 67), is typical of tyrannosaurids (Holtz, 2001, 2004). This is also seen in other basal coelurosaurs (e.g., *Gallimimus*: ZPAL MgD/I-1; *Mirischia*: SMNK 2349 PAL). However, the ilia clearly were not in contact dorsal to the sacrum, because the sacral neural spines rise above the ilium and separate the opposing ilia. The ilia make contact in several tyrannosaurids (Holtz, 2004) and there are often distinct striations on the dorsal margin of the

medial surface marking this articulation (e.g., Lambe, 1917: fig. 39). However, the ilia do not meet in more basal taxa (e.g., *Guanlong*: Xu et al., 2006; *Stokesosaurus*: Benson, 2008), and it is unclear whether this feature is individually variable or changes throughout ontogeny in tyrannosaurids.

Ischium: Both left and right ischia are preserved (measurements in Table 10). The right ischium is well preserved and nearly complete, missing only part of the distal end (figs. 69-70). The left ischium is missing the peduncles proximally and much of the distal end. The ischium is comprised of two principal regions: the ischial plate proximally, which contains the peduncles and the obturator process, and the shaft distally. The entire bone, from the acetabular contribution proximally to the most distal preserved tip of the shaft, is 77% of the length of the femur. This is similar to the ratios in other tyrannosaurids (e.g., Brochu, 2003), and although the pubis is unavailable for comparison, suggests that the ischium was most likely "short" relative to the pubis, a condition diagnostic of tyrannosaurids (e.g., Holtz, 2001).

Proximally, the ischial plate region is divided into separate peduncles for articulation with the pubis and ilium (fig. 69, pp, ip). These articulations are unfused in *A. altai*, but fusion between pelvic elements (usually the pubis and ischium, but sometimes also involving the ilium) is present in some large tyrannosaurid specimens (e.g., *Daspletosaurus*: AMNH FARB 5438; *Tyrannosaurus*: Brochu, 2003). The two peduncles are separated by a smooth, concave surface that comprises the ischial contribution to the acetabulum. This margin is 37 mm long anteroposteriorly and 25 mm thick mediolaterally. The smooth articular surface covers the entire region of the ischium between the peduncles in proximal view, and continues distally onto the lateral surface of the bone as a shallow, triangular fossa (fig. 69, fos). It is shallowest anteriorly,

immediately posterior to the pubic peduncle, and deepens posteriorly before terminating against the raised, laterally-convex surface of the ischial peduncle (the antitrochanter region). This fossa is separated from an additional fossa on the lateral surface of the obturator process by a raised region extending posteriorly from the midpoint of the pubic peduncle (fig. 69, rid).

The lateral portion of the acetabular surface is continuous with the more extensive, proximally-facing region, as the two are separated by only a change in surface orientation and not a discrete ridge like is sometimes present in other tyrannosaurids (e.g., *Daspletosaurus*: AMNH FARB 5438). However, the smooth surface for the acetabulum does not continue onto the medial surface of the ischium. Instead, the proximally-facing acetabular surface strongly overhangs the medial surface of the ischial plate (fig. 69, lam). This overhang is present in other tyrannosaurids and was described as a "thin lamina of bone extending along the ventromedial rim of the acetabulum" by Brochu (2003:107).

The pubic peduncle is teardrop shaped in anterior view: it is widest proximally (35 mm mediolaterally) and then tapers to a distal rounded point (fig. 69, pp). At its midpoint the articular surface is 30 mm wide mediolaterally and 42 mm tall proximodistally. The lateral margin of the peduncle is convex and the medial margin is slightly concave. The articular surface itself would have been oriented approximately vertically in life, and would have met the pubis along a straight contact. Unfortunately erosion has removed details of the surface texture of the articular surface.

The iliac peduncle faces entirely proximally (=dorsally) and is ovoid in proximal view, with a 48 mm long axis that trends mediolaterally and a 37 mm minor axis oriented anteroposteriorly (fig. 69, ip). The peduncle has a funnel-like morphology: it expands proximally towards the articular contact with the ilium and its articular surface is excavated by a large pit

that would have received a projection from the ilium to stabilize the contact. The pit occupies nearly the entire surface of the peduncle, and there are not separate fossae as described in *Tyrannosaurus* (Brochu, 2003). Concave depressions in the iliac peduncle are present in other tyrannosauroids (e.g., *Gorgosaurus*: Lambe, 1917; *Stokesosaurus*: Benson, 2008; *Tarbosaurus*: ZPAL MgD-I/38), as well as the potential tyrannosauroid *Bagaraatan* (Osmólska, 1996). In proximal view the lateral margin of the peduncle is thickened and extends lateral to the smooth acetabular surface. This is the ischial contribution to the antitrochanter (fig. 69, anti), which is robust in other tyrannosaurids (e.g., *Tyrannosaurus*: AMNH FARB 5027). The antitrochanter of *A. altai* was clearly large and prominent, but erosion of its lateral surface prevents definitive comparisons with other taxa.

Immediately distal to the iliac peduncle, and present along the posterior margin of the ischial plate, is a laterally and slightly posteriorly facing ovoid fossa that is marked by a rugose bulge at its center (fig. 69, it). This is the ischial tubercle, which likely was an attachment site for the flexor tibialis musculature (Hutchinson, 2001; Carrano and Hutchinson, 2002). The tubercle is 60 mm long proximodistally and 21 mm wide anteroposteriorly. In lateral view this region projects posteriorly from the ischial plate as a convex bulge. Proximal to the bulge is the concave posterior margin of the iliac peduncle and distally is the smoothly convex posterior margin of the ischial shaft. The tubercle is not expressed on the medial surface of the ischium, which is smooth in this region. Two additional rugosities distal to the tubercle, described as present in *Tyrannosaurus* by Brochu (2003), are not visible but this may be due to surface erosion.

Robust and rugose ischial tubercles are characteristic of tyrannosaurids and other coelurosaur groups (Hutchinson, 2001; Brochu, 2003; Benson, 2008), whereas they are often expressed as shallow grooves in more basal tetanurans (e.g., Brusatte et al., 2008). The shape,

size, and degree of rugosity of the tubercle are similar in *A. altai* and juvenile *Gorgosaurus* (AMNH FARB 5664). In contrast, adult *Tyrannosaurus* has a larger, more robust, and triangular flange (AMNH FARB 5027; Brochu, 2003) and more basal tyrannosauroids (e.g., *Stokesosaurus*: Benson, 2008: fig. 10) have a less pronounced bulge that is only slightly differentiated from the posterior margin of the ischial shaft. This latter condition appears to be figured for *Dilong* (Xu et al., 2004: fig. 2), whereas *Guanlong* (Xu IVPP V14531) possesses the grooved condition.

Distal to the peduncles is the obturator process, which is a long triangular flange that projects anteriorly (fig. 69, obt). The process is 230 mm long proximodistally, 80 mm long anteroposteriorly at its midpoint, and 5 mm thick mediolaterally at its anterior end. It is positioned proximally on the ischium: the apex of the process (the "maximum extension" of Brochu 2003:109) is located at approximately one third of the length of the bone. The obturator process is separated from the pubic peduncle by an elongate (50 mm) concave margin, the obturator notch (fig. 69, on). Notches are seen in tyrannosaurids and tetanurans in general (e.g., *Daspletosaurus*: CMN 8506; *Gorgosaurus*: CMN 2120; *Tarbosaurus*: PIN 551-2; *Tyrannosaurus*: FMNH PR2081), but *Guanlong* exhibits a plesiomorphic condition in which the obturator process is continuous with the pubic peduncle, forming an extensive flange penetrated by a foramen (Xu et al., 2006: fig. 2).

The obturator process gradually tapers distally to eventually merge with the shaft. Thus, the distal end of the process is not separated from the shaft by a second discrete notch, as is sometimes the case in basal tetanurans (e.g., Madsen, 1976: pl. 49; Currie and Zhao, 1993: fig. 21). In *A. altai* the obturator process curves somewhat as it extends distally: it begins as a thin flange that is perpendicular to the shaft proximally, but distally it terminates in a long, thin ridge

on the medial surface of the shaft (fig. 69, ma). This ridge is the medial apron (see below). The lateral surface of the obturator process is broken and reconstructed with plaster, but preserved regions exhibit a smooth surface texture. The process was clearly concave on its lateral surface, where it was excavated by a shallow fossa as is common in other tyrannosaurids (e.g., *Gorgosaurus*: AMNH FARB 5664; *Tyrannosaurus*: AMNH FARB 5027). The fossa is deepest at the anterodorsal corner of the obturator process, where a robust lip overhangs the lateral surface.

The ischial shaft is essentially straight, with very slightly convex anterior and posterior margins. This is similar to the condition in adult *Gorgosaurus* (Lambe, 1917: fig. 38) and *Tyrannosaurus* (Brochu, 2003: fig. 93). In contrast, the anterior margin is concave in *Dilong* (Xu et al., 2004: fig. 2), *Guanlong* (IVPP V14531), and *Stokesosaurus* (Benson, 2008: fig. 10). It is also concave, but more subtly, in *Appalachiosaurus* (Carr et al., 2005: fig. 15), and juveniles of *Gorgosaurus* (AMNH FARB 5664) and *Tarbosaurus* (Carr et al., 2005). The distal end of the shaft is broken in both specimens of *A. altai*, so it is unclear whether the ischium expanded into a distal expansion as is typical of some basal coelurosaurs (Benson, 2008). However, the entire preserved portions of both specimens keep a relatively constant anteroposterior thickness, so if an expansion was present it was likely small. We predict that, should complete ischia be found of *A. altai*, that the tip of the shaft will not be expanded, which is the condition that is seen in all other tyrannosaurids.

The shaft of *A. altai* is robust and convex laterally, with a generally smooth surface. The anterior margin of the shaft develops into a ridge distal to where it merges with the obturator process. In this region, the lateral surface is still convex but the medial surface is flattened. This region of the medial surface is covered with a fine series of proximodistally oriented striations,

which begin slightly proximal to the point where the tapering obturator process is reduced to a thin ridge on the medial surface. It is likely that these striations mark the contact with the opposing ischium, and articulated tyrannosaurid ischia seem to have broad contact in this region (e.g., *Tyrannosaurus*: AMNH FARB 5027). However, in the absence of articulated specimens this conclusion must be tentative because the basal tetanuran *Neovenator* has flattened, striated medial ischial surfaces that clearly are not in contact (Brusatte et al., 2008) and may have instead anchored the the fibrous pubo-ischiadic membrane (Hutchinson, 2001).

Regardless of whether the shafts were in broad contact medially, it is clear that the distal extent of the obturator process, which is present as a medial ridge, formed a thin medial apron what would have contacted the opposing ischium at the midline (fig. 69, ma). In *A. altai* the medial apron is located along the anterior margin of the medial surface of the shaft, whereas it is positioned along the posterior edge in *Stokesosaurus* (Benson, 2008) and *Guanlong* (IVPP V14531). Thus, in *A. altai*, the apron would have formed the anterior margin of the contact between the left and right ischia.

Femur: The left femur is complete but badly weathered (figs. 71, 73, 74; measurements in Table 10). It is split into three large fragments: one comprising the head and the lesser and greater trochanters (fig. 71), another that includes most of the midshaft region (fig. 74), and a distal fragment that includes the articular condyles (fig. 73) These fragments are contiguous and fit together well but in most places their surface texture is obliterated. This is especially true of the midshaft fragment, where most of the bone is shattered into small fragments that have been consolidated. A better preserved proximal fragment of the right femur is also preserved but it is broken distal to the lesser trochanter and the medial surface of the head is eroded (fig. 72).

Because of damage the external surface is heavily eroded and textural details are generally not preserved. For instance, there is no clear cranial intramuscular line on the anterior surface of the shaft as is often the case in well-preserved theropod femora (e.g., Brochu, 2003; Brusatte et al., 2008) and most of the muscle attachment scars described by Hutchinson (2001), Carrano and Hutchinson (2002) and Brochu (2003) are not visible. The shaft is not strongly bowed anteriorly, but this may be an artifact of anteroposterior crushing. The femur is extensively hollow and well-preserved regions of the broken surfaces between the three fragments show that the medullary cavity walls were approximately 10 mm thick. The cavity itself is approximately 40 mm in mediolateral width and 27 mm in anteroposterior breadth. In contrast, large specimens of *Tarbosaurus* (e.g., ZPAL D-I/109) have a relatively smaller cavity with thicker walls: the walls can reach a thickness of 60 mm in a femur that is only about 2.5 times as wide mediolaterally as that of *A. altai*.

The head of the femur projects mostly medially but also slightly proximally (dorsally) and anteriorly (figs. 71, 72, h). Thus, it can be described as "anteroproximomedially" oriented. In anterior view the head is separated from the shaft by an angle slightly greater than 90 degrees. This differs from the generalized dinosaurian condition (Sereno, 1991; Benton, 2004) in which the head is perpendicular to the shaft. In *A. altai* this morphology is produced by the slightly proximomedially inclined proximal margin of the head. The ventral margin of the head, on the other hand, arises from the shaft roughly perpendicularly. Not only is the head oriented anteroproximomedially, but it is also "elevated," as it extends further proximally (dorsally) relative to the greater trochanter. A similar condition, in which the head is anteroproximomedially oriented and elevated, is present in *Albertosaurus* (AMNH FARB 5423), *Bistahieversor* (NMMNH P-25049), *Dilong* (IVPP 14243), *Daspletosaurus* (AMNH

FARB5438), and *Guanlong* (IVPP V14531), as well as the basal coelurosaurs (possible tyrannosauroids) *Bagaraatan* (Osmólska, 1996: fig. 11) and *Tanycolagreus* (Carpenter et al., 2005a: fig. 2.14). *Tarbosaurus* (ZPAL D-I/109; Maleev,1974: fig. 40), and *Tyrannosaurus* (Brochu, 2003: fig. 95) possess an anteroproximomedially oriented head, but it is not elevated relative to the greater trochanter (see below; it is elevated by a short distance in one specimen of the subadult *Tyrannosaurus* LACM 23845). An elevated and anteroproximomedially head has been described as present in *Dryptosaurus* (Carpenter et al., 1997), but erosion renders this conclusion uncertain (Brusatte et al., 2011). In contrast, the head of *Appalachiosaurus* is proximomedially oriented but not elevated above the greater trochanter (RMM 6670; Carr et al., 2005), and in some specimens of juvenile *Tarbosaurus* (Currie and Dong, 2001a) it is neither proximomedially oriented nor elevated.

The proximal surface of the head is smoothly rounded and is not excavated by a groove (figs. 71-72). In proximal view the head keeps a relatively constant width as it extends medially. This is variable in basal tetanurans, as specimens of the same taxon often exhibit either constant or medially expanding heads (Brusatte et al., 2008). It may be variable in tyrannosaurids as well: specimens of *Gorgosaurus* (Lambe, 1917: fig. 41) and *Tarbosaurus* (ZPAL D-I/109) possess heads with constant widths, whereas specimens of *Bistahieversor* (NMMNH P-25049), *Dilong* (IVPP V14243), *Guanlong* (IVPP V14531), and *Tyrannosaurus* (Brochu, 2003: fig. 95) exhibit the medially expanding condition.

In *A. altai* the anterior margin of the head is a smooth, convex arc when viewed proximally. It is not marked by any clear tubera or muscle attachment scars. On the other hand, the posterior margin is marked by a slight convexity at its midpoint (fig. 71, pcon), which continues down the posterior surface of the shaft as a distolaterally trending ridge. This ridge

forms the lateral boundary of a fossa for the femoral head ligament (fig. 71, sl), which excavates the medial half of the posterior surface of the head, and is represented in proximal view by a concave margin. However, the fossa itself is not strongly visible in proximal view, but is instead obscured by an overhanging lip, which comprises the visible concave margin (fig. 71, lip). The posteromedial region of the head is broken in both specimens, making it is impossible to determine the strength of the lip that demarcated the fossa medially. The convexity, lip, and fossa are also seen in *Albertosaurus* (CMN 11315), *Bistahieversor* (NMMNH P-25049), and *Tarbosaurus* (PIN 552-2). A similar condition is seen in adult *Tyrannosaurus* (FMNH PR2081; Brochu, 2003:fig. 95), but the lip is bisected into dorsal and ventral parts by a groove that extends laterally from the fossa.

The greater trochanter is eroded on the left femur but better preserved on the right fragment, although the proximal margin in both specimens is missing (figs. 71-72, gt). The trochanter nearly extends to the same proximal level of the head itself, but falls short due to the "elevated" dorsomedial trend of the head. In adult *Tyrannosaurus* (Brochu, 2003: fig. 95) and *Tarbosaurus* (ZPAL D-I/109; Maleev, 1974: fig. 40) the greater trochanter extends slightly past the proximal level of the lateral region of the head. Therefore, in adults of these taxa, the proximal margin of the head appears as a highly concave surface in posterior view, due to the elevated medial region of the head and the elevated greater trochanter laterally (Brusatte et al., 2010a: character 285). There does appear to be some potential ontogenetic variation in this character, however: the proximal margin in subadult *Tyrannosaurus* (LACM 23845) is gently convex, and the greater trochanter is a low and wide ridge lateral to it. In *A. altai* the trochanter appears to be smoothly confluent with the head and the two are not separated by a groove or

cleft. The greater trochanter is most pronounced in lateral view, is visible in posterior view as a thin flange, and is barely distinguishable from the head in anterior view.

In posterior view, the flange-like profile of the greater trochanter is separated from the median ridge that demarcates the ligament fossa (see above) by a second fossa, the trochanteric fossa (fig. 71, tf). This depression is 25 mm wider mediolaterally than the ligament fossa, but is much less inset into the bone. It is not apparent as a concave surface in proximal view, but is clearly present as a smooth indentation on the posterior surface in posterior view. The trochanteric fossa is plesiomorphic for dinosaurs (Novas, 1996) and is present as a deep and discrete structure in *Dilong* (IVPP 14243), *Guanlong* (IVPP V14531), *Tarbosaurus* (ZPAL D-I/109) and *Tyrannosaurus* (Brochu, 2003: fig. 95A). In the latter two taxa it is a much wider, more triangular depression than it is in *A. altai*. This fossa may be an attachment site for the M. puboischiofemoralis, which is reconstructed as attaching to the greater trochanter itself in *Tyrannosaurus* (Carrano and Hutchinson, 2002).

In lateral view the greater trochanter is a semiovoid, flattened structure. It is distinctly separated from the lesser trochanter: the two are divided by a narrow cleft (fig. 71, cl), which continues posteriorly on the lateral surface of the femur as a thin and deep groove (fig. 71, gr). The lesser and greater trochanters extend to approximately the same level proximally when seen in lateral view, although this may be a preservational artifact. Both trochanters are also approximately the same size and have an anteroposterior breadth of approximately 45 mm.

The lesser trochanter is a pronounced process extending anteriorly from the shaft as a flange, which curves medially as it projects anteriorly (figs. 71-72, lt). It is 120 mm in proximodistal length, and rises nearly to the level of the head proximally. The trochanter continues distally and thickens before gradually merging with the anterolateral margin of the

shaft. It projects 38 mm farther anteriorly than the head and the two are separated by a smooth, concave depression, the interotrochanteric fossa (figs. 71-72, itf). The entire medial surface of the trochanter is smoothed by the fossa. On the right element the fossa is pierced by a nutrient foramen (fig. 72E, for), as has been described in *Tyrannosaurus* (Brochu, 2003). However, it is clear that no such foramen is present on the left femur (fig. 71). The extreme proximal region of the fossa, at the spot where the head and greater and lesser trochanters meet, is indented as a deep notch. The notch is essentially a ventral continuation of the cleft between the greater and lesser trochanters, which is expressed on the medial surface of the femur.

The lateral surface of the lesser trochanter is strongly convex immediately anterior to where it meets the greater trochanter. The lateral surface becomes slightly concave laterally as the flange thins and continues anteriorly before terminating as a plate-like structure. This concave surface (fig. 71, ltcon) is scoured by numerous proximodistally trending striations that are especially pronounced at the proximal extent of the lesser trochanter. These are some of the best preserved surface details on the entire femur, and are also seen in other derived tyrannosaurids (e.g., Brochu, 2003). The anterior margin of the lesser trochanter is eroded on the left femur but better preserved on the right bone. It was evidently slightly convex as in *Tyrannosaurus* (Brochu, 2003) and other tyrannosaurids.

The anterior margin of the lesser trochanter is thinnest dorsally and thickens ventrally into a robust region that is likely homologous to the accessory trochanter (figs. 71-72, atr). This subsidiary process is described as a "subtle depression on the lesser trochanter's outline" in *Tyrannosaurus* (Brochu, 2003:113), but is figured as a robust ridge in the same region (Brochu, 2003: fig. 109). The accessory trochanter is also positioned here in basal tetanurans, in which this structure is a more robust protuberance that is clearly demarcated from the lesser trochanter as a

flange (e.g., Madsen, 1976: pl. 50; Brusatte et al., 2008: fig. 21). This basal tetanuran morphology is also present in *Guanlong* (IVPP V14531), *Dilong* (IVPP V14243), and *Xiongguanlong* (FRDC-GS JB16-2-1). The presence of a flange-like accessory trochanter in *A. altai* cannot be ruled out because of inadequate preservation. However, the morphology of other tyrannosaurids (Lambe, 1917; Maleev, 1974; Brochu, 2003), in which the accessory trochanter is a slight mound, suggests that the preserved morphology in *A. altai* may be genuine. In *A. altai* the accessory trochanter is bordered laterally by the slightly concave and rugose fossa on the lateral surface of the trochanter (described above), and the presence of rugose lineations on both structures indicate that they jointly participated in a muscle attachment surface.

On the lateral surface of the femur there is a convex bulge distal and slightly posterior to the lesser trochanter. This is the trochanteric shelf (fig. 71, ts), which is often present as a more discrete flange or ridge in basal theropods and close dinosaur outgroups (e.g., Tykoski and Rowe, 2004). In these more primitive taxa the shelf is continuous with the lesser trochanter, but in *A. altai* and other tyrannosauroids (e.g., *Albertosaurus*: AMNH FARB 5423; *Dilong*: IVPP V14243; *Guanlong*: IVPP V14531; *Tarbosaurus*: ZPAL D-I/109; *Tyrannosaurus*: Brochu, 2003: fig. 95) it is a separate structure. The surface around the trochanter is too damaged to identify any of the various muscle attachment sites described by Hutchinson (2001), Carrano and Hutchinson (2002), and Brochu (2003). However, the surface of the shelf itself is scoured by fine lineations in those regions that are well preserved.

The fourth trochanter is a pronounced ridge on the posteromedial margin of the shaft, beginning approximately 50 mm distal to the head (fig. 74, 4tr). It resembles a narrow ridge and is approximately 95 mm long proximodistally. Proximally it gradually becomes confluent with the shaft, whereas distally it joins the shaft at a more abrupt transition. In many other

tyrannosaurids the trochanter is larger, more offset, and triangular in shape (e.g., *Albertosaurus*: AMNH FARB 5423; *Appalachiosaurus*: Carr et al., 2005: fig. 16B; *Tarbosaurus*: ZPAL D-I/109; *Tyrannosaurus*: Brochu, 2003: fig. 95). It is possible that the more rounded and less prominent trochanter of *A. altai* may be partially an artifact of erosion. Original bone surface is present, however, on the trochanter so any damage would be the result of abrasion and not breakage. In medial and lateral views the outline of the fourth trochanter is similar to those of *Tarbosaurus* and *Tyrannosaurus*: all are sigmoid, with a nearly proximodistally oriented proximal region of the posterior edge and a more obliquely oriented distal region, which meet at a posteriorly-projecting point (fig. 75; ZPAL D-I/109; Brochu, 2003).

The posterior surface of the shaft immediately lateral to the fourth trochanter is convex. In contrast, the anterior surface of the shaft is concave and excavated by a smooth fossa. This fossa corresponds to the "teardrop-shaped rugosity" of *Tyrannosaurus* (Brochu, 2003:113). Here it faces strongly medially and slightly anteriorly, and excavates the medialmost third of the shaft directly lateral to the trochanter. It is bounded anteroventrally by a slight lip, which is in the same position as a rugosity that may be an attachment site for part of the puboischiofemoralis musculature in *Tyrannosaurus* (Brochu, 2003). The external surface of the trochanter is well preserved in some regions, which invariably are scoured by fine strations. These are especially prominent and densely packed distally.

Most of the midshaft region between the fourth trochanter and the extensor groove distally is heavily weathered. It appears as if the anterior surface of the shaft was convex and the posterior region was slightly convex but flatter, but additional details are not apparent.

Distally the femur expands in mediolateral width and gives rise to separate medial and lateral condyles for articulation with the tibia (fig. 73). The medial condyle is an

anteroposteriorly elongate oval in distal view, 82 mm long by 32 mm wide mediolaterally at its midpoint (fig. 73, mc). A similar shape is present in other tyrannosauroids, including *Albertosaurus* (CMN 11315), *Alectrosaurus* (AMNH FARB 6554), *Appalachiosaurus* (Carr et al., 2005: fig. 16D), *Bistahiversor* (NMMNH P-25049), *Dilong* (IVPP V14243), *Dryptosaurus* (Carpenter et al., 1997: fig. 8C; Brusatte et al., 2011: fig. 15F), *Guanlong* (IVPP V14531), *Stokesosaurus* (Benson, 2008: fig. 11F), *Tarbosaurus* (ZPAL D-I/109), and *Tyrannosaurus* (Brochu, 2003: fig. 95J). Both anterior and posterior margins of the medial condyle are of similar shape and size in *A. altai*, unlike the smaller and more acutely rounded anterior margin of *Alectrosaurus* (AMNH FARB 6554) and *Tyrannosaurus* (Brochu, 2003). The lateral condyle is larger than the medial condyle (fig. 73, lc). It is approximately spherical, with a diameter of 52 mm.

The anterior surface of the medial condyle is planar to slightly concave and slopes posterolaterally, whereas that of the lateral condyle is strongly convex. These two surfaces meet medially to form a pronounced extensor groove that is most prominent distally between the condyles (fig. 73, eg). The groove continues proximally, on the anterior surface of the femur, for at least 145 mm, until the region where the femur is heavily eroded. The more proximal extent of the groove is also referred to as the intercondylar fossa (e.g., Brochu, 2003) or the popliteal fossa (e.g., Carr et al., 2005). The groove proper is widest mediolaterally distally (20 mm) and thins as it extends proximally. The anterior surface of much of the lateral condyle is eroded, but preserved regions show that it was generally smooth, as is the better preserved medial condyle. Unfortunately, erosion proximal to the groove precludes identification of the “large, oval rugosity” in this region that is prominent and perhaps diagnostic of tyrannosaurids or a more

inclusive clade of tyrannosauroids (Brochu, 2003:113). This rugosity is present in *Alectrosaurus* (AMNH FARB 6554) and *Tarbosaurus* (ZPAL D-I/109).

The convex anterior surface of the lateral condyle continues laterally and is smoothly confluent with the lateral surface of the femur here. In lateral view there is a smooth, mediolaterally broad, proximodistally extensive fossa that faces laterally and slightly posteriorly (fig. 73, lfos). This depression separates the lateral condyle from the crista tibiofibularis and terminates distally at the smooth articular surface of the condyle. This fossa is seen in many theropods, including the tyrannosauroids *Albertosaurus* (CMN 11315), *Alectrosaurus* (AMNH FARB 6554), *Bistahieversor* (NMMNH P-25049), *Dilong* (IVPP V14243), *Gorgosaurus* (ROM 1247), *Guanlong* (IVPP V14531), *Tarbosaurus* (PIN 552-2), and *Tyrannosaurus* (Brochu, 2003: fig. 95J). The fossa appears to be present as an indistinct structure in *Dryptosaurus* (ANSP 9995; Brusatte et al., 2011), but this morphology is probably an artifact of erosion.

The medial condyle shows a clear separation between its anterior and lateral surfaces. These surfaces are divided by a pronounced ridge, the medial distal crest, which extends 180 mm proximodistally in total length (fig. 73, mdc). The crest pinches out proximally, and at the region where the femur is heavily eroded the anterior and lateral surfaces are undivided and smoothly confluent. Distally, the crest bifurcates (fig. 73, bif) to enclose a broad, triangular fossa that faces medially (fig. 73, trifos). In medial view this fossa occupies the anterior half of the medial condyle, and continues distally until it terminates agains the smooth articular surface of the condyle. A similar fossa is difficult to observe on other tyrannosaurid femora due to breakage and poor preservation, but it is present in *Albertosaurus* (CMN 11315), *Alectrosaurus* (AMNH FARB 6554), and *Tarbosaurus* (ZPAL D-I/109). The medial distal crest is not nearly as pronounced in *Tyrannosaurus*, in which the surface homologous to the triangular fossa is

reduced and faces more anteriorly than it does in *A. altai* (Brochu, 2003: fig. 95). On the other hand, the mesiodistal crest is thick and almost web-like in *Tarbosaurus* (ZPAL D-I/109), a pronounced condition more like that of *A. altai* than *Tyrannosaurus*.

The posterior surface of the femur is deeply excavated by a flexor groove between the condyles (fig. 73, fg). The groove is 25 mm wide mediolaterally at its distal extent, where it is most deeply inset into the bone. Here, the groove is marked by a series of small furrows that are separated by elongate mound-like eminences. This morphology is a reduced version of the rugosities figured in *Tyrannosaurus* (Brochu, 2003: fig. 95J) and described as "deep proximodistal notches" (Brochu, 2003:115). The flexor groove extends proximally for 105 mm and then abruptly becomes confluent with the shaft. Thus, it is much less extensive proximally than the extensor groove. The flexor groove expands in width as it expands proximally, up to a dimension of 40 mm, but then narrows at its proximalmost extent before joining the shaft. The surface of the groove, where preserved, is covered with a series of fine lineations.

The lateral margin of the groove is demarcated distally by a large, conical shaped crista tibiofibularis (fig. 73, ctf). In distal view this structure is 50 mm wide mediolaterally at its base, which is partially broken, and 37 mm long anteroposteriorly. Posterorly it rounds into a terminal point, as is also the case in other tyrannosauroids (*Alectrosaurus*: AMNH FARB 6554; *Bistahieversor*: NMMNH P-25049; *Dilong*: IVPP V14243; *Guanlong*: IVPP V14531; *Stokesosaurus*: Benson, 2008: fig. 11F; *Tarbosaurus*: ZPAL D-I/109; *Tyrannosaurus* (Brochu, 2003: fig. 95J), as well as *Bagaraatan* (ZPAL MgD-I/108; Osmólska et al., 1996: fig. 11). Thus, the crista is a conical or pyramidal structure that resembles a triangle in distal view. In posterior view it becomes confluent with the shaft proximally, thinning into a ridge that laterally bounds the flexor groove across its entire extent.

In distal view the medial condyle is oriented slightly posteromedially-anterolaterally. Its distal surface is smoothly rounded. The lateral condyle is essentially spherical, with a small anterior bulge that is slightly separated from the remainder of the condyle (fig. 73, ab). A similar bulge is present in other tyrannosauroids (*Alectrosaurus*: AMNH FARB 6554; *Appalachiosaurus*: RMM 6670; *Bistahieversor*: NMMNH P-25049; *Dryptosaurus*: ANSP 9995, Brusatte et al., 2011; *Stokesosaurus*: Benson, 2008: fig. 11F; *Tarbosaurus*: ZPAL D-I/109; *Tyrannosaurus*: Brochu, 2003: fig. 95J; *Xiongguanlong*: FRDC-GS JB16-2-1), but is absent in *Dilong* (IVPP V14243) and *Guanlong* (IVPP V14531). The crista tibiofibularis extends posteriorly to the same level as the medial condyle and its lateral margin is concave where it takes part in the fossa separating the crista from the lateral condyle (described above). The lateral condyle extends 20 mm further laterally than the crista. The distal surfaces of both condyles, as well as the crista, are smooth and rounded for articulation with the tibia. The lateral condyle is much more convex than the medial condyle and the two are separated by a shallow trochlear surface in distal view. This region separates the flexor and extensor grooves. The crista is raised slightly proximally relative to the lateral condyle, and thus there is a slight step between them on the distal surface of the femur. The medial condyle extends slightly further distally than the lateral condyle, and by extension the crista (fig. 73B).

Crus-Tarsal Joint: A single fragment preserves the distal regions of the tibia and fibula, the astragalus, and the calcaneum of the right hindlimb (fig. 75). These four bones are preserved articulated and are tightly appressed to each other. However, there is no fusion between any of these elements; fusion is present in the possible tyrannosauroid *Bagaraatan* (Osmólska, 1996).

Instead, the contact surfaces of the *A*. *altai* holotype are clearly visible, but they are often filled with matrix.

Tibia: The distalmost 160 mm of the right tibia is preserved as part of this fragment (fig. 75, tib). It is ovoid in cross section where it is broken proximally, with a mediolateral width of 51 mm an anteroposterior length of 45 mm, and a circumference of 160 mm. The walls of the tibia are thin in this area, measuring only 10 mm in thickness. The tibia was largely hollow, and the marrow cavity itself was approximately 30 mm by 20 mm (fig. 75, mcav). Distally the tibia expands in length and especially width, and it is 101 mm mediolaterally by 55 mm anteroposteriorly at its distal end where it articulates with the astragalus.

The anterior surface of the tibia fragment is almost entirely covered by the ascending process of the astragalus (fig. 75, asc), whereas the lateral surface is concealed by the fibula (fig. 75, fib). Thus, details of these regions are not observable. However, it is clear that there was a prominent crest on medial margin of the anterior surface that bounded the ascending process medially and slightly dorsally (fig. 75, mcr). This crest sweeps laterodorsally, eventually merging smoothly with the anterior surface of the tibia near the midpoint of the bone. The crest is especially prominent across its distal most 60 mm, where it cups the medioventral corner of the ascending process as a pronounced and slightly overhanging lip. This lip is the anterior and medial margin of the medial malleolus of the tibia, and distally it becomes confluent with the anteromedial corner of the malleolus. However, as the ridge gets smaller and thins out proximally, there is no noticeable rim that demarcates the ascending process dorsally. A similar ridge is also present in other tyrannosauroids, including *Albertosaurus* (AMNH FARB 5218),

Appalachiosaurus (RMM 6670), *Dryptosaurus* (ANSP 9995), *Tarbosaurus* (e.g., PIN 551-2), and *Tyrannosaurus* (Brochu, 2003:fig. 96D).

The distal articular surface of the tibia is covered by the astragalus, but it is clear that the tibia is divided into separate medial and lateral malleoli distally (fig. 75, mm, lm). The entire mediolateral width of the distal end of the tibia is slightly greater than that of the astragalus as in tyrannosaurids in general (Carr et al., 2005). The medial surface of the medial malleolus is flattened but the lateral surface of the lateral malleolus is covered by the astragalus and calcaneum. However, small regions of a laterally-facing, smooth, concave facet are present (but not possible to photograph due to the overlying fibula). Here, the distal end of the fibula would have abutted the tibia. This facet faces almost entirely laterally and only slightly anteriorly, in contrast to the condition in *Albertosaurus* (Parks, 1928: fig. 12), *Appalachiosaurus* (Carr et al., 2005: fig. 16E), *Bistahieversor* (NMMNH P-25049), and especially *Tarbosaurus* (ZPAL MgD-I/38) and *Tyrannosaurus* (Brochu, 2003: fig. 96D), in which it faces almost entirely anteriorly. The strong anterior orientation is even present in small *Tarbosaurus* juveniles approximately the same size as the *Alioramus altai* holotype (e.g., ZPAL MgD-I/29). A more laterally facing facet, similar to that in *A. altai*, is present in *Alectrosaurus* (Gilmore, 1933: fig. 10; AMNH FARB 6554), *Dilong* (IVPP V14243), *Guanlong* (IVPP V14531), and *Stokesosaurus* (Benson, 2008: fig. 12A). In *A. altai* the posterior margin of the lateral malleolus, which is the posterolateral corner of the tibia itself, is partially broken, but evidently it is thick and robust. This region backs the fibula posteriorly.

The more laterally-facing fibular facet in *A. altai* is a result of a poorly expanded lateral malleolus (fig. 75, lm). Although the lateral malleolus is covered by the fibula it clearly is smoothly confluent with the shaft and does not project far laterally relative to the shaft (best seen

in anterior or posterior view). This is also the case in *Alectrosaurus* (although some breakage on the type specimen, AMNH FARB 6554, makes this interpretation tentative), *Dilong* (IVPP V14243), *Dryptosaurus* (Carpenter et al., 1997: fig. 8; Brusatte et al., 2011), *Guanlong* (IVPP V14531), and *Stokesosaurus*, as well as several basal coelurosaurs (e.g., *Coelurus*: Carpenter et al., 2005b: fig. 3.11D; *Garudimimus*: Kobayashi and Barsbold, 2005: fig. 14; *Tanycolagreus*: Carpenter et al. 2005a: fig. 2.14) and very basal theropods (*Dilophosaurus*: Welles, 1984: fig. 33; *Ceratosaurus*: Madsen and Welles, 2000: pl. 22; *Sinraptor*: Currie and Zhao, 1993: fig. 22; *Zupaysaurus*: Ezcurra and Novas, 2007: fig. 5). In contrast, other tyrannosauroids have a lateral malleolus that projects strongly laterally relative to the shaft, thus providing space for an anteriorly-facing fibular facet (e.g., *Albertosaurus*, *Appalachiosaurus*, *Bistahieversor*, *Gorgosaurus*, *Tarbosaurus* juveniles and adults, *Tyrannosaurus*). A strongly projecting malleolus is also present in some basal coelurosaurs (e.g., *Tugulusaurus*: Rauhut and Xu, 2005: fig. 4B) and basal theropods (e.g., *Allosaurus*: Madsen, 1976: pl. 51; *Majungasaurus*: Carrano, 2007: fig. 6; *Torvosaurus*: Britt, 1991: fig. 21). Thus, the strength of the lateral malleolus is extremely variable among theropods.

The external surface of the medial malleolus (fig. 75, mm) is broken and somewhat eroded. However, the area where it merges with the shaft is undamaged, and shows that the two regions were smoothly confluent. In other words, the medial malleolus does not project medially as a lobate structure, separated from the shaft by a pronounced step. This is true of tyrannosauroids in general (*Albertosaurus*: Parks, 1928: fig. 12; *Appalachiosaurus*: Carr et al., 2005: fig. 16E,G; *Bistahievesor*: NMMNH P-25049; *Dilong*: IVPP V14243; *Dryptosaurus*: Carpenter et al., 1997: fig. 8, Brusatte et al., 2011; *Guanlong*: IVPP V14531; *Stokesosaurus*: Benson, 2008: fig. 12A; *Tarbosaurus*: ZPAL MgD-I/38; *Tyrannosaurus*: Brochu, 2003: fig. 96).

In *A. altai* the lateral malleolus extends only slightly distally relative to the medial malleolus. This is an unusual condition among tyrannosaurids that is also present in *Dilong* (IVPP V14243). In contrast, other tyrannosaurids have a lateral malleolus projecting much further distally than the medial malleolus (*Albertosaurus*: Parks, 1928: fig. 12; *Appalachiosaurus*: Carr et al., 2005: fig. 16; *Bistahieversor*: NMMNH P-25049; *Dryptosaurus*: Carpenter et al., 1997: fig. 8, Brusatte et al., 2011; *Guanlong*: IVPP V14531; *Stokesosaurus*: Benson, 2008: fig. 12; *Tarbosaurus*: ZPAL MgD-I/38; *Tyrannosaurus*: Brochu, 2003: fig. 96). The unexpanded lateral malleolus of *A. altai* is similar to the condition in many basal coelurosaurs (e.g., *Coelurus*: Carpenter et al., 2005b: fig. 3.11D; *Garudimimus*: Kobayashi and Barsbold, 2005: fig. 14; *Tanycolagreus*: Carpenter et al., 2005a: fig. 2.14; *Tugulusaurus*: Rauhut and Xu, 2005: fig. 4), as well as basal theropods (e.g., *Ceratosaurus*: Madsen and Welles, 2000: pl. 22; *Dilophosaurus*: Welles, 1984: fig. 33; *Elaphrosaurus*: HMN MB.R.38–44; *Liliensternus*: HMN 2175.7.8.1; *Sinraptor*: Currie and Zhao, 1993: fig. 22; *Zupaysaurus*: Ezcurra and Novas, 2007: fig. 5). However, some allosauroids (Brusatte and Sereno, 2008) and spinosauroids (Britt, 1991) also possess a distally expansive lateral malleolus, and thus this character is variable among theropods as well.

Finally, the posterior surface of the tibia is smooth. It is rounded dorsally but becomes flat distally, across the posterior surface of the malleoli.

Fibula: The distalmost 150 mm of the right fibula is preserved as part of the crurotarsal fragment (fig. 75, fib). The broken proximal end is crescent-shaped in cross section, with a concave groove facing medially for articulation with the tibia. The crescent is 20 mm long anteroposteriorly and 7 mm wide mediolaterally at its midpoint. The fibula expands gradually in

anteroposterior thickness as it continues ventrally, before terminating in a slightly expanded club-shaped prominence that sits on top of the calcaneum (fig. 75, defib). This prominence is 30 mm long anteroposteriorly and is almost identical in form to the distal expansion of *Albertosaurus* (Parks, 1928: fig. 14), *Appalachiosaurus* (RMM 6670), *Bistahieversor* (NMMNH P-25049), *Tarbosaurus* (PIN 551-2), and *Tyrannosaurus* (Brochu, 2003: fig. 97).

The external surface of the fibula is abraded but appears to have been relatively smooth. The anterior margin is smooth and unexpanded at the broken proximal end, but ventrally it develops into a sharp crest that overlaps the tibia and astragalus at their articulation ventrally. Proximally the crest is oriented anteriorly and medially; it curves slightly medially to overhang the tibia, but distally it curves somewhat laterally before merging with the anterior margin of the distal club. This lip is what Brochu (2003:115) is referring to when he describes the fibula of *Tyrannosaurus* as "reorient(ing) toward the distal end as it approaches the articular facet, from an anteroposterior projection, such that the surface faces medially, to one in which the surface faces posteromedially." This expanded and curving edge is also seen in *Alectrosaurus* (AMNH FARB 6554), *Appalachiosaurus* (RMM 6670), and *Bistahieversor* (NMMNH P-25049). It is also present, but seemingly to a lesser extent, in *Albertosaurus* (CMN 11315) and *Tarbosaurus* (PIN 551-2).

Medially, at least the proximal region of the fibula was excavated by a groove, as shown by the shape of the broken proximal surface. The medial concavity, which gives the fibula its crescent shape, is probably homologous to the "deep groove" noted on the fibula of *Tyrannosaurus* and tyrannosaurids in general by Brochu (2003:115). The groove is also seen in *Albertosaurus* (AMNH FARB 5218), *Alectrosaurus* (AMNH FARB 6554), *Appalachiosaurus* (RMM 6670), and *Bistahieversor* (NMMNH P-25049), as well as many other theropods. It is

likely that much of this groove articulated against the tibia, although it is difficult to determine details of this contact in *A. altai*. The fibula is appressed to the tibia across the length of the crurotarsal fragment, but this is clearly a preservational artifact. However, Parks (1928:29) describes a well preserved specimen of *Albertosaurus* in which the "tibia and fibula…fit well together in their distal parts," which was likely the case in *A. altai* based on the clear presence of a medial groove and the close fit of this groove against the tibia when the two are appressed. Indeed, although the tight fit of the tibia and fibula is a taphonomic effect, only a thin region of matrix separates them.

Distally, the expanded club of the fibula sits in an articular cup formed by the confluence of the calcaneum, astragalus, and tibia, as described in *Tyrannosaurus* (Brochu, 2003). The morphology of the cup in *A. altai* is similar to that in *Tyrannosaurus*, except that it is more laterally facing (see above). The calcaneum only makes a narrow contribution to the floor of the cup, which is bounded laterally by a lip on the tibia and medially by the astragalus.

Astragalus: The right astragalus is complete and well preserved (fig. 75, ast). It is comprised of two main regions: a thick hourglass-shaped condylar region distally and a thin, plate-like ascending process proximally (fig. 75, asc). The condylar region does not sit directly below the tibia as in many basal theropods (e.g., Madsen, 1976), but is rotated onto the anterior face of the tibia so that it cups the ventral and anterior surfaces of the distal end of the tibia. This condition is present in other tyrannosauroids (e.g., *Alectrosaurus*: AMNH FARB 6554; *Appalachiosaurus*: RMM 6670; *Dryptosaurus*: ANSP 9995; *Tarbosaurus*: ZPAL MgD-I/29; *Tyrannosaurus*: Brochu, 2003:fig. 96) and is common in coelurosaurs (e.g., Holtz et al., 2004: character 605).

The ascending process is tightly appressed to the tibia but the two bones are unfused (i.e., separate from each other). The process is tall, measuring 110 mm in proximodistal height, and it is 2.34 times the greatest height of the condylar region. The ratio of the ascending process to the condylar region is similar to that of most other tyrannosaurids, but is greater than in *Tyrannosaurus* (Table 11). In *A. altai* the ascending process is thin (anteroposterior dimension): it is 5 mm thick distally where it arises from the condyles and gradually thins to less than 1 mm in thickness at its proximal termination. Distally, the mediolateral width of the process is very nearly as wide as the condylar region, as in other tyrannosaurids and basal coelurosaurs (e.g., Kobayashi and Barsbold, 2005; Carpenter et al., 2005a), but this condition is unlike the one seen in more basal theropods in which the ascending process is a small, tab-like triangular projection that is much narrower than the condyles (e.g., Madsen, 1976; Welles, 1984; Britt, 1991; Currie and Zhao, 1993; Madsen and Welles, 2000; Carrano, 2007; Ezcurra and Novas, 2007). This primitive morphology is also seen in *Guanlong* (IVPP V14531).

The anterior surface of the ascending process is smooth, and distally it is excavated by a large, circular fossa (38 mm diameter) immediately above the midpoint of the condylar region (fig. 75, fos). The ventral margin of the fossa is formed by the dorsal margin of the condyles, and here there is a distinct step between the condyles and the ascending process. Although separated by the step, the fossa is essentially continuous with the trochlear surface of the condyles and the two regions are not separated by a groove as in *Appalachiosaurus* (RMM 6670; Carr et al., 2005). The fossa is more deeply excavated laterally, and its lateroventral region is deeply inset as a pocket. In contrast, the medial margin becomes gradually confluent with the anterior surface, especially medioventrally, as has also been described for *Appalachiosaurus* (Carr et al., 2005).

An anterior fossa is common in tyrannosaurids (Parks, 1928; Gilmore, 1933; Maleev, 1974; Brochu, 2003; Carr et al., 2005) and theropods in general (e.g., Currie and Zhao, 1993:fig. 23J), although it is often smaller and less pronounced in more basal theropods with smaller ascending processes (e.g., Carrano, 2007: fig. 9). It is also unpronounced and present as a broad, shallowly offset depression in *Dilong* (IVPP V14243), very different from the more discrete and indented fossae of other tyrannosauroids. The fossa is a single structure in *A. altai*, and it is not divided into two regions as in *Tyrannosaurus* (Brochu, 2003). The region of the anterior surface of the ascending process medial to the fossa, and extending above it, is slightly convex, whereas the lateral region is shallowly concave.

The ascending process of *A. altai* is triangular in shape (fig. 75, asc). The lateral margin of the triangle parallels the lateral margin of the tibial shaft and the fibula, and appears to be nearly straight proximodistally. The medial margin of the triangle is slightly convex and is oriented strongly proximolaterally-distomedially. Thus, the medial and lateral margins diverge at a strongly acute angle and meet at a sharp point proximally. This point, the apex of the triangle, is located along the the straight lateral margin. The sloping medial margin is separated from the medial edge of the medial condyle by a small notch, and is cupped posteriorly and medially by the strong lip on the medial malleolus of the tibia (see above).

The ascending processes of other tyrannosaurids are also triangular, but their exact shapes often differ. In *Tyrannosaurus* the process is triangular with its apex along the lateral margin (Brochu, 2003: fig. 96), as in *A. altai*. However, the medial margin is more convex in *Tyrannosarus*, is oriented less steeply relative to the lateral margin, and is marked by an inflection point that separates two distinct regions that trend in slightly different orientations. Of these regions, the margin proximal to the inflection point trends more horizontally. An inflection

point, separating a proximal subhorizontal margin and a more distal oblique edge, is also present in *Albertosaurus* (AMNH FARB 5227), which has a much taller ascending process that is more similar in relative height to *A. altai* than to *Tyrannosaurus*. *Appalachisaurus* (Carr et al., 2005: fig. 18) and *Dilong* (IVPP V14243) clearly possess a medial margin that is closer to vertical, although breakage precludes observation of an inflection point and calculation of the total height of the process. *Gorgosaurus* (Lambe, 1917: fig. 42) and juvenile *Tarbosaurus* (Maleev, 1974: fig. 61; ZPAL MgD-I/29) are similar in morphology to *A. altai*, as all three possess an elongate and obliquely inclined medial margin without an inflection point.

The condylar region is 91 mm wide mediolaterally, and is comprised of distinct medial and lateral condyles for articulation with the distal tarsals (fig. 75, mc, lc). The medial condyle is formed entirely by the astragalus, but a small region of the lateral condyle is formed by the calcaneum laterally. When the calcaneum contribution is taken into account the condyles are essentially equal in width (37 mm wide mediolaterally) when they are seen in anterior view. However, the astragalar portion of the lateral condyle is only 25 mm in width. The medial condyle is taller (43 mm proximodistally) than the lateral condyle (37 mm). In distal view the medial condyle is obviously much larger than the lateral condyle, as it is 17 mm long anteroposteriorly, compared to 10 mm for the lateral condyle.

Furthermore, in distal view, the lateral condyle projects straight anteroposteriorly, whereas the medial condyle trends anteromedially. A larger medial condyle that projects anteromedially is common in tyrannosauroids (e.g., *Appalachiosaurus*: Carr et al., 2005: fig. 18E; *Dilong*: IVPP V14243; *Dryptosaurus*: Carpenter et al., 1997: fig. 9, Brusatte et al., 2011; *Guanlong*: IVPP V14531; *Tarbosaurus*: ZPAL MgD-I/29; *Tyrannosaurus*: Brochu, 2003: fig. 96J), as well as theropods in general (e.g., *Allosaurus*: Madsen, 1976: pl. 52E; *Coelurus*:

Carpenter et al., 2005b: fig. 3.12E; *Dilophosaurus*: Welles, 1984: fig. 35E; *Garudimimus*: Kobayashi and Barsbold, 2005: fig. 14F; *Sinornithomimus*: Kobayashi and Lu, 2003: fig. 22F; *Sinraptor*: Currie and Zhao, 1993: fig. 23D; *Torvosaurus*: Britt, 1991: fig. 23M; *Tugulusaurus*: Rauhut and Xu, 2005: fig. 4C; *Zupaysaurus*: Ezcurra and Novas, 2007: fig. 4D).

The lateral and medial condyles are separated by a smooth trochlear surface (fig. 75, tro). This surface is most pronounced on the anterior surface of the condyles, where it is deeply inset and continues distally as a smooth but only slightly inset (gently concave) region. The trochlear surface extends slightly onto the posterior face of the astragalus, but the condyles are not pronounced on this surface. In distal view the two condyles are separated by a deeply concave margin anteriorly, which represents the trochlea proper of the crus-tarsal joint. The medial condyle is smoothly confluent with this margin, but the lateral condyle meets it at an abrupt angle, and thus is separated from the margin by a small notch (fig. 75, not). A less distinct notch is present in *Albertosaurus* (CMN 5601). There appears to be a single concave surface in *Alectrosaurus* (AMNH FARB 6554), *Appalachiosaurus* (Carr et al., 2005: fig. 18E; RMM 6670), *Dilong* (IVPP V14243), *Dryptosaurus* (Carpenter et al,. 1997: fig. 9; Brusatte et al., 2011), *Tarbosaurus* (ZPAL MgD-I/29), and *Tyrannosaurus* (Brochu, 2003: fig. 96J), but the notch is a subtle structure that may easily be eroded.

The posterior margin of the astragalus is only slightly concave in distal view and it is much straighter than the anterior margin that is excavated by the trochlea. A similar condition is present in other tyrannosaurids (Brochu, 2003; Carr et al., 2005) and other theropods in general (e.g., Madsen, 1976; Norell and Makovicky, 1999; Kobayashi and Barsbold, 2005). The lateral surface of the lateral condyle is covered by the calcaneum, but the medial surface of the medial condyle is exposed to view. It is crescent shaped, due to a deep proximal concavity where it cups

the medial malleolus of the tibia. At its midpoint the crescent is only 17 mm deep proximodistally.

Calcaneum: The calcaneum is a small, nearly circular plate of bone (fig. 75, calc). It is approximately 40 mm in diameter in lateral view and is 15 mm thick mediolaterally at its distal margin. It thins proximally, reaching a width of 7 mm at its termination, but this may be exaggerated by mediolateral crushing. The maximum width of the calcaneum is only 16% of the astragalus. This is smaller than in other tyrannosaurids (Carr et al., 2005), but we hesitate to regard it as autapomorphic due to erosion and crushing that may exaggerate the narrow width of the calcaneum.

The medial surface of the calcaneum cannot be seen, as it is tightly affixed to the astragalus. The lateral surface is slightly eroded, but it is clearly excavated by a smooth concavity (fig. 75, calc). This concave surface is referred to as the lateral condylar depression (e.g., Osmólska, 1996, Carr et al., 2005) and is present in other tyrannosauroids (e.g., *Alectrosaurus*: AMNH FARB 6554; *Albertosaurus*: AMNH FARB 5227; *Appalachiosaurus*: RMM 6670, Carr et al., 2005; *Bistahieversor*: NMMNH P-25049; *Guanlong*: IVPP V14531; *Tarbosaurus*: ZPAL MgD-I/4; *Tyrannosaurus*: FMNH PR2081, Brochu, 2003), as well as other basal coelurosaurs (e.g., *Bagaraatan*: Osmólska, 1996).

Only the anterior and ventral margins of the calcaneum are well preserved, and these are both smoothly rounded to participate in the saddle-shaped joint surface for the distal tarsals. The ventral surface is heavily eroded but preserved portions show that its texture matches that of the ventral surface of the astragalus. The calcaneum would have smoothly joined with the astragalus and formed the lateral portion of the lateral articular condyle, which is mostly comprised of the

astragalus. The dorsal and posterior margins of the bone are eroded; these have a more complex shape for articulation with the tibia and fibula (Brochu, 2003; Carr et al., 2005: fig. 18G), but details of these articulations are cannot be seen in the holotype of *A. altai*.

Distal Tarsals: Two distal tarsals are preserved appressed to the right metatarsus, and they appear to be in the approximate life positions (fig. 76). In proximal view, the medial tarsal (tarsal 3) overlies the center of the metatarsus, covering most of metatarsal III, the posterolateral portion of metatarsal II and the posteromedial portion of metatarsal IV (fig. 76, dt3). The lateral tarsal (tarsal 4) is positioned over the posterolateral corner of the metatarsus (fig. 76, dt4), such that metatarsal V, which is articulated with the lateral surface of the tarsal, is placed on the posterior (flexor) side of the metatarsus and cannot be seen in anterior view. A similar configuration of both distal tarsals is seen in an articulated metatarsus of *Gorgosaurus* (Lambe, 1917:fig. 44). Both tarsals overhang the metatarsus posteriorly. Neither approaches the anterior margin of the metatarsus, but instead they fall approximately 27 mm short. This condition may be slightly exaggerated by preservation because matrix separating the tarsals from the metatarsus causes the tarsals to be raised such that they slope anteriorly. However, they clearly would not have approached the anterior margin in life, as is also the case in other tyrannosaurids (e.g., *Albertosaurus*: CMN 11315; *Bistahieversor*: NMMNH P-25049; *Gorgosaurus*: Lambe, 1917; *Tyrannosaurus*: Brochu, 2003).

Distal tarsal 3 has a maximum mediolateral width of 31 mm and a maximum anteroposterior length of 27 mm. It is somewhat ovoid shape in proximal view and similar to the shape figured for *Gorgosaurus* (Lambe, 1917:fig. 44), although its medial and posterior surfaces are eroded. Its proximal surface is convex and smooth, whereas its distal surface, which is mostly

visible due to the posterior overhang of this tarsal relative to the metatarsus, is concave medially and convex laterally. The tarsal is thin proximodistally at its anterior margin (4 mm) compared to the much thicker posterior margin (11 mm). There appears to be a notch in the posterior surface, but this is at least partially due to erosion (fig. 76, not).

Distal tarsal 4 is larger than distal tarsal 3 and is broadly triangular in shape (in proximal view). It has a maximum mediolateral width of 39 mm and a maximum anteroposterior length of 35 mm. The proximal surface is smoothly convex but fine surface details such as those observed by Brochu (2003) are unclear due to poor preservation, and the distal surface is covered by matrix and thus cannot be seen. Tarsal 4 slightly overlaps the lateral edge of tarsal 3, but whether this is natural or a preservational artifact is unclear. The lateral articular surface for metatarsal V is broken and eroded and has been infilled by consolidant, therefore preventing a detailed description of this contact. However, there does appear to have been a discrete notch for the metatarsal, as well as an expanded anterolateral corner of the tarsal (fig. 76, alc), as in *Tyrannosaurus* and other tyrannosaurids (Brochu, 2003:fig. 98). As preserved the tarsal does not cover any portion of metatarsal III, but this may be due to postmortem distortion because other tyrannosaurids exhibit extensive overlap (Brochu, 2003).

Metatarsus: Numerous fragments of metatarsals were collected as eroded surface finds. Unfortunately, most of these are small and poorly preserved, and thus are unassignable to individual metatarsals and unable to be described and compared with other tyrannosaurids. However, a reasonably complete but heavily weathered proximal right metatarsus is preserved (fig. 76), as well as a nearly complete right metatarsal I (fig. 77), large fragments of two left metatarsals III, (fig. 78) and a large piece of the left metatarsal V. Most importantly, these

various pieces show that the metatarsus is arctometatarsalian, with a third metatarsal that is pinched between metatarsals II and IV proximally (Holtz, 1995). This condition is present in all tyrannosaurids (e.g., Lambe, 1917; Holtz, 1995; Brochu, 2003), as well as the non-tyrannosaurid taxa *Appalachiosaurus* (RMM 6670; Carr et al., 2005), *Bistahieversor* (NMMNH P-25049), *Dryptosaurus* (ANSP 9995; Brusatte et al., 2011), and *Raptorex* (Sereno et al., 2009). In contrast, a more normal theropod metatarsus, in which metatarsal III is large and unpinched, is seen in the basal tyrannosauroids *Dilong* (IVPP V14243), *Eotyrannus* (MIWG 1997.550), and *Guanlong* (IVPP V14531).

The distal portion of the right **metatarsal I** is preserved (fig. 77). This fragment is 38 mm long proximodistally, but it is unclear how much of the bone is missing proximally. The broken proximal end is teardrop shaped in cross section, with a 20 mm long axis that trends approximately 45 degrees relative to the long axis of the distal end, in concert with the twisting of the shaft to lie against the medial surface of metatarsal II. The ventral margin of the proximal broken surface is thicker mediolaterally (7.5 mm) than the dorsal margin (2 mm), which thins into a plate-like flange to abut metatarsal II. A portion of the articular surface for the second metatarsal is present on the lateral surface of metatarsal I, and this region is slightly concave and smooth (fig. 77, mtII). The distal end of metatarsal I is triangular, 16 mm deep anteroposteriorly (=extensor-flexor) and 12 mm wide mediolaterally at its midpoint. Anteriorly the distal surface terminates in a pronounced and rounded point that stands out from the remainder of the anterior surface of the bone (fig. 77, ac). Posteriorly it divides into two equal-sized condyles that extend to the same level posteriorly (fig. 77, pc). The condyles diverge at an acute angle and are separated by a deep flexor groove that continues posteriorly as a fossa on the posterior (flexor) surface (fig. 77, fg). The medial ligament pit is reduced to a small fossa (fig. 77, llp), whereas the

lateral pit is an extensive, deep, ovoid depression (fig. 77, mlp). All of these features can be seen in other tyrannosauroids (e.g., *Albertosaurus*: AMNH FARB 5218; *Alectrosaurus*: AMNH FARB 6554; *Bistahieversor*: NMMNH P-25049; *Gorgosaurus*: ROM 1247).

The proximal portion of the right **metatarsal II** is preserved on the articulated metatarsus fragment (fig. 76, mtII). Much of the proximal surface is eroded, but this surface was approximately 80 mm anteroposteriorly by 33 mm mediolaterally at its midpoint. As is normal for arctometatarsalian pedes, the lateral surface of the proximal end is strongly concave to brace metatarsal III, and the anterolateral corner is expanded to contact metatarsal IV and exclude metatarsal III from the anterior margin of the proximal metatarsus. The medial surface of metatarsal II is highly convex in proximal view, and the small preserved regions of the anterior, medial, and posterior surfaces are smooth, with a high degree of surface erosion.

Only a very small fragment of the right **metatarsal III** is preserved on the articulated metatarsus, but it was clearly pinched between metatarsals II and IV and did not contribute to the anterior margin of the metatarsus in proximal view. A large piece of the distal left metatarsal III is present and well preserved (fig. 78). It also clearly exhibits the arctometatarsalian characteristics of a pinched midregion (fig. 78, pin), strong posterior ridge (fig. 78, prid), and an abrupt distal expansion at the condyles. Proximally, where the shaft is broken, the cross section is triangular and very small (8 mm anteroposterior by 7 mm mediolateral). These measurements are partially reduced by erosion, but the shaft is clearly pinched here. Distally the shaft rapidly expands in mediolateral width, such that it is 18 mm anteroposteriorly by 18 mm mediolaterally where it gives rise to the condyles. The posterior surface has a pronounced ridge that is placed more laterally than medially, and bifurcates (fig. 78, bif) and dissipates approximately 13 mm proximal to the condyles. The medial surface of the shaft is eroded, but its thick base suggests

that there was a prominent medial flange as in arctometatarsalian tyrannosauroids (Brochu, 2003:fig. 100C; Li et al., 2010). The condylar region is 25 mm anteroposteriorly by 32 mm mediolaterally. The distal articular surface is weathered, but the lateral and medial ligament pits are equally deep and large (fig. 78, llp, mlp). On the anterior surface, between the condyles, is a shallow and smooth extensor groove (fig. 78, eg). On the posterior (flexor) surface, however, is a raised, non-articular platform (fig. 78, nap), which is another characteristic feature of arctometatarsalian taxa (Sereno et al., 2009).

A distal portion of what appears to be a second left metatarsal III is also present, and its features and size are nearly identical with those of the left bone described above. Because the metatarsals fragments were collected as surface float concentration it is possible that some mixing of specimens could have occurred, as theropod dinosaur bones are quite common at Tsaagan Khuushu. However, based on preservation and proximity to in situ bones, and their clear tyrannosauroid features, most of the metatarsal bones can confidently be assigned to the IGM 100/1844 specimen.

The proximal portion of the right **metatarsal IV** is present on the articulated metatarsus fragment (fig. 76, mt IV). Although much of its proximal surface is covered by the distal tarsal 4, accurate measurements are possible (64 mm anteroposteriorly by 41 mm mediolaterally at the midpoint). The medial surface has a discrete concave notch for metatarsal III, as is usual for arctometatarsalian tyrannosauroids (e.g., Lambe, 1917; Maleev, 1974; Brochu, 2003; Carr et al., 2005). The lateral margin is highly convex in proximal view and the anterior margin is shallowly concave. The exposed region of the proximal articular surface is flat and concave at its center. On the lateral surface there is a central triangular platform proximally, immediately below the proximal articular surface (fig. 76, plat). This may have braced metatarsal V, even though this

latter bone is displaced posteriorly to the platform as preserved. The platform is also seen in other tyrannosauroids (e.g., *Alectrosaurus*: AMNH FARB 6554). Distally, the lateral surface gives rise to a subtle ridge which is strongest at the distal broken edge.

The nearly complete right **metatarsal V** is preserved on the articulated metatarsus fragment (fig. 76, mt V) and a proximal portion of the left metatarsal V is preserved in isolation. The right bone is crescentic in shape and 93 mm long proximodistally, but its distal tip is missing. It is remarkably smooth and gracile for a tyrannosaurid, with midshaft dimensions of 14 mm (anteroposterior) by 8 mm (mediolateral). The proximal end is only slightly expanded relative to the shaft (17 mm anteroposteriorly), and although the distal tip is not preserved, there is no sign that the bone expanded here. There are no rugosities on any of the surfaces. In contrast, the metatarsals V of other tyrannosaurids are stockier, scoured with numerous discrete rugosities, greatly expanded proximally and slightly expanded distally, and possess discrete flanges on their posterior surfaces (e.g., Lambe, 1917:fig. 47; Parks, 1928: fig. 19; Maleev, 1974: fig. 45; Brochu, 2003: fig. 102).

The proximal articular surface is not preserved in either metatarsal V, obscuring details of the articulation with distal tarsal 4. Similar patterns of breakage in both specimens and unfinished bone surfaces suggest that the proximal end of the metatarsal may have had a cartilaginous epiphysis. The anterior tuberosity that is present on this bone in many basal theropods is absent, a condition shared with other tyrannosaurids (Brochu, 2003). The lateral surface is flat and smooth proximally but becomes convex distally. The posterior surface is convex proximally, thins into a sharp ridge, and then distally expands into a flattened facet. The medial surface is flat distally where it articulates with metatarsal IV, which a strong ridge posteriorly to brace this contact. Distally the medial surface becomes convex, and then is

excavated by a deep concavity (fig. 76, fos). A similar concave fossa is also seen in other tyrannosauroids (*Albertosaurus*: CMN 11315; *Alectrosaurus*: AMNH FARB 6554; *Bistahieversor*: NMMNH P-25049; *Gorgosaurus*: ROM 1247). This fossa is non-articular, and was likely a muscle attachment site, although identifying individual muscles that anchored on metatarsal V is difficult (Brochu, 2003).

Pedal Phalanges: Numerous phalanges are present, in various states of completeness and preservation (figs. 79-89). As identified with comparisons to complete tyrannosaurid feet (e.g., Lambe, 1917; Parks, 1928; Maleev, 1974; Brochu, 2003), these include both phalanges of the right digit I (fig. 79), the left non-ungual phalanx I-1, and several phalanges tentatively identified as belonging to digits II, III, and IV (fig. 80).

The phalanges of **digit I** are the smallest and most gracile of the pes (fig. 79). The proximal (non-ungual) phalanx is 48 mm long, with a proximal end that is 21 mm deep by 15 mm wide and a distal end that is 13 by 11 mm. The proximal articular surface is a simple concave cup and the distal surface is trochlear, but does not divide into separate condyles posteriorly. Both distal ligament pits are deep and large. There is a flexor groove on the posterior surface but no extensor pit anteriorly. Proximal to the flexor groove the posterior surface becomes convex for a short region and then is excavated by a deep, ovoid concavity that extends to the proximal articular surface. The lateral side of the shaft is smoothly convex and the medial side is marked by a deep concavity along its ventral half, which thins as it continues distally. All of these features are seen in other derived tyrannosauroids (e.g., *Alectrosaurus*: AMNH FARB 6554; *Bistahieversor*: NMMNH P-25049; *Gorgosaurus*: ROM 1247).

The ungual is 36 mm long, with a proximal articular surface that is 17 mm deep by 8 mm wide (fig. 79). There is a single groove on both the lateral and medial surfaces (fig. 79, lgr, mgr). Both grooves are only distinct on the distal half of the ungual. The medial groove is centrally placed, whereas the lateral groove is centrally placed at its proximal end and then curves dorsally and twists onto the extensor surface of the ungual. Although the proximal articular surface is weathered it does not appear as if the dorsal lip was prominent. Prominent lips are present in most theropods, including the basal tyrannosauroids *Appalachiosaurus* (RMM 6670; Carr et al., 2005), *Dilong* (IVPP V14243), *Eotyrannus* (MIWG 1997.550), and *Guanlong* (IVPP V14531). On the contrary, they absent or reduced to a subtle tuberosity in tyrannosaurids (e.g., *Albertosaurus*: Parks, 1928; *Gorgosaurus*: Lambe, 1917; *Tarbosaurus*: Maleev, 1974; *Tyrannosaurus*: Brochu, 2003).

The non-ungual phalanges of **digits II-IV** are generally similar in structure (fig. 80). The proximal and distal articular surfaces are expanded relative to the midshaft, especially in the more proximal phalanges. The proximal articular surfaces are saddle-shaped, with a strongly overhanging dorsal lip. The distal surface is trochlear and divided into separate condyles, except in what are identified as the first two phalanges of digit III where this surface is a single structure. Those phalanges with separate condyles have a deep flexor groove and most phalanges have at least a subtle extensor pit. This pit is larger and deeper in the more proximal phalanges. Both lateral and medial ligament pits are deep in all phalanges. The lateral pits are larger than the medial pits in the phalanges of digit II, the medial pits larger than the lateral pits in the phalanges of digit IV, and the pits of each side are equal in size in the phalanges of digit III. The proximal phalanges of each digit are more than three times longer than wide at the midpoint, as in most

theropods, but contrasting with the shorter and stockier proximal phalanges of *Tarbosaurus* (Maleev, 1974; ZPAL collection) and *Tyrannosaurus* (Brochu, 2003).

DISCUSSION

THE VALIDITY OF *ALIORAMUS*: *ALIORAMUS* IS NOT JUVENILE *TARBOSAURUS*

Brusatte et al. (2009a) identified the specimen described here, IGM 100/1844, as pertaining to a new taxon, *Alioramus altai*, based on its possession of several autapomorphies. Many derived characters exhibited by IGM 100/1844 are also present in the holotype of *Alioramus remotus* (Kurzanov, 1976), and the two specimens appear to pertain to animals of approximately the same size (3% difference in reconstructed skull length) and ontogenetic stage (subadult). As neither known specimen of *Alioramus* pertains to a mature individual, it is pertinent to ask: could these specimens belong to juveniles of a previously known taxon, most likely the temporally and biogeographically contemporaneous large-bodied and deep-skulled *Tarbosaurus bataar*? This possibility has been raised in the literature (Currie, 2003a) and is intriguing to consider in light of recent work demonstrating that large-bodied tyrannosaurids underwent dramatic changes during ontogeny, including a transformation from an elongate and gracile skull (such as that of *Alioramus*) in juveniles to a deep and robust skull in adults (Carr, 1999; Carr and Williamson, 2004). Several lines of evidence, however, indicate that *Alioramus* is a distinct taxon and the two known specimens do not represent *Tarbosaurus* subadults.

Extreme skull length is a diagnostic feature of *Alioramus*: Although juvenile tyrannosaurids possess proportionally longer and lower skulls than adults, no known tyrannosaurid specimen has a skull nearly as proportionally elongate (compared to skull depth and femur length) as the holotype of *A. altai*. When the *A. altai* holotype is plotted on Currie's (2003b) bivariate logarithmic plot of skull length vs. femur length, it clearly falls above the regression lines defined by all other measured tyrannosaurid specimens (see discussion above). Therefore, the *A. altai* holotype has a longer skull in comparison to femur length (and therefore body size, as femur length is tightly correlated with body mass) than any other tyrannosaurid individual, including both tyrannosaurine and albertosaurine subadults of nearly identical femur length that are shown on the Currie (2003b) plot. Therefore, the extremely long and low skull of *A. altai* (and also the *A. remotus* holotype) is a robust diagnostic character based on current understanding of tyrannosaurid growth and body proportions.

This conclusion is supported by comparisons of skull proportions among tyrannosaurid specimens. The holotype skull of *A. altai* has a length:depth ratio of 3.91 (anteroposterior length measured from anteroventral corner of maxilla to posteroventral corner of quadratojugal; depth measured at level of lacrimal ventral ramus). Subadult *Albertosaurus* and *Tyranosaurus* of similar ontogenetic stage and body size are characterized by ratios of 3.15 and 3.4, respectively (Carr, 1999), and older individuals of both taxa have progressively smaller ratios (Currie, 2003; Carr and Williamson, 2004). Described and available specimens of unequivocal *Tarbosaurus* subadults of similar body size to the *A. altai* holotype (see below) are mostly too fragmentary to permit accurate measurement of skull proportions, but the nearly complete skull of PIN 553-1 (a subadult *Tarbosaurus* which has a maxilla that is 12% longer anteroposteriorly than the *A. altai* holotype: Maleev, 1974) has a ratio of 2.63. Furthermore, the exquisitely preserved skull of a

much younger and smaller *Tarbosaurus* individual (ca. 3 years old) has a ratio of 2.82 (Tsuihiji, et al. 2011). Adult *Tarbosaurus* has a smaller ratio of approximately 2.5 (Hurum and Sabath, 2003).

It is possible that future discoveries of subadult *Tarbosaurus* may reveal that individuals of approximately the same age as the *A. altai* holotype (ca. 9 years old) had similarly elongate skulls. This is unexpected, however, given that *Tarbosaurus* specimens of similar body size to the *A. altai* holotype are known and possess a proportionally much deeper skull (PIN 533-1) and divergent anatomical features (see below for discussion of ZPAL specimens). Furthermore, assuming if *A. altai* was a subadult *Tarbosaurus*, this would mean that *Tarbosaurus* underwent its own unique growth trajectory in which skull length is not isometric as in other tyrannosaurids (Currie, 2003b), but rather increased during early adolescence (from the 3-year-old to 9-year-old phase) and decreased later in ontogeny (from the 9-year-old to mature phase). In sum, therefore, comparisons with other tyrannosaurid specimens clearly show that the skull of *Alioramus* is proportionally the most elongate of any known tyrannosaurid, and we confidently consider it a diagnostic feature that distinguishes *Alioramus* as a taxon and differentiates it from subadult *Tarbosaurus*.

Alioramus* is morphologically different from similarly-sized subadult *Tarbosaurus: Another indication that *Alioramus* is not a juvenile *Tarbosaurus* is that similarly-sized specimens of these genera exhibit clear morphological differences (figs. 81-82). Some differences between the holotype of *A. altai* and various specimens of subadult *Tarbosaurus* from the Nemegt Formation were briefly stated in the supplementary information of Brusatte et al. (2009a). Specifically, Brusatte et al. (2009a) referenced a number of exemplar specimens of subadult *Tarbosaurus*

from the Institute of Paleobiology collection in Warsaw, which are of approximately the same size as corresponding elements of the holotype of *Alioramus altai* but differ substantially in morphology. These specimens are identified as *Tarbosaurus* based on shared characters with adult members of the genus (see Hurum and Sabath 2003). Many of these specimens (maxilla, postorbital, jugal, tibia) belong to a single individual (ZPAL MgD-I/29; figs. 81-82), whose tibia is almost exactly the same size (within 10%, based on the width of the distal end) of the tibia of the *A. altai* holotype, which is firm evidence that the two specimens were of approximately the same body size. However, these specimens were only briefly described by Brusatte et al. (2009a) and were not illustrated.

We illustrate the best preserved and most informative juvenile *Tarbosaurus* exemplars in Figures 81-82 (we note that one of the specimens discussed by Brusatte et al. [2009] and interpreted as a juvenile postorbital, ZPAL MgD-I/175, is here reinterpreted as a quadratojugal and not discussed further). These show several important differences with the holotype of *Alioramus altai*. The maxilla of ZPAL MgD-I/29 (fig. 81A) exhibits a deeper subcutaneous surface of the main body (i.e., that surface below the antorbital fossa) and a ventrally convex profile, unlike the shallower main body and straight profile of *A. altai* (fig. 81B). Additionally, the anterior margin of the maxilla is oriented closer to vertical in juvenile *Tarbosaurus*, in contrast to the more posterodorsally sloping profile of the long-snouted *A. altai*. The postorbital of subadult *Tarbosaurus* (ZPAL MgD-I/29; fig. 81F) have a larger, more prominent, and more rugose cornual process posteroventral to the orbit. Additionally, the ventral ramus does not taper as it does in *A. altai*, but projects into the orbit anteroventrally as a sheet-like flange. The surangular of subadult *Tarbosaurus* (ZPAL MgD-I/31; fig. 81D) possesses a muscular fossa above the surangular foramen that faces mostly laterally, unlike the dorsally facing condition of

A. altai, and lacks the deep pocket behind the foramen that is so prominent in *A. altai* (fig. 81C). The tibia of subadult *Tarbosaurus* (ZPAL MgD-I/31; fig. 82B, D) has a fibular facet that faces strongly anteriorly, not laterally as in *A. altai*, and a lateral malleolus that projects far laterally and distally relative to the shaft, unlike the unexpanded condition in *A. altai* (fig. 82A, C). Finally, although we do not provide a figure, the jugal of ZPAL MgD-I/29 lacks the conspicuous and diagnostic lateral hornlet of *A. altai*.

In sum, these differences between the holotype of *Alioramus altai* and juvenile *Tarbosaurus* of approximately the same size, which are located on bones from across the skull and postcranium, support the taxonomic distinction between these two contemporaneous and sympatric tyrannosaurids.

ALPHA-LEVEL TAXONOMY: *ALIORAMUS ALTAI* AND *ALIORAMUS REMOTUS*

Brusatte et al. (2009a) identified the specimen described herein, IGM 100/1844, as pertaining to a new species of the genus *Alioramus*, which was originally described by Kurzanov (1976) based on a fragmentary specimen. This specimen, the holotype of a species Kurzanov (1976) named *Alioramus remotus*, was the only specimen of the genus *Alioramus* described in the scientific literature until the publication of Brusatte et al.'s (2009) short paper describing IGM 100/1844. This new specimen clearly belongs to the genus *Alioramus* (i.e., is more closely related to *A. remotus* than to any other currently known tyrannosauroid taxon), as the two specimens share numerous derived characters that are otherwise unknown among tyrannosauroids (see below). It was also described as a new species, *A. altai*, because it possesses a handful of clear differences

with the holotype of *A. remotus*. Here, we review the evidence for assigning IGM 100/1844 to *Alioramus* and for separating *A. remotus* and *A. altai* as distinct taxa.

Similarities between IGM 100/1844 and the holotype of *Alioramus remotus*: *Alioramus altai* (based on what is currently the only known specimen, IGM 100/1844) and *A. remotus* (based on what is currently the only known specimen, the holotype PIN 3141/1, described by Kurzanov [1976]) share a combination of characters that distinguish them from all other tyrannosauroids. We note that, unfortunately, at least three other skulls probably referable to *Alioramus* that were undoubtedly collected in Mongolia have surfaced in recent years at the Tucson Fossil show (MAN, pers. obs.), but the disposition of these important specimens is unknown.

Characters that are shared by the two published specimens of *Alioramus* include: a long and low skull and jaws (see above), nasals with a series of distinct rugosities, an elongate maxillary fenestra, a vertical and cleftlike exit for the lacrimal canal, and a high tooth count (16-17 maxillary alveoli; 18-20 dentary alveoli). Therefore, the referral of IGM 100/1844 to *Alioramus* is justified. The laterally-projecting jugal "hornlet," considered an autapomorphy of *A. altai* by Brusatte et al. (2009a), may be present in the holotype of *A. remotus*, based on Kurzanov's (1976) description of a tuberculated growth in the middle of the bone in that specimen. However, as the holotype of *A. remotus* is fragmentary and poorly preserved, further anatomical description is necessary to assess this possibility.

Several characters shared between the two taxa, in addition to their similar size (estimated 3% difference in reconstructed skull length), indicate a similar relative immaturity. Both possess a narrow and straight jugal ramus of the postorbital that does not expand into the orbital fenestra as a flange. This unexpanded condition is present in basal tyrannosauroids and

juvenile tyrannosaurids (e.g., Carr, 1999), whereas a flange is present in adults of most derived tyrannosauroid species. Furthermore, the postorbital cornual process of *A. altai* is small, but thick, and expressed as a ridge along the posterodorsal corner of the orbit (a similar condition may be present in *A. remotus*, judging by Kurzanov's description of this region as "slightly thickened"). The cornual process in derived tyrannosauroids increases in size with growth (Carr, 1999; Carr and Williamson, 2010). Therefore, based on the lack of development of the cornual process of the postorbital and the narrow condition of its jugal ramus, neither specimen represents an adult. Many other features of the holotype skull of *A. altai* also indicate immaturity; these are described in detail in the descriptive portion of this monograph.

Differences between IGM 100/1844 and the holotype of *Alioramus remotus*: The holotypes of *A. remotus* and *A. altai* differ in several details, despite their similar size and ontogenetic stage. The holotype of *A. altai* is a slightly smaller individual than is the holotype of *A. remotus*, and several characters suggest that the *A. altai* holotype was a less mature individual than the holotype of *A. remotus*. Although the size difference between the specimens is not great, the differences are consistent with the growth changes seen in other tyrannosaurids, in which rapid transformations in discrete characters occurred throughout ontogeny (Carr, 1999; Carr and Williamson, 2004). Therefore, similarly-sized individuals of the same or closely related taxa may differ greatly in the relative maturity of their discrete characters. Similarly-sized individuals may also differ due to sexual dimorphism, individual variation, or temporal variation (i.e., they belong to the same species but lived at different times). Unfortunately, current understanding of these sources of variation in tyrannosaurids is limited, but there is a wealth of data on ontogenetic

variation that is available for comparison, and we focus on this here (Carr, 1999; Carr and Williamson, 2004).

Brusatte et al. (2009a) noted eight features that differentiated the holotypes of *A. remotus* and *A. altai*, and recognized that at least three of these may be size or ontogenetically-variable, and thus not strong evidence for taxonomic separation. We review each of these features here.

1) The holotype of *A. altai* possesses a subcutaneous flange on the maxilla (below the antorbital fenestra, the lateral subcutaneous surface of the maxilla extends dorsally to form a narrow slot between itself and the antorbital fossa). Published figures of the holotype of *A. remotus* appear to show that this flange is lacking, although we note that this could be an artifact of poor preservation and/or illustration. Confirmation of this difference awaits further description of the *A. remotus* holotype.

2) The holotype of *A. altai* possesses a line of three nasal rugosities, whereas the holotype of *A. remotus* has twice that number, and the last pair are opposite each other on the midline rather than located in an anterior-posterior sequence (Kurzanov, 1976). This difference is consistent with the ontogenetic increase in coarseness of the nasals that is seen in the ontogeny of *Tyrannosaurus* (Carr, 1999; Carr and Williamson, 2004). However, as no other tyrannosauroid taxa possess discrete nasal rugosities such as those seen in *Alioramus*, it is unclear if and how these features change during ontogeny or vary between individuals. Therefore, the taxonomic utility of three vs. six nasal rugosities is unclear.

3) In the holotype of *A. altai* the anterior process of the quadratojugal extends anterior to the anterior margin of the lateral temporal fenestra, whereas in the *A. remotus* holotype this process is less extensive and terminates posterior to the anterior margin of the fenestra (Kurzanov, 1976:figs. 1, 5). This difference may be ontogenetic. There does not appear to be any

morphological difference between the extent of the quadratojugal anterior process in juvenile and adult albertosaurines (*Albertosaurus* and *Gorgosaurus*: Carr, 1999), but the size and extent of this process is ontogenetically variable in other tyrannosaurids, as well as the more basal tyrannosauroid *Bistahieversor*. The joint surface for the quadratojugal anterior process on the jugal extends ahead of the fenestra in juvenile *Bistahieversor* (NMMNH P-25049) but stops below the anterior margin of the fenestra in adults (NMMNH P-27469). In juveniles and subadults of *Daspletosaurus* (TMP 85.62.1, TMP 94.143.1) the quadratojugal anterior process extends ahead of the fenestra, whereas in mature specimens it extends only a short distance ahead of the fenestra (CMN 11594, CMN 8506) or stops below it (FMNH PR308, TMP 36.2001.1). The process extends far ahead of the fenestra in *Tyrannosaurus* juveniles (BMR 2002.4.1, CMNH7541), whereas it only extends a short distance ahead of it in subadults and in adults (CM 79057, FMNH PR2081). Therefore, this character is ontogenetically variable and not a clear taxonomic difference between the two specimens of *Alioramus*.

4) In the holotype of *A. altai* the anterior process of the squamosal extends slightly anterior to the anterior margin of lateral temporal fenestra, whereas in the holotype of *A. remotus* this process terminates posterior to the fenestra margin (as illustrated by Kurzanov, 1976:figs. 1, 5). The extent of the squamosal anterior process is ontogenetically variable in one tyrannosaurid, *Daspletosaurus*, in which the process extends ahead of the lateral temporal fenestra in juveniles (TMP 94.14.31) but stops above the fenestra in more mature specimens (CMN 8506, CMN 11594, FMNH PR308TMP 85.62.1, TMP 36.2001.1). However, this type of ontogenetic variation is not present in *Albertosaurus*, *Tyrannosaurus*, *Gorgosaurus*, or any other tyrannosauroid more derived than *Appalachiosaurus* (Carr, 1999; Carr, 2004; Carr and Williamson, 2004). Therefore, it is unclear whether this difference between the holotypes of *A.*

altai and *A. remotus* can be explained by ontogeny or taxonomic separation. It is also possible that the condition in *A. remotus* is illustrated incorrectly by Kurzanov (1976).

5) In *A. altai* the epipterygoids are paddle-shaped with convex ventral margins, whereas the corresponding bone of *A. remotus* figured by Kurzanov (1976) has a deeply concave ventral margin (such that the bone is bifurcated ventrally into separate processes). Without seeing the holotype of *A. remotus* it is difficult to know if this difference is the result of damage to that specimen.

6) The holotype of *A. altai* has 17 maxillary and 20 dentary teeth, whereas the holotype of *A. remotus* has 16-17 maxillary teeth and 18 dentary teeth. Although this may be a taxonomically significant feature, the phenomenon of ontogenetic tooth loss has been documented in *Tyrannosaurus* and *Gorgosaurus* (Carr, 1999). Therefore, it is unclear whether these differences between the two holotypes are taxonomically significant.

7) There is a single groove between the basal tubera, on the posterior surface of the occiput, in the *A. altai* holotype, but in the holotype of *A. remotus* this groove is bisected by a ridge. The development of this ridge appears to be ontogenetic in *Tyrannosaurus*: it is absent from juveniles (CMNH 7541) but present in subadults (AMNH FARB 5117) and fully-grown adults (FMNH PR2081). Therefore, its utility as a taxonomically-useful character is questionable.

8) In the holotype of *A. altai* the anterior process of the paired parietals is a long, finger-like, tapering structure that extensively overlaps the frontals along the midline. In the holotype of *A. remotus* this process is shorter, smaller, more rectangular, and has less extensive contact with the frontals. Although this is a clear difference between both specimens, the shape of the anterior process is extremely variable in *Tyrannosaurus*, suggesting that it may not have taxonomic

significance. In *Tyrannosaurus*, the parietal forms a mediolaterally narrow, but relatively long, wedge between the frontals in LACM 28471 and MOR 1125; the wedge is present but shorter in AMNH FARB 5027, AMNH FARB 5117, CM 79057, TMP 81.6.1, and RSM 2523.8. In FMNH PR2081, however the parietal is wide and does not come to a point between the frontals (i.e., the anterior process is nearly absent as a discrete structure). There is also some variability in *Gorgosaurus*, in which the process can be narrow (ROM 1247) or short and blunt (TMP 94.12.602), and *Daspletosaurus*, in which the process is present but short in some juveniles (TMP 94.12.602) but completely eliminated in some adults (FMNH PR308). It may be significant that the anterior process of *A. altai* is extremely finger-like (anteroposteriorly long and mediolaterally narrow), much more so than in all specimens of *Gorgosaurus*, *Daspletosaurus*, or *Tyrannosaurus* that we have studied The most similar morphology that we are aware of is present in the juvenile *Tyrannosaurus* specimen LACM 28471, in which the anterior process is also somewhat finger-like, although it is proportionally wider than the corresponding process in *A. altai*.

Finally, we also note a ninth feature that differs between the holotypes of *A. remotus* and *A. altai*. In *A. altai* the dorsal margin of the quadratojugal extends sharply anteroventrally when seen in lateral view, whereas in *A. remotus* the dorsal margin of the bone is horizontally oriented. This difference also distinguishes juvenile (BMR 2002.4.1) and adult (LACM 23845) *Tyrannosaurus*. Therefore, it may simply be an ontogenetically variable feature in *Alioramus* as well, and not indicative of taxonomic separation of the two specimens.

Unfortunately, although *A. altai* is distinguished by 11 autapomorphies (listed in the diagnosis section of this monograph), only one of these (20 dentary teeth) can be dismissed as absent in the holotype of *A. remotus*. The other 10 characters cannot be assessed in this specimen

because the requisite bones are missing, broken, or poorly preserved. It is hoped here that future preparation and anatomical work on the *A. remotus* holotype will lead to a better understanding of its morphology and enable more direct comparisons with the holotype of *A. altai*. Only additional study of *A. remotus* can definitively answer the question of whether the two known specimesn of *Alioramus* are taxonomically distinct, and pending such work, we provisionally follow the taxonomic conclusions of Brusatte et al. (2009a) and consider the specimens to represent different species based on the anatomical, and potential stratigraphic and temporal, differences between them (see Brusatte et al. [2009] for more details). Furthermore, we suggest that its greater number of teeth, comparatively modest nasal ornamentation, and truncated quadratojugal indicate that the holotype of *A. altai* is less mature than that of *A. remotus*.

NOVEL BODY PLAN AND PRESUMED ECOLOGICAL HABITS

The possession of an autapomorphically long and low skull (especially a long snout) in *Alioramus* suggests that this taxon had a different body plan, and perhaps lifestyle and ecology, compared to contemporary deep-skulled Late Cretaceous tyrannosaurids such as *Tarbosaurus* and *Tyrannosaurus*. Unusual characters of *Alioramus* with potential functional significance are not restricted to skull shape, but also include its generally gracile skull bones, lack of interlocking sutures and/or fusion between skull bones, thin teeth, lack of a robust lacrimal-postorbital bar above the orbit, comparatively small attachment sites for jaw muscles, small body size (compared to similarly-aged tyrannosaurids), extreme levels of postcranial and cranial pneumaticity, and its gracile and long-limbed skeleton. Some of these features likely relate to the juvenile status of both known specimens of *Alioramus*—especially the thin teeth, gracile skull

bones, and lack of interlocking cranial sutures—and it is difficult to predict which of these characters, if any, an adult may have retained.

What is clear, however, is that neither known specimen of *Alioramus* was capable of employing the "puncture-pull" feeding style of large-bodied adult tyrannosaurids, in which the muscular jaws, thick teeth, interlocking skull sutures, and stress-dissipating orbital brow enabled individuals to bite with such strong forces that they could literally crunch through the bones of their prey (Erickson et al., 1996; Molnar, 2000; Rayfield, 2004). This suggests that, at the very least, juvenile and subadult *Alioramus* may have employed a different feeding style than large-bodied adult tyrannosaurids, perhaps focusing on smaller prey and relying on speed more than strong bite forces. This is also probably true of juveniles of *Tarbosaurus*, *Tyrannosaurus*, and other tyrannosaurids, but has yet to be explicitly tested by biomechanical modeling. Whether adult *Alioramus* was capable of tyrannosaurid-style puncture-pull feeding, or fed in the same manner as juveniles, are questions that await further fossil discoveries of adult specimens and more explicit functional and biomechanical analyses.

Alioramus was sympatric with *Tarbosaurus*, as specimens of *Tarbosaurus* have been discovered at the same locale as the holotype of *A. altai* (see Brusatte et al., 2010d). This type of ecological association—a fauna with two large predators—is also characteristic of Late Campanian faunas of North America, which included the tyrannosaurids *Daspletosaurus* and *Gorgosaurus* (Russell, 1970; Holtz, 2004). Russell (1970) hypothesized that the two species were able to coexist because of niche partitioning, because they were likely adapted for hunting different prey. The Mongolian taxa add additional evidence that multiple species of large-bodied tyrannosaurids were able to co-exist, and that their co-existence may have been enabled by niche differentiation. As described above, the long, low skull of *Alioramus* contrasts substantially from

that of similar-sized *Tarbosaurus*, in which the skull is short and deep. It is therefore reasonable to predict that biomechanical studies will show that *Alioramus* had a weaker bite than its stockier counterpart, which would indicate that its foraging behavior was derived relative to that of *Tarbosaurus*, and all other derived tyrannosauroids, which retain the plesiomorphic deep and robust skull form.

The Late Cretaceous faunas of Mongolia and Alberta indicate that sympatry and niche partitioning is an iterative pattern in tyrannosaurid evolution that resulted in morphological specialization and increased diversity. Similarly, the Late Jurassic faunas of North America included sympatric large theropods from different lineages (e.g., *Allosaurus*, *Ceratosaurus*, *Torvosaurus*), as did the Early Cretaceous faunas of North Africa and Europe (spinosaurids, carcharodontosaurians, abelisaurids: Brusatte and Sereno, 2007; Sereno and Brusatte, 2008; Benson et al., 2009). However, tyrannosaurid dominated faunas stand out in that the multiple species of contemporary large-bodied predators all belonged to a single clade (Tyrannosauroidea), and species of other theropod subgroups did not occupy niches at the apex of the trophic period. In summary, *Alioramus* represents a distinct morphotype in Tyrannosauridae, and it is likely that the long and low skull was adaptation that maintained the ecological foothold of the species, and whose function expanded the trophic and dietary abilities of the clade.

TABLES

TABLE 1-1: Measurements of cranial bones (in millimeters) of the holotype of *Alioramus altai* (IGM 100/1844).

Maxilla (left element)
- Anteroposterior length (of ventral margin): 430
- Dorsoventral depth (at anterior margin of antorbital fenestra): 120
- Anteroposterior length of maxillary antorbital fossa: 118
- Anteroposterior length of region anterior to antorbital fenestra: 225

Nasal (fused left and right elements)
- Anteroposterior length: 395
- Mediolateral width at the anterior end: 50
- Mediolateral width at the midpoint: 30
- Mediolateral width at the posterior end: 49

Lacrimal (left element)
- Anteroposterior length of anterior process: 130
- Dorsoventral depth of ventral process: 105
- Anteroposterior length of posterior process: 27

Jugal (left element)
- Anteroposterior length of entire bone: 230
- Anteroposterior length of anterior process: 111
- Dorsoventral depth of anterior process (above antorbital fossa); 32
- Anteroposterior length of posterior process: 55*
- Dorsoventral depth of posteror process (at anterior margin): 27
- Dorsoventral depth of dorsal process: 90

Postorbital (left element)
- Anteroposterior length of dorsal bar: 130
- Anteroposterior length of anterior process: 45
- Anteroposterior length of posterior process: 65
- Dorsoventral depth of ventral process: 80

Squamosal (left element)
- Anteroposterior length of anterior process: 70
- Dorsoventral depth of anterior process (at midpoint): 35
- Long axis length of ventral process: 65
- Long axis length of medial process: 35

Quadratojugal (right element)
- Dorsoventral depth of dorsal process: 70
- Anteroposterior length of dorsal process (at ventral extent): 23
- Dorsoventral depth of anterior process (at posterior extent): 15

Quadrate (left element)
- Dorsoventral depth of shaft (between condyles and head): 110
- Anteroposterior length of quadrate flange (perpendicular to shaft): 70

Palatine (right element)
- Anteroposteror length of entire element: 225
- Dorsoventral depth of waisted region between four processes: 25

Ectopterygoid (right element)

Anteroposterior length: 95
Mediolateral width (posterior margin): 40

Epipterygoid (left element)
Dorsoventral depth: 75
Anteroposterior length (at ventral margin): 30

Dentary (left element)
Anteroposterior length: 425
Dorsoventral depth (at third alveolus) 39
Dorsoventral depth (at surangular articulation): 73

Surangular (left element)
Anteroposterior length: 290
Dorsoventral depth (at surangular foramen): 65

Angular (right element)
Anteroposterior length: 204
Dorsoventral depth (maximum): 41

Prearticular (right element)
Anteroposterior length: 285

Splenial (right element)
Anteroposterior length: 255
Dorsoventral depth (maximum): 62

Supradentary/Coronoid (right element)
Anteroposterior length: 380*

Note: asterisk denotes incomplete measurement due to breakage.

TABLE 1-2: Measurement ratios of the maxilla for various tyrannosauroids

Taxon	Depth: Length Ratio	Source
A. altai	0.28	IGM 100/1844
Albertosaurus (juvenile)	0.42	Carr 1999
Albertosaurus (adult)	0.40	Carr 1999
Appalachiosaurus	0.33	RMM 6670
Bistahieversor	0.39	NMMNH P-27469
Daspletosaurus (adult)	0.40	Russell 1970
Dilong	0.34	IVPP V14243
Gorgosaurus (adult)	0.37	Currie 2003a
Guanlong (juvenile)	0.40	IVPP V14532
Tarbosaurus (adult)	0.47	ZPAL MgD-I/4
Tarbosaurus (juvenile)	0.40	Currie and Dong 2001a
Tyrannosaurus (adult)	0.45	AMNH FARB 5027
Tyrannosaurus (juvenile)	0.37	CMNH 7541

Note: length is the anteroposterior length of the ventral margin, depth is the perpendicular dorsoventral measurement at the anterior margin of the antorbital fenestra.

TABLE 1-3: Measurement ratios of the depth of the ventral curvature of the maxillary tooth row.

Taxon	Depth:Length Ratio	Source
A. altai	0.05	IGM 100/1844
Albertosaurus (adult)	0.09	TMP 81.10.1
Daspletosaurus (adult)	0.12	CMN 8506
Gorgosaurus	0.11	CMN 2120
Raptorex	0.06	LH PV18
Tyrannosaurus (juvenile)	0.10	BMR 2002.4.1

Note: depth is the vertical depth of the ventral curvature, perpendicular and below a straight line drawn between the anterior and posterior extemes of the tooth row.

TABLE 1-4: Measurement ratios of the maxillary fenestra for various tyrannosauroids

Taxon	Length: Depth Ratio	Source
A. altai	1.90	IGM 100/1844
Albertosaurus (juvenile)	1.10	Carr 1999
Albertosaurus (subadult)	1.20	CMN 5601
Albertosaurus (adult)	1.75	Carr 1999
Appalachisaurus	1.20	RMM 6670
Bistahieversor	0.93	NMMNH P-27469
Daspletosaurus (subadult?)	1.40	Currie 2003a
Dilong	2.50	IVPP V14243
Gorgosaurus (subadult)	1.60	ROM 1247
Gorgosaurus (adult)	1.43	Currie 2003a
Guanlong (juvenile)	1.30	IVPP V14532
Raptorex	1.3	LH PV18
Tarbosaurus (adult)	1.20	ZPAL MgD-I/4
Tarbosaurus (juvenile)	1.00	Currie and Dong 2001a
Tyrannosaurus (adult)	1.33	AMNH FARB 5027
Tyrannosaurus (juvenile)	1.25*	CMNH 7541
Tyrannosaurus (type, adult)	1.60	CM 9380

Note: length is the anteroposterior length of the fenestra at its midpoint, depth is the perpendicular dorsoventral measurement of the greatest dimension. Asterisk denotes estimate due to breakage.

TABLE 1-5: Measurements of the maxillary (left element) and dentary (left element) alveoli (mesiodistal, labiolingual) and teeth (CBL, CBW, CH) (in millimeters) of the holotype of *Alioramus altai* (IGM 100/1844). CBL = crown base length; CBW = crown base width; CH = crown height (see Smith and Dodson 2003; Smith 2006).

Maxilla

Alveolus	Mesio-distal	Labio-lingual	CBL	CBW	CH
1	7	8	-	-	-
2	11	8	12	7	31
3	18	10	11	7	25
4	19	11	16	8	40
5	24	12	15	7	28
6	23	11	18	7	41
7	22	11	16	5	26
8	19	10	16	5	-
9	10	10	15	6	28
10	17	9	-	-	-
11	17	9	15	6	27
12	17	9	12	4	10
13	16	8	12	5	25
14	14	7	10	4	11
15	13	7	10	5	19
16	12	5	-	-	-
17	8	5	-	-	-

Dentary

Alveolus	Mesio-distal	Labio-lingual	CBL	CBW	CH
1	3	4	-	-	-
2	5	7	-	-	-
3	9	9	4	3	6
4	16	9	-	-	-
5	16	9	-	-	-
6	16	9	-	-	-
7	15	9	13	6	29
8	15	10	-	-	-
9	15	9	10	5	13
10	15	8	-	-	-
11	14	7	9	4	10
12	14	7	-	-	-
13	14	7	11	5	17
14	14	7	12	5	23
15	12	7	-	-	-

16	11	6	-	-	-
17	11	5	-	-	-
18	10	5	-	-	-
19	7	5	-	-	-
20	5	4	-	-	-

TABLE 1-6: Measurement ratios of the anterior ramus of the lacrimal for various tyrannosauroids.

Taxon	Length anterior ramus:height ventral ramus	Source
A. altai	1.40	IGM 100/1844
Daspletosaurus	1.10	CMN 8506, TMP 2001.36.1
Tyrannosaurus (adult)	0.90	RSM 2523.8

Note: The anteroposterior length of the anterior ramus is from the posterior margin of the lacrimal pneumatic recess to the anterior tip of the ramus; the height of the ventral ramus is from the ventral margin of the lacrimal pneumatic recess to the ventral extent of the ventral ramus.

TABLE 1-7: Measurement ratios of the dentary for various tyrannosauroids

Taxon	Depth: Length Ratio	Source
A. altai	0.13	IGM 100/1844
Albertosaurus (adult)	0.28	Currie 2003a,b
Appalachiosaurus	0.25	RMM 6670
Daspletosaurus (adult)	0.26	Currie 2003a,b
Dilong	0.11	IVPP V14243
Gorgosaurus (juvenile)	0.15	Currie 2003a,b
Gorgosaurus (adult)	0.26	Currie 2003a,b
Tarbosaurus (adult)	0.29	Currie 2003a,b
Tarbosaurus (juvenile)	0.26	Currie and Dong 2001a
Tyrannosaurus (adult)	0.29	Currie 2003a,b

Note: measurements following Currie 2003b), depth is the minimum dorsoventral depth of the main body, length is the anteroposterior length of the tooth row

TABLE 1-8: Measurement ratios of the anterior mylohyoid foramen (splenial) for various tyrannosauroids

Taxon	Length: Depth Ratio	Source
A. altai	4.29	IGM 100/1844
Appalachisaurus	3.00	RMM 6670
Bistahieversor	1.40	NMMNH P-27469
Daspletosaurus (subadult?)	2.14	Currie 2003a
Tarbosaurus (adult)	1.70	ZPAL MgD-I/34
Tarbosaurus (juvenile)	1.80	Currie and Dong 2001a
Tyrannosaurus (adult)	1.50	Brochu 2003
Tyrannosaurus (juvenile)	2.85*	Carr 1999

Note: length is the longest dimension of the foramen and width is the perpendicular axis. Asterisk denotes slightly overstated measurement due to orientation of published figures (Carr 1999: fig. 6) that exaggerates long axis relative to shorter axis.

TABLE 1-9: Measurements of the vertebrae (in millimeters) of the holotype of *Alioramus altai* (IGM 100/1844). Asterisks denote minimum measurement due to breakage; ampersand (&) denotes measurement biased by crushing; dollar sign ($) denotes measurement reconstructed due to breakage. 1: measured parallel to the long axis of the spine from the dorsal surface of the transverse processes

Specimen Identification	Antero-posterior length of centrum	Minimum Transverse Width of Centrum	Dorso-ventral height of anterior surface of centrum	Medio-lateral width of anterior surface of centrum	Dorso-ventral height of posterior surface of centrum	Medio-lateral width of posterior surface of centrum	Dorso-ventral height of neural spine[1]	Minimum antero-posterior breadth of neural spine
Cervical 2 (Axis)	36	18	23&	27&	33	30	70	21
Cervical 3	42	27	25$	35$	38	42	?	?
Cervical 4	42	25	35$	41	45	?	?	?
Cervical 5	65	27	35	35	37	39*	?	?
Cervical 6	75	35	29&	43&	?	?	?	?
Cervical 7	57	36	41	51	46	50	?	?
Cervical 8	60	35	48	59	50	53	?	?
Cervical 9	67	37	44	50	?	65	?	?
Cervical 10	51	35	51	55	56	57	?	?
Dorsal A	55	?	49$	?	55$	?	?	?
Dorsal C	55	26	46	46$	53	50	58	30
Sacral 3	75	26	?	?	?	?	104	51
Sacral 4	79	26	?	?	?	?	101	66
Sacral 5	97	?	?	?	65	46*	93	60
Caudal A	87	32	77	51	75	55	66*	36
Caudal B	82	27	81	55$	83	53	72	37
Caudal C	84	16	37	30	35	37	30	63

TABLE 1-10: Measurements of pelvic and hind limb bones (in millimeters) of the holotype of *Alioramus altai* (IGM 100/1844).

Ilium (right element)
- Depth (dorsoventral) above the acetabulum: 160
- Depth (dorsoventral) at the posterior end of the postacetabular process: 100

Ischium (right element)
- Length (proximodistally): 430
- Midshaft width (mediolaterally): 15
- Midshaft length (anteroposteriorly): 17
- Midshaft circumference: 60
- Length of obturator process (proximodistally) at midpoint: 80

Femur (left element)
- Length (proximodistally): 560
- Midshaft width (mediolaterally): 57
- Midshaft length (anteroposteriorly): 44
- Midshaft Circumference: 170
- Proximal width: 122
- Proximal length: 44
- Distal width: 110
- Distal length: 40

TABLE 1-11: Measurement ratios of the ascending process of the astragalus for various tyrannosauroids

Taxon	Apr:Condyles Ratio	Source
A. altai	2.34	IGM 100/1844
Albertosaurus	1.97	AMNH FARB 5227
Alectrosaurus	2.42	AMNH FARB 6554
Dilong	2.08*	IVPP V14243
Gorgosaurus	2.60	Lambe 1917
Guanlong	1.67	IVPP V14531
Tarbosaurus (juvenile)	2.25	Maleev 1974
Tarbosaurus (juvenile)	2.20	ZPAL MgD-I/29
Tyrannosaurus (adult)	1.88	Brochu 2003

Note: “apr” is the greatest proximodistal height of the ascending process, “condyles” is the greatest proximodistal height of the distal condylar region of the astragalus. Asterisk denotes minimum ratio due to breakage of the ascending process proximally.

FIGURES

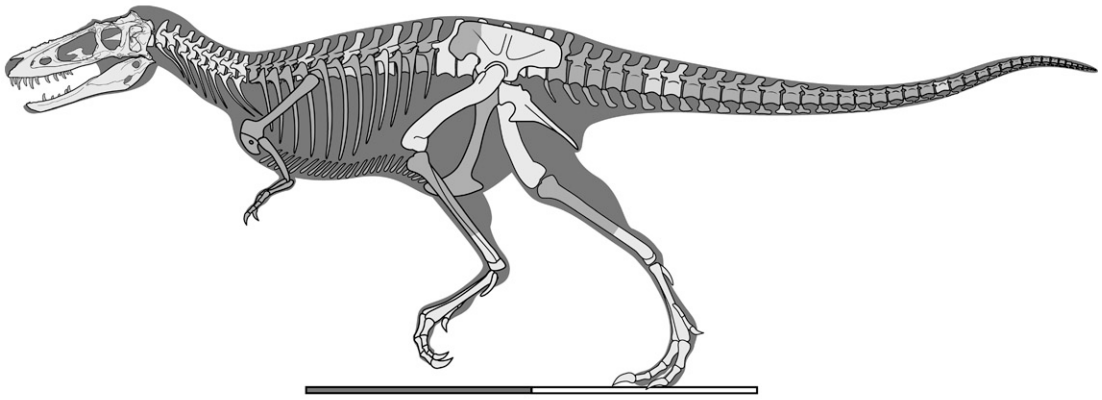

Figure 1-1. Skeletal reconstruction of the holotype specimen of the Late Cretaceous tyrannosaurid *Alioramus altai* (IGM 100/1844). Bones in light gray (e.g., skull) are preserved and those in dark gray (e.g., forearm) are absent but reconstructed based on comparison to close relatives (*Appalachiosaurus*, *Tarbosaurus*, and *Tyrannosaurus* of similar body size). Entire scale bar equals 2 meters. Reconstruction delineated by Frank Ippolito, American Museum of Natural History.

Figure 1-2. The Tsaggan Khushuu locality in the Gobi Desert of Mongolia, where the holotype of *Alioramus altai* (IGM 100/1844) was discovered in Maastrichtian-aged rocks of the Nemegt Formation (top). The right maxilla, in medial view, as preserved in the field (bottom).

Figure 1-3. The holotype skull of *Alioramus altai* (IGM 100/1844) partially prepared in the original field jacket.

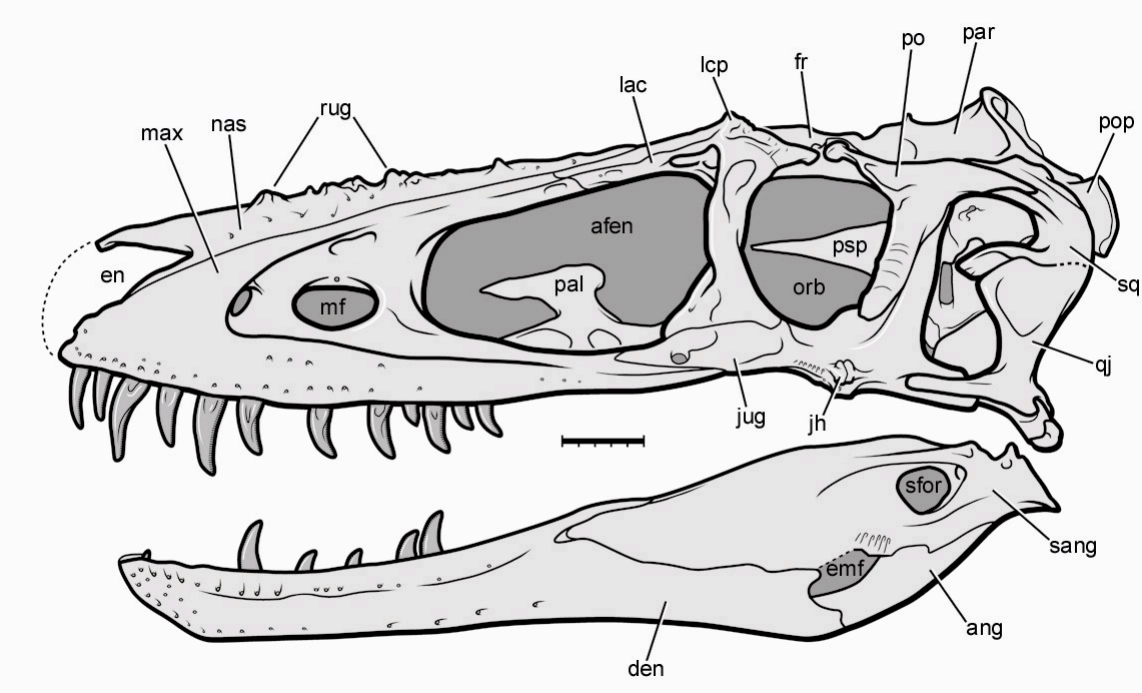

Figure 1-4. Skull reconstruction of the holotype specimen of the Late Cretaceous tyrannosaurid *Alioramus altai* (IGM 100/1844). Scale bar equals 5 cm. Abbreviations: afen, antorbital fenestra; ang, angular; den, dentary; emf, external mandibular fenestra; en, external naris; fr, frontal; jh, jugal horn; jug, jugal; lac, lacrimal; lcp, lacrimal cornual process; max, maxilla; mf, maxillary fenestra; nas, nasal; orb, orbit; pal, palatine; par, parietal; po, postorbital; pop, paroccipital process; psp, parasphenoid rostrum; qj, quadratojugal; rug, rugosities on the nasal; sang, surangular; sfor, surangular foramen; sq, squamosal. Reconstruction delineated by Frank Ippolito, American Museum of Natural History.

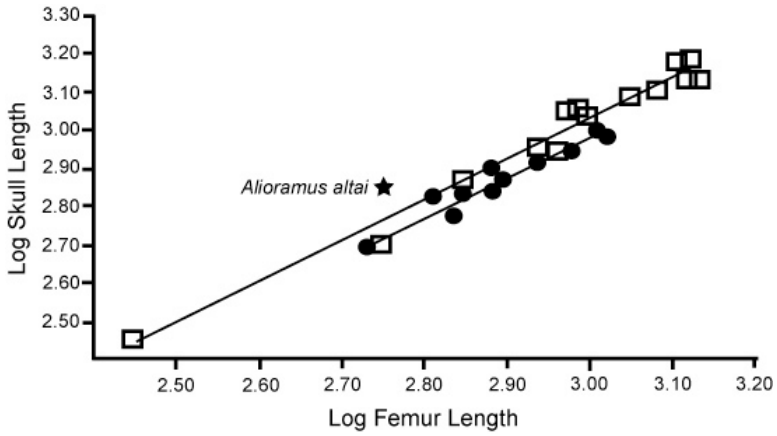

Figure 1-5. Plot of total skull length vs. femur length (logarithmic scale) for several tyrannosaurid specimens, based on Currie (2003b). Squares represent tyrannosaurine specimens (*Tarbosaurus*, *Tyrannosaurus*); closed circles represent albertosaurines (*Albertosaurus*, *Gorgosaurus*); star represents holotype of *Alioramus altai* (IGM 100/1844). Note that the *A. altai* holotype falls above the regression lines, demonstrating that its skull is longer than those of other tyrannosaurids with a similar femur length (and hence body size, as femur length and body size are tightly correlated in theropods). The *Alioramus* data point is closer to the tyrannosaurine regression line, which is consistent with its phylogenetic position as a tyrannosaurine.

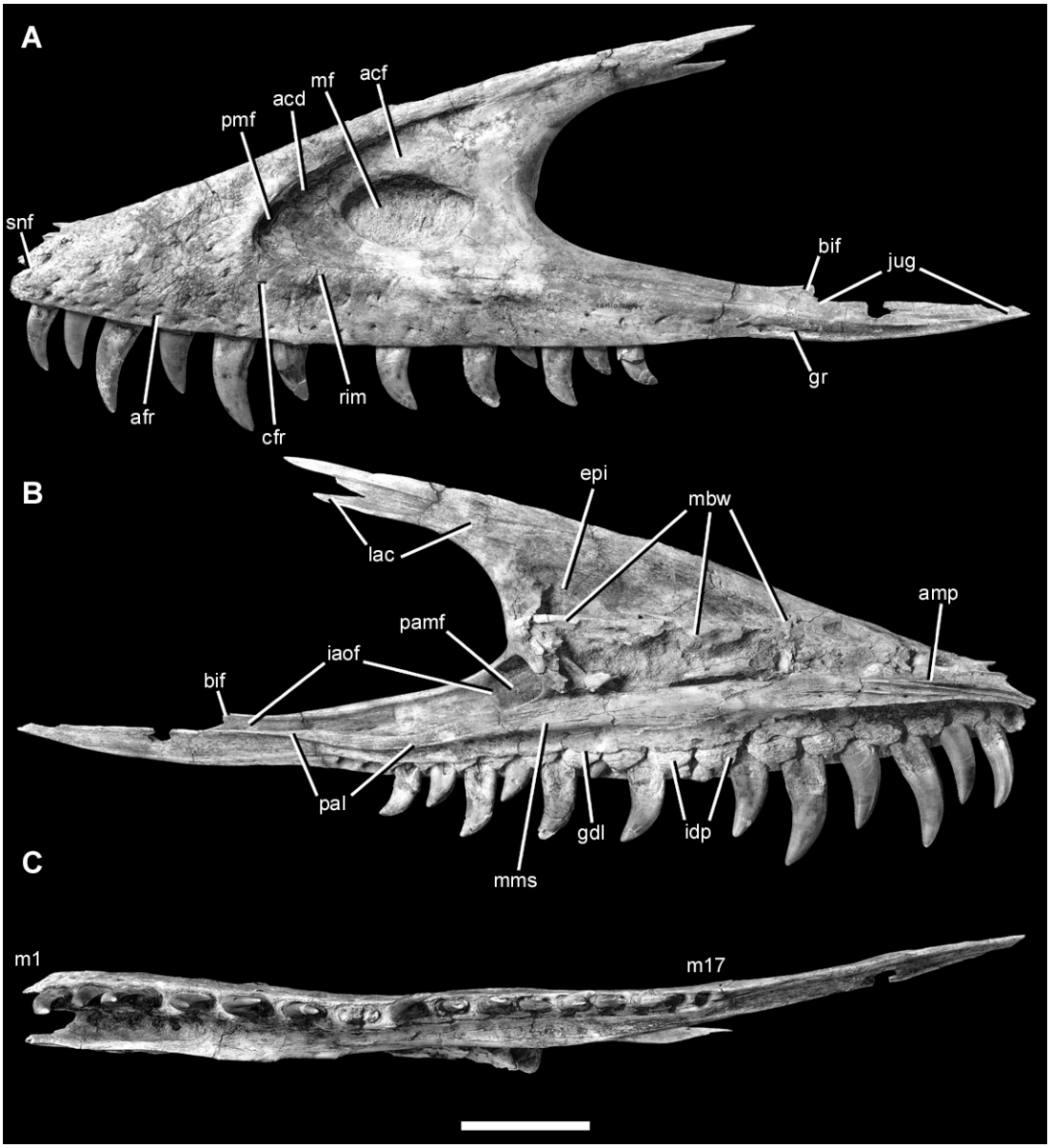

Figure 1-6. Left maxilla of the holotype specimen of *Alioramus altai* (IGM 100/1844) in lateral (A), medial (B), and ventral (C) views. Scale bar equals 5 cm. Abbreviations: acd, accessory depression posterodorsal to promaxillary fenestra; acf, accessory fossa on ascending ramus of maxilla; afr, alveolar foramina row; amp, anteromedial process; bif, bifurcated accessory process for articulation with jugal; cfr, circumfenestral foramina row; epi, epiantral recess; gdl, groove for the dental lamina; gr, groove extending posteriorly from the final foramen of the merged

alveolar and circumfenestral rows; iaof, internal antorbital fossa; idp, interdental plates; jug, jugal articular furrow; lac, lacrimal articular facet; mbw, medial bounding wall of the maxillary antrum; mf, maxillary fenestra; mms, medial maxillary shelf; pal, articular facet for palatine; pamf, posterior anteromaxillary fenestra; pmf, promaxillary fenestra; rim, swollen rim surrounding antorbital fossa; snf, subnarial foramen.

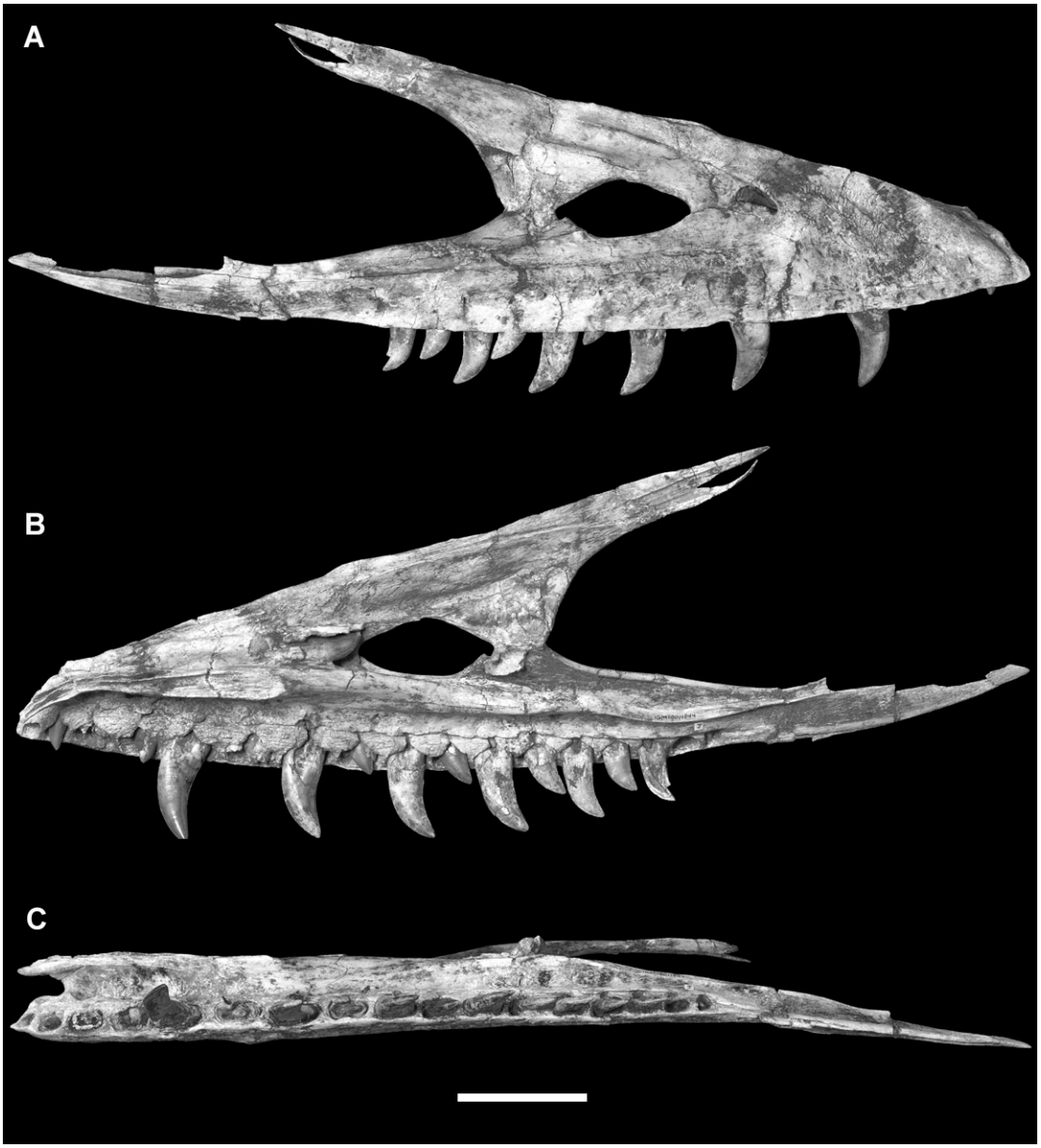

Figure 1-7. Right maxilla of the holotype specimen of *Alioramus altai* (IGM 100/1844) in lateral (A), medial (B), and ventral (C) views. Scale bar equals 5 cm.

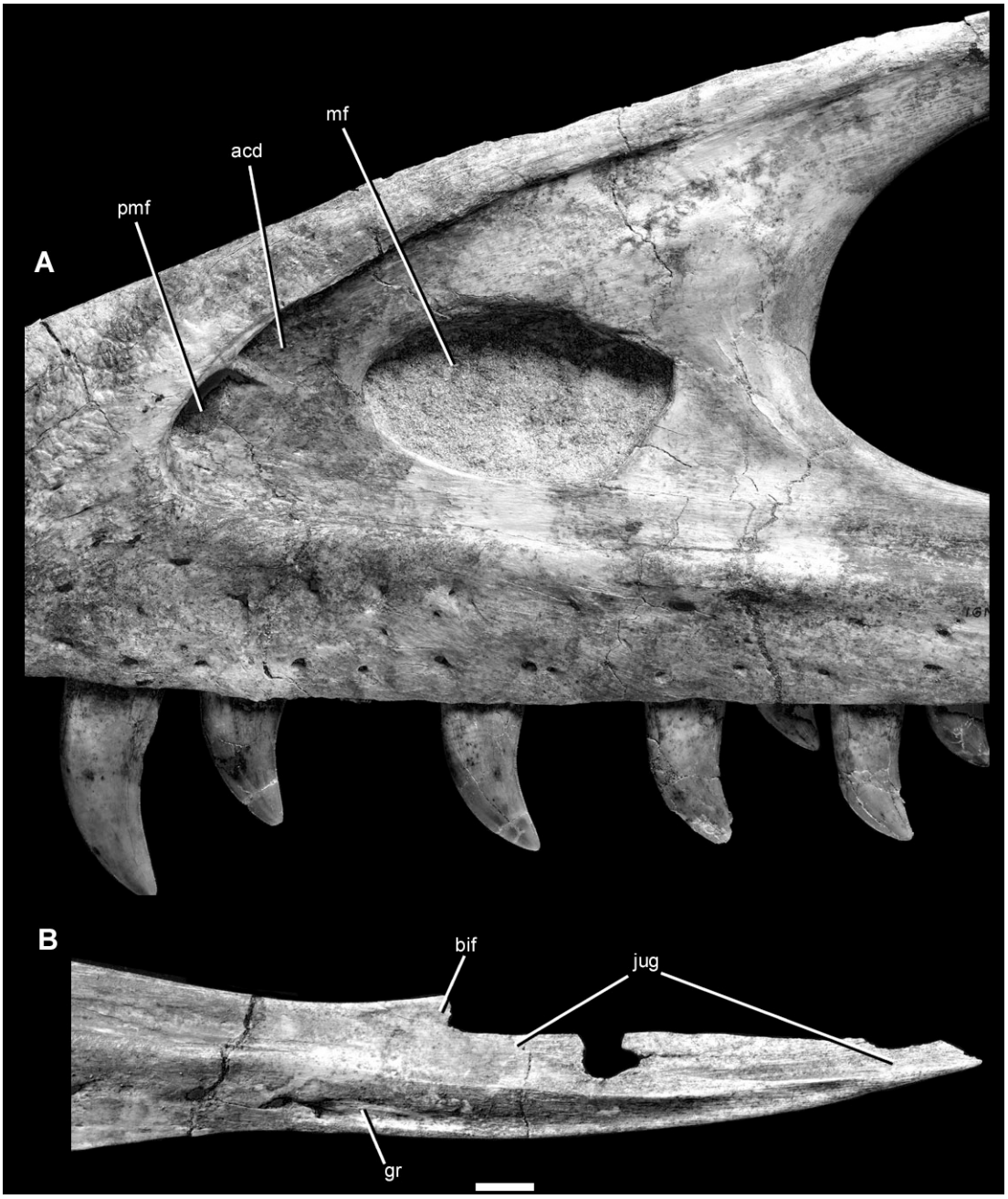

Figure 1-8. Closeup photos of the left maxilla of the holotype specimen of *Alioramus altai* (IGM 100/1844) in lateral view. A: antorbital fossa region; B: posterior end of maxilla. Scale bar equals 2 cm. Abbreviations as in figure 6.

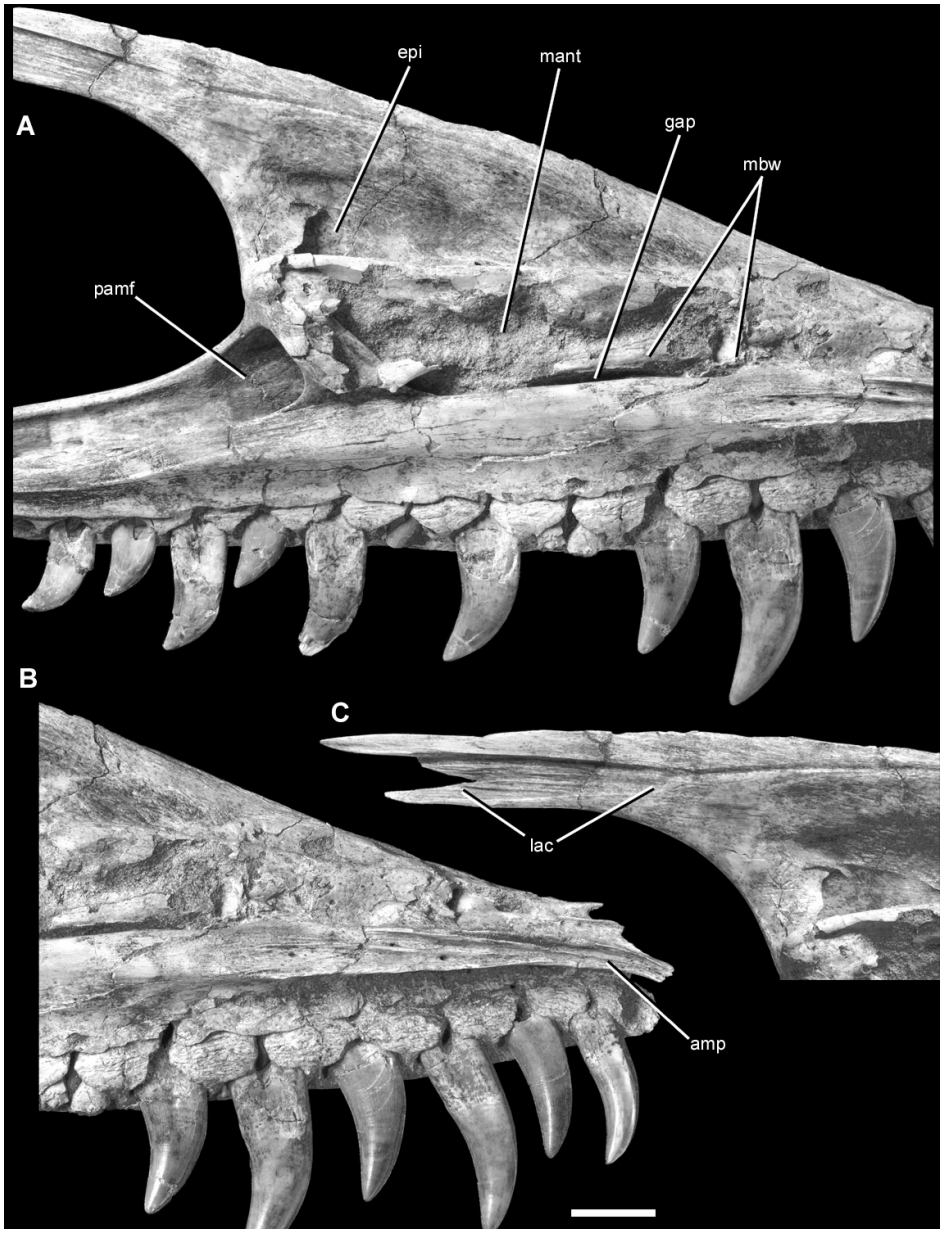

Figure 1-9. Closeup photos of the left maxilla of the holotype specimen of *Alioramus altai* (IGM 100/1844) in lateral view. A: medial antorbital sinus region; B: posterior end of ascending ramus; C: anterior end of maxilla Scale bar equals 2 cm. Abbreviations as in figure 6, plus: gap: apparent gap between the medial bounding wall of the maxillary antrum and the medial maxillary shelf (but probably a result of damage and not genuine); mant, maxillary antrum.

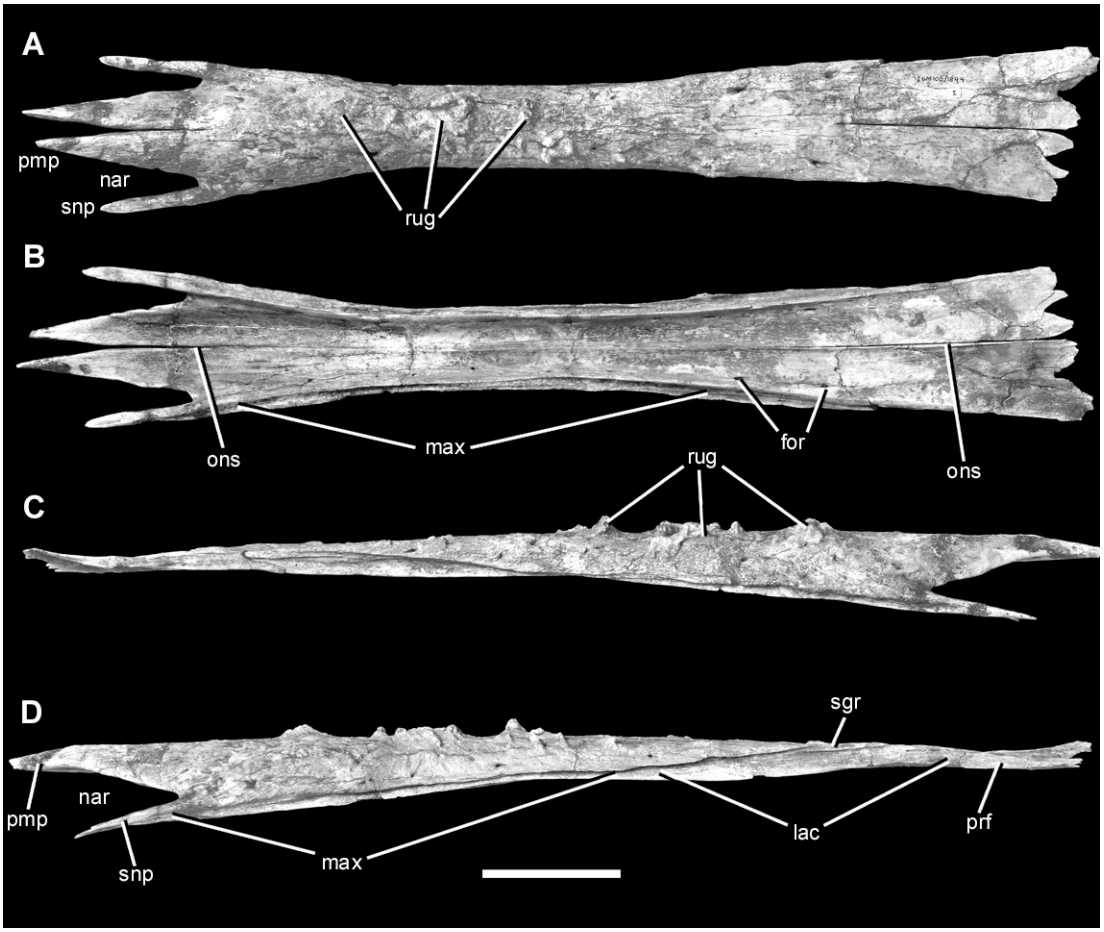

Figure 1-10. Conjoined nasals of the holotype specimen of *Alioramus altai* (IGM 100/1844) in dorsal (A), ventral (B), right lateral (C), and left lateral (D) views. Scale bar equals 5 cm. Abbreviations: for, foramina; lac, lacrimal articular facet; max, maxillary articular facet; nar, external naris; ons, open internarial suture; pmp, premaxillary process; prf, prefrontal articular facet; rug, discrete rugosities; sgr, secondary groove of lacrimal facet; snp, subnarial process.

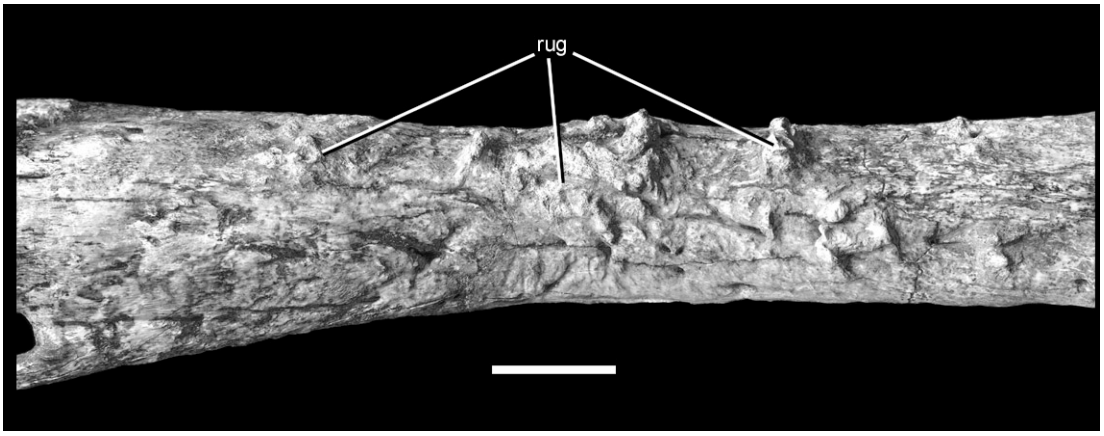

Figure 1-11. Closeup photo of the conjoined nasals of the holotype specimen of *Alioramus altai* (IGM 100/1844) in left lateral oblique view. Scale bar equals 2 cm. Abbreviations as in Figure 10.

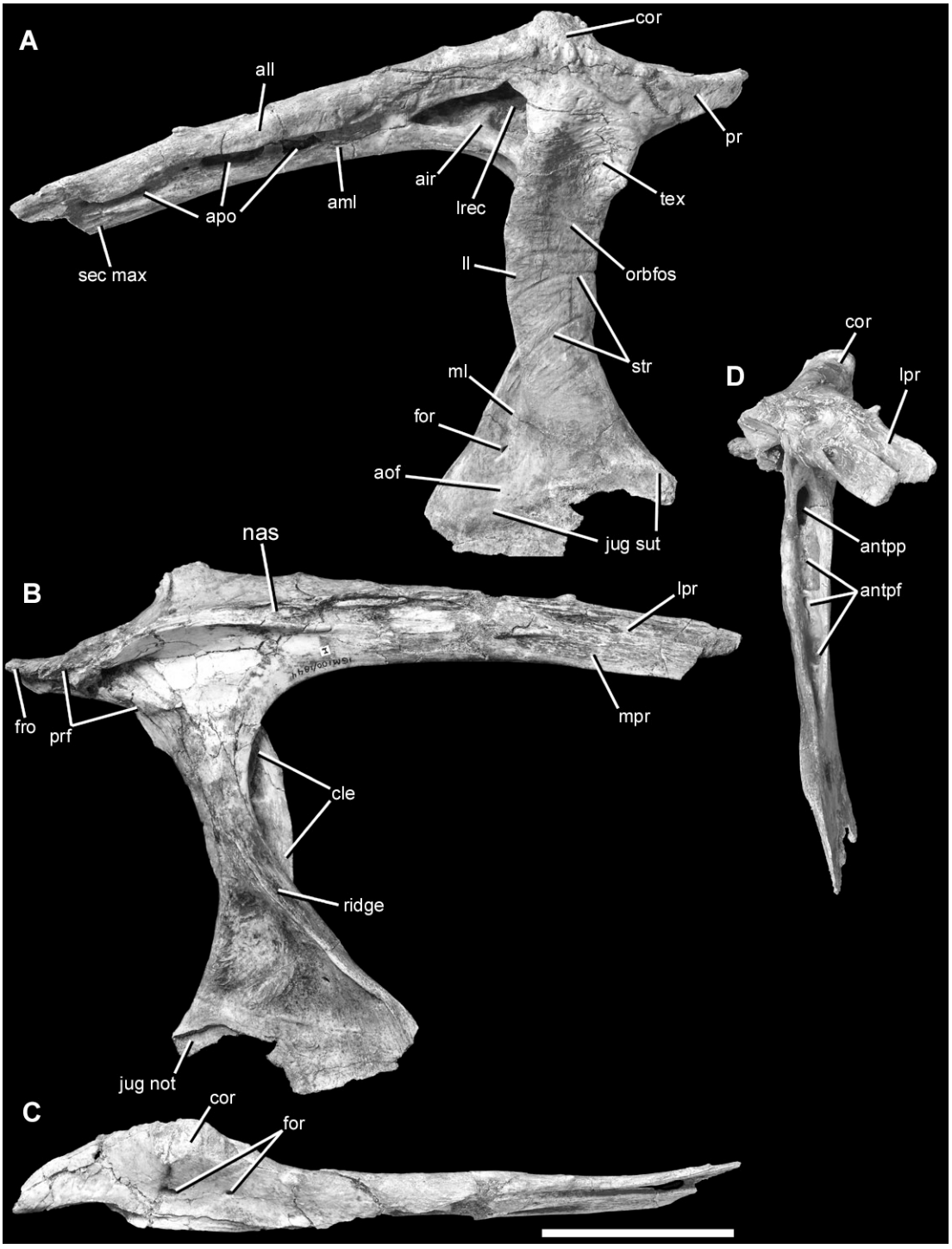

Figure 1-12. Left lacrimal of the holotype specimen of *Alioramus altai* (IGM 100/1844) in lateral (A), medial (B), dorsal (C), anterior (D) views.Scale bar equals 5 cm. Abbreviations: air, arcuate internal ridge within lacrimal recess; all, lateral lamina of anterior ramus; aml, medial lamina of

anterior ramus; aof, antorbital fossa; antpf, pneumatic fossae on anterior surface of ventral ramus; antpp, pneumatic pocket at posteroventral corner of antorbital fossa; apo, accessory pneumatic openings on anterior ramus; cle, cleft between lateral and medial laminae of ventral ramus; cor, cornual process; for, foramen; fro, frontal contact; jug not, notch where the lacrimal overlaps the jugal laterally; jug sut, jugal suture trace; ll, lateral lamina of ventral ramus; lpr, lateral process of anterior bifurcation of anterior ramus; lrec, lacrimal recess; ml, medial lamina of ventral ramus; mpr, medial process of anterior bifurcation of anterior ramus; nas, nasal contact; orbfos, orbital fossa; ovo, ovoid excrescences on lateral surface of cornual process; pr, posterior ramus; prf, prefrontal contact; ridge, orbitonasal ridge; sec max, secondary articulation between lacrimal and maxilla, where a small portion of the maxilla overlaps the lacrimal laterally; str, arcuate striations; tex, region of heavy external texturing at anterodorsal corner of orbit.

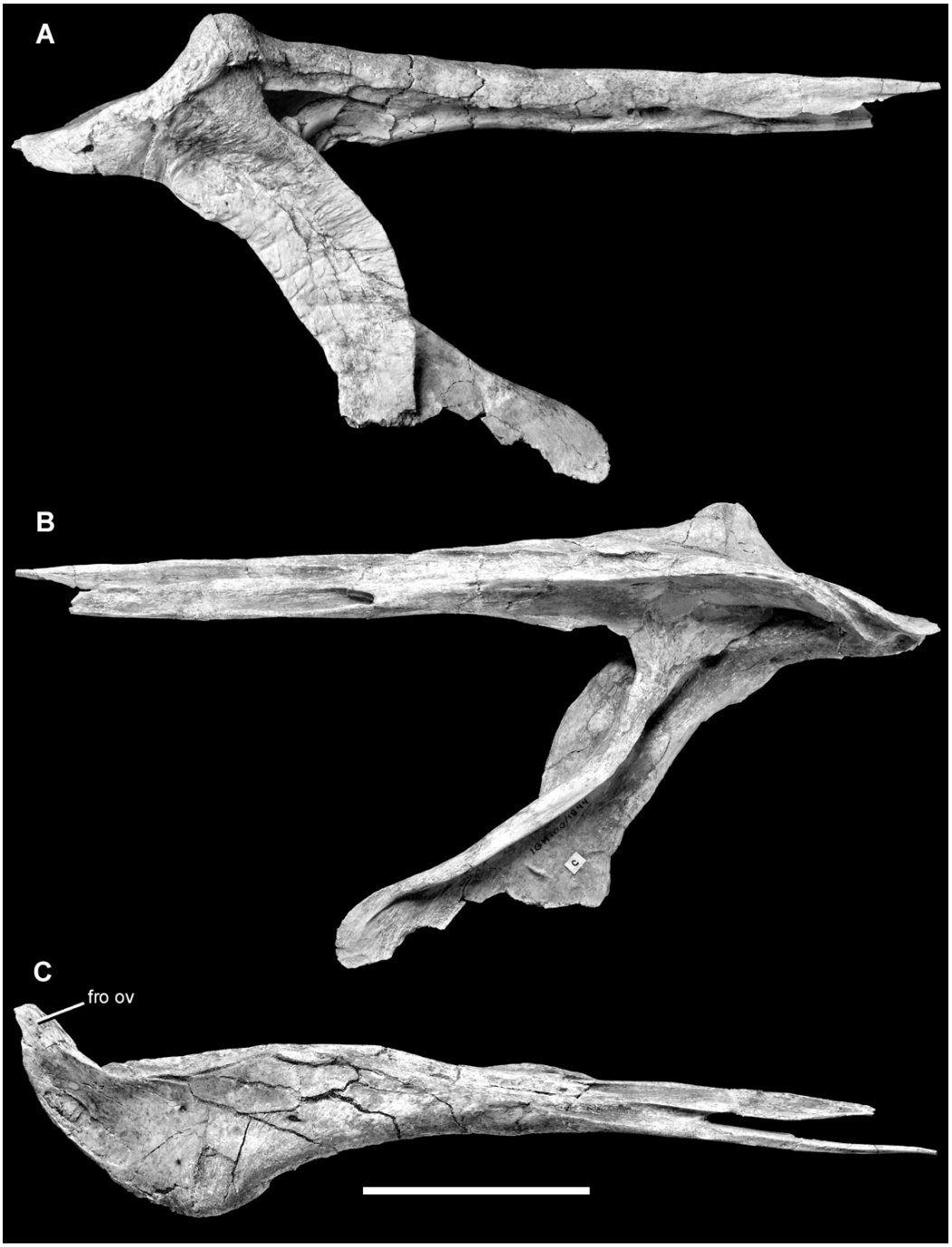

Figure 1-13. Right lacrimal of the holotype specimen of *Alioramus altai* (IGM 100/1844) in lateral (A), medial (B), and dorsal (C) views.Scale bar equals 5 cm. Abbreviations as in Figure 12, plus: fro ov: facet on dorsal surface of posterior ramus of lacrimal that is overlapped by the frontal.

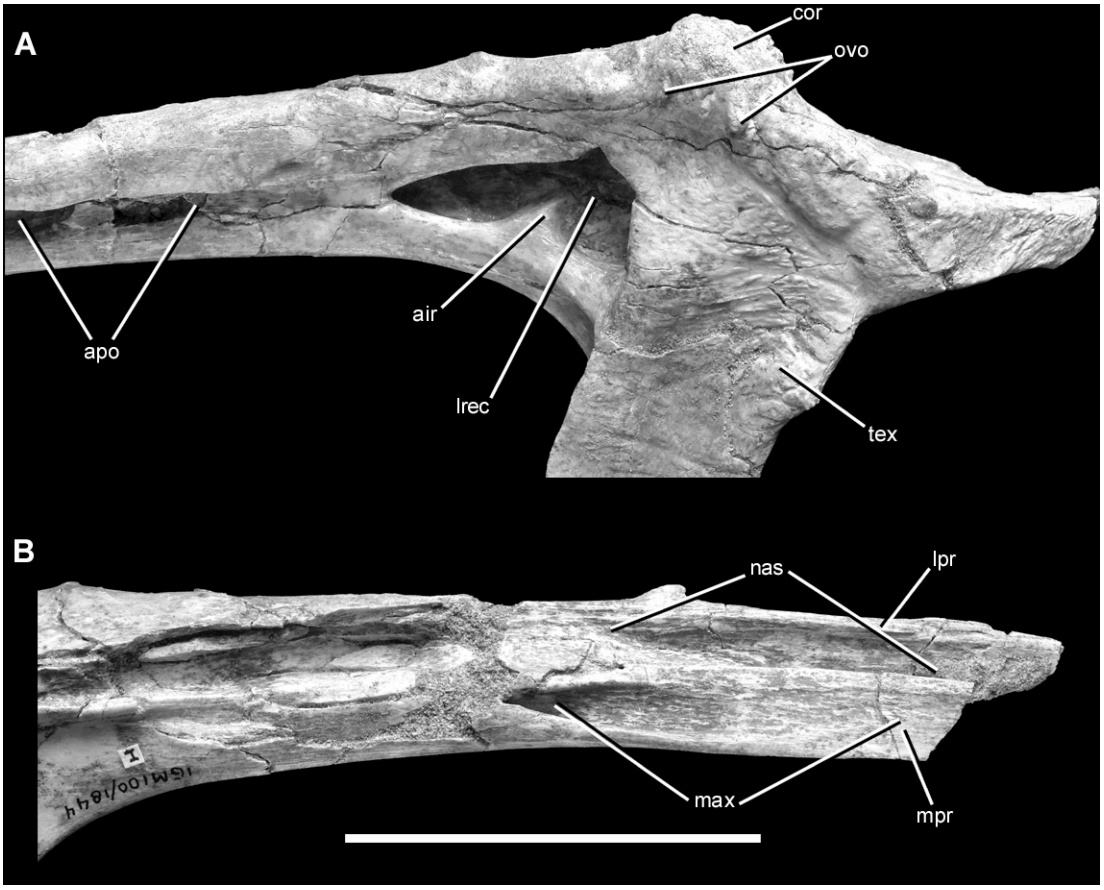

Figure 1-14. Closeup photos of the left lacrimal of the holotype specimen of *Alioramus altai* (IGM 100/1844) in left lateral (A) and medial (B) views. A: pneumatic region where anterior and dorsal processes meet; B: anterior end of anterior process. Scale bar equals 5 cm. Abbreviations as in Figure 12.

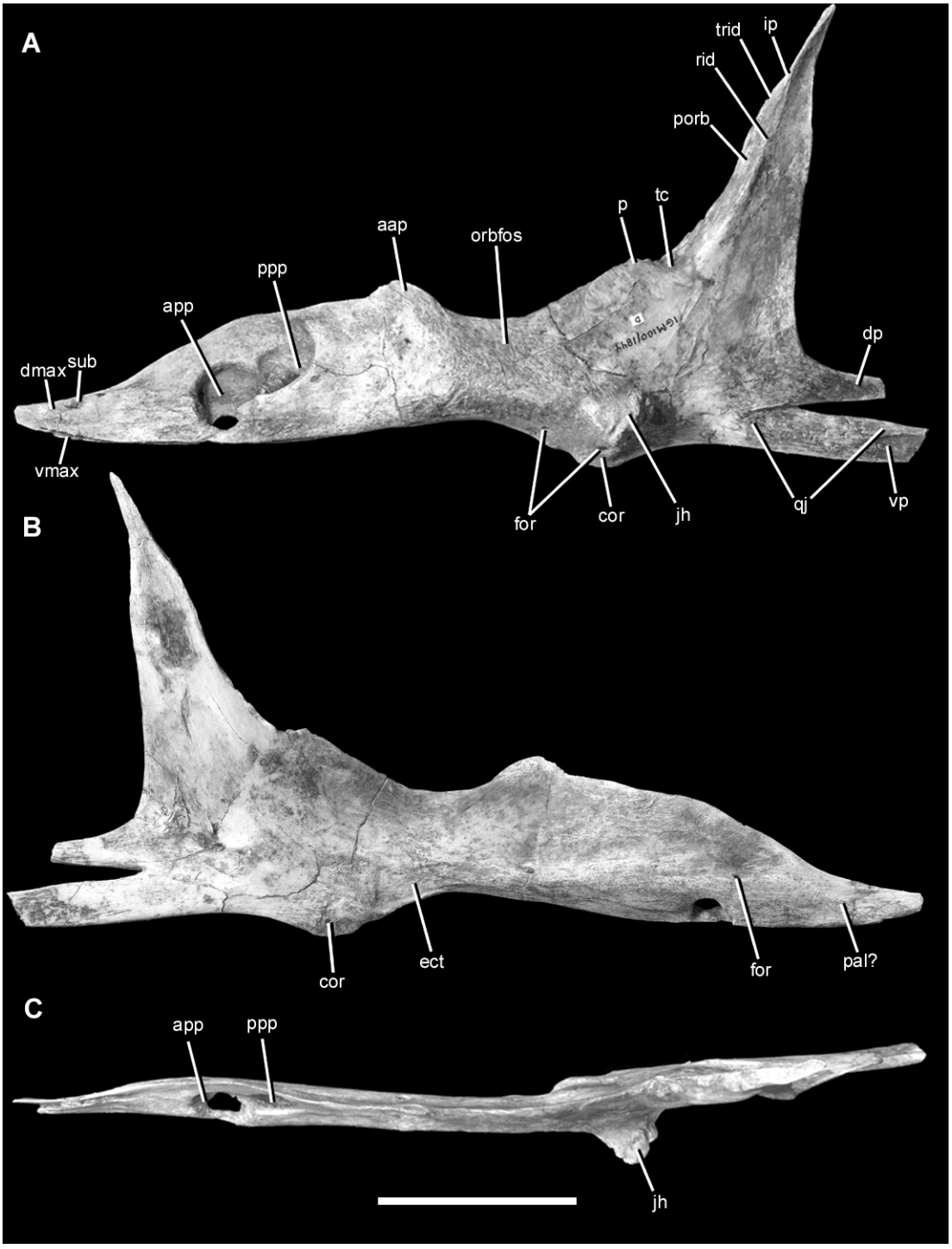

Figure 1-15. Right jugal of the holotype specimen of *Alioramus altai* (IGM 100/1844) in lateral (A), medial (B), and dorsal (C) views. Scale bar equals 5 cm.Abbreviations: aap, anterior ascending process; app, anterior pocket of jugal pneumatic recess; cor, cornual process; dmax,

dorsally-positioned groove for maxilla contact; dp, dorsal prong of posterior ramus; for, foramen; ect, ectopterygoid contact; ip, inflection point; jh, jugal hornlet; orbfos, orbital fossa; p, projection anterior to terminal concavity of postorbital contact; pal, palatine contact; ppp, posterior pocket (main recess) of jugal pneumatic recess; qj, quadratojugal contact; rid, prominent ridge demarcating posterior edge of postorbital contact on dorsal ramus; sub, subsidiary process of anterior ramus; tc, terminal concavity of postorbital contact; trid, thin ridge within postorbital contact surface separating anteriorly and laterally facing portions (the anteriorly-facing portion is not visible here); vmax, ventrally positioned groove for maxilla contact; vp, ventral prong of posterior ramus.

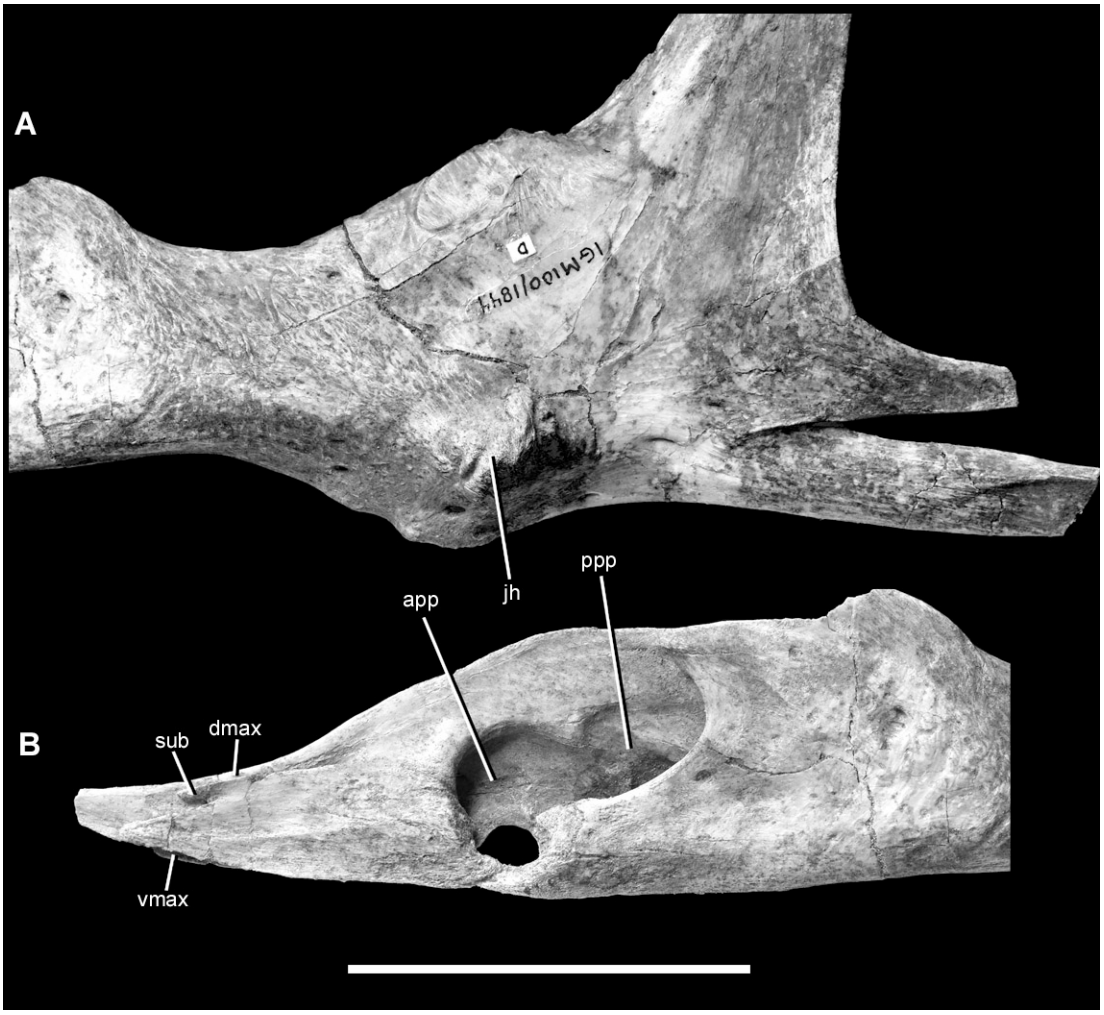

Figure 1-16. Closeup photo of the right jugal of the holotype specimen of *Alioramus altai* (IGM 100/1844) in left lateral view. A: suborbital region; B: region surrounding jugal pneumatic recess. Scale bar equals 5 cm. Abbreviations as in Figure 15.

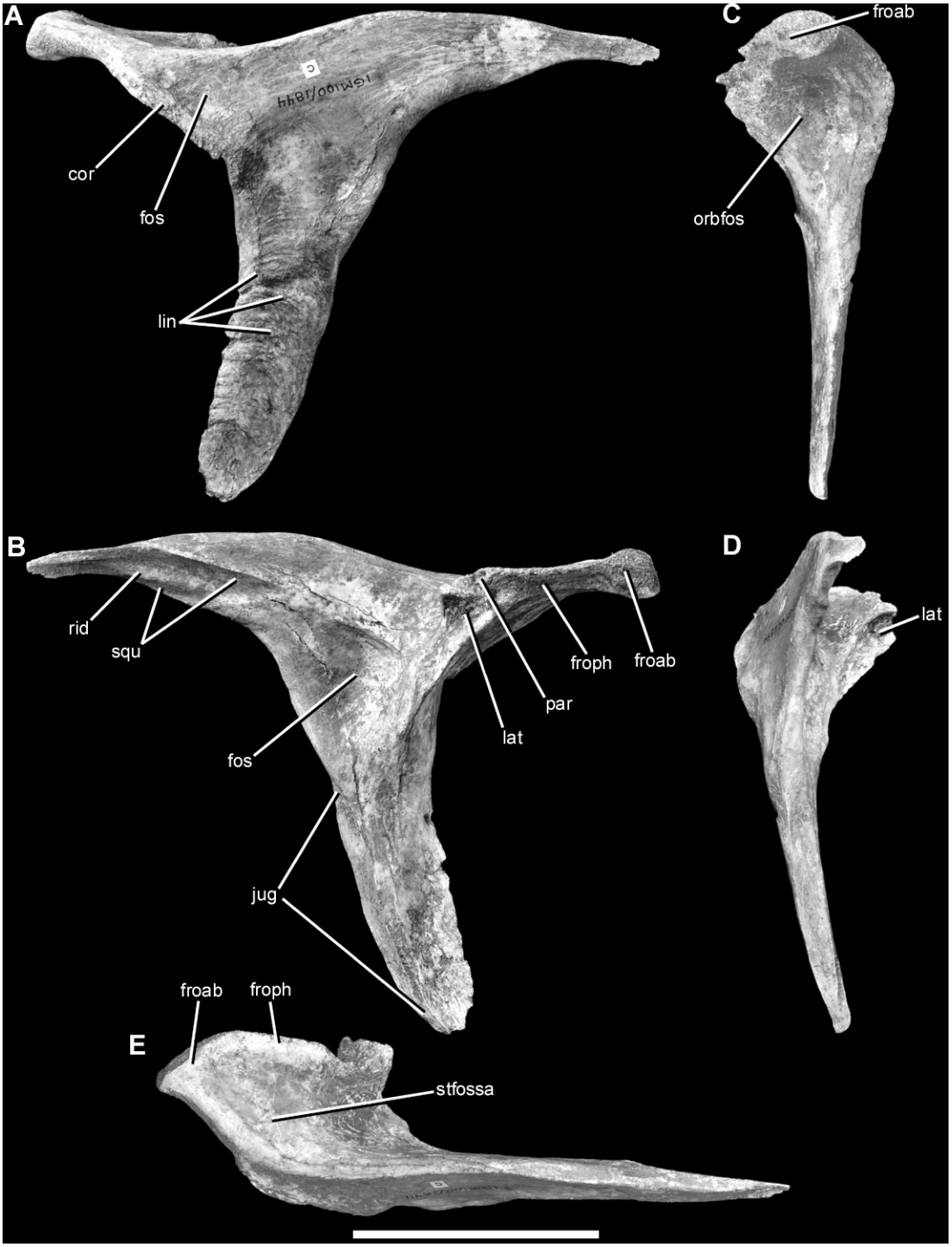

Figure 1-17. Left postorbital of the holotype specimen of *Alioramus altai* (IGM 100/1844) in lateral (A), medial (B), anterior (C), posterior (D), and dorsal (E) views. Scale bar equals 5 cm. Abbreviations: cor, cornual process; fos, fossa; froab, anterior bulge of frontal articulation; froph,

posterior horizontal portion of frontal articulation; jug, jugal contact; lat, laterosphenoid contact; lin, arcuate lineations on lateral surface of ventral ramus; orbfos, orbital fossa; par, parietal contact; rid, ridge separating dorsal and ventral portions of squamosal contact; squ, squamosal contact; stfossa, supratemporal fossa.

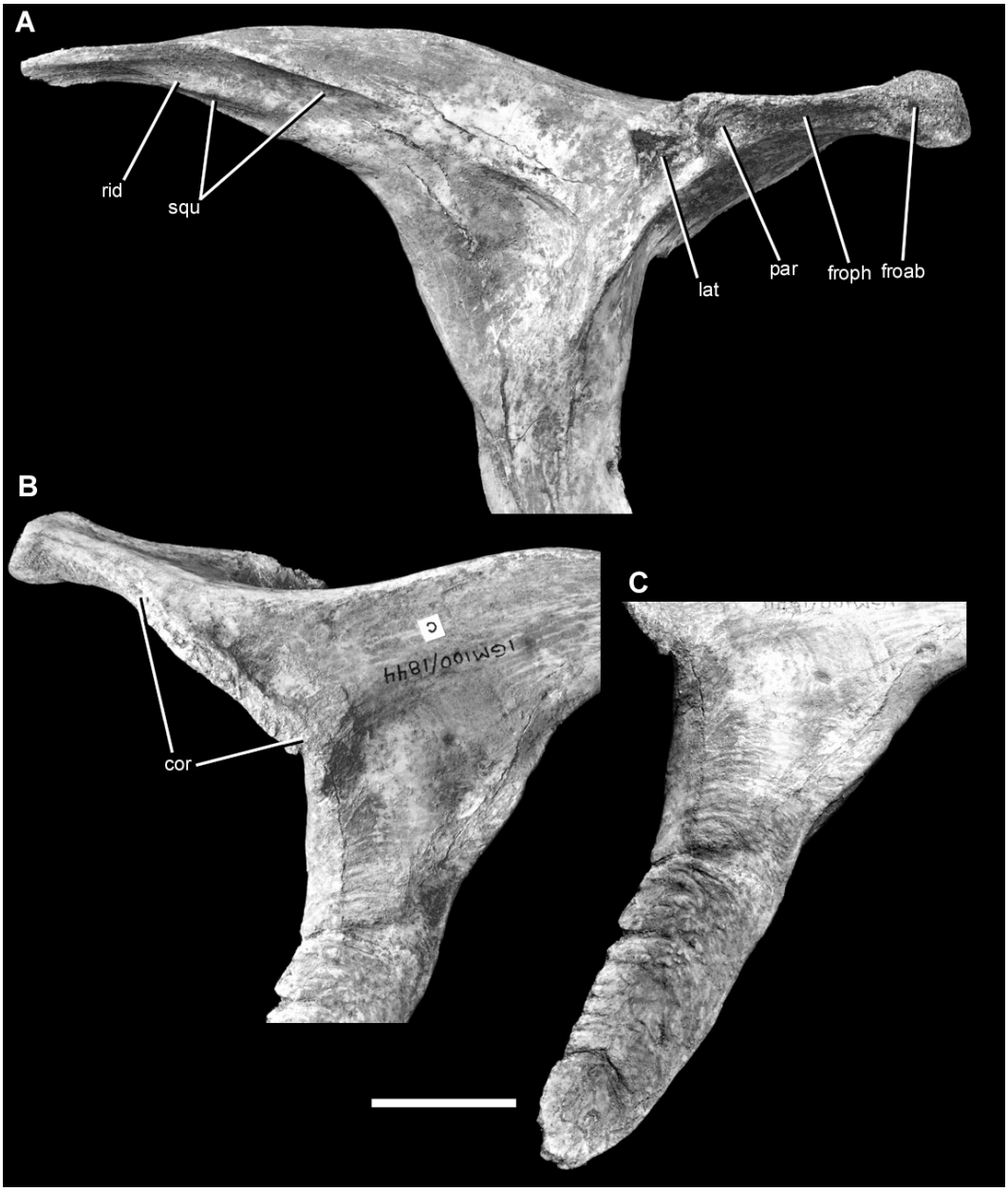

Figure 1-18 Closeup photos of the left postorbital of the holotype specimen of *Alioramus altai* (IGM 100/1844) in medial (A) and lateral (B,C) views. A: region articulating with various cranial bones; B: region of cornual process at posterodorsal corner of orbit; C: ventral ramus. Scale bar equals 2 cm. Abbreviations as in figure 17.

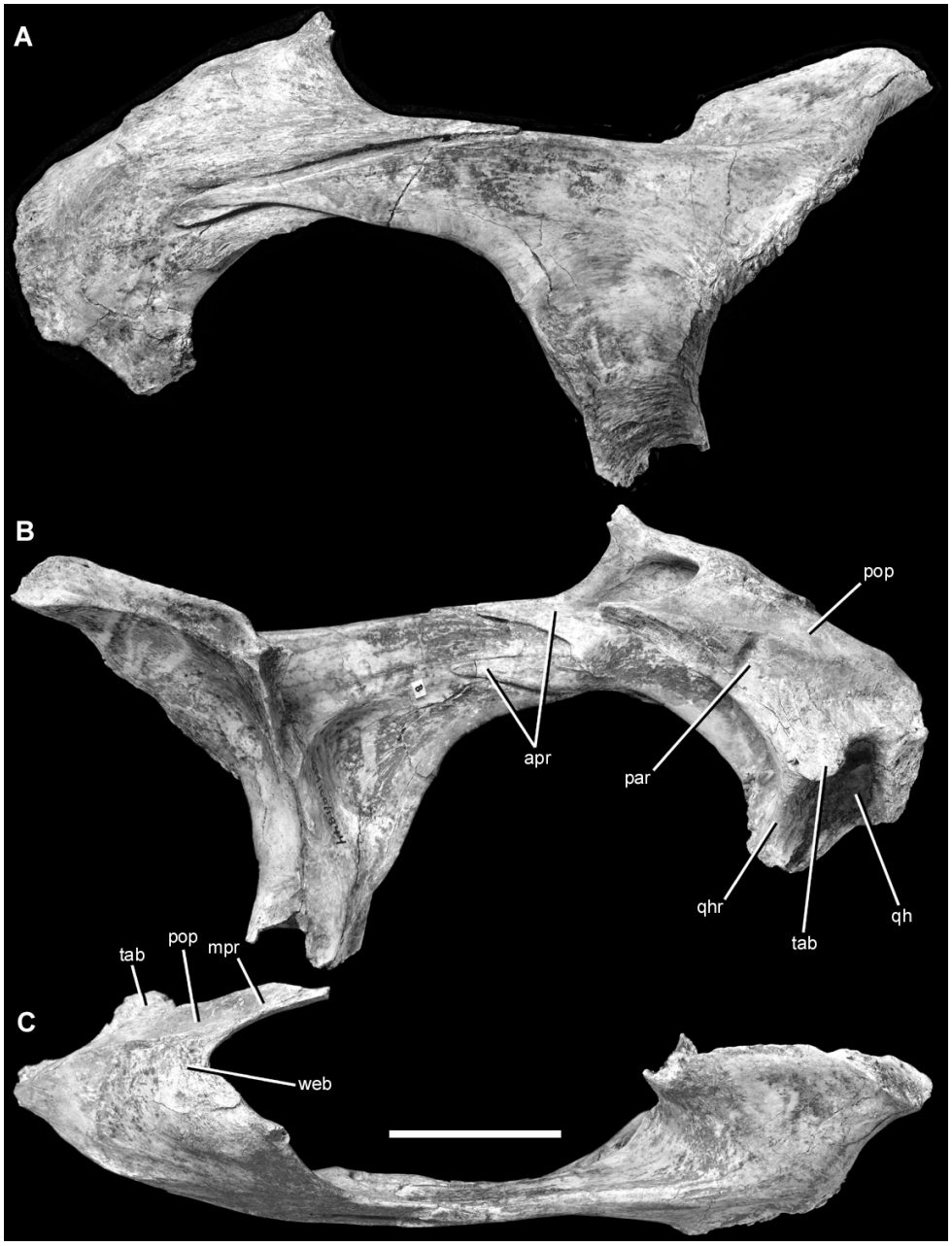

Figure 1-19. Right postorbital and squamosal (in articulation) of the holotype specimen of *Alioramus altai* (IGM 100/1844) in lateral (A), medial (B), and dorsal (C) views. Scale bar equals 3 cm. Abbreviations as in Figure 18, plus: qhr, ridge on squamosal anterior to articulation of quadrate head; web, web of bone connecting anterior and medial processes.

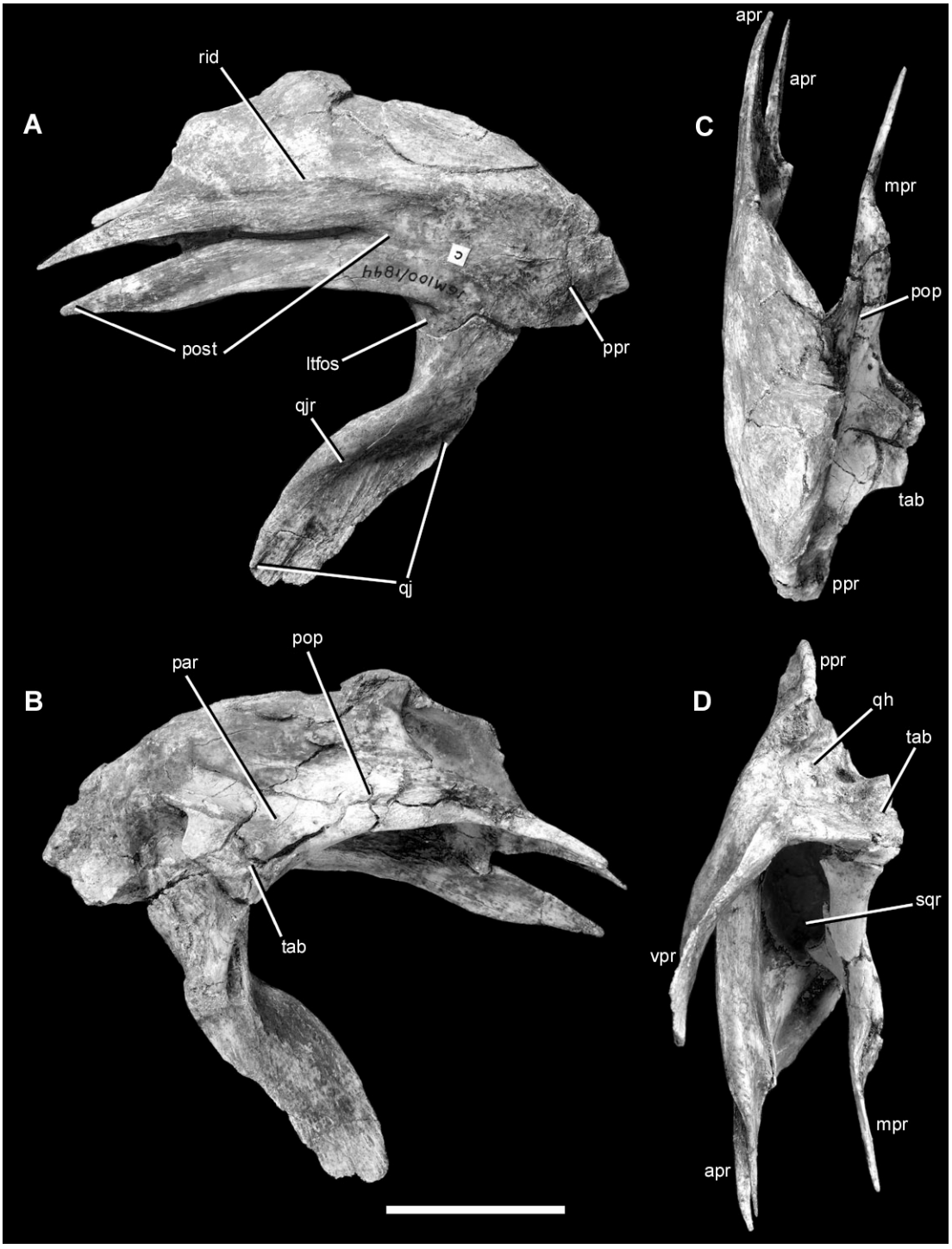

Figure 1-20. Left squamosal of the holotype specimen of *Alioramus altai* (IGM 100/1844) in lateral (A), medial (B), dorsal (C), and ventral (D) views. Scale bar equals 3 cm. Abbreviations: apr, anterior process; ltfos, lateral temporal fossa; mpr, medial process; par, parietal contact

surface; pop, contact surface for paroccipital process; post, postorbital contact surface; ppr, posterior process; qh, socket for articulation with quadrate head; qj, quadratojugal contact surface; qjr, ridge demarcating dorsal extent of suture with quadrate; rid, ridge on lateral surface of anterior process; sqr, squamosal recess; tab; medially projecting tab on medial process; vpr, ventral process.

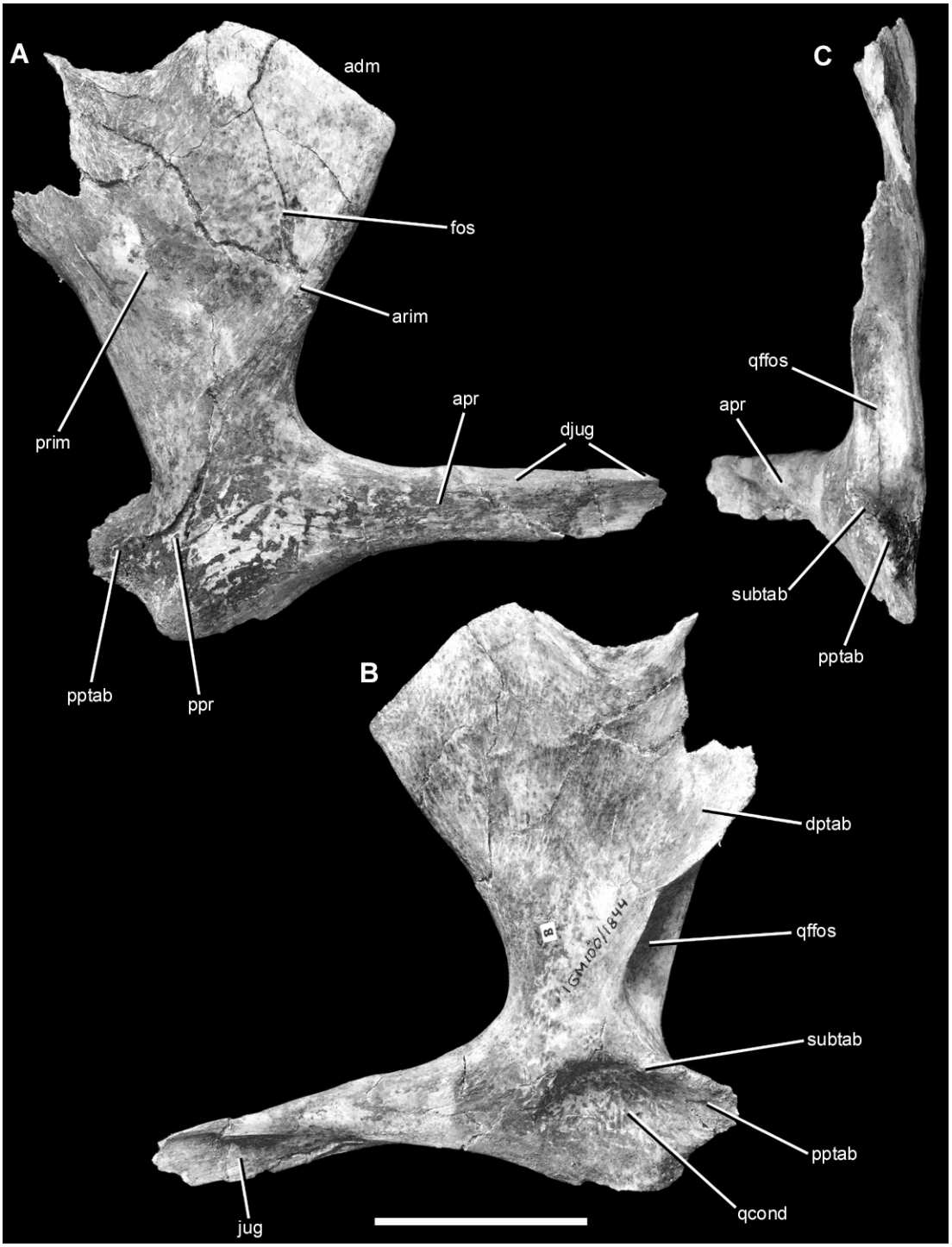

Figure 1-21. Right quadratojugal of the holotype specimen of *Alioramus altai* (IGM 100/1844) in lateral (A), medial (B), and posterior (C) views. Scale bar equals 3 cm. Abbreviations: adm, anterodorsal margin of dorsal process; arim, anterior rim of lateral fossa; apr, anterior process;

djug, groove for jugal on dorsal surface of anterior process; dptab, tab on dorsal process for articulation with quadrate; fos, fossa on lateral surface of dorsal process; jug, jugal contact surface; ppr, posterior process; pptab, tab on posterior process for articulation with quadrate condyle; prim, posterior rim of lateral fossa; qcond, surface for articulation with quadrate condyle; qffos, fossa lateral to quadrate foramen; subtab, subsidiary tab on the larger tab of the posterior process that articules with the quadrate condyle.

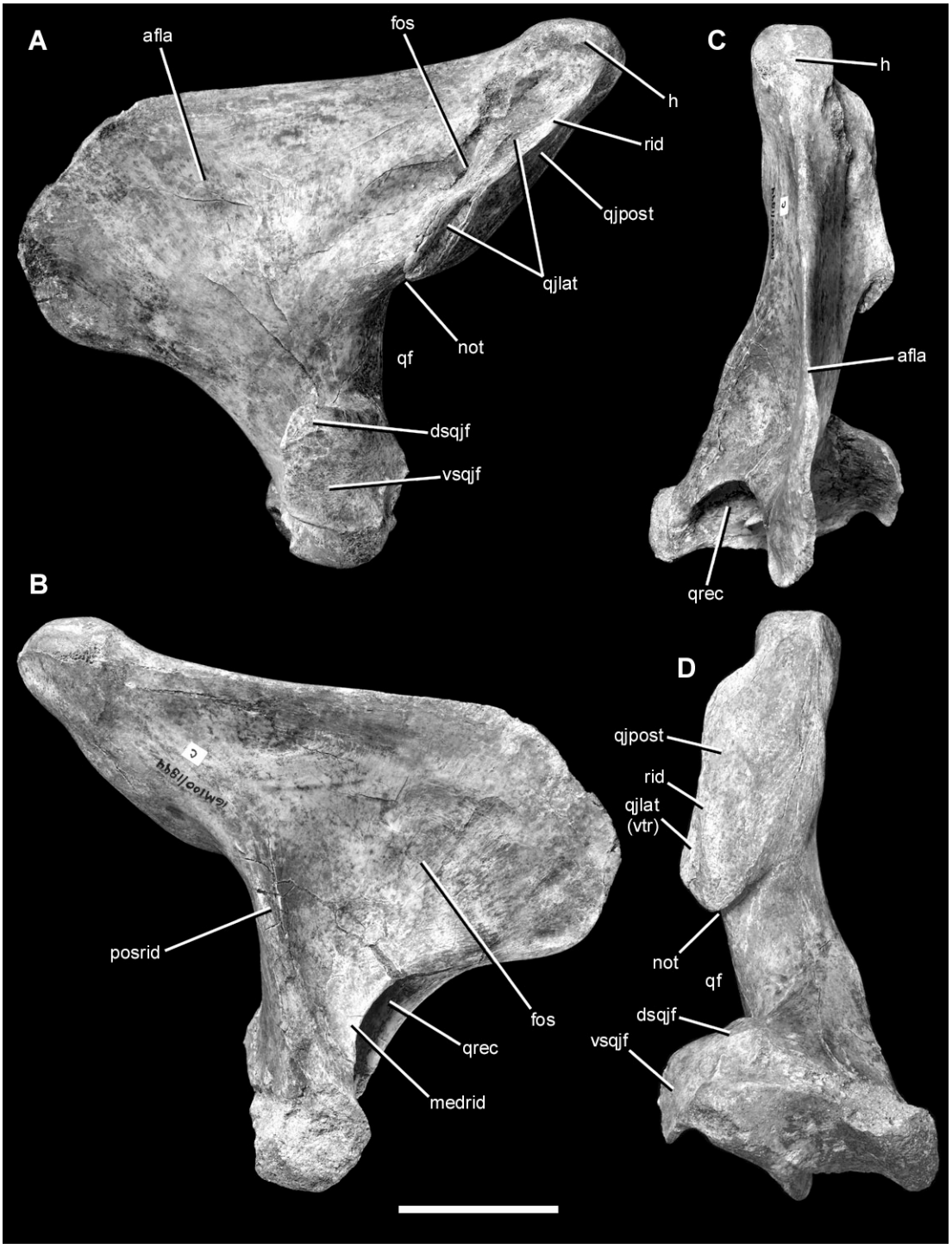

Figure 1-22. Left quadrate of the holotype specimen of *Alioramus altai* (IGM 100/1844) in lateral (A), medial (B), anterior (C), and posterior (D) views. Scale bar equals 3 cm. Abbreviations: afla, anterior flange; dsqjf, dorsal region of quadratojugal contact surface on

lateral condyle; fos, fossa; h, head; not, notch between lateral articular surface for quadrate and quadrate foramen; icqrec, internal chambers of quadrate recess; lc, lateral condyle; mc, medial condyle; medridge, ridge connecting anterior flange to medial condyle; posrid, ridge on posterior surface linking anterior flange and medial condyle to quadrate head; qf, quadrate foramen; qjlat, laterally facing articular surface for quadratojugal on quadrate shaft; qjpost, posteriorly facing articular surface for quadratojugal on quadrate shaft; qrec, quadrate recess; rid, ridge separating lateral and posterior articular surfaces for quadratojugal on quadrate shaft; vsqjf, ventral region of quadratojugal contact surface on lateral condyle; vtr, ventral trochlea on quadrate condyles.

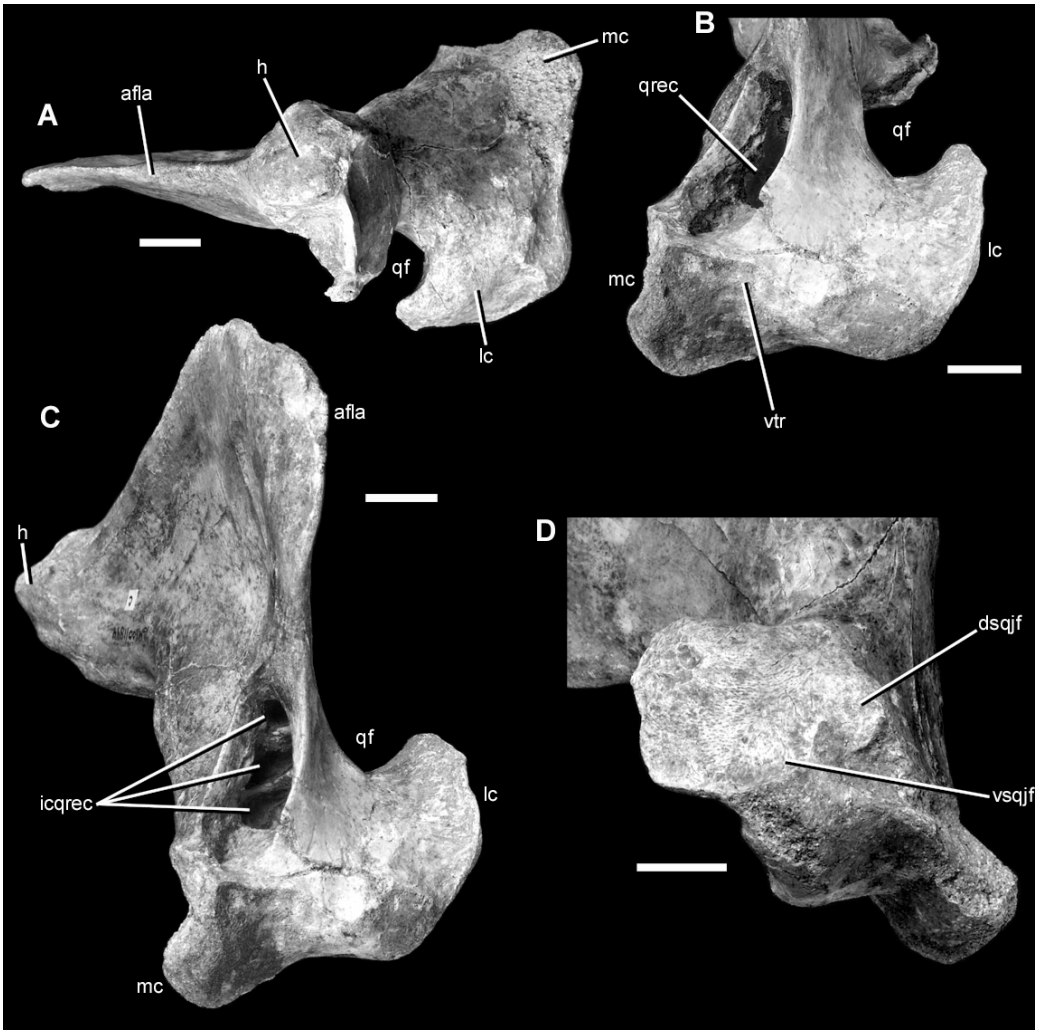

Figure 1-23. Closeup photos of the left quadrate of the holotype specimen of *Alioramus altai* (IGM 100/1844). A: dorsal view of quadrate head; B: ventral and slightly oblique anterior view showing quadrate condyles; C: anteroventral oblique view, showing details of the quadrate recess; D: ventrolateral oblique view, showing details of the quadratojugal articular facet on lateral surface of quadrate condyle. Scale bars equal 1 cm. Abbreviations as in Fig 22.

Figure 1-24. Left quadratojugal and quadrate (in articulation) of the holotype specimen of *Alioramus altai* (IGM 100/1844) in posterior view. Scale bar equals 1 cm. Abbreviations as in Figs. 21 and 22.

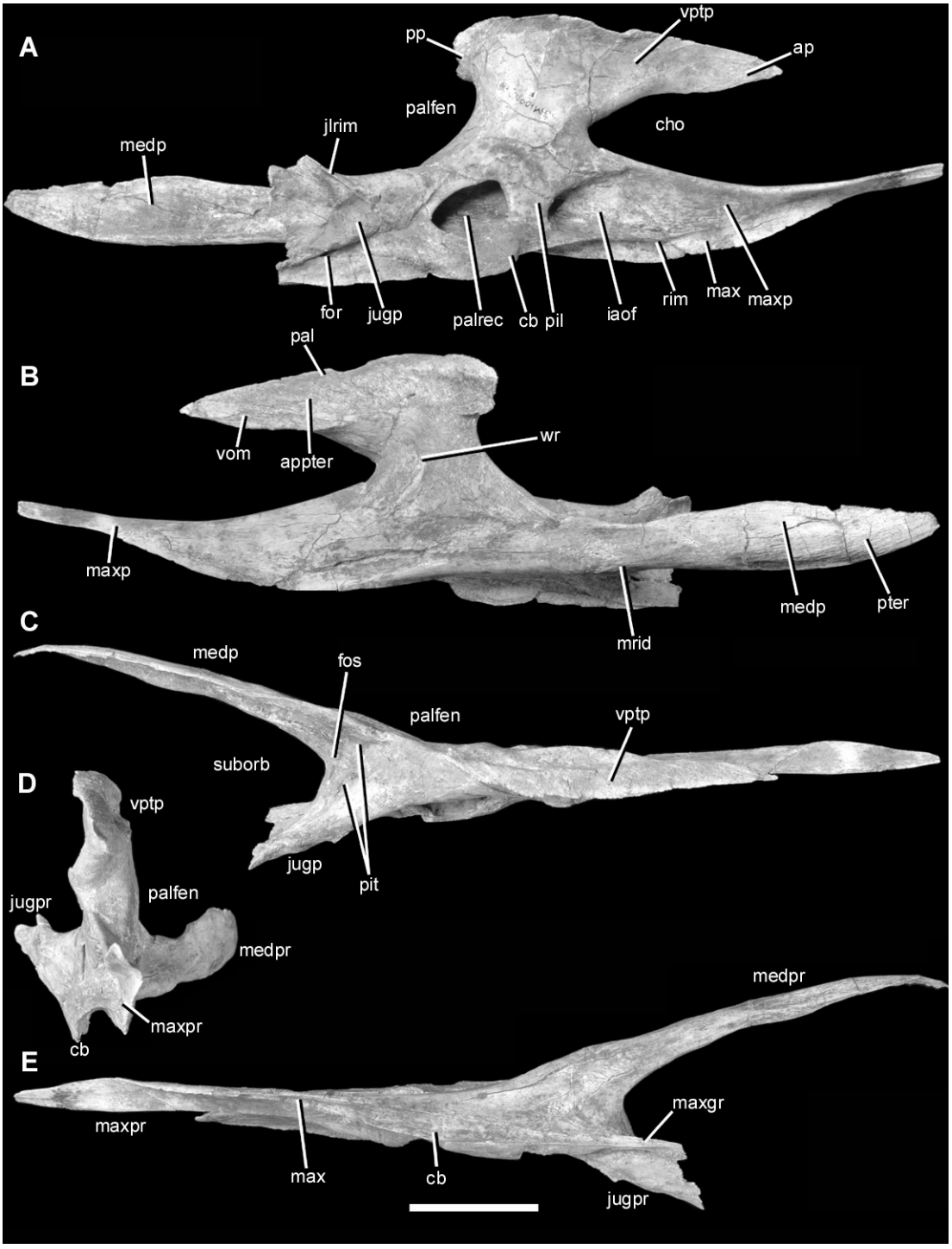

Figure 1-25. Right palatine of the holotype specimen of *Alioramus altai* (IGM 100/1844) in lateral (A), medial (B), dorsal (C), anterior (D), and ventral (E) views. Scale bar equals 3 cm. Abbreviations: ap, anterior projection of vomeropterygoid process; appter, articular surface for

anterior process of pterygoid; cb, convex bulge where maxillary and jugal processes meet; cho, internal choana; for, foramen on lateral surface of jugal process, demarcating the separation between the dorsal and ventral subordinate processes (the foramen would not have been completely enclosed in life, but rather is a slot that is open posteriorly); fos, fossa; iaof, internal antorbital fossa; jlrim, rim separating jugal and lacrimal articular facets on lateral surface of jugal process; jugpr, jugal process; max, contact surface for maxilla on lateral surface of maxillary process; maxgr, groove on ventral surface of jugal process for articulation with the maxilla; maxpr, maxillary process; medpr, medial process; mrid, ridge on medial surface of medial process; pal, articular surface for opposing palatine; palfen, palatine fenestra; palrec, palatine recess; pil, pillar between palatine recess and internal antorbital fossa; pits, pit-like pockets at anterior margin of fossa bordered the suborbital fenestra; pp, posterior projection of vomeropterygoid process; pter, contact surface for pterygoid on medial surface of medial process; rim, rim separating internal antorbital fenestra and maxillary contact surface on lateral surface of maxillary process; suborb, suborbital fenestra; vom, articular surface for vomen; vptp, vomeropterygoid process; wr, waisted region where all four processes of the palatine meet.

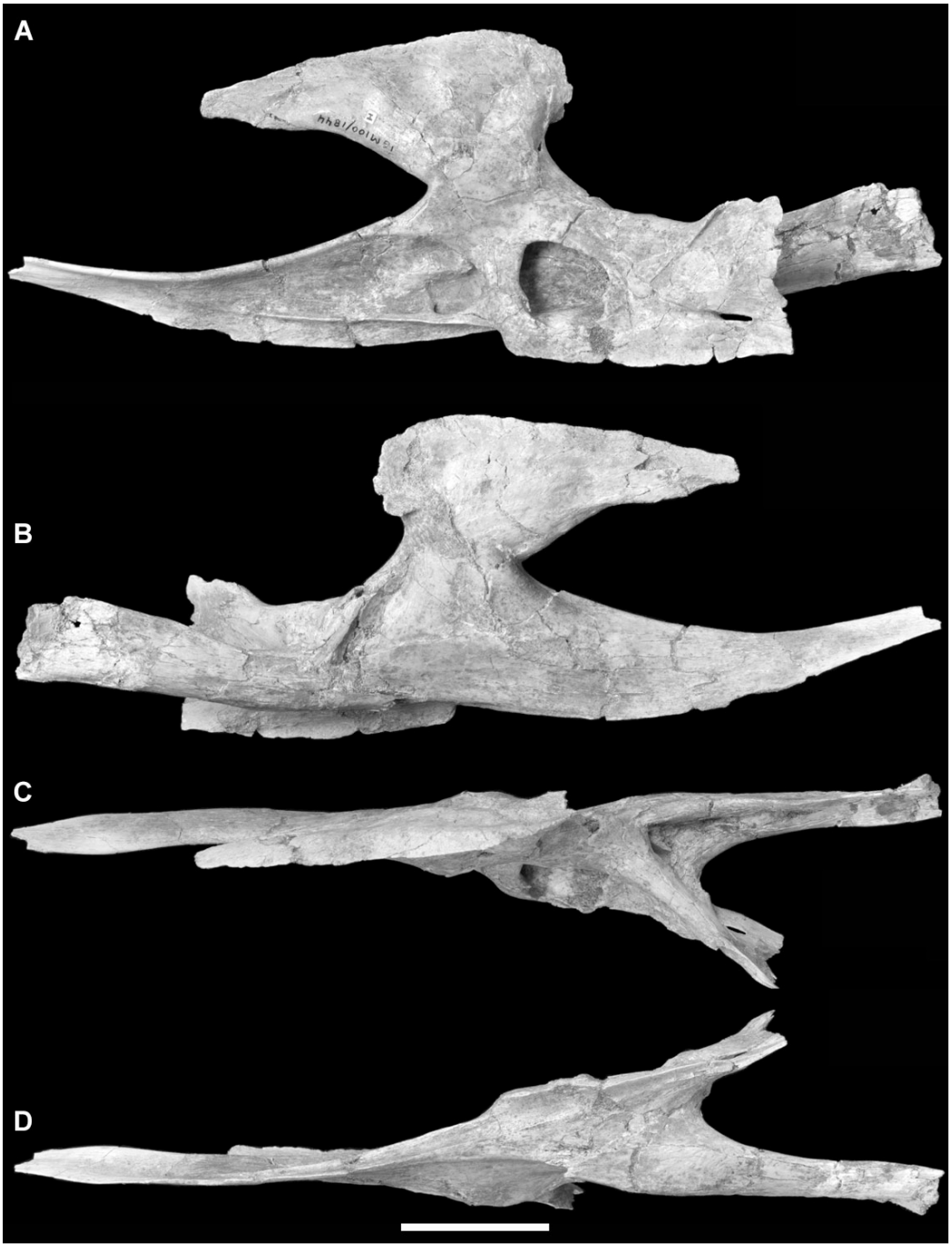

Figure 1-26. Right palatine of the holotype specimen of *Alioramus altai* (IGM 100/1844) in lateral (A), medial (B), dorsal (C), and ventral (D) views. Scale bar equals 3 cm. This figure is not labeled, but refer to figure 25 for corresponding labels on the right palatine.

Figure 27. Closeup photo of the right palatine of the holotype specimen of *Alioramus altai* (IGM 100/1844) in lateral view. Scale bar equals 2 cm. This figure is not labeled, but refer to figure 25 for corresponding labels on the right palatine.

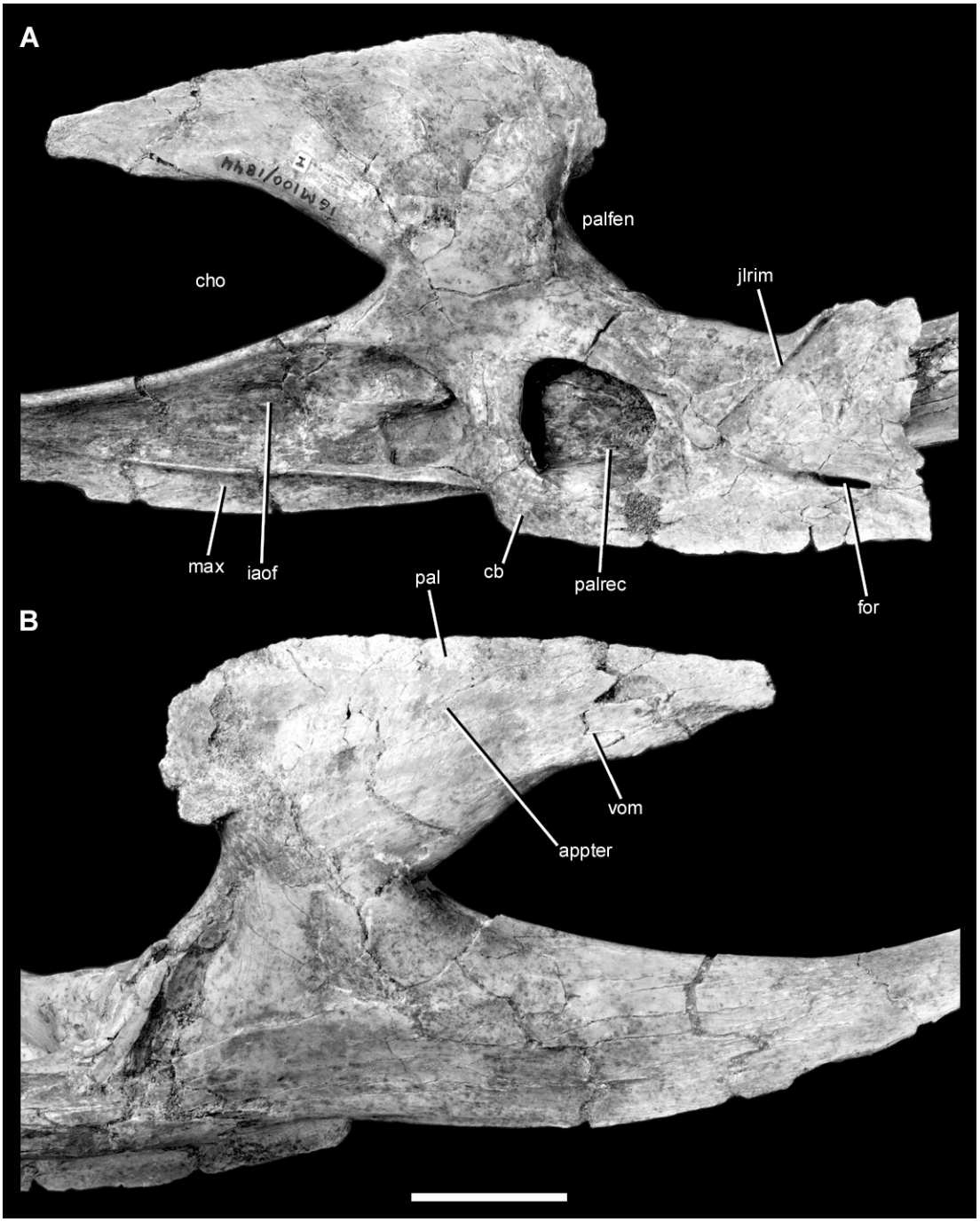

Figure 1-28. Closeup photos of the left palatine of the holotype specimen of *Alioramus altai* (IGM 100/1844) in lateral (A) and medial (B) views. Scale bar equals 2 cm. Abbreviations as in Fig. 25.

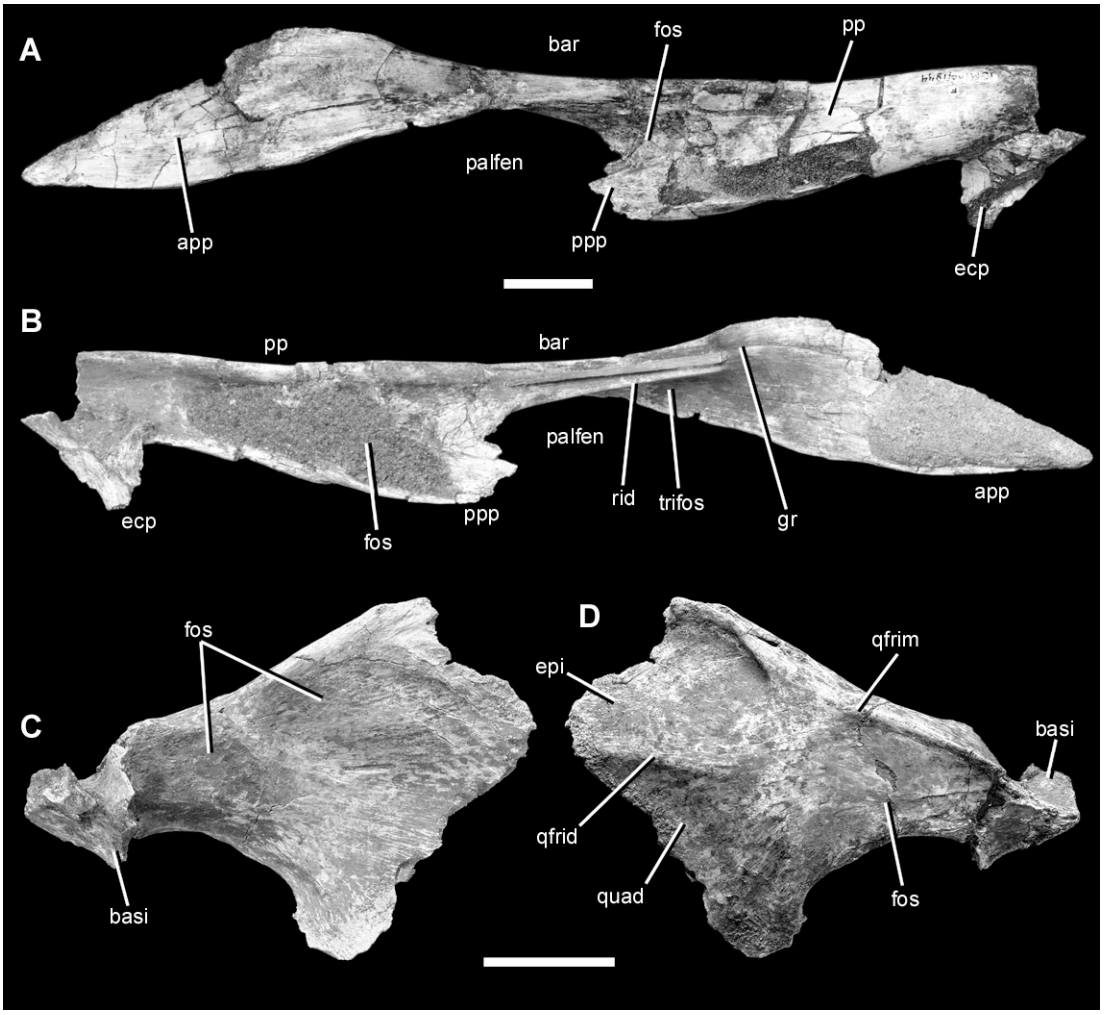

Figure 1-29. Right pterygoid of the holotype specimen of *Alioramus altai* (IGM 100/1844) in medial (A,C), and lateral (B,D) views. A, B: anterior segment that articulated with palatine and ectopterygoid; C,D: posterior segment that articulated with quadrate and epipterygoid. Scale bars equal 2 cm. Abbreviations: app, anterior palatine process; bar, bar linking anterior and posterior palatine processes; basi, process for articulation with basipterygoid process of braincase; ecp, ectopterygoid process; epi, epipterygoid contact surface; fos, fossa; palfen, gr, groove above ridge on bar between anterior and posterior palatine processes; palatine fenestra; pp, palatal plate region of pterygoid; ppp, posterior palatine process; qfrid, ridge on lateral surface of quadrate flange separating articular surfaces for quadrate and epipterygoid; qfrim, rim delimiting anterior

margin of epipterygoid contact surface that continues anteriorly along dorsal margin of bone; quad, quadrate contact surface; rid, ridge on lateral surface of bar between anterior and posterior palatine processes; trifos, triangular fossa on lateral surface.

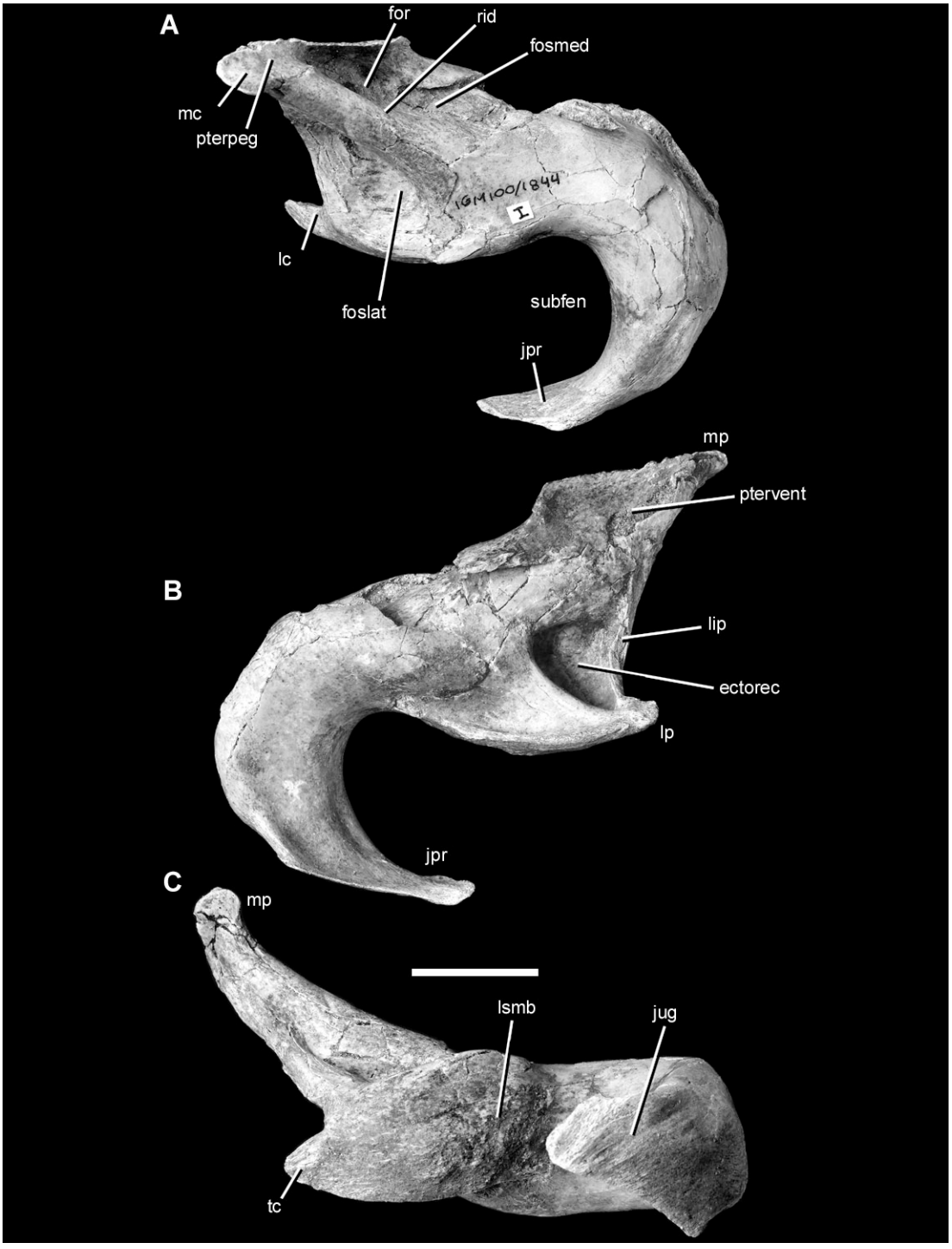

Figure 1-30. Right ectopterygoid of the holotype specimen of *Alioramus altai* (IGM 100/1844) in dorsal (A), ventral (B), and lateral (C) views. Scale bar equals 3 cm. Abbreviations: ectorec,

ectopterygoid recess; for, foramen within medial fossa on dorsal surface of bone; foslat, lateral fossa on dorsal surface of bone; fosmed, medial fossa on dorsal surface of bone; jpr, jugal process; jug, jugal articular surface; lip, lip between ectopterygoid recess and posterior edge of bone; lp, lateral projection of posterior end of main body; lsmb, lateral surface of main body of bone; mp, medial projection of posterior end of main body; pterpeg, peg on medial projection of main body for articulation with the pteygoid; ptervent, articular surface for pterygoid on ventral surface of ectopterygoid; rid, ridge on dorsal surface of bone; subfen, subtemporal fenestra (floor of lateral temporal fenestra); tc, triangular corner of lateral projection of posterior end of main body.

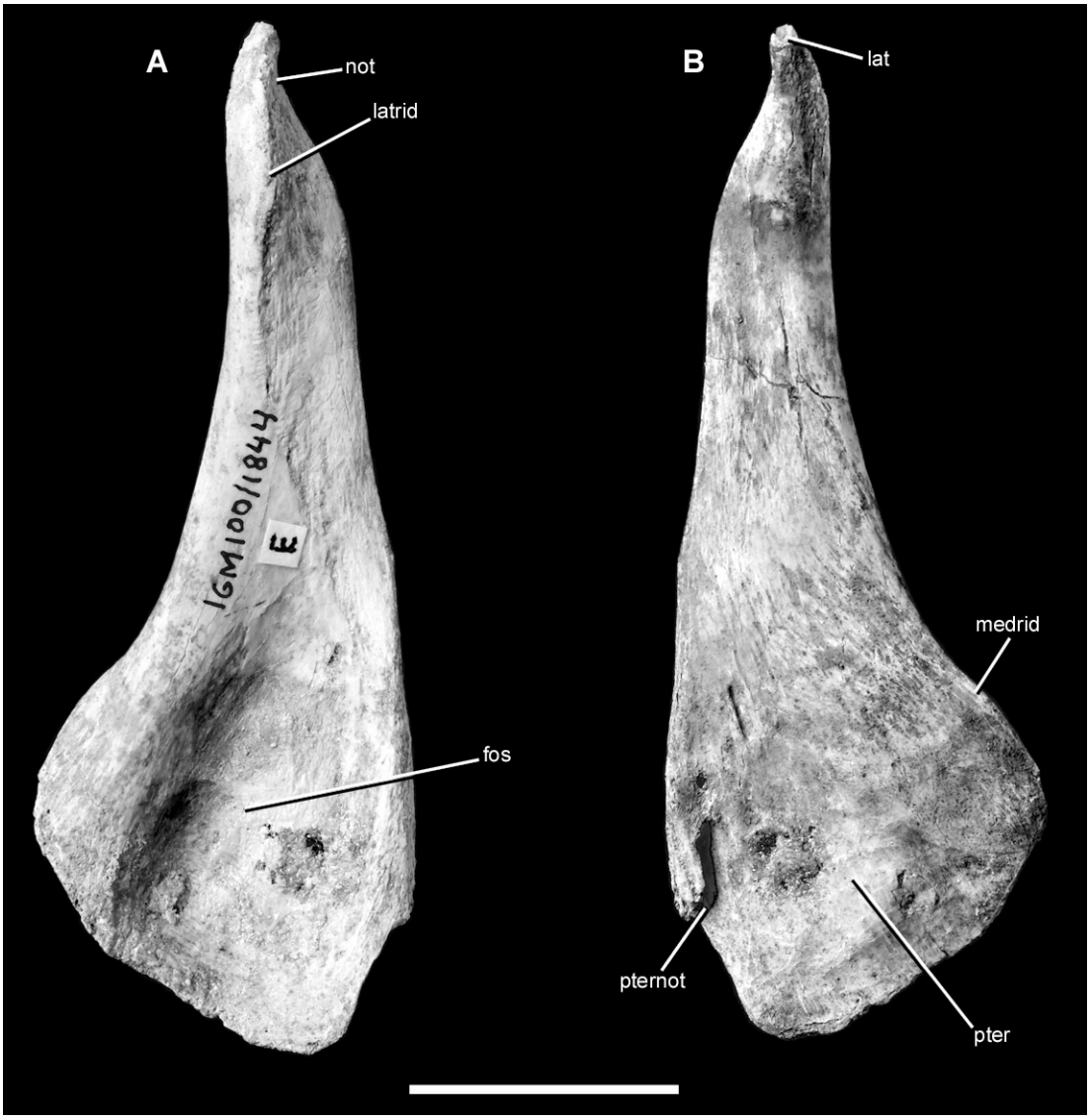

Figure 1-31. Right epipterygoid of the holotype specimen of *Alioramus altai* (IGM 100/1844) in lateral (A) and medial (B) views. Scale bar equals 2 cm. Abbreviations: fos, fossa on lateral surface; lat, articular peg for laterosphenoid; latrid, ridge on lateral surface; medrid, ridge on medial surface; not, notch on anterior margin of bone; pter, pterygoid articular contact on medial surface; pternot, notch on medial surface that reinforced contact with pterygoid.

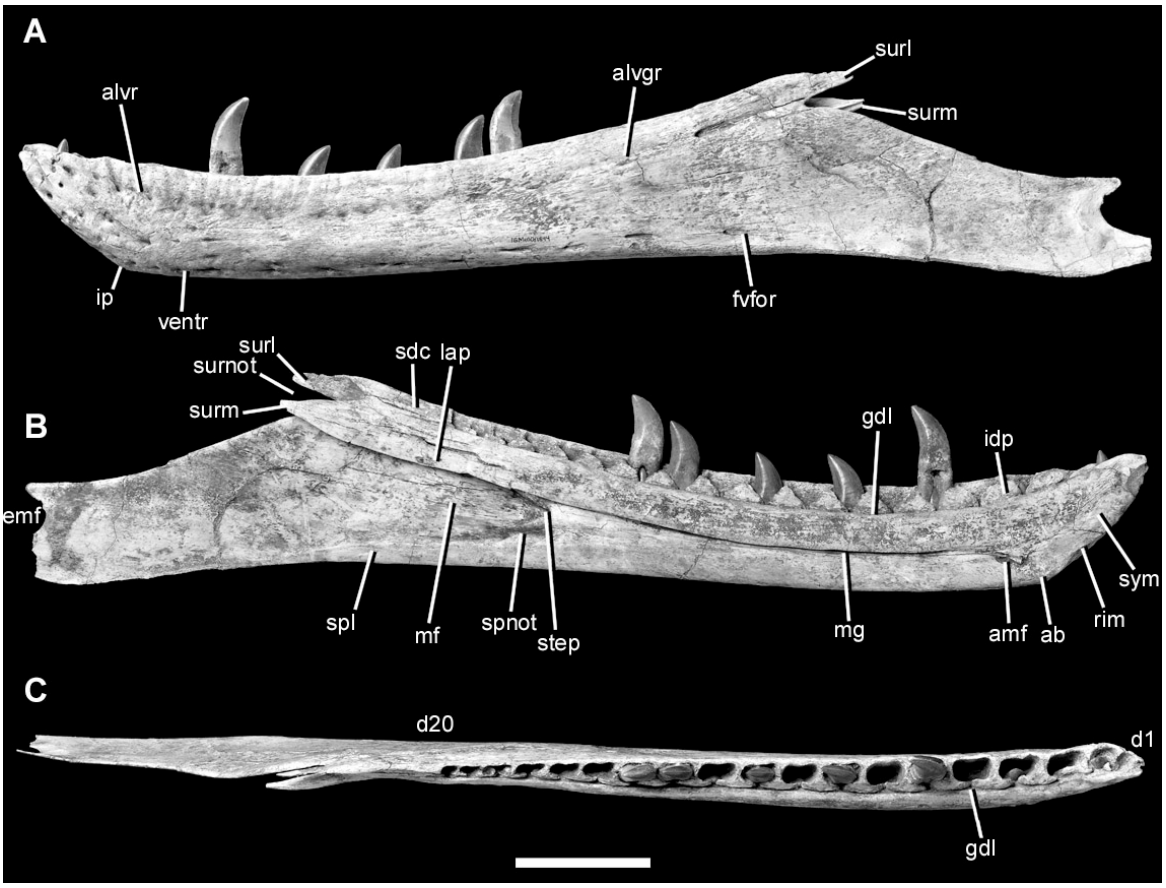

Figure 1-32. Left dentary of the holotype specimen of *Alioramus altai* (IGM 100/1844) in lateral (A) medial (B), and dorsal (C) views. Scale bar equals 5 cm. Abbreviations: ab, convex articular brace ("chin") on the dentary symphysis; alvgr, inset groove that continues posteriorly from the alveolar row of foramina; alvr, alveolar row of foramina; amf, anterior Meckelian foramen; d1, d20, dentary tooth positions; emf, external mandibular fenestra; fvfor, final foramina in the ventral row; gdl, groove for the dental lamina; idp, interdental plates; ip, inflection point where anterior and ventral margins of dentary meet; lap, lappet of main body that covers the Meckelian fossa medially; mf, Meckelian fossa; mg, Meckelian groove; rim, sinuous rim continuing anterodorsally from articular brace of symphysis; sdc, articular surface for supradentary/coronoid element posterior to tooth row; spl, flat articular facet for splenial along ventral margin of medial surface of dentary; spnot, notch for articulation of splenial; step, step between Meckelian groove

and Meckelian fossa; surl, lateral prong for articulation with surangular; surm, medial prong for articulation with surangular; surnotch, articular notch between lateral and medial prongs for articulation with surangular; sym, dentary symphysis; ventr, ventral row of foramina.

Figure 1-33. Closeup photos of the left dentary of the holotype specimen of *Alioramus altai* (IGM 100/1844) in medial view. A: posterior region; B: middle region; C: anterior region. Scale bars equal 5 cm. This figure is not labeled, but refer to figure 32 for corresponding labels on the dentary overview figure.

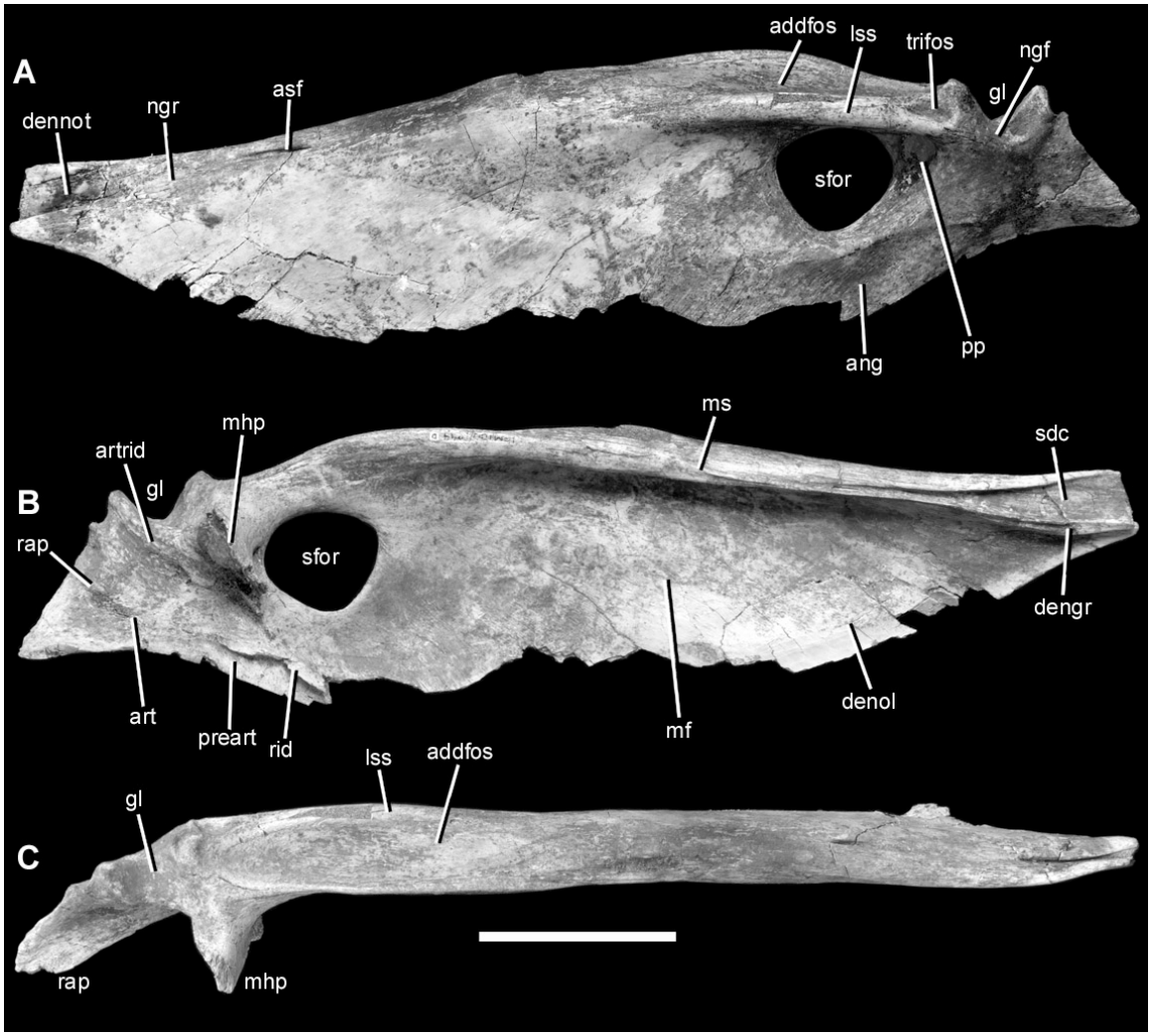

Figure 1-34. Left surangular of the holotype specimen of *Alioramus altai* (IGM 100/1844) in lateral (A) medial (B), and dorsal (C) views. Scale bar equals 5 cm. Abbreviations: addfos, adductor fossa; artrid, ridge on medial surface of retroarticular process to strengthen articulation with articular; ang, region of lateral surface of surangular overlapped by angular; art, articular contact surface; asf, anterior surangular foramen; dengr, groove for articulation with dentary; dennot, notch for articulation with dentary; denol, medial surface of surangular that overlaps dentary laterally; gl, glenoid; lss, lateral surangular shelf; mf, Meckelian fossa; mhp, medial hook process; ms, medial shelf; ngf, non-glenoid fossa on lateral surface of surangular below

glenoid; ngr, neurovascular groove; pp, pneumatic pocket posterodorsal to surangular foramen; preart, groove for articulation with prearticular; rap, retroarticular process; rid, ridge separating articular facets for articular and prearticular on medial surface of retroarticular process; sdc, contact surface for supradentary/coronoid; sfor, surangular foramen; trifos, triangular fossa on lateral surface.

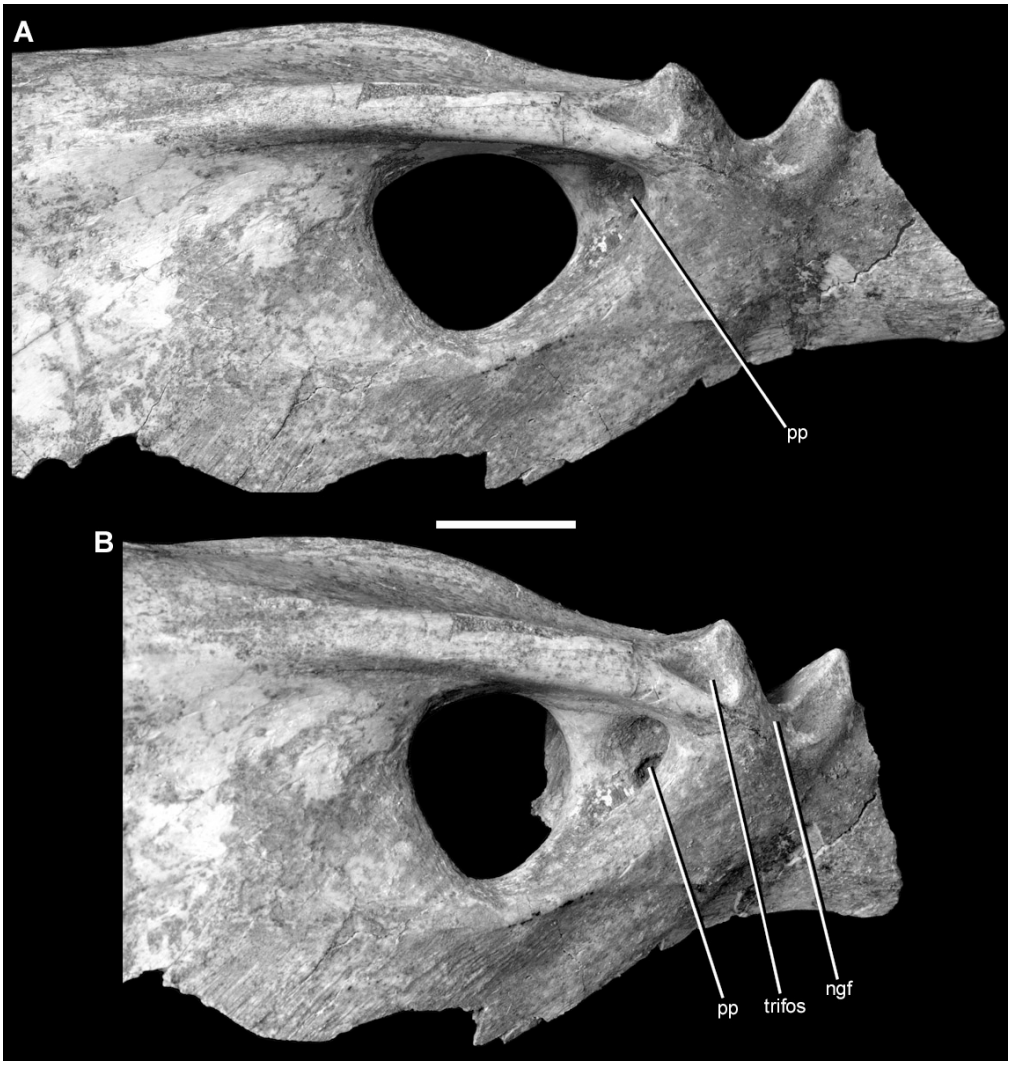

Figure 1-35. Closeup photos of the left surangular of the holotype specimen of *Alioramus altai* (IGM 100/1844) in lateral (A) and anterolateral oblique (B) views. Scale bar equals 2 cm. Abbreviations as in Figure 34.

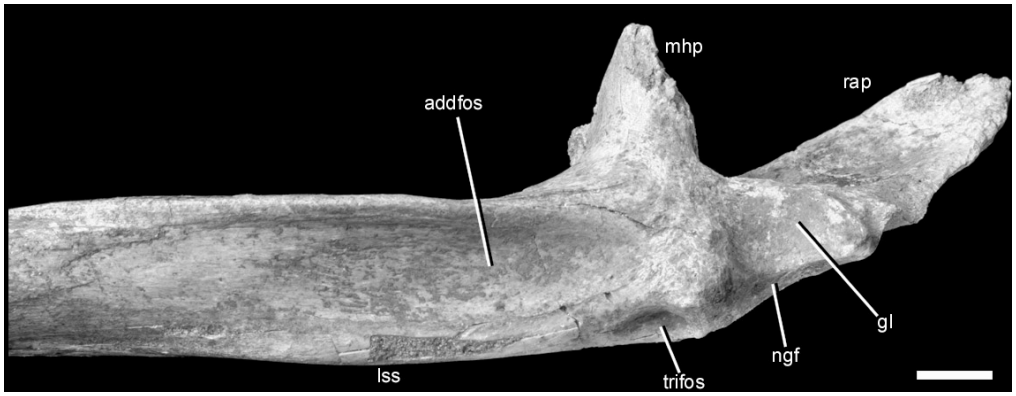

Figure 1-36. Closeup photo of the left surangular of the holotype specimen of *Alioramus altai* (IGM 100/1844) in dorsal view. Scale bar equals 1 cm. Abbreviations as in Figure 34.

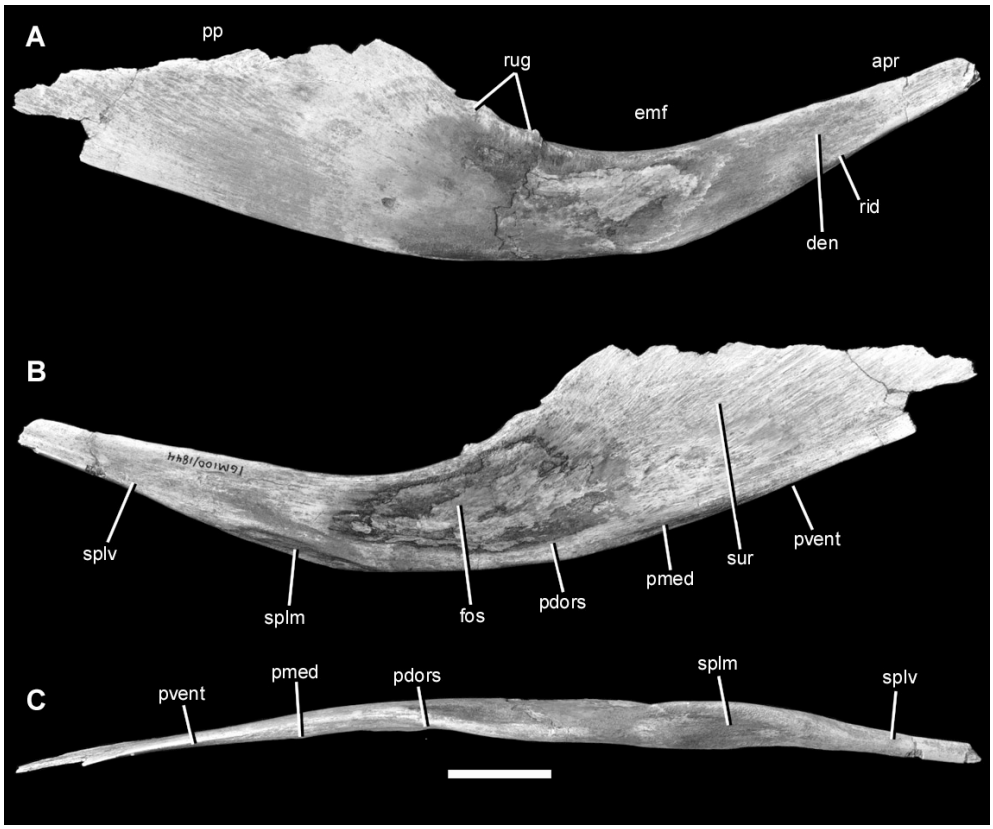

Figure 1-37. Right angular of the holotype specimen of *Alioramus altai* (IGM 100/1844) in lateral (A) medial (B), and ventral (C) views. Scale bar equals 2 cm. Abbreviations: apr, anterior rprocess; den, contact surface for dentary; emf, external mandibular fenestra; fos, fossa; pdors, dorsally facing region of prearticular contact; pmed, medially facing region of prearticular contact; pp, posterior plate, pvent, ventral facing region of prearticular contact; rig, ridge delimiting ventral margin of dentary contact on lateral surface; rug, rugosities; splm, medially facing region of splenial contact; splv, ventrally facing portion of splenial contact; sur, contact surface for surangular.

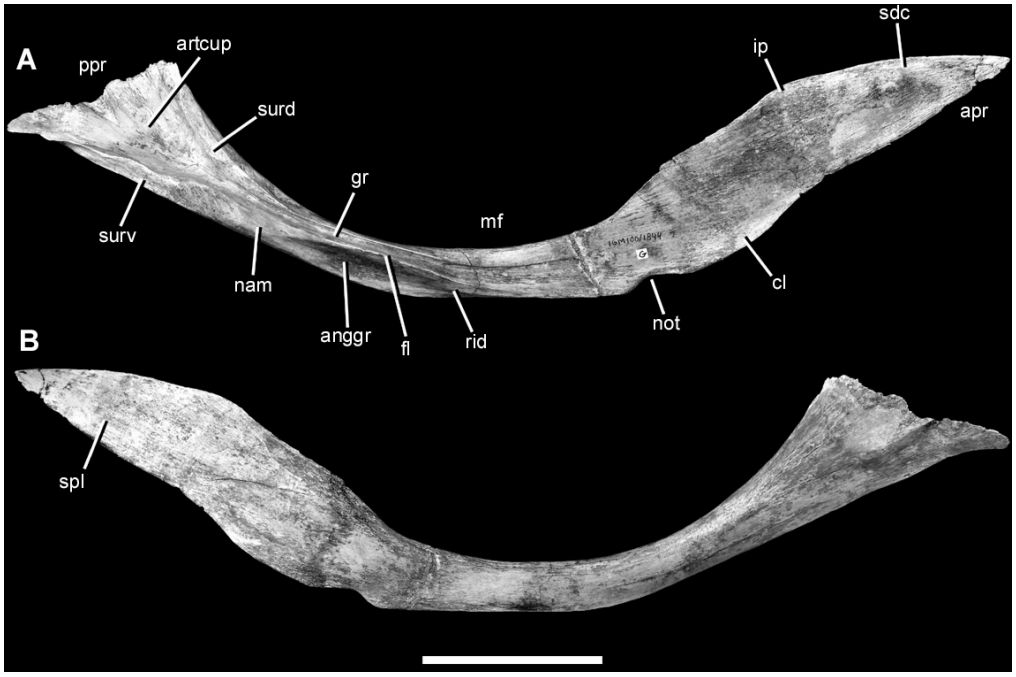

Figure 1-38. Right prearticular of the holotype specimen of *Alioramus altai* (IGM 100/1844) in lateral (A) and medial (B) views. Scale bar equals 5 cm. Abbreviations: anggr, groove for articulation with angular; apr, anterior process; artcup, concave cup for articulation with articulate; cl, convex lobe; fl, flange delimiting dorsal border of groove for angular; gr, groove continuing posteriorly from articular cup; ip, inflection point; mf, Meckelian fossa; nar, non-articular region; not, notch; ppr, posterior process; rid, ridge bisecting groove for angular; sdc, contact surface for supradentary/coronoid; spl, contact surface for splenial; surd, dorsally positioned contact region for surangular; surv, ventrally positioned contact region for surangular.

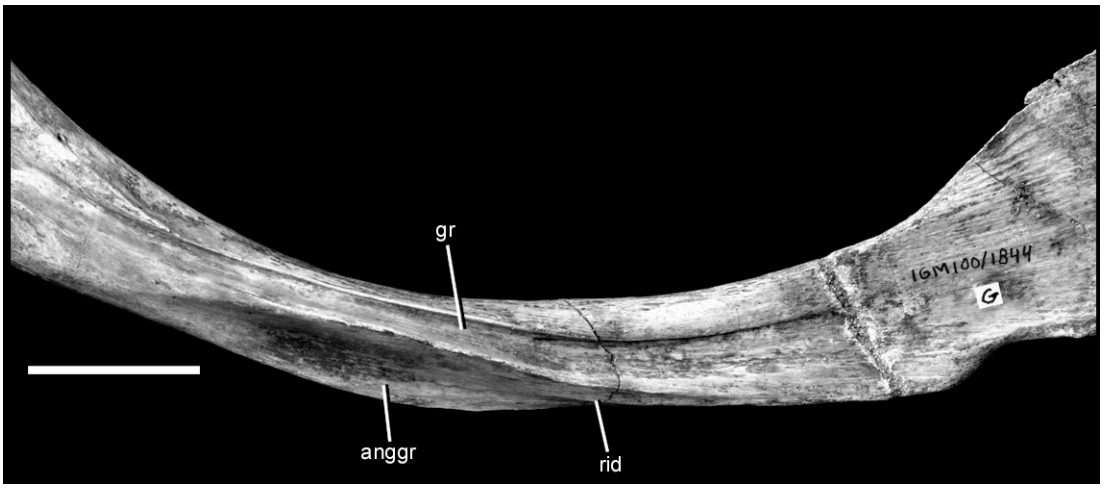

Figure 1-39. Closeup photo of the right prearticular of the holotype specimen of *Alioramus altai* (IGM 100/1844) in lateral view. Scale bar equals 2 cm. Abbreviations as in Figure 38.

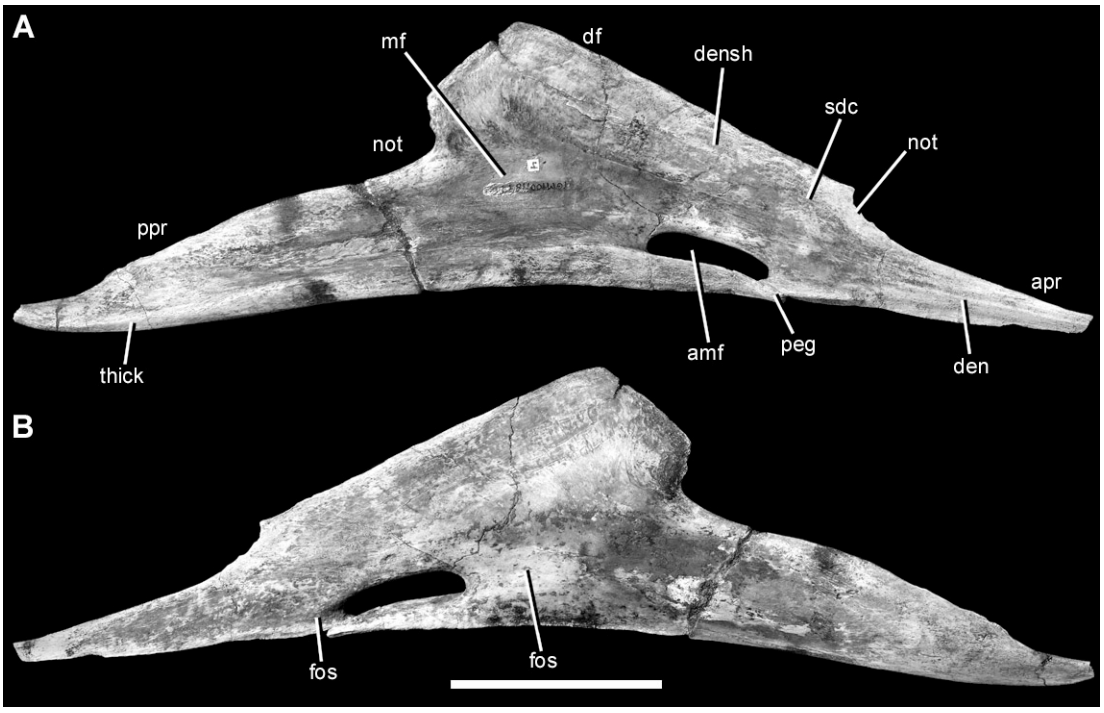

Figure 1-40. Right splenial of the holotype specimen of *Alioramus altai* (IGM 100/1844) in lateral (A) and medial (B) views. Scale bar equals 5 cm. Abbreviations: amf, anterior mylohyoid foramen; apr, anterior process; den, dentary articular contact; densh, articular contact for medial dentary shelf; df, dorsal flange; fos, fossa; mf, Meckelian fossa; not, notch; peg, peg to fit into socket on dentary; ppr, posterior process; thick, thickened region on ventral margin of lateral surface of posterior process (probably for ligamentous attachment).

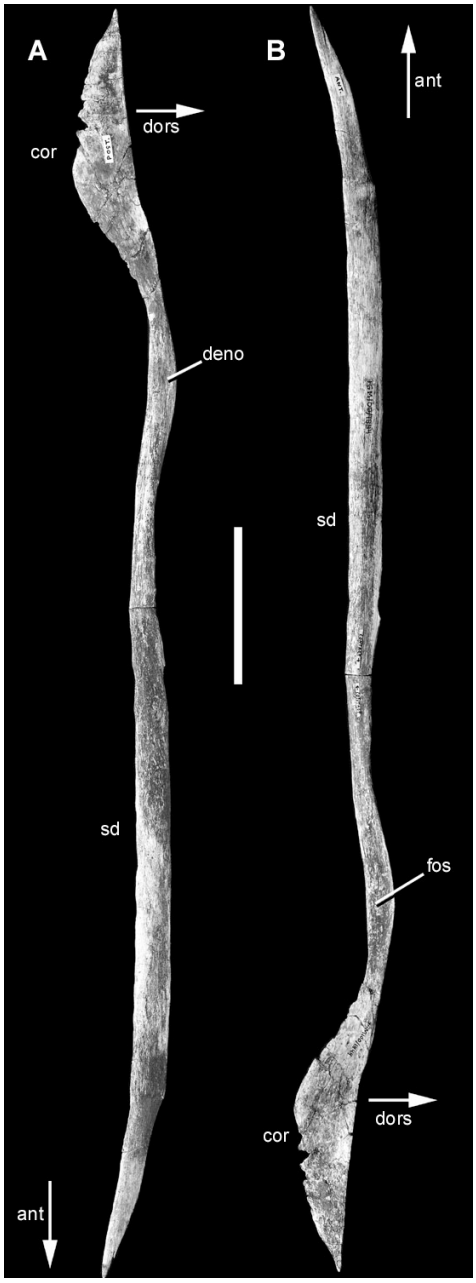

Figure 1-41. Right supradentary-coronoid of the holotype specimen of *Alioramus altai* (IGM 100/1844) in lateral (A) and medial (B) views. Arrows denote anterior and dorsal directions. Scale bar equals 5 cm. Abbreviations: cor, coronoid portion; deno, portion of bone that overlaps dentary medially; fos, fossa; sd, supradentary portion.

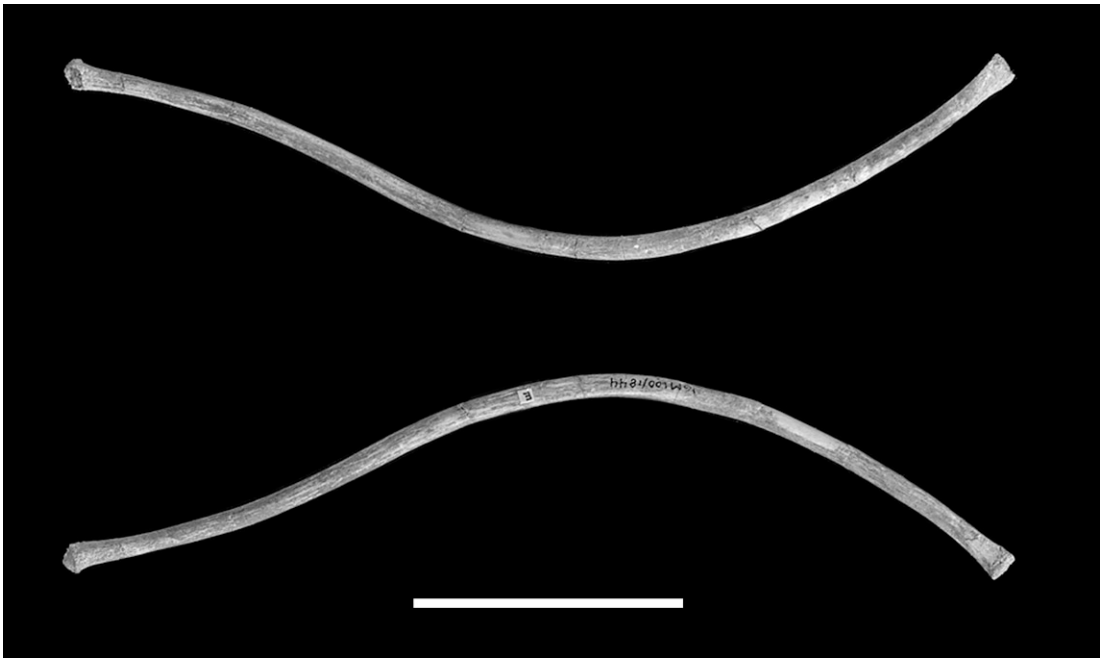

Figure 1-42. Hyoid of the holotype specimen of *Alioramus altai* (IGM 100/1844) in opposing views. Scale bar equals 5 cm.

Figure 1-43. Lateral (maxillary or dentary) teeth of the holotype specimen of *Alioramus altai* (IGM 100/1844) in (from left to right for each tooth) lingual, distal, labial, and mesial views. Scale bar equals 2 cm.

Figure 1-44. Lateral (maxillary or dentary) teeth of the holotype specimen of *Alioramus altai* (IGM 100/1844) in (from left to right for each tooth) lingual, distal, labial, and mesial views. Scale bar equals 2 cm.

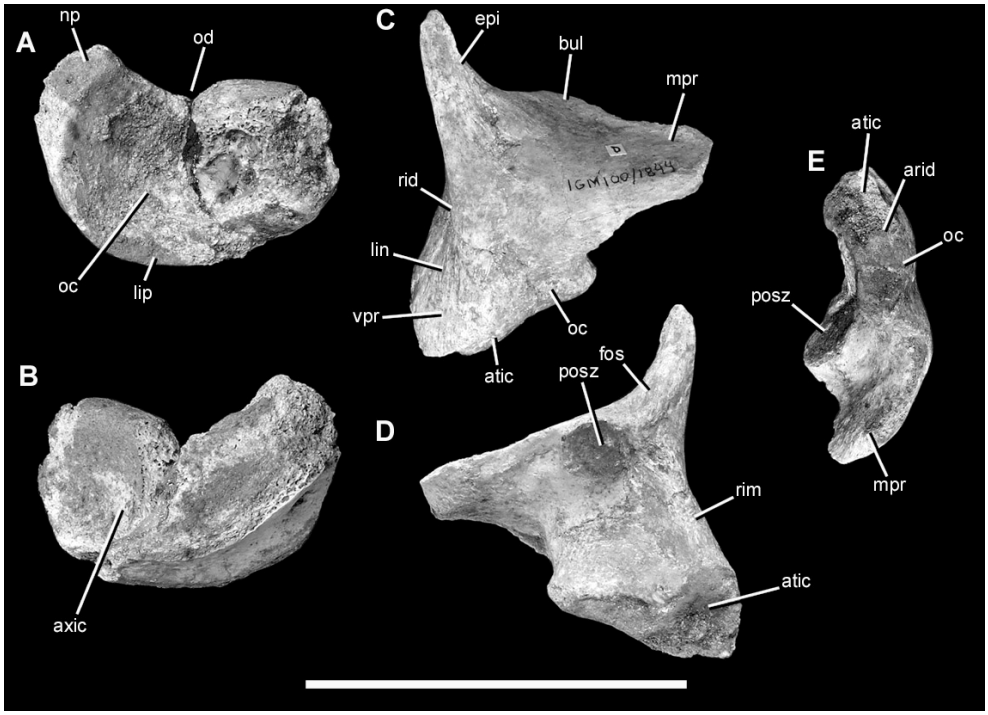

Figure 1-45. Atlas of the holotype specimen of *Alioramus altai* (IGM 100/1844). Atlantal intercentrum in anterior (A) and posterior (B) views; right neurapophysis in oblique anterolateral (C), oblique posteromedial (D), and ventral (E) views. Scale bar equals 5 cm. Abbreviations: arid, ridge between articular surfaces for occipital condlye and atlantal intercentrum on ventral surface of ventral process of neurapophysis; atic, articular surface for atlantal intercentrum; axic, articular surface for axial intercentrum; bul, bule on midline of dorsal web between epipophysis and medial process; epi, epipophysis; fos, fossa on posteromedial margin of dorsal surface of neurapophysis, between epipophysis and postzgygapophysis; lin, lineations on lateral surface of ventral process; lip, lip projecting anteriorly from atlantal intercentrum to underlie occipital condyle; mpr, medial process; np, pedicle for neurapophysis; oc, articular surface for occipital condyle; od, articular surface for odontoid; posz, postzygapophysis; rid, ridge on anterior surface of epipophysis; rim, rim on anterolateral edge of medial surface of neurapophysis; vpr, ventral process.

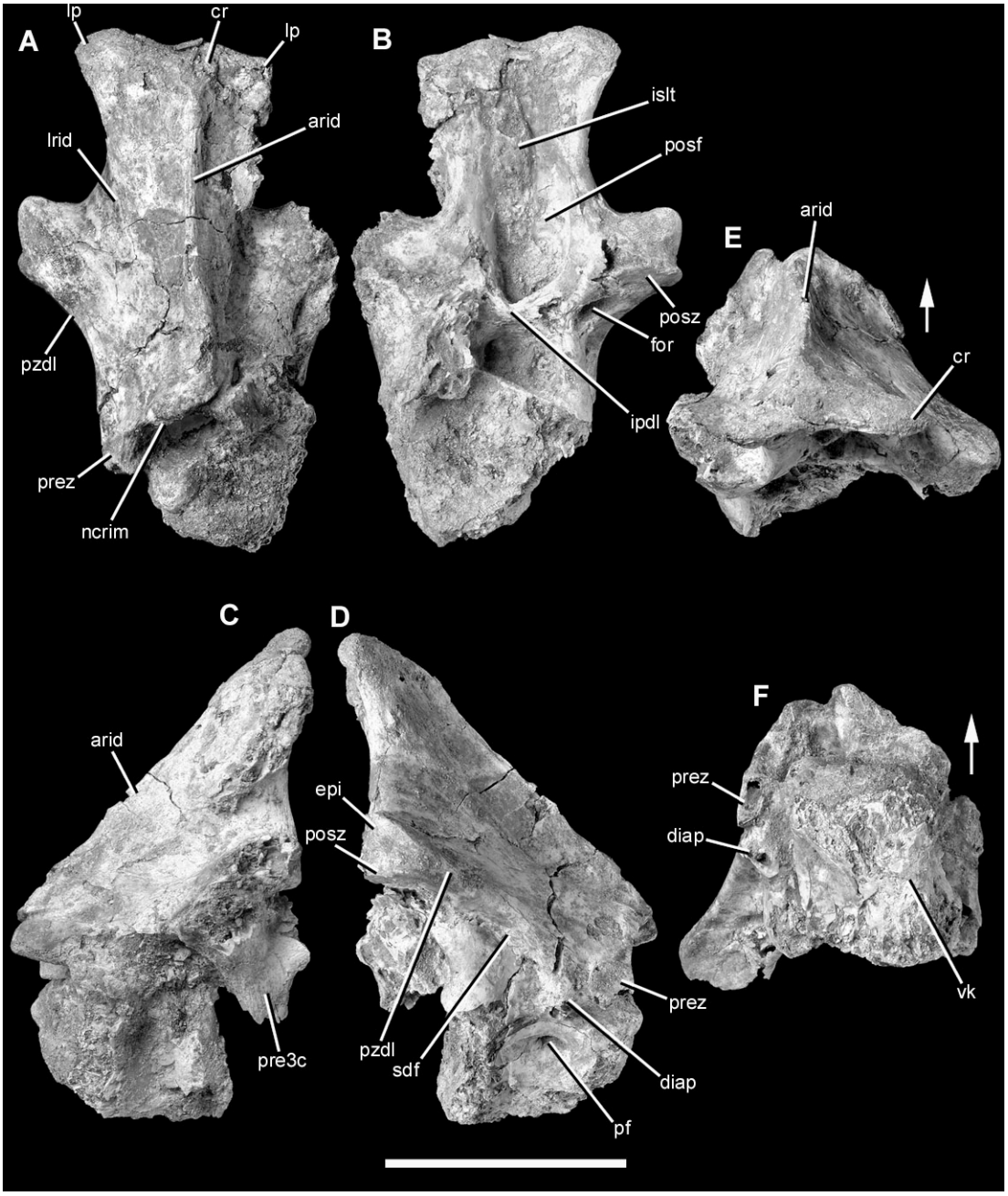

Figure 1-46. Axis of the holotype specimen of *Alioramus altai* (IGM 100/1844) in anterior (A), posterior (B), left lateral (C), right lateral (D), dorsal (E), and ventral (F) views. Arrows indicate anterior direction in E and F. Scale bar equals 5 cm. Abbreviations: arid, anterior ridge; cr, crown of neural spine; diap, diapophysis; epi, epipophysis; for, foramen; ipdl, intrapostzygapophyseal lamina; istl, interspinous ligament tuberosity; lp, lateral projection of crown; lrid, lateral ridge of

neural spine; pf, pneumatic foramen; posf, postspinal fossa; posz, postzygapophysis; pre3c, prezygapophysis of third cervical appressed to postzygapophysis of axis; prz, prezygapophysis; pzdl, postzygapodiapophyseal lamina; sdf, supradiapophyseal fossa; vk, ventral keel.

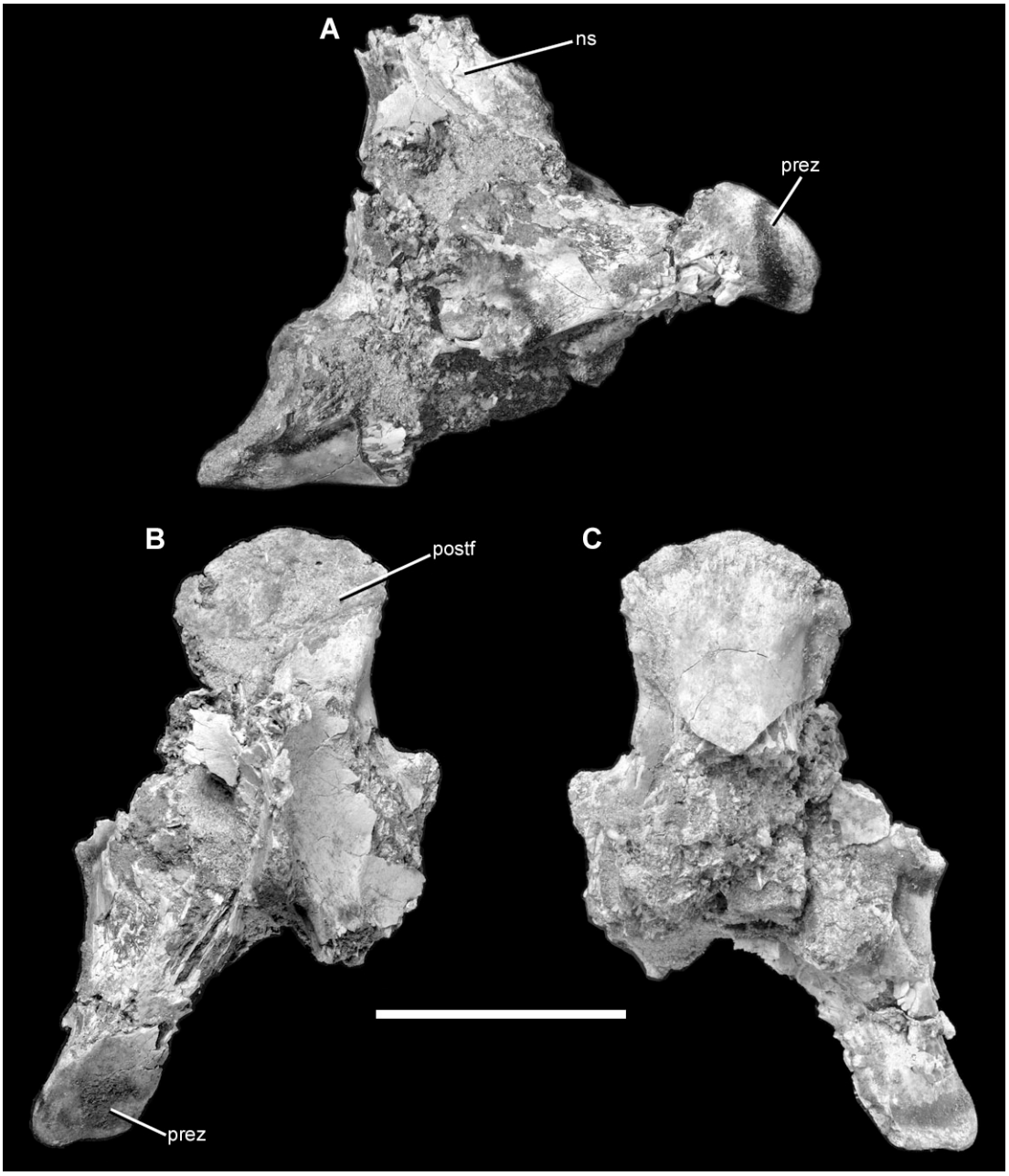

Figure 1-47. Cervical vertebra 3 of the holotype specimen of *Alioramus altai* (IGM 100/1844) in right lateral (A), dorsal (B), and ventral (C) views. Scale bar equals 5 cm. Abbreviations for this and all cervical vertebrae figures: accl, accessory lamina on anterior surface of transverse process; atvpfos, fossa on anterior surface of transverse process; diap, diapophysis; dmf,

dorsomedial fossa on anterior surface of transverse process; dorsfos, fossa on dorsal surface of web of bone between pre- and postzygapophyses; dtvpfos, fossa on dorsal surface of transverse process; epi, epipophysis; epl, epipophyseal-prezygapophyseal lamina; for, foramen within ventrolateral fossa on anterior surface of transverse process; hyp, hypapophysis; ipodl, infrapostzygapophyseal lamina; iprdl, infraprezygapophyseal lamina; keel, keel on ventral surface of centrum; ns, neural spine; para, parapophysis; pcdl, posterior centrodiapophyseal lamina; pcdlfd, fossa dorsal to posterior centrodiapophyseal lamina; pcdlfv, fossa ventral to posterior centrodiapophyseal lamina; pf, pneumatic foramen ("pleurocoel"); posdl, postzygapodiapophyseal lamina; posf, postspinal fossa; posz, postzygapophysis; postf, posterior centrum face; predl, prezygapodiapophyseal lamina; pref, prespinal fossa; prez, prezygapophysis; sposl, spinoprezygapophyseal lamina; sprel, spinoprezygapophyseal lamina; tvp, transverse process; vlf, ventrolateral fossa on anterior surface of transverse process.

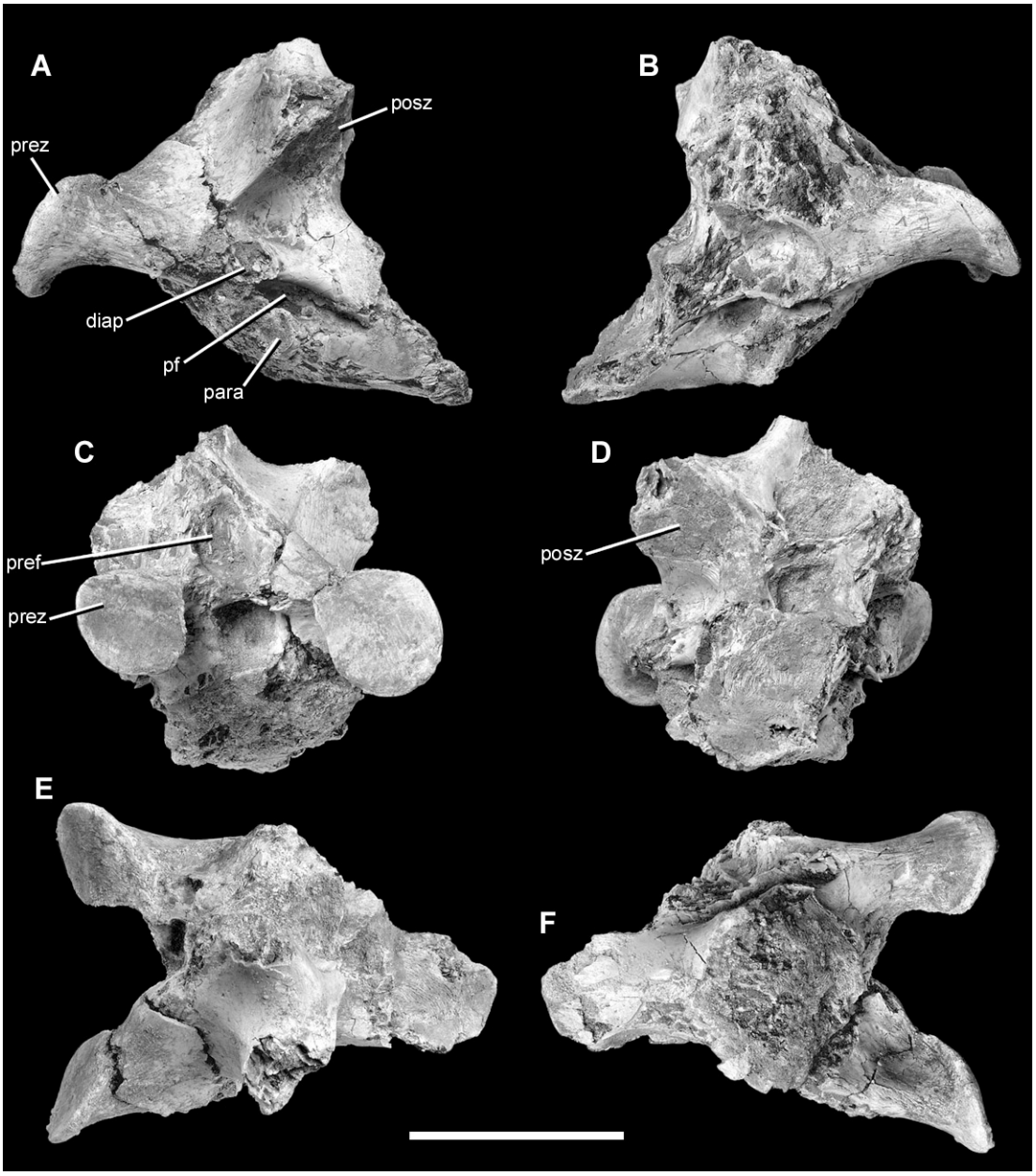

Figure 1-48. Cervical vertebra 4 of the holotype specimen of *Alioramus altai* (IGM 100/1844) in left lateral (A), right lateral (B), anterior (C), posterior (D), dorsal (E), and ventral (F) views. Scale bar equals 5 cm. Abbreviations as in Figure 47.

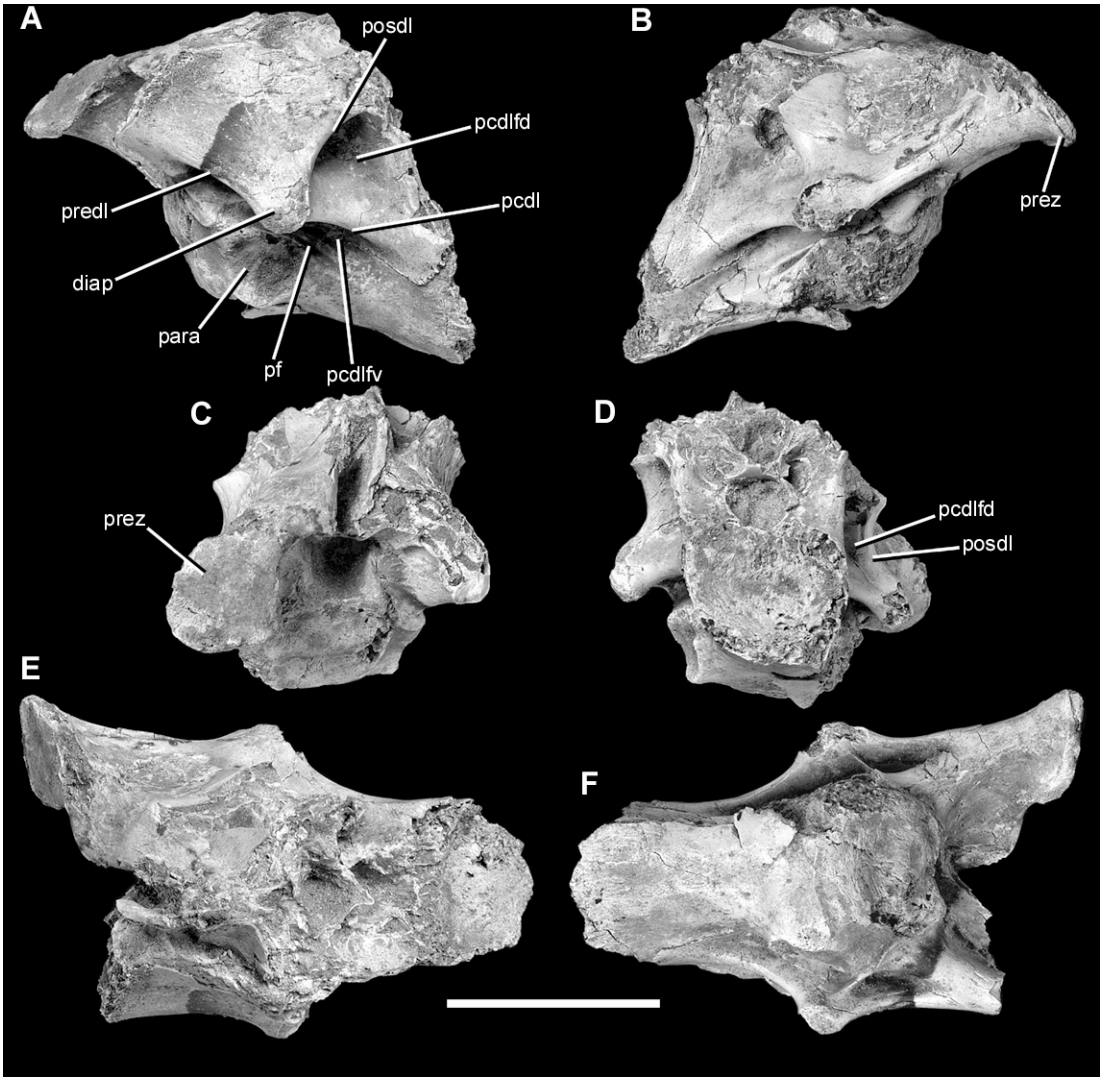

Figure 1-49. Cervical vertebra 5 of the holotype specimen of *Alioramus altai* (IGM 100/1844) in left lateral (A), right lateral (B), anterior (C), posterior (D), dorsal (E), and ventral (F) views. Scale bar equals 5 cm. Abbreviations as in Figure 47.

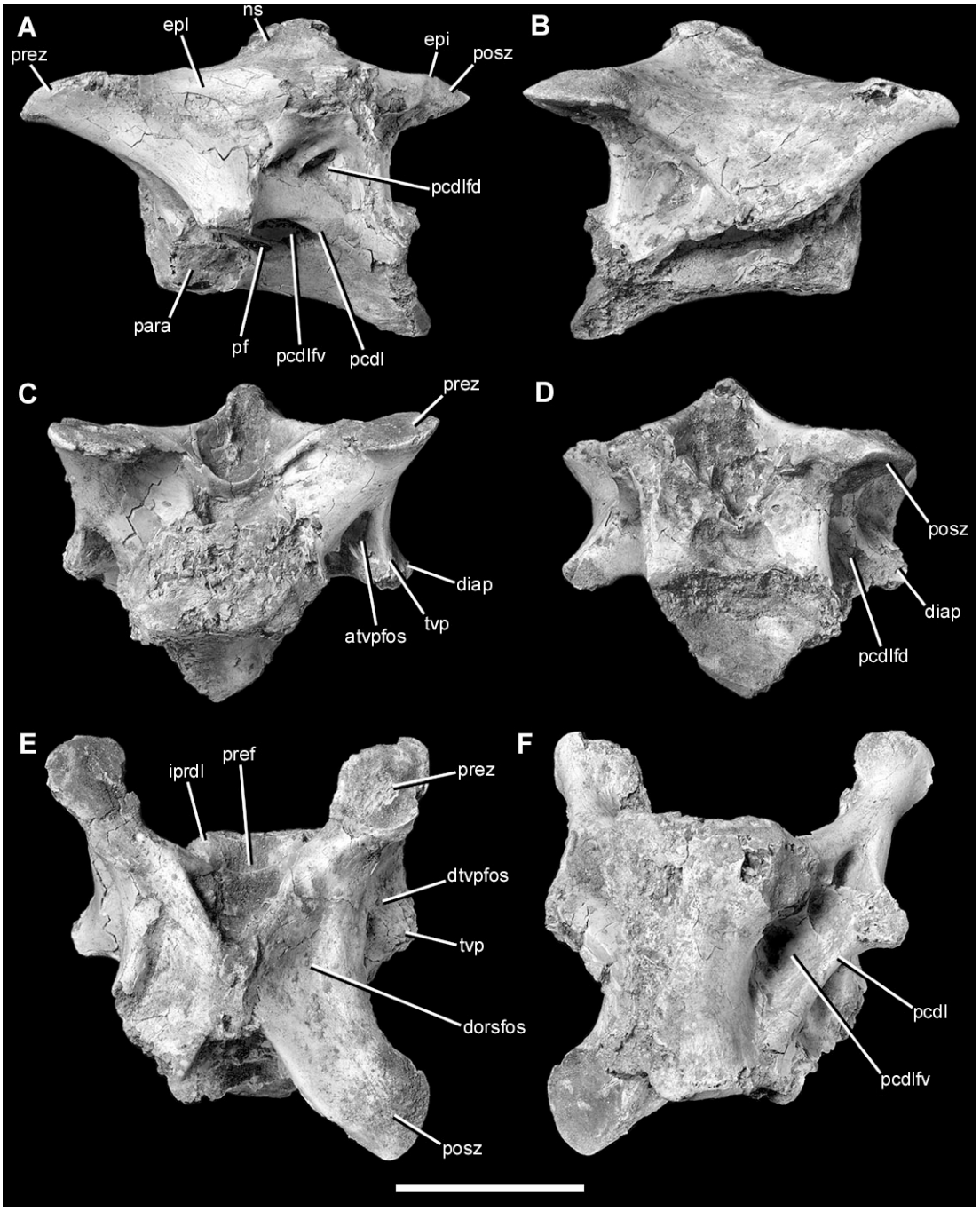

Figure 1-50. Cervical vertebra 6 of the holotype specimen of *Alioramus altai* (IGM 100/1844) in left lateral (A), right lateral (B), anterior (C), posterior (D), dorsal (E), and ventral (F) views. Scale bar equals 5 cm. Abbreviations as in Figure 47.

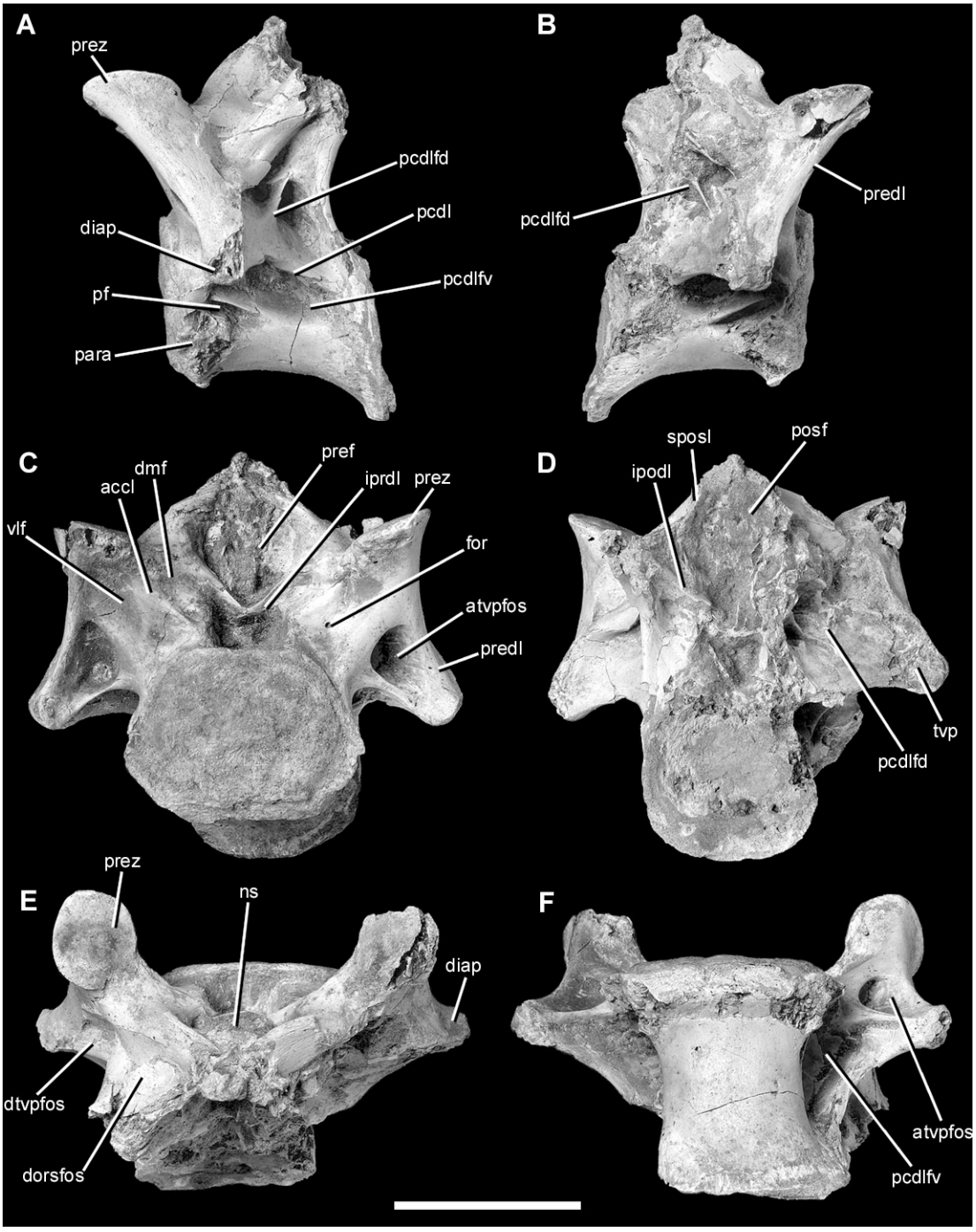

Figure 1-51. Cervical vertebra 7 of the holotype specimen of *Alioramus altai* (IGM 100/1844) in left lateral (A), right lateral (B), anterior (C), posterior (D), dorsal (E), and ventral (F) views. Scale bar equals 5 cm. Abbreviations as in Figure 47.

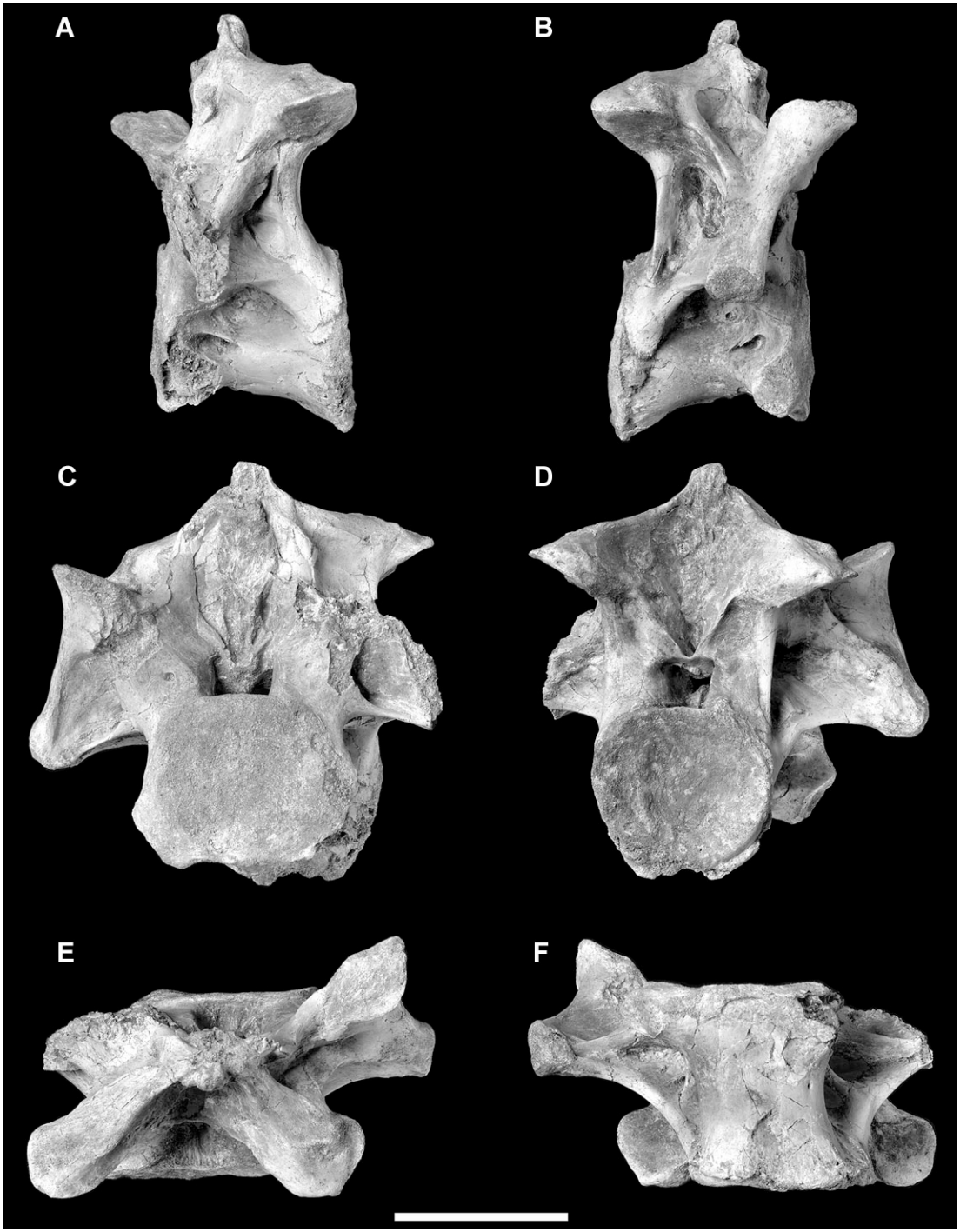

Figure 1-52. Cervical vertebra 8 of the holotype specimen of *Alioramus altai* (IGM 100/1844) in left lateral (A), right lateral (B), anterior (C), posterior (D), dorsal (E), and ventral (F) views. Scale bar equals 5 cm.

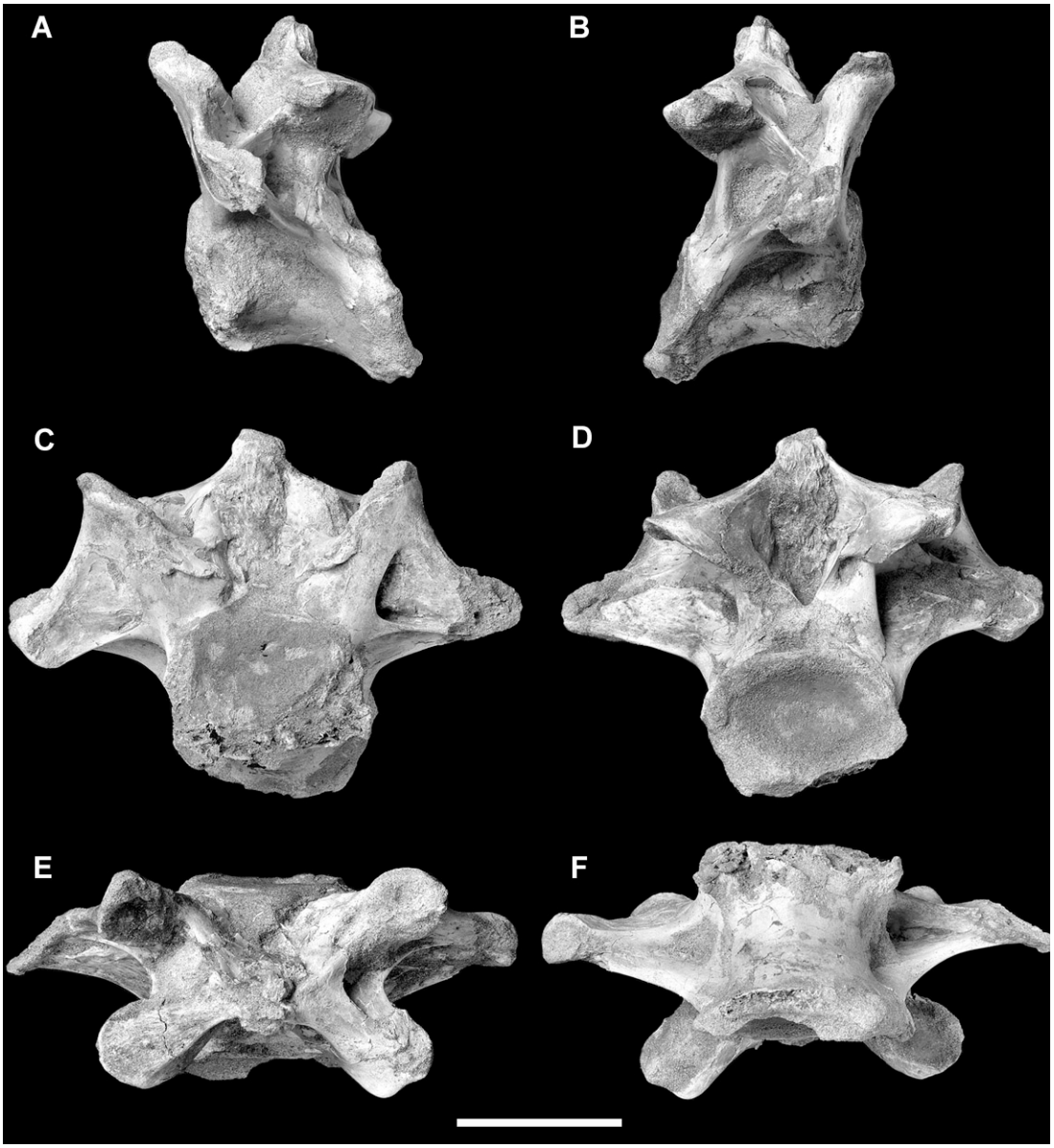

Figure 1-53. Cervical vertebra 9 of the holotype specimen of *Alioramus altai* (IGM 100/1844) in left lateral (A), right lateral (B), anterior (C), posterior (D), dorsal (E), and ventral (F) views. Scale bar equals 5 cm.

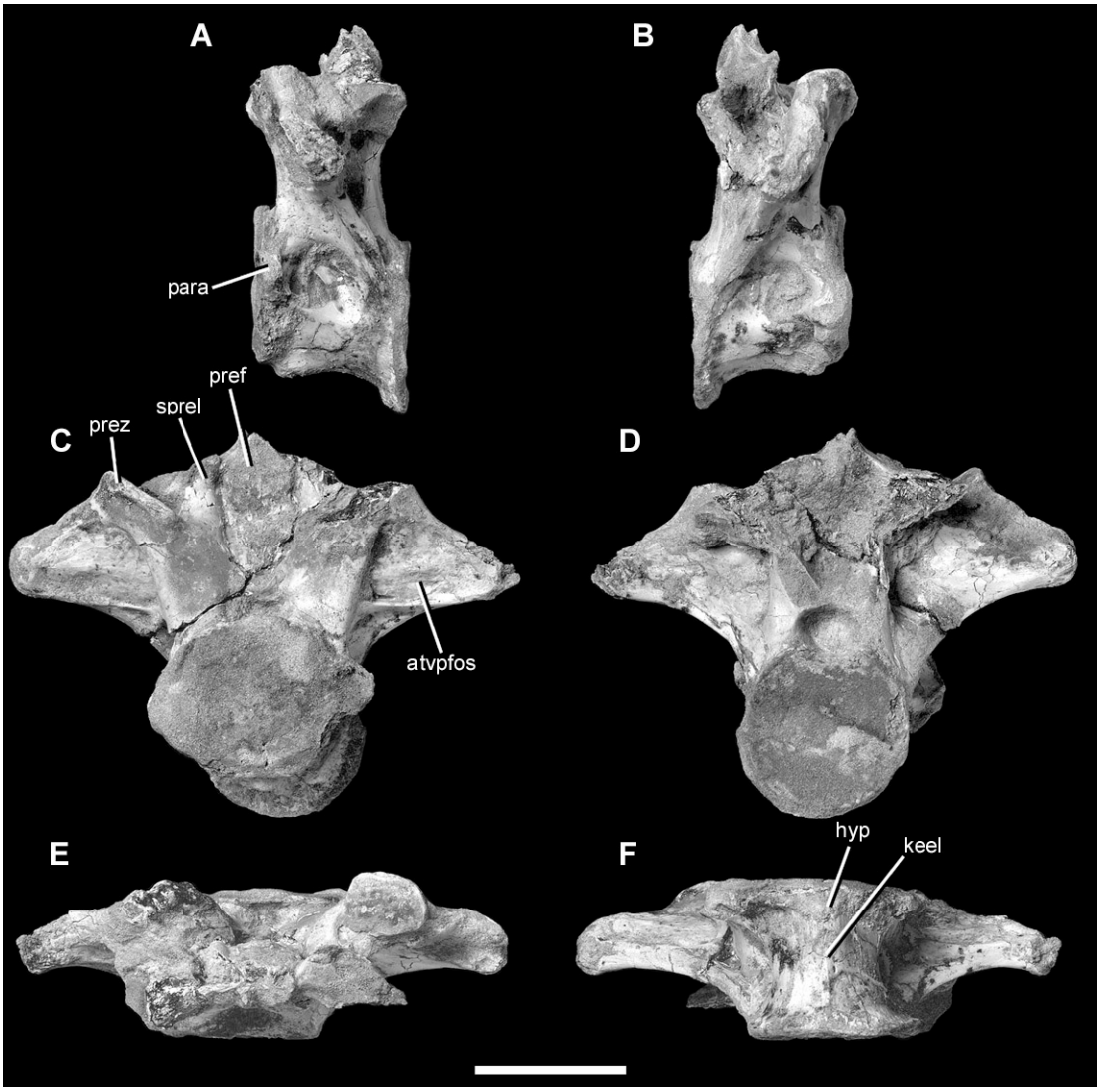

Figure 1-54. Cervical vertebra 10 of the holotype specimen of *Alioramus altai* (IGM 100/1844) in left lateral (A), right lateral (B), anterior (C), posterior (D), dorsal (E), and ventral (F) views. Scale bar equals 5 cm. Abbreviations as in Figure 47.

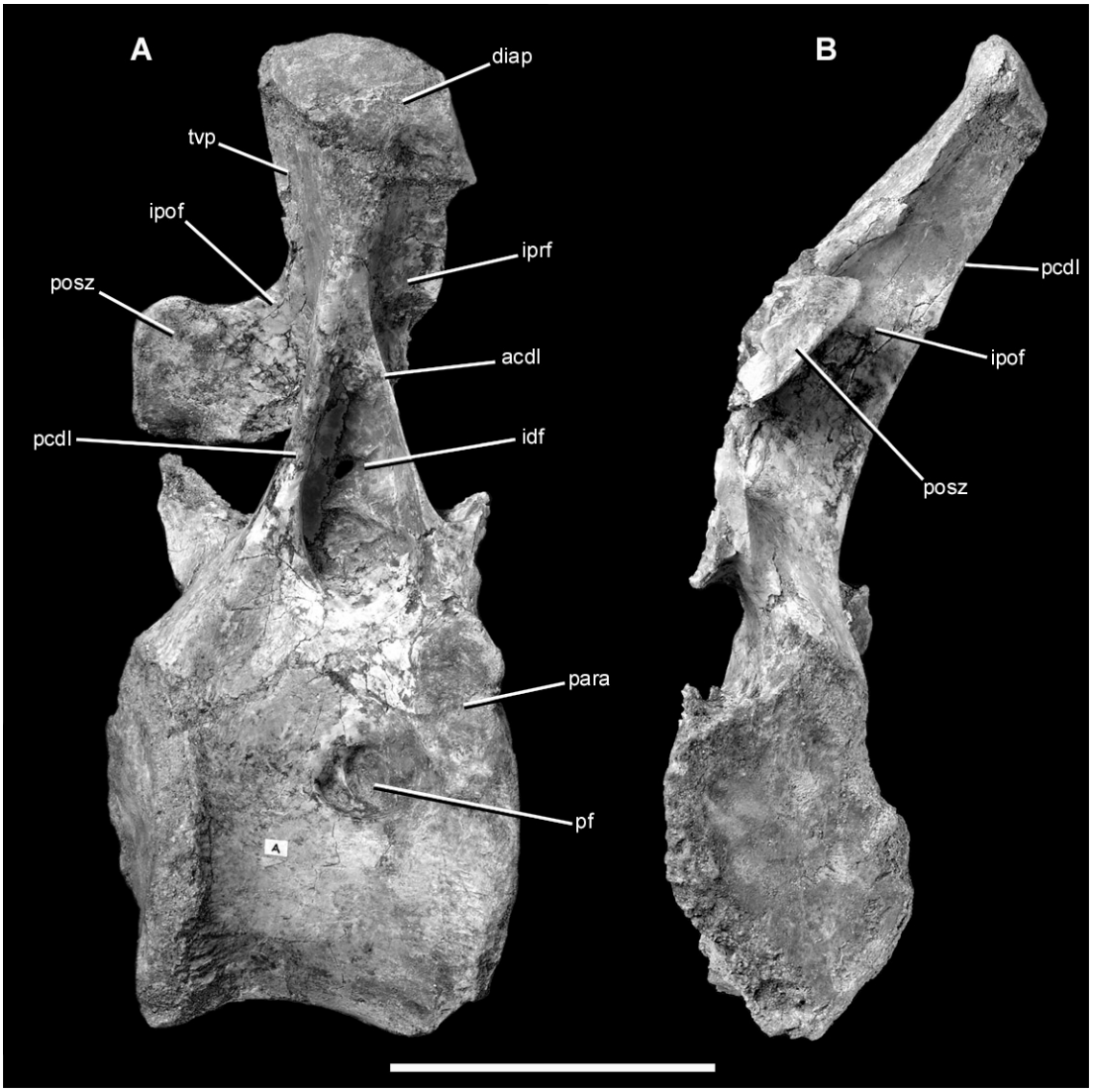

Figure 1-55. Dorsal vertebra A of the holotype specimen of *Alioramus altai* (IGM 100/1844) in right lateral (A) and posterior (B) views. Scale bar equals 5 cm. Abbreviations as in Figure 57.

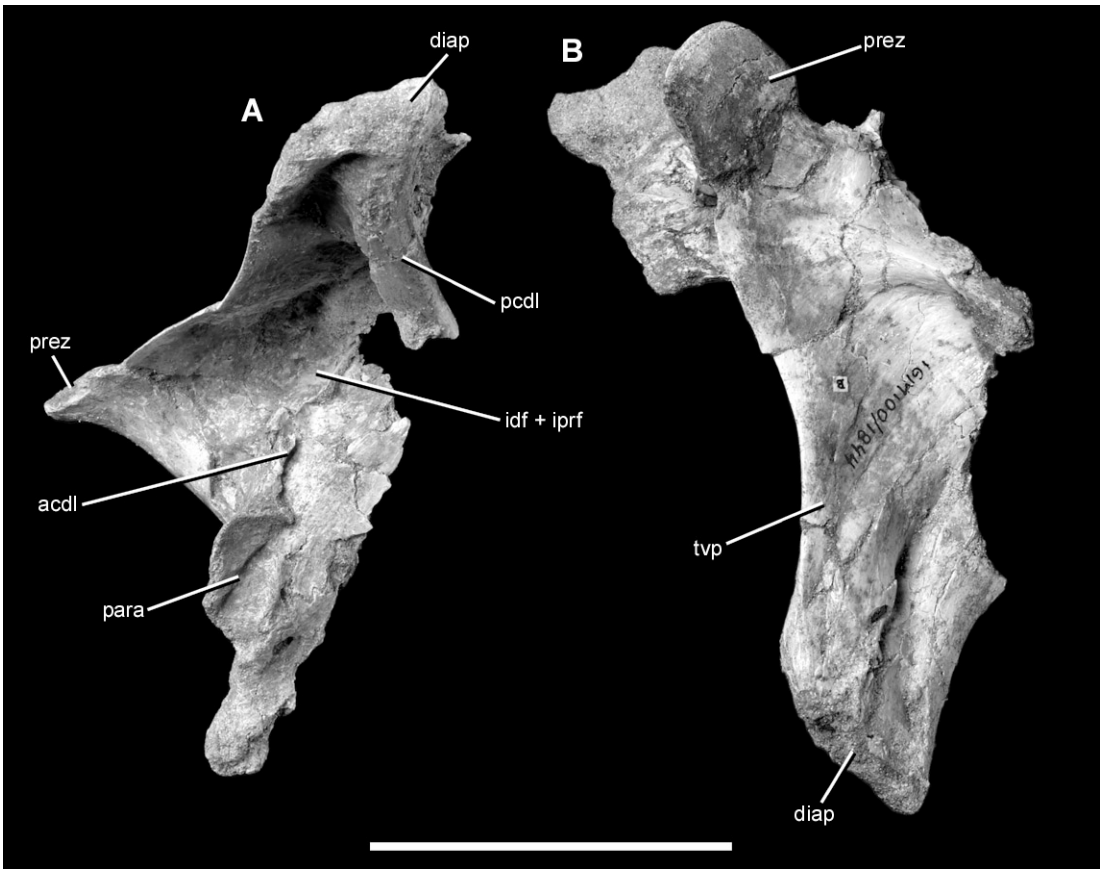

Figure 1-56. Dorsal vertebra B of the holotype specimen of *Alioramus altai* (IGM 100/1844) in left lateral (A) and dorsal (B) views. Scale bar equals 5 cm. Abbreviations as in Figure 57.

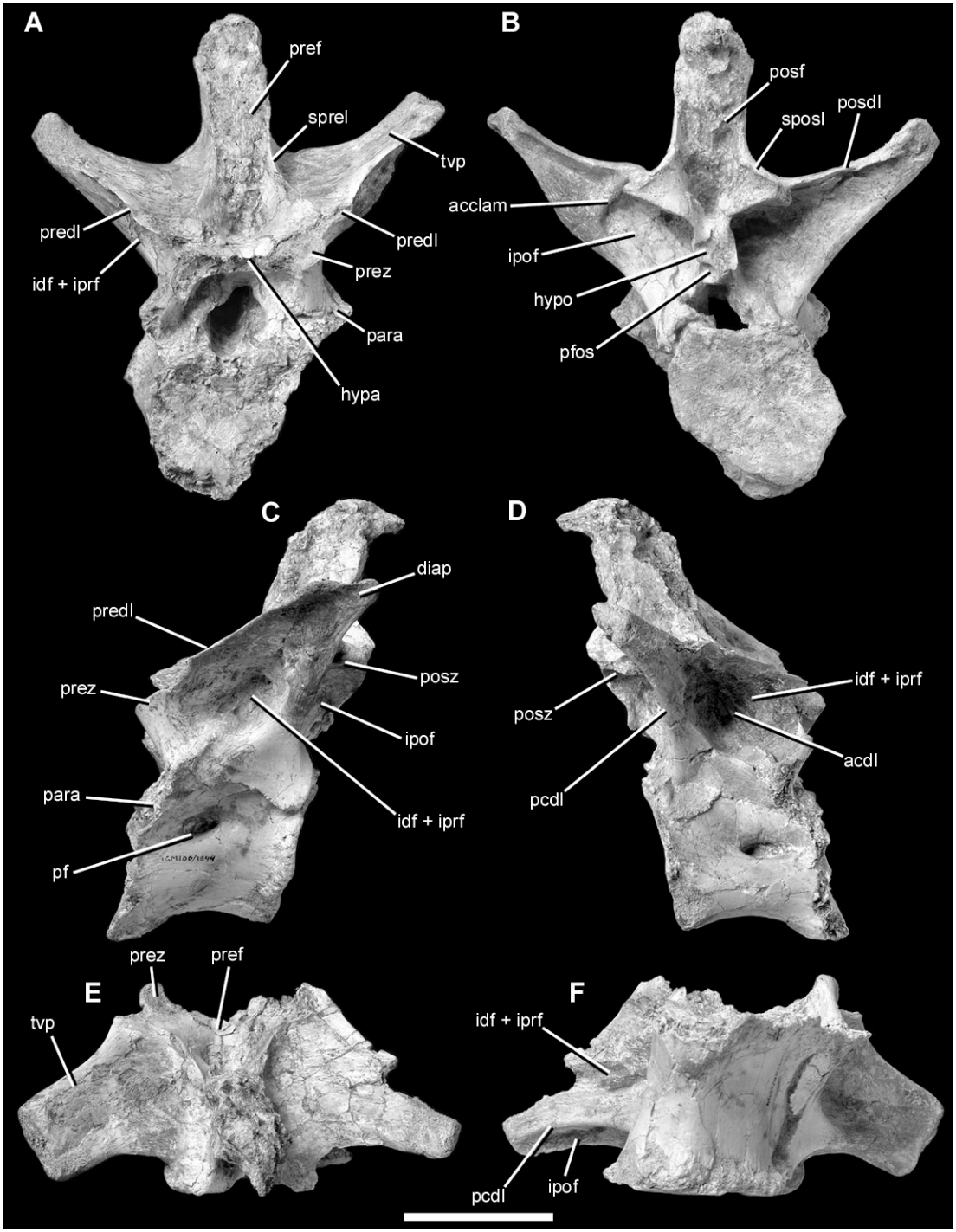

Figure 1-57. Dorsal vertebra C of the holotype specimen of *Alioramus altai* (IGM 100/1844) in anterior (A), posterior (B), left lateral (C), right lateral (D), dorsal (E), and ventral (F) views. Scale bar equals 5 cm. Abbreviations for this and other dorsal vertebrae figures: acclam, accessory lamina; acdl, anterior centrodiapophyseal lamina; diap, diapophysis; hypa, hypantrum;

ho, hyposphene; idf, infradiapophyseal fossa; ipof, infarpostzygapophyseal fossa; iprf, infraprezygapophyseal fossa; para, parapophysis; pcdl, posterior centrodiapophyseal lamina; pf, pneumatic foramen; pfos, pneumatic fossa; posdl, posyzygapodiapophyseal lamina; posf, postspinal fossa; posz, postzygapophysis; predl, prezygapodiapophyseal lamina; pref, prespinal fossa; prez, prezygapophysis; sposl, spinopostzygapophyseal lamina; sprel, spinoprezygapophyseal lamina; tvp, transverse process.

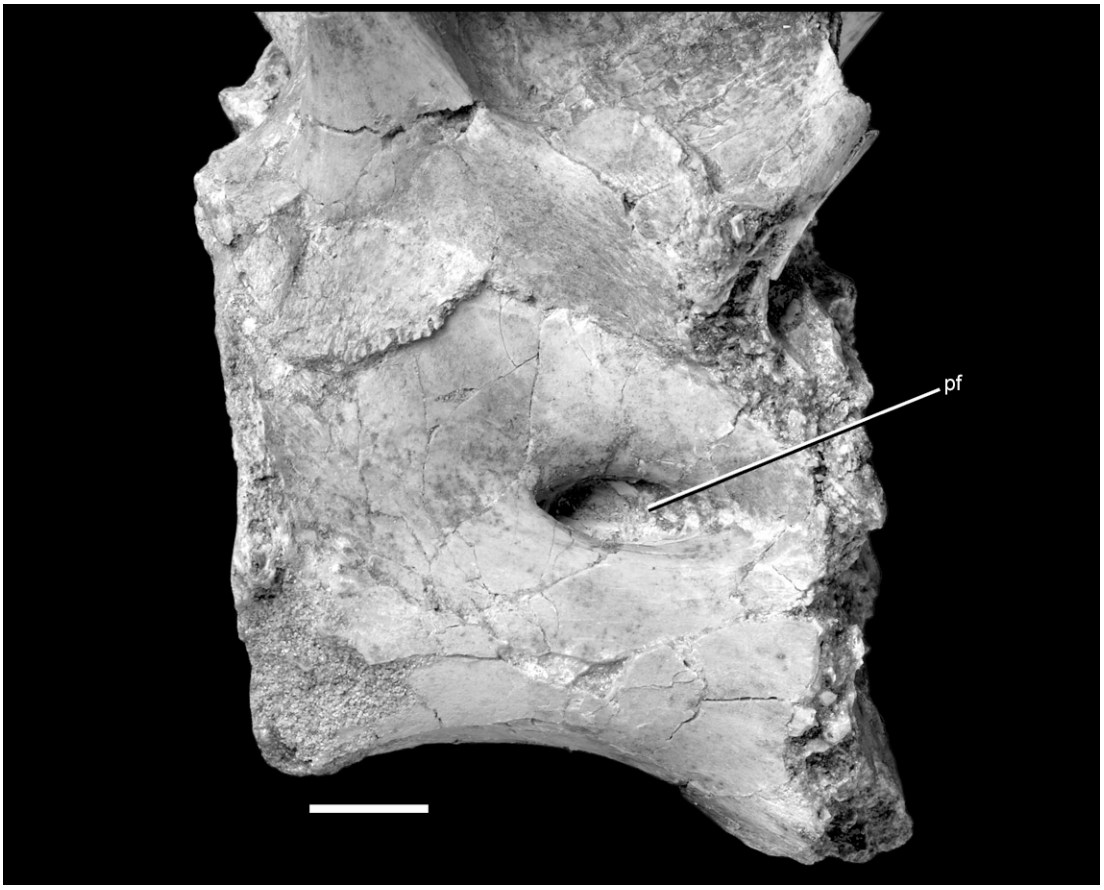

Figure 1-58. Closeup photo of dorsal vertebra C of the holotype specimen of *Alioramus altai* (IGM 100/1844) in right lateral view, showing the pneumatic foramen on the lateral surface of the centrum. Scale bar equals 1 cm. Abbreviations as in Figure 57.

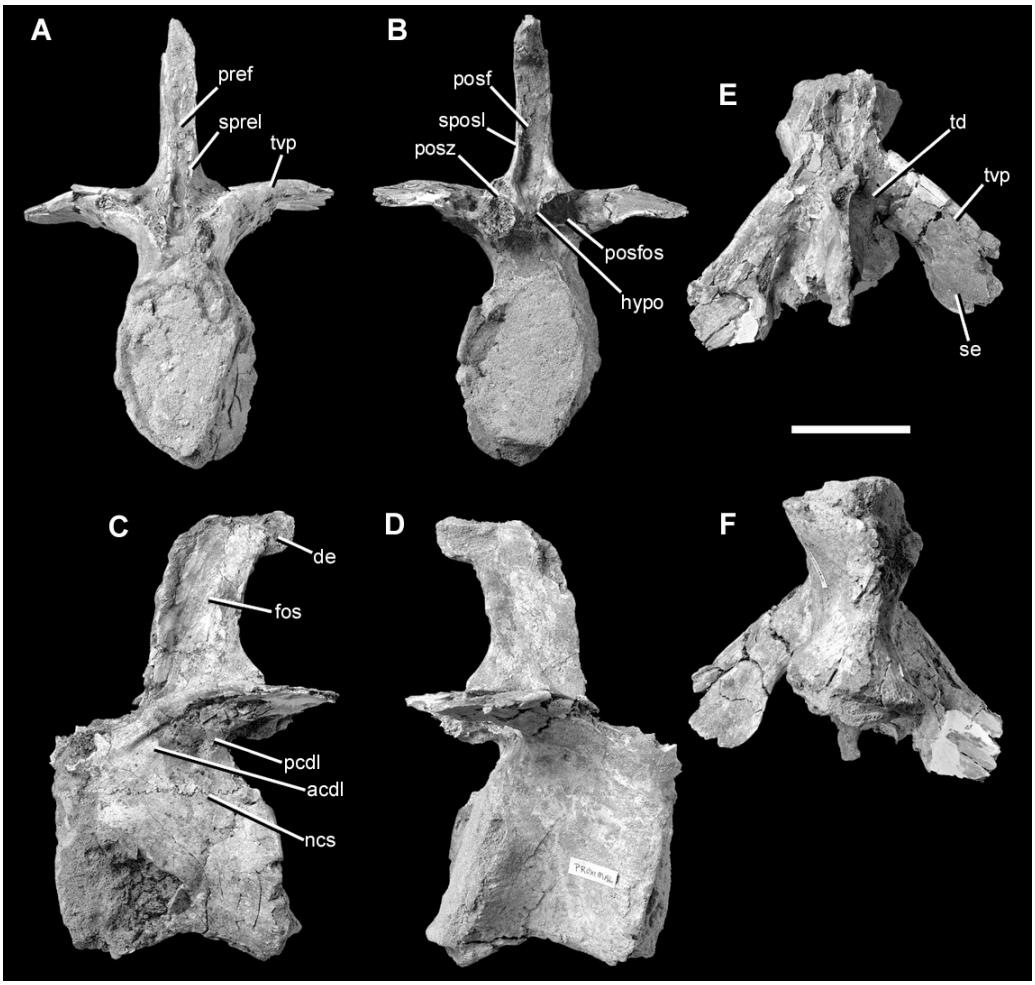

Figure 1-59. Caudal vertebra A of the holotype specimen of *Alioramus altai* (IGM 100/1844) in anterior (A), posterior B), left lateral (C), right lateral (D), dorsal (E), and ventral (F) views. Scale bar equals 5 cm. Abbreviations: acdl, anterior centrodiapophyseal lamina; de, dorsal expansion of neural spine; fos; fossa on lateral surface of neural spine; hypo, hyposphene; ncs, neurocentral suture; pcdl, posterior centrodiapophyseal lamina; posf, postspinal fossa; posfos, posteriorly-facing fossa ventral to postzygapophysis; pref, prespinal fossa; se, spatulate distal expansion of transverse process; spoel, spinopostzygapophyseal lamina; sprel, spinoprezygapophyseal lamina; td, triangular depression on dorsal surface of vertebra where neural spine and transverse processes meet; tvp, transverse process.

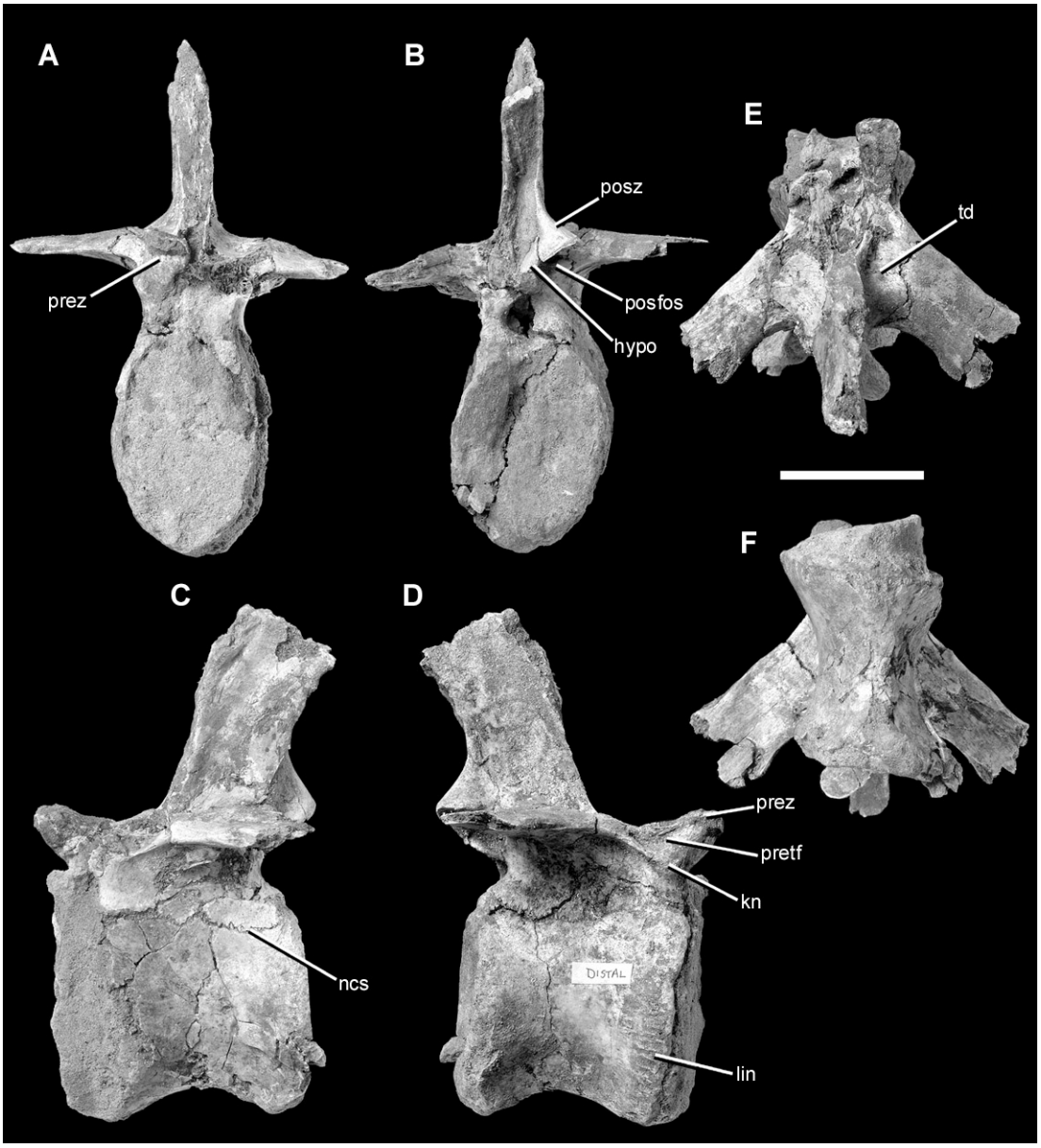

Figure 1-60. Caudal vertebra B of the holotype specimen of *Alioramus altai* (IGM 100/1844) in anterior (A), posterior (B), left lateral (C), right lateral (D), dorsal (E), and ventral (F) views. Scale bar equals 5 cm. Abbreviations as in Figure 59, plus: kn, knob anteroventral to triangular fossa on lateral surface of prezygapophysis; lin, lineations on surface of vertebra; pretf, triangular fossa on lateral surface of prezygapophysis; prez, prezygapophysis.

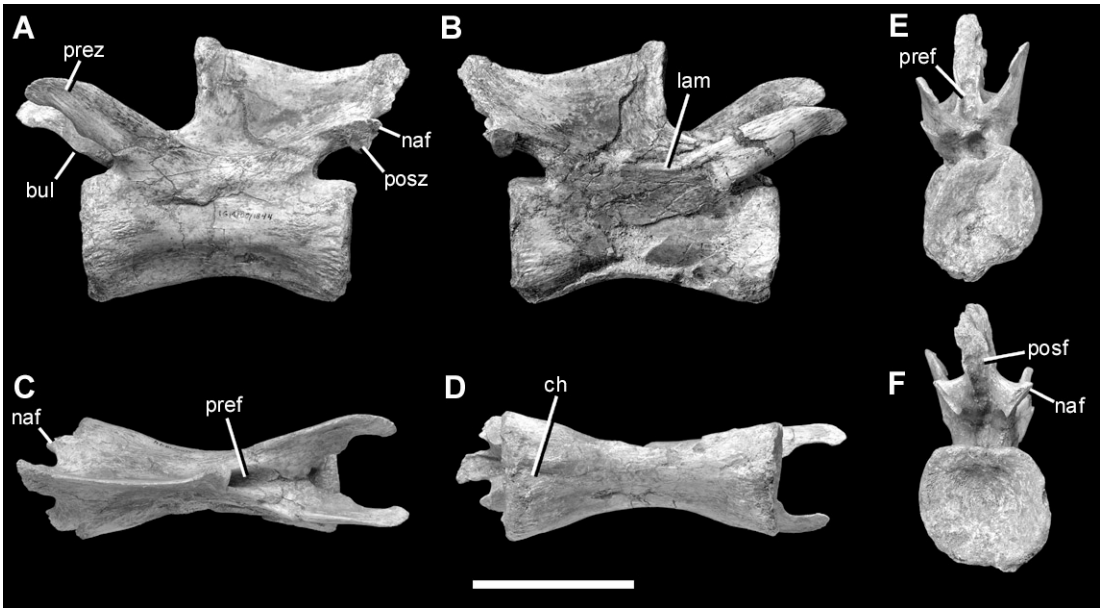

Figure 1-61. Caudal vertebra C of the holotype specimen of *Alioramus altai* (IGM 100/1844) in left lateral (A), right lateral B), dorsal (C), ventral (D), anterior (E), and posterior (F) views. Abbreviations: bul, ventral bulge on prezygapophysis; ch, chevron facet; lam, lamina linking pre- and postzygapophyses; naf, non-articular flange on postzygapophysis; posf, postspinal fossa; posz, postzygapophysis; pref, prespinal fossa; prez, prezygapophysis.

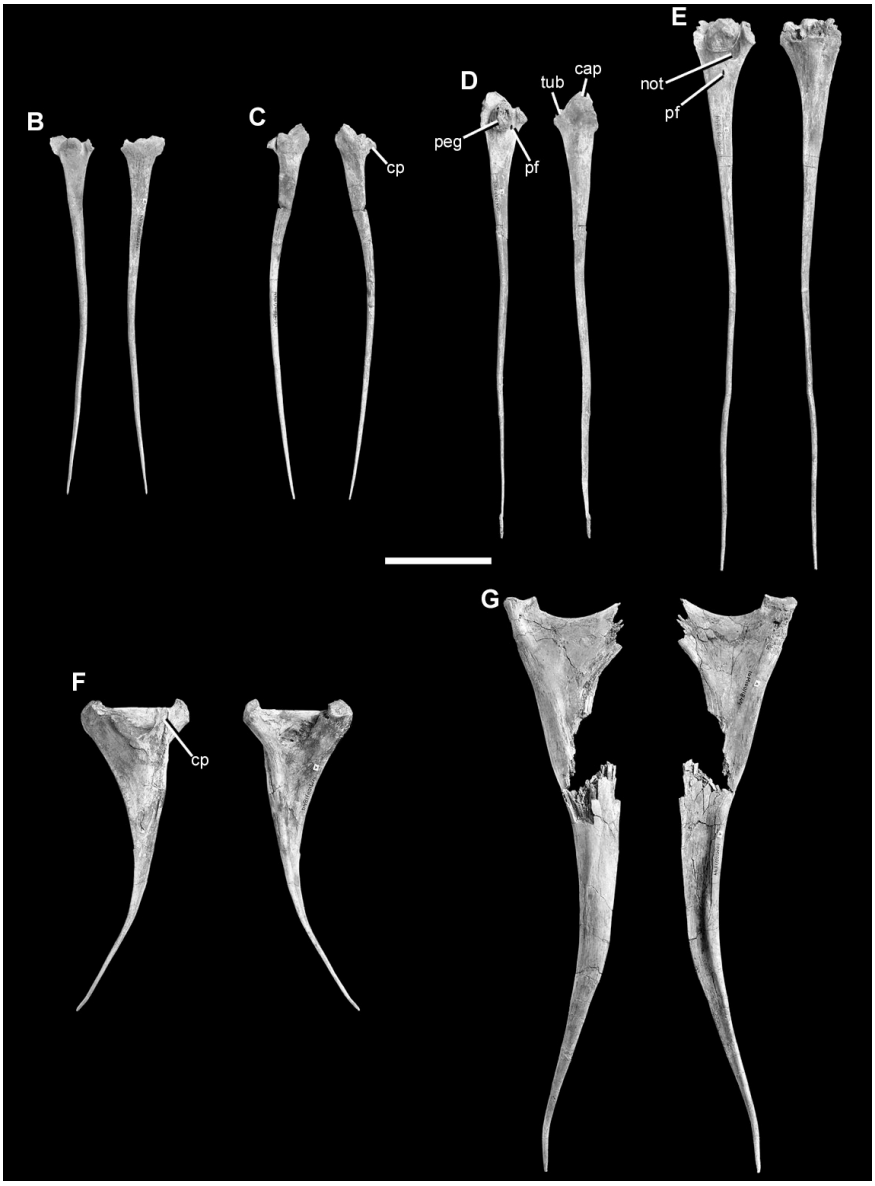

Figure 1-62. Cervical ribs of the holotype specimen of *Alioramus altai* (IGM 100/1844) in anterior and posterior views. Letters correspond to the ordered series of anterior-to-posterior ribs described in the text (lettering starts at B because the small, broken rib A is not figured). Scale bar equals 5 cm. Abbreviations: cap, capitulum; cp, cranial process; not, notch between capitulum and tuberculum; peg, peg on capitulum; pf, pneumatic foramen; tub, tuberculum.

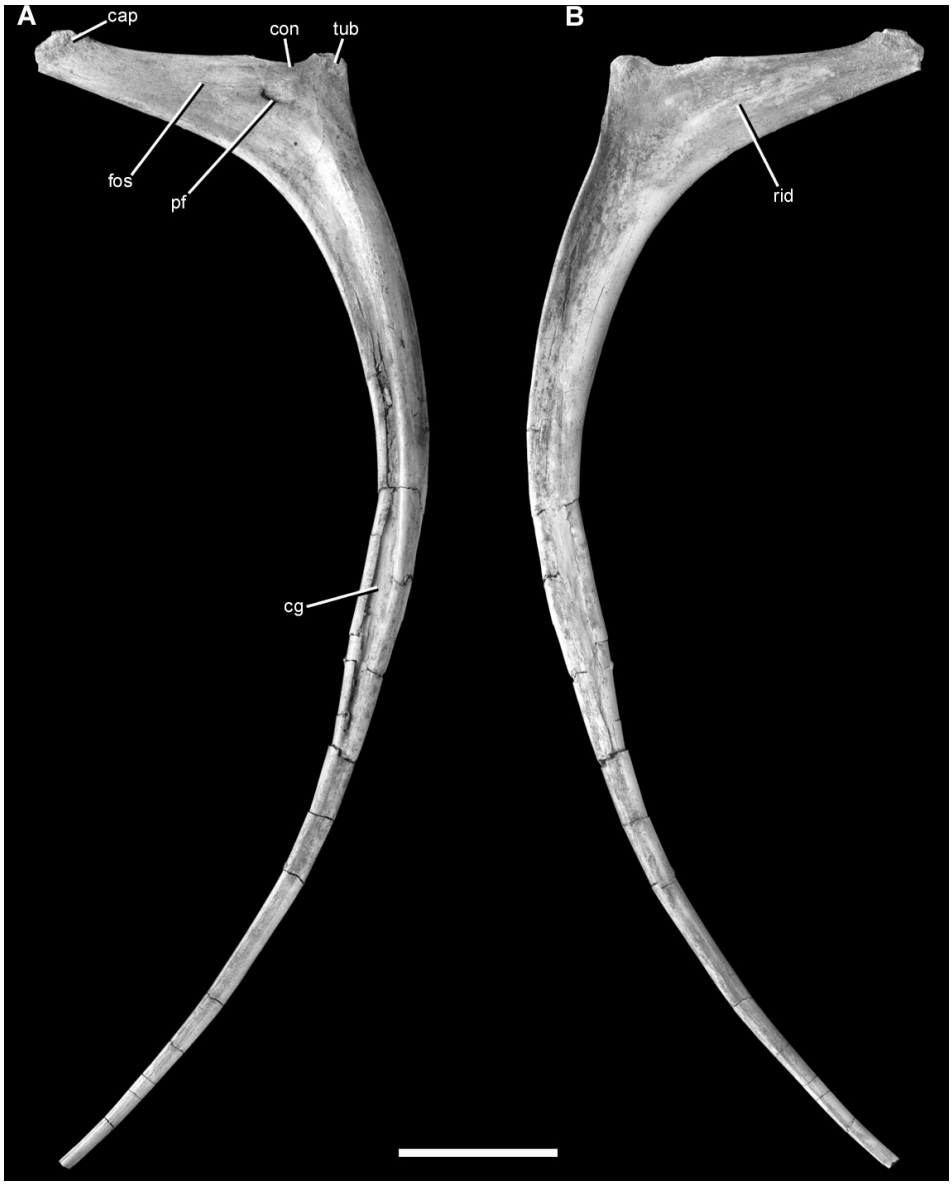

Figure 1-63. Left dorsal rib of the holotype specimen of *Alioramus altai* (IGM 100/1844) in lateral (A) and medial (B) views. Scale bar equals 5 cm. Abbreviations: cap, capitulum; cg, costal groove; conc, concavity on medial margin of neck between tuberculum and capitulum; fos, fossa confluent with pneumatic foramen; pf, pneumatic foramen; rid, ridge on medial surface of proximal region; tub, tuberculum.

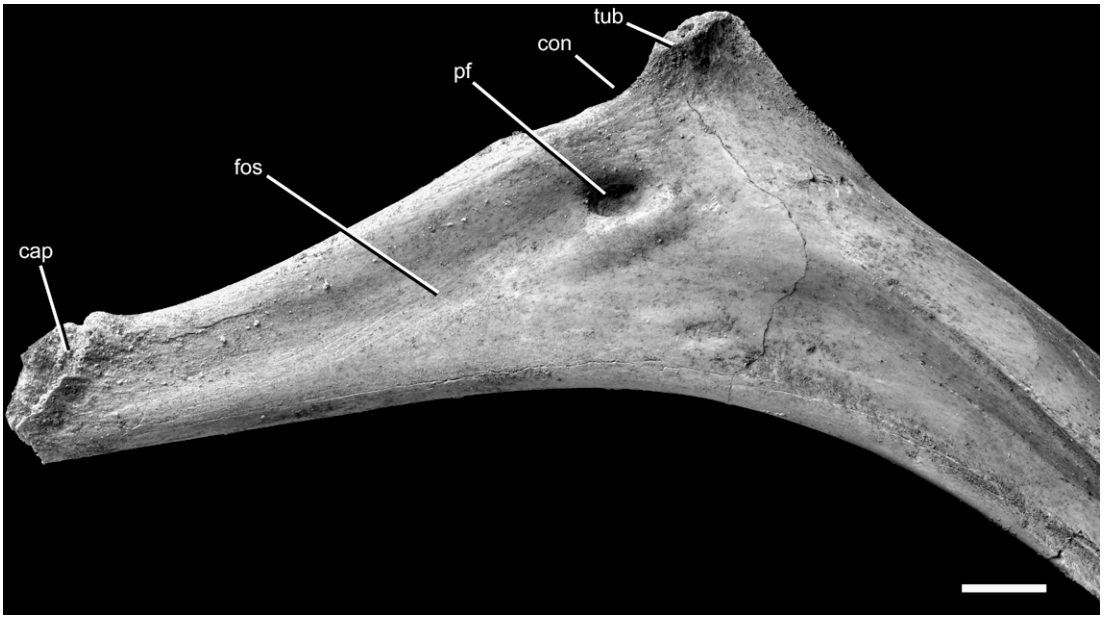

Figure 1-64. Closeup photo of left dorsal rib of the holotype specimen of *Alioramus altai* (IGM 100/1844) in lateral view. Scale bar equals 1 cm. Abbreviations as in Figure 63.

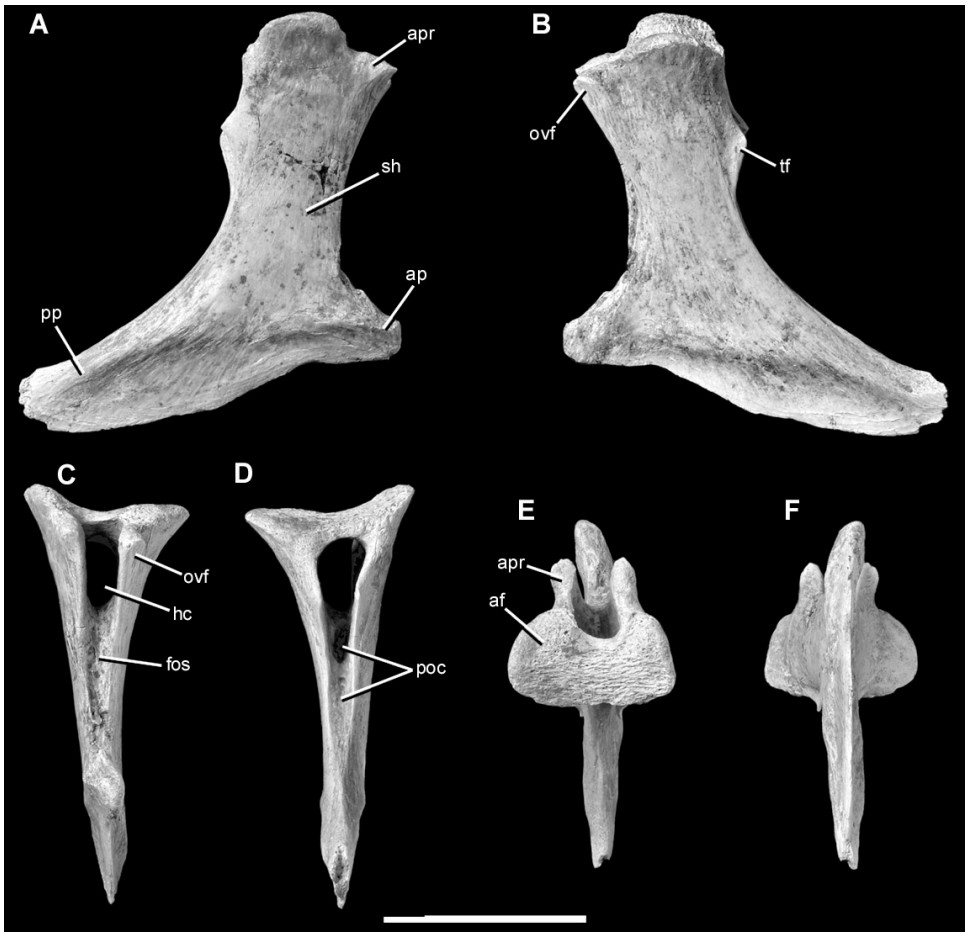

Figure 1-65. Chevron of the holotype specimen of *Alioramus altai* (IGM 100/1844) in right lateral (A), left lateral (B), anterior (C), posterior (D), dorsal (E), and ventral (F) views. Scale bar equals 3 cm. Abbreviations: af, articular facet; ap, anterior process; apr, anterior prong; fos, fossa beneath haemal canal; hc, haemal canal; ovf, ovoid facet on lateral surface of anterior prong; poc, pockets within fossa beneath haemal arch; pp, posterior process; sh, shaft; tf, triangular flange.

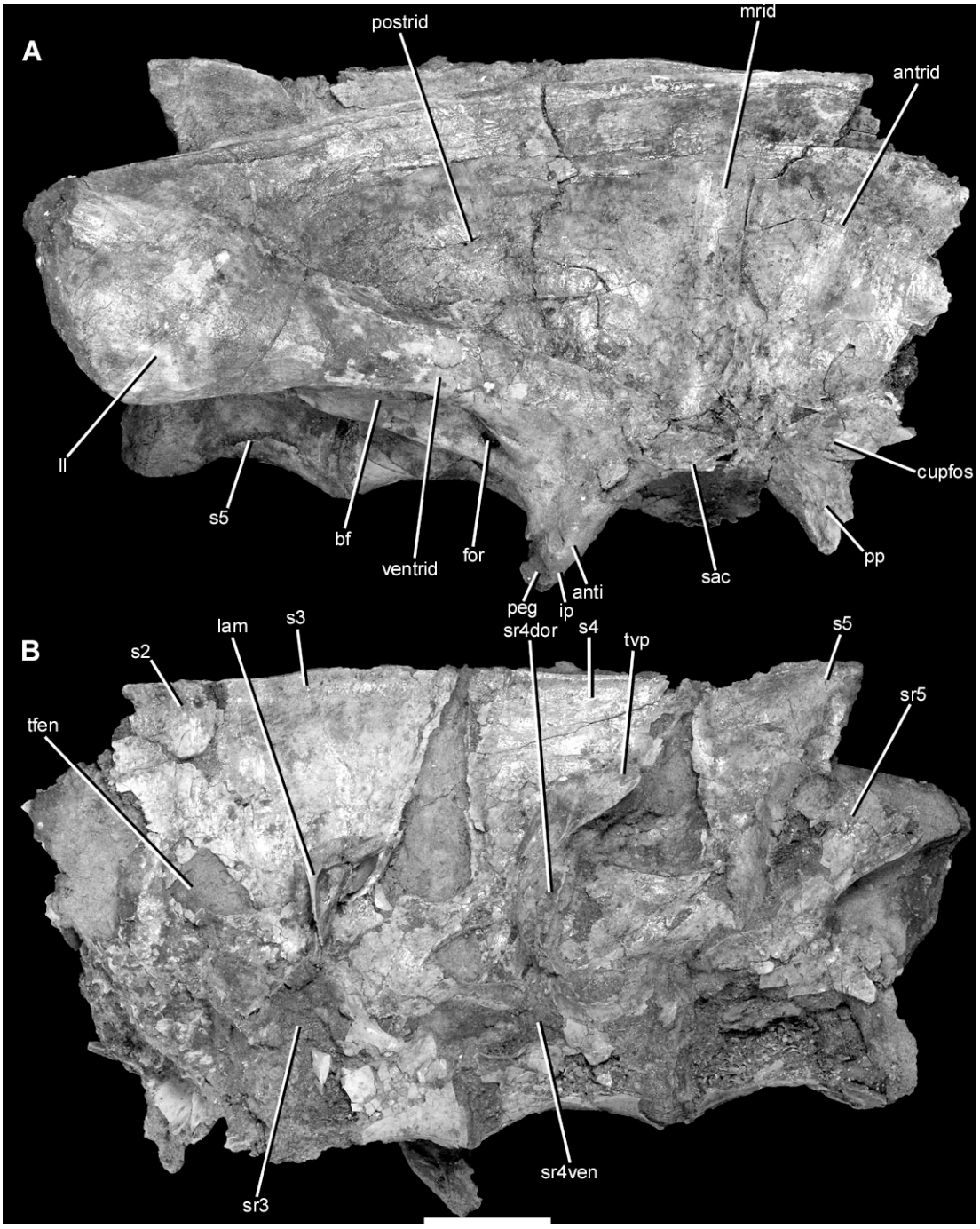

Figure 1-66. Right ilium of the holotype specimen of *Alioramus altai* (IGM 100/1844) in lateral (A) and medial (B) views, with B showing the left lateral surface of the sacrum. Scale bar equals 5 cm. Abbreviations: anti, antitrochanter; antridge, anterior ridge on lateral surface; bf, brevis fossa; cupfos, cuppedicus fossa; for, foramen; ip, ischial peduncle; lam, lamina linking sacral rib

and transverse process; ll, lateral lamina of postacetabular process concealing brevis fossa in lateral view; mrid, medial (primary) ridge on lateral surface; peg, ventral peg on ischial peduncle; postrid, posterior ridge on lateral surface; pp, pubic peduncle; s2-5, sacral vertebrae; sac, supracetabular crest; sr, sacral ribs (dor and ven refer to separate dorsal and ventral portions of sacral rib four); trifen, triangular fenestra; tvp, transverse process; ventrid, ventral ridge on lateral surface of ilium.

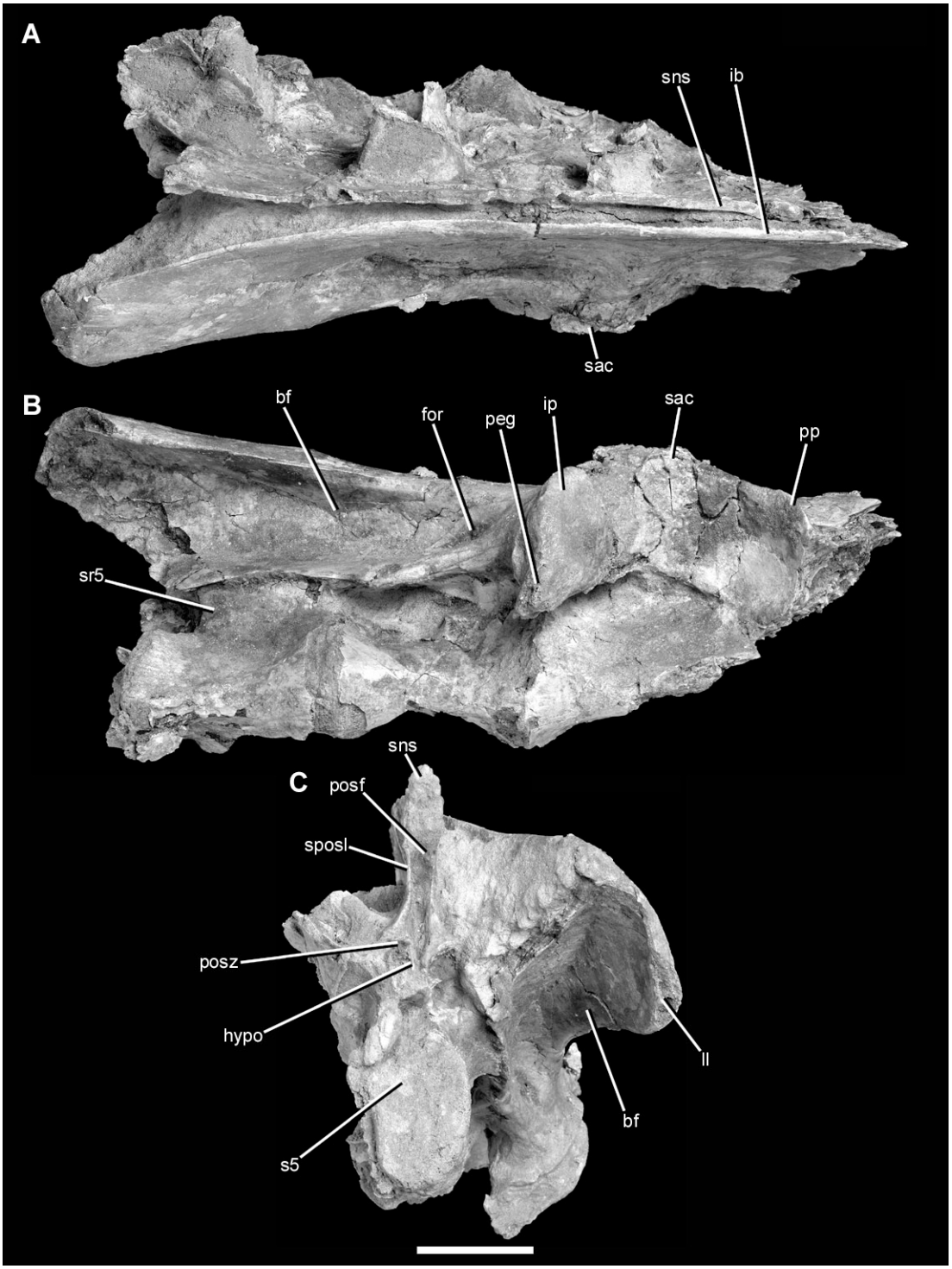

Figure 1-67. Right ilium and sacrum of the holotype specimen of *Alioramus altai* (IGM 100/1844) in dorsal (A), ventral (B), and posterior (C) views. Scale bar equals 5 cm. Abbreviations: bf, brevis fossa; for, foramen; hypo, hyposphene; ib, iliac blade; ip, ischial

peduncle; ll, lateral lamina of postacetabular process; peg, ventral peg on ischial peduncle; posf, postspinal fossa; posz, postzygapophysis; pp, pubic peduncle; s5, fifth sacral vertebra; sac, supracetabular crest; sns, sacral neural spine; sposl, spinopostzygapophyseal lamina; sr5, fifth sacral rib.

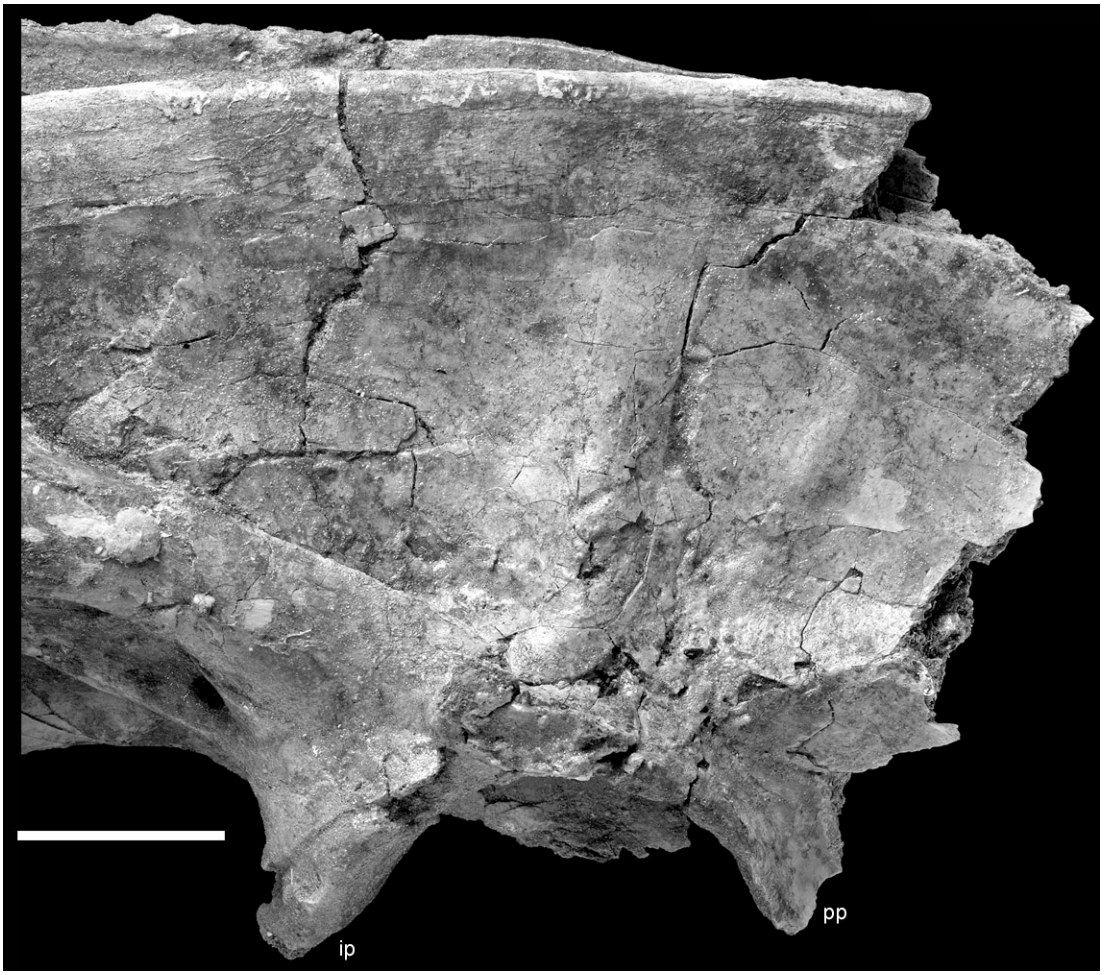

Figure 1-68: Closeup of right ilium of the holotype specimen of *Alioramus altai* (IGM 100/1844) in lateral view. Scale bar equals 5 cm. Abbreviations as in Figure 66.

Figure 1-69. Right ischium of the holotype specimen of *Alioramus altai* (IGM 100/1844) in lateral (A), medial (B), anterior (C), posterior (D), and proximal (E) views. Scale bar equals 5 cm. Abbreviations: acet, acetabulum; anti, antitrochanter; fos, fossa; ip, iliac peduncle; it, ischial tuberosity; lam, lamina; ma, medial apron; obt, obturator process; on, obturator notch; pp, pubic peduncle; rid, ridge.

Figure 1-70. Closeup photo of right ischium of the holotype specimen of *Alioramus altai* (IGM 100/1844) in lateral view. Scale bar equals 5 cm. Refer to labels in Figure 69 for specific anatomical structures.

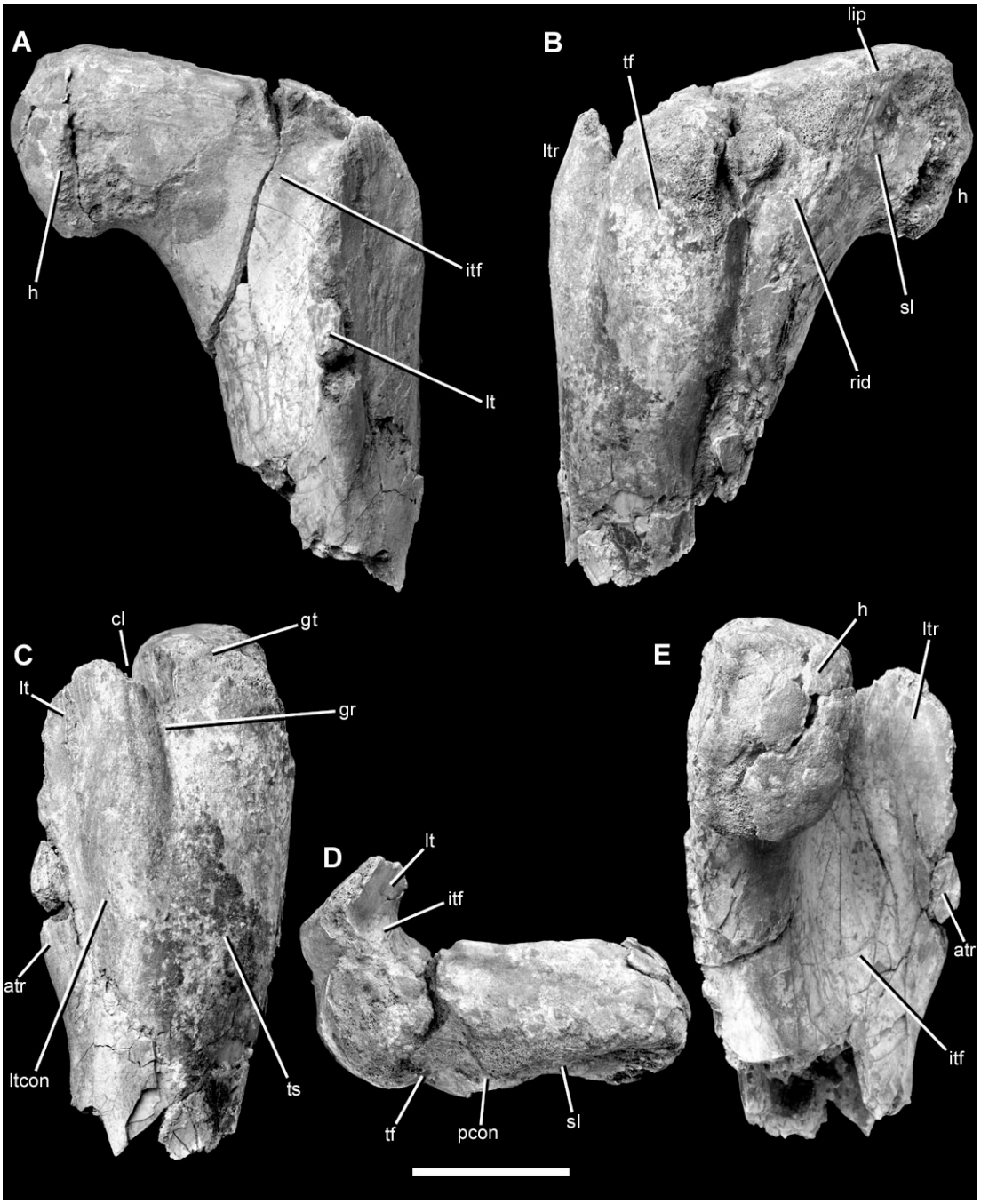

Figure 1-71. Left proximal region of the femur of the holotype specimen of *Alioramus altai* (IGM 100/1844) in anterior (A), posterior (B), lateral (C), proximal (D), and medial (E) views. Scale bar equals 5 cm. Abbreviations: atr, accessory trochanter; cl, cleft between lesser and greater trochanters; for, foramen; gr, groove between greater and lesser trochanters on lateral surface of femur; h, head; itf, intertrochanteric fossa; lip, lip of bone separating the ligament

sulcus from the proximal surface of the femur; ltcon, concavity on the lateral surface of the lesser trochanter; pcon, convexity on the posterior margin of the proximal femur; rid, ridge separating ligament sulcus and trochanteric fossa; sl, sulcus for femoral head ligament; tf, trochanteric fossa; ts, trochanteric shelf.

Figure 1-72. Right proximal region of the femur of the holotype specimen of *Alioramus altai* (IGM 100/1844) in anterior (A), posterior (B), lateral (C), medial (D), and proximal (E) views. Scale bar equals 5 cm. Abbreviations as in Figure 71.

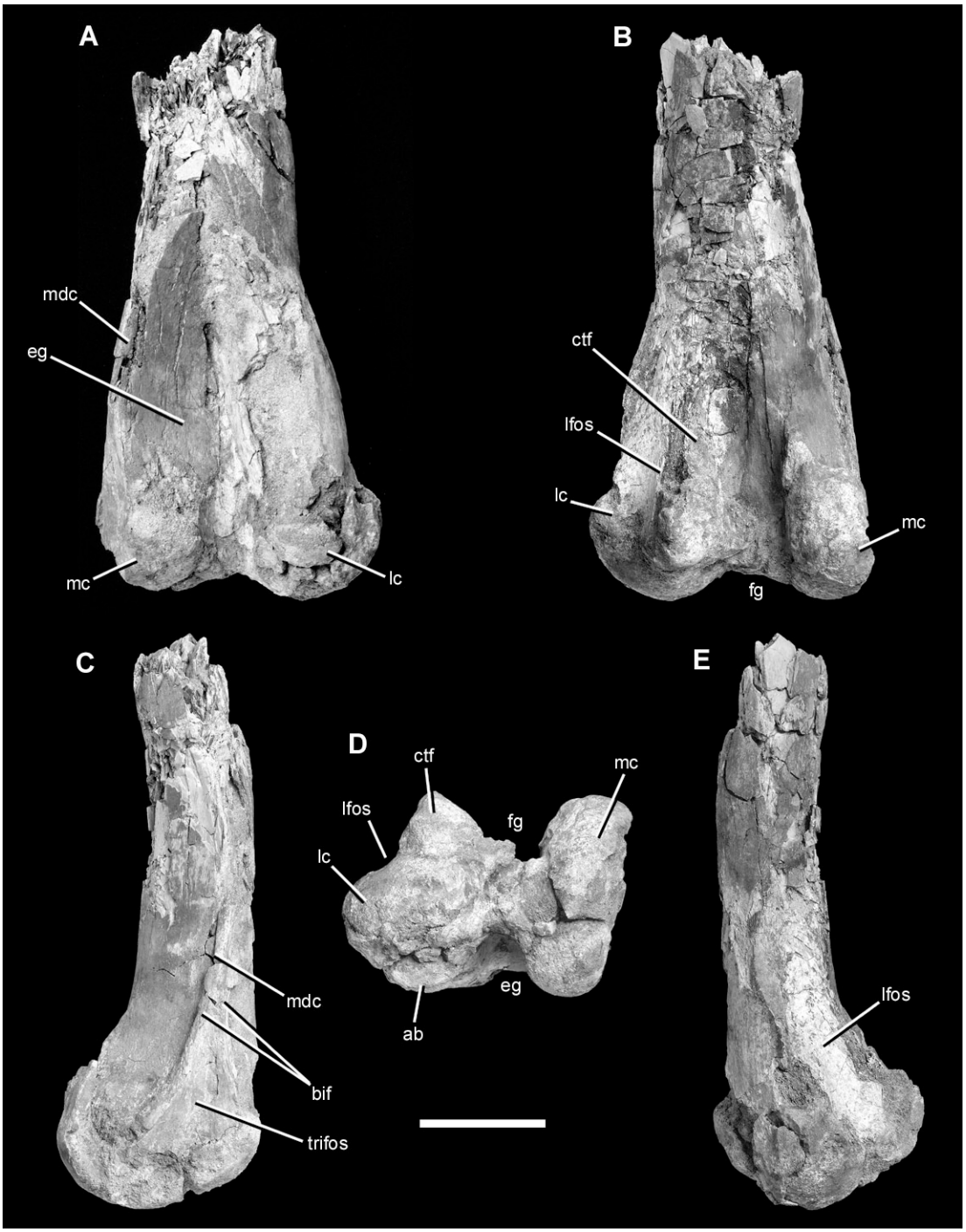

Figure 1-73. Left distal region of the femur of the holotype specimen of *Alioramus altai* (IGM 100/1844) in anterior (A), posterior (B), medial (C), distal (D), and lateral (E) views. Scale bar equals 5 cm. Abbreviations: ab, anterior bulge on anterior surface of lateral condyle; bif, bifurcation of medial distal crest on medial surface; ctf, crista tibiofibularis; eg, extensor groove;

fg, flexor groove; lc, lateral condyle; lfos, fossa on lateral surface between lateral condyle and crista tibiofibularis; mc, medial condyle; mdc, medial distal crest; trifos, triangular fossa defined by bifurcation of medial distal crest on medial surface.

Figure 1-74. Left shaft of the femur of the holotype specimen of *Alioramus altai* (IGM 100/1844) in anteromedial oblique (A) and medial (B) views. Scale bar equals 5 cm. Abbreviations: 4tr, fourth trochanter.

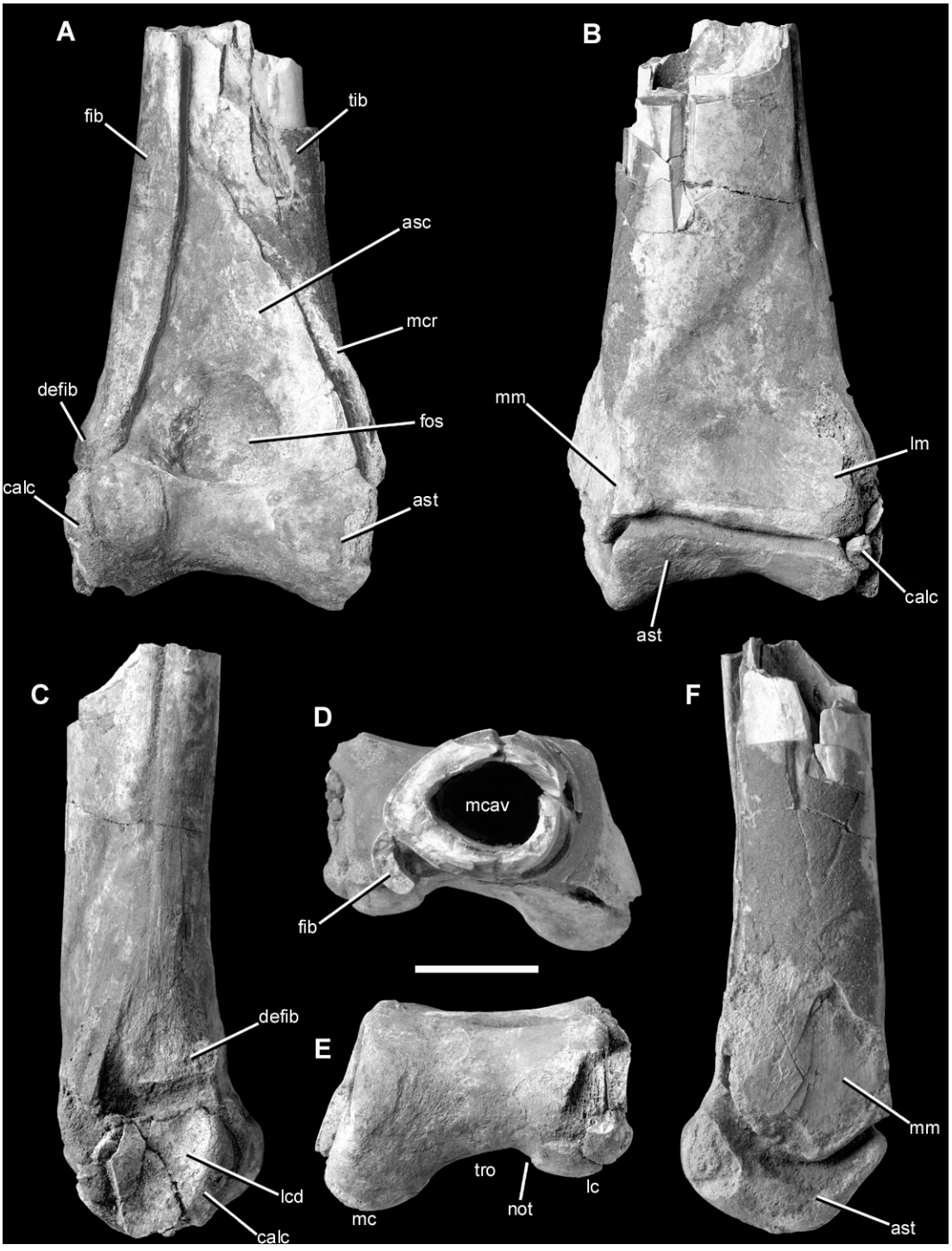

Figure 1-75. Right ankle (crus-tarsal joint) fragment of the holotype specimen of *Alioramus altai* (IGM 100/1844) in anterior (A), posterior (B), lateral (C), proximal (D), distal (E), and medial (F) views. Scale bar equals 4 cm. Abbreviations: asc, ascending process of the astragalus; ast,

astragalus; calc, calcaneum; defib, distal expansion of fibula; fib, fibula; fos, fossa on anterior surface of ascending process of astragalus; lc, lateral condyle of astragalus and calcaneum; lcd, lateral condylar depression of calcaneum; lm, lateral malleolus of the tibia; mc, medial condyle of the astragalus; mcav, marrow cavity; mcr, medial crest of the tibia; mm, medial malleolus of the tibia; not, notch between lateral condyle and trochlear surface of astragalus; tib, tibia; tro, trochlear surface of astragalus.

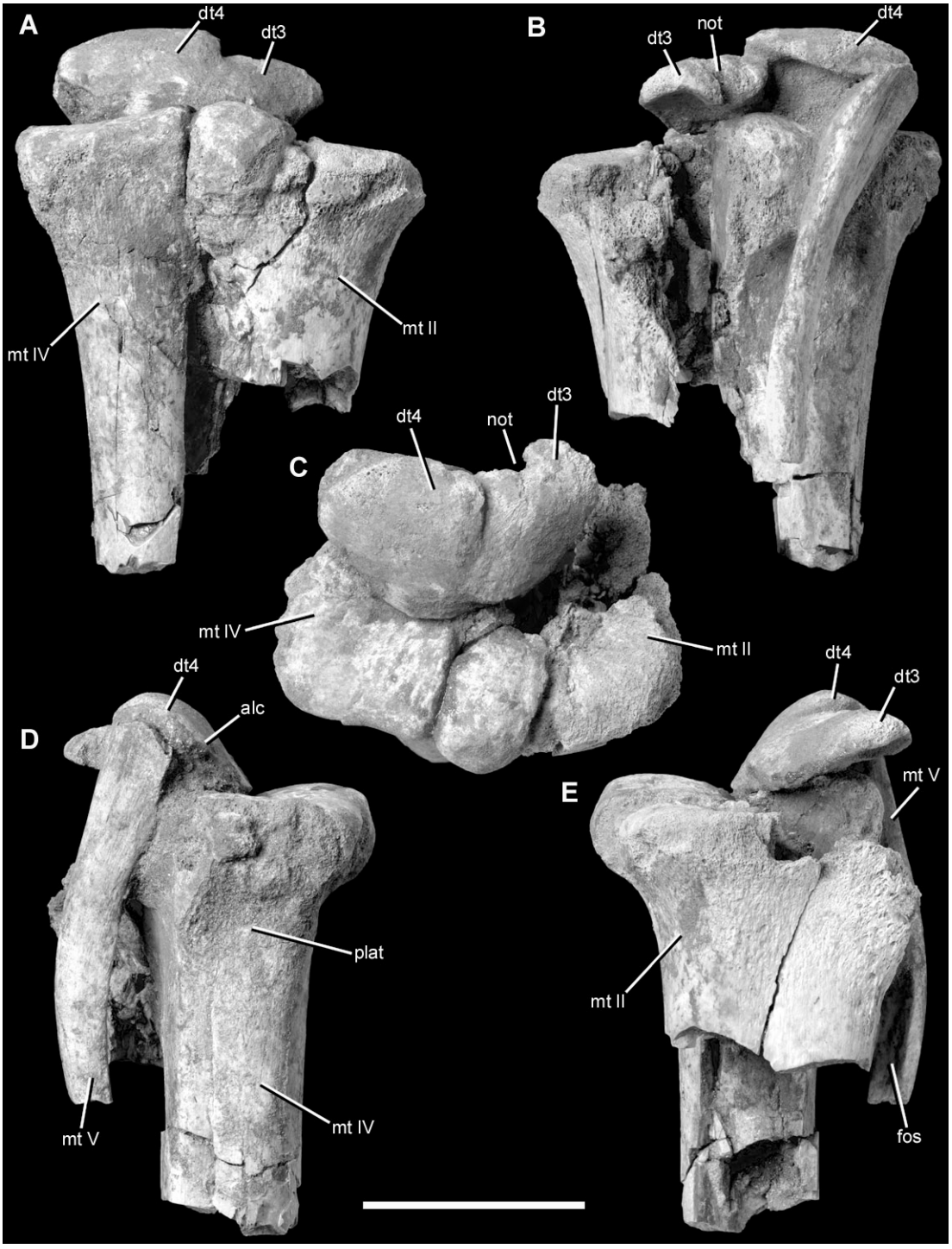

Figure 1-76. Right proximal metatarsus and distal tarsals of the holotype specimen of *Alioramus altai* (IGM 100/1844) in anterior (extensor) (A), posterior (flexor) (B), proximal (C), lateral (D), and medial (E) views. Scale bar equals 5 cm. Abbreviations: alc, anterolateral corner of distal

tarsal 4; dt3, distal tarsal 3; dt4, distal tarsal 4; fos; fossa on medial surface of metatarsal V; mt II, IV, V, metatarsals II, IV, and V, respectively; not, notch on posterior margin of distal tarsal 3; plat, triangular platform on lateral surface of metatarsal IV.

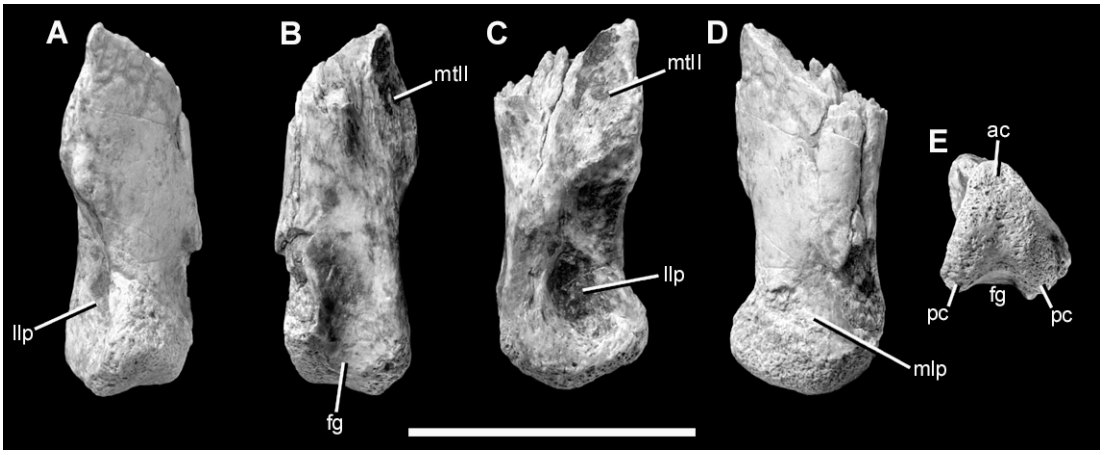

Figure 1-77: Right metatarsal I of the holotype specimen of *Alioramus altai* (IGM 100/1844) in anterior (extensor) (A), posterior (flexor (B), lateral (C), medial (D), and distal (E) views. Scale bar equals 3 cm. Abbreviations: ac, anterior condyle; fg, flexor groove; llp, lateral ligament pit; mlp, medial ligament pit; mtII, articular facet for metatarsal II; pc, posterior condyle.

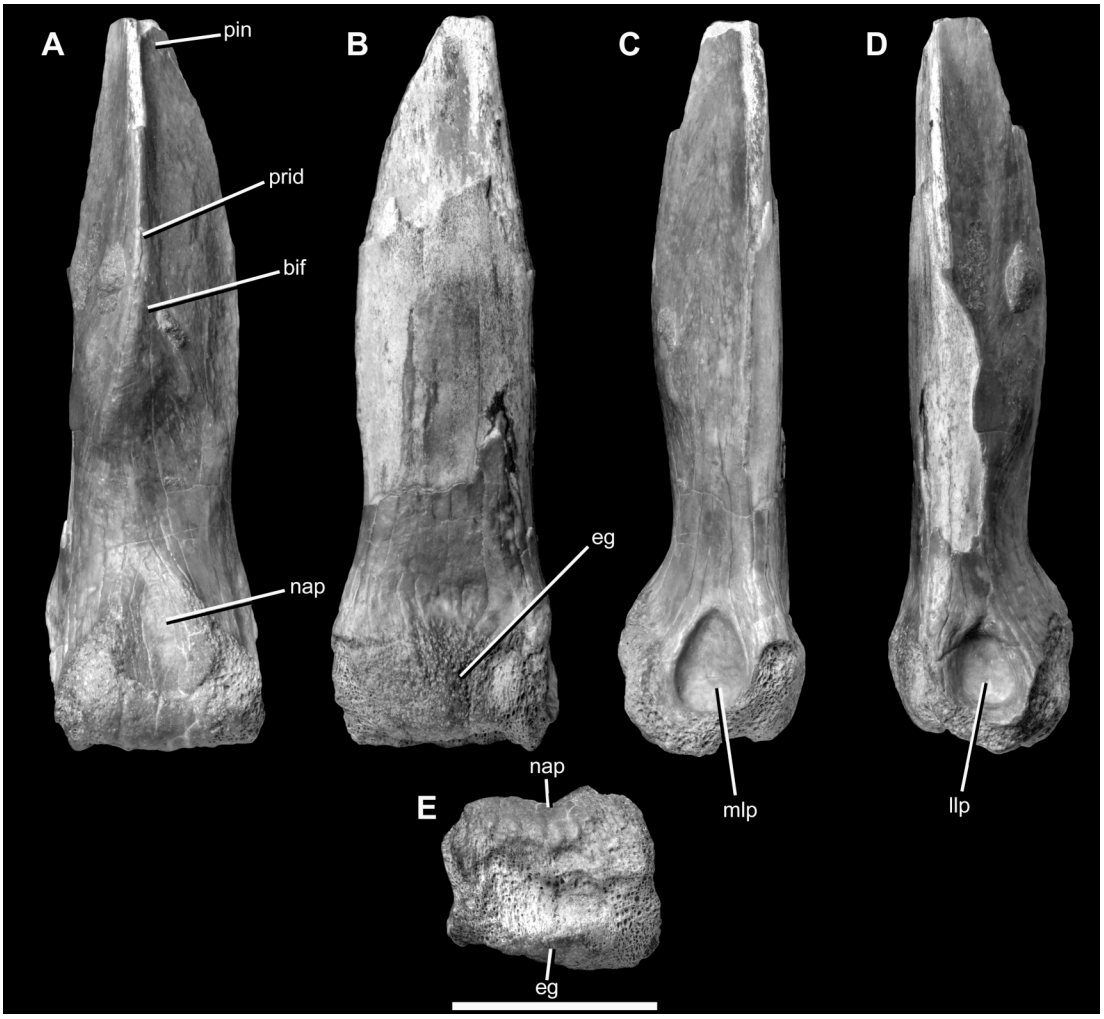

Figure 1-78: Left metatarsal III of the holotype specimen of *Alioramus altai* (IGM 100/1844) in anterior (extensor) (A), posterior (flexor) (B), lateral (C), medial (D), and distal (E) views. Scale bar equals 3 cm. Abbreviations: bif, bifurcation of posterior ridge; eg, extensor groove; llp, lateral ligament pit; mlp, medial ligament pit; nap, non-articular platform; pin, pinched proximal region of bone; prid, posterior ridge.

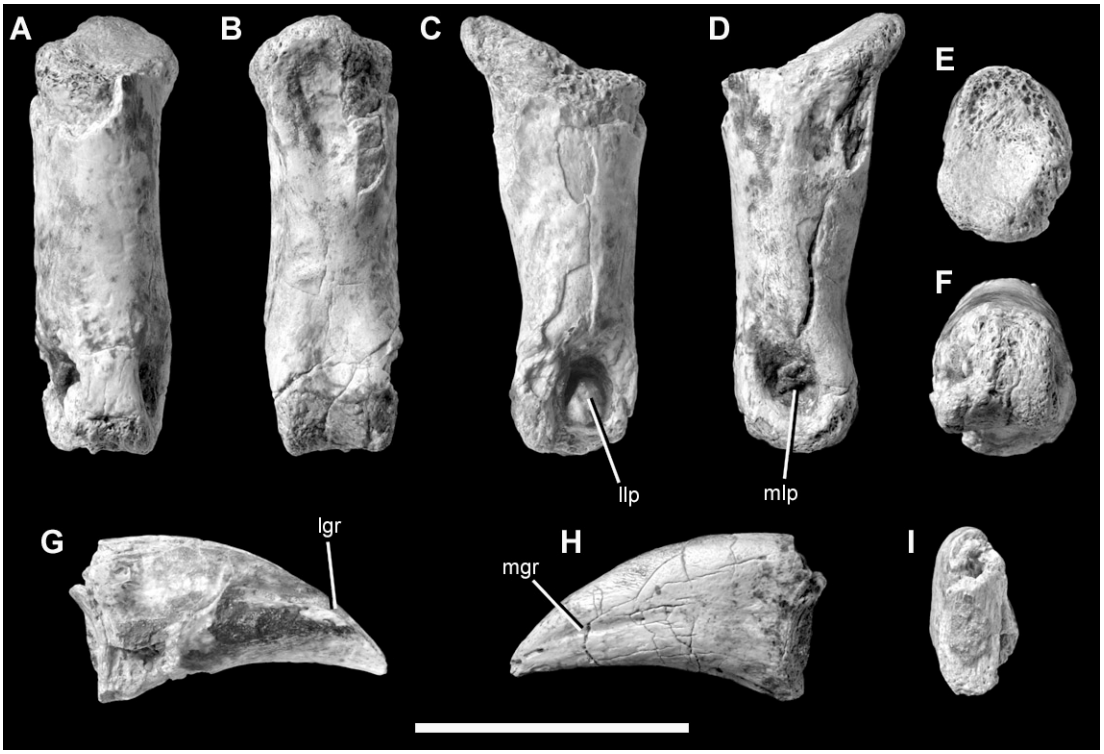

Figure 1-79. Right digit I of the holotype specimen of *Alioramus altai* (IGM 100/1844). Scale bar equals 3 cm. Phalanx I-1 (A-F) in anterior (extensor) (A), posterior (flexor) (B), lateral (C), medial (D), proximal (E), and distal (F) views. Ungual phalanx I-2 (G-I) in lateral (G), medial (H), and proximal (I) views. Abbreviations: lgr, lateral groove on ungual; llp, lateral ligament pit; mgr, medial groove on ungual; mlp, medial ligament pit.

Figure 1-80. Pedal phalanges: Phalanx III-1 (A-F) and two additional phalanges (G-L; M-R). Each phalanx in anterior (extensor) (A,G,M), posterior (flexor) (B,H,N), lateral/medial (C,I,O), opposite lateral/medial (D,J,P), distal (E,K,Q), and proximal (F,L,R) views. Scale bars equal 5 cm.

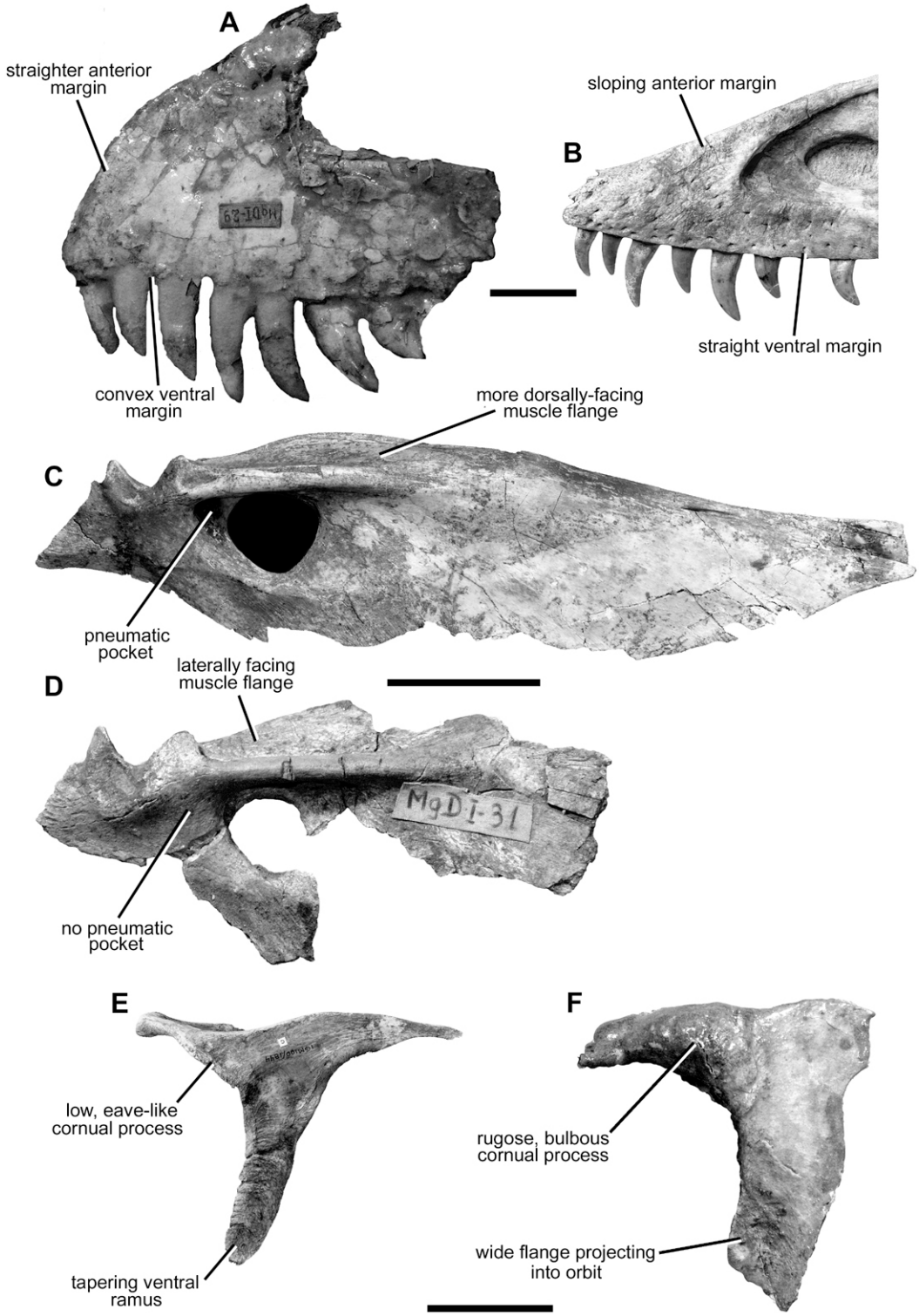

Figure 1-81. Comparison between the holotype of *Alioramus altai* (B,C,E) and bones of subadult *Tarbosaurus* from the Institute of Paleobiology (Warsaw) collection (A,D,F). A,B: left maxillae

in lateral view (*Tarbosaurus*: ZPAL MgD-I/29; size comparison difficult because of proportional disparity between specimens, but *Tarbosaurus* specimen approximately 1.3 times size of *A*. *altai* holotype, based on size comparison of third tooth crown); C,D: surangulars in lateral view (C is left element reversed; D is right element of *Tarbosaurus*: ZPAL MgD-I/31; these two bones are almost exactly the same size, based on the depth of the retroarticular process); E-F: postorbitals in lateral view (E is a left element and F a right element that has been reversed; F is ZPAL MgD-I/29 and is approximately 1.29 times size of *A*. *altai* holotype, based on size comparison of dorsal margin of ventral ramus where it meets the anterior and posterior rami). Major differences between subadult *Tarbosaurus* and *A*. *altai* are indicated in the figure and described more fully in the text. Scale bars equal 5 cm.

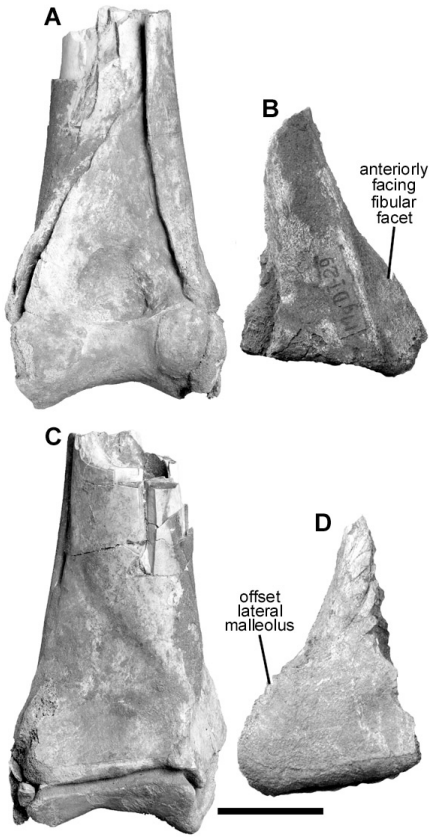

Figure 1-82. Comparison between the holotype of *Alioramus altai* (A,C) and bones of subadult *Tarbosaurus* from the Institute of Paleobiology (Warsaw) collection (ZPAL MgD-I/29) (B,D). A,B: tibia (and additional tarsal bones in A) in anterior view; C,D: tibia (and additional tarsal bones in C) in posterior view. A and C are right elements that are shown reversed; B and D are left elements. Major differences between subadult *Tarbosaurus* and *A*. *altai* are indicated in the figure (distinctive features of subadult *Tarbosaurus* are listed) and described more fully in the text. Scale bar equals 5 cm. The *Tarbosaurus* tibia is from the same individual as the maxilla and the postorbital depicted in Figure 81, and its near identical size to that of the *A*. *altai* holotype suggests that the body size of the two individuals was similar.

CHAPTER 2:

THE SYSTEMATICS AND PHYLOGENY OF BASAL COELUROSAURIAN THEROPODS, BASED ON A COMPREHENSIVE PHYLOGENY OF MESOZOIC COELUROSAURS

INTRODUCTION

Coelurosaurian theropods include all dinosaurs that are more closely related to birds than to *Allosaurus* (see Sereno et al. 2005). Currently this clade includes approximately 175-200 known Mesozoic species, including avialans (birds). Numerous cladistic analyses have focused on coelurosaurian phylogeny over the past decade (e.g., Norell et al. 2001, 2006; Rauhut 2003; Clark et al. 2002a; Hwang et al. 2002, 2004; Makovicky et al. 2003; Holtz et al. 2004; Novas and Pol 2005; Rauhut and Xu 2005; Senter 2007, 2010, 2011; Turner et al. 2007a, 2012; Zhang et al. 2008; Hu et al. 2009; Zanno et al.2009; Choiniere et al. 2010a,b, 2012; Csiki et al. 2010; Rauhut et al. 2010; Zanno 2010b; Dal Sasso and Maganuco 2011; Novas et al. 2012).

Much of this previous work has been conducted by Mark Norell's research group at the American Museum of Natural History (and collaborators) as part of the "Theropod Working Group (TWiG)" project, which has focused on steadily building larger and more comprehensive phylogenetic datasets as the coelurosaurian fossil record expands. This previous TWiG work, as well as the majority of other studies, has focused particularly on the phylogeny of the derived coelurosaurs—the subclade Maniraptora—which includes avialans, the dromaeosaurids (sickle-clawed species such as *Velociraptor*), troodontids (*Troodon* and relatives), oviraptorosaurs (mostly crested and toothless forms, such as *Citipati* and *Oviraptor*),

therizinosauroids (aberrant, herbivorous theropods such as *Nothronychus* and *Alxasaurus*), and alvarezsauroids (cursorial, possibly fossorial theropods such as *Shuvuuia* and *Mononykus*). As a result of this focus, the phylogeny of derived coelurosaurs is generally well understood and most current analyses agree on the general pattern of relationships: dromaeosaurids and troodontids form a monophyletic Deinonychosauria, which is the sister taxon to Avialae (birds), whereas oviraptorosaurs and therizinosaurs are more basally positioned on the tree.

Considerably less research attention has focused on the basal coelurosaurs, a primitive grade of non-maniraptoran taxa that includes the tyrannosauroids (large, bipedal predators such as *Tyrannosaurus* and *Albertosaurus*), compsognathids (small, sleek predators such as *Compsognathus*), ornithomimosaurs (swift, bipedal forms, most of which were toothless and possessed beaks, such as *Gallimimus* and *Struthiomimus*), and puzzling singleton genera such as *Ornitholestes*, *Coelurus*, *Zuolong*, *Tanycolagreus*, and *Nqwebasaurus*. One surprising statistic illustrates this point: in the most recent published version of the TWiG coelurosaur matrix, which includes 111 total taxa, only eight out of 19 known tyrannosauroid species are included, and the mysterious singletons *Tanycolagreus*, *Zuolong*, *Tugulusaurus*, and *Nqwebasaurus* are excluded (Turner et al. 2012).

Although its taxon and character sampling for basal coleurosars is far from complete, Turner et al.'s (2012) study is nevertheless one of the most comprehensive analyses of basal coelurosaurs in the literature. Most other studies include even fewer basal coelurosaur taxa and few characters relevant to the most basal divergences in the clade. It is no surprise, therefore, that published analyses disagree on several critical points. Focusing on six of the largest and most recent analyses, the differences between these phylogenies are substantial (fig. 1). Tyrannosauroids are recovered near the base in all analyses, but Holtz et al. (2004) placed

Compsognathidae as the basal-most coelurosaurian subclade. Compsognathids occupy several positions among the other five studies: Senter (2007) and Turner et al. (2012) place them intermediate between tyrannosauroids and ornithomimosaurs, whereas Zanno et al. (2009) groups them together with tyrannosauroids, Choiniere et al. (2012) recovers them as basal maniraptorans more closely related to birds than to either tyrannosauroids or ornithomimosaurs, and Rauhut et al. (2010) fails to even recover a monophyletic Compsognathidae. The singleton genera *Ornitholestes* and *Coelurus* are found in a wide array of positions in these analyses, and not all analyses agree that *Dilong* and *Proceratosaurus* are basal members of the tyrannosauroid clade. Senter (2007) places *Dilong* within Tyrannosauroidea and Rauhut et al. (2010) finds both *Dilong* and *Proceratosaurus* to be tyrannosauroids, but Turner et al. (2012) finds both genera to be outside of the tyrannosauroid clade and more closely related to birds. These are only some examples of the many disagreements between these studies.

Although these differences may seem trivial, poor resolution at the base of Coelurosauria is problematic for several reasons. First, and most importantly, poor understanding of basal coelurosaurian phylogeny precludes the construction of a complete, species-level tree of birds and their closest dinosaur relatives. Such a tree is a necessary framework for examining major macroevolutionary trends in morphological evolution during the rise of birds. Second, the lack of resolution near the base of the coelurosaur tree makes it difficult to determine character polarity, which has an accumulative effect when optimizing characters higher in the tree (including those characters that change at or near the avialan node, which we are particularly interested in understanding). Third, poor basal resolution hinders our ability to reconstruct patterns of character evolution, and makes it difficult to assess when

certain characters of interest (such as feathers, a mobile wrist, extensive air sacs, etc.) originated.

To provide a comprehensive phylogeny of coelurosaurs and a more robust test of basal coelurosaurian relationships, this chapter presents a new cladistic dataset and analysis. This study is the latest iteration of the TWiG project and is build upon iterative published versions of the TWiG dataset, with the addition of several new taxa and over 300 new characters. The end result is the largest and most comprehensive phylogeny of Coelurosauria yet compiled, which will provide a valuable framework for studying coelurosaurian evolution, including the dinosaur-bird transition.

TAXON SAMPLING

The cladistic analysis presented here includes 150 taxa scored for 853 characters. This analysis is an expanded version of the American Museum of Natural History's Theropod Working group (TWiG) dataset. This dataset has grown iteratively over the past decade with the addition of new taxa and characters, and previous versions have been presented by Norell et al. (2001, 2006), Clark et al. (2002a), Hwang et al. (2002, 2004), Makovicky et al. (2003, 2005), Turner et al. (2007a, 2012), and Csiki et al. (2010). The most recent versions include a large amount of data relevant to avialan phylogeny that was originally presented by Clarke et al. (2006). These studies are considered precursors to the current analysis and many of the character data employed here were first established in these earlier works. Several other authors have also used published TWiG phylogenies as a backbone for additional phylogenetic work, especially analyses targeting the interrelationships of certain coelurosaurian subgroups (e.g., Senter 2007,

2010, 2011; Zhang et al. 2008; Zanno et al. 2009; Zanno 2010b; Choiniere et al. 2010a, 2010b, 2012; Xu et al. 2011a).

The focus of most previous work from the Theropod Working Group, and the focal point of all published TWiG phylogenies, is maniraptoran theropods (therizinosauroids, oviraptorosauroids, paravians, most likely alvarezsauroids). More specifically, the overwhelming focus has been on the paravian theropods, which include dromaeosaurids, troodontids, and avialans (birds). This focus reflects longstanding interest in the origin of birds and the relationships of birds and their closest dinosaurian relatives. This dissertation, on the other hand, focuses on non-maniraptoran "basal" coelurosaurs (tyrannosauroids, ornithomimosaurs, and many singleton taxa, including species often referred to as "compsognathids" that may or may not form a monophyletic Compsognathidae). The cladistic analysis presented here includes a nearly complete sample of Mesozoic coelurosaurs, but the majority of new data (new characters and taxa, revised character scores) is relevant to basal coelurosaurs.

Compared to the most recent TWiG dataset (Turner et al. 2012), this analysis includes 39 new taxa, all of which are basal coelurosaurs. This section includes a list of basal coelurosaur taxa included in the analysis, sources of coding data, notes relevant to individual taxa, and comments on published work that has stemmed from this dissertation project but is not included in the dissertation itself.

General Comments: The starting point for this analysis was the latest published version of the TWiG dataset, which was presented by Turner et al. (2012) and stems from the dissertation work of Alan Turner. Turner's dissertation focused on the paravian theropods and included a comprehsive phylogenetic and systematic revision of the group. Therefore, character scores for

paravian theropods in the Turner et al. (2012) dataset were accepted without revision. In some cases, however, paravian taxa had to be rescored when characters were modified (e.g., by the addition of one or more new states to encapsulate wider variation among coelurosaurs). Character scores for non-paravian maniraptorans were also largely accepted without critical revision, although scores relevant to therizinosauroids and alvarezsauroids were carefully checked. Character scores for non-maniraptoran "basal" coelurosaurs, however, were carefully checked and in some cases modified. Several new basal coelurosaurs, alvarezsauroids, and therizinosauroids were added to the dataset of Turner et al. (2012), but no new oviraptorosauroids or paravians were added. Amy Balanoff's dissertation focused on oviraptorosauroids and new data relevant to their relationships (new characters, modified character scores, additional taxa) will be included in future TWiG analyses. The analysis presented here includes several new characters and these were scored for both basal coelurosaurs and maniraptorans.

Outgroup Taxa: The outgroups employed here are the non-coelurosaurian tetanurans *Allosaurus* and *Sinraptor*. These taxa were scored based on the literature and personal observation of specimens. The Utah Museum of Natural History, American Museum of Natural History, and Carnegie Museum of Natural History collections of *Allosaurus* were studied firsthand, as was the holotype of *Sinraptor* (IVPP 10600). Monographs of both taxa were also used to score characters (*Allosaurus*: Madsen 1976; *Sinraptor*: Currie and Zhao 1993). Much of my previous work has focused on the anatomy and phylogeny of non-coelurosaurian tetanurans, and character data gleaned from past studies was utilized here (e.g., Brusatte and Sereno 2008; Brusatte et al. 2008, 2009; Benson et al. 2010a).

Paravians, Oviraptorosaurs, and Therizinosauroids: Maniraptorans were scored for new characters based on the literature and personal observation of specimens. Several maniraptorans were studied firsthand as part of this project. The complete Utah Museum of Natural History collection of the basal therizinosauroid *Falcarius* was studied, as was the American Museum of Natural History temporary collection of IGM Gobi oviraptorosauroid material (although specimen-by-specimen character scoring was not undertaken, so as to not infringe on the dissertation work of Balanoff). Characters were also scored directly for some Mongolian troodontids from the AMNH and IGM collections (*Byronosaurus*: IGM 100/983; *Saurornithoides*: AMNH FARB 6516), although most new scores for troodontids were based on the literature. Several dromaeosaurids were studied firsthand, including *Austroraptor* (MML 195), *Balaur* (EME PV.313), *Bambiraptor* (AMNH FR 30556), *Buitreraptor* (MPCA 245, 238), *Deinonychus* (YPM 5025 and hypodigm series), *Dromaeosaurus* (AMNH FARB 5356), *Tsaagan* (IGM 100/1015), *Unenlagia*/*Neuquenraptor* (MCF PVPH 77, 78), and *Velociraptor* (AMNH temporary collection of IGM specimens: see Norell and Makovicky 1997, 1999). Finally, the basal avialan *Archaeopteryx* was also observed firsthand (Berlin and Eichstatt specimens), as was the enigmatic *Epidexipteryx* (IVPP V15471).

Note that for all new characters, the five extant bird taxa included in the dataset (*Crypturellus*, *Chauna*, *Anas*, *Crax*, and *Gallus*) were scored in a very conservative manner, due to the great morphological differences between extant birds and basal coelurosaurs (which all new characters relate to). This was a pragmatic decision because it is often very difficult to confidently score living taxa for characters relevant to taxa such as tyrannosauroids and therizinosauroids, and therefore the possibility of making incorrect primary homology

hypotheses is high. The extant birds have essentially been scored for only those characters that relate to skeletal ratios or measurements, or straightforward anatomical features that require no ambiguity to score in the living species.

As part of dissertation tenure at the American Museum, I was part of a collaborative team that named and described the aberrant Late Cretaceous Romanian dromaeosaurid *Balaur bondoc*. *Balaur* is represented by a well preserved holotype that represents the most complete theropod dinosaur from the final 60 million years of the Cretaceous of Europe (EME PV.313), as well as a series of larger specimens referred to *Balaur* sp. (LVP [FGGUB] R.1580-1585). These specimens were originally described in a short paper by Csiki, Vremir, Brusatte, and Norell (2010) and a monograph of the taxon was published by Brusatte et al. (in press).

Alvarezsauroids: The alvarezsauroids *Mononykus* (AMNH IGM collection, including casts), *Patagonykus* (MCF PVPH 37), and *Shuvuuia* (IGM 100/975, 100/99, 100/10001) were studied firsthand. The basal alvarezsauroid *Haplocheirus* was scored based on extensive photographs provided by Jonah Choiniere, as well as the initial description of the taxon (Choiniere et al. 2010a). Other alvarezsauroids were scored based on the literature and on notes and advice provided by Choiniere, whose dissertation and postdoctoral work focused largely on alvarezsauroids. Character scores for TWiG characters and some new characters were taken from Choiniere's published work (Choiniere et al. 2010a, b, 2012) as well as an unpublished character database that he is building at the AMNH. These scores were carefully checked and in rare cases modified. Literature sources for scores include: *Alvarezsaurus* (Bonaparte 1991), *Patagonykus* (Novas 1997), *Achillesaurus* (Martinelli and Vera 2007), *Mononykus* (Perle et al. 1993, 1994), *Shuvuuia* (Chiappe et al. 1998, 2002; Sereno 2001; Suzuki et al. 2002), *Parvicursor* (Kahru and

Rautian 1996), *Albertonykus* (Longrich and Currie 2009), *Albinykus* (Nesbitt et al. 2011), *Bonapartenykus* (Salgado et al. 2009; Agnolin et al. 2012), *Ceratonykus* (Averianov and Barsbold 2009), *Linhenykus* (Xu et al. 2011b, in press), *Xixianykus* (Xu et al. 2010).

Tyrannosauroids: A particular focus of this dissertation work is the anatomy, systematics, and ingroup phylogeny of tyrannosauroids. As part of this dissertation I compiled a new phylogenetic dataset for tyrannosauroids, which was used to generate a species-level phylogeny for the clade (Brusatte et al. 2010a). The characters used in this analysis have been incorporated into the cladistic dataset used in this dissertation, and all characters new to the 2010 analysis are described fully below. Additionally, a considerable amount of alpha taxonomic, anatomical, and systematic research on tyrannosauroids has stemmed from this dissertation project, including the description of two new taxa (*Alioramus altai*: Brusatte et al. 2009a; *Raptorex kriegsteini*: Sereno, Tan, Brusatte et al. 2009), the revision of European basal tyrannosauroids that resulted in the erection of the new genus *Juratyrant* (Brusatte and Benson in press), a review of the Asian Late Cretaceous tyrannosauroid record (Brusatte et al. 2010d), and osteological monographs of two taxa (*Alioramus altai*: Brusatte et al. 2012a; *Dryptosaurus aquilunguis*: Brusatte et al. 2011).

Kileskus aristotocus

Age: Middle Jurassic (Bathonian, ca. 168-165 million years old). See Averianov et al. (2010) for information on the age of the taxon.

Occurrence: Itat Formation, Siberia, Russia

Scoring Sources: Averianov et al. (2010)

Sinotyrannus kazuoensis

Age: Early Cretaceous (Aptian, ca. 120 million years old). See He et al. (2004) for information on the age of the Jiufotang Formation.

Occurrence: Jiufotang Formation, China

Scoring Sources: Ji et al. (2009)

Proceratosaurus bradleyi

Age: Middle Jurassic (late Bathonian, ca. 166.5-165 million years old).

Occurrence: Great Oolite, England, United Kingdom

Scoring Sources: The holotype and only known specimen was studied firsthand (NHMUK R4860). Additional information was gleaned from Rauhut et al. (2010).

Guanlong wucaii

Age: early Late Jurassic (Oxfordian, ca. 161-156 million years old).

Occurrence: Shishugou Formation, Xinjiang, China

Scoring Sources: The holotype (IVPP V14531) and referred specimen (IVPP V14532) were studied firsthand. Additional information was taken from Xu et al. (2006).

Remarks: The cladistic analysis of Brusatte et al. (2010a) includes several character scores gleaned solely from observation of the holotype and referred material, as this taxon has yet to be fully described in the literature. As a monograph is currently in preparation by Jonah Choiniere, Xu Xing, Mark Norell, and colleagues, no further comments on the anatomy are presented here. However, some primary anatomical observations of the braincase, and comparisons with other tyrannosauroid taxa, are presented by Bever, Brusatte et al. (in press).

Dilong paradoxus

Age: Early Cretaceous (Barremian-Early Aptian, ca. 125-121 million years old).

Occurrence: Yixian Formation, China

Scoring Sources: The holotype (IVPP V14243) was studied firsthand. Additional information was taken from Xu et al. (2004).

Eotyrannus lengi

Age: Early Cretaceous (Barremian, ca. 130-125 million years old).

Occurrence: Wessex Formation, Isle of Wight, England, United Kingdom

Scoring Sources: The holotype (MIWG 1997.550) was studied firsthand. Additional information was taken from Hutt et al. (2001) and Naish et al. (2001).

Remarks: The cladistic analysis of Brusatte et al. (2010a) includes several character scores gleaned solely from observation of the holotype and referred material, as this taxon has yet to be fully described in the literature. As a monograph is currently in preparation by Darren Naish and Andrea Cau, no further comments on the anatomy are presented here. However, some primary anatomical observations of the pelvis, and comparisons with other tyrannosauroid taxa, are presented by Brusatte and Benson (in press).

Juratyrant langhami

Age: Late Jurassic (early Tithonian, ca. 151-148.25 million years old). See Benson (2008) for information on the age of the taxon.

Occurrence: Kimmeridge Clay, England, United Kingdom

Scoring Sources: The holotype (OUMNH J.3311-1–J.3311-30) was studied firsthand. Additional information was taken from Benson (2008).

Remarks: The species *Juratyrant langhami* was originally named by Benson (2008) as a new species of *Stokesosaurus*, a tyrannosauroid from the Late Jurassic of North America that is represented by a small amount of fragmentary material (e.g., the holotype of *Stokesosaurus clevelandi* is a sole bone: an ilium) (Madsen 1974). Brusatte and Benson (in press) showed that the characters used by Benson (2008) to unite the British and American specimens in a monophyletic *Stokesosaurus* are more widely distributed among tyrannosauroids, and based on this reasoning and the results of a cladistic analysis removed the British material from *Stokesosaurus* and transferred it to a new genus, *Juratyrant*. It is likely that the British *Juratyrant langhami* and the American *Stokesosaurus clevelandi* are close relatives, but the incredibly fragmentary nature of the American material makes comparison difficult. *Stokesosaurus clevelandi* is not included in the current phylogenetic analysis because it can only be scored for a few characters (those relating to the ilium). However, its holotype ilium is shown in Figure 2.33 to illustrate a handful of new characters in the analysis, as it is a good and well preserved exemplar of a basal tyrannosauroid ilium.

Xiongguanlong baimoensis

Age: Early Cretaceous (Aptian-Albian, ca. 125-99.6 million years old). See Li et al. (2010) for information on the age of the taxon.

Occurrence: White Ghost Castle, Yujingzi Basin, China

Scoring Sources: Li et al. (2010). Many characters were also scored based on high resolution photographs provided by Peter Makovicky.

Dryptosaurus aquilunguis

Age: Late Cretaceous (Maastrichtian, ca. 70.6-65.5 million years old). See Brusatte et al. (2011) for information on the age of the taxon.

Occurrence: New Egypt Formation, New Jersey, United States

Scoring Sources: All character scores are based on the holotype, which was studied firsthand (ANSP 9995, plus one bone that was transferred to the American Museum of Natural History and is catalogued as AMNH FARB 2438). Additional information was gleaned from a historic cast in the collections of the Natural History Museum (London), as well as the description of Carpenter et al. (1997).

Remarks: A monographic redescription of the holotype specimen of *Dryptosaurus* stemmed from this dissertation project (Brusatte et al. 2011), as did an in-progress revision of other tyrannosauroid material from the Late Cretaceous of eastern North America, some of which may be referable to *Dryptosaurus*. The monograph presents a comprehensive anatomical revision of the holotype specimen and makes comparisons with other tyrannosauroids. This information was included in the phylogenetic analysis of Brusatte et al. (2010a), and is also included in the current cladistic analysis.

Appalachiosaurus montgomeriensis

Age: Late Cretaceous (middle Campanian, ca. 78-76 million years old). See Carr et al. (2005) for information on the age of the taxon.

Occurrence: Demopolis Chalk Formation, Alabama, United States

Scoring Sources: Carr et al. (2005). Thomas Carr, a collaborator on the Brusatte et al. (2010a) phylogenetic analysis, also provided scores for characters used in that analysis based on his own firsthand study of the holotype (RMM 6670). For all characters in the current study that also appeared in Brusatte et al. (2010), the scores for *Appalachiosaurus* were carefully checked by Carr.

Bistahieversor sealeyi

Age: Late Cretaceous (Campanian, ca. 83.5-70.6 million years old). See Carr and Williamson (2010) for information on the age of the taxon.

Occurrence: Kirtland Formation, New Mexico, United States

Scoring Sources: Carr and Williamson (2010). Thomas Carr, a collaborator on the Brusatte et al. (2010a) phylogenetic analysis, also provided scores for characters used in that analysis based on his own firsthand study of the holotype (NMMNH P-27469) and referred specimens (NMMNH P-25049, NMMNH P-32824, OMNH 10131). For all characters in the current study that also appeared in Brusatte et al. (2010a), the scores for *Bistahieversor* were carefully checked by Carr.

Albertosaurus sarcophagus

Age: Late Cretaceous (late Campanian-Maastrichtian, ca. 73-65.5 million years old). See Arbour et al. (2009) for information on the range of this taxon in Dinosaur Provincial Park and the Paleobiology Database (http://www.pbdb.org) for information on other occurrences.

Occurrence: Dinosaur Park Formation, Horseshoe Canyon Formation, Alberta, Canada, as well as material from the United States (see the relevant entry in the Paleobiology Database)

Scoring Sources: The American Museum of Natural History collection of *Albertosaurus* material was examined firsthand, and additional information was gleaned from Parks (1928), Carr (1999, 2010), and Currie (2003). Thomas Carr, a collaborator on the Brusatte et al. (2010a) phylogenetic analysis, also provided scores for characters used in that analysis based on his own firsthand study of a vast amount of *Albertosaurus* material in collections in the United States and Canada (e.g., Carr 2010). For all characters in the current study that also appeared in Brusatte et al. (2010a), the scores for *Albertosaurus* were checked by Carr.

Remarks: It is often unclear if individual specimens from western North America (especially from the Dinosaur Park Formation) belong to *Albertosaurus sarcophagus* or the closely related *Gorgosaurus libratus*, and it is possible that future taxonomic work shows that some specimens used to derive *Albertosaurus* scores here actually belong to *Gorgosaurus*, or vice versa. Recent systematic work on the holotype of *Albertosaurus sarcophagus* (Carr 2010) and other anatomical descriptions of this taxon in the same volume are helping to clarify the anatomy and systematics of *Albertosaurus*, but additional specimen-level work is needed, especially regarding *Gorgosaurus*.

Gorgosaurus libratus

Age: Late Cretaceous (middle Campanian, ca. 77-74 million years old). See Arbour et al. (2009) for information on the range of this taxon in Dinosaur Provincial Park.

Occurrence: Dinosaur Park Formation, Alberta, Canada

Scoring Sources: The American Museum of Natural History collection of *Gorgosaurus* material was examined firsthand, and additional information was gleaned from Lambe (1917), Carr (1999), Currie (2003), and Witmer and Ridgely (2009). Thomas Carr, a collaborator on the

Brusatte et al. (2010a) phylogenetic analysis, also provided scores for characters used in that analysis based on his own firsthand study of *Gorgosaurus* material in collections in the United States and Canada. For all characters in the current study that also appeared in Brusatte et al. (2010), the scores for *Gorgosaurus* were checked by Carr.

Remarks: See note above in entry for *Albertosaurus*.

Teratophoneus curriei

Age: Late Cretaceous (middle Campanian, ca. 77-74 million years old).

Occurrence: Kaiparowits Formation, Utah, United States

Scoring Sources: Carr et al. (2011). Thomas Carr, a collaborator on the Brusatte et al. (2010a) phylogenetic analysis, also provided scores for characters used in that analysis based on his own firsthand study of the holotype (BYU 8120/9396, 8120/9397, 826/9402, 9398, 13719). For all characters in the current study that also appeared in Brusatte et al. (2010a), the scores for *Teratophoneus* were carefully checked by Carr. In the Brusatte et al. (2010a) analysis, *Teratophoneus* (which had yet to be formally named at the time) is referred to as the "Utah Taxon".

Daspletosaurus torosus

Age: Late Cretaceous (middle Campanian, ca. 77-74 million years old). See Arbour et al. (2009) for information on the range of this taxon in Dinosaur Provincial Park and the Paleobiology Database (http://www.pbdb.org) for information on other occurrences.

Occurrence: Dinosaur Park Formation, Oldman Formation, Canada, as well as material from the United States (see the relevant entry in the Paleobiology Database)

Scoring Sources: AMNH FARB 6458. Additional information was gleaned from Russell (1970) and Currie (2003). Furthermore, Thomas Carr, a collaborator on the Brusatte et al. (2010a) phylogenetic analysis, also provided scores for characters used in that analysis based on his own firsthand study of a vast amount of *Daspletosaurus* material in collections in the United States and Canada. For all characters in the current study that also appeared in Brusatte et al. (2010a), the scores for *Daspletosaurus* were checked by Carr.

Remarks: The alpha level taxonomy of specimens referred to *Daspletosaurus* is confusing and in dire need of revision. Russell (1970) erected this genus based on a specimen from the Oldman Formation of Alberta (NMC 8506), and in the ensusing four decades researchers referred to *Daspletosaurus* additional material from the Dinosaur Park Formation of Alberta, the Two Medicine Formation of Montana, and other units. It is unclear which, if any, of this material can be referred to the same species as the holotype. The anatomy and systematics of *Daspletosaurus* is currently under revision by Philip Currie, Thomas Carr, and colleagues. Until their taxonomic revision is published, all of the aforementioned material referred to *Daspletosaurus* is considered to represent this genus, although character scores in the present analysis are based entirely on the Canadian specimens (not the Two Medicine specimen).

Alioramus altai

Age: Late Cretaceous (Maastrichtian, ca. 70.6-65.5 million years old). See Brusatte et al. (2009a) for information on the age of this taxon and the closely related, and possibly conspecific, *Alioramus remotus*.

Occurrence: Nemegt Formation, Mongolia

Scoring Sources: The type specimen, IGM 100/1844, was studied firsthand and monographed as part of this dissertation project.

Remarks: The new species *Alioramus altai* was described by Brusatte et al. (2009a), based on an exceptionally preserved specimen discovered by Julia Clarke during the American Museum of Natural History-Mongolian Academy of Sciences expedition in 2001. Brusatte et al. (2009a) presented a brief description of the new species, and this publication was followed by the comprehensive osteological monograph of Brusatte et al. (2012a—included in this dissertation as Chapter 1) and two papers focusing on the braincase (Bever et al. 2011, in press). *Alioramus altai* is the second named species of the genus *Alioramus*. The first, *Alioramus remotus*, is the type species of the genus and was described by Kurzanov (1976) based on a fragmentary specimen that has yet to be carefully described and figured in the literature. Brusatte et al. (2009, 2012a) noted several differences between the holotypes of *A. remotus* and *A. altai* and argued that the two are distinct taxa. However, this conclusion is regarded as tentative because neither I nor other members of the AMNH team have been able to study the material of *A. remotus* firsthand, and all anatomical information has been taken from the short paper of Kurzanov (1976) and photographs provided by Philip Currie and Tetsuto Miyashita. It is possible, and perhaps probable, that future work on the *A. remotus* holotype will show that there are no major differences between it and the holotype of *A. altai*, meaning that the two most likely belong to a single species. Such work is currently being undertaken by Vladimir Alifanov and no further comments will be made here. Regardless, the character scores for *Alioramus* in the current analysis are based solely on specimen IGM 100/1844.

Tarbosaurus bataar

Age: Late Cretaceous (Maastrichtian, ca. 70.6-65.5 million years old).

Occurrence: Nemegt Formation, Mongolia

Scoring Sources: The large Polish Academy of Sciences (ZPAL) collection of *Tarbosaurus* was studied firsthand. Additional information was gleaned from Maleev (1974), Hurum and Currie (2000) and Hurum and Sabath (2003).

Remarks: A great amount of material from the Campanian and Maastrichtian of Asia has been referred to *Tarbosaurus* (see Holtz [2004] and the relevant entry in the Paleobiology Database). It is unclear, however, whether this material all belongs to the same species. This is considered unlikely, given the large number of different tyrannosaurid species that populated western North America during the same time interval (e.g., *Albertosaurus*, *Daspletosaurus*, *Gorgosaurus*, *Tyrannosaurus*). It is also likely that some isolated material referred to *Tarbosaurus* may belong to the closely related and sympatric tyrannosaurid *Alioramus* (Brusatte et al. 2009a, 2012a). In the current analysis *Tarbosaurus* was scored solely based on ZPAL specimens and additional material in the PIN (Moscow) described by Maleev (1974). A specimen-level revision of the taxonomy and anatomy of *Tarbosaurus* is needed and it is hoped that this will be the subject of future work.

Tyrannosaurus rex

Age: Late Cretaceous (Maastrichtian, ca. 70.6-65.5 million years old).

Occurrence: Hell Creek Formation, United States and equivalent (or similar) aged formations in the United States and Canada

Scoring Sources: The *Tyrannosaurus* collection at the American Museum of Natural History (e.g., AMNH FARB 5027), FMNH PR2081, and CMNH 7541 were studied firsthand.

Additional information was gleaned from Osborn (1906, 1912, 1917), Molnar (1991), Brochu (2003), Carr and Williamson (2004), and Witmer and Ridgely (2009).

Ornithomimosaurs: Several ornithomimosaurian taxa were studied firsthand whereas others were scored based on the literature and photographs. Because ornithomimosaurs are a primary focus of this dissertation, those ornithomimosaurs that are included as terminal taxa in the cladistic analysis are described separately here.

Pelecanimimus polydon

Age: Early Cretaceous (Late Barremian, ca. 130-125 million years old)

Occurrence: Calizas de La Huérgina Formation, Las Hoyas, Spain

Scoring Sources: The holotype and only known specimen was observed firsthand (LH 7777). Additional information was taken from Perez-Moreno et al. (1994) and Choiniere et al. (2012).

Remarks: Study of the holotype shows that *Pelecanimimus* possesses several characters that are often thought to be diagnostic of other clades, including D-shaped premaxillary teeth (often said to be a feature of tyrannosauroids, e.g., Holtz [2001]), an elongate palatal process of the maxilla (the "secondary palate," also often said to be a feature of tyrannosauroids, e.g., Brusatte et al. [2011]), and fan-shaped neural spines on the dorsal vertebrae (often said to be a feature of compsognathids, e.g. Chiappe and Göhlich 2010). This species is described in only a short publication (Perez-Moreno et al. 1994) and various abstracts. Additional anatomical observations were recently published by Choiniere et al. (2012). As the specimen is currently under further study by Jose Sanz and colleagues in Madrid it will not be discussed further.

Shenzhousaurus orientalis

Age: Early Cretaceous (Barremian-Early Aptian, ca. 125-121 million years old). See Swisher et al. (1999, 2002) and Yang et al. (2007) for information on the age of the Yixian Formation.

Occurrence: Yixian Formation, China

Scoring Sources: The holotype and only known specimen was observed firsthand (NGMC 97-4-002). Additional information was taken from Ji et al. (2003).

Harpymimus okladnikovi

Age: Early Cretaceous (Hauterivian-Barremian, ca. 136-120 million years old). See Kobayashi and Barsbold (2005b) for information on the age of the taxon.

Occurrence: Shinekhudug Formation, Mongolia

Scoring Sources: Kobayashi and Barsbold (2005b)

Garudimimus brevipes

Age: Late Cretaceous (Cenomanian-Turonian, ca. 99.6-89.3 million years old). See Kobayashi and Barsbold (2005a) for information on the age of the taxon.

Occurrence: Bayanshiree Formation, Mongolia

Scoring Sources: Kobayashi and Barsbold (2005a)

Beishanlong grandis

Age: Early Cretaceous (Aptian-Albian, ca. 125-99.6 million years old). See Makovicky et al. (2010) for information on the age of the taxon.

Occurrence: Xinminpu Group, China

Scoring Sources: Makovicky et al. (2010)

Kinnareemimus khonkaenensis

Age: Early Cretaceous (Valanginian-Barremian, ca. 140-125 million years old). See Buffetaut et al. (2009) for information on the age of the taxon.

Occurrence: Sao Khua Formation, Thailand

Scoring Sources: Buffetaut et al. (2009)

Archaeornithomimus asiaticus

Age: Late Cretaceous (Campanian-Maastrichtian, ca. 83.5-65.5 million years old). The Late Cretaceous age for the Iren Dabasu Formation is based on recent work by van Itterbeeck et al. (2005), which contrasts with previous estimates for an older (Cenomanian-Santonian) age.

Occurrence: Iren Dabasu Formation, Inner Mongolia, China

Scoring Sources: The full series of lectotype, paratype, and referred specimens at the American Museum of Natural History were studied firsthand. Additional information was taken from Gilmore (1933) and Smith and Galton (1990).

Anserimimus planinychus

Age: Late Cretaceous (Maastrichtian, ca. 70.6-65.5 million years old). The Maastrichtian age for the Nemegt Formation is based on recent geological reviews of the Mongolian Cretaceous (Dashzeveg et al. 2005; Dingus et al. 2008).

Occurrence: Nemegt Formation, Mongolia

Scoring Sources: Barsbold (1988), Kobayashi and Barsbold (2006)

Sinornithomimus dongi

Age: Late Cretaceous (Turonian, ca. 92 million years old). The Turonian age for the Ulansuhai Formation is based on a radiometric date (see discussion in Kobayashi and Lü [2003], Benson and Xu [2008], and Brusatte et al. [2009]).

Occurrence: Ulansuhai Formation, Inner Mongolia, China

Scoring Sources: Kobayashi and Lü (2003). Original and material and casts were also studied by the author in the Sereno Lab at the University of Chicago before this dissertation project commenced.

Qiupalong henanensis

Age: Late Cretaceous (Campanian-Maastrichtian, ca. 83.5-65.5 million years old). See L. Xu et al. (2011) for information on the age of the taxon.

Occurrence: Qiupa Formation, China

Scoring Sources: L. Xu et al. (2011)

Gallimimus bullatus

Age: Late Cretaceous (Maastrichtian, ca. 70.6-65.5 million years old).

Occurrence: Nemegt Formation, Mongolia

Scoring Sources: The vast Polish Academy of Sciences collection (ZPAL) of *Gallimimus* was studied firsthand, as was an exceptionally preserved skull (IGM 100/1133). Additional information was taken from Osmólska et al. (1972).

Struthiomimus altus

Age: Late Cretaceous (late Campanian-Maastrichtian, ca. 73-65.5 million years old).

Occurrence: Dinosaur Park Formation, Horseshoe Canyon Formation, Canada

Scoring Sources: The American Museum of Natural History collection of *Struthiomimus* specimens was studied firsthand, as was a cast of a well preserved skull (RTMP 90.26.1). Additional information was taken from Russell (1972), Nicholls and Russell (1985), Makovicky and Norell (1998), and Makovicky et al. (2004).

Remarks: There is considerable uncertainty about the alpha level taxonomy of Late Cretaceous ornithomimosaurs from North America, particularly the number of different species among specimens that are commonly referred to as *Struthiomimus*, *Ornithomimus*, and *Dromiceiomimus* (see Makovicky et al. 2004). The likely synonymy of *Ornithomimus* and *Dromiceiomimus* is accepted here, but considerable specimen-level work on North American Late Cretaceous orntihomimosaurs is needed before the systematics of these taxa are resolved. I consider those specimens labeled as *Struthiomimus* in the AMNH collection to belong to this taxon, and consider keystone specimens of *Struthiomimus* and *Ornithomimus* described in publications such as Nicholls and Russell (1985) and Makovicky et al. (2004) to belong to the taxon they are assigned to. I am cognizant, however, that future work may show that some of these assignments are incorrect.

Ornithomimus edmontonicus

Age: Late Cretaceous (late Campanian-Maastrichtian, ca. 73-65.5 million years old).

Occurrence: Dinosaur Park Formation, Horseshoe Canyon Formation, Lance Formation, Canada and United States

Scoring Sources: Russell (1972), Makovicky et al. (2004).

Remarks: See above entry for *Struthiomimus*.

Additional Basal Coelurosaurs: Taxa listed above can be confidently assigned to Tyrannosauroidea and Ornithomimosauria based on possession of clear synapomorphies of these groups, and often these assignments are clear even without the use of cladistic analysis (although they are affirmed here: see below). Many other basal coelurosaurs do not form obvious groupings and their relationships are the subject of particular debate. Because these taxa cannot be easily assigned to higher-level ingroup clades without the use of a phylogenetic analysis, they are listed together here. Note that some of these taxa are often argued to belong to a monophyletic Compsognathidae, but the existence and composition of a potential compsognathid group is here considered an open question that demands testing by phylogenetic analysis.

Bicentenaria argentina

Age: early Late Cretaceous (Cenomanian, ca. 99.6-93.5 million years old).

Occurrence: Candeleros Formation, Argentina

Scoring Sources: Characters were scored based on the published description of Novas et al. (2012) as well as high resolution photographs provided by Christophe Hendrickx.

Coelurus fragilis

Age: Late Jurassic (Kimmeridgian-Tithonian, ca. 156-145.5 million years old). See the Paleobiology Database for information on the age of the taxon.

Occurrence: Morrison Formation, United States

Scoring Sources: The holotype (YPM 2012) was studied firsthand, as were referred specimens considered by Carpenter et al. (2005b) as syntype material (YPM 1991-1993). Additional information was gleaned from Carpenter et al. (2005b).

Remarks: A dentary that is curated at the Yale Peabody Museum with the holotype specimen (YPM 2010) was described by Carpenter et al. (2005b) as possibly belonging to the holotype, due to a similar color and state of preservation. This bone was not originally noted by Marsh (1879) in his description of this taxon and because its provenance is uncertain it is not used to score character data in the current analysis.

Compsognathus longipes

Age: Late Jurassic (late Kimmeridgian-early Tithonian, ca. 153-149 million years old). For information on the age of this taxon see Peyer (2006) and Reisdorf and Wuttke (2012).

Occurrence: Solnhofen Limestone, Germany; Portlandian Limestone, France

Scoring Sources: The holotype German specimen (BSP AS I 563) and the referred French specimen (MNHN CNJ 79) were studied firsthand. Additional information was gleaned from Ostrom (1978), Peyer (2006), and Gishlick and Gauthier (2007).

Huaxiagnathus orientalis

Age: Early Cretaceous (Barremian-Early Aptian, ca. 125-121 million years old).

Occurrence: Yixian Formation, China

Scoring Sources: Hwang et al. (2004)

Juravenator starki

Age: Late Jurassic (latest Kimmeridgian, ca. 153-151 million years old). See Chiappe and Göhlich (2010) for information about the age of the taxon.

Occurrence: Painten Formation, Germany

Scoring Sources: The holotype and only known specimen, JME Sch 200, was studied firsthand. Additional information was gleaned from Göhlich and Chiappe (2006), Göhlich et al. 2006, and Chiappe and Göhlich (2010).

Remarks: The holotype specimen was studied in detail as part of this dissertation project and my notes were passed along to Luis Chiappe and Ursula Göhlich as part of my review of their 2010 monograph of *Juravenator*. Rauhut et al. (2012) have recently raised concerns about the coelurosaurian affinities of *Juravenator*, noting that this taxon groups with the megalosauroid *Sciurumimus* in some versions of their phylogenetic analysis. This is most likely due to the fact that both *Juravenator* and *Sciurumimus* are known from single holotype specimens belonging to very young individuals. *Juravenator* is included in the current analysis, but it is a distinct possibility that future studies may show that this taxon is a non-coelurosaurian tetanuran that groups with coelurosaurs in phylogenetic analyses solely because of its juvenile features. Such a result would not be unexpected if coelurosaurs are paedomorphic versions of more basal, non-coelurosaurian theropods, as argued by Bhullar et al. (2012). In other words, if coelurosaurs are

paedomorphic tetanurans it may be expected that juveniles of non-coelurosaurs group with coelurosaurs in a phylogenetic analysis.

Mirischia asymmetrica

Age: Early Cretaceous (Albian, ca. 112-99.6 million years old).

Occurrence: Santana Formation, Brazil

Scoring Sources: The holotype and only known specimen, SMNK 2349 PAL, was studied firsthand. Additional information was gleaned from Naish et al. (2004).

Remarks: The species name "asymmetrica" refers to the supposedly asymmetric condition of the pelvis, as described by Naish et al. (2004). They noted that the right pubis has a completely enclosed obturator foramen whereas the left bone has an open obturator notch. Similarly, they described the left ischium as bearing an enclosed obturator foramen and the right element as having an open notch. In both cases the "notch" condition is due to the absence of part of the rim of bone surrounding the foramen, which Naish et al. (2004) considered to be a genuine feature of the anatomy. Personal observation of the holotype (SMNK 2349 PAL) reveals that these interpretations are incorrect. The obturator foramen does indeed appear to be reduced to a notch on the left pubis and the right ischium, but in both cases this is an artifact due to breakage of the foramen rim. Breakage on these two bones is confirmed by the presence of broken bone texture on both edges of the supposed notch. Therefore, it is almost certain that an enclosed obturator foramen was present on both left and right pubes and ischia.

Nqwebasaurus thwazi

Age: Early Cretaceous (Berriasian–Valanginian, ca. 145.5-136 million years old). See Choiniere et al. (2012) for information on the age of this taxon.

Occurrence: Kirkwood Formation, South Africa

Scoring Sources: de Klerk et al. (2000), Choiniere et al. (2012).

Remarks: Character scores for earlier TWiG characters were taken directly from Choiniere et al. (2012) and an unpublished database of character scores provided by Jonah Choiniere.

Ornitholestes hermanni

Age: Late Jurassic (Kimmeridgian-Tithonian, ca. 156-145.5 million years old). See the Paleobiology Database for information on the age of the taxon.

Occurrence: Morrison Formation, United States

Scoring Sources: The holotype, AMNH FARB 619, was studied firsthand as part of the dissertation project. Additional information was taken from Osborn (1903, 1916), Carpenter et al. (2005b), and Göhlich and Chiappe (2010).

Remarks: A detailed osteological monograph and systematic revision of *Ornitholestes* will be published at a later date. This project, in collaboration with Mark Norell and Jonah Choiniere, is considered part of the current dissertation project. An isolated specimen of a coelurosaur manus (AMNH FARB 587) was referred to *Ornitholestes hermanni* by Osborn (1903). Carpenter et al. (2005a) argued that this specimen actually belongs to the recently described *Tanycolagreus topwilsoni*, and considered it to be a paratype of this latter species. Although similar to the manus of the *Tanycolagreus* holotype, it is not yet clear whether the two specimens belong to the same taxon. Because of the uncertainty over its identity, AMNH FARB

587 is not used to score any characters in the current analysis, either for *Ornitholestes* or *Tanycolagreus*.

Sinocalliopteryx gigas

Age: Early Cretaceous (Barremian-Early Aptian, ca. 125-121 million years old).

Occurrence: Yixian Formation, China

Scoring Sources: Ji et al. (2007)

Sinosauropteryx prima

Age: Early Cretaceous (Barremian-Early Aptian, ca. 125-121 million years old).

Occurrence: Yixian Formation, China

Scoring Sources: Chen et al. (1998), Currie and Chen (2001). The type specimen, NGMC 2123, was also personally observed.

Tanycolagreus topwilsoni

Age: Late Jurassic (Kimmeridgian-Tithonian, ca. 156-145.5 million years old).

Occurrence: Morrison Formation, United States

Scoring Sources: The holotype, TPII 2000-09-29, was studied firsthand. Additional information was gleaned from Carpenter et al. (2005a).

Remarks: See above remark about AMNH 587, a manus that may belong to either *Ornitholestes* or *Tanycolagreus*. This specimen is not used to score characters for *Tanycolagreus*, nor is a second specimen (UMNH 7821) referred to this taxon by Carpenter et al. (2005a). Only the holotype is used to score *Tanycolagreus* in the current analysis.

Tugulusaurus faciles

Age: Early Cretaceous (?Valanginian-Albian, ca. 140-99.6 million years old). See Rauhut and Xu (2005) for information on the age of this taxon.

Occurrence: Lianmugin Formation, Xinjiang, China

Scoring Sources: The holotype, IVPP V 4025, was studied firsthand. Additional information was gleaned from Rauhut and Xu (2005).

Zuolong salleei

Age: Late Jurassic (early Oxfordian, ca. 161.2-158.7 million years old). See Choiniere et al. (2010b) for information on the age of this taxon.

Occurrence: Shishugou Formation, Xinjiang, China

Scoring Sources: Choiniere et al. (2010b) and high resolution photographs provided by Jonah Choiniere.

Remarks: Character scores for earlier TWiG characters were taken directly from Choiniere et al. (2010b, 2012) and an unpublished database of character scores provided by Jonah Choiniere.

Excluded Taxa: Some basal coelurosaur taxa were excluded from the analysis for various reasons.

Some taxa were excluded because they are represented only by highly immature specimens, and therefore the sub-adult or adult morphologies of these taxa are unknown. It is likely that such immature specimens would not be placed accurately in a phylogenetic analysis,

and thus these taxa were excluded. *Scipionyx* was not included because the holotype and only known specimen is a remarkably young individual, which perhaps died soon after hatchling (Dal Sasso and Signore 1998; Dal Sasso and Maganuco 2011). Similarly, the tyrannosauroid *Raptorex* was excluded because its holotype is also a young individual which probably died within the first five years of life (Sereno et al. 2009). Fowler et al. (2011) recently argued that the holotype of *Raptorex* probably represents a juvenile of a well-known latest Cretaceous tyrannosaurid such as *Tarbosaurus*. This conclusion is not supported here, as the holotype of *Raptorex* can clearly be distinguished from a nearly identically sized specimen of juvenile *Tarbosaurus* (Tsuihiji et al. 2010). For instance, *Raptorex* lacks a midline ridge on the lateral surface of the ilium whereas juvenile *Tarbosaurus*, and all other known tyrannosauroids, possess this feature. The affinities of *Raptorex*, and a more thorough comparison with juvenile *Tarbosaurus*, is in preparation by a team led by Paul Sereno and including the author of this dissertation. Therefore, this issue will not be discussed further here. The pending status of this revision is a major factor in the decision to exclude *Raptorex* from the current analysis, but it is anticipated that *Raptorex* will be re-introduced into future cladistic studies using the current dataset. Note that *Raptorex* was included in the phylogenetic analysis of tyrannosauroids presented by Brusatte et al. (2010) which is part of this dissertation work, and whose characters are included in the current analysis.

Note, however, that a few taxa are included in the analysis even though they are based on young specimens (e.g., *Juravenator* and potentially other compsognathids, *Epidendrosaurus*). All compsognathid taxa are retained because detailed histological data on the ages of the relevant specimens is not yet available. Furthermore, *Juravenator* is retained because it is known from a nearly complete skeleton that can be scored for more characters than nearly any other basal coelurosaur, whereas *Epidendrosaurus* is retained because it is one of the few examples of a

newly discovered and aberrant coelurosaurian subgroup, Scansoriopterygidae, whose phylogenetic placement demands testing in a large-scale analysis. As reported below, however, both *Juravenator* and *Epidendrosaurus* are removed in certain iterations of this analysis to gauge the effect of their inclusion on the results.

Other taxa were excluded because they are known only from highly incomplete remains and/or because they are not described in detail in the literature. These taxa were carefully considered during the initial part of this dissertation work and were excluded when it became clear that they could not be scored for the vast majority of characters in the analysis. Some of these taxa could potentially be included, but were stricken from the analysis because they were not examined firsthand and are the subject of only brief reports in the literature. *Xinjiangovenator* was excluded because it is represented only by fragmentary hindlimb material (tibia and fibula: Rauhut and Xu 2005), whereas *Santanaraptor* (Kellner 1999) and *Yixianosaurus* (Xu and Wang 2003; Dececchi et al. 2012) were excluded because they are known from fragmentary specimens that were not able to be observed firsthand. Finally, the recently described *Yutyrannus* was excluded even though it is known from a reasonably complete specimen (Xu et al. 2012). This decision was made because it has yet to be examined firsthand and the published figures are not adequate for carefully checking the character scores used by the authors in their phylogenetic analysis, which is a variation of the Brusatte et al. (2010) analysis that is part of this dissertation work.

Other taxa are excluded because of serious doubts regarding their coelurosaurian affinities or their taxonomic status. *Aniksosaurus* was not included because it is unclear if it possesses any clear coelurosaurian characters (Martinez and Novas 2006). Material of *Nedcolbertia* was examined firsthand as part of this project (CEUM 5071-5073), but this taxon

was excluded because it is unclear if all of the referred material (which comes from several individuals) belongs to the same taxon. Furthermore, the histological ages of the specimens are uncertain, leaving open the possibility that some or all of them represent very young individuals and/or juveniles of a large-bodied non-coelurosaurian theropod. For more information on this taxon see Kirkland et al. (1998). This material is currently under study as part of this dissertation project and a taxonomic and anatomical revision of *Nedcolbertia* will be published at a later date. *Bagaraatan* was excluded because it is strongly suspected that the holotype material described by Osmólska (1996) is a chimera of tyrannosauroid and non-tyrannosauroid coelurosaurian material, a subject that will be explored in a future paper by Peter Makovicky and others (including the author of this dissertation). This conclusion is tentatively supported by personal observation of some of the holotype material in the Polish Academy of Sciences collection (ZPAL). The tyrannosauroid *Alectrosaurus* is excluded because this taxon is currently under revision by Thomas Carr, and the derived tyrannosaurid *Zhuchengtyrannus* (Hone et al. 2011) is excluded because it is unclear if this taxon, represented only by a few fragmentary skull bones, can be differentiated from *Tarbosaurus*. Finally, note that the Argentine taxon *Orkoraptor*, which appears in many phylogenetic analyses of Coelurosauria, is not included here because recent work convincingly shows that this taxon belongs to the non-coelurosaurian clade Neovenatoridae (Benson et al. 2010a).

CHARACTER SAMPLING AND SCORING

As outlined above, previous versions of the Theropod Working Group (TWiG) matrix have focused predominately on maniraptoran theropods, especially dromaeosaurids, troodontids, and

avialans. A major goal of this dissertation was to expand taxon and character sampling relevant to more basal coelurosaurian theropods such as tyrannosauroids and ornithomimosaurs, so that the TWiG dataset now represents a more-or-less complete coverage of coelurosaurian taxa and characters.

The character list employed here is built upon the most recent published version of the TWiG dataset, which was presented by Turner et al. (2012). The Turner et al. (2012) dataset included 474 characters, among which are characters used in previous TWiG analyses, characters relevant to avialan phylogeny published by Clarke et al. (2006), and new characters outlined by Turner et al. that were gleaned from new research or scrutiny of other published theropod phylogenies. These characters are included in the current dataset. In the current analysis, however, some of these characters have been expanded with the addition of new states or redefined, in order to better account for the full range of morphological variation expressed by coelurosaurs (e.g., so they could be scored in taxa as disparate as tyrannosauroids and basal birds). Some have also been divided into multiple characters, to ensure character independence. For details of these minor modifications, please see Appendix 1. I have also attempted to standardize character statements by subtly rewriting each character so that the relevant bone (or other portion of the anatomy) is listed first, followed by the aspect of that feature that varies among taxa, followed by the category of variation (number, form, etc.), followed by the types of variation (the character states) (Sereno 2007).

In addition to the 474 characters employed by Turner et al. (2012), the current analysis includes an additional 379 characters, resulting in a total of 853 characters. These new characters were compiled from several sources. Most new characters are novel characters stemming from this dissertation project, many of which are relevant to the ingroup relationship of

tyrannosauroids and were published by Brusatte et al. (2010a). Other souces of new characters include recent phylogenetic analyses of basal coelurosaurian subgroups such as ornithomimosaurs (Makovicky et al. 2010; L. Xu et al. 2011), therizinosauroids (Zanno et al. 2009; Zanno 2010b), and alvarezsauroids (Choiniere et al. 2010a,b). The character lists in these analyses were carefully scrutinized and I retained all those characters that were not redundant with current TWiG characters, were understandable, and were consistent with personal observations of specimens. Finally, 27 new characters that were not previously published either by me or by other authors were also included.

The full list of 853 characters is presented in Appendix 1. Characters used by Turner et al. (2012) are listed first, followed by a handful of new characters created when original TWiG characters were divided into two or more characters, and then followed by the characters added to the TWiG dataset in this dissertation. Among these new characters, those presented by Brusatte et al. (2010a) are listed first, followed by those added from other published datasets, and finally followed by the 27 characters completely new to this dissertation manuscript. Note that several characters (142 in total) are treated as ordered because they describe numerical transformational sequences (e.g. two vertebrae-three vertebrae-four vertebrae), nested sets of homologies (e.g., small process, medium process, large process), or combine presence/absence and transformational data (e.g., process absent, process small, process large). These decisions were based upon prior TWiG usage and the recent proposals of Sereno (2007) and Brazeau (2011). Each multistate character is denoted as either ordered or unordered in Appendix 1.

DESCRIPTIONS OF NEW CHARACTERS

The numerous new characters employed here were formulated to describe anatomical variation in basal coelurosaurian taxa such as tyrannosauroids, ornithomimosaurs, "compsognathids," and singleton genera of uncertain affinities (e.g., *Bicentenaria*, *Coelurus*, *Mirischia*, *Nqwebasaurus*, *Ornitholestes*, *Tanycolagreus*, *Tugulusaurus*, *Zuolong*). Most of these characters are relevant to the interrelationships of tyrannosauroids and were originally published by Brusatte et al. (2010a), a paper that stemmed from this dissertation project. Many other characters are new to this dissertation and are used in a cladistic analysis for the first time here. In this section I describe all characters new to this dissertation project, including those characters employed by Brusatte et al. (2010a) that were not previously used before the publication of that analysis. Note that I do not describe here those characters employed by Brusatte et al. (2010a) that originally appeared in earlier published analyses of tyrannosauroid phylogeny (e.g., Holtz 2001, 2004; Currie et al. 2003; Carr et al. 2005; Sereno et al. 2009; Carr and Williamson 2010). Character numbering in this section follows numbering in the full list of characters used in the present analysis (Appendix 1).

478. Skull, anteroposterior length: less than (0) or greater than (1) 40% trunk length**.**

This character was inspired by discussion in the supplementary information of Sereno et al. (2009) and first utilized as character 3 in Brusatte et al. (2010a). Skull length is measured from the anterior end of the premaxilla to the posterior end of the quadrate condyle or quadratojugal, whichever is further posteriorly when the skull is visible in lateral view. Trunk length is measured from the anterior extremity of the pectoral girdle (usually the anterior edge of the coracoid) to the posterior extremity of the pelvic girdle (usually the posterior edge of the iliac postacetabular process or the ischium). Sereno et al. (2009) noted that coelurosaurian outgroups,

some basal coelurosaurs (*Ornitholestes*), and basal tyrannosauroids (*Guanlong*) have a skull that is less than 40% of the length of the trunk, whereas more derived tyrannosauroids such as *Albertosaurus* and *Tyrannosaurus* possess a proportionally larger skull that is greater than 40% of the trunk length. We here score a suite of derived tyrannosauroids, including tyrannosaurids (e.g., Brochu 2003; Brusatte et al. 2012a) and non-tyrannosaurid taxa such as *Xiongguanlong* (Li et al. 2010) and *Appalachiosaurus* (Carr et al. 2005), for state 1. We also note that state 1 is present in a handful of more derived coelurosaurs, including dromaeosaurids (e.g., *Bambiraptor*: Burnham et al. 2000; *Tianyuraptor*: Zheng et al. 2010) and troodontids (e.g., *Anchiornis*: Hu et al. 2009; *Mei*: Xu and Norell 2004). State 1 is also present in several compsognathids (*Huaxiagnathus*: Hwang et al. 2004; *Juravenator*: Chiappe and Göhlich 2010; *Sinocalliopteryx*: Ji et al. 2007; *Sinosauropteryx*: Currie and Chen 2001), but not in *Compsognathus* itself (Peyer 2006).

479. Lateral temporal fenestra, orientation of long axis relative to long axis of orbit: posterodorsal (0) or approximately parallel (1).

In coelurosaurian outgroups such as *Allosaurus* (Madsen 1976) and most coelurosaurian taxa, the long axis of the lateral temporal fenestra is oriented obliquely relative to the long axis of the orbit. In most such taxa, the long axis of the orbit is approximately dorsoventrally oriented whereas that of the lateral temporal fenestra is posterodorsally-anteroventrally oriented. This condition is seen in taxa such as dromaeosaurids (e.g., *Tsaagan*: Norell et al. 2006), troodontids (e.g., *Saurornitholestes*: Norell et al. 2009), therizinosauroids (e.g., *Erlikosaurus*: Clark et al. 1994), derived alvarezsauroids (e.g., *Shuvuuia*: Chiappe et al. 1998), ornithomimosaurs (e.g., *Gallimimus*: Osmólska et al. 1972), and basal tyrannosauroids such as *Dilong* (Xu et al. 2004),

Guanlong (Xu et al. 2006), *Proceratosaurus* (Rauhut et al. 2010), and *Xiongguanlong* (Li et al. 2010). In some taxa, however, the long axes of the orbit and lateral temporal fenestra are approximately parallel, and in most of these cases both long axes are oriented approximately dorsoventrally. This condition is seen in oviraptorosaurs (e.g., *Citipati*: Clark et al. 1999), the basal alvarezsauroid *Haplocheirus* (Choiniere et al. 2010a), *Compsognathus* (Peyer 2006), *Juravenator* (Chiappe and Göhlich 2010), *Ornitholestes* (AMNH FARB 619), and derived tyrannosauroids such as *Bistahieversor* (Carr and Williamson 2010), *Gorgosaurus* (Currie 2003), *Alioramus* (Brusatte et al. 2012a), and *Tyrannosaurus* (Brochu 2003).

This character was first used by Brusatte et al. (2010a, character 5). States 0 and 1 are illustrated in Figure 2-2.

483. Premaxilla: form of narial fossa ventral to external naris: shallowly excavated (0) or deeply excavated, with the anterior margin invaginated as a deep groove (1).

Most theropods have a smooth fossa surrounding the external naris, which usually excavates part of the lateral surface of the premaxilla, as well as adjoining regions of the nasal and, in some cases, the maxilla. In the vast majority of theropods this fossa is shallowly excavated and its anterior margin merges smoothly and gradually with the subcutaneous surface of the premaxilla. This condition is seen in coelurosaurian outgroups such as *Allosaurus* (Madsen 1976; UMNH 5427), as well as most coelurosaurian ingroup taxa (e.g., *Byronosaurus*: Makovicky et al. 2003; *Citipati*: Clark et al. 1999; *Garudimimus*: Kobayashi and Barsbold 2005a; *Huaxiagnathus*: Hwang et al. 2004; *Ornitholestes*: AMNH FARB 619; *Shuvuuia*: Chiappe et al. 1998; *Tsaagan*: Norell et al. 2006; *Tyrannosaurus*: Brochu 2003; *Zuolong*: Choiniere et al. 2010b). In some taxa, however, the narial fossa is deeply embayed and its

anterior margin is invaginated as a sharp groove, which is distinctly offset from the subcutaneous surface of the premaxilla. This condition is seen in the basal tyrannosauroids *Guanlong* (IVPP V14531; Xu et al. 2006), *Kileskus* (Averianov et al. 2010), *Proceratosaurus* (NHMUK R4860; Rauhut et al. 2010), and *Sinotyrannus* (Ji et al. 2009). It is also present in the basal coelurosaurs *Compsognathus* (Peyer 2006) and *Tanycolagreus* (TPII 2000-09-29), as well as the ornithomimosaur *Sinornithomimus* (Kobayashi and Lü 2003), the therizinosauroid *Erlikosaurus* (Clark et al. 1994), and the troodontid *Xixiasaurus* (Lü et al. 2010).

This character was first used by Brusatte et al. (2010a, character 11). States 0 and 1 are illustrated in Figure 2.3.

484. Premaxilla: extent of narial fossa: limited to region immediately ventral to external naris (0) or extensive, covering most of the main body of the premaxilla (1).

The narial fossa of most theropods is limited to the region of the lateral surface of the premaxilla immediately adjacent to the external naris. Usually, in taxa possessing this condition, the fossa is a narrow band immediately ventral to the external naris or a small pocket at the anteroventral corner of the naris. This condition is present in coelurosaurian outgroups such as Allosaurus (Madsen 1976) and nearly all coelurosaurs, with the exception of the basal ornithomimosaur *Pelecanimimus* (LH 7777) and the basal tyrannosauroids *Guanlong* (IVPP V14531; Xu et al. 2006), *Kileskus* (Averianov et al. 2010), and *Proceratosaurus* (NHMUK R4860; Rauhut et al. 2010). In these latter taxa the narial fossa is extensive and covers nearly the entire lateral surface of the main body of the premaxilla. This character is not redundant with character 483 above, referring to a deeply excavated fossa invaginated anteriorly as a groove, because *Pelecanimimus* possesses an extensive but shallowly excavated fossa (state 0 for

character 483 and state 1 for character 484), whereas the basal coelurosaurs *Compsognathus* and *Tanycolagreus* possess deeply excavated fossae that are restricted to the region of the premaxilla immediately ventral to the naris (state 1 for character 483 and state 0 for character 484). This character was first used by Brusatte et al. (2010a, character 12). States 0 and 1 are illustrated in Figure 2.3.

485. Premaxilla: orientation and shape of anterior margin: smoothly curved and projecting posterodorsally, angle between ventral margin of premaxilla and anterior margin is less than 90 degrees (0); smoothly curved and projecting vertically or slightly anterodorsally, angle between ventral margin of premaxilla and anterior margin is equal to or greater than 90 degrees (1); projecting vertically or slightly anterodorsally, with a discrete inflection point between a more vertical ventral portion and a more horizontal dorsal portion (2).

Most theropods possess a premaxilla in which the anterior margin is both smoothly curved and projects posterodorsally relative to the ventral (alveolar) margin. In other words, the anterior and ventral margins are separated by an acute angle at the anteroventral corner of the premaxilla. This condition is seen in coelurosaurian outgroups such as *Allosaurus* (Madsen 1976) as well as most coelurosaurian taxa (e.g., *Compsognathus*: Peyer 2006; *Erlikosaurus*: Clark et al. 1994; *Gallimimus*: Osmólska et al. 1972; *Incisivosaurus*: Balanoff et al. 2009; *Shuvuuia*: Chiappe et al. 1998; *Sinornithosaurus*: Xu and Wu 2001; *Zanabazar*: Norell et al. 2009). In contrast, some coelurosaurs have a nearly vertical anterior margin of the premaxilla, which forms a right angle, or in some cases a slightly obtuse angle, with the ventral margin of the bone. This condition is seen in all tyrannosauroids, including basal taxa such as *Guanlong* (Xu et al. 2006), "intermediate" taxa such as *Eotyrannus* (MIWG 1997.550), and derived genera such as

Tyrannosaurus (Brochu 2003). It is also present in some dromaeosaurids (e.g., *Deinonychus*: Ostrom 1969; *Velociraptor*: Barsbold and Osmólska 1999), derived oviraptorosaurs (e.g., *Citipati*: Clark et al. 1999), the basal alvarezsauroid *Haplocheirus* (Choiniere et al. 2010a), and the basal coelurosaur *Sinocalliopteryx* (Ji et al. 2007).

Among those taxa with a vertical anterior margin, two distinct conditions are present. Most of these taxa have a smooth anterior margin of the premaxilla; this condition is seen, for example, in the aforementioned dromaeosaurids, oviraptorosaurs, *Haplocheirus*, *Sinocalliopteyx*, and most tyrannosauroids (e.g., *Albertosaurus*, *Eotyrannus*, *Xiongguanlong*, *Tyrannosaurus*). Some basal tyrannosauroids, on the other hand, possess a distinct condition in which the anterior and vertical margins of the premaxilla are separated from each other by a right or obtuse angle at the anteroventral corner of the premaxilla, but only the ventral portion of the anterior margin of the premaxilla is vertical. This vertical portion is separated from a more horizontally-oriented dorsal portion of the anterior margin by a distinct inflection point. This morphology is present in *Dilong* (IVPP V14243), *Guanlong* (IVPP V14531; Xu et al. 2006), *Kileskus* (Averianov et al. 2010), *Proceratosaurus* (NHMUK R4860; Rauhut et al. 2010), and *Sinotyrannus* (Ji et al. 2009). Because this morphology is a special condition of state 1, this character is treated here as an ordered multistate.

This character is an expanded version of character 13 in Brusatte et al. (2010a). The original Brusatte et al. (2010a) character was a binary character that distinguished a smoothly curved anterior margin of the premaxilla (original state 0) from one that has an inflection point separating a nearly vertical ventral portion from a nearly horizontal dorsal portion (original state 1). Thus, the character as worded in this dissertation separates the original state 0 into states referring to a posterodorsally inclined and smoothly curved anterior margin of the premaxilla

(state 0 here) and a vertically inclined and smoothly curved anterior margin of the premaxilla (state 1 here). State 2 here is equivalent to the original state 1 in Brusatte et al. (2010a). States 0 and 2 are illustrated in Figure 2.3.

486. Premaxilla: position of palatal process: immediately above interdental plates (0) or separated from interdental plates by deep lingual surface of premaxilla (1).

The palatal process on the medial surface of the premaxilla, which articulates with the opposite premaxilla and in some cases the vomer, is positioned immediately above the interdental plates in many coelurosaurs (e.g., *Compsognathus*: Peyer 2006; *Dromaeosaurus*: Currie 1995; *Garudimimus*: Kobayashi and Barsbold 2005a; *Ornitholestes*: AMNH FARB 619; *Sinocalliopteryx*: Ji et al. 2007; *Sinornithosaurus*: Xu and Wu 2001; *Tanycolagreus*: TPII 2000-09-29; *Zuolong*: Choiniere et al. 2010b). This is also the condition in the basal tyrannosauroids *Eotyrannus* (MIWG 1997.550), *Guanlong* (IVPP V14531), *Kileskus* (Averianov et al. 2010), as well as the more derived taxa *Albertosaurus*, *Bistahieversor*, and *Gorgosaurus* (Currie 2003; T.D. Carr, pers. comm.). The derived tyrannosaurine tyrannosaurids *Daspletosaurus*, *Tarbosaurus*, and *Tyrannosaurus* possess a distinct condition in which the palatal process is elevated above the interdental plates, such that there is a deep region of the medial surface of the maxilla between them (e.g., ZPAL MgD-I/75; T.D. Carr, pers. comm.). Both conditions are seen among outgroup taxa, as *Sinraptor* possesses state 0 (Currie and Zhao 1993) and *Allosaurus* state 1 (Madsen 1976). Unfortunately, this condition is difficult to score in many coelurosaurian taxa, because the medial surface of the premaxilla is rarely visible in articulated skulls and slab specimens.

This character was first used by Brusatte et al. (2010a, character 14). States 0 and 1 are illustrated in Figure 2.4.

487. Maxilla, promaxillary fenestra, position: anterior margin of antorbital fossa (0); extreme anteroventral corner of antorbital fossa (1).

Most coelurosaurs possess a promaxillary fenestra, an opening in the external surface of the maxilla which leads into an internal sinus (Witmer 1997). The promaxillary fenestra is usually located near the anterior margin of the antorbital fossa but elevated above the ventral margin of the fossa. This condition is seen in the coelurosaurian outgroup *Sinraptor* (Currie and Zhao 1993), as well as many coelurosaurian ingroup taxa (e.g., *Anchiornis*: Hu et al. 2009; *Garudimimus*: Kobayashi and Barsbold 2005a; *Juravenator*: Chiappe and Göhlich 2010); *Ornitholestes*: AMNH FARB 619; *Sinornithosaurus*: Xu and Wu 2001; *Tyrannosaurus*: Brochu 2003; *Zuolong*: Choiniere et al. 2010b). In some taxa, on the other hand, the promaxillary fenestra is located at the extreme anteroventral corner of the antorbital fossa. This is the condition in several basal tyrannosauroids, including *Dilong* (IVPP V14243), *Eotyrannus* (MIWG 1997.550), *Guanlong* (IVPP V14531), *Kileskus* (Averianov et al. 2010), *Proceratosaurus* (NHMUK R4860; Rauhut et al. 2010), and *Sinotyrannus* (Ji et al. 2009). This state is also present in some dromaeosaurids (e.g., *Deinonychus*: Ostrom 1969; *Tsaagan*: Norell et al. 2006; *Velociraptor*: Barsbold and Osmólska 1999), as well as the coelurosaurian outgroup *Allosaurus* (Madsen 1976).

This character was originally used by Brusatte et al. (2010a, character 16). States 0 and 1 are illustrated in Figure 2.5.

489. Maxilla, maxillary fenestra, position within maxillary antrum: does not (0) or does (1) abut dorsal border of antrum in medial view.

The maxillary fenestra of theropods leads internally into a sinus called the maxillary antrum (Witmer 1997). The dimensions and shape of the maxillary antrum are often visible on the medial surface of the maxilla, and in poorly preserved specimens the size and shape of the antrum can be reconstructed from broken bone surfaces. In the coelurosaurian outgroups *Allosaurus* (Madsen 1976) and *Sinraptor* (Currie and Zhao 1993) the maxillary fenestra is centered within the maxillary antrum. In other words, when the maxillae of these taxa are observed in medial view, the maxillary fenestra does not abut, or even closely approach, the dorsal bounding wall of the antrum. This condition is also present in several tyrannosauroids, such as *Albertosaurus*, *Appalachiosaurus*, *Daspletosaurus*, and *Gorgosaurus* (Carr et al. 2005; T. D. Carr, pers. comm.). The tyrannosaurine tyrannosaurids *Alioramus* (Brusatte et al. 2012), *Tarbosaurus* (Hurum and Sabath 2003), and *Tyrannosaurus* (Molnar 1991) possess a distinct condition in which the maxillary fenestra is dorsally placed within the antrum, such that the dorsal edge of the fenestra abuts the dorsal border of the antrum in medial view. This character state is not illustrated here, but can be seen in figures 8 and 9 in Brusatte et al. (2012a). Unfortunately, this character is difficult to score in most coelurosaurs because the medial surface of the maxilla is either not visible (due to the articulation of bones or because the specimen is preserved on a slab). State 0, however, is clearly present in *Nqwebasaurus* (Choiniere et al. 2012), *Ornitholestes* (AMNH FARB 619), and *Zuolong* (Choiniere et al. 2010b). This character was first used by Brusatte et al. (2010a, character 20).

498. Maxilla, anterior ramus, absent (0) or present (1).

The maxillae of many non-coelurosaurian theropods are marked by a discrete anterior ramus, which is offset from the ascending ramus by a concave step on the anterior margin of the maxilla. This condition is typified by the coelurosaurian outgroup *Allosaurus* (Madsen 1976), and many other allosauroids, megalosauroids, and non-coelurosaurian theropods exhibit a maxillary anterior ramus (e.g., Sereno et al. 1996; Benson 2010; Benson et al. 2010a). The possession of an anterior ramus, however, is much rarer among coelurosaurs. It is absent in most taxa, including dromaeosaurids (e.g., *Deinonychus*: Ostrom 1969), oviraptorosaurs (e.g., *Incisivosaurus*: Balanoff et al. 2009; *Citipati*: Clark et al. 1999), therizinosauroids (e.g., *Falcarius*: Zanno 2010a; *Erlikosaurus*: Clark et al. 1994), alvarezsauroids (e.g., *Haplocheirus*: Choiniere et al. 2010a; *Shuvuuia*: Chiappe et al. 1998), ornithomimosaurs (e.g., *Pelecanimimus*: LH 7777; *Gallimimus*: Osmólska et al. 1972), most tyrannosauroids (e.g., *Dilong*: Xu et al. 2004; *Alioramus*: Brusatte et al. 2012a; *Tyrannosaurus*: Brochu 2003), and the singleton genera *Ornitholestes* (AMNH FARB 619) and *Zuolong* (Choiniere et al. 2010b). A distinct anterior ramus is present, however, in a handful of basal tyrannosauroids (*Guanlong*: Xu et al. 2006; *Proceratosaurus*: Rauhut et al. 2010; *Sinotyrannus*: Ji et al. 2009), compsognathids (*Compsognathus*: Peyer 2006; *Huaxiagnathus*; Hwang et al. 2004; *Juravenator*: Chiappe and Göhlich 2010; *Sinosauropteryx*: Currie and Chen 2001), and several troodontids (e.g., *Mei*: Xu and Norell 2004; *Zanabazar*: Norell et al. 2009).

This character was originally used by Brusatte et al. (2010a, character 30), and is also often used in phylogenetic analyses of non-coelurosaurian theropods (e.g., Sereno et al. 1996; Benson 2010; Benson et al. 2010a). States 0 and 1 are illustrated in Figure 2.5.

500. Maxilla, form of external subcutaneous surface texturing: random foramina and shallow grooves and ridges (0); deep, prominent, dorsoventrally trending grooves and ridges (1).

The external (lateral) surface of the maxillae of most theropods is ornamented with a variety of foramina, grooves, ridges, and tubercles, but in almost all taxa the degree of external texturing is subtle. Among coelurosaurs and close outgroups, only the derived tyrannosaurine tyrannosaurids *Daspletosaurus* (Currie 2003), *Tarbosaurus* (Hurum and Sabath 2003), and *Tyrannosaurus* (Molnar 1991; Brochu 2003) possess an extreme degree of texturing characterized by especially deep grooves and prominent ridges, which are generally aligned in a regular dorsoventral orientation. This character was first utilized by Brusatte et al. (2010a, character 32) and the derived condition (state 1) is figured well by Molnar (1991), Brochu (2003), and Hurum and Sabath (2003).

501. Maxilla, swollen rim separating antorbital fossa and subcutaneous surface: present (0); absent (1).

In most theropods the smooth and inset antorbital fossa is separated from the textured subcutaneous surface of the lateral maxilla by a discrete rim, which variably takes the form of a sharp ridge, a convex shelf, or a subtle but distinct change in surface relief. This condition is present in coelurosaurian outgroups such as *Allosaurus* (Madsen 1976) and *Sinraptor* (Currie and Zhao 1993), as well as many coelurosaurs (e.g., *Citipati*: Clark et al. 1999; *Compsognathus*: Peyer 2006; *Deinonychus*: Ostrom 1969; *Erlikosaurus*: Clark et al. 1994; *Falcarius*: Zanno 2010a; *Guanlong*: IVPP V14531; *Huaxiagnathus*: Hwang et al. 2004; *Ornitholestes*: AMNH FARB 619; *Pelecanimimus*: LH 7777; *Shenzhousaurus*: Ji et al. 2003; *Shuvuuia*: Chiappe et al. 1998; *Sinornithosaurus*: Xu and Wu 2001; *Zuolong*: Choiniere et al. 2010b).

Some coelurosaurs, however, do not exhibit a rim, ridge, shelf, or other discrete separation between the antorbital fossa and the subcutaneous surface. Instead, in these taxa the fossa and subcutaneous surface gradually and subtly merge into each other. This condition is seen in several tyrannosauroids, including *Eotyrannus* (MIWG 1997.550), *Xiongguanlong* (Li et al. 2010), *Appalachiosaurus* (Carr et al. 2005), and tyrannosaurids (e.g., *Alioramus*: Brusatte et al. 2012a; *Gorgosaurus*: Currie 2003; *Tyrannosaurus*: Brochu 2003). Note that some specimens of juvenile tyrannosaurids, as well as non-tyrannosaurids such as *Appalachiosaurus*, have a subtle rim separating the fossa and subcutaneous surface, but this is treated as equivalent to state 1 because this rim is much less pronounced than the distinct rim in outgroups and most coelurosaurs (e.g., Brusatte et al. 2012a; Carr et al. 2005). An absent rim is also seen in some dromaeosaurids (*Austroraptor*: MML 195, Novas et al. 2009; *Buitreraptor*: MPCA 245, Makovicky et al. 2005), troodontids (e.g., *Byronosaurus*: Makovicky et al. 2003; *Zanabazar*: Norell et al. 2009), the basal alvarezsauroid *Haplocheirus* (IVPP V15988; Choiniere et al. 2010a), and derived ornithomimosaurs (e.g., *Garudimimus*: Kobayashi and Barsbold 2005a; *Sinornithomimus*: Kobayashi and Lü 2003).

This character was first used by Brusatte et al. (2010a, character 33). States 0 and 1 are illustrated in Figure 2.5.

502. Maxilla, size of ascending ramus, anteroposterior chord directly above maxillary fenestra: greater than 1.75 times (0) or less than 1.60 times (1) dorsoventral depth of maxilla below anterior edge of antorbital fenestra

This character quantifies the relative size of the ascending ramus of the maxilla, using a comparison between the anteroposterior width of the ascending ramus and the depth of the main

body of the maxilla. In essence, it distinguishes taxa with large (state 0) and small (state 1) ascending rami, or put another way, taxa with anteroposteriorly thick (state 0) and thin (state 1) rami. The outgroups *Allosaurus* and *Sinraptor* possess small/thin rami (state 1), as does the basal coelurosaur *Zuolong* (Choiniere et al. 2010b) and derived tyrannosauroids (e.g., *Alioramus*: Brusatte et al. 2009a, 2012a; *Appalachiosaurus*: Carr et al. 2005; *Gorgosaurus*: Currie 2003; *Tarbosaurus*: Hurum and Sabath 2003; *Tyrannosaurus*: Brochu 2003). The basal tyrannosauroids *Dilong* (Xu et al. 2004), *Guanlong* (Xu et al. 2006), *Kileskus* (Averianov et al. 2010), and *Proceratosaurus* (Rauhut et al. 2010) possess large/thick ascending rami (state 0), as does every other coelurosaur that can be affirmatively scored for the dataset.

Although the landmarks utilized in this character may appear convoluted or complicated, they present the most straightforward means for quantifying the relative size of the anterior ramus, instead of relying on vague terms such as "large" or "small", or "thick" or "thin". Note that the "anteroposterior chord" measurement of the ascending ramus is the anteroposterior measurement of the thickness of the ramus, in lateral view, immediately above the maxillary fenestra. If a maxillary fenestra is not present then this measurement is taken at the midpoint of the ascending ramus, and if a fenestra of uncertain homology is present the measurement is taken at the dorsal margin of this fenestra (e.g., in oviraptorosaurs such as *Citipati*: Clark et al. 1999). This character was first utilized by Brusatte et al. (2010a, character 34).

503. Maxilla, posterior region of the main body (portion including the final 3-5 teeth and anterior to the jugal process), shape: maintains a relatively constant dorsoventral depth (0) or tapers in depth posteriorly (1).

The main body of the maxilla is that portion of the bone beneath the antorbital fenestra that includes most of the tooth row. Two general shapes of the main body are present in coelurosaurs: this portion of the bone either maintains a nearly constant dorsoventral depth across most of its length (state 0) or gradually decreases in depth by tapering posteriorly (1). Note that even in taxa with state 0 there is often a distinct jugal process at the posterior end of the maxilla that usually tapers, but this character refers solely to the shape of the main body and not the jugal process. Therefore, some taxa scored for state 0 may appear to possess maxillae that taper posteriorly, but in these cases the taper is caused solely by the jugal process while the main body itself maintains a constant depth.

The outgroups *Allosaurus* and *Sinraptor* possess state 1 (Madsen 1976; Currie and Zhao 1993), as do several derived tyrannosauroids (e.g., *Alioramus*: Brusatte et al. 2012a; *Appalachiosaurus*: Carr et al. 2005; *Gorgosaurus*: Currie 2003; *Tyrannosaurus*: Brochu 2003), some dromaeosaurids (e.g., *Tsaagan*: Norell et al. 2006; *Velociraptor*: Osmólska and Barsbold 1999), the troodontid *Anchiornis* (Hu et al. 2009), and derived oviraptorosaurs (e.g., *Caudipteryx*: Ji et al. 1998; *Citipati*: Clark et al. 1999). All other coelurosaurs that can be scored affirmatively possess a tapering main body, including other troodontids (e.g., *Zanabazar*: Norell et al. 2009), the basal oviraptorosaur *Incisivosaurus* (Xu et al. 2002a; Balanoff et al. 2009), several dromaeosaurids (e.g., *Dromaeosaurus*: Currie 1995; *Sinornithosaurus*: Xu and Wu 2001; *Shanag*: Turner et al. 2007b), therizinosauroids (e.g., *Falcarius*: Zanno 2010a; *Erlikosaurus*: Clark et al. 1994), alvarezsauroids (e.g., *Haplocheirus*: Choiniere et al. 2010a; *Shuvuuia*: Chiappe et al. 1998), ornithomimosaurs (e.g., *Gallimimus*: Osmólska et al. 1972; *Garudimimus*: Kobayashi and Barsbold 2005a), compsognathids (e.g., *Compsognathus*: Peyer 2006; *Huaxiagnathus*: Hwang et al. 2004), basal tyrannosauroids (e.g., *Dilong*: Xu et al. 2004;

Guanlong: Xu et al. 2006), and the singleton genera *Ornitholestes* (AMNH FARB 619) and *Zuolong* (Choiniere et al. 2010b).

This character was originally used by Brusatte et al. (2010a, character 35). States 0 and 1 are illustrated in Figure 2.5.

504. Maxilla, primary row of neurovascular foramina, form: continues as a row posteriorly (0) or transitions posteriorly into a sharp groove, paralleling the antorbital fossa rim (1).

Most coelurosaurs possess numerous neurovascular foramina on the lateral surface of the maxilla, which would have allowed for the passage of nerves and blood vessels to the overlying skin and muscles. Although many of these foramina are seemingly randomly oriented, most species possess a primary row of foramina that parallels the ventral (alveolar) margin of the maxilla and is located directly above the tooth row (the degree of separation between the teeth and and the primary row of foramina ranges from only a few millimeters to a centimeter or more). The foramina in this primary row are arranged in an orderly sequence and are often larger than many of the remaining foramina on the lateral surface of the maxilla, and in some cases there is an orderly number of one or two foramina per tooth alveolus.

In most taxa the primary row of foramina is simply an orderly sequence of foramina, which may be set into a shallow groove. This condition is present in the coelurosaurian outgroups *Allosaurus* (Madsen 1976) and *Sinraptor* (Currie and Zhao 1993), as well as nearly all coelurosaurian ingroup taxa (e.g., *Compsognathus*: Peyer 2006; *Dilong*: Xu et al. 2004; *Dromaeosaurus*: Currie 1995; *Falcarius*: Zanno 2010a; *Garudimimus*: Kobayashi and Barsbold 2005a; *Ornitholestes*: AMNH FARB 619; *Shuvuuia*: Chiappe et al. 1998; *Tyrannosaurus*: Brochu 2003; *Zanabazar*: Norell et al. 2009; *Zuolong*: Choiniere et al. 2010b). The basal

tyrannosauroids *Guanlong* (IVPP V14532) and *Proceratosaurus* (NHMUK R4860) possess a different condition in which the primary row is expressed as a series of discrete foramina anteriorly on the maxilla but then transitions into a deep, sharp groove underneath the antorbital fenestra. This groove parallels the rim of the fenestra, and discrete foramina are not visible within the groove.

This character was originally used by Brusatte et al. (2010a, character 36). States 0 and 1 are illustrated in Figure 2.5, and a closeup of state 1 is shown in *Proceratosaurus* in Figure 2.6.

505. Maxilla, extent of antorbital fossa on the main body: covers more (0) or less (1) than half of the depth of the main body of the maxilla beneath the anterior margin of the antorbital fenestra.

In most theropods there is a band of smooth fossa underneath the antorbital fenestra along the main body of the maxilla. In the outgroups *Allosaurus* (Madsen 1976) and *Sinraptor* (Currie and Zhao 1993) this band of fossa is deep, and it covers more than half of the dorsoventral depth of the main body immediately underneath the anterior edge of the antorbital fenestra. This condition is also seen in basal coelurosaurs such as *Ornitholestes* (AMNH FARB 619) and *Zuolong* (Choiniere et al. 2010b), basal tyrannosauroids (e.g., *Dilong*: Xu et al. 2004; *Guanlong*: Xu et al. 2006; *Proceratosaurus*: Rauhut et al. 2010; *Xiongguanlong*: Li et al. 2010), compsognathids (e.g., *Compsognathus*: Peyer 2006; *Huaxiagnathus*: Hwang et al. 2004), ornithomimosaurs (e.g., *Gallimimus*: Osmóolska et al. 1972; *Pelecanimimus*: LH 7777), alvarezsauroids (e.g., *Haplocheirus*: Choiniere et al. 2010a), basal oviraptorosaurs (e.g., *Caudipteryx*: Ji et al. 1998; *Incisivosaurus*: Xu et al. 2002a, Balanoff et al. 2009), and some troodontids and dromaeosaurids (e.g., *Anchiornis*: Hu et al. 2009; *Sinornithosaurus*: Xu and Wu 2001).

Many other coelurosaurs, however, exhibit a different condition in which the band of antorbital fossa underneath the antorbital fenestra is reduced. In these taxa, the dorsoventral depth of the fossa underneath the anterior edge of the antorbital fenestra is less than half of the dorsoventral height of the entire main body. This condition is seen in derived tyrannosauroids such as *Alioramus* (Brusatte et al. 2009a, 2012a), *Appalachiosaurus* (Carr et al. 2005), *Gorgosaurus* (Currie 2003), *Tarbosaurus* (Hurum and Sabath 2003), and *Tyrannosaurus* (Molnar 1991; Brochu 2003). It is also present in therizinosauroids (e.g., *Falcarius*: Zanno 2010a; *Erlikosaurus*: Clark et al. 1994), derived oviraptorosaurs (e.g., *Citipati*: Clark et al. 1999), most troodontids (e.g. *Byronosaurus*: Makovicky et al. 2003; *Zanabazar*: Norell et al. 2009), and most dromaeosaurids (e.g., *Austroraptor*: Novas et al. 2009; *Tsaagan*: Norell et al. 2006; *Velociraptor*: Barsbold and Osmólska 1999).

The distinction between these two conditions was first formulated as a character by Brusatte et al. (2010a, character 37). States 0 and 1 are illustrated in Figure 2.5.

512. Nasal, thin, low, and laterally projecting crest at the corner where lateral and dorsal surfaces meet: absent (0) or present (1).

Xu et al. (2004) described a "Y-shaped crest formed by the nasals and lacrimals" as an autapomorphy of *Dilong*, based on the presence of this unusual feature in the holotype skull (IVPP V14243). This feature is visible in both lateral and dorsal views and is well illustrated by Xu et al. (2004: figure 1). In lateral view, the crest appears as a sharp and pronounced rim along the dorsal surface of the skull, beginning on the nasal posterior to the external naris and continuing onto the lacrimal. In dorsal view, the crest appears as a Y-shaped structure, as it begins anteriorly as a single midline ridge on the nasal and then bifurcates posteriorly (beginning

at the level of the anterior margin of the antorbital fenestra) into separate crests that parallel the left and right lateral sides of the skull. Between the left and right crests, on the dorsal surface of the nasal, is a noticeable fossa. A similar condition is present in *Eotyrannus*, in which the dorsal surface of the bone is excavated by a deep fossa whose lateral margins are formed by ridges (MIWG 1997.550). These ridges are not as pronounced as in *Dilong*, and they are not visible in lateral view but only in dorsal view. Regardless, we hypothesize primary homology between the ridges of both taxa due to their similar position along the edges of the skull and the fact that they enclose a midline fossa. Under this interpretation, the especially pronounced crest of *Dilong*, which is visible in lateral view as well as dorsal view, is an autapomorphy of that taxon. The coelurosaur outgroups *Allosaurus* (Madsen 1976) and *Sinraptor* (Currie and Zhao 1993) possess sharp crests along the lateral margins of the nasals and we score these taxa as equivalent to *Dilong* and *Eotyrannus* (state 1). All other taxa that can be affirmatively scored in the dataset are scored for state 0.

This character was first used by Brusatte et al. (2010a, character 47). States 0 and 1 are illustrated in Figure 2.7.

526. Lacrimal, posterior process for articulation with frontal, inflated by pneumatic recess: no (0) or yes (1).

A lacrimal pneumatic recess is present in many coelurosaurs and non-coelurosaurian theropods, but only in the derived tyrannosaurine tyrannosaurids *Daspletosaurus* (Currie 2003), *Tarbosaurus* (ZPAL MgD-I/109; Hurum and Sabath 2003), and *Tyrannosaurus* (CM 9380; Molnar 1991, Brochu 2003) is this recess so extensive within the interior of the lacrimal that it inflates the region of the bone that articulates with the frontal (the posterior process). The

presence of an inflated posterior process can usually be confidently assessed without the use of CT scanning or other imagining technology, as the external morphology of this process appears inflated or "puffy" in these three tyrannosaurids in which it is inflated by the lacrimal recess. This character was first used by Brusatte et al. (2010a, character 62). States 0 and 1 are illustrated in Figure 2.8.

527. Lacrimal, extent of antorbital fossa on ventral ramus: covers greater (0) or less than (1) 60% of the anteroposterior length along the contact with the jugal.

The ventral ramus of the lacrimal, which forms the preorbital bar separating the antorbital fenestra and the orbit, is usually at least partially covered by the antorbital fossa in theropods. The extent of the fossa, however, differs. This character differentiates an extensive (state 0) and limited (state 1) fossa by quantifying the percentage of the anteroposterior length of the ventral edge of the lacrimal ventral ramus that is excavated by the fossa. The measurement is taken along the ventral-most preserved margin of the lacrimal in lateral view, which in nearly all taxa is the suture between the lacrimal and jugal. Therefore, the measurement in question is taken by identifying the transition point between the antorbital fossa and subcutaneous surface of the lacrimal ventral ramus along the trace of the lacrimal-jugal suture. The percentage of the anteroposterior length of the ventral edge of the ventral ramus covered by the fossa is then calculated.

The coelurosaurian outgroups *Allosaurus* (Madsen 1976) and *Sinraptor* (Currie and Zhao 1993) possess an extensive fossa (state 0). This state is also seen in the basal coelurosaurs *Ornitholestes* (AMNH FARB 619) and *Tanycolagreus* (TPII 2000-09-29), several basal tyrannosauroids (e.g., *Dilong*: Xu et al. 2004; *Eotyrannus*: MIWG 1997.550; *Guanlong*: Xu et al.

2006; *Proceratosaurus*: Rauhut et al. 2010), compsognathids (*Compsognathus*: Peyer 2006; *Juravenator*: Göhlich and Chiappe 2010), therizinosauroids (*Erlikosaurus*: Clark et al. 1994), oviraptorosaurs (*Citipati*: Clark et al. 1999; *Incisivosaurus*: Balanoff et al. 2009), and dromaeosaurids (e.g., *Tsaagan*: Norell et al. 2006; *Velociraptor*: Barsbold and Osmólska 1999). On the contrary, a limited fossa (state 1) is present in several derived tyrannosauroids, such as *Alioramus* (Brusatte et al. 2012a), *Bistahieversor* (Carr and Williamson 2010), *Gorgosaurus* (Currie 2003), *Tarbosaurus* (Hurum and Sabath 2003), and *Tyrannosaurus* (Brochu 2003). It is also present in ornithomimosaurs (e.g., *Pelecanimimus*: LH 7777; *Shenzhousaurus*: Ji et al. 2003; *Garudimimus*: Kobayashi and Barsbold 2005a; *Gallimimus*: Osmólska et al. 1972) and alvarezsauroids (e.g., *Ceratonykus*: Alifanov and Barsbold 2009; *Haplocheirus*: Choiniere et al. 2010a; *Shuvuuia*: Chiappe et al. 1998).

This character was first utilized by Brusatte et al. (2010a, character 63). States 0 and 1 are illustrated in Figure 2.8.

537. Jugal, articulation with postorbital, extent of scarf joint on lateral surface of postorbital ramus: limited, occupies less than 50% of anteroposterior length of the process (0); extensive, occupies approximately 50-75% of the anteroposterior length of the process (1).

In most theropods the ventral ramus of the postorbital and the dorsal (postorbital) ramus of the jugal contact each other along a scarf joint. The postorbital overlaps the jugal laterally along this joint, and as a result, there is often a smooth articular facet along the anterior edge of the lateral surface of the dorsal ramus of the jugal. In most theropods this facet is small and covers only a small portion of the lateral surface of the dorsal ramus of the jugal. At its greatest

anteroposterior length, the fossa occupies less than 50% of the total anteroposterior length of the dorsal ramus in close coelurosaurian outgroups (e.g., *Allosaurus*: Madsen 1976) and nearly all coelurosaurs. The only exceptions are the derived tyrannosaurine tyrannosaurids *Tarbosaurus* (Hurum and Sabath 2003) and *Tyrannosaurus* (Molnar 1991; Brochu 2003). In these two large-bodied tyrannosaurids the facet for the postorbital on the dorsal ramus of the jugal is extensive and widely visible in lateral view, as it occupies between 50-75% of the entire anteroposterior length of the lateral surface of the ramus. This character was first used by Brusatte et al. (2010a, character 73). States 0 and 1 are illustrated in Figure 2.9.

538. Jugal, articulation with postorbital, braced by a pronounced ridge on the lateral surface of the postorbital ramus, which borders the postorbital posteriorly: no (0) or yes (1).

In most theropods the articular facet for the postorbital on the anterior portion of the lateral surface of the dorsal ramus of the jugal is separated from the subcutaneous surface of the posterior portion of the ramus by a subtle change in surface texture. This is the case in the coelurosaurian outgroups *Allosaurus* (Madsen 1976) and *Sinraptor* (Currie and Zhao 1993), as well as nearly every coelurosaurian ingroup taxon. The sole exceptions are a handful of derived tyrannosauroids, including *Alioramus* (Brusatte et al. 2012a), *Albertosaurus* (Currie 2003), *Daspletosaurus* (Currie 2003), *Gorgosaurus* (Currie 2003), *Tarbosaurus* (Hurum and Sabath 2003), and *Tyrannosaurus* (Molnar 1991; Brochu 2003). In these taxa there is a strong, sharp, and distinctive ridge that parallels the posterior edge of the postorbital facet, thereby separating the facet from the subcutaneous surface of the jugal. This ridge would have served to brace the articulation between the postorbital and jugal. This character was first utilized by Brusatte et al. (2010a, character 74). States 0 and 1 are illustrated in Figure 2.9.

539. Jugal, postorbital ramus, orientation relative to ventral margin of jugal: approximately perpendicular (0) or posterodorsal, with an obtuse angle between the long axis of the process and the ventral margin of the jugal (1).

In the coelurosaurian ougroups *Allosaurus* (Madsen 1976) and *Sinraptor* (Currie and Zhao 1993) the dorsal (postorbital) ramus of the jugal is approximately perpendicular to the ventral margin of the jugal. In other words, there is (approximately) a right angle between the long axis of the dorsal ramus and the long axis of the ventral margin. This state is retained in some coelurosaurs, whereas others possess a ramus that is oriented distinctly posterodorsally relative to the ventral margin, such that there is an obtuse angle between them anteriorly. This distinction was first formalized as a phylogenetic character by Brusatte et al. (2010a, character 75). States 0 and 1 are illustrated in Figure 2.9.

State 0, referring to a perpendicular dorsal ramus, is present in the basal coelurosaur *Ornitholestes* (AMNH FARB 619), most tyrannosauroids (e.g., *Alioramus*: Brusatte et al. 2012a; *Bistahieversor*: Carr and Williamson 2010; *Gorgosaurus*: Currie 2003; *Tyrannosaurus*: Brochu 2003; *Xiongguanlong*: Li et al. 2010), and compsognathids (*Compsognathus*: Peyer 2006; *Huaxiagnathus*: Hwang et al. 2004; *Juravenator*: Chiappe and Göhlich 2010; *Sinocalliopteryx*: Ji et al. 2007; *Sinosauropteryx*: Currie and Chen 2001). It is also present in most oviraptorosaurs, including *Caudipteryx* (Ji et al. 1998), *Citipati* (Clark et al. 1999), and *Oviraptor* (Osborn 1924; Clark et al. 1999). On the contrary, state 1, referring to a posterodorsally oriented dorsal ramus, is present in several basal tyrannosauroids, including *Dilong* (Xu et al. 2004), *Guanlong* (Xu et al. 2006), and *Proceratosaurus* (Rauhut et al. 2010). It is also seen in ornithomimosaurs (e.g., *Pelecanimimus*: LH 7777; *Gallimimus*: Osmólska et al. 1972; *Garudimimus*: Kobayashi and

Barsbold 2005a), alvarezsauroids (*Haplocheirus*: Choiniere et al. 2010a), therizinosauroids (Erlikosaurus: Clark et al. 1994), the basal oviraptorosaur *Incisivosaurus* (Xu et al. 2002a, Balanoff et al. 2009), troodontids (e.g., *Anchiornis*: Hu et al. 2009; *Zanabazar*: Norell et al. 2009), and most dromaeosaurid (e.g., *Deinonychus*: Ostrom 1969; *Tsaagan*: Norell et al. 2006).

544. Jugal, raised rim on the lateral surface, paralleling the ventral margin of the bone and anteriorly confluent with the antorbital fossa rim of the maxilla: absent (0); present (1).

In most coelurosaurs and their closest outgroups the lateral surface of the jugal is either flat or smoothly convex, without any distinctive ornamentation. The tyrannosaurid *Alioramus* is an obvious exception, as it uniquely possesses a conical "hornlet" on the lateral surface of the jugal, which projects straight laterally (Brusatte et al. 2009a, 2012a). Some other tyrannosauroids also possess their own distinctive feature of the lateral surface. In *Dilong* (IVPP V14243; Xu et al. 2004), *Gualong* (IVPP V14531; Xu et al. 2006), and *Proceratosaurus* (NHMUK R4860; Rauhut et al. 2010) there is a sharp, pronounced rim on the lateral surface that parallels the ventral margin of the jugal. The rim is positioned only a few millimeters dorsal to the ventral edge of the bone, and therefore essentially occupies the region where the lateral and ventral surfaces of the bone meet. A similar feature is also seen on the skull of *Incisivosaurus* (Balanoff et al. 2009: figure 3), although it is located at a slightly more dorsal position than in the aforementioned tyrannosauroids, as it is positioned nearly at the midpoint of the lateral surface of the jugal. It is unclear if this structure is primarily homologous to that of basal tyrannosauroids, but because the structures in both tyrannosauroids and *Incisivosaurus* are generally similar to each other these taxa are all scored for state 1. *Alioramus*, on the other hand, is scored for state 0 because the laterally projecting hornlet in this taxon is neither topologically nor morphologically

similar to the lateral ridges of taxa like *Guanlong* and *Incisivosaurus*. This character was first used by Brusatte et al. (2010a, character 80). States 0 and 1 are illustrated in Figure 2.9.

565. Quadratojugal, posterior process, length and orientation: short, oriented mostly laterally (0); elongate, wraps onto the posterior surface of the quadrate condyles (1).

In most theropods the quadratojugal is essentially L-shaped, with nearly perpendicular anterior and dorsal processes that form the posteroventral margins of the lateral temporal fenestra. Most taxa also possess a small posterior process at the extreme posteroventral corner of the quadratojugal, whose medial surface articulates against the lateral condyle of the quadrate, thus preventing the condyle from being visible in lateral view. This posterior process is usually a flat plate that sits against the lateral surface of the quadrate lateral condyle. This morphology is present in coelurosaurian outgroups such as *Allosaurus* (Madsen 1976) and *Sinraptor* (Currie and Zhao 1993) as well as most coelurosaurs. A different morphology is seen in some derived tyrannosauroids, including *Alioramus* (Brusatte et al. 2012a), *Bishtahieversor* (T.D. Carr, pers. comm.), *Daspletosaurus* (Currie 2003), *Xiongguanlong* (FRDC-GS JB16-2-1), *Tarbosaurus* (Hurum and Sabath (2003), and *Tyrannosaurus* (Brochu 2003). In these and closely related tyrannosauroids the posterior process is proportionally elongate (longer relative to the anterior ramus than in other taxa) and, most distinctly, it wraps around the posterior surface of the quadrate lateral condyle. Therefore, the posterior process both sits against the lateral surface of the quadrate lateral condyle and makes contact with posterior surface of the condyle.

Unfortunately, it is difficult to score this character in many coelurosaurs that are preserved on slabs, have broken posterior regions of the quadratojugal, or do not preserve quadrates. It is clear, however, that basal tyrannosauroids such as *Dilong* (IVPP V14243),

Guanlong (IVPP V14531), and *Proceratosaurus* (NHMUK R4860) do not possess an elongate quadratojugal posterior process that wraps around the posterior surface of the quadrate condyles, nor do other basal (non-paravian) coelurosaurs that are phylogenetically proximate to tyrannosauroids (e.g., *Citipati*: Clark et al. 1999; *Erlikosaurus*: Clark et al. 1994; *Gallimimus*: IGM 100/1133; *Garudimimus*: Kobayashi and Barsbold 2005a; *Haplocheirus*: IVPP V15988; *Ornitholestes*: AMNH FARB 619; *Tanycolagreus*: TPII 2000-09-29; *Zuolong*: Choiniere et al. 2010b).

This character was first utilized by Brusatte et al. (2010a, character 104). This character is not illustrated here, but state 1 is figured by Brusatte et al. (2012a: figures 21 and 24).

569. Quadrate, quadratojugal articulation, extent on lateral surface of lateral condyle: limited, occupies only part of the surface (0); extensive, covers entire lateral surface and extends dorsally to partially enclose quadrate foramen laterally (1).

As outlined above, the posterior process of the quadratojugal (and adjoining regions of the "main body" of the bone, where the anterior and dorsal processes meet) cover the quadrate condyles laterally. There is a pronounced articular facet on the medial surface of the quadratojugal and the lateral surface of the quadrate lateral condyle marking this contact. In most coelurosaurs these contact facets are small, and in particular, the articular surface on the lateral condyle of the quadrate does not cover the entire lateral surface of the condyle. This condition is seen in the basal tyrannosauroid *Guanlong* (IVPP V14531), the basal coelurosaurs *Ornitholestes* (AMNH FARB 619) and *Tanycolagreus* (TPII 2000-09-29), ornithomimosaurs (e.g., *Gallimimus*: IGM 100/1133; *Garudimimus*: Kobayashi and Barsbold 2005a; *Sinornithosaurus*: Kobayashi and Lü 2003), alvarezsauroids (*Haplocheirus*: IVPP IVPP V15988), therizinosauroids

(e.g., *Erlikosaurus*: Clark et al. 1994; *Falcarius*: Zanno 2010a), and dromaeosaurids (e.g., *Tsaagan*: Norell et al. 2006). These taxa can be scored for state 0 even if their skulls are in articulation, as the limited articular surface is associated with a quadate foramen that is not partially enclosed by a dorsal flange of the quadratojugal articular surface on the quadrate lateral condyle.

Some taxa exhibit a distinct morphology in which the articular surface for the quadratojugal covers the entire lateral surface of the quadrate lateral condyle. In these taxa the articular surface on the condyle is so large that it continues dorsally onto a small flange extending from the lateral condyle, which is seen to partially enclose the quadrate foramen laterally when the skull is seen in posterior view (e.g., Brusatte et al. 2012a: figures 22-23). This condition is present in the coelurosaurian outgroups *Allosaurus* (Madsen 1976) and *Sinraptor* (Currie and Zhao 1993), as well as the basal coelurosaur *Zuolong* (Choiniere et al. 2010b). It is also seen in several tyrannosauroids, including *Eotyrannus* (MIWG 1997.550), *Xiongguanlong* (FRDC-GS JB16-2-1), *Alioramus* (Brusatte et al. 2012a), *Daspletosaurus* (Currie 2003), *Tarbosaurus* (Hurum and Sabath 2003), and *Tyrannosaurus* (Brochu 2003). The basal tyrannosauroid *Guanlong*, however, lacks this morphology and is scored for state 0 (IVPP V14531).

This character was first utilized by Brusatte et al. (2010a, character 108). States 0 and 1 are illustrated in Figure 2.10.

571. Prefrontal, contacts nasal: yes (0); no, excluded by frontal-lacrimal contact (1).

The presence and morphology of the prefrontal varies considerably among coelurosaurs. In most coelurosaurs, as well as close outgroups such as *Allosaurus* (Madsen 1976) and

Sinraptor (Currie and Zhao 1993), the prefrontal is exposed on the skull roof and makes contact with the nasal. The size and shape of the prefrontal may be different in taxa, but the contact between this bone and the nasal is consistently present. Among coelurosaurs, this condition is seen in *Ornitholestes* (AMNH FARB 619), most tyrannosauroids (e.g., *Alioramus*: Brusatte et al. 2009a, Bever et al. 2011; *Gorgosaurus*: Currie 2003), ornithomimosaurs (e.g., *Garudimimus*: Kobayashi and Barsbold 2005a; *Sinornithosaurus*: Kobayashi and Lü 2003), alvarezsauroids (e.g., *Ceratonykus*: Alifanov and Barsbold 2009; *Shuvuuia*: IGM 100/977), therizinosauroids (e.g., *Erlikosaurus*: Clark et al. 1994), and dromaeosaurids (e.g., *Sinornithosaurus*: Xu and Wu 2001). A different morphology is present in a handful of basal coelurosaurs, including the basal tyrannosauroid *Guanlong* (IVPP V14531), *Compsognathus* (Peyer 2006), *Juravenator* (Chiappe and Göhlich 2010), and *Sinocalliopteryx* (Ji et al. 2007). In these taxa the prefrontal is reduced in size and is excluded from contacting the nasal by a frontal-lacrimal suture, which restricts the prefrontal to a lateral position at the anterodorsal corner of the orbit.

This character was first used by Brusatte et al. (2010a, character 110). State 0 is well illustrated in the literature, and is clearly shown, for example, by Clark et al. (1994: figure 3), Xu and Wu (2001: figure 4), and Currie (2003: figure 2). State 1 is figured here in *Guanlong* in Figure 2.11.

574. Frontal, size of single frontal: ratio of anteroposterior length of exposed portion on skull roof to mediolateral width at midpoint: greater than 2.0 (usually greater than 2.5) (0); less than 2.0 (1).

In most coelurosaurs the frontals are anteroposteriorly elongate elements that are more than twice as long anteroposteriorly as wide transversely at their midpoints. This condition is

seen in a range of taxa, including the basal coelurosaurs *Ornitholestes* (AMNH FARB 619) and *Zuolong* (Choiniere et al. 2010b), the basal tyrannosauroids *Guanlong* (IVPP V14531; Xu et al. 2006) and *Dilong* (IVPP V14243; Xu et al. 2004), compsognathids (e.g., *Compsognathus*: Peyer 2006; *Sinocalliopteryx*: Ji et al. 2007), ornithomimosaurs (e.g., *Garudimimus*: Kobayashi and Barsbold 2005a; *Sinornithomimus*: Kobayashi and Lü 2003), alvarezsauroids (e.g., *Shuvuuia*: Chiappe et al. 1998), therizinosauroids (e.g., *Erlikosaurus*: Clark et al. 1994), troodontids (e.g., *Xixiasaurus*: Lü et al. 2010; *Zanabazar*: Norell et al. 2009), and dromaeosaurids (e.g., *Sinornithosaurus*: Xu and Wu 2001; *Velociraptor*: Barsbold and Osmólska 1999). In most of these taxa the frontals are more than 2.5 times as long as their midpoint width.

In some taxa, however, the frontals are proportionally shortened relative to their widths. This condition is quantitatively characterized by an individual frontal that is less than twice as long anteroposteriorly than wide at the midpoint. The close coelurosaurian outgroups *Allosaurus* (Madsen 1976) and *Sinraptor* (Currie and Zhao 1993) possess this condition, as do two clusters of coelurosaurs: many derived tyrannosauroids (e.g., *Bistahieversor*: Carr and Williamson 2010; *Gorgosaurus*: Currie 2003; *Tarbosaurus*: Hurum and Sabath 2003; *Tyrannosaurus*: Brochu 2003) and oviraptorosaurs (e.g., *Caudipteryx*: Ji et al. 1998; *Citipati*: Clark et al. 1999; *Incisivosaurus*: Xu et al. 2002a, Balanoff et al. 2009).

The possession of short frontals is correlated in some way to the possession of a short and deep skull, which is represented by character 477 in the current analysis. These two characters are not redundant, however, as several taxa that possess elongate frontals (state 0 for the current character) are scored for having a short and deep skull with a length-to-height ratio of less than 3.2 (state 1 for character 477). These taxa include several troodontids (e.g., *Anchiornis*: Hu et al. 2009; *Mei*: Xu and Norell 2004) and the therizinosauroid *Erlikosaurus* (Clark et al. 1994).

Furthermore, the tyrannosauroid *Bistahieversor* is scored for a shortened frontal (state 1 for the current character) but a long skull with a length-to-height ratio of more than 3.2 (state 0 for character 477). The remaining tyrannosauroids scored for a short frontal (state 1 for the current character) are scored for a short and deep skull (state 1 for character 477), as are the outgroups *Allosaurus* and *Sinraptor*. The current character relating to the proportions of the frontal was first used by Brusatte et al. (2010a, character 114). This character used 2.5 instead of 2.0 as the numerical cutoff for state 0, but this has been modified here so that a broader range of coelurosaurs can be scored confidently for the character.

This character is not illustrated here, but states 0 and 1 can be clearly seen in many published figures. For example, state 0 can be seen in Clark et al. (1994: figure 3) and Peyer (2006: figure 4), whereas state 1 can be seen in Currie (2003: figure 2) and Hurum and Sabath (2003: figure 1).

600. Palatine, maxillary articulation, form: maxilla abuts lateral surface of maxillary process and anterior region of jugal process (0); contact reinforced by a "brace" at the anteroventral corner of the jugal process, which sits within the internal antorbital fossa (1).

The palatines of most coelurosaurs are either unknown, poorly preserved, or poorly described in the literature. Those taxa that are represented by well-preserved palatines, however, exhibit two general conditions of the maxillary articulation. In some taxa the maxilla simply abuts the lateral surface of the maxillary (anterior) process of the palatine and the anterior region of the lateral surface of the jugal (posterior) process. This condition is seen in the outgroup *Allosaurus* (Madsen 1976; UMNH VP8925), the dromaeosaurids *Austroraptor* (MML 195), *Deinonychus* (Ostrom 1969) and *Velociraptor* (Barsbold and Osmólska 1999), and the non-

tyrannosaurid tyrannosauroids *Appalachiosaurus* (Carr et al. 2005) and *Eotyrannus* (MIWG 1997.550). Other taxa, however, possess a discrete, convex "brace" at the corner where the maxillary and jugal processes meet. This brace may project laterally or ventrally (see character 601 below), but in all cases braces the palatine-maxilla articulation by sitting within the antorbital fossa and helping to "lock" the two bones together when they are articulated. This "brace" is present in the outgroup *Sinraptor* (Currie and Zhao 1993) as well as derived tyrannosauroids such as *Albertosaurus* (Currie 2003), *Alioramus* (Brusatte et al. 2012a), *Bistahieversor* (T.D. Carr, pers. comm.), *Tarbosaurus* (Hurum and Sabath 2003; ZPAL MgD-I/4), and *Tyrannosaurus* (Molnar 1991). This character was first used by Brusatte et al. (2010a, character 143). States 0 and 1 are illustrated in Figure 2.12.

601. Palatine, morphology of maxillary articulation brace: projects ventrally due to a jugal process that extends further ventrally than the maxillary process, such that there is a discrete corner between the two processes in lateral view (0); projects laterally, with no discrete corner between the smoothly confluent jugal and maxillary processes in lateral view (1).

Those taxa that possess a "brace" on the palatine to strengthen the articulation with the maxilla (i.e., those scored for state 1 for character 600 above) possess one of two morphologies. In the outgroup *Sinraptor* (Currie and Zhao 1993) and the tyrannosauroids *Albertosaurus* (Currie 2003) and *Alioramus* (Brusatte et al. 2012a) the brace projects strongly ventrally such that it is widely visible in lateral view. In these taxa the jugal process extends further ventrally than the maxillary process, creating a discrete corner between the two processes. This corner is the "brace". In the derived tyrannosaurine tyrannosaurids *Daspletosaurus*, *Tarbosaurus*, and *Tyrannosaurus*, however, the palatine "brace" projects straight laterally (e.g., ZPAL MgD-I/4).

As a result, it is visible in dorsal view but barely perceptible in lateral view. In these taxa the maxillary and jugal processes of the palatine extend to approximately the same level ventrally and there is no discrete corner between them in lateral view. However, the jugal process does extend further laterally than the maxillary process when the palatine is seen in dorsal view, which results in the laterally projecting brace. This character was first used by Brusatte et al. (2010a, character 144). States 0 and 1 are illustrated in Figure 2.12.

602. Internal choana, shape: anteroposteriorly elongate oval (0); nearly circular (1).

The internal choana is a palatal opening continuous with the external naris in the living animal, which is visible when the skull is seen in both lateral and ventral (palatal) views. The posterior margin of this opening is formed by the diverging maxillary and vomeropterygoid processes of the palatine. In most theropods the choana is an anteroposteriorly elongate oval, and this shape can be inferred from the shape of the region between the divergent maxillary and vomperopterygoid processes of the palatine even if a complete or near-complete palate is not preserved. This condition is seen in the outgroups *Allosaurus* (Madsen 1976) and *Sinraptor* (Currie and Zhao 1993), the basal coelurosaur *Ornitholestes* (AMNH FARB 619), most tyrannosauroids (e.g., *Albertosaurus*: Currie 2003; *Alioramus*: Brusatte et al. 2012a; *Eotyrannus*: MIWG 1997.550; *Proceratosaurus*: Rauhut et al. 2010), compsognathids (e.g., *Compsognathus*: Peyer 2006; *Sinocalliopteyx*: Ji et al. 2007), ornithomimosaurs (e.g., *Garudimimus*: Kobayashi and Barsbold 2005a; *Pelecanimimus*: LH 7777), alvarezsauroids (e.g., *Haplocheirus*: Choiniere et al. 2010a), therizinosauroids (e.g., *Erlikosaurus*: Clark et al. 1994), the basal oviraptorosaur *Incisivosaurus* (Balanoff et al. 2009), troodontids (e.g., *Saurornithoides*: Norell et al. 2009), and dromaeosaurids (e.g., *Austroraptor*: MML 195; *Velociraptor*: Barsbold and Osmólska 1999). A

distinct condition is seen in the derived tyrannosaurine tyrannosaurids *Tarbosaurus* (Hurum and Sabath 2003) and *Tyrannosaurus* (Molnar 1991; Brochu 2003), as well as the oviraptorosaur *Citipati* (Clark et al. 1999). In these taxa the internal choana is nearly circular in shape.

This character was first used by Brusatte et al. (2010a, character 145). States 0 and 1 are illustrated in Figure 2.12, which shows the shape of the choana when the palatine is seen in lateral view. These conditions are also clearly visible on palatal view reconstructions of some taxa published in the literature (e.g., Currie 2003: figure 2; Hurum and Sabath 2003: figure 15).

603. Suborbital fenestra, shape: anteroposteriorly elongate oval (0); nearly circular (1).

The suborbital fenestra is a separate palatal opening beneath the orbit, which is visible when the skull is seen in ventral (palatal) view. Its anterior margin is formed by the diverging jugal and medial processes of the posterior end of the palatine. In most theropods the suborbital fenestra is an anteroposteriorly elongate oval, and this shape can be inferred from the shape of the region between the divergent jugal and medial processes of the palatine even if a complete or near-complete palate is not preserved. This condition is seen in the outgroups *Allosaurus* (Madsen 1976) and *Sinraptor* (Currie and Zhao 1993), the basal coelurosaur *Ornitholestes* (AMNH FARB 619), most tyrannosauroids (e.g., *Albertosaurus*: Currie 2003; *Alioramus*: Brusatte et al. 2012a; *Eotyrannus*: MIWG 1997.550; *Proceratosaurus*: Rauhut et al. 2010), ornithomimosaurs (e.g., *Garudimimus*: Kobayashi and Barsbold 2005a), therizinosauroids (e.g., *Erlikosaurus*: Clark et al. 1994), oviraptorosaurs (e.g., Citipati: Clark et al. 1999; *Incisivosaurus*: Balanoff et al. 2009), troodontids (e.g., *Saurornithoides*: Norell et al. 2009), and dromaeosaurids (e.g., *Austroraptor*: MML 195; *Velociraptor*: Barsbold and Osmólska 1999). The derived tyrannosaurids *Tarbosaurus* (Hurum and Sabath 2003) and *Tyrannosaurus* (Molnar 1991;

Brochu 2003), on the other hand, possess a nearly circular suborbital fenestra. This character was first used by Brusatte et al. (2010a, character 146). States 0 and 1 are not illustrated here, but they can be seen on palatal view reconstructions of some taxa published in the literature (e.g., state 0: Currie 2003: figure 2; state 1: Hurum and Sabath 2003: figure 15).

607. Exoccipital-opisthotic, paroccipital process, ventral flange at distal end: absent (0); present (1).

This was a new character established by Brusatte et al. (2010a, character 150) to codify the derived presence of a ventrally expansive flange at the distal end of the paroccipital process in a subclade of tyrannosauroids. The flange, which often takes the form of a discrete lobe-like structure, is absent in the non-tyrannosaurid tyrannosauroid *Xiongguanlong* (Li et al. 2010), present in the non-tyrannosaurid *Bistahieversor*, and present in all known tyrannosaurids (*Albertosaurus*, *Daspletosaurus*, *Gorgosaurus*: Currie 2003; *Alioramus*: Bever et al. 2011, IGM 100/1844; *Tarbosaurus*: Hurum and Sabath 2003; *Teratophoneus*: Carr et al. 2011; *Tyrannosaurus*: Osborn 1912, Brochu 2003). This condition is illustrated in Figure 2.14.

The presence or absence of the flange is variable in non-tyrannosauroid coelurosaurs as well. The outgroups *Allosaurus* (Madsen 1976) and *Sinraptor* (Currie and Zhao 1993) lack the flange, as do the basal coelurosaurs *Nqwebasaurus* (Choiniere et al. 2012) and *Ornitholestes* (AMNH FARB 619), ornithomimosaurs (e.g., *Garudimimus*: Kobayashi and Barsbold 2005a; *Gallimimus*: IGM 100/1133; *Sinornithomimus*: Kobayashi and Lü 2003), alvarezsauroids (e.g., *Ceratonykus*: Alifanov and Barsbold 2009; *Haplocheirus*: IVPP V15988; *Shuvuuia*: Chiappe et al. 1998), theizinosauroids (e.g., *Erlikosaurus*: Clark et al. 1994; *Falcarius*: Smith et al. 2011), oviraptorosaurs (e.g., *Citipati*: Clark et al. 1999; *Incisivosaurus*: Balanoff et al. 2009), and

troodontids (e.g., *Byronosaurus*: Makovicky et al. 2003). A flange is present, however, in several dromaeosaurids, including *Dromaeosaurus* (Currie 1995), *Mahakala* (Turner et al. 2011), *Tsaagan* (Norell et al. 2006), and *Velociraptor* (Barsbold and Osmólska 1999; Norell et al. 2004).

608. Exoccipital-opisthotic, paroccipital process, deep fossa on posterior surface dorsolateral to the foramen magnum: present (0); absent (1).

This character, established by Brusatte et al. (2010a, character 151), scores for the presence or absence of a deep, smooth fossa on the posterior surface of the paroccipital process, immediately dorsolateral to the foramen magnum. This fossa does not bear any noticeable pneumatic foramina in any specimen in which it is resent, and therefore does not appear to be associated with any of the pneumatic sinuses of the braincase, but it may conceivably be related to the cervical airsac system. Alternatively, it may be a muscle attachment site, although Snively and Russell (2007), in their study of tyrannosaurid neck muscles, did not reconstruct a muscle as attaching in this region.

The fossa is absent in the coelurosaurian outgroups *Allosaurus* (Madsen 1976) and *Sinraptor* (Currie and Zhao 1993). Among tyrannosauroids, the fossa is present in *Guanlong* (IVPP V14531) and *Dilong* (IVPP V14243), but it is absent in more derived tyrannosauroids, including *Xiongguanlong* (FRDC-GS JB16-2-1) *Bistahieversor* (T.D. Carr, pers. comm.), *Albertosaurus* (T.D. Carr, pers. comm.), *Gorgosaurus* (Witmer and Ridgely 2009), *Alioramus* (Bever et al. 2011; IGM 100/1844), *Teratophoneus* (T.D. Carr, pers. comm.), *Daspletosaurus* (Currie 2003), *Tarbosaurus* (Hurum and Sabath 2003; ZPAL MgD-I/3), and *Tyrannosaurus* (Brochu 2003; Witmer and Ridgely 2009). The fossa appears to be present in all other

coelurosaurs in which it can be affirmatively scored, although the size and depth of the fossa differ among taxa. The morphology of the fossa in *Guanlong* is shown in Figures 2.14 and 2.15.

609. Exoccipital-opisthotic, crista tuberalis (=metotic strut), extent in posterior view: limited, mediolateral width across opposing cristae less than one half the dorsoventral depth of the braincase from the dorsal tip of the supraoccipital to the ventral tip of the basal tubera (0); extensive, width greater than one half braincase depth (1).

The crista tuberalis, which is often referred to as the metotic strut in the theropod literature, is the pronounced crest of bone that separates the posterior (occipital) and lateral surfaces of the braincase. It is visible in posterior view as a flange projecting lateral to each side of the occipital condyle, which spans the distance between the paroccipital process and basal tuber. The size of the cristae can be quantified by measuring the mediolateral width across the opposing cristae (i.e., the mediolateral width of the entire posterior surface of the braincase at the dorsoventral level of the midpoint of the cristae) and comparing this to the dorsoventral depth of the entire braincase. The distinction between wide and narrow cristae was first used as a phylogenetic character by Brusatte et al. (2010a, character 152).

In most theropods the cristae are visible in posterior view but do not extend far laterally. This condition is explicitly quantified by a ratio of cristae width to braincase depth that is less than 0.5. The outgroups *Allosaurus* (Madsen 1976) and *Sinraptor* (Currie and Zhao 1993) are scored for this condition, as are a range of coelurosaurs including the basal coelurosaur *Ornitholestes* (AMNH FARB 619), most tyrannosauroids (e.g., *Alioramus*: Bever et al. 2011; *Tarbosaurus*: Hurum and Sabath 2003; *Tyrannosaurus*: Brochu 2003; *Xiongguanlong*: FRDC-GS JB16-2-1), some ornithomimosaurs (e.g., *Garudimimus*: Kobayashi and Barsbold 2005a),

alvarezsauroids (e.g., *Ceratonykus*: Alifanov and Barsbold 2009; *Haplocheirus*: Choiniere et al. 2010a; *Shuvuuia*: Chiappe et al. 1998), some therizinosauroids (e.g., *Falcarius*: Smith et al. 2011), oviraptorosaurs (e.g., *Citipati*: Clark et al. 1999; *Incisivosaurus*: Balanoff et al. 2009), troodontids (e.g., *Byronosaurus*: Makovicky et al. 2003; *Zanabazar*: Norell et al. 2009), and dromaeosaurids (e.g., *Tsaagan*: Norell et al. 2006; *Velociraptor*: Barsbold and Osmólska 1999).

Some coelurosaurs, however, have mediolaterally expansive cristae, quantified by a width-to-depth ratio of greater than 0.5. This condition is seen in the basal tyrannosauroids *Guanlong* (IVPP V14531) and *Dilong* (IVPP V14243), as well as some derived ornithomimosaurs (e.g., *Gallimimus*: IGM 100/1133; *Struthiomimus*: Makovicky and Norell 1998) and derived therizinosauroids (e.g., *Erlikosaurus*: Clark et al. 1994; *Nothronychus*: Kirkland et al. 2005, Smith et al. 2011). These taxa are all scored for state 1 here, although the morphologies of *Guanlong* and *Dilong* deserve further comment. Note that the *Guanlong* condition is illustrated in Figures 2.14 and 2.15.

In *Guanlong* and *Dilong*, the great lateral extent of each crista tuberalis is due to the presence of pronounced "corners" at the lateroventral edge of each basal tuber. Because the crista tuberalis links the basal tuber to the paroccipital process, the extreme lateral extent of these projecting "corners" results in a laterally extensive crista. It is unclear, however, if the conditions in *Guanlong* and *Dilong* are truly homologous. In *Guanlong* the "corner" is formed entirely by the basisphenoid, in the form of an ovoid process that is located immediately lateral to, and confluent with, the basal tuber in occipital view. In *Dilong*, on the other hand, the "corner" is formed entirely from a novel process of the basioccipital and located above the ventral level of the basal tuber, thus producing a notch between the "corner" and the tuber. Furthermore, if homologous between *Dilong* and *Guanlong*, it is unclear if the wide condition is a

synapomorphy of these taxa or a tyrannosauroid plesiomorphy lost in more derived taxa. The latter is suggested by the presence of wide cristae tuberalis in a close outgroup, ornithomimosaurs, although in these coelurosaurs the width of the cristae is caused by especially wide basal tubera and not additional "corner"-like contributions from the basioccipital or basisphenoid (Makovicky and Norell 1998).

Per the interpretation of Brusatte et al. (2010a) and Bever et al. (in press), the "corners" at the lateroventral edge of each basal tuber at least could be homologous, despite variation in the bones comprising them. In this case, the bones forming this "corner" would be considered an additional character. Brusatte et al. (2010a) did not employ this character because each condition ("corner" comprised of either basisphenoid or basioccipital) is currently only known in a single taxon each, and thus this character is phylogenetically uninformative at this time. Future discoveries, however, may reveal that other taxa share the basisphenoid or basioccipital condition with *Guanlong* or *Dilong*, respectively. When or if this happens, an additional character would then be warranted.

610. Basioccipital, basal tubera, dorsoventral depth: less than (0) or greater than (1) depth of occipital condyle.

The basal tubera are the portion of the braincase extending below the occipital condyle as a sheet. In the outgroups *Allosaurus* (Madsen 1976) and *Sinraptor* (Currie and Zhao 1993) the tubera are short, vertical sheets that project only slightly below the occipital condyle. The dorsoventral depth of the tubera is less than that of the condyle. This condition is seen in many coelurosaurs, including the basal coelurosaur *Ornitholestes* (AMNH FARB 619), basal tyrannosauroids (*Dilong*: IVPP V14243; *Guanlong*: IVPP V14531; *Xiongguanlong*: Li et al,

2010), some ornithomimosaurs (*Garudimimus*: Kobayashi and Barsbold 2005a), alvarezsauroids (e.g., *Ceratonykus*: Alifanov and Barsbold 2009; *Haplocheirus*: Choiniere et al. 2010a; *Shuvuuia*: Chiappe et al. 1998), oviraptorosaurs (e.g., *Citipati*: Clark et al. 1999; *Incisivosaurus*: Balanoff et al. 2009), troodontids (e.g., *Byronosaurus*: Makovicky et al. 2003; *Zanabazar*: Norell et al. 2009), and some dromaeosaurids (e.g., *Dromaeosaurus*: Currie 1995).

In contrast, some other coelurosaurs possess a distinct condition in which the tubera are much larger and more ventrally extensive, with dorsoventral dimensions greater than that of the corresponding occipital condyle. This morphology is present in several derived tyrannosauroids, including *Albertosaurus* (Currie 2003), *Alioramus* (Bever et al. 2011; IGM 100/1844), *Bistahieversor* (NMMNH P-27469), *Daspletosaurus* (Currie 2003), *Gorgosaurus* (ROM 1247), *Tarbosaurus* (Hurum and Sabath 2003), *Teratophoneus* (BYU 8120/9396), and *Tyrannosaurus* (Osborn 1912; Molnar 1991; Brochu 2003). It is also present in some derived ornithomimosaurs (e.g., *Gallimimus*: IGM 100/1133; *Struthiomimus*: Makovicky and Norell 1998), therizinosauroids (e.g., *Erlikosaurus*: Clark et al. 1994; *Falcarius*: Smith et al. 2011; *Nothronychus*: Kirkland et al. 2005, Smith et al. 2011), and some dromaeosaurids (e.g., *Tsaagan*: Norell et al. 2006; *Velociraptor*: Barsbold and Osmólska 1999, Norell et al. 2004). Note that in therizinosauroids, we consider the region of the braincase ventral to the occipital condyle to be homologous to the basal tubera even though it has been apomorphically modified into an expanded bulla that is a phylogenetically informative character of the group (and is used as a separate character in the current analysis).

The distinction between short and deep basal tubera was first used by Brusatte et al. (2010a, character 154). States 0 and 1 are illustrated in Figures 2.14 and 2.15.

611. Basioccipital, basal tubera, concave notch ventrally between opposing tubera: shallow, less than 40% of the dorsoventral depth of the tubera (0); deep, approximately 50% of the depth of the tubera (1).

In most theropods the left and right basal tubera are separated along their ventral margins by a concave notch. In other words, the ventral margin of the lamina formed by the conjoined tubera is concave. The depth of this notch differs among coelurosaurs and other theropods. The outgroups *Allosaurus* (Madsen 1976) and *Sinraptor* (Currie and Zhao 1993) have a subtle notch whose dorsoventral depth is less than 40% of the depth of the tubera themselves (the depth of the tuber is the maximum depth, which is usually along the lateral edge of the structure, not the depth at the level of the notch). This condition is also seen in the basal coelurosaur *Ornitholestes* (AMNH FARB 619), basal tyrannosauroids (*Guanlong*: IVPP V14531; *Proceratosaurus*; Rauhut et al. 2010; *Xiongguanlong*: Li et al. 2010), some ornithomimosaurs (e.g., *Garudimimus*: Kobayashi and Barsbold 2005a; *Struthiomimus*: Makovicky and Norell 1998), alvarezsauroids (e.g., *Haplocheirus*: IVPP V15988; *Shuvuuia*: Chiappe et al. 1998), therizinosauroids (e.g., *Erlikosaurus*: Clark et al. 1994; *Falcarius*: Smith et al. 2011; *Nothronychus*: Kirkland et al. 2005, Smith et al. 2011), oviraptorosaurs (e.g., *Citipati*: Clark et al. 1999; *Incisivosaurus*: Balanoff et al. 2009), troodontids (e.g., *Byronosaurus*: Makovicky et al. 2003; *Zanabazar*: Norell et al. 2009), and dromaeosaurids (e.g., *Dromaeosaurus*: Currie 1995; *Tsaagan*: Norell et al. 2006; *Velociraptor*: Barsbold and Osmólska 1999, Norell et al. 2004).

A few coelurosaurs possess basal tubera notches that are proportionally deep. In these taxa the depth of the notch is approximately 50% of the depth of the basal tubera. Among these taxa are the single ornithomimosaur genus *Gallimimus* (IGM 100/1133) and several derived tyrannosauroids, including *Bistahieversor* (Carr and Williamson 2010; NMMNH P-27469),

Albertosaurus, *Gorgosaurus*, and *Daspletosaurus* (Currie 2003), *Alioramus* (Bever et al. 2011; IGM 100/1844), *Tarbosaurus*: (Hurum and Sabath 2003), *Tyrannosaurus* (Osborn 1912; Molnar 1991; Brochu 2003). The distinction between the small tubera of basal tyrannosauroids such as *Guanlong* and derived taxa such as *Tyrannosaurus* is marked. In *Guanlong*, for instance, the notch is only approximately 10% of the depth of the tubera, whereas in *Tyrannosaurus* the notch is approximately 50% of the depth of the tubera.

The original character of Brusatte et al. (2010a, character 155) was created to encapsulate this striking difference. States 0 and 1 are illustrated in Figures 2.14 and 2.15.

615. Basisphenoid, basisphenoid recess, shape in ventral view: funnel-like, expands in mediolateral width posteriorly (0); ovoid or circular, no posterior expansion (1).

The basisphenoid recess is a pneumatic region on the ventral surface of the braincase, filling the space between the basal tubera posteriorly and the basipterygoid processes anteriorly. It is present in many theropods, including most but not all coelurosaurs (Rauhut 2004). When the recess is observed in ventral view it is seen to either funnel out in mediolateral with posteriorly (i.e., become mediolaterally wider as it continues posteriorly) or to keep a relatively constant width across its entire anteroposterior length. The distinction between these conditions was first encapsulated in a phylogenetic character by Brusatte et al. (2010a, character 160). States 0 and 1 are illustrated in Figure 2.16.

State 0, in which the recess funnels out posteriorly, is present in the basal tyrannosauroids *Guanlong* (IVPP V14531) and *Proceratosaurus* (NHMUK R 4860), as well as ornithomimosaurs (e.g., *Gallimimus*: IGM 100/1133; *Struthiomimus*: Makovicky and Norell 1998), oviraptorosaurs (e.g., *Citipati*: Clark et al. 1999; *Incisivosaurus*: Balanoff et al. 2009), and dromaeosaurids (e.g.,

Tsaagan: Norell et al. 2006; *Velociraptor*: Barsbold and Osmólska 1999). State 1, in which the recess is ovoid or circular without any posterior expansion, is present in the outgroups *Allosaurus* (Madsen 1976) and *Sinraptor* (Currie and Zhao 1993). It is also seen in a number of derived tyrannosauroids, including *Bistahieversor* (Carr and Williamson 2010; NMMNH P-27469), *Albertosaurus*, *Gorgosaurus*, *Daspletosaurus* (Currie 2003), *Alioramus* (Bever et al. 2011; IGM 100/1844), *Tarbosaurus* (Hurum and Sabath 2003), and *Tyrannosaurus* (Brochu 2003). Note that in *Tarbosaurus* and *Tyrannosaurus* the basisphenoid recess faces more strongly posteriorly than ventrally, so the lack of a posterior expansion may not be clear in ventral view. The ovoid condition without a posterior expansion is also seen in *Dromaeosaurus* (Currie 1995) and *Falcarius* (Smith et al. 2011).

617. Parasphenoid, shape of rostrum: anteroposteriorly expanded, ventral margin is a smooth concave arch (0); dorsoventrally expanded, ventral margin is nearly vertical posteriorly and then abruptly transitions to horizontal trend anteriorly (1).

This character was originally devised by Brusatte et al. (2010a, character 162) to refer to differences in the parasphenoid shape among tyrannosauroids. *Guanlong* (IVPP V14531) and *Alioramus* (IGM 100/1844; Bever et al. 2011) exhibit a distinctive condition, also seen in the outgroup *Allosaurus* (Madsen 1976) and all other coelurosaurs that can be scored affirmatively, in which the parasphenoid rostrum is anteroposteriorly elongate, with a ventral margin that transcribes a single, smoothly convex arch (Figure 2.13). Other tyrannosauroids, however, have a proportionally shorter but deeper rostrum, with a ventral margin whose posterior portion trends vertically in its posterior part and then rapidly changes to a horizontal trend more anteriorly. Taxa possessing this morphology include *Bistahieversor* (Carr and Williamson 2010; NMMNH

P-27469), *Albertosaurus*, *Gorgosaurus*, *Daspletosaurus* (Currie 2003), *Tarbosaurus* (Hurum and Sabath 2003), and *Tyrannosaurus* (Brochu 2003).

The possession of state 0 in *Alioramus* may appear unusual, as the weight of additional character evidence shows this taxon to be a more derived tyrannosauroid closely related to taxa such as *Tarbosaurus* and *Tyrannosaurus* that possess state 1 (Brusatte et al. 2009a, 2010a). The specimen of *Alioramus* used to score this character, IGM 100/1844, belongs to an immature invidual. In a similar vein, state 0 is also present in the ontogenetically immature holotype of *Raptorex*, which clearly pertains to a derived tyrannosauroid closely related to taxa with state 1 (Sereno et al. 2009). Therefore, it is possible (perhaps likely) that the shape of the parasphenoid rostrum is ontogenetically controlled, with younger individuals retaining the primitive condition. Testing this hypothesis awaits future discoveries, especially of more mature individuals of *Alioramus*. It is interesting to note, however, that a seemingly intermediate condition between the primitive and derived states is seen in juvenile *Tyrannosaurus* (CMNH 7541; Witmer and Ridgely 2009), and possibly also *Tarbosaurus* (MPC-D 107/7; Tsuihiji et al. 2011), where the rostrum is positioned relatively close to the basipterygoid processes. At the very least, these specimens indicate that the shape of the rostrum changed during postnatal ontogeny, as the condition in the juveniles is different than that in adult *Tyrannosaurus* and *Tarbosaurus* (see above).

619. Laterosphenoid, antotic crest, form: single structure (0); bifurcates ventrally (1).

This antotic crest is a ridge of bone that separates the lateral wall of the braincase (prootic, laterosphenoid, exoccipital-opisthotic) from the orbital and temporal spaces, which would have been filled with the eyeball and jaw adductor muscles, respectively. Brusatte et al.

(2010a, character 165) utilized a character differentiating the form of the crest within tyrannosauroids. In the basal tyrannosauroid *Guanlong* (IVPP V14531), the antotic crest is a single structure across its entire length. This condition is also seen in the coelurosaur outgroup *Allosaurus* (Madsen 1976; UMNH VP7415) as well as the few non-tyrannosauroid coelurosaur ingroup taxa that can be scored affirmatively for this character (*Tsaagan*: Norell et al. 2006; *Velociraptor*: Barsbold and Osmólska 1999; *Zanabazar*: Norell et al. 2009). The crest exhibits a unique morphology, in which it bifurcates ventrally, in the derived tyrannosauroids *Bistahieversor* (Carr and Williamson 2010; NMMNH P-27469), *Albertosaurus*, *Gorgosaurus*, *Daspletosaurus* (Currie 2003), *Alioramus* (Bever et al. 2011; IGM 100/1844), *Tarbosaurus* (Hurum and Sabath 2003; ZPAL MgD-I/3), and *Tyrannosaurus* (Osborn 1912; Brochu 2003). State 1 is shown in *Alioramus* in Figure 2.13.

620. Laterosphenoid, fossa on lateral surface that houses head of epipterygoid: absent or very shallow (0); present, deep and rugose (1).

The head of the epipterygoid contacts the lateral surface of the laterosphenoid (and sometimes the prootic) in theropods, and usually this contact is marked by a flat surface or subtle depression on the lateral side of the braincase. This is the case in the coelurosaurian outgroups *Allosaurus* (Madsen 1976; UMNH VP7415) and *Sinraptor* (Currie and Zhao 1993), as well as the few non-tyrannosauroid coelurosaur ingroup taxa that can be scored affirmatively for this character (*Tsaagan*: Norell et al. 2006; *Velociraptor*: Barsbold and Osmólska 1999; *Zanabazar*: Norell et al. 2009). It is also present in the basal tyrannosauroid *Guanlong* (IVPP V14531). Many derived tyrannosauroids, however, exhibit a deep and rugose contact surface for the epipterygoid, between the bifurcated portions of the antotic crest. These taxa include

Bistahieversor (Carr and Williamson 2010; NMMNH P-27469), *Albertosaurus*, *Gorgosaurus*, *Daspletosaurus* (Currie 2003), *Alioramus* (Bever et al. 2011; IGM 100/1844), *Tarbosaurus* (Hurum and Sabath 2003; ZPAL MgD-I/3), and *Tyrannosaurus* (Osborn 1912; Brochu 2003). Because the epipterygoid articulation is associated with the antotic crest, and because the distribution of character scores for this and the previous character are identical, it is possible that the two characters (619 and 620) are correlated. Further testing awaits the description of more specimens. The current character was first utilized by Brusatte et al. (2010a, character 166). State 1 is shown in *Alioramus* in Figure 2.13.

625. Dentary, ventrally projecting rugose process ("chin") where the anterior and ventral margins of the dentary meet: absent (0) or present, visible as a pointed projection in lateral view and convex in medial view, braces dentary symphysis (1).

In most theropods the anterior and ventral margins of the dentary smoothly merge. This is the case in coelurosaurian outgroups such as *Allosaurus* (Madsen 1976) and *Sinraptor* (Currie and Zhao 1993), as well as most coelurosaurs, including the basal coelurosaur *Ornitholestes* (AMNH FARB 619), the basal tyrannosauroid *Eotyrannus* (MIWG 1997.550), compsognathids (e.g., *Compsognathus*: Peyer 2006; *Huaxiagnathus*: Hwang et al. 2004; *Juravenator*: Chiappe and Göhlich 2010; *Sinocalliopteryx*: Ji et al. 2007; *Sinosauropteryx*: Currie and Chen 2001), ornithomimosaurs (e.g., *Gallimimus*: Osmólska et al. 1972; *Pelecanimimus*: LH 7777), alvarezsauroids (e.g., *Haplocheirus*: Choiniere et al. 2010a; *Shuvuuia*: Chiappe et al. 1998), the basal therizinosauroid *Falcarius* (Zanno 2010a), the basal oviraptorosaur *Incisivosaurus* (Xu et al. 2002a; Balanoff et al. 2009), most troodontids (e.g., *Byronosaurus*: Makovicky et al. 2003;

Zanabazar: Norell et al. 2009), and dromaeosaurids (e.g., *Buitreraptor*: Makovicky et al. 2005; *Dromaeosaurus*: Currie 1995; *Sinornithosaurus*: Xu and Wu 2001; *Tsaagan*: Norell et al. 2006).

Some coelurosaurs, however, possess a discrete and rugose projection that extends from the anteroventral corner of the dentary. This feature, which is often referred to as a "chin," is present in most tyrannosauroids, including *Dilong* (IVPP V14243), *Appalachiosaurus* (Carr et al. 2005), *Bistahieversor* (Carr and Williamson 2010), *Albertosaurus* and *Gorgosaurus* (Currie 2003), *Alioramus* (Brusatte et al. 2009a, 2012a), *Teratophoneus* (Carr et al. 2011), *Daspletosaurus* (Russell 1970), *Tarbosaurus* (Hurum and Sabath 2003), and *Tyrannosaurus* (Brochu 2003). This process is small and subtle in basal tyrannosauroids such as *Dilong* and *Appalachiosaurus*, but it is larger and more robust in colossal taxa such as *Tyrannosaurus* (Brochu 2003). In all tyrannosauroids, however, the "chin"is visible laterally, convex in medial view, and helps brace the dentary symphysis. The distinction between this condition and the normal theropod condition in which a "chin"-like process is lacking was first utilized as a cladistic character by Brusatte et al. (2010a, character 172). States 0 and 1 are illustrated in Figure 2.17.

A "chin"-like projection is also present in derived therizinosauroids (*Erlikosaurus*: Clark et al. 1994), derived oviraptorosaurs (*Caudipteryx*: Ji et al. 1998; *Citipati*: Clark et al. 1999), and the single troodontid taxon *Xixiasaurus* (Lü et al. 2010). It is unclear if the condition in these taxa is homologous to that in tyrannosaurids, as it is not possible to confirm whether the "chin"-like process is convex medially and helps brace the symphysis. Nevertheless, because of general morphological and topological similarity we consider these taxa to possess state 1 as defined here, in the absence of any contrary information.

626. Dentary, symphysis texture: generally smooth (0); strongly rugose and beveled, with interlocking ridges and convexities for articulation with the opposing symphysis (1)

In most theropods the dentary symphysis—the surface on the medial portion of the anterior dentary that articulates against the corresponding surface on the opposing dentary—is generally smooth. Small ridges, grooves, and convexities may be present, but in general the symphysis is a facet-like feature that lies against the opposing symphysis when the dentaries are in articulation. This condition is present in the coelurosaurian outgroups *Allosaurus* (Madsen 1976; UMNH VP9351) and *Sinraptor* (Currie and Zhao 1993), as well as nearly every coelurosaur that can be scored affirmatively for this character. The three exceptions are the derived tyrannosaurine tyrannosaurids *Tarbosaurus* (Hurum and Sabath 2003; ZPAL MgD-I/5) and *Tyrannosaurus* (Molnar 1991; Brochu 2003), as well as the large-bodied dromaeosaurid *Austroraptor* (MML 195). In these taxa the symphyseal surface is exceptionally rugose, as it is marked by pronounced ridges, grooves, and convexities that would have strengthened the articulation between the dentaries. This character was originally used by Brusatte et al. (2010a, character 173). States 0 and 1 are illustrated in Figures 2.17 and 2.18.

627. Dentary, articular surface for splenial along ventral region of dentary ramus below the Meckelian fossa, form: dorsoventrally shallow and smooth (0); dorsoventrally deep (nearly as deep as anterior depth of fossa) and rugose (1).

In most theropods the splenial articulates broadly against much of the medial surface of the dentary, covering much of the dentary from visibility when the articulated lower jaw is seen in medial view. There are several individual contact sites for the splenial on the medial surface of the dentary, including an anteroposteriorly elongate articular facet paralleling the ventral margin

of the dentary below the Meckelian fossa. This contact surface is dorsoventrally shallow and smooth in most theropods, including the coelurosaurian outgroups *Allosaurus* (Madsen 1976; UMNH VP9351) and *Sinraptor* (Currie and Zhao 1993) and nearly every coelurosaur that can be scored affirmatively for this character. The two exceptions are the derived tyrannosaurine tyrannosaurids *Tarbosaurus* (Hurum and Sabath 2003; ZPAL MgD-I/5) and *Tyrannosaurus* (Molnar 1991; Brochu 2003). In these taxa the splenial contact surface underneath the Meckelian fossa is dorsoventrally deep, so much so that it is nearly the same dorsoventral depth as the anterior portion of the Meckelian fossa. Furthermore, in these two large-bodied tyrannosaurids the contact surface is rugose instead of smoothly flat. This character was originally used by Brusatte et al. (2010a, character 174). States 0 and 1 are illustrated in Figure 2.17.

628. Dentary, anterior alveoli, size in comparison to alveoli in middle of tooth row: approximately same size (0); first two alveoli substantially smaller (1); first alveolus substantially smaller (2).

In most theropods the first two alveoli of the lower jaw are approximately the same size, or larger, than the following several alveoli, including those alveoli in the middle of the tooth row. This is the case in the coelurosaurian outgroups *Allosaurus* (Madsen 1976; UMNH VP9351) and *Sinraptor* (Currie and Zhao 1993) and nearly every coelurosaur that can be scored affirmatively for this character. The condition in many tyrannosauroids, however, is distinct. In most tyrannosauroids the first two alveoli are substantially smaller than the following alveoli. This condition is seen in *Proceratosaurus* (Rauhut et al. 2010; NHMUK R4860), *Dilong* (Xu et al. 2004; IVPP V14243), *Eotyrannus* (MIWG 1997.550), *Albertosaurus* and *Gorgosaurus* (Currie 2003), *Alioramus* (Brusatte et al. 2012a), and *Daspletosaurus* (Russell 1970). This

morphology is referred to as state 1 here. The derived tyrannosaurine tyrannosaurids *Tarbosaurus* (Hurum and Sabath 2003; ZPAL MgD-I/5) and *Tyrannosaurus* (Brochu 2003) possess a similar but slightly different condition in which only the first alveolus is markedly smaller than the following alveoli. Because so many characters from across the skeleton unite *Tarbosaurus* and *Tyrannosaurus* as sister taxa nested within a suite of tyrannosauroids with state 1 (e.g., Holtz 2001 2004; Currie 2003; Carr et al. 2005; Brusatte et al. 2009a, 2010a; Carr and Williamson 2010), we hypothesize that their morphology (scored for state 2) is a special case of state 1. Therefore, in order to preserve synapomorphy between these two conditions of alveolar size reduction in the anterior dentary, we consider this an ordered character here.

This character was first utilized by Brusatte et al. (2010a, character 175), but treated as unordered in that analysis. States 0, 1, and 2 are illustrated in Figure 2.18.

629. Dentary, dorsal margin of bone in lateral view, profile: straight (0); strongly concave (1); strongly convex (2).

In most theropods the dorsal (alveolar) margin of the dentary is straight (or nearly straight) when the lower jaw is seen in lateral view. This is the case in close coelurosaurian outgroups such as *Allosaurus* (Madsen 1976) and *Sinraptor* (Currie and Zhao 1993) and many coelurosaurs, including the basal coelurosaur *Ornitholestes* (AMNH FARB 619), basal tyrannosauroids (*Guanlong*: Xu et al. 2006; *Proceratosaurus*: Rauhut et al. 2010; *Dilong*: Xu et al. 2004; *Eotyrannus*: MIWG 1997.550), compsognathids (*Compsognathus*: Peyer 2006; *Huaxiagnathus*: Hwang et al. 2004; *Juravenator*: Chiappe and Göhlich 2010; *Sinocalliopteryx*: Ji et al. 2007; *Sinosauropteryx*: Currie and Chen 2001), ornithomimosaurs (e.g., *Gallimimus*: Osmólska et al. 1972; *Pelecanimimus*: LH 7777), alvarezsauroids (e.g., *Haplocheirus*: Choiniere

et al. 2010a; *Shuvuuia*: Chiappe et al. 1998), basal therizinosauroids (e.g., *Beipiaosaurus*: Xu et al. 1999; *Falcarius*: Zanno 2010a), some troodontids (e.g.., *Byronosaurus*: Makovicky et al. 2003; *Xixiasaurus*: Lü et al. 2010; *Zanabazar*: Norell et al. 2009), and most dromaeosaurids (e.g., *Buitreraptor*: Makovicky et al. 2005; *Dromaeosaurus*: Currie 1995; *Shanag*: Turner et al. 2007b; *Tsaagan*: Norell et al. 2006; *Velociraptor*: Barsbold and Osmólska 1999).

Some theropods, however, possess a dentary in which the dorsal margin is strongly concave. This is perhaps most notable in derived tyrannosauroids, including *Appalachiosaurus* (Carr et al. 2005), *Bistahieversor* (Carr and Williamson 2010), *Albertosaurus* and *Gorgosaurus* (Currie 2003), *Alioramus* (Brusatte et al. 2012a), *Teratophoneus* (Carr et al. 2011), *Daspletosaurus* (Russell 1970), *Tarbosaurus* (Hurum and Sabath 2003), and *Tyrannosaurus* (Brochu 2003). A concave dorsal margin is also seen in some troodontids (*Anchiornis*: Hu et al. 2009; *Xiaotingia*: Xu et al. 2011a) and some dromaeosaurids (*Microraptor*: Hwang et al. 2002; *Sinornithosaurus*: Xu and Wu 2001).

Furthermore, some theropods exhibit a third distinct condition in which the dorsal margin of the dentary is strongly convex. This is seen in all oviraptorosaurs, including *Caudipteryx* (Ji et al. 1998), *Citipati* (Clark et al. 1999), *Incisivosaurus* (Xu et al. 2002a; Balanoff et al. 2009), and *Oviraptor* (Osborn 1924; Clark et al. 1999). It is also present in the derived therizinosauroids *Alxasaurus* (Russell and Dong 1993), *Erlikosaurus* (Clark et al. 1994), and *Neimongosaurus* (Zhang et al. 2001), but not in the basal taxon *Falcarius* (see above).

This character was originally used by Brusatte et al. (2010a, character 177). The original character was binary and recognized the difference between a flat and a concave dorsal margin. A third state is added to the present analysis to refer to the convex condition (state 2). This resulting multistate character is left unordered because there is no clear nested hierarchy of

homologies between straight, concave, and convex conditions. States 0 and 1 are illustrated in Figure 2.17. State 2 is not illustrated here but can be seen in published figures, such as figure 10 in Clark et al. (1994).

630. Dentary, Meckelian groove, form: dorsoventrally deep and shallowly inset into medial surface of bone (0); dorsoventrally shallow and deeply inset into bone, groove appears as a thin, sharp structure (1).

The Meckelian groove is a longitudinal depression that extends anteroposteriorly on the medial surface of the dentary, beginning posteriorly at its confluence with the Meckelian fossa and continuing anteriorly until its termination at one or more foramina close to the anterior end of the dentary, in the region of the symphysis. In most theropods the groove is fairly dorsoventrally deep (approximately 20% or greater than the dorsoventral depth of the dentary) and shallowly inset. This condition is seen in the close coelurosaurian outgroups *Allosaurus* (Madsen 1976; UMNH VP9351) and *Sinraptor* (Currie and Zhao 1993), as well as nearly every coelurosaur that can be scored affirmatively for this character. A few coelurosaurs possess a distinctive condition in which the Meckelian groove is exceptionally dorsoventrally thin (less than 10% of the depth of the entire dentary) and deeply inset as a sharp groove. As a result, the Meckelian groove has the appearance of a thin incision on the medial surface of the dentary. This morphology is present in several tyrannosauroids, including *Bistahieversor* (NMMNH P-27469), *Daspletosaurus* (Currie 2003), *Alioramus* (Brusatte et al. 2012a), *Tarbosaurus* (Hurum and Sabath 2003), and *Tyrannosaurus* (Brochu 2003). The only tyrannosauroid that can be scored affirmatively but lacks this sharp, incision-like groove is *Eotyrannus* (MIWG 1997.550).

A sharp groove (state 1) is also present in a single troodontid, *Zanabazar* (Norell et al. 2009), and it is possible that it is present in other coelurosaurs but cannot be observed due to the rarity of exposed and well preserved medial dentaries in most taxa. The deep and shallow groove (state 0) is clearly present, however, in the basal coelurosaur *Ornitholestes* (AMNH FARB 619), *Compsognathus* (Peyer 2006), ornithomimosaurs (e.g.., *Gallimimus*: IGM 100/1133; *Garudimimus*: Kobayashi and Barsbold 2005a; *Harpymimus*: Kobayashi and Barsbold 2005b), therizinosauroids (e.g., *Alxasaurus*: Russell and Dong 1993; *Beipiaosaurus*: Xu et al. 1999; *Erlikosaurus*: Clark et al. 1994; *Falcarius*: Zanno 2010a), the troodontid *Xixiasaurus* (Lü et al. 2010), and several dromaeosaurids (e.g., *Austroraptor*: MML 195; *Dromaeosaurus*: Currie 1995; *Sinornithosaurus*: Xu and Wu 2001).

This character was first used by Brusatte et al. (2010a, character 178). States 0 and 1 are illustrated in Figure 2.17.

634. Surangular, surangular shelf on lateral surface, orientation relative to the long axis of the lower jaw: anterodorsal (0); anteroventral (1); straight anteroposteriorly (2).

In most theropods there is a shelf on the lateral surface of the surangular, above which the jaw adductor muscles attach. The presence/absence and position of the shelf is encapsulated by other characters in this dataset. The current character, which was first used by Brusatte et al. (2010a, character 182), refers to differences in the orientation of the shelf. This is an unordered multistate because there is no clear nested set of hierarchial homologies between the states. The three states are illustrated in Figure 2.19.

State 2, referring to a shelf that is approximately straight anteroposteriorly and roughly parallel to the long axis of the lower jaw, is present in the coelurosaurian outgroups *Allosaurus*

(Madsen 1976) and *Sinraptor* (Currie and Zhao 1993). It is also seen in the basal coelurosaurs *Ornitholestes* (AMNH FARB 619) and *Compsognathus* (Peyer 2006), several derived tyrannosauroids (e.g., *Dryptosaurus*: Brusatte et al. 2011; *Bistahieversor*: Carr and Williamson 2010; *Gorgosaurus*: Currie 2003; *Alioramus*: Brusatte et al. 2012a; *Tarbosaurus*: Hurum and Sabath 2003; *Tyrannosaurus*: Brochu 2003), and dromaeosaurids (e.g., *Buitreraptor*: Makovicky et al. 2005; *Dromaeosaurus*: Currie 1995; *Sinornithosaurus*: Xu and Wu 2001; *Tsaagan*: Norell et al. 2006).

State 0, referring to a shelf that is oriented anterodorsal-posteroventral relative to the long axis of the lower jaw, is present in many coelurosaurs. This condition is seen in basal tyrannosauroids, including *Dilong* (Xu et al. 2004; IVPP V14243), *Guanlong* (Xu et al. 2006; IVPP V14531), *Kileskus* (Averianov et al. 2010), and *Proceratosaurus* (Rauhut et al. 2010; NHMUK R4860). It is also present in ornithomimosaurs (e.g., *Garudimimus*: Kobayashi and Barsbold 2005a; *Sinornithomimus*: Kobayashi and Lü 2003), alvarezsauroids (*Haplocheirus*: IVPP V15988), theizinosauroids (*Erlikosaurus*: Clark et al. 1994), and oviraptorosaurs (e.g., *Citipati*: Clark et al. 1999; *Incisivosaurus*: Balanoff et al. 2009).

State 1, referring to a shelf that is oriented anteroventral-posterodorsal relative to the long axis of the lower jaw, is present only in the basal tyrannosauroid *Eotyrannus* (MIWG 1997.550) among the taxa scored for the current phylogenetic analysis. Therefore, this character currently optimizes as an autapomorphy of *Eotyrannus*, but we retain it in the dataset because *Eotyrannus* cannot otherwise be scored for either state 0 or state 2, and because we anticipate future discoveries will show that other taxa shared this condition.

635. Surangular, pneumatic fossa posterodorsal to posterior surangular foramen: absent (0); present and shallow (1); present and deeply invaginated (2).

In most theropods there is no noticeable pneumaticity on the lateral surface of the surangular posterior to the surangular foramen (or in taxa without a surangular foramen, on the lateral surface of the surangular underneath and slightly anterior to the glenoid). Several tyrannosauroids, however, possess signs of pneumaticity in this region. This takes the form of a shallow fossa-like impression in *Albertosaurus* and *Gorgosaurus* (Currie 2003) and *Tarbosaurus* (Hurum and Sabath 2003; ZPAL MgD-I/4). This subtle condition is encapsulated by state 1. The pneumatic fossa is expanded into a deep, invaginated opening in *Alioramus* (Brusatte et al. 2012a) and *Tyrannosaurus* (Brochu 2003; CM 9380), which is referred to as state 2. Brochu (2003) used CT scans to show that this opening leads into a large internal recess in *Tyrannosaurus*, and unpublished data also shows that this is the case in *Alioramus* (Gold, Brusatte, and Norell unpub. data). A large, invaginated fossa also appears to be present in *Bistahieversor* (Carr and Williamson 2010; NMMNH P-27469) and *Daspletosaurus* (Currie 2003; T.D. Carr, pers. comm.), although CT scans are needed to confirm whether this leads into a large internal recess as in *Alioramus* and *Tyrannosaurus*. Regardless, *Bistahieversor* and *Daspletosaurus* are scored for state 2 because their pneumatic regions are similar in external morphology to those of *Alioramus* and *Tyrannosaurus*.

This character was first used by Brusatte et al. (2010a, character 183) and is treated as ordered because the three states form a nested hierarchy of homology (absent-small-large). Brusatte et al. (2012a) described how a juvenile specimen of *Tarbosaurus* (ZPAL MgD-I/31) lacks any sign of pneumaticity posterodorsal to the surangular foramen, and therefore it is likely that the presence and extent of pneumaticity in this region is ontogenetically variable. However,

the immature holotype specimen of *Alioramus altai* (IGM 100/1844), which is nearly exactly the same size as the juvenile *Tarbosaurus* specimen in question (ZPAL MgD-I/31), possesses a large and deeply invaginated pneumatic pocket posterodorsal to the surangular foramen. Therefore, there is no clear correlation between ontogeny/body size and the presence/absence or extent of surangular pneumaticity across all tyrannosauroids. The three states are illustrated in Figure 2.19, and states 1 and 2 are shown in closeup in Figure 2.20.

636. Surangular, adductor muscle attachment site dorsal to surangular shelf, orientation: faces primarily dorsally (0); faces almost equally dorsally and laterally (1); faces primarily laterally (2).

A large portion of the jaw adductor musculature attaches to the dorsolateral surface of the surangular in many theropods. The attachment facet is usually either a flat or depressed surface located above the lateral ridge on the surangular, or if this ridge is absent, on the dorsolateral edge of the posterior part of the bone. The orientation of this attachment surface differs among coelurosaurs.

State 0 describes an attachment surface that faces almost entirely dorsally. Therefore, in taxa that possess this character state, the muscle attachment facet is not strongly visible in lateral view but is widely visible in dorsal view. The coelurosaurian outgroups *Allosaurus* (Madsen 1976) and *Sinraptor* (Currie and Zhao 1993) are scored for this condition, as are many coelurosaurs, including the basal coelurosaur *Ornitholestes* (AMNH FARB 619), the basal tyrannosauroids *Guanlong* (IVPP V14531) and *Proceratosaurus* (NHMUK R4860), compsognathids (*Compsognathus*: Peyer 2006; *Juravenator*: Chiappe and Göhlich 2010), ornithomimosaurs (e.g.., *Garudimimus*: Kobayashi and Barsbold 2005a; *Sinornithomimus*:

Kobayashi and Lü 2003), alvarezsauroids (e.g., *Haplocheirus*: IVPP V15988; *Shuvuuia*: IGM 100/977), therizinosauroids (e.g., *Erlikosaurus*: Clark et al. 1994; *Falcarius*: Zanno 2010a), and oviraptorosaurs (e.g., *Citipati*: Clark et al. 1999; *Incisivosaurus*: Balanoff et al. 2009). This condition is also seen in the tyrannosauroid *Bistahieversor* (Carr and Williamson 2010), which is unusual for a derived tyrannosauroid (see below).

State 1 describes an intermediate condition between states 0 and 2, in which the attachment facet faces almost equally laterally and dorsally. Therefore, it is equally visible in lateral and dorsal views. This condition is seen in several tyrannosauroids, including *Kileskus* (Averianov et al. 2010), *Eotyrannus* (MIWG 1997.550), *Dryptosaurus* (Brusatte et al. 2011), *Albertosaurus* and *Gorgosaurus* (Currie 2003), *Alioramus* (Brusatte et al. 2012a), and *Daspletosaurus* (Russell 1970). It is also present in several dromaeosaurids, including *Bambiraptor* (Burnham et al. 2000), *Deinonychus* (Ostrom 1969), *Dromaeosaurus* (Currie 1995), *Velociraptor* (Barsbold and Osmólska 1999), *Sinornithosaurus* (Xu and Wu 2001), and *Tsaagan* (Norell et al. 2006).

State 2 refers to a condition in which the attachment facet faces primarily laterally. In taxa possessing this state the facet is visible strongly in lateral view, as a discrete dorsally projecting flange eminating from the dorsal edge of the surangular, but is not widely observable in dorsal view. This condition is seen in the basal tyrannosauroid *Dilong* (IVPP V14243) and the derived tyrannosaurine tyrannosaurids *Tarbosaurus* (Hurum and Sabath 2003) and *Tyrannosaurus* (Brochu 2003).

This character was first utilized by Brusatte et al. (2010a, character 184). It is treated as an ordered multistate because the three conditions describe a hierarchial set of homologies (dorsal-dorsolateral-lateral). The three states are illustrated in Figure 2.19.

637. Surangular, triangular fossa on the lateral surface of the surangular shelf immediately anteroventral to glenoid: absent (0); present (1).

Several tyrannosauroids possess a shallow triangular fossa on the lateral surface of the surangular shelf, below and slightly anterior to the glenoid. This feature is seen in *Bistahieversor* (Carr and Williamson 2010; NMMNH P-27469), *Albertosaurus* and *Gorgosaurus* (Currie 2003), *Alioramus* (Brusatte et al. 2012a), *Daspletosaurus* (Currie 2003), and *Tyrannosaurus* (Brochu 2003; CM 9380). It is most likely present in *Tarbosaurus*, based on its presence in several close relatives, but none of the specimens observed in the Warsaw ZPAL collection as part of this dissertation work were well preserved enough to score this character affirmatively (therefore, *Tarbosaurus* is scored as "?"). The fossa is demonstrably absent in the basal tyrannosauroids *Guanlong* (IVPP V14531), *Proceratosaurus* (NHMUK R4860), *Kileskus* (Averianov et al. 2010), and *Eotyrannus* (MIWG 1997.550). It is also absent in all other coelurosaurs that could be scored affirmatively, as well as the outgroups *Allosaurus* (Madsen 1976) and *Sinraptor* (Currie and Zhao 1993). This character was first used by Brusatte et al. (2010a, character 185). States 0 and 1 are shown in Figure 2.19 and state 1 is shown in close-ups in Figure 2.20.

638. Surangular, fossa on the lateral surface of the bone immediately ventral to, and separated from, the glenoid: absent (0); present (1).

In addition to the triangular fossa on the surangular shelf, several tyrannosauroids also possess a distinct fossa on the lateral surface of the surangular immediately ventral to the glenoid. This fossa is separated from the glenoid fossa by a smooth and subtle lip of bone. The lateral surface fossa is present on all tyrannosauroids that possess the triangular fossa (character

637), and it is also observable in *Dryptosaurus* (Brusatte et al. 2011) and *Tarbosaurus* (Hurum and Sabath 2003; ZPAL MgD-I/4, MgD-I/31), both of which are scored as uncertain for the triangular fossa character. Among tyrannosauroids, the lateral surface fossa is demonstrably absent in the basal taxa *Guanlong* (IVPP V14531), *Proceratosaurus* (NHMUK R4860), *Dilong* (IVPP V14243), and *Eotyrannus* (MIWG 1997.550). It is also absent in all other coelurosaurs that could be scored affirmatively, as well as the outgroups *Allosaurus* (Madsen 1976) and *Sinraptor* (Currie and Zhao 1993). This character was first used by Brusatte et al. (2010a, character 186). States 0 and 1 are illustrated in Figure 2.19 and close-ups of state 1 are shown in Figure 2.20..

639. Surangular, anteroposterior length of anterior flange (region anterior to anterior margin of external mandibular fenestra) compared to overall length of surangular: less than (0) or greater than (1) 30%.

In most theropods there is only a small region of the surangular that projects anterior to the anterior edge of the external mandibular fenestra. In these taxa, the anteriorly projecting region (referred to as the "anterior flange") has an anteroposterior length that is less than 30% of the anteroposterior length of the entire surangular. The length of the anterior flange is taken to be the length of the surangular anterior to the anteriormost tip of the external mandibular fenestra, whereas the length of the entire surangular is the maximum anteroposterior length of the bone. The small anterior flange (state 0) is present in the coelurosaurian outgroups *Allosaurus* (Madsen 1976) and *Sinraptor* (Currie and Zhao 1993), and nearly every coelurosaur for which this character can be scored affirmatively. In contrast, the anterior flange is greater than 30% of the length of the surangular in the basal tyrannosauroids *Guanlong* (Xu et al. 2006; IVPP V14531),

Proceratosaurus (Rauhut et al. 2010; NHMUK R4860), as well as the more derived tyrannosaurid tyrannosauroid *Alioramus* (Brusatte et al. 2012a) and the ornithomimosaur *Ornithomimus* (Makovicky et al. 2004). This character was first used by Brusatte et al. (2010a, character 187). The character states are not illustrated here but they can be seen in published skull reconstructions (e.g., state 0: Hurum and Sabath 2003: figure 1; state 1: Brusatte et al. 2012: figure 4).

640. Angular, ventral margin, form: smoothly convex (0); anterior region "flexed" relative to posterior region, such that there is a discrete step between them (1).

In most theropods the angular has a convex ventral margin, and the anterior and posterior processes merge with each other smoothly, without any offset of one process relative to the other. This is the case in the coelurosaurian outgroups *Allosaurus* (Madsen 1976) and *Sinraptor* (Currie and Zhao 1993), as well as nearly every coelurosaur for which this character can be scored affirmatively. In contract, the derived tyrannosaurine tyrannosaurids *Daspletosaurus* (Russell 1970), *Tarbosaurus* (Hurum and Sabath 2003; ZPAL MgD-I/4), and *Tyrannosaurus* (Brochu 2003) exhibit a different morphology. In these taxa the anterior region is offet dorsally relative to the posterior process, and therefore, there is a discrete notch between them along the ventral margin of the angular. This character was originally used by Brusatte et al. (2010a, character 188). States 0 and 1 are illustrated in Figure 2.21.

641. Articular, mediolateral width of jaw muscle attachment site: less than width of glenoid for articulation with quadrate (0); approximateily equal to width of glenoid (1)

There is a distinctive attachment site for the jaw depressor muscles on the dorsal surface of the articular in most theropods. In most coelurosaurs the mediolateral width of the attachment site is less than the mediolateral width of the glenoid fossa (note that the glenoid fossa is usually shared between the articular and surangular, and this character refers to the width of the entire fossa on both bones). This is the case in the coelurosaurian outgroup *Allosaurus* (Madsen 1976), and it is also observed in nearly every coelurosaur that can be scored affirmatively for this character. The exceptions are nearly all tyrannosauroids, in which the width of the muscle attachment site is approximately equal to that of the glenoid. This morphology is present in *Dilong* (IVPP V14243), *Bistahieversor* (Carr and Williamson 2010; NMMNH P-27469), *Gorgosaurus* (Currie 2003), *Teratophoneus* (T.D. Carr, pers. comm.), *Daspletosaurus* (Currie 2003), *Tarbosaurus* (Hurum and Sabath 2003; ZPAL MgD-I/4), and *Tyrannosaurus* (Brochu 2003). The only tyrannosauroid that can be scored affirmatively that lacks this character state (i.e., that is scored for state 0 instead of state 1) is *Proceratosaurus* (Rauhut et al. 2010; NHMUK R4860).

This character was first used in a cladistic analysis by Brusatte et al. (2010a, character 189) and was inspired by discussion in Rauhut et al. (2010). The two character states are not illustrated here, but each is figured in the literature (e.g., state 0: Madsen 1976: plate 7; state 1: Currie 2003: figure 4). It is likely that this character is related to the reduced retroarticular process of the articular in tyrannosauroids, which is expressed by a separate character in this analysis (character 76). However, these two characters are not redundant, as *Proceratosaurus* (along with all tyrannosauroids that can be scored affirmatively) are scored for a reduced retroarticular process in character 76, but *Proceratosaurus* is not scored for the proportionally

large muscle attachment site (opposite of the condition in all other tyrannosauroids) in the present character.

642. Articular, smooth non-articular region between glenoid and attachment site for depressor mandibular muscles: present (0); absent (1).

In most theropods there is a distinct non-articular surface between the smooth glenoid fossa and the attachment site for the jaw depressors on the dorsal surface of the articular. This is the case in coelurosaurian outgroups *Allosaurus* (Madsen 1976) and *Sinraptor* (Currie and Zhao 1993) and is also present in nearly all coelurosaurs that can be scored affirmatively for this character. The exceptions are nearly all tyrannosauroids, in which the glenoid fossa and muscle attachment site abut each other, with no intervening non-articular surface between them. This condition is seen in *Dilong* (IVPP V14243), *Bistahieversor* (Carr and Williamson 2010; NMMNH P-27469), *Albertosaurus* and *Gorgosaurus* (Currie 2003), *Teratophoneus* (T.D. Carr, pers. comm.), *Daspletosaurus* (Currie 2003), *Tarbosaurus* (Hurum and Sabath 2003; ZPAL MgD-I/4), and *Tyrannosaurus* (Brochu 2003). The only tyrannosauroid that can be scored affirmatively that lacks this character state (i.e., that is scored for state 0 instead of state 1) is *Proceratosaurus* (Rauhut et al. 2010; NHMUK R4860).

This character was first used in a cladistic analysis by Brusatte et al. (2010a, character 190) and was inspired by discussion in Rauhut et al. (2010). The two character states are not illustrated here, but each is figured in the literature (e.g., state 0: Madsen 1976: plate 7; state 1: Currie 2003: figure 4). It is likely that this character is related to the reduced retroarticular process of the articular in tyrannosauroids (character 76 in the current analysis) and the character relating to the enlarged muscle attachment site on the articular (character 641 above). This

character is not redundant with character 76, because *Proceratosaurus* is scored for a reduced retroartcular process but still retains a non-articular region between the glenoid and muscle attachment site. Whether this character is redundant with character 641 is less certain. All taxa that can be scored affirmatively are scored identically for both characters, including *Proceratosaurus* (which is scored for state 0 for both characters 641 and 642 whereas all other tyrannosauroids are scored for state 1). We provisionally retain both of these characters here, until future discoveries will help clarify their relationship.

644. Splenial, dorsal region overlapped medially by prearticular: absent (0); present (1).

In most theropods in which the splenial and prearticular are preserved together and in articular (or near articulation), the posterodorsal region of the splenial abuts the anterodorsal edge of the prearticular. At most, the prearticular only slightly overlaps the splenial medially. This condition is present in the coelurosaur outgroup *Allosaurus* (Madsen 1976) and most of the handful of coelurosaurs that can be positively assessed for this character (*Alioramus*: Brusatte et al. 2012a; *Citipati*: Clark et al. 1999; *Dromaeosaurus*: Currie 1995; *Erlikosaurus*: Clark et al. 1994; *Gallimimus*: Osmólska et al. 1972; *Garudimimus*: Kobayashi and Barsbold 2005a; *Ornitholestes*: AMNH FARB 619; *Shuvuuia*: IGM 100/977). The derived tyrannosaurine tyrannosaurids *Tarbosaurus* (Hurum and Currie 2000; Hurum and Sabath 2003) and *Tyrannosaurus* (Brochu 2003) possess a distinct morphology in which the prearticular broadly overlaps the splenial in this region. This character was originally utilized by Brusatte et al. (2010a, character 192). The character states are not figured here, but the unusual condition 1 is figured for *Tarbosaurus* and *Tyrannosaurus* by Hurum and Currie (2000: figures 1-2), Hurum and Sabath (2003: figure 19), and Brochu (2003: figure 40).

645. Prearticular, ventral bar, series of ridges on lateral surface to strengthen articulation with angular: absent (0); present (1).

In many theropods the lateral surface of the prearticular abuts the medial surface of the angular, and at the very least, there are only small ridge and grooves to strengthen this contact. This is the case in the coelurosaur outgroup *Allosaurus* (Madsen 1976; UMNH VP499), the dromaeosaurid *Deinonychus* (Ostrom 1969), and the tyrannosauroid *Alioramus* (Brusatte et al. 2012a). In other tyrannosauroids, however, the lateral surface of the prearticular bears a series of pronounced ridges to strengthen contact with the angular (Hurum and Currie 2000). This condition is present in *Bistahieversor* (NMMNH P-27469), *Albertosaurus* and *Gorgosaurus* (Currie 2003), *Daspletosaurus* (T.D. Carr, pers. comm.), *Tarbosaurus* (Hurum and Currie 2000; Hurum and Sabath 2003), and *Tyrannosaurus* (Brochu 2003). It seems unusual that state 1 is absent in *Alioramus* given that it is present in many close relatives. The specimen of *Alioramus* that is used to score the taxon, IGM 100/1844, is an immature individual (Brusatte et al. 2009a, 2012a). Therefore, it may be that the pronounced ridges are ontogenetically variable and develop only late in ontogeny in concert with the development of the robust skull and jaws of adult tyrannosaurids. This character was originally used by Brusatte et al. (2010a, character 163). States 0 and 1 are illustrated in Figure 2.22.

646. Supradentary ossification, shape: elongate, shallow strip (0); deep, crescentic shape (1).

Very few theropod specimens preserve a complete or near complete supradentary bone on the medial surface of the lower jaw. This is likely because the supradentary is a thin plate in most taxa and susceptible to breakage. Among those theropods that preserve supradentaries, two

general shapes of this bone are apparent. In the coelurosaur outgroup *Allosaurus* (Madsen 1976), the basal coelurosaur *Ornitholestes* (AMNH FARB 619), the dromaeosaurid *Dromaeosaurus* (Currie 1995), and several tyrannosauroids the supradentary is an elongate, shallow strip that maintains a relatively constant dorsoventral depth across its anteroposterior length, with a relatively straight ventral margin. Tyrannosauroids with this morphology include *Bistahieversor* (NMMNH P-27469), *Albertosaurus* and *Gorgosaurus* (Currie 2003; T.D. Carr, pers. comm.), *Daspletosaurus* (Currie 2003), and *Alioramus* (Brusatte et al. 2012a). The derived tyrannosaurine tyrannosaurids *Tarbosaurus* and *Tyrannosaurus* possess a distinctive morphology in which the supradentary is exceptionally deep and crescentic in shape, with a convex ventral margin (Hurum and Currie 2000; Brochu 2003; Hurum and Sabath 2003). This character was first utilized by Brusatte et al. (2010a, character 194). The character states are not figured here but are well illustrated in the literature (e.g., state 0: Madsen 1976: plate 9; state 1: Hurum and Sabath 2003: figures 19 and 20).

647. Supradentary and coronoid ossifications, form of contact at their zone of fusion: smoothly confluent (0); offset by a concave notch (1).

In those few non-avian theropods that preserve a supradentary and coronoid these bones are usually indistinguishably fused (Brochu 2003). In the coelurosaur outgroup *Allosaurus* (Madsen 1976), the basal coelurosaur *Ornitholestes* (AMNH FARB 619), and the tyrannosauroids *Alioramus* (Brusatte et al. 2012) and *Daspletosaurus* (Currie 2003) the supradentary and coranoid are smoothly confluent where they meet and the ventral margin of this region is shallowly concave. In *Tarbosaurus* and *Tyrannosaurus*, however, the supradentary and coronoid portions are fused by offset from each other by a concave notch along the ventral

margin where they meet (Hurum and Currie 2000; Brochu 2003; Hurum and Sabath 2003). This character was first utilized by Brusatte et al. (2010a, character 195). The character states are not figured here but are well illustrated in the literature (e.g., state 0: Brusatte et al. 2012a: figure 41; state 1: Hurum and Sabath 2003: figures 19 and 20).

650. Premaxillary teeth, curvature of distal (posterior) teeth: recurved (0); straight (1).

The premaxillary teeth of most theropods are recurved distally (posteriorly), and this curvature ranges from pronounced to subtle. This is true of both mesial (anterior) and distal (posterior) premaxillary teeth. Such curvature is present in the coelurosaurian outgroups *Allosaurus* (Madsen 1976) and *Sinraptor* (Currie and Zhao 1993), as well as most coelurosaur taxa, including the basal coelurosaur *Ornitholestes* (AMNH FARB 619), the basal tyrannosauroids *Guanlong* (Xu et al. 2006; IVPP V14531) and *Proceratosaurus* (Rauhut et al. 2010; NHMUK R4860), compsognathids (*Compsognathus*: Peyer 2006; *Huaxiagnathus*: Hwang et al. 2004; *Juravenator*: Chiappe and Göhlich 2010; *Sinosauropteryx*: Currie and Chen 2001), the basal ornithomimosaur *Pelecanimimus* (Perez-Moreno et al. 1994; LH 7777), the basal oviraptorosaur *Caudipteryx* (Ji et al. 1998), troodontids (e.g., *Byronosaurus*: Makovicky et al. 2003; *Saurornithoides* and *Zanabazar*: Norell et al. 2009), and dromaeosaurids (e.g., *Dromaeosaurus*: Currie 1995; *Sinornithosaurus*: Xu and Wu 2001; *Tsaagan*: Norell et al. 2006; *Velociraptor*: Barsbold and Osmólska 1999).

In some coelurosaurs, however, the distal (posterior) premaxillary teeth are essentially straight, with no pronounced distal recurvature. This morphology is present in several tyrannosauroids, including *Dilong* (IVPP V14243), *Albertosaurus* and *Gorgosaurus* (Currie 2003), *Daspletosaurus* (Russell 1970), *Tarbosaurus* (Hurum and Sabath 2003), and

Tyrannosaurus (Molnar 1991; Brochu 2003; Smith 2005). It is also present in the basal oviraptorosaur *Incisivosaurus* (Xu et al. 2002a; Balanoff et al. 2009) and the scansoriopterygid *Epidexipteryx* (Zhang et al. 2008).

This character was first used by Brusatte et al. (2010a, character 199). States 0 and 1 are shown in Figure 2.23.

654. Axis, pneumatic foramen (pleurocoel), position: near midheight of centrum (0); dorsally located, directly underneath neurocentral suture and directly posterior to diapophysis (1).

The axial centrum of most theropods is excavated by a pneumatic foramen ("pleurocoel") on its lateral surface. In some taxa the foramen is located at approximately the dorsoventral midheight of the centrum, and may be placed either centrally or anteriorly relative to the anteroposterior center of the centrum. This condition is seen in some tyrannosauroids (e.g., *Alioramus*: Brusatte et al. 2012a; *Daspletosaurus*: AMNH FARB 6458; *Dilong*: IVPP V14243), the basal coelurosaur *Sinocalliopteryx* (Ji et al. 2007), some ornithomimosaurs (e.g., *Pelecanimimus*: LH 7777), and dromaeosaurids (e.g., *Deinonychus*: Ostrom 1969; *Mahakala*: Turner et al. 2011). A different condition is present in a handful of other taxa, in which the pneumatic foramen is positioned dorsal to the dorsoventral midheight of the centrum, immediately below and abutting the neurocentral suture and directly posterior to the diapophysis. This morphology is seen in the coelurosaurian outgroups *Allosaurus* (Madsen 1976) and *Sinraptor* (Currie and Zhao 1993) and the derived tyrannosaurine tyrannosaurids *Tarbosaurus* (ZPAL MgD-I/09) and *Tyrannosaurus* (Brochu 2003). It also appears to be present in *Ornithomimus* (Makovicky et al. 2004). This character was first utilized by Brusatte et al. (2010a, character 203). States 0 and 1 are shown in Figure 2.24.

655. Axis, pneumatic foramen, extent of surrounding fossa: limited to margins of foramen (0); extensive, occupies most of lateral surface of centrum (1).

In most theropods the pneumatic foramen on the axis is surrounded by a narrow fossa, which is restricted to the immediate region around the margins of the foramen. This condition is present in the outgroups *Allosaurus* (Madsen 1976) and *Sinraptor* (Currie and Zhao 1993), as well as some tyrannosauroids (e.g., *Alioramus*: Brusatte et al. 2012a; *Daspletosaurus*: AMNH FARB 6458; *Dilong*: IVPP V14243), the basal coelurosaur *Sinocalliopteryx* (Ji et al. 2007), ornithomimosaurs (e.g., *Garudimimus*: Kobayashi and Barsbold 2005a; *Pelecanimimus*: LH 7777), and dromaeosaurids (e.g., *Deinonychus*: Ostrom 1969; *Mahakala*: Turner et al. 2011). The tyrannosaurids *Tarbosaurus* (ZPAL MgD-I/09) and *Tyrannosaurus* (Brochu 2003) exhibit an unusual condition in which the fossa surrounding the pneumatic foramen is so extensive that it covers much of the lateral surface of the axial centrum. This character was first utilized by Brusatte et al. (2010a, character 204). States 0 and 1 are shown in Figure 2.24.

656. Axis, ridge on ventral surface of centrum: absent (0); present (1).

The ventral surface of the axial centrum is smooth in the coelurosaurian outgroups *Allosaurus* (Madsen 1976) and *Sinraptor* (Currie and Zhao 1993), the dromaeosaurid *Deinonychus* (Ostrom 1969), the ornithomimosaur *Gallimimus* (Osmólska et al. 1972), and some tyrannosauroids (e.g., *Daspletosaurus*: AMNH FARB 6458; *Dilong*: IVPP V14243; *Xiongguanlong*: FRDC-GS JB16-2-1). In contrast, the ventral surface bears a pronounced midline longitudinal ridge (sometimes referred to as a keel) in the tyrannosauroids *Alioramus* (Brusatte et al. 2012a), *Tarbosaurus* (ZPAL MgD-I/09), and *Tyrannosaurus* (Brochu 2003).

Unfortunately this character cannot be scored in most coelurosaurs, because few taxa are represented by well preserved axes that can be observed in ventral view. It is also worth noting that, although absent in the two outgroups used in the current analysis, the ventral ridge is present in some basal tetanuran outgroups to coelurosaurs (e.g., Brusatte and Sereno 2008). This character was first utilized in a phylogenetic analysis of coelurosaurs by Brusatte et al. (2010a, character 205). States 0 and 1 are shown in Figure 2.24.

657. Axis, pneumatic foramina and fossae on each side of the anterior ridge on the neural spine: absent (0); present (1).

The axial neural spine of most theropods is ornamented by a pronounced dorsoventrally-trending ridge on its anterior surface, which separated muscle attachment sites on the left and right sides of the surface. Some tyrannosauroids possess a distinctive condition in which large pneumatic foramina and fossae are positioned on each side of this anterior ridge. Taxa with this morphology include *Bistahieversor* (T.D. Carr, pers. comm.), *Daspletosaurus* (AMNH FARB 6458), *Tarbosaurus* (ZPAL MgD-I/09), and *Tyrannosaurus* (Brochu 2003). This condition is also present in one non-tyrannosauroid coelurosaur: the basal ornithomimosaur *Pelecanimimus* (LH 7777). In contrast, these pneumatic foramina and fossae are absent in the tyrannosauroids *Alioramus* (Brusatte et al. 2012a), *Dilong* (IVPP V14243), *Eotyrannus* (MIWG 1997.550), and *Xiongguanlong* (FRDC-GS JB16-2-1). They are also absent in the outgroups *Allosaurus* (Madsen 1976) and *Sinraptor* (Currie and Zhao 1993) and all other coelurosaurs that can be scored affirmatively for this character, including most ornithomimosaurs (e.g., *Garudimimus*: Kobayashi and Barsbold 2005a; *Sinornithomimus*: Kobayashi and Lü 2003), oviraptorosaurs (e.g., *Microvenator*: Makovicky and Sues 1998), and dromaeosaurids (e.g., *Deinonychus*:

Ostrom 1969; *Tsaagan*: Norell et al. 2006). This character was first utilized by Brusatte et al. (2010, character 206). States 0 and 1 are illustrated in Figure 2.24

658. Axis, neural spine, texture of dorsal region of anterior surface: generally smooth or with subtle texture (0); highly rugose, with series of grooves, ridges, and eminences (1).

The dorsal region of the axial neural spine is generally smooth in most theropods, and at most it is marked by a subtle and random array of small pits and grooves. This morphology is characteristic of the coelurosaurian outgroups *Allosaurus* (Madsen 1976) and *Sinraptor* (Currie and Zhao 1993), as well as some tyrannosauroids (e.g., *Alioramus*: Brusatte et al. 2012a; *Dilong*: IVPP V14243; *Eotyrannus*: MIWG 1997.550; *Xiongguanlong*: FRDC-GS JB16-2-1), the basal coelurosaur *Sinocalliopteryx* (Ji et al. 2007), ornithomimosaurs (e.g., *Garudimimus*: Kobayashi and Barsbold 2005a; *Pelecanimimus*: LH 7777), oviraptorosaurs (e.g., *Microvenator*: Makovicky and Sues 1998), and dromaeosaurids (e.g., *Deinonychus*: Ostrom 1969; *Tsaagan*: Norell et al. 2006). A noticeably different morphology is seen in some derived tyrannosauroids, including *Bistahieversor* (T.D. Carr, pers. comm.), *Daspletosaurus* (AMNH FARB 6458), *Tarbosaurus* (ZPAL MgD-I/09), and *Tyrannosaurus* (Brochu 2003). In these taxa the dorsal region of the neural spine is heavy rugose and ornamented by a marked series of grooves, ridges, and protuberances. This character was originally used by Brusatte et al. (2010a, character 207). States 0 and 1 are shown in Figure 2.24.

659. Axis, dorsal region of neural spine, number of projections on “crown” region: two lateral projections, dorsal surface of spine smoothly concave (0); two lateral projections and one dorsal projection on the midline (1).

Some theropods have a mediolaterally broad axial neural spine, whose dorsal region is mediolaterally flared relative to the remainder of the spine. The presence or absence of this morphology is encapsulated by character 92, and the mediolaterally broad condition is generally seen in tyrannosauroids and outgroups, but absent in most other coelurosaurs. Among those taxa with a mediolaterally broad spine, two variable conditions of the dorsal tip of the spine (the so-called "crown region") are observable. Some taxa possess a crown region with lateral projections on the left and right dorsolateral tips of the crown, and as a result, the dorsal margin of the crown is smoothly concave or nearly straight. This is seen in the outgroup *Allosaurus* (Madsen 1976), as well as the tyrannosauroids *Alioramus* (Brusatte et al. 2012a), *Tyrannosaurus* (Brochu 2003), and *Xiongguanlong* (FRDC-GS JB16-2-1). A different condition is present in *Bistahieversor* (T.D. Carr, pers. comm.), *Daspletosaurus* (AMNH FARB 6458), and *Dilong* (IVPP V14243). In these taxa the crown is marked by the two aforementioned lateral projections and also by a third, central, dorsally-extending projection. Therefore, the dorsal margin of the crown region is not a smooth concave or straight edge. This character was first utilized by Brusatte et al. (2010a, character 208). State 0 is illustrated in Figure 2.24.

660. Axis, supradiapohyseal fossa (fossa posterodorsal to diapophysis): absent or shallow (0); deeply excavated and funnel-like (1).

In some theropods there is a distinctive fossa on the lateral surface of the axial neural arch, posterodorsal to the diapophysis and bounded dorsally by a lamina linking the diapophysis and postzygapophysis (the postzygapodiapophyseal lamina). This fossa is referred to as the supradiapophyseal fossa (Brochu 2003). The fossa is shallow, or absent entirely, in many theropods, including the coelurosaurian outgroups *Allosaurus* (Madsen 1976) and *Sinraptor*

(Currie and Zhao 1993), many tyrannosauroids (e.g., *Alioramus*: Brusatte et al. 2012a; *Daspletosaurus*: AMNH FARB 6458; *Dilong*: IVPP V14243; *Xiongguanlong*: FRDC-GS JB16-2-1), ornithomimosaurs (e.g., *Garudimimus*: Kobayashi and Barsbold 2005a; *Sinornithomimus*: Kobayashi and Lü 2003), and dromaeosaurids (e.g., *Deinonychus*: Ostrom 1969; *Tsaagan*: Norell et al. 2006). Note that absent and shallow fossae are considered equivalent here, because in practice it is often difficult to distinguish a very shallow fossa from one that is genuinely absent. The derived tyrannosaurine tyrannosaurids *Tarbosaurus* (ZPAL MgD-I/09) and *Tyrannosaurus* (Brochu 2003) possess an unusual condition in which the supradiapophyseal fossa is broadly exposed in lateral view and deeply excavated, such that it appears funnel-like. This character was first used by Brusatte et al. (2010a, character 209). States 0 and 1 are shown in Figure 2.24.

662. Cervical vertebrae, morphology of posterior centrodiapophyseal laminae in anterior-middle cervicals: absent or present as a weak ridge (0); present as a thick, laterally offset lamina that demarcates a deep infradiapophyseal fossa anteriorly (1).

Most theropods exhibit anterior and posterior centrodiapophyseal lamina on some or all of the cervical and dorsal vertebrae (Wilson 1999). These strut-like ridges of bone are present on the lateral surface of the vertebra and link the diapophysis dorsally with the centrum ventrally. In most theropods the posterior centrodiapophyseal lamina of the anterior-middle cervicals is present as a thin ridge, which is clearly offset from the lateral surface of the vertebra but not especially robust. This condition is present in the coelurosaurian outgroups *Allosaurus* (Madsen 1976) and *Sinraptor* (Currie and Zhao 1993) as well as nearly every coelurosaur that can be scored affirmatively for this character, including the tyrannosauroids *Dilong* (IVPP V14243),

Eotyrannus (MIWG 1997.550), *Guanlong* (IVPP V14531), *Juratyrant* (Benson 2008), and *Xiongguanlong* (FRDC-GS JB16-2-1). The derived tyrannosauroids *Alioramus* (Brusatte et al. 2012a), *Daspletosaurus* (AMNH FARB 6458), *Tarbosaurus* (Maleev 1974), and *Tyrannosaurus* (Brochu 2003) have a distinctive condition in which the posterior centrodiapophyseal lamina is expressed as a dorsoventrally thick shelf that overhangs the lateral surface of the centrum far laterally as a web, demarcating a deep infradiapophyseal anteroventrally. This character was first used by Brusatte et al. (2010a, character 213). States 0 and 1 are shown in Figure 2.25.

663. Cervical vertebrae, hypapophysis on anterior region of ventral surface: absent (0); present (1).

Some derived tyrannosauroids possess a hypapophysis—a pronounced process that projects anteriorly and ventrally—at the anterior edge of the ventral surface of the centrum of some or all cervical vertebrae. These structures are observable on some cervicals of *Alioramus* (Brusatte et al. 2012a) and the anterior cervicals, but not those posterior to cervical 5, in *Tyrannosaurus* (Brochu 2003). They are also present in *Daspletosaurus* (AMNH FARB 6458) and *Xiongguanlong* (FRDC-GS JB16-2-1). These structures are absent on all known cervicals of the tyrannosauroids *Dilong* (IVPP V14243), *Eotyrannus* (MIWG 1997.550), *Guanlong* (IVPP V14531) and *Juratyrant* (Benson 2008), as well as the cervicals of coelurosaurian outgroups (e.g., Madsen 1976; Currie and Zhao 1993) and all coelurosaurs that can be scored affirmatively for this character, with the exception of the four tyrannosauroids listed above. This character was originally utilized by Brusatte et al. (2010a, character 214). State 0 is illustrated in Figure 2.25 and state 1 can be seen in Brochu (2003: figures 50-51).

664. Cervical vertebrae, position of prezygapophysis in middle cervicals: slightly overhangs centrum laterally (0); strongly overhangs centrum laterally, entire prezygapophyseal facet placed lateral to centrum (1).

In almost all coelurosaurs the prezygapophyses of the middle cervicals (and often the anterior and posterior cervicals) are placed far laterally, such that the entire articular facet of the zygapophysis is positioned lateral to the centrum. This condition, codified by state 1, is readily observable in dorsal and ventral views, where it can be seen that the prezygapophyses are offset substantially laterally relative to the lateral margins of the centrum. Derived tyrannosauroids such as *Xiongguanlong* (FRDC-GS JB16-2-1), *Alioramus* (Brusatte et al. 2012a), and *Tyrannosaurus* (Brochu 2003) possess this morphology, as do the vast majority of coelurosaurs that can be scored affirmatively for this character. The few exceptions include the basal coelurosaurs *Coelurus* (YPM 2010), *Dilong* (Xu et al. 2004; IVPP V14243), *Guanlong* (IVPP V14531), and *Zuolong* (Choiniere et al. 2010b). In these taxa the prezygapophyses are not positioned far laterally relative to the centrum in dorsal view, and when the vertebrae are seen in anterior view much of the articular facet of the zygapophysis is seen not to extend laterally past the level of the lateral edge of the centrum. This morphology is also present in the coelurosaurian outgroups *Allosaurus* (Madsen 1976) and *Sinraptor* (Currie and Zhao 1993). This character was first used by Brusatte et al. (2010a, character 215). States 0 and 1 are shown in Figure 2.25.

665. Cervical vertebrae, orientation of posterior centrodiapophyseal lamina in anterior-middle cervicals: projects posteroventrally, infrapostzygapophyseal fossa located primarily posterior to lamina (0); nearly horizontal, fossa located primarily dorsal to lamina (1).

In most theropods, the posterior centrodiapophyseal lamina, which connects the diapophysis and lateral surface of the centrum, projects strongly posteroventrally when seen in lateral view (Wilson 1999). As a result, the infrapostzygapophyseal fossa is positioned posterior to the lamina. This is the case in the coelurosaurian outgroups *Allosaurus* (Madsen 1976) and *Sinraptor* (Currie and Zhao 1993), most tyrannosauroids (e.g., *Alioramus*: Brusatte et al. 2012a; *Tyrannosaurus*: Brochu 2003; *Xiongguanlong*: FRDC-GS JB16-2-1), and nearly every other coelurosaur that can be scored affirmatively for this character (e.g., *Deinonychus*: Ostrom 1969; *Falcarius*: Zanno 2010a; *Gallimimus*: ZPAL MgD-I/1; *Ornitholestes*: AMNH FARB 619). A subset of basal coelurosaurs possesses a different morphology in which the posterior centrodiapophyseal lamina is nearly horizontal in orientation, which results in an infrapostzygapophyseal fossa that is positioned dorsal to the lamina. This condition is seen in *Coelurus* (YPM 2010), *Dilong* (Xu et al. 2004; IVPP V14243), *Guanlong* (IVPP V14531), and *Juratyrant* (Benson 2008). This character was first utilized by Brusatte et al. (2010a, character 216). States 0 and 1 are shown in Figure 2.25.

666. Cervical and dorsal vertebrae, rugose ligament attachment scars in pre- and postspinal fossae: absent or weakly developed (0); present as prominent, rectangular flanges that extend outside of the fossae and are visible in posterior view, but on the dorsal vertebrae only (1); prominent in dorsals and cervicals (2).

Ligaments supporting the neck and trunk attach to the anterior and posterior surfaces of the vertebral neural spines in all dinosaurs (e.g., Tsuihiji 2004), and often these attachment sites are marked by subtle lineations and faint rugosities (state 0). This is the case in the vast majority of coelurosaurs, including taxa such as *Coelurus* (YPM 2010), *Deinonychus* (Ostrom 1969),

Dilong (IVPP V14243), *Eotyrannus* (MIWG 1997.550), *Gallimimus* (ZPAL MgD-I/1), *Guanlong* (IVPP V14531), *Juratyrant* (Benson 2008), *Microvenator* (Makovicky and Sues 1998), *Mononykus* (Perle et al. 1994), *Ornitholestes* (AMNH FARB 619), and *Xiongguanlong* (FRDC-GS JB16-2-1).

In some theropods, however, there are extensive, rugose, rectangular flanges that extend from the anterior and posterior surfaces of the neural spines to provide additional attachment area for the neck and trunk ligaments. These structures are limited to the dorsal vertebrae (state 1) in some taxa, including the tyrannosauroid *Gorgosaurus* (Lambe 1917; AMNH FARB 5458, 5664) and derived therizinosauroids (e.g., *Alxasaurus*: Russell and Dong 1993; *Nothronychus*: Zanno et al. 2009; *Suzhousaurus*: Li et al. 2008). A third condition, in which the rugose flanges are present in the cervical and dorsal vertebrae (state 2), is present in the derived tyrannosaurine tyrannosaurids *Daspletosaurus* (AMNH FARB 6458), *Tarbosaurus* (Maleev 1974), and *Tyrannosaurus* (Brochu 2003), as well as the coelurosaurian outgroups *Allosaurus* (Madsen 1976) and *Sinraptor* (Currie and Zhao 1993).

This character was first utilized by Brusatte et al. (2010a, character 217) and is treated as an ordered multistate because the three states describe a sequence of nested homologies (absent-limited-widespread). The character states are not figured here, but good examples of the rugose, prominent, rectangular flanges can be seen in Brochu (2003: figure 60).

669. Dorsal vertebrae, middle-posterior dorsals, position of postzygapophysis relative to prezygapophysis: at same level (0); elevated dorsally (1).

Benson (2008) recognized a "dorsally raised postzygapophyses on (the) last dorsal vertebra" as an unusual feature and potential autapomorphy of the tyrannosauroid *Juratyrant*. In

this taxon, the postzygapophysis is elevated noticeably dorsally relative to the prezygapophysis (state 1), whereas in most theropods the two zygapophyses are positioned at approximately the same level (state 0; e.g., *Allosaurus*: Madsen 1976; *Compsognathus*: Peyer 2006; *Deinonychus*: Ostrom 1969; *Falcarius*: Zanno 2010a; *Ornitholestes*: AMNH FARB 619). The unusual elevated condition is not unique to *Juratyrant*, however, as it is also present in other tyrannosauroids, including *Alioramus* (Brusatte et al. 2012a), *Daspletosaurus* (AMNH FARB 6458), *Gorgosaurus* (Lambe 1917), *Tarbosaurus* (Maleev 1974), *Tyrannosaurus* (Brochu 2003), and *Xiongguanlong* (FRDC-GS JB16-2-1). In fact, among tyrannosauroids only the basal taxa *Dilong* (IVPP V14243) and *Guanlong* (IVPP V14531) possess the unelevated condition of state 0. A broad survey of coelurosaurs reveals that the elevated condition (state 1) is also present in the ornithomimosaurs *Gallimimus* (ZPAL MgD-I/1; Osmólska et al. 1972), *Garudimimus* (Kobayashi and Barsbold 2005a), and *Ornithomimus* (Makovicky et al. 2004). It is not present in all ornithomimosaurs, however, as *Archaeornithomimus* (Smith and Galton 1990) and *Harpymimus* (Kobayashi and Barsbold 2005b) possess the unelevated condition. This character was first used by Brusatte et al. (2010a, character 221) and its wider distribution in tyrannosauroids was discussed by Brusatte and Benson (in press). States 0 and 1 are shown in Figure 2.26.

670. Dorsal vertebrae, middle-posterior dorsals, form of anterior and posterior centrodiapophyseal laminae: discrete laminae absent, or laminae present but do not demarcate a deep infradiapophyseal fossa between them (0); present and make contact on ventral surface of transverse process, demarcating a triangular infradiapophyseal fossa (1); present and do not

make contact but roughly parallel each other, infraprezygapophyseal and infradiapophyseal fossa merged into a single fossa (2).

As reviewed above, most theropods possess anterior and posterior centrodiapophyseal laminae that link the diapophysis with the lateral surface of the centrum in the dorsal vertebrae (Wilson 1999). In many theropods both laminae are distinctive, meet each other dorsally on the ventral surface of the transverse process, and funnel out ventrally, with the anterior lamina projecting anteroventrally and the posterior lamina posteroventrally, to demarcate a depressed infradiapophyseal lamina between them. This morphology is codified as state 1 and is present in the coelurosaurian outgroups *Allosaurus* (Madsen 1976) and *Sinraptor* (Currie and Zhao 1993), along with many coelurosaurs, including most tyrannosauroids (e.g., *Dilong*: IVPP V14243; *Tyrannosaurus*: Brochu 2003; *Xiongguanlong*: FRDC-GS JB16-2-1), the basal coelurosaur *Tanycolagreus* (TPII 2000-09-29), ornithomimosaurs (e.g., *Gallimimus*: ZPAL MgD-I/1; *Garudimimus*: Kobayashi and Barsbold 2005a), basal alvarezsauroids (e.g., *Bonapartenykus*: Agnolin et al. 2012; *Patagonykus*: Novas 1997), therizinosauroids (e.g., *Falcarius*: Zanno 2010a; *Suzhousaurus*: Li et al. 2008), oviraptorosaurs (e.g., *Microvenator*: Makovicky and Sues 1998), and some dromaeosaurids (e.g., *Austroraptor*: MML 195; *Unenlagia*: MCF 075).

Two alternative conditions are seen in some coelurosaurs. First, some taxa possess pronounced anterior and posterior centrodiapophyseal laminae, but these do not make contact with each other underneath the diapophysis. Instead, the two laminae roughly parallel each other, and as a result, the infraprezygapophyseal and infradiapophyseal fossae are merged into a single fossa (within which is the anterior centrodiapophyseal lamina). This unusual morphology, which is codified as state 2, is present in the basal tyrannosauroid *Guanlong* (IVPP V14531), the

derived tyrannosauroids *Alioramus* (Brusatte et al. 2012a) and *Tarbosaurus* (Maleev 1974), and the basal coelurosaurs *Coelurus* (YPM 2010) and *Ornitholestes* (AMNH FARB 619).

Second, some coelurosaurs possess remarkably weak anterior and centrodiapophyseal laminae that do not demarcate a deep infradiapophyseal fossa between them. In some taxa with this condition the laminae are so weak that they are essentially absent, whereas in others they are more prominent but fail to define a deep infradiapophyseal fossa. Therefore, the defining characteristic of this state, which is codified as state 0, is the lack of the fossa and its corresponding well-defined anterior and posterior rims (which are formed by the laminae). This morphology is present in derived alvarezsauroids, including *Linhenykus* (Xu et al. in press), *Mononykus* (Perle et al. 1994), *Parvicursor* (Kahru and Rautian 1996), *Shuvuuia* (IGM 100/977), and *Xixianykus* (Xu et al. 2010). It is also present in several dromaeosaurids, including *Balaur* (Csiki et al. 2010; Brusatte et al. in press; EME PV.313), *Buitreraptor* (Makovicky et al. 2005; MPCA 245), *Deinonychus* (Ostrom 1969), *Microraptor* (Hwang et al. 2002), and *Velociraptor* (Norell and Makovicky 1999).

This character was originally used by Brusatte et al. (2010a, character 222). It is treated as an ordered multistate, because the three states describe a hierarchial series of homologies (subtle-pronounced-pronounced but modified). States 0, 1, and 2 are shown in Figure 2.26.

671. Sacral vertebrae, fenestrae between fused neural spines: neural spines unfused (0); spines fused but fenestrae absent (1); spines fused and fenestrae present (2).

The sacral neural spines of most coelurosaurs are fused together into a broad apron. The only taxa in which this is not the case (state 0) are the therizinosauroids *Falcarius* (Zanno 2010a) and *Nanshiungosaurus* (Dong 1979) and the basal coelurosaurs *Compsognathus* (Peyer 2006)

and *Mirischia* (Naish et al. 2004; SMNK 2349 PAL). Additionally, some, but not all, specimens of the outgroup *Allosaurus* exhibit unfused sacral neural spines (Madsen 1976; UMNH VP collection).

Those taxa in which the neural spines are fused into an apron exhibit two distinctive morphologies. In many taxa the spines are smoothly fused together along their margins, without any intervening fenestrae or other openings between what were the original individual neural spines. This condition is codified as state 1, and is seen in some specimens of *Allosaurus*, the basal tyrannosauroid *Guanlong* (IVPP V14531), ornithomimosaurs (e.g., *Garudimimus*: Kobayashi and Barsbold 2005a; *Harpymimus*: Kobayashi and Barsbold 2005b), alvarezsauroids (e.g., *Shuvuuia*: IGM 100/99), some therizinosauroids (e.g., *Enigmosaurus* and *Segnosaurus*: Zanno 2010b; *Suzhousaurus*: Li et al. 2008), and dromaeosaurids (e.g., *Microraptor*: Hwang et al. 2002; *Rahonavis*: Forster et al. 1998; *Unenlagia*: MCF 010; *Velociraptor*: Norell and Makovicky 1997, 1999). Some taxa, however, exhibit large fenestrae between the fused neural spines (state 2). In these taxa, the neural spines are fused at their dorsal ends, and in some cases ventrally, but the open fenestrae remain between them at their midpoints. This is seen in the tyrannosauroids *Alioramus* (Brusatte et al. 2012a) and *Tyrannosaurus* (Brochu 2003). Some specimens of *Gallimimus* exhibit this condition, whereas others exhibit state 1 (ZPAL collection).

This character was first used by Brusatte et al. (2010a, character 224). It is treated as an ordered multistate because the three states describe a hierarchial series of homologies (fusion absent-fusion present-fusion present with fenestrae), and the ordered nature of the character allows taxa with different conditions of fusion (entirely fused or fused but with fenestrae) to be

united by the synapomorphy of sacral neural spine fusion. The unusual state 1 is illustrated in Figure 2.27 and can also be seen in Brochu (2003: figure 57).

672. Sacral ribs, position of central ribs on sacrum: span two sacrals (0); limited to a single sacral (1).

In most theropods the sacral rib attachment sites are not limited to a single sacral, but rather span across the suture between two adjoining sacrals. This is the case in the coelurosaurian outgroup *Allosaurus* (Madsen 1976) as well as nearly every coelurosaur that can be scored in the affirmative for this character, including the basal tyrannosauroids *Guanlong* (IVPP V14531) and *Juratyrant* (Benson 2008), the basal coelurosaur *Mirischia* (Naish et al. 2004), ornithomimosaurs (e.g., *Garudimimus*: Kobayashi and Barsbold 2005a), alvarezsauroids (e.g., *Patagonykus*: Novas 1997; *Xixianykus*: Xu et al. 2010), therizinosauroids (e.g., *Falcarius*: Zanno 2010a; *Suzhosaurus*: Li et al. 2008), troodontids (e.g., *Zanabazar*: Norell et al. 2009), and dromaeosaurids (e.g., *Balaur*: EME PV. 313). The derived tyrannosauroids *Alioramus* (Brusatte et al. 2012a) and *Tyrannosaurus* (Osborn 1906, 1916; Brochu 2003) exhibit a distinctive morphology in which the sacral rib attachment sites are limited to a single vertebra each, and do not span across the suture between two adjacent vertebrae. This unusual condition is also seen in the basal coelurosaur *Ornitholestes* (AMNH FARB 619). This character was first employed by Brusatte et al. (2010a, character 225). The unusual state 1 is illustrated in Figure 2.27 and can also be seen in Brochu (2003: figure 57).

673. Sacral ribs, position of rib attachment for central ribs on individual sacrals: span centrum and neural arch (0); limited to neural arch only (1).

In most theropods the sacral rib attachment sites are large and span the neurocentral suture between the centrum and neural arch. Therefore, the rib attachment is shared between these two portions of the vertebrae. This morphology is present in the coelurosaurian outgroup *Allosaurus* (Madsen 1976) as well as nearly every coelurosaur that can be scored in the affirmative for this character, including the basal tyrannosauroids *Guanlong* (IVPP V14531) and *Juratyrant* (Benson 2008), the derived tyrannosauroid *Alioramus* (Brusatte et al. 2012a), the basal coelurosaurs *Mirischia* (Naish et al. 2004), *Ornitholestes* (AMNH FARB 619), and *Zuolong* (Choiniere et al. 2010b), ornithomimosaurs (e.g., *Garudimimus*: Kobayashi and Barsbold 2005a), therizinosauroids (e.g., *Falcarius*: Zanno 2010a; *Suzhosaurus*: Li et al. 2008), and dromaeosaurids (e.g., *Buitreraptor*: MPCA 245). In contrast, the derived tyrannosaurine tyrannosaurids *Tarbosaurus* (Maleev 1974) and *Tyrannosaurus* (Osborn 1906, 1916; Brochu 2003) possess a distinct condition in which the rib attachment site is restricted to the neural arch. Therefore, in these taxa the sacral ribs are positioned further dorsally on the sacrum than in other coelurosaurs. This unusual morphology is also present in alvarezsauroids (*Patagonykus*: Novas 1997; *Shuvuuia*: IGM 100/99). This character was first used by Brusatte et al. (2010, character 226). State 0 is illustrated in Figure 2.27 and state 1 can be seen in Brochu (2003: figure 57).

674. Sacral vertebra five, position of ventral margin of posterior articular face in lateral view: at same level as ventral margin of anterior articular face (0); positioned ventral to ventral margin of anterior articular face (1).

In many theropods the ventral margin of the posterior articular surface of sacral vertebra 5 extends to approximately the same ventral level as the ventral margin of the anterior articular surface when this vertebra is seen in lateral view. This is the case in the outgroup *Allosaurus*

(Madsen 1976), the basal coelurosaur *Zuolong* (Choiniere et al. 2010b), the basal tyrannosauroid *Guanlong* (IVPP V14531), ornithomimosaurs (e.g., *Garudimimus*: Kobayashi and Barsbold 2005a; *Sinornithomimus*: Kobayashi and Lü 2003), and dromaeosaurids (e.g., *Balaur*: EME PV.313; *Rahonavis*: Forster et al. 1998; *Velociraptor*: Norell and Makovicky 1997, 1999). In some taxa, however, the ventral edge of the posterior articular face extends substantially farther ventrally than the ventral edge of the anterior articular face. This condition is seen in several tyrannosauroids, including *Juratyrant* (Benson 2008), *Gorgosaurus* (Lambe 1917), *Alioramus* (Brusatte et al. 2012a), and *Tyrannosaurus* (Osborn 1906, 1916; Brochu 2003). It is also present in the alvarezsauroids *Patagonykus* (Novas 1997) and *Shuvuuia* (IGM 100/99; Chiappe et al. 1996) and the therizinosauroids *Enigmosaurus* (Zanno 2010b) and *Suzhousaurus* (Li et al. 2008). This character was originally used by Brusatte et al. (2010a, character 227). States 0 and 1 are shown in Figure 2.27.

675. Sacral vertebrae, form of hyposphene in posteriormost sacral: absent or present as a single midline structure (0); present and comprised of two parallel-sided sheets (1).

The posterior surface of the last sacral is not frequently observable in coelurosaurs, because many taxa are known from slab specimens or because this vertebra often remains in articulation with the first caudal vertebrae. Those coelurosaurs in which this surface can be observed possess one of two general conditions regarding the shape of the hyposphene. In some taxa the hyposphene is present as a single, peg-like midline structure. This is the case in the outgroup *Allosaurus* (Madsen 1976), the basal tyrannosauroids *Guanlong* (IVPP V14531) and *Juratyrant* (Benson 2008), the basal coelurosaur *Ornitholestes* (AMNH FARB 619), ornithomimosaurs (e.g., *Gallimimus*: ZPAL MgD-I/94; *Garudimimus*: Kobayashi and Barsbold

2005a), alvarezsauroids (*Patagonykus*: Novas 1997; MCF PVPH 37), and therizinosauroids (*Suzhousaurus*: Li et al. 2008). In the derived tyrannosauroids *Alioramus* (Brusatte et al. 2012a) and *Tyrannosaurus* (Brochu 2003), on the other hand, the hyposphene is a prominent structure comprised of two parallel sheets, with a cleft between them. This character was first used by Brusatte et al. (2010a, character 228). States 0 and 1 are illustrated in Figure 2.27.

676. Caudal vertebrae, anterior caudals, position of base of neural spine: anterior to (0) or level with or posterior to (1) posterior surface of centrum.

The posterior edge of the neural spine base is anterior to the posterior edge of the centrum in the anterior caudal vertebrae of most theropods. In other words, the neural spine is approximately centered (or slightly displaced posteriorly) on the vertebra (state 0). This is not the case in the outgroups *Allosaurus* (Madsen 1976) and *Sinraptor* (Currie and Zhao 1993), the derived tyrannosaurids *Alioramus* (Brusatte et al. 2012a), *Tarbosaurus* (Maleev 1974) and *Tyrannosaurus* (Brochu 2003), and the therizinosauroids *Falcarius* (Zanno 2010a) and *Alxasaurus* (Russell and Dong 1993). In these taxa the posterior edge of the neural spine is level with, or even is placed posterior to, the posterior edge of the centrum (state 1). Note that this morphology is not present in other tyrannosauroids and therizinosauroids; for example, taxa such as *Gorgosaurus* (Lambe 1917) and *Juratyrant* (Benson 2008) among tyrannosauroids, and *Neimongosaurus* (Zhang et al. 2001) and *Suzhousaurus* (Li et al. 2008) among therizinosauroids, are scored for state 0. This character was first utilized by Brusatte et al. (2010a, character 229). States 0 and 1 are illustrated in Figure 2.28.

677. Caudal vertebrae, anterior caudals, shape of transverse processes in dorsal view: rectangular, with parallel anterior and posterior sides, or slightly ovoid with a gradual expansion in width distally (0); distal end expanded into a spatulate bulb (1)

In the vast majority of coelurosaurs and close outgroups the transverse processes of the anterior caudal vertebrae are roughly rectangular when seen in dorsal view. At most, they may expand slightly in anteroposterior width at their distal terminations (e.g., *Allosaurus*: Madsen 1976; *Deinonychus*: Ostrom 1969; *Falcarius*: Zanno 2010a; *Gallimimus*: ZPAL MgD-I/9). The derived tyrannosauroids *Alioramus* (Brusatte et al. 2012a) and *Tyrannosaurus* (Brochu 2003) exhibit a peculiar condition in which the transverse processes of the anterior caudals expand in anteroposterior width greatly as they extent laterally, such that the distal end is elaborated into a spatulate-shaped bulb. This morphology is not present in basal tyrannosauroids such as *Guanlong* (IVPP V14531) and *Appalachiosaurus* (Carr et al. 2005), which are scored for state 0. This character was first used by Brusatte et al. (2010a, character 230). States 0 and 1 are illustrated in Figure 2.28.

678. Caudal vertebrae, anterior caudals, two laminae linking prezygapophysis and transverse process, between which is a deep, triangular fossa: absent (0); present (1).

A subset of derived tyrannosauroids exhibit an unusual feature on the anterior caudals: the presence of two discrete laminae linking the prezygapophysis and transverse process on the lateral surface of the neural arch. Between these two laminae is a deep fossa. This character state is seen in *Alioramus* (Brusatte et al. 2012a), *Daspletosaurus* (AMNH FARB 6458), *Tarbosaurus* (ZPAL MgD-I/226), and *Tyrannosaurus* (Brochu 2003). It is also apparently present in *Bistahieversor* (T.D. Carr pers. comm.), but is absent in the tyrannosauroids *Gorgosaurus*

(AMNH FARB 5458, 5664), *Juratyrant* (Benson 2008), and *Dilong* (IVPP V14243), as well as all other coelurosaurs that can be given an affirmative score for this character. It is also absent in both outgroups, *Allosaurus* (Madsen 1976) and *Sinraptor* (Currie and Zhao 1993). This character was originally used by Brusatte et al. (2010a, character 231). Note that they accidentally swapped the scores for *Gorgosaurus* and *Albertosaurus*; the proper scores for these genera are "0" and "?", respectively. States 0 and 1 are illustrated in Figure 2.28.

684. Coracoid, coracoid foramen: present (0); absent or extremely small (1).

The coracoids of most theropods are penetrated by a large foramen on the lateral surface. This feature, the coracoid foramen, is present in the outgroup *Allosaurus* (Madsen 1976) and most coelurosaurs, including some tyrannosauroids (e.g., *Gorgosaurus*: Lambe 1917; *Tyrannosaurus*: Brochu 2003), the basal coelurosaur *Tanycolagreus* (TPII 2000-09-29), compsognathids (*Compsognathus*: Peyer 2006; *Huaxiagnathus*: Hwang et al. 2004; *Sinocalliopteryx*: Ji et al. 2007), some ornithomimosaurs (e.g., *Beishanlong*: Makovicky et al. 2010; *Sinornithosaurus*: Kobayashi and Lü 2003), alvarezsauroids (e.g., *Alvarezsaurus*: Bonaparte 1991; *Haplocheirus*: Choiniere et al. 2010a; *Mononykus*: Perle et al. 1994), oviraptorosaurs (e.g., *Microvenator*: Makovicky and Sues 1998), troodontids (e.g., *Sinornithoides*: Currie and Dong 2001b), and dromaeosaurids (e.g., *Bambiraptor*: Burnham 2004; *Buitreraptor*: MPCA 245; *Deinonychus*: Ostrom 1969). In contrast, the foramen is absent or remarkably small in some coelurosaurs. This character does not distinguish between absence and presence because it is likely that a genuinely small foramen may be mistaken for absence on specimens that are not well preserved. Coelurosaurs with a small or absent foramen include some basal tyrannosauroids (*Dilong*: IVPP V14243; *Eotyrannus*: MIWG 1997.550; *Guanlong*: IVPP

V14532) and therizinosauroids (*Beipiaosaurus*: Xu et al. 1999; *Falcarius*: Zanno 2006; *Suzhosaurus*: Li et al. 2007; *Therizinosaurus*: Barsbold 1976). This character was first used by Brusatte et al. (2010a, character 238). States 0 and 1 are figured in Figure 2.29.

686. Humerus, additional muscle attachment tubera at the corner of the anterior and lateral surfaces distal to the deltopectoral crest: absent (0); present (1).

As described by Brochu (2003), the humeri of the derived tyrannosaurids *Daspletosaurus* (Russell 1970), *Tarbosaurus* (Maleev 1974), and *Tyrannosaurus* (Brochu 2003) exhibit a pronounced, rugose muscle attachment tuber distal to the deltopectoral crest, along the region where the anterior and lateral surfaces of the bone meet. This feature is unknown in the outgroup *Allosaurus* (Madsen 1976) or in any other coelurosaur that can be scored in the affirmative. This character was used by Brusatte et al. (2010a, character 243). The unusual state 1 is illustrated by Brochu (2003: figure 85).

687. Humerus, concave notch between external tuberosity and deltopectoral crest: present, two structures clearly separated (0); absent, two structures smoothly confluent (1).

In most theropods there is a distinct notch separating the deltopectoral crest and the external tuberosity on the proximal surface of the humerus. This notch is visible as a concave indentation in anterior and lateral views. Such a notch is present in the outgroup *Allosaurus* (Madsen 1976), the basal tyrannosauroids *Guanlong* (IVPP V14531) and *Dilong* (IVPP V14243), and the basal coelurosaurs *Coelurus* (YPM 2010), *Ornitholestes* (AMNH FARB 619), *Tanycolagreus* (TPII 2000-09-29), and *Zuolong* (Choiniere et al. 2010b). It is also seen in ornithomimosaurs (e.g., *Beishanlong*: Makovicky et al. 2010; *Struthiomimus*: Nicholls and

Russell 1985), alvarezsauroids (e.g., *Mononykus*: Perle et al. 1994), therizinosauroids (e.g., *Falcarius*: Zanno 2006; *Suzhousaurus*: Li et al. 2007), and oviraptorosaurs (e.g., *Microvenator*: Makovicky and Sues 1998).

Some coelurosaurs, however, exhibit a distinct condition in which the deltopectoral crest and external tuberosity are smoothly confluent with each other. In other words, a notch between the two structures is missing. This morphology is clearly visible when the humerus is seen in lateral view, as the deltopectoral crest and external tuberosity meet each other and merge smoothly to create a broad, convex anterior outline of the proximal region of the humerus in lateral view. This condition is seen in several tyrannosauroids, including *Eotyrannus* (MIWG 1997.550), *Albertosaurus* and *Gorgosaurus* (Lambe 1917; Parks 1928), *Daspletosaurus* (Russell 1970), *Tarbosaurus* (Maleev 1974), and *Tyrannosaurus* (Brochu 2003). It is also present in paravian theropods, including troodontids such as *Mei* (Xu and Norell 2004) and *Sinornithoides* (Currie and Dong 2001b) and dromaeosaurids such as *Austroraptor* (MML 195), *Bambiraptor* (Burnham et al. 2000), *Deinonychus* (Ostrom 1969), and *Velociraptor* (Norell and Makovicky 1999).

This character was originally used by Brusatte et al. (2010a, character 244). States 0 and 1 are illustrated in Figure 2.30.

688. Humerus, form of distal condyles: lateral and medial condyles expanded equally (offset from shaft in anterior or posterior view is equal) (0); medial condyle expanded further medially than the lateral condyle is laterally (1).

The lateral and medial condyles of the distal humerus are approximately equally offset from the shaft in most coelurosaurs. In other words, the distance between the medial edges of the

medial condyle and shaft is approximately equal to the distance between the lateral edge of the lateral condyle and shaft. This is the case in the outgroup *Allosaurus* (Madsen 1976) and most coelurosaurs, including the basal coelurosaur *Zuolong* (Choiniere et al. 2010b), derived tyrannosauroids (*Gorgosaurus*: Lambe 1917; *Tarbosaurus*: Maleev 1974; *Tyrannosaurus*: Brochu 2003), most alvarezsauroids (e.g., *Haplocheirus*: Choiniere et al. 2010b; *Mononykus*: Perle et al. 1994), therizinosauroids (e.g., *Falcarius*: Zanno 2006; *Suzhousaurus*: Li et al. 2007), oviraptorosaurs (e.g., *Microvenator*: Makovicky and Sues 1998), and dromaeosaurids (e.g., *Bambiraptor*: Burnham et al. 2000; *Microraptor*: Hwang et al. 2002; *Velociraptor*: Norell and Makovicky 1999).

Many basal coelurosaurs possess a different condition in which the medial condyle is more strongly offset relative to the medial edge of the shaft than the lateral condyle is relative to the lateral edge of the shaft. This is seen in the basal tyrannosauroids *Dilong* (IVPP V14243), *Eotyrannus* (MIWG 1997.550), and *Guanlong* (IVPP V14531), as well as the basal coelurosaurs *Coelurus* (YPM 2010), *Ornitholestes* (AMNH FARB 619), and *Tanycolagreus* (TPII 2000-09-29). It is also present in ornithomimosaurs, including *Archaeornithomimus* (Smith and Galton 1990), *Beishanlong* (Makovicky et al. 2010), *Gallimimus* (ZPAL MgD-I/2), and *Harpymimus* (Kobayashi and Barsbold 2005b).

This character was first used by Brusatte et al. (2010a, character 245). States 0 and 1 are illustrated in Figure 2.30.

692. Metacarpal I, medial margin, shape in proximal view: concave (0); smoothly convex or straight (1).

In the coelurosaurian outgroup *Allosaurus* (Madsen 1976) and some basal coelurosaurs, metacarpal I has a deeply concave medial margin in proximal view. This morphology is seen in *Eotyrannus* (MIWG 1997.550), *Guanlong* (IVPP V14531), *Tugulusaurus* (IVPP V4025), and *Tanycolagreus* (TPII 2000-09-29). In contrast, all other coelurosaurs in which this character can be scored do not have a concave medial margin, but rather a straight or convex one. This is the case in derived tyrannosauroids such as *Gorgosaurus* (Lambe 1917) and *Tyrannosaurus* (Brochu 2003), as well as ornithomimosaurs (e.g., *Archaeornithomimus*: Smith and Galton 1990; *Gallimimus*: ZPAL MgD-I/2), therizinosauroids (e.g., *Alxasaurus*: Russell and Dong 1993; *Falcarius*: Zanno 2006), and dromaeosaurids (e.g., *Bambiraptor*: Burnham 2004; *Deinonychus*: Ostrom 1969). Note that in some of these taxa there is a strongly concave anterior edge of metacarpal in proximal view, and sometimes this concavity faces anteromedially (e.g., Ostrom 1969, figure 62; Zanno 2006, figure 5). This is not considered equivalent to state 0, however, as it is not equivalent to the deep medially facing concavity that occupies the entire medial surface of the bone in *Allosaurus* and the aforementioned basal coelurosaurs. This character was first used by Brusatte et al. (2010a, character 251). States 0 and 1 are illustrated in Figure 2.32.

700. Ilium, ventral margin of postacetabular process, shape: straight to slightly convex (0); highly convex, forming a discrete “lobe”-like flange (1).

In some theropods the brevis fossa is widely visible in lateral view, because the lateral flange of the postacetabular process (which encloses the fossa laterally) does not extend as far ventrally as the medial flange of the postacetabular process (which encloses the fossa medially). Therefore, a wide portion of the fossa on the lateral surface of the medial flange is visible in lateral view. In some tyrannosauroids the portion of the exposed medial flange is highly convex

and forms a “lobe”-like structure. This feature is present in *Albertosaurus* (Parks 1928: figure 10), *Daspletosaurus* (CMN 8506), *Tarbosaurus* (Maleev 1974: figure 38), and *Tyrannosaurus* (AMNH FARB 5027). The “lobe”-like condition of the flange is absent in other tyrannosauroids, including *Alioramus* (Brusatte et al. 2012a), *Dilong* (IVPP V14243), *Gorgosaurus* (Lambe 1917), and *Guanlong* (IVPP V14531). In these taxa the ventral edge of the medial flange of the postacetabular process is nearly straight, not highly convex. The “lobe”-like condition is also absent in the outgroups *Allosaurus* (Madsen 1976) and *Sinraptor* (Currie and Zhao 1993), as well as all other coelurosaurs that can be scored affirmatively for this character. This character was initially utilized by Brusatte et al. (2010a, character 265). States 0 is illustrated in Figure 2.33 and state 1 is illustrated in the aforementioned figures (e.g., Maleev 1974: figure 38).

701. Ilium, dorsal margin, shape: smoothly convex or straight across entire length (0); convex anteriorly and straightens out posteriorly (1).

In most coelurosaurs and close outgroups the dorsal margin of the ilium is either smoothly convex or approximately straight across its entire length when the ilium is seen in lateral or medial views. This is the case in outgroups such as *Allosaurus* (Madsen 1976), as well as many coelurosaurs, including the basal coelurosaurs *Ornitholestes* (AMNH FARB 619) and *Zuolong* (Choiniere et al. 2010b), several basal tyrannosauroids (e.g., *Dilong*: IVPP V14243, Xu et al. 2004; *Guanlong*: IVPP V14243, Xu et al. 2006; *Juratyrant*: Benson 2008, Brusatte and Benson in press; *Sinotyrannus* Ji et al. 2009; *Xiongguanlong*: FRDC-GS JB16-2-1), compsognathids (e.g., *Huaxiagnathus*: Hwang et al. 2004; *Sinocalliopteryx*: Ji et al. 2007; *Sinosauropteryx*: Currie and Chen 2001), basal ornithomimosaurs (e.g., *Archaeornithomimus*: Smith and Galton 1990; *Shenzhousaurus*: Ji et al. 2003), alvarezsauroids (e.g., *Alvarezsaurus*:

Bonaparte 1991; *Xixianykus*: Xu et al. 2010), therizinosauroids (e.g., *Falcarius*: Zanno 2010a; *Suzhousaurus*: Li et al. 2008), oviraptorosaurs (e.g., *Caudipteryx*: Ji et al. 1998), troodontids (e.g., *Anchiornis*: Hu et al. 2009), and dromaeosaurids (e.g., *Deinonychus*: Ostrom 1969; *Microraptor*: Hwang et al. 2002; *Rahonavis*: Forster et al. 1998).

Some coelurosaurs exhibit a different condition in which the dorsal surface of the ilium is convex anteriorly, on the preacetabular process and over the region dorsal to the acetabulum, but then straightens out horizontally on the postacetabular process. This condition is seen in derived tyrannosauroids such as *Albertosaurus* (Parks 1928), *Alioramus* (Brusatte et al. 2012a), *Daspletosaurus* (CMN 8506), *Gorgosaurus* (Lambe 1917), *Tarbosaurus* (Maleev 1974), and *Tyrannosaurus* (Brochu 2003). It is also seen in several derived ornithomimosaurs, including *Garudimimus* (Kobayashi and Barsbold 2005a), *Gallimimus* (Osmólska et al. 1972; ZPAL MgD-I/94), *Harpymimus* (Kobayashi and Barsbold 2005b), and *Sinornithomimus* (Kobayashi and Lü 2003).

This character was first used by Brusatte et al. (2010a, character 266). States 0 and 1 are illustrated in Figure 2.33. Note that some dromaeosaurids, such as *Unenlagia* (MCF 001; Novas and Puerta 1997), possess a separate posterior tab-like process of the postacetabular process, which is encapsulated in a separate character in the current analysis. These dromaeosaurids are scored for state 0 for the current character, which in these taxa refers to that portion of the ilium excluding the posterior tab (which is a neomorphic process).

702. Ilium, ratio of anteroposterior length to dorsoventral depth above acetabulum: greater than 3.0, ilium is long and low (0); less than 2.8, ilium is subovoid in shape (1).

The shape and proportions of the ilium vary greatly among theropods. Many theropods possess an ilium that is long and low, with a ratio of maximum anteroposterior length to dorsoventral depth above the acetabulum that is greater than 3.0 (state 0). In many taxa this ratio is even larger: in *Shuvuuia*, for instance, the ratio approaches 5.0 (Chiappe et al. 2002). This condition is seen in almost all coelurosaurs, with only two notable exceptions: a suite of basal tyrannosauroids and derived therizinosauroids, both of which have subovoid-shaped ilia that are abnormally deep relative to their anteroposterior lengths. In these taxa the ratio of length to depth is less than 2.8. In some taxa this ratio is even smaller: in *Suzhousaurus*, for instance, the ratio is only slightly larger than 2.0. Taxa with this unusual condition (state 1) include *Dilong* (IVPP V14243), *Juratyrant* (Benson 2008; Brusatte and Benson in press), *Sinotyrannus* (Ji et al. 2009), and *Xiongguanlong* (FRDC-GS JB16-2-1) among tyrannosauroids, as well as *Alxasaurus* (Russell and Dong 1993), *Beipiaosaurus* (Xu et al. 1999; Zanno 2010b), *Enigmosaurus* (Zanno 2010b), *Nanshiungosaurus* (Dong 1979), *Nothronychus* (Zanno et al. 2009), *Segnosaurus* (Barsbold and Perle 1980), and *Suzhousaurus* (Li et al. 2008) among therizinosauroids. It is also present in the outgroup taxa *Allosaurus* (Madsen 1976) and *Sinraptor* (Currie and Zhao 1993).

This character was originally used by Brusatte et al. (2010a, character 268) and discussed in more detail by Brusatte and Benson (in press). States 0 and 1 are illustrated in Figure 2.23.

703. Pubis, pubic tubercle: absent (0); present as a convexity on the anterior margin of the pubis (1); present as a rugose flange that is discretely offset from the anterior margin of the pubis and is bordered posteriorly by heavy rugosities on the lateral surface on the obturator region of the pubis (2).

Some theropods possess a pubic tubercle: a rugose muscle attachment site along the anterior margin of the lateral surface of the proximal portion of the pubis. This feature is absent in the outgroups *Allosaurus* (Madsen 1976) and *Sinraptor* (Currie and Zhao 1993), as well as many coelurosaurs such as the basal taxa *Coelurus* (YPM 2010), *Ornitholestes* (AMNH FARB 619), and *Zuolong* (Choiniere et al. 2010b), compsognathids (*Compsognathus*: Peyer 2006; *Mirischia*: Naish et al. 2004), ornithomimosaurs (e.g., *Garudimimus*: Kobayashi and Barsbold 2005a; *Qiupalong*: L. Xu et al. 2011; *Shenzhousaurus*: Ji et al. 2003), and alvarezsauroids (e.g., *Patagonykus*: Novas 1997; *Shuvuuia*: Chiappe et al. 1996). These taxa are scored for state 0.

In contrast, a pubic tubercle is present in all known tyrannosauroids and many dromaeosaurids. Taxa possessing a tubercle generally exhibit one of two discrete conditions. First, many taxa have a small, subtle pubic tubercle that is offset from the anterior margin of the pubis as a small bulge (state 1). This is the condition in all dromaeosaurids that possess the tubercle, such as *Balaur* (EME PV.313) and *Velociraptor* (Norell and Makovicky 1999), as well as the basal tyrannosauroids *Guanlong* (IVPP V14531) and *Juratyrant* (Benson 2008). More derived tyrannosauroids have a different morphology in which the tubercle is large, rugose, and offset from the anterior margin of the pubis as a discrete flange (state 2). This state is present in *Albertosaurus* (Parks 1928), *Gorgosaurus* (Lambe 1917), *Tarbosaurus* (Maleev 1974), and *Tyrannosaurus* (Brochu 2003).

This character was first utilized in the cladistic analysis of Carr and Williamson (2010, character 255). It is being discussed here because it was modified when used by Brusatte et al. (2010a, character 270), and because it is relevant to explaining the next character (704) below. Differences in the morphology of the pubic tubercle, and its usage as a systematically informative character, were discussed in detail by Benson et al. (2010b). The character here, as

well as in the original Brusatte et al. (2010a) analysis, is treated as an ordered multistate because the three conditions are hierarchically nested (absent-present but subtle-present and large). States 0 and 2 are illustrated in Figure 2.35, whereas state 1 is illustrated in several dromaeosaurid descriptions (e.g., Norell and Makovicky 1997: figure 13).

704. Pubis, pubic tubercle, position: distally positioned, located ventral to the level of the obturator notch (0); proximally positioned, located level with or dorsal to the obturator notch (1).

The position of the pubic tubercle varies in those few coelurosaurian taxa that possess this feature (see character 703 above). In the basal tyrannosauroids *Guanlong* (IVPP V14531) and *Juratyrant* (Benson 2008) the tubercle is distally positioned, such that it is located ventral to the level of the obturator notch (state 0). In contract, the tubercle is positioned proximal to the obturator notch (state 1) in the tyrannosauroids *Albertosaurus* (Parks 1928), *Gorgosaurus* (Lambe 1917), *Tarbosaurus* (Maleev 1974), and *Tyrannosaurus* (Brochu 2003), and most likely *Daspletosaurus* (T.D. Carr, pers. comm.). The proximal position is also seen in those dromaeosaurids with a pubic tubercle, such as *Velociraptor* (Norell and Makovicky 1999). This character was first used by Brusatte et al. (2010a, character 271). States 0 and 1 are shown in Figure 2.35.

705. Pubis, pubic boot, anteroposterior length relative to total long axis length of pubis: less than (0) or greater than (1) 60%.

Many theropods have an expanded “boot” at the distal end of the pubis, and several characters in the analysis concern the presence and shape of the boot. This character quantifies

the size of the boot compared to the size of the pubis. The size of the boot is taken to be its maximum anteroposterior length, whereas the size of the pubis is quantified as the proximodistal long axis length of the entire bone, including the pubic boot portion. In most theropods the length of the boot is less than 60% of the length of the pubis, including in the outgroups *Allosaurus* (Madsen 1976) and *Sinraptor* (Currie and Zhao 1993) and nearly every coelurosaur that is scored affirmatively for this character. The exceptions are the derived tyrannosauroids *Albertosaurus* (Parks 1928), *Daspletosaurus* (T.D. Carr, pers. comm.), *Gorgosaurus* (Lambe 1917), *Tarbosaurus* (Maleev 1974), and *Tyrannosaurus* (Brochu 2003), as well as the derived therizinosauroids *Enigmosaurus* (Zanno 2010b) and *Nothronychus* (Zanno et al. 2009). In these taxa the boot is enlarged, such that it is greater than 60% of the length of the pubis. This character was first used by Brusatte et al. (2010a, character 272). States 0 and 1 are shown in Figure 2.35.

707. Pubis, anteroposterior expansion of proximal obturator plate region relative to the anterior edge of the pubis shaft at its midpoint: less than (0) or greater than (1) twice the anteroposterior thickness of the shaft at its midpoint.

The derived tyrannosaurine tyrannosaurids *Tarbosaurus* (Maleev 1974) and *Tyrannosaurus* (Brochu 2003) share a peculiar condition of the proximal pubis. In these large-bodied tyrannosauroids the proximal obturator plate region of the pubis—the region that participates in the acetabulum and makes contact with the ischium—is greatly expanded anteriorly relative to the shaft. The degree of expansion can be quantified my measuring the anteroposterior dimension of the portion of the obturator plate region that projects further anteriorly than the anterior edge of the pubis shaft at its midpoint. This value is less than two

times the anteroposterior dimension of the shaft (at the midpoint of the bone) in the outgroups *Allosaurus* (Madsen 1976) and *Sinraptor* (Currie and Zhao 1993) and all other coelurosaurs that can be affirmatively scored for this character, but is greater than twice midshaft dimension in these two giant tyrannosauroids. This character was first used by Brusatte et al. (2010a, character 276). States 0 and 1 are shown in Figure 7.35 (note that state 1 is not labeled in *Tyrannosaurus* in this figure because it is obscured slightly by overlying armature on the mounted specimen, but it is present here). This character may be related to the enlarged pubic tubercle of some tyrannosauroids, which projects anteriorly from the obturator plate region of the pubis (character 703). Indeed, *Tarbosaurus* and *Tyrannosaurus* have both the enlarged tubercle and expanded obturator region. However, *Albertosaurus* (Parks 1928) and *Gorgosaurus* (Lambe 1917) both possess an enlarged and flange-like pubic tubercle but do not possess an obturator plate region that is expanded (state 0 for the current character), illustrating that this character is not redundant with character 703 that relates to the pubic tubercle.

708. Pubis, obturator notch, form: discrete structure, demarcated ventrally by extensive obturator flange (0); essentially absent, no ventral flange (1).

Several non-coelurosaurian theropods have either an enclosed fenestra in the proximal obturator region of the pubis, or this fenestra is partially open as a notch that is demarcated ventrally by a flange of bone. This condition is seen in the outgroup taxon *Sinraptor* (Currie and Zhao 1993). An enclosed fenestra is present in only a single coelurosaurian taxon: *Mirischia* (Naish et al. 2004; SMNK 2349 PAL). Naish et al. (2004) described the left and right pubes of *Mirischia* as being asymmetrical, in that an enclosed obturator foramen is present on the right side but it is open as a notch on the left side. However, examination of the holotype specimen

(SMNK 2349 PAL) shows that the supposedly open notch on the left side is a result of breakage of part of the margin of the fenestra. Therefore, *Mirischia* is here considered to possess a closed fenestra on both left and right pubes. Two other coelurosaurs, *Guanlong* (IVPP V14531; Xu et al. 2006) and *Juratyrant* (Benson 2008; OUMNH J.3311-22), possess a discrete notch in the obturator process, which is open posteriorly but enclosed ventrally by a flange of bone. These two taxa, along with *Mirischia*, are scored for state 0, whereas all other coelurosaurs and the outgroup *Allosaurus* (Madsen 1976) are scored for state 1. In the future, if additional coelurosaurs are found to possess the *Mirischia*-like condition of a closed obturator foramen then this character should be expanded into an ordered multistate, with different states representing a closed foramen and open notch. This character was originally utilized by Brusatte et al. (2010a, character 277). States 0 and 1 are shown in Figure 2.35.

709. Ischium, position of medial apron: along posterior margin of shaft (0); along anterior margin of shaft (1).

Among coelurosaurs there is variability in the placement of the medial apron on the medial shaft of the ischium. In the outgroup *Allosaurus* (Madsen 1976) the medial apron arises from the posterior end of the medial surface of the ischium, and this condition is also seen in the basal tyrannosauroids *Guanlong* (IVPP V14531; Xu et al. 2006) and *Juratyrant* (Benson 2008; OUMNH J.3311-24, 25), the basal coelurosaur *Ornitholestes* (AMNH FARB 619), and the ornithomimosaur *Sinornithomimus* (Kobayashi and Lü 2003). In contrast, the apron arises from the anterior margin of the medial surface in the derived tyrannosauroids *Alioramus* (Brusatte et al. 2012a), *Tarbosaurus* (Maleev 1974; ZPAL MgD-I/29), and *Tyrannosaurus* (Brochu 2003). This character state is also seen in *Gallimimus* (ZPAL MgD-I/8). Unfortunately, this character is

difficult to score in most coelurosaurs, especially those taxa known from slab specimens in which the medial surface of the ischium is concealed. Several derived coelurosaurs also lack an ischial apron (character 171) and must be scored as inapplicable ("?") for the current character. This character was first used by Brusatte et al. (2010a, character 282). States 0 and 1 are illustrated in Figure 2.36.

712. Femur, proximal margin in anterior view: approximately straight and perpendicular to the long axis of the shaft (0); approximately straight and oriented at an obtuse angle to the long axis of the shaft (=dorsally or proximally inclinded head) (1); concave and oriented at an obtuse angle to the long axis of the shaft, due to a head that is proximally inclined and a greater trochanter that is elevated substantially relative to the central portion of the proximal surface of the femur (2).

Differences in the inclination of the femoral head among theropod taxa are often discussed in the literature and are sometimes used as phylogenetic characters in cladistic datasets (e.g., Harris 1998; Brusatte and Sereno 2008 for an example in non-coelurosaurian theropods). In practice, however, it is often difficult to develop a standard protocol to quantify the orientation of the femoral head in a consistent, repeatable way among a wide range of taxa. This character is an attempt to provide an explicit and standard means of quantifying the degree of femoral head inclination, using the angle between the trace of the proximal margin of the head and the shaft when the femur is seen in anterior view. This character can sometimes be scored in femora that are only visible in posterior view or specimens that lack much or all of the femoral shaft (see below). The three conditions are illustrated in Figures 2.37 and 2.38

Most coelurosaurs and close outgroups possess femora in which the proximal margin of the head and the shaft are nearly perpendicular to each other. These taxa are said to possess

medially projecting femoral heads, and this condition is codified as state 0. This condition is seen in the outgroups *Allosaurus* (Madsen 1976) and *Sinraptor* (Currie and Zhao 1993) and most coelurosaur ingroup taxa, including basal coelurosaurs (e.g., *Coelurus*: YPM 2010; *Mirischia*: SMNK 2349 PAL; Naish et al. 2004; *Tanycolagreus*: TPII 2000-09-29; *Tugulusaurus*: IVPP V4025; Rauhut and Xu 2005; *Zuolong*: Choiniere et al. 2010b), ornithomimosaurs (e.g., *Garudimimus*: Kobayashi and Barsbold 2005a; *Beishanlong*: Makovicky et al. 2010), alvarezsauroids (e.g., *Parvicursor*: Kahru and Rautian 1996; *Xixianykus*: Xu et al. 2010), basal therizinosauroids (e.g.., *Beipiaosaurus*: Xu et al. 1999; *Falcarius*: Zanno 2010a), most oviraptorosaurs (e.g., *Avimimus*: Vickers-Rich et al. 2002), troodontids (e.g., *Saurornithoides*: Norell et al. 2009), and dromaeosaurids (e.g., *Microraptor*: Hwang et al. 2002; *Rahonavis*: Forster et al. 1998; *Velociraptor*: Norell and Makovicky 1999).

Some other coelurosaurs possess a different condition in which the proximal margin of the head and the long axis of the shaft form an obtuse angle relative to each other. These taxa are said to have proximally inclined (=dorsally inclined) femoral heads, and this condition is seen in taxa scored for both states 1 and 2 in this character. These two states refer to two distinct morphologies of the proximally inclined head. In some taxa (state 1) the proximal margin of the femur is straight. This condition is seen in basal tyrannosauroids (e.g., *Dilong*: IVPP V14243; *Guanlong*: IVPP V14531; *Xiongguanlong*: FRDC-GS JB16-2-1; *Appalachiosaurus*: Carr et al. 2005; *Bistahieversor*: T.D. Carr, pers. comm.; *Gorgosaurus*: Lambe 1917; *Alioramus*: Brusatte et al. 2012; *Teratophoneus*: T.D. Carr, pers. comm.). In other taxa (state 2) the proximal margin is distinctly concave, due to the fact that both the head and the greater trochanter are elevated substantially relative to the central portion of the proximal surface of the femur. This condition is often most clearly apparent when the femur is seen in posterior view. Taxa with this condition

include the derived tyrannosaurine tyrannosaurids *Tarbosaurus* (Maleev 1974; ZPAL MgD-I/09) and *Tyrannosaurus* (Brochu 2003), as well as derived therizinosauroids (e.g., *Alxasaurus*: Russell and Dong 1993; *Erliansaurus*: Xu et al. 2002b; *Neimongosaurus*: Zhang et al. 2001; *Nothronychus*: Zanno et al. 2009; *Segnosaurus*: Zanno 2010b; *Suzhousaurus*: Li et al. 2008).

A version of this character was originally used by Brusatte et al. (2010a, character 285) for tyrannosauroids and Zanno et al. (2009, characters oZCD 320, 339) for therizinosauroids. The current character is a modified version of these previous characters that has been expanded into an ordered multistate. This character is ordered because the three states describe a hierarchial sequence of homologies (perpendicular-inclined-inclined and modified), which allows taxa with different conditions of an inclined head (states 1 and 2) to be united by a primary homology statement.

The original Brusatte et al. (2010a) character referred only to the shape (straight vs. concave) of the proximal margin, and stipulated that this character be scored when the femur is seen in posterior view, because the concave margins of *Tarbosaurus* and *Tyrannosaurus* are usually best seen in this view. The language of the current character has been substantially modified relative to the original Brusatte et al. (2010) character, and now it is stipulated that the measurement between the trace of the proximal margin and the long axis of the shaft be taken in anterior view. We note, however, that if an anterior view is not possible, then this character can usually confidently be scored by measuring the femur in posterior view (although caution must be exercised, because in some cases a proximally inclined head may appear to arise from the shaft perpendicularly in posterior view: e.g., *Tyrannosaurus*: Brochu 2003). Furthermore, this character can often be scored confidently in taxa that are lacking much or all of the shaft, because taxa with a proximally inclined femoral head (states 1 and 2) have a proximomedially

projecting proximal surface of the femur when seen in anterior view. Additionally, taxa with a proximally inclined femoral head usually possess a head that is elevated proximally relative to the greater trochanter, which is another means for recognizing the inclined condition in specimens that do not preserve the shaft.

Finally, note that Brusatte et al. (2012a) stated that *Tanycolagreus* (TPII 2000-09-29; Carpenter et al. 2005) possesses a proximally inclined femoral head, but we note here that this is incorrect and that this taxon is properly scored for a head that is perpendicular to the shaft (state 0).

713. Femur, trochanteric fossa on the posterior surface of the head, lateral to the ligament sulcus (for the capital ligament), form: absent or shallow (0); deep fossa (1); deep, extensive triangular depression that covers most of the posterior surface of the femur proximally and is demarcated medially and ventrally by a pronounced, curving, swollen ridge (2).

There are two distinctive fossae on the posterior surface of the proximal region of the femur in most theropods: a ligament sulcus (for the capital ligament) that excavates the posterior surface of the head and a trochanteric fossa that is placed further medially. The trochanteric fossa is present but shallow in most theropods, including the coelurosaurian outgroups *Allosaurus* (Madsen 1976) and *Sinraptor* (Currie and Zhao 1993) and nearly every coelurosaur that can be scored affirmatively for this character (e.g., *Buitreraptor*: MPCA 245; *Coelurus*: YPM 2010; *Garudimimus*: Kobayashi and Barsbold 2005a; *Velociraptor*: Norell and Makovicky 1999; *Zuolong*: Choiniere et al. 2010b). Some coelurosaurs, however, possess an especially deep trochanteric fossa, including the alvarezsauroid *Patagonykus* (Novas 1997) and several tyrannosauroids (e.g., *Dilong*: IVPP V14243; *Guanlong*: IVPP IVPP V14531; *Xiongguanlong*:

FRDC-GS JB16-2-1; *Appalachiosaurus*: Carr et al. 2005; *Alioramus*: Brusatte et al. 2012a). These taxa are scored for state 1. The derived tyrannosaurine tyrannosaurids *Tarbosaurus* (Maleev 1974; ZPAL MgD-I/09) and *Tyrannosaurus* (Brochu 2003) exhibit a further unique condition in which the fossa is not only deep, but it is so extensive that it covers most of the posterior surface of the proximal femur medial to the ligament sulcus. In these taxa the trochanteric fossa is triangular in shape and clearly offset by robust, curved, and swollen ridges medially and ventrally. This character was originally used by Brusatte et al. (2010a, character 286), who mistakenly described the fossa in question (which is properly the trochanteric fossa) as the fossa "lateral to the trochanteric fossa". This character is ordered because the three states form a nested sequence of subtle-deep-deep and extensive. The three conditions are illustrated in Figure 2.38.

714. Femur, fourth trochanter, position, measurement from proximal margin of head to distal termination of trochanter relative to total length of the femur: 40% or less (0); greater than 40% (1).

The length of the fourth trochanter varies among coelurosaurs and their immediate outgroups. This variation is quantified by noting where on the femoral shaft the fourth trochanter terminates, and then comparing the distance between the proximal end of the femur and this point to the overall proximodistal length of the femur. In many taxa the trochanter terminates at a position that is less than 40% of the total length of the femur. This is seen in many coelurosaurs, including basal taxa (e.g., *Coelurus*: YPM 2010; *Sinosauropteryx*: Currie and Chen 2001; *Tanycolagreus*: TPII 2000-09-29; *Tugulusaurus*: IVPP V4025; Rauhut and Xu 2005; *Zuolong*: Choiniere et al. 2010b), basal tyrannosauroids (e.g., *Dilong*: IVPP V14243; *Guanlong*: IVPP

IVPP V14531; *Xiongguanlong*: FRDC-GS JB16-2-1; *Appalachiosaurus*: Carr et al. 2005; *Dryptosaurus*: Brusatte et al. 2011), ornithomimosaurs (e.g., *Garudimimus*: Kobayashi and Barsbold 2005a; *Sinornithosaurus*: Kobayashi and Lü 2003), alvarezsauroids (e.g., *Mononykus*: Perle et al. 1994), some therizinosauroids (e.g.., *Erliansaurus*: Xu et al. 2002b; *Falcarius*: Zanno 2010a), oviraptorosaurs (e.g., *Microvenator*: Makovicky and Sues 1998), and dromaeosaurids (e.g., *Buitreraptor*: MPCA 245; *Mahakala*: Turner et al. 2011; *Velociraptor*: Norell and Makovicky 1999).

Some coelurosaurs, however, possess a proportionally longer fourth trochanter that terminates at a position further distally than 40% of the total shaft length. This is seen in the outgroups *Allosaurus* (Madsen 1976) and *Sinraptor* (Currie and Zhao 1993), derived tyrannosauroids (e.g., *Albertosaurus*: Parks 1928; *Alioramus*: Brusatte et al. 2012a; *Gorgosaurus*: Lambe 1917; *Tarbosaurus*: Maleev 1974; *Teratophoneus*: T.D. Carr, pers. comm.; *Tyrannosaurus*: Brochu 2003), the basal coelurosaur *Mirischia* (SMNK 2349 PAL; Naish et al. 2004), and the derived therizinosauroids *Neimongosaurus* (Zhang et al. 2001) and *Suzhousaurus* (Li et al. 2008).

This character was first utilized by Brusatte et al. (2010a, character 288). It has been slightly modified here so that the cutoff for state 0 is 40%, not 35% as in the original character. States 0 and 1 are illustrated in Figure 2.39.

715. Femur, lateral condyle, shape in distal view: circular or ovoid (0); ovoid, but with an anterior bulge that is slightly separated from the remainder of the condyle (1).

The standard condition for theropods is a lateral distal condyle of the femur that is circular or ovoid in shape when seen in distal view. This is the case in the outgroups *Allosaurus*

(Madsen 1976) and *Sinraptor* (Currie and Zhao 1993), and nearly every coelurosaur that can be scored affirmatively for this character. The few exceptions are several derived tyrannosauroids, including *Juratyrant* (Benson 2008), *Xiongguanlong* (FRDC-GS JB16-2-1), *Dryptosaurus* (Brusatte et al. 2011), *Alioramus* (Brusatte et al. 2012a), *Tarbosaurus* (ZPAL MgD-I/09), and *Tyrannosaurus* (Brochu 2003). In these taxa the condyle is ovoid in distal view, but it is also marked by a discrete bulge on the anterior surface that is slightly offset from the remainder of the condyle. This character was first used by Brusatte et al. (2010a, character 289). States 0 and 1 are illustrated in Figure 2.40.

716. Femur, extensor groove on anterior surface of distal end, form: absent or extremely shallow, anterior surface flat between the condyles in distal view (extensor groove may be present but does not manifest itself as a groove on the anterior margin in distal view) (0); groove present but shallow, expressed as a broad concave margin in distal view but present as an extensive depression on the anterior surface of the femur (1); groove present and deep, expressed as a deep, U-shaped cleft in distal view and present as an extensive depression on the anterior surface of the femur (2).

An extensor groove on the anterior surface of the distal end of the femur is often recognized as a synapomorphy of tetanuran theropods (e.g., Holtz 2000; Benson et al. 2009), but its size, shape, and depth differs greatly among taxa. This character does not concern the general absence or presence of an extensor groove, but rather how this groove is or is not expressed on the anterior margin of the femur in distal view. In most coelurosaurs the extensor groove, if present, is separated from the distal end of the femur. Therefore, when the femur is seen in distal view the anterior margin is straight or smoothly convex, with no sign of a concave margin that

represents the inset extensor groove. This condition, which is codified as state 0, is seen in several basal coelurosaurs, including *Coelurus* (YPM 2010), *Ornitholestes* (AMNH FARB 619), *Tanycolagreus* (TPII 2000-09-29), *Tugulusaurus* (IVPP V4025; Rauhut and Xu 2005), and *Zuolong* (Choiniere et al. 2010b). It is also present in the basal tyrannosauroids *Dilong* (IVPP V14243) and *Guanlong* (IVPP V14531), ornithomimosaurs (e.g., *Garudimimus*: Kobayashi and Barsbold 2005a; *Sinornithomimus*: Kobayashi and Lü 2003), alvarezsauroids (e.g., *Haplocheirus*: IVPP V15988; *Patagonykus*: Novas 1997; *Mononykus*: Perle et al. 1994), the basal therizinosauroid *Falcarius* (Zanno 2010a), and dromaeosaurids (e.g., *Mahakala*: Turner et al. 2011; *Rahonavis*: Forster et al. 1998; *Velociraptor*: Norell and Makovicky 1999).

Some coelurosaurs possess an extensor groove that reaches the distal margin of the femur, and thus is expressed as a concave margin on the anterior edge of the femur in distal view. Among these taxa are two distinct conditions. In the basal tyrannosauroid *Juratyrant* (Benson 2008; Brusatte and Benson in press) and the therizinosauroids *Nothrohynchus* (Zanno et al. 2009) and *Suzhousaurus* (Li et al. 2008), the concave surface for the groove is shallow and expressed as a broad margin covering much of the anterior surface of the femur. This is referred to as state 1. It is also apparently present in the derived tyrannosauroid *Teratophoneus* (T.D. Carr, pers. comm.). A second condition, referred to as state 2, is seen in the outgroups *Allosaurus* (Madsen 1976) and *Sinraptor* (Currie and Zhao 1933), as well as several derived tyrannosauroids such as *Xiongguanlong* (FRDC-GS JB16-2-1), *Dryptosaurus* (Brusatte et al. 2011), *Gorgosaurus* (Lambe 1917), *Alioramus* (Brusatte et al. 2012a), *Daspletosaurus* (T.D. Carr, pers. comm.), *Tarbosaurus* (ZPAL MgD-I/09), and *Tyrannosaurus* (Brochu 2003). In these taxa the extensor groove is remarkably deep and is expressed as a deep, U-shaped cleft on the anterior surface of the femur in distal view.

This character was first used by Brusatte et al. (2010a, character 290). It is considered an ordered multistate because the three conditions describe a nested hierarchy: no expression on the anterior surface-shallow expression-deep expression. The distribution of this character in tyrannosauroids has been discussed by Brusatte et al. (2011, 2012a) and Brusatte and Benson (in press). The three character states are illustrated in Figure 2.40.

717. Femur, mesiodistal crest, form: single structure (0); bifurcates distally to enclose fossa on the medial surface of the medial condyle (1).

The mesiodistal crest on the medial surface of the distal femur is variably expressed as either a weak or strongly overhanging structure in coelurosaurs, as described by character 186. There is also variability in the shape of the crest when it is seen in medial view. In the outgroups *Allosaurus* (Madsen 1976) and *Sinraptor* (Currie and Zhao 1993) and most coelurosaurs the crest is a single structure. This is the case, for example, in the basal tyrannosauroids *Dilong* (IVPP V14243), *Guanlong* (IVPP V14531), and *Juratyrant* (Benson 2008). A different morphology is seen in the derived tyrannosauroids *Alioramus* (Brusatte et al. 2012a), *Tarbosaurus* (ZPAL MgD-I/09), and *Tyrannosaurus* (Brochu 2003), as well as the alvarezsauroid *Mononykus* (Perle et al. 1994). In these taxa the crest bifurcates distally when it reaches the medial surface of the medial condyle, and the two bifurcating arms of the crest enclose a deep fossa between them. This character was first used by Brusatte et al. (2010a, character 291). States 0 and 1 are illustrated in Figure 2.41.

721. Tibia, lateral malleolus, position relative to medial malleolus: extend to approximately the same level distally (0); lateral malleolus extends substantially further distally than medial malleolus (1).

The lateral and medial malleoli of the distal end of the tibia extend to the same approximate level ventrally in the majority of coelurosaurs, as well as the outgroup *Allosaurus* (Madsen 1976). In some taxa, however, the lateral malleolus extends much further distally than the medial malleolus, such that there is a noticeable step between them on the ventral margin of the tibia when the bone is seen in anterior view. This condition is present in the outgroup *Sinraptor* (Currie and Zhao 1993), the basal therizinosauroid *Falcarius* (Zanno 2010a), the alvarezsauroids *Mononykus* (Perle et al. 1994) and *Parvicursor* (Kahru and Rautian 1996), and most tyrannosauroids (e.g., *Guanlong*: IVPP V14531; *Eotyrannus*: MIWG 1997.550; *Juratyrant*: Benson 2008; *Dryptosaurus*: Brusatte et al. 2011; *Appalachiosaurus*: Carr et al. 2005; *Albertosaurus*: Parks 1928; *Gorgosaurus*: Lambe 1917; *Tarbosaurus*: ZPAL MgD-I/29, I-38; *Tyrannosaurus*: Brochu 2003). The only tyrannosauroids lacking the expanded lateral malleolus are *Dilong* (IVPP V14243), *Alioramus* (Brusatte et al. 2012a), and apparently *Bistahieversor* (T.D. Carr, pers. comm.). This character was originally used by Brusatte et al. (2010a, character 295). States 0 and 1 are illustrated in Figure 2.42.

723. Astragalus, fossa on anterior surface of ascending process, form: shallow concavity that covers most of the ventral region of the ascending process (0); deep, triangular or ovoid fossa immediately above midpoint of condyles, set within a broad fossa that covers most of the ventral region of the ascending process (1).

There is a depressed, smooth fossa on the anterior surface of the ascending process of the astragalus in most theropods, and this depression usually takes the form of a small, impressed region located immediately above the condyles at the approximate midpoint of the ascending process. This condition is codified as state 0 and is seen in the outgroup *Allosaurus* (Madsen 1976) and most coelurosaurs that can be scored affirmatively for this character, including basal coelurosaurs (e.g., *Tanycolagreus*: TPII 2000-09-29; *Tugulusaurus*: IVPP V4025, Rauhut and Xu 2005; *Zuolong*: Choiniere et al. 2010b), some basal tyrannosauroids (*Dilong*: IVPP V14243; *Guanlong*: IVPP V14531), compsognathids (e.g., *Compsognathus*: Peyer 2006; *Sinosauropteryx*: Currie and Chen 2001), ornithomimosaurs (e.g., *Beishanlong*: Makovicky et al. 2010; *Garudimimus*: Kobayashi and Barsbold 2005a), basal alvarezsauroids (e.g., *Alvarezsaurus*: Bonaparte 1991; *Achillesaurus*: Martinelli and Vera 2007), therizinosauroids (e.g., *Falcarius*: Zanno 2010a), oviraptorosaurs (e.g.., *Microvenator*: Makovicky and Sues 1998), troodontids (e.g., *Zanabazar*: Norell et al. 2009), and dromaeosauris (e.g., *Deinonychus*: Ostrom 1969; *Rahonavis*: Forster et al. 1998; *Velociraptor*: Norell and Makovicky 1999).

Some coelurosaurs possess a different condition, which is codified as state 1 here. In these taxa the fossa is especially deep and triangular or ovoid in shape, and it is set within a broader fossa that covers nearly the entire anteroposterior length of the ascending process above the condyles of the astragalus. This morphology is present in the outgroup *Sinraptor* (Currie and Zhao 1993), derived alvarezsauroids (e.g., *Albinykus*: Nesbitt et al. 2011; *Mononykus*: Perle et al. 1994; *Xixianykus*: Xu et al. 2010), and derived tyrannosauroids (e.g., *Dryptosaurus*: Brusatte et al. 2011; *Appalachiosaurus*: Carr et al. 2005; *Bistahieversor*: T.D. Carr, pers. comm.; *Albertosaurus*: Parks 1928; *Gorgosaurus*: Lambe 1917; *Alioramus*: Brusatte et al. 2012a; *Tarbosaurus*: ZPAL MgD-I/29; *Tyrannosaurus*: Brochu 2003).

This character was first used by Brusatte et al. (2010a, character 298). States 0 and 1 are illustrated in Figure 2.44.

726. Pes, metatarsals II-IV, distal separation when in articulation: metatarsals closely appressed and distance between II-III and III-IV is approximately equal (0); distal ends of II and IV diverge from III, and distance between III-IV greater than that between II-III (1).

In most theropods the central metatarsals of the foot (metatarsals II, III, and IV) are closely appressed to each other throughout most of their lengths and only diverge from each other slightly at their distal ends, where they articulate with the first phalanges of the digits. Usually the distal ends of metatarsals II and IV diverge to an approximately equal degree relative to the distal end of metatarsal III. This condition is present in the outgroups *Allosaurus* (Madsen 1976) and *Sinraptor* (Currie and Zhao 1993) as well as the vast majority of coelurosaurs that can be scored affirmatively for this character. The only exceptions are derived tyrannosauroids, including *Appalachiosaurus* (Carr et al. 2005), *Albertosaurus* (Parks 1928), *Gorgosaurus* (Lambe 1917), *Tarbosaurus* (Maleev 1974), and *Tyrannosaurus* (Brochu 2003). In these taxa the distal ends of metatarsals II and IV diverge from the distal end of metatarsal III to a substantial degree, and the degree of divergence between III and IV is noticeably greater than that between II-III. This character was first used by Brusatte et al. (2010a, character 302). The character states are not illustrated here, but the unusual state 1 is figured in the literature (e.g., Brochu 2003: figure 104).

727. Pes, metatarsal II, articular scar for metatarsal III on distal portion of lateral surface of shaft, form: subtle or absent (0); enlarged as a rugose fossa that occupies more than half of the proximodistal length of the shaft and expands in anteroposterior width distally (1).

In many theropods the lateral surface of metatarsal II and the medial surface of metatarsal III make contact along much of their shafts. This contact continues distally in many taxa, and sometimes there is a noticeable articular scar on the lateral surface of metatarsal II immediately above the distal condylar region. If present, this scar is usually subtle and its surface is not especially rugose. This is the condition in the outgroups *Allosaurus* (Madsen 1976) and *Sinraptor* (Currie and Zhao 1993), basal coelurosaurs (e.g., *Ornitholestes*: AMNH FARB 619; *Tanycolagreus*: TPII 2000-09-29), some basal tyrannosauroids (e.g., *Eotyrannus*: MIWG 1997.550; *Appalachiosaurus*: Carr et al. 2005), ornithomimosaurs (e.g., *Kinnareemimus*: Buffetaut et al. 2009; *Qiupalong*: L. Xu et al. 2011), alvarezsauroids (e.g., *Albinykus*: Nesbitt et al. 2011; *Mononykus*: Perle et al. 1994), therizinosauroids (e.g., *Falcarius*: Zanno 2010a; *Neimongosaurus*: Zhang et al. 2001), and dromaeosaurids (e.g., *Balaur*: EME PV.313; *Deinonychus*: Ostrom 1969; *Velociraptor*: Makovicky and Norell 1999).

A distinct condition is seen in some large-bodied arctometatarsalian tyrannosauroids (i.e., those taxa in which metatarsal III is "pinched" between metatarsals II and IV: Holtz 1995). In these taxa the articular surface for metatarsal III on the distal end of the lateral surface of the shaft of metatarsal II is enormous. It is enlarged relative to the condition in other taxa such that it occupies more than half of the proximodistal length of the shaft. It is highly rugose, defined by sharp rims around its margins, and expands in anteroposterior (extensor-flexor) width as it continues distally. This morphology is seen in *Albertosaurus*, *Bistahieversor*, and *Daspletosaurus* (T.D. Carr, pers. comm.), *Alioramus* (additional material belonging to IGM

100/1844 not described by Brusatte et al. 2012a), *Tarbosaurus* (ZPAL MgD-I/76), and *Tyrannosaurus* (Brochu 2003). Possession of this character state is not uniquely correlated with the possession of an arctometatarsalian pes, either within tyrannosauroids or among coelurosaurs more broadly. For example, the arctometatarsalian tyrannosauroid *Appalachiosaurus* (Carr et al. 2005) and ornithomimosaur *Qiupalong* (L. Xu et al. 2011) lack the expanded and rugose articular surface on metatarsal II.

This character was first used by Brusatte et al. (2010a, character 303). States 0 and 1 are illustrated in Figure 2.44.

728. Pes, metatarsal II, lateral surface in proximal view, shape: flat or weakly concave (0); moderately concave (1); strongly concave (deep concave notch is present) (2).

When seen in proximal view, the lateral surface of metatarsal II is flat or very weakly concave in most theropods. Among taxa with this condition are the outgroups *Allosaurus* (Madsen 1976) and *Sinraptor* (Currie and Zhao 1993), the basal coelurosaurs *Ornitholestes* (AMNH FARB 619) and *Zuolong* (Choiniere et al. 2010b), some basal tyrannosauroids (e.g., *Dilong*: IVPP V14243; *Eotyrannus*: MIWG 1997.550; *Guanlong*: IVPP V14531), some ornithomimosaurs (e.g., *Kinnareemimus*: Buffetaut et al. 2009), alvarezsauroids (e.g., *Achillesaurus*: Martinelli and Vera 2007; *Patagonykus*: Novas 1997; *Mononykus*: Perle et al. 1994), therizinosauroids (e.g., *Falcarius*: Zanno 2010a; *Neimongosaurus*: Zhang et al. 2001), and dromaeosaurids (e.g., *Deinonychus*: Ostrom 1969; *Mahakala*: Turner et al. 2011; *Velociraptor*: Norell and Makovicky 1999).

A different morphology is present in a handful of other coelurosaurs, in which the lateral surface of metatarsal II is concave in proximal view. Among taxa with a concave margin two

discrete conditions are apparent: either the margin is moderately concave (state 1) or strongly concave, with a deep notch (state 2). The first state is seen in several ornithomimosaurs (e.g., *Garudimimus*: Kobayashi and Barsbold 2005a; *Qiupalong*: L. Xu et al. 2011), whereas the second is seen in derived tyrannosauroids (e.g., *Appalachiosaurus*: Carr et al. 2005; *Gorgosaurus*: Lambe 1917; *Tarbosaurus*: ZPAL MgD-I/76; *Tyrannosaurus*: Brochu 2003). The possession of a notch is related to the possession of an arctometatarsalian pes, but there is not a one-to-one correlation between these characters. For instance, both subarctometatarsalian and fully arctometatarsalian ornithomimosaurs possess state 1, whereas some arctometatarsalian taxa such as *Mononykus* (Perle et al. 1994) do not possess a concave lateral margin of metatarsal II (state 0).

This character was originally used by Brusatte et al. (2010a, character 304), which was a multistate character that distinguished between a flat or weakly concave surface and a strongly concave surface. The character is expanded into a multistate here to take into account the subtly concave condition of ornithomimosaurs, which differs discretely from the flat condition in most coelurosaurs and the deeply concave condition of derived tyrannosauroids. This character is ordered because the three states describe a nested sequence of homologies (flat-subtly concave-deeply concave). The three character states are illustrated in Figure 2.44.

729. Pes, metatarsal IV, distal end, ratio between anteroposterior long axis (measured from midpoint of condyles posteriorly to anterior surface of bone) and mediolateral width (measured at midpoint: greater than 1.40, distal surface is elongate anteroposteriorly (0); between 1.40 and 1.20 (1); less than 1.20, distal surface nearly square shaped with nearly flat anterior surface (2).

The proportions of the distal end of metatarsal IV vary among coelurosaurs and close outgroups. The general shape of the distal end can be quantified by calculating a ratio of the anteroposterior (extensor-flexor) length of the surface to the mediolateral width of the surface. The anteroposterior length is measured between the condyles (i.e., it is not a maximum length), whereas the mediolateral width is measured at the midpoint of the mediolateral margin.

State 0, in which this ratio is greater than 1.4, represents taxa in which the anteroposterior length of the distal surface of metatarsal IV is substantially longer than the mediolateral width. This condition is seen in several basal coelurosaurs, including *Coelurus* (YPM 2010), *Ornitholestes* (AMNH FARB 619), *Tanycolagreus* (TPII 2000-09-29), *Zuolong* (Choiniere et al. 2010b), and the basal tyrannosauroid *Guanlong* (IVPP V14531). It is also seen in ornithomimosaurs (e.g., *Garudimimus*: Kobayashi and Barsbold 2005a; *Harpymimus*: Kobayashi and Barsbold 2005b) and dromaeosaurids (e.g., *Deinonychus*: Ostrom 1969; *Velociraptor*: Norell and Makovicky 1999). It is also apparently present in the derived tyrannosauroid *Bistahieversor* (T.D. Carr, pers. comm.)

State 1, in which this ratio is between 1.4 and 1.2, is present in the outgroups *Allosaurus* (Madsen 1976) and *Sinraptor* (Currie and Zhao 1993). Among coelurosaurs, it is seen in several basal tyrannosauroids (e.g., *Appalachiosaurus*: Carr et al. 2005; *Dilong*: IVPP V14243; *Dryptosaurus*: Brusatte et al. 2011; *Eotyrannus*: MIWG 1997.550), the basal therizinosauroid *Falcarius* (Zanno 2010a), and alvarezsauroids (e.g., *Mononykus*: Perle et al. 1994; *Parvicursor*: Kahru and Rautian 1996).

State 2, in which the ratio is less than 1.2, is present in the therizinosauroid *Alxasaurus* (Russell and Dong 1993) and several derived tyrannosauroids, including *Albertosaurus* (Parks 1928), *Gorgosaurus* (Lambe 1917), *Tarbosaurus* (ZPAL MgD-I/206), and *Tyrannosaurus*

(Brochu 2003). In these taxa the anterior surface of the distal end of metatarsal IV is nearly straight and the entire distal surface appears nearly square shaped when seen in distal view.

This character was first used by Brusatte et al. (2010a, character 305). It is an ordered multistate because the three states describe an orderly numerical progression of ratios. The three character states are illustrated in Figure 2.44.

730. Pes, proximal pedal phalanges of digits II and III, ratio of length to midshaft width: greater than 3.0 (0); less than 3.0 (1).

In the vast majority of coelurosaurs the proximal phalanges of pedal digits II and III are elongate and gracile. This condition is characterized numerically by a length-to-width ratio that is greater than 3.0. In these measurements length describes the proximodistal long axis of the phalanx and width the mediolateral dimension at the midpoint of the shaft. This condition is seen, for example, in taxa such as the basal coelurosaur *Ornitholestes* (AMNH FARB 619), the basal tyrannosauroid *Guanlong* (IVPP V14531), the compsognathid *Compsognathus* (Peyer 2006), the ornithomimosaur *Garudimimus* (Kobayashi and Barsbold 2005a), the alvarezsauroids *Haplocheirus* (Choiniere et al. 2010a) and *Mononykus* (Perle et al. 1994), the therizinosauroids *Falcarius* (Zanno 2010a) and *Alxasaurus* (Russell and Dong 1993), the oviraptorosaurs *Caudipteryx* (Ji et al. 1998) and *Citipati* (Clark et al. 2002b), the troodontid *Saurornithoides* (Norell et al. 2009), and the dromaeosaurids *Deinonychus* (Ostrom 1969), *Microraptor* (Hwang et al. 2002), and *Rahonavis* (Forster et al. 1998). A different morphology is present in a few taxa, however, which are characterized by short and stout proximal pedal phalanges with a length-to-width ratio of less than 3.0. This character state is seen in the derived tyrannosaurine tyrannosaurids *Tarbosaurus* (Maleev 1974) and *Tyrannosaurus* (Brochu 2003), the derived

therizinosauroids *Neimongosaurus* (Zhang et al. 2001) and *Nothronychus* (Zanno et al. 2009), and the outgroups *Allosaurus* (Madsen 1976) and *Sinraptor* (Currie and Zhao 1993). This charater was first used by Brusatte et al. (2010a, character 306). The possession of stout phalanges may be generally associated with large body size, although large-bodied tyrannosauroids such as *Alioramus* (Brusatte et al. 2012a) and *Gorgosaurus* (Lambe 1917) possess elongate and gracile phalanges. This character is not illustrated here, but the unusual state 1 is figured in the literature (e.g., Brochu 2003: figure 105).

731. Pes, pedal unguals, lip overhanging proximal articular surface dorsally (on extensor surface): present (0); absent or reduced to a subtle tuber (1).

Most theropods exhibit a pronounced lip on the dorsal (extensor) surface of the proximal end of the pedal unguals, which helps form the articulation with the penultimate phalanx. This lip is absent or extremely reduced, however, in a subset of derived tyrannosauroids, including *Bistahieversor* (T.D. Carr, pers. comm.), *Albertosaurus* (Parks 1928), *Gorgosaurus* (Lambe 1917), *Alioramus* (Brusatte et al. 2012a and additional material of IGM 100/1844 not described in that paper), *Tarbosaurus* (Maleev 1974), and *Tyrannosaurus* (Brochu 2003). This character was first used by Brusatte et al. (2010a, character 307) and was inspired by discussion in Carr et al. (2005). This character is not illustrated here, but the unusual state 1 is figured in the literature (e.g., Brochu 2003: figure 107).

827. Premaxilla, anteroposterior length compared to that of maxilla: length of ventral (alveolar) margin greater (0) or less than (1) 10% total anteroposterior length of maxilla.

In the majority of coelurosaurs the anteroposterior length of the premaxilla (measured along the tooth row) is greater than 10% of the total anteroposterior length of the maxilla. This is the case in the outgroups *Allosaurus* (Madsen 1976) and *Sinraptor* (Currie and Zhao 1993), the basal coelurosaurs *Ornitholestes* (AMNH FARB 619) and *Zuolong* (Choiniere et al. 2010b), most compsognathids (*Compsognathus*: Peyer 2006; *Huaxiagnathus*: Hwang et al. 2002; *Juravenator*: Chiappe and Göhlich 2010; *Sinosauropteryx*: Currie and Chen 2001), most ornithomimosaurs (e.g., *Garudimimus*: Kobayashi and Barsbold 2005a; *Sinornithomimus*: Kobayashi and Lü 2003), therizinosauroids (e.g., *Erlikosaurus*: Clark et al. 1994), oviraptorosaurs (e.g., *Citipati*: Clark et al. 1999; *Incisivosaurus*: Xu et al. 2002a, Balanoff et al. 2009), some troodontids (e.g., *Anchiornis*: Hu et al. 2009; *Mei*: Xu and Norell 2004), and dromaeosaurids (e.g., *Sinornithosaurus*: Xu and Wu 2001; *Tsaagan*: Norell et al. 2006).

In some taxa, however, the premaxilla is markedly reduced relative to the maxilla. In these coelurosaurs the anteroposterior length of the premaxillary tooth row is less than 10% of the total length of the maxilla. This condition is seen in all tyrannosauroids that can be affirmatively scored for this character, including *Dilong* (IVPP V14243; Xu et al. 2004), *Guanlong* (IVPP V14531; Xu et al. 2006), *Kileskus* (Averianov et al. 2010), *Proceratosaurus* (Rauhut et al. 2010), *Xiongguanlong* (Li et al. 2010), and tyrannosaurids (e.g., Brochu 2003; Hurum and Sabath 2003). It is also seen in the compsognathid *Sinocalliopteryx* (Ji et al. 2007) and the basal ornithomimosaur *Pelecanimimus* (LH 7777), but not in more derived ornithomimosaurs. Finally, it is present in alvarezsauroids (e.g., *Haplocheirus*: Choiniere et al. 2010a; *Shuvuuia*: Chiappe et al. 1998) and some troodontids (e.g., *Byronosaurus*: Makovicky et al. 2003; *Saurornithoides* and *Zanabazar*: Norell et al. 2009; *Xixiasaurus*: Lü et al. 2010).

States 0 and 1 are illustrated in Figure 2.2

828. Supraoccipital, tab-like processes on left and right sides of dorsal margin of bone: absent (0); present (1).

In most theropods, including the basal tyrannosauroids *Guanlong* (IVPP V14531), *Dilong* (IVPP V14243), and *Xiongguanlong* (Li et al., 2010), the dorsal margin of the supraoccipital is a flat plate that abuts (sits directly behind) the posterior surface of the parietal. As first noted by Bakker et al. (1988), this is not the condition in more derived tyrannosauroids. In these taxa, the dorsal margin of the supraoccipital is not flat and does not sit directly against the parietal, but rather is folded (like a vertical fold in a partially drawn curtain) and curves posteriorly to overlie the remainder of the supraoccipital (like a quiff hairstyle). The posterior surface of the "quiff" is depressed at its center, and as a result, the left and right sides both appear as discrete "tab-like" processes that project posteriorly. Therefore, these "tabs" are symmetrical along the dorsoventral midline of the supraoccipital. This morphology is present in *Bistahieversor* (NMMNH P-27469), *Albertosaurus* (Currie, 2003), *Gorgosaurus* (Currie, 2003; Witmer and Ridgely, 2009; ROM 1427), *Alioramus* (IGM 100/1844), *Daspletosaurus* (Currie, 2003), *Tarbosaurus* (Hurum and Sabath, 2003), and *Tyrannosaurus* (Bakker et al., 1988; Brochu, 2003; MOR 1125). States 0 and 1 are figured in Figure 2.14.

There has been confusion in the literature relating to the "tab-like" processes, their phylogenetic utility, and their possible relationship with other phylogenetic characters relating to the supraoccipital. Bakker et al. (1988) noted that a peculiar set "tab-like" processes was present on the dorsal margin of the supraoccipital in all tyrannosaurids. Subsequently, Holtz (2001, character 8) and Currie et al. (2003, character 71) both considered the presence of the "tab-like" processes to be synapomorphies of Tyrannosauridae (their analyses were published before basal

tyrannosauroids such as *Guanlong* and *Dilong* were known). Carr and Williamson (2010: character 172) also utilized this character, but Brusatte et al. (2010a, character 149) combined the character relating to the "tab-like" processes with another character relating to the forking of the supraoccipital at its dorsal margin into a single character. This decision was made because at the time some of the authors felt that these two character states were equivalent (i.e., that the bifurcation of the supraoccipital into two "forks" produced the "tab-like" processes). However, recent observations by Thomas Carr (pers. comm.) reveal that the two characters are distinct from each other. The two characters can clearly be distinguished from each other on well-preserved tyrannosauroid specimens, and some taxa (such as *Alioramus altai*) possess the "tab-like" processes but lack a forked supraoccipital. Therefore, a separate character for the "tab-like" processes is included here (note that the character for the dorsal forking of the supraoccipital is also included here as character 606). All of the above discussion is presented in Bever et al. (in press).

829. Nasal, premaxillary processes (=supranarial processes), extent of their apposition to each other on the midline in dorsal view: apposed for nearly their entire length (may abruptly separate from each other at their tips) (0); not apposed for most of their length, and therefore do not abruptly separate from each other at their tips (1).

Most tyrannosauroids, such as *Guanlong* (IVPP V14531), *Dilong* (IVPP V14243), *Appalachiosaurus* (Carr et al. 2005), and *Albertosaurus* and *Gorgosaurus* (Currie 2003), possess left and right premaxillary processes of the nasal that are closely appressed for most of their lengths and only diverge from each other at their anterior tips. This is also seen in the outgroups *Allosaurus* (Madsen 1976) and *Sinraptor* (Currie and Zhao 1993) and nearly every coelurosaur

that can be affirmatively scored for this character. The few exceptions are some derived tyrannosauroids, as well as a few other coelurosaurs, which exhibit an unusual condition in which the left and right premaxillary processes of the nasal do not lie against each other for most of their lengths, but rather are widely separated like two tines on a fork. This feature is seen in *Alioramus* (Brusatte et al. 2012a), *Daspletosaurus* (Russell 1970), *Tarbosaurus* (Hurum and Sabath 2003), and *Tyrannosaurus* (Brochu 2003), as well as the therizinosauroid *Erlikosaurus* (Clark et al. 1994) and the alvarezsauroid *Shuvuuia* (Chiappe et al. 1998). It is unclear if this condition is representative of all therizinosauroids and alvarezsauroids, however, as no other members of these groups can be scored affirmatively for this character. States 0 and 1 are shown in Figure 2.7.

830. Dentary, Meckelian groove, position: approximately centered at dorsoventral midheight of dentary (0); positioned ventrally, located closer to the ventral margin than the dorsal margin (1).

This character was originally used by Carr and Williamson (2010, character 211), who scored state 0 as present in all tyrannosauroids that could be scored in the affirmative. We note here that this character state, representing a Meckelian groove that is positioned at approximately the dorsoventral midheight of the medial surface of the dentary, is also present in the coelurosaurian outgroups *Allosaurus* (Madsen 1976) and *Sinraptor* (Currie and Zhao 1993), as well as *Compsognathus* (Peyer 2006), one derived therizinosauroid (*Erlikosaurus*: Clark et al. 1994), and one aberrant dromaeosaurid (*Austroraptor*: MML 195). All other coelurosaurs that can be assessed in the affirmative are scored for state 1, referring to a Meckelian groove that is positioned closer to the ventral margin of the dentary than the dorsal margin (i.e., ventrally deflected relative to midheight of the dentary. Examples include *Ornitholestes* (AMNH FARB

619), ornithomimosaurs (e.g., *Harpymimus*: Kobayashi and Barsbold 2005b), most therizinosauroids (e.g., *Falcarius*: Zanno 2010a; *Neimongosaurus*: Zhang et al. 2001), oviraptorosaurs (e.g., *Citipati*: Clark et al. 1999), troodontids (e.g., *Zanabazar*: Norell et al. 2009), and dromaeosaurids (e.g., *Deinonychus*: Ostrom 1969). States 0 and 1 are illustrated in Figure 2.17.

831. Dentary, row of foramina on lateral surface paralleling ventral margin: absent or limited to a small series of foramina at the anterior end of the dentary (at the level of the first 1-4 alveoli) (0); present as a distinct row that extends along most of the lateral surface of the dentary (across the entire length of the tooth row at the very least) (1).

Most theropods possess a primary row of neurovascular foramina on the dentary which approximately parallels the tooth row and is located close to the alveolar (dorsal) margin of the bone. Additionally, several other randomly placed foramina are also usually present. Some coelurosaurs exhibit a peculiar condition in which there is a discrete secondary row of foramina that parallels the ventral margin of the dentary, and is located only a few millimeters above the ventral edge of the bone. This character state is seen in all tyrannosauroids that can be scored in the affirmative, including *Proceratosaurus* (Rauhut et al. 2010; NHMUK R4860), *Dryptosaurus* (Brusatte et al. 2011), *Bistahieversor* (T.D. Carr, pers. comm.), *Albertosaurus* and *Gorgosaurus* (Currie 2003), *Alioramus* (Brusatte et al. 2012a), *Teratophoneus* (Carr et al. 2011), *Daspletosaurus* (Russell 1970), *Tarbosaurus* (Hurum and Sabath 2003), and *Tyrannosaurus* (Brochu 2003). It is also present in *Compsognathus* (Peyer 2006) and many dromaeosaurids, including *Shanag* (Turner et al. 2007b), *Sinornithosaurus* (Xu and Wu 2001), *Dromaeosaurus* (Currie 1995), *Deinonychus* (Ostrom 1969), *Velociraptor* (Barsbold and Osmólska 1999),

Tsaagan (Norell et al. 2006), and *Austroraptor* (MML 195). All other coelurosaurs that can be affirmatively scored lack this secondary row, including taxa such as ornithomimosaurs (e.g., *Pelecanimimus*: LH 7777; *Sinornithosaurus*: Kobayashi and Lü 2003), alvarezsauroids (e.g., *Haplocheirus*: Choiniere et al. 2010a; *Shuvuuia*: Chiappe et al. 1998), therizinosauroids (e.g., *Falcarius*: Zanno 2010a; *Erlikosaurus*: Clark et al. 1994), oviraptorosaurs (e.g., *Citipati*: Clark et al. 1999; *Incisivosaurus*: Balanoff et al. 2009), and troodontids (e.g., *Zanabazar*: Norell et al. 2009). It is also absent in the outgroups *Allosaurus* (Madsen 1976) and *Sinraptor* (Currie and Zhao 1993). States 0 and 1 are illustrated in Figure 8.17.

832. Splenial, notch along dorsal margin of anterior process, where the splenial contacts the supradentary (if present): absent (0); present (1).

Some tyrannosauroids exhibit a distinctive condition in which the splenial is marked by a notch along the dorsal margin of its anterior process, where this bone makes contact with the supradentary. This morphology is present in *Albertosaurus* (CMNH 5601), *Alioramus* (Brusatte et al. 2012a), *Daspletosaurus* (CMN 8506), *Gorgosaurus* (ROM 1247), *Tarbosaurus* (Hurum and Sabath 2003), and *Tyrannosaurus* (Brochu 2003). It is absent in the outgroup *Sinraptor* (Currie and Zhao 1993) as well as all other coelurosaurs that can be scored in the affirmative, including the basal coelurosaurs *Compsognathus* (Peyer 2006) and *Tanycolagreus* (TPII 2000-09-29), ornithomimosaurs (e.g., *Garudimimus*: Kobayashi and Barsbold 2005a), therizinosauroids (e.g., *Erlikosaurus*: Clark et al. 1994), oviraptorosaurs (e.g., *Citipati*: Clark et al. 1999), troodontids (e.g., *Zanabazar*: Norell et al. 2009), and dromaeosaurids (e.g., *Dromaeosaurus*: Currie 1995). The character states are not figured here but are illustrated in the literature (e.g., state 0: Currie and Zhao 1993: figure 11; state 1: Brusatte et al. 2012a: figure 40).

833. Cervical vertebrae, position of prezygapophyses in anterior-middle cervicals: prezygapophyseal facet approximately level with anterior face of centrum (0); prezygapophyseal facet entirely anterior to anterior face of centrum (1).

In the coelurosaurian outgroups *Allosaurus* (Madsen 1976) and *Sinraptor* (Currie and Zhao 1993), the prezygapophyses in the anterior-middle cervicals do not extend far anteriorly. In these taxa the articular facet is located at a level that is approximately even with the anterior face of the centrum. This is not the case in all coelurosaurs that can be affirmatively scored. In these taxa, as exemplified for example by *Deinonychus* (Ostrom 1969) and *Tyrannosaurus* (Brochu 2003), the articular facet of the prezygapophysis is positioned anterior to the anterior face of the centrum. States 0 and 1 are illustrated in Figure 2.25.

834. Caudal vertebrae, morphology of dorsal portion of neural spines of anterior caudals: unexpanded (0); expanded anteroposteriorly relative to the remainder of the neural spine (and often mediolaterally as well) (1).

Most theropods exhibit neural spines of the anterior caudals that are approximately rectangular in shape, and which do not expand in anteroposterior length at their dorsal tip. This condition is exemplified by the outgroups *Allosaurus* (Madsen 1976) and *Sinraptor* (Currie and Zhao 1993), as well as by coelurosaurs such as *Falcarius* (Zanno 2010a), *Shenzhousaurus* (Ji et al. 2003), and *Velociraptor* (Norell and Makovicky 1999). A few coelurosaurs possess a different character state in which the dorsal tips of the anterior caudal neural spines are anteroposteriorly expanded relative to the remainder of the spine. Oftentimes the dorsal tips are expanded in the mediolateral dimension as well. The only taxa in which this morphology is present are several

derived tyrannosauroids (e.g., *Alioramus*: Brusatte et al. 2012a; *Gorgosaurus*: Lambe 1917; *Tyrannosaurus*: Brochu 2003) and derived therizinosauroids (e.g., *Neimongosaurus*: Zhang et al. 2001; *Suzhousaurus*: Li et al. 2008). States 0 and 1 are illustrated in Figure 2.28.

835. Ulna, morphology of distal end: expanded mediolaterally at least 1.5x relative to midshaft mediolateral width (0); expanded less than 1.5x midshaft mediolateral width (1).

The ulna of most theropods is expanded mediolaterally at its distal end, such that it is at least 1.5 times as wide here as at the midpoint of the shaft. This is the case in the outgroup *Allosaurus* (Madsen 1976), as well as many coelurosaurs, including basal coelurosaurs (*Coelurus*: YPM 2010; *Tanycolagreus*: TPII 2000-09-29; *Zuolong*: Choiniere et al. 2010b), tyrannosauroids (e.g., *Guanlong*: IVPP V14531; *Tyrannosaurus*: Brochu 2003), compsognathids (e.g., *Compsognathus*: Peyer 2006; *Juravenator*: Chiappe and Göhlich 2010; *Sinosauropteryx*: Currie and Chen 2001), the basal therizinosauroid *Falcarius* (Zanno 2006), oviraptorosaurs (e.g., *Microvenator*: Makovicky and Sues 1998), troodontids (e.g., *Sinornithoides*: Currie and Dong 2001b), and dromaeosaurids (e.g., *Bambiraptor*: Burnham 2004; *Deinonychus*: Ostrom 1969). A distinctive condition is seen in some non-paravian theropods, characterized by an ulna whose distal end is less than 1.5 times as wide mediolaterally as the shaft midpoint. In essence, the ulnae of these taxa are unexpanded distally. This character state is seen in ornithomimosaurs (e.g., *Archaeornithomimus*: Smith and Galton 1990; *Beishanlong*: Makovicky et al. 2010; *Struthiomimus*: Nicholls and Russell 1985), alvarezsauroids (e.g., *Haplocheirus*: IVPP V15988; *Patagonykus*: Novas 1997; *Mononykus*: Perle et al. 1994), and most therizinosauroids (e.g., *Erliansaurus*: Xu et al. 2002b; *Nothronychus*: Zanno et al. 2009).

Note that all measurements discussed here are mediolateral dimensions, and thus can be measured in photographs of the ulna in anterior or posterior views. There is variability in the degree of anteroposterior expansion, as seen in lateral or medial views, but this is not encapsulated by this character. Expansion in this dimension is likely related to expansion in the mediolateral dimension, so it is not scored as a separate character. However, if an ulna is only visible in lateral or medial views and is seen to possess an expanded distal end, this is not considered sufficient to score the specimen in question for state 1, and instead this specimen would be scored as questionable ("?").States 0 and 1 are illustrated in Figure 2.31.

836. Ilium, medial surface of preacetabular process, pronounced horizontal shelf continuing from anterior margin of pubic peduncle to demarcate the cuppedicus fossa dorsally: absent (0); present (1).

As originally described by Holtz (2001), several tyrannosauroids possess a distinctive feature on the medial surface of the ilium: a pronounced horizontal shelf that borders the cuppedicus fossa dorsally. This shelf begins at the anterior margin of the pubic peduncle, with which it is continuous, and then extends posteriorly and dorsally before orienting itself into a horizontal structure. It is absent in the basal tyrannosauroid *Guanlong* (IVPP V14531), but is present in all other tyrannosauroids that can be scored affirmatively, including *Dilong* (IVPP V14243), *Juratyrant* (Benson 2008; OUMNH J.3311), *Albertosaurus* and *Gorgosaurus* (Holtz 2001), *Alioramus* (Brusatte et al. 2012a), *Tarbosaurus* (Maleev 1974; ZPAL MgD-I/204), and *Tyrannosaurus* (Brochu 2003). It is absent in almost all other coelurosaurs in which it can be positively scored, including close tyrannosauroid relatives such as the basal coelurosaur *Mirischia* (SMNK 2349 PAL) and ornithomimosaurs (e.g.., *Gallimimus*: ZPAL MgD-I/1, I/94;

Qiupalong: L. Xu et al. 2011). One exception, however, is that it is present in the ovirpatorosaur *Microvenator* (AMNH FARB 3041). It is also absent in the outgroups *Allosaurus* (Madsen 1976) and *Sinraptor* (Currie and Zhao 1993), but is present in the neovenatorid allosauroids (Benson et al. 2010a). Based on current phylogenies of basal tetanuran theropods, this feature is optimized as evolving convergently in tyrannosauroids and neovenatorids (Benson et al. 2010a). However, if neovenatorids are later found to be basal coelurosaurs, or closer to coelurosaurs than to *Allosaurus* and *Sinraptor*, then the medial shelf may be a synapomorphy of coelurosaurs that is lost in more derived taxa. States 0 and 1 are illustrated in Figure 2.34.

837. Metatarsal III, mediolateral width of distal end compared to mediolateral widths of distal ends of metatarsals II or IV (whichever of the latter is greater): less than (0) or greater than (1) 1.3 times as wide.

In most coelurosaurs the mediolateral width of the distal end of metatarsal III is approximately the same width as the distal ends of metatarsals II and IV. This is expressed by state 0, and is present in coelurosaurian outgroups (*Allosaurus*: Madsen 1976; *Sinraptor*: Currie and Zhao 1993) and most coelurosaurs, among them some basal tyrannosauroids (e.g., *Dilong*: IVPP V14243; *Eotyrannus*: MIWG 1997.550), derived tyrannosauroids (e.g., *Tyrannosaurus*: Brochu 2003), most ornithomimosaurs (e.g., *Garudimimus*: Kobayashi and Barsbold 2005a; *Harpymimus*: Kobayashi and Barsbold 2005b), alvarezsauroids (e.g., *Haplocheirus*: IVPP V15988; *Alvarezsaurus*: Bonaparte 1991; *Mononykus*: Perle et al. 1994), therizinosauroids (e.g., *Falcarius*: Zanno 2010a; *Neimongosaurus*: Zhang et al. 2001), troodontids (e.g., *Mei*: Xu and Norell 2004; *Sinornithoides*: Currie and Dong 2001b), and dromaeosaurids (e.g., *Deinonychus*: Ostrom 1969; *Mahakala*: Turner et al. 2011; *Rahonavis*: Forster et al. 1998; *Sinornithosaurus*:

Xu and Wu 2001). Some basal coelurosaurs exhibit a modified condition in which the mediolateral width of the distal end of metatarsal III is expanded relative to those of II and IV, so that it is more than 1.3 times as wide. Taxa exhibiting this condition include *Coelurus* (YPM 2010), *Guanlong* (IVPP V14531), *Tanycolagreus* (TPII 2000-09-29), and *Zuolong* (Choiniere et al. 2010b). It is also present in the oviraptorosaur *Citipati* (Clark et al. 1999) and some ornithomimosaurs (e.g., *Gallimimus*: ZPAL MgD-I/32). Note that to score this character, the mediolateral measurement of metatarsal III is compared to that of either II or IV, whichever is larger. In those cases where only one of II or IV is preserved, then this character is scored by comparing the width of metatarsal III to whichever of II or IV is present. States 0 and 1 are illustrated in Figure 2.44.

838. Lacrimal, extent of antorbital fossa on region where anterior and ventral rami meet: extensive, fossa excavates nearly entire region and nearly extends to the posterodorsal corner of the lacrimal (the lacrimal angle), leaving only a thin region of bone at the posterodorsal corner of the lacrimal (0); reduced, fossa stops well short of the posterodorsal corner of the lacrimal (1).

In most theropods the antorbital fossa excavates the lateral surface of the lacrimal where the anterior and ventral processes meet. This excavation is bordered dorsally and posteriorly by thick regions of subcutaneous bone surface in most taxa, such that the antorbital fossa does not approach the posterodorsal corner of the lacrimal (the "lacrimal angle"). This condition is codified as state 1 and is present in the outgroups *Allosaurus* (Madsen 1976) and *Sinraptor* (Currie and Zhao 1993), as well as nearly every coelurosaur that can be scored in the affirmative. A few exceptions are scored for state 0, which refers to an antorbital fossa that is so extensive that it approaches the posterodorsal corner of the lacrimal, and is separated from breaching this

corner by only a very thin strut of bone. This morphology is seen in the basal coelurosaurs *Tanycolagreus* (TPII 2000-09-29) and *Zuolong* (Choiniere et al. 2010b), as well as oviraptorosaurs (e.g., *Citipati* and *Oviraptor*: Clark et al. 1999; *Incisivosaurus*: Xu et al. 2002a, Balanoff et al. 2009). States 0 and 1 are illustrated in Figure 2.8.

839. Scapula and coracoid, deep fossa on lateral surfaces of both bones in the region of their suture (covering the posterior half of the coracoid and anterior portion of the acromion plate region of the scapula): present (0); absent (1).

The closest outgroups of coelurosaurs exhibit a deep fossa that covers much of the lateral surfaces of the scapula and coracoid in the region where they meet (e.g., Madsen 1976; Currie and Zhao 1993). This fossa covers the posterior half of the coracoid and the anterior portion of the acromion plate region of the scapula, including some of the lateral surface of the acromion itself. The fossa, which is scored as state 0 here, is also seen in several coelurosaurs, including the basal coelurosaurs *Coelurus* (YPM 2001) and *Tanycolagreus* (TPII 2000-09-29), basal alvarezsauroids (e.g., *Haplocheirus*: IVPP V15988; *Alvarezsaurus*: Bonaparte 1991), therizinosauroids (e.g., *Falcarius*: Zanno 2006; *Neimongosaurus*: Zhang et al. 2001; *Suzhousaurus*: Li et al. 2007), and troodontids (e.g., *Sinornithoides*: Currie and Dong 2001b). Several coelurosaurs, however, lack a fossa (state 1). These taxa include all tyrannosauroids that can be scored affirmatively (e.g., *Dilong*: IVPP V14243; *Eotyrannus*: MIWG 1997.550; *Tyrannosaurus*: Brochu 2003), ornithomimosaurs (e.g., *Beishanlong*: Makovicky et al. 2010; *Sinornithomimus*: Kobayashi and Lü 2003; *Struthiomimus*: Nicholls and Russell 1985), derived alvarezsauroids (e.g., *Patagonykus*: Novas 1997; *Mononykus*: Perle et al. 1994), and dromaeosaurids (e.g., *Microraptor*: Hwang et al. 2002; *Rahonavis*: Forster et al. 1998;

Velociraptor: Norell and Makovicky 1999). Some of these taxa possess a subtle fossa covering much of the coracoid-scapula suture and adjacent regions, but this is not as deep, discrete, and extensive as the condition scored as state 0. States 0 and 1 are illustrated in Figure 2.29.

840. Scapula and coracoid, contribution of each bone to the glenoid: both bones contribute approximately equally in the anteroposterior dimension (0); scapula contribution markedly anteroposteriorly longer than coracoid contribution (1); coracoid contribution markedly anteroposteriorly longer than scapula contribution (2).

The relative contributions of the coracoid and scapula to the glenoid are variable among coelurosaurs, and this unordered multistate distinguishes three discrete conditions. These are not considered to represent an ordered sequence because there is no clear set of nested hierarchies or a numerical sequence between them. Each condition refers to the proportion of the total anteroposterior length of the glenoid, as measured in lateral or ventral views, that is formed by the scapula and coracoid. The three character states are illustrated in Figure 2.29.

State 0 refers to the condition in which the coracoid and scapula contribute essentially equally to the glenoid (i.e., the anteroposterior lengths of the portions of the glenoid formed by the coracoid and scapula are essentially equal). This state is seen in the outgroup *Allosaurus* (Madsen 1976), the compsognathid *Compsognathus* (Peyer 2006), ornithomimosaurs (e.g., *Gallimimus*: Osmólska et al. 1972, ZPAL MgD-I/2; *Struthiomimus*: Nicholls and Russell 1985), alvarezsauroids (e.g., *Bonapartenykus*: Agnolin et al. 2012; *Mononykus*: Perle et al. 1994), and some dromaeosaurids (e.g., *Balaur*: Csiki et al. 2010; *Deinonychus*: Ostrom 1969; *Sinornithosaurus*: Xu and Wu 2001; *Velociraptor*: Norell and Makovicky 1999).

State 1 refers to the condition in which the scapular contribution to the glenoid is markedly longer anteroposteriorly than the coracoid contribution. This is present in most tyrannosauroids (e.g., *Guanlong*: IVPP V14532; *Tyrannosaurus*: Brochu 2003), the basal coelurosaur *Tanycolagreus* (TPII 2000-09-29; Carpenter et al. 2005a), therizinosauroids (e.g., *Falcarius*: Zanno 2006; *Suzhosaurus*: Li et al. 2007), troodontids (e.g., *Sinornithoides*: Currie and Dong 2001b), and some dromaeosaurids (e.g., *Buitreraptor*: MPCA 245; *Rahonavis*: Forster et al. 1998; *Unenlagia*: Novas and Puerta 1997). It is also inferred to be present in *Microvenator* even though the scapula is unknown for this taxon, because of the very small glenoid surface present on the coracoid (Makovicky and Sues 1998).

Finally, state 2 refers to the condition in which the coracoid contribution is much longer anteroposteriorly than the scapular contribution. This is currently known in only a single coelurosaur: the basal tyrannosauroid *Dilong* (Xu et al. 2004; IVPP V14243). Although currently an autapomorphy of *Dilong*, it is included in the dataset in anticipation of future taxa being discovered with this feature.

841. Femur, shape of anterior margin in proximal view: strongly convex, due to a midline tubercle (0); essentially straight or slightly concave (1).

When seen in proximal view, the anterior margin of the femur is broadly convex in the coelurosaurian outgroups *Allosaurus* (Madsen 1976) and *Sinraptor* (Currie and Zhao 1993), due to a midline tubercle that projects anteriorly. This morphology is also seen in some basal coelurosaurs, including *Guanlong* (IVPP V14531), *Tanycolagreus* (TPII 2000-09-29), *Tugulusaurus* (IVPP V4025), and *Zuolong* (Choiniere et al. 2010b). It is also present in ornithomimosaurs, including *Archaeornithomimus* (Smith and Galton 1990), *Garudimimus*

(Kobayashi and Barsbold 2005a), *Gallimimus* (ZPAL MgD-I/94), *Harpymimus* (Kobayashi and Barsbold 2005b), and *Sinornithomimus* (Kobayashi and Lü 2003). In contrast, the anterior margin of the femur is essentially straight in anterior view in many other coelurosaurs, due in part to the absence of the discrete anterior tuber. These taxa include derived tyrannosauroids (e.g., *Alioramus*: Brusatte et al. 2012a; *Gorgosaurus*: Lambe 1917; *Tarbosaurus*: ZPAL MgD-I/09; *Tyrannosaurus*: Brochu 2003), the basal coelurosaur *Coelurus* (YPM 2010), alvarezsauroids (e.g., *Mononykus*: Perle et al. 1994; *Xixianykus*: Xu et al. 2010), therizinosauroids (e.g., *Falcarius*: Zanno 2010a; *Suzhousaurus*: Li et al. 2008), and dromaeosaurids (e.g. *Mahakala*: Turner et al. 2011; *Unenlagia*: MCF 045; *Velociraptor*: Norell and Makovicky 1999). States 0 and 1 are illustrated in Figure 2.41.

842. Femur, horizontal ridge on the anterior surface of the head and neck, demarcating a deep fossa ventrally: absent (0); present (1).

The basal coelurosaurs *Coelurus* (YPM 2010) and *Tanycolagreus* (TPII 2000-09-29) share a distinctive feature on the anterior surface of the head of the femur. In these two taxa there is a pronounced horizontal ridge on the ventral portion of the head, which begins medially at approximately the medioventral corner of the head and then continues laterally across most of the lateral surface of the head as a straight structure. Beneath this ridge is a deep ventral fossa. The associated ridge and fossa are unknown in other coelurosaurs or close outgroups (e.g., *Allosaurus*: Madsen 1976). States 0 and 1 are illustrated in Figures 2.37 and 2.38.

843. Femur, extent of crista tibiofibularis in distal view: projects further posteriorly than medial condyle (0); extends to the same approximate posterior level as medial condyle (1); terminates

well short of the posterior level of the medial condyle (medial condyle projects substantially further posteriorly) (2).

The crista tibiofibularis is a large crest or tubercle of bone that continues posteriorly from the posterior surface of the lateral distal condyle of the femur. It demarcates the lateral extent of the flexor groove on the posterior surface of the femur and is especially visible in distal view, where it appears as a discrete structure affixed to the posterior side of the lateral condyle. The posterior extent of the crista relative to the medial condyle is variable among coelurosaurs and outgroups, and this ordered character describes a nested series of homologies (projects further-projects to same level-stops short). The three character states are illustrated in Figure 2.40.

State 0 refers to a crista tibiofibularis that projects further posteriorly than the medial condyle when the femur is seen in distal view. This condition is present in the outgroups *Allosaurus* (Madsen 1976) and *Sinraptor* (Currie and Zhao 1993), the basal coelurosaurs *Tugulusaurus* (IVPP V4025) and *Zuolong* (Choiniere et al. 2010b), most ornithomimosaurs (e.g., *Archaeornithomimus*: Smith and Galton 1990; *Gallimimus*: ZPAL MgD-I/94; *Sinornithomimus*: Kobayashi and Lü 2003), alvarezsauroids (e.g., *Patagonykus*: Novas 1997; *Mononykus*: Perle et al. 1994), and dromaeosaurids (e.g., *Buitreraptor*: MPCA 245; *Unenlagia*: MCF 045; *Velociraptor*: Norell and Makovicky 1999).

State 1 refers to a crista tibiofibularis that projects to approximately the same posterior level as the medial condyle. This morphology is seen in several tyrannosauroids, including *Guanlong* (IVPP V14531), *Juratyrant* (Benson 2008), *Xiongguanlong* (FRDC-GS JB16-2-1), *Alioramus* (Brusatte et al. 2012a), *Tarbosaurus* (ZPAL MgD-I/09), and *Tyrannosaurus* (Brochu 2003). It is also present in the ornithomimosaur *Garudimimus* (Kobayashi and Barsbold 2005a) and the basal therizinosauroid *Falcarius* (Zanno 2010a).

State 2 refers to a crista tibiofibularis that terminates well short of the posterior edge of the medial condyle. In other words, those taxa that are scored for state 2 possess a crista that is much less extensive posteriorly than the medial condyle. This is a highly unusual condition and is only currently known in the basal coelurosaurs *Coelurus* (YPM 2010) and *Tanycolagreus* (TPII 2000-09-29), as well as the single therizinosauroid *Suzhousaurus* (Li et al. 2008). Because very few therizinosauroids can be assessed for this character it is possible that state 2 may be more widely present among these aberrant theropods.

844. Tibia, position of medial ridge on posterior surface of distal end: displaced laterally, positioned lateral to the medial edge of the distal tibia by approximately 25-33% of the mediolateral width of the distal tibia (0); positioned lateral to the medial edge of the distal tibia approximately 10-20% of the mediolateral width of the distal tibia (1); positioned medially, positioned at approximately the posteromedial corner of the distal tibia in distal view (2).

The posterior surface of the distal tibia in most theropods is marked by a ridge, which is clearly visible in distal view. The presence of this ridge gives the distal tibia a triangular shape when seen in distal view, with the ridge representin the shortest apex of the triangle. The ridge is always located medial to the midpoint of the tibia, but its precise position varies among taxa. This character is an ordered multistate distinguishing three discrete conditions that together describe a hierarchial sequence of homologies (lateral-somewhat lateral-far medial). This character is scored by identifying the position of the ridge, calculating the distance between the medial edge of the tibia and the ridge, and then comparing this distance to the overall mediolateral width of the distal tibia in distal view. The three character states are illustrated in Figure 2.42.

State 0 refers to the condition in which the ridge is positioned at a distance from the medial edge of the tibia that is 25-35% of the total mediolateral width of the tibia. This is the state in which the ridge is most laterally positioned among taxa (states 1 and 2 refer to ridges that are located progressively further medially). State 0 is present in the outgroups *Allosaurus* (Madsen 1976) and *Sinraptor* (Currie and Zhao 1993) but is not currently scored in any coelurosaurian ingroup taxa.

State 1 refers to the condition in which the ridge is positioned at a distance from the medial edge of the tibia that is approximately 10-20% of the total mediolateral width of the tibia. This state is seen in the basal coelurosaur *Tugulusaurus* (IVPP V4025), tyrannosauroids (e.g., *Juratyrant*: OUMNH J.3311; *Dryptosaurus*: Brusatte et al. 2011; *Tyrannosaurus*: Brochu 2003), ornithomimosaurs (e.g., *Garudimimus*: Kobayashi and Barsbold 2005a; *Qiupalong*: L. Xu et al. 2011), therizinosauroids (e.g., *Falcarius*: Zanno 2010a; *Neimongosaurus*: Zhang et al. 2001), troodontids (e.g., *Zanabazar*: Norell et al. 2009), and some dromaeosaurids (e.g., *Austroraptor*: MML 195; *Neuquenraptor*: MCF PVPH 77).

State 2 refers to a ridge that is placed at nearly the posteromedial corner of the distal tibia in distal view. In other words, the ridge is basically aligned with the medial edge of the bone. This unusual morphology is present in the basal coelurosaurs *Coelurus* (YPM 2010) and *Tanycolagreus* (TPII 2000-09-29) and some dromaeosaurids (e.g., *Balaur*: EME PV.313; *Deinonychus*: Ostrom 1969; *Velociraptor*: Norell and Makovicky 1999).

845. Scapula, fossa on lateral surface of bone immediately above glenoid, which is demarcated dorsally by a convex bulge or ridge spanning the scapula-coracoid suture: absent (0); present (1).

The basal coelurosaurs *Coelurus* (YPM 2010) and *Tanycolagreus* (TPII 2000-09-29) share a distinctive feature on the lateral surface of the scapula. In these two taxa there is a deep fossa on the lateral scapula immediately above the glenoid, which is bordered dorsally by a convex ridge or bulge that crosses the scapula-coracoid suture. The associated ridge and fossa are unknown in other coelurosaurs or close outgroups (e.g., *Allosaurus*: Madsen 1976). States 0 and 1 are illustrated in Figure 2.29.

846. Humerus, deltopectoral crest, orientation relative to mediolateral long axis of proximal end of humerus in proximal view:straight, approximately perpendicular to long axis of proximal end of humerus (0); curves strongly medially as it continues anteriorly, such that anterior end of crest is oblique to long axis of proximal end of humerus (1).

In most coelurosaurs the deltopectoral crest projects anteriorly from the anterolateral corner of the humerus, forming a perpendicular angle with the long axis of the proximal end of the bone. This is not true of some taxa, which possess a deltopectoral crest that projects laterally and is thus in line with the long axis of the head, as is scored in character 358. Among those taxa that possess the more standard anteriorly projecting crest, two conditions are present. In most taxa the crest maintains a relatively straight orientation as ir extends anteriorly. This is seen in the outgroup *Allosaurus* (Madsen 1976) and most coelurosaurs that can be scored affirmatively for this character. In contrast, a small subset of taxa possess a crest tha curves strongly medially as it continues anteriorly, such that the anterior end of the crest is oriented obliquely relative to the long axis of the head. This morphology is seen in *Coelurus* (YPM 2010), *Guanlong* (IVPP V14531), *Eotyrannus* (MIWG 1997.550), and tyrannosaurids (e.g., *Tyrannosaurus*: Brochu 2003). States 0 and 1 are illustrated in Figure 2.30.

847. Femur, position of fourth trochanter: along posteromedial corner of shaft along its entire length (0); positioned near center of posterior surface of shaft distally and extending proximomedially to become confluent with posteromedial corner of shaft proximally (1); positioned near center of posterior surface of shaft distally and extending proximolaterally to bcome confluent with the greater trochanter (2).

In most theropods the fourth trochanter is a proximodistally elongate ridge positioned along the posteromedial corner of the shaft across its entire length. A fourth trochanter of this morphology is therefore widely visible in both posterior and medial views. This condition, codified as state 0, is seen in the outgroups *Allosaurus* (Madsen 1976) and *Sinraptor* (Currie and Zhao 1993), as well as most coelurosaurian ingroups. Two modified conditions are present in a small sample of coelurosaurs. State 1 refers to a fourth trochanter that is placed at the center of the posterior surface of the shaft at its distal end but angles proximomedially as it extends proximally, ultimately terminating proximally along the posteromedial surface of the shaft. This morphology is present in the basal coelurosaurs *Coelurus* (YPM 2010), *Tanycolagreus* (TPII 2000-09-29), *Tugulusaurus* (IVPP V4025; Rauhut and Xu 2005), and *Zuolong* (Choiniere et al. 2010b). Therizinosauroids possess another distinctive condition, referred to as state 2, in which the fourth trochanter is positioned near the center of the posterior surface of the shaft distally and then extends proximolaterally to become confluent with the greater trochanter at its proximal end (e.g., *Falcarius*: Zanno 2010a; *Suzhousaurus*: Li et al. 2008). Because there is no clear sequence of nested homologies, this multistate character is considered unordered. The three states are illustrated in Figure 2.39.

848. Fibula, anteroposterior width of the minimum point of the midshaft compared to the maximum anteroposterior width of the proximal end: 20% or greater (0); less than 18%, fibula shaft exceptionally gracile (1).

State 0, denoting a fibular shaft that is relatively robust compared to the proximal end, is present in the outgroups *Allosaurus* (Madsen 1976) and *Sinraptor* (Currie and Zhao 1993), all tyrannosauroids that can be scored affirmatively (e.g., *Guanlong*: IVPP V14531; *Dilong*: IVPP V14243; *Dryptosaurus*: Brusatte et al. 2011; *Appalachiosaurus*: Carr et al. 2005; *Albertosaurus*: Parks 1928; *Gorgosaurus*: Lambe 1917; *Tarbosaurus*: Maleev 1974, ZPAL MgD-I/188: *Tyrannosaurus*: Brochu 2003), ornithomimosaurs (e.g., *Beishanlong*: Makovicky et al. 2010; *Garudimimus*: Kobayashi and Barsbold 2005a), and the basal alvarezsauroid *Haplocheirus* (Choiniere et al. 2010a; IVPP V15988). A reduced fibular shaft, which at (or near) midshaft has an anteroposterior width that is less than 18% of the anteroposterior width of the proximal end, is present in several other coelurosaurs. This condition is seen in the basal coelurosaurs *Coelurus* (YPM 2010) and *Tanycolagreus* (TPII 2000-09-29; Carpenter et al. 2005a), derived alvarezsauroids (e.g., *Shuvuuia*: Chiappe et al. 1996; *Xixianykus*: Xu et al. 2010), therizinosauroids (e.g., *Erliansaurus*: Xu et al. 2002b; *Nothronychus*: Zanno et al. 2009), oviraptorosaurs (e.g., *Caudipteryx*: Ji et al. 1998; *Citipati*: Clark et al. 1999; *Microvenator*: Makovicky and Sues 1998), and dromaeosaurids (e.g., *Balaur*: Csiki et al. 2010; *Buitreraptor*: MPCA 245; *Deinonychus*: Ostrom 1969; *Mahakala*: Turner et al. 2011; *Microraptor*: Hwang et al. 2002). States 0 and 1 are illustrated in Figure 2.43.

849. Maxillary teeth, posterior (distal) extent of tooth row: extensive, extends posterior to the level of the maxillary ascending ramus and underneath the antorbital fenestra (if present) (0); limited, terminates posteriorly at the level of the maxillary ascending ramus (1).

This character was described by Choiniere et al. (2012). They noted that the basal ornithomimosaurs *Nqwebasaurus* (Choiniere et al. 2012) and *Pelecanimimus* (Perez-Moreno et al. 1994; LH 7777) and the derived alvarezsauroid *Shuvuuia* (Chiappe et al. 1998) are unsual among coelurosaurs, close outgroups, and theropods in general because their maxillary tooth row is restricted to the anterior end of the bone. In these taxa the tooth row terminates at approximately the level of the maxillary ascending ramus, whereas in all other theropods with teeth the maxillary tooth row is more posteriorly extensive and it terminates far behind the ascending ramus and underneath the antorbital fenestra. The basal alvarezsauroid *Haplocheirus* possesses the normal theropod condition (Choiniere et al. 2010a) and no other alvarezsauroids can be scored in the affirmative, so it is unclear if this character state is a synapomorphy of alvarezsauroids and ornithomimosaurs that may be reversed in *Haplocheirus*. All ornithomimosaurs other than *Nqwebasaurus* and *Pelecanimimus* lack maxillary teeth so this character must be scored as inapplicable in these taxa. The character states are not illustrated here but are figured in Choiniere et al. (2012).

850. Dentary, shape of ventral margin in lateral view: approximately straight or slightly convex (0); broadly concave (1).

In most theropods the ventral margin of the dentary is approximately straight or ever so slightly convex in lateral view. This is the case in the coelurosaurian outgroups *Allosaurus* (Madsen 1976) and *Sinraptor* (Currie and Zhao 1993), as well as most coelurosaurs that can be

scored affirmatively. In contrast, the ventral margin of the dentary is broadly concave in some coelurosaurs, including *Ornitholestes* (AMNH FARB 619), ornithomimosaurs (e.g., *Garudimimus*: Kobayashi and Barsbold 2005a; *Gallimimus*: Osmólska et al. 1972; *Pelecanimimus*: LH 7777), all therizinosauroids more derived than *Falcarius* (e.g., *Beipiaosaurus*: Xu et al. 1999; *Alxasaurus*: Russell and Dong 1993; *Erlikosaurus*: Clark et al. 1994), and the oviraptorosaur *Caudipteryx* (Ji et al. 1998). Several taxa with states 0 are illustrated in Figure 2.17 along with one taxon with state 1, whereas other taxa with state 1 are well illustrated in the literature (e.g., Kobayashi and Barsbold 2005a: figures 2-3).

851. Maxilla, posterior extent of the ascending ramus relative to that of the main body (jugal ramus): the two rami extend to approximately the same level posteriorly, distance between posterior tip of ascending ramus and posterior tip of main body no more than 1/3 of the anteroposterior length of the entire maxilla (0); main body extends considerably further posteriorly relative to the ascending ramus, distance between the posterior tips of the two rami is greater than 1/3 of the length of the maxilla (1).

This character was described by Choiniere et al. (2012). They noted that the basal ornithomimosaurs *Nqwebasaurus* (Choiniere et al. 2012), *Pelecanimimus* (Perez-Moreno et al. 1994; LH 7777), and *Garudimimus* (Kobayashi and Barsbold 2005a), as well as the derived alvarezsauroid *Shuvuuia* (Chiappe et al. 1998), are unsual among coelurosaurs in possessing an ascending ramus of the maxilla that terminates far anteriorly relative to the posterior edge of the main body (the tooth-bearing region of the bone in those taxa with teeth). In these four taxa the distance between the posterior ends of the ascending ramus and the main body is greater than one third of the anteroposterior length of the entire maxilla. All other coelurosaurs and close

outgroups that can be scored affirmatively possess an ascending ramus that extends to the same approximate level posteriorly as the main body. The main body often extends slightly further posteriorly, but the distance between the posterior ends of the two processes never approaches 33% of the length of the maxilla. The character states are not illustrated here but are figured in Choiniere et al. (2012).

852. Tibia, proximal surface, proximal extent of cnemial crest relative to the proximal extent of the posterior condyles: cnemial crest extends further proximally than condyles (0); cnemial crest and condyles extend to same approximate level proximally (1).

Variation in the proximal extent of the cnemial crest of the tibia relative to the posterior condyles of the proximal region of the tibia was described by Choiniere et al. (2010b). In the coelurosaurian outgroups *Allosaurus* (Madsen 1976) and *Sinraptor* (Currie and Zhao 1993) the proximal surface of the cnemial crest extends further proximally than the proximal surface of the posterior condyles. This can be clearly observed when the tibia is seen in lateral or medial views, and in these views there is a noticeable step between the higher cnemial crest and the more distally placed proximal condyles. This condition, codified as state 0, is also present in some derived tyrannosauroids, including *Albertosaurus* (Parks 1928), *Gorgosaurus* (Lambe 1917), *Dryptosaurus* (Brusatte et al. 2011; *Tarbosaurus* (Maleev 1974; ZPAL MgD-I/188). All other coelurosaurs for which this character can be scored affirmatively, including basal tyrannosauroids such as *Guanlong* (IVPP V14531) and *Eotyrannus* (MIWG 1997.550) and basal coelurosaurs such as *Tugulusaurus* (Rauhut and Xu 2005) and *Zuolong* (Choiniere et al. 2010b), exhibit a cnemial crest that extends to the same approximate level proximally as the posterior

condyles. In these taxa, therefore, there is no noticeable step between the crest and condyles when the tibia is seen in lateral or medial views. States 0 and 1 are illustrated in Figure 2.42

853. Prootic, prominent fossa on the lateral surface of the bone, anterior to the otic recess and posterior to the preotic pendant, that houses the external foramina of the trigeminal and facial nerves and pneumatic openings: absent (0); present (1).

The lateral surface of the prootic of several tyrannosauroids exhibits an unusual morphology, as explained by Bever et al. (in press) and described in well-preserved specimens by Witmer and Ridgely (2009, 2010), Tsuihiji et al. (2011), and Bever et al. (2011). In these taxa there is a deep and prominent fossa on the lateral surface of the prootic, anterior to the otic recess and posterior to the preotic pendant. Within this fossa are several foramina, including the entrances for the trigeminal and facial nerves and a number of pneumatopores. This so-called "prootic fossa" (terminology of Bever et al. in press) is seen in *Albertosaurus* (CMN 5600), *Bistahieversor* (NMMNH P-27469), *Daspletosaurus* (CMN 8506), *Gorgosaurus* (ROM 1247), *Tarbosaurus* (ZPAL MgD-I/4), *Teratophoneus* (BYU 8120/9396), and *Tyrannosaurus* (AMNH FARB 5117). Unfortunately, its presence or absence cannot currently be assessed in *Dilong* (IVPP V14243) because the lateral surface of the prootic is concealed by other bones, or in *Guanlong* (IVPP V14531) because of poor preservation of the holotype. The fossa is clearly absent in the basal coelurosaur *Ornitholestes* (AMNH FARB 619), ornithomimosaurs (e.g., *Struthiomimus*: Makovicky and Norell 1998), alvarezsauroids (e.g., *Shuvuuia*: Chiappe et al. 1998), therizinosauroids (e.g., *Falcarius*: Smith et al. 2011; *Erlikosaurus*: Clark et al. 1994), oviraptorosaurs (e.g., *Citipati*: Clark et al. 2002b; *Incisivosaurus*: Balanoff et al. 2009), troodontids (e.g., *Byronosaurus*: Makovicky et al. 2003), and dromaeosaurids (e.g., *Tsaagan*:

Norell et al. 2006). State 1 is shown in Figure 2.13 and is figured in full in Bever et al. (2011, in press).

CLADISTIC ANALYSIS: METHODOLOGICAL PROTOCOLS

The full dataset of 853 characters scored in 150 taxa was analyzed with equally weighted parsimony in the phylogenetic program TNT v. 1.1 (Goloboff et al. 2008). Following previous TWiG protocol, the outgroup *Allosaurus* was used to root the tree because it the best known, most extensively studied, and best described of the two outgroup taxa. Because of the large size of the dataset a heuristic search strategy was necessary. As a first step the data matrix was analyzed under the "New Technology" search options, using sectorial search, ratchet, tree drift, and tree fuse options with default parameters. The minimum length tree was found in 10 replicates, a procedure that aims to initially sample as many tree islands as possible. The generated trees were then analyzed under traditional TBR branch swapping, a procedure that aims to more fully explore each tree island. Zero-length branches were collapsed following Rule 1 of Coddington and Scharff (1994).

CLADISTIC ANALYSIS: RESULTS

Most Parsimonious Topologies: The initial New Technology search recovered 73 most parsimonious trees (MPTs) of 3352 steps (consistency index=0.323; retention index=0.776). Additional TBR branch swapping on these 73 trees resulted in 99999 total MPTs. 99999 trees is the memory limit in the utilized version of TNT, so it is likely that several other MPTs are left

unrecovered, which is always the reality under a heuristic search. To further check the results, therefore, several additional searches using identical protocols were run, as was a different type of heuristic search using the protocol outlined in Turner et al. (2012), in which 1000 replicates of Wagner trees are followed by TBR branch swapping. All of these analyses returned an identical strict consensus of recovered MPTs, suggesting that this consensus topology is more-or-less representative of the full range of most parsimonious trees.

Tree Summary: The 99999 individual most parsimonious trees were combined into a strict consensus topology (figure 2.45). Portions of the strict consensus are highly resolved and the monophyly of several major coelurosaurian subgroups is corroborated (e.g., Tyrannosauroidea, Compsognathidae, Alvarezsauroidea, Therizinosauroidea, Troodontidae). The ingroup relationships of some of these clades are also well resolved. However, several portions of this consensus phylogeny are unresolved. Perhaps surprisingly, Ornithomimosauria is not found to be monophyletic and there is a large polytomy at the base of the clade that includes all coelurosaurs more derived (closer to avialans) than tyrannosauroids. This lack of resolution is due to the uncertain phylogenetic position of a small handful of taxa, including the fragmentary basal coelurosaur *Kinnareemimus* (a purported ornithomimosaur: Buffetaut et al. 2009), the aberrant coelurosaur *Epidendrosaurus* (which is known only from two juvenile individuals: Zhang et al. 2002), the paravians *Pyroraptor* and *Hesperonychus*, and the avialan *Limenavis*. *Pyroraptor* and *Limenavis* were also found to be unstable in the analysis of Turner et al. (2012), whereas *Epidendrosaurus* was excluded from the primary version of that analysis. The “wildcard” nature of these five taxa is largely due to enormous amounts of missing data—each taxon can only be scored for a small fraction of the 853 characters in the analysis.

In order to ameliorate the effects of these fragmentary wildcard taxa, a reduced strict consensus topology was created based on the 99999 most parsimonious trees. This procedure uses the original MPTs as source trees but simply excludes these five taxa when calculating the strict consensus. This is preferred to excluding these taxa from the analysis a priori, as it allows the taxa (and their character scores) to contribute information to the analysis and prevents the somewhat subjective decision of discarding taxa that seem too fragmentary from the outset. The reduced strict consensus topology is shown in Figures 2.46-2.47 and is used here as the preferred phylogeny and basis for character optimization and discussion of coelurosaurian phylogeny and evolution. This topology is considerably more resolved than the strict consensus, and recovers a monophyletic Ornithomimosauria and better resolution among basal coelurosaurs and paravians.

Clade Support Values: The degree of support for individual clades was assessed in two ways. First, Bremer support values were calculated. These values, sometimes referred to as decay indices, denote the number of extra steps required for the clade to fall apart in the strict consensus of less optimal topologies. In the current case, a Bremer support value of 1 indicates that the clade in question is not recovered in the strict consensus of all trees of length 3353 or less (i.e., one step longer than the MPT length of 3352). Second, jackknife percentages were calculated. The jackknife is a resampling technique, in which the phylogeny is systematically reanalyzed as characters are randomly deleted. The jackknife percentage of each clade indicates the percent of trees recovered in the jackknife analysis that includes the clade in question. Both Bremer supports and jackknife percentages were calculated in TNT using standard scripts. The jackknife was run using the default parameter of 36% character removal probability and 1000 replicates.

Salient Phylogenetic Results and Discussion: All of the major coelurosaurian subgroups that have long been considered monophyletic are also found to be monophyletic here. These include Tyrannosauroidea, Compsognathidae, Ornithomimosauria, Alvarezsauroidea, Therizinosauroidea, Oviraptorosauria, Dromaeosauridae, Troodontidae, and Avialae. Relationships within these clades are relatively well resolved in most cases. The exceptions include: Compsognathidae, whose ingroup relationships are completely unresolved; Ornithomimosauria, in which several intermediate taxa such as *Harpymimus* and *Garudimimus* fall into a polytomy; and Therizinosauroidea, in which the basal relationships are well resolved but numerous more derived taxa fall into a polytomy. Corroborating recent studies, *Haplocheirus* is found to be the basal-most alvarezsauroid (Choiniere et al. 2010a), *Nqwebasaurus* is recovered as a basal ornithomimosaur (Choiniere et al. 2012), *Xiaotingia* and *Anchiornis* are recovered as basal troodontids (Turner et al. 2012), *Mahakala* is a basal dromaeosaurid (Turner et al. 2007a, 2012), and *Archaeopteyx* is the basal-most availan (as traditionally found, contra Xu et al. 2011a). These results indicate that the phylogenetic positions of these taxa are robust to the inclusion of a large amount of new data relevant to basal coelurosaurs.

Among basal coelurosaurs, *Bicentenaria* is found to be the basal-most coelurosaurian taxon. Its position at the base of the clade is well supported: the clade of all other coelurosaurs is recovered in 67% of jackknife replicates and has a Bremer support value of 2. This is largely concordant with the phylogenetic analysis of Novas et al. (2012), which recovered *Tugulusaurus* as the most basal coelurosaur, followed by *Bicentenaria*. Here, *Tugulusaurus* and *Zuolong* are recovered in a slightly more derived position (i.e., they are more closely related to avialans than

is *Bicentenaria*). *Tugulusaurus* and *Zuolong* comprise a polytomy with two other groups: Tyrannosauroidea and the clade of all other coelurosaurs.

The small-bodied basal coelurosaurs *Guanlong*, *Dilong*, and *Proceratosaurus* are members of the clade Tyrannosauroidea, defined as all taxa more closely related to *Tyrannosaurus* than to *Ornithomimus*, *Velociraptor*, and *Troodon* (Sereno et al. 2005). This corroborates previous arguments in favor of the tyrannosauroid affinities of these taxa, which were largely based on shared, derived characters but were often not tested with large-scale phylogenetic analyses that included a broad array of basal coelurosaurs (e.g., Xu et al. 2004, 2006; Brusatte et al. 2010a). More recent analyses with increased basal coelurosaur taxon and character sampling have found some or all of *Guanlong*, *Dilong*, and *Proceratosaurus* to group with tyrannosauroids (e.g., Senter 2007, 2010, 2011; Zanno et al. 2009; Choiniere et al. 2010a, 2010b; Li et al. 2010; Rauhut et al. 2010; Dal Sasso and Maganuco 2011), but the Turner et al. (2012) phylogeny found *Dilong* and *Proceratosaurus* to be closer to avialans than to taxa such as *Eotyrannus* and *Tyrannosaurus*, and therefore not part of the tyrannosauroid clade. Here, the clade consisting of *Guanlong*, *Dilong*, *Proceratosaurus*, and traditionally recognized tyrannosauroids is strongly supported by a jackknife percentage of 81% and a Bremer support of 2.

Furthermore, *Coelurus* and *Tanycolagreus* form a sister taxon pair at the base of the tyrannosauroid lineage. This result was also recovered by Senter (2007, 2010, 2011), Dal Sasso and Maganuco (2011), and Novas et al. (2012), whereas *Coelurus* occupies a range of other positions in other phylogenetic analyses (see below). *Tanycolagreus* has been included in only a few phylogenetic analyses; it groups with *Coelurus* as a basal tyrannosauroid in the studies of Senter (2007, 2010, 2011) and Novas et al. (2012) but is placed elsewhere in other studies

(Choiniere et al. 2010b; Li et al. 2010; Rauhut et al. 2010) (see below). In the current analysis the sister taxon grouping of *Coelurus* and *Tanycolagreus* is well supported, as it is characterized by a jackknife percentage of 72% and a Bremer support of 2. The tyrannosauroid placement of these two genera is less supported, however, as the clade Tyrannosauroidea (*Coelurus*, *Tanycolagreus*, and all other tyrannosauroids) is characterized by a jackknife percentage of less than 50% and a Bremer value of 2).

Relationships within Tyrannosauroidea are well resolved and largely follow those reported by Brusatte et al. (2010a) in their tyrannosauroid-specific phylogenetic analysis. This is not surprising considering that the Brusatte et al. (2010a) character set has been integrated into the present analysis. The current study, however, reports slightly less resolution than the Brusatte et al. (2010a) analysis, which had recovered a single most parsimonious tree. Here *Proceratosaurus*, *Sinotyrannus*, and *Guanlong* fall into a polytomy within Proceratosauridae. Furthermore, Proceratosauridae, *Dilong*, and the *Eotyrannus* + Tyrannosauridae clade also fall into a polytomy, and *Eotyrannus* and *Juratyrant* are in a polytomy at the base of the *Eotyrannus* + Tyrannosauridae clade. Many tyrannosauroid ingroup clades are well supported by high jackknife and Bremer support values.

All other coelurosaurs form a clade exclusive of *Bicentenaria*, *Tugulusaurus*, *Zuolong*, and tyrannosauroids. This clade—Maniraptoriformes—is only poorly supported (Bremer support of 1 and jackknife percentage of less than 50%), and relationships at is base are unresolved. There is a basal polytomy consisting of four clades: *Ornitholestes*, Compsognathidae, Ornithomimosauria, and Maniraptora (i.e., the clade of all taxa more closely related to birds than to *Ornithomimus*: Sereno et al. 2005).

Maniraptora—the clade defined as all taxa closer to birds than to *Ornithomimus*—is comprised in the present study of Alvarezsauroidea, Therizinosauroidea, Oviraptorosauria, and Paraves. This clade is supported by a Bremer value of 2 but a jackknife percentage of less than 50%.

The clade consisting of Oviraptorosauria and Paraves is supported by a Bremer value of 2 and a jackknife percentage of less than 50%. Paraves—consisting of dromaeosaurids, troodontids, and avialans—is even more poorly supported, as it has a Bremer value of 1 and a jackknife of less than 50%.

One intriguing result of the present analysis is that *Epidexipteryx* and *Pedopenna*, which together comprise a sister taxon group usually referred to as Scansoriopterygidae, are placed as the basal-most lineage of oviraptorosaurs. This result occurs in the reduced strict consensus after *Epidendrosaurus*, which is also usually placed in Scansoriopterygidae, is excluded a posteriori because of its status as a wildcard taxon. Scansoriopterygids are usually considered very basal avialans, possibly the basal-most members of the group (i.e., more basal than *Archaeopteryx*). This result is recovered, for example, by Senter (2007, 2010, 2011), Zhang et al. (2008), Choiniere et al. (2010a, 2012), Xu et al. (2011a), and Novas et al. (2012). Turner et al. (2012) reported a different result in which *Epidexipteryx* is placed as the immediate outgroup of the clade consisting of dromaeosaurids, troodontids, and paravians, but also discussed how a grouping of *Epidexipeteryx* and oviraptorosaurs is only slightly less parsimonious. As far as can be discerned, the placement of scansoriopterygids as basal oviraptorosaurs is recovered here in a most parsimonious topology for the first time. Characters supporting this grouping, which are discussed below, largely relate to features of the short and deep skull shared by scansoriopterygids and oviraptorosaurs. It must be stated, however, that the scansoriopterygid +

oviraptorosaur clade is poorly supported (Bremer support of 1, jackknife percentage of less than 50%).

The Status of *Juravenator*: As mentioned above, *Juravenator* was retained in the phylogenetic analysis even though its holotype and only known specimen is a very young individual. To assess any possible bias this may cause, *Juravenator* was excluded from the strict consensus tree construction a posteriori. Other than the omission of *Juravenator*, the resulting reduced strict consensus is identical to the reduced strict consensus that includes *Juravenator*. This exercise indicates that the phylogeny of Coelurosauria is robust to the inclusion or exclusion of *Juravenator* and that the monophyly and placement of Compsognathidae are not dependant on the inclusion of *Juravenator*.

CLADES AND SYNAPOMORPHIES

In this section the synapomorphies uniting major basal coelurosaurian clades are briefly discussed. All synapomorphies discussed here are unambiguous synapomorphies of the clade in question, as optimized onto the reduced strict consensus tree in TNT. For each clade that has a formal name the requisite phylogenetic definition is given. These definitions follow Sereno et al. (2005). Please consult that publication, as well as the corresponding online TaxonSearch database (www.taxonsearch.org), for a full discussion of authorship of clade names and conflicting definitions. In this section character numbers are followed by a period and then the synapomorphic character state number.

COELUROSAURIA

Definition: The most inclusive clade containing *Passer domesticus* but not *Allosaurus fragilis*, *Sinraptor dongi*, *Carcharodontosaurus saharicus.*

Synapomorphies: 35.0; 194.1; 543.0; 847.1

Comments: Perhaps surprisingly, Coelurosauria is only supported by four unambiguous synapomorphies. These include an L-shaped quadratojugal without a prominent posterior process (35.0), an astragalus whose ascending process is separated from the condyles by a transverse groove or fossa (194.1), a jugal with a weakly concave orbital margin that is not deeply U-shaped (543.0), and a femoral fourth trochanter that is positioned near the center of the posterior surface of the shaft distally and extends proximomedially to become confluent with the posteromedial corner of the shaft proximally (847.1). Turner et al. (2012) and other previous analyses have often reported greater character support for Coelurosauria, but the relative lack of coelurosaurian synapomorphies in the present analysis is due to three primary factors. First, the inclusion of basal coelurosaurs like *Bicentenaria*, *Tugulusaurus*, and *Zuolong* cause many previous coelurosaurian synapomorphies to become spread across several branches near the base of Coelurosauria. Second, the fragmentary nature of many basal coelurosaurian taxa included here, but excluded in previous studies, leads to ambiguous optimization of potential coelurosaurian synapomorhpies. Third, the current analysis is not actually a strong test of coelurosaurian monophyly or character support, because only two outgroup taxa are employed and characters relevant to immediate coelurosaurian outgroups are not included.

UNNAMED CLADE: COELUROSAURS MORE DERIVED THAN *BICENTENARIA*

Synapomorphies: 99.0; 176.1; 676.0; 716.0

Comments: The group of all coelurosaurs to the exclusion of *Bicentenaria* are united by four synapomorphies. These include: amphiplatyan or weakly opisthocoelous cervical vertebrae (99.0), a pubic apron that extends medially from the anterior edge of the shaft (176.1), anterior caudal vertebrae with neural spines positioned anterior to the posterior surface of the centrum (676.0), and a femur with an absent or extremely shallow extensor groove on the anterior surface of the distal end (716.0). These features would optimize as coelurosaurian synapomorphies if *Bicentenaria* were not included in the analysis.

TYRANNOSAUROIDEA

Definition: The most inclusive clade containing *Tyrannosaurus rex* but not *Ornithomimus edmontonicus*, *Troodon formosus*, *Velociraptor mongoliensis*.

Synapomorphies: 75.1; 256.1; 665.1; 840.1; 843.1

Comments: Tyrannosauroids, including *Coelurus* and *Tanycolagreus*, are united here by five synapomorphies. These are the characters that support *Coelurus* and *Tanycolagreus* as members of the tyrannosaur lineage. These synapomorphies include: an elongate medial process extending from the retroarticular process of the articular (75.1), a premaxilla with a main body that is between 1.0-1.9 times deep dorsoventrally than long anteroposteriorly (256.1), anterior-middle cervical vertebrae with posterior centrodiapophyseal laminae that are nearly horizontal instead of projecting posteroventrally (665.1), a glenoid in which the scapula makes a larger anteroposterior contribution than the coracoid (840.1), and a femur in which the crista tibiofibularis and medial

condyle extend to approximately the same posterior level in distal view (843.1, an intermediate state in an ordered character that is modified in *Coelurus* and *Tanycolagreus*). Three of these five synapomorphies stem from characters new to this phylogenetic analysis.

COELURIDAE

Definition: The most inclusive clade containing *Coelurus fragilis* but not *Allosaurus fragilis*, *Tyrannosaurus rex*, *Ornithomimus edmontonicus*, *Passer domesticus*.

Definition Comment: The family-level taxon Coeluridae was originally erected by Marsh (1881b) and for many years was used to group together several small theropods that are now considered distantly related. For example, Steel (1970) included numerous coelurosaurs in this group, including taxa today considered as dromaeosaurids, troodontids, and oviraptorosaurs. Rauhut (2003) recovered a grouping of *Coelurus* and some compsognathid taxa, which he termed Coeluridae. Later, Senter (2007) used Coeluridae to refer to a grouping of *Coelurus* and *Tanycolagreus* recovered by his phylogenetic analysis. As far as can be discerned, however, Coeluridae has never been phylogenetically defined. When applied to the current phylogeny, the above definition refers only to the sister grouping of *Coelurus* and *Tanycolagreus*, but because taxa such as *Ornitholestes*, compsognathids, and non-tyrannosaurid tyrannosaurines are not included as external specifiers this leaves open the possibility that other coelurosaurs may fall within Coeluridae in future analyses.

Synapomorphies: 142.1; 685.1; 837.1; 842.1; 843.2; 844.2; 845.1

Comments: The sister grouping of *Coelurus* and *Tanycolagreus* is supported by seven synapmorphies here, including: an ulna whose proximal surface is divided into two distinct

fossae separated by a median ridge (142.1), a humeral deltopectoral crest that extends for 25-35% of the length of the bone (685.1), a metatarsal III with a distal end whose mediolateral width is greater than 1.3 times that of the adjacent metatarsals (837.1), a horizontal ridge on the anterior surface of the femoral head that demarcates a deep fossa ventral to it (842.1), a medial condyle of the femur that projects further posteriorly than the crista tibiofibularis in distal view (843.2), a tibia in which the posterior ridge of the distal end is positioned at approximately the posteromedial corner of the bone in distal view (844.2), and a deep fossa on the lateral surface of the scapula immediately above the glenoid (845.1). Six of these synapomorphies relate to characters that are new to this analysis. Furthermore, none of these seven character states were recovered as synapomorphies of the *Coelurus* + *Tanycolagreus* clade by Senter (2007); rather, Senter recovered five other character states to be synapomorphic of this clade, none of which are corroborated here.

UNNAMED CLADE: ALL TYRANNOSAUROIDEA OTHER THAN COELURIDAE

Synapomorphies: 24.1; 76.2; 481.1; 485.1,2; 514.3; 684.1; 703.1; 712.1; 713.1; 746.1; 791.1; 839.1; 847.0

Comments: These characters are synapomorphies that unite what has become the traditional concept of Tyrannosauroidea over the past decade: the group that includes *Guanlong*, *Dilong*, and derived large-bodied taxa such as *Albertosaurus* and *Tyrannosaurus*. The monophyly of this group, and thus the tyrannosauroid affinities of small-bodied Middle Jurassic-Early Cretaceous taxa such as *Guanlong* and *Dilong*, is well supported by 13 synapomorphies. Among these are: conjoined premaxillae that are rounded in ventral view, with at least the first two teeth oriented

mediolaterally (24.1), an extremely reduced retroarticular process of the articular (76.2); a premaxilla with a deep foramen or fossa on the lateral surface of the base of the nasal process (481.1); a premaxilla with an anterior margin that is oriented vertically or slightly anterodorsally relative to the ventral margin (485.1,2); a lacrimal with at least a small cornual process (514.3); a coracoid foramen that is absent or extremely small (684.1); a pubic tubercle expressed as a convexity on the anterior margin of the pubis (703.1); a femur with a proximally inclined head (712.1); a deep trochanteric fossa on the femur (713.1); a pubic boot with an anterior edge that is markedly anterior to the anterior margin of the pubic shaft (746.1); dorsal vertebrae with hypertrophied parapophyses (791.1); the lack of a deep fossa on the lateral surface of the scapula and coracoid where the two bones meet (839.1); and a femoral fourth trochanter positioned along the posteromedial corner of the shaft (847.0). All but two of these characters are new to the present analysis, which helps to explain why *Dilong* and *Proceratosaurus* were not recovered as tyrannosauroids by Turner et al. (2012).

PROCERATOSAURIDAE

Definition: The most inclusive clade containing *Proceratosaurus bradleyi* but not *Tyrannosaurus rex*, *Allosaurus fragilis*, *Compsognathus longipes*, *Coelurus fragilis*, *Ornithomimus edmontonicus*, *Deinonychus antirrhopus*.

Definition Comment: We follow the definition proposed by Rauhut et al. (2010). Averianov et al. (2010) argued that Rauhut et al. (2010) did not validly name Proceratosauridae because, as a taxon ending in the traditional ICZN family-level suffix “idae,” they needed to formally diagnose it, which they did not do. Averianov et al. (2010) proceeded to diagnose a group containing

Proceratosaurus, *Guanlong*, and *Kileskus*, which they termed Proceratosauridae and then defined phylogenetically. However, they provided an alternative definition to that of Rauhut et al. (2010): "a node based taxon icluding *Proceratosaurus*, *Kileskus*, their most recent common ancestor, and all its descendants." We prefer the definition of Rauhut et al. (2010) and utilize it both because it was established first and because we feel that it better encapsulates the concept of a clade focused on *Proceratosaurus*, regardless of whether they named Proceratosauridae properly under the regulations of the ICZN. Averianov et al.'s (2010) definition on some trees could exclude *Guanlong* and *Sinotyrannus* from Proceratosauridae even though they are extremely similar morphologically to *Proceratosaurus* and despite the strong character support for a *Proceratosaurus*-*Guanlong*-*Kileskus*-*Sinotyrannus* clade.

Synapomorphies: 270.1; 483.1; 484.1

Comments: A discrete grouping of the basal tyrannosauroids *Proceratosaurus*, *Guanlong*, *Kileskus*, and *Sinotyrannus* is supported by three synapomorphies: a large external naris whose long axis is approximately equal to that of the antorbital fenestra (270.1); a narial fossa on the lateral surface of the premaxilla that is deeply excavated and invaginated anteriorly as a groove (483.1); and a narial fossa that covers nearly the entire lateral surface of the premaxilla.

UNNAMED CLADE: *PROCERATOSAURUS* + *GUANLONG* + *SINOTYRANNUS*

Synapomorphies: 498.1; 632.0; 636.0

Comments: Within Proceratosauridae, the three genera *Proceratosaurus*, *Guanlong*, and *Sinotyrannus* are united to the exclusion of *Kileskus* by three character states: a maxillary

anterior ramus (498.1); a surangular shelf reduced to a low ridge (632.0); and an adductor muscle scar on the surangular that faces almost entirely dorsally (636.0).

UNNAMED CLADE: ALL TYRANNOSAUROIDS EXCEPT COELURIDS AND PROCERATOSAURIDS

Synapomorphies: 23.0; 72.1; 89.2; 169.1; 262.1; 263.1; 296.0; 501.1; 507.1; 514.1; 632.2; 649.2; 669.1; 674.1; 685.1; 687.1; 695.1; 706.1; 715.1; 716.1; 752.1; 774.0; 785.0

Comments: All tyrannosauroids other than coelurids and proceratosaurids are united by a number of synapomorphies. The majority of these (16 out of 23) relate to characters new to this study. Among these characters are conjoined nasals that maintain a relatively constant mediolateral width across their length (507.1), all premaxillary teeth with a median vertical ridge on the lingual surface (649.2), postzygapophyses elevated relative to the prezygapophyses on the middle-posterior dorsal vertebrae (669.1), a humerus with a smoothly confluent deltopectoral crest and external tuberosity (687.1), an anterior bulge on the lateral condyle of the femur in distal view (715.1), and a deep extensor groove on the anterior surface of the distal femur (716.1).

UNNAMED CLADE: *XIONGGUANLONG* + *TYRANNOSAURUS*

Synapomorphies: 24.2; 30.0; 154.1; 155.2; 496.1; 566.1; 663.1; 665.0; 696.1; 697.1; 716.2

Comments: A total of 11 character states unite the clade of all tyrannosauroids exclusive of coelurids, proceratosaurids, *Eotyrannus*, and *Juratyrant*. Among these synapomorphies are hypapophyses on the cervical vertebrae (663.1), ilia that are medially inclined so that their

medial surfaces lie against the sacral neural spines (696.1), and a deep U-shaped extensor groove on the distal femur in distal view (716.2).

UNNAMED CLADE: *DRYPTOSAURUS* + *TYRANNOSAURUS*

Synapomorphies: 182.1; 185.0; 852.0

Comments: Three synapomorphies unite *Dryptosaurus*, *Appalachiosaurus*, *Bistahieversor*, and tyrannosaurids. Among these are: a non-alariform femoral lesser trochanter that is reduced to approximately the same anteroposterior width as the greater trochanter (182.1); the absence of an accessory trochanter on the lesser trochanter (185.0); and a cnemial crest that extends further proximally than the posterior condyles on the proximal end of the tibia (852.0).

UNNAMED CLADE: *APPALACHIOSAURUS* + *TYRANNOSAURUS*

Synapomorphies: 720.1

Comments: The sole character supporting the position of *Appalachiosaurus* as closer to tyrannosaurids than *Dryptosaurus* is a tibial lateral malleolus that is expansive laterally, such that its mediolateral width is greater than 40% of the width of the adjacent shaft (720.1).

UNNAMED CLADE: *BISTAHIEVERSOR* + *TYRANNOSAURUS*

Synapomorphies: 235.2; 596.1; 597.1; 598.1; 600.1; 643.2; 727.1; 731.1

Comments: Eight features unite *Bistahieversor* and tyrannosaurids as a clade. These include a palatine with a palatine recess whose anterior margin is located far anterior to the anterior margin of the neck of the vomeropterygoid process (596.1), a "brace" on the palatine where the maxillary and jugal processes meet (600.1), and an enormous rugose fossa on the lateral surface of the distal shaft of metatarsal II that articulates with metatarsal III (727.1).

TYRANNOSAURIDAE

Definition: The least inclusive clade containing *Tyrannosaurus rex* and *Gorgosaurus libratus*, *Albertosaurus sarcophagus*.

Synapomorphies: 491.1; 515.1; 538.1; 588.1; 729.2

Comments: The iconic clade Tyrannosauridae, which includes *Albertosaurus*-like and *Tyrannosaurus*-like taxa, is linked by five synapomorphies. All are states of characters new to the current analysis, as characters synapomorphic of this node in previous TWiG datasets are now smeared across several tyrannosauroid branches due to the increased taxon sampling employed here. The five characters supporting Tyrannosauridae here are: a maxilla with an interfenestral strut whose anteroposterior length is less than 50% of the long axis of the maxillary fenestra (491.1), a lacrimal cornual process marked by a discrete apex (515.1), a pronounced ridge on the lateral surface of the postorbital ramus of the jugal (538.1), an ectopterygoid with a jugal process that is inflated by a pneumatic sinus (588.1), and a metatarsal IV whose distal end has a ratio of anteroposterior length: mediolateral width less than 1.20 (729.2).

ALBERTOSAURINAE

Definition: The most inclusive taxon containing *Albertosaurus sarcophagus* but not *Tyrannosaurus rex*.

Synapomorphies: 533.0; 534.1; 542.1; 548.1; 549.1; 570.1; 592.1; 614.1; 652.1

Comments: The sister taxon grouping of *Albertosaurus* and *Gorgosaurus* is supported by eight synapomorphies, all of which are states of characters that are new to the current analysis. Among these are: a jugal-lacrimal suture whose posterior half is steep (534.1), a squamosal ramus of the postorbital that is emarginated by a discrete concave notch that houses a projection of the squamosal (548.1), and a vomeropterygoid process of the palatine with a vertically inclined neck (592.1).

TYRANNOSAURINAE

Definition: The most inclusive taxon containing *Tyrannosaurus rex* but not *Albertosaurus sarcophagus*.

Synapomorphies: 482.2; 497.1; 522.1; 529.1; 554.1; 555.1; 560.2; 586.1; 589.1; 590.1; 618.1; 676.1; 829.1

Comments: A total of 13 synapomorphies unite *Alioramus*, *Teratophoneus*, *Daspletosaurus*, *Tarbosaurus*, and *Tyrannosaurus* as a monophyletic tyrannosaurine clade. As with albertosaurine synapomorphies, all of these are character states of characters that are first included in the TWiG analysis in this dissertation. These features include a maxillary process of the premaxilla that is oriented mostly dorsally and thus not widely visible in lateral view (482.2), a deep joint surface

for the palatine on the maxilla (491.1), and a jugal maxillary ramus that is deeper dorsoventrally relative to the suborbital portion of the bone (529.1).

UNNAMED CLADE: *TERATOPHONEUS* + *DASPLETOSAURUS* + *TARBOSAURUS* + *TYRANNOSAURUS*

Synapomorphies: 91.1; 518.0; 562.2; 573.1; 577.1; 578.2

Comments: Among the features linking all tyrannosaurines other than *Alioramus* are a frontal whose posterior end is expanded into a retangular shape with a small anterior triangle (573.1) and a postorbital suture that is dorsoventrally deep and differentiated into vertical and horizontal regions (578.2).

UNNAMED CLADE: *DASPLETOSAURUS* + *TARBOSAURUS* + *TYRANNOSAURUS*

Synapomorphies: 28.0; 234.0; 488.2; 517.1; 519.1; 524.1; 535.1; 553.1; 557.2; 579.2; 606.1; 652.1

Comments: *Daspletosaurus*, *Tarbosaurus*, and *Tyrannosaurus* are united by 12 features, including a lacrimal anterior ramus inflated by an extension of the lacrimal pneumatic recess (517.1) and a squamosal pneumatic recess that is present as a deep, concave depression on the ventral surface of the bone (557.2).

UNNAMED CLADE: *TARBOSAURUS* + *TYRANNOSAURUS*

Synapomorphies: 3.2; 9.1; 10.1; 242.2; 256.2; 476.1; 490.0; 514.0; 537.1; 541.1; 543.1; 576.2; 579.3; 580.0; 587.1; 591.1; 602.1; 603.1; 612.0; 626.1; 627.1; 628.2; 636.2; 646.1; 647.1; 652.2; 654.1; 655.1; 660.1

Comments: The sister taxon relationship between the colossal Late Cretaceous tyrannosaurids *Tarbosaurus bataar* and *Tyrannosaurus rex* is one of the best supported clades in the analysis. These taxa are united by 29 character states, all but six of which are new to the current analysis. Among these synapomorphies are a supratemporal fossa that extends across more than 60% of the anteroposterior length of the frontal (242.2), a deep U-shaped orbital margin on the jugal (543.1), internal choanae and suborbital fenestrae that are circular instead of ovoid (602.1, 603.1), a strong rugose and beveled dentary symphysis (626.1), and an adductor muscle scar on the surangular that faces primarily laterally (636.2).

MANIRAPTORIFORMES

Synapomorphies: 19.0; 30.0; 38.0; 60.1; 81.2; 97.1; 110.1; 117.1; 159.1; 235.0; 247.0; 252.0; 258.0; 275.1; 443.0; 460.0; 529.0; 605.0; 613.0; 632.0; 664.1; 692.1; 702.0; 741.1; 757.0; 781.1; 830.1; 847.0

Comments: A total of 28 synapomorphies unite all coelurosaurs other than *Bicentenaria*, *Tugulusaurus*, *Zuolong*, and tyrannosauroids within a monophyletic Maniraptoriformes. These include a braincase in which the exits of cranial nerves X-XII are flush with the surface of the exoccipital and not located within a deep depression (19.0); nasals that lack external pneumatopores leading into an internal recess (30.0, 38.0); a palatine and ectopterygoid that contact each oher (60.1); maxillary and dentary teeth without serrations (81.2); cervical vertebrae

with short neural spines that are centered on the neural arch, giving each vertebra an "X" shape in dorsal view (97.1); flattened ventral surfaces on the sacral vertebrae (110.1); distal caudal vertebrae without neural spines (117.1); a prominent antitrochanter on the ilium (159.1); a shallow main body of the maxilla (235.0); a splenial without a notch along the dorsal surface of its posterior end (247.0); a quadratojugal and squamosal that do not constrict the lateral temporal fenestra (252.0); a jugal anterior process that tapers underneath the lacrimal (258.0); the absence of vomer-premaxilla contact (275.1); the absence of a preotic pendant on the braincase (443.0); vertical to subvertical articular facets on the cervical vertebrae (460.0); a shallow jugal maxillary ramus (529.0); a supraoccipital that forms the entire rim of the foramen magnum (605.0); a vertically oriented basisphenoid recess that is not visible in posterior view (613.0); a low or absent ridge on the lateral surface of the surangular (632.0); middle cervical vertebrae in which the prezygapophyses strongly overhang the centrum laterally (664.1); a smoothly convex or straight medial margin of metacarpal I in proximal view (692.1); a long and low ilium (702.0); manual unguals with distally placed flexor tubercles (741.1); square-shaped neural spines in the posterior dorsal vertebrae (757.0); a foramen magnum that is approximately equal in size to the occipital condyle (781.1); a Meckelian groove positioned ventrally along the medial surface of the dentary (830.1); and a fourth trochanter positioned along the posteromedial corner of the shaft (847.0).

COMPSOGNATHIDAE

Definition: The most inclusive clade containing *Compsognathus longipes* but not *Passer domesticus*.

Synapomorphies: 76.1; 81.1; 89.0; 94.1; 122.2; 174.1; 175.2; 206.1; 207.1; 452.0; 478.1; 479.1; 498.1; 551.1; 571.1; 622.2; 671.0; 683.1

Comments: The monophyly of Compsognathidae is supported by a number of character states. These include an elongate and slender retroarticular process of the articular (76.1), hair-like cervical ribs (122.2), a pubic shaft that projects vertically (174.1), a pubic boot without an anterior process (175.2), fan-shaped neural spines on the dorsal vertebrae (206.1), a manual phalanx I-1 with a greater shaft diameter than the radius (207.1), a lateral temporal fenestra whose long axis is approximately parallel to the long axis of the orbit (479.1), a maxilla with an anterior ramus (498.1), a long and slender anterior ramus of the postorbital (551.1), a prefrontal excluded from the nasal by frontal-lacrimal contact (571.1), an absent external mandibular fenestra (622.2), unfused sacral neural spines (671.0), and an elongate coracoid (683.1).

It is possible that some of these characters, such as the unfused sacral neural spines, may be related to the immaturity of some compsognathid specimens. Furthermore, some characters long considered unequivocal compsognathid synapomorphies, such as the absence of the anterior process of the pubic boot and fan-shaped dorsal neural spines, are now known to be more widely distributed among coelurosaurs (e.g., the anterior process of the pubic boot is absent in some dromaeosaurids; fan-shaped spines are present in *Pelecanimimus*). These are optimized as compsognathid synapomorphies here because the strict consensus is used for optimization, but some of these features may characterize more inclusive clades depending on the resolution of polytomies (e.g., the fan-shaped neural spines could be a synapomorphy of a compsognathid + ornithomimosaurian clade lost in later ornithomimosaurs). With that being said, the monophyly of Compsognathidae is well supported here, both in terms of character support (18 synapomorphies) and clade support (Bremer support of 2). The monophyly of the group is also

found regardless of whether or not *Juravenator* is included in construction of the strict consensus tree (see above).

ORNITHOMIMOSAURIA

Definition: The most inclusive clade containing *Ornithomimus edmontonicus* but not *Tyrannosaurus rex*, *Shuvuuia deserti*, *Therizinosaurus cheloniformis*, *Oviraptor philoceratops*, *Troodon formosus*, *Passer domesticus*.

Synapomorphies: 11.1; 20.2; 21.1; 23.0; 28.0; 68.0; 132.1; 134.2; 146.1; 148.1; 190.1; 209.1; 386.0; 475.1; 523.1; 527.1; 685.1; 694.1; 733.1; 736.1; 740.1; 755.2; 769.1; 779.1; 849.1; 850.1

Comments: *Nqwebasaurus* is more closely related to *Ornithomimus* than to other coelurosaurs such as *Tyrannosaurus*, *Shuvuuia*, and *Oviraptor*, and is therefore an ornithomimosaur by definition (see also Choiniere et al. 2012). The ornithomimosaur clade is united by a number of synapomorphies, listed above. Among these is a clear character that unites *Nqwebasaurus* with the unequivocal basal ornithomimosaur *Pelecanimimus*: maxillary teeth that are limited to the far anterior end of the maxilla (849.1). This character is subsequently lost in later ornithomimosaurs that lose their maxillary teeth. It is unclear if *Nqwebasaurus* or *Pelecanimimus* is the basal-most ornithomimosaur, a topic that was discussed in detail by Choiniere et al. (2012). Both of these taxa possess tooth rows on the upper and lower jaws, which are reduced in later ornithomimosaurs. *Pelecanimimus*, however, possesses several derived character states of the manus that are shared with some, but not all, derived Late Cretaceous ornithomimosaurs. It may be that *Pelecanimimus* is more derived than taxa such as *Beishanlong*, as reported by Choiniere et al. (2012). This would require that tooth loss proceeded independently in different lineages of

ornithomimosaurs. This phylogenetic scenario is not corroborated by the present analysis, as *Nqwebasaurus* and *Pelecanimimus* are both placed as basal ornithomimosaurs and not part of a more derived clade that includes all other ornithomimosaurian taxa. Charater conflict at and near the base of Ornithomimosauria, however, almost certainly plays a large role in the massive polytomy among most taxa more derived than *Shenzhousaurus*.

UNNAMED CLADE: *SHENZHOUSAURUS* + MORE DERIVED ORNITHOMIMOSAURS

Synapomorphies: 78.1; 80.1; 212.1; 217.1

Comments: All ornithomimosaurs with the exception of *Nqwebasaurus* and *Pelecanimimus* are united as a clade that is supported by four synapomorphies. These include: the absence of premaxillary and maxillary teeth (78.1, 80.1); upper and lower jaws that diverge anteriorly due to the downward deflection of the dentary (212.1); and dentary teeth restricted to the anterior tip (217.1). Dentary teeth are present at the tip of the lower jaw in some basal members of this clade (e.g., *Harpymimus*, *Shenzhousaurus*), but are lost entirely in more derived members (e.g., *Gallimimus*, *Garudimimus*).

UNNAMED CLADE: *BEISHANLONG* + MORE DERIVED ORNITHOMIMOSAURS

Synapomorphies: 108.1; 151.1; 164.1; 501.1; 624.1; 701.1; 732.1

Comments: All ornithomimosaurs with the exception of *Nqwebasaurus*, *Pelecanimimus*, and *Shenzhousaurus* are united as a clade that is supported by seven synapomorphies. These include: six or more sacral vertebrae (108.1); an ilium that is subquadrate in shape with a recurved

anterior margin (151.1); an ischial shaft that is curved anteriorly at its ventral end (164.1); the absence of a swollen rim separating the antorbital fossa from the subcutaneous surface of the maxilla (501.1); a dentary with a transition point between the ventral and anterior margins located far posteriorly (624.1); an ilium with a dorsal margin that is convex anteriorly and flattens out posteriorly (701.1); and the absence of a discrete row of foramina along the ventral edge of the lateral surface of the maxilla (732.1).

ORNITHOMIMIDAE

Definition: The most inclusive clade containing *Ornithomimus edmontonicus* but not *Garudimimus brevipes*, *Harpymimus okladnikovi*, *Shenzhousaurus orientalis*, *Pelecanimimus polyodon*.

Synapomorphies: 31.1; 50.1; 72.1; 92.1; 133.1; 146.2; 200.2; 210.1; 214.1; 252.1; 260.0; 397.2; 442.1; 561.1; 563.1; 609.1; 610.1; 669.1; 690.1; 724.1; 743.1; 837.1

Comments: The "intermediate" grade ornithomimosaurs *Beishanlong*, *Sinornithomimus*, *Garudimimus*, *Harpymimus*, and *Archaeornithomimus* fall into a large polytomy with the lineage leading to the clade of derived ornithomimosaurs that include *Gallimimus*, *Anserimimus*, *Ornithomimus*, *Struthiomimus*, and *Qiupalong*. This latter clade, which fits the definition of Ornithomimidae, is united by a large number of synapmorphies. These include an ascending process of the jugal that is reduced (31.1); a quadrate with a broad, triangular process along its shaft (51.1); a small surangular foramen (72.1); an axis neural spine that is compressed mediolaterally (92.1); a metatarsal III with a bulge along the medial surface of the distal part of

the shaft (724.1); the absence of pedal digit I (743.1); and a metatarsal III with a distal end that is more than 1.3 times as wide mediolaterally as the adjacent metatarsals (837.1).

The loss of dentary teeth is optimized basal to Ornithomimidae, somewhere within the large polytomy of "intermediate" ornithomimosaurs. One member of this polytomy (*Harpymimus*) possesses dentary teeth but all other taxa subsumed by this polytomy do not (as far as is known, as some of these taxa are not known from skull material, e.g., *Archaeornithomimus*). Depending on the resolution of the polytomy, dentary teeth may have been lost convergently in different ornithomimosaur subclades (including, in one scenario, at the base of Ornithomimidae itself).

UNNAMED CLADE: *GALLIMIMUS* + *ANSERIMIMUS*

Synapomorphies: 737.1; 738.1

Comments: The Asian Late Cretaceous ornithomimids *Gallimimus* and *Anserimimus* are united by two synapomorphies: a coracoid biceps tubercle positioned closer to the anterior edge of the bone than to the coracoid-scapula suture (737.1); and an infraglenoid buttress of the coracoid that is offset laterally relative to the posterior process (738.1).

UNNAMED CLADE: *ORNTIHOMIMUS* + *STRUTHIOMIMUS* + *QIUPALONG*

Synapomorphies: 208.1; 285.1; 732.0; 735.1; 742.1; 745.1; 746.1

Comments: The North American Late Cretaceous ornithomimids *Ornithomimus* and *Struthiomimus* are united with the Asian taxon *Qiupalong* by seven characters. These include the

absence of an anterior surangular formaen (735.1); a strongly convex ventral margin of the pubic boot (742.1); an approximately 90 degree angle between the anterior process of the pubic boot and the pubic shaft (745.1); and a pubic boot whose anterior process extends markedly anterior to the anterior margin of the pubic shaft (746.1). Many of these characters were outlined by L. Xu et al. (2012), who also found a *Qiupalong*-*Struthiomimus*-*Ornithomimus* clade to the exclusion of all other ornithomimosaurs.

MANIRAPTORA

Definition: The most inclusive clade containing *Passer domesticus* but not *Ornithomimus edmontonicus*.

Synapomorphies: 4.1; 20.1; 41.1; 46.1; 86.1; 89.0; 100.1 115.1; 118.2; 143.1; 145.0; 156.1; 158.0; 161.1; 171.1; 185.0; 186.0; 214.1; 280.1; 464.1; 552.2; 681.1; 752.1; 764.1; 781.2; 841.1

Comments: Alvarezsauroids, therizinosauroids, oviraptorosaurs, and paravians are united within a monophyletic Maniraptora, which is supported by a number of synapomorphies. The vast majority of these characters have appeared in previous versions of the TWiG analysis and many were discussed by Turner et al. (2012), who found them to be synapomorphies of either Maniraptora (including *Ornitholestes*) or the slightly more derived clade of all maniraptorans except for *Ornitholestes*. Because maniraptoran phylogeny is not a major focus of the current dissertation, and the addition of new taxa and characters was not focused on untangling maniraptoran phylogeny, these characters will not be discussed in detail. Similarly, the characters supporting various clades within Maniraptora will not be listed or discussed here, with a few exceptions concering clades whose taxon sampling is greatly increased relative to previous

TWiG analyses (Alvarezsauroidea and Therizinosauroidea) and the novel Scansoriopterygidae + Oviraptorosauria clade.

ALVAREZSAUROIDEA

Definition: The most inclusive clade containing *Alvarezsaurus calvoi* but not *Passer domesticus*.

Definition Comment: This definition follows that proposed by Choiniere et al. (2010a). Refer to the supplementary information of that paper for more information on this definition and the history of the clade name Alvarezsauroidea.

Synapomorphies: 18.2; 21.1; 39.2; 66.1; 71.1; 75.1; 93.1; 101.1; 104.0; 134.2; 140.2; 141.1; 149.1; 207.1; 208.1; 222.1; 351.1; 406.1; 527.1; 679.1; 683.1; 758.1; 768.1; 827.1; 835.1

Comments: *Haplocheirus* is united with taxa such as *Alvarezsaurus*, *Patagonykus*, *Shuvuuia*, and *Mononykus* to comprise a monophyletic Alvarezsauroidea.

UNNAMED CLADE: ALL ALVAREZSAUROIDS MORE DERIVED THAN *HAPLOCHEIRUS*

Synapomorphies: 154.1; 161.2; 181.1; 759.1

UNNAMED CLADE: ALL ALVAREZSAUROIDS MORE DERIVED THAN *HAPLOCHEIRUS* AND *ACHILLESAURUS*

Synapomorphies: 195.1

UNNAMED CLADE: ALL ALVAREZSAUROIDS MORE DERIVED THAN *HAPLOCHEIRUS*, *ACHILLESAURUS*, AND *ALVAREZSAURUS*

Synapomorphies: 99.1; 195.2; 698.1; 723.1; 839.1

UNNAMED CLADE: ALL ALVAREZSAUROIDS MORE DERIVED THAN *HAPLOCHEIRUS*, *ACHILLESAURUS*, *ALVAREZSAURUS*, *BONAPARTENYKUS*, AND *PATAGONYKUS*

Synapomorphies: 102.0; 178.3; 181.2; 184.1; 187.1; 188.1; 189.1; 191.1; 192.1; 193.2; 200.3; 345.1; 407.1; 667.1; 670.0; 747.1; 756.1; 764.0; 765.1; 771.1

UNNAMED CLADE: *BONAPARTENYKUS* + *PATAGONYKUS*

Synapomorphies: 161.1; 762.1

PARVICURSORINAE

Definition: The least inclusive clade containing *Parvicursor remotus* and *Mononykus olecranus*.

Definition Comment: This definition follows that presented by Choiniere et al. (2010a).

Synapomorphies: 138.3; 337.1; 721.1; 777.0

UNNAMED CLADE: *SHUVUUIA* + *LINHENKYUS* + *PARVICURSOR*

Synapomorphies: 104.1; 779.0

UNNAMED CLADE: *LINHENKYUS* + *PARVICURSOR*

Synapomorphies: 186.0

THERIZINOSAUROIDEA

Definition: The most inclusive clade containing *Therizinosaurus cheloniformis* but not *Tyrannosaurus rex*, *Ornithomimus edmontonicus*, *Mononykus olecranus*, *Oviraptor philoceratops*, *Troodon formosus*.

Definition Comment: This definition follows that presented by Zanno (2010b). Refer to that paper for discussion on the history of definitions pertaining to therizinosauroids and arguments about nomenclatural synonymy.

Synapomorphies: 8.1; 13.1; 63.1; 68.0; 81.0; 90.1; 98.1; 111.2; 117.0; 193.1; 348.1; 352.1; 366.1; 505.1; 610.1; 684.1; 746.1; 755.1; 776.1; 789.1; 790.1; 797.1; 799.1; 803.1; 816.1; 825.0; 843.1; 847.2

Comments: *Falcarius* is united with taxa such as *Beipiaosaurus*, *Therizinosaurus*, and *Suzhousaurus* to comprise a monophyletic Therizinosauroidea.

UNNAMED CLADE: ALL THERIZINOSAUROIDS MORE DERIVED THAN *FALCARIUS*

Synapomorphies: 64.1; 67.1; 84.0; 85.1; 165.2; 212.1; 462.1; 702.1; 805.1; 807.1; 814.1; 818.1; 824.1; 850.1

UNNAMED CLADE: ALL THERIZINOSAUROIDS MORE DERIVED THAN *FALCARIUS* AND *BEIPIAOSAURUS*

Synapomorphies: 151.2; 154.1; 167.1; 182.1; 203.1; 629.2; 712.2; 800.1; 806.1; 808.1

UNNAMED CLADE: ALL THERIZINOSAUROIDS MORE DERIVED THAN *FALCARIUS*, *BEIPIAOSAURUS*, AND *ALXASAURUS*

Synapomorphies: 741.0; 798.1; 801.1; 802.1

UNNAMED CLADE: ALL THERIZINOSAUROIDS MORE DERIVED THAN *FALCARIUS*, *BEIPIAOSAURUS*, *ALXASAURUS*, AND *ERLIANSAURUS*

Synapomorphies: 133.1; 185.1; 714.1; 764.2; 806.2; 812.1; 819.2

OVIRAPTOROSAURIA

Definition: The most inclusive clade containing *Oviraptor philoceratops* but not *Therizinosaurus cheloniformis*, *Ornithomimus edmontonicus*, *Troodon formosus*, *Tyrannosaurus rex*, *Passer domesticus*.

Synapomorphies: 64.1; 68.0; 113.1; 217.1; 248.2; 623.2; 629.2

Comments: The novel finding that scansoriopterygids (*Epidexipteyx* and *Pedopenna*) are united with oviraptorosaurs, and by definition the basal-most members of the clade Oviraptorosauria, deserves further comment. This relationship is supposed by seven synapomorphies, including: a dentary whose dorsal margin is downturned anteriorly (64.1); a dentary that is subtriangular in lateral view (68.0); caudal vertebrae that are homogeneous along the tail, without a transition point (113.1); dentary teeth present only at the far anterior tip of the bone (217.1); a first premaxillary tooth that is much larger in cross section than the more distal premaxillary teeth (248.2); a glenoid on the lower jaw that is positioned far ventral to the alveolar margin of the dentary (623.2); and a dentary dorsal margin that is strongly convex in lateral view (629.2). Five of these synapomorphies are states relating to previous TWiG characters whereas only two relate to characters new to this analysis.

DISCUSSION

Consensus on Basal Coelurosaur Relationships

With the flurry of phylogenetic analyses focused on theropods over the past decade, including numerous iterative analyses published by the TWiG consortium, consensus has emerged on several aspects of coelurosaurian phylogeny. For the first time in the TWiG research program, the current dataset includes a broad sample of basal coelurosaurian taxa and characters pertinent to their relationships. This dataset offers the strongest test yet of basal coelurosaurian relationships among TWiG analyses and, along with analyses published by other research

groups, helps clarify several longstanding debates regarding the phylogeny and early evolution of coelurosaurs. In regards to the relationships of non-paravian taxa, there are many general areas of agreement between the current phylogeny and recently published coelurosaur phylogenies (those published over the past 10 years, e.g., Holtz et al. 2004; Rauhut and Xu 2005; Senter 2007, 2010, 2011; Zanno et al. 2009; Choiniere et al. 2010a,b, 2012; Li et al. 2010; Rauhut et al. 2010; Zanno 2010b; Dal Sasso and Maganuco 2011; Xu et al. 2011a; Novas et al. 2012; Turner et al. 2012). These similarities are highlighted here.

Monophyly of Coelurosaurian Subgroups: The monophyly of major basal coelurosaurian subgroups is almost universally agreed upon. Clades such as Tyrannosauroidea, Compsognathidae, Ornithomimosauria, Alvarezsauroidea, and Therizinosauroidea are consistently recovered in phylogenetic analyses and are usually well supported by character data. One slight exception is Compsognathidae, which is recovered as a monophyletic group in most analyses, usually containing the core genera *Compsognathus*, *Sinosauropteryx*, *Huaxiagnathus*, and occasionally other taxa such as *Juravenator*, *Sinocalliopteryx*, and *Mirischia* if these are included in the analysis. This result is recovered here, but it is only moderately supported (Bremer value of 2, jackknife percentage of 57%). A monophyletic Compsognathidae has also been recovered by Turner et al. (2012) and previous versions of the TWiG analysis and many other studies (Holtz 2004; Senter 2007, 2010, 2011; Zanno et al. 2009; Choiniere et al. 2010a,b, 2012; Li et al. 2010; Zanno 2010b; Dal Sasso and Maganuco 2011; Xu et al. 2011; Novas et al. 2012). On the contrary, Rauhut et al. (2010) found *Compsognathus* and *Mirischia* to group together as sister taxa, but *Sinosauropteryx* as a more derived taxon more closely related to maniraptorans. In that analysis, therefore, the three compsognathid taxa comprise a paraphyletic

grade among basal coelurosaurs. It is also worth noting that Dal Sasso and Maganuco (2011) recovered a monophyletic Compsognathidae consisting of *Compsognathus*, *Huaxiagnathus*, *Juravenator*, *Sinocalliopteyx*, and *Sinosauropteryx*, but found *Mirischia* at the base of Coelurosauria, several nodes closer to the root of the tree than Compsognathidae. These few exceptions aside, the consistent recovery of Compsognathidae in many alternative studies comprises a clear consensus, although the monophyly of this clade may still be open to question (see below).

Tyrannosauroid Affinities of *Dilong*, *Guanlong*, and *Proceratosaurus*: There is now a near universal consensus that small-bodied basal coelurosaurian taxa such as *Dilong*, *Guanlong*, and *Proceratosaurus* are basal members of an inclusive Tyrannosauroidea. The various analyses of Senter (2007, 2010, 2011) and others based on this dataset (e.g., Dal Sasso and Maganuco 2011; Xu et al. 2011a; Novas et al. 2012) have been consistent in placing *Dilong*, and when included *Guanlong*, within the tyrannosauroid lineage. This is also the case in other recent analyses (e.g., Zanno et al. 2009; Choiniere et al. 2010a,b, 2012; Li et al. 2010; Rauhut et al. 2010; Zanno 2010b). Rauhut et al. (2010), in their redescription of *Proceratosaurus*, argued that this long-enigmatic basal coelurosaur is morphologically similar to *Guanlong* and also a basal member of Tyrannosauroidea, a result corroborated by their phylogenetic analysis. In agreement with these previous studies, *Dilong*, *Guanlong*, *Proceratosaurus*, and a handful of other taxa (*Sinotyrannus*, *Kileskus*, *Juratyrant*, *Eotyrannus*) are recovered as basal tyrannosauroids in the current analysis and these relationships are all well supported by character data and clade support values. Many of these relationships were also reported in the tyrannosauroid-specific phylogenetic analysis of Brusatte et al. (2010a) and their recovery here, in a larger dataset that allows for a better test of

tyrannosauroid membership and relationships within the context of all coelurosaurs, corroborates these earlier results. The tyrannosauroid affinities of taxa such as *Dilong* and *Guanlong*, therefore, are largey agreed upon and robustly supported.

Perhaps surprisingly, Turner et al. (2012) found *Dilong* and *Proceratosaurus* to be closer to avialans than to taxa such as *Eotyrannus* and *Tyrannosaurus*, and therefore not part of the tyrannosauroid clade. Similar results were found in some previous TWiG datasets (e.g., Turner et al. 2007a). However, this result is almost certainly due to poor character and taxon sampling near the base of Coelurosauria. This point was explicitly mentioned by Turner et al. as something that would be improved upon in future versions of the TWiG dataset such as this dissertation analysis. For example, Turner et al. (2012) did not include the non-tyrannosaurid tyrannosauroids *Guanlong*, *Juratyrant*, *Xiongguanlong*, *Dryptosaurus*, and *Applachiosaurus* in their dataset, and also did not include the 200+ characters relative to tyrannosauroid phylogeny outlined by Brusatte et al. (2010a) that are included here. With these new data added into the TWiG matrix, the tyrannosauroid affinities of *Guanlong*, *Dilong*, and *Proceratosaurus* appear strong.

Basal Coelurosaur Position of *Bicentenaria*, *Tugulusaurus*, and *Zuolong*: Few analyses have included the singleton genera *Bicentenaria*, *Tugulusaurus*, and *Zuolong*, but there is an emerging consensus that these taxa are all placed close to the base of Coelurosauria. *Zuolong* was originally described by Choiniere et al. (2010b), who recovered it in a large polytomy at the base of Coelurosauria. The later analysis of Choiniere et al. (2012) was able to better resolve the position of *Zuolong*, and placed this genus as the most basal coelurosaur. Novas et al. (2012), on the other hand, found *Zuolong* as phylogenetically intermediate between tyrannosauroids and

compsognathids (i.e., as more closely related to birds than to tyrannosauroids). All of these results are consistent with the results of the current analysis, as *Zuolong* is here found within a small polytomy near the base of Coelurosauria, which also includes *Tugulusaurus*, Tyrannosauroidea, and the clade of all more derived coelurosaurs (e.g., compsognathids, ornithomimosaurs, maniraptorans). Regardless of its exact phylogenetic position, the consensus is that *Zuolong* is among the most basal coelurosaurs known. This is generally consistent with its Callovian-Oxfordian geological age, which is among the oldest known of any coelurosaur (although *Zuolong* is not the oldest coelurosaur—tyrannosauroids such as *Proceratosaurus* and *Kileskus* are known from earlier in the Middle Jurassic). The basal position of *Zuolong* is also well supported by character data, as *Zuolong* retains many primitive character states that are shared with the outgroup taxa but are modified into synapomorphies that unite all, or most, other coelurosaurs. These include, for example, cervical prezygapophyses with flat (not convex) facets that extend only slightly laterally (not far laterally) relative to the centrum.

The small-bodied *Tugulusaurus* is represented solely by a fragmentary holotype specimen that comprises some vertebrae and parts of the manus and hindlimb (Rauhut and Xu 2005). It has been included in only a select number of phylogenetic analyses but is universally found to be among the most basal coelurosaurs (Rauhut and Xu 2005; Choiniere et al. 2010b; Rauhut et al. 2010; Novas et al. 2012). In all of the aforementioned analyses, with the exception of Choiniere et al. (2010b), *Tugulusaurus* is positioned as the most basal member of Coelurosauria. This placement is generally consistent with the results of the current study, which find *Bicentenaria* to be the most basal coelurosaur but *Tugulusaurus* and *Zuolong* one node more derived (i.e., closer to birds). Of all previous studies, only the analysis of Novas et al. (2012) includes both *Bicentenaria* and *Tugulusaurus*, as the latter genus was established in that

publication. The relative positions of *Bicentenaria* and *Tugulsaurus* are swapped relative to those found in the current analysis, as Novas et al. (2012) finds *Tugulusaurus* to be the most basal coelurosaur and *Bicentenaria* positioned one node more derived (closer to birds). The basal-most coelurosaur position of *Bicentenaria* is well supported in the current study, as the clade of all other coelurosaurs is characterized by high clade support values (Bremer of 2; jackknife percentage of 94%) and is united by clear synapomorphies that are absent in *Bicentenaria* and the outgroups, including amphiplatyan or weakly opisthocoelous cervical vertebrae and a femur with a shallow or absent extensor groove. Regardless of the exact placements of *Bicentenaria* and *Tugulusaurus*, however, there is general agreement that these genera are among the most primitive coelurosaurs known, and this is considered to be current consensus.

Ornithomimosaurian Affinities for *Nqwebasaurus*: Another problematic singleton taxon, *Nqwebasaurus*, has been included in a few cladistic analyses but has been recovered in a widely varying number of positions. In the original description of *Nqwebasaurus*, de Klerk et al. (2000) did not present a phylogenetic analysis but argued, based on the distribution of synapomorphies in published cladistic analyses, that this new taxon was a very basal member of Coelurosauria. Later, Holtz et al. (2004) explicitly included *Nqwebasaurus* in a phylogenetic analysis and found it to group with *Ornitholestes* and *Proceratosaurus* within a small subclade of basal coelurosaurs, placed between compsognathids and a clade of more derived coelurosaurs including tyrannosauroids, ornithomimosaurs, and maniraptorans. Rauhut and Xu (2005) found *Nqwebasaurus* to be more derived than *Tugulusaurus*, *Coelurus*, and compsognathids, but part of a large polytomy that also included tyrannosauroids, ornithomimosaurs, and maniraptorans. Dal Sasso and Signore (2011) reported a novel result in which *Nqwebasaurus* grouped with

alvarezsauroids, whereas Li et al. (2010) and Novas et al. (2012) found *Nqwebasaurus* to be a member of Compsognathidae.

Although the position of *Nqwebasaurus* has widely fluctuated, and every analysis seems to recover a different result, the recent comprehensive redescription of this taxon has clarified its phylogenetic affinities (Choiniere et al. 2012). This clarification is based on both extensive comparisons with other coelurosaurs and the description of new portions of the holotype that were previously unprepared, which possess phylogenetically useful characters. Choiniere et al. (2012) identified unequivocal characters shared between *Nqwebasaurus* and ornithomimosaurs, and recovered *Nqwebasaurus* as the basal-most member of Ornithomimosauria. This result is also found here, and based on this agreement and the strong character support, the ornithomimosaurian affinities of *Nqwebasaurus* are considered robust.

The Ornithomimosauria + Maniraptora + *Ornitholestes* Clade: There is general agreement that ornithomimosaurs, maniraptorans, and *Ornitholestes* are more closely related to each other than any of these taxa are to tyrannosauroids or basal forms such as *Zuolong* and *Tugulusaurus*. Put another way, the consensus is that tyrannosauroids are among the most basal coelurosaurs and that most other major coelurosaur subclades (or all, depending on the position of compsognathids) form a group exclusive of tyrannosauroids. This group is termed Maniraptoriformes. This result is found here and has been recovered by most recent studies, including Senter (2007, 2010, 2011), Zanno et al. (2009), Choiniere et al. (2010a, 2012), Li et al. (2010), Rauhut et al. (2010), Zanno (2010b), Dal Sasso and Maganuco (2011), Novas et al. (2012), and Turner et al. (2012) and previous TWiG analyses. The only recent studies that do not recover this result only do so because of the uncertainty of polytomies. Rauhut and Xu (2005),

for example, find tyrannosauroids, ornithomimosaurs, *Ornitholestes*, and maniraptorans to fall into a large polytomy. Choiniere et al. (2010b) reported a similar result, in which more taxa are also part of this polytomy. It is also worth noting that Holtz et al. (2004) found an ornithomimosaur + maniraptoran clade exclusive of tyrannosauroids, but recovered *Ornitholestes* (and compsognathids) closer to the base of Coelurosauria than tyrannosauroids.

These few exceptions aside, there is strong consensus that tyrannosauroids are the most basal major coelurosaurian subgroup and that ornithomimosaurs, maniraptorans, and *Ornitholestes* form a clade of more derived taxa. Therefore, although some tyrannosauroids and some ornithomimosaurs share characters (e.g., medially inclined iliac blades, dorsal margin of ilium convex anteriorly but straightens out posteriorly), these are optimized as convergences. With that being said, however, it must be pointed out that the ornithomimosaur + maniraptoran subclade is characterized by low clade support values in the current study. This is most likely due to uncertainty regarding the position of compsognathids, which are part of the ornithomimosaur + maniraptoran subclade here but some of which share characters with tyrannosauroids (see below).

Maniraptora: A major point of agreement between the current study and most alternative analyses is the existence of a maniraptoran clade that includes alvarezsauroids, therizinosauroids, oviraptorosaurs, and paravians (and potentially compsognathids and *Ornitholestes*: see below) to the exclusion of tyrannosauroids, ornithomimosaurs, and basal taxa such as *Zuolong* and *Tugulusaurus*. The existence of a "derived" coelurosaur clade exclusive of ornithomimosaurs and tyrannosauroids was first articulated by Gauthier (1986) and has been consistently found in most subsequent cladistic analyses, although the relationships within this clade often differ (see

below). Additionally, as is the case in most recent studies, the current analysis recovers a subclade of oviraptorosaurs and paravians the latter of which includes dromaeosaurids, troodontids, and avialans. Because this part of the phylogeny is not a major focus of this dissertation the relationships among oviraptorosaurs and paravians will not be discussed further, and the reader is referred to Turner et al. (2012) for a full discussion of these topics.

Summary of Consensus: In summary, the current phylogeny is similar to recent published analyses in many regards. Because the current study includes a large sample of characters and taxa relevant to basal coelurosaurs, and incorporates a large amount of data from other studies, these areas of agreement are considered as the current "consensus" view. The most salient aspects of the consensus are: 1) Major coelurosaurian subclades such as Ornithomimosauria, Tyrannosauroidea, and Compsognathidae are monophyletic; 2) the singleton genera *Zuolong*, *Tugulusaurus*, and *Bicentenaria* are among the most basal coelurosaurs and are not clearly linked to major subclades based on shared, derived characters; 3) the small-bodied *Dilong*, *Guanlong*, and *Proceratosaurus* are basal members of Tyrannosauroidea; 4) tyrannosauroids are the most basal major coelurosaur subgroup, with ornithomimosaurs and maniraptorans united in a monophyletic Maniraptoriformes; 5) alvarezsauroids, therizinosauroids, oviraptorosaurs, and paravians form a monophyletic Maniraptora to the exclusion of tyrannosauroids and ornithomimosaurs.

AREAS OF UNCERTAINTY

Although there are many areas of general agreement between the current study and previous phylogenies, there are also a handful of disagreements. These disagreements are not between the current study and the pool of all previous studies, but rather are disagreements that have persisted between alternative published studies and reflect primary areas of uncertainty in coelurosaur phylogeny. The continuation of these disagreements illustrates that even with great increases in character and taxon sampling, such as employed in the current study, substantial amounts of homoplasy and character conflict still plague certain areas of coelurosaur phylogeny. The issues highlighted below will likely only be resolved with the discovery of new taxa with unique character combinations.

Compsognathidae: A major uncertainty regards the position of Compsognathidae. Here, compsognathids are placed within a polytomy that also includes *Ornitholestes*, Ornithomimosauria, and Maniraptora. Depending on the resolution of this polytomy compsognathids could be maniraptorans, or they could be closer to the root of the tree than ornithomimosaurs. The position of compsognathids fluctuates greatly among previous studies. Holtz (2004) found them to be the most basal coelurosaurs; in other words, he reported a clade comprised of tyrannosauroids, ornithomimosaurs, and maniraptorans to the exclusion of compsognathids. A similar result was reported by Rauhut and Xu (2005) and Rauhut et al. (2010), the latter of which recovered compsognathids as a paraphyletic grade near the base of Coelurosauria. The various analyses of Senter (2007, 2010, 2011) place compsognathids as phylogenetically intermediate between tyrannosauroids and ornithomimosaurs, the latter of which are closer to birds. This is also recovered in several analyses based on the Senter datasets, including Dal Sasso and Maganuco (2011), Xu et al. (2011a), and Novas et al. (2012), as well as

in recent versions of the TWiG analyses such as Turner et al. (2007a, 2012). In contrast, some previous versions of the TWiG analysis (e.g., Hwang et al. 2004) found compsognathids to be basal maniraptorans (in other words, more closely related to birds than are tyrannosauroids and ornithomimosaurs). This was also reported by Choiniere et al. (2010a, 2012). The analyses of Zanno et al. (2009) and Zanno (2010b), on the contrary, recovered a dramatically different result in which compsognathids and tyrannosauroids form a sister-taxon pair at the base of Coelurosauria.

The current analysis is consistent with compsognathids being placed either intermediate between tyrannosauroids and ornithomimosaurs, or in a more derived position at the base of Maniraptora. It is not consistent, however, with the Holtz et al. (2004) and Rauhut et al. (2010) hypothesis that compsognathids are the most basal clade (or grade) of coelurosaurs, or the results of Zanno et al. (2009) and Zanno (2010b) linking tyrannosauroids and compsognathids together as a subclade. Although some compsognathids do share characters with some tyrannosauroids (e.g., *Sinocalliopteyx* has an ilium with a concave anterodorsal corner and a premaxilla that is less than 10% of the anterior length of the skull, as in tyrannosauroids), these characters are optimized as convergences. There is genuine character conflict in the ornithomimosaur-compsognathid-maniraptoran zone of the tree and both an ornithomimosaur + maniraptoran group and a compsognathid + maniraptoran clade are supported by some characters. One potentially complicating factor is that resolution with Compsognathidae is poor, as all members of the clade degrade into a basal polytomy. This does not allow relationships within Compsognathidae to confidently inform character polarity at the base of the clade, which is important for placing compsognathids among coelurosaurs more generally. Furthermore, some (or all) compsognathids likely are represented by only juvenile specimens, meaning that adult

morphologies are not being sampled, which can be strongly problematic in phylogenetic analyses (e.g., Bever and Norell 2009). Better understanding of the higher-level placement of compsognathids among coelurosaurs will likely follow better resolution of compsognathid ingroup phylogeny, new discoveries that reveal adult morphologies, and histological and ontogenetic work on compsognathids that may help reveal which characters are ontogenetically variable within the group and thus phylogenetically problematic.

It is also important to reiterate that, although compsognathids are found to be a monophyletic group in both the current study and nearly all previous cladistic analyses of coelurosaurs, this result may not be convincing. The fundamental problem with compsognathids is that most specimens likely belong to very young individuals (including some that are probably immediate post-hatchlings: Dal Sasso and Signore 1998; Dal Sasso and Maganuco 2011), but histological work has yet to shed light on the actual ages of the individuals. It is worrying that the recent phylogenetic analysis of Rauhut et al. (2012) placed the putative compsognathid *Juravenator*, known only from a very young individual, with the megalosauroid *Sciurumimus*, also known from a very young individual. This suggests that the juvenile nature of both specimens is causing them to link together in the phylogenetic analysis, and this may also explain why Compsognathidae is found to be monophyletic in the current analysis and elsewhere (e.g., *Compsognathus*, *Sinosauropteyx*, and other taxa may unite together in a clade only because they share juvenile features). The only way to test whether this is the case is with a better understanding of compsognathid growth and ontogeny, which can only come with histological sampling of specimens and the discovery of clear adult material of *Compsognathus*, *Sinosauropteryx*, and other putative compsognathid taxa.

One particularly interesting possibility is that some or all compsognathids may not even be coelurosaurs. This cannot be adequately tested in the current study because non-coelurosaur taxa are not included in the analysis (except for the two outgroups). Bhullar et al. (2012) recently showed that there is a paedomorphic trend throughout coelurosaur evolution, meaning that progressively more derived (bird-like) coelurosaurs resemble the juveniles of more basal taxa. It could be that many supposed compsognathid specimens are actually juveniles of megalosauroids, allosauroids, or other non-coelurosaurian taxa, but they group with coelurosaurs in phylogenetic analyses because they resemble adult coelurosaurs due to the paedomorphic trend. This is simply a hypothesis that is mentioned here in passing, but it deserves to be tested with additional study. Once again, only histological data, the discovery of adult compsognathid specimens, and wider taxonomic sampling in phylogenetic analyses (including coelurosaurs and non-coelurosaurs simultaneously) can adequately test this hypothesis.

Coelurus* and *Tanycolagreus: Another point of disagreement among studies is the position of two problematic singleton genera, *Coelurus* and *Tanycolagreus*. *Coelurus* has been known for over a century (Marsh 1879), whereas *Tanycolagreus* was described only recently (Carpenter et al. 2005a), but both have been included in only a few phylogenetic analyses. *Coelurus*, for example, was added to the TWiG analysis only very recently (Turner et al. 2007a) and *Tanycolagreus* is first incorporated into the TWiG dataset in the current study. Holtz et al. (2004) found *Coelurus* to be phylogenetically intermediate between tyrannosauroids and ornithomimosaurs and Rauhut and Xu (2005) placed *Coelurus* in a polytomy near the base of Coelurosauria that also included Compsognathidae. Turner et al. (2007a, 2012) recovered *Coelurus* as intermediate between tyrannosauroids and compsognathids, and thus generally

concordant with the results of Holtz (2004). Zanno et al. (2009) and Zanno (2010b) placed *Coelurus* in a more derived position: as a basal member of Maniraptora and thus more closely related to birds than tyrannosauroids, ornithomimosaurs, and compsognathids. Choiniere et al. (2010a) and Rauhut et al. (2010), on the other hand, found *Coelurus* to be among the most basal coelurosaurs, and closer to the root of the tree than are tyrannosauroids and ornithomimosaurs.

Most of these aforementioned analyses, however, did not include *Tanycolagreus*. Senter (2007, 2010, 2011) included both *Coelurus* and *Tanycolagreus* and found these genera to form a sister taxon pair at the base of Tyrannosauroidea, a result also recovered in later analyses using Senter's dataset as a base (e.g., Dal Sasso and Maganuco 2011; Xu et al. 2011a; Novas et al. 2012). Similarly, Li et al. (2010) found both genera to group together as sister taxa, but this lineage was placed at the base of Coelurosauria and not with tyrannosauroids. Choiniere et al. (2012) included only *Tanycolagreus* but found it as a basal tyrannosauroid. Choiniere et al. (2010b) included both genera and found them to form part of a large polytomy at the base of Coelurosauria, whereas Rauhut et al. (2010) placed *Tanycolagreus* in a much more derived position than *Coelurus*, as a member of an ornithomimosaur + *Ornitholestes* + Maniraptora clade to the exclusion of tyrannosauroids.

The current analysis is consistent with Senter's (2007, 2010, 2011) finding that *Coelurus* and *Tanycolagreus* comprise a sister taxon pair, which is the basal-most lineage of tyrannosauroids (i.e., *Guanlong*, *Dilong*, and tyrannosaurids form a clade exclusive of *Coelurus* and *Tanycolagreus*). The placement of *Tanycolagreus* and *Coelurus* within Tyrannosauroidea is well supported by synapomorphies and moderately supported by clade robusticity metrics (Bremer support of 2). The sister grouping of these two genera, regardless of their higher-level position among coelurosaurs, is even better supported (Bremer support of 2, jackknife percentage

of 72%). The current analysis is inconsistent with Rauhut et al.'s (2010) finding that *Coelurus* and *Tanycolagreus* are phylogenetically distant from each other. It is worth noting, however, that the position of *Coelurus* as a basal tyrannosauroid is only one or a few nodes removed from the basal-most (or near basal-most) coelurosaur position reported by Rauhut and Xu (2005) and Rauhut et al. (2010), as well as its position near tyrannosauroids, but not grouping with them, in Holtz (2004), Turner et al. (2007a, 2012), and other analyses. In the current analysis the addition of new characters relevant to basal coelurosaurian phylogeny, especially several new features shared explicitly by *Tanycolagreus* and *Coelurus* and by these genera and tyrannosauroids (see above), has swung the balance of character support in favor of tyrannosauroid affinities. This has caused *Coelurus* to move one or two nodes relative to previous studies and group with tyrannosauroids.

Ornitholestes: In addition to *Coelurus* and *Tanycolagreus*, the phylogenetic position of a third singleton genera has been the subject of considerable debate. This taxon, *Ornitholestes*, has been known for over a century (Osborn 1903) and has been included in numerous phylogenetic analyses, dating back to the seminal analysis of Gauthier (1986). The strinking consistency among most of these analyses is that *Ornitholestes* is usually placed as its own branch interspersed within a pectinate set of major clades leading to birds. In other words, *Ornitholestes* usually does not group with any of the major coelurosaurian subclades such as ornithomimosaurs, compsognathids, alvarezsauroids, or therizinosauroids. This is because the overall anatomy of *Ornitholestes* is quite generalized and it does not share any clear, unequivocal synapomorphies with the major coelurosaurian subgroups, at least based on current understanding of its osteology. One exception to this general trend is that Choiniere et al. (2012)

recently found *Ornitholestes* to group with compsognathids, as the most basal member of a monophyletic Compsognathidae that also includes *Compsognathus*, *Huaxiagnathus*, and *Sinosauropteryx*. This relationship is only weakly supported, however, by a Bremer value of 1, meaning that it is not found in the strict consensus of all trees up to one step longer than the most parsimonious trees.

Not only does *Ornitholestes* usually fail to group with major coelurosaurian subclades in most analyses, but its phylogenetic position is labile as well. Holtz et al. (2004) recovered it as among the most basal coelurosaurs, closer to the root of the coelurosaur tree than were tyrannosauroids, ornithomimosaurs, and the other primary subclades. Rauhut and Xu (2005) found *Ornitholestes* as part of a major polytomy near the base of Coelurosauria that also includes tyrannosauroids, ornithomimosaurs, and maniraptorans, and Rauhut et al. (2010) later better resolved this portion of the tree and placed *Ornitholestes* as the outgroup to an ornithomimosaur + maniraptoran clade. Li et al. (2010) reported a similar result in which *Ornitholestes*, Ornithomimosauria, and Maniraptora form a polytomy. Most analyses, however, have been consistent in placing *Ornitholestes* as a basal member of Maniraptora, the major clade that includes all coelurosaurs more closely related to birds than to ornithomimosaurs. Usually *Ornitholestes* is found to be the most basal maniraptoran (Senter 2007, 2010, 2011; Zanno et al. 2009; Choiniere et al. 2010a; Zanno 2010b; Dal Sasso and Maganuco 2011; Xu et al. 2011a; Novas et al. 2012; Turner et al. 2012). The results of the current analysis are consistent with many of these scenarios, including a basal maniraptoran placement, a position as the outgroup to an ornithomimosaur + maniraptoran clade, and even a linkage with compsognathids. The only major recent hypothesis that is inconsistent with the current analysis is Holtz et al.'s (2004)

placement of *Ornitholestes* as basal to a tyrannosauroid + ornithomimosaur + maniraptoran clade.

Uncertainty in the phylogenetic position of *Ornitholestes* is likely due to several primary factors. First, its anatomy is genuinely "generalized" in overall gestalt and it does not share obvious derived characters with major coelurosaurian subgroups. The possibility that *Ornitholestes* may group with compsognathids is intriguing (Choiniere et al. 2012) and worthy of further study, although it is obviously not yet supported by a preponderance of character data. Second, uncertainty in the higher-level placement of ornithomimosaurs and compsognathids (discussed above) has bearing on the placement of *Ornitholestes*, and character conflict at the base of Maniraptora (between compsognathids, ornithomimosaurs, and more derived maniraptorans) is currently a vexing issue. The holotype of *Ornitholestes* is currently being redescribed as part of this dissertation project and it is hoped that a careful examination of its anatomy, and comparisons with a range of coelurosaurs, will reveal new character support that better resolves the phylogeneic position of this long-enigmatic taxon.

Ornithomimosauria: A monophyletic Ornithomimosauria has been universally recovered in recent phylogenetic analyses, but few analyses have included a large suite of ornithomimosaurian taxa and those that do often disagree on the relationships of these species.

The current study finds *Pelecanimimus* (and *Nqwebasaurus*) at the base of Ornithomimosauria, followed by *Shenzhousaurus*, and then a clade of more derived ornithomimosaurs that includes all other known taxa. Some published studies also find *Pelecanimimus* at or near the base of Ornithomimosauria (e.g., Kobayashi and Lü 2003; Makovicky et al. 2004, 2010; Turner et al. 2012 and previous TWiG analyses), but several other

analyses have placed *Pelecanimimus* in a basal polytomy with many other taxa such as *Shenzhousaurus* and *Harpymimus* (Zanno et al. 2009; Choiniere et al. 2010a,b, 2012; Zanno 2010b; L. Xu et al. 2011). These uncertain relationships are due to character conflict between the cranial and postcranial skeleton: *Pelecanimimus* possesses a full suite of teeth, which are absent in other ornithomimosaurs, but has a hand that shares many derived character states with taxa like *Gallimimus* and *Struthiomimus* but not other taxa such as *Harpymimus*. Therefore, the dental characters indicate that all ornithomimosaurs other than *Pelecanimimus* (and *Nqwebasaurus*) can be united into a clade based on the apomorphic loss of teeth, whereas manual characters indicate that *Pelecanimimus* may be more closely related to taxa such as *Gallimimus* than to taxa such as *Shenzhousaurus* and *Harpymimus*. The results of the current analysis, which places *Pelecanimimus* basally, are congruent with the dental characters and indicate that the manual characters evolved homoplastically. However, resolution of the conflict between dental and manual characters requires additional work, and likely the discovery of new taxa with important character combinations.

The relationships among more derived ornithomimosaurs are poorly resolved in the current analysis. There is a major polytomy at the base of the clade that unites all taxa more derived than *Pelecanimimus*, *Nqwebasaurus*, and *Shenzhousaurus*. This basal polytomy includes several genera (*Archaeornithomimus*, *Beishanlong*, *Garudimimus*, *Harpymimus*, *Sinornithomimus*) and the lineage that leads to the derived clade of *Anserimimus*, *Gallimimus*, *Ornithomimus*, *Qiupalong*, and *Struthiomimus*. The relationships of taxa such as *Harpymimus* and *Garudimimus* differ among published studies, although many (but not all) studies find *Garudimimus* more closely related to *Gallimimus* and *Ornithomimus*-like taxa than is *Harpymimus* (Kobayashi and Lü 2003; Makovicky et al. 2004, 2010; Choiniere et al. 2010a, b;

L. Xu et al. 2011; Turner et al. 2012 and previous TWiG studies). Other studies, however, report a similar polytomy to that recovered here (e.g., Zanno et al. 2009; Zanno 2010b; Choiniere et al. 2012). Most published studies do not include the full suite of taxa employed here, and the polytomy in the current analysis indicates that taxa such as *Archaeornithomimus*, *Beishanlong*, and *Sinornithomimus* contribute to character conflicts in this region of the tree. Unfortunately, cranial material is currently unknown for some of these taxa (e.g., *Archaeornithomimus*, *Beishanlong*), and this likely causes some of the uncertainty in this part of the tree.

It is largely agreed upon that *Anserimimus*, *Gallimimus*, *Ornithomimus*, and *Struthiomimus* form a clade of derived taxa exclusive of more basal forms such as *Harpymimus*, *Garudimimus*, and *Pelecanimimus*, as this result has been recovered in nearly every published study (e.g., Kobayashi and Lü 2003; Makovicky et al. 2004, 2010; Choiniere et al. 2010a; L. Xu et al. 2011; Turner et al. 2012 and previous TWiG studies). One slight exception is the analysis presented by Zanno et al. (2009) and Zanno (2010b), which finds *Anserimimus*, *Struthiomimus*, and *Ornithomimus* as a clade but places *Gallimimus* within a large basal polytomy. Zanno et al. (2009), however, also presented an agreement subtree (in which the wildcard taxon *Pelecanimimus* is not included) that placed *Gallimimus* in the *Anserimimus* + *Ornithomimus* + *Struthiomimus* clade, indicating substantial underlying character support for this relationship in the dataset. The recent study of L. Xu et al. (2011) also showed the newly described taxon *Qiupalong* to belong to the *Ornithomimus* and *Gallimimus* clade. The existence of this derived clade, in summary, can be considered a consensus result.

There is debate about the interrelationships of taxa within the *Anserimimus* + *Gallimimus* + *Ornithomimus* + *Struthiomimus* clade, however, with previous studies often finding all members to fall into a polytomy (e.g., Makovicky et al. 2004, 2010; Choiniere et al. 2010a,

2012). TWiG studies such as Turner et al. (2007a, 2012), as well as the Zanno et al. (2009) and Zanno (2010b) analyses that included a large amount of TWiG data, have found support for an *Ornithomimus* + *Anserimimus* grouping within this subclade, whereas Kobayashi and Lü (2003) and L. Xu et al. (2012) have recovered subclades of *Ornithomimus* + *Struthiomimus* and *Gallimimus* + *Anserimimus*. This latter result is found here. The current analysis also places the Asian taxon *Qiupalong* within the *Ornithomimus* + *Struthiomimus* subclade, consistent with the results of L. Xu et al. (2011), until now the only published study to have included *Qiupalong*.

Basal Maniraptora: The current analysis returns poor resolution at the base of Maniraptora, as alvarezsauroids, therizinosauroids, and the clade of Oviraptorosauria + Paraves fall into a polytomy. Because the interrelationships of these groups are largely outside the scope of this dissertation they will not be commented on extensively here.

Many previous versions of the TWiG matrix recovered a sister group relationship of Therizinosauroidea and Oviraptorosauria, but the current analysis agrees with recent studies (e.g., Zanno et al. 2009; Turner et al. 2012) that do not recover such a clade. As discussed by Zanno et al. (2009) and Zanno (2010b), this is because recent discoveries of basal oviraptorosaurs and therizinosaurs illustrate that several characters once thought to be shared by these two groups are lacking in basal members of each clade and therefore likely evolved independently. The position of alvarezsauroids is labile in recent phylogenetic studies. They are found to be the basal-most maniraptorans (not counting *Ornitholestes*) in studies such as Senter (2011), Choiniere et al. (2012), Turner et al. (2012), and previous TWiG analyses, but placed as more closely related to oviraptorosaurs and paravians than therizinosauroids by Senter (2007), Zanno et al. (2009), and Dal Sasso and Signore (2011). The current analysis is consistent with

both scenarios, as well as a scenario in which therizinosauroids and alvarezsauroids form a clade that is sister taxon to Oviraptorosauria + Paraves. The current analysis is not consistent with the results of Novas et al. (2012), who found alvarezsauroids to be the sister taxon to Paraves, and thus more closely related to birds than oviraptorosaurs. As with most every published analysis over the past decade, the current analysis also does not corroborate previous studies from the 1990s which placed alvarezsauroids as basal avialans (e.g., Perle et al. 1993). Nor is the current study consistent with Sereno's (2001) hypothesis that alvarezsauroids and ornithomimosaurs form a clade.

What is clear is that the newly discovered basal members of Alvarezsauroidea (*Haplocheirus*: Choiniere et al. 2010a) and Therizinosauroidea (*Falcarius*: Kirkland et al. 2005) are generally quite primitive in overall morphology compared to the drastically derived body plans of later members of their group, and similar in many features with basal ornithomimosaurs, *Ornitholestes*, and even more basal coelurosaurs. The current analysis shows that there is rampant homoplasy in this part of the phylogeny and current taxon and character sampling is not adequate to resolve relationships at the base of Maniraptora. Related to this problem is the major polytomy located one node closer to the root, which subsumes Maniraptora, Ornithomimosauria, Compsognathidae, and *Ornitholestes*. Resolving these major polytomies should be a primary focus of future work.

Finally, the polytomy between dromaeosaurids, troodontids, and avialans at the base of Paraves indicates uncertainty in the relationships of birds and their closest relatives. Turner et al. (2012) and previous TWiG analyses have recovered a monophyletic Deinonychosauria, comprised of dromaeosaurids and troodontids, which is sister to Avialae. This is usually recovered in other analyses as well (e.g., Senter 2007, 2010, 2011; Zanno et al. 2009; Choiniere

et al. 2010a,b; Dal Sasso and Signore 2011). The recent analysis of Xu et al. (2011a), on the contrary, found the iconic *Archaeopteryx*—long considered the basal-most avialan—to be more closely related to dromaeosaurids and troodontids than avialans, but still recovered a monophyletic group of troodontids and dromaeosaurids that is sister taxon to Avialae. The current analysis indicates that troodontids may be more closely related to avialans than are dromaeosaurids, or that dromaeosaurids and avialans comprise a clade exclusive of troodontids. Ongoing work by Rui Pei, Mark Norell, and others in the Theropod Working Group will hopefully resolve this portion of coelurosaur phylogeny based on the analysis of several important new specimens.

Character Conflict and Uncertainty: The current analysis, in concert with previous studies, indicates that several major relationships among basal coelurosaurs are consistently found and well supported. Among these are the basal position of taxa like *Zuolong* and *Tugulusaurus*, the placement of tyrannosauroids as the most basal major coelurosaur subclade, the tyrannosauroid affinities of *Guanlong* and *Dilong*, and the existence of an ornithomimosaur + maniraptoran clade. But many areas of uncertainty still remain, most notably the relationships of clades that fall into two major polytomies: one consisting of Ornithomimosauria, Compsognathidae, *Ornitholestes*, and Maniraptora, and the other one node crownward (at the base of Maniraptora) and consisting of Alvarezsauroidea, Therizinosauroidea, and the Oviraptorosauria + Paraves clade.

In these cases of uncertainty, the great increase in taxon and character sampling in the current analysis has only served to muddy the picture and reveal hitherto unrecognized character conflict. Interestingly, major alternative hypotheses of relationships reported by previous

studies—such as the position of compsognathids as either intermediate between tyrannosauroids and ornithomimosaurs or as basal maniraptorans—are equally parsimonious in the current study. This is likely because the current dataset includes a broad sample of characters from previous studies. This indicates that disagreements between previous studies were caused by genuine character conflicts—for example, there really are characters placing compsognathids as intermediate between tyrannosauroids and ornithomimosaurs, but also characters linking compsognathids with maniraptorans. Although careful study of specimens and constant reanalysis, redescription, and recomparisons will always reveal new character data, we may be getting to a point where the addition of new characters, which are mostly ever-finer subtleties of anatomy, may not hold the key to better resolving coelurosaur phylogeny. The addition of more characters instead seems to cause a greater degree of homoplasy. Instead, it is likely that resolution may only come with the discovery of new taxa with unique character combinations.

Implications for Early Coelurosaur Evolution

The phylogeny reported here provides an explicit framework for studying the evolution of coelurosaurs in general, and especially the early evolution of the clade.

Coelurosaurs originated by the Middle Jurassic (Bathonian), approximately 168-165 million years ago. The two oldest known coelurosaurs, the basal tyrannosauroids *Kileskus* (Averianov et al. 2010) and *Proceratosaurus* (Rauhut et al. 2010), are known from this time. The entire Middle Jurassic is a fairly poorly sampled time in dinosaur evolution (Barrett et al. 2009), so it is likely that coelurosaurs originated earlier than their first fossil appearances, and that much of the early history of the clade is unrecorded (thus far) in the fossil record. This is strkingly

corroborated by a cursory look at ghost lineages on the phylogeny. *Bicentenaria*, which is found here to be the most basal coelurosaur, dates from the Late Cretaceous (Cenomanian, ca. 99.6-93.5 million years ago: Novas et al. 2012). This means that, if the phylogeny is correct, there is a minimum ghost lineage of at least 65 million years linking *Bicentenaria* to the fossil calibrated origination date of Coelurosauria. There is also a long ghost lineage linking the basal taxon *Tugulusaurus* to the base of Coelurosauria, but because *Tugulusaurus* may be up to 140 million years old this ghost lineage may potentially be as short as 25 million years long. In any case, both *Bicentenaria* and *Tugulusaurus* most likely are the only currently known representatives of basal coelurosaur lineages that were present during the early history of the group and persisted, likely at low diversity, deep into the Cretaceous.

The early history of tyrannosauroids was once one of the great mysteries of coelurosaurian evolution. The most familiar tyrannosauroids are colossal, megapredators such as *Tyrannosaurus* and *Albertosaurus* that lived during the final 20 million years of the Cretaceous. For many decades these were the only known members of the group and little was known about the origin and development of the unusual tyrannosaurid bauplan. Beginning in the early 1990s cladistic analyses began to place tyrannosauroids among coelurosaurs and over the next two decades most analyses consistently found this group to be the most basal, or one of the most basal, major coelurosaurian subclades. This led to an obvious conundrum: almost all tyrannosauroids were known from the latest Cretaceous and the group must have originated much earlier, up to 65 million years before the evolution of iconic species such as *T. rex*. The recent discovery of Middle-Late Jurassic tyrannosauroids such as *Guanlong* and *Kileskus* (Xu et al. 2006; Averianov et al. 2010), as well as the redescription of *Proceratosaurus* as a basal tyrannosauroid (Rauhut et al. 2010), has largely filled this once lengthy stretch of missing fossil

record. Furthermore, these taxa show that tyrannosauroids originated as small-bodied animals and for most of their evolutionary history, until the final 20 million years of the Cretaceous, were mostly moderate-sized predators about the size of a human, which lived in the shadow of other giant predators that belonged to more primitive theropod clades (Brusatte et al. 2010a,d). These early tyrannosauroids had cursorial body proportions, indicating a relatively high level of locomotor ability, and had elongate forearms that could be swung in a wide range of motion and that were capped with three or four digits. The classic *Tyrannosaurus*-like body plan—characterized by enormous size (up to 6 tons in mass), less cursorisal limb proportions, and reduced forelimbs with two digits—seems to have evolved only during the very end of the Cretaceous, beginning in or slightly prior to the Campanian. It was only at this point that tyrannosauroids were the unequivocal apex predators in all well-sampled dinosaur-bearing ecosystems in North America and Asia.

The current phylogeny reiterates the growing realization that the ancestral coelurosaur was likely a small-bodied animal, no more than a few meters in total head-tail length. The basal-most coelurosaurs in the current phylogeny—*Bicentenaria*, *Zuolong*, *Tugulusaurus*, basal tyrannosauroids—do not exceed a few meters in total length, and some are considerably smaller. This is in stark contrast to the large body sizes of immediate coelurosaur outgroups such as *Allosaurus* and *Sinraptor*, which grew to lengths of up to 10-12 meters and probably had masses surpassing a ton (Madsen 1976; Currie and Zhao 1993). A quantitative optimization of the ancestral coelurosaur body size, a comparison between the estimated size of the ancestral coelurosaur and close outgroups, and a study of body size trends across Coelurosauria must necessarily wait for a more complete theropod phylogeny with better outgroup sampling (but see Novas et al. 2012). With that being said, the size discrepancy between the earliest coelurosaurs

and their closest outgroups is striking, and size reduction may have been a major evolutionary event associated with the origin, early radiation, and evolutionary success of Coelurosauria.

As has been discussed in detail by Zanno et al. (2009), Zanno and Makovicky (2011), and many other authors, coelurosaurs exhibit a wide range of different dietary strategies and morphological features (especially those of the skull) that are likely related to diet. Because of several polytomies, the phylogeny presented here does not offer any substantial new insight into the dietary evolution of coelurosaurs beyond what has already been discussed by Zanno and colleagues. Depending on the resolution of polytomies and on how diet is optimized onto the phylogeny—which is never straightforward because diet is not necessarily divisible into discrete categories and is difficult to explicitly determine in fossil taxa—a non-carnivorous diet may have potentially developed once at or near the base of the Ornithomimosauria + Maniraptora clade, with one or more reversals to carnivory occurring later among paravians.

CONCLUSIONS

This chapter presents a comprehensive new phylogenetic analysis of coelurosaurian theropods, which is an updated version (and thus the latest iteration) of the long-standing Theropod Working Group analysis. The current study incoroporates a wealth of new taxa and character data into the TWiG matrix for the first time, most of which is relevant to basal (non-maniraptoran) coelurosaurs, which had previously been the subject of only cursory character and taxon sampling in TWiG studies. Much of this new information is novel data gleaned as part of this dissertation project, along with characters added from recent phylogenies of coelurosaurian ingroup clades such as ornithomimosaurs, alvarezsauroids, and therizinosauroids. All characters

new to this dissertation are described and illustrated. The full dataset was analyzed under parsimony and a strict consensus of most parsimonious source trees is presented. This phylogeny includes several well supported relationships and agrees with previous analyses in many aspects. As a result, it is argued that a consensus view of basal coelurosaurian relationships has emerged, including: 1) the monophyly of major subclades such as Tyrannosauroidea, Compsognathidae, and Ornithomimosauria; 2) the position of the singleton genera *Bicentenaria*, *Zuolong*, and *Tugulusaurus* near the base of Coelurosauria; 3) the placement of Tyrannosauroidea as the most basal major coelurosaurian subclade; 4) the inclusion of *Guanlong*, *Dilong*, and *Proceratosaurus* within Tyrannosauroidea; 5) the existence of a derived maniraptoran clade that includes alvarezsauroids, therizinosauroids, oviraptorosaurs, and paravians to the exclusion of ornithomimosaurs and tyrannosauroids. Remaining areas of uncertainty include the phylogenetic position of Compsognathidae and the singleton genus *Ornitholestes*, the relationships at the base of the Ornithomimosauria + Maniraptora clade and the base of Maniraptora itself, and the positions of the genera *Coelurus* and *Tanycolagreus*, although they are strongly supported as tyrannosauroids in the present analysis. The phylogeny reported here indicates that much of the early history of Coelurosauria has yet to be sampled in the fossil record, that coelurosaurs originated at small body size, that the evolution of the iconic *Tyrannosaurus*-like bauplan occurred only towards the end of the Cretaceous, and that non-carnivorous diets may have potentially evolved only once among coelurosaurs.

FIGURES

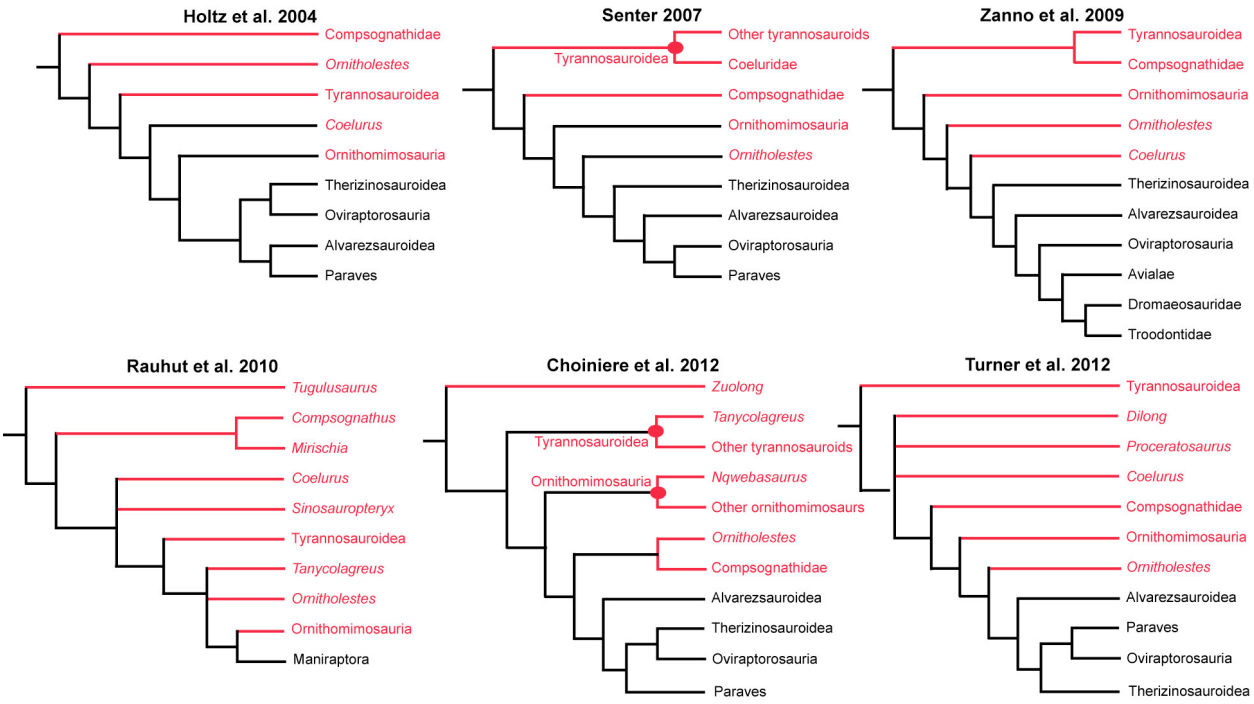

Figure 2-1. Six major recent analyses of coelurosaur phylogeny. Lineages in red denote the "basal coelurosaurs" (i.e., non-maniraptoran taxa) that are the primary focus of this dissertation. There is essentially no consistency among the relationships of basal coelurosaurs in these analyses.

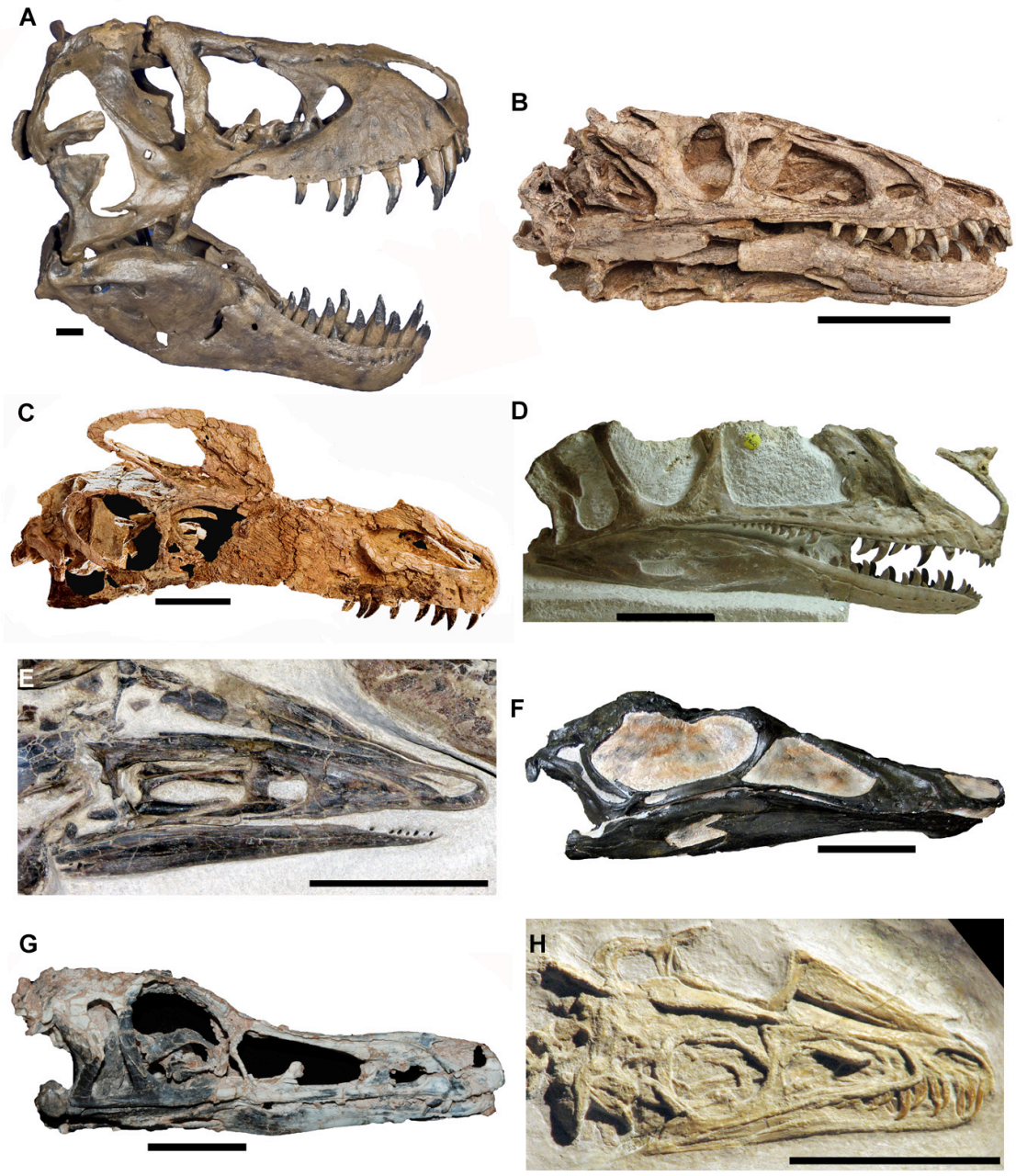

Figure 2-2. Monatage of the skulls of basal coelurosaurian theropods. *Tyrannosaurus rex*, BHI 3033 cast (A); *Dilong paradoxus*, IVPP V14243 (B); *Guanlong wucaii*, IVPP V14531 (C); *Proceratosaurus bradleyi*, NHMUK R4860 (D); *Shenzhousaurus orientalis*, NGMC 97-4-002 (E); *Struthiomimus altus*, RTMP 90.26.1 cast (F); *Zuolong salleei*, IVPP V15912 (G);

Juravenator starki, JME Sch 200. Photo in A courtesy of Larry Witmer; C from Brusatte et al. (2010), originally from I. Block, National Geographic stock; G courtesy of Jonah Choiniere. Scale bars equal 4 cm.

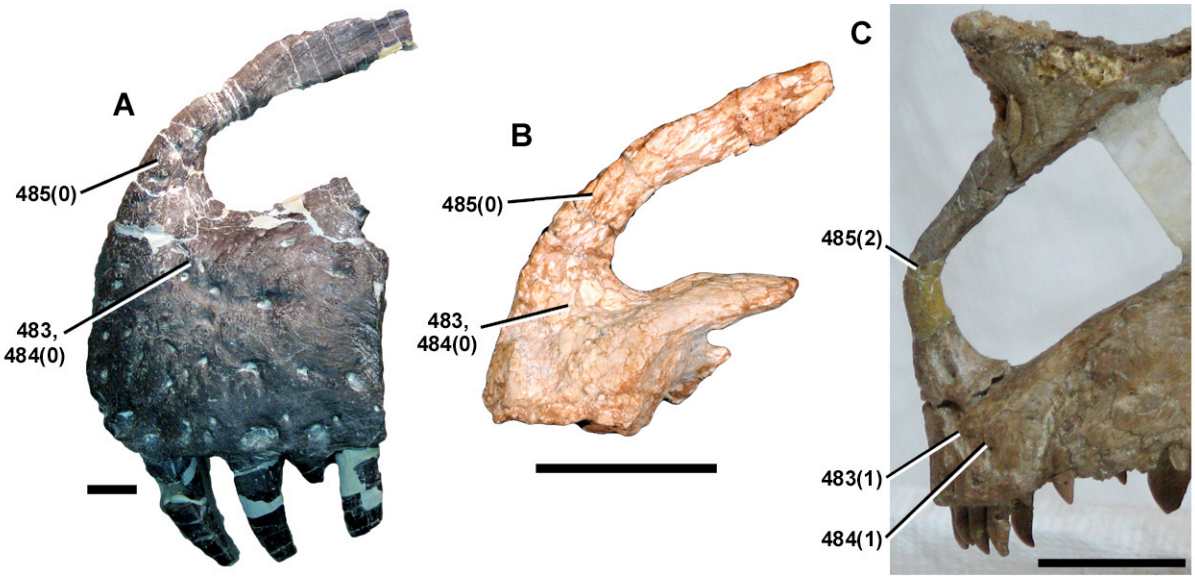

Figure 2-3. Premaxillae of theropod dinosaurs in left lateral view. *Allosaurus fragilis*, UMNH UUVP 5427 (reversed) (A); *Zuolong salleei*, IVPP V15912 (B); *Proceratosaurus bradleyi*, NHMUK R4860 (C). Photo B courtesy of Jonah Choiniere. Scale bars equal 2 cm.

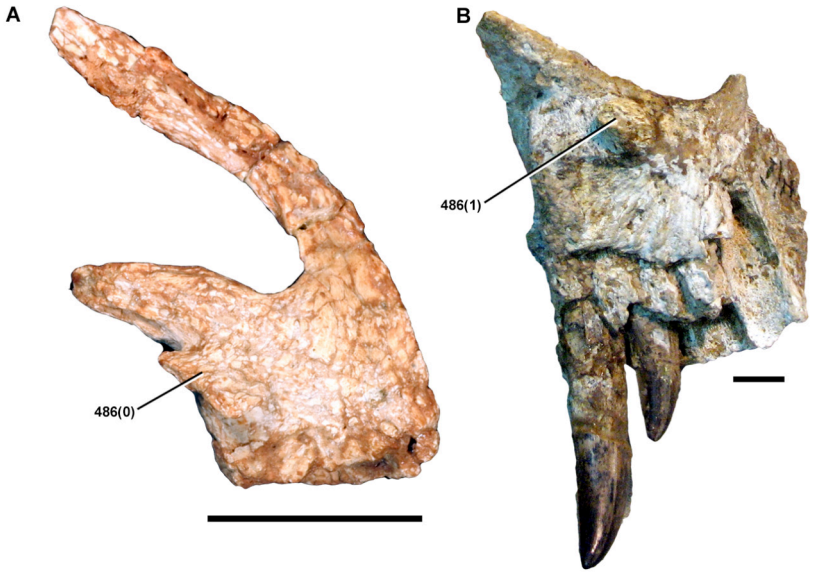

Figure 2-4. Premaxillae of theropod dinosaurs in left medial view. *Zuolong salleei*, IVPP V15912 (A); *Tarbosaurus bataar*, ZPAL MgD-I/5 (B). Scale bars equal 2 cm.

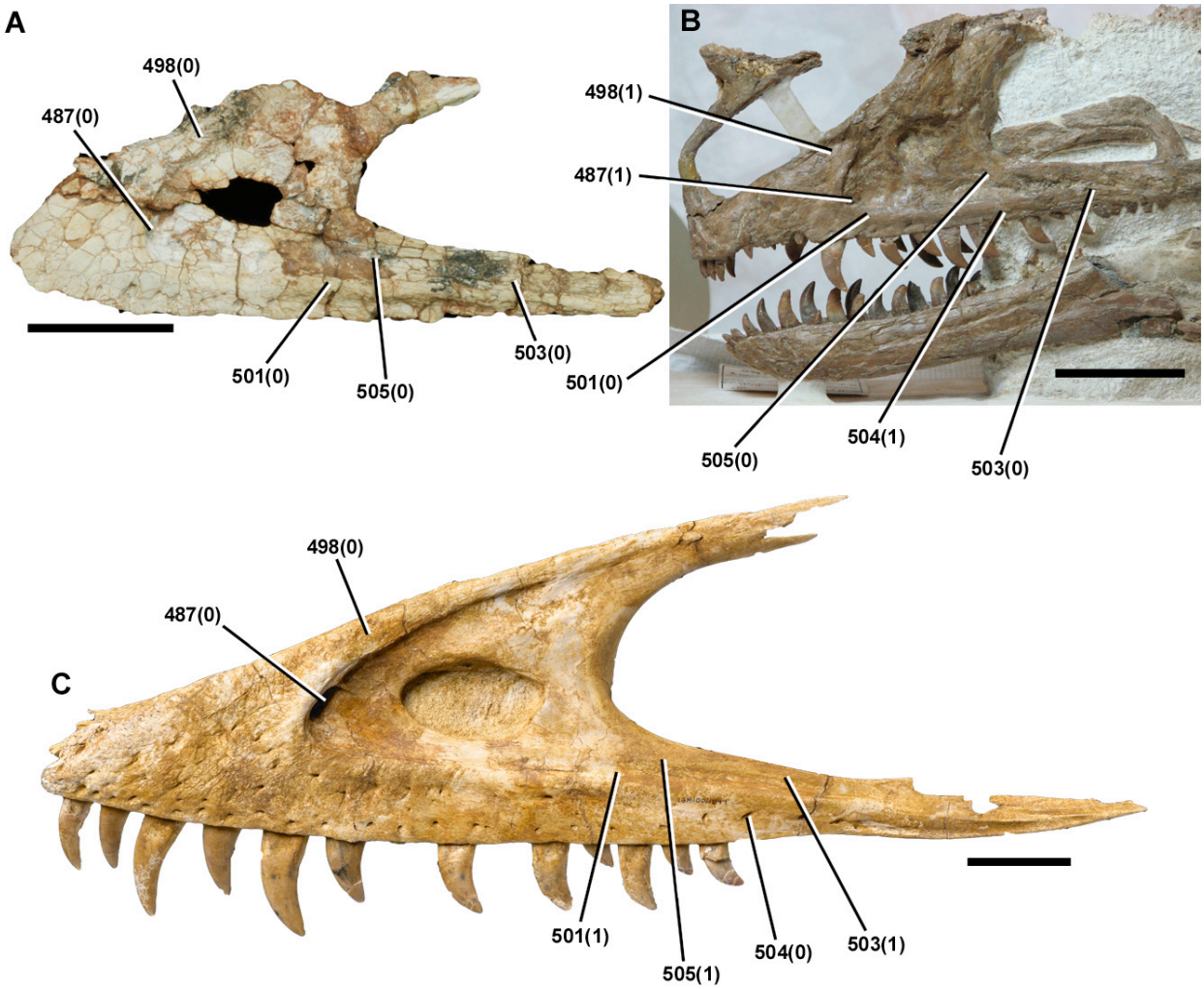

Figure 2-5. Maxillae of theropod dinosaurs in left lateral view. *Zuolong salleei*, IVPP V15912 (A); *Proceratosaurus bradleyi*, NHMUK R4860 (B); *Alioramus altai* IGM 100/1844 (C). Photo A courtesy of Jonah Choiniere, C by Mick Ellison. Scale bars equal 4 cm.

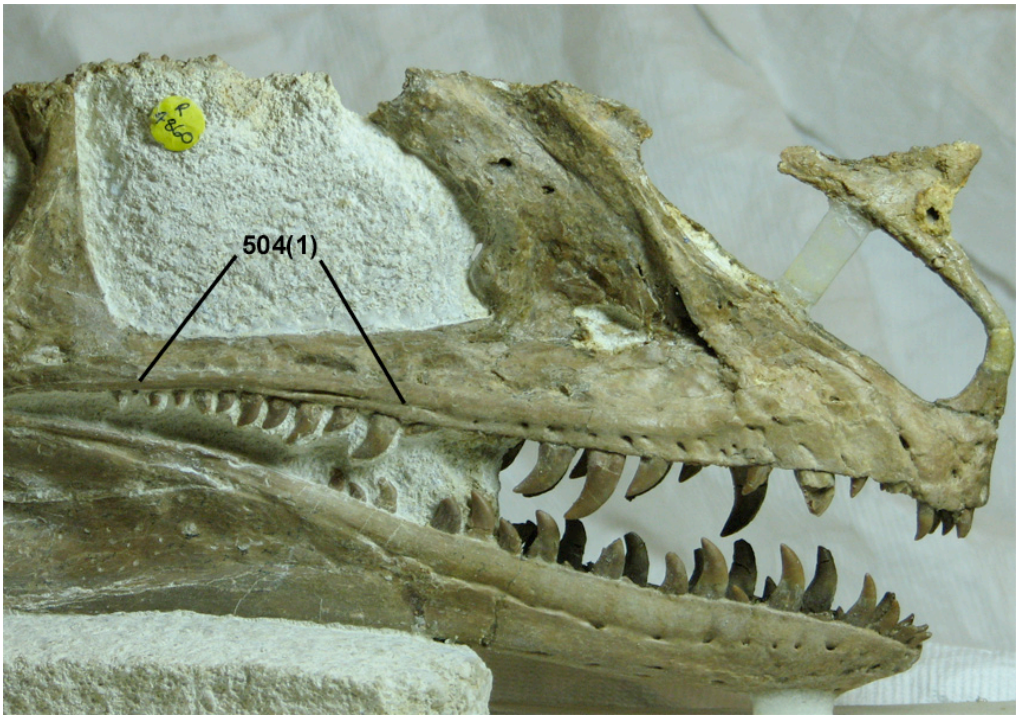

Figure 2-6. Anterior snout of *Proceratosaurus bradleyi* (NHMUK R4860) in right lateral view, showing the apomorphic condition of the primary row of maxillary neurovascular foramina transitioning into a deep groove posteriorly. See figure 4 for scale.

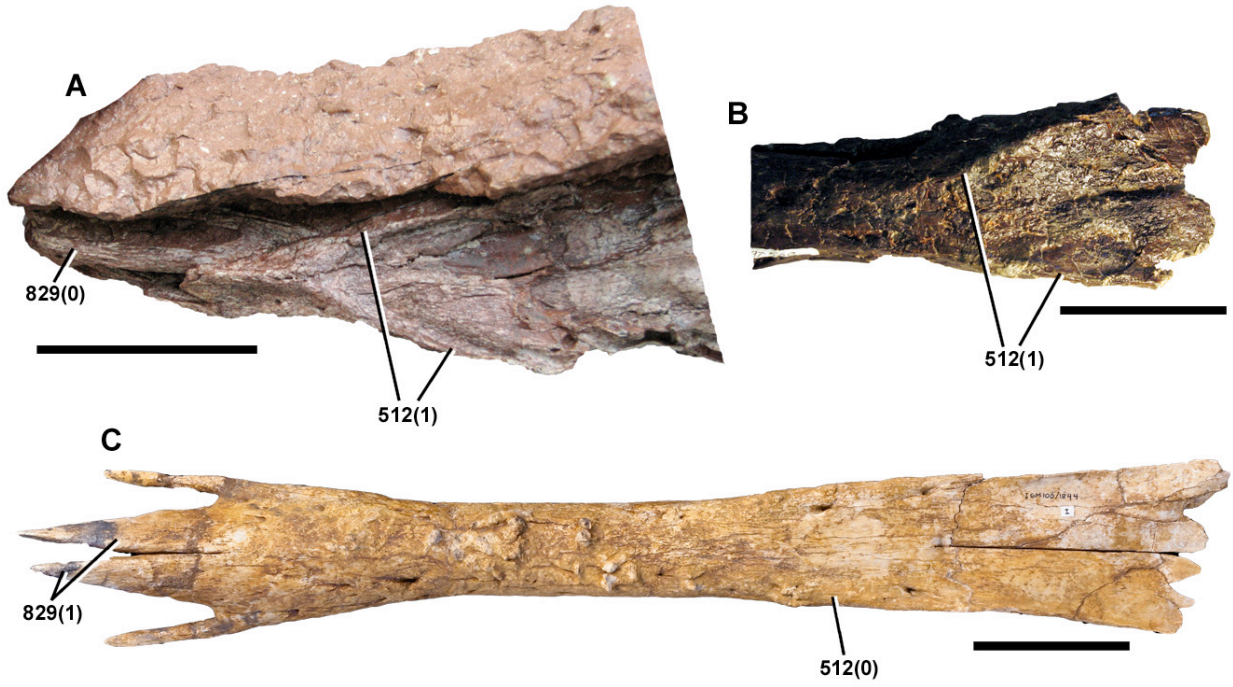

Figure 2-7. Nasals of theropod dinosaurs in dorsal view. *Dilong paradoxus*, IVPP V14243 (A); *Eotyrannus lengi*, MIWG 1997.550 (B); *Alioramus altai* IGM 100/1844 (C). Photo C by Mick Ellison. Scale bars equal 5 cm.

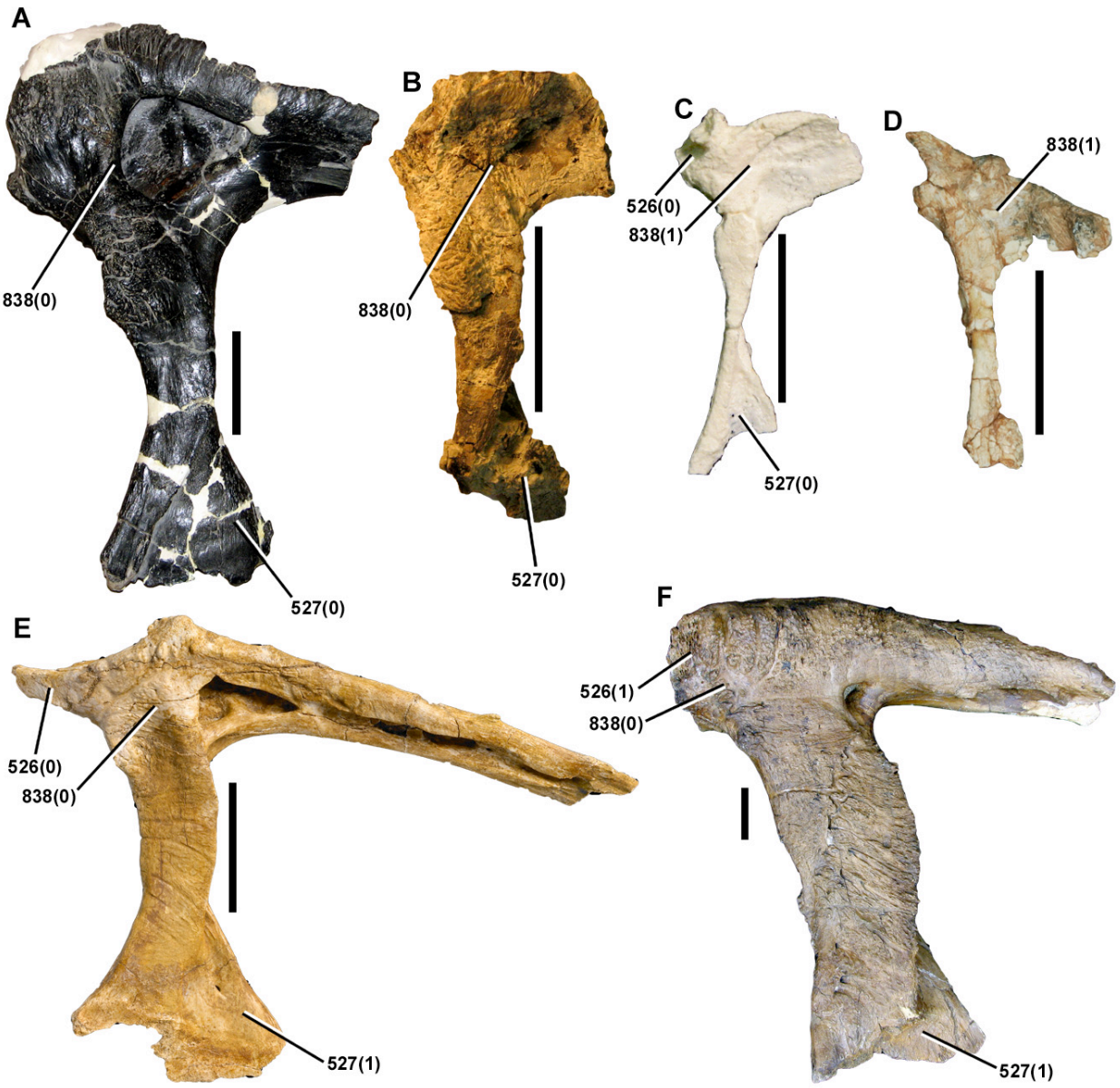

Figure 2-8. Lacrimals of theropod dinosaurs in right lateral view. *Allosaurus fragilis*, UMNH 6838 (A); *Eotyrannus lengi*, MIWG 1997.550 (B); *Tanycolagreus topwilsoni*, TPII 2000-09-29 cast (reversed) (C); *Zuolong salleei*, IVPP V15912 (D), *Alioramus altai* IGM 100/1844 (reversed) (E); *Tyrannosaurus rex*, CM 9380 (F). Photo D courtesy of Jonah Choiniere, E by Mick Ellison. Scale bars equal 4 cm.

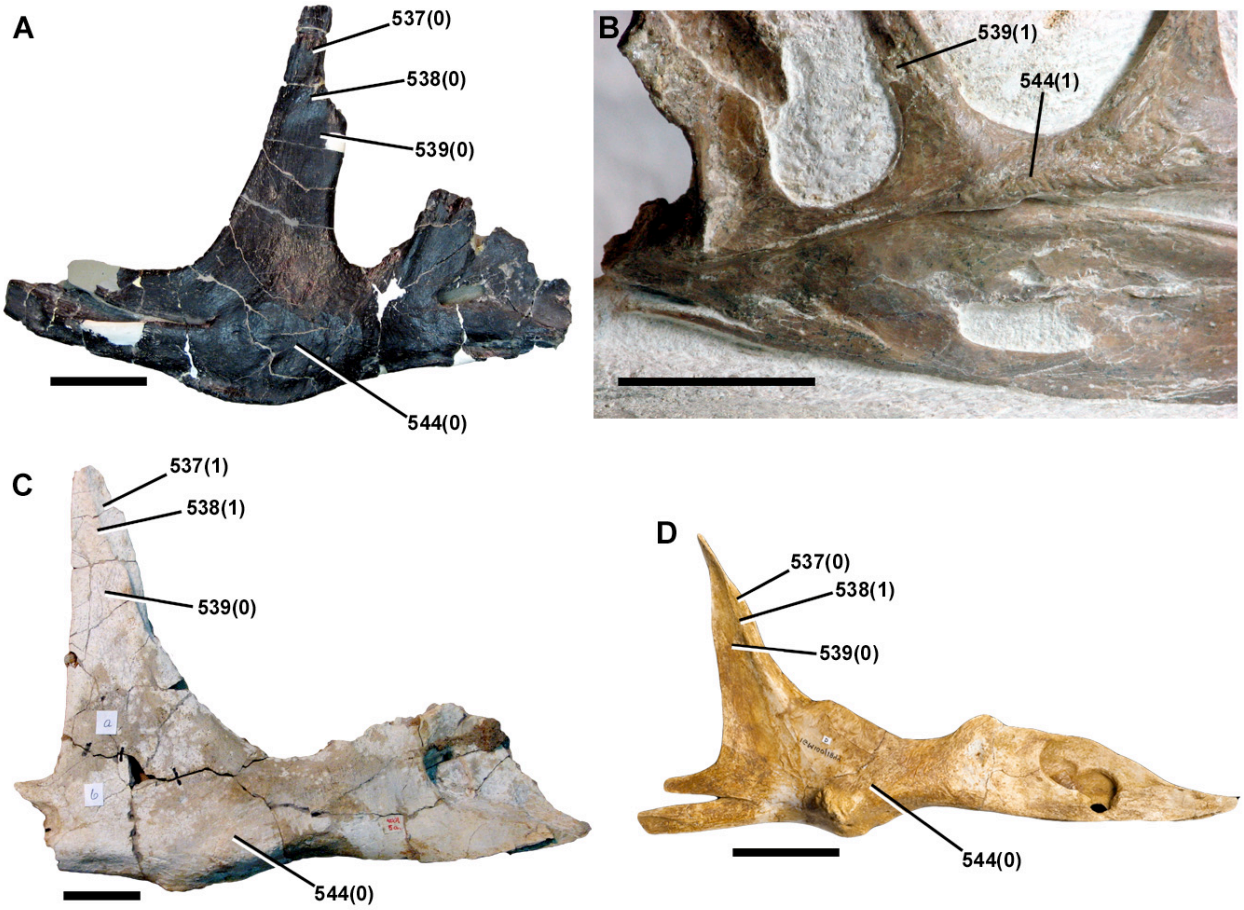

Figure 2-9. Jugals of theropod dinosaurs in right lateral view. *Allosaurus fragilis*, UMNH 3981 (reversed) (A); *Proceratosaurus bradleyi*, NHMUK R4860 (B); *Tarbosaurus bataar*, ZPAL MgD-I/175 (C); *Alioramus altai* IGM 100/1844 (reversed) (D). Photo D by Mick Ellison. Scale bars equal 4 cm.

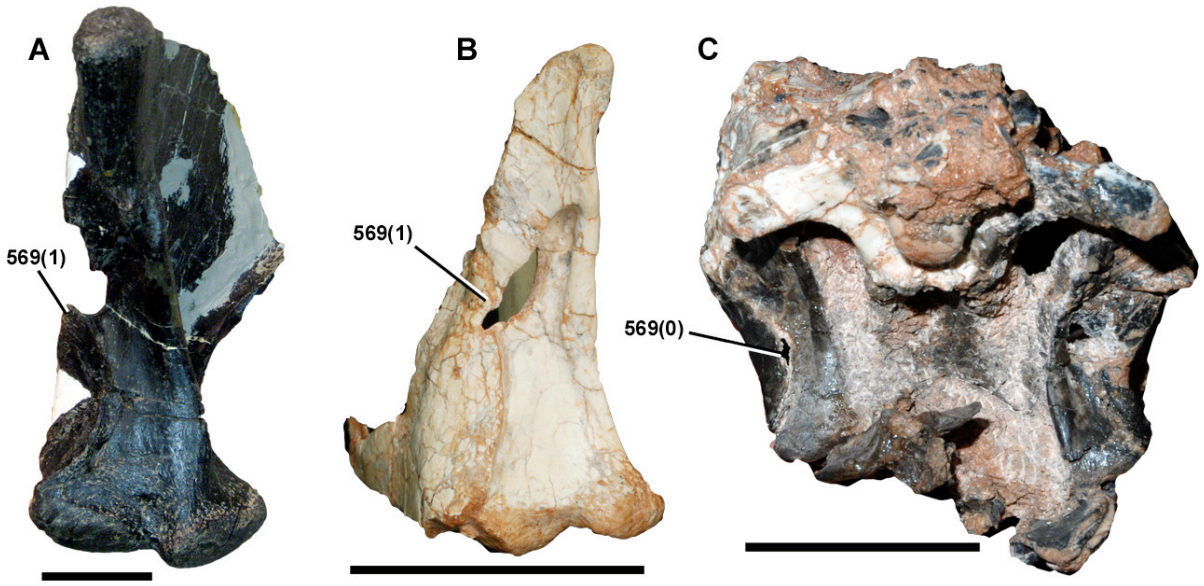

Figure 2-10. Quadrates (and in some cases surrounding bones) of theropod dinosaurs in posterior view. *Allosaurus fragilis*, UMNH VP9569 (A); *Zuolong salleei*, IVPP V15912 (B); *Haplocheirus sollers*, IVPP V15988 (C). Photos B and C courtesy of Jonah Choiniere. Scale bars equal 4 cm.

Figure 2-11. Orbital region of *Guanlong wucaii* (IVPP V14531) in left lateral view, showing an apomorphic condition of the prefrontal. Scale bar equals 4 cm.

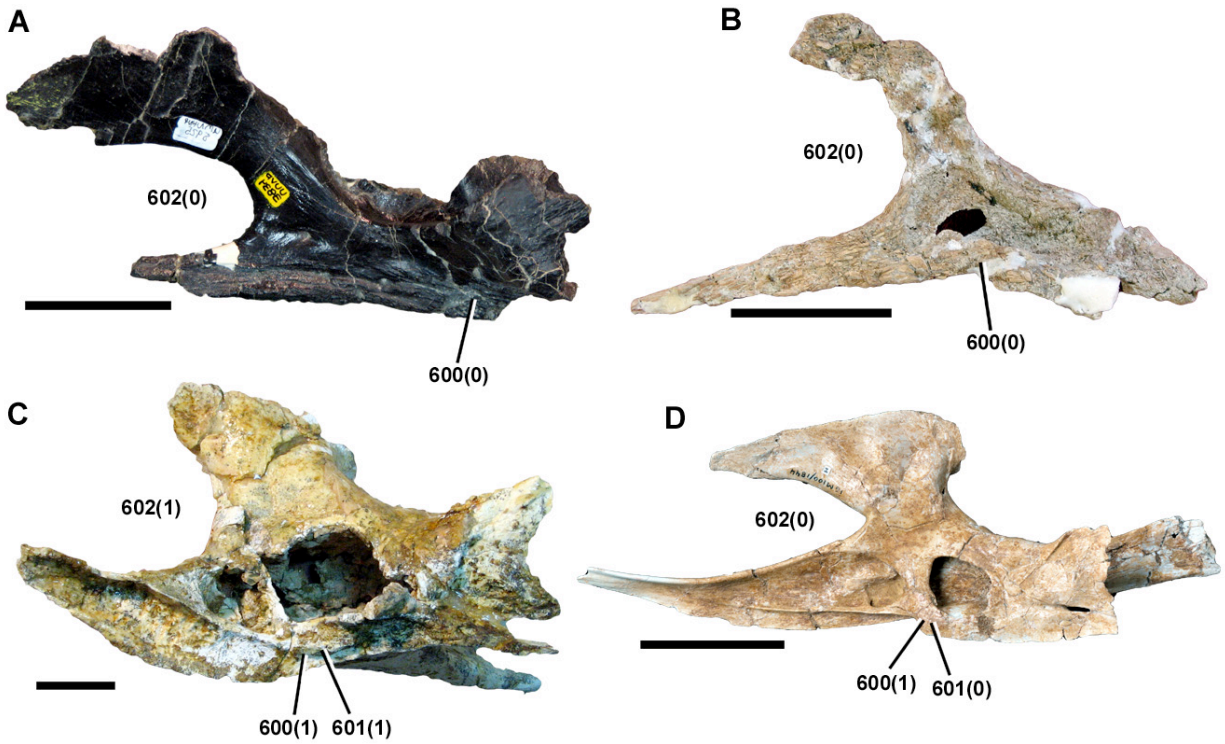

Figure 2-12. Palatines of theropod dinosaurs in left lateral view. *Allosaurus fragilis*, UMNH VP8925 (reversed) (A); *Austroraptor cabazai*, MML 195 (reversed) (B); *Tarbosaurus bataar*, ZPAL MgD-I/4 (C); *Alioramus altai* IGM 100/1844 (D). Photo D by Mick Ellison. Scale bars equal 4 cm.

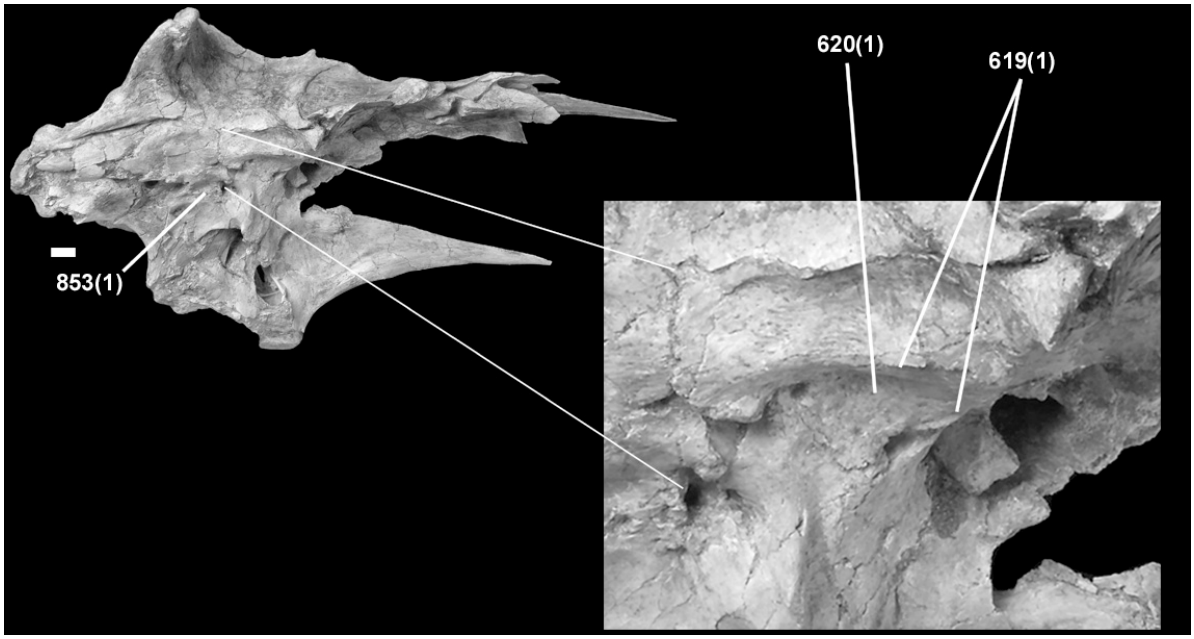

Figure 2-13. Braincase of *Alioramus altai* (IGM 100/1844) in right lateral view, with a closeup of the laterosphenoid and surrounding bones. Photos by Mick Ellison. Scale bar equals 2 cm.

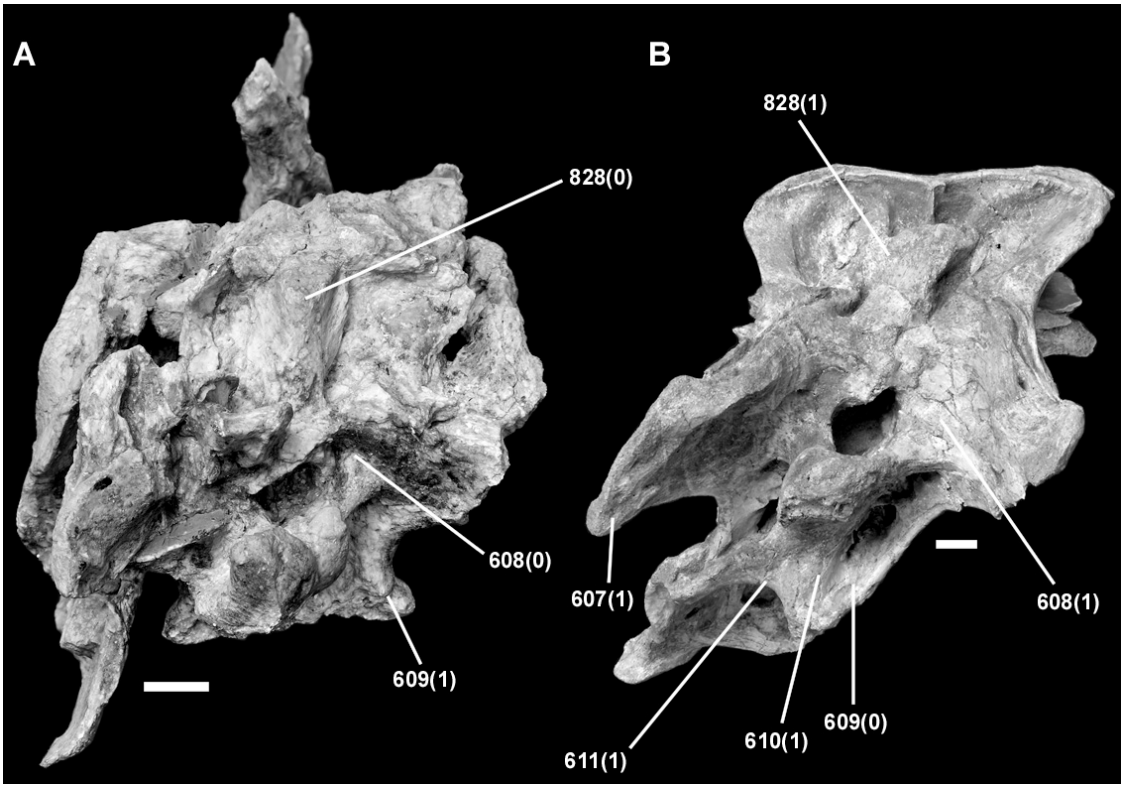

Figure 2-14. Braincases of theropod dinosaurs in posterior (occipital) view. *Guanlong wucaii*, IVPP V14531 (A); *Alioramus altai* IGM 100/1844 (B). Photos by Mick Ellison. Scale bars equal 2 cm.

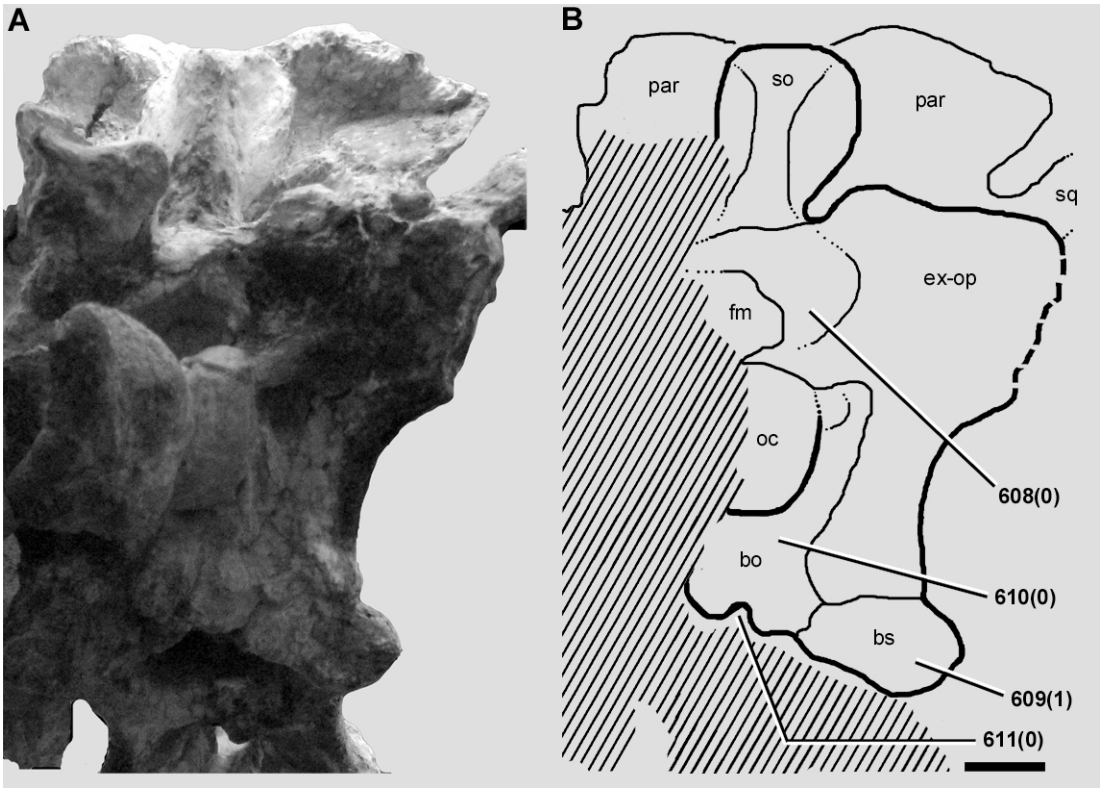

Figure 2-15. Braincase of *Guanlong wucaii* (IVPP V14531) in posterior (occipital view): photograph (A) and line drawing (B). Scale bars equal 2 cm. Abbreviations: bo, basioccipital; bs, basisphenoid; ex-op, exoccipital-opisthotic; fm, foramen magnum; oc, occipital condyle; par, parietal; so, supraoccipital; sq, squamosal.

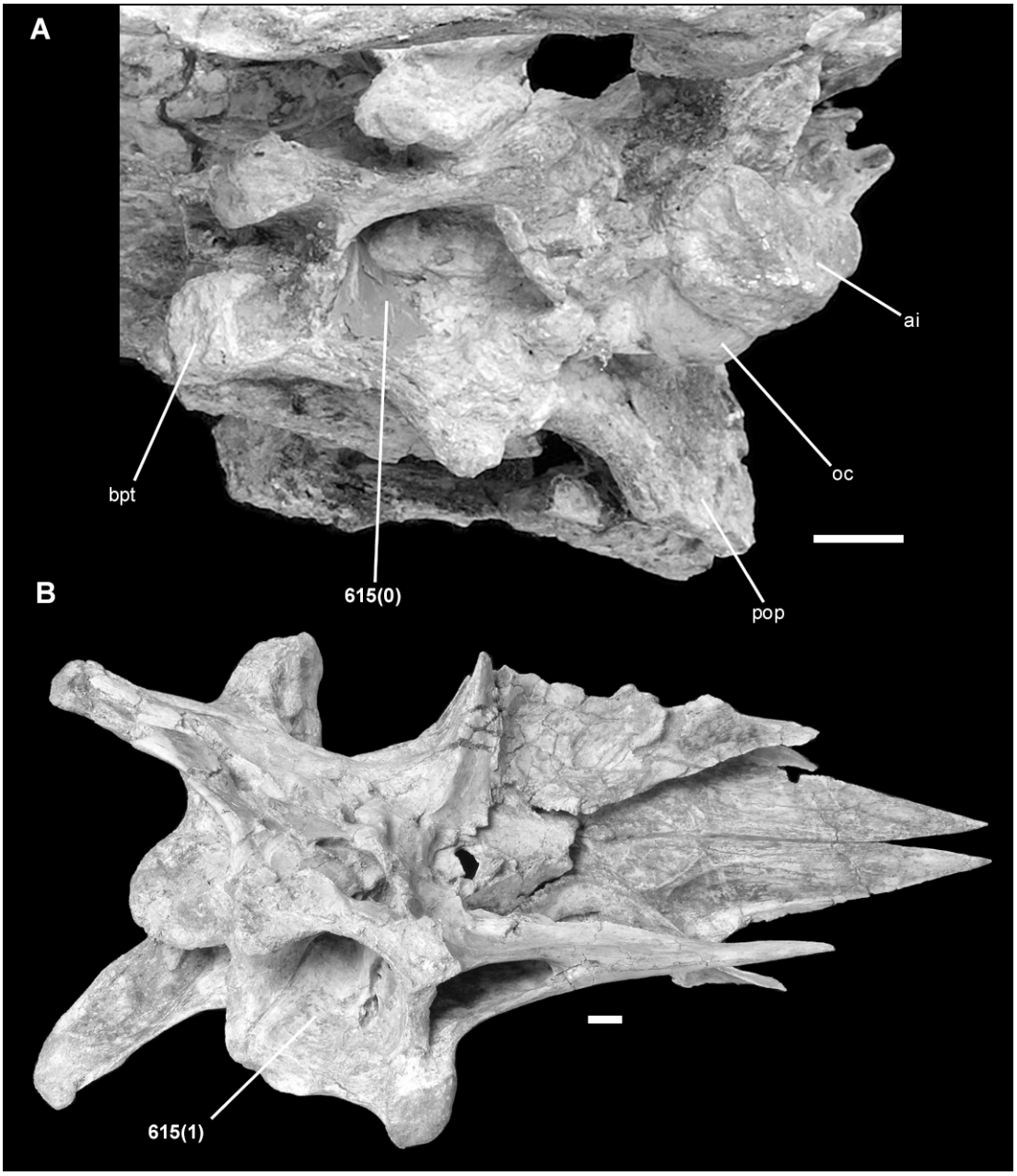

Figure 2-16. Braincases of theropod dinosaurs in ventral or oblique ventrolateral view. *Guanlong wucaii*, IVPP V14531 (A); *Alioramus altai* IGM 100/1844 (B). Photos by Mick Ellison. Scale bars equal 2 cm. Abbreviations, ai: axial intercentrum; bpt, basipterygoid process; oc, occipital condyle; pop, paroccipital process.

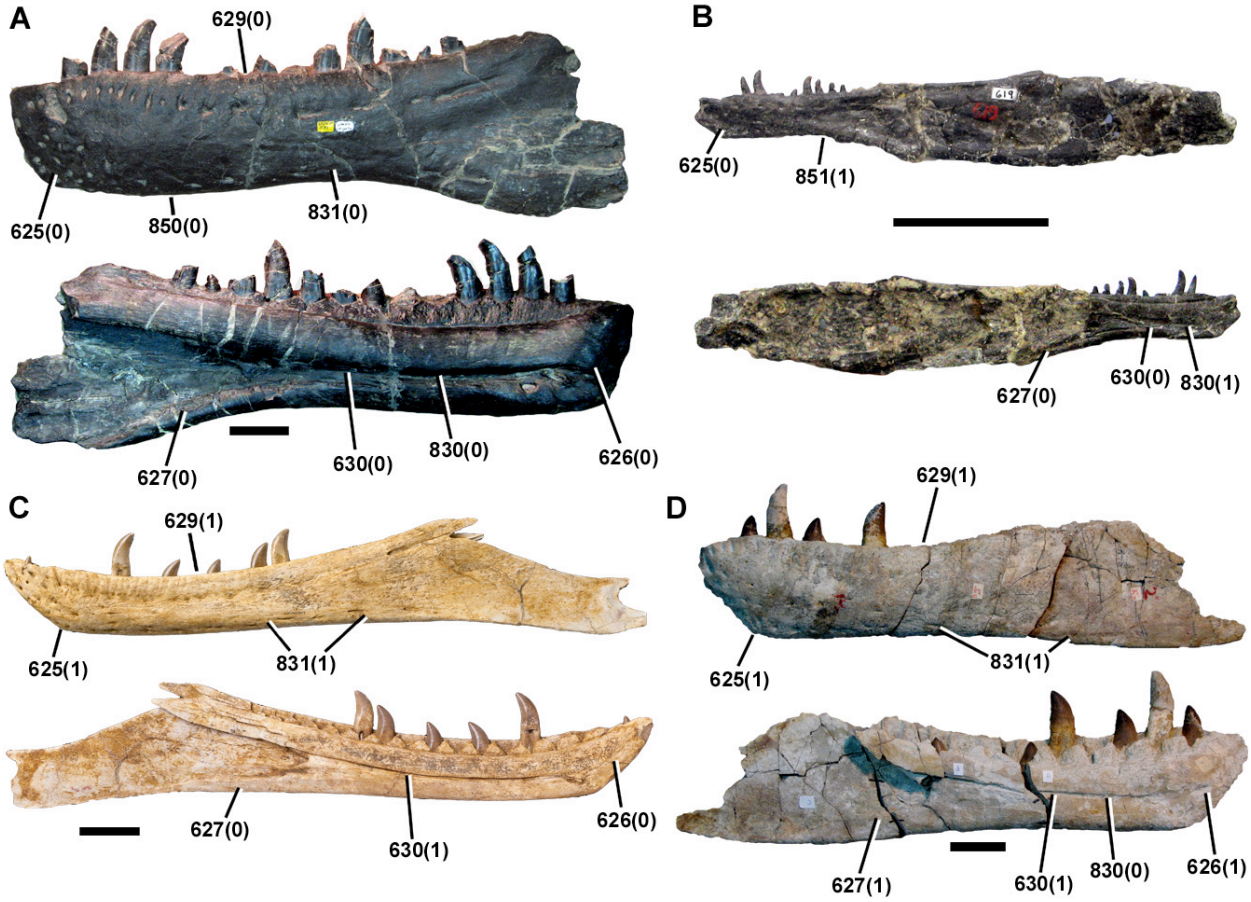

Figure 2-17. Dentaries of theropod dinosaurs in lateral (top of each pair) and medial (bottom of each pair) views. *Allosaurus fragilis*, UMNH VP6476 (A); *Ornitholestes hermanii*, AMNH FARB 619 (B); *Alioramus altai*, IGM 100/1844 (C); *Tarbosaurus bataar*, ZPAL MgD-I/175 (reversed) (D). Photos in C by Mick Ellison. Scale bars equal 4 cm.

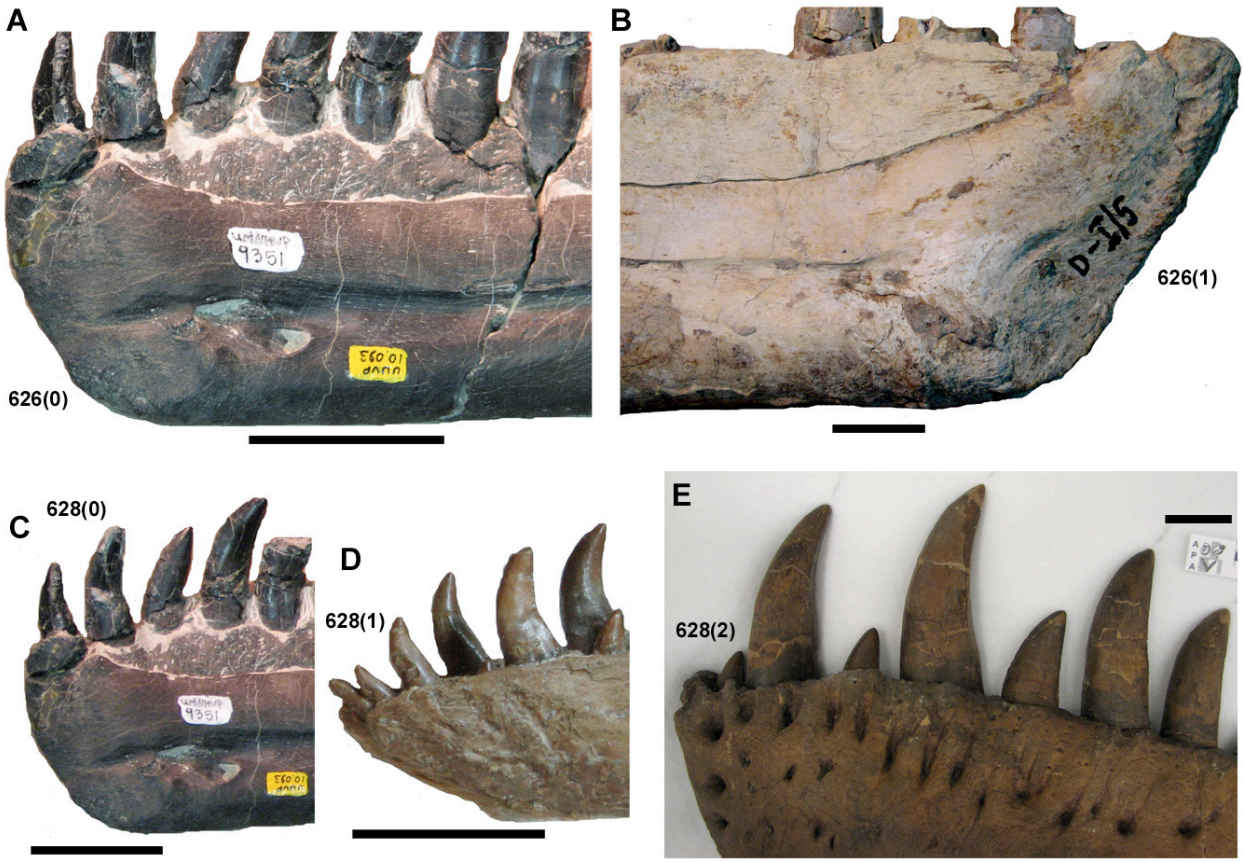

Figure 2-18. Dentaries of theropod dinosaurs in medial (A, B, C) and lateral (D, E) views. *Allosaurus fragilis*, UMNH VP9351 (A, C); *Tarbosaurus bataar*, ZPAL MgD-I/5 (B); *Proceratosaurus bradleyi*, NHMUK R4860 (D); *Tyrannosaurus rex*, CM 9380 (E). Scale bars equal 4 cm, except for that in D which equals 2 cm.

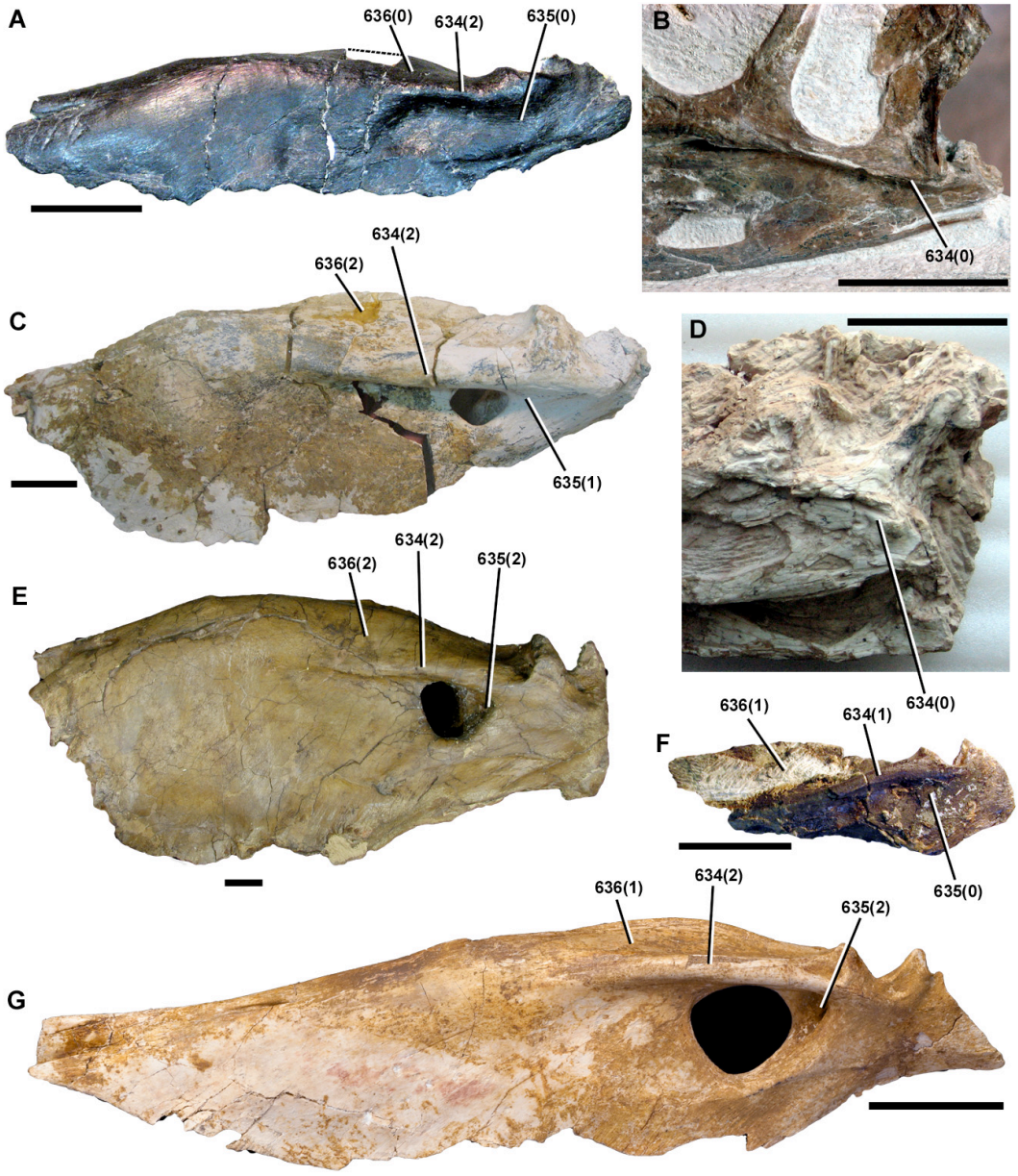

Figure 2-19. Surangulars of theropod dinosaurs in left lateral views. *Allosaurus fragilis*, UMNH UUVP 5902 (A); *Proceratosaurus bradleyi*, NHMUK R4860 (reversed) (B); *Tarbosaurus bataar*, ZPAL MgD-I/4 (reversed) (C); *Guanlong wucaii*, IVPP V14532 (D); *Tyrannosaurus rex*, CM 9380 (E); *Eotyrannus lengi*, MIWG 1997.550 (F); *Alioramus altai*, IGM 100/1844 (G). Photo G by Mick Ellison. Scale bars equal 4 cm.

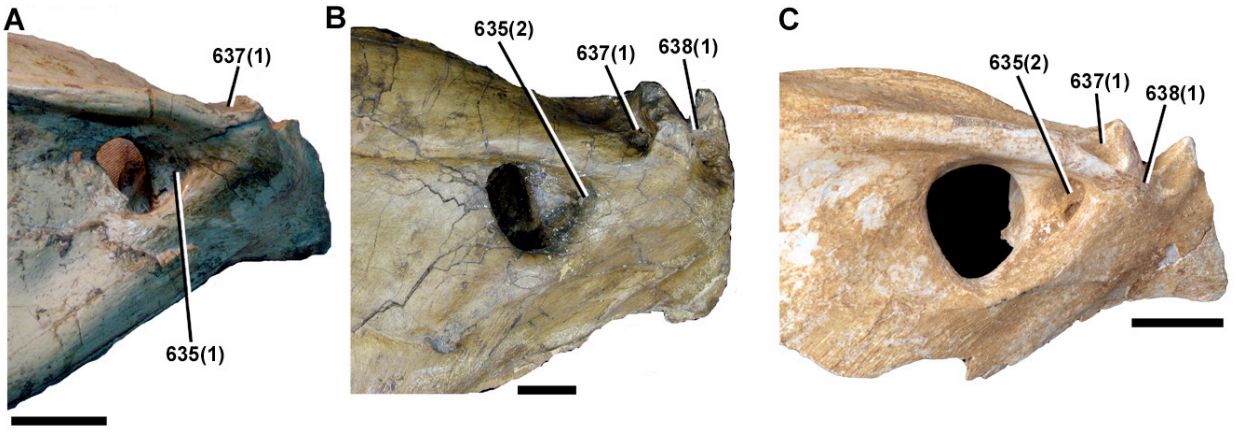

Figure 2-20. Surangulars of theropod dinosaurs in left anterolateral oblique views. *Tarbosaurus bataar*, ZPAL MgD-I/3 (A); *Tyrannosaurus rex*, CM 9380 (B); *Alioramus altai*, IGM 100/1844 (C). Photo C by Mick Ellison. Scale bars equal 4 cm, except for that in C which equals 2 cm.

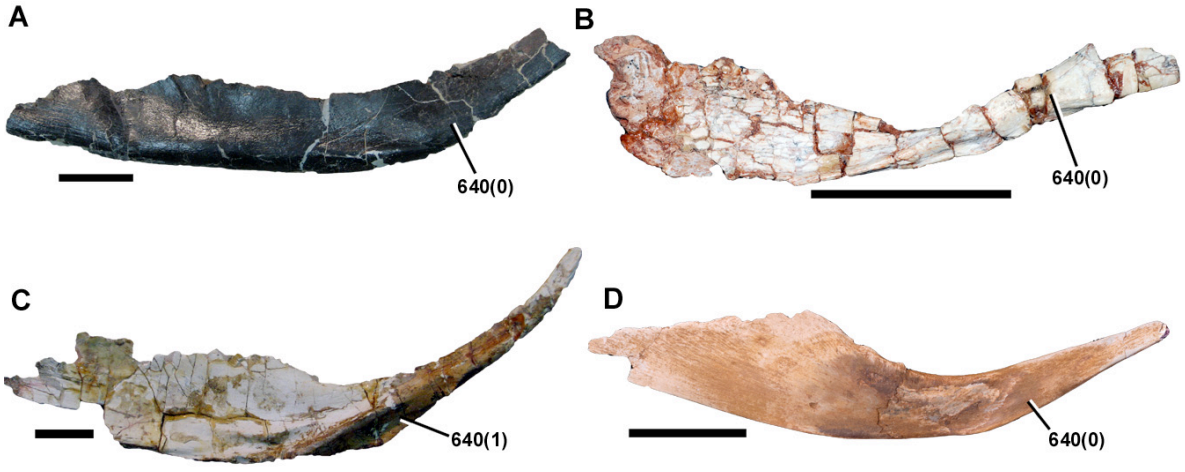

Figure 2-21. Angulars of theropod dinosaurs in lateral (A, D) and medial (B, C) views. *Allosaurus fragilis*, UMNH VP9311; *Zuolong salleei*, IVPP V15912 (B); *Tarbosaurus bataar*, ZPAL MgD-I/4 (C); *Alioramus altai*, IGM 100/1844 (D). Photo B courtesy of Jonah Choiniere and C by Mick Ellison. Scale bars equal 4 cm.

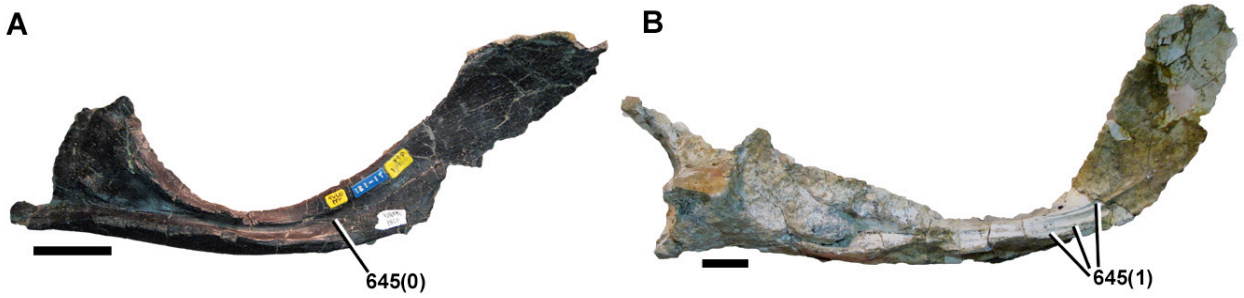

Figure 2-22. Prearticulars of theropod dinosaurs in lateral view. *Allosaurus fragilis*, UMNH VP9284; *Tarbosaurus bataar*, ZPAL MgD-I/4 (B). Photo B includes the fused articular. Scale bars equal 4 cm.

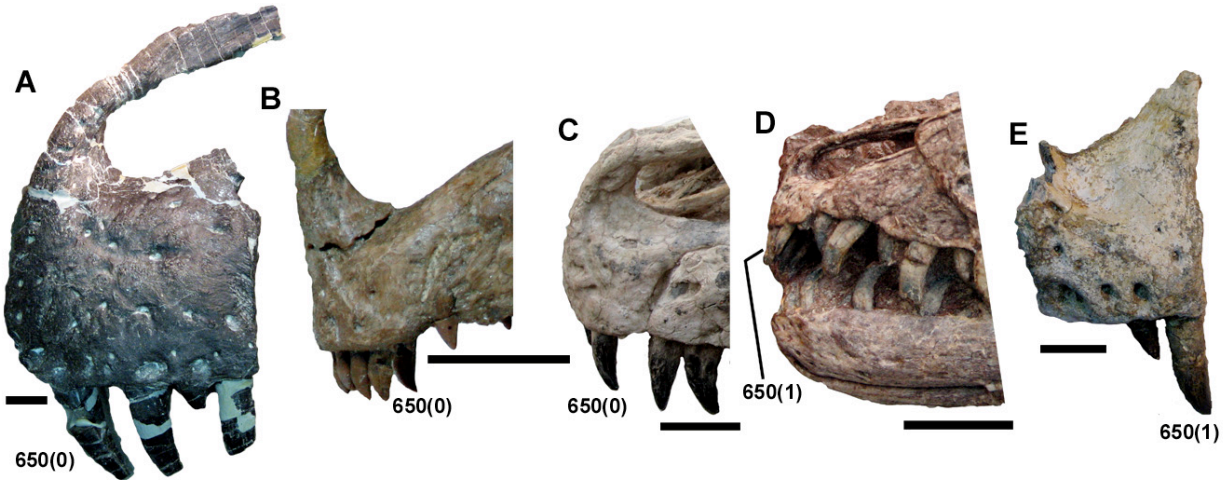

Figure 2-23. Premaxillary teeth of theropod dinosaurs in left lateral view. *Allosaurus fragilis*, UMNH UUVP 5427 (reversed) (A); *Proceratosaurus bradleyi*, NHMUK R4860 (B); *Guanlong wucaii*, IVPP V14531 (C); *Dilong paradoxus*, IVPP V14243 (D); *Tarbosaurus bataar*, ZPAL MgD-I/5 (reversed) (E). Scale bars equal 4 cm, except for those in A and E that equal 2 cm.

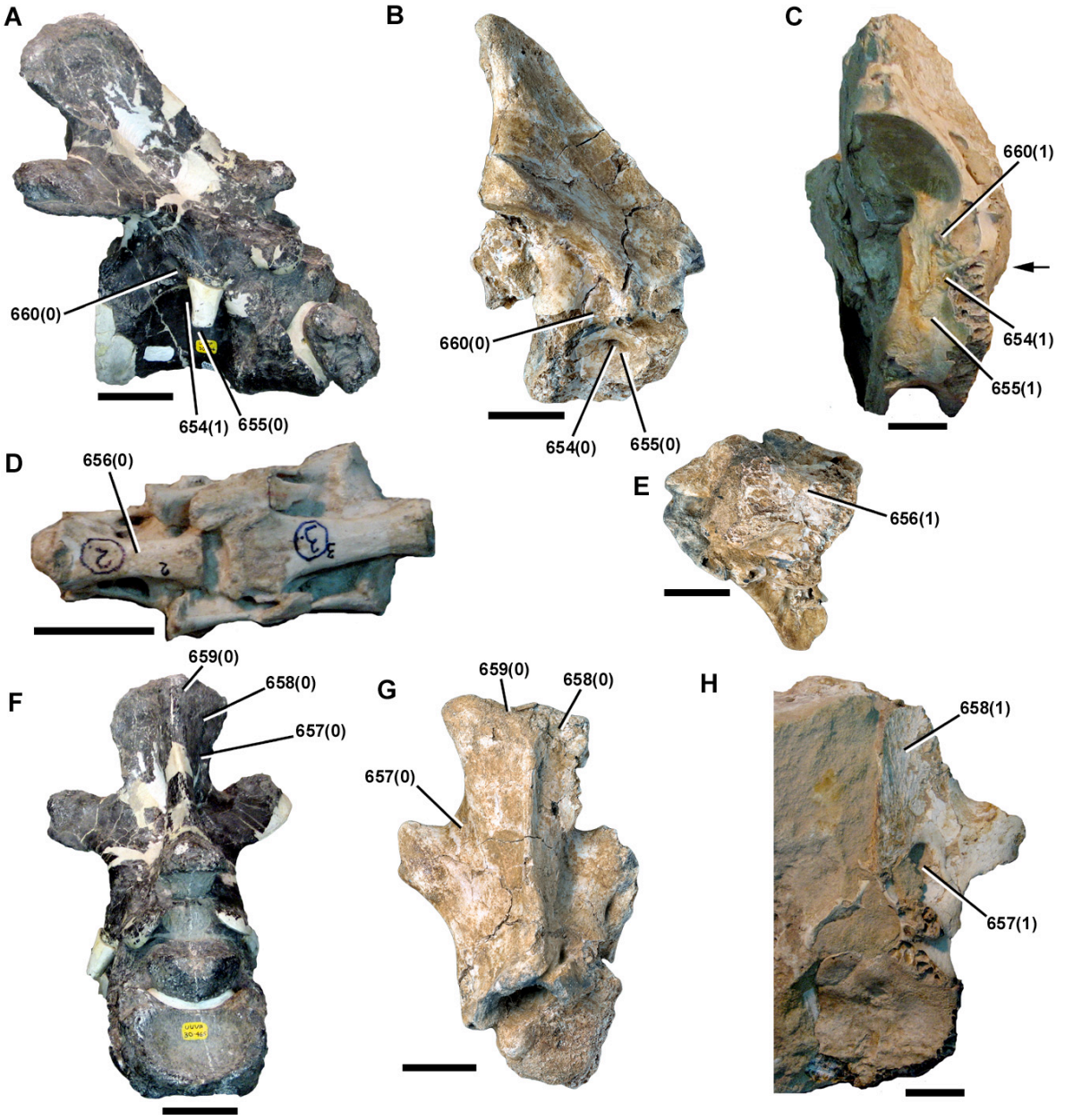

Figure 2-24. Axes of theropod dinosaurs in right lateral (A, B, C), ventral (D, E), and anterior (F, G, H) views. *Allosaurus fragilis*, UMNH VP30466 (A, F); *Alioramus altai*, IGM 100/1844 (B, E, G); *Tarbosaurus bataar*, ZPAL MgD-I/09 (reversed) (C, H); *Gallimimus bullatus*, ZPAL MgD-I/94 (D). Scale bars equal 4 cm for A, C, F, H; 2 cm for B, D, E, G. Arrow in C denotes neurocentral suture.

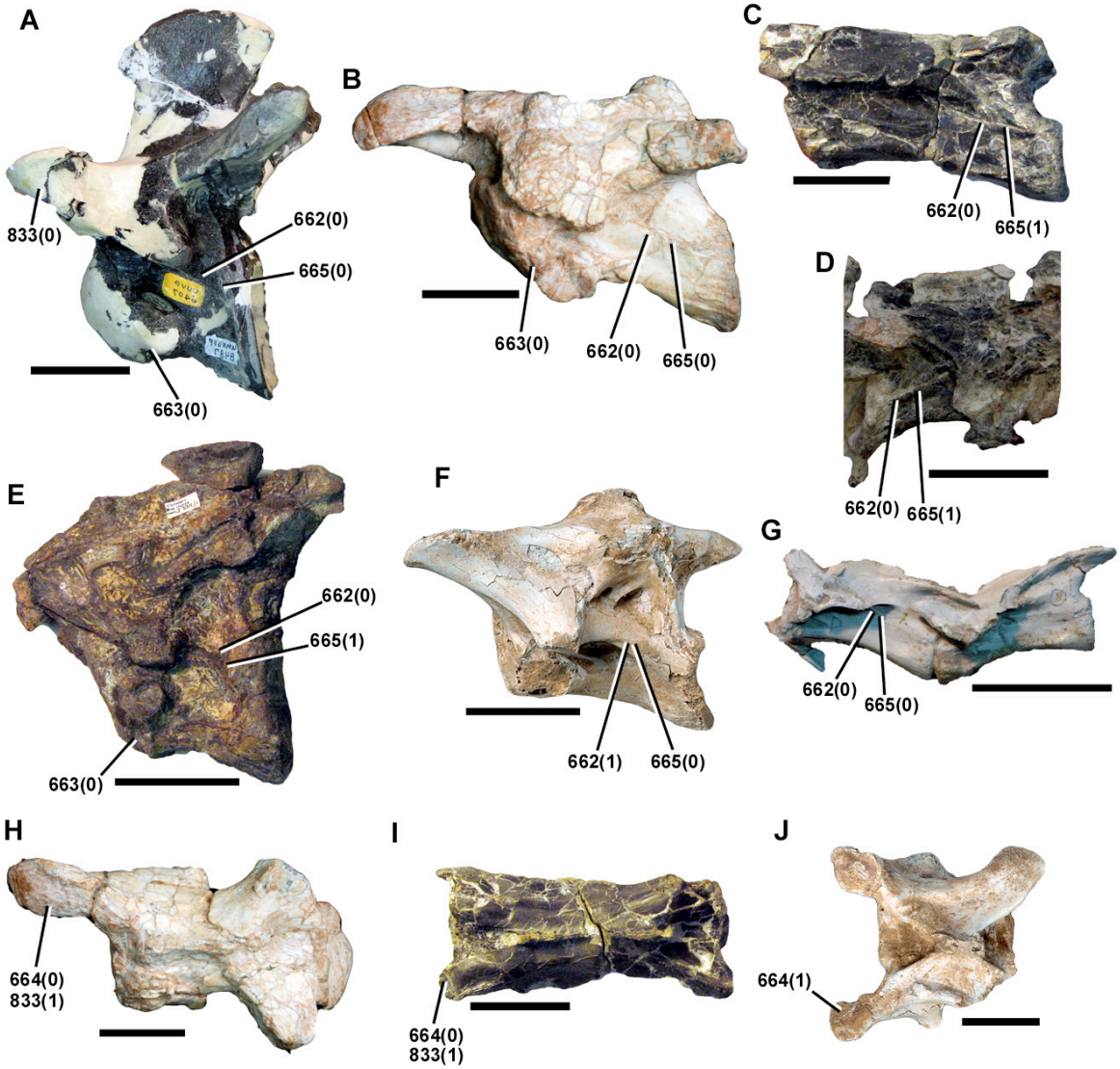

Figure 2-25. Postaxial cervical vertebrae of theropod dinosaurs in left lateral (A-G) and dorsal (H-J) views. *Allosaurus fragilis*, UMNH VP8487 (reversed) (A); *Zuolong salleei*, IVPP V15912 (B, H); *Coelurus fragilis*, YPM 2010 (C, I); *Guanlong wucaii*, IVPP V14531 (D); *Juratyrant langhami*, OUMNH J.3311 (E), *Alioramus altai*, IGM 100/1844 (F); *Gallimimus bullatus*, ZPAL MgD-I/94 (G, J). Photos B and H courtesy of Jonah Choiniere; F and J by Mick Ellison.Scale bars equal 4 cm except for B, C, H, and I, in which they are 2 cm. The *Gallimimus* vertebrae are middle-posterior cervicals (cervicals 7-8) but they possess the same morphology of the posterior centrodiapophyseal laminae as the anterior-middle cervicals and are therefore illustrated here.

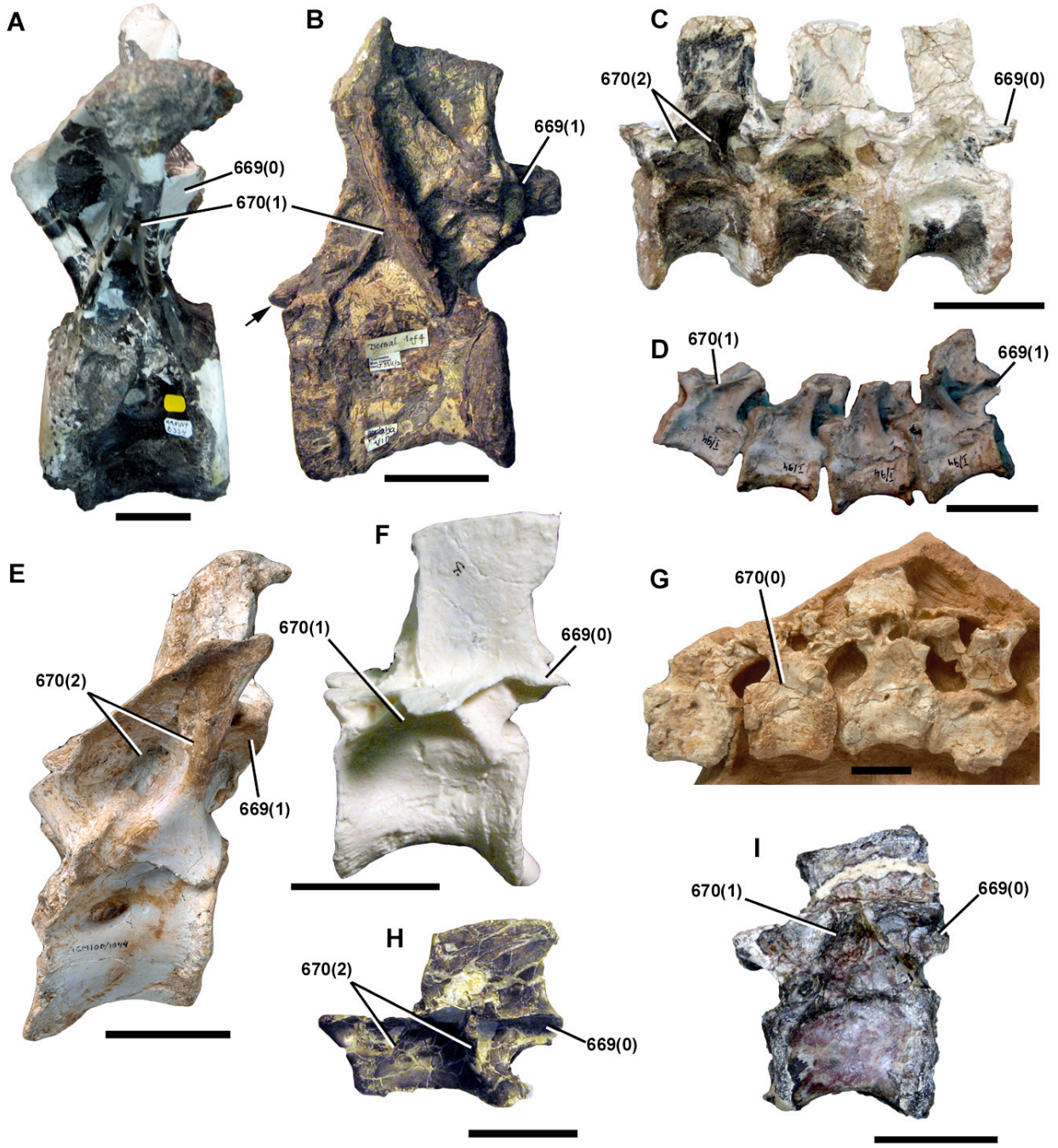

Figure 2-26. Dorsal vertebrae of theropod dinosaurs in left lateral views. *Allosaurus fragilis*, UMNH VP8334 (A); *Juratyrant langhami*, OUMNH J.3311 (B); *Guanlong wucaii*, IVPP V14531 (C); *Gallimimus bullatus*, ZPAL MgD-I/94 (D); *Alioramus altai*, IGM 100/1844 (E); *Tanycolagreus topwilsoni*, TPII 2000-09-29 cast (reversed) (F); *Balaur bondoc*, EME PV.313

(G); *Coelurus fragilis*, YPM 2010 (reversed) (H); *Falcarius utahensis*, UMNH Falcarius paratype (I). Photos E and G by Mick Ellison. Scale bars equal 4 cm except for those in G and H, which equal 2 cm. Arrow denotes prezygapophysis in *Juratyrant* in (B).

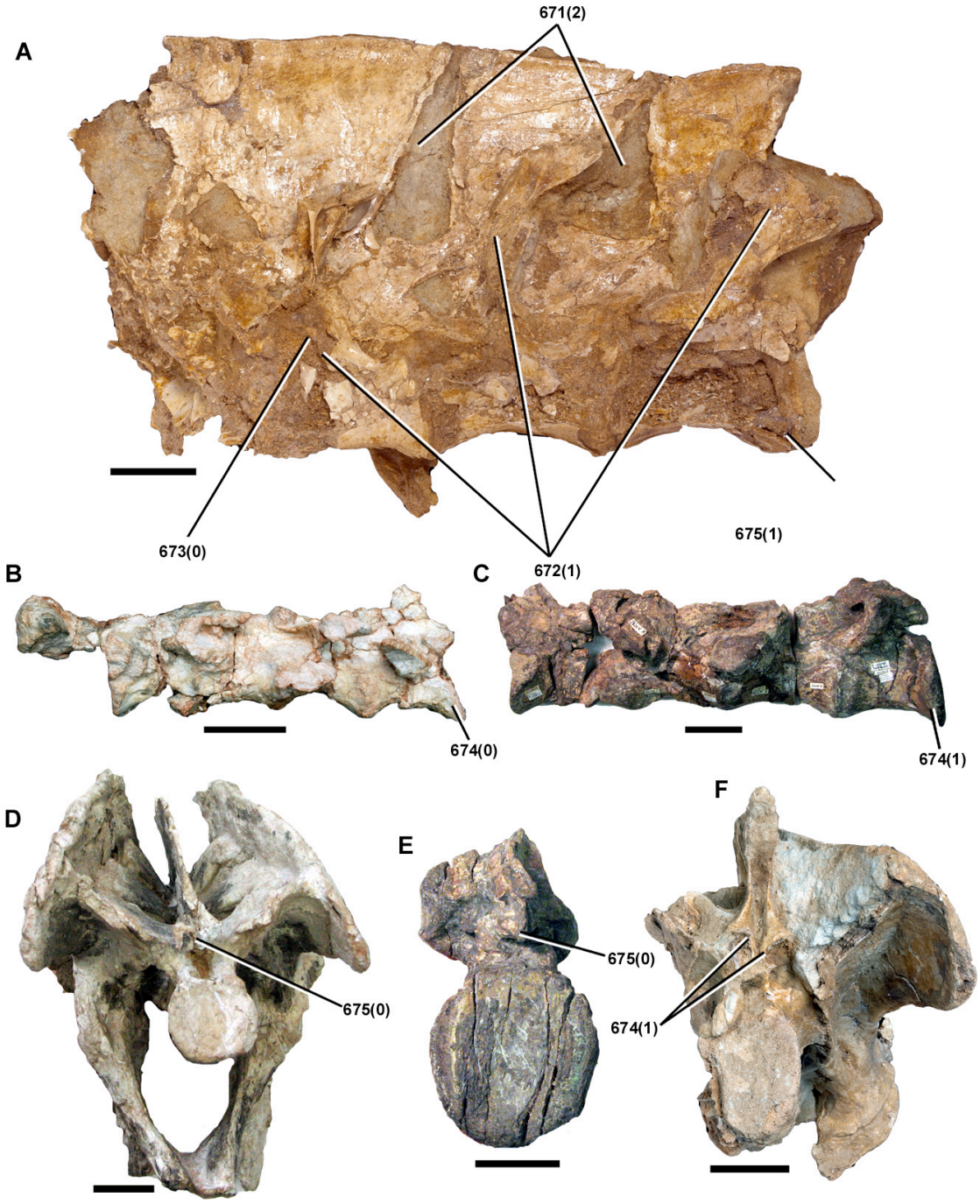

Figure 2-27. Sacral vertebrae of theropod dinosaurs in lateral (A-C) and posterior (D-F) views. *Alioramus altai*, IGM 100/1844 (A, F); *Zuolong salleei*, IVPP V15912 (reversed) (B); *Juratyrant langhami*, OUMNH J.3311 (C, E); *Guanlong wucaii*, IVPP V14531 (D). Photo B courtesy of Jonah Choiniere and A and F by Mick Ellison. E and G by Mick Ellison. Scale bars equal 4 cm.

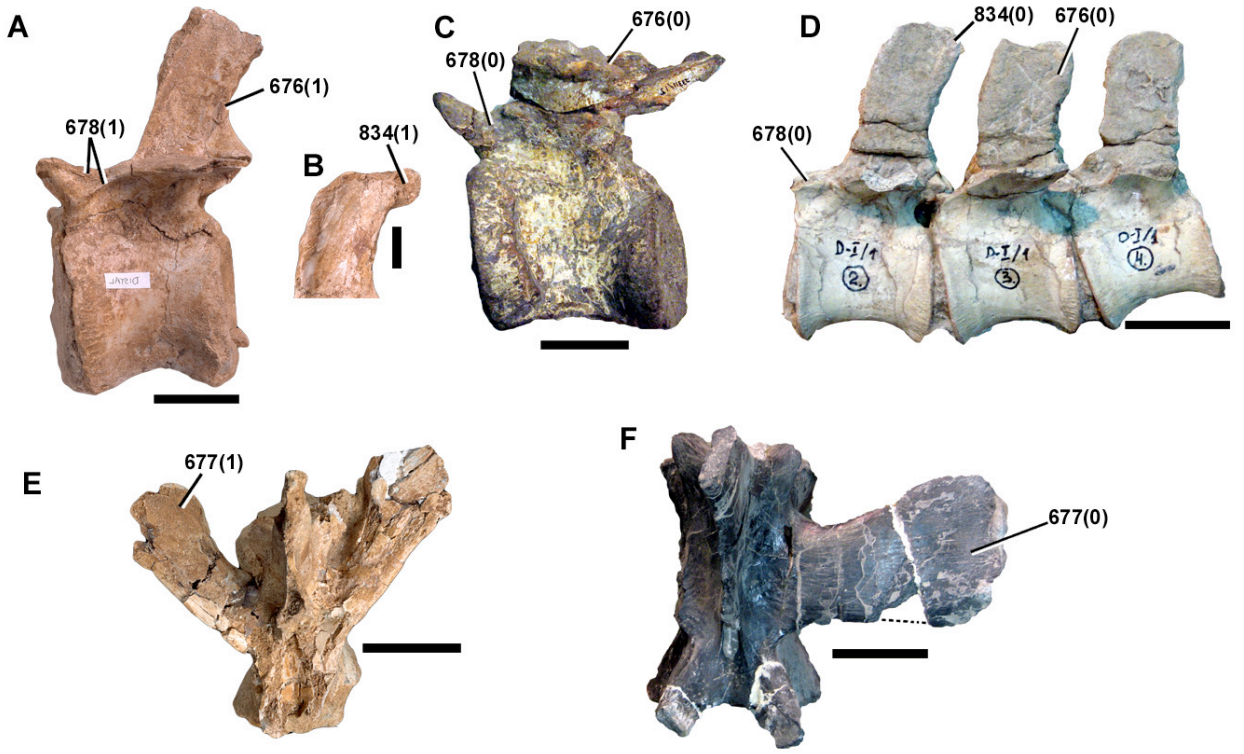

Figure 2-28. Caudal vertebrae of theropod dinosaurs in left lateral (A-D) and dorsal (E-F) views. *Alioramus altai*, IGM 100/1844 (A is reversed) (A, B, E); *Juratyrant langhami*, OUMNH J.3311 (reversed) (C); *Gallimimus bullatus*, ZPAL MgD-I/9 (D); *Allosaurus fragilis*, UMNH uncatalogued (F). Photos A, B, E by Mick Ellison. Scale bars equal 4 cm. Photo B is a closeup of the neural spine of a caudal vertebra of *Alioramus*; this vertebra is not the same as figured in photo A.

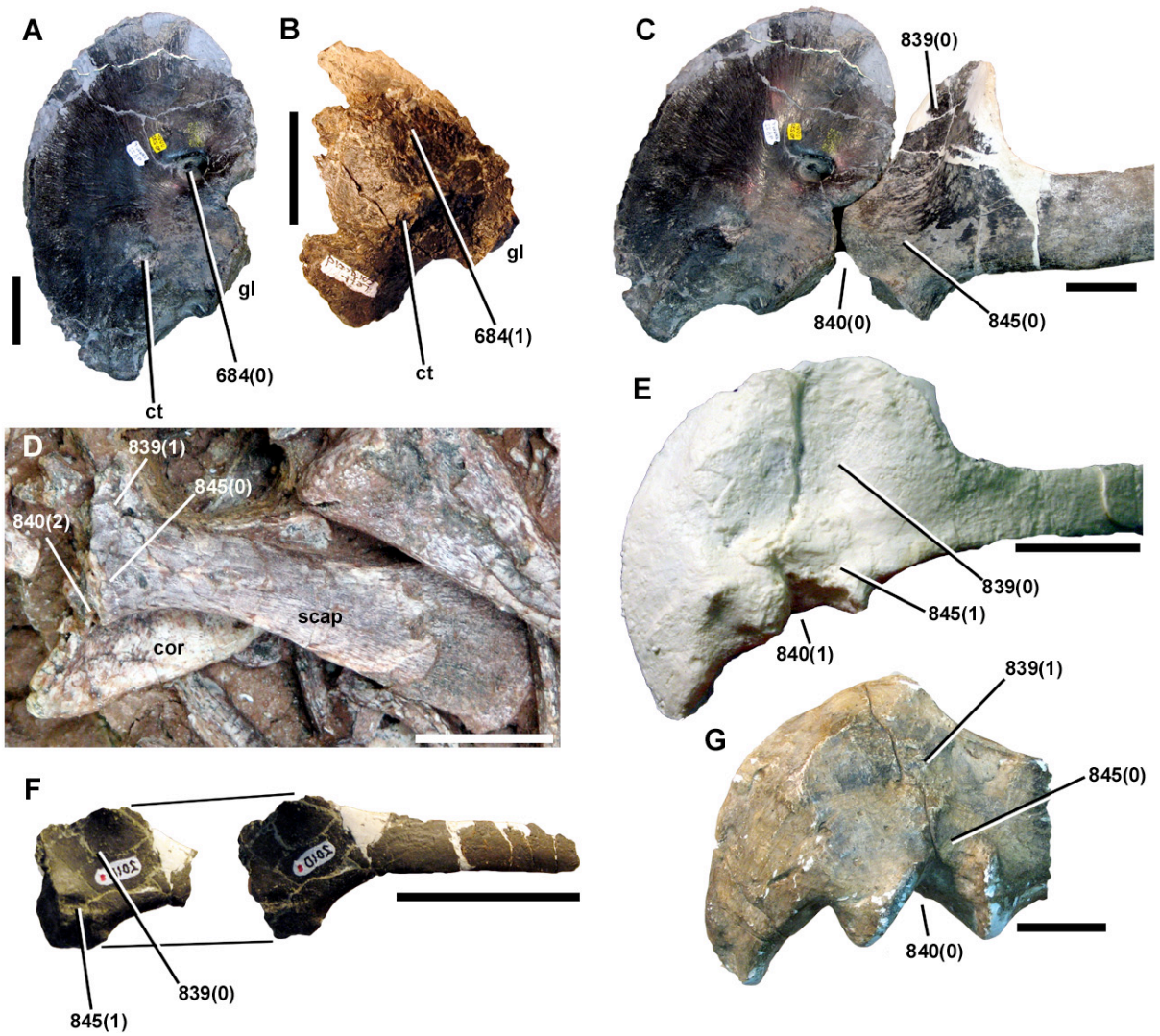

Figure 2-29. Coracoids and scapulae of theropod dinosaurs in left lateral (A-G), medial (coracoid in D), and anterolateral oblique (left image in F) views. *Allosaurus fragilis*, UMNH VP9822 (reversed) (A, C); *Eotyrannus lengi*, MIWG 1997.550 (B); *Dilong paradoxus*, IVPP V14243 (D); *Tanycolagreus topwilsoni*, TPII 2000-09-29 cast (E); *Coelurus fragilis*, YPM 2010 (reversed) (F); *Gallimimus bullatus*, ZPAL MgD-I/2 (G). Scale bars equal 4 cm, except for that in D which equals 2 cm. Abbreviations: cor, coracoid; ct, coracoid tubercle; gl, glenoid; scap, scapula. Note that coracoid of *Dilong* is disarticulated and lies underneath the scapula in B.

Figure 2-30. Humeri of theropod dinosaurs in anterior and lateral (left and right of paired images) (A-F) and proximal (G-J) views. *Allosaurus fragilis*, UMNH UUVP 1334 (A, G); *Zuolong salleei*, IVPP V15912 (B); *Falcarius utahensis*, UMNH VP12284 (C); *Coelurus*

fragilis, YPM 2010 (reversed) (D); *Guanlong wucaii*, IVPP V14531 (reversed) (E, I); *Eotyrannus lengi*, MIWG 1997.550 (F, J); *Gallimimus bullatus*, ZPAL MgD-I/2 (reversed) (H). Photos in B courtesy of Jonah Choiniere. Scale bars equal 4 cm.

Figure 2-31. Ulnae of theropod dinosaurs in anterior view. *Coelurus fragilis*, YPM 2010 (A); *Gallimimus bullatus*, ZPAL MgD-I/2 (B). Scale bars equal 4 cm.

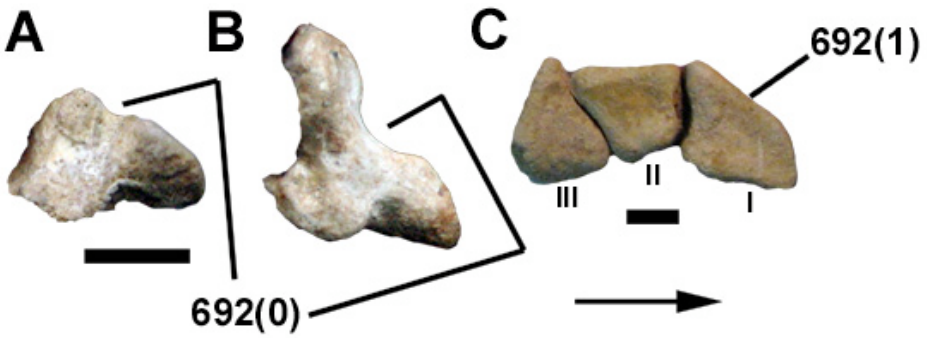

Figure 2-32. Metacarpals I of theropod dinosaurs in proximal view, with II and III also pictured in C. *Tugulusaurus faciles*, IVPP V4025 (A); *Guanlong wucaii*, IVPP V14531 (B); *Gallimimus bullatus*, ZPAL MgD-I/82 (reversed) (C). Scale bars equal 1 cm. Arrow points to the medial direction.

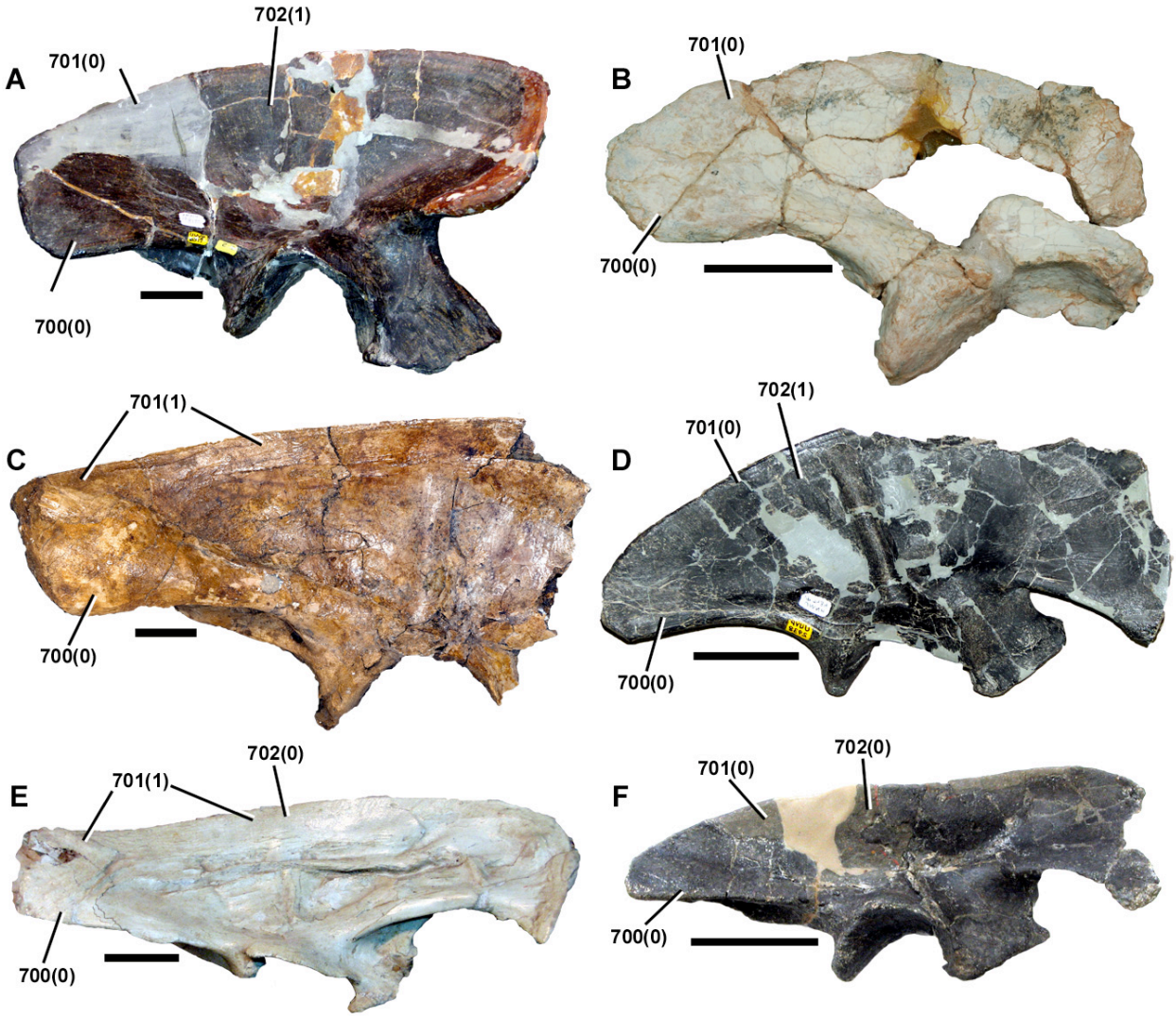

Figure 2-33. Ilia of theropod dinosaurs in right lateral view. *Allosaurus fragilis*, UMNH VP8122 (A); *Zuolong salleei*, IVPP V15912 (reversed) (B); *Alioramus altai*, IGM 100/1844 (C); *Stokesosaurus clevelandi*, UMNH VP7434 (reversed) (D); *Gallimimus bullatus*, ZPAL MgD-I/94 (E); *Ornitholestes hermanni*, AMNH FARB 619 (reversed) (F). Scale bars equal 4 cm.

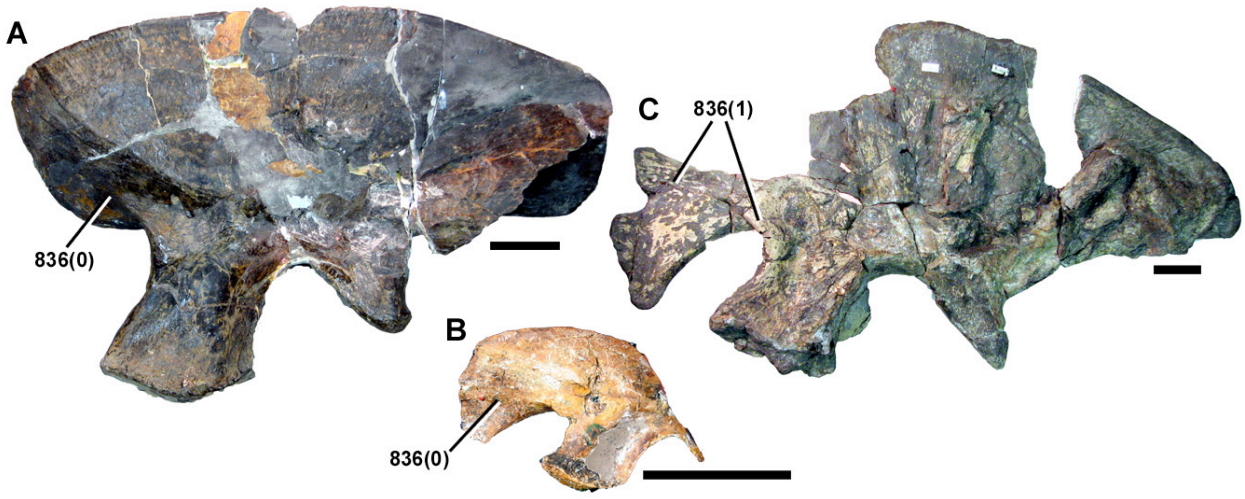

Figure 2-34. Ilia of theropod dinosaurs in medial view, with anterior to the left. *Allosaurus fragilis*, UMNH VP8122 (A); *Mirischia asymmetrica*, SMNK 2349 PAL (B); *Juratyrant langhami*, OUMNH J.3311 (C). Scale bars equal 4 cm.

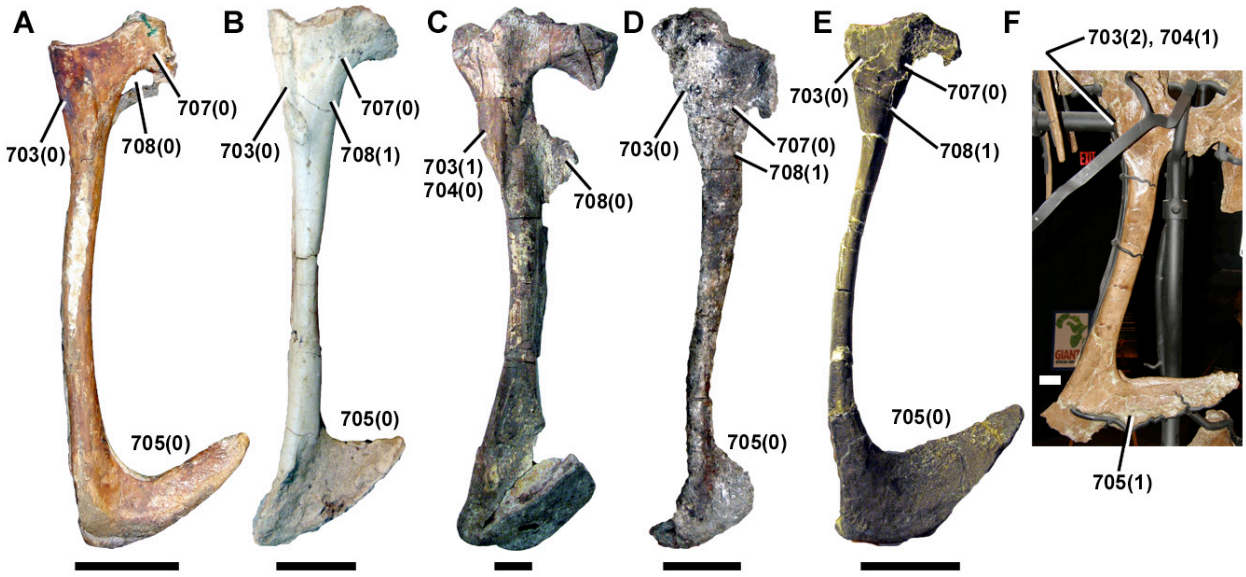

Figure 2-35. Pubes of theropod dinosaurs in left lateral view. *Mirischia asymmetrica*, SMNK 2349 PAL (A); *Gallimimus bullatus*, ZPAL MgD-I/94 (reversed) (B); *Juratyrant langhami*, OUMNH J.3311 (reversed) (C); *Falcarius utahensis*, UMNH VP14539 (D); *Coelurus fragilis*, YPM 2010 (reversed) (E); *Tyrannosaurus rex*, BMR 2002.4.1 (F). Photo F courtesy of Thomas Carr. Scale bars equal 4 cm.

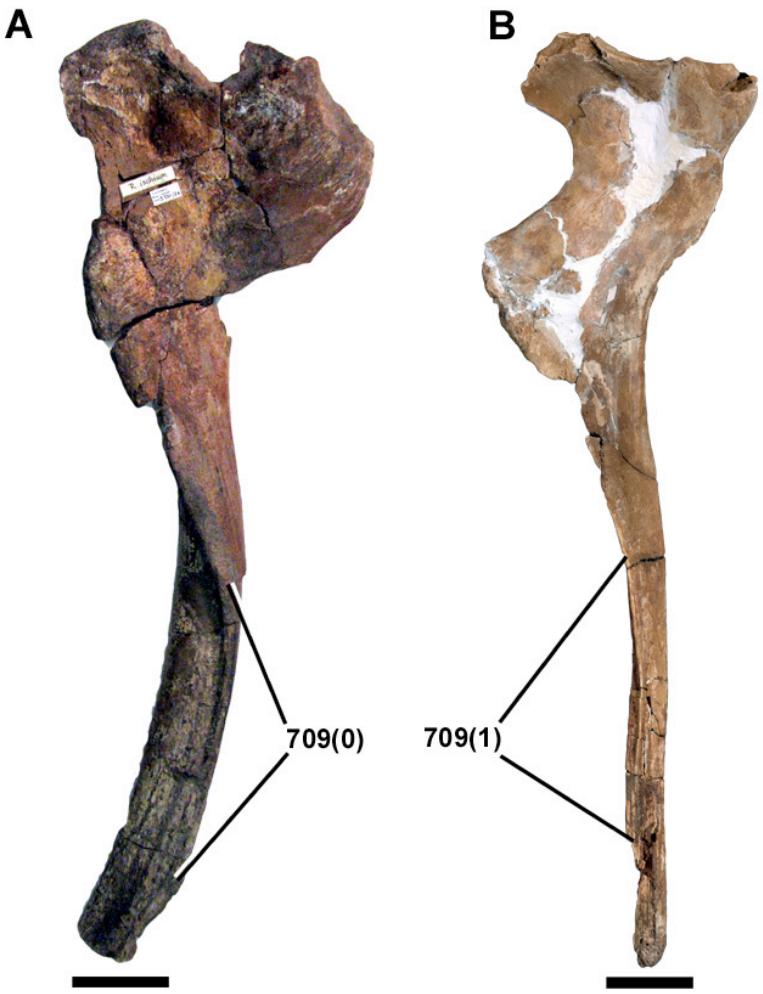

Figure 2-36. Right ischia of theropod dinosaurs in medial view. *Juratyrant langhami*, OUMNH J.3311 (A); *Alioramus altai*, IGM 100/1844 (B). Photo B by Mick Ellison. Scale bars equal 4 cm.

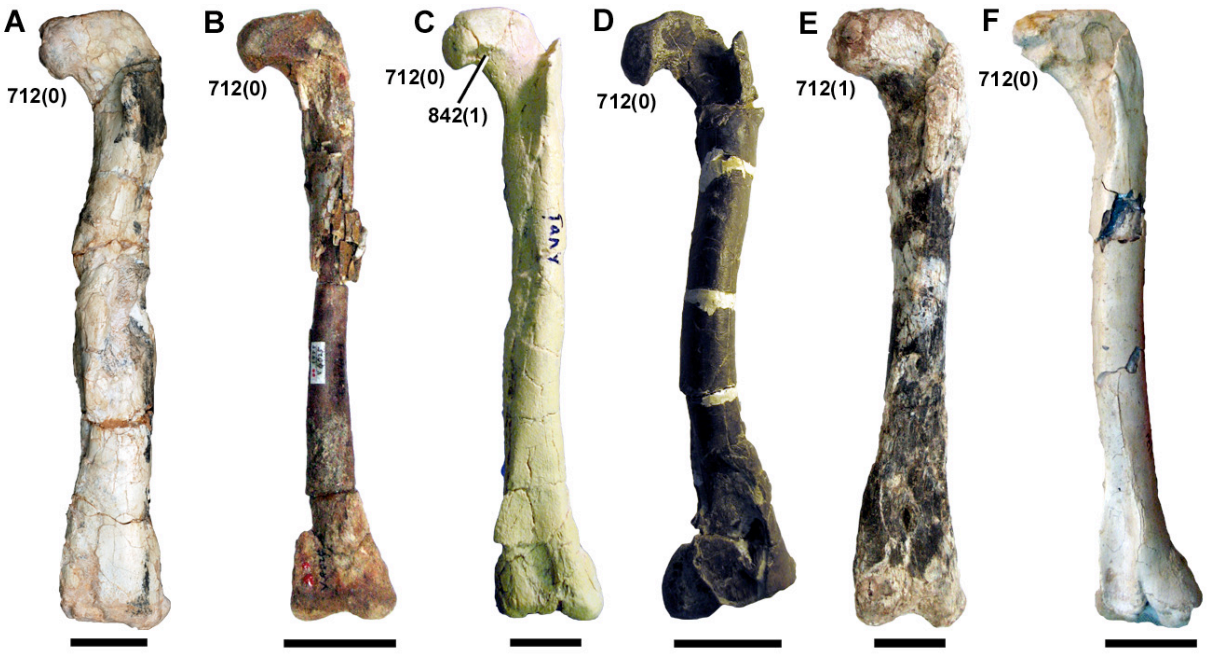

Figure 2-37. Femora of theropod dinosaurs in anterior view. *Zuolong salleei*, IVPP V15912 (reversed) (A); *Tugulusaurus faciles*, IVPP V4025 (B); *Tanycolagreus topwilsoni*, TPII 2000-09-29 cast (C); *Coelurus fragilis*, YPM 2010 (D); *Guanlong wucaii*, IVPP V14531 (E); *Gallimimus bullatus*, ZPAL MgD-I/94 (reversed) (F). Photo A courtesy of Jonah Choiniere. Scale bars equal 4 cm.

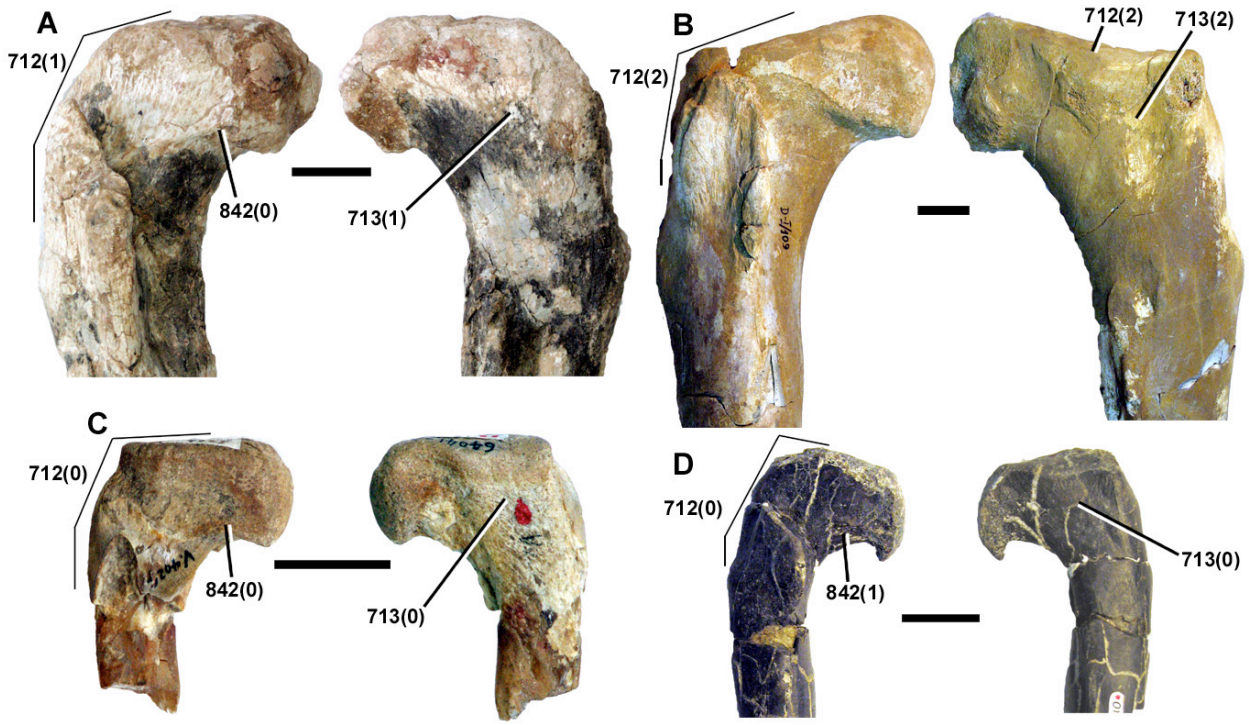

Figure 2-38. Femora of theropod dinosaurs in anterior (left photo of each pair) and posterior (right photo of each pair) view. *Guanlong wucaii*, IVPP V14531 (reversed) (A); *Tarbosaurus bataar*, ZPAL MgD-I/09 (B); *Tugulusaurus faciles*, IVPP V4025 (C); *Coelurus fragilis*, YPM 2010 (D). Scale bars equal 2 cm except for that in B, which equals 4 cm. Series of three connected lines denote the angle of the femoral head. Taxa with an inclined head have an obtuse angle between the top line and the bottom line. The middle line links the top and bottom line to save space.

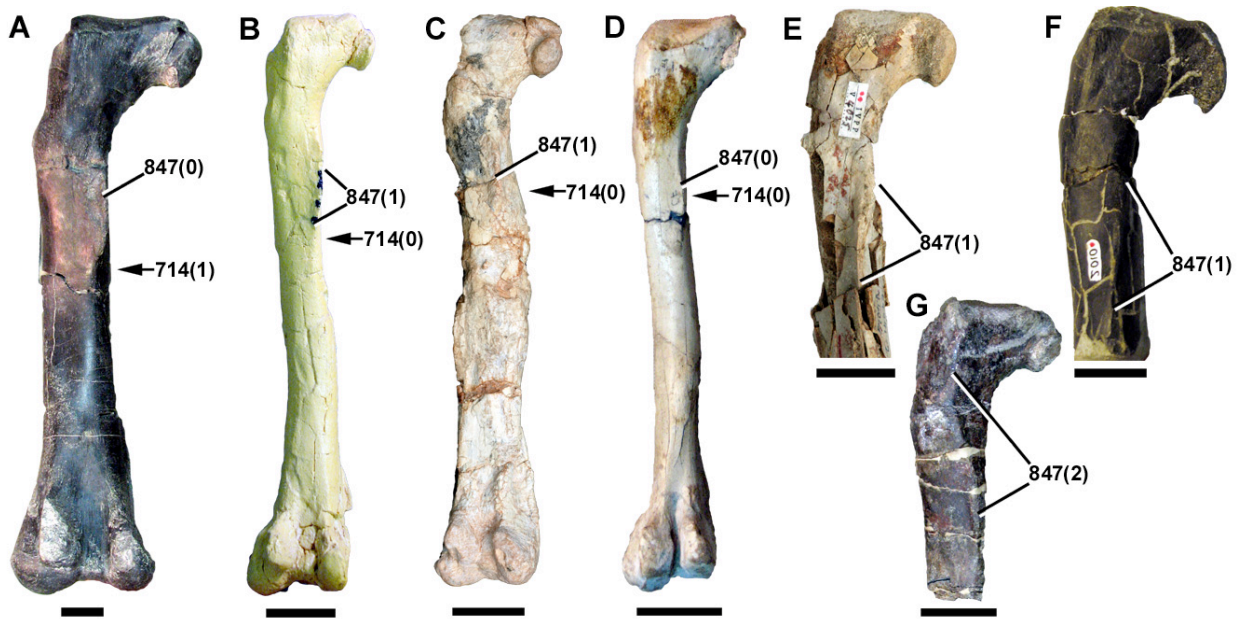

Figure 2-39. Femora of theropod dinosaurs in posterior view. *Allosaurus fragilis*, UMNH VP12231 (A); *Tanycolagreus topwilsoni*, TPII 2000-09-29 cast (B); *Zuolong salleei*, IVPP V15912 (C); *Gallimimus bullatus*, ZPAL MgD-I/94 (reversed) (D); *Tugulusaurus faciles*, IVPP V4025 (E); *Falcarius utahensis*, UMNH paratype (reversed) (G); *Coelurus fragilis*, YPM 2010 (reversed) (F). Photograph C courtesy of Jonah Choiniere. Scale bars equal 4 cm except for those in E and F, which equal 2 cm. Arrows denote the distal extent of the fourth trochanter.

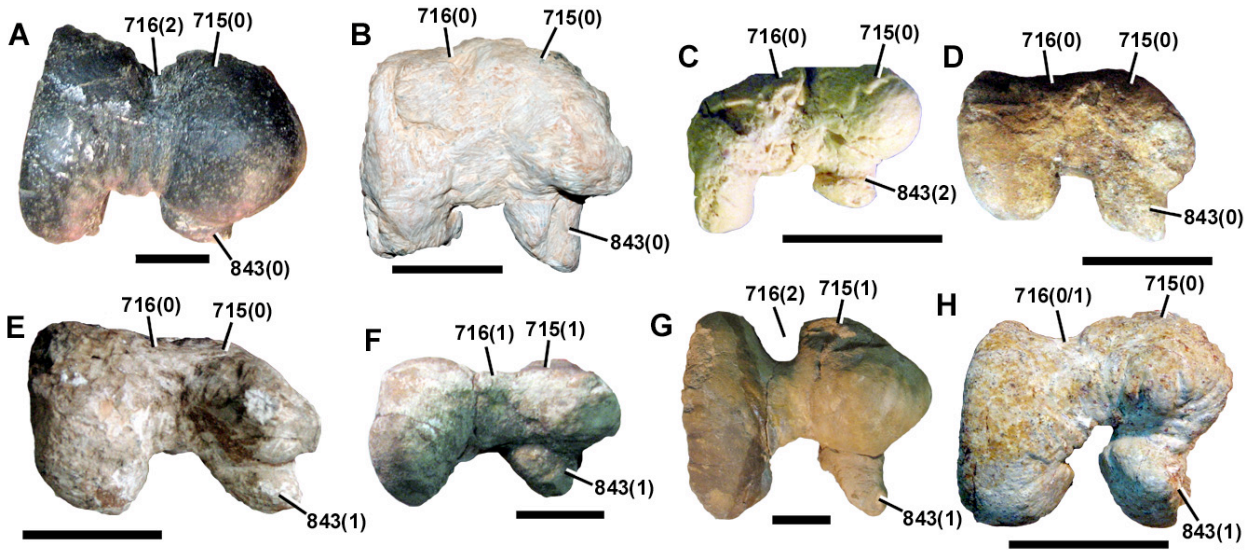

Figure 2-40. Femora of theropod dinosaurs in distal view. *Allosaurus fragilis*, UMNH VP12231 (A); *Zuolong salleei*, IVPP V15912 (B); *Tanycolagreus topwilsoni*, TPII 2000-09-29 cast (C); *Tugulusaurus faciles*, IVPP V4025 (D); *Guanlong wucaii*, IVPP V14531 (E); *Juratyrant langhami*, OUMNH J.3311 (F); *Tarbosaurus bataar*, ZPAL MgD-I/09 (reversed) (G); *Gallimimus bullatus*, ZPAL MgD-I/29 (reversed) (H). Photograph B courtesy of Jonah Choiniere. Scale bars equal 4 cm except for that in D which equals 2 cm.

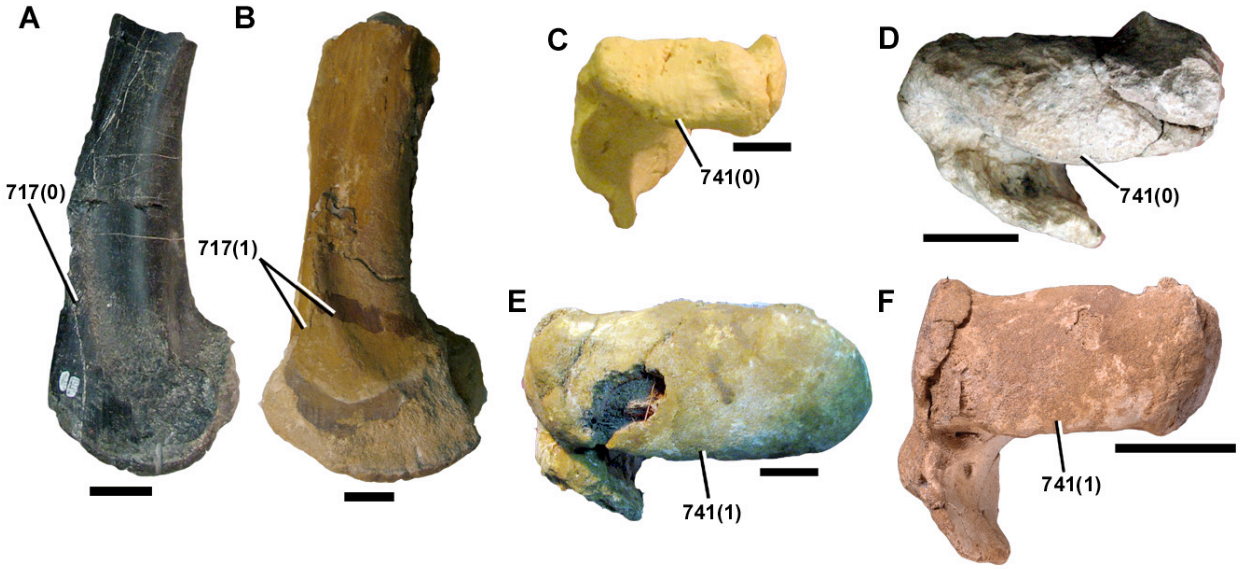

Figure 2-41. Femora of theropod dinosaurs in medial (A-B) and proximal (C-F) views. *Allosaurus fragilis*, UMNH VP12231 (reversed) (A); *Tarbosaurus bataar*, ZPAL MgD-I/09 (B, E); *Tanycolagreus topwilsoni*, TPII 2000-09-29 cast (C); *Guanlong wucaii*, IVPP V14531 (D); *Alioramus altai*, IGM 100/1844 (F). Photo F by Mick Ellison. Scale bars equal 4 cm, except for those in C and D which equal 2 cm.

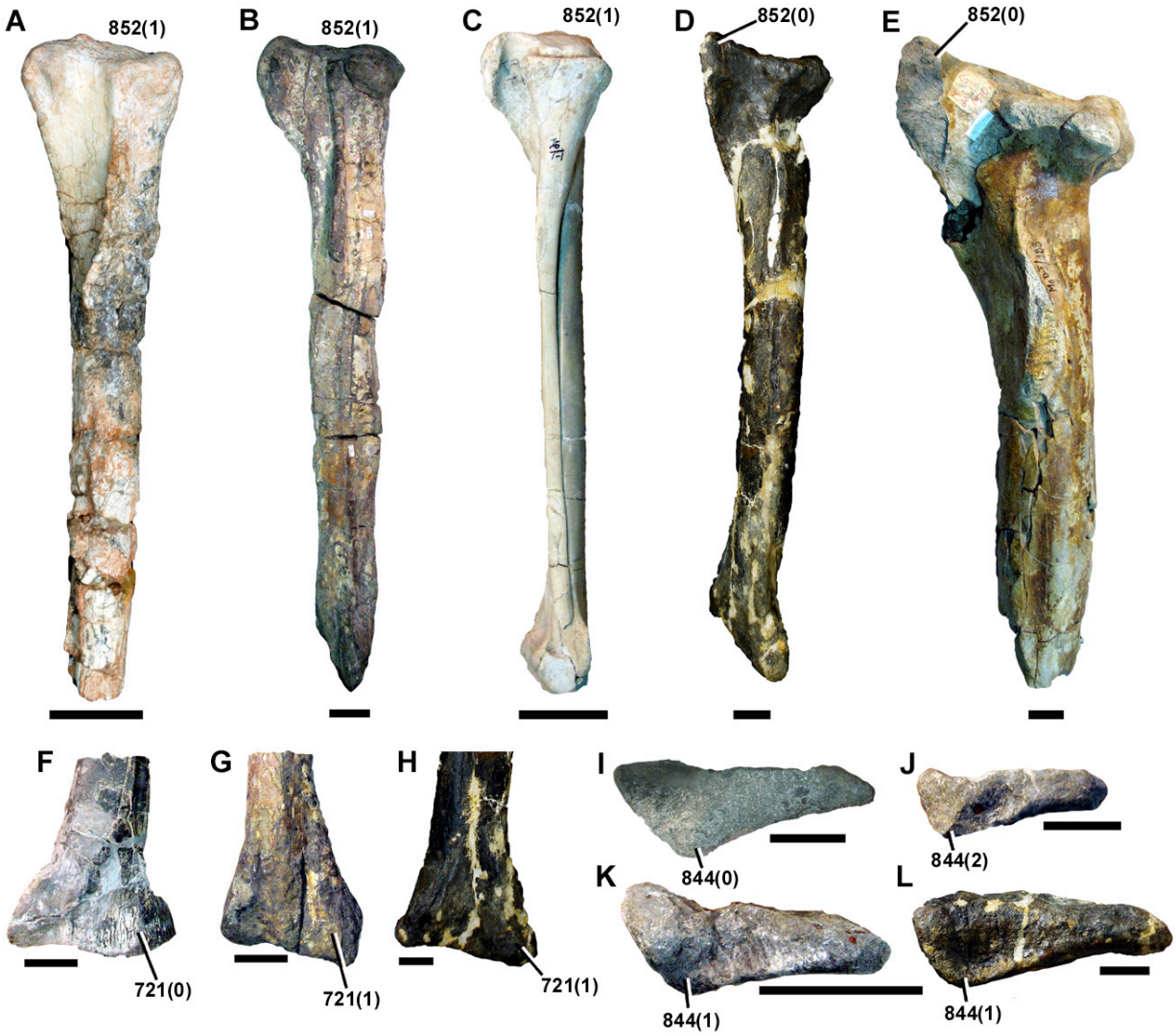

Figure 2-42. Tibiae of theropod dinosaurs in left lateral (A-E, C with fibula), anterior (F-H, all distal end), and distal (I-L) views. *Zuolong salleei*, IVPP V15912 (reversed) (A); *Juratyrant langhami*, OUMNH J.3311 (B, G); *Gallimimus bullatus*, ZPAL MgD-I/94 (reversed) (C); *Dryptosaurus aquilunguis*, ANSP 9995 (D, H, L); *Tarbosaurus bataar*, ZPAL MgD-I/188 (E); *Allosaurus fragilis*, UMNH VP7922 (F, I); *Coelurus fragilis*, YPM 2010 (J); *Falcarius utahensis*, UMNH VP12362 (K). Photograph A courtesy of Jonah Choiniere and D, H, and L courtesy of Roger Benson. Scale bars equal 4 cm, except that in J which equals 2 cm.

Figure 2-43. Fibulae of theropod dinosaurs in lateral view. *Tarbosaurus bataar*, ZPAL MgD-I/188 (A); *Dryptosaurus aquilunguis*, ANSP 9995 (B); *Coelurus fragilis*, YPM 2010 (C). Photograph B courtesy of Roger Benson. Scale bars equal 4 cm.

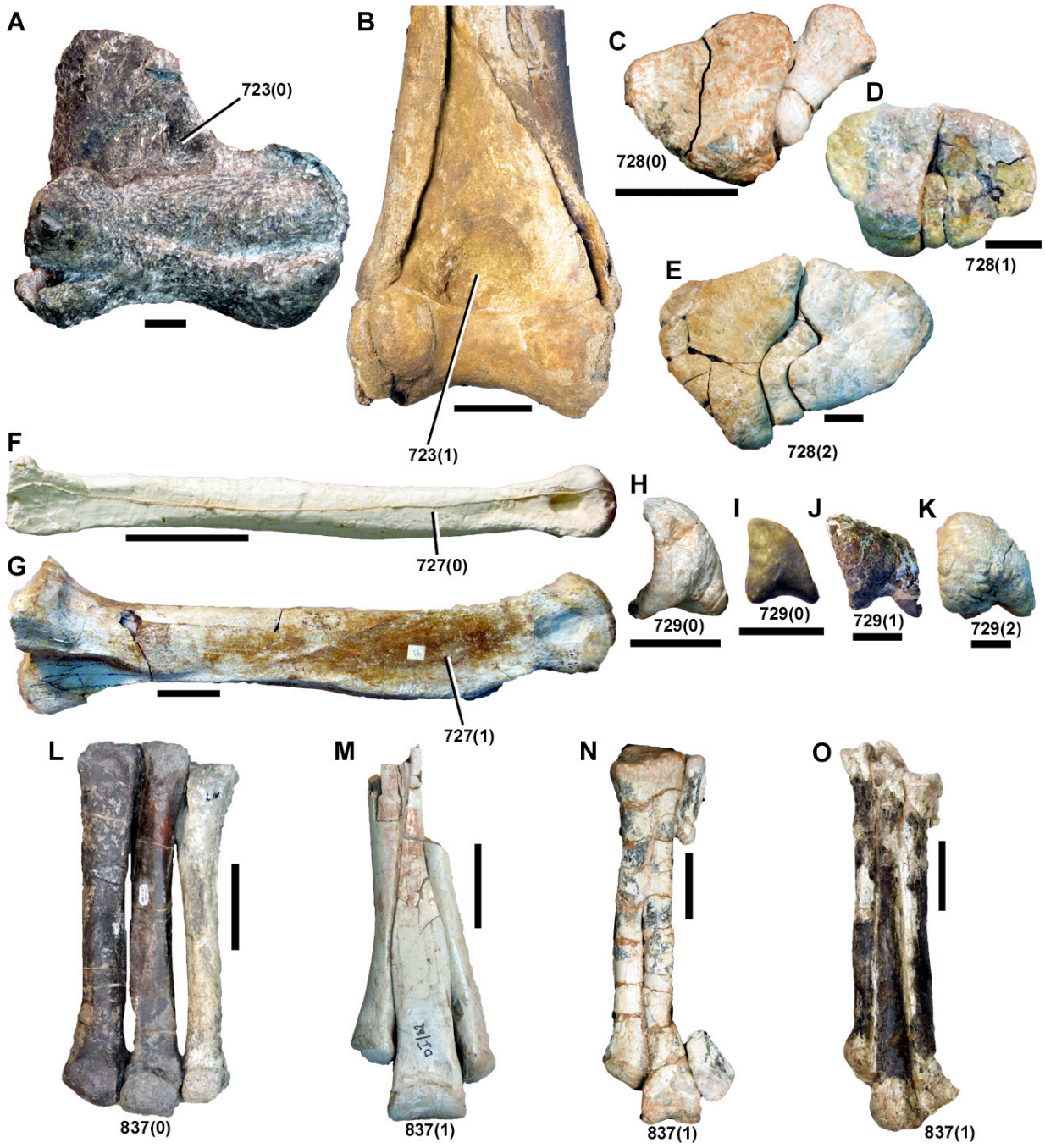

Figure 2-44. Tarsals and metatarsals of theropod dinosaurs in anterior (A-B, L-O), proximal (C-E), lateral (F-G), and distal (H-K) views. Bones figured include: astragalus (A-B), articulated metatarsals (C-E, L-O), metatarsal II (F-G), and metatarsal IV (H-K). *Allosaurus fragilis*, UMNH VP11456 (A); *Alioramus altai*, IGM 100/1844 (B); *Zuolong salleei*, IVPP V15912 (C, H, N; H and N are reversed); *Gallimimus bullatus*, ZPAL MgD-I/181 (reversed) (D);

Tarbosaurus bataar, ZPAL MgD-I/76 (E, G); *Tanycolagreus topwilsoni*, TPII 2000-09-29 cast (F); *Coelurus fragilis*, YPM 2010 (I); *Eotyrannus lengi*, MIWG 1997.550 (J); *Tarbosaurus bataar*, ZPAL MgD-I/206 (K); *Falcarius utahensis*, UMNH VP12366 (L); *Gallimimus bullatus*, ZPAL MgD-I/32 (M); *Guanlong wucaii*, IVPP V14531 (O). Photograph B by Mick Ellison; photographs C, H, and N courtesy of Jonah Choiniere. Scale bars equal 2 cm except for images F-G and L-O, in which they equal 4 cm.

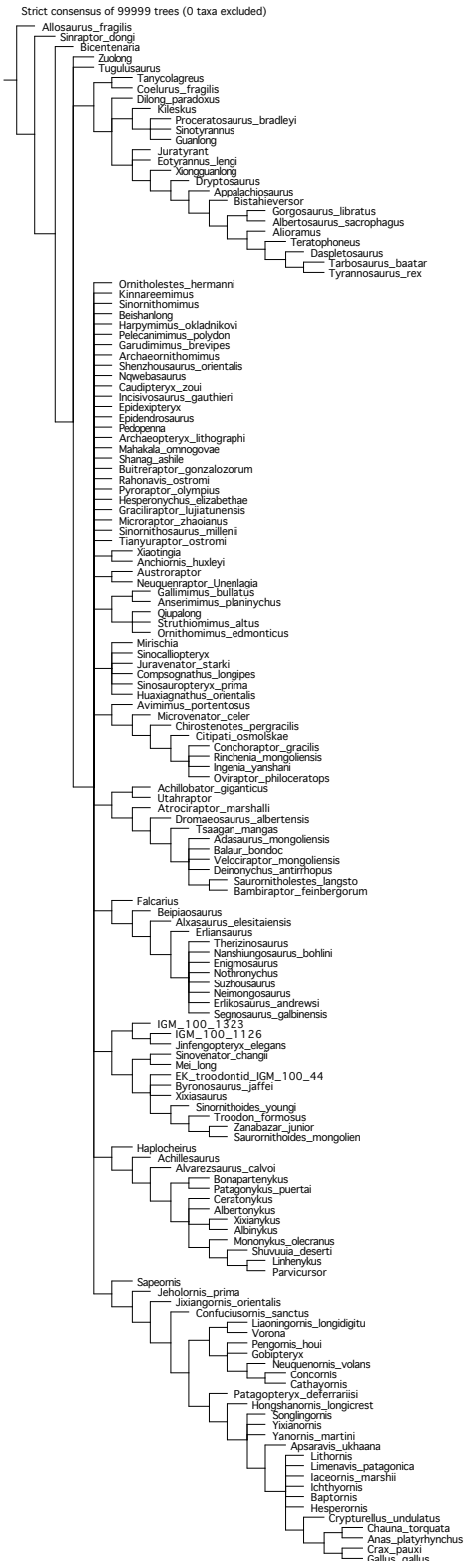

Figure 2-45. Strict consensus of 99999 most parsimonious trees recovered by the cladistic analysis (consistency index=0.323; retention index=0.776). This is the TNT output of the strict

consensus, which is poorly resolved in several areas. This is due to the wildcard nature of five taxa, which are removed in the reduced strict consensus topology below (Figures 2.46 and 2.47). It is the reduced strict consensus that is used as the preferred phylogeny in this dissertation, and which is used for character optimization and discussion of coelurosaurian evolution.

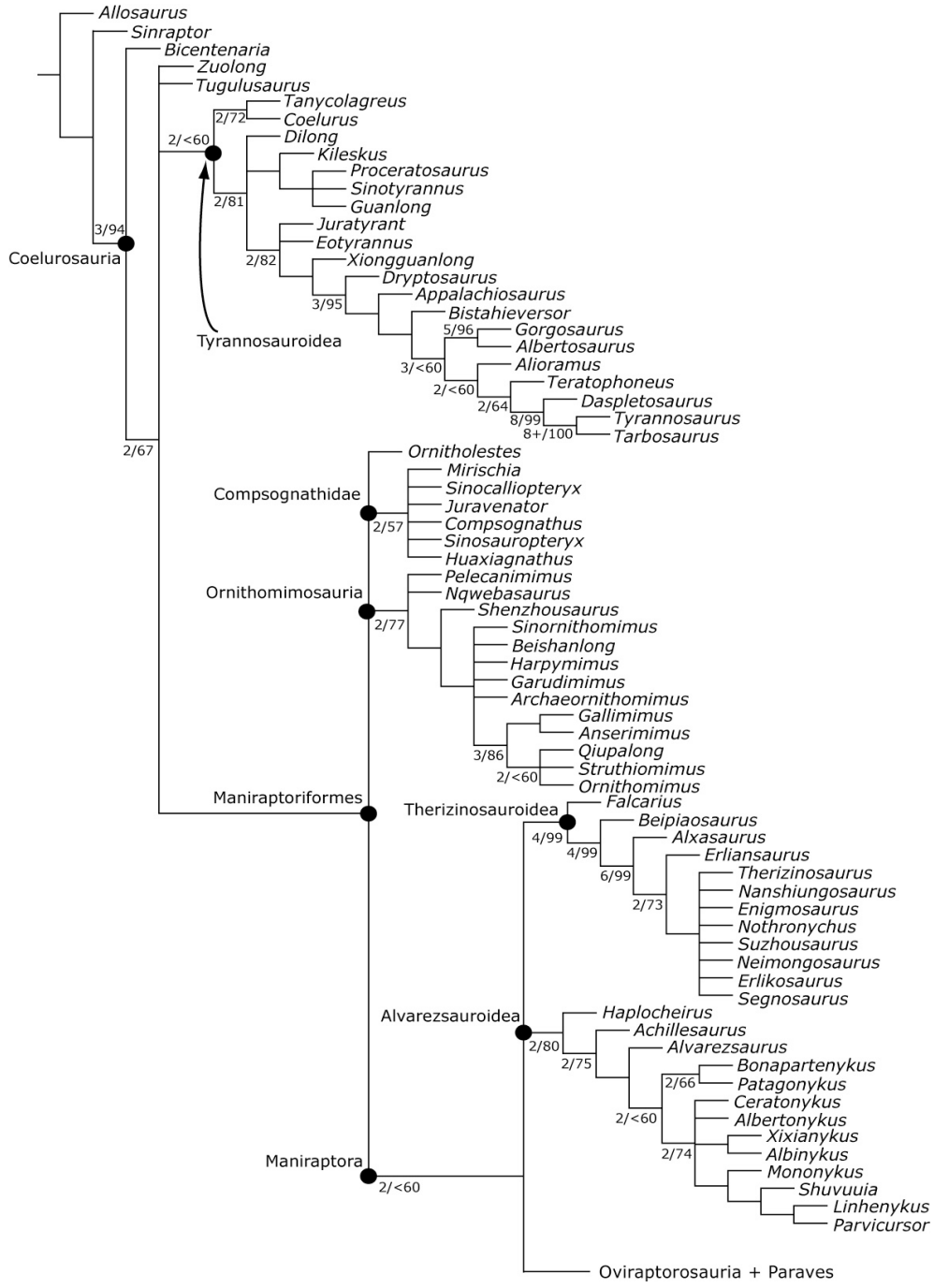

Figure 2-46. Reduced strict consensus of the 99999 most parsimonious trees recovered by the cladistic analysis (consistency index=0.323; retention index=0.776). The reduced strict

consensus is calculated after the a posteriori removal of five taxa: *Kinnareemimus*, *Epidendrosaurus*, *Pyroraptor*, *Hesperonychus*, and *Limenavis*. Numbers next to nodes denote Bremer support value/jackknife percentage. Those nodes without any numbers are characterized by Bremer values of 1 and a jackknife percentage of less than 60%. The Oviraptorosauria + Paraves clade is collapsed here for space reasons but is fully shown in the following figure (Figure 2.47).

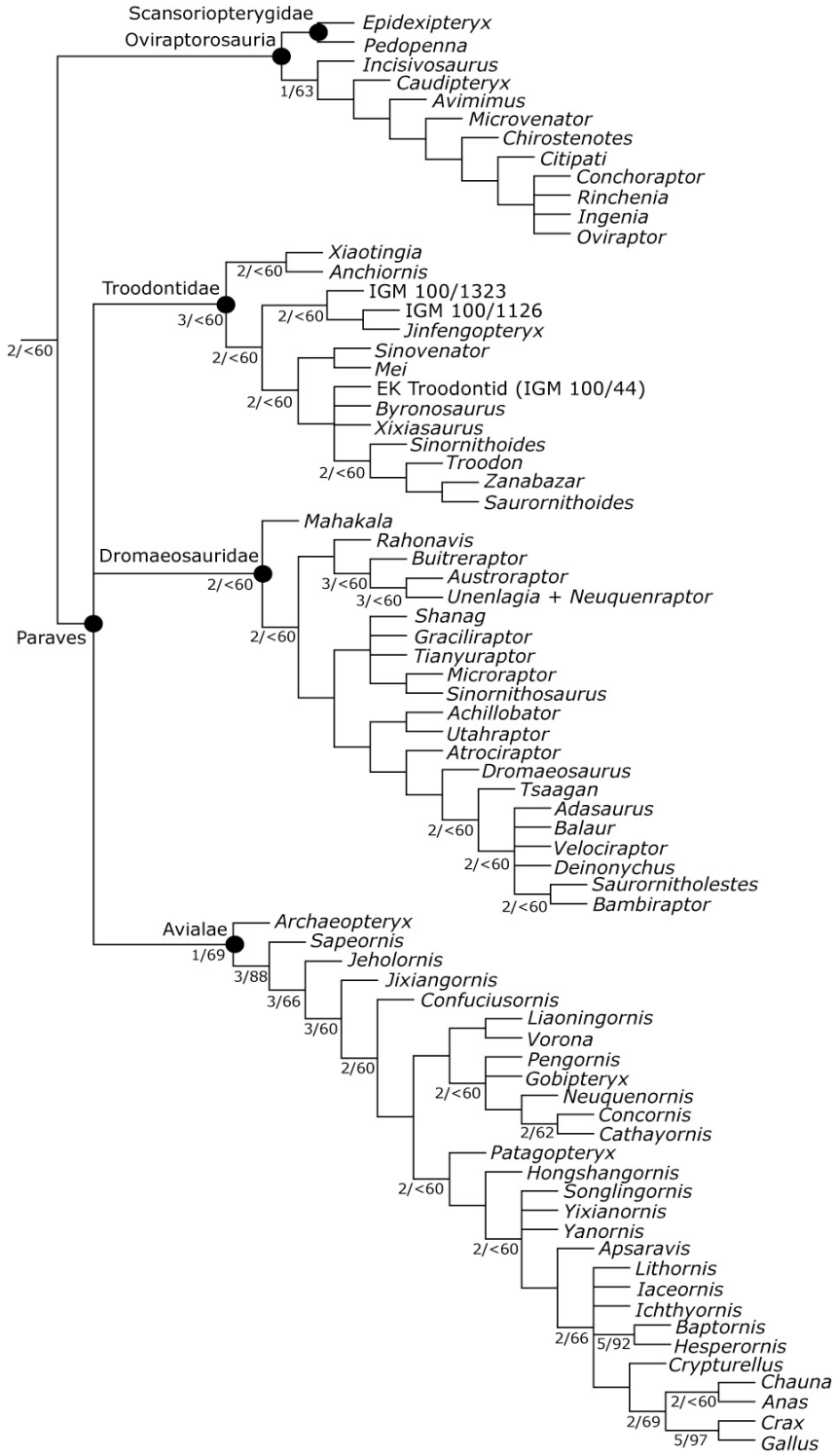

Figure 2-47. Reduced strict consensus relationships within the Oviraptorosauria + Paraves clade (see the placement of this clade among higher-level coelurosaur phylogeny in Figure 2.46 above). Refer to the caption of Figure 2.46 for explanation.

CHAPTER 3:

THE EVOLUTION OF CRANIAL FORM AND FUNCTION IN THEROPOD DINOSAURS: INSIGHTS FROM GEOMETRIC MORPHOMETRICS

PREFACE NOTE: This chapter was published as Brusatte et al. (2012b). This publication was a collaboration between me, Manabu Sakamoto, Shaena Montanari, and Will Harcourt-Smith. As first author, the majority of this chapter was my original work. I designed the project, collected all relevant theropod cranial images for analysis (along with Shaena Montanari), plotted all landmarks, performed the morphometric analysis, performed the disparity analyses, and wrote and formatted the paper. Manabu Sakamoto's major contribution was the collection and analysis of theropod biting function data, which was first reported in Sakamoto (2010). He also performed the phylogenetic comparative statistical tests (as outlined in the sections "Phylogenetic comparative methods", "Form vs. function", and "Primary determinants of theropod skull shape"). For this reason these results are reported here, as they form an integral part of the published paper, but they are not discussed in detail. They are fully acknowledged to be Manabu Sakamoto's part of the project. For more information on these statistical tests, as well as full details of the input data and methods, please consult the supplementary information of Brusatte et al. (2012b). Shaena Montanari's contribution was in helping to plan the project, collecting some theropod skull images, and collaborating in determining the landmark plotting strategy. Will Harcourt-Smith provided methodological advice and checked the morphometric analyses.

Some formatting points are important to note. First, the full text of the supplementary information associated with the original paper is included here as Appendix 3. All supplementary

tables and figures, however, are included in the main text of this dissertation because they are referred to in the main text of the paper itself. These supplementary tables and figures are denoted with the prefix "S". Note that Tables S7-S11 and Figures S6 and S22-S27 were compiled by Manabu Sakamoto and summarize the statistical analyses that he performed as part of this project.

INTRODUCTION

Theropod dinosaurs have captured the public imagination because they include some of the largest terrestrial predators in earth history, most notably the iconic *Tyrannosaurus rex* (Paul 1988; Brusatte et al. 2010a). Not all theropods were colossal megapredators, however. Over their 160+ million year evolutionary history, non-avian theropods developed a great diversity of body size, skull morphologies, and feeding habits (Weishampel et al. 2004). Species ranged from a few kilograms to over six tons in mass (Christiansen and Farina 2004; Carrano 2006; Therrien and Henderson 2007), possessed an array of skull morphologies (including long-snouted, deep-skulled, crested, and toothless forms: Weishampel et al. 2004), and experimented with a wide variety of diets (including pure carnivory, omnivory, and obligate herbivory) (Barrett 2005; Zanno et al. 2009; Zanno and Makovicky 2011). New fossil discoveries are consistently revealing novel body plans and presumed ecological behaviors for Mesozoic theropods (Brusatte et al. 2009a; Longrich and Currie 2009; Novas et al. 2009; Xu et al. 2009, 2011; Csiki et al. 2010), leading to an ever-greater understanding of this remarkable group of fossil organisms.

Although theropods are archetypal dinosaurs in the public eye, and perhaps the most intensely studied dinosaur group, there has been little work on large-scale macroevolutionary

patterns across theropod phylogeny and evolutionary history. In particular, there has been no quantitative documentation of broad patterns of skull shape variation in theropods, and little examination of how differences in cranial morphology relate to feeding behaviour (but see Rayfield 2005; Sakamoto 2010). As a result, several major questions remain unanswered. What are the principal ways in which theropod skulls vary, and which subgroups have the most atypical morphologies? Is cranial morphology tightly correlated to phylogeny and functional behaviour, and which of the two was more important in shaping theropod skull evolution? Did the evolution of non-carnivorous diets allow theropods to explore new, and perhaps larger, regions of morphospace, as has been suggested but not yet tested (Zanno et al. 2009)? Conversely, are colossal large-bodied theropods (a body type that independently evolved several times: Carrano 2006) morphologically constrained relative to other species, as has been noted in some living mammals that solely eat meat (Holliday and Steppan 2004)? Do distantly-related taxa with similar feeding styles converge on the same regions of morphospace?

We attempt to answer these questions with an integrated toolkit of morphological, functional, and phylogenetic data. As the basis for this study, we utilise geometric morphometrics to study variability in the shape of the theropod skull. These techniques, which model a series of specimens using homologous landmarks and utilise multivariate statistics to elucidate major patterns of shape variation, are commonly used in studies of fossil and living organisms (e.g., O'Higgins 2000; Zelditch et al. 2004; Stayton and Ruta 2006; Pierce et al. 2008, 2009; Young et al. 2010, 2011). However, geometric morphometrics have infrequently been used to study dinosaurs, and most studies have employed these methods to examine ontogenetic variation (Chapman 1990; Egi and Weishampel 2002), inform taxonomic decisions (Chapman 1990), and study locomotory behaviour (Bonnan 2004, 2007; Chinnery 2004), rather than

quantify large-scale macroevolutionary patterns over long time scales and within a phylogenetic context (but see Young and Larvan 2010). Here, we present a novel landmark-based morphometric analysis that reveals major patterns of theropod skull variation and allows species to be plotted into a morphospace. The positions of taxa in morphospace are compared to phylogeny and quantitative measures of theropod biting performance (Sakamoto 2010), giving insight into large-scale patterns and processes of theropod cranial evolution during the Mesozoic.

MATERIALS AND METHODS

Geometric Morphometrics: We analyzed morphological variation in the cranium of non-avian Mesozoic theropod dinosaurs using two-dimensional geometric morphometrics, a quantitative technique utilised to summarize and study shape variation across a collection of specimens (Bookstein 1991: O'Higgins 2000; Zelditch et al. 2004). These methods are held to be superior to traditional morphometric techniques, often based on multivariate analysis of length and angle measurements, because they preserve geometry, are better able to separate shape from size-related variation, and better capture subtle sources of variation that are not easily summarized by simple measurements (O'Higgins 2000; Rohlf 2000).

We encapsulated the cranial geometry of 51 species of theropod using 24 type 1 and 2 homologous landmarks (Bookstein 1991; O'Higgins 2000), which were plotted on photographs and published reconstructions using the program tpsDig2 (Rohlf, 2010) (fig. 1a). After plotting landmarks on all 51 specimens (one specimen per species) it became apparent that many specimens had a large number of landmarks that could not be plotted because of poor preservation or missing bones. Missing data are not ideal, because they reduce the statistical

power of the analysis. Therefore, we proceeded with two datasets: a 26-taxon dataset that could be scored for all landmarks and a 36-taxon dataset that could be scored for a reduced set of 13 landmarks. The decision to use a 36 taxon/13 landmark dataset aimed to maximize both the number of taxa and landmarks that could be included, as well as permit inclusion of representatives of all major theropod subclades.

For both the 26- and 36-taxon datasets, landmark coordinates were superimposed using Generalized Procrustes Analysis (GPA) in MorphoJ (Klingenberg 2011), which serves to minimize non-shape variation between specimens, such as that caused by size, position, and rotation. This procedure produced a set of GPA "corrected" landmark coordinates, which were then converted into a covariance matrix and subjected to Principal Components Analysis (PCA), also using MorphoJ. This multivariate analysis assimilates data from all landmarks and reduces them into a distilled set of PC scores that summarize the skull shape of each taxon. Because our PCA of both the 26- and 36-taxon datasets revealed that one particular group of theropods, the short-and-deep-skulled oviraptorosaurs (Osmólska et al. 2004), were outliers relative to all other taxa on PC1, we also performed supplementary analyses of each dataset with oviraptorosaurs excluded from the PCAs. These additional datasets included 24 and 31 taxa, respectively. Therefore, in the remainder of this paper, we will discuss four separate datasets: the 26- and 36-taxon datasets that include oviraptorosaurs and the 24- and 31-taxon datasets that do not.

Theropod Skull Function: As part of this study, we wish to compare theropod skull form (based on the morphometric analysis) with a measure of cranial function. We quantify theropod functional performance with a straightforward and well-established metric: the mechanical advantage (MA), defined as the ratio of the muscle moment arm (effort) to the biting moment, of

three major cranial muscle groups (Westneat 1994). MA measurements for several theropods were recently presented by Sakamoto (2010), and we built upon this study by adding measurements for 25 additional taxa (total of 60 taxa), thereby compiling a dataset of functional metrics for 35 of the 36 taxa included in the morphometric analysis. The MA measures for each muscle group were subjected to PCA (see Sakamoto [2010] for details), resulting in a set of PC scores for each taxon, which are useful proxies for function. We reiterate that the MA quantifies a very specific aspect of skull function, namely the strength and speed of the bite, and that other functional metrics may relate to skull shape in different ways. We chose MA because it is straightforward to measure, it can be measured in a wide range of theropod specimens (unlike, for instance, estimates of skull strength generated from finite element analysis, which has only been conducted on a handful of taxa: Rayfield [2005]), has well understood mechanical properties (Westneat 1994), and can be measured using two-dimensional skull images (and thus is roughly an equivalent type of proxy to the form proxies generated from the morphometric analysis). We note that mechanical advantage measurements utilize information from both the cranium and mandible (the latter of which is not included in the morphometric analysis), but a sensitivity analysis shows that the overriding factor in mechanical advantage calculations is the shape of the cranium (see online supporting information in the published version of this paper).

Morphological Disparity: Morphological disparity measures the anatomical variety exhibited by a group of organisms (Foote 1993; Wills et al. 1994; Ciampaglio et al. 2001). Disparity calculations require some measure of morphological form for each organism being assessed, and we used PC scores from the PCA of the GPA corrected coordinates as a proxy for theropod skull shape. Comparative disparity is assessed by binning taxa into various pre-defined groups (e.g.,

taxonomic, temporal, ecological) and calculating disparity metrics for each, which can then be compared to determine whether certain groups have a greater variety of morphological form than others.

We divided our taxa into dietary and taxonomic categories. Dietary categories included carnivores and non-carnivores, as well as large-bodied carnivores, carnivorous theropods that are not large-bodied, and all theropods that are not-large bodied (regardless of diet). Large-bodied is here defined as all taxa with skulls greater than 65 cm in length, a category that includes several independent radiations of colossal theropods such as abelisaurids, tyrannosauroids, and allosauroids (Carrano 2006). Non-carnivorous theropods are identified based on published studies of theropod diet (see Zanno and Makovicky [2010] for an overview), and are here held to include the aberrant toothless ceratosaur *Limusaurus* (Xu et al. 2009), as well as four clades: the ornithomimosaurs (Kobayashi et al. 1999; Norell et al. 2001; Barrett 2005; Zanno and Makovicky 2011), therizinosauroids (Zanno et al. 2009; Zanno and Makovicky 2011), alvarezsaurids (Senter 2005; Longrich and Currie 2009; Zanno and Makovicky 2011), and oviraptorosaurs (Zanno and Makovicky 2011). Finally, taxonomic categories included: Basal Theropoda (paraphyletic), Ceratosauria, Basal Tetanurae (paraphyletic), Tyrannosauroidea, Oviraptorosauria, and Dromaeosauridae; categories at this taxonomic level were selected so that sample sizes were approximately equivalent, and so that groups were not nested within each other.

Four disparity metrics were calculated for each category: the sum and product of the ranges and variances on the first 5 PC axes generated from the 36-taxon morphometric dataset, using the program RARE (Wills 1998). These same measures were then calculated for identical categories using the 31-taxon morphometric dataset in which oviraptorosaurs were excluded

(disparity was not calculated using the 24- and 26-taxon datasets, because all taxa in these analyses are also included in the more inclusive 31- and 36-taxon datasets, respectively). The first five PC axes were chosen in both cases because these axes were deemed significant by reference to the "broken-stick" method, in which a scree plot (percentage of total variance against number of principal components) is examined for a significant break in its slope (following Wills et al. 1994). Range measures summarize the entire spread of morphospace occupied by the taxa in question, whereas variance denotes mean dissimilarity among the taxa (their spread in morphospace) (Wills et al. 1994). Statistical significance of disparity comparisons was assessed by the overlap or non-overlap of 95% confidence intervals, generated by bootstrapping, and rarefaction was used to assess whether disparity differences are robust to sample size differences between categories (variance metrics are usually more robust to sample size bias: Wills et al. 1994; Butler et al. 2012).

Phylogenetic Comparative Methods: One major question is: is theropod skull shape significantly correlated with phylogeny? A strong phylogenetic signal means that closely related species tend to fall out closer in morphospace than more distantly related species (Klingenberg and Gidaszewski 2010).

We used three methods to assess phylogenetic signal in the morphometric dataset, in each case using a composite theropod phylogeny for reference (see online supporting information). First, we performed a permutation test in MorphoJ in which the phylogeny is held constant and the PC scores for each taxon are randomly swapped across the tree 10,000 times (Klingenberg and Gidaszweski 2010). The null hypothesis of no phylogenetic signal is discarded if less than 5% of permutations result in a tree length (calculated using squared change parsimony) that is

shorter or equal to the value obtained from the original data. Second, we performed a multivariate phylogenetic eigenvector regression (MPVR) (Diniz-Filho et al. 1998), in which phylogeny, represented by principal coordinate axes derived from a phylogenetic distance matrix, is regressed against form metrics (significant axes of PC scores from the morphometric analyses). The multivariate R^2 value and *p*-value represent the strength and significance of the correlation, respectively, between the form and phylogeny proxies. Third, we used the techniques of Blomberg et al. (2003), which compare the variance in phylogenetically independent contrasts (PICs) (Felsenstein 1985) in PC1 scores with those computed from permutations of those scores across the same tree topology. If the variances for the original data are lower than those derived from the permutations, then there is a significant phylogenetic signal in the morphometric data (see online supporting information for full explanation).

Form vs. Function: Another major question is: is theropod skull shape significantly correlated with function? We performed three correlation analyses on form and function metrics to assess this question. First we performed a two-block partial least squares (2B-PLS) analysis in MorphoJ, using Procrustes coordinates from the geometric morphometric analysis as the form metric block and the biomechanical coefficients standardized by their respective standard deviations as the function metric block. The RV coefficient was determined and the *p*-value was computed through 10000 permutations; these represent the strength and significance of the correlation, respectively, between the form and function proxies. Second, we performed a multivariate multiple regression (MMR) analysis in R, on the significant axes of PC scores for form (PC1 to PC5 or PC1 to PC7) and function (PC1 and PC2). The multivariate R^2 value and *p*-value represent the strength and significance of the correlation, respectively, between the two

matrices. Third, we performed PIC correlation analyses on PC1 and PC2 of both form and function. Both sets of metrics were transformed into PICs and an ordinary least squares regression model was fitted through the origin for all pairwise comparisons of form and function metrics (i.e., PICs of PC1 and PC2 of form and function). Once again, R^2 value and p-value represent the strength and significance of the correlation, respectively. We also used the disparity methods described above to calculate measures of functional disparity for several dietary and taxonomic categories (based on PC1 and PC2 function scores), to assess whether clades with high morphological disparity also exhibit high functional variety.

Primary Determinants of Theropod Skull Shape: Finally, following from the above assessment of phylogenetic and functional signals in the morphometric data, another major question of interest is: does phylogeny or function better explain the range of variation in theropod skull shape? We addressed this question by performing a series of MPVR that partition variance in morphometric form metrics (a matrix of PC scores) into components related solely to function, a combination of function and phylogeny, solely to phylogeny, and to other sources not explained by either function or phylogeny, following published protocols (Desedivses et al. 2003) (see online supporting information in the published version of this chapter for full explanation of this procedure).

RESULTS

Morphospace Occupation and Major Shape Changes: The PCAs show that the majority of shape variation in both the 26- and 36-taxon datasets is summarized by the first two PC axes

(46.2% and 18.6% of total variance, respectively, for the 26-taxon dataset; 56.9% and 16.5% for the 36-taxon dataset). A two-dimensional morphospace (PC1 vs. PC2) for the 36-taxon dataset is depicted in Figure 2 and the major changes in skull shape along the two primary PC axes, based on all 24 landmarks for the 26-taxon dataset, are shown in Figure 1b-c. The online supporting information includes plots of PC3 vs. PC4 for the 36-taxon study, as well as PC1-4 plots for the 26-taxon study and a diagram of major shape changes on the 13 landmarks in the 36-taxon study (Fig. S2, S3, S7). PC1 largely describes variation in the anteroposterior length of the skull, as well as the dorsoventral depth of the snout and the depth and size of the external naris. PC2 largely describes the size of the orbit (length and depth), the depth of the cheek region (the area underneath and slightly anterior to the orbit), and to a lesser extent, the depth of the temporal region (the area surrounding the lateral temporal fenestra). The caption for Figure 2 itemizes the specific changes (from negative to positive) along the two primary PC axes. In both the 26- and 36-taxon morphospaces, the most salient observation is that oviraptorosaurs are placed in a unique position on PC1, far separate from all other theropods. This is not true of PC2-4, however.

The PCAs for the two supplementary datasets excluding oviraptorosaurs (the 24- and 31-taxon datasets) also show that the majority of shape variation is summarized by the first two PC axes (38.6% and 19.5% of total variance, respectively, for the 24-taxon dataset; 37.9% and 23.13% for the 31-taxon dataset). A two-dimensional morphospace (PC1 vs. PC2) for the 31-taxon dataset is depicted in Figure 3; four-dimensional morphospaces (PC1 vs. PC2, PC3 vs. PC4) for both datasets are depicted in the online supporting information, along with diagrams depicting major shape changes on each landmark (fig. S4, S5, S8, S9). With oviraptorosaurs excluded, PC1 in the 24-taxon dataset describes the depth of the snout and the size of the

external naris (Figure S4), as it does in the full 26-taxon dataset with oviraptorosaurs included (fig. S2). However, this axis now also describes a large amount of variation in the depth of the orbit, cheek, and temporal region, which were summarized by PC2 when oviraptorosaurs were included. Furthermore, when oviraptorsaurs are excluded, PC2 largely describes the anteroposterior length of the snout, which was mainly a component of PC1 when oviraptorosaurs were included.

Both the outlying position of oviraptorosaurs on PC1 in the original 26- and 36-taxon analyses and the changes in PC loadings between the datasets that include and exclude oviraptorosaurs suggest that these short-skulled theropods contribute disproportionately to the PC analysis. PC1 of the original 26- and 36-taxon datasets largely, but not entirely, summarizes major shape differences between oviraptorosaurs and other theropods (but this is not true of successive PC axes). In other words, oviraptorosaurs are clearly the most aberrant theropods in terms of their skull shape (see further discussion of this point below).

Relationship Between Specimen Size and PC Scores: Although Procrustes Analysis largely factors out non-shape differences between specimens, such as those caused by size, there is still the possibility that some relationship between size and PC scores remains (i.e., that some PC axes may be allometry, not shape, axes). Therefore, we tested whether the first three PC axes of all four datasets are significantly correlated with the centroid size of each specimen (Table S3). There is no significant relationship between size and PC3 for all datasets and between size and PC1 for the two datasets that include oviraptorosaurs (26- and 36-taxon datasets), but there is for the two datasets excluding oviraptorosaurs (24- and 31-taxon datasets). Similarly, there is a significant relationship between size and PC2 for all datasets. However, all of these significant

relationships (except PC2 for the 31-taxon dataset) disappear when large-bodied taxa are removed. Therefore, although some relationship between size and PC scores remains, none of the axes (except perhaps for PC2 in the 31-taxon dataset) can be interpreted simply as allometry axes. PC1 and PC2 retain some information on body size in some datasets, but this is primarily because many of the largest theropods in the analysis have a similar skull shape. We interpret this as evidence of morphological convergence of the several independent radiations of large-bodied theropods.

Morphological Disparity: When oviraptorosaurs are included, the most salient result of the disparity calculations is that non-carnivores have higher disparity than carnivores based on all four disparity metrics, but these results are statistically significant only for sum of variances and marginally insignificant for product of variances (there is only a very slight overlap of error bars; see online supporting information) (Table 1; fig. S10). Although there is a clear sample size difference between the two categories (n=26 for carnivores, n=10 for non-carnivores), rarefaction analysis shows that when samples are equalized and disparity is subsampled, non-carnivores still have a greater disparity than carnivores at all sample sizes (fig. S11). Similarly, large-bodied carnivores have significantly lower disparity than all other theropods, but this pattern is almost entirely driven by the presence of non-carnivorous taxa (especially oviraptorosaurs) in the "other theropods" dataset (fig. S13, S14). Indeed, when large-bodied carnivores are compared to all other (non-large-bodied) carnivores, the two groups are found to have statistically indistinguishable disparity (fig. S13).

With that being said, the comparatively high disparity of non-carnivorous taxa compared to carnivorous taxa and the low disparity of large-bodied carnivores compared to other theropods

seem to be driven largely by the presence of the highly aberrant oviraptorosaurs in the "non-carnivore" and "non-large-bodied carnivore" categories. When disparity metrics are calculated using the 31-taxon dataset that excludes oviraptorosaurs from the PCA, carnivores are now found to have higher disparity based on the range metrics and non-carnivores higher disparity based on the variance metrics, but none of these differences are statistically significant (fig. S12). Furthermore, although large-bodied carnivores still have lower disparity than all other theropods, these results are no longer significant (fig. S15).

In sum, therefore, these results indicate that non-carnivorous theropods as a whole do have higher disparity than carnivores (based on the significant and marginally insignificant results generated from the variance calculations), but this is mostly the result of the peculiar skull shapes of one particular non-carnivorous subclade, the oviraptorosaurs. When all other non-carnivores are binned together (ornithomimosaurs, alvarezsaurids, therizinosauroids, *Limusaurus*), they collectively have indistinguishable disparity from all carnivores. Oviraptorosaurs also largely cause the relatively high disparity of non-large-bodied theropods relative to large-bodied taxa. Therefore, large-bodied carnivores do have significantly lower disparity than all other theropods, but only if oviraptorosaurs are included and only if the "other theropod" category includes both carnivores and non-carnivores. The disparity of large-bodied taxa is indistinguishable from that of smaller carnivores, or smaller carnivores plus all non-oviraptorosaur non-carnivores.

Disparity comparisons between taxonomic categories are mostly non-significant due to small sample sizes, but oviraptorosaurs and ceratosaurs (two groups including non-carnivorous taxa) have higher disparity than the entirely-carnivorous basal theropods, basal tetanurans, tyrannosauroids, and dromaeosaurids (fig. S16). Some of the comparisons involving

oviraptorosaurs are significant, which is strong evidence that this aberrant non-carnivorous clade exploited a greater swath of morphospace than other theropod subclades (see online supporting information). Tyrannosauroids, despite their great range of body size and noticeable differences in skull form between gracile and crested basal taxa and robust and deep-skull derived species, have similar measures of disparity as other carnivorous groups (basal theropods, basal tetanurans, dromaeosaurids). When these calculations are repeated using the 31-taxon dataset excluding oviraptorosaurs no significant differences between clades are found, although ceratosaurs still have relatively (but insignificantly) high disparity compared to other groups (fig. S17).

Phylogenetic Comparative Methods: All three analyses indicate that theropod cranial form is significantly correlated with phylogeny. When subjected to the permutation test in MorphoJ, all four datasets are found to have significant phylogenetic signal (24-taxon dataset: tree length=0.16899822, $p<0.001$; 26-taxon dataset: tree length=0.24750721, $p<0.0001$; 31-taxon dataset: tree length=0.17546221, $p<0.001$; 36-taxon dataset: tree length=0.26278840, $p<0.0001$). Multivariate phylogenetic eigenvector regression reveals that form metrics (PC scores) exhibit significant correlations with phylogeny in all four datasets (all sample sizes, both with and without oviraptorosaurs) (Table S7). Finally, Blomberg's methods show that PC1 of form has a significant phylogenetic signal (Table S8) in all datasets, whereas PC2 of form usually is significantly correlated with phylogeny. We also note that MPVR and Blomberg's methods show that function is strongly correlated with phylogeny (see Tables S7, S8).

Form vs. Function: 2B-PLS reveals no significant correlations between Procrustes coordinates (form) and standardized biomechanical coefficients (function), whereas MMR reveals significant but weak correlations between morphospace and function space (PC scores of form and function; Table S9). This indicates that multivariate correlation between form and function is either nonexistent or weak, based on the form and function metrics that we use as proxies. The least squares regression of PICs of form and function metrics reveals that there is no significant correlation between the single most important (most explanatory) PC values of form and function ($PC1_{form}$ vs. $PC1_{function}$) for all but one dataset, the correlation of which is extremely small (figs. S23-25). Regressions of other form and function metrics ($PC2_{form}$ and $PC2_{function}$) against each other and PC1s are marginally significant but weak, with all r^2 values less than 0.44. This indicates that major patterns of variation in form and function are only weakly correlated.

Measures of functional disparity, calculated using the PC scores from the mechanical advantage analysis, indicate that carnivorous theropods have greater disparity than non-carnivorous taxa (significant only for sum of ranges, however), and rarefaction shows that this relationship holds at all sample sizes (figs. S18-S20). Therefore, opposite to the relationship in form disparity, carnivores are more functionally diverse than non-carnivores.

Primary Determinants of Theropod Skull Shape: The series of MPVR reveals that two sources of variation, phylogeny and a combination of phylogeny and function, together explain about 71~85% of total variance in form (morphospace variance) (Tables S10-S11). The phylogenetically structured functional variance is only 17~36%, whereas variance attributed to phylogeny alone is 49~60%. Further, the lack of significantly strong correlation between form and function (see above) indicates that any proportion of variance in form explained by function

is almost entirely due to phylogenetic constraint rather than phylogenetically structured adaptive evolution. Therefore, based on these results, as well as the strong correlations between phylogeny and form but weak correlations between function and form, phylogeny is considered to be a greater determinant of theropod skull shape than biting function.

DISCUSSION

Major Patterns in Theropod Cranial Shape: Theropod skulls vary greatly in length, depth, and in the size of the orbit, naris, and lateral temporal fenestra. The largest amount of variation, which is encapsulated by PC1 in the analyses that include oviraptorosaurs, involves skull length and snout depth, whereas there is also great variance in the size (depth and length) of the orbit and depth of the temporal (posterior) portion of the skull (encapsulated by PC2). Interestingly, the depth of the snout, a major component of PC1, is not necessarily associated with the depth of the posterior portion of the skull, which is a large component of PC2. This is intuitively reasonable, as these regions are under different biomechanical, functional, and developmental constraints. Whereas snout depth is associated with the size of the naris and the antorbital fenestra (a sinus that probably lightened the skull: Witmer [1997]), posterior skull depth is closely tied to the size of the orbit, the configuration of the endocranial cavity, and the attachment area for jaw musculature (Holliday 2009).

Based on the PCA with oviraptorosaurs included, most theropods cluster fairly closely together in cranial morphospace, in the vicinity of the origin (fig. 2). The most significant outliers are oviraptorosaurs, the bizarre toothless and crested theropods that are closely related to birds (Osmólska et al. 2004). They occupy a highly positive region on PC1, reflecting their

especially anteroposteriorly shortened skulls, and a relatively negative position on PC2, reflecting their large, circular orbits. Other distinctly placed taxa include the toothless ceratosaur *Limusaurus* (Xu et al. 2009), which is among the most negatively-placed taxa on PC2 due to its enormous orbit and shallow cheek region, and the large-bodied carnivorous abelisaurids, which are positively positioned on PC1 due to their shortened skulls. In general, the morphospace occupation patterns show that oviraptorosaurs have an extreme cranial shape, and deviate most strongly from both the "typical" and the ancestral theropod morphology. This is reiterated by the fact that the major shape changes on PC1 and PC2 change dramatically between the PCAs that include and exclude oviraptorosaurs (see above).

When the PCAs are repeated after excluding oviraptorosaurs, it is now seen that large-bodied theropods, including distantly-related groups such as tyrannosaurids, abelisaurids, and allosauroids, preferentially occupy a highly positive region of PC1. In this dataset, PC1 largely summarizes variation in the depth of the orbit, cheek, and temporal region, and large-bodied taxa are positioned here due to their deep posterior skulls and narrow, keyhole-shaped orbits. The most positively placed taxon, the abelisaurid *Carnotaurus*, occupies an extreme position on PC1 due to its remarkably short and deep skull and constricted orbit (Bonaparte et al. 1990). The toothless ceratosaur *Limusaurus* still occupies a unique position, this time in a highly positive region on PC2, due to its elongate skull and large orbit and shallow cheek region (which also contribute to PC2, although less extremely than to PC1). These observations indicate that, with oviraptorosaurs excluded, large-bodied theropods (especially abelisaurids) deviate most from the "typical" and ancestral theropod morphologies.

Theropod Cranial Shape and Diet: Although the ancestral theropod was almost certainly carnivorous, more derived members of the clade developed a variety of dietary strategies, including omnivory, possible insectivory, and obligate herbivory (Barrett 2005; Senter 2005; Zanno et al. 2009; Zanno and Makovicky 2011). Our PCA results that include oviraptorosaurs show that non-carnivorous species have a greater disparity than carnivorous forms, and are also mostly positioned in separate regions of morphospace. There is no single "non-carnivorous" portion of morphospace, but rather each non-carnivorous clade occupies its own distinct swath. The non-carnivorous oviraptorosaurs, and to a lesser extent *Limusaurus*, are set well apart from carnivores, including their closest carnivorous relatives, and the non-carnivorous ornithomimosaurs and alvarezsaurids (*Shuvuuia*) are positioned at the lower left hand corner of the morphospace, as they possess among the most negative scores on both PC1 and PC2. The single therizinosauroid exemplar, *Erlikosaurus*, is the only non-carnivore that is interspersed within a "carnivorous" region of morphospace. It is noteworthy that the various clades of non-carnivores mostly occupy different regions of morphospace (the exception being that ornithomimosaurs and *Shuvuuia* are close together), indicating that different radiations of non-herbivorous taxa are associated with distinctly different cranial morphologies. In sum, these patterns suggest that the acquisition of non-carnivorous diets enabled theropods to explore different, and larger (due to their higher collective disparity), regions of morphospace, which is consistent with Zanno et al.'s (2009) hypothesis that dietary plasticity was an important driver of theropod morphological evolution.

This conclusion is tempered somewhat by the PCAs that exclude oviraptorosaurs. The collective disparity of non-carnivorous taxa is no longer greater than that of carnivores, meaning that non-oviraptorosaurian non-carnivores did not exploit a greater swath of morphospace than

carnivores. However, *Limusaurus* is still set apart from all other theropods due to its highly positive score on PC2, and the non-carnivorous ornithomimosaurs and alvarezsaurids (*Shuvuuia*) are still positioned at the lower left hand corner of the morphospace. Furthermore, the therizinosauroid *Erlikosaurus* is still positioned within a "carnivorous" region of morphospace. These results indicate that the relative morphospace positions of other non-carnivorous taxa are insensitive to the inclusion or exclusion of oviraptorosaurs, and that some non-carnivorous clades did explore different (although perhaps not larger) regions of morphospace compared to carnivores. In other words, the distinct cranial morphology of non-carnivores is not entirely due to the highly aberrant nature of oviraptorosaurs, even if the overall higher disparity of non-carnivores relative to carnivores may be.

In contrast to non-carnivorous theropods, large-bodied theropods cluster together in morphospace, both when oviraptorosaurs are included and excluded. These taxa—tyrannosaurids, allosauroids, and the carnivorous ceratosaurs—overlap almost completely on PC2 when oviraptorosaurs are included and PC1 when oviraptorosaurs are excluded, as they all have small, ovoid eyes and deep cheeks. They do, however, exhibit some variation in skull length (PC1 when oviraptorosaurs are included, PC2 when excluded). Each group represents an independent acquisition of large body size, and each has a most recent non-large-bodied ancestor close to the root of the theropod tree, yet they converge on the same region of morphospace, contra to the overall pattern of strong phylogenetic signal in skull shape (i.e., non-convergence). This is not simply due to the fact that PC1 and PC2 are allometric (body size) axes, as there is almost always no significant relationship between PC scores and specimen size in the non-large-bodied taxa (see above). Furthermore, when oviraptorosaurs are included, the large-bodied taxa have significantly lower disparity than all other theropods (although this relationship does not

hold when oviraptorosaurs are excluded). In total, these patterns suggest that there is a limited morphological toolkit for building (through evolution) a large-bodied dinosaurian hyperpredator (although perhaps no more limited than for building a smaller carnivore, as large-bodied carnivores and smaller carnivores have indistinguishable disparity). Low disparity and morphological convergence have also been noted among mammalian hypercarnivores (those taxa that solely eat meat) (Holliday and Steppan 2004), and may be more general evolutionary phenomena unique to large-bodied carnivores and/or taxa that solely consume meat.

Form, Function, and Phylogeny: Theropod skull form is strongly correlated with phylogeny but only weakly correlated with the measure of function that we utilise (mechanical advantage of the jaw muscles), and our statistical tests show that phylogeny explains a substantially greater amount of variance in skull shape than does function. In other words, closely related species are more similar in morphology than with distantly related species, and distances in morphospace are more congruent with phylogenetic distances than with distances in function space. Therefore, phylogeny is the primary determinant of broad patterns in theropod skull shape, and theropod cranial anatomy was apparently subject to strong phylogenetic constraint. It is important to keep in mind that our study is a broad-scale analysis that examines the range of skull shapes across Mesozoic non-avian theropods, rather than a focused analysis that looks at subtle differences between many individual species. Therefore, our results show that higher-level theropod phylogeny is the best correlate of large-scale variation in theropod skull shape, but it is possible that this correlation would be weaker at lower taxonomic levels (i.e., within individual theropod subclades). A disconnect between strong higher-level, but weak lower-level, correlations between phylogeny and shape has been noted in extant pinniped mammals (Jones and Goswami

2010), and whether this holds true for theropods awaits the compilation of larger morphometric datasets as more fossils are discovered.

Although our statistical tests show weak correlation between skull shape and function, we do not argue that function played no role in shaping theropod cranial anatomy. The function metric that we use, mechanical advantage, specifically quantifies the biting performance and efficiency of theropods (Westneat 1994; Sakamoto 2010). This is only one of numerous possible functional metrics, and other measures, such as skull strength, may exhibit stronger correlations with skull shape. Testing this proposition awaits further biomechanical studies of theropods, and it would be especially interesting to determine whether estimates of skull strength generated from finite element modeling (Rayfield 2005, 2007) and beam theory (Henderson 2002) correlate with broad-scale patterns in theropod skull shape. A previous study that noted a correlation between theropod orbit size (form) and skull strength generated from beam theory models (function) suggests that this may be the case (Henderson 2002).

Furthermore, we note that our function metric is based on both cranial and mandibular measurements, whereas our form metric solely encapsulates the geometric shape of the cranium. These slightly different data sources may explain the weak correlation between the two metrics, and future studies may wish to examine the relationship between mandible shape and biting performance. Our sensitivity analysis, however, shows that cranial shape, not mandibular shape, is the overriding factor in our functional (mechanical advantage) calculations (see online supplementary information). Therefore, we suspect that the different measurement sources for the form and function metrics are not driving their weak correlation.

Finally, it is possible that we do not find a strong correlation between form and function because biting performance (and perhaps other function metrics) may not correlate with major

sources of skull variation, such as variance in length, snout depth, and cheek depth, but rather correlate with other, more subtle features that are not captured by the morphometic analysis. As our morphometric study quantifies cranial shape using two-dimensional coordinates plotted only on the lateral surface of the skull, it is possible that future studies using different protocols (three-dimensional coordinates, landmarks on the dorsal and palatal surfaces, etc.) may find different results.

The Evolution of Skull Shape in Theropods: By plotting phylogeny into morphospace, with the position of internal nodes calculated using squared change parsimony, it is possible to examine broad patterns in theropod cranial evolution. The following description utilises the full morphospace with oviraptorosaurs (fig. 2), as it contains the largest sample of theropod taxa, but similar (although slightly different) patterns are evident by examining the morphospace ordinated without oviraptorosaurs (fig. 3). Interestingly, the common ancestors of theropods, tetanurans, coelurosaurs, and maniraptorans are all located fairly closely in morphospace. The common ancestor of all theropods had a long skull, shallow snout, and a horizontal naris (negative position PC1), and a large, circular orbit and shallow cheek region (quite negative position on PC2). Moving progressively up the tree, the tetanuran common ancestor had a similar skull length as the theropod ancestor (nearly identical score on PC1), but a smaller orbit and deeper cheek region (more positive position on PC2). Finally, the coelurosaurian and maniraptoran common ancestors had proportionally longer skulls and a larger orbit and shallower cheek region (reversal to more negative scores on PC2).

It is difficult to confidently assess the amount of evolution between sister taxa (branch lengths in morphospace), because large jumps in morphospace may reflect either great bursts of

cranial evolution or be a figment of missing data (most theropods do not preserve complete or near-complete skulls and could not be included in this study, but if included they may fill gaps between widely separated clades). With this in mind, two patterns appear to be robust.

First, although non-carnivorous taxa generally occupy distinct regions of morphospace, only half of them in the current study (the oviraptorosaurs and *Limusaurus*) are far separated from their closest carnivorous relatives. The other half, including ornithomimosaurs, alvarezsaurids, and therizinosauroids, are only marginally separated from their closest carnivorous relatives. In other words, branch lengths between these taxa and their carnivorous relatives are on the same order of magnitude as branch lengths between carnivorous sister taxa (see Figures 2 and 3 for quantification of branch lengths). Therefore, although these taxa may have unusual skull morphologies that do not overlap with those of carnivorous taxa (hence their distinct positions in morphospace), it did not require great amounts (and perhaps rates) of evolution to acquire these. This supports the notion that phylogeny is a greater influence on skull shape than function, as even many dietarily aberrant clades are, at least based on branch lengths, morphologically similar to close relatives with different feeding habits. Dietary and ecological habits do play a supporting role in shaping skull morphology, however, as shown by the larger relative disparity of non-carnivorous taxa (with oviraptorosaurs included) and the mostly distinct positions of most herbivorous clades in morphospace (even if they are located near carnivorous relatives).

Second, distantly-related large-bodied theropods converge on the same region of morphospace (especially on PC2 when oviraptorosaurs are included and PC1 when excluded). Along with the observations about the high disparity and distinct morphospace positions of non-carnivores, this shows that although phylogeny is a major constraint on theropod skull form,

function (especially relating to feeding ecology) still played a role in shaping theropod cranial evolution.

The relative importance of phylogeny, function, and other potential drivers of theropod skull shape should become clearer as morphometric techniques become more refined and especially as datasets expand with the discovery of new theropod taxa. Unfortunately, many of our statistical comparisons are non-significant due to the overlap of large error bars, which is almost certainly a function of small sample sizes in many cases. Small sample sizes also preclude the use of some additional statistical techniques, such as Discriminant Function Analysis, to more confidently test whether non-carnivorous subclades inhabited distinct regions of morphospace (alvarezsaurids and therizinosauroids, for instance, are only represented by a single taxon each in this analysis, because complete or near-complete skull material for these clades is so rare). The overriding hypothesis that we present in this paper, which our overall sample size of 36 taxa and cocktail of multivariate methods are adequate to address, is that phylogeny and not biting function better explains broad patterns in theropod skull shape. We look forward to additional tests of this hypothesis as more data become available, as well as similar studies of other clades. Only studies such as these can address a fundamental, but largely unsolved, question in the evolution of many groups: was phylogenetic constraint or functional adaptation more important in shaping morphology?

TABLES

TABLE 3-1: Comparisons of morphological disparity, based on four metrics (the sums and products of the ranges and variances on the first five PC axes from the morphometric analysis), in different categories of taxa. Comparisons are shown between carnivores and non-carnivores, as well as large-bodied carnivores vs. both smaller carnivores (all other carnivores) and all other theropods (small carnivores + non-carnivores). Disparity metrics are calculated twice, first using the 36-taxon/13-landmark analysis that includes oviraptorosaurs and secondly with the 31-taxon/13-landmark analysis that excludes oviraptorosaurs (denoted by "no ovi." in the table). The two numerical values for each comparison indicate the disparity metric for the group in question. For example, in the first comparison, carnivores have a sum of ranges of 0.81 and non-carnivores 0.99. Significant comparisons are denoted by SIG and one marginally significant comparison (in which the error bars for both measures ever so slightly overlap) is denoted by MSIG. Please see the online supporting information for more details, an explanation of the statistical significance tests, and graphical plots of all disparity metrics and their associated error bars.

Comparison	**Sum of Ranges**	**Prod of Ranges**	**Sum of Variances**	**Prod of Variances**
Carnivore vs. non-carnivore	0.81/0.99	0.15/0.17	0.011/0.044 **SIG**	0.0018/0.0035 **MSIG**
Carnivore vs. non-carnivore (no ovi.)	0.79/0.56	0.15/0.11	0.012/0.015	0.0017/0.0023
Large carn. vs. small carn.	0.54/0.57	0.10/0.11	0.006/0.006	0.0012/0.0012
Large carn. vs. all others	0.54/1.06 **SIG**	0.10/0.18 **SIG**	0.006/0.029 **SIG**	0.0012/0.0026 **SIG**
Large carn. vs. small carn. (no ovi.)	0.56/0.54	0.11/0.10	0.0069/0.0069	0.0014/0.0011
Large carn. vs. all others (no ovi.)	0.56/0.73	0.11/0.14	0.0069/0.009	0.0014/0.0016

TABLE 3-S1: Sources for skull images used in morphometric analysis.

Taxon	Source
Acrocanthosaurus	Eddy and Clarke 2011, PLoS ONE
Alioramus	Brusatte et al. 2009a, PNAS
Allosaurus	Rayfield et al. 2001, Nature
Austroraptor	Novas et al. 2008, Proceedings of the Royal Society, Series B
Bambiraptor	Burnham et al. 2000, Univ of Kansas Paleontological Contributions
Bistahieversor	Carr and Williamson 2010, Journal of Vertebrate Paleontology
Byronosaurus	Makovicky et al. 2003, American Museum Novitates
Carcharodontosaurus	Sereno et al. 1996, Science
Carnotaurus	Sampson & Witmer 2007, Society of Vertebrate Paleontology Memoir
Ceratosaurus	Sampson & Witmer 2007, Society of Vertebrate Paleontology Memoir
Citipati	Osmólska, Currie, and Barsbold 2004, The Dinosauria 2nd Edition (Univ. of California Press)
Coelophysis	Colbert 1989, Museum of Northern Arizona Bulletin
Compsognathus	Peyer 2006, Journal of Vertebrate Paleontology
Conchoraptor	Osmólska, Currie, and Barsbold 2004, The Dinosauria 2nd Edition (Univ. of California Press)
Daspletosaurus	Holtz 2004, The Dinosauria 2nd Edition (Univ. of California Press)
Deinonychus	Ostrom 1969, Bulletin of the Peabody Museum of Natural History
Dilong	Xu et al. 2004, Nature
Dilophosaurus	Welles 1984, Palaeontographica Abteilung A
Dromaeosaurus	Currie 1995, Journal of Vertebrate Paleontology
Dubreuillosaurus	Allain 2002, Journal of Vertebrate Paleontology
Eoraptor	Sereno et al. 1993, Nature
Erlikosaurus	Currie 2000, The Age of Dinosaurs in Russia and Mongolia (Cambridge Univ. Press)
Gallimimus	Osmólska et al. 1972, Palaeontologica Polonica
Garudimimus	Kobayashi and Barsbold 2005, Canadian Journal of Earth Sciences
Gorgosaurus	Currie 2003, Acta Palaeontologica Polonica
Guanlong	Xu et al. 2006, Nature
Haplocheirus	Choiniere et al. 2010, Science
Herrerasaurus	Sereno and Novas 1994, Journal of Vertebrate Paleontology
Incisivosaurus	Balanoff et al. 2009, American Museum Novitates
Juravenator	Gohlich and Chiappe 2006, Nature
Khaan	Clark et al. 2001, Journal of Vertebrate Paleontology
Limusaurus	Xu et al. 2009, Nature
Majungasaurus	Sampson and Witmer 2007, Society of Vertebrate Paleontology Memoir
Monolophosaurus	Brusatte et al. 2010b, Zoological Journal of the Linnean Society
Ornitholestes	Osborn 1916, Bulletin of the American Museum of Natural History
Ornithomimus	Currie 2005, Dinosaur Provincial Park (Indiana Univ. Press)
Rinchenia	Osmólska, Currie, and Barsbold 2004, The Dinosauria 2nd Edition (Univ. of California Press)
Saurornithoides	Norell et al. 2009, American Museum Novitates
Shuvuuia	Sereno 2001, New Perspectives on the Origin and Early Evolution of Birds (Peabody Museum, Yale)
Sinornithosaurus	Xu and Wu 2001, Canadian Journal of Earth Sciences
Sinornithomimus	Kobayashi et al. 2003, Acta Palaeontologica Polonica
Sinraptor	Currie and Zhao 1993, Canadian Journal of Earth Sciences
Skorpiovenator	Canale et al. 2009, Naturwissenschaften
Syntarsus	Tykoski and Rowe 2004, The Dinosauria 2nd Edition (Univ. of California Press)
Tarbosaurus	Currie 2000, The Age of Dinosaurs in Russia and Mongolia (Cambridge Univ. Press)
Tawa	Nesbitt et al. 2009, Science
Tsaagan	Norell et al. 2006, American Museum Novitates
Tyrannosaurus	Rayfield 2004, Proceedings of the Royal Society of London, Series B
Velociraptor	Currie 2000, The Age of Dinosaurs in Russia and Mongolia (Cambridge Univ. Press)
Zanabazar	Norell et al. 2009, American Museum Novitates
Zupaysaurus	Ezcurra 2007, Historical Biology

TABLE 3-S2: Table showing which taxa are included in the four PCA datasets. The 13 landmarks in the 36 and 31-taxon analyses are landmarks 1,2,4,5,7,10,11,12,15,16,17,19,21.

	26-taxon/24-landmarks	24-taxon/24-landmarks	36-taxon/13-landmarks	31-taxon/13-landmarks
Acrocanthosaurus	x	x	x	x
Allosaurus	x	x	x	x
Bambiraptor			x	x
Bistahieversor			x	x
Carnotaurus	x	x	x	x
Ceratosaurus	x	x	x	
Citipati	x		x	x
Coelophysis	x	x	x	x
Compsognathus	x	x	x	
Conchoraptor	x		x	
Daspletosaurus	x	x	x	x
Dilong	x	x	x	x
Eoraptor	x	x	x	x
Erlikosaurus	x	x	x	x
Gallimimus			x	x
Garudimimus			x	x
Gorgosaurus	x	x	x	x
Guanlong	x	x	x	x
Herrerasaurus	x	x	x	x
Incisivosaurus			x	
Juravenator			x	x
Khaan			x	
Limusaurus	x	x	x	x
Majungasaurus	x	x	x	x
Monolophosaurus	x	x	x	x
Ornitholestes			x	x
Rinchenia			x	
Shuvuuia			x	x
Sinornithosaurus	x	x	x	x
Sinraptor	x	x	x	x
Syntarsus	x	x	x	x
Tarbosaurus	x	x	x	x
Tawa	x	x	x	x
Tsaagan	x	x	x	x
Tyrannosaurus	x	x	x	x
Velociraptor	x	x	x	x

TABLE 3-S3: Linear correlation between specimen centroid size and PC loadings for the four PC datasets. In parentheses, it is indicated whether the relationship between centroid size and PC score is positive (positive allometry, positive correlation coefficient) or negative (negative allometry, negative correlation coefficient).

26-taxon/24-landmarks
PC1: r^2=0.014, p=0.563 (positive relationship)
PC2: r^2=0.569, p<0.001 (positive relationship)
PC2 minus large-bodied theropods: r^2=0.108, p=0.232
PC3: r^2=0.058, p=0.234 (negative relationship)

24-taxon/24-landmarks (no oviraptorosaurs)
PC1: r^2=0.206, p=0.026 (negative relationship)
PC1 minus large-bodied theropods: r^2=0.188, p=0.139
PC2: r^2=0.442, p<0.001 (negative relationship)
PC2 minus large-bodied theropods: r^2=0.250, p=0.082
PC3: r^2=0.030, p=0.420 (negative relationship)

36-taxon/13-landmarks
PC1: r^2=0.053, p=0.177 (negative relationship)
PC2: r^2=0.646, p<0.001 (positive relationship)
PC2 minus large-bodied theropods: r^2=0.155, p=0.06
PC3: r^2=0.002, p=0.773 (positive relationship)

31-taxon/13-landmarks (no oviraptorosaurs)
PC1: r^2=0.417, p<0.001 (positive relationship)
PC1 minus large-bodied theropods: r^2=0.0277, p=0.496
PC2: r^2=0.269, p=0.003 (negative relationship)
PC2 minus large-bodied theropods: r^2=0.361, p=0.007
PC3: r^2=0.006, p=0.665 (negative relationship)

TABLE 3-S4: Table showing the dietary categories into which the 36 theropod taxa are binned.

	Carnivores	Non-Carnivores	Large-Bodied Carnivores	Non-Large Carnivores
Acrocanthosaurus	x		x	
Allosaurus	x		x	
Bambiraptor	x			x
Bistahieversor	x		x	
Carnotaurus	x		x	
Ceratosaurus	x		x	
Citipati		x		
Coelophysis	x			x
Compsognathus	x			x
Conchoraptor		x		
Daspletosaurus	x		x	
Dilong	x			x
Eoraptor	x			x
Erlikosaurus		x		
Gallimimus		x		
Garudimimus		x		
Gorgosaurus	x		x	
Guanlong	x			x
Herrerasaurus	x			x
Incisivosaurus		x		
Juravenator	x			x
Khaan		x		
Limusaurus		x		
Majungasaurus	x		x	
Monolophosaurus	x		x	
Ornitholestes	x			x
Rinchenia		x		
Shuvuuia		x		
Sinornithosaurus	x			x
Sinraptor	x		x	
Syntarsus	x			x
Tarbosaurus	x		x	
Tawa	x			x
Tsaagan	x			x
Tyrannosaurus	x		x	
Velociraptor	x			x

TABLE 3-S5: Table showing the phylogenetic categories into which the theropod taxa are binned.

A) Basal Theropods	
	Coelophysis
	Eoraptor
	Herrerasaurus
	Syntarsus
	Tawa
B) Ceratosaurs	
	Carnotaurus
	Ceratosaurus
	Majungasaurus
	Limusaurus
C) Basal Tetanurans	
	Acrocanthosaurus
	Allosaurus
	Monolophosaurus
	Sinraptor
D) Tyrannosauroids	
	Bistahieversor
	Daspletosaurus
	Dilong
	Gorgosaurus
	Guanlong
	Tarbosaurus
	Tyrannosaurus
E) Dromaeosaurids	
	Bambiraptor
	Sinornithosaurus
	Tsaagan
	Velociraptor
F) Oviraptorosaurs	
	Citipati
	Conchoraptor
	Incisivosaurus
	Khaan
	Rinchenia

TABLE 3-S6: First occurrence dates (millions of years ago, Ma) of the 36 taxa, used to calculate branch lengths in some of the phylogenetically-informed statistical analyses.

TAXON	AGE
Herrerasaurus	229.165
Eoraptor	229.165
Tawa	214
Coelophysis	216
Syntarsus	195.6
Limusaurus	158.45
Ceratosaurus	150.6
Carnotaurus	77.05
Majungasaurus	68.05
Monolophosaurus	162.95
Sinraptor	158.45
Allosaurus	150.6
Acrocanthosaurus	118.5
Guanlong	158.45
Dilong	125
Bistahieversor	73.825
Gorgosaurus	77.05
Daspletosaurus	77.05
Tarbosaurus	70.6
Tyrannosaurus	70.6
Compsognathus	148.15
Juravenator	153.25
Ornitholestes	150.6
Gallimimus	73.825
Garudimimus	94.45
Shuvuuia	77.05
Erlikosaurus	94.45
Incisivosaurus	125
Conchoraptor	77.05
Khaan	77.05
Rinchenia	77.05
Citipati	77.05
Sinornithosaurus	125
Bambiraptor	77.05
Tsaagan	77.05
Velociraptor	77.05

TABLE 3-S7: Overall strengths and significances of the multivariate phylogenetic eigenvector regressions of form/function matrix against phylogenetic eigenvector matrix. R^2-values and *p*-values are shown. Significance codes: 0.01, **; 0.001, ***.

Response	R^2	*p*-value
36-Taxa form	0.847	$2.18\times10^{-3**}$
35-Taxa form	0.848	$1.12\times10^{-3**}$
35-Taxa func	0.869	$1.48\times10^{-3**}$
31-Taxa form	0.776	$3.64\times10^{-4***}$
30-Taxa form	0.769	$1.19\times10^{-3**}$
30-Taxa func	0.853	$9.67\times10^{-3**}$
26-Taxa form	0.817	$1.03\times10^{-6***}$
26-Taxa func	0.782	$4.70\times10^{-3**}$
24-Taxa form	0.705	$4.47\times10^{-4***}$
24-Taxa func	0.756	$4.31\times10^{-3**}$

TABLE 3-S8: Significance and strength of phylogenetic signal using Blomberg's *K*. *K*-statistic indicating strength of phylogenetic signal, observed variance of the PIC ($PIC_{var.obs}$), mean variance of PIC from the permutation ($PIC_{var.rnd}$), *Z*-score of observed vs. random variance of PIC and *p*-value of observed vs. random variance of PIC (Kembel *et al.*, 2009) are shown for each variable on the various trees. Significance codes: 0.05, *; 0.01, **; 0.001, ***.

Dataset		*K*	$PIC_{var.obs}$	$PIC_{var.rnd}$	Z-score	*p*-value
36-taxa	$PC1_{form}$	0.664	2.24×10^{-4}	9.37×10^{-4}	-2.74	$1.00\times10^{-4***}$
	$PC2_{form}$	0.468	1.47×10^{-4}	2.71×10^{-4}	-2.08	$4.10\times10^{-3**}$
	$PC3_{form}$	0.297	7.48×10^{-5}	1.01×10^{-4}	-1.00	0.125
	$PC4_{form}$	0.165	9.76×10^{-5}	8.54×10^{-5}	0.545	0.766
	$PC5_{form}$	0.302	4.65×10^{-5}	7.16×10^{-5}	-1.41	$3.56\times10^{-2*}$
35-taxa	$PC1_{form}$	0.66	2.30×10^{-4}	9.27×10^{-4}	-2.6	$1.00\times10^{-4***}$
	$PC2_{form}$	0.469	1.50×10^{-4}	2.65×10^{-4}	-1.92	$1.00\times10^{-2*}$
	$PC3_{form}$	0.317	7.12×10^{-5}	9.70×10^{-5}	-0.988	0.119
	$PC4_{form}$	0.163	1.00×10^{-4}	8.49×10^{-5}	0.68	0.802
	$PC5_{form}$	0.296	4.77×10^{-5}	7.13×10^{-5}	-1.26	$5.02\times10^{-2*}$
	$PC1_{func}$	1.62	6.47×10^{-2}	1.47×10^{-1}	-2.17	$5.00\times10^{-4***}$
	$PC2_{func}$	0.39	8.42×10^{-3}	1.68×10^{-2}	-1.86	$2.20\times10^{-3**}$
31-taxa	$PC1_{form}$	0.575	1.11×10^{-4}	3.66×10^{-4}	-2.57	$1.00\times10^{-4***}$
	$PC2_{form}$	0.304	2.49×10^{-4}	2.23×10^{-4}	0.389	0.714
	$PC3_{form}$	0.274	5.71×10^{-5}	9.26×10^{-5}	-1.18	0.0535
	$PC4_{form}$	0.383	4.01×10^{-5}	7.86×10^{-5}	-1.76	$3.80\times10^{-3**}$
	$PC5_{form}$	0.361	3.66×10^{-5}	4.65×10^{-5}	-0.821	0.193
30-taxa	$PC1_{form}$	0.575	1.14×10^{-4}	3.59×10^{-4}	-2.46	$1.00\times10^{-4***}$
	$PC2_{form}$	0.302	2.57×10^{-4}	2.19×10^{-4}	0.534	0.768
	$PC3_{form}$	0.287	5.49×10^{-5}	8.93×10^{-5}	-1.12	0.0603
	$PC4_{form}$	0.393	3.99×10^{-5}	7.78×10^{-5}	-1.72	$4.40\times10^{-3**}$
	$PC5_{form}$	0.358	3.75×10^{-5}	4.62×10^{-5}	-0.698	0.248
	$PC1_{func}$	1.43	7.46×10^{-2}	1.71×10^{-1}	-1.98	$1.10\times10^{-3**}$
	$PC2_{func}$	0.25	8.14×10^{-3}	1.16×10^{-2}	-1.02	0.114
26-taxa	$PC1_{form}$	0.554	2.36×10^{-4}	7.85×10^{-4}	-1.76	$1.10\times10^{-3**}$
	$PC2_{form}$	0.443	1.53×10^{-4}	3.17×10^{-4}	-1.76	$6.20\times10^{-3**}$
	$PC3_{form}$	0.409	1.14×10^{-4}	1.55×10^{-4}	-0.827	0.187
	$PC4_{form}$	0.221	6.91×10^{-5}	9.27×10^{-5}	-0.758	0.213
	$PC5_{form}$	0.376	3.53×10^{-5}	6.68×10^{-5}	-1.44	$1.65\times10^{-2*}$
	$PC1_{func}$	1.14	8.42×10^{-2}	1.68×10^{-1}	-1.65	$1.25\times10^{-2*}$
	$PC2_{func}$	0.34	7.61×10^{-3}	1.33×10^{-2}	-1.28	$3.65\times10^{-2*}$
24-Taxa	$PC1_{form}$	0.509	1.54×10^{-4}	4.71×10^{-4}	-1.88	$5.00\times10^{-4***}$
	$PC2_{form}$	0.307	2.51×10^{-4}	2.37×10^{-4}	0.166	0.667
	$PC3_{form}$	0.248	7.26×10^{-5}	1.11×10^{-4}	-1.04	0.102
	$PC4_{form}$	0.425	3.63×10^{-5}	7.84×10^{-5}	-1.61	$4.90\times10^{-3**}$
	$PC5_{form}$	0.601	4.88×10^{-5}	6.24×10^{-5}	-0.607	0.28
	$PC6_{form}$	0.199	4.38×10^{-5}	5.25×10^{-5}	-0.553	0.323
	$PC7_{form}$	0.409	3.09×10^{-5}	3.86×10^{-5}	-0.66	0.267
	$PC1_{func}$	1.03	9.16×10^{-2}	1.81×10^{-1}	-1.62	$1.55\times10^{-2*}$
	$PC2_{func}$	0.285	7.60×10^{-3}	1.21×10^{-2}	-1.05	0.0868

TABLE 3-S9: Results of two-block partial least squares and multivariate multiple regression analyses. Correlation between Procrustes coordinates and standardized biomechanical coefficients and *p*-values were determined using two-block partial least squares in MorphoJ. A multivariate equivalent of the R^2 value and *p*-value were computed in R. Significance codes: 0.01, **; 0.001, ***.

Sample size	*RV* (2B-PLS)	*p*-value	R^2 (MMR)	*p*-value
35-taxa	0.107	0.0861	0.415	$7.73\times10^{-7***}$
30-taxa	0.138	0.0908	0.319	$6.01\times10^{-5***}$
26-taxa	0.121	0.166	0.328	$3.68\times10^{-4***}$
24-taxa	0.133	0.206	0.306	$2.79\times10^{-3**}$

TABLE 3-S10: Results of PVR on the various combinations of response and predictors. Proportion of variance explained by the MMR model (R^2), *p*-value, and Akaike weights (w_i) are shown for each sample size. R^2 values from each sample size were further used to partition morphospace variance (Table S10). Significance codes: 0.01, **; 0.001, ***.

Sample size	MMR model	R^2	*p*-value	Akaike weights (w_i)
35-taxa	form vs function	0.415	$7.73\times10^{-7***}$	1.53×10^{-59}
	form vs phylogeny	0.848	$1.12\times10^{-3**}$	1.58×10^{-16}
	form vs func+phylo	0.902	$2.09\times10^{-4***}$	1.00
30-taxa	form vs function	0.319	$6.01\times10^{-5***}$	1.24×10^{-51}
	form vs phylogeny	0.769	$1.19\times10^{-3**}$	6.93×10^{-23}
	form vs func+phylo	0.886	$1.94\times10^{-5***}$	1.00
26-taxa	form vs function	0.328	$3.68\times10^{-4***}$	3.65×10^{-56}
	form vs phylogeny	0.817	$1.03\times10^{-6***}$	3.49×10^{-24}
	form vs func+phylo	0.923	$3.80\times10^{-8***}$	1.00
24-taxa	form vs function	0.306	$2.79\times10^{-3**}$	8.66×10^{-50}
	form vs phylogeny	0.705	$4.47\times10^{-4***}$	1.77×10^{-22}
	form vs func+phylo	0.841	$1.69\times10^{-4***}$	1.00

TABLE 3-S11: Proportion of variance in morphospace for each sample size. Variance in morphospace (PC1-PC5 or PC1-PC7) are partitioned into four compartments: a, proportion of variance attributed to function ($PC1_{func}$ and $PC2_{func}$); b, proportion of variance attributed to a combination of function and phylogeny (phylogenetically structured variance); c, proportion of variance attributed to phylogeny alone; and d, proportion of variance unexplained by the model.

Sample size	a	b	c	d
35-taxa	0.0539	0.361	0.487	0.0979
30-taxa	0.117	0.202	0.567	0.114
26-taxa	0.106	0.222	0.595	0.0772
24-taxa	0.136	0.170	0.535	0.159

FIGURES

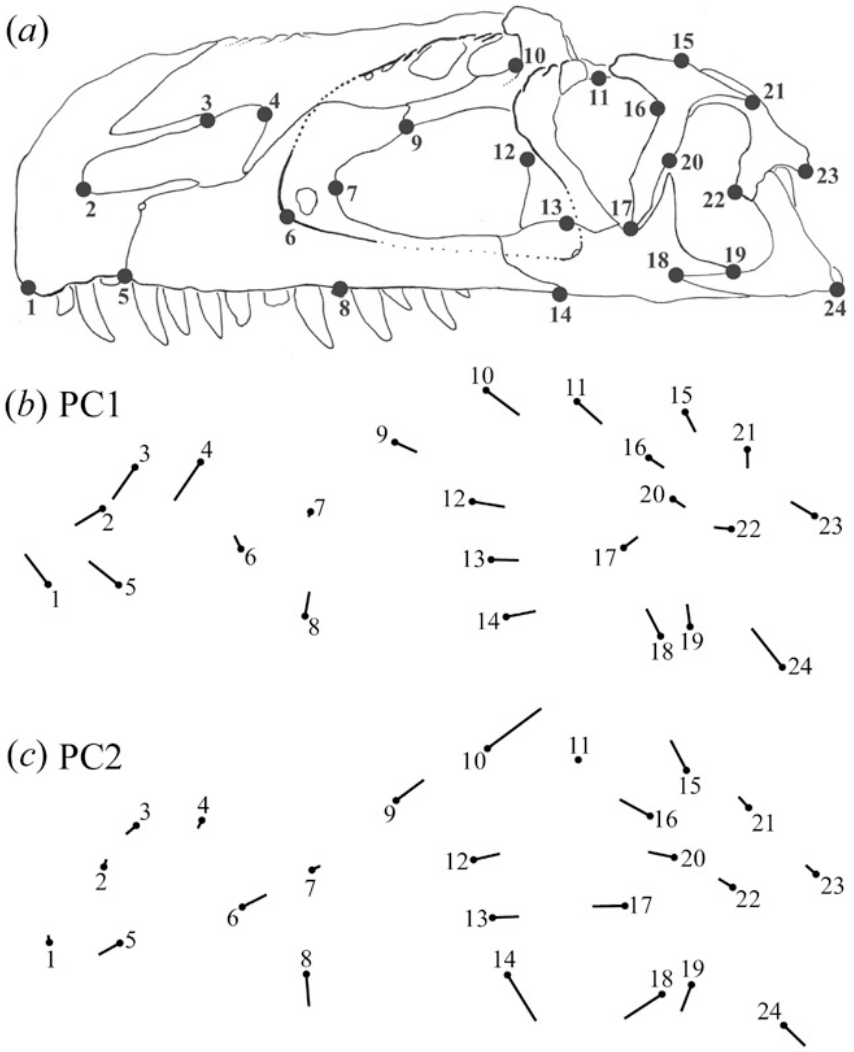

Figure 3.1. Theropod skull shape analyzed using geometric morphometrics. (a) Homologous landmarks plotted on all skulls in the study. (b) Major changes in skull shape (based on each landmark) on principal component (PC) axis 1 for the 26-taxon, 24-landmark analysis. (c) Major changes in skull shape based on principal component axis 2 for the same analysis. Skull depicted in (a) is the basal tetanuran *Monolophosaurus*.

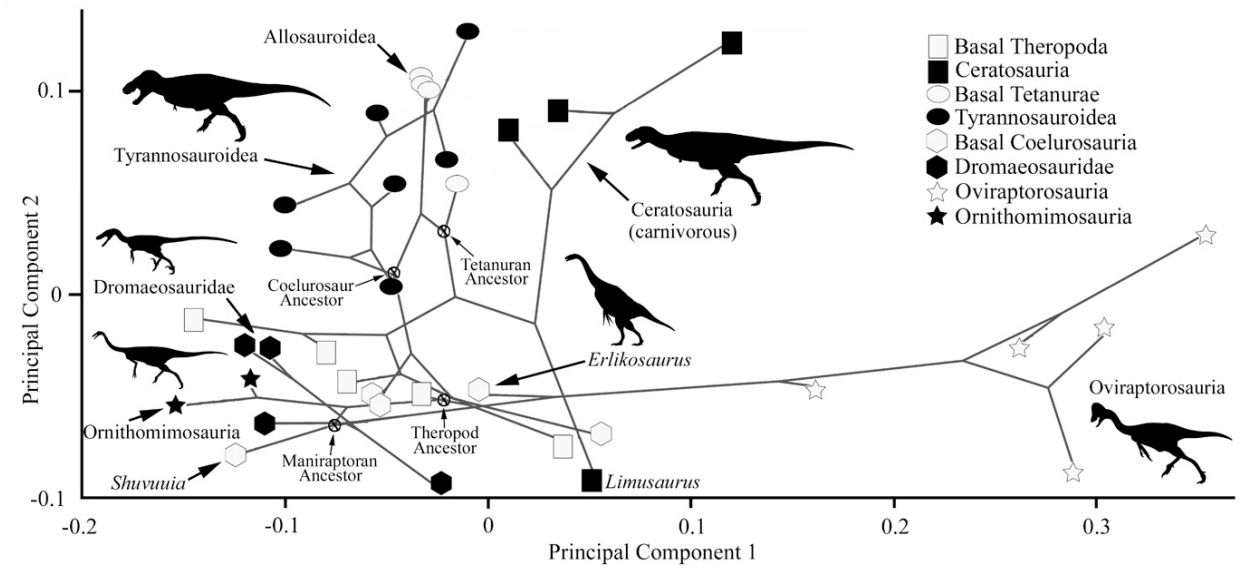

Figure 3.2. Two-dimensional theropod skull shape morphospace, based on the first two PC axes generated by the 36-taxon, 13-landmark analysis. The phylogenetic tree is mapped into morphospace, with internal nodes placed according to a squared-change parsimony optimization. Four major nodes (most recent common ancestor of Theropoda, Tetanurae, Coelurosauria, and Maniraptora) are labeled. Major changes in skull shape along the two PC axes are depicted in Figure S7. Changes along PC1 (negative to positive) reflect an anteroposterior shortening of the skull, a dorsoventral deepening of the snout, and reorientation of the long axis of the naris from a horizontal to an oblique orientation. Changes along PC2 (negative to positive) reflect a reduction in the area of the orbit, the development of a proportionally taller and shorter orbit, and a deepening of the cheek region. Theropod silhouettes courtesy of Scott Hartman (http://www.skeletaldrawing.com/).

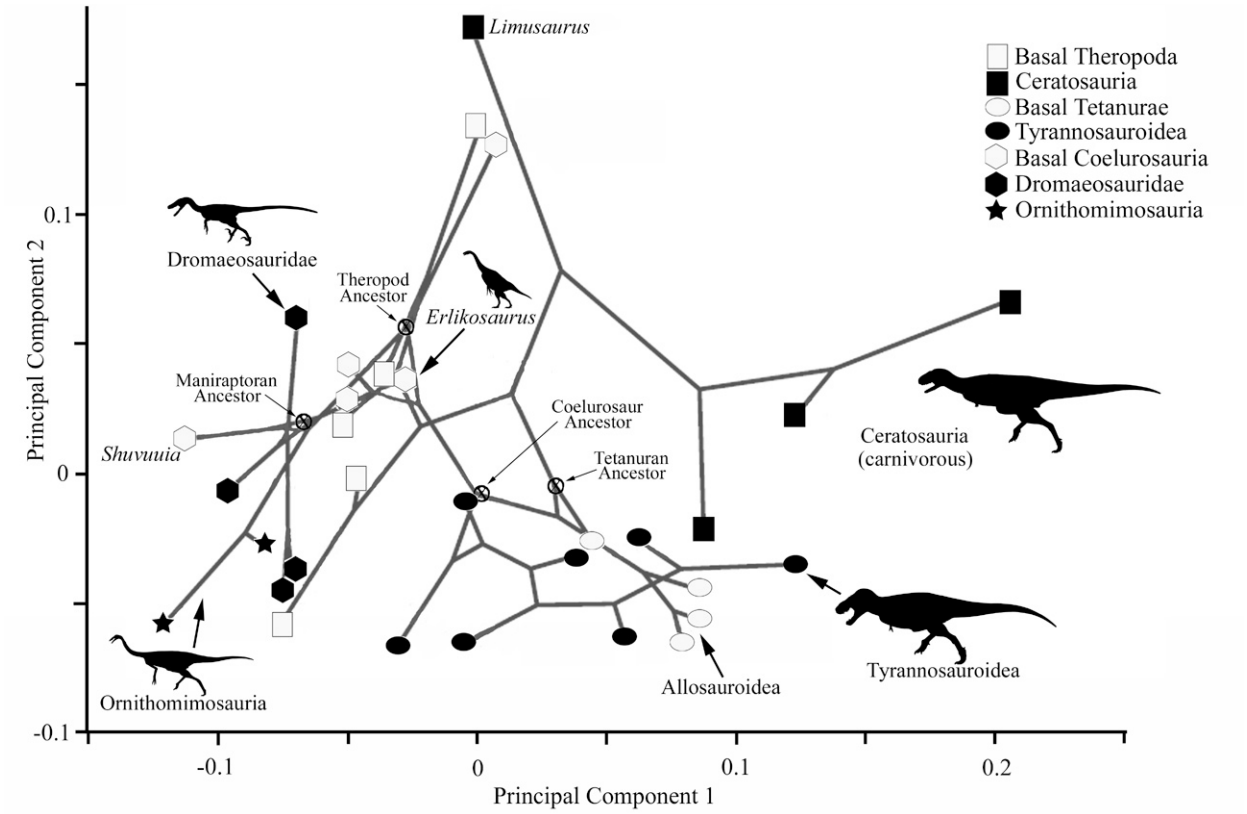

Figure 3.3. Two-dimensional theropod skull shape morphospace, based on the first two PC axes generated by the 31-taxon, 13-landmark analysis (excluding oviraptorosaurs). The phylogenetic tree is mapped into morphospace, with internal nodes placed according to a squared-change parsimony optimization. Four major nodes (most recent common ancestor of Theropoda, Tetanurae, Coelurosauria, and Maniraptora) are labeled. Major changes in skull shape along the two PC axes are depicted in Figure S9. Changes along PC1 (negative to positive) reflect a dorsoventral deepening of the snout, orbit, and temporal region, and anteroposterior constriction of the orbit. Changes along PC2 (negative to positive) largely reflect a proportionally longer skull and anteroposterior lengthening of the orbit, as well as some changes in the depth of the temporal portion of the skull. Theropod silhouettes courtesy of Scott Hartman (http://www.skeletaldrawing.com/).

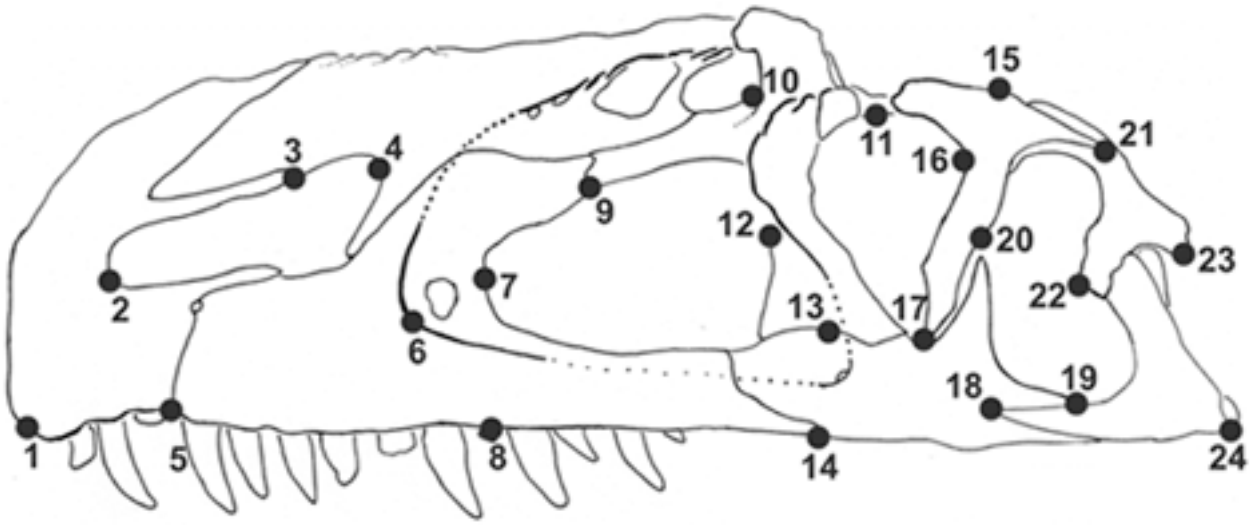

Figure 3-S1. Landmarks plotted on all theropod skulls analyzed in this study. Definition of landmarks is as follows: 1) anteroventral corner of premaxilla (anteroventral corner of skull); 2) anteroventral corner of external naris; 3) contact of premaxilla and nasal above external naris; 4) posterodorsal corner of external naris; 5) contact of premaxilla and maxilla along tooth row; 6) anteroventral corner of antorbital fossa; 7) anterior-most point of antorbital fenestra; 8) point on ventral margin of maxilla immediately below point 7; 9) contact of maxilla and lacrimal above antorbital fenestra; 10) dorsal-most point of lacrimal above ventral ramus; 11) midpoint of dorsal margin of orbit (usually midpoint of frontal contribution to orbital rim); 12) midpoint of posterior margin of antorbital fenestra (usually where medial and lateral laminae of lacrimal meet; 13) midpoint of lacrimal-jugal suture on lateral surface of skull; 14) contact of maxilla and jugal along ventral margin of skull; 15) dorsal-most point of postorbital above ventral ramus; 16) posterodorsal corner of the orbit; 17) contact of postorbital and jugal on the orbital margin; 18) anterior tip of quadratojugal anterior proecess; 19) contact of jugal and quadratojugal on lateral temporal fenestra margin; 20) contact of jugal and postorbital on lateral temporal fenestra

margin; 21) posterior tip of postorbital posterior ramus; 22) anteroventral tip of squamosal on lateral temporal fenestra margin; 23) posteroventral tip of squamosal posterior process; 24) posteroventral corner of quadratojugal (posteroventral corner of skull).

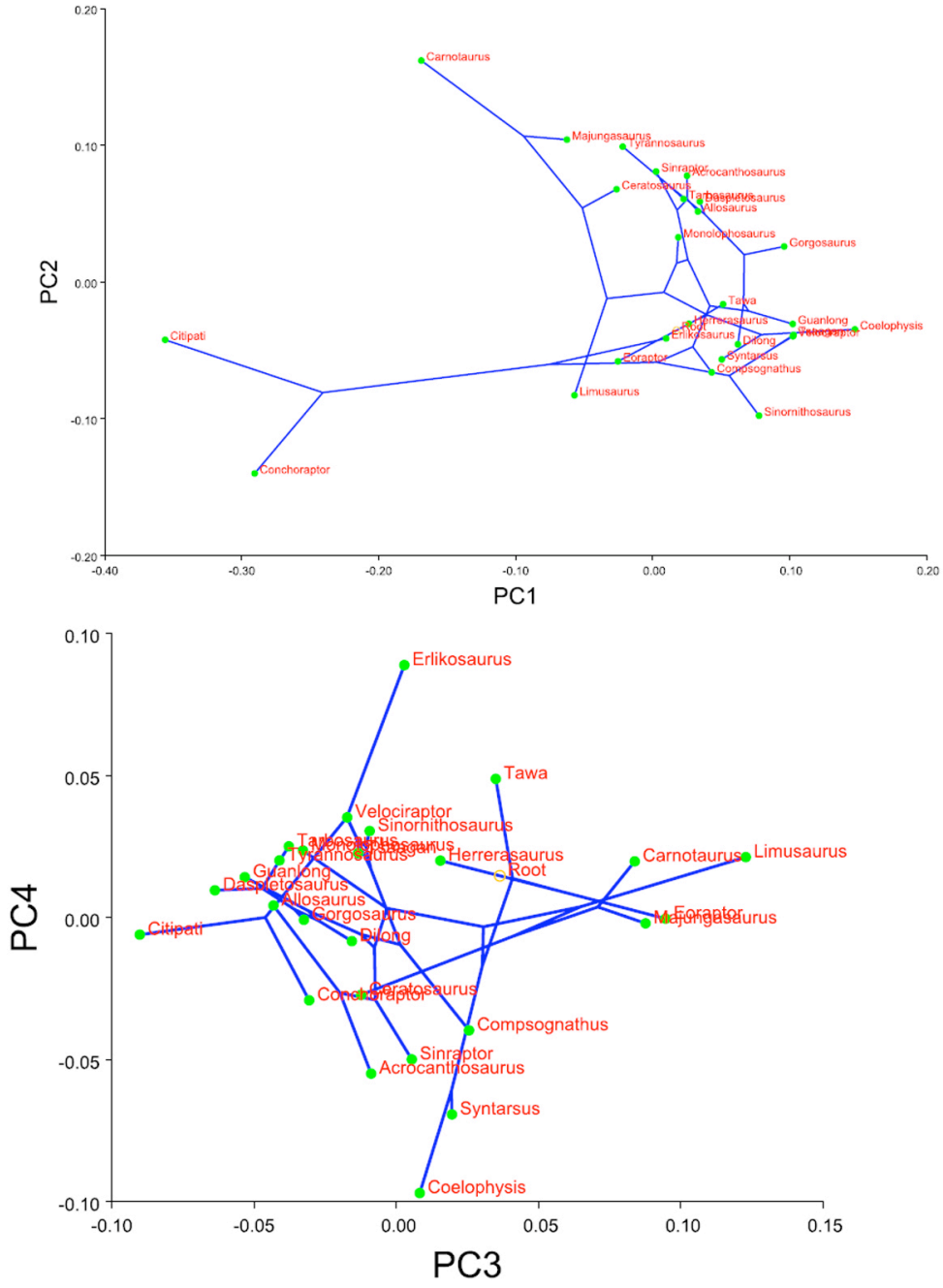

Figure 3-S2. Two-dimensional morphospaces, with phylogenetic tree mapped according to squared change parsimony optimization (see Section S4) above, for the 26-taxon, 24-landmark dataset.

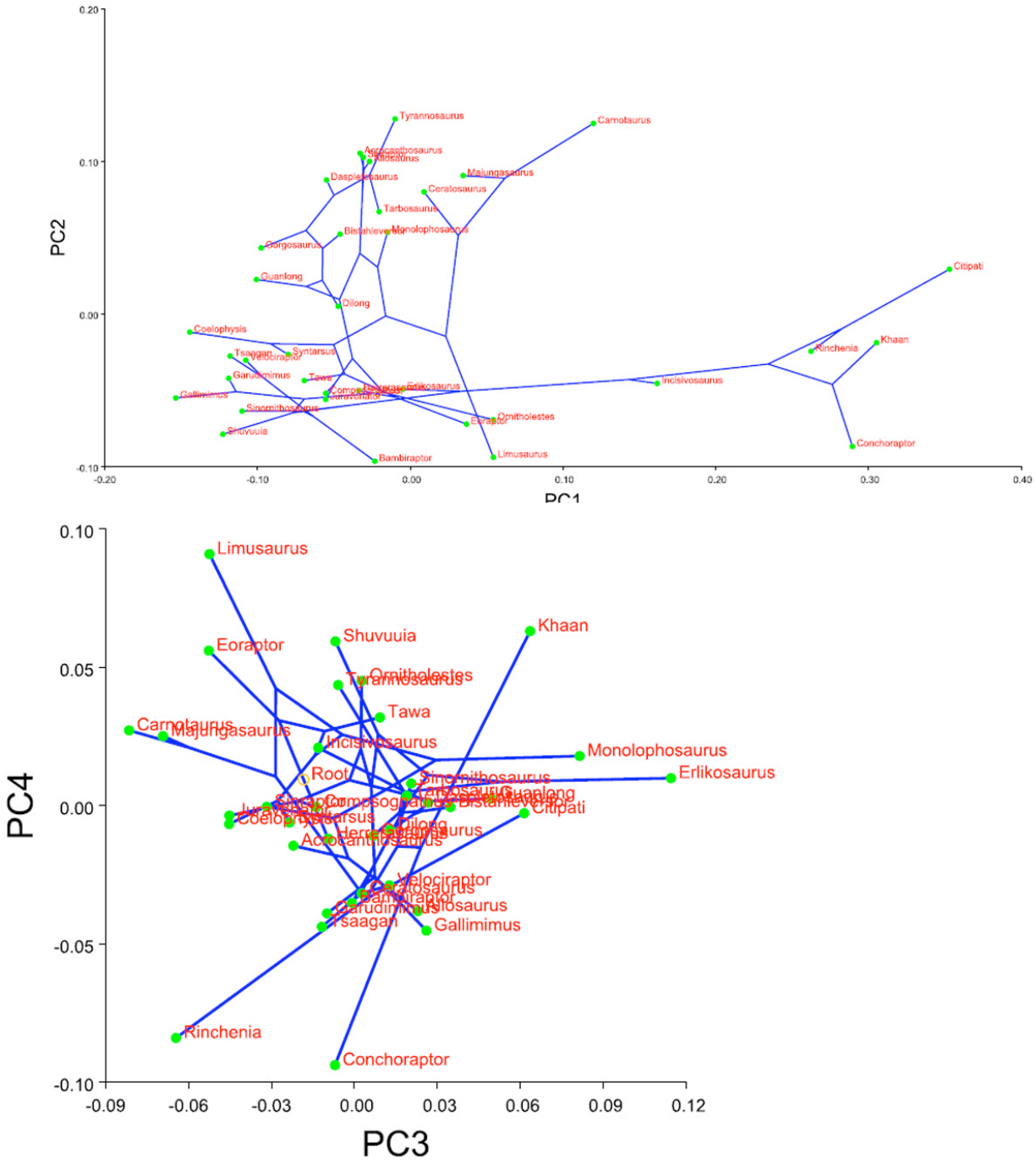

Figure 3-S3. Two-dimensional morphospaces, with phylogenetic tree mapped according to squared change parsimony optimization (see Section S4) above, for the 36-taxon, 13-landmark dataset.

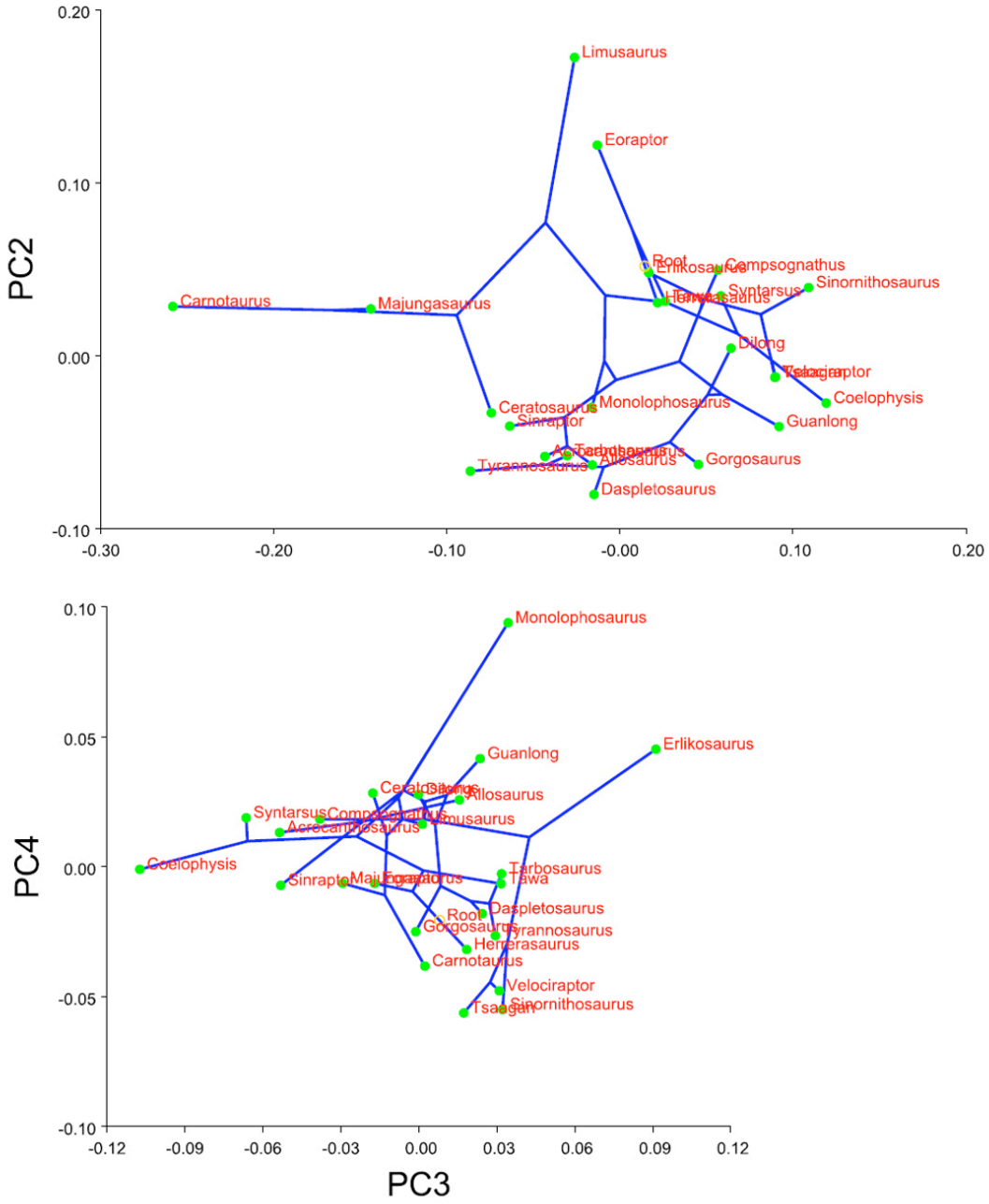

Figure 3-S4. Two-dimensional morphospaces, with phylogenetic tree mapped according to squared change parsimony optimization (see Section S4) above, for the 24-taxon, 24-landmark dataset (i.e., the 26 taxon/24 landmark dataset with oviraptorosaurs excluded).

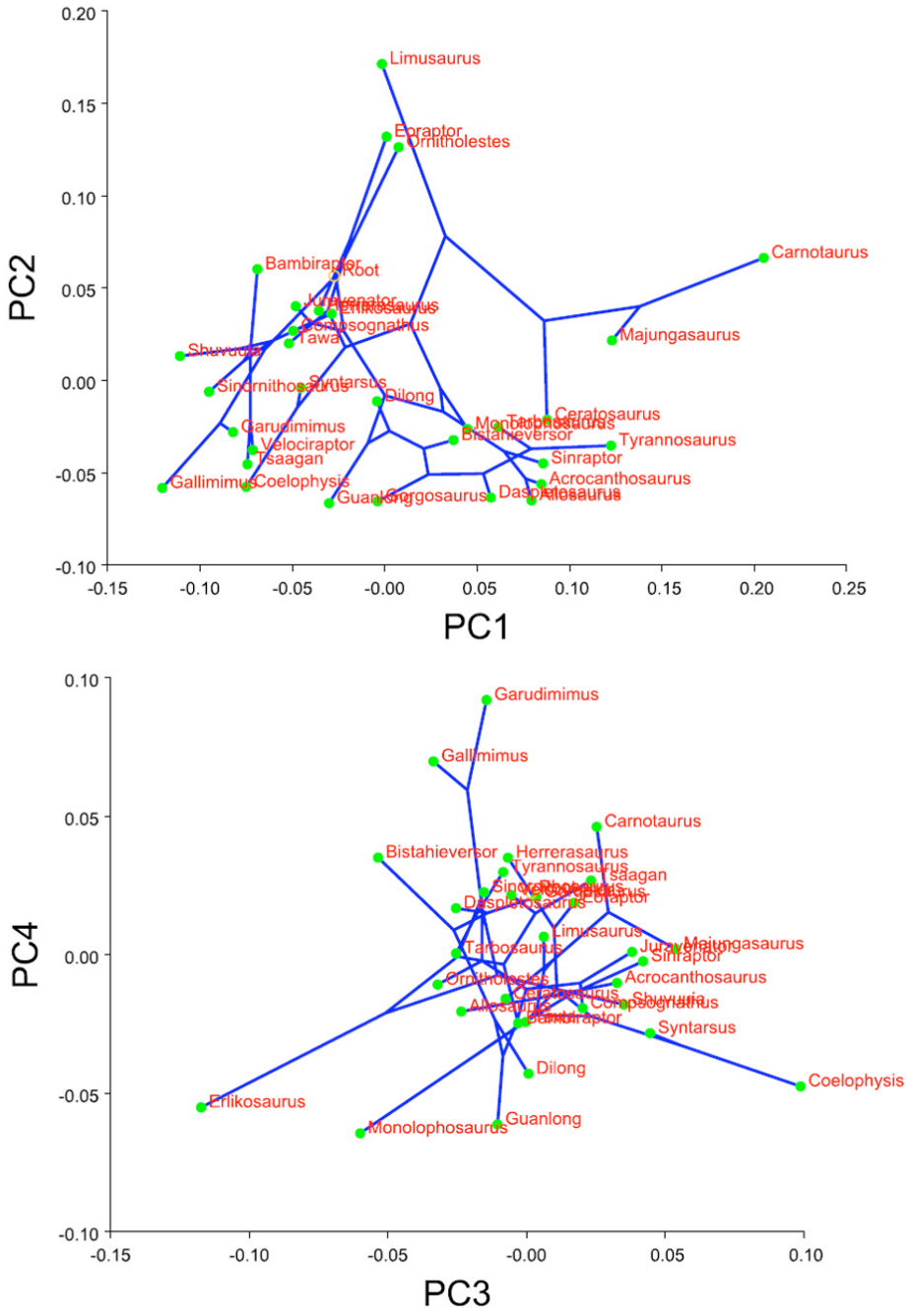

Figure 3-S5. Two-dimensional morphospaces, with phylogenetic tree mapped according to squared change parsimony optimization (see Section S4) above, for the 31-taxon, 13-landmark dataset (i.e., the 36 taxon/13 landmark dataset with oviraptorosaurs excluded).

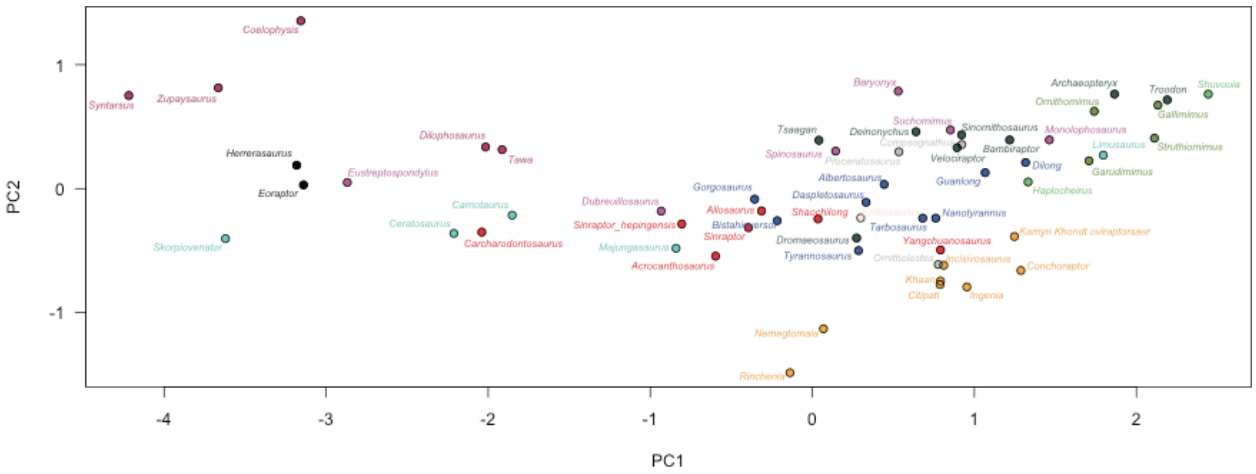

Figure 3-S6. Two-dimensional function space for the 60-taxon biomechanical dataset. All but one taxon (*Juravenator*) from the 36-taxon, 13-landmark morphometric dataset are represented (and, therefore, all taxa in the 26-taxon, 24-landmark dataset are included). Jaw function was quantified through biomechanical profiling and the resulting polynomial coefficients were ordinated using PCA. The first PC accounts for 90.1% while the second PC accounts for 9.67% of total variance. Together, PC1 and PC2 capture 99.8% of total variance in functional disparity. Phylogenetic groups (not all monophyletic; only for graphical purposes) are shown in different colours: black, Basal Theropoda; maroon, Coelophysoidea; turquoise, Ceratosauria; magenta, Basal Tetanurae; red, Allosauroidea; gray, Basal Coelurosauria; blue, Tyrannosauroidea; olive, Ornithomimosauria; pink, Therizinosauroidea; orange, Oviraptorosauria; spring green, Alvarezsauridae; dark green, Paraves (Deinonychosauria+*Archaeopteryx*). Axes are to scale.

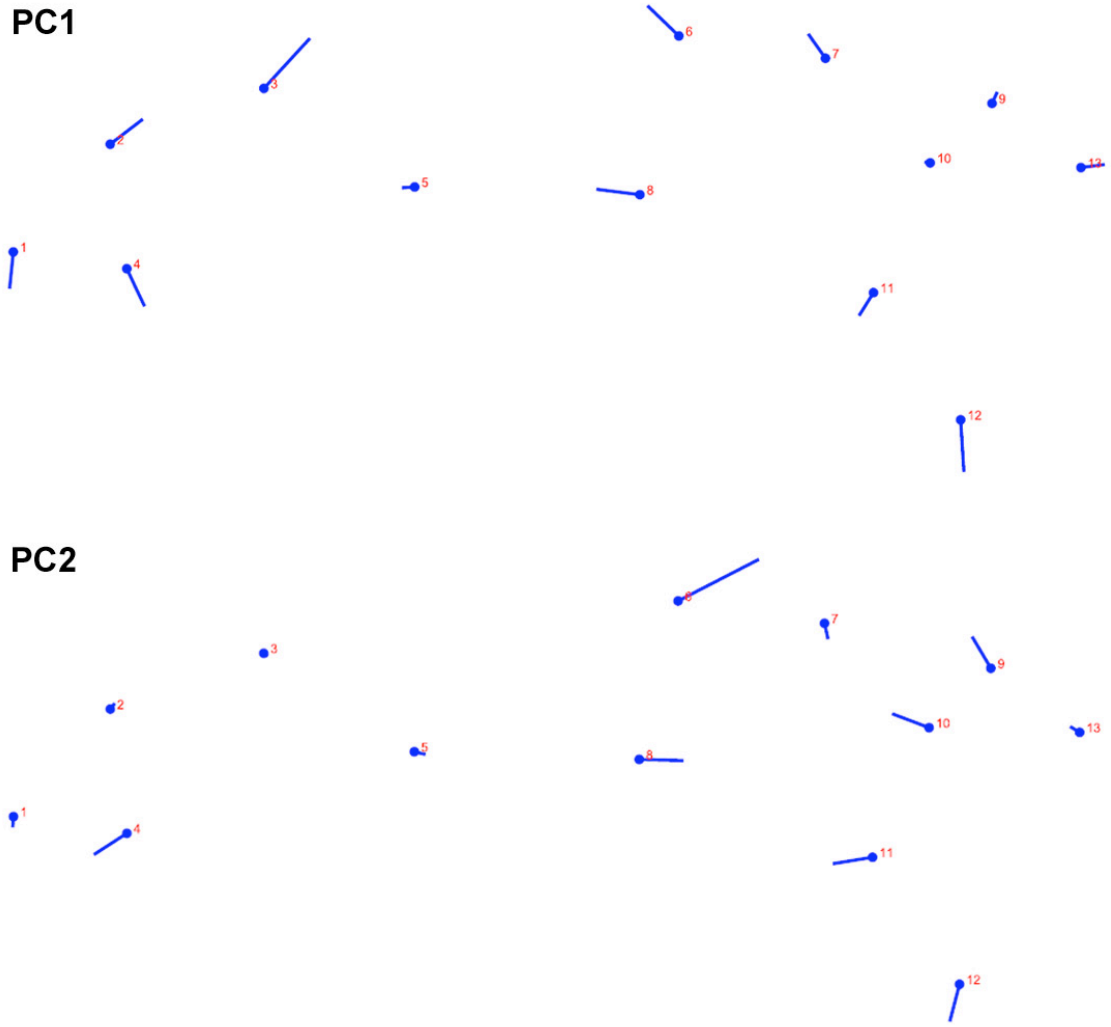

Figure 3-S7. Major changes in skull shape based on the 13 landmarks for the for the 36-taxon, 13-landmark dataset. Landmarks are labeled 1-13; this numbering does not match that in the original landmark list, but rather landmarks 1,2,4,5,7,10,11,12,15,16,17,19,21 in the original dataset, respectively.

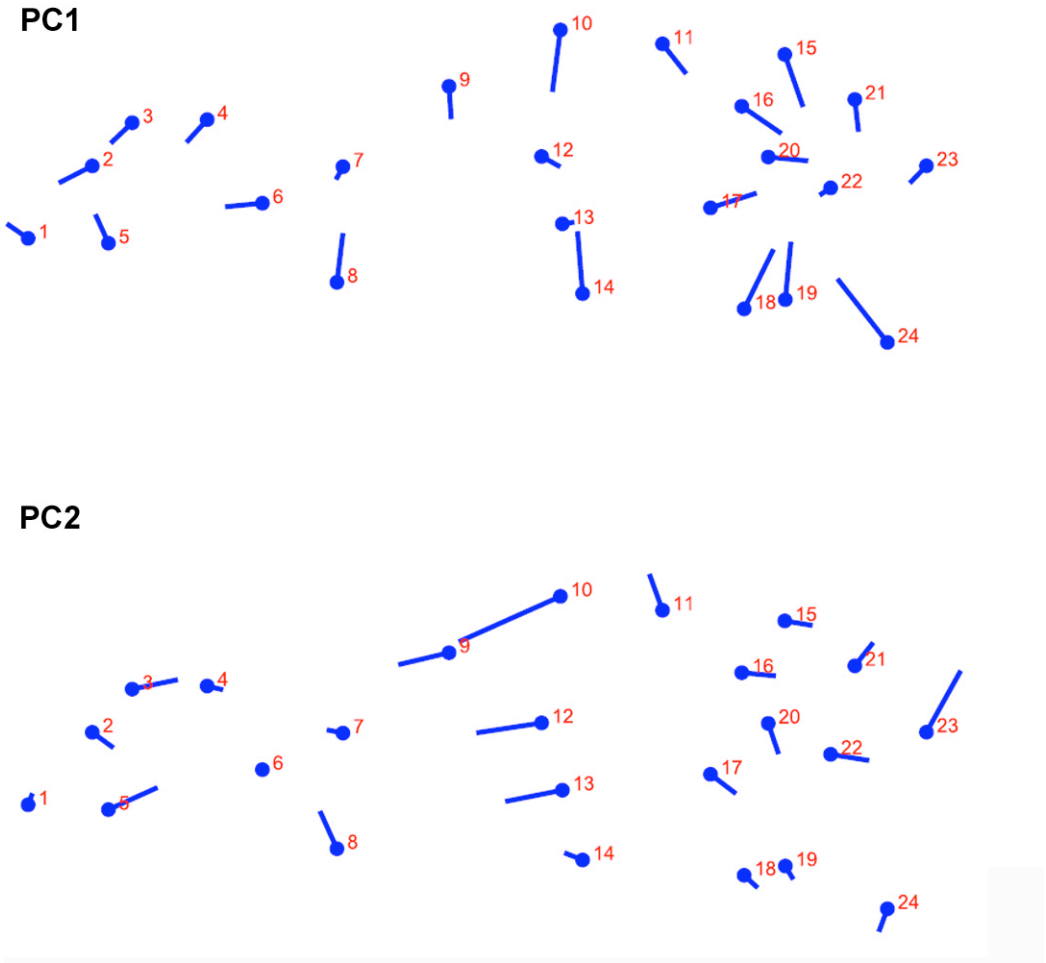

Figure 3-S8. Major changes in skull shape based on the 24 landmarks for the for the 24-taxon, 24-landmark dataset (i.e, the 26-taxon/24-landmark dataset without oviraptorosaurs). Landmarks are labeled 1-13; this numbering does not match that in the original landmark list, but rather landmarks 1,2,4,5,7,10,11,12,15,16,17,19,21 in the original dataset, respectively.

Figure 3-S9. Major changes in skull shape based on the 24 landmarks for the for the 31-taxon, 13-landmark dataset (i.e, the 36-taxon/13-landmark dataset without oviraptorosaurs). Landmarks are labeled 1-13; this numbering does not match that in the original landmark list, but rather landmarks 1,2,4,5,7,10,11,12,15,16,17,19,21 in the original dataset, respectively.

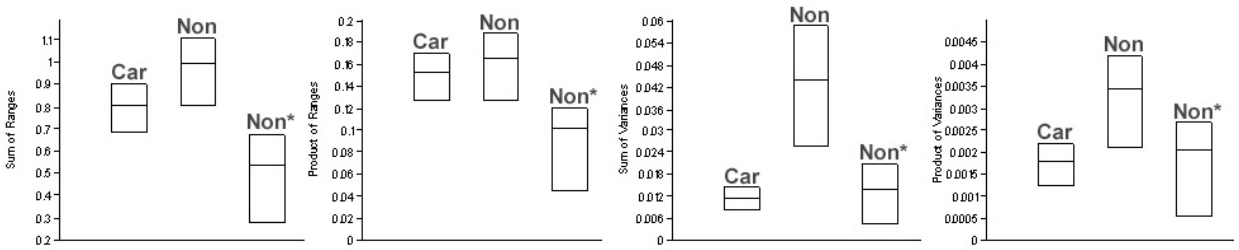

Figure 3-S10. Four disparity metrics (disparity of form) compared in carnivorous theropods (denoted by "Car") and non-carnivorous theropods (full set of 10 taxa denoted by "Non"; set of 5 taxa after oviraptorosaurs removed after the PCA denoted by "Non*"). The boxes represent the extent of 95% error bars and the horizontal line inside the box is the disparity measure for the group in question. The overlap or non-overlap of the error bars denotes statistical significance. For example, for the sum of variances plot, the non-carnivorous species are significantly more disparate than the carnivorous species, because the error bars do not overlap on the y axis. However, the non-carnivorous species with oviraptorosaurs removed are not significantly more disparate than the carnivorous taxa, because the error bars overlap on the y axis.

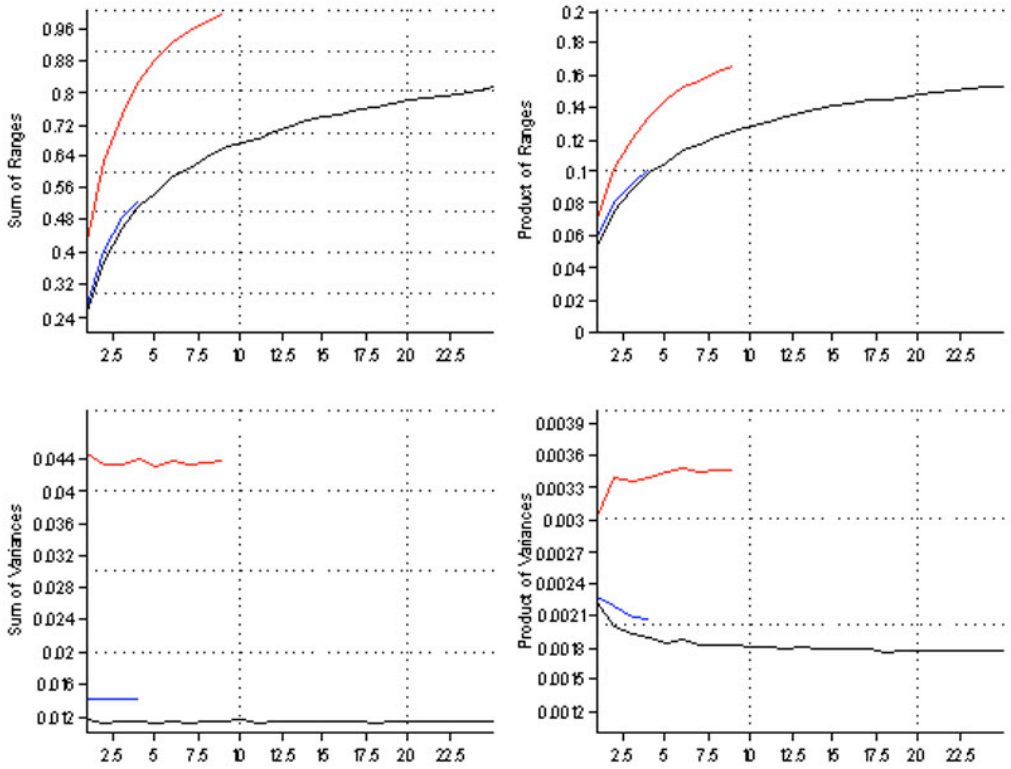

Figure 3-S11. Rarefaction profiles for the four disparity metrics (disparity of form) calculated for non-carnivorous species (red), non-carnivorous species minus oviraptorosaurs (blue), and carnivorous species (black). Note that for all metrics the non-carnivorous species have a higher disparity than the carnivorous species at all subsampled sample sizes.

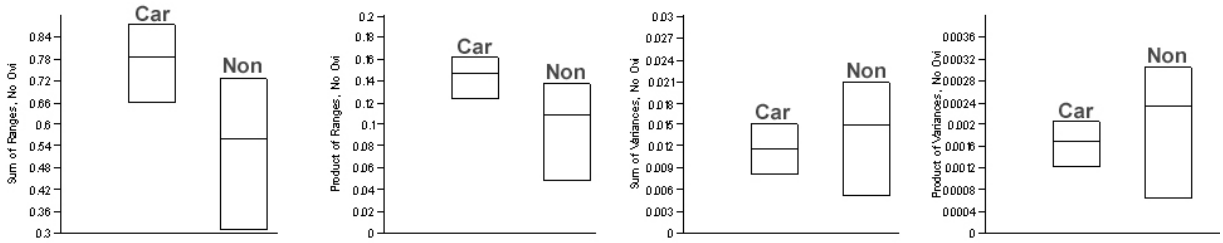

Figure 3-S12. Four disparity metrics (disparity of form) compared in carnivorous theropods (denoted by "Car") and non-carnivorous theropods (denoted by "Non"; n=5), based on the 31-taxon/13-landmark dataset that completely excludes oviraptorosaurs from the PCA. The boxes represent the extent of 95% error bars and the horizontal line inside the box is the disparity measure for the group in question. The overlap or non-overlap of the error bars denotes statistical significance.

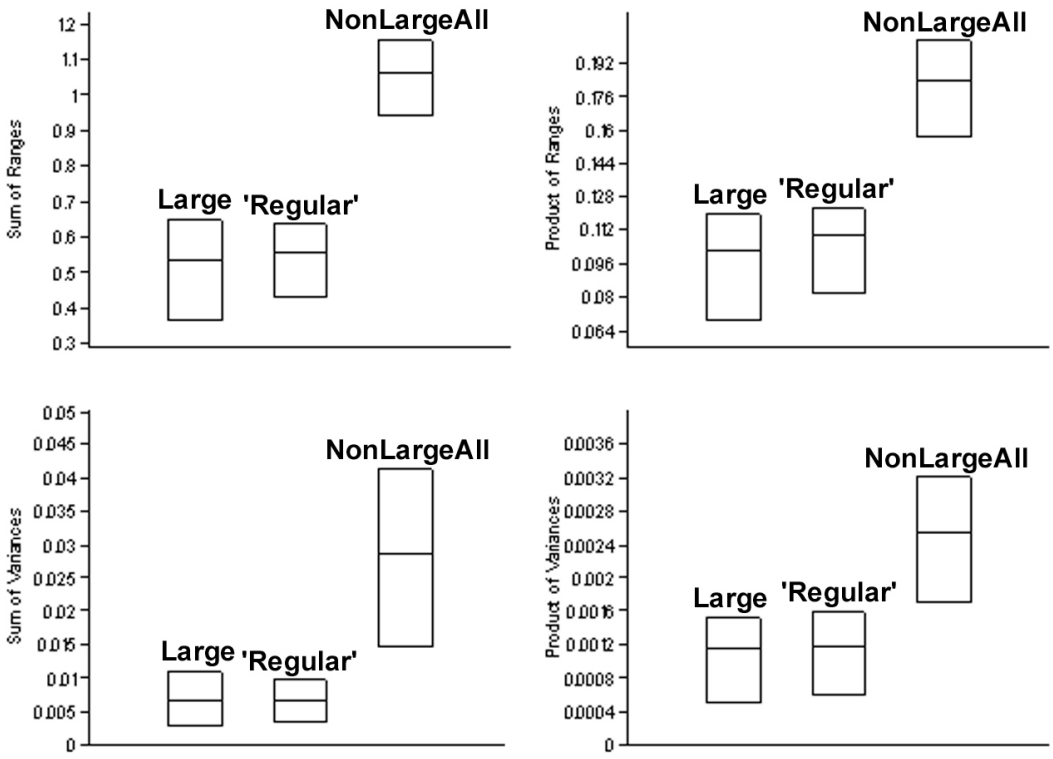

Figure 3-S13. Four disparity metrics (disparity of form) compared in large-bodied theropods ("Large," all taxa with a skull length greater than 65 cm) and two clusters of non-large-bodied theropods: non-large-bodied carnivorous theropods ("'Regular'") and all non-large-bodied theropods in general (i.e., also including non-carnivorous taxa; "NonLargeAll"). The boxes represent the extent of 95% error bars and the horizontal line inside the box is the disparity measure for the group in question. The overlap or non-overlap of the error bars denotes statistical significance.

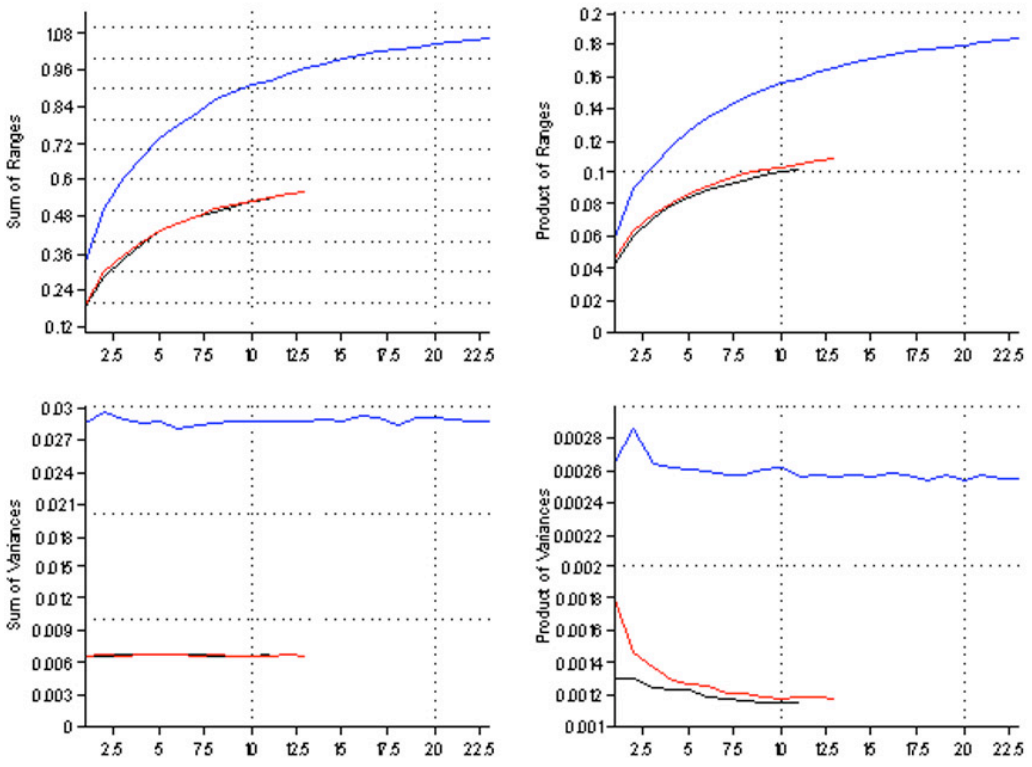

Figure 3-S14. Rarefaction profiles for the four disparity metrics (disparity of form) calculated for large-bodied theropods (black), non-large-bodied carnivorous theropods (‘regular’ carnivores) (red), and all non-large-bodied theropods (blue). Note that for all metrics the non-large-bodied species have a higher disparity than the carnivorous species at all subsampled sample sizes.

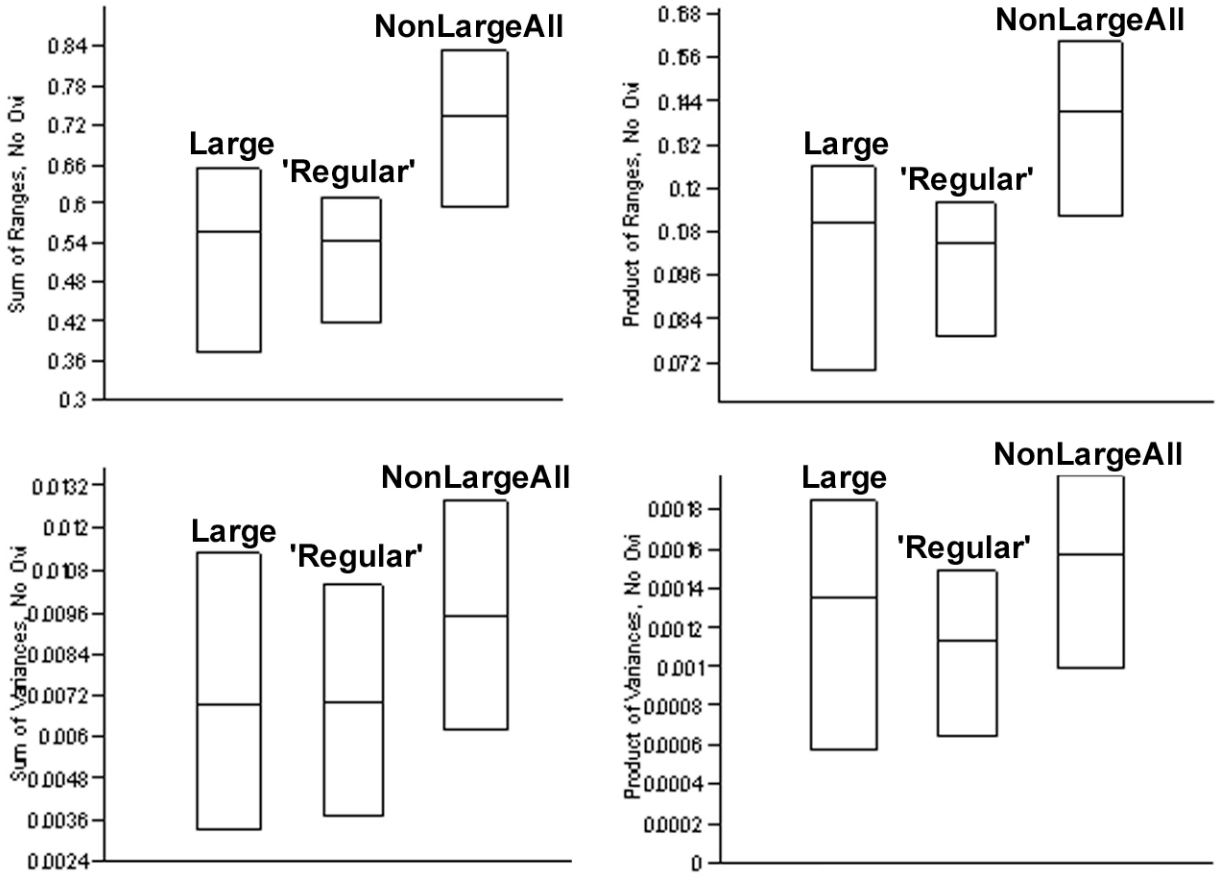

Figure 3-S15. Four disparity metrics (disparity of form) based on the 31-taxon/13-landmark dataset that completely excludes oviraptorosaurs from the PCA. Plot compares the disparity of large-bodied theropods ("Large," all taxa with a skull length greater than 65 cm) and two clusters of non-large-bodied theropods: non-large-bodied carnivorous theropods ("'Regular'") and all non-large-bodied theropods in general (i.e., also including non-carnivorous taxa; "NonLargeAll"). The boxes represent the extent of 95% error bars and the horizontal line inside the box is the disparity measure for the group in question. The overlap or non-overlap of the error bars denotes statistical significance.

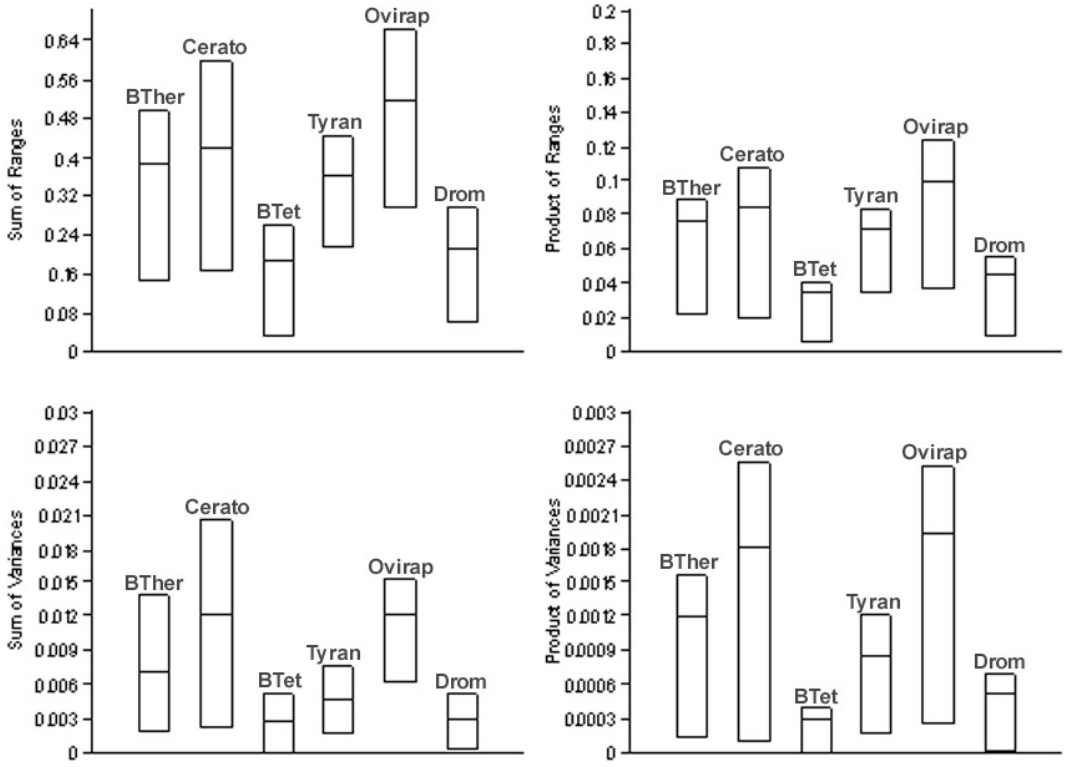

Figure 3-S16. Four disparity metrics (disparity of form) compared in six taxonomic groups of taxa (basal theropods: BTher; ceratosaurs: Cerato; basal tetanurans: BTet; tyrannosauroids: Tyran; oviraptorosaurs: Ovirap; dromaeosaurids: Drom). Sample sizes are: Basal Theropoda (5), Ceratosauria (4), Basal Tetanurae (4), Tyrannosauroidea (7), Oviraptorosauria (5), and Dromaeosauridae (4). The boxes represent the extent of 95% error bars and the horizontal line inside the box is the disparity measure for the group in question. The overlap or non-overlap of the error bars denotes statistical significance.

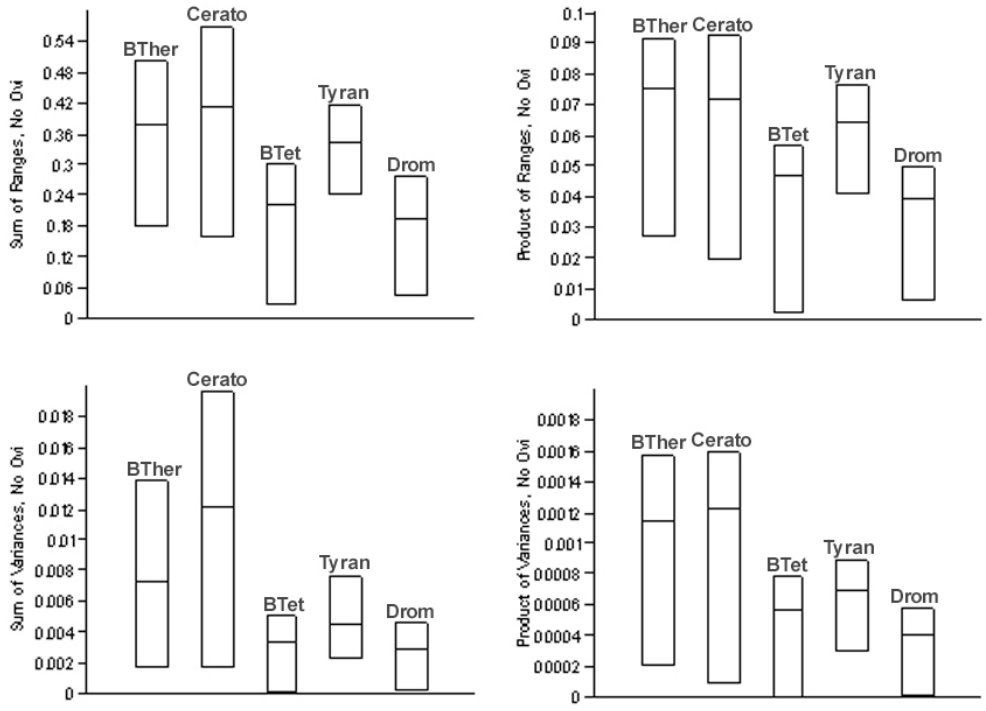

Figure 3-S17. Four disparity metrics (disparity of form) compared in five taxonomic groups of taxa, based on the 31-taxon/13-landmark dataset that completely excludes oviraptorosaurs from the PCA. Clusters denoted by: basal theropods: BTher; ceratosaurs: Cerato; basal tetanurans: BTet; tyrannosauroids: Tyran; oviraptorosaurs: Ovirap; dromaeosaurids: Drom. Sample sizes are the same as listed in Figure S16. The boxes represent the extent of 95% error bars and the horizontal line inside the box is the disparity measure for the group in question. The overlap or non-overlap of the error bars denotes statistical significance.

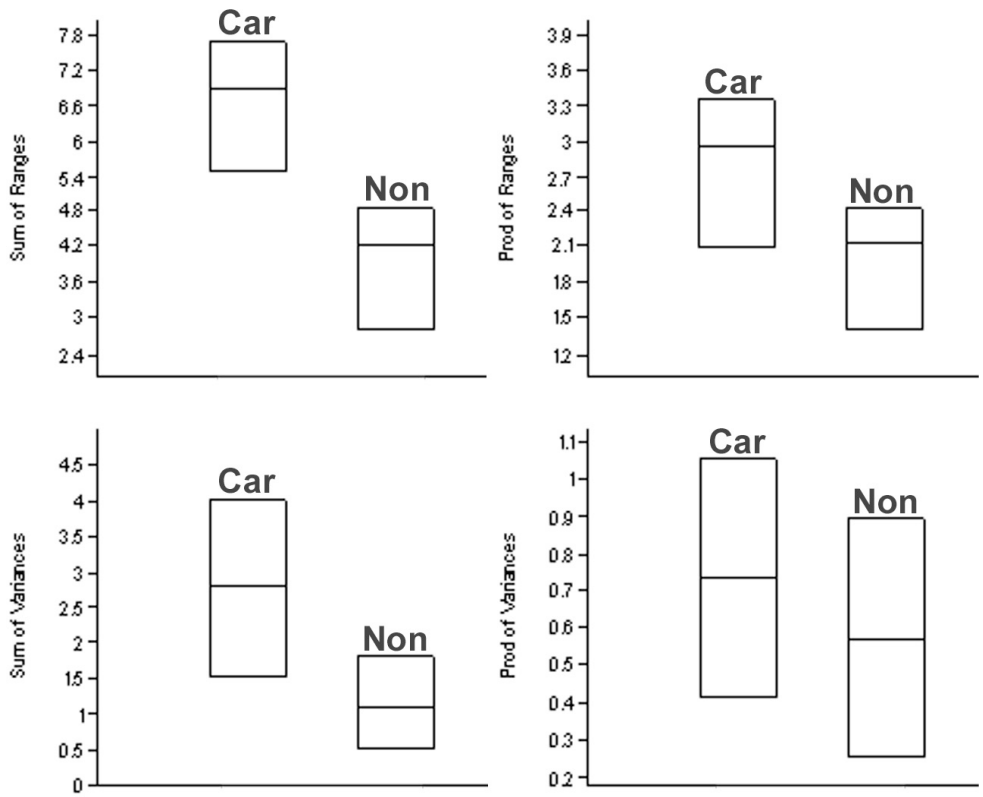

Figure 3-S18. Four disparity metrics (disparity of function) compared in carnivorous theropods (denoted by "Car") and non-carnivorous theropods (denoted by "Non"). The boxes represent the extent of 95% error bars and the horizontal line inside the box is the disparity measure for the group in question. The overlap or non-overlap of the error bars denotes statistical significance.

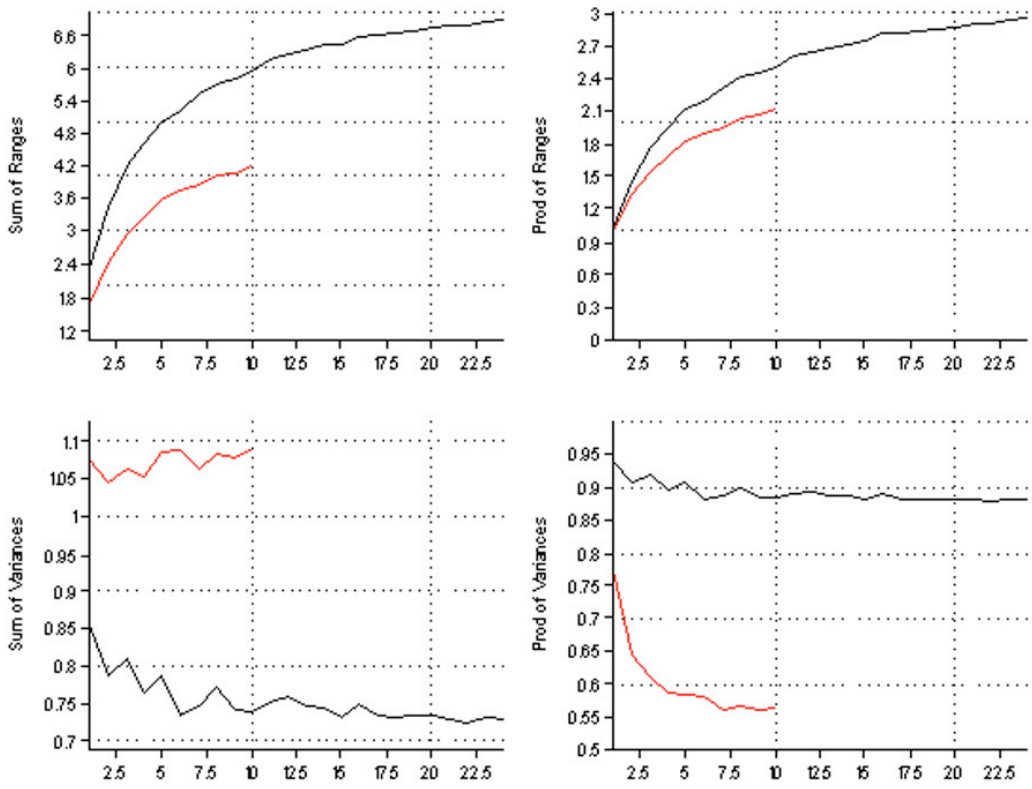

Figure 3-S19. Rarefaction profiles for the four disparity metrics (disparity of function) calculated for non-carnivorous species (red) and carnivorous species (black). Note that for all metrics the carnivorous species have a higher disparity than the carnivorous species at all subsampled sample sizes.

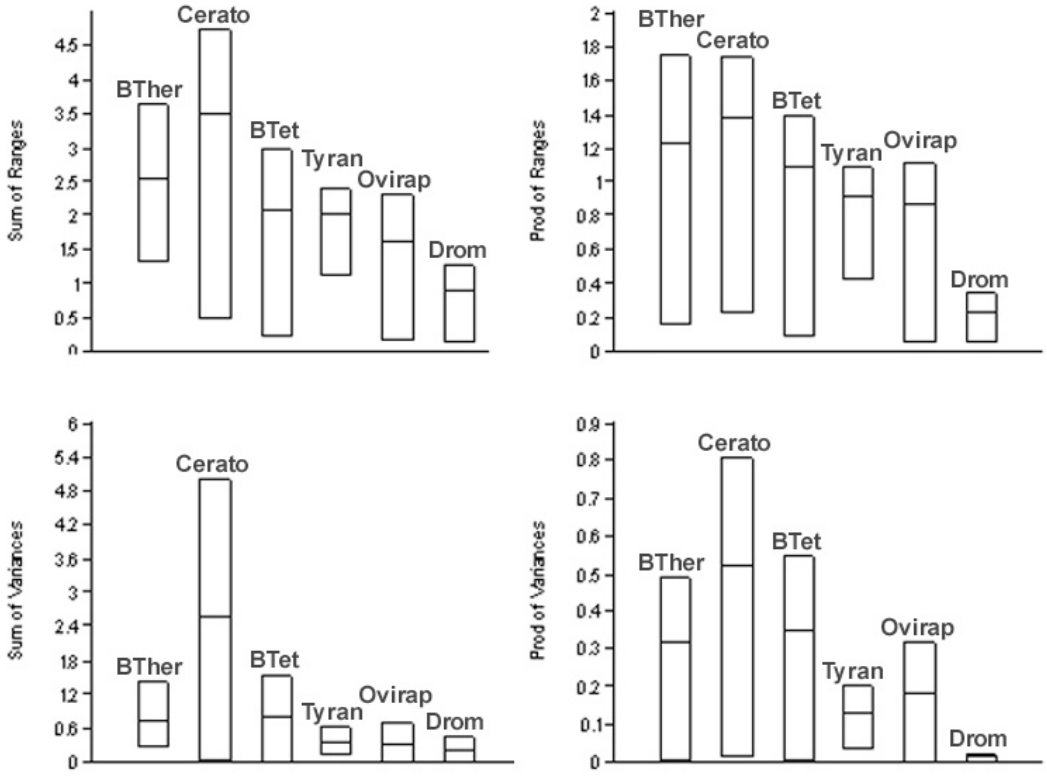

Figure 3-S20. Four disparity metrics (disparity of function) compared in six taxonomic groups of taxa (basal theropods: BTher; ceratosaurs: Cerato; basal tetanurans: BTet; tyrannosauroids: Tyran; oviraptorosaurs: Ovirap; dromaeosaurids: Drom). The boxes represent the extent of 95% error bars and the horizontal line inside the box is the disparity measure for the group in question. The overlap or non-overlap of the error bars denotes statistical significance.

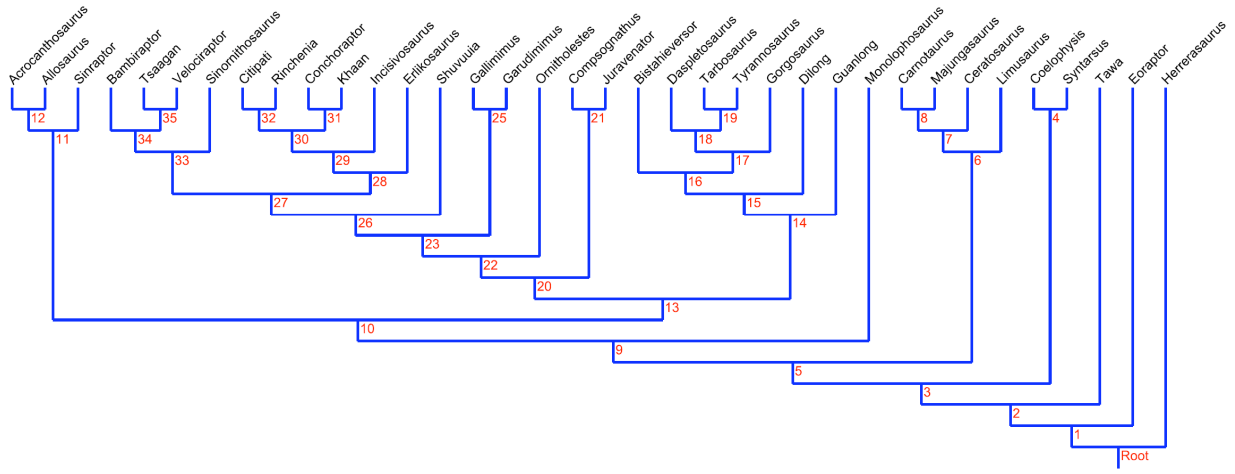

Figure 3-S21. The informal supertree used in all phylogenetic comparative analyses (see below).

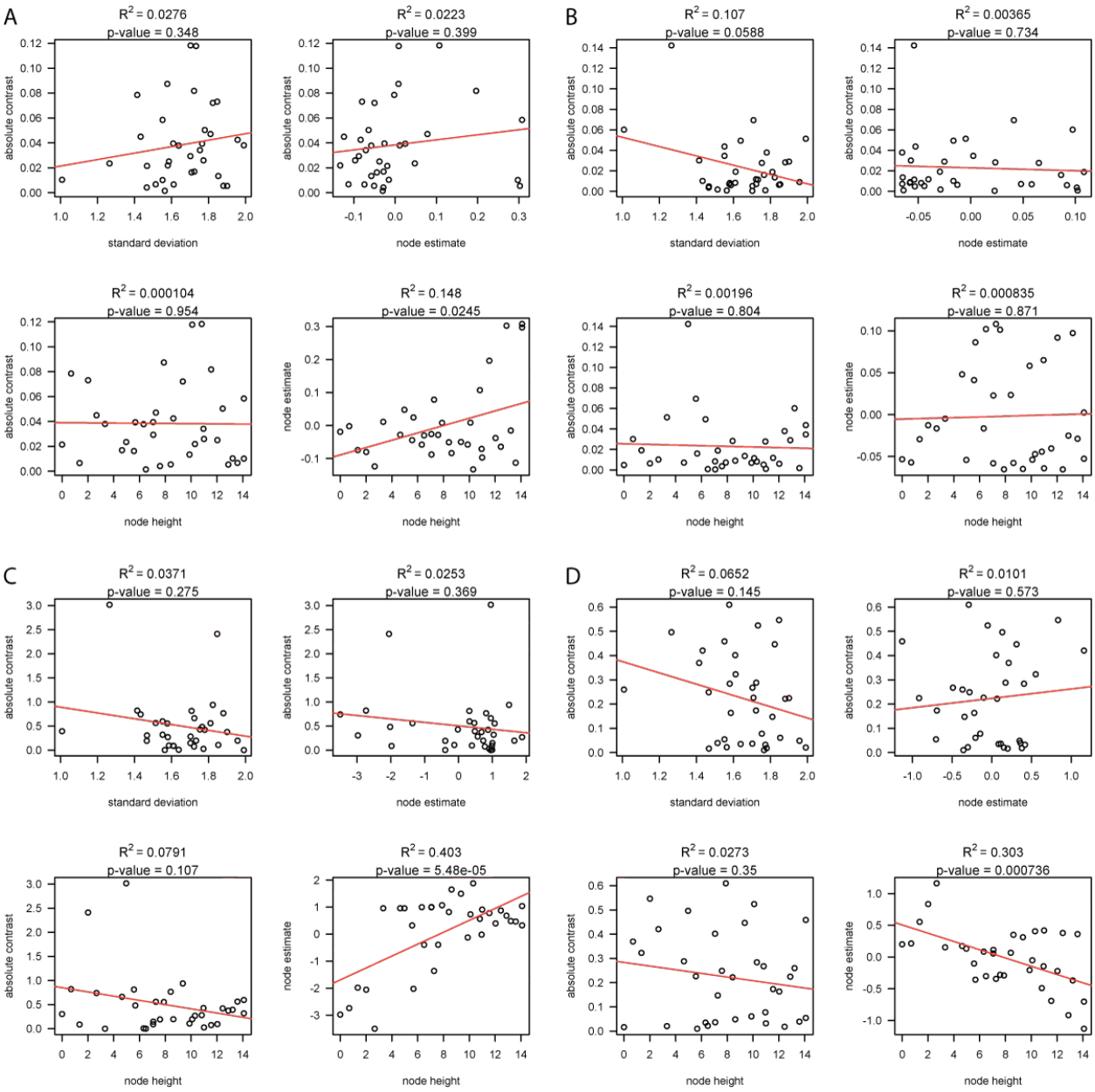

Figure 3-S22. PIC diagnostic plots and statistics for the 35-taxa dataset and tree. A, $PC1_{form}$; B, $PC2_{form}$ on $\log_{10}$ transformed branch lengths; C, $PC1_{func}$; D, $PC2_{func}$ on $\log_{10}$ transformed branch lengths. The four diagnostic tests are described in the text of the supplementary information. Only diagnostics for the 35-taxa dataset and tree are shown. Coefficient of determination (R^2) and p-value is shown for each regression

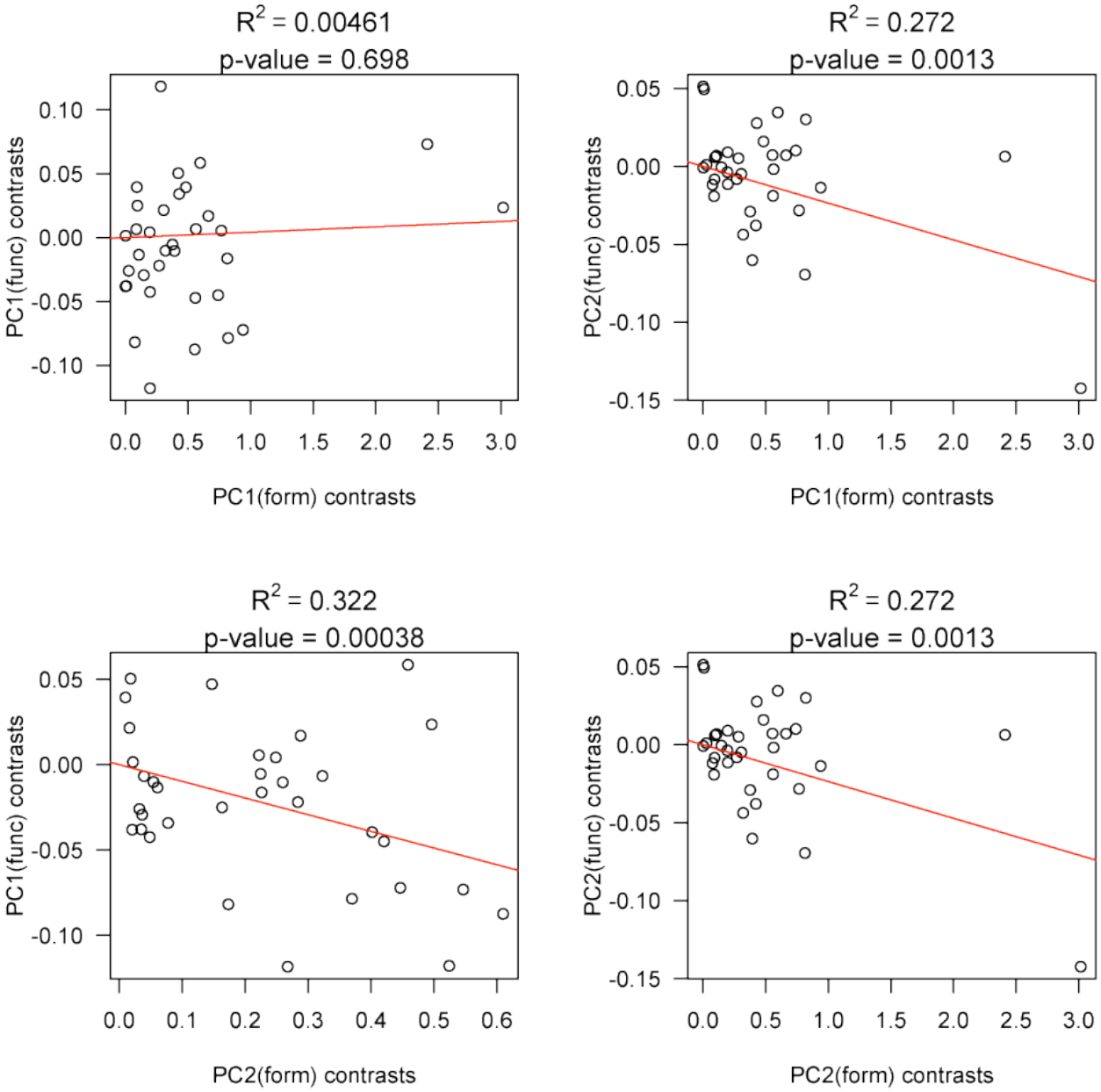

Figure 3-S23.Correlations of positivized PICs in the 35-taxon tree. Pairs of PICs were 'positivized' following Garland et al. (1992) and fitted with an ordinary least squares regression through the origin. Coefficient of determination (R^2) and p-value is shown for each pair.

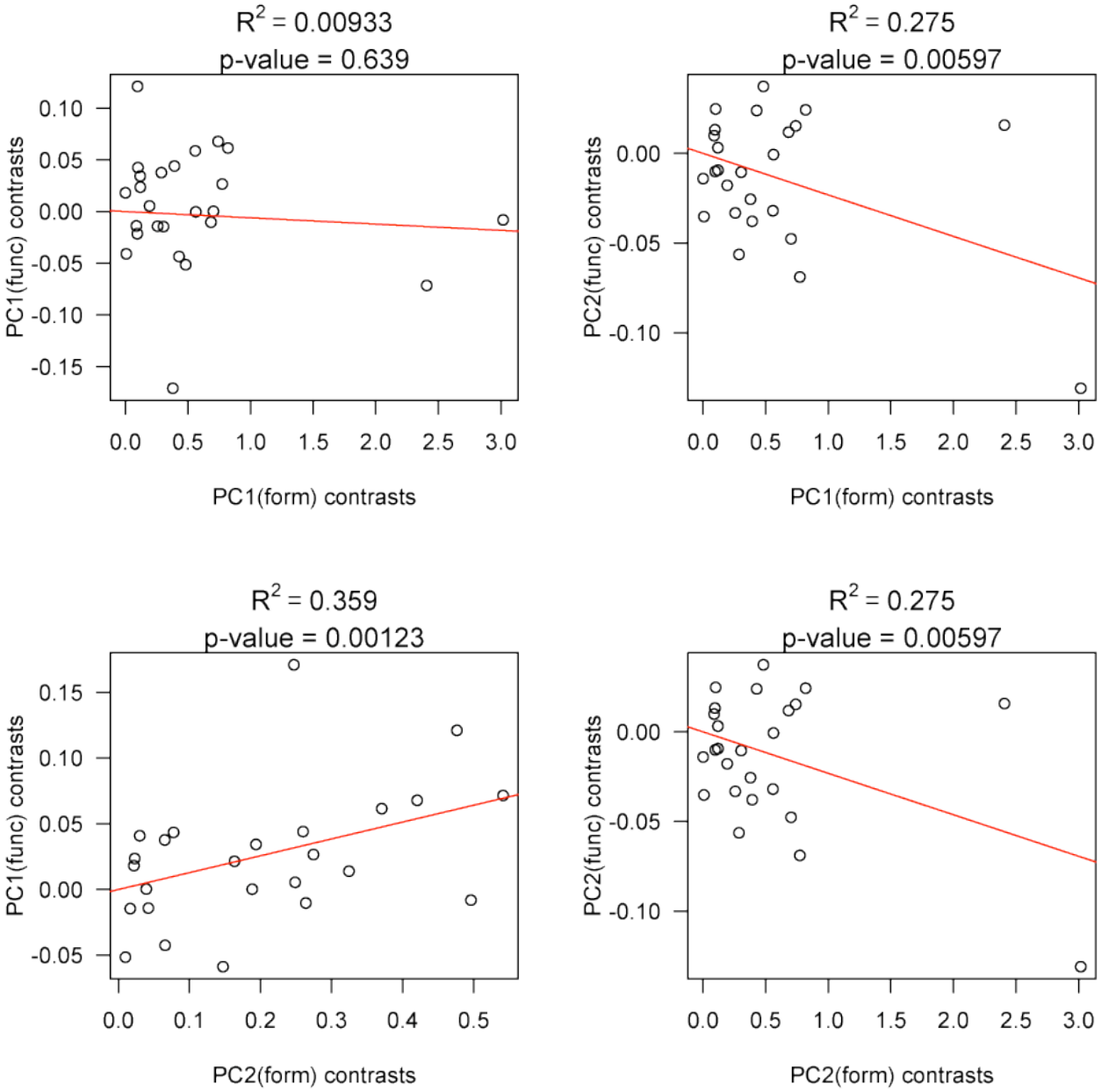

Figure 3-S24. Correlations of positivized PICs in the 26-taxon tree. Pairs of PICs were 'positivized' following Garland et al. (1992) and fitted with an ordinary least squares regression through the origin. Coefficient of determination (R^2) and p-value is shown for each pair.

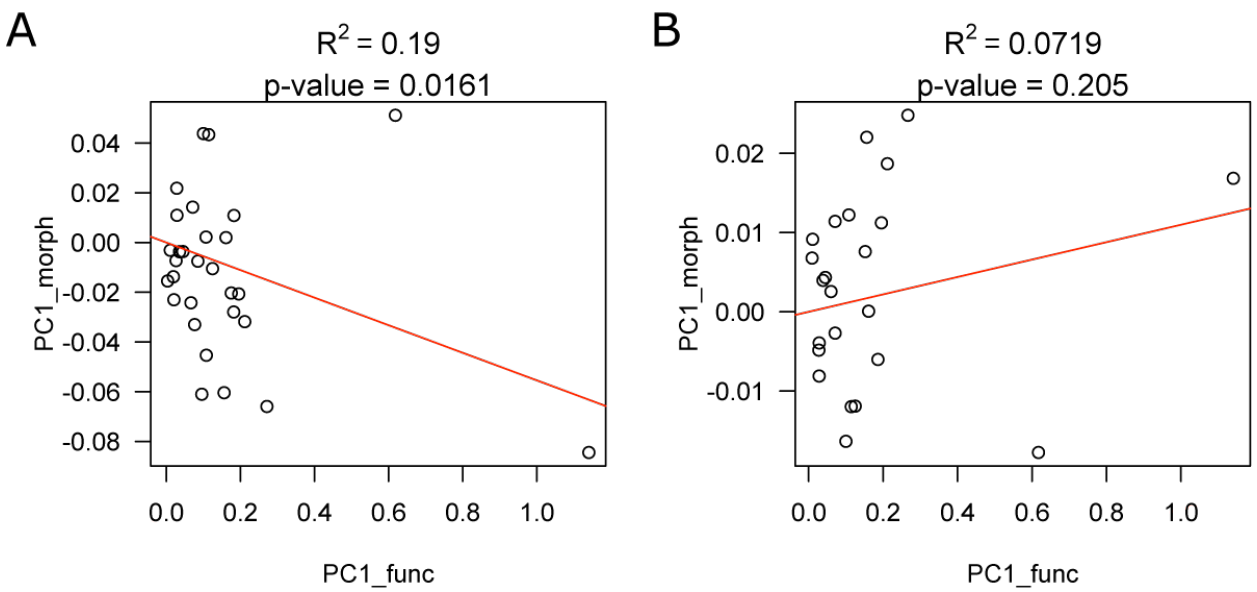

Figure 3-S25. Correlations of positivized PICs for $PC1_{form}$ and $PC1_{func}$ in the 30- (A) and 24-taxon trees (B). Pairs of PICs were 'positivized' following Garland et al. (1992) and fitted with an ordinary least squares regression through the origin. Coefficient of determination (R^2) and *p*-value is shown for each pair.

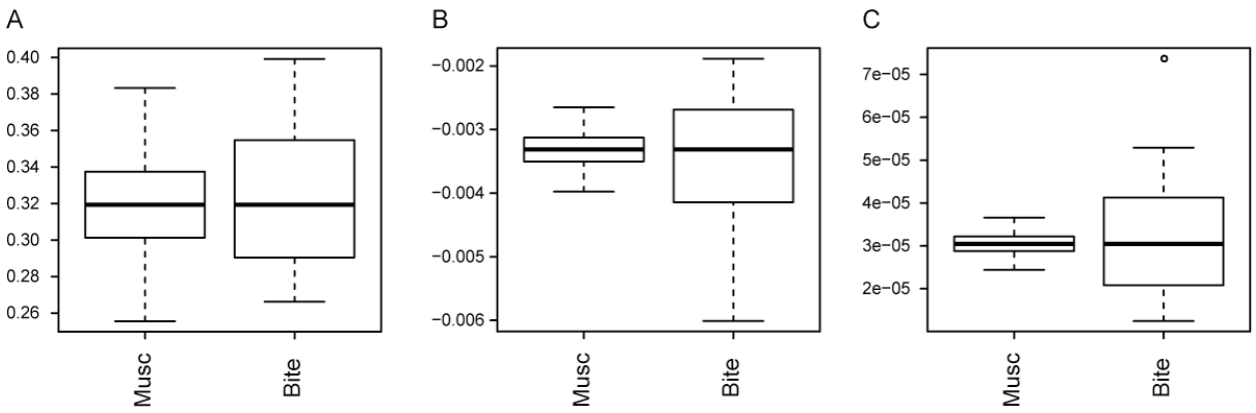

Figure 3-S26.Comparisons of polynomial coefficients from the sensitivity analyses of muscle and biting levers. Box plots show the pooled values of polynomial coefficients, β_0 (A), β_1 (B), and β_2 (C), of the polynomial best fit lines to the mechanical advantage profile along the tooth row computed when either muscle or biting levers are increased or reduced by 10% and 20%. Changes to either muscle or biting levers have a similar amount of effect to the intercept β_0 while both the slope β_1 and the curvature β_2 are greatly sensitive to alterations in biting levers.

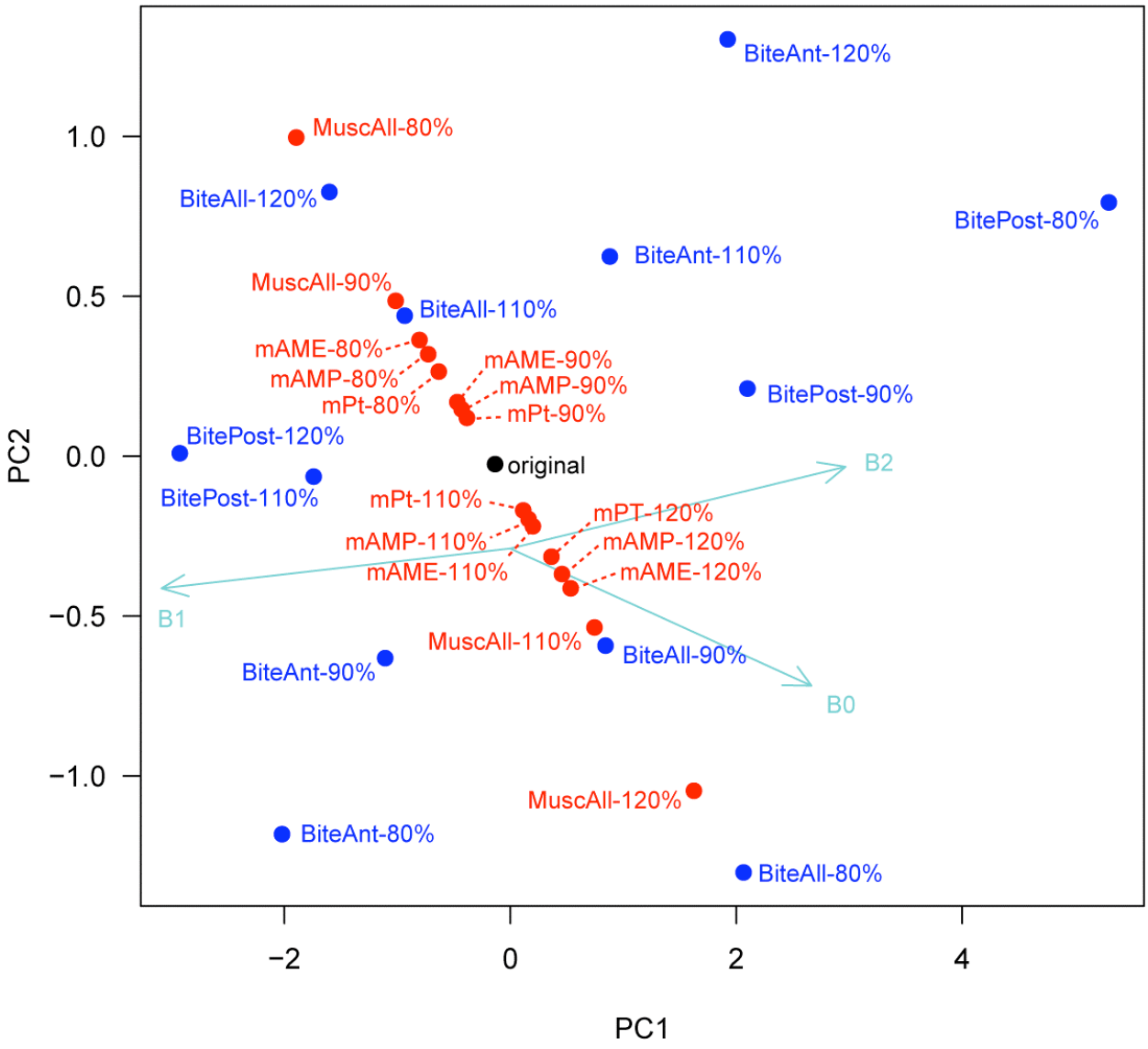

Figure 3-S27. A plot of the first two principal components from Principal Components Analysis on the various sets of coefficients as a result of different iterations of lever adjustments. Red points are coefficients of muscle lever alterations while blue points are those of bite lever alterations. The black point is the original set of coefficients from the unaltered muscle and bite levers. A biplot is superimposed to aid in interpretations of axes. See text (section S7) for abbreviations and explanations of the various combinations of lever length adjustments.

SUMMARY, AND PROSPECTUS

Summary: The three chapters presented here reveal new information on coelurosaurian theropod anatomy, phylogeny, and macroevolution. Chapter 1 presents a thorough description of a well preserved and nearly complete tyrannosauroid skeleton, the holotype specimen of *Alioramus altai*. This description reiterates the diagnostic features of the skeleton and confirms that it is distinct from the sympatric *Tarbosaurus bataar*, and provides further evidence that *Alioramus* is an unsual long-snouted, slender-limbed, gracile tyrannosaurid. Perhaps most importantly, exhaustive comparisons between *Alioramus* and other tyrannosauroids reveals an abundance of new character data (variable features of the anatomy among tyrannosauroids) that can be included in phylogenetic analyses. These data were included in the tyrannosauroid-specific phylogeny of Brusatte et al. (2010a) and in this dissertation are integrated (along with other new characters) into the larger Theropod Working Group matrix, to create a 150-taxon and 853-character dataset that is the largest and most comprehensive source of coelurosaurian phylogenetic data yet compiled.

This new dataset is presented and analyzed in Chapter 2. The resulting phylogeny is a more-or-less complete genealogy of Mesozoic coelurosaurs that helps clarify the problematic basal relationships of the group. It finds strong support for the monophyly of major coelurosaurian subgroups, the basal position of singleton genera such as *Bicentenaria* and *Zuolong*, the placement of tyrannosauroids as the most basal major coelurosaurian subgroup, the position of *Guanlong* and coelurids near the base of Tyrannosauroidea, and the existence of a maniraptoran clade comprised of alvarezsauroids, therizinosauroids, oviraptorosaurs, and paravians. Some areas of the phylogeny, however, are poorly resolved. Major areas of

uncertainty surround the basal relationships of Maniraptora and the interrelationships of Ornithomimosauria, Compsognathidae, *Ornitholestes*, and Maniraptora, the four of which fall into a polytomy. This phylogeny provides a valuable framework for better understanding coelurosaurian evolution. It indicates that much of the earliest history of coelurosaurs is currently unsampled in the fossil record, that the unusual body plan of colossal predators like *Tyrannosaurus* was established only very late in dinosaurian history, and that coelurosaurs originated as small-bodied animals.

The final chapter, Chapter 3, is a geometric morphometric analysis of theropod crania that quantifies major patterns in evolution during the 150+ million year Mesozoic history of the group. This analysis finds that theropod skulls differ primarily in relative anteroposterior length and snout depth and that oviraptorosaurs deviate most substantially from the "typical" and ancestral theropod cranial morphologies. Cranial shape is strongly correlated with phylogeny—that is, taxa that are closely related have more similar skull shapes than predicted by chance. On the other hand, skull shape is only weakly correlated with a quantitative measure of biting function. This suggests that phylogeny, not differences in feeding function, was the major driver of theropod cranial evolution during the Mesozoic.

Prospectus: Along with helping clarify some aspects of coelurosaur anatomy, phylogeny, and macroevolution, this dissertation has also exposed at least as many questions that deserve future research. On the subject of coelurosaur anatomy, it is critical that many important but poorly described taxa are comprehensively monographed. Our current work on *Ornitholestes*, which began as part of this dissertation project, is the most pressing concern, as this taxon falls into an unresolved polytomy in the current phylogenetic analysis, is recovered in different positions in

alternative published analyses, and seems to lack clear anatomical features linking it with other coelurosaur clades. Other important basal coelurosaurs such as *Guanlong*, *Dilong*, *Xiongguanlong*, and *Eotyrannus* will be monographed soon by other workers, but other taxa such as *Coelurus*, *Tanycolagreus*, *Pelecanimimus*, and *Sinocalliopteryx* are in dire need of restudy and would benefit from detailed, well illustrated monographic redescriptions.

Along with simply redescribing various taxa, it will also be useful to use CT technology and other anatomical imaging techniques to expand the sample of basal coelurosaur characters, more accurately score specimens, and fill in questionable scores (especially those relating to pneumaticity and braincase anatomy). It is clarification of primary homology statements and more accurate character scoring, rather than the addition of numerous new characters, that is the most likely key for better phylogenetic resolution among basal coelurosaurs. It goes without saying, however, that the discovery of new taxa with important character combinations is almost certainly most critical, especially because there are currently major gaps in the sampling of basal coelurosaur fossils.

The ingroup relationships of tyrannosauroids (Brusatte et al. 2010a), alvarezsauroids (Choiniere et al. 2010a, 2012), and therizinosauroids (Zanno et al. 2009; Zanno 2010b) have been the subject of recent intensive focus, and character data from these studies has been incorporated into the dataset presented in this dissertation. Two other clades—Ornithomimosauria and Compsognathidae—have been the subject of less recent work, and there are major questions about the anatomy and alpha-level systematics of these groups. Perhaps the most pressing issue of all is uncertainty over the histological ages and ontogenetic status of most compsognathid specimens. A better understanding of how compsognathid morphology changes during ontogeny, and better identification of the adult morphologies of taxa, is critical. Only new

specimens can solve some of these problems, but at the very least, future work should focus on the histology and ontogeny of available specimens. Additional specimen-level work is also needed on the anatomy of ornithomimosaurs and compsognathids, to compile new character data that may better resolve the ingroup relationships of these clades, which largely disintegrate into polytomies in the present analysis.

Very little work has been done on theropod macroevolution, and it is this area of research that I am most interested in exploring as a continuation of my dissertation work. My colleagues and I will use the coelurosaur phylogenetic dataset presented here, as well as the resulting phylogeny, to quantify two aspects of coelurosaurian macroevolution: morphological disparity and rates of discrete character change. This will address two fundamental questions: Was the origin of birds was associated with an elevated rate of character change, or was character evolution consistent across coelurosaurian phylogeny? Did early birds occupy a distinct region of morphospace or did they overlap with their closest relatives, indicative of little overall morphological variety (disparity) between them? Other interesting questions regard rate of evolution in different regions of the coelurosaur skeleton and the effects of sampling biases on our understanding of coelurosaur phylogeny, as well as quantifying various evolutionary trends (body size, skull shape, etc.) and testing whether these conform to different models of evolutionary change (driven trends, stasis, etc.). This type of work can only proceed once a large anatomical dataset and a phylogeny are available, and the work done for this dissertation puts us in a good position to examine Mesozoic theropod evolution in great detail.

REFERENCES

Agnolin, F.L.., J.E. Powell, F.E. Novas, and M. Kundrat. 2012. New alvarezsaurid (Dinosauria, Theropoda) from uppermost Cretaceous of north-western Patagonia with associated eggs. Cretaceous Research 35: 33-56.

Alifanov, V.R., and R. Barsbold. 2009. *Ceratonykus oculatus* gen. et sp. nov., a new dinosaur (?Theropoda, Alvarezsauria) from the Late Cretaceous of Mongolia. Paleontological Journal 43: 94-106.

Allain, R. 2005. The postcranial anatomy of the megalosaur *Dubreuillosaurus valesdunensis* (Dinosauria Theropoda) from the Middle Jurassic of Normandy, France. Journal of Vertebrate Paleontology 25: 850-858.

Arbour, V.M., M.E. Burns, and R.L. Sissons. 2009. A redescription of the ankylosaurid dinosaur *Dyoplosaurus acutosquameus* Parks, 1924 (Ornithischia: Ankylosauria) and a revision of the genus. Journal of Vertebrate Paleontology 29: 1117-1135.

Bakker, R.T., M. Williams, and P.J. Currie. 1988. *Nanotyrannus*, a new genus of pygmy tyrannosaur, from the latest Cretaceous of Montana. Hunteria 1: 1-30.

Balanoff, A.M., X. Xing, Y. Kobayashi, Y. Matsufune, and M.A. Norell. 2009. Cranial osteology of the theropod dinosaur *Incisivosaurus gauthieri* (Theropoda: Oviraptorosauria). American Museum Novitates 3651: 1-35.

Barrett, P.M. 2005. The diet of ostrich dinosaurs (Theropoda: Ornithomimosauria). Palaeontology 48: 347-358.

Barrett, P.M., A.J. McGowan, and V. Page. 2009. Dinosaur diversity and the rock record. Proceedings of the Royal Society of London, Series B 276: 2667-2674.

Barsbold, R. 1976. [New data on Therizinosaurus (Therizinosauridae, Theropoda)] Transactions, Joint Soviet-Mongolian Paleontological Expedition 3 76-92. [Russian]

Barsbold, R. 1988. A new Late Cretaceous ornithomimid from the MPR. Paleontologicheskii Zhurnal 1: 122-124.

Barsbold, R., and H. Osmólska. 1999. The skull of *Velociraptor* (Theropoda) from the Late Cretaceous of Mongolia. Acta Palaeontologica Polonica 44: 189–212.

Barsbold, R., and A. Perle. 1980. Segnosauria, a new infraorder of carnivorous dinosaurs. Acta Palaeontologica Polonica 25: 185–195.

Benson, R.B.J. 2008. New information of *Stokesosaurus*, a tyrannosauroid (Dinosauria: Theropoda) from North America and the United Kingdom. Journal of Vertebrate Paleontology 28: 732–750.

Benson, R.B.J. 2009. An assessment of variability in theropod dinosaur remains from the Bathonian (Middle Jurassic) of Stonesfield and New Park Quarry, UK and taxonomic implications for *Megalosaurus bucklandii* and *Iliosuchus incognitus*. Palaeontology 52: 857-877.

Benson, R.B.J. 2010. A description of *Megalosaurus bucklandii* (Dinosauria: Theropoda) from the Bathonian of the UK and the relationships of Middle Jurassic theropods. Zoological Journal of the Linnean Society 158: 882-935.

Benson, R.B.J., P.M. Barrett, H.P. Powell, and D.B. Norman. 2008. The taxonomic status of *Megalosaurus bucklandii* (Dinosauria, Theropoda) from the Middle Jurassic of Oxfordshire, UK. Palaeontology 51: 419–424.

Benson, R.B.J., P.M. Barrett, T.H. Rich, and P. Vickers-Rich. 2010b. A southern tyrant reptile. Science 327: 1613.

Benson, R.B.J., S.L. Brusatte, S. Hutt, and D. Naish. 2009. A new large basal tetanuran (Dinosauria: Theropoda) from the Wessex Formation (Barremian) of the Isle of Wight, England. Journal of Vertebrate Paleontology 29: 612-615.

Benson, R.B.J., M.T. Carrano, and S.L. Brusatte. 2010a. A new clade of archaic large-bodied predatory dinosaurs (Theropoda: Allosauroidea) that survived to the latest Mesozoic. Naturwissenschaften 97: 71–78.

Benson, R.B.J., and X. Xu. 2008. The anatomy and systematic position of the theropod dinosaur *Chilantaisaurus tashuikouensis* Hu, 1964 from the Early Cretaceous of Alanshan, People's Republic of China. Geological Magazine 145: 778-789.

Benton, M.J. 2004. Origin and relationships of Dinosauria. *In* D. B. Weishampel, P. Dodson, and H. Osmólska (editors), The Dinosauria, 2nd Edition:7-19. Berkeley: University of California Press.

Bever, G.S., S.L. Brusatte, A.M. Balanoff, and M.A. Norell. 2011. Variation, variability, and the origin of the avian endocranium and inner ear: insights from the anatomy of *Alioramus altai* (Theropoda: Tyrannosauroidea). PLoS ONE 6(8): e23393 (pp. 1-10).

Bever, G.S., S.L. Brusatte, T.D. Carr, X. Xu, A.M. Balanoff, and M.A. Norell. In press. The braincase anatomy of the Late Cretaceous dinosaur *Alioramus* (Theropoda: Tyrannosauroidea). American Museum Novitates.

Bever, G.S. and M.A. Norell. 2009. The perinate skull of Byronosaurus (Troodontidae) with observations on the cranial ontogeny of paravian theropods. American Museum Novitates 3657: 1–51.

Bhullar, B.-A.S., J. Marguán-Lobón, F. Racimo, G.S. Bever, T.B. Rowe, M.A. Norell, and A. Abzhanov. 2012. Birds have paedomorphic dinosaur skulls. Nature 487: 223-226.

Blomberg, S.P., T. Garland, and A.R. Ives. 2003. Testing for phylogenetic signal in comparative data: behavioral traits are more labile. Evolution 57: 717-745.

Bonaparte, J. F. 1991. Los vertebrados fosiles de la Formacion Rio Colorado, de la ciudad de Neuquen y cercanias, Cretacico Superior, Argentina. Revista Museo Argentino Ciencias Naturales "Bernardino Rivadavia" Paleontologia 4: 17–123.

Bonaparte, J.F., F.E. Novas, and R.A. Coria. 1990. *Carnotaurus sastrei* Bonaparte, the horned, lightly built carnosaur from the Middle Cretaceous of Patagonia. Contributions in Science, Natural History Museum of Los Angeles County 416: 1–41.

Bonnan, M. F. 2004. Morphometric analysis of humerus and femur shape in Morrison sauropods: implicatiosn for functional morphology and paleobiology. Paleobiology 30: 444-470.

Bonnan, M.F. 2007. Linear and geometric morphometric analysis of long bone scaling patterns in Jurassic neosauropod dinosaurs: their functional and paleobiological implications. The Anatomical Record 290: 1089-1111.

Bookstein, F.L. 1991. Morphometric Tools for Landmark Data. Cambridge University Press, Cambridge.

Brazeau, M.D. 2011. Problematic character coding methods in morphology and their effects. Biological Journal of the Linnean Society 104: 489-498.

Britt, B.B. 1991. Theropods of Dry Mesa Quarry (Morrison Formation, Late Jurassic), Colorado, with emphasis on the osteology of *Torvosaurus tanneri*. BYU Geology Studies 37: 1–72.

Brochu, C.A. 2003. Osteology of *Tyrannosaurus rex*: insights from a nearly complete skeleton and high-resolution computed tomographic analysis of the skull. Society of Vertebrate Paleontology Memoir 7: 1-138.

Brochu, C.A. 2007. Morphology, relationships, and biogeographical significance of an extinct horned crocodile (Crocodylia, Crocodylidae) from the Quaternary of Madagascar. Zoological Journal of the Linnean Society 150: 835-863.

Brochu, C.A., J. Njau, R.J. Blumenschine, and L.D. Densmore. 2010. A new horned crocodile from the Plio-Pleistocene hominid sites at Olduvai Gorge, Tanzania. PLoS ONE 5(2): e9333.

Brusatte, S.L., and R.B.J. Benson. In press. The systematics of Late Jurassic tyrannosauroids (Dinosauria: Theropoda) from Europe and North America. Acta Palaeontologica Polonica.

Brusatte, S.L., R.B.J. Benson, T.D. Carr, T.E. Williamson, and P.C. Sereno. 2007. The systematic utility of theropod enamel wrinkles. Journal of Vertebrate Paleontology 24: 1052-1056.

Brusatte, S.L., R.B.J. Benson, D.J. Chure, X. Xu, C. Sullivan, and D. Hone. 2009b. The first definitive carcharodontosaurid (Dinosauria: Theropoda) from Asia and the delayed ascent of tyrannosaurids. Naturwissenschaften 96: 1051-1058.

Brusatte, S.L., R.B.J. Benson, P.J. Currie, and X.-J. Zhao. 2010b. The skull of *Monolophosaurus jiangi* (Dinosauria: Theropoda) and its implications for early theropod phylogeny and evolution. Zoological Journal of the Linnean Society 158: 573-607.

Brusatte, S.L., R.B.J. Benson, and S. Hutt. 2008. The osteology of *Neovenator salerii* (Dinosauria: Theropoda) from the Wealden Group (Barremian) of the Isle of Wight. Monograph of the Palaeontographical Society 162(631): 1–166.

Brusatte, S.L., R.B.J. Benson, and M.A. Norell. 2011. The anatomy of *Dryptosaurus aquilunguis* (Dinosauria: Theropoda) and a review of its tyrannosauroid affinities. American Museum Novitates 3717, 1-53.

Brusatte, S.L., R.B.J. Benson, and X. Xu. 2010d. The evolution of large-bodied theropod dinosaurs during the Mesozoic in Asia. Journal of Iberian Geology 36: 275-296.

Brusatte, S.L. M.J. Benton, J.B. Desojo, and M.C. Langer. 2010c. The higher-level phylogeny of Archosauria (Tetrapoda: Diapsida). Journal of Systematic Palaeontology 8: 3-47.

Brusatte, S.L., T.D. Carr, G.M. Erickson, G.S. Bever, and M.A. Norell. 2009a. A long-snouted, multi-horned tyrannosaurid from the Late Cretaceous of Mongolia. Proceedings of the National Academy of Sciences (USA) 106: 17261-17266.

Brusatte, S.L., T.D. Carr, and M.A. Norell. 2012a. The osteology of Alioramus, a gracile and long-snouted tyrannosaurid (Dinosauria: Theropoda) from the Late Cretaceous of Mongolia. Bulletin of the American Museum of Natural History 366: 1-197.

Brusatte, S.L., M.A. Norell, T.D. Carr, G.M. Erickson, J.R. Hutchinson, A.M. Balanoff, G.S. Bever, J.N. Choiniere, P.J. Makovicky, and X. Xu. 2010a. Tyrannosaur paleobiology: new research on ancient exemplar organisms. Science 329: 1481-1485.

Brusatte, S.L., M. Sakamoto, S. Montanari, and W.E.H. Harcourt-Smith. 2012b. The evolution of cranial form and function in theropod dinosaurs: insights from geometric morphometrics. Journal of Evolutionary Biology 35: 365-377.

Brusatte, S.L., and P.C. Sereno. 2007. A new species of *Carcharodontosaurus* (Dinosauria: Theropoda) from the Cenomanian of Niger and a revision of the genus. Journal of Vertebrate Paleontology 27: 902–916.

Brusatte, S.L., and P.C. Sereno. 2008. Phylogeny of Allosauroidea (Dinosauria: Theropoda): comparative analysis and resolution. Journal of Systematic Palaeontology 6: 155–182.

Brusatte, S.L., M. Vremir, Z. Csiki-Sava, A.H. Turner, A. Watanabe, G.M. Erickson, and M.A. Norell. In press. The osteology of *Balaur bondoc*, an island-dwelling dromaeosaurid (Dinosauria: Theropoda) from the Late Cretaceous of Romania. Bulletin of the American Museum of Natural History.

Buffetaut, E., V. Suteethorn, and H. Tong. 2009. An early 'ostrich dinosaur' (Theropoda: Ornithomimosauria) from the Early Cretaceous Sao Khua Formation of NE Thailand. Geological Society of London, Special Publications 315: 229-243.

Burnham, D.A. 2004. New information on *Bambiraptor feinbergi* (Theropoda: Dromaeosauridae) from the Late Cretaceous of Montana. *In* P.J. Currie, E.B. Koppelhus, M.A. Shugar, and J.L. Wright (editors), Feathered Dragons: Studies on the Transition from Dinosaurs to Birds, 67–111. Bloomington: Indiana University Press.

Burnham, D.A., K.L. Derstler, P.J. Currie, R.T. Bakker, Z. Zhou, and J.H. Ostrom. 2000. Remarkable new birdlike dinosaur (Theropoda: Maniraptora) from the Upper Cretaceous of Montana. University of Kansas Paleontological Contributions 13: 1–14.

Butler, R.J., S.L. Brusatte, B. Andres, and R.B.J. Benson. 2012. How do geological sampling biases affect studies of morphological evolution in deep time? A case study of pterosaur (Reptilia: Archosauria) disparity. *Evolution* 66: 147-162.

Carpenter, K. 1992. Tyrannosaurids (Dinosauria) of Asia and North America. *In* N. Mateer and P.J. Chen (editors), Aspects of Nonmarine Cretaceous Geology: 250–268. Beijing: China Ocean Press.

Carpenter, K., C. Miles, and K. Cloward. 2005a. New small theropod from the Upper Jurassic Morrison Formation of Wyoming. *In* K. Carpenter (editor), The Carnivorous Dinosaurs: 23–48. Bloomington: Indiana University Press.

Carpenter, K., C. Miles, J. H. Ostrom, and K. Cloward. 2005b. Redescription of the small maniraptoran theropods *Ornitholestes* and *Coelurus* from the Upper Jurassic Morrison Formation of Wyoming. *In* K. Carpenter (editor), The Carnivorous Dinosaurs: 49-71. Bloomington: Indiana University Press.

Carpenter, K.D., D. Russell, D. Baird, and R. Denton. 1997. Redescription of the holotype of *Dryptosaurus aquilunguis* (Dinosauria: Theropoda) from the Upper Cretaceous of New Jersey. Journal of Vertebrate Paleontology 17: 561–573.

Carr, T.D. 1999. Craniofacial ontogeny in Tyrannosauridae (Dinosauria, Coelurosauria). Journal of Vertebrate Paleontology 19: 497–520.

Carr, T.D. 2004. Phylogeny of Tyrannosauroidea (Dinosauria: Coelurosauria) with special reference to North American Forms. Unpublished PhD Dissertation, University of Toronto, 1270 pp.

Carr, T.D. 2010. A taxonomic assessment of the type series of *Albertosaurus sarcophagus* and the identity of Tyrannosauridae (Dinosauria, Coelurosauria) in the *Albertosaurus* bonebed from the Horseshoe Canyon Formation (Campanian-Maastrichtian, Late Cretaceous). Canadian Journal of Earth Sciences 47: 1213-1226.

Carr, T.D., and T. E. Williamson. 2004. Diversity of late Maastrichtian Tyrannosauridae (Dinosauria: Theropoda) from western North America. Zoological Journal of the Linnean Society 142: 479–523.

Carr, T.D., and T.E. Williamson. 2010. *Bistahieversor sealeyi*, gen. et sp. nov., a new tyrannosauroid from New Mexico and the origin of deep snouts in Tyrannosauroidea. Journal of Vertebrate Paleontology 30: 1-16.

Carr, T.D., T.E. Williamson, B.B. Britt, and K. Stadtman. 2011. Evidence for high taxonomic and morphologic tyrannosauroid diversity in the Late Cretaceous (Late Campanian) of the American Southwest and a new short-skulled tyrannosaurid from the Kaiparowits Formation of Utah. Naturwissenschaften 98: 241-246.

Carr, T.D., T.E. Williamson, and D.R. Schwimmer. 2005. A new genus and species of tyrannosauroid from the Late Cretaceous (Middle Campanian) Demopolis Formation of Alabama. Journal of Vertebrate Paleontology 25: 119–143.

Carrano, M.T. 2006. Body-size evolution in the Dinosauria. *In* M.T. Carrano, R.W. Blob, T.J. Gaudin, and J.R. Wible (editors), Amniote Paleobiology: 225-268. Chicago: University of Chicago Press.

Carrano, M.T. 2007. The appendicular skeleton of Majungasaurus crenatissimus (Theropoda: Abelisauridae) from the Late Cretaceous of Madagascar. Society of Vertebrate Paleontology Memoir 8: 163-179.

Carrano, M.T., and J.R. Hutchinson. 2002. Pelvic and hindlimb musculature of *Tyrannosaurus rex* (Dinosauria: Theropoda). Journal of Morphology 253: 207-228.

Chapman, R.E. 1990. Shape analysis in the study of dinosaur morphology. In K. Carpenter and P.J. Currie (editors), Dinosaur Systematics: Approaches and Perspectives: 21-42. Cambridge: Cambridge University Press.

Charig, A.J., and A.C. Milner. 1997. *Baryonyx walkeri*, a fish-eating dinosaur from the Wealden of Surrey. Bulletin of the Natural History Museum, Geology Series 53: 11–70.

Chatterjee, S. 1985. *Postosuchus*, a new thecodontian reptile from the Triassic of Texas and the origin of tyrannosaurs. Philosophical Transactions of the Royal Society of London, B 309: 395–460.

Chen, P., Z. Dong, and S. Zhen.1998. An exceptionally well-preserved theropod dinosaur from the Yixian Formation of China. Nature 391: 147-152.

Chiappe, L.M., and U.B. Göhlich. 2010. Anatomy of Juravenator starki (Theropoda: Coelurosauria) from the Late Jurassic of Germany. Neues Jahrbuch für Geologie und Paläontologie Abhanglungen 248: 257-296.

Chiappe, L.M., M.A. Norell, and J.M. Clark. 1996. Phylogenetic position of *Mononykus* (Aves: Alvarezsauridae) from the Late Cretaceous of the Gobi Desert. Memoirs of the Queensland Museum 39: 557−582.

Chiappe, L.M., M. Norell, and J.M. Clark. 1998. The skull of a relative of the stem-group bird *Mononykus*. Nature 392: 275–278.

Chiappe, L.M., M.A. Norell, and J.M. Clark. 2002. The Cretaceous, short-armed Alvarezsauridae: *Mononykus* and its kin. *In*: L.M. Chiappe and L.M. Witmer (editors), Mesozoic Birds: Above the Heads of Dinosaurs: 87-120. Berkeley: University of California Press.

Choiniere, J.N., J.M. Clark, C.A. Forster, and X. Xu. 2010b. A basal coelurosaur (Dinosauria: Theropoda) from the Late Jurassic (Oxfordian) of the Shishugou Formation in Wucaiwan, People's Republic of China. Journal of Vertebrate Paleontology 30: 1773-1796.

Choiniere, J.N., C.A. Forster, W.J. de Klerk. 2012. New information on *Nqwebasaurus thwazi*, a coelurosaurian theropod from the Early Cretaceous Kirkwood Formation in South Africa. Journal of African Earth Sciences 71-72: 1-17.

Choiniere, J.N., X. Xu, J.M. Clark, C.A. Forster, Y. Guo, and F. Han. 2010a. A basal alvarezsauroid theropod from the Early Late Jurassic of Xinjiang, China. Science 327: 571–573.

Chinnery, B.J. 2004. Morphometric analysis of evolutionary trends in the ceratopsian postcranial skeleton. Journal of Vertebrate Paleontology 24: 591-609.

Christiansen, P. and R.A. Farina 2004. Mass prediction in theropod dinosaurs. Historical Biology 16: 85–92.

Chure, D.J. 2000. On the orbit of the theropod dinosaurs. Gaia 15: 233–240.

Ciampaglio, C.N., M. Kemp, and D.W. McShea. 2001. Detecting changes in morphospace occupation patterns in the fossil record: characterization and analysis of measures of disparity. Paleobiology 27: 695-715.

Claessens, L.P.A.M. 2004. Dinosaur gastralia; origin, morphology, and function. Journal of Vertebrate Paleontology 24: 89-106.

Clark, J. M., M. A. Norell, and L. M. Chiappe. 1999. An oviraptorid skeleton from the Late Cretaceous of Ukhaa Tolgod, Mongolia, preserved in an avian-like brooding position over an oviraptorid nest. American Museum Novitates 3265: 1–36.

Clark, J.M., M.A. Norell, and P.J. Makovicky. 2002a. Cladistic approaches to the relationship of birds to other theropod dinosaurs. In L.M. Chiappe and L.M. Witmer (editors), Mesozoic Birds: Above the Heads of Dinsoaurs: 31-64. Berkeley: University of California Press.

Clark, J.M, M.A Norell, and T. Rowe. 2002b. Cranial anatomy of *Citipati osmolskae* (Theropoda, Oviraptorosauria), and a reinterpretation of the holotype of *Oviraptor philoceratops*. American Museum Novitates 3364: 1–24.

Clark J.M., A. Perle, and M.A. Norell. 1994. The skull of *Erlicosaurus andrewsi*, a Late Cretaceous "segnosaur" (Theropoda: Therizinosauroidea) from Mongolia. American Museum Novitates 3115: 1-39.

Clarke, J.A., Z. Zhou, and F. Zhang. 2006. Insight into the evolution of avian flight from a new clade of Early Cretaceous ornithurines from China and the morphology of *Yixianornis grabaui*. Journal of Anatomy 208: 287-308.

Coddington, J. A., and N. Scharff. 1994. Problems with zero-length branches. Cladistics 10: 415–423.

Colbert, E.H. 1989. The Triassic dinosaur *Coelophysis*. Museum of Northern Arizona Bulletin 57: 1-160.

Coria R.A., and P.J. Currie. 2006. A new carcharodontosaurid (Dinosauria, Theropoda) from the Upper Cretaceous of Argentina. Geodiversitas 28: 71-118.

Csiki, Z., M. Vremir, S.L. Brusatte, and M.A. Norell. 2010. An aberrant island-dwelling theropod dinosaur from the Late Cretaceous of Romania. Proceedings of the National Academy of Sciences (USA) 107: 15357-15361.

Currie, P.J. 1995. New information on the anatomy and relationships of *Dromaeosaurus albertensis* (Dinosauria: Theropoda). Journal of Vertebrate Paleontology 15: 576- 591.

Currie, P.J. 2003a. Cranial anatomy of tyrannosaurid dinosaurs from the late Cretaceous Alberta, Canada. Acta Palaeontologica Polonica 48: 191–226.

Currie, P.J. 2003b. Allometric growth in tyrannosaurids (Dinosauria: Theropoda) from the Upper Cretaceous of North America and Asia. Canadian Journal of Earth Sciences 40: 651–665.

Currie, P.J., and P. Chen. 2001. Anatomy of *Sinosauropteryx prima* from Liaoning, northeastern China. Canadian Journal of Earth Sciences 38: 1705–1727.

Currie, P.J. and Z. Dong. 2001a. New information on *Shanshanosaurus huoyanshanensis*, a juvenile tyrannosaurid (Theropoda, Dinosauria) from the Late Cretaceous of China. Canadian Journal of Earth Sciences 38: 1729–1737.

Currie, P J. and Z. Dong. 2001b. New information on Cretaceous troodontids (Dinosauria, Theropoda) from the People's Republic of China. Canadian Journal of Earth Sciences 38: 1753–1766.

Currie, P.J., J.H. Hurum, and K. Sabath. 2003. Skull structure and evolution in tyrannosaurid dinosaurs. Acta Palaeontologica Polonica 48: 227–234.

Currie, P.J., J.K. Rigby, Jr., and R.E. Sloan. 1990. Theropod teeth from the Judith River Formation of southern Alberta, Canada. *In* K. Carpenter and P.J. Currie (editors), Dinosaur Systematics: Perspectives and Approaches: 107-125. Cambridge: Cambridge University Press.

Currie, P.J., and X.-J. Zhao. 1993. A new large theropod (Dinosauria, Theropoda) from the Jurassic of Xinjiang, People's Republic of China. Canadian Journal of Earth Sciences 30: 2037-2081.

Dal Sasso, C., and S. Maganuco. 2011. *Scipionyx samniticus* (Theropoda: Compsognathidae) from the Lower Cretaceous of Italy. Osteology, ontogenetic assessment, phylogeny, soft tissue anatomy, taphonomy and palaeobiology. Memorie della Società Italiana di Scienze Naturali e del Museo Civico di Storia di Milano XXXVII: 1-281.

Dal Sasso, C., and M. Signore. 1998. Exceptional soft-tissue preservation in a theropod dinosaur from Italy. Nature 392: 383-387.

Dashzeveg, D., L. Dingus, D.B. Loope, C.C. Swisher III, T. Dulam, and M.R. Sweeney. 2005. New stratigraphic subdivision, depositional environment, and age estimate for the Upper Cretaceous Djadokhta Formation, southern Ulan Nur Basin, Mongolia. American Museum Novitates 3498: 1-31.

Davidson, A.R. 2008. Removing fossil ribs: the thread technique. Journal of Vertebrate Paleontology 28(3):69A.

Davidson, A.R. 2009. Temporary gap-filling to stabilize an exploded matrix for fossil preparation: the sand and Butvar B-76 technique. Journal of Vertebrate Paleontology 29(3): 85A.

Davidson, A., S. Alderson, and M. Fox. 2006. Assembling an archival marking kit for paleontological specimens. Journal of Vertebrate Paleontology 26(3):54A.

Dececchi, T.A., H.C.E. Larsson, and D.W.E. Hone. 2012. *Yixianosaurus longimanus* (Theropoda: Dinosauria) and its bearing on the evolution of Maniraptora and ecology of the Jehol Fauna. Vertebrata PalAsiatica 50: 111-139.

de Klerk, W.J., C.A. Forster, S.D. Sampson, A. Chinsamy, and C.F. Ross. 2000. A new coelurosaurian dinosaur from the Early Cretaceous of South Africa. Journal of Vertebrate Paleontology 20: 324-332.

Desdevises, Y., P. Legendre, L. Azouzi, and S. Morand. 2003. Quantifying phylogenetically structured environmental variation. Evolution 57: 2647-2652.

Dingus, L., D.B. Loope, D. Dashzeveg, C.C. Swisher III, C. Minjin, M.J. Novacek, M.A. Norell. 2008. The geology of Ukhaa Tolgod (Djadokhta Formation, Upper Cretaceous, Nemegt Basin, Mongolia). American Museum Novitates 3616: 1-40.

Diniz-Filho, J.A.F., C.E.R. De Sant'ana, and L.M. Bini. 1998. An eigenvector method for estimating phylogenetic inertia. Evolution 52: 1247-1262.

Dodson, P., C.A. Forster, and S.D. Sampson, S.D. 2004. Ceratopsidae. *In* D.B. Weishampel, P. Dodson, and H. Osmólska (editors), The Dinosauria, 2nd edition: 494-513. Berkeley, CA: University of California Press.

Dong, Z.-M. 1979. Cretaceous dinosaurs of Hunan, China. Mesozoic and Cenozoic Red Beds of South China. Selected Papers from the "Cretaceous-Tertiary Workshop", Institute of Vertebrate Paleontology and Paleoanthropology & Nanjing Institute of Paleontology (editors.), Science Press, Nanxiong, China, 342-350.

Eddy, D.R. 2008. A Re–Analysis of the Skull of *Acrocanthosaurus atokensis* (NCSM 14345): Implications for Allosauroid Morphology, Phylogeny, and Biogeography. Unpublished MSc Thesis, North Carolina State University.

Eddy, D.R., and J.A. Clarke. 2011. New information on the cranial anatomy of *Acrocanthosaurus atokensis* and its implications for the phylogeny of Allosauroidea (Dinosauria: Theropoda). PLoS ONE 6(3): e17932.

Egi, N., and D.B. Weishampel. 2002. Morphometric analyses of humeral shape in hadrosaurids (Ornithopoda, Dinosauria). Senckenbergiana Lethaea 82: 43-58.

Ezcurra, M.D. 2007. The cranial anatomy of the coelophysoid theropod *Zupaysaurus rougieri* from the Upper Triassic of Argentina. Historical Biology 19: 185-202.

Ezcurra, M.D., and F.E. Novas. 2007. Phylogenetic relationships of the Triassic theropod *Zupaysaurus rougieri* from NW Argentina. Historical Biology 19: 35-72.

Farlow, J.O., D.L. Brinkman, W.L. Abler, and P.J. Currie. 1991. Size, shape and serration density of theropod dinosaur lateral teeth. Modern Geology 16: 161–198.

Felsenstein, J. 1985. Phylogenies and the comparative method. American Naturalist 125: 1-15.

Foote, M. 1993. Discordance and concordance between morphological and taxonomic diversity. Paleobiology 20: 185-204.

Forster, C.A., S.D. Sampson, L.M. Chiappe, and D.W. Krause. 1998. The theropod ancestry of birds: new evidence from the Late Cretaceous of Madagascar. Science 279: 1915–1919.

Fowler, D.W., H.N. Woodward, E.A. Freedman, P.L. Larson, and J.R. Horner. 2011. Reanalysis of "*Raptorex kriegsteini*": a juvenile tyrannosaurid dinosaur from Mongolia. PLoS ONE 6(6): e21376.

Gauthier, J. 1986. Saurischian monophyly and the origin of birds. Memoirs of the California Academy of Sciences 8: 1–55.

Gianechini, F.A., F.L. Angolin, and M.D. Ezcurra. 2011. A reassessment of the purported venom delivery system of the bird-like raptor *Sinornithosaurus*. Paläontologische Zeitschrift 85: 103-107.

Gilmore, C.W. 1933. On the dinosaurian fauna of the Iren Dabasu Formation. Bulletin of the American Museum of Natural History 67: 23-95.

Gilmore, C.W. 1946. A new carnivorous dinosaur from the Lance Formation of Montana. Smithsonian Miscellaneous Collections 106: 1-19.

Gishlick, A.D., and J.A. Gauthier. 2007. On the manual morphology of *Compsognathus longipes* and its bearing on the diagnosis of Compsognathidae. Zoological Journal of the Linnean Society 149: 569-581.

Göhlich, U.B., and L.M. Chiappe. 2006. A new carnivorous dinosaur from the Late Jurassic Solnhofen archipelago. Nature 440: 329-332.

Göhlich, U.B., H. Tischlinger, and L.M. Chiappe. 2006. *Juravenator starki* (Reptilia, Theropoda), ein neuer Raubdinosaurier aus dem Oberjura der südlichen Frankenalb (Süddeutschland): Skelettanatomie und Weichteilbefunde). Archaeopteryx 24: 1-26.

Goloboff, P.A., J.A. Farris, and K.C. Nixon. 2008. TNT, a free program for phylogenetic analysis. Cladistics 24: 774-786.

Gong, E., L.D. Martin, D.A. Burnham, and A.R. Falk (2010) The birdlike raptor *Sinornithosaurus* was venomous. Proceedings of the National Academy of Sciences (USA) 107: 766-768.

Gower, D.J. 1999. Cranial osteology of a new rauisuchian archosaur from the Middle Triassic of southern Germany. Stuttgarter Beiträge zur Naturkunde, Serie B (Geologie und Palaeontologie) 280: 1–49.

Harris, J.D. 1998. A reanalysis of *Acrocanthosaurus atokensis*, its phylogenetic status, and Paleobiogeographic implications, based on a new specimen from Texas. New Mexico Museum of Natural History and Science Bulletin 13: 1-75.

He, H.Y., X.L. Wang, Z.H. Zhou, F. Wang, A. Boven, G.H. Shi, and R.X. Zhu. 2004. Timing of the Jiufotang Formation (Jehol Group) in Liaoning, northeastern China, and its implications, Geophysical Research Letters 31: L12605, doi:10.1029/2004GL019790.

Henderson, D.M. 2002. The eyes have it: sizes, shapes, and orientations of theropod orbits as indicators of skull strength and bite force. Journal of Vertebrate Paleontology 22: 766-778.

Hieronymus, T.L., L.M. Witmer, D.H. Tanke, and P.J. Currie. 2009. The facial integument of centrosaurine ceratopsids: morphological and histological correlates of novel skin structures. The Anatomical Record 292: 1370-1396.

Holliday, C.M. 2009. New insights into dinosaur jaw muscle anatomy. The Anatomical Record 292: 1246-1265.

Holliday, J.A., and S. J. Steppan. 2004. Evolution of hypercarnivory: the effect of specialization on morphological and taxonomic diversity. Paleobiology 30: 108-128.

Holtz, T.R. 1995. The arctometatarsalian pes, an unusual structure of the metatarsus of Cretaceous Theropoda (Dinosauria: Saurischia). Journal of Vertebrate Paleontology 14: 480–519.

Holtz, T.R. 2000. A new phylogeny of the carnivorous dinosaurs. Gaia 15: 6–61.

Holtz, T.R. 2001. The phylogeny and taxonomy of the Tyrannosauridae. *In* D.H. Tanke and K. Carpenter (editors), Mesozoic Vertebrate Life: 64–83. Bloomington: Indiana University Press.

Holtz, T.R. 2004. Tyrannosauroidea. *In* D. B. Weishampel, P. Dodson, and H. Osmólska (editors), The Dinosauria, 2nd Edition:111–136. Berkeley: University of California Press.

Holtz, T.R., R.E. Molnar, and P.J. Currie. 2004. Basal Tetanurae. *In* D.B. Weishampel, P. Dodson, and H. Osmólska (editors), The Dinosauria (2nd edition): 71-110. Berkeley: University of California Press.

Hone, D.W.E., K. Wang, C. Sullivan, X.-J. Zhao, S. Chen, D. Li, S. Ji, Q. Ji, and X. Xu 2011.A new, large tyrannosaurine theropod from the Upper Cretaceous of China. Cretaceous Research 32: 495-503.

Hu, D., L. Hou, L. Zhang, and X. Xu. 2009. A pre-*Archaeopteryx* troodontid theropod from China with long feathers on the metatarsus. Nature 461: 640-643.

Huene, F. von 1914. Das natürliche System der Saurischia. Zentralblatt Mineralogie, Geologie, und Palaeontologie B 1914: 154–158.

Hurum, J.H. and P.J. Currie. 2000. The crushing bite of tyrannosaurids. Journal of Vertebrate Paleontology 20: 619–621.

Hurum, J.H. and K. Sabath. 2003. Giant theropod dinosaurs from Asia and North America: Skulls of *Tarbosaurus bataar* and *Tyrannosaurus rex* compared. Acta Palaeontologica Polonica 48: 161–190.

Hutchinson, J.R. 2001. The evolution of pelvic osteology and soft tissue on the line to extant birds (Neornithes). Zoological Journal of the Linnean Society 131: 123–168.

Hutt, S., D.W. Naish, D.M. Martill, M.J. Barker, and P. Newberry. 2001. A preliminary account of a new tyrannosauroid theropod from the Wessex Formation (Early Cretaceous) of southern England. Cretaceous Research 22: 227–242.

Hwang, S.H., M.A. Norell, Q. Ji, and K.-Q. Gao. 2002. New specimens of *Microrapto zhaoianus* (Theropoda: Dromaeosauridae) from Northeastern China. American Museum Novitates 3381: 1–44.

Hwang, S.H., M.A. Norell, Q. Ji, and K.-Q. Gao.2004. A large compsognathid from the Early Cretaceous Yixian Formation of China. Journal of Systematic Palaeontology 2: 13–30.

Ji, Q., P.J. Currie, M.A. Norell, and S.A. Ji. 1998. Two feathered dinosaurs from northeastern China. Nature 393: 753-761.

Ji, Q., S.-A. Ji, and L.-J. Zhang. 2009. First large tyrannosauroid theropod from the Early Cretaceous Jehol Biota in northeastern China. Geological Bulletin of China 28: 1369-1374.

Ji, Q., M.A. Norell, P.J. Makovicky, K. Gao, S. Ji, and C. Yuan. 2003. An early ostrich dinosaur and implications for ornithomimosaur phylogeny. American Museum Novitates 3420:1–19.

Ji, S., Q. Ji, J. Lü, and C. Yuan. 2007. A new giant compsognathid dinosaur with long filamentous integuments from Lower Cretaceous of Northeastern China.Acta Geologica Sinica, 81: 8-15.

Jones, K.E., and A. Goswami. 2010. Quantitative analysis of the influences of phylogeny and ecology on phocid and otariid pinniped (Mammalia; Carnivora) cranial morphology. Journal of Zoology 280: 297-308.

Karhu, A. A., and A. S. Rautian. 1996. A new family of Maniraptora (Dinosauria: Saurischia) from the Late Cretaceous of Mongolia. Paleontological Journal 30: 583–592.

Kellner, A.W.A. 1999. Short Note on a new dinosaur (Theropoda, Coelurosauria) from the Santana Formation (Romualdo Member, Albian), northeastern Brazil". Boletim do Museu Nacional (Serie Geologia) 49: 1–8.

Kirkland, J.I., B.B. Britt, C.H. Whittle, S.K. Madsen, and D.L. Burge. 1998.A small coelurosaurian theropod from the Yellow Cat Memeber of the Cedar Mountain Formation

(Lower Cretaceous, Barremian) of Eartern Utah. New Mexico Museum of Natural History and Science Bulletin 14: 239-248.

Kirkland, J. I., L.E. Zanno, S.D. Sampson, J.M. Clark, and D.D. DeBlieux. 2005. A primitive therizinosauroid dinosaur from the Early Cretaceous of Utah. Nature 7038: 84-87.

Klingenberg, C.P. 2011. MorphoJ: an integrated software package for geometric morphometrics. Molecular Ecology Resources 11: 353-357.

Klingenberg, C.P., and N.A. Gidaszewski. 2010. Testing and quantifying phylogenetic signals and homoplasy in morphometric data. Systematic Biology 59: 245-261.

Kobayashi, Y., and J.-C. Lu. 2003. A new ornithomimid dinosaurian with gregarious habits from the Late Cretaceous of China. Acta Palaeontologica Polonica 48: 235–259.

Kobayashi, Y., J.-C. Lü, Z.-M. Dong, R. Barsbold, and Y. Azuma. 1999. Herbivorous diet in an ornithomimid dinosaur. Nature 402: 480-481.

Kobayashi, Y., and R. Barsbold. 2005a. Reexamination of a primitive ornithomimosaur, *Garudimimus brevipes* Barsbold, 1981 (Dinosauria: Theropoda), from the Late Cretaceous of Mongolia. Canadian Journal of Earth Sciences 42: 1501-1521.

Kobayashi, Y., and R. Barsbold. 2005b. Anatomy of *Harpymimus okladnikovi* Barsbold and Perle 1984 (Dinosauria; Theropoda) of Mongolia. *In* K. Carpenter (editor), The Carnivorous Dinosaurs: 97-126. Bloomington: Indiana University Press.

Kobayashi, Y., and R. Barsbold. 2006. Ornithomimids from the Nemegt Formation of Mongolia. Journal of the Paleontological Society of Korea 22: 195-207.

Kurzanov, S.M. 1976. [A new Late Cretaceous carnosaur from Nogon-Tsav, Mongolia]. Joint Soviet-Mongolian Paleontological Expedition Transactions 3: 93–104. [Russian with English summary].

Lambe, L.M. 1917. The Cretaceous theropodous dinosaur *Gorgosaurus*. Memoirs of the Geological Survey of Canada 100: 1–84.

Li, D., M.A. Norell, K. Gao, N.D. Smith, and P.J. Makovicky. 2010. A longirostrine tyrannosauroid from the Early Cretaceous of China. Proceedings of the Royal Society Series B, 277: 183-190.

Li, D., C. Peng, H. You, M.C. Lamanna, J.D. Harris, K.J. Lacovara, and J. Zhang. 2007. A large therizinosauroid (Dinosauria: Theropoda) from the Early Cretaceous of northwestern China. Acta Geologica Sinica 85: 539-549.

Li, D., H. You, and J. Zhang. 2008. A new specimen of *Suzhousaurus megatherioiides* (Dinosauria: Therizinosauroidea) from the Early Cretaceous of northwestern China. Canadian Journal of Earth Sciences 45: 769-779.

Longrich, N.R., and P.J. Currie. 2009. *Albertonykus borealis*, a new alvarezsaur (Dinosauria: Theropoda) from the Early Maastrichtian of Alberta, Canada: implications for the systematics and ecology of the Alvarezsauridae. Cretaceous Research 30: 239-252.

Lü, J., L. Xu, Y. Liu, X. Zhang, S. Jia, and Q. Ji. 2010. A new troodontid theropod from the Late Cretaceous of central China, and the radiation of Asian troodontids. Acta Palaeontologica Polonica 55: 381-388.

Madsen, J.H. 1974. A new theropod dinosaur from the Upper Jurassic of Utah. Journal of Paleontology 48: 27–31.

Madsen, J.H. 1976. *Allosaurus fragilis*: a revised osteology. Utah Geological Survey Bulletin 109: 1-163.

Madsen, J.H., and S.P. Welles. 2000. *Ceratosaurus* (Dinosauria, Theropoda). A revised osteology. Utah Geological Survey Miscellaneous Publication 2: 1–80.

Makovicky, P.J., S. Apesteguía, and F.L. Agnolín. 2005. The earliest dromaeosaurid theropod from South America. Nature 437: 1007–1011.

Makovicky, P.J., Y. Kobayashi, and P.J. Currie. 2004. Ornithomimosauria. *In* D.B. Weishampel, P. Dodson, and H. Osmólska (editors), The Dinosauria, Second Edition: 137–150. Berkeley: University of California Press.

Makovicky, P.J., D. Li, K.-Q. Gao, M. Lewin, G.M. Erickson, and M.A. Norell. 2010. A giant ornithomimosaur from the Early Cretaceus of China. Proceedings of the Royal Society of London, Series B 277: 191-198.

Makovicky, P.J., and Norell, M.A. 1998. A partial ornithomimid braincase from Ukhaa Tolgod (Upper Cretaceous, Mongolia). American Museum Novitates 3247: 1-16.

Makovicky, P.J., M.A. Norell, J.M. Clark, and T. Rowe. 2003. Osteology and relationships of *Byronosaurus jaffei* (Theropoda: Troodontidae). American Museum Novitates 3402: 1-32.

Makovicky, P.J., and H.-D. Sues. 1998. Anatomy and phylogentic relationships of the theropod dinosaur *Microvenator celer* from the Lower Cretaceous of Montana. American Museum Novitates 3240: 1-27.

Maleev, E.A. 1974. [Gigantic carnosaurs of the family Tyrannosauridae]. Joint Soviet-Mongolian Palaeontological Expedition, Transactions 1: 132–191. [Russian with English summary].

Marsh, O.C. 1879. Notice of new Jurassic reptiles. American Journal of Science, 3rd ser., 18: 501-505.

Marsh, O.C. 1881a. Principal characters of American Jurassic dinosaurs. Part V. American Journal of Science (Series 3) 21: 417-423.

Marsh. O.C. 1881b. A new order of extinct Jurassic reptiles (Coeluria). American Journal of Science 21: 339-340

Martinelli, A.G., and E.I. Vera. 2007. *Achillesaurus manazzonei,* a new alvarezsaurid theropod (Dinosauria) from the Late Cretaceous Bajo de la Carpa Formation, Río Negro Province, Argentina. Zootaxa 1582: 1–17.

Martínez, R.D., and F.E. Novas. 2006. *Aniksosaurus darwini* gen. et sp. nov., a new coelurosaurian theropod from the early Late Cretaceous of central Patagonia, Argentina. Revista del Museo Argentino de Ciencias Naturales 8: 243-259.

Molnar, R.E. 1991. The cranial morphology of *Tyrannosaurus rex*. Palaeontographica Abteilung A 217: 137–176.

Naish, D., S. Hutt, and D. M. Martill. 2001. Saurischian dinosaurs 2: Theropods; pp. 242–309 in D.M. Martill and D. Naish (editors), Dinosaurs of the Isle of Wight: 242-309. London: The Palaeontological Association.

Naish, D., D.M. Martill, and E. Frey. 2004. Ecology, systematics and biogeographical relationships of dinosaurs, including a new theropod, from the Santana Formation (?Albian, Early Cretaceous) of Brazil. Historical Biology 2004: 1-14.

Nesbitt, S.J., J.A. Clarke, A.H. Turner, and M.A. Norell. 2011. A small alvarezsaurid from the eastern Gobi Desert offers insight into evolutionary patterns in the Alvarezsauroidea. Journal of Vertebrate Paleontology 31:144–153.

Nesbitt, S.J., A.H. Turner, M. Spaulding, J.L. Conrad, and M.A. Norell. 2009. The theropod furcula. Journal of Morphology 270: 856-879.

Nicholls, E.L., and A.P. Russell. 1985. Structure and function of the pectoral girdle and forelimb of *Struthiomimus altus* (Theropoda: Ornithomimidae). Palaeontology 28: 638-677.

Norell, M.A., J.M. Clark, L.M. Chiappe, L.M., and D. Dashzeveg. 1995. A nesting dinosaur. Nature 378: 774-776.

Norell, M.A., J.M. Clark, and P.J. Makovicky. 2001. Relationships among Maniraptora: problems and prospects. *In* J.A. Gauthier and L.F. Gall (editors), New Perspectives on the Origin and Early Evolution of Birds: 49-67. New Haven, CT: Peabody Museum of Natural History.

Norell, M.A., J.M. Clark, A.H. Turner, P.J. Makovicky, R. Barsbold, and T. Rowe. 2006.

A new dromaeosaurid theropod from Ukhaa Tolgod (Ömnögov, Mongolia). American Museum Novitates 3545: 1–51.

Norell, M.A., and S.H. Hwang. 2004. A troodontid dinosaur from Ukhaa Tolgod (Late Cretaceous Mongolia). American Museum Novitates 3446: 1–9.

Norell, M.A., and P.J. Makovicky. 1997. Important features of the dromaeosaur skeleton: information from a new specimen. American Museum Novitates 3215: 1–28.

Norell, M.A. and P.J. Makovicky. 1999. Important features of the dromaeosaur skeleton II: information from newly collected specimens of *Velociraptor mongoliensis*. American Museum Novitates 3282: 1–45.

Norell, M.A., P.J. Makovicky, G.S. Bever, A.M. Balanoff, J.M. Clark, R. Barsbold, and T. Rowe. 2009. A review of the Mongolian Cretaceous dinosaur *Saurornithoides* (Troodontidae: Theropoda). American Museum Novitates 3654: 1-63.

Norell, M.A, P.J Makovicky, and J.M Clark. 2004. The braincase of *Velociraptor*. *In*: P.J. Currie, E.B Koppelhus, M.A Shugar, and J.L Wright (editors). Feathered Dragons: Studies on the Transition from Dinosaurs to Birds: 133–143. Bloomington, Indiana: University Press.

Norell, M.A., P.J. Makovicky, and P.J. Currie. 2001. The beaks of ostrich dinosaurs. Nature 412: 874.

Norell, M.A., and X. Xu. 2005. Feathered dinosaurs. Annual Review of Earth and Planetary Sciences 33: 277-299.

Novas, F.E. 1996. Dinosaur monophyly. Journal of Vertebrate Paleontology 16: 723-741.

Novas, F.E. 1997. Anatomy of *Patagonykus puertai* (Theropoda, Maniraptora, Alvarezsauridae) from the Late Cretaceous of Patagonia. Journal of Vertebrate Paleontology 18: 137–166.

Novas, F.E., M.D. Ezcurra, F.L. Agnolin, D. Pol, and R. Ortiz. 2012. New Patagonian Cretaceous theropod sheds light about the early radiation of Coelurosauria. Revista del Museo *Argentino* de Ciencias Naturales 14: 57-81.

Novas, F.E., M.D. Ezcurra, M.D, and A. Lecuona. 2008. *Orkoraptor burkei* nov. gen. et sp., a large theropod from the Maastrichtian Pari Aike Formation, Southern Patagonia, Argentina. Cretaceous Research 29: 468-480.

Novas, F.E., and D. Pol. 2005. New evidence on deinonychosaurian dinosaurs from the Late Cretaceous of Patagonia. Nature 433: 858–861.

Novas, F.E., D. Pol, J.I. Canale, J.D. Porfiri, and J.O. Calvo. 2009. A bizarre Cretaceous theropod dinosaur from Patagonia and the evolution of Gondwanan dromaeosaurids. Proceedings of the Royal Society of London, Series B 276: 1101-1107.

Novas, F.E., and P.F. Puerta. 1997. New evidence concerning avian origins from the Late Cretaceous of Patagonia. Nature 387: 390–392.

O'Connor, P.M. 2007. The postcranial axial skeleton of *Majungasaurus crenatissimus* (Theropoda: Abelisauridae) from the Late Cretaceous of Madagascar. Society of Vertebrate Paleontology Memoir 8: 127-162.

O'Higgins, P. 2000. The study of morphological variation in the hominid fossil record: biology, landmarks and geometry. Journal of Anatomy 197: 103-120.

Osborn, H.F. 1905. *Tyrannosaurus* and other Cretaceous carnivorous dinosaurs. Bulletin of the American Museum of Natural History 21: 259–265.

Osborn, H.F. 1906. Tyrannosaurus, Upper Cretaceous carnivorous dinosaur. (Second communication. Bulletin of the American Museum of Natural History 22: 281-296.

Osborn, H.F. 1912. Crania of *Tyrannosaurus* and *Allosaurus*. Memoirs of the American Museum of Natural History 1: 3–30.

Osborn, H.F. 1916. Skeletal adaptations of *Ornitholestes*, *Struthiomimus*, *Tyrannosaurus*. Bulletin of the American Museum of Natural History 35: 733-771.

Osborn, H.F. 1924. Three new Theropoda, Protoceratops zone, central Mongolia. American Museum Novitates 144: 1–12.

Osmólska, H. 1996. An unusual theropod dinosaur from the Late Cretaceous Nemegt Formation of Mongolia. Acta Palaeontologica Polonica 41: 1-38.

Osmólska, H., Currie, P.J. & Barsbold, R. 2004. Oviraptorosauria. *In* D. B. Weishampel, P. Dodson, and H. Osmólska (editors), The Dinosauria, 2nd Edition: 165-183. Berkeley: University of California Press.

Osmólska, H., E. Roniewicz, and R. Barsbold. 1972. A new dinosaur, *Gallimimus bullatus* n. gen., n. sp. (Ornithomimidae) from the Upper Cretaceous of Mongolia. Palaeontologica Polonica 27: 103-143.

Ostrom, J.H. 1969. Osteology of *Deinonychus antirrhopus*, an unusual theropod from the Lower Cretaceous of Montana. Bulletin of the Peabody Museum of Natural History 30: 1–165.

Ostrom, J.H. 1978. The osteology of *Compsognathus longipes* Wagner. Zitteliana Abhandlungen der Bayerischen Staatssammlung für Paläontologie und historische Geologie 4: 77-118.

Padian, K., and L.M. Chiappe. 1998. The origin and early evolution of birds. Biological Reviews 73: 1-42.

Parks, W.A. 1928. *Albertosaurus arctunguis*, a new species of theropodous dinosaur

from the Edmonton Formation of Alberta. University of Toronto Studies (Geological Series) 25: 3–42.

Paul, G.S. 1988. Predatory Dinosaurs of the World. Simon & Schuster, New York.

Perez-Moreno, B.P., J.L. Sanz, A.D. Buscalioni, J.J. Moratalla, F. Ortega, and D. Rasskin-Gutman. 1994. A unique multitoothed ornithomimosaur dinosaur from the Lower Cretaceous of Spain. Nature 370: 363-367.

Perle, A. 1979. Segnosauridae—a new family of theropods from the Late Cretaceous of Mongolia. Transactions, Joint Soviet-Mongolian Palaeontological Expedition 15: 28–39.

Perle, A., L.M. Chiappe, R. Barsbold, J.M. Clark, and M.A. Norell. 1994. Skeletal morphology of *Mononykus olecranus* (Theropoda: Avialae) from the Late Cretaceous of Mongolia. American Museum Novitates 3105: 1–29.

Perle, A., M.A. Norell, L.M. Chiappe, and J.M. Clark. 1993. Flightless bird from the Cretaceous of Mongolia. Nature 362: 623-626.

Perle, A., M.A. Norell, and J.M. Clark. 1999. A new maniraptoran theropod - *Achillobator giganticus* (Dromaeosauridae) - from the Upper Cretaceous of Burkhant, Mongolia. Contribution no. 101 of the Mongolian-American Paleontological Project: 1–105.

Peyer, K. 2006. A reconsideration of *Compsognathus* from the Upper Tithonian of Canjeurs, Southeastern France. Journal of Vertebrate Paleontology 26: 879–896.

Pierce, S.E., K.D. Angielczyk, and E.J. Rayfield. 2008. Patterns of morphospace occupation and mechanical performance in extant crocodilian skulls: a combined geometric morphometric and finite element modeling approach. Journal of Morphology 269: 840-864.

Pierce, S.E., K.D. Angielczyk, and E.J. Rayfield. 2009. Morphospace occupation in thalattosuchian crocodylomorphs: skull shape variation, species delineation, and temporal patterns. Palaeontology 52: 1057-1097.

Rauhut, O.W.M. 2003a. The interrelationships and evolution of basal theropod dinosaurs. Special Papers in Palaeontology 69: 1-213.

Rauhut, O.W.M. 2003b. A tyrannosauroid dinosaur from the Late Jurassic of Portugal. Palaeontology 46: 903-910.

Rauhut, O.W.M. 2005. Osteology and relationships of a new theropod dinosaur from the Middle Jurassic of Patagonia. Palaeontology 48: 87-110.

Rauhut, O.W.M., C. Foth, H. Tischlinger, and M.A. Norell. 2012. Exceptionally preserved juvenile megalosauroid theropod dinosaur with filamentous integument from the Late Jurassic of Germany. Proceedings of the National Academy of Sciences 109: 11746-11751.

Rauhut, O.W.M., A.C. Milner, and S. Moore-Fay. 2010. Cranial osteology and phylogenetic position of the theropod dinosaur *Proceratosaurus bradleyi* (Woodward, 1910) from the Middle Jurassic of England. Zoological Journal of the Linnean Society 158: 155-195.

Rauhut, O.W.M., and X. Xu. 2005. The small theropod dinosaurs *Tugulusaurus* and *Phaedrolosaurus* from the Early Cretaceous of Xinjiang, China. Journal of Vertebrate Paleontology 25: 107-118.

Rayfield, E.J. 2004. Cranial mechanics and feeding in *Tyrannosaurus rex*. Proceedings of the Royal Society of London Series B 271: 1451-1459.

Rayfield, E.J. 2005. Aspects of comparative cranial mechanics in the theropod dinosaurs *Coelophysis*, *Allosaurus* and *Tyrannosaurus rex*. Zoological Journal of the Linnean Society 144: 309-316.

Rayfield, E.J. 2007. Finite element analysis and understanding the biomechancis and evolution of living and fossil organisms. Annual Review of Earth and Planetary Sciences 35: 541-576.

Residorf, A.G., and M. Wuttke. 2012. Re-evaluating Moodie's opisthotonic-posture hypothesis in fossil vertebrates part I: reptiles—the taphonomy of the bipedal dinosaurs *Compsognathus longipes* and *Juravenator starki* from the Solnhofen Archipelago (Jurassic, Germany). Palaeobiodiversity and Palaeoenvironments 92: 119-168.

Rohlf, F.J. 2000. Statistical power comparisons among alternative morphometric methods. American Journal of Physical Anthropology 111: 463-478.

Rohlf, F.J. 2010. TpsDig 2. Department of Ecology and Evolution, State University of New York, Stony Brook, NY.

Rodríguez-Vázquez, J.F., J.R. Mérida-Velasco, J.A. Mérida-Velasco, I. Sánchez-Montesinos, J. Espín-Ferra, and J. Jiménez-Collado. 1997. Development of Meckel's cartilage in the symphyseal region in man. The Anatomical Record Part A 249: 249-254.

Rowe, T. 1989. A new species of the theropod dinosaur *Syntarsus* from the Early Jurassic Kayenta Formation of Arizona. Journal of Vertebrate Paleontology 9: 125-136.

Russell, D.A. 1970. Tyrannosaurs from the Late Cretaceous of western Canada. National Museum of Natural Science, Publications in Paleontology 1: 1–34.

Russell, D.A., 1972. Ostrich dinosaurs from the Late Cretaceous of western Canada. Canadian Journal of Earth Sciences 9: 375-402.

Russell, D.A. and Z.M. Dong. 1993. The affinities of a new theropod from the Alxa Desert, Inner Mongolia, People's Republic of China. Canadian Journal of Earth Sciences 30: 2107-2127.

Salgado, L., R.A. Coria, A.B. Arcucci, and L.M. Chiappe. 2009. Restos de Alvarezsauridae (Theropoda, Coelurosauria) en la Formación Allen (CampanianoeMaastrichtiano), en Salitral Ojo de Agua, Provincia de Río Negro, Argentina. Andean Geology 36: 67-80.

Sampson, S.D., and M.A. Loewen. 2005. Tyrannosaurus rex from the Upper Cretaceous (Maastrichtian) North Horn Formation of Utah: biogeographic and paleoecologic implications. Journal of Vertebrate Paleontology 25: 469–472.

Sampson, S.D., M.J. Ryan, and D.H. Tanke. 1997. Craniofacial ontogeny in centrosaurine dinosaurs (Ornithischia: Ceratopsidae): taxonomic and behavioral implications. Zoological Journal of the Linnean Society 121: 293-337.

Sampson, S.D., and L.M. Witmer. 2007. Craniofacial anatomy of *Majungasaurus crenatissimus* (Theropoda: Abelisauridae) from the Late Cretaceous of Madagascar. Journal of Vertebrate Paleontology Memoir 8: 32–102.

Sakamoto, M. 2010. Jaw biomechanics and the evolution of biting performance in theropod dinosaurs. Proceedings of the Royal Society of London, Series B 277: 3327-3333.

Senter, P. 2005. Function in the stunted forelimbs of *Mononykus olecranus* (Theropoda), a dinosaurian anteater. Paleobiology 31: 373-381.

Senter, P. 2007. A new look at the phylogeny of Coelurosauria (Dinosauria: Theropoda). Journal of Systematic Palaeontology 5: 429-463.

Senter, P. 2010. Using creation science to demonstrate evolution: application of a creationist method for visualizing gaps in the fossil record to a phylogenetic study of coelurosaurian dinosaurs. Journal of Evolutionary Biology 23: 1732-1743.

Senter, P. 2011. Using creation science to demonstrate evolution 2: morphological continuity within Dinosauria. Journal of Evolutionary Biology 24: 2197-2216.

Sereno, P.C. 1991. Basal archosaurs: phylogenetic relationships and functional implications. Society of Vertebrate Paleontology Memoir 2: 1-53.

Sereno, P.C. 2001. Alvarezsaurids: birds or ornithomimosaurs?. *In*: J.A. Gauthier and L.F. Gall (eds.), New Perspectives on the Origin and Early Evolution of Birds: 69-88. New Haven, CT: Peabody Museum of Natural History.

Sereno, P.C. 2007. Logical basis for morphological characters in phylogenetics. Cladistics 23: 565-587.

Sereno, P.C., and S.L. Brusatte. 2008. Basal abelisaurid and carcharodontosaurid theropods from the Lower Cretaceous Elrhaz Formation of Niger. Acta Palaeontologica Polonica 53: 15–46.

Sereno, P.C., D.B. Dutheil, M. Iarochene, H.C.E. Larsson, G.H. Lyon, P.M. Magwene, C.A. Sidor, D.J. Varricchio, and J.A. Wilson. Predatory dinosaurs from the Sahara and Late Cretaceous faunal differentiation. Science 272: 986-991.

Sereno, P.C., S. McAllister, and S.L. Brusatte. 2005. TaxonSearch: a relational database for documenting taxa and their phylogenetic definitions. Phyloinformatics 8: 1-21.

Sereno, P.C. and F. Novas. 1993. The skull and neck of the basal theropod *Herrerasaurus ischigualastensis*. Journal of Vertebrate Paleontology 13: 451–476.

Sereno, P.C., L. Tan, S.L. Brusatte, H.J. Kriegstein, X. Zhao, and K. Cloward. 2009. Tyrannosaurid skeletal design first evolved at small body size. Science 326: 418-422.

Sereno, P.C., D.B. Dutheil, M. Iarochene, H.C.E. Larsson, G.H. Lyon, P.M. Magwene, C.A. Sidor, D.J. Varricchio, and J.A. Wilson. 1996. Predatory dinosaurs from the Sahara and Late Cretaceous faunal differentiation. Science 272: 986-991.

Smith, D., and P. Galton. 1990. Osteology of *Archaeornithomimus asiaticus* (Upper Cretaceous, Iren Dabasu Formation, People's Republic of China). Journal of Vertebrate Paleontology 10: 255-265.

Smith, D.K., L.E. Zanno, R.K. Sanders, D.D. DeBlieux, and J.I. Kirkland. 2011. New information on the braincase of the North American therizinosaurian (Theropoda, Maniraptora) *Falcarius utahensis*. Journal of Vertebrate Paleontology 31: 387-404.

Smith, J.B. 2006. Heterodonty in *Tyrannosaurus rex*: implications for the taxonomic and systematic utility of theropod dentitions. Journal of Vertebrate Paleontology 25: 865-887.

Smith, J.B. 2007. Dental morphology and variation in *Majungasaurus crenatissimus* (Theropoda: Abelisauridae) from the Late Cretaceous of Madagascar. Society of Vertebrate Paleontology Memoir 8: 103-126.

Smith, J.B., and P. Dodson. 2003. A proposal for a standard terminology of anatomical notation and orientation in fossil vertebrate dentitions. Journal of Vertebrate Paleontology 23: 1-12.

Snively, E., D.M. Henderson, and D.S. Phillips. 2006. Fused and vaulted nasals of tyrannosaurid dinosaurs: implications for cranial strength and feeding. Acta Palaeontologica Polonica 51: 435-454.

Snively, E., and A.P. Russell. 2007. Functional variation of neck muscles and their relation to feeding style in Tyrannosauridae and other large theropod dinosaurs. The Anatomical Record 290: 934–957.

Stayton, C.T., and M. Ruta. 2006. Geometric morphometrics of the skull roof of stereospondyls (Amphibia: Temnospondyli). Palaeontology 49: 307-337.

Steel, R. 1970. Saurischia. Handbuch der Paläoherpetologie/Encyclopedia of Paleoherpetology. Stuttgart: Gustav Fischer Verlag.

Sullivan, C., D.W.E. Hone, X. Xu, and F. Zhang. 2010. The asymmetry of the carpal joint and the evolution of wing folding in maniraptoran theropod dinosaurs. Proceedings of the Royal Society of London, Series B 277: 2027-2033.

Suzuki, S., L.M. Chiappe, G.J. Dyke, M. Watabe, R. Barsbold, and K. Tsogtbataar. 2002. A new specimen of *Shuvuuia deserti* Chiappe et al., 1998 from the mongolian Late Cretaceous with a discussion of the relationships of alvarezsaurids to other theropod dinosaurus. Contributions in Science, Natural History Museum of Los Angeles County 494: 1-18.

Swisher, C.C., X. Wang, Z. Zhou, Y. Wang, F. Jin, J. Zhang, X. Xu, F. Zhang, and Y. Wang. 2002. Further support for a Cretaceous age for the feathered-dinosaur beds of Liaoning, China: new $^{40}Ar/^{39}Ar$ dating of the Yixian and Tuchengzi Formations. Chinese Science Bulletin 47: 136-139.

Swisher, C.C. Y.Q. Wang, X.L. Wang, X. Xu, Y. Wang. 1999. Cretaceous age for the feathered dinosaurs of Liaoning, China. Nature 400: 58-61.

Tahara, R., and H.C.E. Larsson. 2011. Cranial pneumatic anatomy of *Ornithomimus edmontonicus* (Ornithomimidae: Theropoda). Journal of Vertebrate Paleontology 31: 127-143.

Therrien, F., and D.M. Henderson. 2007. My theropod is bigger than yours…or not: estimating body size from skull length in theropods. Journal of Vertebrate Paleontology 27: 108-115.

Tsuihiji, T. 2004. The ligament system in the neck of *Rhea americana* and its implications for the bifurcated neural spines of sauropod dinosaurs. Journal of Vertebrate Paleontology 24: 165-172.

Tsuihiji, T., M. Watabe, K. Togtbaatar, T. Tsubamoto, R. Barsbold, S. Suzuki, A.H. Lee, R.C. Ridgely, Y. Kawahara, and L.M. Witmer. 2011. Cranial osteology of a juvenile specimen of *Tarbosaurus bataar* from the Nemegt Formation (Upper Cretaceous) of Bugin Tsav, Mongolia. Journal of Vertebrate Paleontology 31: 497-517.

Turner, A.H., S.H. Hwang, and M.A. Norell. 2007b. A small derived theropod from Öösh, Early Cretaceous, Baykhangor Mongolia. American Museum Novitates 3557:1–27

Turner, A.H., P.J. Makovicky, and M.A. Norell. 2012. A review of dromaeosaurid systematics and paravian phylogeny. Bulletin of the American Museum of Natural History 371: 1-206.

Turner, A.H., D. Pol, J.A. Clarke, G.M. Erickson, and M.A. Norell. 2007a. A basal dromaeosaurid and size evolution preceding avian flight. Science 317: 1378–1381.

Turner, A.H., D. Pol, and M.A. Norell. 2011. Anatomy of *Mahakala omnogovae* (Theropoda: Dromaeosauridae), Tögrögiin Shiree, Mongolia. American Museum Novitates 3722: 1–66.

Tykoski, R.S., T. and Rowe. 2004. Ceratosauria. *In* D. B. Weishampel, P. Dodson, and H. Osmólska (editors), The Dinosauria, 2nd Edition: 47-70. Berkeley: University of California Press.

Urban, M.A., and M.C. Lamanna. 2006. Evidence of a giant tyrannosaurid (Dinosauria: Theropoda) from the Upper Cretaceous (?Campanian) of Montana. Annals of Carnegie Museum 75: 231-235.

van Itterbeeck, J., D.J. Horne, P. Bultynick, and N. Vandenberghe. 2005. Stratigraphy and palaeoenvironment of the Upper Cretaceous dinosaur-bearing Iren Dabasu Formation (Inner Mongolia, People's Republic of China). Cretaceous Research 26, 699-725.

Vickers-Rich, P., L.M. Chiappe, and S.M. Kurzanov. 2002. The enigmatic birdlike dinosaur *Avimimus portentosus*: comments and a pictorial atlas. *In*: L.M. Chiappe and L.M. Witmer (editors), Mesozoic Birds: Above the Heads of Dinosaurs: 65-86. Berkeley: University of California Press.

Weinbaum, J.C. 2011. The skull of *Postosuchus kirkpatricki* (Archosauria: Paracrocodyliformes) from the Upper Triassic of the United States. PaleoBios 30: 18-44.

Weishampel, D.B., P. Dodson, and H. Osmólska. 2004. *The Dinosauria* (2nd Ed.) Berkeley: University of California Press.

Welles, S. P. 1984. *Dilophosaurus wetherilli* (Dinosauria, Theropoda). Osteology and comparisons. Palaeontographica A 185: 85–180.

Westneat, M.W. 1994. Transmission of force and velocity in the feeding mechanisms of labrid fishes (Teleostei, Perciformes). Zoomorphology 114: 103-118.

Wills, M.A. 1998. Crustacean disparity through the Phanerozoic: comparing morphological and stratigraphic data. Biological Journal of the Linnean Society 65: 455–500.

Wills, M.A., D.E.G. Briggs, and R.A. Fortey. 1994. Disparity as an evolutionary index: a comparison of Cambrian and Recent arthropods. Paleobiology 20: 93–130.

Wilson, J.A. 1999. A nomenclature for vertebral laminae in sauropods and other saurischian dinosaurs. Journal of Vertebrate Paleontology 19: 639-653.

Wilson, J.A., P.C. Sereno, S. Srivastava, D.K. Bhatt, A. Kholsa, and A. Sahni. 2003. A new abelisaurid (Dinosauria, Theropoda) from the Lameta Formation (Cretaceous, Maastrichtian) of India. Contributions from the Museum of Paleontology, University of Michigan 31: 1-42.

Witmer, L.M. 1997. The evolution of the antorbital cavity of archosaurs: a study in soft-tissue reconstruction in the fossil record with analysis of the function of pneumaticity. Society of Vertebrate Paleontology Memoir 3: 1-73.

Witmer, L. M., and R.C. Ridgely. 2009. New insights into the brain, braincase, and ear region of tyrannosaurs (Dinosauria, Theropoda), with implications for sensory organization and behavior. The Anatomical Record 292: 1266–1296.

Witmer, L.M., and R.C. Ridgely. 2010. The Cleveland tyrannosaur skull (*Nanotyrannus* or *Tyrannosaurus*): New findings based on CT scanning, with special reference to the braincase. Kirtlandia 57: 61–81.

Yang, W., S. Li, and B. Jiang. 2007. New evidence for Cretaceous age of the feathered dinosaurs of Liaoning: zircon U-Pb SHRIMP dating of the Yixian Formation in Sihetun, northeast China. Cretaceous Research 28: 177-182.

Young, M.T., M.A. Bell, an S.L. Brusatte. 2011. Craniofacial form and function in Metriorhynchidae (Crocodylomorpha: Thalattosuchia): modelling phenotypic evolution with maximum-likelihood methods. Biology Letters 7: 913-916.

Young, M.T., S. L. Brusatte, M. Ruta, and M.B. Andrade. 2010. The evolution of Metriorhynchoidea (Mesoeucrocodylia: Thalattosuchia): an integrated approach using geometric morphometrics, analysis of disparity and biomechanics. Zoological Journal of the Linnean Society 158: 801-859.

Young, M.T., and M.D. Larvan. 2010. Macroevolutionary trends in the skull of sauropodomorph dinosaurs—the largest terrestrial animals to have ever lived. *In* A.M.T. Elewa (editor), Morphometrics for Nonmorphometricians: 259-269. Heidelberg: Spring-Verlag.

Xu, L., Y. Kobayashi, J. Lü, Y.-N. Lee, Y. Liu, K. Tanaka, X. Zhang, S. Jia, and J. Zhang. 2011. A new ornithomimid dinosaur with North American affinities from the Late Cretaceous Qiupa Formation in Henan Province of China. Cretaceous Research 32: 213-222.

Xu, X, Y.N Chieng, X.-L Wang, and C.-H Chang. 2002a. An unusual oviraptorosaurian dinosaur from China. Nature 419: 291–293.

Xu, X., J.M. Clark, C.A. Forster, M.A. Norell, G.M. Erickson, D.A. Eberth, C. Jia, and Q. Zhao. 2006. A basal tyrannosauroid dinosaur from the Late Jurassic of China. Nature 439: 715–718.

Xu, X., J.M. Clark, J. Mo, J. Choiniere, C.A. Forster, G.M. Erickson, D.W.E. Hone, C. Sullivan, D.A. Eberth, S. Nesbitt, Q. Zhao, R. Hernandez, C.-K. Jia, F. Han, and Y. Guo. 2009. A Jurassic ceratosaur from China helps clarify avian digital homologies Nature 459: 940-944.

Xu, X., and Y. Guo. 2009. The origin and early evolution of feathers: insights from recent paleontological and neontological data. Vertebrata PalAsiatica 47: 311-329.

Xu, X., and M.A. Norell. 2004. A new troodontid dinosaur from China with avian-like sleeping posture. Nature 431: 838-841.

Xu, X., M.A. Norell, X. Kuang, X. Wang, Q. Zhao, and C. Jia. 2004. Basal tyrannosauroids from China and evidence for protofeathers in tyrannosauroids. Nature 431: 680–684.

Xu, X., C. Sullivan, M. Pittman, J.N. Choiniere, D. Hone, P. Upchurch, Q. Tan, D. Xiao, L. Tan, and F. Han. 2011b. A monodactyl nonavian dinosaur and the complex evolution of the alvarezsaurid hand. Proceedings of the National Academy of Sciences (USA) 108: 2338-2342.

Xu, X., Z.-L. Tang, and X.-L.Wang. 1999. A therizinosauroid dinosaur with integumentary structures from China. Nature 399: 350-354.

Xu, X., P. Upchurch, Q. Ma, M. Pittman, J. Choiniere, C. Sullivan, D.W.E Hone, Q. Tan, L. Tan, D. Xiao, and F. Han. In press. Osteology of the alvarezsauroid *Linhenykus monodactylus* from the Upper Cretaceous Wulansuhai Formation of Inner Mongolia, China, and comments on alvarezsauroid biogeography. Acta Palaeontologica Polonica.

Xu, X., D.Y. Wang, C. Sullivan, D.W.E. Hone, F.L. Han, R.H. Yan, and F.M. Du. 2010. A basal parvicursorine (Theropoda: Alvarezsauridae) from the Upper Cretaceous of China. Zootaxa 2413: 1-19.

Xu, X., K. Wang, K. Zhang, Q. Ma, L. Xing, C. Sullivan, D. Hu, S. Cheng, and S. Wang. 2012. A gigantic feathered dinosaur from the Lower Cretaceous of China. Nature 484: 92-95.

Xu, X., and X. Wang, X. 2003. A new maniraptoran from the Early Cretaceous Yixian Formation of western Liaoning. Vertebrata PalAsiatica 41: 195–202.

Xu, X., and X.-C. Wu. 2001. Cranial morphology of *Sinornithosaurus millenii* Xu et al. 1999 (Dinosauria: Theropoda: Dromaeosauridae) from the Yixian Formation of Liaoning, China. Canadian Journal of Earth Sciences 38: 1739-1752.

Xu, X., H. You, K. Du, and F. Han. 2011a. An *Archaeopteryx*-like theropod from China and the origin of Avialae. Nature 475: 465-470.

Xu, X., X.-H. Zhang, P.C. Sereno, X.-L. Zhao, X.-W. Kuang, J. Han, and L. Tan. 2002b. A new therizinosauroid (Dinosauria, Theropoda) from the Upper Cretaceous Iren Dabasu Formation of Nei Mongol. Vertebrata PalAsiatica 40: 228-240.

Zanno, L.E. 2006. The pectoral girdle and forelimb of the primitive therizinosauroid *Falcarius utahensis* (Theropoda, Maniraptora): analyzing evolutionary trends within Therizinosauroidea. Journal of Vertebrate Paleontology 26: 636–650.

Zanno, L.E. 2010a. Osteology of *Falcarius utahensis* (Dinosauria: Theropoda): characterizing the anatomy of basal therizinosaurs. Zoological Journal of the Linnean Society 158: 196-230.

Zanno, L.E. 2010b. A taxonomic and phylogenetic re-evaluation of Therizinosauria (Dinosauria: Maniraptora). Journal of Systematic Palaeontology 8: 503-543.

Zanno, L.E., D.D. Gillette, L.B. Albright, and A.L. Titus. 2009. A new North American therizinosaurid and the role of herbivory in 'predatory' dinosaur evolution. Proceedings of the Royal Society of London, Series B 276: 3505-3511.

Zanno, L.E., and P.J. Makovicky. 2011. Herbivorous ecomorphology and specialization patterns in theropod dinosaur evolution. Proceedings of the National Academy of Sciences (USA) 108: 232-237.

Zelditch, M.L., H.D. Sheets, H.D., and W.L. Fink. 2004. Geometric Morphometics for Biologists: A Primer. San Diego: Elsevier Academic Press.

Zhang, F., Z. Zhou, X. Xu, and X. Wang. 2002. A juvenile coelurosaurian theropod from China indicates arboreal habits. Naturwissenschaften 89: 394-398.

Zhang, F., Z. Zhou, X. Xu, X. Wang, and C. Sullivan. 2008. A bizarre Jurassic maniraptoran from China with elongate ribbon-like feathers. Nature 455: 1105-1108.

Zhang, X.-H., X., Xing, X.-J. Zhao, P.C. Sereno, X.-W. Kuang, and L. Tan. 2001. A long-necked therizinosauroid dinosaur from the Upper Cretaceous Iren Dabasu Formation of Nei Mongol, People's Republic of China. Vertebrata PalAsiatica 10: 282-290.

Zhao, X.-J, R.B.J. Benson, S.L. Brusatte, and P.J. Currie. 2010. The postcranial skeleton of *Monolophosaurus jiangi* (Dinosauria: Theropoda) from the Middle Jurassic of Xinjiang, China, and a review of Middle Jurassic Chinese theropods. Geological Magazine 147: 13-27.

Zhao, X.-J., and P.J. Currie. 1993. A large crested theropod from the Jurassic of Xinjiang, People's Republic of China. Canadian Journal of Earth Sciences 30: 2027-2036.

Zheng, X., X. Xu, H. You, Q. Zhao, and Z. Dong. 2010. A short-armed dromaeosaurid from the Jehol Group of China with implications for early dromaeosaurid evolution. Proceedings of the Royal Society of London, Series B 277: 211-217.

Zhou, Z., P.M. Barrett, and J. Hilton. 2003. An exceptionally preserved Lower Cretaceous ecosystem. Nature 421: 807-814.

APPENDICES

APPENDIX 1: LIST OF CHARACTERS IN THE PHYLOGENETIC ANALYSIS

This character list was compiled by first beginning with the current, most updated version of the Theropod Working Group (TWiG) data set, which was presented by Turner et al. (2012) and included 111 taxa scored for 474 characters. To this I added several new basal coelurosaurian taxa and several new characters relevant to the relationships of these new taxa, as well as basal coelurosaurs generally. Most new characters were novel characters gleaned as part of this PhD project, many of which are relevant to the ingroup relationships of tyrannosauroids and were published by Brusatte et al. (2010a). Other souces of new characters include recent phylogenetic analyses of basal coelurosaurian subgroups such as ornithomimosaurs (Makovicky et al. 2010; L. Xu et al. 2011), therizinosauroids (Zanno et al. 2009), and alvarezsauroids (Choiniere et al. 2010). In total, the current analysis includes 150 taxa scored for 853 characters.

The list below is formatted in the same style as the character list in Turner et al. (2012), and I have noted where I have made character and scoring changes relative to that study. Five characters listed in Turner et al. (2012) have been deleted; these are characters 50, 52, 147, 258, and 280 in the original analysis. Characters 50, 52, and 147 were originally dismissed by Turner et al. (2012) but retained in the matrix so as to keep character ordering consistent with previous TWiG analyses. They are stricken from the dataset here because I feel that retaining dismissed characters, which must be manually tagged for dismissal in phylogenetic programs such as TNT, may be confusing (or easy to forget) when analyzing such a large dataset. Character 258 was deleted because it was combined with another character to create an ordered multistate (character

72 here, character 74 in the original Turner et al. analysis). Character 280 was deleted because it was redundant with an ordered multistate character already in the dataset (the character originally numbered 76, but numbered 74 here).

Character 1: Feathers, vaned feathers on forelimb, form:

0: symmetric

1: asymmetric

Character 2: Orbit, shape

0: circular in lateral or dorsolateral view

1: dorsoventrally elongate

Note: A "dorsoventrally elongate" orbit was not explicitly defined by Turner et al. (2012) or previous versions of the TWiG dataset, but is here held to be any orbit that is greater than 1.5 times deeper dorsoventrally than long anterposteriorly at its midpoint. This character state is only present in some adult tyrannosauroid specimens among coelurosaurs. The presence of a circular orbit in *Alioramus* may be a consequence of the juvenile status of the one quality specimen of this taxon (IGM 100/1844), or alternatively, it could be a product of the dorsoventrally shallow and anteroposteriorly elongated snout of this taxon.

Character 3: Postorbital, ventral ramus, projection into orbit: (ORDERED)

0: does not project into orbit, suborbital process absent

1: projects into orbit, suborbital process present and large in adults and small and unpronounced in sub-adults

2: projects into orbit, suborbital process present and large in sub-adults and adults

Note: Turner et al. (2012) and previous TWiG datasets utilized a binary character relating to the presence/absence of an anterior process projecting into the orbit. We here modify this character by splitting the "presence" state into two states, relating to the varying degree of postorbital projection in tyrannosauroids (to distinguish the hypertrophied condition in *Tyrannosaurus* and *Tarbosaurus* in which the postorbital projects strongly into the orbit in both sub-adults and adults). We have also reversed the 0 and 1/2 designation relative to Turner et al. (2012) so that "0" now refers to the lack of postorbital projection and "1" and "2" refer to the two

conditions of postorbital projection, following Brusatte et al. (2010a). We have changed the score of *Haplocheirus* from present to absent based on Choiniere et al. (2010a).

Character 4: Postorbital, shape of anterior (frontal) process in lateral view:

0: straight

1: curving anterodorsally, such that dorsal border of temporal bar is dorsally concave

Character 5: Postorbital, ventral ramus, orientation: (UNORDERED)

0: parallels quadrate, lower temporal fenestra rectangular in shape

1: oriented strongly obliquely relative to quadrate, jugal and postorbital approach or contact quadratojugal to constrict lower temporal fenestra

2: oriented anteroventrally relative to the long axes of the quadrate and lacrimal, angle of postorbital ventral ramus long axis with the lacrimal long axis (if lacrimal is approximately vertical) greater than 30 degrees

Note: This is a modified version of the original TWiG character, which adds a third state denoting the anteroventrally oriented postorbital ventral rami of some basal coelurosaurs (e.g., tyrannosauroids).

Character 6: Braincase, otosphenoidal crest, form and position:

0: vertical on basisphenoid and prootic, and does not border an enlarged pneumatic recess

1: well developed, crescent shaped, thin crest forms anterior edge of enlarged pneumatic recess

Character 7: Braincase, crista interfenestralis, location:

0: confluent with lateral surface of prootic and opisthotic

1: distinctly depressed within middle ear opening

Character 8: Braincase, subotic recess (pneumatic fossa ventral to fenestra ovalis):

0: absent

1: present

Note: Carr et al. (2011) described a "subotic fossa and recesses" in *Teratophoneus*, but these are not similar to the large, invasive subotic recess of ornithomimosaurs and troodontids.

Character 9: Basisphenoid recess: (UNORDERED)

0: present between basisphenoid and basioccipital

1: entirely within basisphenoid

2: absent

Note: This multistate character is not considered ordered because there is not a clear nested set of primary homologies. The basisphenoid recess is primitive for coelurosaurs, so it is not clear whether the reduced and absent conditions form a transformational sequence. Therefore, the character is left unordered. The reduction of the basisphenoid recess to lie entirely within the basisphenoid in *Tyrannosaurus* and *Tarbosaurus* is most likely due to the extreme anterposterior foreshortening of the recess in these taxa (character 158 in Brusatte et al. 2010a).

Character 10: Basisphenoid recess, posterior opening, form:

0: single opening

1: divided into two small, circular foramina by a thin bar of bone

Character 11: Parasphenoid, base of cultriform process (parasphenoid rostrum), pneumatization:

0: not highly pneumatized

1: expanded and pneumatic (parasphenoid bulla present)

Character 12: Braincase, basipterygoid processes, direction of projection: (UNORDERED)

0: ventral or anteroventrally projecting

1: lateroventrally projecting

2: laterally projecting

Character 13: Braincase, basipterygoid processes, form:

0: well developed, extending as a distinct process from the base of the basisphenoid

1: processes abbreviated or absent

Character 14: Braincase, basipterygoid processes, pneumatization:

0: absent or very subtle, process solid

1: processes hollow, invaded by pneumatic recess (anterior tympanic recess and/or basisphenoid recess)

Note: Turner et al. (2012) scored hollow basipterygoid processes as absent in several tyrannosauroids. However, these are indeed present in taxa that have been CT scanned, including *Alioramus* (Bever et al. 2011), *Gorgosaurus* (Witmer and Ridgely 2009), and *Tyrannosaurus* (Witmer and Ridgely 2009). Therefore, we have scored the character as present in these tyrannosauroids and considered it questionable "?" in all tyrannosauroids (and other basal coelurosaurs) that have not been studied using CT. We anticipate that this character state will eventually be identified in many taxa once they have been the subject of CT study. We also suggest that there may be a difference between the extensively hollow basipterygoid processes of ornithomimosaurs and troodontids (which

have long been noted without CT) and more subtle, less invasive recesses in other taxa (such as tyrannosauroids). For the time being, however, we consider these conditions homologous because it is difficult to differentiate them in a discrete manner.

Character 15: Basisphenoid, basipterygoid recesses on dorsolateral surfaces of basipterygoid processes:

0: absent

1: present

Note: This character refers only to the presence of discrete external pneumatic foramina or fenestrae on the lateral surface of the basipterygoid processes (or immediately above). Brusatte et al. (2010a, character 157) utilized a different character relevant to the ingroup relationships of tyrannosauroids, concerning the presence or absence of a single large, window-like fenestra in this region, which is present in juveniles of *Bistahieversor*, *Alioramus*, and *Daspletosaurus* (but not adults of *Bistahieversor* and *Daspletosaurus*). Because of its ontogenetically variable nature, we do not use the Brusatte et al. (2010a) character here, although we incorporate it into a character relating to the anterior tympanic recess below. Rather, we retain the original character of the TWiG dataset which refers to the simple presence or absence of pneumatic foramina on the basipterygoid processes.

Character 16: Prootic, depression for pneumatic recess (Dorsal Tympanic Recess): (ORDERED)

0: absent

1: present as dorsally open fossa on prootic/opisthotic

2: present as deep, posterolaterally directed concavity

Note: Brusatte et al. (2010a, character 163) utilized a similar character for tyrannosauroids, and we use those character scores here. Most notably, *Dilong* is scored as uncertain (not as possessing a dorsally open recess as in Turner et al. [2012]). *Guanlong*, however, does possess a dorsal tympanic recess.

Character 17: Braincase, accessory tympanic recess dorsal to crista interfenestralis: (ORDERED)

0: absent

1: small pocket present

2: extensive with indirect pneumatization

Character 18: Braincase, caudal (posterior) tympanic recess: (ORDERED)

0: absent

1: present as opening on anterior surface of paroccipital process

2: extends into opisthotic posterodorsal to fenestra ovalis, confluent with this fenestra

Note: Derived tyrannosauroids possess state "2", as can be seen by their inflated and heavily pneumatized paraoccipital processes (Witmer and Ridgely 2009; Bever et al. 2011, in press). *Guanlong* clearly does not possess such extensively inflated paroccipital processes, but in the absence of CT data it is uncertain whether it possesses state 0 or state 1. Because of this uncertainty we conservatively score it as "[01]".

Character 19: Braincase, exits of cranial nerves X-XII, location and form: (ORDERED)

0: flush with surface of exoccipital

1: located together in a shallow bowl-like depression

2: located together in a deep, funnel-like depression

Note: We have modified the original binary character of Turner et al. (2012) and previous TWiG versions into an ordered multistate, to differentiate between two conditions of the "bowl-like depression". The first condition, a shallow depression, is commonly seen in coelurosaurs. The second, an extremely deep funnel-like morphology, is present in some derived tyrannosauroids (Brusatte et al. 2010a, character 153). *Bistahieversor* and *Teratophoneus*, which were scored as "?" in Brusatte et al. (2010a), are now scored as possessing the funnel-like morphology based on recent reexaminations of both specimens by Thomas Carr (as noted in Bever et al. in press).

Character 20: Premaxilla, maxillary process, extent and articulation: (UNORDERED)

0: contacts nasal to form posterior border of nares

1: reduced so that maxilla participates broadly in external naris

2: extends posteriorly to separate maxilla from nasal posterior to nares

Character 21: Premaxilla and nasal, internarial bar, morphology of external surface:

0: rounded

1: flat

Character 22: Premaxilla, crenulated margin on buccal edge of bone:

0: absent

1: present

Character 23: External naris, position of posterior margin:

0: farther anterior than antorbital fossa

1: nearly reaching or overlapping the anterior border of the antorbital fossa

Character 24: Premaxilla, shape of conjoined left and right bones in ventral view: (ORDERED)

0: acute, V-shaped

1: rounded, U-shaped, first two teeth oriented mediolaterally and third and fourth teeth oriented parasagitally

2: rounded, U-shaped, entire tooth row oriented mediolaterally

Note: We have expanded this character into consider this character into an ordered multistate to take into account variation in the "rounded" condition in tyrannosauroids, as denoted by Brusatte et al. (2010a, character 10). All non-tyrannosauroids with rounded snouts are scored for state 1, as are basal tyrannosauroids. Derived tyrannosauroids in which the entire premaxillary tooth row is oriented mediolaterally are scored for state 2.

Character 25: Maxilla, anteromedial process (= "secondary palate"): (ORDERED)

0: short

1: long, with extensive palatal shelves on maxilla

2: extremely elongated, extending back at least to the level of alveolus 4

Note: We have added a second derived state to the character of Turner et al. (2012) and previous TWiG analyses, to differentiate the extremely elongated anteromedial processes of tyrannosauroids, which extend back to at least the level of alveolus 4. The second derived state is present in all score-able tyrannosauroids, as well as basal ornithomimosaurs (*Pelecanimimus*, *Nqwebasaurus*) and the long-snouted dromaeosaurid *Austroraptor*). It is possible that this character may eventually diagnose a more inclusive clade of basal coelurosaurs, given that elongate anteromedial processes are present in nearly all coelurosaurs. However, it is currently difficult to distinguish between the long and extremely long processes of many coelurosaurs, because many specimens are preserved on slabs and therefore fine details of the medial maxilla are not visible. It is clear, however, that derived paravians such as *Dromaeosaurus* and *Deinonychus*, while possessing long anteromedial processes, do not possess the extremely elongate morphology of tyrannosauroids (e.g.., Currie 1995). This is also true of basal coelurosaurs such as *Zuolong* (Choiniere et al. 2010b). Whether compsognathids and ornithomimosaurs may have possessed the tyrannosauroid condition is somewhat unclear, because most preserved specimens are either preserved on slabs or are not preserved in disarticulation (precluding observation of the medial surface of the maxilla). However, high resolution photographs of *Compsognathus* published by Göhlich et al. (2006) indicate that this taxon had a somewhat elongate palatal process, and definitely did not possess the extremely elongated condition of

tyrannosauroids (therefore, we score it for state 1). Furthermore, based on known material, it seems as if most derived ornithomimosaurs at the very least had shorter anteromedial processes than tyrannosauroids (e.g., Osmólska et al. 1972), and we also score these taxa for state 1.

Character 26: Maxilla, palatal shelf, midline ventral "tooth-like" projection:

0: absent, palatal shelf flat

1: present

Character 27: Maxilla, maxillary fenestra: (ORDERED)

0: absent

1: present, fenestra occupies less than half of the depressed area between the anterior margins of the antorbital fossa and antorbital fenestra

2: present, fenestra large and takes up most of the space between the anterior margins of the antorbital fenestra and fossa

Note: the second derived state refers only to the huge fenestrae of some troodontids, which are so large that they take up nearly the entire antorbital fossa region anterior to the antorbital fenestra, with only a thin strut of bone separating the two openings. Other characters referring to nuances of the size and position of the fenestrae are given below.

Character 28: Maxilla, maxillary fenestra, location:

0: situated at anterior border of antorbital fossa

1: situated posterior to anterior border of fossa

Note: This is equivalent to character 17 in Brusatte et al. (2010a). Among tyrannosauroids, *Daspletosaurus*, *Tarbosaurus*, *Tyrannosaurus*, and *Sinotyrannus* have state 0. We here score *Dilong* for state 1, contra Turner et al. (2012). In *Dilong* the maxillary fenestra approaches the anterior border of the antorbital fossa, but it doesn't reach the border.

Character 29: Maxilla, promaxillary fenestra:

0: absent

1: present

Note: We score *Eotyrannus* as possessing the fenestra, based on personal observation of the holotype (MIWG 1997.550)

Character 30: Nasal, pneumatization: (UNORDERED)

0: apneumatic or poorly pneumatized

1: with extensive pneumatic fossae, especially along posterodorsal rim of naris

2: with 2-3 large pneumatic openings, set into a fossa, on the lateral surface above the antorbital fenestra, leading into an extensive internal pneumatic cavity

NOTE: Turner et al. (2012) utilized a binary character, and we added a new state based on Brusatte et al. (2010a, character 43). We do not consider the two pneumatic states to be directly homologous or form a nested series of homology, because of distinct differences in the region of the external pneumatopores (posterodorsal rim of naris vs. midpoint of bone) and the form of the pneumatopores (several pneumatopores posterodorsal to the rim of the naris and within the narial fossa vs. 2-3 discrete pneumatic openings centered in a fossa). The outgroups and some basal tyrannosauroids possess condition 2, whereas oviraptorosaurs possess condition 1. Turner et al. (2012) scored the outgroups (*Allosaurus* and *Sinraptor*) for state 0, and this was correct when the character was a simple binary distinction between no/poor pneumaticity and the extreme pneumaticity of oviraptorosaurs. The new condition added here recognizes morphological similarity between the outgroups and some basal coelurosaurs (basal tyrannosauroids), and probably optimizes as the ancestral condition for Coelurosauria.

Character 31: Jugal and postorbital, contribution to postorbital bar:

0: contribute equally to postorbital bar

1: ascending process of jugal reduced and descending process of postorbital ventrally elongate

Character 32: Jugal, dorsoventral height beneath lower temporal fenestra:

0: tall, twice or more as tall dorsoventrally as it is wide transversely

1: very short, jugal rod-like

Character 33: Jugal, pneumatic recess in posteroventral corner of antorbital fossa:

0: present

1: absent

Note: This character refers to an internal pneumatic recess of the jugal, which hollows out some or all of the bone internally. As shown by Tahara and Larsson (2011), the presence of a discrete jugal diverticulum (located in the jugal portion of the antorbital fossa) does not always equate to the presence of an internal recess hollowing the jugal. The presence of an internal recess can be confidently assessed by the presence of a discrete pneumatopore

externally, which leads into the recess. *Pelecanimimus* possesses this pneumatopore (LH 7777) and is here scored for state 0, whereas all other ornithomimosaurs are scored for state 1 because they lack the external pneumatopore, and in the case of *Ornithomimus* are known to lack the internal recess based on CT scans (Tahara and Larsson 2011).

Character 34: Jugal, medial jugal foramen:

0: present on medial surface ventral to postorbital bar

1: absent

Note: Turner et al. (2012) scored the foramen as absent in *Dilong*, but the medial surface of the jugal is obscured in the holotype specimen, which has not yet been the subject of CT study. Therefore, we have changed the score to "?".

Character 35: Quadratojugal, shape:

0: without horizontal process posterior to ascending process (reversed "L" shape)

1: with horiziontal posterior process (i.e., inverted 'T' or 'Y' shape)

Character 36: Jugal and quadratojugal, fusion:

0: absent

1: present, the two bones are not distinguishable from one another

Character 37: Lacrimal, supraorbital crests in adult individuals: (UNORDERED)

0: absent

1: dorsal crest above orbit

2: lateral expansion anterior and dorsal to orbit

Note: Following Turner et al. (2012), we consider this an unordered character because we do not hypothesize primary homology between state 1 (discrete crests or tubercles along the dorsal margin of the lacrimal, as present in outgroups and tyrannosauroids) and state 2 (a lamina-like triangular sheet that expands laterally above the orbit, as present in troodontids). Turner et al. (2012) scored *Shuvuuia* for state 1, but we have rescored this as state 0 because this taxon does not possess the discrete crest/tubercle along the dorsal margin of the lacrimal as in outgroups and tyrannosauroids.

Character 38: Lacrimal, pneumatic foramina opening laterally at the junction of the anterior and ventral processes above the antorbital fenestra: (ORDERED)

0: absent

1: present, extent of pneumaticity limited to partially hollowing the bone in the region where the anterior and ventral rami meet

2: present and extensive, completely hollowing the bone where the anterior and ventral rami meet

Note: Turner et al. (2012) used a binary character to distinguish between the presence/absence of lacrimal pneumaticity, and we add a third state to distinguish the greatly extensive pneumatic recess of some tyrannosauroids. Therefore, this is now an ordered character. Turner et al. (2012) scored *Eotyrannus* as lacking lacrimal pneumaticiy, but observation of the type specimen shows that it has a shallow pneumatic recess with external pneumatopores, as in *Guanlong*, *Dilong*, and other basal tyrannosauroids.

Character 39: Lacrimal, posterodorsal process: (ORDERED)

0: absent, lacrimal is inverted 'L' shaped or '7' shaped in lateral view

1: present, lacrimal 'T' shaped in lateral view

2: present but reduced, anterodorsal process much longer than posterodorsal process

Note: Turner et al. (2012) and previous TWiG datasets have referred to the presence of an "anterodorsal process", which creates a T-shaped lacrimal, in this character. This T-shaped condition contrasts with the "inverted L" shape of most theropod lacrimals. However, the inverted L shape is due to a pronounced anterior process along the dorsal margin of the bone (the anterodorsal process) and the lack of any posterior process along the dorsal margin (the posterodorsal process). Therefore, we have reworded the character to refer specifically to the posterodorsal process. We also consider this an ordered character, because state 2 (the presence of a posterodorsal process that is much shorter than the anterodorsal process) is a sub-condition of state 1, meaning that there is a nested primary homology hypothesis. Brusatte et al. (2010a, character 48) utilized a character distinguishing the T-shaped and 7-shaped lacrimals of tyrannosauroids. We utilize this as a separate character below. *Zulong*, which possesses a small posterodorsal process that appears large because of the presence of an autapomorphic notch ventral to it, is scored for state 0.

Character 40: Prefrontal, exposure in dorsal view: (ORDERED)

0: large, dorsal exposure similar to that of lacrimal, forms much of orbital rim and usually separates or nearly separates frontal and lacrimal

1: greatly reduced in size, not exposed widely along the orbital rim and allows for wide contact between frontal and lacrimal

2: absent

Note: We have slightly reworded this character based on language in Brusatte et al. (2010a, character 111). Turner et al. (2012) scored *Dilong* for a reduced frontal, based on the description in Xu et al. (2004). However, personal observation of the holotype (IVPP V14243) reveals that it is difficult to distinguish the prefrontal from surrounding bones, so we conservatively score this taxon as "?" following Brusatte et al. (2010a).

Character 41: Frontals, shape of conjoined left and right elements in dorsal view:

0: triangular, narrowing anteriorly as a wedge between nasals

1: rectangular, end abruptly anteriorly, suture with nasal transversely oriented

Note: Brusatte et al. (2010a, character 113) distinguished between the broad triangular shape of most tyrannosauroid frontals and the anteroposteriorly foreshortened shape of derived tyrannosaurid frontals. However, the frontals of all tyrannosauroids are triangular, so we retain the current character and add a new character below to distinguish between the tyrannosauroid morphologies.

Character 42: Frontal, outline of anterior emargination of supratemporal fossa:

0: straight or slightly curved

1: strongly sinusoidal and reaching onto postorbital process

Character 43: Frontal, form of articulation between postorbital process and frontal orbital margin in dorsal view:

0: smooth transition from orbital margin

1: sharply demarcated from orbital margin

Note: Turner et al. (2012) scored some derived tyrannosaurids for state "1", but we here rescore these as state "0," because they do not possess the strongly demarcated and discrete postorbital processes that are seen in some dromaeosaurids (which state "1" refers to).

Character 44: Frontal, form of lateral margin of lacrimal (or prefrontal) suture:

0: smooth

1: with discrete notch

Character 45: Parietals, form of dorsal surface and presence of sagittal crest(s): (ORDERED)

0: flat, lateral ridge borders supratemporal fenestra, sagittal crest (or crests) absent

1: convex with very low sagittal crest (or crests) along midline

2: convex with well developed sagittal crest (or crests)

Note: This character was unordered in Turner et al. (2012), but we here make it an ordered character because states 1 and 2 are a nested series of homologies defining progressively more prominent sagittal crests, whereas state 0 refers to the absence of a crest. This character subsumes character 122 in Brusatte et al. (2010a), which referred to the presence/absence of sagittal crests in tyrannosauroids.

Character 46: Parietals, fusion of left and right elements:

0: unfused

1: fused on the midline in sub-adults and adults (when known)

Note: This character is equivalent to character 127 in Brusatte et al. (2010a).

Character 47: Squamosal, quadratojugal (descending) process, orientation of long axis:

0: dorsoventral or slightly oblique, essentially parallels quadrate shaft

1: anteroposterior, nearly perpendicular to quadrate shaft

Note: This character is equivalent to character 92 of Brusatte et al. (2010a). Brusatte et al. (2010a) scored *Bistahieversor* for state 0, but we here change this to state 1. This miscoding was an error in the Brusatte et al. (2010a) analysis.

Character 48: Squamosal, contact of descending (ventral) process with quadratojugal:

0: present

1: absent, squamosal does not contact quadratojugal

Character 49: Squamosal, posterolateral shelf overhanging quadrate head:

0: absent

1: present

Character 50: Quadrate, orientation of shaft when in articulation:

0: vertical

1: strongly inclined anteroventrally so that ventral end lies far forward of dorsal end

Character 51: Quadrate shaft, form of lateral surface:

0: straight, without any prominent processes projecting laterally; quadrate foramen not visible in lateral view

1: with broad, triangular process along lateral edge of shaft contacting squamosal and quadratojugal above an enlarged quadrate foramen, which is often partially or largely visible in lateral view

Note: We have slightly reworded the character to explain it more clearly.

Character 52: Foramen magnum, shape:

0: subcircular, slightly wider than tall

1: oval, taller than wide

Character 53: Occipital condyle, mediolateral width and dorsoventral height of neck linking condyle to remainder of braincase:

0: approximately the same width and height as the condyle

1: constricted in width and height relative to the condyle

Note: We have reworded this character to make it clearer here, so that it refers specifically to a discrete neck that is constricted in width and height relative to the width of the condyle.

Character 54: Paroccipital processes, shape:

0: elongate mediolaterally and slender dorsoventrally compared to mediolateral length, with dorsal and ventral edges nearly parallel

1: process short mediolaterally, deep dorsoventrally compared to mediolateral length, with convex distal end

Character 55: Paroccipital processes, orientation in posterior view:

0: straight, projects laterally or slightly posterolaterally

1: downturned, distal end curves ventrally and is pendant

Note: This character is not equivalent to character 150 in Brusatte et al. (2010a), which refers to a distinct ventral flange at the distal end of the paroccipital processes of some tyrannosauroids. This character is utilized below.

Character 56: Paroccipital process, orientation of dorsal edge:

0: straight

1: twisted anterolaterally at distal end

Character 57: Ectopterygoid, form of the opening into the pneumatic fossa on the ventral surface:

0: constricted opening relative to fossa

1: widely opened fossa

Note: Turner et al. (2012) scored *Albertosaurus* and *Gorgosaurus* for state "0", which is unusual among coelurosaurs. Our observations of tyrannosauroids do not reveal any discrete differences between these taxa and other tyrannosauroids, both basal (e.g., *Guanlong*, *Xiongguanlong*) and derived (e.g., *Alioramus*, *Tarbosaurus*, *Tyrannosaurus*) forms. Therefore, all tyrannosauroids are scored "1" here.

Character 58: Ectopterygoid: dorsal recess:

0: absent

1: present

Note: This character does not refer to the principal pneumatic recess of the ectopterygoid, which hollows out much of the bone and opens via a large pneumatopore on the ventral surface. Rather, it refers to a separate dorsal recess present in some dromaeosaurids.

Character 59: Pterygoid, morphology of the posterior flange for articulation with quadrate and epipterygoid:

0: well developed

1: reduced in size or absent

Note: This character has been reworded here for clarity. See Balanoff et al. (2009) for a good description of state 1, which is present in oviraptorosaurs and a handful of other coelurosaurs.

Character 60: Palatine and ectopterygoid, articulation between the two bones:

0: absent, the two bones separated from each other by the pterygoid

1: present, the two bones contact each other

Character 61: Palatine, jugal process:

0: present, palatine tetraradiate in shape

1: absent, palatine triradiate in shape

Character 62: Skull, suborbital fenestra, size:

0: large, similar in anteroposterior length to the anteroposterior length of the orbit

1: reduced in size (less than one quarter orbital length) or absent

Character 63: Dentary, form of symphyseal region in dorsal or ventral view: (ORDERED)

0: approximately straight anteroposteriorly, paralleling lateral margin of the remainder of bone; conjoined dentaries narrow

1: recurved slightly medially relative to remainder of bone, conjoined dentaries U-shaped

2: recurved strongly medially relative to remainder of bone, conjoined dentaries forming broad U-shaped muzzle

Note: This character has been reworded for clarity.

Character 64: Dentary, orientation of dorsal margin of symphyseal region in lateral view:

0: in line with the remainder of the dorsal (alveolar) margin of the dentary

1: downturned relative to the remainder of the dorsal margin

Character 65: Lower Jaw, coronoid prominence (usually located on surangular):

0: absent

1: present

Character 66: Dentary, contribution to the dorsal margin of the external mandibular fenestra: (ORDERED)

0: absent or slight, without discrete posterodorsal process

1: present, with discrete posterodorsal process above anterior end of fenestra

2: present and extensive, with elongate posterodorsal process extending over most of fenestra

Character 67: Dentary, morphology of lateral surface:

0: flat, tooth row approximately in line with the remainder of the lateral surface

1: bearing lateral ridge, tooth row inset from remainder of lateral surface

Character 68: Dentary, shape:

0: subtriangular in lateral view, with dorsoventral depth expanding posteriorly

1: strap-like in lateral view, with subparallel dorsal and ventral edges and a consistent dorsoventral depth across its length

Note: Turner et al. (2012) scored some derived tyrannosauroids (*Eotyrannus*, *Gorgosaurus*, *Tyrannosaurus*, *Daspletosaurus*) for state "1", whereas the basal tyrannosauroids *Dilong* and *Proceratosaurus* were scored for state "0". This character was introduced to the TWiG matrix based on the descriptions of Currie (1995), who noted that some dromaeosaurids (and other coelurosaurs) had dentaries that maintained an approximately even depth across their entire lengths, unlike the dentaries of most theropods that funnel out in depth posteriorly (so-called

"subtriangular" dentaries). The subtriangular condition is indeed present in basal tyrannosauroids, but also in more derived tyrannosauroids, contra Turner et al. (2012) (e.g., Brochu 2003; Currie 2003; Carr et al. 2011; Brusatte et al. 2012a). We here score all tyrannosauroids for state "0". Turner et al. (2012) scored *Eotyrannus* for state "1", seemingly because the preserved portions of the left and right dentaries of the holotype (MIWG 1997.550) are gracile and do not expand posteriorly. However, neither of these dentaries are complete posteriorly, so the degree of expansion cannot be assessed. Therefore, we here score *Eotyrannus* as "?".

Character 69: Dentary, primary neurovascular foramina on lateral surface, arrangement:

0: distinct but superficial foramina

1: distinct foramina lie within a deep and sharp groove across the middle and posterior regions of the dentary

Note: This character is equivalent to character 176 in Brusatte et al. (2010a). It has long been utilized in the TWiG matrix, with state 1 scored for a handful of coelurosaurs. Brusatte et al. (2010a) recognized that a distinct and sharp groove is also present in the basal tyrannosauroids *Guanlong*, *Proceratosaurus*, and *Sinotyrannus*.

Character 70: Lower jaw, external mandibular fenestra, shape

0: oval

1: subdivided by a spinous anterior process of the surangular

Character 71: Lower jaw, internal mandibular fenestra (opening between splenial and prearticular on medial surface of mandible), size and shape:

0: small and slit-like

1: large and rounded

Note: This character was introduced into the TWiG dataset based on Currie (1995), who describe an unusual morphology of the internal mandibular fenestra in some dromaeosaurids, in which this opening is large and circular. This contrasts with the smaller and more ovoid opening of most theropods, which is often reduced to a small slit. Turner et al. (2012) scored *Tyrannosaurus* for a large and rounded fenestra, but as shown by Brochu (2003) this opening, although absolutely large due to the large size of Tyrannosaurus, is not circular and is smaller in relation to the size of the dentary than in dromaeosaurids. Therefore, *Tyrannosaurus* and all other tyrannosauroids with known splenials are here scored for state 0. This state can be inferred in isolated splenials by the size and shape of the notch along the posterior margin, which forms the anterior margin of the internal mandibular fenestra.

Character 72: Surangular, foramen in lateral surface of surangular anterior to the mandibular articulation: (ORDERED)

0: absent

1: present but small

2) present and large, approximately 30% of the dorsoventral depth of the posterior surangular

Note: This multistate ordered character combines two characters in the Turner et al. (2012) dataset: character 74 that scores the presence or absence of the surangular foramen and character 258 that scores variability in size of the foramen. The latter character is also used by Brusatte et al. (2010a, character 179) to distinguish between the small and extremely large foramina of some tyrannosauroids. This ordered multistate better encapsulates the full range of variation among not only coelurosaurs, but also tyrannosauroids (basal taxa such as *Guanlong* lack the foramen all together, whereas intermediate taxa such as *Eotyrannus* have a small foramen and derived tyrannosauroids have a derived enlarged foramen). Turner et al. (2012) scored *Eotyrannus* as "?", but the recent realization that the holotype (MIWG 1997.550) includes surangular material shows that *Eotyrannus* has a small foramen.

Character 73: Splenial, exposure in lateral view:

0: not widely exposed on lateral surface of mandible

1: exposed as a broad triangle between dentary and angular on lateral surface of mandible

Character 74: Lower jaw, coronoid ossification, presence and shape: (ORDERED)

0: present as a large, triangular bone (fused with the supradentary)

1: present but reduced to a thin splint

2: absent

Character 75: Articular, elongate and slender medial process emanating from retroarticular process (can project medially, posteromedially, or dorsomedially):

0: absent

1: present

Note: Turner et al. (2012) scored *Dilong* and *Daspletosaurus* as lacking the process, and *Gorgosaurus* and *Tyrannosaurus* as possessing it. We could not confirm any observation of the articular medial process on *Dilong*, so we score this taxon as "?". *Daspletosaurus* has the same general morphology of *Tyrannosaurus* and *Gorgosaurus*,

which a pronounced dorsally and medially extending process at the posteromedial corner of the retroarticular process (Currie 2003). Therefore, we score it for state 1. We also have identified this process in *Tarbosaurus* and *Proceratosaurus*.

Character 76: Articular, retroarticular process, presence and shape: (UNORDERED)

0: present, short and stout, with a distinct region between the glenoid and the portion of the retroarticular process to which the jaw depressors attached

1: present, elongate and slender

2: present but extremely reduced, with no (or only a very short) margin between the glenoid and the muscle attachment region

Note: We have modified this character to include an additional state signifying the extremely reduced retroarticular processes of tyrannosauroids. In tyrannosauroids, including basal taxa such as *Guanlong* and *Dilong*, the retroarticular process is so short that there is essentially no separation between the mandibular glenoid and the attachment site (on the retroarticular process) for the jaw depressor muscles. This is not the case in *Tanycolagreus*, which has a longer retroarticular process and a wider margin between the glenoid and muscle attachment site (Carpenter et al. 2005a, fig. 2.4). In tyrannosauroids lacking an articular, the short retroarticular process can be inferred with a high degree of confidence by the short retroarticular region of the surangular, which articulates with the angular. This inferral is based on the one-to-one correspondence of the short surangular process and short articular retroarticular process in all known tyrannosauroids.

Character 77: Lower jaw, glenoid articular surface for mandible, anteroposterior length:

0: approximately as long as distal quadrate condyles

1: twice or more as long as distal quadrate condyles, allowing anteroposterior movement of mandible

Note: This character can usually be confidently inferred from the shape of all or part of the glenoid articular surface on the surangular and articular. Oviraptorosaurs, which possess state 1, have a radically different morphology compared to other theropods. In oviraptorosaurs, the quadrate condyles do not tightly articulate with the mandibular glenoid, and the lack of a clear, corresponding fit can be seen by observing the surangular and articular.

Character 78: Premaxilla, teeth:

0: present

1: absent

Character 79: Premaxillary dentition, size of second premaxillary tooth:

0: approximately equivalent in size to other premaxillary teeth

1: markedly larger than third and fourth premaxillary teeth

Character 80: Maxilla, teeth:

0: present

1: absent

Character 81: Maxillary and dentary teeth, serrations: (UNORDERED)

0: present on all known teeth

1: some teeth without serrations on mesial (anterior) carina (except at base in *S. mongoliensis*)

2: all known teeth without serrations on both mesial and distal carinae

Note: This character is considered unordered, because we do not hypothesize a nested sequence of primary homology. In other words, we do not hypothesize that there is a clear transformational sequence from serrations to only distal serrations to no serrations, although we recognize that this is a possibility that needs testing without assuming that the character is ordered. We score *Zuolong* for state 1. Choiniere et al. (2010b) described the mesial carina of an isolated lateral tooth as lacking serrations, but considered it difficult to rule out the absence of serrations across the entire carina because of the missing apical tip of the tooth. We feel that enough of the tooth is preserved to show that serrations certainly weren't present across most of the length of the carina, and if were present, were restricted to the very apical tip of the tooth. We consider this equivalent to state 1.

Character 82: Maxillary and dentary teeth, size:

0: large

1: small (25-or more teeth in dentary when complete series is observable)

Note: The "large" condition is the normal condition for theropods in which 10-20 distinct maxillary teeth and 10-20 distinct dentary teeth are present. The "small" condition refers to the higher number of tightly packed teeth in the maxillae and dentaries of some coelurosaurs. Although a complete or near-complete maxilla and/or dentary are needed to score this character confidently, usually the size of individual teeth can be used to predict the state of this character.

Character 83: Dentary teeth, implantation:

0: in separate alveoli

1: set in open groove

Character 84: Maxillary and dentary teeth, serrations (denticles):

0: large

1: small

Note: Turner et al. (2012) and previous versions of the TWiG matrix have followed Farlow et al. (1991) in quantifying this difference. In the current dataset, along with previous TWiG matrices, the "large" condition refers only to the pronounced, coarse denticles of therizinosauroids and troodontids (~1-5 serrations per millimeter), whereas other coelurosaurs are scored for the "small" condition (~more than 5 serrations per millimeter).

Character 85: Maxillary and dentary teeth, serrations, form:

0: simple, convex, and approximately perpendicular to the long axis of the tooth

1: large, hooked and pointing toward the tip of the crown on the distal and often mesial carinae

Character 86: Maxillary and dentary teeth, constriction between root and crown:

0: present

1: absent, root and crown confluent

Character 87: Dentary teeth, spacing between teeth:

0: evenly spaced across tooth row

1: anterior dentary teeth smaller, more numerous, and more closely appressed than those in middle of tooth row

Character 88: Dentary, interdental plates, form:

0: distinct internal plates absent (although a homologue to the plates is probably present)

1: distinct, clearly demarcated interdental plates medially between teeth

Note: As reviewed by Turner et al. (2012), state 0 refers to the condition in dromaeosaurids and troodontids in which clear, distinct, unambiguously demarcated interdental plates are absent. It is likely, however, that bony tissue homologous to the interdental plates is present in this region but has been morphologically transformed.

Character 89: Premaxillary tooth crowns, position of mesial carina: (ORDERED)

0: along mesial margin of tooth, tooth cross section sub-oval to sub-circular

1: rotated distally on premaxillary teeth 1 and 2, such that anterior teeth have an asymmetrical cross section (D-shaped, with highly convex labial surface and flat lingual surface, with narrow spacing between mesial and distal carinae)

2: rotated distally on all premaxillary teeth, such that all teeth are D-shaped in cross section.

Note: Turner et al. (2012) and previous TWiG matrices have utilized a binary character relating to tooth cross sectional shape, differentiating "sub-oval" and "sub-circular" teeth, which are present in the outgroups and most coelurosaurs, from "D-shaped" teeth, which are present in tyrannosauroids and a few other coelurosaurs. We note that some outgroups (allosauroids) and many coelurosaurs do possess premaxillary teeth that are roughly D-shaped in cross section, due to a labial margin that is somewhat convex and a lingual margin that is somewhat flat (and always flatter than the labial margin). For this character, however, we define D-shaped teeth based on the morphology of the mesial carina. A "D-shaped" tooth is held to be a tooth in which the mesial carina is rotated strongly distally, such that it is present on the lingual surface of the tooth. This condition is seen almost exclusively in tyrannosauroids, and roughly follows the definition of D-shaped teeth by Currie et al. (1990), Choiniere et al. (2010b), and previous authors. This condition is always associated with a highly convex labial surface and a flat lingual surface, on which the two carinae are only very narrowly separated. In contrast, the somewhat D-shaped teeth of allosauroids and other coelurosaurs exhibit wider separation between both carinae on the lingual surface and a less convex labial surface. Therefore, these morphologies are not considered homologous to the "D-shaped" condition as defined here, although we recognize that there may be some homology shared between these taxa and coelurosaurs with true D-shaped teeth that is not present in more basal theropods such as coelophysoids, ceratosaurs, and some basal tetanurans (assessing this hypothesis awaits further study of theropod teeth more generally). Furthermore, following Brusatte et al. (2010a, character 196), we divide the "D-shaped" condition into two character states, which we consider to be nested homologies. Although these characters refer to the presence "D-shaped" morphology of either some (state 1) or all (state 2) of the tooth row, we here score all taxa lacking any sign of "D-shaped" teeth with rotated mesial carinae for state 0. It is possible that some of these taxa that do not preserve entire premaxillary tooth rows may eventually be scored for state 1, but we conservatively score them 0 here to minimize missing data.

Character 90: Cervical vertebrae, number:

0: ≤10

1: 12 or more

Character 91: Axis, epipophyses, form:

0: absent or poorly developed as a small pyramidal mound, not extending past posterior edge of postzygapophyses

1: large, rugose, and posteriorly directed flange, extending far beyond postzygapophyses

Note: This character is equivalent to Brusatte et al. (2010a, character 210). The form of the axial epipophyses in tyrannosauroids conforms to the form of the epipophyses in the anterior-middle postaxial cervicals, so if these cervicals are well preserved they can be used as a confident proxy for scoring this character. Because this correspondence is not necessarily clear for coelurosaurs as a whole, we only use anterior-middle cervicals as a proxy for tyrannosauroids.

Character 92: Axis, neural spine, form of dorsal portion:

0: flared transversely

1: compressed mediolaterally

Character 93: Cervical vertebrae, epipophyses, position:

0: placed distally on postzygapophyses, above postzygapophyseal facets

1: placed proximally, anterior to postzygapophyseal facets

Character 94: Cervical vertebrae, position of centrum in anterior cervical vertebrae:

0: terminates level with or anterior to the posterior extent of the neural arch

1: extending beyond the posterior limit of the neural arch

Character 95: Cervical vertebrae, carotid process on posterior cervical vertebrae:

0: absent

1: present

Character 96: Cervical vertebrae, shape of anterior articular surface of anterior cervical centra:

0: subcircular or square in anterior view

1: distinctly wider than high, kidney shaped

Character 97: Cervical vertebrae, neural spines, shape in dorsal view:

0: anteroposteriorly long

1: short and centered on neural arch, giving arch an “X” shape in dorsal view

Note: This is equivalent to character 211 in Brusatte et al. (2010).

Character 98: Cervical vertebrae, number of pneumatic foramina on lateral surface of centra:

0: one on each side

1: two on each side

Character 99: Cervical and anterior trunk vertebrae, form: (UNORDERED)

0: amphiplatyan or weakly opisthocoelous (anterior surface flat or weakly convex, posterior surface is flat or weakly concave)

1: strongly opisthocoelous (anterior surface is convex and posterior surface concave)

2: at least partially heterocoelous

Note: Although the cervicals of tyrannosauroids and some other coelurosaurs are often referred to as "opisthocoelous," this character distinguishes between very weak opisthocoely in which the anterior surface is only very slightly convex (state 0, considered homologous to the amphiplatyan condition) and strong opisthocoely in which the anterior face is strongly convex and fits into a deep concave socket on the posterior surface of the preceding vertebra (state 1). This latter condition is present in *Dilong* and *Eotyrannus* among tyrannoauroids, *Compsognathus*, some alvarezsaurids, and rarely among other coelurosaurs.

Character 100: Dorsal vertebrae, hypapophyses in anterior trunk vertebrae:

0: absent or very small

1: large and pronounced

Character 101: Dorsal vertebrae, parapophyses in posterior trunk vertebrae, form:

0: flush with neural arch

1: distinctly projected on pedicels

Character 102: Dorsal vertebrae, hyposphene-hypantrum articulations:

0: absent

1: present

Character 103: Dorsal vertebrae, opposing zygapophyses on the same vertebra: (ORDERED)

0: abutting or nearly abutting one another above neural canal, opposite hyposphenes (if present) meet to form a single structure (lamina or rectangular projection)

1: zygapophyses placed distinctly lateral to neural canal and hyposphenes (if present) separated as two widely-spaced laminae, which are joined medially by an inset web of bone

2: zygapophyses placed distinctly lateral to neural canal and hyposphenes (if present) separated as two widely-spaced lamina, which are separated medially by a deep groove (the inset web of bone in state 1 is absent)

Note: We have modified this character by dividing state 1 of Turner et al. (2012), which scores for the absence/presence of abutting postzygapophyses, into two states. Both of these states are applicable to taxa with widely separated postzygapophyses and hyposphenes on the midline. Most coelurosaurs have this condition, in which separate left and right hyposphenes take the form of vertical sheets, which are distinctly separated from each other. However, the region between the separated hyposphenes can either house a web of bone, which is only slightly inset from the hyposphenes (state 1), or the web of bone is lost and the hyposphenes and zygapophyses are separated by a deep groove (state 2). Some coelurosaurs have left and right hyposphenes that are appressed to each other on the midline due to closely appressed left and right zygapophyses (*Alxasaurus*, derived tyrannosauroids). This is also the condition in outgroups (e.g., *Allosaurus*), and these taxa and the outgroups are scored for state 0. This character is ordered because the states describe a progressive sequence of conjoined-separation-loss of separating web.

Character 104: Cervical vertebrae, pneumaticity:

0: absent

1: present

Character 105: Dorsal vertebrae, transverse processes of anterior dorsals, form:

0: long (in mediolateral direction) and thin (in anteroposterior direction)

1: short (in mediolateral direction), wide (in anteroposterior direction), and only slightly inclined

Character 106: Dorsal vertebrae, neural spines, mediolateral expansion of dorsal end:

0: absent

1: present, expanded to form ‘spine table’

Character 107: Dorsal vertebrae, scars for interspinous ligaments, position:

0: terminate at apex of neural spines

1: terminate below apex of neural spine

Character 108: Sacral vertebrae, number: (ORDERED)

0: 5 or less

1: 6

2: 7

3: 8

4: 9

5: 10

6: 11 or more

7: 15 or more

Character 109: Sacral vertebrae, fusion of zygapophyses:

0: absent, or zygapophyses partially fused to each other but still retaining the morphology of the original discrete structures

1: present, completely fused zygapophyses forming a sinuous ridge in dorsal view

Character 110: Sacral centra, ventral surface of posterior sacrals, form: (UNORDERED)

0: gently rounded, convex

1: ventrally flattened, sometimes with shallow sulcus

2: centrum strongly constricted transversely, ventral surface keeled

Character 111: Sacral vertebrae, pneumatic foramina on lateral surfaces of centra: (ORDERED)

0: absent on sacral vertebrae

1: present on anterior sacrals only

2: present on all sacrals

Character 112: Sacral vertebrae, morphology of the posterior articular face of the last sacral centrum:

0: flat or slightly concave

1: convex

Character 113: Caudal vertebrae, change in morphology of free caudals along the tail:

0: present, with distinct transition point from shorter centra with long transverse processes proximally to longer centra with small or no transverse processes distally

1: absent, vertebrae homogeneous in shape, without transition point

Character 114: Caudal vertebrae, location of transition point along the tail: (ORDERED)

0: begins distal to the 10th caudal vertebra

1: between the 7th and 10th caudal vertebra

2: or proximal to the 7th caudal vertebra

Character 115: Caudal vertebrae, morphology of anterior caudal centra: (UNORDERED)

0: tall, oval in cross section

1: with box-like centra in caudals I-V

2: anterior caudal centra laterally compressed with ventral keel

Character 116: Caudal vertebrae, neural spines, form:

0: simple, undivided

1: separated into anterior and posterior alae throughout much of caudal sequence

Character 117: Caudal vertebrae, neural spines on distal caudals (distal to ~caudal 15), form: (ORDERED)

0: present as a low ridge

1: absent

2: absent and location of spine replaced by midline sulcus in center of neural arch

Note: Turner et al. (2012) scored *Dilong* for state 1, but we conservatively rescore this taxon as "?" because we have been unable to observe the caudal vertebrae directly, and also based on the illustrations in Xu et al. (2004), which seem to indicate that there may indeed be remnants of the neural spines on caudals in the vicinity of caudal 15 (state 0). Turner et al. (2012) may have scored this taxon as state 1 based on Xu et al.'s (2004) illustrations of extreme distal caudal vertebrae, which do lack neural spines. However, this is also the case in the extreme distal caudals of tyrannosaurids (e.g., *Tyrannosaurus*) and outgroups (*Allosaurus*), both of which Turner et al. (2012) scored for state 0. What we recognize as state 1 here is the condition in taxa such as *Compsognathus* (Peyer 2006), in which neural spines cease to be recognizable as discrete structures around ca. caudal 15 (in *Tyrannosaurus* and *Allosaurus* this happens much more posteriorly in the tail, ca. caudal 30: Brochu 2003).

Character 118: Caudal vertebrae, length of prezygapophyses of distal caudals: (UNORDERED)

0: between 1/3 and whole centrum length

1: extremely long (up to 10 vertebral segments long in some taxa)

2: strongly reduced or absent, terminate at approximately the anterior level of the centrum

3: prezygapophyses present but negligible in size, clasping the posterior surface of neural arch of preceding vertebrae, postzygapophyses negligible (this is an autapomorphy of *Ichthyornis dispar*)

Note: Turner et al. (2012) scored *Dilong* for state 2, but personal observation of the holotype and the figures of Xu et al. (2004) show that state 0 is the correct score.

Character 119: Caudal vertebrae, number: (ORDERED)

0: more than 40

1: 35-40

2: 25-35

3: 8-25

4: less than 8 free caudal vertebrae, tail very short

Note: We have modified this character by breaking down what was previously a single state (25-40 caudals) into two states, which better allows this character to differentiate the moderately elongate tails of ornithomimosaurs and alvarezsauroids (which have approximately 35 vertebrae) from the shortened tails of therizinosauroids, ornithomimosaurs, and many paravians (which have approximately 25 vertebrae).

Character 120: Chevrons, form of chevrons from proximal part of tail:

0: long and slender, proximal end short anteroposteriorly and shaft cylindrical

1: short and stout, proximal end elongate anteroposteriorly and shaft flattened and plate-like

Note: Turner et al. (2012) scored various compsognathids for state 1, but we have rescored these taxa for state 0, as their proximal chevrons are elongate bones (with anteroposteriorly short proximal ends) that are proportionally similar to other taxa with state 0, such as outgroups (*Allosaurus*) and tyrannosauroids (e.g., *Tyrannosaurus*), and distinct from the short and stout proximal chevrons of other taa scored for state 1 (such as dromaeosaurids).

Character 121: Chevrons, form of chevrons from distal part of tail: (ORDERED)

0: simple

1: anteriorly bifurcate

2: bifurcate at both ends

Character 122: Cervical ribs, shaft: (UNORDERED)

0: slender and longer than vertebra to which they articulate

1: broad and shorter than vertebra

2: extremely thin and slender, hair-like

Note: We have modified this character to include a third state designating the extremely thin and hair-like cervical ribs of compsognathid-grade theropods, as recognized by Göhlich and Chiappe (2006). This character is unordered because there is no clear set of nested homologies or no clear character transformation sequence.

Character 123: Ossified uncinate processes: (ORDERED)

0: absent

1: present and unfused to ribs

2: present and fused to ribs

Character 124: Ossified ventral (sternal) rib segments:

0: absent

1: present

Character 125: Gastralia, lateral gastral segment, size:

0: shorter than medial one in each lateral-medial gastralium set

1: longer than the medial one

Note: We have modified this character following Claessens (2004). Claessens showed that in outgroups (*Allosaurus*) and tyrannosaurids (*Gorgosaurus*, *Tyrannosaurus*) the medial gastral segment is longer than the lateral gastral segment (state 0), contra the scores in Turner et al. (2012) and previous TWiG matrices. Furthermore, Norell and Makovicky (1997) showed that in *Velociraptor* the lateral segment is longer than the medial segment (state 1), which was affirmed by Claessens (2004) but contra the score in Turner et al. (2012). We suspect that scores 0 and 1 may have been swapped for some or all taxa accidentally in the TWiG matrix. Because of the confusion of scores in the original TWiG matrix, we conservatively take all character scores from Claessens (2004) and leave all other taxa as "?", unless observed personally by S. Brusatte or specifically reported in the literature.

Character 126: Sternum, ossified sternal plates, fusion:

0: absent, left and right plates separate in adults

1: present, left and right plates fused

Character 127: Sternum, lateral xiphoid process posterior to costal margin:

0: absent

1: present

Character 128: Sternum, groove on anterior edge for reception of coracoid:

0: present

1: absent

Character 129: Sternum, position of articular facet for coracoid (conditions may be determined by the position of the the articular facet on coracoid in taxa without ossified sternum):

0: anterolateral or more lateral than anterior

1: almost anterior

Character 130: Furcula, hypocledium: (**ORDERED)**

0: absent

1: present as tubercle

2: present as an elongate process

Character 131: Scapula, orientation of acromion margin:

0: continuous with blade

1: anterior edge laterally everted relative to blade

Character 132: Coracoid, expansion of posterolateral surface ventral to glenoid fossa:

0: unexpanded

1: posterolateral edge of coracoid expanded to form triangular subglenoid fossa bounded laterally by enlarged coracoid tuber

Character 133: Scapula and coracoid, fusion:

0: absent, two bones separate

1: present, two bones fused into scapulacoracoid

Character 134: Coracoid, shape in lateral view: (UNORDERED)

0: subcircular, with shallow ventral blade

1: subquadrangular with extensive ventral blade

2: shallow ventral blade with elongate posteroventral process

3: height more than twice width, coracoid strut-like

Character 135: Scapula and coracoid, form of their articulation:

0: form a continuous arc in posterior and anterior views

1: coracoid inflected medially relative to scapula, scapulocoracoid 'L' shaped in lateral view

Character 136: Scapula and coracoid, glenoid fossa, orientation of articular surface:

0: faces posteriorly or posterolaterally

1: faces laterally

Character 137: Scapula, length compared to length of humerus:

0: longer

1: approximately same length or shorter

Note: In *Guanlong*, the scapula and humerus are approximately the same length (Xu et al. 2006), so this taxon is scored for state 1. The same scoring is used for all ornithomimosaurs, which have humeri that are slightly longer than the scapula (Osmólska et al. 1972) or have humeri and scapulae of approximately the same length (e.g., Nicholls and Russell 1985; Kobayashi and Lü 2003; Kobayashi and Barsbold 2005b; Makovicky et al. 2010).

Character 138: Humerus, deltopectoral crest, extent and morphology: (UNORDERED)

0: large and distinct, proximal end of humerus quadrangular or triangular in anterior view

1: deltopectoral crest less pronounced, forming an arc rather than being quadrangular

2: deltopectoral crest very weakly developed, proximal end of humerus with rounded edges

3: deltopectoral crest extremely long and rectangular

Character 139: Humerus, deltopectoral crest, form of anterior surface:

0: smooth

1: with distinct muscle scar near lateral edge along distal end of crest for insertion of biceps muscle

Character 140: Ulna, olecranon process, size:

0: weakly developed

1: distinct and large

Character 141: Ulna, morphology of distal articular surface (dorsal condyle and dorsal trochlea in birds):

0: flat

1: convex, semilunate surface

Character 142: Ulna, morphology of proximal surface:

0: a single continuous articular facet

1: divided into two distinct fossae (one convex, the other concave) separated by a median ridge

Character 143: Lateral proximal carpal (ulnare?), shape in proximal view:

0: quadrangular

1: triangular

Character 144: Distal carpals in contact with metacarpals, number:

0: two separate carpals, one covering the base of metacarpal I (and perhaps contacting metacarpal II) the other covering the base of metacarpal II

1: a single distal carpal capping metacarpals I and II

Character 145: Semilunate distal carpal, size: (UNORDERED)

0: well developed, covering all of proximal ends of metacarpals I and II

1: small, covers about half of base of metacarpals I and II

2: covers bases of all metacarpals

3: covers MC II and MC III

Character 146: Metacarpal I, length: (ORDERED)

0: less than half the length of metacarpal II

1: approximately half of the length (~50-70%) of metacarpal II

2: subequal in length to metacarpal II

Note: We have modified the character of Turner et al. (2012) to include a new state, signifying the condition in some tyrannosauroids (and outgroups and other coelurosaurs) in which metacarpal I is approximately half of the length of metacarpal II. In essence, we have divided the original "half or less of the length of metacarpal II" character into two distinct states. This follows the character of Brusatte et al. (2010a, character 252). We have also removed the state in Turner et al.'s (2012) character that refers to the autapomorphically short and robust metacarpals I of alvarezsaurids, which are wider transversely than long proximodistally. We now provide a separate character denoting the presence or absence of this peculiar morphology below.

Character 147: Third manual digit, size:

0: present and large, phalanges present

1: reduced to no more than metacarpal splint

Note: This character is equivalent to Brusatte et al. (2010, character 249).

Character 148: Manual unguals, curvature: (ORDERED)

0: strongly curved, flexor margin deeply concave

1: weakly curved, flexor margin shallowly concave (third ungual may be straight)

2: all manual unguals straight

Note: We have divided the original character of Turner et al. (2012) and previous TWiG matrices, which related to both the curvature and size of the flexor tubercle, into two separate characters. This character now refers to the degree of curvature, whereas a separate character has been added below for the size of the flexor tubercle. Furthermore, a separate character has also been added to simply denote the presence and absence of manual unguals (to distinguish the condition of derived avialans in which unguals are absent, which was originally one of several unordered character states in Turner et al.'s character). As constructed, this current character on manual ungual curvature subsumes c haracter 255 of Brusatte et al. (2010a). We here score *Dryptosaurus* for state 0 (strongly curved manual unguals) based on the recent redescription of this taxon by Brusatte et al. (2011), contra the "weak curvature" score in Brusatte et al. (2010a). Many ornithomimosaurs have a straight manual ungual 3 but more curved manual unguals 1 and 2. These taxa are here scored for state 1, whereas those ornithomimosaurs with straight manual digits 1-3 are scored as state 2. We do not differentiate state 1 into multiple states for "weak curvature in all unguals" vs. "weak curvature in unguals 1 and 2 and a straight ungual 3," because derived tyrannosauroids do not possess a manual ungual 3, which would make it impossible to score them for this character as currently constructed. Therefore, we conservatively lump together these two conditions into state 1, but recognize that future authors may advocate subdividing this character (but this would necessitate scoring derived tyrannosaurids as inapplicable, or dividing this character into multiple characters).

Character 149: Manual unguals, size of ungual on digit I compared to the other manual unguals in the hand:

0: generally similar in size

1: distinctly larger

Character 150: Manual unguals, a transverse ridge immediately dorsal to the articulating surface ("proximodorsal lip"):

0: absent

1: present

Character 151: Ilium, preacetabular process, anteroventral corner, form: (UNORDERED)

0: subtriangular, ventral margin of preacetabular process is shallowly concave

1: subquadrate with recurved anterior margin, ventral margin of preacetabular process is deeply concave such that the open region between the pubic peduncle and anteroventral region of the preacetabular process defines much of a circle

2: process strongly hooked

Note: This character subsumes Brusatte et al. (2010a, character 259). State 1 is seen in some derived tyrannosauroids and ornithomimosaurs (and a few other coelurosaurs), and specifically refers to an anteroventral corner of the preacetabular process that is so recurved and ventrally projecting that the notch between it and the pubic peduncle is wide and essentially circular. Turner et al. (2012) and previous TWiG matrices scored the ougroups (*Allosaurus* and *Sinraptor*) as possessing state 1. However, although these taxa do have somewhat of a hooked anterior margin of the preactabular process (as do some compsognathids such as *Sinocalliopteryx*), they do not have the extremely pronounced condition of derived tyrannosauroids.

Character 152: Ilium, preacetabular process, length: (ORDERED)

0: roughly as long as postacetabular process

1: markedly longer (more than 2/3 of total ilium length) than postacetabular process

2: postacetabular blade much longer than postacetabular process

Character 153: Ilium, morphology of anterior margin of preacetabular process: (UNORDERED)

0: gently rounded or straight

1: anterior end strongly convex, lobate

2: pointed at anterodorsal corner with concave anteroventral edge

3: distinctly concave dorsally

Note: Turner et al. (2012) scored *Dilong* for state 0, which is unexpected if it is a tyrannosauroid (as all known tyrannosauroids possess state 3). However, based on personal observation of the specimen (IVPP V14243) the anterodorsal margin of the ilium is broken, so we here score this taxon as "?". *Sinocallipteryx* is described as possessing a "slightly concave" anterodorsal margin of the preacetabular process, and this is clearly shown in an accompanying figure (Ji et al. 2007). Although we would prefer to confirm this score based on the original specimen, in order to determine whether it is genuine or a potential artifact of breakage, we here score *Sinocallipteryx* for state 3. Li et al. (2010) noted that *Mirischia* may possess an anterodorsal concavity, but personal

observation of the specimen (SMNK 2349 PAL) shows that this region is broken, and therefore we score this taxon as "?".

Character 154: Ilium, supraacetabular crest on ilium, form: (ORDERED)

0: present as a separate process from the antitrochanter, and forming a "hood" over the femoral head

1: reduced but still separate from the antitrochanter, not forming "hood"

2: absent

Character 155: Ilium, postacetabular process, shape of distal end: (UNORDERED)

0: squared

1: acuminate

2: squared, with nearly vertical posterior margin that is nearly equivalent in depth to the anterior margin of the preacetabular process

Note: We have expanded this character into an unordered multistate, by adding a third state referring to the extremely deep and squared-off postacetabular processes of some derived tyrannosauroids such as *Alioramus* and *Tyrannosaurus*, as noted by Brusatte et al. (2010a, character 267). This condition differs from the shallower postacetabular processes of more basal tyrannosauroids such as *Guanlong*, *Dilong*, and *Juratyrant*. In these taxa the postacetabular process is squared off posteriorly, but is much shallower than the preacetabular process.

Character 156: Ilium, opposing postacetabular blades, orientation in dorsal view:

0: subparallel to each other

1: diverge posteriorly from each other

Note: The "subparallel" condition includes those iliac blades which are oriented medially to contact each other (or nearly contact) above the sacrum (these blades are parallel to each other, but instead of their lateral surfaces being oriented straight laterally they are instead oriented dorsolaterally, hence the convergence above the midline). In some of these taxa, such as the ornithomimosaurs *Gallimimus* and *Garudimimus*, the postacetabular blades diverge from each other when seen in dorsal view, but this is a result of the reorientation of the lateral surface to face dorsolaterally, due to the medial orientation of the two blades to contact each other (or nearly contact) above the acetabulum. Without this medial rotation the postacetabular processes would be parallel or nearly parallel to each other. State 1 refers to the condition in some maniraptorans in which the two iliac blades clearly diverge from each other posteriorly when seen in dorsal view.

Character 157: Ilium, tuber along dorsal edge of ilium dorsal or slightly posterior to acetabulum:

0: absent

1: present

Character 158: Ilium, brevis fossa, form:

0: shallowly inset into bone, brevis shelf projects strongly medially

1: deeply inset into bone, with both lateral lamina and medial brevis shelf curving ventrally to demarcate the deeply concave fossa

Character 159: Ilium, antitrochanter, form:

0: absent or poorly developed

1: prominent

Note: This character is equivalent to Brusatte et al. (2010a, character 261). In scoring this character, we hold that the large antitrochanters of derived tyrannosauroids, which are extensive flanges that are deeply inset from the remainder of the ischial peduncle, are primarily homologous to the prominent antitrochanters of most other coelurosaurs. Therefore, tyrannosauroids with flange-like antitrochanters and other coelurosaurs with prominent antitrochanters are both scored for state 1.

Character 160: Ilium, ridge bounding cuppedicus fossa, extension:

0: terminates anterior to acetabulum or curves ventrally onto anterior end of pubic peduncle

1: extends far posteriorly and to become confluent or almost confluent with acetabular rim

Character 161: Ilium, cuppedicus fossa, form: (ORDERED)

0: deeply inset into the anterior and lateral surfaces of the pubic peduncle, with a pronounced dorsal rim

1: reduced, fossa shallow or flat, with little or no overhanging dorsal rim

2: absent

Character 162: Ischium, prominent median posterior process along posterior edge of bone:

0: absent, posterior edge of bone straight

1: present

Character 163: Ischium, morphology of shaft distal to the acetabular (obturator) region: (ORDERED)

0: extremely rod-like, midshaft diameter 30-50% midshaft diameter of pubis

1: rod-like, midshaft diameter 60-100% midshaft diameter of pubis

2: wide, flat, and plate-like, midshaft diameter greater than midshaft diameter of pubis

Note: This is a modified character that subsumes character 280 in Brusatte et al. (2010a). In essence, we here separate the "rod-like" character into two characters: extremely rod-like (in which the ischial shaft is less than 50% of the width of the pubic shaft, seen in some derived tyrannosauroids) and somewhat rod-like (in which the ischial shaft and pubic shaft are approximately the same diameter, seen in many coelurosaurs). We have rescored *Ornitholestes* for state 1 (somewhat rod-like), from Turner et al.'s (2012) polymorphic score for both a rod-like and a plate-like shaft in this taxon. We also score the tyrannosauroids *Dryptosaurus* and *Alioramus* as polymorphic for states 0 and 1. This is a conservative score, because it is clear that the ischium of these taxa is rod-like but it is unclear how the midshaft diameter compares to the pubic midshaft diameter.

Character 164: Ischium, orientation of shaft: (UNORDERED)

0: straight

1: curved anteriorly at the ventral end

2: hooked posteriorly at the ventral end

Character 165: Ischium, surface morphology of lateral face of ischiadic blade: (UNORDERED)

0: flat or gently rounded

1: concave

2: with longitudinal ridge subdividing lateral surface into anterior (including obturator process) and posterior parts

Character 166: Ischium, obturator process of ischium: (ORDERED)

0: absent

1: proximal in position (midpoint of process positioned at less than 30% of the total length of the ischium)

2: located near middle of ischiadic shaft (midpoint of process positioned at approximately 40-50% of the total length of the ischium)

3: located at distal end of ischium (midpoint of process positioned distal to the midpoint of the ischium)

Note: The language in this character has been modified following the quantitative character description of Brusatte et al. (2010a, character 281).

Character 167: Ischium, obturator process, contact with pubis:

0: absent

1: present

Character 168: Ischium, obturator foramen or notch in proximal portion of obturator process: (ORDERED)

0: enclosed foramen present

1: open notch present (i.e., a foramen that is no longer completely enclosed)

2: notch or foramen absent

Note: This character has been modified to take into account the closed obturator foramen of *Guanlong* and *Mirischia*, which although unusual among coelurosaurs and proximal outgroups (allosauroids) is also seen in more distal basal theropod outgroups. Although Naish et al. (2004) described the left and right obturator foramina in *Mirischia* as asymmetrical (one open as a notch, one enclosed), we interpret the supposedly open notch as a closed foramen that has been broken, based on personal observation of the specimen (SMNK 2349 PAL). Turner et al. (2012) scored derived tyrannosauroids for "notch or foramen absent," whereas *Dilong*, compsognathids, and ornithomimosaurs were scored for "open notch present." However, all tyrannosauroids have an open obturator notch that is essentially identical in morphology to those of ornithomimosaurs and compsognathids. Therefore, these taxa are here scored for state 1.

Character 169: Ischium, ischial tubercle ("semicircular scar") ventral to iliac peduncle on the posterior margin of the proximal end of ischium: (ORDERED)

0: absent or potentially homologous structure present as a groove

1: present as a convex bulge on the posterior surface of the ischium

2: present as a rugose, ovoid or triangular flange whose lateral surface is depressed relative to the remainder of the ischium

Note: This character has been modified, and an additional state added, based on Brusatte et al. (2010a, character 278). We consider the condition in ornithomimosaurs to be equivalent to the "convex bulge" condition of the tyrannosauroid *Juratyrant*, and score more derived tyrannosauroids for a hierarchically nested condition of an especially rugose, flange-like tubercle. We also consider the "groove-like" morphology of this region of the ischium to be homologous, at some level, to the ischial tubercle itself (see Hutchinson 2001). Because it is difficult to distinguish the groove-like condition from true absence of any muscular attachment in this region, we lump together both conditions as state 0 but recognize that future work may be able to subdivide these conditions into separate character states.

Character 170: Ischium, length of bone:

0: greater than two-thirds of pubis length

1: two-thirds or less of pubis length

Character 171: Ischium, morphology of distal ends of opposing ischia: (ORDERED)

0: form symphysis

1: approach one another but do not form symphysis

2: widely separated

Note: We here score all tyrannosauroids for state 0, contra Turner et al. (2012) who score derived taxa for state 1. As discussed by Brusatte et al. (2012a), the distal ischia of tyrannosauroids do make contact with each other, although this contact is unfused. This is equivalent to the condition in ornithomimosaurs and compsognathids, and we here score all of these taxa for state 0.

Character 172: Ischium, distal end, expansion relative to midshaft:

0: present, resulting in an ischial "boot"

1: absent, ischial "boot" absent

Note: This character is equivalent to Brusatte et al. (2010a, character 279).

Character 173: Ischium, tubercle on anterior edge of bone:

0: absent

1: present

Character 174: Pubis, orientation of shaft when in articulation: (UNORDERED)

0: projecting anteroventrally (propubic)

1: vertical

2: projecting posteroventrally (opisthopubic)

3: appressed to ischium

Note: This character subsumes Brusatte et al. (2010a, character 275). We consider this character unordered because there is not a clear transformation sequence or nested set of homologies, although it is possible that future authors may argue for an anteroventral-vertical-posteroventral trend in theropod pelvic evolution.

Character 175: Pubis, pubic boot, anterior projection of boot relative to posterior projection: (ORDERED)

0: equal in size or anterior process larger than posterior process

1: anterior process small, approximately 10-40%

2: anterior process completely absent, posterior process large

3: both anterior and posterior processes absent (i.e., boot present but without distinct anterior and posterior projections)

Note: This character subsumes Brusatte et al. (2010a, character 273). We have added an additional state here, to distinguish between taxa in which the anterior and posterior projections are equal in size (some derived tyrannosaurids) and those taxa in which anterior projections are present but are approximately 10-40% of the length of the posterior projection (many other coelurosaurs). Using our character scoring scheme, compsognathids and various paravians are scored for state 2, which refers to the complete lack of an anterior process and a pubic boot that is often "hook-like" in its morphology.

Character 176: Pubis, shelf on shaft proximal to symphysis ('pubic apron'): (UNORDERED)

0: extends medially from middle of shaft

1: shelf extends medially from anterior edge of shaft

2: strongly reduced (restricted to distal end of pubis) or absent

Note: Turner et al. (2012) scored tyrannosauroids (including *Dilong* and tyrannosaurids) for state 0, but we here rescore all score-able tyrannosauroids for state 1, based on personal observation of specimens. In all known tyrannosauroid pubes the pubic apron arises from the anterior margin of the shaft, not the middle of the shaft as in outgroups like *Allosaurus* (Madsen 1976). We have also removed the language in the original TWiG character relating to the cylindrical or anteroposteriorly flattened nature of the shafts, as these conditions do not correspond 1-to-1 with the location of the apron. Future authors may wish to reintroduce a character relating to the morphology of the shaft (cylindrical vs. flattened), but we could not identify clear, distinct categories of variation among taxa and hence do not utilize such a character here.

Character 177: Pubis, curvature of shaft: (UNORDERED)

0: absent, shaft straight

1: distal end curves anteriorly, anterior surface of shaft concave

2: distal end curves posteriorly, anterior surface of shaft convex

Note: This character subsumes character 269 of Brusatte et al. (2010a). Derived tyrannosauroids are here scored for state 1, a concave anterior margin of the pubic shaft, based on Brusatte et al. (2010a).

Character 178: Pubis, length of pubic apron: (ORDERED)

0: about half of pubic shaft length

1: less than 1/3 of shaft length

2: greatly reduced, restricted to far distal end of pubis

3: absent

Note: We modified this character to make it into an additive multistate referring to the presence/absence and size of the pubic apron. For all other pubic apron characters, those taxa without an apron are scored as inapplicable ("?").

Character 179: Pubic apron, form of contact between opposing pubes distally: (ORDERED)

0: both pubes meet extensively

1: contact between pubes disrupted by a slit (pubic foramen)

2: no contact between pubes distally, pubic apron absent in this part of pubis but present further proximally

Note: The pubic fenestra is usually considered a synapomorphy of Tetanurae (Rauhut 2003; Benson et al. 2009). Turner et al. (2012) scored *Dilong* for state 0, but personal observation of the specimen indicates that the distal portion of the conjoined pubes is too damaged (and not complete enough) to permit observation of the fenestra. Therefore, it is here scored "?". Turner et al. (2012) also scored *Haplocheirus* for state 0, which would be unexpected, but because we cannot confirm this with a personal observation we conservatively score it as "?".

Character 180: Femur, head, fovea capitalis for attachment of capital ligament:

0: absent or subtle

1: present as a distinct circular fovea located in center of the medial surface of the head

Character 181: Femur, interaction of lesser and greater trochanters: (ORDERED)

0: separated from each other by deep cleft

1: separated from each other by small groove

2: completely fused to each other (absent as distinct structures), forming a trochanteric crest

Character 182: Femur, lesser trochanter, shape in lateral view:

0: alariform, projects anteriorly as a broad flange that is anteroposteriorly wider than the greater trochanter

1: reduced to approximately the same anteroposterior width as the greater trochanter, cylindrical in cross section

Character 183: Femur, ridge on lateral surface distal to lesser and greater trochanters (homologous to the trochanteric shelf):

0: absent or represented only by faint rugosity or bulge

1: distinctly raised from shaft as a pronounced, mound-like ridge

Character 184: Femur, fourth trochanter:

0: present

1: absent (or reduced to a subtle and barely distinguishable margin)

Character 185: Femur, accessory trochanteric crest distal to lesser trochanter:

0: absent

1: present

Note: We consider the "accessory trochanteric crest" (identified by Makovicky and Sues [1998] in *Microvenator*) as equivalent to the accessory trochanter that is present in some tetanurans (including some coelurosaurs: e.g., Brusatte et al. 2008), as both structures are accessory flanges or ridges along the anterior margin of the distl portion of the lesser trochanter. Therefore, this character is equivalent to Brusatte et al. (2010a, character 287). Accessory trochanters are large and prominent in basal tyrannosauroids (*Guanlong*, *Xiongguanlong*) but are lost in more derived tyrannosauroids. They are also large and prominent in several basal coelurosaurs (e.g., ornithomimosaurs, *Mirischia*, *Zuolong*, *Coelurus*, *Tanycolagreus*).

Character 186: Femur, mesiodistal crest, form:

0: absent or present as a subtle structure

1: present as a pronounced longitudinal crest extending proximally from medial condyle, which is seen to strongly overhang the remainder of the medial margin of the femur in posterior view (i.e., is visible as a broad flange in posterior view

Note: We have reworded this character to make it refer specifically to the pronounced mesiodistal crest of some coelurosaurs. This crest is either located on the anterior surface of the femur (as described in the original TWiG character) or along the anteromedial corner of the femur, but in all cases extends proximally from the medial condyle.

Character 187: Femur, flexor groove, morphology of distal end:

0: open distally, smoothly confluent with distal articular surface

1: closed off distally by contact between distal condyles, separated from distal articular surface

Character 188: Fibula, distal extent:

0: reaches proximal tarsals

1: short, tapering distally, and not in contact with proximal tarsals

Character 189: Fibula, medial margin of proximal end in proximal view:

0: concave

1: flat

Character 190: Fibula, deep oval fossa, with well defined margins, on medial surface near proximal end:

0: absent

1: present

Note: This character refers specifically to the discrete, ovoid fossa of some tyrannosauroids and ornithomimosaurs, as well as outgroup taxa. Some other basal coelurosaurs such as *Coelurus* and *Zuolong* have a depressed groove excavating much of the medial surface of the proximal fibula, but this is not present as a discrete, indented fossa with well defined margins (instead, the groove has a well defined anterior margin but opens posteriorly). The outgroups are scored for state 0, because they possess an open fossa (without a distinct posterior margin) as in most coelurosaurs.

Character 191: Astragalus and calcaneum, morphology of distal condyles:

0: condyles separated by shallow, indefinite sulcus

1: condyles separated by prominent tendoneal groove on anterior surface

Character 192: Tibia, number of cnemial crests:

0: single pronounced crest

1: two crests (main crest with accessory anterior crest)

Character 193: Astragalus, ascending process, form: (UNORDERED)

0: tall and broad, covering most of anterior surface of distal end of tibia (70% or more of mediolateral width of surface) and dorsoventral height greater than twice the height of the main body of the astragalus

1: process short and slender, covering only lateral half of anterior surface of tibia (includes derived therizinosauroid condition in which a lateral extension of the ascending process contacts the fibula) and dorsoventral height less than twice the height of the main body of the astragalus

2: ascending process tall, but with medial notch that restricts it to lateral side of anterior face of distal tibia

Note: This character includes information on both the dorsoventral height and mediolateral width of the ascending process. Sometimes these measurements are given separate characters, but we here hold that they are generally correlated, in the sense that taxa with a very tall ascending process always have a mediolaterally broad process as well, and taxa such as *Guanlong* and *Falcarius* with a short ascending process also have a mediolaterally restricted process. We recognize, however, that future authors may want to break this character into separate characters referring to length and width, but we hesitate to do so because we do not wish to introduce a second character that is likely correlated with the first.

The ascending processes of compsognathids have been described as somewhat reduced, in that they only cover approximately 70% of the anterior surface of the tibia (Ostrom 1978; Currie and Chen 2001; Hwang et al. 2004). We consider this condition equivalent to state 0 here, but recognize that future authors may want to subdivide state 0 into separate characters for a broad ascending process that covers most of the anterior surface of the tibia and a reduced process that covers approximately 70% of the surface. These could be associated with state 1 here (a process covering half the tibial surface) to create an ordered multistate, and state 2 here (which is unique to some alvarezsaurids) could be made into its own character. We do not do this, however, because we hesitate to divide state 0 into additional states because the "reduced" ascending processes of compsognathids are all based on slab specimens, which are difficult to measure and often prone to misinterpretation. It is clear, however, that these compsognathids do not possess the reduced and laterally restricted ascending processes of some basal coelurosaurs (e.g., *Guanlong*, *Coelurus*, *Tugulusaurus*) and the ougroups (*Allosaurus*, *Sinraptor*), which are denoted by state 1. This character is an equivalent, but expanded, version of Brusatte et al. (2010a, character 297).

Character 194: Astragalus, ascending process, articulation with condyles distally:

0: confluent with condylar region of astragalus

1: separated from condylar region by transverse groove or fossa across base

Character 195: Astragalus and calcaneum, fusion: (ORDERED)

0: absent, astragalus and calcaneum unfused to each other or to tibia in adults

1: present, astragalus and calcaneum fused to each other, unfused to tibia

2: present, astragalus and calcaneum completely fused to each other and to tibia

Character 196: Distal tarsals, fusion with metatarsals:

0: absent, distal tarsals and metatarsals separate

1: present, distal tarsals and metatarsals fused into tarsometatarsus

Character 197: Metatarsals, fusion: (ORDERED)

0: absent, metatarsals not co-ossified

1: present, metatarsals co-ossified proximally

2: present, metatarsals co-ossified proximally and distally

3: present, metatarsals co-ossified proximally and distally, with distal fusion extreme and distal vascular foramen closed

Character 198: Metatarsal II, morphology of distal end:

0: smooth, not ginglymoid

1: with developed ginglymus that extends onto extensor surface, giving the distal end a strongly concave profile in extensor (anterior) view

Character 199: Metatarsal III, morphology of distal end:

0: smooth, not ginglymoid

1: with developed ginglymus: smooth articular region extends proximally onto extensor surface and is broadly exposed

Note: We here consider the condition in some basal coelurosaurs (*Zuolong*, *Tugulusaurus*, *Dilong*, *Guanlong*) to represent a well developed ginglymus, as defined for character state 1. Xu et al. (2004) recognized that *Dilong* was unusual among tyrannosauroids in possessing a gingylmus on metatarsal III (although it is absent on metatarsal II), a character score that was followed by Turner et al. (2012). Later discoveries showed that this character state is also present in some other basal coelurosaurs: Rauhut and Xu (2005) later noted that one was present on *Tugulusaurus* and Choiniere et al. (2010) described and figured it for *Zuolong*. Our personal observations of *Guanlong* show that it is present in this taxon as well. *Bicentenaria* is described by Novas et al. (2012) as lacking a ginglymoid distal end of metatarsal III, but we score this taxon here as "?" because we have not been able to observe it, and therefore cannot assess if it has the basal coelurosaur-style ginglymoid condition of *Guanlong*, *Tugulusaurus*, and *Zuolong*.

Character 200: Metatarsal III, exposure of proximal shaft in extensor view: (ORDERED)

0: prominently exposed between MT II and MT IV along entire metapodium

1: MT III proximal shaft constricted and much narrower than either II or IV, but still exposed along most of metapodium, subarctometatarsal

2: very pinched, not exposed along proximal section of metapodium, arctometatarsal

3: proximal part of MT III lost entirely

Note: We here consider this character ordered, because we hypothesize nested homology between the subarctometatarsal-arctometatarsal-mt III lost states (i.e., these form an ordered, progressive sequence of metatarsal III pinching and eventual loss). This character is equivalent to Brusatte et al. (2010a, Character 299).

Character 201: Pedal digit II, ungual and penultimate phalanx, morphology:

0: similar to those of III

1: penultimate phalanx highly modified for extreme hyper-extension, ungual more strongly curved and significantly larger than that of digit III

Character 202: Metatarsal II, site of articular surface for metatarsal I: (UNORDERED)

0: the middle of the medial surface of metatarsal II

1: the posterior surface of distal quarter

2: the medial surface near the proximal end

3: the medial surface at or near the distal end

Character 203: Metatarsal I, form of proximal end:

0: attenuates proximally, articular surface for metatarsal II is a simple butt joint lying against the shaft of metatarsal II

1: large and robust, similar to those of metatarsals II-IV

Note: Although character states could probably be inferred by the form and position of the metatarsal I articular scar on metatarsal II, we conservatively score taxa for an affirmative score only if we can observe metatarsal I itself.

Character 204: Metatarsal IV, shaft thickness:

0: round or thicker dorsoventrally (extensor-flexor direction) than wide mediolaterally in cross section

1: mediolaterally widened and flat in cross section

Character 205: Foot, symmetry:

0: symmetrical

1: asymmetrical with slender MTII and very robust MT IV, excluding flange

Character 206: Dorsal vertebrae, neural spines on posterior dorsals, shape in lateral view:

0: rectangular or square

1: fan-shaped, anteroposterior length of spine expanding dorsally

Note: State 1 refers specifically to the fan-shaped neural spines of compsognathids and *Pelecanimimus*, whose dorsal extremity is substantially longer anteroposteriorly than is the base of the spine. This is due to a "funneling outwards) in anteroposterior length dorsally across the length of the spine. Some theropods (e.g., *Tanycolagreus*, some ornithomimosaurs in intermediate phylogenetic position between *Pelecanimimus* and derived taxa with rectangular neural spines) have some dorsal vertebrae with neural spines that are moderately expanded at their dorsal tips, but these do not exhibit the striking fan shape of compsognathids, and are thus scored for state 0.

Character 207: Manual phalanx I-1, shaft diameter:

0: less than or approximately equal to the shaft diameter of radius.

1: greater than the shaft diameter of radius.

Note: State 1 of this character refers to a phalanx that is substantially thicker in diameter than the radius. Several coelurosaurs (e.g., *Tanycolagreus*, tyrannosauroids, ornithomimosaurs) have a phalanx I-1 that is approximately the same diameter of the radius, and sometimes is slightly larger (~10%). These taxa are scored for state 0, however, because this condition differs from the condition in compsognathids in which the phalanx is dramatically larger than the radius (state 1).

Character 208: Angular, extent in lateral view:

0: widely exposed, suture between surangular and angular reaches or nearly reaches posterior end of mandible

1: reduced in exposure, suture between surangular and angular does not reach posterior end of the mandible

Character 209: Surangular, laterally inclined flange along dorsal edge of bone for articulation with the lateral process of lateral quadrate condyle:

0: absent

1: present

Character 210: Distal articular ends of metacarpals I + II: (UNORDERED)

0: ginglymoid

1: rounded, smooth

2: II ginglymoid and MC I shelf

Character 211: Radius and ulna, articulation with each other:

0: well separated

1: with distinct adherence or syndesmosis distally

Character 212: Upper and lower jaws, occlusion:

0: occlude for their full length

1: diverge anteriorly due to kink and downward deflection of the dentary (pronounced downward deflection of dentary buccal margin anteriorly)

Character 213: Quadrate, exposure of head in lateral view:

0: absent, covered by squamosal laterally

1: present, exposed because quadrate cotyle of squamosal opens laterally due to a wide notch between the ventral and posterior processes

Character 214: Ilium, brevis fossa, orientation and exposure in lateral view:

0: faces primarily ventrally, but it is widely visible in lateral view (especially anteriorly)

1: faces primarily ventrally and medially, and it is obscured in lateral view across its entire length by a well developed lateral lamina of the postacetabular process of the ilium

Note: This character is equivalent to character 310 in the revised version of the Brusatte et al. (2010a) analysis published by Brusatte and Benson (in press). We have altered the wording here to reflect the character language of Brusatte and Benson (in press), which focuses specifically on whether the fossa is visible or obscured in lateral view.

Character 215: Lesser trochanter, vertical ridge on lateral surface:

0: present

1: absent

Character 216: Supratemporal fossa, extension onto the squamosal:

0: absent, fenestra bounded laterally and posteriorly by the squamosal, with no distinct fossa present on the dorsal surface of the squamosal

1: present, distinct fossa extends onto the dorsal surface of the squamosal

Character 217: Dentary, teeth: (ORDERED)

0: present across much of bone, dentary fully toothed

1: present but only at the far anterior tip

2: absent, dentary edentulous

Character 218: Coracoid, ventral (=anterior) margin of bone anterior (=ventral) to glenoid, form:

0: straight or shallowly indented by a notch

1: deeply indented by a pronounced notch separating the glenoid and postglenoid process, glenoid lip everted

Note: State 1 refers to the deep notch of ornithomimosaurs, which separates the glenoid from a pronounced and hook-shaped postglenoid process anteriorly. Many other coelurosaurs have a shallow notch in this region, but only ornithomimosaurs have a discrete, deep notch, which helps to define the characteristic hook-like postglenoid process in these taxa.

Character 219: Articular, retroarticular process, orientation:

0: points posteriorly

1: curves gently posterodorsally

Character 220: Scapula, flange on supraglenoid buttress:

0: absent

1: present

Character 221: Laterosphenoid, depression (possibly pneumatic) on ventral surface of postorbital process of bone:

0: absent

1: present

Character 222: Braincase, basal tubera, mediolateral width of conjoined tubera relative to occipital condyle: (ORDERED)

0: as wide as or wider than the occipital condyle

1: narrower than occipital condyle, reduced to a set of small processes directly below the condyle and separated by a narrow notch

2: tubera absent

Note: This character is not equivalent to characters 154 and 155 in Brusatte et al. (2010a), which refer to the dorsoventral depth of the basal tubera and the depth of the notch between the tubera, respectively. This character refers solely to the mediolateral width of the tubera, and is considered an ordered character because we hypothesize a nested set of homologies (large-small-absent). The highly modified basal tubera of derived therizinosauroids are here regarded as possessing state 0 and not state 2 (absent), as remnants of the tubera are still present despite their incorporation into the basisphenoidal bulla.

Character 223: Ilium, postacetabular process, morphology of dorsal edge:

0: convex or straight

1: deeply concave, ventral portion of postacetabular process (housing brevis shelf medially) extending posterior to dorsal portion of the postacetabular process as a tab-like structure

Note: State 1 refers to the condition in some dromaeosaurids (e.g., *Unenlagia*), in which the dorsal margin of the postacetabular process is deeply concave, due to the extension of the ventral portion of the postacetabular process posteriorly as a discrete, rectangular, tab-like structure. This tab-like structure is ornamented by the brevis shelf medially, and therefore houses an extension of the brevis fossa itself. Some ornithomimosaurs have a subtly concave dorsal border of the postacetabular process, but this is not considered equivalent to the marked condition of some dromaeosaurids.

Character 224: Ilium, posterior end of postacetabular process, morphology in dorsal view:

0: terminating in rounded or square end, due to a brevis shelf that extends no farther than the posterior margin of the lateral lamina (lateral surface) of the postacetabular process

1: with lobate brevis shelf projecting beyond posterior end of lateral lamina of postacetabular process

Character 225: Pedal phalanx II-2, flexor heel, form:

0: small and asymmetrically developed only on medial side of vertical ridge subdividing proximal articulation

1: heel long and lobate, with extension of midline ridge extending onto its dorsal surface

Note: Taxa without a discrete flexor heel are scored as inapplicable ("?").

Character 226: Metatarsal IV, large, longitudinal flange along posterior or lateral surface of bone:

0: absent

1: present

Character 227: Ischium, proximodorsal process, form:

0: small, tab-like or pointed process along posterior edge of ischium

1: large, proximodorsally hooked, and separated from iliac peduncle of the ischium by a notch

Note: Taxa without a discrete proximodorsal process are scored as inapplicable ("?").

Character 228: Pubis, prominent tubercle on lateral surface of shaft, at approximately the midpoint of the shaft:

0: absent, shaft smooth

1: present

Character 229: Ischium, distally placed dorsal process along posterior edge of shaft:

0: absent

1: present

Character 230: Ischium, obturator process, shape:

0: tab-like, with distal end separated from shaft by a discrete notch

1: triangular, with distal end confluent with shaft

Character 231: Ischium, morphology of triangular obturator process (only in those taxa with a triangular process as defined in character 233):

0: longer proximodistally than wide anteroposteriorly at the center of the process

1: shorter proximodistally than wide anteroposteriorly at the center of the process, resembles an elongate triangle extending anteriorly

Character 232: Metatarsal II, tuber along extensor surface (associated with the insertion of the tendon of the m. tibialis cranialis in Aves): (ORDERED)

0: absent

1: present, on approximately the center of the proximodorsal surface of metatarsal II

2: present, developed on lateral surface of metatarsal II, at contact with metatarsal III or on lateral edge of metatarsal III

Character 233: Ulna: femur length ratio:

0: substantially less than one

1: equal to or greater than one

Character 234: Maxilla, position of maxillary fenestra relative to ventral margin of antorbital fossa: (ORDERED)

0: abuts ventral margin

1: dorsal to ventral margin, at approximately the dorsoventral midpoint of the antorbital fossa

2: far dorsal to the ventral margin, dorsal to the dorsoventral midpoint of the antorbital fossa

Note: This character has been modified to take into account variation in the position of the maxillary fenestra in tyrannosauroids, as noted by Brusatte et al. (2010a, character 18). State 0 here refers to the condition in *Daspletosaurus*, *Tarbosaurus*, and *Tyrannosaurus*, in which the maxillary fenestra abuts the ventral margin of the antorbital fossa.

Character 235: Maxilla, dorsoventral depth of main body of bone (=jugal process) at the midpoint of the antorbital fenestra compared to the depth of the entire skull at this measuring point: (ORDERED)

0: shallow, less than 16% of the depth of the entire skull

1: between 16-22% of skull depth

2: deep, greater than 22% of skull depth

Note: This character has been modified into an ordered multistate to take into account additional variation noted by Brusatte et al. (2010a, character 23).

Character 236: Maxilla, maxillary fenestra, recessed within a shallow, posteriorly or posterodorsally open fossa, which is itself located within the maxillary antorbital fossa:

0: absent

1: present

Character 237: Maxilla, ascending process (=dorsal ramus or nasal process), form:

0: prominent, exposed medially and laterally

1: absent or reduced to a process with slight medial and no lateral exposure

Character 238: Maxilla, participation of the ventral ramus of the nasal process (=ascending process) in the anterior margin of the antorbital fenestra (as seen in lateral view): (ORDERED)

0: present extensively

1: small dorsal projection of the maxilla participates in the anterior margin

2: no dorsal projection of maxilla participates in the anterior margin

Character 239: Antorbital fenestra, composition of the dorsal border (as seen in lateral view):

0: lacrimal and maxilla

1: lacrimal and nasal

Character 240: Antorbital fossa, composition of the dorsal border (as seen in lateral view): (UNORDERED)

0: lacrimal and maxilla

1: lacrimal and nasal

2: maxilla, premaxilla, and lacrimal

Character 241: Maxilla, lateral lamina of the ascending ramus:

0: present and broadly exposed in lateral view

1: present but reduced to small triangular exposure in lateral view

Character 242: Frontal, supratemporal fossa, anteroposterior length compared to overall length of exposed portion of frontal on skull roof: (ORDERED)

0: less than 30%

1: between 30-60%

2: greater than 60%

Note: This character has been modified and transformed into an ordered multistate using the quantitative character descriptions of Brusatte et al. (2010a, character 115). As worded here, this character now refers solely to the extent of the supratemporal fossa onto the frontal, unlike the previous TWiG character that referred to the qualitative extent (minor, extensive) of the fossa onto the frontal and postorbital. We note, however, that taxa with an extensive fossa on the frontal usually also have an extensive fossa on the dorsal surface of the postorbital.

Character 243: Jugal, contribution to antorbital fenestra margin (in lateral view):

0: absent

1: present

Character 244: Maxillary and dentary teeth, size of mesial (=anterior) and distal (=posterior) denticles:

0: not substantially different in size

1: mesial denticles, when present, substantially smaller than distal denticles

Character 245: Maxillary teeth, orientation relative to the long axis of the lower jaw:

0: almost perpendicular to jaw margin

1: inclined strongly posteroventrally

Character 246: Maxillary teeth, apicobasal height of teeth along tooth row:

0: highly variable with gaps evident for replacement

1: almost isodont with no replacement gaps

Character 247: Splenial, posterior margin (anterior margin of internal mandibular fenestra):

0: smooth

1: with distinct notch

Character 248: Premaxillary teeth, cross sectional size of first tooth crown compared with crowns of premaxillary teeth 2 and 3: (UNORDERED)

0: slightly smaller or same size

1: much smaller

2: much larger

Character 249: Maxilla, promaxillary fenestra in adults, visibility in lateral view:

0: visible (either as complete fenestra or portion of the fenestra)

1: completely obscured by ascending ramus of maxilla

Note: This character is equivalent to character 15 in Brusatte et al. (2010).

Character 250: Nasal, shape of dorsal surface: (ORDERED)

0: flat or slightly convex

1: convex (vaulted) anteriorly, above and immediately posterior to the external naris

2: vaulted across most of their length

Note: This character has been modified following Brusatte et al. (2010, character 38). Tyrannosauroids with a midline nasal crest are scored as inapplicable ("?").

Character 251: Nasal, fusion between left and right nasals:

0: absent

1: present

Character 252: Quadratojugal and squamosal, constriction of lateral temporal fenestra: (ORDERED)

0: absent, anterior margins of both bones are approximately vertical

1: present, convex kink along the suture between the two bones that projects into the fenestra, constricting it to approximately one half or less of its maximum anteroposterior length

2: present, dorsal region of quadratojugal moderately expanded anteroposteriorly relative to the remainder of the bone, constricting fenestra to approximately one half of its maximum anteroposterior length

3: present, dorsal region of quadratojugal expanded anteroposteriorly by at least twice the minimum anteroposterior dimension of the bone, forming a flange that meets the ventral ramus of the squamosal to nearly divide the fenestra

Note: This character is expanded into an ordered multistate using the character state definitions of Brusatte et al. (2010a, character 98).

Character 253: Supraoccipital, pronounced and strongly demarcated median ridge on posterior (occipital) surface:

0: absent

1: present

Character 254: Surangular, anteroventral extension divides external mandibular fenestra by contacting angular anteriorly

0: absent

1: present

Character 255: Ilium, vertical ridge on lateral surface of iliac blade above acetabulum: (ORDERED)

0: absent or poorly developed

1: present as a well-developed, linear structure extending vertically or anterodorsally

2: present as a well-developed, linear structure extending posterodorsally

Note: This character is modified into an ordered multistate to take into account variation within tyrannosauroids as noted by Brusatte et al. (2010a, character 258).

Character 256: Premaxilla, main body, dorsoventral depth compared to anteroposterior length: (ORDERED)

0: less than or equal to

1: between 1.0-1.9 times larger

2: greater than 2 times larger

Note: This character is modified into an ordered multistate to take into account variation within tyrannosauroids as noted by Brusatte et al. (2010, character 8).

Character 257: Nasal, external texture of mid section of bone:

0: smooth to slightly rugose

1: pronounced rugosities and accessory vascular foramina present

Note: This character is equivalent to Brusatte et al. (2010, character 40).

Character 258: Jugal, shape of anterior process underneath the lacrimal: (UNORDERED)

0: tapering

1: bluntly squared anteriorly

2: expanded

3: bifurcated

Character 259: Axis, neural spine, morphology in lateral view:

0: extensive and anteroposteriorly elongate, sheet-like

1: anteroposteriorly reduced, rod-like

Character 260: Cervical vertebrae, prezygapophyses in anterior postaxial cervicals, orientation:

0: straight across their lengths

1: anteroposteriorly convex, flexed ventrally anteriorly

Character 261: Dorsal vertebrae, extent of pneumaticity (pneumatic foramina on lateral surfaces): (ORDERED)

0: foramina absent

1: foramina present in anterior dorsals

2: present in all dorsals

Note: This character is equivalent to Brusatte et al. (2010, character 218).

Character 262: Femur/humerus length ratio: (ORDERED)

0: more than 3.3

1: between 3.3-2.5

2: between 1.2 and 2.5

3: less than 1

Note: This character has been modified to include additional variation within tyrannosauroids, following Brusatte et al. (2010, character 239).

Character 263: Humerus, shape in lateral view:

0: sigmoidal

1: straight

Note: We consider this character to be equivalent to character 242 in Brusatte et al. (2010a), which scores for the presence/absence of humeral shaft rotation (quantified by the angle between the long axes of the proximal and distal ends). Brusatte et al. (2010a) scored *Dryptosaurus* for such rotation, but this taxon has a straight humerus in lateral view and is thus scored for state 1 here. It is possible that there is a subtle amount of variation within this character, such that taxa like *Dryptosaurus* have a straight humerus in lateral view but still retain some degree of rotation (a 30-45 degree angle between the long axes of the proximal and distal ends). However, we do not want to subdivide this character too finely, because it makes recognizing homologies across a wide swath of taxa more difficult. Therefore, we retain a simple binary character here.

Character 264: Radius, length compared to that of humerus:

0: more than half the length of humerus

1: less than half the length of humerus

Character 265: Premaxilla, fusion of opposing premaxillae at the symphysis: (ORDERED)

0: unfused in adults

1: fused anteriorly in adults, posterior nasal [frontal] processes not fused to each other

2: fused anteriorly and opposing frontal processes completely fused

Character 266: Dentary, form of articulation between opposing dentaries at the symphysis:

0: joined proximally by ligaments

1: joined by bone

Character 267: Dentary, symphysis region, two strong grooves forming an anteriorly opening 'v' in ventral view:

0: absent

1: present

Character 268: Cranium, facial margin, composition: (ORDERED)

0: primarily formed by the maxilla, with the maxillary process of the premaxilla restricted to the anterior tip

1: maxillary process of the premaxilla extending along half of facial margin

2: maxillary process of the premaxilla extending more than half of facial margin

Character 269: Premaxilla, nasal (frontal) process, length:

0: short

1: long, closely approaching frontal

Character 270: External naris, size compared to the antorbital fenestra: (ORDERED)

0: considerably smaller

1: long axis approximately same length as long axis of antorbital fenestra

2: larger

Note: This character has been expanded into an ordered multistate to take into account variation within tyrannosauroids noted by Brusatte et al. (2010a, character 4). *Sinotyrannus* is here scored for state 1; although the antorbital fenestra is not preserved in this taxon, state 1 is hypothesized because the external naris long axis is as long as the first seven teeth of the maxillary tooth row, similar to the proportions in *Guanlong* and *Proceratosaurus*, which are scored for state 1, but differing from the state in other tyrannosauroids (and most other coelurosaurs) in which the naris is no longer than the first 4-5 teeth.

Character 271: Ectopterygoid:

0: present

1: absent

Character 272: Vomer and pterygoid, form of articulation between bones: (UNORDERED)

0: present, well developed

1: reduced, narrow process of pterygoid passes dorsally over palatine to contact vomer

2: absent, pterygoid and vomer do not contact

Note: This character is left unordered because it is unclear if states 1 and 2 form a nested set of homologies.

Character 273: Palatine and pterygoid, form of articulation between bones:

0: long, anteroposteriorly overlapping contact

1: short, primarily dorsoventral contact

Character 274: Palatine, contacts with bones of the facial region:

0: contacts maxillae only

1: contacts premaxillae and maxillae

Character 275: Vomer, contact with premaxilla:

0: present

1: absent

Character 276: Basisphenoid, projecting articulation with pterygoid via discrete basipterygoid processes:

0: present

1: absent

Character 277: Basisphenoid, location of pterygoid articular surface:

0: located basal on basisphenoid

1: located markedly anterior on basisphenoid (parasphenoid rostrum) such that the articulations are subadjacent on the narrow rostrum

Character 278: Basisphenoid and pterygoid articulation, orientation of contact: (UNORDERED)

0: anteroventral

1: mediolateral

2: entirely dorsoventral

Character 279: Pterygoid, articular surface for basisphenoid, morphology: (ORDERED)

0: concave 'socket' or short groove enclosed by dorsal and ventral flanges

1: flat to convex

2: flat to convex facet, stalked, variably projected

Character 280: Pterygoid, shape of bone:

0: kinked, surface for basisphenoid articulation at high angle to axis of palatal process of pterygoid

1: straight, basisphenoid articulation in line with axis of palatal process

Character 281: Ossified interorbital septum, sphenethmoid:

0: absent

1: present

Note: This character is equivalent to Brusatte et al. (2010a, character 167), which recognizes the presence of an ossified mesethmoid and sphenethmoid in derived tyrannosauroids. In the absence of developmental data, it is

not clear if the ossification referred to as the sphenethmoid in tyrannosauroids is homologous to that in birds. However, we retain a single character scoring for the presence/absence of an ossified sphenethmoid for simplicity. The Brusatte et al. (2010a) character refers to both an ossified sphenethmoid and mesethmoid, but here we consider only the sphenethmoid in defining this character, so that it is equivalent to the original character in Turner et al. (2012). All known tyrannosauroids with an ossisfied sphenethmoid also possess an ossified mesethmoid, so their presence is probably correlated.

Character 282: Ossified interorbital septum, mesethmoid:

0: unossified or small, restricted to the ventral surface of the frontal or marginally extends anteriorly past the premaxillae/frontal contact but does not surpass posterior edge of external nares

1: large, extends anterior to the posterior extent of the frontal processes of premaxillae and anterior to the posterior edge of the external nares

Character 283: Eustachian tubes, morphology: (UNORDERED)

0: paired and lateral

1: paired, close to cranial midline

2: paired and adjacent on midline or single anterior opening

Character 284: Eustachian tubes, ossification:

0: absent

1: present

Character 285: Squamosal, ventral (=zygomatic) process, morphology:

0: large and elongate, dorsally encloses otic process of the quadrate and extends anteroventrally along shaft of quadrate, dorsal head of quadrate not visible in lateral view

1: short, head of quadrate exposed in lateral view

Note: This character is not redundant with Turner et al. (2012, character 216), because this character refers specifically to the size of the ventral process. A reduced ventral process is one means of exposing the quadrate head in lateral view, as is a wide notch between the ventral and posterior processes (which is what is scored in character 216).

Character 286: Quadrate, orbital process (=pterygoid flange) of quadrate, form of articulation with pterygoid:

0: pterygoid broadly overlapping medial surface of orbital process (i.e., 'pterygoid ramus' present)

1: pterygoid contact restricted to anteromedial edge of orbital process

Character 287: Quadrate, form of pterygoid articulation with orbital process in those taxa where the contact is restricted to the anteromedial edge of the process: (ORDERED)

0: pterygoid articulates with anterior-most tip

1: pterygoid articulation does not reach tip

2: pterygoid articulation with no extent up orbital process, restricted to quadrate corpus

Note: All taxa scored for state 0 in the previous character are here scored as inapplicable ("?").

Character 288: Quadrate/pterygoid contact, morphology in those taxa where the contact is restricted to the anteromedial edge of the orbital process:

0: as a facet, variably with slight anteromedial projection cradling base

1: condylar, with a well-projected tubercle on the quadrate

Note: All taxa scored for state 0 for character 286 are here scored as inapplicable ("?").

Character 289: Quadrate, well-developed tubercle on anterior surface of dorsal process:

0: absent

1: present

Character 290: Quadrate, form of articulation with quadratojugal:

0: overlapping

1: peg and socket articulation

Character 291: Quadrate, dorsal process, articulation with other bones:

0: with squamosal only

1: with squamosal and prootic

Character 292: Quadrate, dorsal process, development of intercotylar incisure between prootic and squamosal cotylae: (ORDERED)

0: absent, articular surfaces not differentiated (usually meaning prootic contact was absent)

1: two distinct articular facets, incisure not developed

2: incisure present, 'double headed'

Character 293: Quadrate, mandibular articulation, form:

0: divided into two condyles

1: divided into three condyles, due to additional posterior condyle or broad surface

Character 294: Quadrate, pneumaticity:

0: absent

1: present

Note: This character scores specifically for the presence or absence of an internal pneumatic recess in the quadrate. Many coelurosaurs have an internally pneumatic quadrate, but this recess communicates with the external surface of the bone in two distinct ways (Tahara and Larsson 2011). Most coeluorsaurs have a small foramen, usually on the posterior surface of the quadrate, that leads into the recess. Derived tyrannosauroids, on the other hand, possess a large, deep, funnel-like pneumatic opening on the anterior surface of the quadrate where the pterygoid wing and mandibular condyles meet. Both conditions are considered homologous at the level of absence/presence of quadrate pneumaticity here, but we utilize separate characters below for the absence/presence of the posterior foramen and the absence/presence of the anterior funnel. The homologous nature of both conditions is supported by the morphology of *Dilong*, which clearly has an anterior funnel and also a posterior foramen (IVPP V14243; Xu et al. 2004).

Character 295: Quadrate, cluster of pneumatic foramina on the posterior surface of the tip of the dorsal process:

0: absent

1: present

Note: Because we are uncertain whether this condition may be homologous to the broader condition of quadrate pneumaticity, we score taxa lacking this character for state 0, even if they are also scored for state 0 (absence) for the general character of quadrate pneumaticity.

Character 296: Quadrate, form of pneumatization, large single pneumatic foramen on the posterior or posteromedial surface of the shaft:

0: absent

1: present

Note: See discussion regarding quadrate pneumaticity above. All taxa without quadrate pneumaticity are scored as inapplicable (“?”) for this character.

Character 297: Articular, pneumaticity:

0: absent

1: present

Character 298: Dentary, morphology of posterior end:

0: approximately straight or with a weakly developed separation into dorsal and ventral forks (i.e., small dorsal ramus)

1: strongly forked with the dorsal and ventral rami approximately equal in posterior extent

Character 299: Splenial, anterior extent: (ORDERED)

0: limited, stops well posterior to mandibular symphysis

1: elongate, extends to mandibular symphysis but does not participate in symphysis

2: elongate, extends to anterior tip of mandible to contacting on midline and participate in symphysis

Character 300: Mandibular symphysis, anteroposteriorly extensive, flat to convex, dorsal-facing surface:

0: absent, symphysis concave

1: present

Character 301: Mandibular symphysis, symphyseal foramina:

0: absent

1: present

Character 302: Mandibular symphysis, symphyseal foramina, number:

0: single

1: paired

Character 303: Mandibular symphysis, symphyseal foramina, location:

0: opening on posterior edge of symphysis

1: opening on dorsal surface of symphysis

Character 304: Dentary, Meckelian groove, exposure in medial view:

0: exposed as deep and conspicuous groove, not completely covered by splenial

1: not exposed, covered by splenial

Character 305: Lower jaw, anterior external mandibular fenestra:

0: absent

1: present

Character 306: Jugal, contact with postorbital:

0: present

1: absent

Character 307: Frontal/parietal suture

0: open

1: fused

Character 308: Thoracic vertebrae (with ribs articulating with the sternum, or in the middle-posterior dorsal series of theropods without preserved sterna), one or more with prominent hypapophyses:

0: absent

1: present

Character 309: Thoracic vertebrae, number: (ORDERED)

0: 12 or more

1: 11

2: 10 or fewer

Character 310: Thoracic vertebrae, form of articular surfaces:

0: at least part of series with round or ovoid articular surfaces (e.g. amphicoelous/ opisthocoelous) that lack the dorsoventral compression seen in heterocoelous vertebrae

1: series completely heterocoelous

Character 311: Thoracic vertebrae, parapophysis, position:

0: anterior to transverse process

1: directly ventral to transverse process (close to midpoint of vertebra)

Character 312: Thoracic vertebrae, centrum, proportions:

0: approximately equal in anteroposterior length and midpoint mediolateral width

1: length markedly greater than midpoint width

Character 313: Thoracic vertebrae, morphology of lateral surfaces of centra: (UNORDERED)

0: flat to slightly depressed

1: deep, emarginated fossae

2: central ovoid foramina

Note: Turner et al. (2012) scored some taxa with large pneumatic foramina in the dorsals for character state 2 (e.g., *Balaur*). Because the size and shape of pneumatic foramina are variable, and because dorsal pneumaticity is already scored in other characters, we restrict state 2 to representing the large, ovoid, central foramina of some avialans (and also *Linhenykus*). Turner et al. (2012) also scored *Tyrannosaurus* for state 1, possibly because of the pneumatic foramen and surrounding fossa on the dorsal centra. We do not consider this homologous to the deeply emarginated fossae on the lateral surfaces of some avialan and oviraptorosaur vertebrae, and therefore consider *Tyrannosaurus* (as well as all other tyrannosauroids and non-maniraptoran coelurosaurs) to be scored for state 0.

Character 314: Thoracic vertebrae with ossified connective tissue bridging transverse processes:

0: absent

1: present

Character 315: Notarium:

0: absent

1: present

Character 316: Sacral vertebrae, series of short vertebrae, with dorsally directed parapophyses just anterior to the acetabulum: (ORDERED)

0: absent

1: present, three such vertebrae

2: present, four such vertebrae

Character 317: Caudal vertebrae, anterior free caudals prior to transition point, length of transverse processes:

0: subequal to width of centrum

1: substantially shorter than centrum width

Character 318: Caudal vertebrae, fusion of distal caudals:

0: unfused to each other

1: fused to each other

Character 319: Caudal vertebrae, extent of fused distal caudals: (ORDERED)

0: fused element length equal or greater than 4 free caudal vertebrae

1: length less than 4 caudal vertebrae

2: less than 2 caudal vertebrae in length

Character 320: Gastralia:

0: present

1: absent

Character 321: Sternum, carina or midline ridge, morphology: (ORDERED)

0: absent

1: slightly raised

2: distinctly projected

Character 322: Sternum, position of carina or midline ridge: (UNORDERED)

0: restricted to posterior half of sternum

1: approaches anterior limit of sternum

2: restricted to the anterior half of the sternum

Character 323: Sternum, dorsal surface, pneumatic foramen (or foramina):

0: absent

1: present

Character 324: Sternum, pneumatic foramina in the depressions (loculi costalis) between rib articulations (processi articularis sternocostalis):

0: absent

1: present

Character 325: Sternum, coracoidal sulci spacing on anterior edge: (UNORDERED)

0: widely separated mediolaterally

1: adjacent

2: crossed on midline

Character 326: Sternum, number of processes for articulation with the sternal ribs: (ORDERED)

0: three

1: four

2: five

3: six

4: seven or more

Character 327: Sternum, raised, paired intermuscular ridges (linea intermuscularis) parallel to sternal midline:

0: absent

1: present

Character 328: Sternum, posterior margin, distinct posteriorly projected medial and/or lateral processes, morphology: (ORDERED)

0: absent

1: with distinct posterior processes

2: midpoint of posterior sternal margin connected to medial posterior processes to enclose paired fenestræ

Character 329: Clavicles, fusion:

0: left and right bones fused together

1: left and right bones unfused

Note: We here score *Juravenator* as polymorphic "[01]". Chiappe and Göhlich (2010) described an unfused furcula in *Juravenator*, but because this specimen is such a young individual we cannot rule out that the two clavicles may have later fused in adults. Therefore, we conservatively score it as polymorphic for both conditions.

Character 330: Clavicles, interclavicular angle between left and right clavicles:

0: greater than, or equal, to 90 degrees

1: less than 90 degrees

Character 331: Furcula, lateral excavation:

0: absent

1: present

Character 332: Furcula, dorsal (omal) tip, form:

0: flat or blunt

1: with a pronounced posteriorly pointed tip

Character 333: Furcula, ventral margin of apophysis, form:

0: curved, angling

1: with a truncated or squared base

Character 334: Scapula and coracoid, form of articulation: (UNORDERED)

0: pit-shaped scapular cotyla developed on the coracoid, and coracoidal tubercle developed on the scapula ('ball and socket' articulation)

1: scapular articular surface of coracoid convex

2: flat

Character 335: Coracoid, procoracoid process:

0: absent

1: present

Character 336: Coracoid, lateral margin, form:

0: straight to slightly concave

1: convex

Character 337: Coracoid, dorsal surface (= posterior surface of taxa less derived than Paraves), form:

0: strongly concave

1: flat to convex

Note: This character can be scored by examining the trace of the scapula-coracoid suture in lateral view. Those taxa with state 0 have a strong concavity on the coracoid, whereas those scored for state 1 have either a flat suture or one with a convexity on the coracoid.

Character 338: Coracoid, pneumaticity:

0: absent

1: present

Character 339: Coracoid, position of pneumatic foramen:

0: proximal

1: distal

Character 340: Coracoid, lateral process:

0: absent

1: present

Character 341: Coracoid, ventral surface (=anterior surface of taxa less derived than Paraves), lateral intermuscular line or ridge:

0: absent

1: present

Character 342: Coracoid, position of glenoid facet:

0: dorsal to, or at approximately same level as, acrocoracoid process/'biceps tubercle' (or estimated position of biceps tubercle is a discrete tubercle is absent)

1: far ventral to acrocoracoid process

Character 343: Coracoid, acrocoracoid process, shape:

0: straight

1: hooked medially

Character 344: Coracoid, n. supracoracoideus passes through coracoid (usually via coracoid foramen):

0: present

1: absent

Note: This character is not equivalent to the presence or absence of a large, discrete coracoid foramen (Turner et al. 2012, character 440). Although a noticeable foramen is sometimes absent in non-avialan coelurosaurs, the overall morphology of the coracoid (and pectoral region in general) suggests that the n. supracoracoideus still passes through the coracoid, unlike the condition in some derived avialans. In the absence of soft tissue information in fossil taxa, we consider all non-paravian theropods with a traditional plate-like coracoid to possess state 0.

Character 345: Coracoid, medial surface, area of the foramen n. supracoracoideus (when developed)

0: strongly depressed

1: flat to convex

Note: Turner et al. (2012) scored the outgroup *Allosaurus* and derived tyrannosauroids for state 1, but in these taxa this surface of the coracoid is indeed depressed (the condition in these taxa is basically identical to the ornithomimosaur *Gallimimus*, for instance, which was scored for state 0). Therefore, we score these taxa for state 0. State 1 is now scored only in some avialans, some alvarezsaurids, and *Microvenator*.

Character 346: Coracoid and scapula, angle between bones at glenoid:

0: greater than 90 degrees

1: 90 degrees or less

Character 347: Scapula, ratio of dorsoventral depth of distal end to minimum dorsoventral depth of blade: (ORDERED)

0: greater than 2.5

1: slightly taller or approximately the same depth as proximal dorsoventral shaft width, ratio between 1.0 and 2.5

2: tapering distally, ratio less than 1.0

Note: This character has been modified into an ordered multistate to take into account variation within tyrannosauroids noted by Brusatte et al. (2010a, character 235).

Character 348: Scapula, curvature in lateral view:

0: absent, bone straight

1: present, bone dorsoventrally curved

Note: Turner et al. (2012) scored some basal coelurosaurs (*Haplocheirus*, *Mononykus*, *Archaeornithomimus*, *Gallimimus*) for the curved condition, but these taxa have straight scapular blades that are extremely similar in overall shape to closely related that that were scored for the straight condition. We score them for the straight condition here, meaning that the curved condition is restricted to some derived maniraptorans.

Character 349: Scapula, position of acromion process:

0: extends anteriorly to surpass the articular surface for coracoid (facies articularis coracoidea)

1: does not extend further anteriorly than the articular surface for coracoid

Character 350: Scapula, orientation of acromion process:

0: straight

1: laterally hooked tip

Note: Turner et al. (2012) scored tyrannosauroids for state 1, which is otherwise present only in some derived avialans. We do not recognize any discrete difference in the orientation of the acromion process of derived tyrannosauroids relative to other basal coelurosaurs, and therefore score all tyrannosauroids with well-preserved scapulae for state 0.

Character 351: Humerus and ulna, length comparison: (ORDERED)

0: humerus longer than ulna

1: ulna and humerus approximately the same length (within ~10% of each other)

2: ulna substantially longer than humerus

Character 352: Humerus, head, shape in anterior or posterior view

0: strap-like, articular surface flat or weakly convex, no proximal midline convexity

1: prominent and highly convex (domed) proximally

Note: We consider this character equivalent to character 240 in Brusatte et al. (2010a), which scores for the absence/presence of an enlarged head that occupies the majority of the proximal end, is bulbous in roximal view, and overhangs both anterior and posterior surfaces. This feature, which is seen in some derived tyrannosauroids, is here considered equivalent to state 1.

Character 353: Humerus, proximal end, shape of proximal projection:

0: dorsal edge projected farthest

1: midline projected farthest

Character 354: Humerus, ventral tubercle and capital incisure:

0: absent

1: present

Character 355: Humerus, capital incisure, morphology:

0: an open groove

1: closed by tubercle associated with a muscle insertion just distal to humeral head

Character 356: Humerus, anterior surface, well-developed fossa on midline making proximal articular surface appear v-shaped in proximal view:

0: absent

1: present

Character 357: Humerus, 'transverse groove':

0: absent

1: present, developed as a discrete, depressed scar on the proximal surface of the bicipital crest or as a slight transverse groove

Character 358: Humerus, deltopectoral crest, orientation:

0: projected laterally or dorsally, such that it is in line with the long axis of humeral head

1: projected anteriorly, such that it is approximately perpendicular to the long axis of the head

Character 359: Humerus, deltopectoral crest, thickness compared with thickness of shaft: (ORDERED)

0: less

1: same width

2: dorsoventral thickness greater than shaft thickness

Character 360: Humerus, deltopectoral crest, proximoposterior surface (=proximolateral surface in most non-avialan theropods), form:

0: flat to convex

1: concave

Character 361: Humerus, deltopectoral crest, large fenestra:

0: absent, crest not perforate

1: present, crest perforate

Character 362: Humerus, bicipital crest, pit-shaped scar/fossa for muscular attachment on anterodistal, distal, or posterodistal surface of crest:

0: absent

1: present

Character 363: Humerus, bicipital crest, position of pit-shaped fossa for muscular attachment: (UNORDERED)

0: anterodistal on bicipital crest

1: directly ventrodistal at tip of bicipital crest

2: posterodistal, variably developed as a fossa

Character 364: Humerus, bicipital crest, anterior projection: (ORDERED)

0: absent or subtle

1: present, developed as an anterior projection relative to shaft surface in ventral view

2: present as a hypertrophied, rounded tumescence

Character 365: Humerus, proximal end, one or more pneumatic foramina:

0: absent

1: present

Character 366: Humerus, distal articular condyles, position:

0: on distal surface of bone

1: on anterior surface of bone

Character 367: Humerus, long axis of dorsal (lateral) distal condyle, orientation:

0: at low angle to humeral axis, proximodistally orientated

1: at high angle to humeral axis, almost transversely orientated

Character 368: Humerus, distal condyles, form:

0: prominent, subround and bulbous

1: weakly defined, 'strap-like'

Character 369: Humerus, distal margin, orientation:

0: approximately perpendicular to long axis of humeral shaft

1: oblique (angling strongly ventrally) to long axis of humeral shaft, ventrodistal margin projected significantly distal to dorsodistal margin (sometimes described as a well-projected flexor process)

Character 370: Humerus, distal end, compressed anteroposteriorly and flared dorsoventrally:

0: absent

1: present

Character 371: Humerus, brachial fossa:

0: absent

1: present, developed as a flat scar or as a scar-impressed fossa

Character 372: Humerus, ventral (medial) distal condyle, length of long axis:

0: less than the long axis of the dorsal (lateral) condyle

1: the same or greater than the long axis of the dorsal (lateral) condyle

Character 373: Humerus, demarcation of muscle origins (e.g. m. extensor metacarpi radialis in Aves) on the dorsal (=lateral in non-avialan theropods) edge of the distal humerus:

0: no indication of origin as a scar, a pit, or a tubercle

1: indication as a pit-shaped scar or as a variably projected scar-bearing tubercle or facet

Character 374: Humerus, groove for passage of m. scapulotriceps on distal end of posterior surface:

0: absent

1: present

Character 375: Humerus, m. humerotricipitalis groove:

0: absent

1: present as a ventral depression contiguous with the olecranon fossa

Character 376: Ulna, cotylae, orientation of dorsal (lateral) and ventral (medial) cotylae:

0: dorsoventrally adjacent

1: widely separated by a deep groove

Character 377: Ulna, dorsal cotyla, form: convex

0: flat or non-distinct

1: convex

Character 378: Ulna, distal end, dorsal (lateral) condyle, dorsal trochlear surface, extent along posterior margin:

0: less than transverse measure of dorsal trochlear surface

1: approximately equal in extent

Character 379: Ulna, bicipital scar: (ORDERED)

0: absent

1: present, developed as a slightly raised scar

2: present, developed as a conspicuous tubercle

Character 380: Ulna, brachial scar

0: absent

1: present

Character 381: Radius, posteroventral surface (=posteromedial surface of non-avialans), texture: (UNORDERED)

0: smooth

1: with muscle impression along most of surface

2: deep longitudinal groove

Character 382: Ulnare:

0: absent

1: present

Character 383: Ulnare, shape:

0: circular, triangular, or 'heart-shaped', with no or minimal differentiation into short dorsal and ventral rami

1: V-shaped, well- developed dorsal and ventral rami

Character 384: Ulnare, ventral ramus (crus longus), length: (ORDERED)

0: shorter than dorsal ramus (crus brevis)

1: same length as dorsal ramus

2: longer than dorsal ramus

Character 385: Semilunate carpal and metacarpals, fusion: (ORDERED)

0: separate from each other, no fusion

1: incomplete proximal fusion

2: complete proximal fusion

3: complete proximal and distal fusion

Character 386: Metacarpal III, anteroposterior (extensor-flexor) diameter at midshaft compared to anteroposterior diameter of metacarpal II:

0: approximately equal or greater than 50%

1: less than 50%

Character 387: Metacarpal I, anteroproximally projected muscular process, form: (ORDERED)

0: absent, no distinct process visible

1: present as small knob at anteroproximal tip of metacarpal

2: present, tip of process marginally surpasses the distal articular facet for phalanx 1 in anterior extent

3: present, tip of process conspicuously surpasses articular facet by approximately half the width of the facet, producing a pronounced knob

4: present, tip of process conspicuously surpasses articular facet by approximately the entire width of the facet, producing a pronounced knob

Character 388: Metacarpal I, anterior (extensor) surface, shape:

0: roughly hourglass-shaped proximally, at least moderately expanded anteroposteriorly, and constricted just before flare of articulation for phalanx 1

1: anterior surface broadly convex

Character 389: Carpometacarpus, pisiform process:

0: absent

1: present

Character 390: Carpometacarpus, ventral surface, supratrochlear fossa deeply excavating proximal surface of pisiform process or adjacent region:

0: absent

1: present

Character 391: Carpometacarpus, intermetacarpal space (between metacarpals II and III):

0: reaches proximally as far as the distal end of metacarpal I

1: terminates distal to end of metacarpal I

Note: All taxa without a carpometacarpus are scored as inapplicable ("?").

Character 392: Metacarpals II and III, distal ends, position of articular surfaces for digits:

0: articular surface on metacarpal II located at same distal level as, or surpasses distally, articular surface on metacarpal III

1: articular surface on metacarpal III extends further distally than articular surface on metacarpal II

Character 393: Metacarpals, intermetacarpal process or tubercle: (ORDERED)

0: absent

1: present as scar

2: present as tubercle or flange

Character 394: Manual digit II, phalanx 1, shape:

0: subcylindrical to subtriangular in cross section

1: strongly dorsoventrally compressed, flat posterior surface

Character 395: Manual digit II, length of phalanx II-1 compared to that of II-2:

0: less than or equal to

1: longer

Character 396: Manual digit II, phalanx 2, internal index process on posterodistal edge:

0: absent

1: present

Character 397: Pelvis, ilium, ischium, and pubis, proximal contact between bones in adult individuals: (ORDERED)

0: unfused to each other

1: partially fused to each other (pubis not ankylosed)

2: completely fused to each other

Note: State 0 includes the condition in derived therizinosauroids in which the pubis and obturator process of the ischium meet and fuse ventral to the acetabulum, which does not include fusion between the ilium and other pelvic bones.

Character 398: Ilium/ischium, distal co-ossification to completely enclose the ilioischiadic fenestra:

0: absent

1: present

Character 399: Ischium, dorsal process

0: does not contact ilium

1: contacts ilium

Note: All taxa without a dosrsal process are scored as inapplicable ("?").

Character 400: Ilium, antitrochanter, position:

0: directly posterior to acetabulum

1: posterodorsal to acetabulum

Character 401: Ilium, preacetabular pectineal process: (ORDERED)

0: absent

1: present as a small flange

2: present as a well-projected flange

Character 402: Ilium, preacetabular processes, orientation of left and right processes:

0: approach on midline but do not contact (open space between them, possibly a cartilaginous connection)

1: make contact with each other on midline and fuse, dorsal closure of 'iliosynsacral canals'

Character 403: Ilium, preacetabular process, morphology of process as it extends anterior to first sacral vertebra:

0: no free ribs overlapped

1: one or more ribs overlapped

Character 404: Ilium, postacetabular process, orientation:

0: dorsoventrally orientated, such that broad external surface faces laterally

1: mediolaterally orientated, such that broad external surface faces dorsally

Character 405: Ilium, postacetabular process, ventral surface, renal fossa:

0: absent

1: present

Character 406: Ilium, cuppedicus fossa, form:

0: broad, mediolaterally oriented surface directly anteroventral to acetabulum

1: small and entirely laterally facing fossa anterior to the acetabulum

Note: All taxa without a cuppedicus fossa (scored as absent for the character denoting the absence/presence of the fossa above) are scored here as inapplicable ("?").

Character 407: Pubis, cross section:

0: suboval

1: compressed mediolaterally

Character 408: Pubes, contact of distal ends of left and right pubes:

0: present, variably co-ossified into symphysis

1: absent, pubes noncontacting

Character 409: Femur, posterior trochanter: (ORDERED)

0: present, developed as a slightly projected tubercle or flange

1: present, hypertrophied into a 'shelf-like' conformation (in combination with development of the trochanteric shelf)

2: absent

Character 410: Femur, patellar groove

0: absent

1: present

Note: Turner et al. (2012) scored derived tyrannosauroids for possessing a patellar groove, probably because these taxa have a deep extensor groove for muscle attachment (a feature that is variably developed in tetanurans). We do not consider this feature homologous to the distinct patellar groove of birds, which houses a patella ossification (which is not known for tyrannosauroids or any other non-avialan theropod). Instead, we utilize a separate character (below) to refer to the extensor groove.

Character 411: Femur, ectocondylar tubercle and lateral condyle, separation:

0: present, separated by deep notch

1: absent, form single trochlear surface

Character 412: Femur, posterior projection of the lateral border of the distal end, continuous with lateral condyle:

0: absent

1: present

Character 413: Femur, laterally projected fibular trochlea: (ORDERED)

0: absent

1: present, developed as small notch

2: present, developed as a shelf-like projection

Character 414: Tibia/tarsals, condyles, extent of medial and lateral condyles:

0: medial condyle projecting further anteriorly than lateral

1: equal in anterior projection

Character 415: Tibia/tarsals, condyles, extensor canal: (ORDERED)

0: absent

1: present as an emarginated groove

2: present as a groove bridged by an ossified supratendoneal bridge

Character 416: Tibia/tarsals, condyles, tuberositas retinaculi extensoris indicated by short medial ridge or tubercle proximal to the condyles close to the midline and a more proximal second ridge on the medial edge:

0: absent

1: present

Character 417: Tibia/tarsals, condyles, mediolateral widths of lateral and medial condyles: (ORDERED)

0: medial condyle wider

1: approximately equal

2: lateral condyle wider

Character 418: Tibia/tarsals, condyles, medial constriction of lateral and medial condyles:

0: present, gradual sloping medial constriction of condyles

1: absent, no medial tapering of either condyle

Character 419: Tibia/tarsals, condyles, intercondylar groove, mediolateral width:

0: broad, approximately 1/3 width of anterior surface

1: narrow, less than 1/3 width of total anterior surface

Character 420: Tibia/tarsals, position of articular surface for distal tarsals/tarsometatarsus: (ORDERED)

0: on distal surface or restricted to distal-most edge of posterior surface, no broad extension of trochlear surface onto posterior surface of bone

1: well-developed articular surface extending up the posterior surface of the tibiotarsus (sulcus cartilaginis tibialis of Aves)

2: well-developed articular surface extending up the posterior surface of the tibiotarsus, with well-developed and posteriorly projecting medial and lateral crests

Character 421: Tibia, mediolateral width of distal end:

0: wider than midpoint of shaft, giving distal profile a weakly developed triangular form

1: approximately equal to midshaft width, no distal expansion of whole shaft (although condyles may be variably splayed mediolaterally)

Character 422: Metatarsal V:

0: present

1: absent

Character 423: Metatarsal III, position of proximal end:

0: proximally in same plane with II and IV

1: proximally displaced plantarly (to the extensor surface), relative to metatarsals II and IV

Character 424: Tarsometatarsus or metatarsals, intercotylar eminence:

0: absent

1: well developed, globose

Character 425: Tarsometatarsus or metatarsals, projected surface or grooves on proximoposterior surface (associated with the passage of tendons of the pes flexors in Aves; hypotarsus): (ORDERED)

0: absent

1: developed as posterior projection with flat posterior surface

2: developed as a posterior projection, with distinct crests and grooves

3: developed as a posterior project with distinct crests and grooves, at least one groove enclosed by bone posteriorly

Character 426: Tarsometatarsus or metatarsals, proximal vascular foramina: (ORDERED)

0: absent

1: single foramen present, between metatarsals III and IV

2: two foramina present

Character 427: Metatarsal I, shape: (ORDERED)

0: straight

1: curved or distally deflected but not twisted, ventral surface convex ('J shaped')

2: distally deflected and twisted, such that the ventromedial surface is concave proximal to trochlear surface for phalanx I

Character 428: Metatarsal II, distal extensor surface, fossa for metatarsal I: (ORDERED)

0: absent

1: present as a shallow notch

2: present as a conspicuous ovoid fossa

Character 429: Metatarsal IV, mediolateral width at midshaft: (UNORDERED)

0: metatarsal IV approximately the same width as metatarsals II and III

1: metatarsal IV narrower than MII and MIII

2: metatarsal IV greater in width than either metatarsal II or III

Character 430: Metatarsals, comparative trochlear width (UNORDERED):

0: II approximately the same size as III and/or IV (this includes taxa in which metatarsal III is slightly wider than the other metatarsals disally)

1: II markedly wider than III and/or IV

2: II markedly narrower than III and/or IV

3: IV markedly narrowest.

Character 431: Metatarsus, distal vascular foramen, form:

0: simple, with one exit

1: forked, two exits (plantar and distal) between metatarsals III and IV.

Character 432: Metatarsal III, distal trochlea in extensor view, proximal extent of lateral and medial edges:

0: equally extended proximally

1: lateral edge extends further proximally

Character 433: Metatarsal II, distal extent of metatarsal II relative to metatarsal IV: (ORDERED)

0: approximately equal in distal extent

1: metatarsal II shorter than metatarsal IV, but reaching distally further than base of metatarsal IV trochlea

2: metatarsal II shorter than metatarsal IV, reaching distally only as far as base of metatarsal IV trochlea

Character 434: Caudal vertebrae, middle to posterior caudals, anteroposterior length: (ORDERED)

0: shortened, less than 1.5x length of dorsal vertebrae (where known) and anteroposterior length of centrum less than twice its maximum mediolateral width

1: 1.5x-2x or less the length of dorsal vertebrae

2: 3x-4x length of dorsal vertebrae

Note: This is a modified version of the original Turner et al. (2012) character, which takes into account an additional state (denoted as state 0) noted by Zanno et al. (2009).

Character 435: Coracoid, coracoid fenestra:

0: absent

1: present

Character 436: Metatarsal V, elongated and bowed

0: absent

1: present

Character 437: Chevrons, degree of posterior extension of posterior chevrons:

0: not substantially elongated

1: very elongated

Character 438: Radius, width at midshaft:

0: roughly half or greater than width of ulna

1: less than half width of ulna

Character 439: Manus, combined length of metacarpal I and phalanx I-1:

0: greater than length of MC II

1: equal to or less than length of MC II

Character 440: Metacarpal III, shape:

0: straight

1: bowed

Character 441: Metatarsal I, position of distal trochlea:

0: proximally placed relative to trochleae of other metatarsals

1: inline distally with others

Character 442: Metatarsal I:

0: present

1: absent

Character 443: Braincase, preotic pendant, form: (ORDERED)

0: absent

1: present but small

2: present and robust

Character 444: Braincase, metotic strut, shape:

0: short and robust

1: long and narrow

Character 445: Prootic, pneumatic excavation on lateral surface leading into anterior tympanic recess: (ORDERED)

0: absent

1: present and shallow

2: present and deep

Note: Witmer (1997), Makovicky and Norell (1998), Bever et al. (in press) and others have described lateral pneumatic excavations on the prootic, which are present in some coelurosaurs, to be associated with the anterior tympanic recess, which is present in most theropods. The character here does not code for the absence/presence of the recess, but rather for the absence/presence of discrete external pneumatic openings on the lateral surface of the prootic that lead into the recess. Contra Turner et al. (2012), tyrannosauroids are scored for state 1, as they possess a distinct fossa on the lateral surface of the prootic that includes the external foramina of the trigeminal and facial nerves, along with pneumatic openings that lead into the anterior tympanic recess (Bever et al. in press). This fossa itself is a distinct tyrannosauroid character, which is listed as a separate character below.

Character 446: Braincase, anterior tympanic recess (ATR), manifestation on external surface of basisphenoid: (ORDERED)

0: subtle, external fossa not deeply impressed into the lateral surface of the basisphenoid

1: deeply impressed into the lateral surface of the basisphenoid in juveniles but not adults

2: deeply impressed into the lateral surface of the basisphenoid in adults

Note: Turner et al. (2012) originally scored for the absence/presence of an anterior tympanic recess. Witmer (1997), Bever et al. (in press), and others have shown that this recess is present in most theropods, so we have modified this character to refer specifically to the external manifestation of the recess on the basisphenoid. This character scores for a shallow/deep lateral fossa or fossae on the basisphenoid. We have also subdivided the "deeply impressed" condition into two states, to take into account the recognized loss of a deeply impressed recess during ontogeny in some tyrannosauroids (Bever et al. in press). This character is therefore equivalent to Brusatte et al. (2010a, character 157).

Character 447: Braincase, anterior tympanic recess and anterior tympanic crista (crest marking the posterior and dorsal border of the ATR), location:

0: below the exit foramen of cranial nerve VII exit and just proximal to the otic recess

1: anteriorly, with little or no development of the recess posterior to the basipterygoid processes

Character 448: Braincase, anterior tympanic recess confluent with the subotic recess:

0: absent

1: present, forming the Lateral Depression

Note: All taxa without a subotic recess are scored as inapplicable ("?").

Character 449: Braincase, V-shaped opening between basal tubera (or remnants of tubera):

0: absent

1: present

Character 450: Braincase, small tubera medial to basal tubera (or remnants of basal tubera) and ventral to occipital condyle:

0: absent

1: present

Character 451: Pedal phalanx II-2, size of distal articular surface relative to proximal articular surface:

0: approximately equal in size or distal surface slightly smaller than proximal surface

1: distal surface less than half the size of proximal surface

Character 452: Sternum, ossification of sternal plates:

0: absent, plates unossified

1: present, plates ossified

Character 453: Ulna, size of proximal cotylae:

0: unequal in size, lateral (=dorsal in avialans) condyle smaller

1: equal in size

Character 454: Braincase, middle ear resides within the Lateral Depression (formed by merged anterior tympanic recess and subotic recess):

0: absent

1: present

Character 455: Feathers, filamentous integumentary structures (Stage 1 feathers):

0: absent

1: present

Character 456: Feathers, vaned feathers (Stage 4 feathers):

0: absent

1: present

Character 457: Quadratojugal, size:

0: large

1: greatly reduced

Character 458: Frontal, notch for postorbital contact on postorbital process of frontal:

0: absent, process smooth or facet small

1: large notch present

Character 459: Frontal and parietal, position of fronto-parietal suture relative to postorbital processes of frontal: (ORDERED)

0: well posterior to the postorbital processes

1: at the level of the postorbital processes

2: anterior to postorbital processes

Character 460: Cervical vertebrae, orientation of articular surfaces between cervical vertebrae:

0: surfaces vertical to subvertical

1: strongly slanted anteroventrally

Character 461: Skull roof, accessory depression in supratemporal fossa:

0: absent

1: present

Character 462: Ilium, relative ventral extension of pubic and ischiadic peduncles: (ORDERED)

0: equal

1: pubic peduncle extends farther ventrally

2: pubic peduncle hyperelongate, approximately 2.5-3 times the proximodistal length of the ischial peduncle

Note: This is a modified version of the original Turner et al. (2012) character, which incorporates a second derived state referred to the hyperelongate condition of some derived therizinosauroids (see Zanno et al. 2009: character ZCD 311). We also consider this character to be equivalent to Zanno et al. (2009: character ZCD 309).

Character 463: Parasphenoid, ala parasphenoidalis:

0: absent

1: present, well-developed and crest-shaped forming anterior edge of enlarged pneumatic recess with the ala continuous with the anterior tympanic crista

Character 464: Furcula, cross-section:

0: nearly circular

1: anteroposteriorly compressed near the symphysis

Character 465: Furcula, shape:

0: V-shaped

1: U-shaped

Character 466: Furcula, epicledial processes, form:

0: unexpanded

1: expanded

Character 467: Furcula, lateral expansion of the rami between the hypocledium and the epicledial process:

0: absent

1: present

Character 468: Furcula, hypocledium, shape:

0: rounded

1: keeled

Character 469: Furcula, symmetry:

0: asymmetrical

1: nearly symmetrical

Character 470: Furcula, thickness of rami:

0: thin

1: thick

Character 471: Metatarsal III, extensor (=anterior or dorsal) surface, shape:

0: relatively narrow and flat

1: transversely expanded and slightly concave

Character 472: Metatarsal IV, accessory longitudinal ridge on anterolateral side of the distal end of the bone:

0: absent

1: present

NEW CHARACTERS ADDED TO THE TWiG DATASET HERE:

*Expansions of Turner et al. (2012) Characters:

Character 473: Metacarpal I, width of proximal articular surface compared to proximodistal length of entire metacarpal:

0: shorter

1: wider

Note: This character is a new character, originally part of Turner et al. (2012, character 149), which distinguishes the extremely short and wide metacarpals I of some alvarezsaurids.

Character 474: Manual unguals:

0: present

1: absent

Note: This character is a new character, originally part of Turner et al. (2012, character 151), which distinguishes the absent manual unguals of derived avialans.

Character 475: Manual unguals, form of flexor tubercle: (ORDERED)

0: large, robust, rugose, conical structure

1: reduced to a small convexity

2: absent

Note: This character is a new character, originally part of Turner et al. (2012, character 151), which distinguishes the large flexor tubercles of most coelurosaurs from the small flexor tubercles of some tyrannosauroids, ornithomimosaurs, and other taxa. Some alvarezsauroids have completely absent flexor tubercles, which is denoted by state 2. This character is equivalent to Brusatte et al. (2010a, character 255).

*Characters Relevant to Tyrannosauroidea (from Brusatte et al. 2010a):

Character 476: Skull, occipital region, orientation:

0: posteriorly

1: posteroventrally

Character 477: Skull, general shape:

0: long and low, length: height ratio greater than 3.2

1: deep, length: height ratio less than 3.2

Note: Length is premaxilla-quadrate cotyle length; height is maximum height of the upper jaw, not counting any cranial crests.

Character 478: Skull, anteroposterior length:

0: less than 40% trunk length

1: greater than 40% trunk length

Note: Trunk length is the anterior extremity of the pectoral girdle to the posterior extremity of the pelvic girdle, as defined by Sereno et al. (2009).

Character 479: Lateral temporal fenestra, orientation of long axis relative to long axis of orbit:

0: posterodorsal

1: approximately parallel

Character 480: Premaxilla, nasal process of opposing premaxillae, orientation:

0: divergent from each other, with small process of nasals fitting in between them

1: closely appressed to each other

Character 481: Premaxilla, deep foramen or fossa on the lateral surface of the base of the nasal process, within the anteroventral corner of the narial fossa:

0: absent

1: present

Character 482: Premaxilla, maxillary process orientation: (ORDERED)

0: mostly laterally (and resultantly widely visible in lateral view)

1: dorsolaterally (facing almost equally dorsally and laterally)

2: dorsally (and resultantly mostly hidden in lateral view)

Character 483: Premaxilla, form of narial fossa ventral to external naris:

0: shallowly excavated

1: deeply excavated, anterior margin invaginated as a deep groove

Character 484: Premaxilla, extent of narial fossa:

0: limited to region immediately ventral to external naris

1: extensive, covers most of main body of premaxilla

Character 485: Premaxilla, orientation and shape of anterior margin: (ORDERED)

0: smoothly curved and projecting posterodorsally, angle between ventral margin of premaxilla and anterior margin is less than 90 degrees;

1: smoothly curved and projecting vertically or slightly anterodorsally, angle between ventral margin of premaxilla and anterior margin is equal to or greater than 90 degrees

2: projecting vertically or slightly anterodorsally, with a discrete inflection point between a more vertical ventral portion and a more horizontal dorsal portion

Note: We have transformed the original character of Brusatte et al. (2010a: character 13) into an ordered multistate by adding a new intermediate state referring to an approximately vertical (or slightly anterodorsally inclined) anterior margin of the ventral portion of the premaxilla. State 2 now refers to a special condition of this state, in which the anterior margin is vertical (or anterodorsally inclined) and there is also a discrete inflection point between the more vertical ventral portion of the anterior margin and the more horizontal dorsal portion of the margin. Taxa with this condition, therefore, do not possess a smoothly curved anterior margin of the premaxilla. Tyrannosauroids are characterized by either state 1 or state 2, with state 2 referring to a subset of basal tyrannosauroids (*Dilong*, *Guanlong*, *Kileskus*, *Proceratosaurus*, *Sinotyrannus*).

Character 486: Premaxilla, position of palatal process:

0: immediately above interdental plates

1: separated from interdental plates by deep lingual surface of premaxilla

Character 487: Maxilla, promaxillary fenestra, position:

0: anterior margin of antorbital fossa

1: extreme anteroventral corner of antorbital fossa

Character 488: Maxilla, maxillary fenestra, anteroposterior length compared to the distance between the anterior margins of the antorbital fossa and fenestra: (ORDERED)

0: less than half

1: greater than half

2: greater than half and also greater than half of the length of the eyeball-bearing portion of the orbit

Character 489: Maxilla, maxillary fenestra, position within maxillary antrum:

0: does not abut dorsal border of the antrum in medial view

1: abuts dorsal border of the antrum in medial view

Character 490: Maxilla, antorbital fossa, extent:

0: reaches nasal suture

1: does not reach nasal suture

Character 491: Maxilla, interfenestral strut, anteroposterior length:

0: greater than 50% of long axis of maxillary fenestra

1: less than 50% of long axis of maxillary fenestra

Note: In oviraptorosaurs, the size of the interfenestral strut is measured relative to the "accessory antorbital fenestra," whose homology with the maxillary and/or premaxillary fenestrae of other theropods is not clear (e.g., Balanoff et al. 2009).

Character 492: Maxilla, antorbital fossa, trend of dorsoventral depth across main body:

0: uniform

1: diminishes

Character 493: Maxilla, subcutaneous flange bordering the antorbital fossa laterally on the posterior end of the main body, resulting in the fossa forming a channel between the flange and the main body:

0: absent

1: present

Character 494: Maxilla, dorsolateral process, coverage by antorbital fossa: (ORDERED)

0: process absent

1: process covered by subcutaneous surface only

2: ventral half of process covered by antorbital fossa

3: antorbital fossa completely excluded

Character 495: Maxilla, narrow region of smooth surface texture between anterior margin of antorbital fossa and the subcutaneous surface:

0: absent

1: present

Character 496: Maxilla, ventral margin of the anterior region of the bone, profile:

0: straight

1: convex

Character 497: Maxilla, joint surface for palatine, depth:

0: shallow, does not obscure the tooth root bulges from view

1: deep, obscures tooth root bulges from view

Character 498: Maxilla, anterior ramus (demarcated by concave step in anterior margin of maxilla):

0: absent

1: present

Character 499: Maxilla, form of contact with nasal in subadult to adult specimens: (ORDERED)

0: smooth

1: weakly scalloped

2: deeply scalloped with interlocking transverse ridges on both elements

Character 500: Maxilla, form of external subcutaneous surface texturing:

0: random foramina and shallow grooves and ridges

1: deep, prominent, dorsoventrally trending grooves and ridges

Character 501: Maxilla, swollen rim separating antorbital fossa and subcutaneous surface:

0: present

1: absent

Character 502: Maxilla, size of ascending ramus, anteroposterior chord directly above maxillary fenestra compared to dorsoventral depth of maxilla below anterior edge of antorbital fenestra:

0: greater than 1.75 times (ascending ramus large)

1: less than 1.60 times (ascending ramus small)

Character 503: Maxilla, posterior region of the main body (portion including the final 3-5 teeth and anterior to the jugal process), shape:

0: maintains a relatively constant dorsoventral depth

1: tapers in depth posteriorly

Character 504: Maxilla, primary row of neurovascular foramina, form:

0: continues as a row posteriorly

1: transitions posteriorly into a sharp groove, paralleling the antorbital fossa rim

Character 505: Maxilla, antorbital fossa, extent on main body:

0: covers more than half of the depth of the main body beneath the anterior margion of the antorbital fenestra

1: covers less than half of this depth

Character 506: Nasals, midline crest on dorsal surface:

0: absent

1: present

Character 507: Nasal, shape in dorsal view: (UNORDERED)

0: expands in width posteriorly

1: relatively constaint width across the length of the bone, due to subparallel lateral sides

2: tapers in width posteriorly

Character 508: Nasal, frontal process, mediolateral width:

0: unconstricted

1: constricted, less than ½ width of widest point of nasal

Character 509: Nasal, posterolateral process that overlaps the lateral surface of the lacrimal:

0: absent

1: present

Character 510: Nasal, extent of narial fossa on premaxillary process:

0: limited to ventral margin of process

1: covers entire process, and thus meets opposite fossa on dorsal midline

Character 511: Nasal, medial processes of frontal articulation, shape: (UNORDERED)

0: processes absent or very subtle

1: lanceolate

2: tapered

Character 512: Nasal, thin, low, and laterally projecting crest at the corner where lateral and dorsal surfaces meet:

0: absent

1: present

Character 513: Lacrimal, angle between anterior and ventral rami

0: 90 degrees (=inverted L shaped) or greater

1: approximately 70-80 degrees (=7 shaped)

Character 514: Lacrimal, cornual process on dorsal surface, form: (UNORDERED)

0: barely perceptible ridge across entire length of anterior ramus (equivalent to the state "cornual process absent" in tyrannosauroid-specific datasets)

1: broad, shallow, dorsally convex, laterally overhanging swelling across most of the length of the anterior ramus

2: discrete conical projection

3: small, conical, smooth projection that rises 2-3 millimeters from skull roof

Note: All taxa without a cornual process (those scored as absent for character 37) are here scored as inapplicable ("?").

Character 515: Lacrimal, cornual process, form:

0: smoothly rounded

1: discrete apex present

Note: All taxa without a discrete cornual process (those scored as absent for character 37 and those scored as 0 for character 514) are here scored as inapplicable ("?").

Character 516: Lacrimal, cornual process, position of apex:

0: dorsal to ventral ramus

1: anterior to ventral ramus

Note: All taxa without a discrete cornual process (those scored as absent for character 37 and those scored as 0 for character 514 and 515) are here scored as inapplicable ("?").

Character 517: Lacrimal, anterior ramus, pneumaticity:

0: not inflated

1: inflated by pneumatic recess

Character 518: Lacrimal, size of primary external opening for lacrimal recess:

0: small, anterior end located approximately at the same level as the anterior end of the ventral ramus

1: large, anterior end located far anterior to the ventral ramus

Character 519: Lacrimal, interaction of primary external opening for lacrimal recess and antorbital fossa:

0: separate

1: blend

Character 520: Lacrimal, accessory external openings for lacrimal recess on the anterior ramus: (ORDERED)

0: absent

1: present and proximally located (i.e., near to primary recess)

2: present and distally located

Character 521: Lacrimal, pneumatic recess opening internally onto medial surface of bone:

0: absent

1: present

Character 522: Lacrimal, dorsal prong of anterior ramus for articulation with maxilla ("anterodorsal process"), size:

0: absent or small

1: present and elongate

Note: We have combined "absent" and "small" into a single character statement, because the subtle process can easily be mistaken for absent if it is broken or poorly preserved.

Character 523: Lacrimal, ventral ramus, extent of medial lamina:

0: greater than half of the dorsoventral depth of the ramus

1: half or less of the dorsoventral depth of the ramus

Character 524: Lacrimal, orbitonasal ridge on medial surface, position:

0: anterior to posterior margin of ventral ramus

1: adjacent to or contacting posterior margin of ventral ramus

Character 525: Lacrimal, articulation with frontal, form:

0: squamous

1: conical lacrimal process set into deep pit in frontal

Character 526: Lacrimal, posterior process for articulation with frontal, inflated by pneumatic recess:

0: no

1: yes

Character 527: Lacrimal, extent of antorbital fossa on ventral ramus:

0: covers greater than 60% of anteroposterior length along the contact with the jugal

1: covers less than this measure

Character 528: Lacrimal, maxillary process of anterior ramus, visibility in lateral view:

0: both dorsal and ventral margins visible

1: dorsal margin concealed by subcutaneous surface abouve antorbital fossa and only ventral margin visible

Note: Those taxa without a maxillary process ("dorsal prong" in character 522) are here scored as inapplicable ("?").

Character 529: Jugal, maxillary ramus, depth:

0: shallow, not expanded relative to subortibal portion of bone

1: deep, expanded relative to suborbital portion of bone

Character 530: Jugal, antorbital fossa, extent on maxillary ramus:

0: edge of fossa undercut and continues posterodorsal to jugal recess

1: fossa edge does not extend past the jugal recess

Note: Those taxa without a jugal recess (e.g., most ornithomimosaurs) are here scored as inapplicable ("?") for this character.

Character 531: Jugal, pneumatic recess, location relative to ventral ramus of lacrimal:

0: ventral

1: anterior

Note: Those taxa without a jugal recess (e.g., most ornithomimosaurs) are here scored as inapplicable ("?") for this character.

Character 532: Jugal, pneumatic recess, orientation of long axis:

0: approximately horizontal

1: inclined at approximately 45 degrees relative to the ventral skull margin

Note: Those taxa without a jugal recess (e.g., most ornithomimosaurs) are here scored as inapplicable ("?") for this character.

Character 533: Jugal, secondary fossa for pneumatic recess, position relative to recess:

0: ventral

1: dorsal

Note: Those taxa without a jugal recess (e.g., most ornithomimosaurs) are here scored as inapplicable ("?") for this character.

Character 534: Jugal, suture with lacrimal, angle of the posterior half of the contact

0: low

1: steep

Character 535: Jugal, fossa on lateral surface of postorbital ramus, depth inset into bone:

0: shallow

1: deep

Character 536: Jugal, articulation with postorbital, form of ventral extremity of suture:

0: tapering scarf joint

1: interlocking notch for postorbital

Character 537: Jugal, articulation with postorbital, extent of scarf joint on lateral surface of postorbital ramus:

0: limited, occupies less than 50% of anteroposterior length of the process

1: extensive, occupies approximately 50-75% of the anteroposterior length of the process

Character 538: Jugal, articulation with postorbital, braced by a pronounced ridge on the lateral surface of the postorbital ramus, which borders the postorbital posteriorly:

0: no

1: yes

Character 539: Jugal, postorbital ramus, orientation relative to ventral margin of jugal:

0: approximately perpendicular

1: posterodorsal (obtuse angle between the long axis of the process and the ventral margin)

Character 540: Jugal, cornual process: (ORDERED)

0: absent

1: present

2: present and distinctive (mediolaterally wide and heavily rugose)

Character 541: Jugal, dorsal prong of quadratojugal ramus, slope in lateral view:

0: horizontal

1: posterodorsal

Character 542: Jugal, ventral prong of quadratojugal ramus, slope of joint surface in lateral view:

0: approximately anteroposteriorly oriented, angled less than 45 degrees from horizontal

1: angled anterodorsally at greater than 45 degrees from horizontal

Character 543: Jugal, shape of orbital margin:

0: weakly concave, approximately level with lacrimal-jugal suture

1: U-shaped, extends ventral to lacrimal-jugal suture

Character 544: Jugal, raised rim on the lateral surface, paralleling the ventral margin of the bone and anteriorly confluent with the antorbital fossa rim of the maxilla:

0: absent

1: present

Character 545: Postorbital, cornual process: (ORDERED)

0: absent

1: limited to rugose rim at posterodorsal corner of orbit

2: present as a rugose, convex boss

Character 546: Postorbital, cornual process, position:

0: separated from dorsal margin of postorbital by a smooth, convex region

1: approaches or extends past dorsal margin of bone

Note: Those taxa without a cornual process are scored as inapplicable ("?").

Character 547: Postorbital, cornual process, position:

0: located at orbital margin

1: located posterodorsal to orbital margin

Note: Those taxa without a cornual process are scored as inapplicable ("?").

Character 548: Postorbital, squamosal ramus, form of posterodorsal margin:

0: uninterrupted convex arc

1: emarginated by squamosal (discrete concave notch within the margin)

Character 549: Postorbital, squamosal ramus, extent relative to posterior margin of lateral temporal fenestra:

0: reaches or extends posterior to

1: terminates anterior to

Character 550: Postorbital, suborbital process, position:

0: at ventral end of ventral process

1: flange-like, separated from ventral tip of the ventral process by a notch

Note: Taxa without a suborbital process are here scored as inapplicable ("?").

Character 551: Postorbital, anterior ramus, form:

0: short and stout, long axis is approximately half the length of the ventral ramus and the thickness at the base is approximately the same as the thickness of the midpoint of the ventral ramus

1: long and slender, long axis is greater than 60% of the length of the ventral ramus and the thickness at the base is approximately half that of the midpoint of the ventral ramus

Character 552: Postorbital, ventral ramus, anteroposterior width at midpoint: (UNORDERED)

0: approximately the same width as ventral ramus of the lacrimal

1: substantially wider than ventral ramus of lacrimal

2: substantially narrower than ventral ramus of lacrimal

Character 553: Squamosal, lateral ridge delimiting supratemporal fossa, form:

0: ridge unpronounced or undivided

1: divided

Character 554: Squamosal, supratemporal fossa, surface morphology:

0: flat or concave

1: convex

Character 555: Squamosal, quadratojugal process, morphology of anterior tip in those taxa with horizontal processes:

0: tapered point

1: squared off

Character 556: Squamosal, quadratojugal process, flange that is covered laterally by the quadratojugal, dorsoventral depth of entire process compared to portion of process that is exposed in lateral view when in articulation with quadratojugal: (ORDERED)

0: flange absent

1: thinner

2: substantially thicker

Character 557: Squamosal, pneumaticity: posterior process, inflated by squamosal recess: (ORDERED)

0: absent

1: present as a deep, concave depression on the ventral surface of the main body

2: present as a deep, concave depression on the ventral surface of the main body, and extending posteriorly to inflate the squamosal posterior process

Note: This is a modified version of the original character in Brusatte et al. (2010a, character 95) which includes a second derived state referring to squamosal pneumaticity in general. This character is ordered, as state 2 is a special condition of state 1 in which the pneumatic recess that invades the ventral surface of the main body of the squamosal also extends posteriorly into the posterior process of the squamosal.

Character 558: Squamosal, posterior process, length of the long axis:

0: long, approximately 1/3-1/2 length of quadratojugal process

1: short, approximately 1/6 length of quadratojugal process

Character 559: Squamosal, anterior process, flange that extends dorsal to the postorbital posterior process:

0: absent

1: present

Character 560: Quadratojugal, dorsal process, ridge along anterior margin of lateral surface: (ORDERED)

0: absent

1: present, subtle and fades in strength dorsally

2: present, robust and extends to the dorsal margin of the bone

Character 561: Quadratojugal, form of jugal articulation, dorsal prong of posterior process of jugal approaching the base of the quadratojugal (the corner where the anterior and dorsal processes of the quadratojugal meet):

0: absent

1: present

Character 562: Quadratojugal, anterior process for articulation with jugal, form of anterior region: (UNORDERED)

0: tapered

1: rounded

2: squared off or double pronged

Character 563: Quadratojugal, anterior process, extent related to anterior margin of lateral temporal fenestra:

0: terminates posterior to fenestra margin

1: level with or anterior to fenestra margin

Character 564: Quadratojugal, curvature of bone:

0: mediolaterally compressed and flat

1: posterior region flexed so that it curves posteriorly, thus delimiting the lateral edge of a deep pocket that borders the quadrate foramen laterally in posterior view

Character 565: Quadratojugal, posterior process, length and orientation:

0: short, oriented mostly laterally

1: elongate, wraps onto the posterior surface of the quadrate cotyles

Character 566: Quadrate foramen, size:

0: small, long axis approximately 10% of the dorsoventral depth of the quadrate shaft

1: large, long axis greater than 20% of the dorsoventral depth of the quadrate shaft

Character 567: Quadrate, form of pneumatization, deep recess on the anterior surface where the psterygoid wing and condyles meet:

0: absent

1: present

Character 568: Quadrate, condyles, position relative to occipital condyle when skull is in articulation:

0: aligned (i.e., quadrate condyles approximately ventral to occipital condyle, or slightly anterior to condyle)

1: completely posterior

Character 569: Quadrate, quadratojugal articulation, extent on lateral surface of lateral condyle:

0: limited, occupies only part of the surface

1: extensive, covers entire lateral surface and extends dorsally to partially enclose quadrate foramen laterally

Character 570: Quadrate, articular surface for quadratojugal on quadrate lateral condyle, orientation of medial margin as seen in posterior view where quadratojugal wraps around quadrate:

0: vertical or dorsomedial

1: dorsolateral

Character 571: Prefrontal, contacts nasal:

0: yes

1: no, excluded by frontal-lacrimal contact

Character 572: Prefrontal, ventral process, extent:

0: large, extends 1/2-1/4 of the way down the ventral ramus of the lacrimal to make an extensive contribution to the preorbital bar

1: reduced or absent, ventral process is a thin flange that is continuous with the crista cranii of the frontal, and does not extend more than approximately ¼ of the length of the preorbital bar

Character 573: Frontal, shape (in those taxa with frontals that narrow anteriorly as a wedge between the nasals):

0: triangular

1: posterior end expanded into a rectangular shape, with a small anterior triangle

Note: Taxa with frontals that do not narrow anteriorly between the nasals (scored in character 41) are scored here as inapplicable ("?").

Character 574: Frontal, size of single frontal, ratio of anteroposterior length of exposed portion on skull roof to mediolateral width at midpoint:

0: greater than 2.0 (usually greater than 2.5)

1: less than 2.0

Character 575: Frontal, supratemporal fossa, medial extension:

0: fossa restricted to posterolateral corner of frontal

1: meets opposing fossa at the midline

Character 576: Frontal, sagittal crest: (UNORDERED)

0: absent or subtle, only discernable as a slight midline bulge

1: present and pronounced (dorsoventrally tall), single structure

2: present and pronounced (dorsoventrally tall), paired structure

Note: This charater is not equivalent to a parietal sagittal crest. Rather, it refers specifically to raised crests on the dorsal surface of the frontal, which may or may not be continuous with a sagittal crest on the parietal.

Character 577: Frontal, sagittal crest, anteroposterior length:

0: short, less than 15% length of the frontal

1: extensive, approximately 25% of the length of the frontal

Note: Those taxa without a frontal sagittal crest are scored as inapplicable ("?").

Character 578: Frontal, postorbital suture: (ORDERED)

0: dorsoventrally shallow and undifferentiated

1: dorsoventrally shallow (approximately 6 times longer than deep) and differentiated into a vertical region anteriorly and a horizontal region posteriorly

2: dorsoventraly deep (approximately twice as long as deep) and subtly differentiated into vertical and horizontal regions

Character 579: Frontal, contribution to orbital rim: (ORDERED)

0: extensive

1: present but limited to a small notch

2: excluded by postorbital-lacrimal contact in large specimens

3: exclueed by postorbital-lacrimal articulation and oval “palpebral” ossification

Character 580: Parietal-frontal suture, form:

0: transversely smooth

1: tab-like wedge from parietal extends anteriorly to overlie frontal on mindline

Character 581: Parietal, sagittal crest, form:

0: comprised of two parallel crests

1: comprised of a single midline crest

Note: Those taxa without a parietal sagittal crest are here scored as inapplicable (“?”).

Character 582: Parietal, skull table between supratemporal fossae, width:

0: broad, more than 10% of the mediolateral width of the fossa

1: extremely reduced, sagittal crest or crests (if present) pinched between opposing fossae

Character 583: Parietal, sagittal crest, dorsoventral depth:

0: consistent across length of crest

1: peaked anteriorly at frontal-parietal suture

Note: Those taxa without a parietal sagittal crest are here scored as inapplicable (“?”).

Character 584: Parietal, nuchal crest, dorsoventral depth:

0: as low as or lower than dorsal surface of the interorbital region

1: extends higher than the dorsal surface of the interorbital region

Character 585: Vomer, shape of anterior end:

0: lanceolate (lateral margins parallel-sided)

1: expanded into a diamond

Character 586: Ectopterygoid, extent of internal recess:

0: does not inflate body of the bone and the pterygoid process

1: inflates body of the bone and the pterygoid process

Character 587: Ectopterygoid, jugal process, external pneumatic foramina leading into jugal recess:

0: absent

1: present

Character 588: Ectopterygoid, jugal process, pneumaticity:

0: is not inflated by the internal recess

1: is visibly inflated by the internal recess

Character 589: Ectopterygoid, external opening of pneumatic recess, shape:

0: thin ovoid slot

1: large, round or triangular

Character 590: Ectopterygoid, surface posteriorly adjacent to external opening of pneumatic recess, form:

0: flat, recess grade smoothly into the floor of the lateral temporal fenestra (=subtemporal fenestra)

1: lip, recess separated from lateral temporal fenestra (=subtemporal fenestra)

Character 591: Palatine, vomeropterygoid process, ratio of anteroposterior length of dorsal margin to length of greatest constriction of process neck:

0: greater than 2.0

1: less than 2.0

Character 592: Palatine, vomeropterygoid process, orientation of neck:

0: inclined anterodorsally

1: vertical

Character 593: Palatine, pneumaticity:

0: absent

1: present

Character 594: Palatine, pneumatic recess, number of external pneumatic openings:

0: one

1: two

Character 595: Palatine, primary external opening of palatine recess, location of posterior margin:

0: level with or extends posterior to posterior margin of the vomeropterygoid process neck

1: located far anterior to posterior margin of the vomeropterygoid process neck

Character 596: Palatine, primary opening of palatine recess, location of anterior margin:

0: level with or extends posterior to anterior margin of the vomeropterygoid process neck

1: located far anterior to anterior margin of the vomeropterygoid process neck

Character 597: Palatine, jugal process, location of contact surface for lacrimal:

0: posterior ("distal"), separated from opening of palatine recess by wide margin

1: anterior ("proximal'), closely approaches opening of palatine recess

Character 598: Palatine, maxillary process, form of maxillary articulation:

0: flat

1: deeply excavated as a slot, demarcated dorsally by a pronounced lip of bone

Character 599: Palatine, extension of pneumatic recess into jugal process:

0: no

1: yes, process visibly inflated

Character 600: Palatine, maxillary articulation, form:

0: maxilla abuts lateral surface of maxillary process and anterior region of jugal process

1: contact reinforced by a "brace" at the anteroventral corner of the jugal process, which sits within internal antorbital fossa

Character 601: Palatine, morphology of maxillary articulation brace:

0: projects ventrally due to a jugal process that extends further ventrally than the maxillary process, such that there is a discrete corner between the two processes in lateral view

1: projects laterally, with no discrete corner between the smoothly confluent jugal and maxillary processes in lateral view

Character 602: Internal choana, shape:

0: anteroposteriorly elongate oval

1: nearly circular

Character 603: Suborbital fenestra, shape:

0: anteroposteriorly elongate oval

1: nearly circular

Character 604: Braincase, orientation of occipital surface:

0: faces posteriorly

1: faces posteroventrally

Character 605: Supraoccipital, contribution to dorsal rim of foramen magnum (ORDERED)

0: forms entire rim

1: makes limited contribution to rim via triangular ventral process

2: completely excluded from rim

Character 606: Supraoccipital, form of dorsal margin

0: smoothly convex and undivided

1: divided into two processes ("forked")

Character 607: Exoccipital-opisthotic, paroccipital process, ventral flange at distal end:

0: absent

1: present

Character 608: Exoccipital-opisthotic, paroccipital processes, deep fossa on posterior surface dorsolateral to the foramen magnum:

0: present

1: absent

Character 609: Exoccipital-opisthotic, crista tuberalis (=metotic strut), extent in posterior view:

0: limited, mediolateral width across opposing cristae less than one half the dorsoventral depth of the braincase from the dorsal tip of the supraoccipital to the ventral tip of the basal tubera

1: extensive, width greater than one half braincase depth

Character 610: Basioccipital, basal tubera, dorsoventral depth:

0: less than depth of occipital condyle

1: greater than depth of occipital condyle

Character 611: Basioccipital, basal tubera, concave notch ventrally between opposing tubera, dorsoventral depth:

0: shallow, less than 40% depth of tubera

1: deep, approximately 50% depth of tubera

Character 612: Basioccipital, subcondylar recess, depth of pneumatic fossae on posterior surface of basal tubera:

0: absent or shallow

1: deep

Character 613: Basisphenoid, basisphenoid recess, orientation of central axis: (ORDERED)

0: vertical, recess obscured in posterior view

1: posteroventral, recess partially visible in posterior view

2: extremely posteroventral, recess compressed anteroposteirorly and widely visible in posterior view, and basipterygoid processes located beneath the basal tubera

Character 614: Basisphenoid, basisphenoid recess, inflation of the ceiling of the recess:

0: absent

1: present

Character 615: Basisphenoid, basisphenoid recess, shape in ventral view:

0: funnel-like, expands in mediolateral width posteriorly

1: ovoid or circular, no posterior expansion

Character 616: Basisphenoid, shape of basicranium (rectangle defined by positions of both basal tubera and both basipterygoid processes):

0: anteroposteriorly longer than mediolaterally wide

1: wider than long

Character 617: Parasphenoid, shape of rostrum:

0: anteroposteriorly expanded, ventral margin is a smooth concave arch

1: dorsoventrally expanded, ventral margin is nearly vertical posteriorly and then abruptly transitions to horizontal trend anteriorly

Character 618: Laterosphenoid, antotic crest separating lateral wall of braincase from orbital and temporal spaces:

0: absent or indistinct

1: present, robust and rugose

Character 619: Laterosphenoid, antotic crest, form:

0: single structure

1: bifurcates ventrally

Character 620: Laterosphenoid, fossa on lateral surface that houses head of epipterygoid:

0: absent or shallow

1: present, deep and rugose

Character 621: Mandibular ramus, dorsoventral depth of dentary at level of dentary-surangular contact on the dorsal margin of the lower jaw:

0: less than 18% of the total anteroposterior length of the lower jaw

1: greater than 18% of the total anteroposterior length of the lower jaw

Character 622: External mandibular fenestra, dorsoventral depth relative to depth of mandible at midpoint of fenestra: (ORDERED)

0: greater than 25% depth of mandible

1: less than 25% depth of mandible

2: absent

Character 623: Lower jaw, articulation, glenoid position relative to level of alveolar margin of dentary: (UNORDERED)

0: approximately level with

1: dorsal to

2: strongly ventral to

Character 624: Dentary, position of the transition point between the ventral and anterior margins of the bone in lateral view:

0: below alveoli 1-3, anterior margin of bone rounded (or in some cases nearly straight)

1: below alveolus 4 (or more posteriorly), anterior margin nearly straight and projects posteroventrally

Character 625: Dentary, ventrally projecting rugose process ("chin") where the anterior and ventral margins of the dentary meet:

0: absent

1: present, visible as a pointed projection in lateral view and convex in medial view, braces dentary symphysis

Character 626: Dentary, symphysis, texture:

0: generally smooth

1: strongly rugose and beveled, with interlocking ridges and convexities for articulation with the opposing symphysis

Character 627: Dentary, articular surface for splenial along ventral region of dentary ramus below the Meckelian fossa, form:

0: dorsoventrally shallow and smooth

1: dorsoventrally deep (nearly as deep as anterior depth of fossa) and rugose

Character 628: Dentary, anterior alveoli, size in comparison to alveoli in middle of tooth row: (ORDERED)

0: approximately same size

1: first two alveoli substantially smaller

2: first alveolus substantially smaller

Note: This character is ordered here, because we hypothesize that state 2 (which is seen only in a small subset of derived tyrannosaurids: *Tarbosaurus* and *Tyrannosaurus*) is a special condition of state 1 (which is present in all score-able tyrannosauroids except for the derived subset).

Character 629: Dentary, dorsal margin of bone in lateral view, profile: (UNORDERED)

0: straight

1: strongly concave

2: strongly convex

Character 630: Dentary, Meckelian groove, form:

0: dorsoventrally deep and shallowly inset into medial surface of bone

1: dorsoventrally shallow and deeply inset into bone, groove appears as a thin, sharp structure

Character 631: Surangular, posterior surangular foramen, size:

0: absent or small foramen

1: large fenestra, approximately 30% depth of posterior surangular

Character 632: Surangular, surangular shelf on lateral surface, form: (ORDERED)

0: low ridge or absent

1: prominent ridge that is offset laterally from the bone but dorsoventrally thin

2: prominent shelf that is dorsoventrally deep

Note: The “low ridge” and “absent” conditions are considered primarily homologous here, because a very low ridge may appear absent on a specimen due to poor preservation. Taxa that genuinely appear to lack a ridge

(e.g., *Shuvuuia*) are scored as inapplicable ("?") for the following characters related to the form and the position of the ridge.

Character 633: Surangular, surangular shelf on lateral surface, position and form: (ORDERED)

0: placed far dorsal to posterior surangular foramen

1: foramen abuts shelf but shelf projects laterally and does not overhang foramen

2: shelf projects ventrolaterally to overhang foramen

Character 634: Surangular, surangular shelf on lateral surface, orientation relative to the long axis of the lower jaw: (UNORDERED)

0: anterodorsal

1: anteroventral

2: straight anteroposteriorly

Character 635: Surangular, pneumatic fossa posterodorsal to posterior surangular foramen: (ORDERED)

0: absent

1: present and shallow

2: present and deeply invaginated

Character 636: Surangular, adductor muscle attachment site dorsal to surangular shelf, orientation: (ORDERED)

0: faces primarily dorsally

1: faces almost equally dorsally and laterally

2: faces primarily laterally

Character 637: Surangular, triangular fossa on the lateral surface of the surangular shelf immediately anteroventral to glenoid:

0: absent

1: present

Character 638: Surangular, fossa on the lateral surface of the bone immediately ventral to, and separated from, the glenoid:

0: absent

1: present

Character 639: Surangular, anteroposterior length of anterior flange (region anterior to anterior margin of external mandibular fenestra) compared to overall length of surangular:

0: less than 30%

1: greater than 30%

Character 640: Angular, ventral margin, form:

0: smoothly convex

1: anterior region "flexed" relative to posterior region, such that there is a discrete step between them

Character 641: Articular, mediolateral width of jaw muscle attachment site:

0: less than width of glenoid for articulation with quadrate

1: approximateily equal to width of glenoid

Character 642: Articular, smooth non-articular region between glenoid and attachment site for depressor mandibular muscles:

0: present

1: absent

Character 643: Splenial, anterior mylohoid foramen, shape and size: (ORDERED)

0: small circular or ovoid opening, or absent

1: large, anteroposteriorly ovoid shape

2: extremely large, approximately as deep dorsoventrally as the anterior process of the splenial

Note: The small and absent conditions are here treated as a single character state, because poor preservation often makes a very small foramen appear absent.

Character 644: Splenial, dorsal region overlapped medially by prearticular:

0: absent

1: present

Character 645: Prearticular, ventral bar, series of ridges on lateral surface to strengthen articulation with angular:

0: absent

1: present

Character 646: Supradentary ossification, shape:

0: elongate, shallow strip

1: deep, crescentic shape

Character 647: Supradentary and coronoid ossifications, form of contat at their zone of fusion:

0: ossifications smoothly confluent

1: ossifications offset by a concave notch

Character 648: Premaxillary tooth crown 4, apicobasal height relative to largest maxillary crown:

0: subequal

1: approximately 50%

Character 649: Premaxillary teeth, median vertical ridge on lingual surface: (ORDERED)

0: absent

1: present as a subtle structure in anterior (mesial) premaxillary teeth

2: present as pronounced structure in all premaxillary teeth

Character 650: Premaxillary teeth, curvature of distal (posterior) teeth:

0: recurved

1: straight

Character 651: Maxillary teeth, number:

0: 13 or more

1: less than 13 (in the largest adult specimens when growth series are known)

Character 652: Maxillary and dentary teeth, form: (ORDERED)

0: ziphodont, transverse width of base less than 60% of mesiodistal length

1: incrassate, width greater than 60% of length

2: incrassate, width nearly equal to length

Note: Those taxa with conical or leaf-like teeth are scored as inapplicable ("?") for this character (e.g., therizinosauroids, most alvarezsauroids).

Character 653: Axis and postaxial cervicals, anteroposterior length of centrum compared to dorsoventral height of posterior centrum face:

0: greater

1: less than or equal to

Character 654: Axis, pneumatic foramen (pleurocoel), position:

0: near midheight of entrum

1: dorsally located, directly underneath neurocentral suture and directly posterior to diapophysis

Character 655: Axis, pneumatic foramen (pleurocoel), extent of surrounding fossa:

0: limited to margins of foramen

1: extensive, occupies most of lateral surface of centrum

Character 656: Axis, ridge on ventral surface of centrum:

0: absent

1: present

Character 657: Axis, pneumatic foramina and fossae on each side of the anterior ridge on the neural spine:

0: absent

1: present

Character 658: Axis, neural spine, texture of dorsal region of anterior surface:

0: generally smooth or with subtle texture

1: highly rugose, with series of grooves, ridges, and eminences

Character 659: Axis, dorsal region of neural spine, number of projections on "crown" region:

0: two lateral projections, dorsal surface of spine smoothly concave

1: two lateral projections and one dorsal projection on the midline

Note: Only those taxa scored for a mediolaterally broad ("transversely flared") neural spine for character 92 are relevant to this charater. All taxa with a mediolaterally compressed neural spine are scored as inapplicable ("?").

Character 660: Axis, supradiapophyseal fossa (fossa posterodorsal to diapophysis), form:

0: absent or shallow

1: deeply excavated and funnel-like

Character 661: Cervical vertebrae, neural spines in middle-posterior cervicals, dorsoventral height:

0: substantially shorter than height of posterior centrum face

1: approximately same length as or longer than height of posterior centrum face

Character 662: Cervical vertebrae, morphology of posterior centrodiapophyseal laminae in anterior-middle cervicals:

0: absent or present as a weak ridge

1: present as a thick, laterally offset lamina that demarcates a deep infradiapophyseal fossa anteriorly

Character 663: Cervical vertebrae, hypapophysis on anterior region of ventral surface:

0: absent

1: present

Character 664: Cervical vertebrae, position of prezygapophysis in middle cervicals:

0: slightly overhangs centrum laterally

1: strongly overhangs centrum laterally, entire prezygapophyseal facet placed lateral to centrum

Character 665: Cervical vertebrae, orientation of posterior centrodiapophyseal lamina in anterior-middle cervicals:

0: projects posteroventrally, infrapostzygapophyseal fossa located primarily posterior to lamina

1: nearly horizontal, fossa located primarily dorsal to lamina

Character 666: Cervical and dorsal vertebrae, rugose ligament attachment scars in pre- and postspinal fossae: (ORDERED)

0: absent or weakly developed

1: present as prominent, rectangular flanges that extend outside of the fossae and are visible in posterior view, but on the dorsal vertebrae only

2: prominent in dorsals and cervicals

Character 667: Dorsal vertebrae, neural spine, level of posterior termination:

0: at approximately the same level as the posterior centrum face

1: far posterior to the posterior centrum face

Character 668: Dorsal vertebrae, anteroposterior length of middle-posterior dorsal centra compared to dorsoventral height of posterior centrum face:

0: greater

1: less than or equal

Character 669: Dorsal vertebrae, middle-posterior dorsals, position of postzygapophysis relative to prezygapophysis:

0: at same level

1: elevated dorsally

Character 670: Dorsal vertebrae, middle-posterior dorsals, form of anterior and posterior centrodiapophyseal laminae: (ORDERED)

0: discrete laminae absent, or laminae present but do not demarcate a deep infradiapophyseal fossa between them

1: present and make contact on ventral surface of transverse process, demarcating a triangular infradiapophyseal fossa

2: present and do not make contact but roughly parallel each other, infraprezygapophyseal and infradiapophyseal fossa merged into a single fossa

Character 671: Sacral vertebrae, fenestrae between fused neural spines: (ORDERED)

0: neural spines unfused

1: spines fused but fenestrae absent

2: spines fused and fenestrae present

Character 672: Sacral ribs, position of central ribs on sacrum:

0: span two sacrals

1: limited to a single sacral

Character 673: Sacral ribs, position of rib attachment for central ribs on individual sacrals:

0: span centrum and neural arch

1: limited to neural arch only

Character 674: Sacral vertebra five, position of ventral margin of posterior articular face in lateral view:

0: at same level as ventral margin of anterior articular face

1: positioned ventral to ventral margin of anterior articular face

Character 675: Sacral vertebrae, form of hyposphene in posteriormost sacral:

0: absent or present as a single midline structure

1: present and comprised of two parallel-sided sheets

Character 676: Caudal vertebrae, anterior caudals, position of base of neural spine:

0: anterior to posterior surface of centrum

1: level with or posterior to posterior surface of centrum

Character 677: Caudal vertebrae, anterior caudals, shape of transverse processes in dorsal view:

0: rectangular, with parallel anterior and posterior sides, or slightly ovoid with a gradual expansion in width distally

1: distal end expanded into a spatulate bulb

Character 678: Caudal vertebrae, anterior caudals, two laminae linking prezygapophysis and transverse process, between which is a deep, triangular fossa:

0: absent

1: present

Character 679: Scapula, angle between posterior margin of glenoid and dorsal margin of blade:

0: greater than 90 degrees

1: approximately 90 degrees

Character 680: Scapula, acromion, dorsoventral depth:

0: less than 3.0 times minimum dorsoventral depth of blade

1: greater than 3.0 times minimum dorsoventral depth of blade

Character 681: Scapula, ratio of anteroposterior length of bone to minimum dorsoventral depth of blade:

0: less than 10.0

1: greater than 10.0

Character 682: Scapula and coracoid, glenoid, position relative to posteroventral margin of blade:

0: offset posteroventrally (by a distance equivalent to the width of the neck of the blade to ½ of the width of neck of the blade)

1: offset only slightly posteroventrally (less than 50% the width of the neck of the blade)

Character 683: Coracoid, anteroposterior length at midpoint:

0: approximately 100-150% of the length of the scapular acromion at midheight

1: 200% or greater than the length of the scapular acromion at midheight

Character 684: Coracoid, coracoid foramen:

0: present

1: absent or extremely small

Character 685: Humerus, apex of deltopectoral crest, location from proximal end: (ORDERED)

0: 35-50% of the length of the humerus

1: 25-35% of the length of the humerus

2: less than 25% of the length of the humerus

Character 686: Humerus, additional muscle attachment tubera at the corner of the anterior and lateral surfaces distal to the deltopectoral crest:

0: absent

1: present

Character 687: Humerus, concave notch between external tuberosity and deltopectoral crest:

0: present, two structures clearly separated

1: absent, two structures smoothly confluent

Character 688: Humerus, form of distal condyles:

0: lateral and medial condyles expanded equally (offset from shaft in anterior or posterior view is approximately equal)

1: medial condyle expanded further medially than the lateral condyle is laterally

Character 689: Ulna, shaft axis, form:

0: bowed

1: straight

Character 690: Principal distal carpal, shape:

0: semilunate in lateral view with trochlear proximal surface

1: discoid with flat proximal surface

Character 691: Metacarpal I, medial distal condyle, form:

0: well formed and large

1: rudimentary

Character 692: Metacarpal I, medial margin, shape in proximal view:

0: concave

1: smoothly convex or straight

Character 693: Metacarpals, metacarpal II, mediolateral width at midpoint compared to midpoint width of metacarpal I:

0: equal to or narrower than

1: more robust than

Character 694: Manual phalanx II-1, length compared to that of metacarpal 1:

0: longer

1: subequal to

Character 695: Ilium, anteroposterior length compared to length of femur: (ORDERED)

0: 70-85%

1: 95-105%

2: 105-115% (or greater, in some birds)

Character 696: Ilium, dorsal margin of blade, position relative to sacral neural spines: (UNORDERED)

0: separated by a gap

1: lies against neural spines and opposing iliac blaces may make contact above neural spines in some individuals

2: separated by a wide gap

Note: This is a modified version of the Brusatte et al. (2010a) character, which adds a second derived state ("separated by a wide gap") to refer to the condition of some derived therizinosauroids, as used by Zanno et al. (2009, character ZCD 306).

Character 697: Ilium, supraacetabular crest, maximum lateral projection relative to ischial peduncle:

0: significantly greater

1: subequal

Character 698: Ilium, supraacetabular crest, extent on pubic peduncle:

0: extensive, extends along most or all of the edge of the peduncle

1: limited, discretely offset from acetabular edge of pubic peduncle

Character 699: Ilium, pubic and ischial peduncles, anteroposterior lengths at dorsal base: (ORDERED)

0: pubic peduncle substantially longer than ischial peduncle

1: both peduncles approximately the same length

2: ischial peduncle longer than pubic peduncle

Character 700: Ilium, ventral margin of postacetabular process, shape:

0: straight to slightly convex

1: hightly convex, forming a discrete “lobe”-like flange

Character 701: Ilium, dorsal margin, shape:

0: smoothly convex or straight across entire length

1: convex anteriorly and straightens out posteriorly

Note: In dromaeosaurids such as *Unenlagia*, which possess a separate posterior tab-like process of the postacetabular process, this character refers to the shape of the remainder of the ilium (i.e., the entirety of the bone except the tab-like process). Therefore, these taxa are scored for state 0.

Character 702: Ilium, ratio of anteroposterior length to dorsoventral depth above acetabulum:

0: greater than 3.0, ilium is long and low

1: less than 2.8, ilium is subovoid in shape

Character 703: Pubis, pubic tubercle: (ORDERED)

0: absent

1: present as a convexity on the anterior margin of the pubis

2: present as a rugose flange that is discretely offset from the anterior margin of the pubis and is bordered posteriorly by heavy rugosities on the lateral surface on the obturator region of the pubis

Character 704: Pubis, pubic tubercle, position:

0: distally positioned, located ventral to the level of the obturator notch

1: proximally positioned, located level with or dorsal to the obturator notch

Note: All taxa without a pubic tubercle are here scored as inapplicable (“?”).

Character 705: Pubis, pubic boot, anteroposterior length relative to total long axis length of pubis:

0: less than 60%

1: greater than 60%

Character 706: Pubis, pubic boot, position of anterior process relative to posterior process:

0: displaced dorsally, resulting in a highly convex ventral margin of the boot

1: placed at the same level, ventral margin of the boot essentially straight

Note: Taxa without a discrete anterior process (e.g., compsognathids) are here scored as inapplicable (“?”).

Character 707: Pubis, anteroposterior expansion of proximal obturator plate region relative to the anterior edge of the pubis shaft at its midpoint:

0: less than twice the anteroposterior thickness of the shaft at its midpoint

1: greater than twice the anteroposterior thickness of the shaft at its midpoint

Character 708: Pubis, obturator notch, form:

0: discrete structure, demarcated ventrally by extensive obturator flange

1: essentially absent, no ventral flange

Note: The enclosed obturator foramen of *Mirischia* is here scored as equivalent to state 0. The presence of a completely enclosed foramen is autapomorphic of *Mirischia* among coelurosaurs.

Character 709: Ischium, position of medial apron:

0: along posterior margin of shaft

1: along anterior margin of shaft

Character 710: Femur, circular scar on posterior surface of shaft distal to fourth trochanter, position:

0: absent, low, or positioned approximately centrally on the shaft

1: abuts medial edge of shaft

Character 711: Femur, lesser trochanter, height relative to greater trochanter:

0: shorter, terminates further distally

1: subequal or slightly taller, the two structures extend to approximately the same level proximally

Note: This is equivalent to Zanno et al. (2009: character ZCD 325).

Character 712: Femur, proximal margin in anterior view: (ORDERED)

0: approximately straight and perpendicular to the long axis of the shaft

1: approximately straight and oriented at an obtuse angle to the long axis of the shaft (=dorsally or proximally inclined head)

2: concave and oriented at an obtuse angle to the long axis of the shaft, due to head that is proximally inclined and a greater trochanter that is elevated substantially relative to the central portion of the proximal surface of the femur

Note: Characters relating to the inclination of the femoral head are often used in theropod phylogenetic datasets, but it is often difficult to develop a standard system of measurement for quantifying the orientation of the

head. We use the character as defined here, which concerns the angle between the long axis of the shaft and the long axis of the proximal end, as measured in anterior view (note that many taxa with obtuse angles between the head and shaft in anterior view, such as *Tyrannosaurus*, appear to have perpendicular angles when measured in posterior view). Usually, taxa with an obtuse angle between head and shaft (i.e., a dorsally inclined femoral head) have a proximomedially projecting proximal surface of the femur when seen in anterior view, and this may indicate the presence of an inclined head in specimens that do not preserve the shaft. Furthermore, taxa with an obtuse angle between head and shaft (a dorsally inclined femoral head) possess a head that is elevated proximally relative to the greater trochanter, which is another means for recognizing the inclined condition in specimens that do not preserve the shaft. We also recognize a second derived state, encoded by Zanno et al. (2009: character oZCD 339) and Brusatte et al. (2010a: character 285), referring to the deeply concave proximal margins of the derived tyrannosaurids *Tyrannosaurus* and *Tarbosaurus* and some derived therizinosauroids, which have dorsally inclined heads but also greater trochanters that are raised substantially relative to the remainder of the proximal femur (except for the head), giving the proximal margin a deeply concave profile in posterior view. This character is equivalent to Zanno et al. (2009, character oZCD 320), which refers to the distinction between a medially ("perpendicular to shaft") and dorsally inclined femoral head. Brusatte et al. (2012a) stated that *Tanycolagreus* possesses a dorsally inclined (elevated) femoral head, but we here note that this is not correct and that this taxon possesses a head that is perpendicular to the shaft (state 0).

Character 713: Femur, trochanteric fossa on the posterior surface of the head, lateral to the ligament sulcus (for the capital ligament), form: (ORDERED)

0: absent or shallow

1: deep fossa

2: deep, extensive triangular depression that covers most of the posterior surface of the femur proximally and is demarcated medially and ventrally by a pronounced, curving, swollen ridge

Character 714: Femur, fourth trochanter, position, measurement from proximal margin of head to distal termination of trochanter relative to total length of the femur:

0: 40% or less

1: greater than 40%

Character 715: Femur, lateral condyle, shape in distal view:

0: circular or ovoid

1: ovoid, but with an anterior bulge that is slightly separated from the remainder of the condyle

Character 716: Femur, extensor groove on anterior surface of distal end, form: (ORDERED)

0: absent or extremely shallow, anterior surface flat between the condyles in distal view (extensor groove may be present but does not manifest itself as a groove on the anterior margin in distal view)

1: groove present but shallow, expressed as a broad concave margin in distal view but present as an extensive depression on the anterior surface of the femur

2: groove present and deep, expressed as a deep, U-shaped cleft in distal view and present as an extensive depression on the anterior surface of the femur

Character 717: Femur, mesiodistal crest, form:

0: single structure

1: bifurcates distally to enclose fossa on the medial surface of the medial condyle

Character 718: Tibia, length relative to the femur:

0: 1.05 or greater

1: less than 1.00

Character 719: Tibia, lateral condyle of proximal end, anterior process:

0: absent

1: present

Character 720: Tibia, lateral malleolus, lateral extent:

0: limited, mediolateral measure is less than 40% of mediolateral width of adjacent shaft

1: extensive, mediolateral measure greater than 40% of mediolateral width of adjacent shaft

Character 721: Tibia, lateral malleolus, position relative to medial malleolus:

0: extent to approximately the same level distally

1: lateral malleolus extends substantially further distally than medial malleolus

Character 722: Fibula, iliofibularis tubercle, form:

0: single crest

1: large, rugose, and formed by two crests separated by a depressed fossa (“bipartite” condition)

Character 723: Astragalus, fossa on anterior surface of ascending process, form:

0: shallow concavity that covers most of the ventral region of the ascending process

1: deep, triangular or ovoid fossa immediately above midpoint of condyles, set within a broad fossa that covers most of the ventral region of the ascending process

Character 724: Pes, metatarsal III, form of medial surface in anterior or posterior view:

0: straight or subtly convex

1: with medial convex expansion forming a bulge along the distal part of the shaft

Note: This character is equivalent to L. Xu et al. (2011: character 48), who utilized it as a character relevant to ornithomimosaurs.

Character 725: Pes, metatarsal III, ventral nonarticular surface (on the flexor surface) immediately proximal to the distal condyles, form:

0: concave

1: raised subtriangular platform

Character 726: Pes, metatarsals II-IV, distal separation when in articulation:

0: metatarsals closely appressed and distance between II-III and III-IV is approximately equal

1: distal ends of II and IV diverge from III, and distance between III-IV greater than that between II-III

Character 727: Pes, metatarsal II, articular scar for metatarsal III on distal portion of lateral surface of shaft, form:

0: subtle or absent

1: enlarged as a rugose fossa that occupies more than half of the proximodistal length of the shaft and expands in anteroposterior width distally

Character 728: Pes, metatarsal II, lateral surface in proximal view, shape: (ORDERED)

0: flat or weakly concave

1: moderately concave

2: strongly concave (deep concave notch is present)

Note: This is an expanded version of the original Brusatte et al. (2010a, character 304) character, which adds a new derived state to take into account the subtly concave condition in some ornithomimosaurs, which differs from the flat condition in outgroups and many basal coelurosaurs (e.g., *Ornitholestes*) and the deeply concave notched condition of derived tyrannosaurids.

Character 729: Pes, metatarsal IV, distal end, ratio between anteroposterior long axis (measured from midpoint of condyles posteriorly to anterior surface of bone) and mediolateral width (measured at midpoint: (ORDERED)

0: greater than 1.40, distal surface is elongate anteroposteriorly

1: between 1.40 and 1.20

2: less than 1.20, distal surface nearly square shaped with nearly flat anterior surface

Character 730: Pes, proximal pedal phalanges of digits II and III, ratio of length to midshaft width:

0: greater than 3.0

1: less than 3.0

Character 731: Pes, pedal unguals, lip overhanging proximal articular surface dorsally (on extensor surface):

0: present

1: absent or reduced to a subtle tuber

*Characters Relevant to Ornithomimosauria (from L. Xu et al. 2011):

Character 732: Maxilla, series of discrete foramina along ventral edge of lateral surface:

0: present

1: absent

Character 733: Lacrimal, prominence on lateral surface of bone:

0: absent

1: present

Character 734: Dentary, morphology of dorsal border in transverse cross section:

0: rounded and lacks “cutting edge”

1: sharp with a “cutting edge”

Character 735: Surangular, foramen on dorsal edge of bone dorsal to mandibular fenestra (anterior surangular foramen):

0: present

1: absent

Character 736: Neck, length compared to that of skull:

0: less than twice skull length

1: greater than twice skull length

Character 737: Coracoid, biceps tubercle, position:

0: positioned close to base of posterior process (closer to coracoid-scapula suture than to anterior edge of coracoid)

1: positioned more anterior than the base of the posterior process (closer to anterior edge of coracoid than to coracoid-scapula suture)

Character 738: Coracoid, position of infraglenoid buttress relative to that of posterior process when bone is seen in dorsal view:

0: two structures extend to same level laterally

1: buttress offset laterally from posterior process

Character 739: Metacarpal II, length compared to metacarpal III:

0: shorter

1: equal to or longer

Character 740: Manual digit I, length of phalanx I-1 compared to metacarpal II:

0: shorter

1: longer

Character 741: Manual unguals, flexor tubercles, position:

0: near proximal end

1: distal to proximal end

Note: Those alvarezsauroids without discrete flexor tubercles are scored as inapplicable ("?").

Character 742: Pubis, shape of ventral margin of pubic boot:

0: straight or slightly convex

1: strongly convex with ventral expansion

Character 743: Pes, pedal digit I:

0: present

1: absent

Character 744: Pes, phalanx II-2, length:

0: more than 60% of length of pedal phalanx II-1

1: less than 60% of length of pedal phalanx II-1

Character 745: Pubis, angle between anterior process of pubic boot and shaft:

0: greater than 90 degrees

1: approximately 90 degrees

Character 746: Pubis, position of anterior edge of anterior process of pubic boot:

0: approximately same level as anterior margin of pubic shaft

1: markedly anterior to the anterior margin of pubic shaft

Character 747: Pes, pedal unguals, shape:

0: curved in lateral view

1: straight

*Characters Relevant to Basal Coelurosauria (from Li et al. 2010):

Character 748: Premaxillary teeth, size compared to mesial (anterior) maxillary teeth:

0: approximately same size, slightly smaller, or larger

1: considerably smaller

Character 749: Ischium, form of articulation with ilium on proximal surface of iliac peduncle:

0: approximately flat or slightly concave

1: deeply concave as a deep socket to receive a peg-like ischial peduncle of the ilium

Note: Some tyrannosauroids and ornithomimosaurs have been described as possessing an accessory peg-like structure on the distal edge of the ischial peduncle of the ilium, which fits into a deep socket on the ischium (e.g.., *Alioramus*, *Gallimimus*: Brusatte et al. 2012a). Because it is often difficult to determine the presence or absence of this subtle peg-like process, we here consider the peg-like process and a peg-like ischial peduncle itself as primarily homologous. The presence of either of these processes can be clearly determined by the presence of a funnel-like socket on the iliac peduncle of the ischium. Because both structures leave a similar mark on the ischium, this supports the hypothesis of their primary homology (at least at some level).

Character 750: Scapula, acromion process, shape:

0: much deeper dorsoventrally than long anteroposteriorly, generally tapering or triangular in shape

1: approximately as long as or longer anteroposteriorly than deep dorsoventrally, with short reach beyond scapular blade and squared-off profile

Character 751: Basisphenoid, pronounced muscle scars flanking basisphenoid recess:

0: absent

1: present

Character 752: Ilium, form of distal articular surface of pubic peduncle:

0: convex

1: flat or concave (notched)

*Characters Relevant to Alvarezsauroidea (from Choiniere et al. 2010a,b, 2012 and Choiniere, pers. comm.):

Character 753: Lacrimal, orientation of ventral ramus relative to the long axis of the alveolar margin of the upper jaw when the articulated skull is seen in lateral view

0: approximately vertical or inclinded slightly anteroventrally

1: inclined strongly posteroventrally

Character 754: Exoccipital-opisthotic, position of ventral edge of the base of the paroccipital process:

0: level with or dorsal to the dorsal border of the occipital condyle

1: situated at mid-height of occipital condyle or further ventrally

Character 755: Maxillary teeth, shape: (UNORDERED)

0: mediolaterally thin and recurved

1: lanceolate (as in therizinosauroids)

2: conical (as in alvarezsauroids)

Character 756: Dorsal vertebrae, form of opisthocoely in taxa with opisthocoelous dorsals:

0: some dorsal vertebrae opisthocoelous

1: most or all dorsal vertebrae opisthocoelous

Note: Only those taxa with strongly opisthocoelous dorsal vertebrae (character 99) are scored for an affirmative score here. All other taxa are scored as inapplicable ("?").

Character 757: Dorsal vertebrae, shape of neural spine in posterior dorsals:

0: approximately square-shaped or slightly rectangular, with a dorsoventral height that is equal to or slightly greater than the anteroposterior length at the base

1: rectangular, much higher dorsoventrally than long anteroposteriorly at the base

Character 758: Dorsal vertebrae, position of parapophysis in posterior dorsals:

0: distinctly ventral to transverse process

1: at approximately same dorsoventral level as transverse process

Character 759: Caudal vertebrae, morphology of anterior caudals:

0: amphiplatyan

1: procoelous

Character 760: Caudal vertebrae, position of transverse process on anterior caudals:

0: approximately centered (in the anteroposterior dimension) on the centrum

1: anteriorly displaced

Character 761: Coracoid, biceps tubercle:

0: absent or subtle

1: present as a discrete, mound-like structure

Character 762: Coracoid, strong lateral ridge on lateral surface, extending posteriorly from biceps tubercle along posteroventral process:

0: absent

1: present

Character 763: Scapula, tubercle on posterior surface of bone dorsal to glenoid:

0: absent

1: present

Character 764: Humerus, shape of internal tuberosity in anterior view: (ORDERED)

0: triangular or rounded, not discretely separated from remainder of humerus

1: rectangular, separated from the humeral head by a small but distinct notch

2: rectangular and hypertrophied, separated from the humeral head by a large notch

Note: This character is modified into an ordered multistate with the addition of a second derived state, to distinguish between the condition in some therizinosauroids in which the internal tuberosity is rectangular and offset by a small notch (*Falcarius*, *Erliansaurus*) and that in which the internal tuberosity is rectangular but also proportionally hypertrophied and set off by a larger notch (*Segnosaurus*, *Erlikosaurus*, *Neimongosaurus*, *Suzhousaurus*, *Nothronychus*). This distinction follows Zanno et al. (2009, character ZCD 285).

Character 765: Ulna, shape of olecranon process:

0: transversely broad

1: mediolaterally thin and blade-like

Character 766: Ulna, position of distal articular surface:

0: limited to distal end

1: trochlear articular surface extends onto dorsal surface of ulna, bulbous in shape

Character 767: Metacarpal III, form of proximal articular surface:

0: flat or slightly convex

1: deeply concave and cup-like

Character 768: Metacarpal III, length:

0: considerably longer than length of metacarpal I

1: approximately same length as, or slightly longer than, metacarpal I

Character 769: Manual digits, paired flexor processes on proximal portion of ventral surfaces of proximal-most phalanges:

0: absent

1: present

Character 770: Manus, shape of proximal articular surface of ungual of first digit:

0: ovoid, dorsoventrally taller than mediolaterally wide

1: approximately square shaped, as mediolaterally wide as dorsoventrally tall

Character 771: Manus, form of lateral groove on ungual of first digit:

0: unenclosed or partially enclosed proximally by small flange

1: proximal end of grooves passes through foramena on ventral surface of ungual

Character 772: Femur, interaction of head and greater trochanter:

0: confluent

1: separated by a cleft

Character 773: Femur, shape of lateral distal condyle:

0: distally rounded

1: distally conical, projecting substantially further distally than medial condyle

Character 774: Tibia, shape of medial posterior condyle of proximal end in proximal view:

0: posteriorly rounded

1: posteriorly conical, projecting substantially further posteriorly than lateral condyle

Character 775: Fibula, orientation of proximal margin (as seen in lateral view):

0: horizontal or nearly horizontal

1: anterior portion of proximal margin extends substantially further proximally than posterior portion

Note: This character is equivalent to Zanno et al. (2009: character ZCD 329).

Character 776: Fibula, shape of proximal surface in proximal view:

0: anterior and posterior portions of surface with nearly equal mediolateral widths

1: anterior portion markedly wider mediolaterally than posterior portion

Note: This character is equivalent to Zanno et al. (2009: character ZCD 331).

Character 777: Astragalus, fossa on anterior surface of lateral portion of base of ascending process, sometimes bearing accessory fenestrations:

0: absent

1: present

Character 778: Astragalus, horizontal groove on proximal portion of anterior surface of condyles, separating condyles from ascending process:

0: present

1: absent

Character 779: Pes, phalanges of pedal digit IV, shape:

0: anteroposteriorly long, proximal and distal articular surfaces well separated

1: anteroposteriorly short, with proximal and distal articular surfaces very close together, particularly in distal elements

*Characters Relevant to Therizinosauroidea (from Zanno et al. 2009 and Zanno 2010b):

Character 780: Basisphenoid, inflated basisphenoidal bulla:

0: absent

1: present

Character 781: Braincase, foramen magnum, size (area): (ORDERED)

0: smaller than size of occipital condyle

1: approximately equal in size with occipital condyle

2: larger than size of occipital condyle

Character 782: Ectopterygoid, position:

0: posterior to palatine

1: lateral to palatine

Character 783: Dentary, mediolateral width of symphyseal region of conjoined dentaries:

0: narrower than width of post-symphyseal region

1: broader than width of post-symphyseal region

Character 784: Premaxillary teeth, serrations:

0: present

1: absent

Note: It has been shown that unserrated premaxillary teeth are present in some juvenile tyrannosaurids, but serrations are gained during ontogeny (Carr and Williamson 2004). Taxa in which this ontogenetic shift occurs are scored for the present condition (state 0). Any taxa with any trace of serrations on any premaxillary tooth (whether all teeth are serrated or not) are also scored for the present condition. Only those taxa in which all known premaxillary teeth are lacking serrations are scored for the absent condition (state 1). It is likely that there is positional variation in serration presence/absence along the premaxillary tooth row, but this is difficult to parse out because complete dentitions are not known for most taxa. We recognize that future authors may wish to divide this

character into additional states referring to serration presence/absence on individual premaxillary teeth or regions of the premaxillary dentition.

Character 785: Dentary teeth, shape of mesial (anterior) teeth:

0: not conical (i.e., ziphodont or lanceolate)

1: conical

Note: Although the first one or two dentary teeth of derived tyrannosauroids such as *Alioramus* and *Tyrannosaurus* are small and somewhat conical (in comparison to the remainder of the dentary tooth row), these taxa are here scored for state 0. State 1 refers to taxa in which the first several teeth of the dentary (at least the first four, where visible) are distinctly conical compared to the more posterior (distal) dentary teeth, but are of approximately the same size as the more distal premaxillary teeth. Oftentimes this condition is referred to in the literature as "anterior dentary teeth that are similar to the premaxillary teeth in shape".

Character 786: Dentary, extent of tooth row:

0: teeth present at anterior (mesial) tip of dentary

1: teeth absent at anterior dentary but present further posteriorly (distally)

Note: This character encapsulates Zanno et al.'s (2009) revision of the original TWiG character number 220, which is character number 217 in the current analysis. We retain character 217 in the original language of Turner et al. (2012) here, as it refers to an ordered progression of fully toothed-posteriorly edentulous-completely edentulous, and therefore the addition of a fourth state for an anteriorly edentulous dentary (which is unique to some derived therizinosauroids) would disrupt this ordered sequence. Our preference is to include the therizinosauroid condition as a separate character, with those taxa that are completely edentulous scored as inapplicable ("?").

Character 787: Cervical vertebrae, length of anterior centra:

0: up to three times longer anteroposteriorly than the minimum transverse centrum width in ventral view (or the height of the anterior articular surface in lateral view, if the centrum cannot be viewed ventrally)

1: hyperelongate, approximately five times longer than wide

Note: Zanno et al. (2009) presented a three-state character, but we do not want to over divide a ratio character such as this, and therefore recognize the major distinction among coelurosaurs as between a centrum that is fairly anteroposteriorly short (somewhere between 1-3 times longer than wide) and the so-called "hyperelongate"

condition in which the centrum is approximately five times longer than wide. Those taxa that do not preserve anterior cervical, but have middle cervical that are hyperelongate, are scored for state 1.

Character 788: Cervical vertebrae, morphology of ventral surface of centrum:

0: smoothly flat or convex

1: with distinct depression anteriorly (at the level of the parapophyses)

Character 789: Cervical vertebrae, posterolateral margins of ventral surface of centrum, form:

0: unpronounced

1: developed into prominent crests (ventrally projecting "fins")

Note: Zanno (2010b) notes that less pronounced crests, potentially homologous to state 1, are present on the cervical vertebrae of some ornithomimosaurs, but Zanno et al. (2009) scores all score-able ornithomimosaurs for state 0. We agree that ornithomimosaurs should be scored for state 0, as taxa such as *Gallimimus* (ZPAL MgD/I-94) clearly do not possess the prominent "fin-like" crests of therizinosauroids and some basal oviraptorosaurs.

Character 790: Dorsal vertebrae, anterior dorsals, dorsoventral depth of neural arch compared to that of centrum:

0: depth of region between prezygadiapophyseal lamina and base of neural spine less than or equal to depth of anterior and/or posterior articular surface of centrum

1: depth of region between prezygadiapophyseal lamina and base of neural spine greater than depth of anterior and/or posterior articular surface of centrum (neural arch hypaxially inflated relative to centrum)

Character 791: Dorsal vertebrae, size of parapophyses on anterior dorsals:

0: moderate in size, articular facet of parapophysis less than half dorsoventral depth of anterior articular surface of centrum

1: hypertrophied, articular facet greater than two thirds of the dorsoventral depth of the anterior articular surface of centrum

Character 792: Caudal vertebrae, pneumatic foramina on the centra of anterior caudals:

0: absent

1: present

Character 793: Scapula, dorsal flange on dorsal margin of scapular blade:

0: absent

1: present

Character 794: Humerus, crest on posteromedial surface of humeral shaft:

0: absent

1: present

Character 795: Humerus, tuberosity on anterior surface of distal humerus, proximal to entepicondyle:

0: absent

1: present

Character 796: Humerus, entepicondyle:

0: present and prominent as a spherical, conical, or crest-like structure in cranial view

1: extremely reduced or absent

Note: This is a modified version of Zanno et al. (2009: character ZCD 291). We find it difficult to distinguish between Zanno et al.'s discrete conditions of "spherical" and "crest-like," which are given separate states in the original analysis. Therefore, we combine these conditions into a single "present and prominent" state, and recognize the major difference between coelurosaurs as the presence or absence of a prominent entepicondyle. Taxa with a prominent entepicondyle usually, if not always, exhibit a prominent groove proximal to the entepicondyle, whereas those that have a reduced or absent condyle do not. Therefore, we do not utilize Zanno et al.'s (2009: character oZCD 292) separate character for the groove.

Character 797: Humerus, mediolateral width of distal end:

0: greater than 2x minimum width of shaft

1: less than 2x minimum width of shaft

Note: This is a modified version of Zanno et al. (2009: character oZCD 293), which combines two of the original states ("moderately expanded" and "significantly expanded") into a single state of "greater than 2x minimum width of shaft. Therefore, the character as worded here distinguishes the aberrantly unexpanded distal humeri of ornithomimosaurs and some tyrannosauroids from the standard condition among theropods.

Character 798: Humerus, morphology of distal humerus in anterior view:

0: medial aspect of distal humerus unexpanded, entepicondyle situated proximal to ulnar condyle

1: medial aspect of distal humerus expanded and subtriangular in anterior view, entepicondyle located well medial to ulnar condyle

Character 799: Metacarpal I, rectangular buttress on ventrolateral aspect of proximal surface that underlies ventromedial surface of metacarpal II:

0: absent

1: present

Character 800: Manus, ratio of the proximodistal length of metacarpal II to that of the combined proximodistal lengths of phalanges II-1 and II-2:

0: less than or equal to 1.0

1: greater than 1.0 (i.e., metacarpal II longer than combined lengths of phalanges II-1 and II-2)

Character 801: Manus, ligament pits on manual phalanges:

0: strongly developed

1: weakly developed or absent

Character 802: Manus, manual unguals, proximodistal length:

0: shorter to, equal to, or slightly longer than length of penultimate phalanx

1: elongate, twice or more as long as penultimate phalanx

Character 803: Ilium, orientation of ventral portion of preacetabular process:

0: parasagittal, in line with dorsal portion of process

1: laterally deflected, extends nearly perpendicular from sagittal plane of ilium

Character 804: Ilium, size of preacetabular process:

0: moderately developed, anteroposterior length of process subequal with dorsoventral height of ilium directly dorsal to the center of the acetabulum

1: hyperelongate, length of process at least twice the height of ilium above acetabulum

Character 805: Ilium, orientation of blade:

0: parallel or gently inclined relative to dorsoventral plane passing through the pubic and ischial peduncles (the ventral portion of the ilium)

1: angled laterally relative to the ventral portion of the ilium, rising steeply at at least a 30 degree angle from the dorsoventral plane passing through the peduncles

Character 806: Ilium, morphology of dorsal surface of postacetabular process in dorsal view: (ORDERED)

0: smooth and non-rugose

1: with rugosity causing transverse expansion of the posterior dorsal margin

2: hyperrugose, with hypertrophied posterior tuberosity

Character 807: Ilium, orientation of pubic peduncle: (ORDERED)

0: straight

1: posteriorly recurved, articular face posteroventrally directed

2: posteriorly recurved, articular face posteriorly directed

Character 808: Ilium, morphology of antitrochanter: (ORDERED)

0: separated from ischial peduncle

1: merged with ischial peduncle, both structures together form enlarged ventrolaterally flattened boss

2: merged with ischial peduncle as a boss, which is hypertrophied and spherical

Character 809: Ischium, position of distally placed dorsal process along posterior edge of shaft: (UNORDERED)

0: entirely proximal to obturator process

1: opposite obturator process

2: extending distal to obturator process

Note: This character refers to the position of the dorsal process of the ischium, whose presence or absence is scored in character 226. Those taxa without a process are scored as inapplicable ("?").

Character 810: Ischium, shape of obturator process in those taxa in which the process contacts the pubis:

0: approximately square-shaped

1: elongate anteroposteriorly, approximately twice as long as dorsoventrally deep

Note: The presence/absence of an obturator process contacting the pubis is scored in character 164. Those taxa scored for the absence of this feature in character 164 are scored as inapplicable ("?") for the current character.

Character 811: Ischium and pubis, morphology of contact surfaces between the two bones:

0: flat

1: markedly sinuous

Character 812: Pubis, shape of shaft:

0: rod-like

1: mediolaterally flattened

Character 813: Pubis, morphology of distal shaft:

0: distal portion of shaft approximately equal (or less than) in anteroposterior length to proximal portion of shaft

1: distal portion of shaft greatly enlarged, more than twice the anteroposterior length of the proximal portion of shaft

Character 814: Femur, anteroposterior width of region bridging femoral head and greater trochanter in proximal view:

0: smoothly confluent with head and greater trochanter

1: anteroposteriorly constricted relative to head and greater trochanter

Character 815: Femur, hook-like process at distal edge of femoral head, demarcating a notch between the head and the shaft

0: present

1: absent, shaft and head smoothly confluent

Note: This is equivalent to Zanno et al. (2009: character oZCD 323), which refers to the presence or absence of a "raised ventral rim" that separates the femoral head from the femoral neck (essentially the shaft). The "ventral rim" is equivalent to the hook-like process of the femoral head, which extends further distally relative to the remainder of the head to demarcate a notch between the head and shaft in anterior and posterior views.

Character 816: Tibia, morphology of incisura tibialis (lateral fossa on the tibia in proximal view):

0: deeply inset

1: wide and shallow, nearly absent

Character 817: Tibia, shape of tibia in proximal view:

0: anteroposteriorly longer than mediolaterally wide (measurements taken through midpoint of proximal surface)

1: mediolaterally wider than anteroposteriorly long

Character 818: Tibia, length of fibular crest:

0: short and proximally positioned, extends up to approximately 1/3 of the length of the tibia

1: long and distally extensive, extends to approximately the midshaft of the tibia

Character 819: Tibia, exposure and morphology of the anteromedial region of the distal tibia: (ORDERED)

0: covered anteriorly by the astragalus

1: not covered anteriorly by the astragalus, exposed

2: exposed and developed into an anterior tuberosity

Character 820: Fibula, iliofibularis tubercle, position:

0: proximal to midshaft of fibula

1: approximately at midshaft of fibula

Note: In those alvarezsauroids with an apomorphically shortened fibula (e.g., *Shuvuuia*, *Xixianykus*, *Parvicursor*), the position of the tubercle is measured relative to the length of the shaft of the tibiotarsus. Therefore, these taxa are scored for state 0 although their tubercles are located near the distal end of the shortened fibula.

Character 821: Astragalus, ascending process position:

0: lateral edge terminates approximately at the lateral edge of the tibia, or medial to the lateral edge of the tibia

1: lateral edge extends lateral to the tibial shaft to contact and overlap the fibula

Character 822: Astragalus, lateral condyle of distal end, morphology:

0: well developed

1: strongly reduced, lateral tibia exposed on distal and anterior surfaces of tibiotarsal region when tibia and astragalus are in articulation

Character 823: Metatarsus, overall shape:

0: elongate, unit comprised of metatarsals II-IV much longer proximodistally than wide mediolaterally

1: short and broad, unit comprised of metatarsals II-IV less than twice as long as wide

Character 824: Metatarsus, proximodistal length: (ORDERED)

0: greater than 45% length of tibia

1: between 44-38% length of tibia

2: less than 36% length of tibia

Note: For those taxa in which only isolated metatarsals are present (i.e., not a complete metatarsus), the length of metatarsals II, III, or IV is taken as a proxy for the length of the metatarsus as a whole.

Character 825: Metatarsus, orientation of individual metatarsals II-IV:

0: not closely appressed, divergent from each other

1: appressed throughout most of metatarsus

Note: The outgroups *Allosaurus* and *Sinraptor* are scored for state 0, as in these taxa metatarsals II and III are closely appressed but metatarsal IV is divergent. *Zuolong* has closely appressed metatarsals II and III, but because only a fragment of metatarsal IV is known it cannot be determined if IV was appressed or divergent, and therefore this taxon is scored as "?". Within coelurosaurs, all therizinosauroids are scored for a divergent metatarsus, following Zanno et al. (2009: character ZCD 335). Taxa without a complete metatarsus can be scored based on the shape of metatarsal IV (a laterally divergent kink along the shaft is indicative of state 0, whereas a straight shaft is indicative of state 1).

Character 826: Pes, pedal unguals of digits III-IV, proximodistal length:

0: approximately the same length as the penultimate phalanx (ungual may be slightly shorter or longer than the penultimate phalanx)

1: twice as long or more than the penultimate phalanx

*New Characters Relevant to Basal Coelurosaurs Established in this Dissertation (Note that some are inspired by published literature, as described in the main text, and others may have been added to published analyses during the time this dissertation was written).

Character 827: Premaxilla, anteroposterior length compared to that of maxilla:

0: length of ventral (alveolar) margin greater than 10% total anteroposterior length of maxilla

1: length of ventral (alveolar) margin less than 10% total anteroposterior length of maxilla

Character 828: Supraoccipital, tab-like processes on left and right sides of dorsal margin of bone:

0: absent

1: present

Note: This character has been included in previous phylogenetic analyses of tyrannosauroid interrelationships (e.g., Carr and Williamson 2010), but Brusatte et al. (2010a) combined this and the absence/presense of a dorsal bifurcation of the supraoccipital into a single character, due to a presumed equivalency between the characters. As outlined by Bever et al. (in press), however, the tabs are separate from the bifurcation, as

many tyrannosauroids have tabs but only a few taxa exhibit a bifurcation. The tabs themselves are created by midline depression of supraoccipital relative to left and right sides, as explained by Bever et al. (in press).

Character 829: Nasal, premaxillary processes (=supranarial processes), extent of their apposition to each other on the midline in dorsal view:

0: apposed for nearly their entire length (may abruptly separate from each other at their tips)

1: not apposed for most of their length, and therefore do not abruptly separate from each other at their tips

Character 830: Dentary, Meckelian groove, position:

0: approximately centered at dorsoventral midheight of dentary

1: positioned ventrally, located closer to the ventral margin than the dorsal margin

Note: This character was originally used by Carr and Williamson (2010: character 211), in which state 0 was scored for all score-able tyrannosauroids. We here note that this condition is also present in outgroups, *Compsognathus*, and derived therizinosauroids (*Erlikosaurus*), whereas state 1 is present in *Ornitholestes*, ornithomimosaurs (*Harpymimus*), basal therizinosauroids (*Falcarius*, *Beipiaosaurus*, *Alxasaurus*), and paravians (e.g.., *Deinonychus*, *Zanabazar*).

Character 831: Dentary, row of foramina on lateral surface paralleling ventral margin:

0: absent or limited to a small series of foramina at the anterior end of the dentary (at the level of the first 1-4 alveoli)

1: present as a distinct row that extends along most of the lateral surface of the dentary (across the entire length of the tooth row at the very least)

Character 832: Splenial, notch along dorsal margin of anterior process, where the splenial contacts the supradentary (if present):

0: absent

1: present

Character 833: Cervical vertebrae, position of prezygapophyses in anterior-middle cervicals:

0: prezygapophyseal facet approximately level with anterior face of centrum

1: prezygapophyseal facet entirely anterior to anterior face of centrum

Character 834: Caudal vertebrae, morphology of dorsal portion of neural spines of anterior caudals:

0: unexpanded

1: expanded anteroposteriorly relative to the remainder of the neural spine (and often mediolaterally as well)

Character 835: Ulna, morphology of distal end:

0: expanded mediolaterally at least 1.5x relative to midshaft mediolateral width

1: expanded less than 1.5x midshaft mediolateral width

Note: The denoted measurements are taken in anterior (extensor) and posteror (flexor) views.

Character 836: Ilium, medial surface of preacetabular process, pronounced horizontal shelf continuing from anterior margin of pubic peduncle to demarcate the cuppedicus fossa dorsally:

0: absent

1: present

Character 837: Metatarsal III, mediolateral width of distal end compared to mediolateral widths of distal ends of metatarsals II or IV (whichever of the latter is greater):

0: less than 1.3 times as wide

1: greater than 1.3 times as wide

Character 838: Lacrimal, extent of antorbital fossa on region where anterior and ventral rami meet:

0: extensive, fossa excavates nearly entire region and nearly extends to the posterodorsal corner of the lacrimal (the lacrimal angle), leaving only a thin region of bone at the posterodorsal corner of the lacrimal

1: reduced, fossa stops well short of the posterodorsal corner of the lacrimal

Character 839: Scapula and coracoid, deep fossa on lateral surfaces of both bones in the region of their suture (covering the posterior half of the coracoid and anterior portion of the acromion plate region of the scapula):

0: present

1: absent

Character 840: Scapula and coracoid, contribution of each bone to the glenoid: (UNORDERED)

0: both bones contribute approximately equally in the anteroposterior dimension

1: scapula contribution markedly anteroposteriorly longer than coracoid contribution

2: coracoid contribution markedly anteroposteriorly longer than scapula contribution

Character 841: Femur, shape of anterior margin in proximal view:

0: strongly convex, due to a midline tubercle

1: essentially straight or slightly concave

Character 842: Femur, horizontal ridge on the anterior surface of the head and neck, demarcating a deep fossa ventrally:

0: absent

1: present

Character 843: Femur, extent of crista tibiofibularis in distal view: (ORDERED)

0: projects further posteriorly than medial condyle

1: extends to the same approximate posterior level as medial condyle

2: terminates well short of the posterior level of the medial condyle (medial condyle projects substantially further posteriorly)

Character 844: Tibia, position of medial ridge on posterior surface of distal end: (ORDERED)

0: displaced laterally, positioned lateral to the medial edge of the distal tibia by approximately 25-33% of the mediolateral width of the distal tibia

1: positioned lateral to the medial edge of the distal tibia approximately 10-20% of the mediolateral width of the distal tibia

2: positioned medially, positioned at approximately the posteromedial corner of the distal tibia in distal view

Character 845: Scapula, fossa on lateral surface of bone immediately above glenoid, which is demarcated dorsally by a convex bulge or ridge spanning the scapula-coracoid suture:

0: absent

1: present

Character 846: Humerus, deltopectoral crest, orientation relative to mediolateral long axis of proximal end of humerus in proximal view:

0: straight, approximately perpendicular to long axis of proximal end of humerus

1: curves strongly medially as it continues anteriorly, such that anterior end of crest is oblique to long axis of proximal end of humerus

Note: Those taxa scored for state 0 for character 358 (a deltopectoral crest that is projected laterally or dorsally, such that it is in line with the long axis of proximal end of the humerus) are here scored as inapplicable ("?").

Character 847: Femur, position of fourth trochanter: (UNORDERED)

0: along posteromedial corner of shaft along its entire length

1: positioned near center of posterior surface of shaft distally and extending proximomedially to become confluent with posteromedial corner of shaft proximally

2: positioned near center of posterior surface of shaft distally and extending proximolaterally to bcome confluent with the greater trochanter

Character 848: Fibula, anteroposterior width of the minimum point of the midshaft compared to the maximum anteroposterior width of the proximal end:

0: 20% or greater

1: less than 18%, fibula shaft exceptionally gracile

Character 849: Maxillary teeth, posterior (distal) extent of tooth row:

0: extensive, extends posterior to the level of the maxillary ascending ramus and underneath the antorbital fenestra (if present)

1: limited, terminates posteriorly at the level of the maxillary ascending ramus

Character 850: Dentary, shape of ventral margin in lateral view:

0: approximately straight or slightly convex

1: broadly concave

Character 851: Maxilla, posterior extent of the ascending ramus relative to that of the main body (jugal ramus):

0: the two rami extend to approximately the same level posteriorly, distance between posterior tip of ascending ramus and posterior tip of main body no more than 1/3 of the anteroposterior length of the entire maxilla

1: main body extends considerably further posteriorly relative to the ascending ramus, distance between the posterior tips of the two rami is greater than 1/3 of the length of the maxilla

Character 852: Tibia, proximal surface, proximal extent of cnemial crest relative to the proximal extent of the posterior condyles:

0: cnemial crest extends further proximally than condyles

1: cnemial crest and condyles extend to same approximate level proximally

Character 853: Prootic, prominent fossa on the lateral surface of the bone, anterior to the otic recess and posterior to the preotic pendant, that houses the external foramina of the trigeminal and facial nerves and pneumatic openings:

0: absent

1: present

APPENDIX 2: CHARACTER SCORES FOR PHYLOGENETIC ANALYSIS

Note: The following are also available as an Excel spreadsheet and TNT file from the author.

Allosaurus_fragilis?10000?0000000100011001000100200111011001 0??000000000000001000000
000010001000000000000101010010000000100101000000000000100000000???000000000000
000?100000000000010000100101000000100010000011000000100000000000000000000001000000
00000?0?000?00110000100000010000111000210110000000002000000000?0000??0000000?0
0000??0000000010000[01]0?0????????0000020?00?0000000101000?0?0010000?00000000000
001000010?01000??0000000?000?00000200000000000000?00000?00?0010000000020000?00010
0??001100000[01]0?0000000010000000011000000000001000110000000211210010000000100?1
????000000000100??10?0000?000000000000011000?100?000?0?1000000000????000?0001001
00001010000000000000000010200000000000000000000100000000000020101[01]000010000000
00000000000100000010?0001000001020110000000000110000000010000000000000010010001
0000000000000000000000000000000000000000000??0000000000000000000000?0000010
00000000000000

Sinraptor_dongi?10000?000?00010001000000010?200001011001 0?00?0000000000010000?000
00100?10?0000000001010100100000001001010000000000001??????0??1?10?0?0??00??0?????
?000000000?010??0100101000001?0?100000110000001000000000000000?000?000?00?000000
?0?000?0011000010010001000000100002101???00000000000000000000?0000??0000000?00000??
0000000010000???00?00??00?????2?????????????1010?????????????????????????????????????1?
?????0??000??0000000020000000000000000000?00?00??0???00020000?0001?0??0011000????
?????000100000000000000000001000001100000002102100000010?00?100000000000000100?
?01?0000?00000000000?11000?100?010?0?100?00?001000?0010000100100001010?0?000000
0000001120000000?00????00000010000?0000000201 01??0??1000000????????????00001001 0?0
000?000010201101010?00011000000??1?00000000000000100 1000??0???00000000100?00000
000000000???????00000000??00000000000000000000000000?0010?00000?0000000

Dromaeosaurus_albertensis?0??001000000000010??0???0?01??01110????1111????101?100110
0??00000010011111000?0000101001???
?????????????1??11?1?0????00??????00?0?00??1???
??????1?00??011000100?0????????????????0???0000?00000??0000??0000000?00000??00?????
??00?????????
?????????????????????????????0????0?????????010121?000??0???00?0?????????0????0??0??0
???0???????0?0100?00?00?????????????????????????0????00000100000???????0???????0001001
?0?0????00??00?????0?0?10????????????000?1000000010????000000000000112010000000?0?
00010??0??000?
0??????????????0??0?010??????????????????????????0200000?????????????????????????????????????
???0?1?0??110??????????????????000?0

Deinonychus_antirrhopus?0010????1???????1??0000?0111000111000111111100?1??00001110
100000?0100111?1000?0100101000?110001100?1121011????0011011112?????1?11011100
1001110000010022111010102022O?01111211201?1111000000000100011010010000000001100
0000?00010?00100021100000111101100O0??000012200000000?0????000????0???????????
00000??000000000000?[01]0?0?????????????20000?000?000111000?0?0010000?000000000000
00101?0???00000??0100000?000?000000000000000000000000000?00100000000????????0?1?
???00111?????????0000?????00001?10?0010001?000001010??00?0???????00??0?0??0?????00
0010000000??01?00?0?00000001?????????????????????????0?0?1001000?000?00?????????????????
?000000000001120100?0000?0?????00000000?0000100010O?????00000?1101010000100??1?0
000?????????????????????00000?000000000?00?100?00??0001?1??0?000010?100000000010?010?
?00?000000000000000000000000??0????000000000100??1101?000110???200?10001?

Velociraptor_mongoliensis?00100100100001201120000101110001110001211l?10?010100001
11010000000100111110001010010100001100011001112101111100011011112111101011111
11001001110000010022111011102022020111122120111l1?000000000111011010010000000
01100000000011?00101021100000111001100000000000011200000000000?000000?0000??00
00000??0000??0000?00000000[01]0?00??000?000000200O?000?000111000?0?001000???000
0000000010100???00000??0100000?000000000000000000000000000000?0110000000010[1
2]21?000110110001110000?100000000?0100001?10?0010001?0?000101010000000???0??0?0
1??00?0????000001000000??01?0000?00000001001?0?0???000??0011010O?0???01000?000?0
0000100100O?000000000000??00?0112010000??????00000?????????????01001000?0000011
10101?0?0?00?0100000110?01?0100000000000000000000000?000100000?000?101010?00001
00100000000010?0100200000000000000000000000000??000010000000001000O?1?10?0011
01002000100010

Balaur_bondoc???
?????????????????????????????1?2??1????0???10??????????0????111[01]1110100l?1?00001???2??
?0111?202?02?0?1?22122?????????????????2110001001000??00??1???????????0?00??0???????
??????????????1?????2?00???00000000?[01]???0?
???????????20??????0???0111000?0?001000???010?00?????010?00???21??0?00000020?100??
0000??????00???0?000000000?00??0?00000????????010????????1????????00000????????????
??
??
????0100?0?0??0?00?1101010000?00?01000?0110?01?????????????000?00??00?????0010000
0?00??1?????000010010O?0000?????0?0???????????000000000000000000??000????0000002
10????????000?10???200?1?????

Tsaagan_mangas?00100100100001201120000101010001?10001211111000101100001O0??000
000100?1111000101001010000110O??1??????0?????????????????1????????11?111??????????
??00??00??00?0000??????????
211000011?00?0000000?00001????0000000????000000?0000??0000000?00000???000??????
??????????????????????20000???0?0?0??10??
?????????????????????????????????????0????????0121?00???0??00011?0????????????00?010000
1?10?0010001?0?000101010O0?00???0??0?01??00?0????000001000000??0??0000?000000010
01?000???000??001101?0?0?????????????????000100100000000000000??00?01120100000000??
??000000???00?00001?????????????????00?110??

?000?000?????????0?10?010?????10?????????????????02?0000000?????????????????????????????
???????????000?1?1????110????0???000?0

Bambiraptor_feinbergorum?0010??001000012010[02]00?010111000?110001211?1000101?00
011?0?0?000?0100?1111000?01001010??1110?1100?1??100?0?1100[01]1011??2????010101
1011110?001?10000011?211?0101?202202?111022100???11100000000010001101?00000000
0001100000000011?0010?021100??11?110??0000?000000122000?00000?0??00000??0000??0
000000?1?000??000000000100??0??0?0?0?0?00000?20000?00000?011?000?0?0?1000??000000
000?00010?????00000??0000000?000?000000000000000000000000?00?011?100000000121?
000110??0001110110?1000000001010000?1?10?0110001?000001000100000???0??0??1??00
?0????000001000000??01?0000?00000001??1?0?????000??001101?????????????????????0?????
???????????0?000??00?0112010?????????????0000000?000010001011000?000001110101000
010?00100000110?01?010000000?00000?000000000?0001?000??00001?10?0?100010?100???
?????????????0?000?????00??00????000000??0000100000000100?0???100001101002007100
01?

Tianyuraptor_ostromi??01?????????????????0????111?????????????0??1?????????????????
??????????0?0?0?1010??0???0?????????0?0?0?1??01?0112???????1??00?011110?001?1100001
112?1??0?1102223?2111022?0???1?110??????????00?11????000??0???1??00?0??01???1011?
0???0??????1?0??????????0????2?000?0?????????????????????????????????????0??????????0
?00?00????00000?0?00?000?0?0???00?1?0?
???10?????????????0?0????????20?101????????????1???????????0000?10??000??1?????????
?????????????????0???
???0?????????????????????????????0?????????
??????????????????01?1?1???00??0?0????000?????????????0?????0?0???00????0????0?0???0
???????0???0?????0??0?????????????????????0?????0???0?????????????????????????0010???????
?0?0????????????0?0??

Sinornithosaurus_millenii0001??????0??????????00???1110????10001111100?1????1??0???????
?00?00100??1????010100??100????????1??1???????0???00?1??1???????01?1?1101111?0?0????
?0000?00?201?01?112023?2?111022?2?1???1?????????110001?1100?0?00010001??0000???01
10111100200000011110?00?00???000???20000?000?????0??000????0????00000??1000??00?
00?0?????0?0??0???????00?0?[12]0000???0?000100?00?0??010?0??00?????????????????????00
00??0000?0000??0?0?00?????000??0?0000?00?0???0111?11000????????01??10000111?1100?
1000000?0101000000000?0000000?0?0000000100020???0??0??1??00?0????000000000000??0
0?0000?00000001??1????0??000??001101????????10?????????????????????????001000?0100
11201000???????100?0?????????????????????????0011101????00?000?????????0?01???????
????????0?0???00000??0??00000?000?1??0?0?????10?????0?00?????0?0???0100??????0????0
0000????001?000?????0??000100?011????0110????0???000??

Microraptor_zhaoianus0?????????????????100?????????????????????????????????????0??
010?0?1????0?01000000?????001?1??01?2100?01???0110?1212111?01?10111111010??1110
000110121111??0112023?2?111022120?11111??00?000111011111?100??000?11?000????10
10111100?0?0???1?110???0?00??0?00???20??0?000?????????????????????????0?0???????00
001000?[01]0?00?0000?0010002000??0?000?01???10?0???10100?000??1?0?000?????????000?
??????0?00?000000000????000?00??000000000??1211111??00?021???011011???1?1?1100?1

000000???????????????????????????????0??
??00???1???????????????
????????00?????????????00001????????01???1?10000?000???0000??0?01??10?????0?0000?0
???00????0????0?00??0????1????0000???10??0?00???0?010???????0???0?00??000??0?000000
?000?10?000000010??????????0?1??0?????1???1?

Graciliraptor_lujiatunensis??
?????????????????020???1???????????????????????????0???11?12?????????????????01011?11000
01??????????????????????????????????????0??0?010?[01]11?1??0??0??00??????????????0??????
?????????????00????????????????200??
????????????????????????????????????0??????10?0???000??0????????????10?0000??00?000????????
????????????????????????????????????10??????????????????????????????????000???????????????
???
??0???????????
?????????????????????1????00?00??????????????????????????????0000???00??????100??0??0??
?????0?????????00?0?00?????01???????????????????0???00?????????????????0?000?10?????????
0?0????????????????

Hesperonychus_elizabethae??
???
????21??010?????????????221211?????????????????????1?????????????1??????????0??1???????
???
???
???0??
???
???
??????????????????????????01000?0110?01???????????????????????????????????0???0????1????
??000?????????????????????????????????????
??????????

Pyroraptor_olympius??
???????????????????????????????????????0????????1?????????????????????????001?????????????
???01??1?????????0?????????????0??????0??????????
???
??010??0????????????????????????????????????
??????????????????????0???
???
???0?
0??????????0???0???????????????0?????????????????
0???
??

Rahonavis_ostromi??
????????????0????????????????011121???1?01?011112?12???????????0??11??011??????0?0111
1?10111120?3?2012101?121??21110001000?011101101?0100????0??1?????0??100010111111?
??0011000[01]0

??????????????2?????????????1100?????????????????????????????010100?????????????????000000?
0000000001000000000?00000000?001??01???0????????0?1?11?????1????????00?????????????
??
??
??????100?1??0?0??0011?????0?????0?100000????01??10???0?0????00?0???00?????????00??0?00?1????0000??0?0???????0???010???????????000?????????0000000?000?10??00?0001?
???????00?0?11?0??0????????

Buitreraptor_gonzalozorum?0010?????????????????0000101?00?????????100?10??01?0???????
??00??001??????????0210??100?00101111001111?110???100011012[012]121??????01101111
010?1?1??0?????11?101??12[02]23??01?1?1?120???11?0??0??1?011?0?1110000?????0??1???
?????11010001100110000???0??????0000??0?00?10200?00?0???????????0????????0?000101???
0????00000000000[01]0??????????0100010?0?0?00??0?10000?0?001100??00000100000001
?100?????????????????000????00???0?00??????????0?00?000?0010?00?????????????1????0010
??1100?0000???00?0?????????1?11?00?0???010?0101?0??0????00000??1100????????0000????0
?0??0??0?????????????100?????000??00?0?????????????????????0?????????????????0?000???
0??1?2?????????????????000???????00010010000??0??0000011101010???0?001??000????????0
1000???00??0?????????0?0?000??????????00????0?1000100?0???????01000?????0?000100000
00000????000000??0??01000?0??001???????10????11100?000100 01?

Neuquenraptor+Unenlagia???
??1121111111111???1????1????????????0??1001????????
??01111?10111120220201 11?12120201 1?10000??0?010??111100000????0??11????0??110110
?110?????????????????????0?????220???0?00000
?0?????????????????1?????????????1100?0?0?0011000?00000????????????0?????????????00
000?000000000000000000?00000000?00???
??
??
???????????11011?0?????0011???01???????00100000110?01?0100000000?00?0100???00??????
????000?00?00?1????10????01???????00???010?????????????00???0????000000??000010??0?
000010?????????0??111001000??????

Austroraptor?0000?????????????????????2?1?0????????12?0001?????????????????????0?011?????
??????210??10?????0011?001????11?????????????????????????????00????????0??????????
??????????????????????????1??????0?0?0?0??[12]1??????????0????0?????????????????11?00??01
??00?????????????1[12]20??0?0?????????????????????????????????????0??00?00???????????
?????????????????????????0?0?001100???00??0000000?????????????????????????????????
??00?0??????????0?1010?0
000010??1???????1?????????????????????????????????0??01?01?????????????????????0?10?00??
??????????00100?000?00?????????????????0??0010000?????????????????????000??????00010
01101?????????????101?????????????????????????????000????????00?00????????????0???
??0?0?????????????????????????????0?0001000?????0???????0000???????00??????0?????01?1??
??1?????1?0??0001?

Shanag_ashile?????????????????????1??1010110?????????????????????????????????00??011????
??????01001011???

??0????0??????????????????21100001???0
0??????????????????00??0??
??
??1?10???00?0?000000
??
??????????????????????????0??00??00????????????????????10????????????????????????????
??0?0??????????????????0???????????
??????????????????00??1??????????????????00???

Mahakala_omnogovae?????????????????101?????????????????????1?00???????0?0011?????????
?????????????02????1???00??0?11?011?211??1?10001101221O??????????????????00??1110000?
100?211101?2?????????????????????0111100????0?01100110?00000??00??11?0?????0000?????
00????????0????????????0????1[01]2?0??????0?????????????????0??1?00??????????0000010
000[01]0????????????????????????????10??[01]0???0?0000???0?????????????100????0??0???0
00000??0??001??0???000000000?00000000?001??00?000????1???0??????011?0????????00000
0????????????????????0???0??
?????0?????000?00????????0??????????????00010?????????????????????0????????????????????
???0000?????0?01?000???????000??????????00????00100000???????0100000?0?000?100?0?0
00?0????0?0?0???0????1?10???00???????????0????010?20????0?0??0???????000000000??0??
0100000000010?0????1?000???10????01????0

Atrociraptor_marshalli?????????????????????[02]00?0??1010????????????????????????????????0
0??010????????0?0000101001???
??0????0??????????????21?
00??0??111?????????1???????????0????????????????????????????0????0????????????????????
??
??00001?1????1???
0?0?000?01??
????????????????????????????????????0?????0?00?????????????????0????????????????????
??0?0?????????????0??????0?
??????????????????????????000??0??1?????????????
?????00???

Utahraptor?????????????????????[02]00?0???????????0?001?????????????????????????????????
???0????0101??1????0?1100?1??1????????0??011?????????????101?1???????????0??????????0?
01?????????????11?????0111?00??0?00100010???10????????11??0???????0?????0???????????
1???0???????0???10???0???0?????????????????????????????????????00000?????????????????
????20000?000000???00???????0??000000
0000000?0000?????0?10?????????????????????????????????????00?????000001?????????????
?????????????1???0??00010?0???
??
??01?????????0?0?????????????0?????0??????
??????????00????????????0?????????????????????????????????0?0?????????????????1????????
???????

Adasaurus_mongoliensis?0010?????0????2?????????????0?????0?1??11?1?0?101??001??0???
??0????0?1???0?????????????01100?11?0111?10?111[01]100??011?1?1??????1?111111??????
????????10221110101?2202?1?1122100l?111000000?000?1010010010??00??00110?0?0?0
001??00100?????????11????????00?0????1??????????0?????????00??00???000?0????????????0
00?0010000[01]0??????????????200?0???00??01110?????????????????????????????????????
????????00?000000000000000000000000?002??11?00???00???21?000??0??0001?1???????
??0???0??0?????????????????????????????0?????????1??00?????0000010??000??0??00?0
?0?00????????0??????????0?????????????????????????0?????????????????0???????111201????
??100000??0?01?????????????0?0
???00?0????????000?00????10?????????????????????????00??????0??00????????????000000??0
00010000??00010???????????01???????????????

Achillobator_giganticus?????????????????????????01?1?????????????????????????????????
????????????????0000101??????0?01100?11210???????0??011?11??????????101????????????00?
?10220??11010102102?011011?001?2111?0?????00?000?101????0???????1???0????001??001
00021100??0??100????????0???0000??
??????????????????20000?0?0?0?0??10???00???
0?00000??000???????0?0000????????0?????????????????0??????????0???????????00??????????
00?001???0?0?000??1???
??10???????
???????0100?????????????????????????????100000??0101?0100000?1000??????????0?????????0?
?01?????1??0??0?????????????01??0?????????0??00?????????0000000???0000100????????1??
?????????????1?1?????0?00?

Saurornitholestes_langsto???111????????????11????0
??????????????????100101?00?11000110011121011011100?1011?1?1????????????111????????
?000111221?1?1?1?2?0?????????????????11??0????00??001101??00???00?0?1??00?00000010?
001000????????1110011??????0????1220???????0?????????????????????0000???????????0????
??????????????????????????????0???00??1???0?
??0???00??????????0???????00111????????00?00?????????
??00?01??0?0?0?000?00???
???000??00?1???0?000?????????????????????????????0??0000000?????????????????????0???
????????????1?0???0??????0?
??????????????0?????????????????1??01????????????0?????????00?????????????????????????????
11?????????????????0???

Saurornithoides_mongolien?00??1?1??1101???0?110001?1000????????2?????????????????1?0
10?100?0010??1????000111010?????????1???0??1?????100??1?????????????????????????????
?????????????????02012020?010??10[01]1?11110???????????0???10?01??????0??1?0????????
????010??11000??0?1?01?0?????0?000??????0??0000????0?1000?0??0???????????0000???0??
??00100?0???
??00????????0?0????0000000000000?20?021000000000020100l?10???1110?1?????????????
00?0100000??2??11?0?0?1?0100010100??00???0??0?????0??0?????????????00?????????????????
?????????????????????????0?????????????????000?????????????????0?????????????????0?????
??00000?????????????????0????????0?0?????????????????????????????1?010???????????00????0

0000?????????00??00????0?0???00???????????1??????0??000?0?????0?????????????????????0?00
???????0?101?0????????1???0??????0?0?0

Zanabazar_junior?00101?12?110100?001?000??100000????2022000?21??0??11100??????100?
001???1????0001110101000?????????????????????1?1000?1020?1?????????????????????????????
????????????2?????????????????????????????????011????2???????????00??00???11????????0??110
000000100000????1??00????????00?000?????001??0?00?????????????0000??0?00?????????0[01
]0???
????????000100000??000??2????1??0???00000201001?11???1110?1?????????????00??100000?
?2??11?0?0?1?0100010100?000???0??0?????0??0?????????10??000??00?0?????????????????????
???000?00011010?????????????????????000?00000????0000???000?001?????????????0????00000?
?????????????????0?????????????????????????????????0?????????????0?0????????000??????
???????0?????00???0?????????????????01?00?0000?????????????????????????????0?00????
100100???????????1????000?0

Xixiasaurus?????????????????????0100010111?????2?22?????????????????????0?00??001?????
???000201??01?0???00?1??????????
???0???00?????????????????????1?000000???01
?0000????00???????000000???00?????????????????????????0????????????????????????????????
??0??????0??????????????????????????
??????????????????0?0?????????????????????????????????00????110100??2?01100?0?1?01000
101000000???0??0???000??0???????????
?????????????????????????????????????010?000?????????????????0000?????????????????????????
??000??????0??????0????0?0????????
??????0????????????0100??????????????0?????????????????????????1?010??????1??????????0
00??

Byronosaurus_jaffei?????101???101?1100110001011?0??????20220??????????1?100??????000
0001??11????000211??01?0?0???????010121????????0??02?????????????????????????????????
????????????????????????????????????1????0?0??0????????21?????????0????0????1???????????11
000000?1?00????0??0?000??0???000000?????????????0?????????????????0?0????0????0010??????
??
????000?????????????????????????????????00020001 1??0????????1????????????00??100000??2?0
11?0?0?1?0100010100??00???0??0?????0??0?????????????00?????????????????????????????0?
??????????0????????????????????00?000000????????0??00??00?0????????0???????0?0000??????
????1??000????????????
?0????000?????????????????????????????00?0100?????????????????????????????00?????????1?0?0?
1????1???????????000?0

Sinornithoides_youngi?0??01?????????????1?000??1??0????00???2???????1?????????????????00?
?0010???????0001110?01??????11??001???????????0011?10212101 1???1?00?1?101?0???1000
00????21??01??02??30???11?0??001??1110?????0???1?000110001?0??0?0?1??00?0???0???00
10?0??00000????0??0??0???00???0?2000000?0?????????????????????00?????1?00??000???????
???[01]0?0?????????0??0?20??0?00000?0??1000???0?1000???00?0?????????0??010?0000???00
0000??00??0??000????000000000000000020?021000000000????????101??????1?010100??1??00
0???0??

???????????000??0???0
?0?00?????????0?????????????????00?110101?000?000?????????????????1??????0?????000???00?
0???0???0?00??0??1????0?????100????0?0????????0???000?000???00??10?000?????0??00???0
000000001 0????0?1?0?0101????0????0???

Mei_long?0????????0????????11010?????0?11?00201210000 1?1010??100??????00010010??1?
0000?021???01?00110111000 11?2110?01???0110222111?1?????111?11100?0?1?1000001?012
111?1??1200302?1110221?[01]?0111100?0101001000??110011?0?0000???00000??000100?1?
?0?1?000000?001?0?0000?000001020000?000??????????00?0??0??00??0101????????0?000001
0000[01]0?0????????0100020?00?00000?0111000?0?0000000?0000000?000?01?1?0???00000?
???00000?000000 10000??000000000000?000021?01100000??0???20???1010??101100?1100?10
?0000?110??0??0???????????0?1?01????0?????00?????????????0?????????????00??????????
???????1???0??????0????0????0?????????????????????????????????0?000?????????????0?
??????0?0000?????????0?????????????????????1?1?0?????????????????????????????0??????00?
??00?00?0??????0????0????1?0?000?1001??00?0001?0?010???0???0?000000000?000????00?
??0???00?000000100?????????01???????????0?0??

Jinfengopteryx_elegans?0?????????????????1?01???2000????????1??00?0????1???100??????00
?00??0??1??0?000?1???0???1?????????????????????02????2?200???????1101110??????10000
0?????1?????????????????????2??0??????????0?????????????????0?0??00????00??????????????01
?000001???0??0?0??????0????200?0?000?????????????????????????0??????0?000???0?0??0
?0?????????????00?0???0?0?01???0???
??????????????????????????????10?0000???????????0??11?01?????????????000?110?????0?01?
?1????0?????????0?????00?????????????????????????????0?????????????????????????????0??
??0????0?????????????????????????????????????0??00?????????????????????????0??????????
???0????????0????1??0????00????0?????????????????????0?????????????0?0??00??????00?
???1?0???0????????0?????????????????000?????????????0?0???????00?????????001?0????????
?????????????000??

Anchiornis_huxleyi000100?????????????11010??11100?????0?2?000??1???11???????????000?
?01??1?????00020???01??0?101???00?0??010?01???0110122 0??01?????0111111 10000??1000
00010?21?1001102 0?202?1?1122121???1?1?000??1?01?000121100010?1000?1??00?0???????
0?11?011000001???0??00?????000???030000?000??????????0??????0????0??????0??????0000
0?0000[01]0?0????????0000020000?0?00??0?10000?????10?0???0???????????????10?01000?
?0?00?00??00?00000????????????00000?0?00??0100000000????????00??1110?1?1?1100010??
000?110??0??0?01?010?0?0?1??101?00??0??00?????????????0?????????1???000??0???2????
??????1?????????00????0????0?????????????????????????????????0?000??01?0?????????0??
?????0?0000?????????0???000??????000??????1???00??0000100000??0?01????????0?????0?0
???00?00?0??100?00??00???11?0?0000???????0??????????0????1000????0????0??0?0000000?
??00?0???????00100???0???0?01???????????000??

Xiaotingia?00?????????????????1?1???111000????0?2??????????11?????????????001001??1???
00??020???01??0??0???1?0?????10?01?????1??????10??????01?01111?10???10000010111?111
0?1102122?????102?12[01]??????????10????????1?0100010100001?1??0?10??00???0010?0110
00??1???00??0?????000???22000??000?????????????????????0000?????????0??000?10000???0
????????010002?????????????11?000?0?00???0???0?0?0????0???????????0100??1?00000???0?0

000?????????????????????0??0?02????10000????????00??1??????1?1100?10??000?110??0??0?0
1??1????0?????0???0?????0?????????????????0??????????1???00?????????????????????????????
0????0????0?????????????????????????????????????0??00???1?0????????0???????????00??????
???0?????????????????0011??????0???000010?000?????????????????0???????0???00000?0??100?0
0??00?1??1?0???????0????0??????????0?????000?????0???0??000?000?????0??????????0?100
???0?????0101????0???000??

Troodon_formosus???1?1112?1101000001???0?011?0??????2022000210?0??01100????0?10?
?001??????????01110101001??1111100101211111?1000?1020??11?????????????1?010?????00
0010??????????0?0?2?20?11001?0??0111100???000100000210??01????000??1?0??010???1??0
??0?1?00000?0?0????????00?????????????????????????001??0?000?????0??1?1?????????00????????
??
????????????????????????????????0?????000002010010??0???1110?1?????????0000??????????
??0?????0
000??00110?????????????????????0000001000??000000??0000000?????????????????????00???
????0?0??00?????????????????????0?????????????????????????????????????00000?000??0????????
00??0???0??0????00??01??0000?0?1??01?01?00?0?????????????0?0?????????????????0?000?10
?0?10?0?0?0?????????????0??0

Sinovenator_changii?0???0002?000011110010101?1110?011?02??2??0011???1?10100????0?0
00?001?????000001111O?1?????11?1010001211O?0010001102222?1?????????110111???????1
00?0???0?211?010112[02]0302?111022120l?11110000??100110001111??110?000000???00001
1000100011001100O??1??011??0000?00000??0??000000000000?000000?00?0??0000010100[12
]00??00000?0010000?????????????????20000??00?0101?10?????????????????????????????
??????????????00?10000001000000000000?0?00?020?0110?000000000?0?010?10??101100
0??????000000?????0000?02?011??00?1?0100010?????0?????????????????????????????
?????????????????????0????????0?00????1?????????????????????0????????0???00000??00???0???
??????????????????00?????????????00????0??????00111?????????????0000?0??0?01???????1?
?0????0?0?0???0?0???????????0?0?1?1??0?????100????????0????0??01?01?0?0000?00??????0
?00??0???0000?000000001?1???0?????0??1??1?????000?0

EK_troodontid_IGM_100/44?????0012???0???????
????????1??11??????????1??????0???1?0
0000???01?1?001???00??????0?0??1?????????
0???1?1?????????????????????
???
???0?????????000?????????????????
???0????????????
???
???
??????????????????0??????????1????0????????????0000?????????????????????0?1?????????????
??????????????

IGM_100/1126?0????002?0000?11[12]01?010??2000?011?02012100011O?01010100??0??0000
00000?11?000000211??00?0?????????????????0????01102?????????????????????0??10000
01???211?010?020020200010131012??111000????0??2?00121000l?00000011?00?0?020000?0

0100?1?00000111?01?0?00?000003??????000000?????00??00?00?0??0??0000?00?00???0?0??
???????0???0?00???0000???0100
000?00??0???0?00?00?????00?1?000?20?02????00000010?0?111??0??101?001???????0?000??
??
??
??
??
??????????????????????????

IGM_100/1323?00???????0???11???1?000??20000?1??020121?00?1??0?0??????00?0?000?0??
??1??00000021???0000?????????????????????????011?????????????????????????????????00??
1??????020?20200[12]102?1011???????00???0????0??2???01??00??0????0?0???00?0?00100?1
?000000?1?01?0?00?00?003??????0000000????00?000?00?0?????0000?0?000??0?00?????????
??00?????
00?00?0?00?????????1000??2?????????????????????????????01?????????????????????????
??
??
??
??
??????????????????

Archaeopteryx_lithographi100?0000??000??112010010??1110?0110000121?0?10?0000??1001
11?0?000001000002?00000200??00100?1?1???00?0??1?0?0???00210123110?0????101111111
1000?1100000000112111010?120030201210222?2?2?111100000?000100000003?00000000011
00000??00?000110011100001001?01000000???0000?030000?0000000?00110??00?0??000?00
??000???00?000000000[01]000?0????????00000?0000?0000000100000000?0011000?000??000?
0000100000??00000?000000000000?0?00000000?00?0?[01]1000000?00???0000010000102?0
0001011101?0101100?10000000110?00000?01?01?0000?0?0100?10100?000???0000?01??00?
0????00???10??000?????????000000?0?0????????000??0011000?????0?????????0000000011?
?????00000?000000000??00???0???0???0?0100???????000?0000????????0?0011101?10000?0
00?100000??0?01?01??????0????00?0???00?00?00?100000?000?1?1000?0?0010010??000000?
0?010020?1000?000000??0?000000?0000?000?????0?0000100001001???0111????00?100010

Confuciusornis_sanctus10010?????????????1?000?00??0001???0??2??0??0??00??01???????00
0010000?10?0001?1?????????0??????????1021?0?2???0?2????4??111?11010??1311100?1111
0000001121?1?1??12000?2?111023?2??12??10??11??120211010030?000000000110200??00?
0101??11?10001100?????0?????000?123001[01]00120?????????10??00??011200??01[12]01
1111000000110000100100012000?00?0000?0??0??0100000000?000211??00100000000101021
01011[01]?10?000000101000000000101010010001100001100?0000000[01]000???200000110
1110?00??1100?10?0000?110?00000??1?00?0000?0?01?0?10100?00??????????1??00?0????00
00000??000??01?02???00100000?0????????000??00???0?????????????????????????????????
?00010???0?00??00??10????????????0???????0001?000???0????0?00111?0?1?000?100??????0
??0??1?????????0????00?0???00?00?0??100000??0??1??0?????0?????0??00???????010?????
0?????0?0000?0?0??????0??0??????0?0000100?0?0?????01???????????1???

Jeholornis_prima10????0????????1???0???0?????001?????????????????0???????????0000?1??
?00?00?1?1?????????0????????0????1?0?11???0211103 1??01?0???0110311100 01??100000101
1?1??0??01?0???2???1?221?10???????01????0101101003000000000??0??1000??00?010????1?
??000?1?????0???0??0??0??12300?10010?????????????????????0????00?00000??00?0000001000
00?0??001???0000?00000?0?10001200010 00?0010000?000?0000?000010000101100 00?00000
0000000?00000?0100000000100000100 0?00000001100????????011?1110???1?1100?10?0000
?110?00000??????????0?0???????0?????????????????????0??????????0??00?????????????????
????????????000??00?????????????????????????????????????0??00???0?????????????????
?????????????0?0??0000???????0?0011101?1?0???000???0000??0?01?????????0????00?0???0
0?0??0??100000?00??1?10???0?00???????00???????010???????0?????0???0??0?000?00???000
?????0?0000100???0?????0??????????1?1?1?

Jixiangornis_orientalis100?????????????????0010????001????0?0??00000??????0100?????00
0001????0?0??1??0????????00?0???1?00????1??20???02??1031??11?1?000110311100011010 0
000111210101021200002010 1?221?10?2?11?001??1?01[12]1101003000?00?000?0??1000??0
0?0100??111?001?1?????????00?000000?12300?00010?????????????????????0?????000??00?
0000?11?0?10?11?0?????000000000?00100112100 10?0?0000000?000???0??0????0??010?00
100??0000?00100000?00??0000??00000100000?00?0000?001100????????00??11????01?110
0?10?0000?11??00000??????????0?0???????0?????????????????????0??????????0??0????????
??????????????????????????0???00010???0?????????
????????????????0?????????????????????????????0?1?00??00?????????????????????0?????0
?0???00?0??0??100?00??0?????0?????????????00?????????0?????????????????0??0?0???????
?????????????00100???0?????0????????????1???

Yanornis_martini?00?????????????????1?010?????0?11???0??2??0??????00???????????0000011
???0????000?1???00??0????1???0????????4?1???????04??????110?0110311 10?011?130010???
?????????????????????23?010?2??10??1??0?0121[23]0000300000??0001???00?0???????0???2
1?1?0?????????????????????0?????300100012??????????10???????1?????????????????0?0011?00?
??0210?[12]??10100001010?1?11?112100111??0101?0101?10000?0?????021[01]101311[01]11
00[01]100?0?1?0??0?00??????0??00?1110[01]?1?00??1?0??01100????????01??1????????1100
?11??001?11??????0??????????0?0???????0?????0?????????????????0??????????0??0??????????
??0???0???0???????????
????????????0???????0?0??0?0??????????00111?0?1?00??100???0000??0?01?????????0?????0
?0???00?0??0??100000??00?1??0?????????????00?????????0?????000?????0????????000?00?
?????????????00100?????????0??1?????????0?1?

Apsaravis_ukhaana?????????????????????????0?????????????????????????????????????0002?1?
0??0?????????????????1??11??10200??1???5?100021??24??????1?0101103110000111 13003??0
00?1???1?201000?2?021?23?03?12?010?????1??1213010 0?00000??20???1?20?0?????0?00??2
1?????????????????????????????300?10?????????????????????0?1[01]?????1?0????????20010?[
01]001??21??1????????00000?0?1000121011111?01011010[12]011111000010102 1110?[23]12
0100?11??20?1[01]0010?11?110?1012112111111?0000?1?0??01101????????011??????0?1????
????0001???
??
???????????0?????????01???0?????0??0?0011100010001?1?0?1?0000????01?010??????????0

000??000?????????????0??0??1????????00?00100?????0??????0???????0????0000000????00000
????000????0?000?10????????0?0?11????0????????

Yixianornis100?????2?021??1?????0?01????0?1?1?0??????????????????0100??????000?010???0
?00?00120???10?01???1???0000??1?0?40??0???0024???11?1100011031110?00101300001000
21?101?212003020001023?23?0211?0??1??????213010010000??000?0??1000?20??0?000001
???????????0??0??0???0??0?1230010001???????01??1????????11[01]?????1?0?????10?200110
00?11021??[12]??10100001010?111101121001111001?0110???01?000???0?01021[01]10?31201
100[01]100?00100?00?002?101??????11110[01]?1?00??1?0?001100?????00011?11?01????01
00?10??000??1???0???????????
?????????????????????0???0????????
?????????????0?????????????00?0????????00111?0???000?100?1??000????01????????0?????
0?0???00????0??100?00??0??1????????0???0????00?????0???0???????0?????0???0????000?00
????00??????0??00100?????????0?11????0??1?????

Sapeornis?001?????????????????0?010??11000????00??21?0?00????0??????0????0000010??10?0
0000020?????00????1???000????0?211??0210004??100?????2110111101001110000101121?
?00?212000?201[01]00221210????1??01??1001210?1003000000000????2000??0??0100??011
1?000???1???00??0???0000??230000000000?????????????????????????0?00???000000001000
0100????????000002000?00000?01000100?0?01010?0010000?0???010?1[01]10?11100??0[0
1]00?0000?0000?00?000??00?00??000001?00??0?00001000????????001?1?1011?1?110001000
000??1?000000??????????0?0???????010??00?????????01??00?0?????????00??0???????????0??
???000??0????????000??00?????????????????????????????????????0000???0??????0????0?
??????0?0100???????000??000?0??????0?00111?1?1?000?000???0000??0?01?0???????0?????0
?0???00?0??0??100000?000?1?10?0?0?0??0?1???000000?0???0????1??0???0?0??????0?000?0
00??000?????0000010?0?0?1???00?1?????????1?1?

Neuquenornis_volans???????12????????20?????????????????????????00?????00?????????????
????????????????????????????????00?????????????????????1?11011?1031110?01111000?????
????????????????????????????????010???????????[01]010030??0????0??????0?00???????????1??
?????????????????0???????0200??0110???????21
1?????10110??0100?001?001?0??[12]??1???01?0???0?????[01]?????????2???20?1??01???????
?????????10?1????????1?0???1011???????0?000???20000011?????????????????0??0???????
??
????00???0????????????????????????000??0100??
????????????????????????0111?????0????????????????????????????????????0?0???00????????????
00??0??1???0????????????????????????????2???????????????0?????????????????????0010?0
????????0???????????????

Patagopteryx_deferrariisi?0???0010?????????????????
????????????????????????????????????2?????????????????????????????????????0?1?????????
??211101?????????????????????2?010001??10012130100l?000???????1????????00?0?????1??
?????????????????????0?????0?????????????????00?1??????00??1111100000?????????0100000000??
??????0????????000????0101?1210[01]00???[01]?10?0???01000001[01]0001?[12]00???30????
???00?2000000?010120????0?000[12]11001100000?[01]?0??0?100?1?200??01?0???0?001????
????00???0?1???

????????????0??????0?0??0?110?????????????????????0?????????????????????????????00020000
??00???????????0?0?00??0001?00000????????00111?00100???????1?0000???????0100??0?0???
0?000???00????0??????00??0??1??????0?10???????????00???010???????00000000??0?????000
000???00?1???0000001 0??????1???0????0???0?1???10

Cathayornis?0?????????????????1?010?????0?1??????????0?????????????????????00???????????
??00001???????0????????[02]????????3?????2????4???0??11?02?1031110?011?1300?0?01111
?0?00?12000?201?1022?23?????????1???0??[12]1[01]1?0?3000?0???00????0??1??0??0100???
111?????????0??0???????0????2300[01]0?012?????????????????????????????0??????0????0111?
?0010?20??1??10110?101????010?0120001001011 0[01]?01020111110?[01]?1?????210120?11
?01?0101011?0?000001???1?0?0?1[01]1?0???????????0??01110????????01????????01????????
??0???110?00000??????????0?0?0100?10100?000?????????????????0??????????0??00??????????
?????????????????????000??00?0?0?????????????????????????????????????0??00??00??????????
???????0?0100???????0?????????????????????00111?0???0?????????0000?????????????????0?????0?
0???00?0??0??????00??00?1?1??0?????????????????????????0????100??????0???0?????00?00???
???????????00100?????????0????????????000??

Concornis???
??????????????????????00?????????????????????0??11?02?1031110?0?1???0030?????????????120
?102??11?23??3?0???1???1???0?1[02]11??0?3000?0???0?????????????????001??1???????????
??????????????????2300???0111????10?20??1?010
1100101?0?0010001?0??[01]001?110??0102?1???10???1[01]1?[12]??????????????[01]???????
?????00?????0?100??1?00??1?[01]1??0??????110?????????????????????1100110??01?????????
??
??
??????????0??????????00111?0?1?0?????????????????????????0?????0?0???00???????100?
00??0??1?????????????????????????????0?????????????0????????0?????????????????0??0010??
????????0???????????????

Gobipteryx?0?????????????????1?01010?0?0?????????????????????????????11?000?0????????
??1?1???2????????????????????????????????
??????????????????????????????????11?????????????????????????????????1????0????????????
??????0????????1100100?00110?10?????00?????0???0??0??1?????????????10??????????11??
10000?0?100012000[12]001?1?0110???0????????????1?121??[012]0?????1?0??1????????000?
0???10?0011111000?1?11?0???00000?????????
?0?1?01????0???0?0???
???0?????????????????0?????????????????????0?01000?00?0??00???000?????????????????????
??0????????????????
??????????????????????????????????0?????????????????????????????????????0???0?????????
?????????0???

Vorona???
??
??????????12?0100111010011211 0???00?????????????????????0?????2????????????????????
??
??101011110000

1?000000?????????????????????????????????????00?????????????????????????????????????
??
??
??????????????????????????1??????00000000?00?????????????????????????????????????
0?10001?????????????????????????????????????110?0000001?????????0????0?????1???1?

Songlingornis?????????????????????0?0????????????????????????????????????00??????????
???000?0????0????????????????????????????????????11??[01]???3????????????????????
??0????0?????0?????00????????????????????
??0???????0?????????0?01????????????????????????????????0?????????????21??[12]?00
0100?010???1?11011???
?????????????????????0??0?????????????1??1?????????????????????????????0????????????
??
??????????????????????????????????0??00??00?????????????????????0?0?0????????????????????
??????1?1?????0??1???????????
??????????????????????????00????????????????????????????????????0?1?????????????????
?0???

Pengornis_houi?0010?????????????10010??0?00??????0?12??0??????0?????0?????000?001?
???????0?0?00??00???01??????20???0???2??????????4????1?????2?1031111?0??????03??001?
1?????????????????2??2??????????1??????211???0?000??0??000???0??0??00???0???11?1?00
0??????????00????0000123000?000?????????????????????????????0?????0???0011??00100??
??????01[01]00?00??????0??1??012111[01]0?011010001[01][01]1?????1??1???10[12][12]0??1
??1?11??????0????00?0????0??0[01]?1?00??1?11??0?0??0?100????????01????00?01?100101
1???1??110?00000????0??0??0?0?0100??0?????00?????????????0??????????0??000??????2?
??????????????????????0?0??0?????????????????????????????????????0?0?0???0??0??00???
0???????0?0100??0?0??0??1?0?????????????00111?0?1000????0???0000?????????????????0?????
0?0???00?0??0??????00??00?1??0?0???0????1?????????????????0????1?00??????????0??????0?0??
???00?1???????00100??????????1?1????????000??

Hesperornis?0?????????????????00010100?00?????00021?001????00???00????1?000?001???1
?0001?021???00??1010110?2100??11?50100?210?24??11??10??00103111??????????3??0202
100?1??01000???021023?03?12???0001??11?1213110010??0?00??01?1?0000?000???00??2??1
?1111????0???????10000??10?1?10?1121200110?1010??1110011100??00?0???101012101100
0012?0?000100100?0???10?0???00011??0?????????0???0????0?????????????????????????20?
1100001112110211110021111122122002?0?????00??????0001?0???0?000?0100?11???1??01?
?00000??????????0?1?0100??0?????00????????0???0??0??????????0??00?????????????????00??
0????????0?0??0????0?????????????????????????????????????0?000???0?????????????????????
000????????0?0??000????????0???01?????????????201??000????01?????????0????00?0???0??00
?0??????00?????1??0?0?0?0???0?????????????????0?????000?????????0?????0000?????00??????
???001?0??????0???1???????????000??

Baptornis???
??????????????????????2?????????5?????????24??
??????????????????????????????212??????????????????????????????????2????????????????????
???????????[12]?????????????????????11001??00??1???????????12101100001?????012?0?????0

1?10?0???000????0?????????0???0??????????01?[01]1[01]???????????????20?1100001112110
2111100211111?21020?2???
???
???0???????0?0??000???
????0???01???????0?????201??000????01?????????0????0000???0????????????00?????1??????
0?0???0???????????????0???????0?????????0?????0000?????00?????????0210???????0???????
????????????

Ichthyornis?????00????????1220????????????????????000111????0???????????000??1?????10
00??0210??10???1?01111?2100?1???5?000?21??34???01?100?001031110?011113003??0102?
1??10212000????21023??3?12??10011??11?1213110???00?0??20?????00????0??00????21????
???????0?????????????012300[12]0?11???????????10[01]1?111011101001020???101?1200111
?101[12]?2110220101000001010?1111011211011110010110111010000101[01]1011211112312
0110011?12001[01]0010?11211021111002111l[12]2?100002?0??011?100?20???0110??1??00?
00100?11??01??01???????????????????????????0?00?00?????????????????????????????????
???????????????????1?0?????00??????????????????????????0????0100?????0?00?0000?00???
??????000?0??????00??000??0?01?0000??????0??00111?00100?0?10201??000???01?0????
???0????0000?0?0???0?0??1???00??0??1??????000??00100?0???001??01??2?0?00000?000000
00????0000?????00?111?0?00001????10?1?0?0?11?0??0????0??0

Iaceornis_marshii??
??1101?010311??????113?03?????????
???????????????????????2??1??1???????21?????????????20???1??0????????????????????????
???21?02[23]1
1???1101010?111101121O1?????????????????????????????111314011101110200l0??1?1?12
110212110021?????????????????????????????????????0100?11???1???????????????????
???
??
??????????00111???????0?10???????????????0??0??0??????0???????????????1??????????1????
???????00????0???00???01???????????????0??????1??????????????1???0?00??????????????11
?0??0????????

Limenavis_patagonica???
??011?13?????????
???20????????????????????????????
???
????????????????????????????????????10000[01]010101011?11[12]313011?011?????????????
???
???
???
???????????????????0?0??
???????????????????????????????????????0000??
???????????

Lithornis100????????????????01010100?00?111??2?02?00?0???????????????10000?00????02?
101?1?????????1????????2????????[67]?1????????????[12]??11000010311110011?13003??000

210101?20200102??2102?????12?01000???11?1213010?????0??200?01?2010???0?0?0???21?
??12???????????00???00000??300?1121210?000111110101?0?11[01]1101?1111?01?1012101
2?0111[12]12111221101?0?0101101111011210111110011?0001[12]111000010101010111111?3
130110[01]11102[01]0120110?11211020110002111122210010[01]?000011?1????????011?111
??00???????????01???1???
??0??????????????0?????????????????????????
????????????????????????0???????0?0?????????????????????????????????1??000????????????????
??????????????????0??0?????????????????000
0???

Hongshanornis_longicrest101?????????????????11010?????0?11???0????00?????????????????????
000?001??00????1?1?10???0??0??01??1?0????????[234]??????????4???1??11?0111031110001
1113002?0112???01?20????????2??23?23??2??100?1??????21[23]0100000000?000?01?1???
?????0?0????1?1?0?????????????0????0000?1?300???012?????????????????????????????00??????
1?????0?????110????????01?0??11???0?10???2100?111???110???2????0????????????1??2000?
?000100?0??0?0??000????????1???1100??[01]?00??2?0???1?????????????????????????0100?11
??001?11??????0??????????0?????????0??????0?????????????????0??????????0??0?????????????
????????????????????????0??0?0?0???0??????????0???
?????????0????????0?????????????????????01?1?0?000?0?10?????????????????????0?????0?0???
00????0??100?00??0?????0??????????1???00?????????0?????????????????0??0?0?????????0??
????????00100?????????0?????????????1???

Liaoningornis_longidigitu???
??3??1??0??????????
??????????????????????????????????100?1????0?2121100300?????0????????????????????????
????????????0??011?
01??????????0???0?????????????????????????????0?????01???2?????????????????????????01
?1?0??00111111020100?00???
??
??
????????????????????0?????????????????????????????0?????0?0???00??????????00??0???????
????????????????????????0??0010??????????0????
??????????1?

Crypturellus_undulatus10????012?020002?2001010100?00?111?12002100001011100010???1?
10000?000??102?001?1?????????1110111122100?01107?110??12?24??121?1101001031101101
1113003??00121001?2022011200210?3?23?12?0100010011012130?0???01000200001?200
00200?0?001021???120??01??????0????000001030021121?1[01]0100011111010110011011111
1111100101012101011211212111112?1010002101101011111210011111101100012011000011?0
1010111110314010111110?0?120110?112110202110021111222100101?0??011?10102000001
111110000??1100?10??01??11???
????????????????????????????0??0???
??2?????????????????
??????0??
???????????0?????????????0?????????????????????????

Gallus_gallus100???102?021002?20000101 00?00?111?120021?0001?1000001????1?10010000
0000021101?1?????????101[01]1111221?0?01007?120??12?24??1[12]1?110120103110200111
13003??00121111?2?2001120021023?23?12?0100011011??213010010001000200100?201002
00?0?0???21???121??01???0??00???0000010300110212121111122110111111111111101100011
0101112101011201112111121101000210111111111121001111101100012011000010111010111
1111314010012110 21?121111?112110202110021111322200111?00?011000102 0?0001111 1?
000??0010110??01??11??
????????????????????0??0?????????
??2?????????????????????0
??
????0????????????????0??????????????????????????????

Crax_pauxi1001011?2?021000??00101010 0?00?111?120021000011100000100??1?100000000
0000021101?1?????????1000111122100?111?7?120??12?24??121?1100201031112101111 3003?
?0002100?1?2?2001120021023?03?12?0100011011?121301001000100020 01?1?20100200?0?0
???21???121??01??????00???0000010300210212121111122110111111111111101100011011011
1210101120111211112110100021011111111112100111110110001201100001011101011111131
1401011211021?111111?112110202110021111322200110100001100 0?020?00011111100 00?1
1100011??01??11??
????????????????????0??0?????????
??2?????????????????????0?????
??0
????????????????0??????????????????????????????

Anas_platyrhynchus100???102?021002?2101001100?00?111?10002??00?1?100010?0???1?102
0000010 0?021101?1?????????101?1111221?0?011?7?11???10?2410121?1101111031111110111
13003??0012000?1?2?2001120021023?13?12?0100011011?121311?0???0100021 01?1?20100?
00?0?0?1021???121??????????00???0000011300210212111111122110211121111111101100011
1101112101010201112111131201001010 10?1[01]1111121000111001100012011000010111 01
1111112314010101110 21?111110?1111101021100 21111[23]2210010210?0011?10?020?00011
1111?000??0100?11??01??11??
????????????????????????????0??0????
??2?????????????????
?????0??
??????????0?????????????0??????????????????????????

Chauna_torquata000??1012?0210002?10101010 0?00?111?100021?000101000101 00??1?10000
0000??0021101?1?????????10111011121 00?111?7?11???10124121 11?1000010311111011113
103??0012101?1?2?200102?021023?23?12?0100011011??213010010000000200101?20100000
?0?0?1021???121??01??????00???0000012300110212 1[12]1111022110111121111111011000 1
1110111210121020111211114010100101011111101112110211100110001201100001011101 01
1111231401011111021?111111?112110202120021111222200100100001100010200010111111
0000?11101?11??01??11??
????????????????????????0??0?????????
??2?????????????????????

0??
??????????????????0??????????????????????????????

Pedopenna??
??
??????????????????????????0?0?0??0010??
??
??00?00
0?????0??0????00????????0???11?????????????????0??
??
??
??????????????????????????????????00????0???00???????????00??0????????????????????????????
??????0??0?10??????????????????????????

Epidendrosaurus??0??1??????????????????10????????
??01?????0???????0??????1????????????????????????????????????001??1??0?????001????????
??????????????????????????????0????????0000030?0?0???0?????1?????????????????1???????????
??????????????????3?0??0???????0?????????????????
???0??0?0??????1???0?????????0???0???0?????????????????0??????000?????????????????????
????100?00000??0?0??0?010????????00??????1???????????0??00????????????????????????????
??0????0??????????
??
??0011??????0????????????????????????????0?????0?0???00?????????0?00??0?????????????????
??????????????????0????????????0????????0??????????????????????0010??????????0???????????
?????

Epidexipteryx?01?????????????????????1?????00?????0??2??0011?????????????????100?0?0???
?00001020???10000?????????????????0?[01]????1?1?123??10??0????0101?010?0??????00?1???
????????022?????011?03?0??????????0????011?0??0?10?000???00??1?1?0???00?0?00???0?0?
????????1??2?????0???????2?0?????0??????????0?????????????????????000?0????00??0?0??
????????????0??0?0??????1???0?????????????00?[01]0??????????????????????????????????
??????????????????10?0?0?0????10?00???0?????????1??11??1????????????0?00?100?????0??????
????0?????????0?????0??0????
0??00200??02??????????0???????0?1??????????????
??????????????0011??1???0?????00??????????01?????????0?????0?0?????????0????0?0????0?
???????0??????????????????????0???????00??????0???0????0?????????0??????????001?00???????
??????????????0???

Incisivosaurus_gauthieri?00?00?01?001??1??10001110100100 1?010?120000110001010110101
1112101000010 01?1?000210??00?0??
??00??00??01?0??0?0?????
????10000000100010 2?00010?100??????000000000010000 1??0000???0000101?1100??0000??
??
??01020?00???0??000?0?0?????????????11?110
0000????1000000?0?0000?000?0?000???1000??1??00?0????000?110??010??01?0000?00000??
?00?00????0100??0111000??????????????????00100000010000????00200??02?01?0000000000?

????00110???
?100??????????????0??0?001????????????????????????0201100?????????????????????????????
??????????0?0?0??????0??????????000?0

Citipati_Osmólskae?001001001001??2210001011111?01011?00010210001100001000100011O1
21120?010001011 1?1?????????10111011001012110O1??201??002200111?01112001101001OO
?1100000100021100 1??02012020??1011111 1?2101000000000?00000000000000000000110200
00000?0?001000?000002011???0???[01]000020001220001000000001102?1??0000??00000100
01010??0000020011000[01]0?00?0010000101020??????0????111000?0?0010000?0000000000
00?00100?0??0?0???0000000????00000?2000000000000000000002?000?000000000020?0001
10??00[01]10?0110110000000 11?1100001????1000001?0?0001?11000?001???1002??0???0?0?
???000?000??000??01?0000?000000000100?????100??0111000????????????????1010000000
10000????10201???2?01?0000000???0???10???00?00?
?????????????????????????0?0?0???00100???000?00??0???0?00?????????0?0?0?00?0???0?0
0211??????????0??00?000?0???????0??????0?0000100?0100????10??????????1?00?0

Oviraptor_philoceratops?00?0??????01?1????0??1??111?1011???0???1?0?11???01?0???0?11?1
21120?01?00?01?1?1?????????????????????????????????0????????????????12??1?????00???10??
00?00??1??0?????????????????????????????0????0????0??0?????00?00000???2?00?0??????????
??10000?0?0???????0??0???0????00???0?00????????10?0?00??0??00?00?1?1????00???00?100
????0????????01010?0?00?0?0????1?100??????1100???0????????00?????????000?0??00000???
??????????????????????????????????0??000?????20????1?0???02?0??1101100???0011?1?????
1????10????1???0?01????????01????????????????0??????0???00??0?0??0??00?????00??????????
?????????0???1020????2?01?0000000??????????????
?????????????????????????1???1???0???100????000
???????????0?????????????????0??0????????211??????????00??????0??0??????????????????????0
0??0??????0????????????00??

Microvenator_celer???21?20?0
?????????????????????011?0?11000121100???0?1?1002?????????????00?000?11000?????00100
02???0000?????????????1110??0101100?0000010???????0??0???00??11?20?0??00???0?1??0??
??????????????????0???0?2200000???????????????????????????????????????0?0001????????
????????????20000?000?01?????00?0??010?00?00000000000010000?????00????????0???0??
00000200000000000????????????10??0???????????????1????????0???????????00????????????
??
???0???00??0
001?01001?????????????010000?0?????100???????01?01??0000???00??????????????0?????0??
??????1????000?10?000???0010?0001????1??????00??00?10??00000000??000?0??00000?????
?????1?01??11100??001?????

Caudipteryx_zoui00010???????????????0?111??10?0001?10???21000???0?0?????????????21120?
0????????0?1??0?????00????0??00????1???0???01?????30?????0???0??0???01?0???100000?00
0?1??????0201202???1????101?11?????0????01000??1?00?0?000000?1102000??00?0?001000
100000?00????0???00?00000?1[01]2000000000???????????0??????0000????1000???0000?00?
0000?0?0??????????????20??0?0?000?11??00???????0?0???00?00?????????????1??0000???0000
000?000000000??0?0?00????0000000??0??2000000??0????????01101100??01?110???0??000?

10???0000?????0????0?0?0001?00?????0?????????????????0????00???00??0?0??0??0?????????
000?0????????1????0???00201???2???????????0??????
???0??0?????????????????????????????1???????00??000???0000?????????????????0?00??0?0???00
1?0?0???00?0???0????10?????0???000??0?00?0???0?0???11??0????00????0?000?0000???0?0?
????0?0?00100???0?????????????????1?10??

Ingenia_yanshani?00?0?????????????????1?1?????1?????????????????????????????????21120?01
000?0111?1?????????????????????????????1???01????2?00???10111200112??00000??100000100
021??????020120200110112?1110110?0000?00011?000000000??0000??11?2000?000?0?00100
0?????????????????????0002?0??2200?1000000??1?????0?0??0??0000?00??1?10???000??0??1??
0[01]0??02??????0101??0??0???0?0?0101000?????1100???00?0?????????????????00????0?00?
00?000?0?000??0?0?000?0?0?0??00?0????00?000000????????0110??00?1?0?1101000??000?1
??
??
??????????????????????????0011000?001?0?01??101000??0101??11??0??????00000???00???
??1?000000010??1?1?0??????10???0???0??0?000????11???0???0100000001000000000??00010
0?000000010???????????0??1?0??00?1???1?

Rinchenia_mongoliensis?00?0????0??????????0111?1???1?11?00010??00???0000?????00??1?1
2112??01000??111?1?????????????????1?????????????????0?????220??????????2??1???00?0???1??
0001000?1?????1?????????????????1?????????0????0??0?0???????0??00??001???2?00???????????
???0??????00????????00??210??????2??0120????????10?0?10??0???0?????????????0?????????
??00???0?
00???002?0????????????00?1?1?00001????
1??0001?0?0001?11??0??01???1????????????0????000?000??000??01?00???0?00000?0???????
?100??0????0?????????????????????????????????0??
??1?1001?????????????????????????????0?????????????
??????0?????????????????0???????????11?????????????????????0??????????????????????0??????
????0?????????????0??

Conchoraptor_gracilis?0010??????????1???00111?1???1?11?000??2100011?00????1?0????12
1120?010?0?0111?1?????????0101011001??1?012?110??10????01?1?????2001100001?0????
???00100021000101020020??101101[01]1?11010000??000100000?000??000?001102?0?0
000?0?00100010000200?1???????0?0?0200012??????000000000????????10???0100100??????
??000??0?010??
???????00?00??000002000000000000?0000?002?01?????????0?020?000??0??002?00?????????
??0011?1?00001????1??00?1?0?0?01?11??0??01????0?2????????0????0?0??00??0?0??01?00??
?0?00?000?0?0??????100??0???00?????????????????10???0???????0?????????????????????
??0?0?????????????????????????0?0
????010?????010?????0?????0???????10??????00?0???????21?????????????????0?000000????
???????????0?1?00????????00?????????????0?0

Chirostenotes_pergracilis?????1??01?01101??0???1?110?0?????????????????????01010??????
21120?00000201???1?????????????????1101?12????1?12???0?????????????????101?1?????????
00?100021?00101022120201110?111[01]??01??100???00?100000200000??000?0?1??20?0?00
0?0?00100?????????????????????000?????[12]????10????????001????00?????????????01?10???0

????0011??00?????????????????20000?00000??
???00000?00??00000?00?0????????000000?0???0000?????001020?00???0????????1????????0?
001?????????????????????1?0?00???0??
??10000010000??????00200???2?01?000??0000?
?????????0???????0?0??00???1000?0?????????????0??0??101000?????1?0100?0??0?00??0000
0?001?0??1?1?000?01?????1?0??????10?????000??0??????02?1???0110?1???????000000000??
?00????00??00010?0??0?????1?0??0????????0?1?

Avimimus_portentosus?00?0???10011?00??0??1?1???????1???1????00?11??00100110??????2
?1???00?0??0111????????????011010110101?1?00??100?????????????????????0100???????
???00?211?01??02012020102011?0?1000100?0???0001111002O???00??0?0?01?02?000000?0?
001000????????0?????????00?01??0?02001?????????????????????0??0???00??0??????????0200
1000?????????????????????????????0?????0?0?0010000?000000000????????????2??????????
?[02]0?000?0000020?0100000000000000??00?01??0??????0?????????????????????????????
1?0??
???????????100??0?1100?????????????????????0000001?0?00????????????????????????????
?????0???????0001000001?????????????00001??????101001??0101?0100?0?000??001000??
00???????0??0?1001??101????0000100000?????1001101102?????101010000000????00?000??
?00100000000010?0????1??01????0??00?1???1?

Falcarius??01?11100001111010?????1????00??????????00??????0000000??????100?000??0???
????001010001?1??000111010121010001200010O??0000?????000001000100010?000010O?0
11001010220301010100100010000000000001100000000000O??000?10?00?0?000?0?00100
0?????????0?001???00?0?0?0??11?0??000???????000??00???0??00?00100?0?00??0000??00100
00[01]0??????????0100020000?000000001110?1?0?0010000?00100000000010000???0100???0
000000?000000000200000000000?00000000?0000??00000?0?200000??0???00000?1100?000
00000?????????????????????000?00?00100????0?????????????????????????????0?????0?????
?????????00?00????00?00?????????????????????????0000001010010????0??0000000?1???0????
??????????0?0???????000100000100O??1000??101000000010000000000?0101?01000000000
1?000001000?0??00101000010?1?01?11?10001001000000000111010O2?0?101111000001010
000100000??000001000?000000?0?10?10000?01101100O?00?10

Beipiaosaurus0??1???10?10??????
???????1001001?100????1?????????????000??0220????????0000??0????0?1000000?0000??0
01???20220??0??0????0??00?0??00??????0000????0???0??00111???0?0??0????0010?0???????
???0??????????0???0??????0?????????????????????????????????????00????001000???????????
??00?00?????????????????????????????????10000??????????1??0100???000000???0??0??0????
?0???????000000000???0?0?00000????????????10?????1?1100??0??000?1?0?????0?????????
???????????0???
??0??0?00?????????????????????0???????0???????
???????????????1???0?00??00???00?1????????10?????0?0?????????00???????1?1?0????????1?
?1?????10???000?0?00?????????????????????0??0?01000?0101O???0?11??10??0?1?0???1???????
?????????????1???

Segnosaurus_galbinensis???21?
?10?0000?000???0100?001????????1??????????1?0?0?????????????????????0?10?1?00000????0??

?2001110010202022 1??0110201101?11001?00?00?1100000002 1?0??00?01?1??0?0???00?0?01
0?00??????????0?????????00???????0?????????????????????????????????????0?0????0???????????
????????????????????0??????0????1????1???0010000?00100000?????????????????????????00?0
0000??10??????00?????000000000??21?0????00?????????????????2??????????0???????????
??
??
???????????10?????????????0?00???????2102001 0?0101??02????????????0?00?????????????0?
?01??0??1??1????????2????????0??110????????1???????10100??1?111222101111111112?11120
1??????????0???1????????????

Erlikosaurus_andrewsi?0012???2?0?1?1??10100111 00??0001?100000100001000000000??111
12100100000020001?001001001???0???????
??0000?021?0??00??11??00?0?00????????
????0?0000001001 0??00000?000????0?000002000001???10?0100???0000?0?10000??0000????
??1?0?0010000?00100000 00?????????????????????
????????????????????????????00000000????????0000?0????000?????000?0?????????0????01?00
01100????1?10000?0?00?0?100000000???0??0?00??00?0????00000100000??00?0200?00000
101000?00001?000??00?0?00?????????????????00000001101????0???0100100020000000000000
000??????0????????????????????????????????0?00??
???0000???????00??0???0?011????????2??????????????11210?11????????1?0?1??????????????
?????????1?0100100 0????01??????????010?0

Alxasaurus_elesitaiensis???210
?100????????????1001001?????????0?0101 0000?1?0101002?0?1???????????0?000??0?10?00
00120?11??0??1?20?21???11?????????1????0?????????00000?10000??001?1??00?0??00?0?0??
?00??????????0??????????0?????0????0????????????????????????????0??00????0??00??
[01]0????????????????0????????0??11??01??????0?0???010000??????????10?0100???000000
???0??0?????????????????????????????1000000?0????????0?????????????????????000????????
??
??0??0020?????????????????????0????
???????11101?????1??0?11??0?00??010?0?????01?????????2??????????????200??0????1?1
??0??0????1??1?100???????0000000??1??0???0?00???11?0????01100??11?1????1111?????1?
00???10?1???0?????????????1???

Neimongosaurus???21????0???
??????????0??001?1??000?110101?1?0?10?2?1?1?02200????????0001010000??????????????11
1001?2?????????????????????0??00????0??00000002 1?00????0??1??00?0??00?0?????0???????
????0????????????????1[12]200?0????????????????????????????????????0?????00?0000?0????
??????0000020 0?0?00000?0?11001?0?0?10?0???010000?0?00?????????????????????0????????
???20?00???????0?00000000?0210??????0????????0???????????2?1100?000?????????????????
??
??0????2?????????????????????0???????0??
1??11???????0??01?10?0?00???????21?2?????????????2?1???1?00??00000?1???0??00????00???
?00??????100010?2???????00?????1???0?0111?1110010 11????1?1121?????111111????10????
1??11??0?0??0?100???1?1?

Erliansaurus??
??????????????????????????10??1??????????1??????????????????0?0???10?0?0???00000????1?0?1??
????????????2??1????10?00?0?0001?0??00??????????00??????????????????????0?????????????
????????0??????200??0????0????????????????????
??????????????????01?0?0?10?0???010000???00010???????100???000000???????????20?00????
???0?????????????????0??????????????????????????????????000??????????????????????????????
??
??0????????????????????????
??????0?0?1?0?01?????????????????02?0???1?000?????????????00100???????0?????????00???
100?????00?11??????????????????011?111111??11?1???0?1?1111101l?0?????????1??????????0
?1?????

Suzhousaurus??
??????????????????????????0101??01000??0??1????0??????????001010000???????????200l11001
?2020?2?1001002011010110?00?????????????????????0???????1????????00???010?????????????
???????????0?????0?0???20010000[01]?????????
???????20000?00000?01010?1?0?0010?0???0100000??00?????????????????????00?000?00?10
20000?????????????????????0?????????????????????????????2????????????????????????????????
??
??
??1011
1100100000?11010?00??????021020010?0101?00201010?????????????????????0???0??01??00?
1????1000?0?2????????00?????????????????11?10001l????111221211110?????????????????????1?
0??01102?0?2???????

Nothronychus?????1112??11?1?0?0?????????????????????????????????00000?????????????????
???????????1?????????????10101?10?01?1?00?100220?001?????00000?100?00????000020??
10?1?2020221100100201101?1100100?10001100000002l?00???00??????0?0?000?0?010?00??
?????????????????????0????1[12]200??????????1?????????????????????????????????0010000[0
1]0??????????00000200?0?00000?0211001?0?0?10?0???010000???00010???????000???00???0
0?000000?1020??000000000?00000000?0210??0?000?0????000????????0???1100?000?000???
??
????????????????????????????????????000?01100??
?0????????0?0??1010110???0000?110?00001?0?0?021?20010?1101??02???1?10000?0?000?10?
????0?1?0000010?0??1?11?1?00100200000?00001110?1?2??????1?1110?0001???11112221011
1111?1210112O??0????1?1?0???10?????1???10

Enigmosaurus??
??111?01?20
20221100??0201101?????????????????????????????????1????????00???010?????????????????
??
??00?000000?10?????????????
??2??
??
??1??1???????
??????????????2?020?10?1101?????????????????????????????0??01?????1?????????????????
????????????????????????????????????1?122121100??

Nanshiungosaurus_bohlini???
?????????????????????????1???????101?121???0??
??
??????????????????0?????1???200??0?????????
??0?????????????
??2????????????????????????????????????
??
??0??????????1???1??0
??????????????????????21?2??10???01????????????????????????????????01??0??1?????
????????????????????????????????1?????????????11222??11????????????????????????????
?????????

Therizinosaurus???
??0010?0000????0?00200?????????
??????????????????????????????0??0?11000000021?0????00????????????????????????????
??????????????????00??0?????????????????
??2000??00000?01?1001?0?0?10?0???010000?????010???????100???00000?????????????????
?????????????????????0??0100?????????????????????????????????00????????????????????
??
??
???00?1010?00100101???001?0????????0??????????
10??0000?????????????????????????1110111111?????????????????2?111?0?????????1???01????
0????????

Haplocheirus?0010???00010?0?120110111011120 01?0000201 00?0?1010??0001?00100000101
10110?1000001101010100??10??0?0111201??0?00001?0???0?00???????1002100012 10?0?000
10???001?00?10100201001 0?011000?00000000?0000?0000000??00?1110001100010001?0???
0010?0100000000??0000001?00000?1020000000000????00???00???0???000000??0??0??0000
?000?000????0?????????????20000?000000010101?????100???000?00???????????0???00000?
?0000000?00?000100200000???????000?0??0???0100?000???0?0??????????00?0??????????0?
0000001?00001??0?0000000?0?0100000 0?0??11???0??0?01??01?0????000001000000??00??1
00?000000000000?000????00??0??0?0??????001????????0?0??0?0000????0???00000??00?0000
00??00??????????000???????0??1????????????00?1010100??0100?00?0????????0?01??0???00?
0?????0?????00000?00?101000??00?0??010?1100100100010000011 0??00??0?101???00000???
0000?????????000????????00101???0?1?1?010?????0??0000??

Alvarezsaurus_calvoi???
????????????????????????????01000???0???0?20?0?2012???????????000?00????????0??1?000
0101?00?2?????????????????????01?000??0??0??11000000??00????????1???0?0??00?0?????0????
?????????????????0????10???00100???0????
???????????2?000?????0?0?0???0??000?00???
2????0000000?000???00?02???0?????????????0????????0??????????00?????????????????????
??
??0???????0001?00
????????00?10?0?0???????????000?000?????????????????0??00?????00?????????????0??0??0??

??????1000???????10?????101???????1????00?????????00000??????1???0?000?10??????1???
0?0??0??0????????

Patagonykus_puertai??
?????????????????????????1?01?112????012010?2?2??????????????00210???210?????1?0???
1????1010?????20????21202??11000000000001210??0????001??0???????0?????????0????0???
??????????????????0?????01???0?00100???????
???????????20000?000?00??????0?0?0000??0?0010000???0??????????1???????????0???0????1
0020000000000??00?0???????10??0??????????????????????????????????0????????????????
???
???
00001?01100?0?????000?1100??????11???0?0?01?01?1?000?10??1????0?00?????0????00?000
?0??1???0??1001?101??1?0?1111111?????????????0?00000??0?????00??0000?00?0?00??1?????
????10??1???0???0?????1?

Achillesaurus??
???????????????????????????????020???2????????????????????????????????????10??01?2
???????????????????1??????0??1?01000??0???00????????1???????????0?????0??????????????
???????0???
???0???????????2????0000000
0?0??0??0??
???
???
???????????????00?0???????????0????????00?0????0??????????????????????????????11???????
?????????11??????????????0?????????????000????????1???0?00???????????????0??????0???????????

Mononykus_olecranus??????00???????112???????????????????????????????????100??????????
??????????????2????00???????1?1?11102001???2?10?2???????1???1000?000200030210?02201
100??1????1?201000?2?????3??0??021010011101121200003000000l??00???1??0?0??00?0?0?
??00???????????????????????????00011???0?0010?0
?????210???00?????2?010?0?0?0?010?011?0?0001000?001000000000??0000???30000???0???
0??00????????2000000000000??0000??0?00?0??0??000???????01?0?????0?0????????11102????
???
??0
???????1001001000????????1010100000100?????011???0???01?010000010101?100000100???
?0??????00??1??0???021?1110010111111111101011???????0100000000000?000?0000??0000
10000?000?10????????100?10100?0?01???1?

Shuvuuia_deserti?00101002?01011112011000101l?01111?100201000010100100l0???1110?00
1010010021 00??0211??000??01111110111021 00?0?20101201211 0100?1000?0002000302 1??0
220110000101001?201000?2002203??03?021010011101121200003000000110000011000000 1
0000?00??00100000001?010??000000000?000100000000?101000?10000110?0111000??0[12]
0????0100?0010000[01]0?0210?0?00?????20010?000?01010101 1?0?0001000?00100000?000??
???????30000??000??00?000?00?1020000000000000?0000000?00100000?0000020?0001?01?1
010001???????1110200?000?000??0?1??0000?0?00000?00000100???0??0?00??01?0????0????
?0??000??00?0200?000000??0?0?0??00?000?001?0?0???????????????????000000000????????

00000?000?00??000000??00??????0?0???????0001001000101 1?0001010100000100??0?01110
000???01??1??????????0???0????00001????1??00??1??00110210?110010?1111111??0?01002?
0??00??0?0000000?000000000??000?????00000010101?0??0?00110????00?1101?0

Parvicursor??
??????????????????????10?????????1??2??1????2?1
000???02203??03??2??100011?11211000030??00?????????1??????????0?00??0?????????????
????????0?????0??0?00?00??????????????????
???0????????1?20000000000
00??000?000?00?0????????????????0???????????????????11??????????????????????????????
??
???1000?????00??
??????????????????????0???01??10??00?0?01??000??100???????????00??1????????1?111????
???????11100010?????????????0?????????????0?????000??00000000010??????????0???1?0????1
???1?

Albertonykus??
???211?????1?0????????????
??030?????????0???????????????????????????????????????
???
???
??0??02???????????????????????????????????
???
???
????1????????????????????????????????0???00????0??????????????????????????????????11???1
1??1??0????0???????????1??????????????????

Albinykus??
???0??????????
??????????????????????1101??121100300000????????????????0000?????0?????????????????
???
??0??????0????????000000000?
0000000?00??0????00????????0???????????????????11???????????????????????????????????
???
???
???????????????????????????????????0?010000??00???????????00??1?????????????????????
???00000?10??????????0??????????1?????

Bonapartenykus???
??????????????????????????112??0????????????????????????000210??????????????????????
01????????????212?2??1????????????????????????0???????????0?0???????0????????????????
??????????????0??00100?????????????????
?20000?000?000??10??100?????????
?????????????????0??
???
???0?1000??1?????0?

010?010?????????????????????0?0?01?????????????????????????00?????00???????????0???????1???0l
1?????????????????????????????????0?????????????????????0?????0?????????????????????10????0????
????

Ceratonykus?0010???2??10?????????????????11???10?201?0?0?0100??0?????????????01?0???
?????????????????????????1?1?????????????????????????????10????0?2???0????????????????????????
?????????????????????????1????????212?0003???00?????????????????????0?????0?????????????????
?????0?????????????????????????00???????1????111?????????????????????????????21?????0????
??0000?0???01?????????????????????0???00000
000??000?000?00?0?????????????????1????10?0?????????????????0??0?????????????????????????
?????????0?????????????????1?0????0?????0??000??0??02???0?0000??0?0?0??00?000??0????0???
?????????????????0??0?00?????????0?0?????????????????????????????0???????000l?????????
???0?0??1000???????0?????????????????1?????1
?00?0?????????????1???00?00001???????????01???????
????????

Linhenykus???
?????????????????111?101?1??1?0???2010020?2???????10?0???1??????????0?21110???????????2
?????????????????????0?1010001????2?2?0?030?0000???0????1??????????0?????0?????????????????
?????????????01???0?0012?0?????210????0????
?20??0???0?0?0?????????????????????10000???0??????????31?????00??0?????????1?20000000
00000??000?000?001?????0?0?????????1???????0?????????????02????????????????????????????
???
???0???????0001?01000????
?0??????1?????????????????????????????0?0??00?0?0???000???00?0??????1??0?????????????1011
????????1111?1???0?????????????0????????00???????????01??00?00001???????????0?1?110?
0????????

Xixianykus???
?????????????????????????102?00?21201??0?????????????????????????????????????0?01?1??1?20
0000?20022?3??03?02?0100111011212l1??3???000???????11???????00?0?00??0???????????????
??????????0???0?0010000?????????????????
???00?000000?1?2000000
000000??000?000?0?????????????????????????????0???
???
???1000?0???
?????????????????????0001100000???01?010??00?0?00010?0?????????????????????0??1???1011
????????????111??11?????????????0???????????0?0000??0000100000000001??????????0????100
????1???1?

Nqwebasaurus?0?????????????????02????2010????????0100?00??1?????0?00?????????????????
???????02????1??????00?11001???1?????????????????????????0102?000??0?00?10110??????
?????????????????????00?????0?0000100010000000?000?1??00??????0?0?0?????0????01?00??
?00?????????????????10200?????????????????????????????00?????????????????????????0?????
????????20????0?0???0101?0??????10?0?????????????????????00000??00000?????????00?
???????????00?0????00??0?0??00000????????0???????0?0??????????0?001?????????????0?0???

???0???0???????????0???0??????0??????????????????????????1?????????????????????000??0?
?0?0?????????????????????????00???0?????????????
???????????000??01?0?1?0?0?????????????????????????0????00?0???00?????0?111?0???1??0??
012?????100??000100001000011???????0?????????????0?????????????????0?000010??????????
0????????????1?1??

Shenzhousaurus_orientalis???0?????????????????210001?10?0??1???000??00?000?0????????????0
?00000000??0??0?1?12?0??1?????????????000??1???0???00000???0?????????????????????????????
?010000000??1100010010 1?000001100??00001?0??????????????????0??1??1?0011?????00???
0010??10000010????????00??0?00???0???00?000?????????????????????00?????0??????0?00?0?
100?0?0?0???0?????0?0000
0?00000?0002?000?????????????????????????00?????????????????00000???????????01?00??0
0000??0?0000?00?0?000000000??00???0??0??1???1?????????????????????????????????????
??????????????????????????????10???????0?????????????????????00?00??00?000?0????0???????????
??????????????000????????00?????????????????010100000?0001?00??0?????????????????01???
??0?10??00??1??00?2?0000????????100?0????????00?10????00????????00000000???00??????
???????0???0??0???1???????????1???

Ornithomimus_edmonticus?00010?1101101?10102100010101010110000000000000001000000
??????000000000010?1001?1????????0?001?10110000111000101000000010010000??????011200
12000000?2020010000001100011010110000011001000001100010001000002 0??00?01111111
012111000?0?0010001000000001?????0001?000000002100000000?????????0?0?10???00001
0110??????000000010000[01]0?0?????????????????0??0?0?0?0?01?1001?0?00?000???0000000??
00??????1??00000??0000020?000?000002000000000000?0??0?????0??0??000?1???????0???0?
?0000000????????00010000?00000?00?0000?01?0?0100000??0??00???0??0?01??01?0????000
001000000??01?00????0000101?0000??000000??0????0?????????????????????1??????????????
?00210???0?000000?010?????????????010?00?0000100001 1?????????????????????10?00???1????
?????????????????????1???????011110011111111?11000???????100??0???00?01????101?0??
?1??0?0000?10000000000????000000000000100?0????????1???????????10?0

Archaeornithomimus_asiati???
??????????????????????????????00?10110000111000 1?10000000?0??????????010200?2000?0
110[12]0???000?0110001101011000001020100000 1100??000?0000020??0000?10??10??1?1??
00??0?001000???
0?001000?[01]0??????????????????20?00?00000?0?0??01?0?0010000?000000000000010000???0
0000??000??00???0000000200000000000?0000??00?0?10?000?????????????0??????0?0?????
???00001???
??
???????????0???????0??1?00001?00??00000?0002001 0?010?01010000?01011?00000000000?
000001000????? 001?101?001?11?0????000010000001100001??011???????110?000001100000
000000??000000000?000?10?????101?0?1?000?000????1?

Anserimimus_planinychus???
??1??????????????????0??????????1?200?2????00?2020
0100000011000110101????001?001?????????????????00002???00????11??10??1?1??00?0?0010
00???

????????????????0????????0??1????????????????????????????????????01000??00000????????
????????????????10000??00??0??0??00?1????????????????????????????001??????????????
??
??
??????????????????????????10?0??1?1????????????????????????1?0??????????110110110012?
1?0????????100???01?00????????????????????????000?10?000????????????????????010????????
??????????????????

Struthiomimus_altus?00010?110??0??10102100010111012?1100000000000000010??0001?01??
000100000102000 1?1?????????001?10110000111000101000000001001005?????01120012000
000120100100000001100011010110000012?001000001100010001000002 0??0000111111101211
10000?0?001000100000000 1?????00?1?0000??2210????0???????????0?0?1????000?????0?00
???00?0000?0000[01]0?0?????????????200?0?0?000?0101001?0?0010000??000000000002?100
000??00000??0000000?000000000200?000000000000000??00?02100000 0?1002200000 0?0??0?
00?00?????????00100000000000?00?0000?01?0?0100000000000???0??0?01??01?0????000001
0?0000??01?0000??0000101?00?0??000000??00?0?0?????????????????????10000110102?00????0
0210???0?000000000?????????????00??00?0000100001 1????000000000200?110101?101001
00?01011?000000000000010001000001110011111111?1?110000??000010000001100001000110
0100???1??0?000011000000000???000?000000000100?0?0?101?1110000?0000?1010

Gallimimus_bullatus?00010?1101101010102100010112?0101100000000000000010000001?010
000000000010200 01?1?????????0011101100001110001010000000010010 0?????0112001200
000??201001000000110001101011000001100100000110001000100000 20??000001111110121
110000?0?001000100000000 1?????0001100000002210 00?000000100000 0?0000??00000?0?1
0200??1000000010000[01]0?0?????????????20010?000000010100 1?0?0010000?00000000000
00100001??00000??0000020?000000000200000000000000000?000?02100000 0?1002??0000?0
0??0000000??????? 0000100000000000??0?0000?01?0?0100000000000???0??0?01??01?0????0
00001000000??01?0000?00000101000?000000000?000?0?000?????????????????0010000111100
000???00210?0?000000000000000????????000000?00001000011[12]0000000000002001 1?0
1010101001 00?0101100000000000000100?1000111011111101100 1?110001??0000100000011
000010001101 00???1100000001100000000000??000000000000001000 0?0010101110000100 0
0?1010

Garudimimus_brevipes?000?????01101????02?00010101000??000000000000000000?00001?01
000000000000002?001?1???????0??0111????0001?10001?100??00?????10?????????????????
????????0000001100?????????????0??001000001?000?000?000001000000?01??1110?2?1?0?0
0?0?0??000100000000?????0000100000010???00?0000?00100000 0?0000??000001011000 0??
000000001000 0???0???
???????00?000000000200000000000000000000?021?0????0000????00???0??001000????????
00???000000000000 2?0000?00?0?0100000000000???0??0?01??01?0????000001000000??01?
0000??000000000000000000??00?0?000??00?010???????00100000010???0???00210???00
000000000000000????????0?0?00?0000??0001110000000?????????????????0101001 00?0101?00
00000?000000100?1000111?????001000?1?0001??0000???????????0000101101 00?????000
?????????? 000000??000000000000001 0000?0010??01??0011??00?111?
Pelecanimimus_polydon?00???????1????????2100?2?1??0000??000000?0000?????????????0?
000?0000??????000211??0001??000???0?0?111?00?????????????????0??0?00???120????00??0?

2010???1001010????0?????0?????0??
??10000??0?1?0????00????0000?0?10???0?0??????????0?0??????????????????????00???0?10??
????0?????????????????0??0?0?0???0?????????????????????????????????????1??00000??00000????
?????????????????????????????????????0??000???????????1?????0?00???????????001?00??00010
??0?0000?00?000000000000??00???0??0?01??01?00?0?0000011??000?????????????????????
????00??0?000?????????0010000????0?????????????????0??00??00?????????????????????0000
0000?10???????0?0?????????????????????0?01?????????????????????????????????????010?1?
?111??????0????0?2?0?????000001100???????????0?1101???????????0?000?????????????????
?????1???0??????1???????????111??

Harpymimus_okladnikovi?0?????????????????2100??????0??????000000000000?????????????
?000000?0000????1?1200??1???0???1???0?00??10001?100000?00?001????????0?1?00120000
0000010?10??00???????1?????????????00?00??????0??0?0100000010??00000101 1????1?0???00
?0?0???001??0000??1?0????00??0000??11?10000000?????????????0?????????????0000??00?0
0000?0000[01]0??????????????????????????????10??01?0?0010000?000000000000???0?010?000
00??0000000?0?0000?00?????00000000?00000?00??11??0000?0????????0???????000????????
?0?001?000000000????0????0??0?0?????0000?000???0??0?01??0?????????????????0???1?00
??????0????????????00000??00?0?????????????????????????????????????00210??0000??????
??0????????????0???????000??0000?1??0????0000??2001?00?01?1??0010?????????0?????????
?00?0??0001100100011??0??0?11?00????000???00000100?????011???0??01???00000110?000
000000???0?00???0?000?100?01??1?1?01??00??00???1???

Beishanlong???
???0102001200 0????0100??????????
??10???1??00?????000001100?1000100?01??000?0???1???0??1?1????????01000??????????
???????????????????210???0??0????????????
??20010?0000000101001?0?0010?00?000000000000010?????????????????????0??????????20000
00000000?00000?00????0??0?0?0????????0?0?????????????????????00?01?????????????????????
??
??
??????000000200 11?????????????????????????00?????0?00000?0???00?????00??1?0???0??1?????
?????1000000?1??00?0?011?????????????000100??00?????????????000000000001?????????1???
10?0??0??0???1?

Sinornithomimus?0001?????1?0????1?21000??1010001?000000000000000000?000??0???0000
0000?00????1?1?????????0001?0?10?0???100?1?1??0?00?0?0?100??????0102001200 0?01101
0010000001100011010110000001?00?000001100010000?000?010??000001011100121?1??00?0?
0010?0100000000 1?????0000100000?02100000000?????????????00??000001?1?0??????0000
0001?000?0?0?????????????20010?00?00?0101001?0?0010000?0000000000??0100001 0?0000
0??0000000?000000000200000000000000000??00??1100?0000?????????000???000000???????
?0?0010000000100?00?0000?01?000100000??0?000???0??0?01??01?0????000??10??000??01?
0000??000?????000000000000??00?0?0?0?????????????????10000????????????00210???0?000
0000000?????????????0???00?00001?000?????0?0??000000200?100?0101010010 0?0?01000?0
00?00?0??1?0?1?00111?1001110?1001?11?00???000010000001100001 00?11??00???11000000
0110?000000000???000000000000001000??0?101?011?000?0?00?101?

Qiupalong??
??00??1100????
????????01100?????????0??0001000002???00????????1????????00?0?0???0????????????????
??0??????????????????????
???20?0?0?00000????00000000
?0000?000?02?????????1????????0??????????0????????00??????????????????????????????????
???
???
??????????????10100?00?0001??????????000?010001??0??????????1??110????0????????????
????????1??01?????????????????????????0000??000??0000?00001??????????01??????1??????
?1?

Kinnareemimus??
???
??????????????????????????????0???00001???00???????????????????0?????0?????????????
???0???????????????
???0?????????0?????000000
0000000?000?02????????????????????????????????????00????????????????????????????????
???
???
??????????????????????0???????????????000??00000?00?????????????????????????????????
????????00???1??????????????????????????????????0???0000???001???????????0??????????????
1?

Huaxiagnathus_orientalis?00?0?????????????0001???1???0?????00??0???????????????????0
0?0010????????00010?1010?00??0???1????????0??????00???0?002010????000000000?00??01
000000020?0??000100201?000012?0???0??????0??0?010000000?0?011??000???00?0??00?0
?0010?0100000?0?1?00????0????0000??200???0000?????????????????????????????????00?00
?1??0?[01]0?0????????0000020?00?0?0?0?010100??????10?0???0????????????????????010????
000??00?00??00000??????000?0??00??0??0????100000000????????000????00000?0?00??0000
00?01??00000??0?00?0?00?10000000000???1?????????????????????????????00?00?????????????
?????????????????????0??02?00???0?????????????????
???1?0?00????????0?0??0000??????0??0001100???1?0?000??00000??0?????????????0??????0?0?
??0?0?0?00?101000??01?0?00?0?00001000?000??0????????0?????10?????00????0?0?0?0000??
??0???0????0000100??????????????????????000??

Sinosauropteryx_prima000?0??????????????0001???1???0?????0000??????00??0?????????????00
??01????????1?0001001010?000?01??100????1?0?0????00?110000201??????00000000?10??01
0000?00020??????0100201?000?11?0?1?00?0??000?0?0100000000?011??0000??000?0??00?
0?000??010000000?1?00?00?????000?0??20000?000??????????????0????????0101????????000
0?0??0?00[01]0?0???????????????0?00?0?00??010?000?????10?0???00?00??????????????1??0100
???0000000?00000??0?2?????00??0??00??00?0???0100000000????????000?10???000????????
?0000?01???0000??1??1????0?1?0?00??0???????0???????????????????????????00??0?????????????
??????????????????????0???02?00???0?????????????
?????000100????????0?0??0010???????0??00111?0???110?000??00000??0?0???0??0???0??0?00?

0???0?000?00?11100???0000?00?0?0?001000?0?0?0??????010????1100???0000???0?000?000
00??000???????0000100?????100???????????????000??

Compsognathus_longipes?00?0?????????????????00101?1??00???00000????000????000???????0
?00000100?1?00100001001010100?01??1010???1?0?0???000?012000201O?????0?000000?10
????0?000000??????0?0100201000001?2?0???????????00?000100000000000110O?00????0?0???
00?0?00100011000000?1?00000000?0?000??020000?0000??0?0??0??????0???0000????01?0??
0000000010000[01]0?0????????00?0?20000?0?0?0?010100????0?1000???0???00?????????????
?010????0?0??00??0?000?00??????00??0?0000?00000?00100000000?????????00????000000???
?????00000?001?001000?1?0100?000100000000000??0???0??0?000?00?0????0000000?00?0?
?01?12????????000???????11?000?????????????????????????????0?????????????????02000?00000
0020000?0???????1?0000??????000??0000?0????0???????01???1????00????0??0?0?0???0???
???0??0000?0???0?000000?101000??00?0??0?000?0010???0?0????0????10????1100??0000???
?0???0?00??????00???????0000100?0010100??1?0????????001??

Juravenator_starki0000?????????????????00010??11000?1???00000?0000?0?????00?????0?00000
10???0????00100101??00??0???1???????0???????00??10002010????000000000000????0000
000000?01100?????????????????????0?????00??????0?0??000000?10?000?0??0??0??00?0??????
010000000?1?00?0?000??0000???20000?000?????????????0????????????0??????000?00???00
??0?0????????[01]00002???0???????0101000?0?0010000??000?000?000???0?0????100???000
0?0???00?000??2??00?????000??0?0000?0010000000???????00???00?0?00???00??0?0000?
011000?00?01?0100?00?1?000000000000?00???0??0?00??00?0????0000000??000??01?10????0
00??00???????11?000??00?0????????00?????????0?????????????????????02000???0??????0???0??
?????0?010?????????????????????????????0000??00??1?0?000?????0????????0??????0?????0?0?
??00000?0??101?00??00?0??0?0???0????0?0?0??0?0?????0????0?0?????000???0?000?0??????
?0??????????00100?0????00?1??????0???00???

Sinocalliopteryx0000?????????????????0001??0???000???00?000?000??0??????????0?0?0000001?
??????1?000100101010O0?01??10?????1?0???????00??1000020?0?????0000000??00??0100000
003?0?0??000110201?000012?0?????????00???0??000??0000?011??000?1??0000??00????010
?01?000000???00?0000???00000??20000?0000?00?????0????00?????0???????????000000010
00?[01]0?0????????00?0?20000?0?000?010100??????10?0????0??00???????????1??010???00
00000?0000000002??00?0????00?0??00?00??0100000000????????00??10?00000???00??00?00
0?01???0?010?0?0000?000??000000000???0???0??0?00?????0????0????00?00?0??0???2????
?00???????????11?0????0?????????????0?????????0??????????????????????2?00??00?000????????
0?????1???0000??0??000?00010??????0??000010????1?0?000??00000??0?0???0??????0??0??0
?0???0?000?00?100000??01?0?00?0?0?0010?0?0?0????0?0???0??0?0?00??0??0???00?000?000
0????00????????000101?????10???1???????????000??

Mirischia???
??????????????????????????0??0?0??0????????0001?0
2000???0121001000101l0????0?????????????1?????????????????????0010?????????????????
???0?1?0?????????????????????
???0???00?0?000?????????????????
??
??

??0???000???????????
???????????1??????0?0?00?000?1??0?0?????????????????????0??????0??0????0????0???????
????1?????????????????????????????000?0????00??00?????????????????0??????????0????1?

Ornitholestes_hermanni?0002???0?0?00?1???0?010?0111000 1?100101?0??1000001?01011????
0000001000?0?000010?00101001?????011?0101210000??000?0010??1?????????????????01?00?
????????00001??1?0?0100101000001??0?1???????0????????00?00????00000?0010?00?0?0000
?0?0000?0100000000 1?01?0000100000 2?1120000000 10?0??000000?0?00???0000?0?0000???0
000000010000[01]0??????????????????????????????????0?0?0010000?000000000000??0??0???
?1000??0000000?000?00000?0000?????????0000?000?001??00?0????????00??0???0001?0????
?????00??00?1?000000000000000?000000000??00??0???0000?000?00?0????0000000?0000??
01?0000?00?0000100??00001?000?0001100?00000?01000?????000000000000???0???0200000
0000002000?00000?00000000???????0001000002?10?00?0?????? 10010?01??000000000???0
100????000????0?00?0000?0000???????????001??1010?0000???0???0????0?00??00100000?0
0???000000???000000??000?????????0?1000?1001?0001????0??0?1010?0

Coelurus_fragilis???
??????????????????0??0100100001210 00?????0?0002?????????????0?0??0?10001????0?????????
?????????????????01100?000001?0?0000110?0?0????0?00??00???0??????????0?0????0???????
?????????????????????11200???001000???????????
???????2?????????????01000?0?0010000?000000000000010000???0????????0000?????????00
2000000000000??000???????????0000???????????0??????0??????????0?????????????????????
???
??0???????000010
0002?????0?000?0??100100?????????????0?0001?000000000?0000?????0?????????????1??00???
???????0000??000???0??00?0100????????1100000000000?00?????????00000??00000001??????
???0?1?0?11221111?????

Tanycolagreus?000?????????????????00?0??????0???00110????????0?00????????????????????
??10?00??????1?????????????0011?000?????0????0?0??0???????000000000011?1000000?????
?????????????????????1100100000110000000100000000000000??00???0??000?????0?0???00????
?????????????1???1????[01]2000???0?????????????????????00??0?0??????????0?00001000??0?
0?????????????20000?000000010100 0?0?0010000?000000000000010000??01000??00000???
???????00200000000000000000000?00100?00000????????0?0?????????????????00000?????0
01000?????????????????????0??????021000000?000?0?????????????????0??0??00???????0?0?00
0??00???0?????????
?????????????00001????????00110010010000 00??????????00???000000000000000000?000???
??00100000000??0??0?0?100?1000000000000101000?????????????000000000?????????0?00
000000000010?????0??0?10010122101 1???1?

Tugulusaurus???
?????????????????????????????????????0?????????????????????????????????0?0????????????
??????????????????000?0?100??00110?0?1????0?????0?????????????????????????????????????
???
???200000000000
0???01?????????????????????????????????

??
??
????????00??????????????????000000000000?0???????0?????????0??????????????????????????????
??000001???1??0?????00????????????????????0001??1????
1?

Zuolong?0000?????????????????0000010111?0???000?0000001100000?????1000?????????????????
??00010?101??1?0100010000???1???000000?0000?????????????????????000?0??????0?????00?01
00?????????????011001100001l0?00?0???00010?0?00?????0?0100?????00???0???001100000
0??0???00??1???0??0002000??0000?????????????00??0000000?????????010?0?10??0?0?????
??????????????????????????????0??????10000?000000000000010000?????????????????00?0?0?00?0
020000?????????0000?000?0?1???0?????????????????0???000100????????0??00?????0000000000
000?000000001000???????1???0??00?0000?????????????????????0?????0000?00000?0?000??10??
0010?0001101?00000???0??????????100????
???00000??0???000???0??????00000?????0?00000?0?0?0??000000000????000?000?00??0???
?0?????000??00?0???0???????????000011?????0?0??0000?0?00000??00???0?0???0000000?????
00??0?????1?0?10??000??01?0?01?

Bicentenaria???????????00?1??????0?0??????00??00?????????????00?????????????????????
0?000000001?????????????100?????????0?????????????????????0?00???????????0?1????0??10?
??????????????0???00000?10???0?110???????0??????????1????0?????????????????00??0???0
???????????????1???0??????????00????????0??????00???????????0???0010????0????????????
??2???0???0???0?????0?0?001??????00000000?0?????????????????????0??0???0????2000?00
000000?????????????0?????????????????????0?????????????????00????????0???????????0???00
??0?????????????????????????????????0?0000000?????????????????00000000?1?????????????????
??1?2?00??000??0??????0?????????????????????
???1?00??0????00?????????0??0?????????0000?02???00?0???????00????????0?????00??????0??
?00???0???????00???00?????0??????00??00?0??????0??0?????00?????00???????????0?????0?0
??0?1?0????

Kileskus?????????????????????0?01120111???0
0000?101???
??????????????????????????????????00?00??0?????????????????????????????????1?0000?0???0??00??
????1????????0??001???
??
??
??1011201???000?0000?0000?0?????
??
??????????????????????????????????????0100010?????????????00????????????????????????????
??00?????00?????????????????1??????0?????????????
?????????????0???1?????????????????????0????

Guanlong?00020?000000?010[01]10001120111200?00110000001000000000?10????000000
10?00??2000000010l0?100?000000000111000000000000?0???00??????0000001000000?0100
000003000010000100200000001110010000011000?00110000100000000000000000000000000?
0?00100011000000011100?00?11101102?1120000?0010????0000?000?00??0000000??0?0????0
0000001000?0?????????????????20000?0?????0101?00?0?0010000?000000000000010000???01

000??0000000?000000000200000000000000000000?00100?000002020?000?00??0001000??
????0000000000001120102?1000?00?1000001010000?003??0000??0??00?1000100000110001
0??01?1000?000000000000000?1000011?000000?00000?????????????020?0100010000000000
????0?000000001?0???????010100???????000010000210000?0?000001000100000000000001000
00000?011000000010000?0000000?000110000010?010010?1000100000000000010000000000
00?00100100000000000000000??000000000000010100???1?0011?1001??1000001?

Sinotyrannus?????????????????????0?01???101?????????????????????????????????????00??0?1?????
???0?0000101?????????????????0??0??00??0?0?0
00???0??0?????00?????????1?0000?0??10
0??0?????11????????00?001?????????????????????????????0????????????????????????????????
??00?000?0?0????????????
??0???????????00??????01?2?1??10???0??1?00???
?1??
????????????????????????????????0??????????????????????????0????????????????????????
????????????????????0001?????????????????????????????0?0??????0???????????0?1???????
????????????????????0???00?
??

Proceratosaurus_bradleyi?00?2?????????????00011?01112000?00??????????00?00???????000
?0000001?00?120000000101011???
??00??0????0?0??0??????????
?110000?0?1100?00?11?0?1?2??????000001000000?????????00???0??00??10?0????00????????
??
??0???????0?????????????????????00?0010112?1
0?1000?00?1?0000101???0?????????????????0?1000100000110001???????0???0???000000000??
0?0?????????????0000??000?????0??0?0??????00100????0001???10?000000001000?????1100
0??0?00???
?????????1????0?0????????????????????????0??0010?????????????????????????????????
??1?0?1?????????????????000??

Dilong_paradoxus?0002??000000???0?100011??1112000?00110?000010000000100???????000
00000?00??2000000001010?1?0000?0001?0??1000?????0??0?0?0??0???????000000110?????0
000000?00??1??00110201?0?0001?00?000?0??00??000100001000?0000?00000?0?00000?000?0
?00100010000000001100?001111?110201?20?000000????00000???0?0???00000101100000??00
0??00??00????0?????????????20000?0?0?0?0101000?0?0010000?000000000000?0??0????10
00??0000000???0?00000200000000000000000??00?0?1000?0000?0?20?00???0100001000?????
???000000000010002?11?1000100?0?000000000000103??0100?00??000101111000011000107
?00?1100??000000000010????00000?000100?????????????????????020?010?010?0????01001??1
0?010002?00?11?????011100000001000001000001??????000001100017????10000?0001??000?
??0110000000000000??010000000??11000????1?01?01001?????00??00???00???00000?00100?0
0?0000010?0?000000????00??0?000?0001?100???1??10112????0??0000??

Eotyrannus_lengi?????????????????????000120??12??0???110???????????0?????????0?000?0?0
??1???2000000010101 2?00?????01?0??1?????????????????????????0000000107????????0?0??
??0???00000?0?00???00?0????00?0?????0?????0?1?00

0?00??10??0121???111?0?211?0000?0??????????????0??00?00100???00??0???0?0010?0??0?
????????????????200?0?0?000?0?0?0?0?0?0010000?0000000?0000??????????00?????????????
?0??????????????????????????????0??????????????????????1???????????0?00?????1?00101?
??????00?0?01????01000?1010??1??0?00?00?????????????????0?????????????????????01?1??0
??????????????????001??????0?00?????????????????????000?10002110100??????????2??00???
00???00????0??????????00??011011?000?????????????????????????01??00?00100?000?0???
0??????1?0??0?00????1000??????0?00????????0000?00???0000100?00??0??????????0000???0
?1????0??????011??????1???0?1?

Juratyrant???
????????????0?00?0000001?10??00000??0????????????????????????????????????00?00?010000
11010110000011?01???0??10????0?????????????????????1????????00???0010?????????????????
????????2????11???0?00100?0?0?????????????
??00?000000000?0?00?000
??00?????????????1?????????????????????????1?0???
??
??
??0????????00?100011?00100?
0?????????????????10000001100100?????1100001?????????????????????0??01??1??1?????000?
???????????0?????????????0000?0?????????000000??000??0000?????????????1??1??????11??
0????1?

Xiongguanlong?0002???00000?????1?000220???0000?00110100?2100000?0001??000??????
????????00000?101??2000000000001110000???0
?12?01000?????????????????????0000110?????????????????????0??????0?00?????000?????????1?0
00000???00?0?1121?2102011???0??0000?00?000??????00???0??000???????????00?00100????
??00?00000
00??20000???????0?????????????????????????????0???????000100?????????????0010?10001???
?1?00?01?0?01?0000100??0010?0100??0??0??0?????0???01000?0???0?0100???001?11111001
0????100?1?11??00?100????????????00100100001?1?????????????????????????????2?000
??0000000110000011?????????????????????????111??001???????0111012?????????????????00??0?
??????????1??1?010?10?????????????00??????000?0??00001???????????000000?????000000??
?????10????1?????????1???0?0?01?

Dryptosaurus?????????????????????????20?????????????????????????????????????0?0?0??2???
????0000101?1?????????????????????????0???00?????????????????????10???????10?0??????????
??[01]?0?0?2???????101?010001000100010002???2???0??????????0?0????????0?0?????????????
??00?????????????????11????0?????????????????????????????????????0????????????0??????????
?????????????????????????0?0?0010000?00?????????????????????????????0????????00200000
00000000??000??0???00?01?????????????????????????
?0???
???1212?1?1?????????????????????????????????
????????????10?????????????????????1?0???012?1?0111?????1????0??????0?????????????0??
?????????????000000?????????????????00?1???00?????????00??0000?00001????01?????????
0?1??00?0?0?

Appalachiosaurus?????????????????????0?0?20111?????120?????????????????????????00000?000
?0????????0000101?2?????????????????????????0?0?00?????????????????????????????????????
??????0000101?0?10???10??0100010001000100000?2?0?00??????0????0????????0?00100?110
00000?1???1?021?????????????????000??0??????000?????0???????????0000???0?????????????0??
??00????????0
020000000000000?0000?000?00???00?????1????????000?0
00?01?010111?101??1?0020?01?10??0?0???
?????????????0000000101000?00?????????????????11?110??1??????????0??1?????2?0????????
??????????????????0?????????????????????????????1?01110???111111111021?0000??????????
??0?????0?0???00??????????0000000???00??0?????0?????????????????00?0??00000001???
0???????01?????1??00000??

Bistahieversor?1102?????????10?2200002?0111000?00120100?2110000?????????0000000
0?20??2?000000101012??0???
??????????????????????????????0?????????????2???????10??00??00?0??0???????????120000
0011?00?00213?0?112?????0000000?????????10??0????00001???0?0????00?????????????????
??????????????????????????00???
??????????????????????????????????11?????????0?????????????????0?1011001000?10101
01?0101110101010100201000100 1???10000??000000200002110000100 00??1111111?1?10010
1100121111 1?01000?0100111 11??????11?111101?1011111 1100?1112122011001 12?10??2?00
????111?????????????????0111?1?????????????????????????011?????0110111 1?120010000?
???????????1??1?0?0?????????????????????????0??0?????????????????????????????????
???11001??????1???????????000?1

Albertosaurus_sacrophagus?1102??000000?100220000220111000000012010000211000 00?000
1000000000000020??2000000010101 20????0?10?001?100?0????000??0????0???????0000000
10000???0110010312001100000010120010001 10??0?00?1000??00100000200000001000000000
0000?000?0?0010?012000000110 00?002131011121020110000000???00000100?00??0000010
010000??000000001000 0?0?????????000020000?00000?0001001?0?0010000?00000000000
0010??0?????000???00??00?000000000200000000000000000?00??0100000??020100?000??0
??001100?0110?000000101110110010000[01]1001[01]100101110102011100211[01]1[01]1?01
?00100000010001020100200110010001111101111111110101100111111 1000[01]000110[01][
01]1111000010110111111110111111100111121211 1100?12?10?121011???????1????????????
????111110201111 1?10211111102111 01??1???1???111111111220100000 00??00000101?011
010?100010?000??00?000000100?000000??0?00??110??00000000??0000?0000000001011001
111010111????010000001

Gorgosaurus_libratus?11020?000000110022000022011100000001201000021100000100010000
0000000000200120000000101012 0?000010000101000000?000000000000?000010000000010
0000010110010312001100000010120010001101001000100 0?0001000020000000100000000
0000000?0?001000120000001100010021310111210201100000000000000000100000??0000010
?10000??0000000010000[01]0?0????????0000020000?00000?0001001?0?0010000?000000000
000010000010??1000??0000000?000000000200000000000000000000?00100000000201 00?00
0100??00110000110?000000101110110010000[01]100101001011101020112002 1101[02]1001
000100000010001020100200110010001111101111111110101100111111100010001101111 1??
001101101111111101111111001111212111100112?10?121011???????1????1101????1?0?0111

1102010111110211110102111012011?1?2?111111111?22010000000100000010110110102100
010?000010000000001000000000000?0000110?000000000??0000?000000000101100111101011110??0?0000001

Alioramus?01020?000000110022002?0?201110000000120100002110000010001000000000000
0200?20??000010101?000000010000111000000?00?00?0??000?????????????????????????????
?120011000[01]001012?010?????001000100??0?01000?02??000??10??000000?0?0000????010??110000001100012?0213101?12102????000?000000000000100000??00000100?0000??00000?00100?0?0???00?0???000??2000000000000000000?0??0?1?0????002011?00???0??0011000???????0????00111?2????0011101111102011101010012012100102111010111000100001020000100000010110111201111111100101100111111?10111001001110100011011011110110111011101111001112122111102??10000???000001000011110?10122101111?????????????????1111010?????1?1111121??00?111?12?0100000??????0???0?1?1?010??000?????????0????01?0000?000000?0????????????0000??0??00???0?000?1??1101111?1?1??1011??0?000?1

Teratophoneus?1?0???0???????0??2??????0111?00????1201???????0000???????????00??000????????0000101012??1???0?????????????????????????????0?????????????????????????????0????0?????????????0000?01?????????3?????????0???000?????????????10??0???00?001???0?????0???1???100???0????0?01???????????????2?021?00010?10??????????0???01?1??????0???01??1?1??21?111?10011110121122?????????????????????011?1?120?1????1??1100?11?????????11????????10???????????1???????????????1?01???1?????????????????????011?1?1?????????????000?????????????????0?0??????????????????????????0??0???1??????1??????????00??1

Daspletosaurus?11020?000000?10022000022010100000001201000021100000100010000000000000020012000000010101201000001000012100?0????000??0????0???????000000010000???1111001031200110000001012001000110??0100?1000??00100000200000001000000000000000?0?0010?00200000011000101213101112102011000000000???00000100?00???00001001000000??000000001000?0?0????????0000020000?00000?0001001?0?0010000?000000000000010??0??????1000??000??00?000000000200000000000000000?00??01000000?020110?000??0??00110000110?000000101110120011020110021110211110102101201210101[12]111111111111101101020000211001011[01]112112121111111100?111012211111110111001101111[01]1001111101111011111111111100111122221110111?2100121011000111011110211112222222?11?1?11?112111??1??111?1??1????2?11????11?12???00000??11000????1??1?010?1000???000?1000?0??????0?000000000???0011000?0?????????????????????????1110111102?1?????????000?1

Tyrannosaurus_rex?12020?011000110022000022010100000001201000021100000100010000000000020012000000010101201000001000010100000010000000000?0????000000001000???11100103120011000000101200100011010010001000100010000020000000100000000000000?0?00100002000000210001012131012121020110000000000000000100000??000001001000??0000000010000[01]0?0????????000002000?000000000100?0?0010000?000000000001000000????1000??000??00?000000000200000000000000000000?00100000000201002000?

00??00110000110?000000111111120011021 01[0]1[3]0110211110102111201 0??101210111
11011[01]1101111021010211001011111211[12]12111111100111121230111111111110110111
11111111110110201111111111111121112222211011121111121121111101111021111211111
11111102110111111211111102111111112211211111111111221100000001000000101101101
0?1000100000??000000000110000000000010000110 0?10000000??000000000000000010111011
11010111011010000001

Tarbosaurus_baatar??2020?011000?10022000022010100000001201000021100000100010000
00000000020012000000010101201000001000010100000?100000000000???????0000000100
00?01111001031200110000001012001000110100100010001000100000200000001000000000
000000?0?00100002000000210001012131012121020110000000000000000010000??00000100
10000??000000001000?0?0?????????????20000?00000?0001001?0?0010000?0000000000000
10000????1000??0000000?000000000200000?000000000000000?00100000000201 0?000?00?
?00110000??????000011111112001102101113011021111010210120 0??10121111110111110
11110210102110010111112112121111111000111212301111111111101101111111111111 0110
20111111111111121112221 2?10111211111211211111?111?1021112??1??1?1111110211011
1?11211111102111111112211211111111111221100000001000000101101101 0?1000?0000001
000000000110000000000010000110??10000000??000000000000001011101111010111101 1??
0000001

APPENDIX 3: SUPPLEMENTARY TEXT FOR CHAPTER 3

1) Morphometric Analysis

a) General methods

We analyze morphological variation in the cranium of theropod dinosaurs using a geometric morphometric approach. Geometric morphometric techniques are commonly used to quantify and study shape variation across a collection of specimens, usually based on either outline or landmark data that encapsulate the geometry of the specimens in question. They are held to be superior to traditional morphometric techniques, based on multivariate analysis of length and angle measurements, because they preserve geometry, are better able to separate shape from size-related variation, and better capture subtle sources of variation that are not easily summarized by simple measurements (Rohlf 2000). Geometric morphometric techniques have been reviewed extensively by Bookstein (1991), Rohlf and Marcus (1993), O'Higgins (2000), MacLeod and Forey (2002), Adams and Rohlf (2004), Elewa (2004), and Zelditch et al. (2004), among many others.

b) Specimens

We digitized landmarks (see below) on two-dimensional images of the cranium of 51 species of theropod dinosaur. Of the ~200 known, valid species of non-avian Mesozoic theropods, these 51 represent all species for which a complete (or near-complete) cranium is known from well-preserved, adult (or near-adult) fossil material that has been described in the literature and was accessible to us (we note that spinosaurids, an aberrant group of large-bodied and long-snouted theropods, could not be included because none is known from a nearly complete or well preserved skull). Landmarks were plotted on published drawings, reconstructions, and photos in lateral view (Table S1). In all possible cases we checked these images against original specimens, and used the original material to more accurately plot landmarks that would be difficult to locate on the image alone. All but seven of the specimen images were reconstructed line drawings, which we carefully selected and vetted for accuracy (often based on our own observation of specimens). The seven taxa represented by photographs are: *Byronosaurus*, *Dubreuillosaurus*, *Haplocheirus*, *Incisivosaurus*, *Khaan*, *Saurornithoides*, *Tsaagan*.

As theropod skulls are three-dimensional structures, the use of two-dimensional images is not ideal but necessary due to data availability. Almost every species in our analysis is represented by a single fossilized skull, and these specimens are spread throughout museum collections across the globe. Acquiring high-resolution, three-dimensional data for each skull is currently not possible, but as laser-scanning technology becomes cheaper and more widely available it is anticipated that future work can build upon the two-dimensional study presented here (see Souter et al. 2010). A similar rationale has been used to support two-dimensional morphometric studies of various other fossil vertebrate groups (e.g., Bonnan 2004, 2007; Chinnery 2004; Stayton and Ruta 2006; Pierce et al. 2008, 2009a,b; Young et al. 2010; Young and Larvan 2010).

c) Landmarks

We chose 24 landmarks to describe the overall geometry of the theropod skull (Figure S1). These represent equivalent (homologous) points that can be plotted on each specimen, thereby allowing each specimen to be mathematically modeled and compared to every other specimen in the analysis. Landmark selection aimed to encapsulate both the overall shape of each individual skull and the diverse range of skull shapes across Mesozoic theropods, while at the same time minimizing the number of total landmarks (so that it is less than the number of specimens in the analysis) and ensuring that landmarks were not bunched together in certain regions of the skull (thus overemphasizing those regions in the analysis). All landmarks are either Type 1 (strong evidence for biological homology, such as the meeting point of two or more bones) or Type 2 (good evidence for geometric homology, such as the endpoints of bones) in the terminology of Bookstein (1991).

Landmarks were digitized on all 51 species images using the program tpsDig2 (Rohlf 2010), which outputs a tps (thin plate spline) file with two-dimensional landmark coordinates and scale (size) data for each specimen. All landmarks were plotted by one of us (SLB) for consistency and then checked by another author (SM).

d) Two datasets

After plotting landmarks on all 51 specimens it became apparent that many specimens had a large amount of missing data (landmarks that could not be plotted because of poor preservation or missing bones). Although some geometric morphometric software can handle small amounts of missing data, such missing information is not ideal because it reduces the statistical power of the analysis and requires that fewer landmarks be used to align specimens in shape space (see below). In sum, 26 of our specimens could be scored for the full complement of 24 landmarks, and missing landmarks in the other 25 specimens ranged from 1 to 15. Therefore, we decided to proceed with two datasets: 1) a dataset including the 26 taxa that could be scored for all 24 landmarks (Table S2); 2) a dataset including 36 taxa that could be scored for a reduced set of 13 landmarks that could be plotted on all specimens (landmarks: 1,2,4,5,7,10,11,12,15,16,17,19,21) (Table S2). The decision to use a 36 taxon/13 landmark dataset aimed to maximize both the number of taxa and landmarks that could be included, as well as permit inclusion of representatives of all major theropod subclades. Taxa shared between both datasets fall out in a similar pattern in morphospace when each dataset is analyzed separately (see below; Figures S2-S3), indicating that the reduced set of 13 landmarks is capturing the same basic signal in skull shape as the full set of 24 landmarks.

e) Superimposition

For both the 26 and 36-taxon datasets, landmark coordinates were superimposed using Generalized Procrustes Analysis (GPA), in which each specimen is scaled to a common size and rotated to minimize the squared differences between corresponding landmarks (Rohlf and Slice 1990). This serves to eliminate (or minimize) non-shape variation between specimens, such as that caused by size, location, orientation, and rotation. The Procrustes alignment produces a revised set of GPA "corrected" landmark coordinates for each landmark on each specimen. We performed the Procrustes alignment, and generated an output of "corrected" landmark coordinates, using MorphoJ (Klingenberg 2011).

f) Principal Components Analysis

For both the 26 and 36-taxon datasets, the "corrected" landmark coordinates were then converted into a covariance matrix, which was subjected to Principal Components Analysis (both were conducted using MorphoJ). This procedure is essentially equivalent to a Relative Warps Analysis (see MacLeod 2010). The 26-taxon dataset was summarized by 25 PC axes and the 36-taxon dataset by 22 axes. In each case the first five axes were deemed significant by the "broken stick method," in which a scree plot (percentage of total variance against number of principal components) is examined for a significant break in its slope. For the 26-taxon dataset these first five components describe 83.3% of the total variance, and the first two components are particularly explanatory (46.2% and 18.6% of total variance, respectively). For the 36-taxon dataset the first five components describe 88.9% of the total variance, with the first two components explaining 56.9% and 16.5%, respectively. Therefore, for both datasets the first five axes are used to calculate disparity metrics (see below). Two-dimensional morphospaces showing the first four PC components (PC1 vs. PC2; PC3 vs. PC4) for the 26 and 36-taxon datasets are shown in Figures S2 and S3. The major changes in skull shape based on the included landmarks are shown in Figure 1 of the main text (26 taxon/24 landmark dataset) and Figure S7 (36 taxon/13 landmark dataset).

Because the PCA for both the 26 and 36-taxon datasets showed oviraptorosaurs in their own highly divergent position on PC1, we ran additional analyses with oviraptorosaurs excluded. This was done both as a heuristic exercise to gauge whether oviraptorosaurs, as an outlier, have a disproportionate statistical influence on the PCA, as well as provide a second source of PC loadings to be used in disparity analyses (see below). Excluding oviraptorosaurs from the 26-taxon dataset resulted in a 24-taxon/24-landmark dataset, whereas excluding oviraptorosaurs from the 36-taxon dataset resulted in a 31-taxon/13-landmark dataset. The 24-taxon dataset was summarized by 23 PC axes and the 31-taxon dataset by 22 axes. For the 24-taxon dataset the first seven axes were deemed significant by the broken-stick method; these components together describe 86.2% of total variance, with the first two explaining 38.6% and 19.5%, respectively. For the 31-taxon dataset the first five axes were deemed significant and together describe 83.6% of total variance, with the first and second axes explaining 37.9% and 23.1%, respectively. Two-dimensional morphospaces showing the first four PC components (PC1 vs. PC2; PC3 vs. PC4) for the 24 and 31-taxon datasets are shown in Figures S4 and S5. Shape changes on the included landmarks in these datasets are shown in Figures S8 and S9.

g) Relationship between specimen size and PC scores

Although the Procrustes Analysis largely factors out non-shape differences between specimens, such as those caused by size, there is still the possibility that some relationship between size (allometry) and PC scores remains. Therefore, we tested whether the first three PC axes of all four datasets (24, 26, 31, and 36-taxon datasets) are significantly correlated with the centroid size of each specimen. Statistical results are presented in Table S3. There is no significant correlation between size and PC1 for the two datasets that include oviraptorosaurs (26 and 36-taxon datasets), but there is a significant relationship for the two datasets excluding oviraptorosaurs (24 and 31-taxon datasets). However, this relationship is largely the result of large-bodied theropods (those with a skull length greater than 65 cm) clustering close together on PC1. Indeed, when large-bodied taxa are removed the correlations are no longer significant. Similarly, there is a

significant correlation between size and PC2 scores for all four datasets, but these too are deemed insignificant when large-bodied taxa are excluded (except for the 31-taxon dataset). There is no significant relationship between size and PC3 for any dataset. Therefore, although some relationship between size and PC scores remains, none of the axes (except perhaps PC2 in the 31-taxon dataset) can be interpreted simply as an allometry axis. PC1 and PC2 retain some information on body size in some datasets, but this is because many of the largest theropods in the analysis (which differ in body size by an order of magnitude or more from the smallest taxa) have a similar skull shape (see discussion in main text about morphological convergence of large-bodied taxa).

h) A note on sample size and missing data

Our goals with this project are to describe broad-scale patterns in cranial shape variation across theropods, assess major changes in skull form in a phylogenetic context, and test whether theropod skull shape is strongly correlated with function and phylogeny. Our results, of course, depend intimately on the empirical dataset that we are using. Ideally, a study such as this would use a complete species-level dataset of all Mesozoic theropods, but that is not possible for various reasons. First, only a fraction of all Mesozoic theropods have currently been sampled in the fossil record. Second, we must exclude several species because they are not known from complete, or near-complete, skulls that have been well-prepared, well-described, and published in the literature. Both forms of missing data are unavoidable for this study, or indeed, for any macroevolutionary or phylogenetic study of fossil taxa. All published morphometric analyses of fossil vertebrates are hampered by the same missing data bias (e.g., Bonnan 2004, 2007; Chinnery 2004; Stayton and Ruta 2006; Pierce et al. 2009a,b; Young et al. 2010; Young and Larvan 2010). We have endeavored to include as many theropods in our analysis as possible, but acknowledge the obvious fact that additional discoveries may expand the known variety of theropod skull shape and lead to different results in the morphometric and correlation analyses that we provide here. We note, however, that our 26 taxon/24 landmark and 36 taxon/13 landmark datasets return similar PCA results (similar major changes on PC axes 1 and 2) and morphospace plots (Figures S2-S3), and both are significantly correlated with phylogeny (see below). Similarly, the two datasets excluding oviraptorosaurs also return similar PCA results (similar major changes on PC axes 1 and 2) and are both significantly correlated with phylogeny. This suggests that our dataset captures robust patterns of theropod cranial variation, and that the level of sampling we include is enough to give a consistent signal even when substantial data (both taxa and landmarks) are excluded. When interpreting our results, however, it must be kept in mind that our results are contingent on the sample available to us.

2) Theropod Skull Function

As part of this study, we wish to compare theropod skull form (derived from the morphometic analysis) with cranial function. Just as a geometric morphometric analysis is only one approach for quantifying the overall shape of a structure (in this case the theropod skull), there are many methods for encapsulating the functional performance or capabilities of a structure. One of the most straightforward, useful, and well-established approaches is to quantify the efficiency of translating muscle moment to biting moment: the mechanical advantage (MA) (Westneat 1994). Mechanical advantage measurements for several theropods were recently presented by Sakamoto

(2010), and we built upon this study to compile a database of functional metrics for 35 of the 36 taxa included in our final morphometrics analysis. This involved adding several new taxa to the dataset of Sakamoto (2010).

The methods of Sakamoto (2010) involve calculating the MA of each muscle group along the entirety of the tooth row. Three functional muscle groups, the temporal muscle group (incuding musculus (m.) adductor mandibulae externus [mAME] and m. pseudotemporalis superficialis [mPsTS]), the quadrate muscle group (or the m. adductor mandibulae posterior [mAMP]/m. pseudotemporalis profundus [mPsTP] complex), and the pterygoid muscle group (m. pterygoideus), were identified. The anterior- and posterior-most extremities of the respective attachment sites were mapped on a lateral image of the skull and mandible for each taxon in ImageJ 1.43u (Rasband, 1997-2011), and their landmark coordinates were recorded. Coordinates of biting points were also recorded at either the tips of the teeth or along beak margins in toothless forms. Lever arms were computed from these coordinates (for further information see the electronic supplementary information of Sakamoto [2010]). MA is defined as the ratio of the inlever (muscle lever arm) and outlever (biting lever arm), and this value was calculated for each muscle group along each biting point. Ultimately, the mean of each muscle was used to represent average MA for all 35 taxa in the dataset (the full 36-taxon dataset minus *Juravenator*, which was not entirely suitable for biomechanical profiling because of missing bones at the posterior end of the upper and lower jaws). A best-fit polynomial curve was fitted to the MA profile using R (see Sakamoto 2010) and the three common coefficients (intercept, slope, and curvature) were taken as the biomechanical variables, which were then subjected to PCA (scaled to have unit variance). Polynomial coefficients for an additional 25 theropod taxa were included in this multivariate ordination (thus a 60-taxon biomechanical dataset) to better quantify the overall theropod function space. The first PC accounts for 90.1% while the second PC accounts for 9.67% of total variance. Together, PC1 and PC2 capture 99.8% of total variance in functional disparity in the 60-taxon biomechanical dataset. Therefore, the PC1 and PC2 coordinates for each taxon are useful proxies for "function," which can be compared to similar proxies (PC values from the morphometric analysis) for "form." A functional plot (function space: PC1 vs. PC2) of the 60-taxon dataset is shown in Figure S6.

3) Morphological Disparity

Morphological disparity measures the overall anatomical variety exhibited by a group of organisms (Foote 1993; Wills et al. 1994; Ciampaglio et al. 2001; Erwin 2007). In essence, it is a morphological equivalent to taxonomic diversity. Disparity calculations require some measure of morphological form for each organism being assessed. The most common methods for quantifying form are based on discrete characters or morphometric data (see Wills et al. [1994] for a detailed review). In the present analysis we use the PC scores as a proxy for the form of each taxon. Comparative disparity is assessed by binning taxa into various groups and calculating several disparity metrics for each group. These metrics can then be compared to determine whether certain groups are more disparate—have a greater variety of morphological form—than others.

We utilized a set of procedures that have been employed in many recent studies of disparity in extinct vertebrate groups (e.g., Brusatte et al. 2008a,b, 2011a,b; Ruta 2009; Cisneros and Ruta 2010). Disparity metrics were calculated using the first five PC axes generated from the 36-taxon morphometric dataset (the 26-taxon dataset was not used for this exercise because

sample size for some groups was too low to rigorously assess statistical significance in disparity). The same metrics were then calculated for the 31-taxon dataset that excludes oviraptorosaurs. Species, with their requisite PC scores, were binned into both dietary and phylogenetic clusters. Dietary groupings included carnivores and non-carnivores, as well as large-bodied carnivores (defined here as all taxa with a skull length greater than 65 cm), non-large-bodied carnivores ('regular' carnivores), and all non-large-bodied-carnivore theropods (i.e., 'regular' carnivores plus non-carnivores) (Table S4). For the carnivore vs. non-carnivore comparison based on the 36-taxon dataset, separate analyses were also run in which oviraptorosaurs were excluded from the disparity calculations (although the PC scores used in the disparity calculations are generated from a PCA that includes oviraptorosaurs). This was done in order to gauge whether these taxa, which occupy their own discrete regions of morphospace, are contributing disproportionately to the disparity values for non-carnivores. These same tests were also run with oviraptorosaurs completely excluded from the PCA, using the 31-taxon dataset; both results are presented here. Phylogenetic clusters included: Basal Theropoda, Ceratosauria, Basal Tetanurae, Tyrannosauroidea, Dromaeosauridae, and Oviraptorosauria (Table S5). The taxonomic clusters were selected so that sample sizes were approximately equivalent (n=5, 4, 4, 7, 4, and 5 taxa, respectively), and it should be noted that two of these groups (Basal Theropoda, Basal Tetanurae) are not monophyletic.

Four disparity metrics were then calculated for each cluster: the sum and product of the ranges and variances on the five PC axes (Wills et al. 1994), using the software program RARE (Wills 1998). Multiplicative measures were normalized by taking the fifth root (corresponding to the number of PC axes used). Range measures summarize the entire spread of morphospace occupied by the taxa in question, whereas variance measures denote mean dissimilarity among the taxa (the spread of taxa in morphospace compared to its center). Statistical significance of each pairwise disparity comparison between groups was assessed by the overlap or non-overlap of 95% confidence intervals, calculated by bootstrapping (1000 replicates) in RARE. Subsampled disparity curves were produced with rarefaction analysis, also implemented by RARE, to assess whether differences in disparity are robust to sample size differences between groups.

The most salient results of the disparity analysis include the following:

1) Non-carnivores (n=10 taxa) have higher disparity than carnivores (n=26 taxa) based on all four disparity metrics (Figure S10). This result is statistically significant for sum of variances and marginally significant for product of variances (there is an ever so slight overlap of the error bars for this metric). When oviraptorosaurs are excluded, non-carnivores still have higher disparity than carnivores for the variance metrics, although these comparisons are not statistically significant, but significantly lower disparity than carnivores for the range metrics (Figure S10). Similar results are seen when disparity is measured using the 31-taxon/13-landmark dataset that completely excludes oviraptorosaurs from the PCA (i.e., they have no influence whatsoever on the morphospace ordination) (Figure S12). This is clear evidence that oviraptorosaurs are primarily contributing to the pattern of greater non-carnivore disparity. Although there is a clear sample size difference between the carnivorous and non-carnivorous groups, rarefaction analysis (when applied to the 36-taxon metrics calculated with oviraptorosaurs) shows that when samples are equalized and disparity is subsampled, non-carnivores still have a greater disparity than carnivores at all sample sizes (i.e., for n=2 to n=10) (Figure S11). In sum, there is evidence that non-carnivorous theropods exploited a greater range

of morphospace than carnivorous theropods, but the extreme disparity of oviraptorosaurs is the primary reason for the relatively high disparity of non-carnivores.

2) When oviraptorosaurs are included, large-bodied theropods have significantly lower disparity than non-large-bodied theropods based on all four metrics (Figure S13). Rarefaction shows this result to be robust to sample-size differences, as non-large-bodied taxa have greater disparity than large-bodied species at all sample sizes (Figure S14). However, the disparity of large-bodied taxa is extremely similar to, and statistically indistinguishable from, the disparity of non-large-bodied carnivorous theropods ('regular' theropods). Large-bodied and non-large-bodied carnivores also have very similar rarefaction profiles (Figure S14). Therefore, large-bodied taxa have lower morphological variability than non-large-bodied taxa, but the high relative high disparity of the non-large-bodied forms is due almost entirely to the morphologies of non-carnivorous taxa, most especially oviraptorosaurs. When oviraptorosaurs are completely excluded from the PCA, and disparity metrics are calculated based on the 31-taxon dataset, large-bodied taxa always have lower disparity than non-large-bodied theropods, but this is never statistically significant (Figure S15). Furthermore, using this 31-taxon dataset, the disparity of large-bodied carnivores and 'regular' carnivores is essentially identical for all four metrics. In sum, there is no evidence that non-large-bodied carnivorous theropods had a greater or lesser range of skull morphology than their smaller carnivorous relatives. There is some evidence that large-bodied carnivores had lower disparity than all non-large bodied theropods, but this is largely due to the aberrant disparity of the non-carnivorous oviraptorosaurs. Therefore, it is difficult to interpret this result as anything more than the conclusion, outlined above, that non-carnivores have higher disparity than carnivores (when oviraptorosaurs are included in the calculations).

3) Using the full 36-taxon dataset, oviraptorosaurs and ceratosaurs, two subgroups that include non-carnivorous taxa, have higher ingroup disparity than the entirely-carnivorous basal theropods, basal tetanurans, tyrannosauroids, and dromaeosaurids (Figures S16-S17). Small sample sizes (especially for ceratosaurs) render most comparisons statistically insignificant. However, oviraptorosaurs have significantly higher disparity than basal tetanurans and dromaeosaurids based on sum of variances, and significantly higher disparity than basal tetanurans based on sum of ranges. Oviraptorosaurs also have essentially significantly higher disparity (only slight overlap of error bars) than dromaeosaurids based on sum of ranges and basal tetanurans based on product of ranges. This is strong evidence that oviraptorosaurs exploited more morphospace than most other generally equivalent (in a taxonomic level and sample-size sense) groups of carnivorous theropods. The same is likely true of ceratosaurs, based on the disparity calculations and visual examination of their expansive morphospace occupation (Figures S2-S5), but sample sizes are too small to be certain. It may be noteworthy that ceratosaurs have higher disparity than all groups (except for oviraptorosaurs), despite the fact that they have the smallest sample size of any group analyzed. Because range-based disparity metrics (and sometimes variance metrics) usually increase with sample size (Wills et al. 1994), we predict that additional sampling of ceratosaur skull shape will increase the disparity of the group and decrease the spread of the error bars, therefore adding evidence that this group is anomalously disparate among theropods.

4) Tyrannosauroids, despite their great range of body size and noticeable differences in skull form between gracile and crested basal taxa and robust and deep-skulled derived species, have similar measures of disparity as other carnivorous groups (basal theropods, basal tetanurans, dromaeosaurids). Furthermore, tyrannosaurids have lower disparity (although non

significantly) than the non-carnivorous oviraptorosaurs. The variety of tyrannosauroid cranial shape, therefore, is evidently no greater than that in other generally equivalent (in a taxonomic level and sample-size sense) carnivorous theropod groups. It is worth noting, though, that the aberrant long-snouted tyrannosaurid *Alioramus* is not included in this study, because of several missing landmarks at the anterior end of the snout. Inclusion of this taxon may show that tyrannosauroid morphospace is larger than found here.

5) We also calculated measures of functional disparity, based on the PC1 and PC2 scores of taxa in the biomechanical function space (see above). These were calculated using an identical protocol to that described above, except that multiplicative measures were normalized by taking the square root (because only two PC axes were used in the calculations). Carnivorous theropods were found to have greater functional disparity than non-carnivorous taxa, and this relationship is significant for sum of ranges (Figure S18). Rarefaction shows that carnivores have greater functional disparity than non-carnivores at all subsampled sample sizes (Figure S19). Therefore, opposite to the relationship in form disparity (non-carnivores greater than carnivores), carnivores are more functionally diverse than non-carnivorous theropods.

6) Functional disparity was also calculated for the taxonomic clusters, but in nearly all cases error bars were so large that significant differences between groups were not apparent (Figure S20). With that being said, ceratosaurs had the largest functional disparity value for each of the four metrics, and additional sampling of ceratosaur functional behavior may show that this group genuinely was more functionally disparate than other groups.

4) Phylogenetic Comparative Methods

a) Phylogenetic framework

All phylogenetic comparative analyses described below utilize a single resolved phylogeny for context (Fig. S21). This phylogeny is an informal supertree (sensu Butler and Goswami 2008), based upon the results of several of the most recent, comprehensive, and well-resolved theropod phylogenetic analyses (both higher-level and specific to theropod subgroups). The following analyses formed the basis for the tree: higher level theropod phylogeny (Nesbitt et al. 2009), ceratosaur phylogeny (Carrano and Sampson 2008; Xu et al. 2009), basal tetanuran phylogeny (Brusatte and Sereno 2008; Benson 2010; Benson et al. 2010), tyrannosauroid phylogeny (Brusatte et al. 2010a), higher-level and ingroup coelurosaur phylogeny (Turner et al. 2007; Csiki et al. 2010). One of the authors (SLB) has been involved in the primary data collection and analysis for several of these studies (Brusatte and Sereno 2008; Benson et al. 2010; Brusatte et al. 2010a; Csiki et al. 2010). Because our informal supertree includes only 36 taxa that span the range of theropod phylogeny, and because the higher-level relationships of theropods are generally well-understood and agreed upon by most studies, there are few areas of our phylogeny that are particularly controversial. Our entire informal supertree is used for all phylogenetic comparative analyses based on the 36 taxa/13 landmark dataset, whereas a pruned version is used for all analyses based on the 26 taxa/24 landmark dataset and 24 taxa/24 landmark and 31 taxa/13 landmark datasets without oviraptorosaurs.

b) Permutation test

One major question is: is skull shape significantly correlated with phylogeny? In other words, does the distribution of taxa in cranial morphospace have a strong phylogenetic signal? A strong phylogenetic signal means that closely related species tend to fall out closer in morphospace than more distantly related species (Klingenberg and Gidaszewski 2010). The degree of this correlation, or lack therefore, can be calculated by first mapping the phylogeny into morphospace. This requires reconstruction of the PC scores for each internal node (hypothetical ancestor) on the tree, which is accomplished in MorphoJ using squared change parsimony (Maddison 1991; Klingenberg 2011). The squared change parsimony procedure collates the sum of squared changes in morphometric form data (PCA scores) along all branches of the phylogeny. Then, the most optimal positions of the internal nodes are taken to be those at which the total sum of squared change across the tree is minimized. This optimal configuration is mathematically described by a tree length value, which can then be used to determine the strength of the correlation between phylogeny and morphospace occupation. If there is a strong correlation (closely related species close to each other in morphospace), then the tree length value should be small; conversely, if there is a weaker correlation then the tree length value should be larger.

A permutation test in MorphoJ calculates the significance of the observed tree length by holding the phylogeny constant and randomly swapping the observed form data (PC scores) across the tree. If phylogeny and form are weakly correlated, then randomly exchanging the PC scores across the tree should result in little change to the tree length. On the other hand, if there is a strong correlation between phylogeny and form, then random swapping should result in a longer tree length than observed on the original tree. MorphoJ randomly permutes the PC values across the tips of the tree 10,000 times and calculates an empirical P value, which is the proportion of permuted datasets in which the tree length is shorter or equal to the value obtained for the original data (Klingenberg and Gidaszweski 2010). If the P value is less than 0.05, then the null hypothesis of no phylogenetic signal can be discarded and the phylogeny and form data are considered significantly correlated.

We subjected both the 26 and 36-taxon datasets to the phylogenetic permutation test in MorphoJ. In both cases the null hypothesis of no phylogenetic signal was decisively rejected (tree length=0.24750721, $p<0.0001$ for the 26-taxon dataset; tree length=0.26278840, $p<0.0001$ for the 36-taxon dataset). We also subjected the 24 and 31-taxon datasets (without oviraptorosaurs) to the same permutation test. In both cases, the null hypothesis was also rejected (tree length=0.16899822, $p<0.001$ for the 24-taxon dataset; tree length=0.17546221, $p<0.001$ for the 31-taxon dataset). Therefore, we conclude, theropod cranial shape and phylogeny are strongly correlated to each other.

c) Phylogenetic eigenvector regression

A second test for phylogenetic signal in skull morphospace occupation (as well as position of taxa in functional space) involved subjecting PC scores of form (and PC scores of function) to phylogenetic eigenvector regressions (PVR: Diniz-Filho et al. 1998). In PVR, phylogeny is represented as principal coordinate scores computed through a principal coordinates analysis (PCO) on a pairwise phylogenetic Euclidean distance matrix of appropriately scaled branch lengths. These phylogenetic PCO scores are used as the predictor variables in multiple linear regressions in which the response variable is any quantity of interest such as size (Diniz-Filho et al. 1998; Desdevises et al. 2003), bone microanatomy (Kriloff et al. 2008), and form and/or

function (Sakamoto 2010; Sakamoto et al. 2010). When more than one response variable exists, a multivariate multiple regression (MMR) can be employed (Sakamoto 2010). In this case, the response variable is a matrix of variables instead of a single variable as in standard multiple linear regression. For both form (morphospace occupation) and function (function space occupation), the respective PC values were taken as the response variable matrices while a matrix of phylogenetic PCO scores was taken as the predictor variable matrix. The fit of the MMR on the two matrices was assessed by MANOVA (Sakamoto 2010), and the multivariate R^2 value was computed as the proportion of variance in the response variable matrix explained by the regression model (or variance of the fitted values). Multivariate PVR (MPVR) was performed in R.

Branch lengths were scaled using a 37-taxon phylogeny (which also includes an additional taxon, *Ornithomimus*, which was excluded from the morphometric analysis due to high amounts of missing data) using first-occurrence dates (Table S6), and zero length branches were adjusted by sharing time with adjacent branches following the protocol of Brusatte et al. (2008a) (see also Ruta et al. 2006). An arbitrary length of 10 Ma was added to the root. R functions and descriptions for the branch scaling procedure are available at http://www.graemetlloyd.com/methdpf.html.

In the current study, we began with the dated phylogeny and form PC scores for all 36 theropod taxa included in the morphometric study. From this point, some taxa required deletion. First, because the skull reconstruction of *Juravenator* was not entirely suitable for biomechanical profiling (because of missing bones at the posterior end of the upper and lower jaws), this taxon was pruned from the tree and form PC scores, resulting in a 35-taxon dataset. Second, taxa were further pruned to reflect the taxonomic sampling of the reduced 26-taxon morphometric dataset. Third, oviraptorosaur taxa were pruned from the 36-, 35-, and 26-taxon trees and form/function datasets, resulting in 31-, 30-, and 24-taxon datasets. Therefore, for form metrics, six MPVR analyses were conducted conducted (36-, 35-, 31-, 30-, 26-, and 24-taxon datasets), whereas for function four sets of MPVR were conducted (35-, 30-, 26-, and 24-taxon datasets). In our MPVR analyses, we retained the first *n* PCO axes that account for more than 90% of the total variance in phylogenetic distances. This is necessary because the higher dimensional PCO scores can be degenerate (e.g., negative eigenvalues) and therefore contribute little to the analysis or even, in some cases, give spurious results. In this way, 22, 21, 18, 17, 13, and 11 PCO axes were retained for MPVR in the 36-, 35-, 31-, 30-, 26-, and 24-taxon trees respectively.

As in disparity calculations, morphospace was represented by the first five PC axes in all sample sizes except in the 24-taxon dataset, which was represented by the first seven PC axes (this choice was also based on the broken stick model). Similarly, function space was represented by the first two PC axes, which account for 99.8% of the functional variance.

MPVR revealed that both form and function exhibit significant correlations with phylogeny at all taxonomic sample sizes (Table S7). Therefore, theropod cranial shape and phylogeny are strongly correlated with each other, in agreement with the permutation test described above. Furthermore, theropod function and phylogeny are also strongly correlated.

d) Blomberg's K test

A third and final method for detecting phylogenetic signal is to employ the techniques of Blomberg et al. (2003). These techniques calculate phylogenetically independent contrasts (PIC: Felsenstein 1985) and compares the variances of the contrasts computed from a given variable on

a particular tree topology with those computed from permutations of that variable across the same tree (i.e., randomly reshuffling the values amongst the OTUs while keeping the tree topology constant). If the variances in the contrasts for the data on the "true" tree (i.e., the input phylogeny) are lower than those from permutations, then there is a significant phylogenetic signal in the data (Blomberg et al., 2003). We conducted this test in R using the picante library (Kembel et al. 2009), which also computes Blomberg's *K* statistic. A *K* less than one indicates that closely related OTUs have values that are less similar than expected under Brownian motion (therefore, a departure from Brownian motion, such as adaptive or directional evolution), whereas a *K* greater than one indicates that closely related OTUs have values more similar than expected under Brownian motion (in other words, a strong phylogenetic signal: Blomberg et al. 2003). Therefore, it is possible that a variable of interest may show statistically significant yet weak phylogenetic signal (if the permutation test comes out statistically significant but if *K* is less than 1). A likely scenario in this case is that the variable evolved with phylogenetic inertia but under a different evolutionary process such as the Ornstein-Ulenbeck process.

When applied to our dataset, Blomberg's (2003) methods show that only PC1 of form and function consistently have significant phylogenetic signals in all datasets while other PCs are variable in their significance (Table S8). For instance, $PC2_{form}$ is only significant in the 36- and 35-taxon datasets while $PC2_{func}$ is only significant in the 35- and 26-taxon datasets; functional PC2 only shows significant phylogenetic signal when oviraptorosaurs are included in the analysis. However, only $PC1_{func}$ has $K > 1$, indicating that only this variable has a particularly strong phylogenetic signal, or in other words, that this trait in closely related taxa is more similar than expected under Brownian motion. Conversely, all other significant PCs in closely related taxa are less similar than expected under Brownian motion.

5) Form vs. Function

One major question is: is skull shape (morphometric form) correlated with skull function (mechanical advantage biting profiles)? We employed three tests to assess this question.

First, we chose Procrustes coordinates from the geometric morphometric analysis as a proxy for "form" and biomechanical coefficients standardized according to their standard deviations as a proxy for "function," and performed a correlation analysis on these two matrices in MorphoJ using two-block partial least squares (2B-PLS). 2B-PLS were performed for all taxonomic sample sizes (36-, 31-, 26-, and 24-taxon datasets); the actual sample sizes for the 36- and 31-taxon datasets are 35 and 30, respectively, due to the exclusion of *Juravenator* for which biomechanical data is not available (see above). The multivariate equivalent of the correlation coefficient, the *RV* coefficient, was determined for each sample size and the *p*-value was computed through 10000 permutations. 2B-PLS reveals that at all sample sizes skull shape and skull function are not significantly correlated (Table S9).

Second, we employed multivariate multiple regression (MMR) on morphometric PC scores (first five or first seven axes, see above) against functional PC scores (PC1 and PC2), and the proportion of morphological variance accounted for by the MMR model and *p*-value were computed for the 35-, 30-, 26-, and 24-taxon datasets. MMR reveals that the form PC score matrix is significantly correlated with functional PC score matrix at all sample sizes (Table S9). This discrepancy in results between 2B-PLS and MMR may be due to the differences in the data used; while 2B-PLS was performed on Procrustes coordinates and original biomechanical coefficients, MMR was performed on the ordinated shape/function space.

Third, we chose individual morphometic PC scores as a proxy for "form" and function space PC scores as a proxy for "function," and performed a correlation analysis. Both metrics were transformed into phylogenetically independent contrasts (PICs), because both sets of PCs displayed high levels of phylogenetic signal and therefore the individual PCs are not independent variables (Felsenstein 1985). To reduce the number of comparisons, we focused on the first two PCs—by far the most explanatory of all PC axes—of both form and function for each sample size.

Because the PIC method assumes that character evolution can be modeled as a random walk (i.e., Brownian motion) and that characters change at a uniform rate per unit branch length across all branches (i.e., variance accumulation is assumed to be equal per unit time), the data and/or branch lengths must conform to these assumptions (Garland et al. 1992). There are four widely used diagnostics to test this (Garland et al. 1992; Purvis and Rambaut 1995; Midford et al. 2005): 1, check that there is no significant correlations between the absolute values of the standardized contrasts and their standard deviations; 2, check that there is no correlation between the absolute values of the standardized contrasts and the estimated values of the corresponding nodes (or PIC ancestor reconstructions); 3, check that there is no correlation between the absolute values of the standardized contrasts and the ages of the corresponding nodes; and 4, check that there is no correlation between the node estimates and node ages. An R function was written by one of us (MS) to conduct these four tests. The fourth criterion (no correlation between node estimate and node age) has not strictly been proposed as a diagnostic test and is more a test of trended evolution (Midford et al. 2005). Thus a significant result of the fourth diagnostic test may not necessarily equate to a violation of the assumptions; this may even be expected in fossil trees (which include taxa of many different ages spread through time). For both form and function, PC1 contrasts were adequately standardized on all trees except the 30-taxon tree; a $\log_{10}$ branch length transformation was necessary in the 30-taxon tree for adequate standardization of the $PC1_{form}$ contrasts. On the other hand, PC2 contrasts were only adequately standardized on untransformed branches for $PC2_{form}$ on the 26-taxon tree. A $\log_{10}$ transformation of the branch lengths was necessary for adequate standardization of PC2 contrasts for the 35-taxon tree, while a power transformation (raised to the power of 0.25) of the branch lengths was necessary for $PC2_{func}$ contrasts for the 26-taxon tree. PC2 contrasts for the 30- and 24-taxon trees could not be adequately standardized, so PC2 was ignored for these two datasets.

Pairs of 'positivized' PICs (Garland et al. 1992) were plotted and an ordinary least squares regression model was fitted through the origin, on: 1) $PC1_{form}$ vs $PC1_{func}$; 2) $PC1_{form}$ vs $PC2_{func}$; 3) $PC2_{form}$ vs $PC1_{func}$; and 4) $PC2_{form}$ vs $PC2_{func}$. Contrasts of $PC1_{form}$ and $PC1_{func}$ generally had no significant correlations (Figs S23-S25), except in the 30-taxon tree. Most other combinations of PC contrasts (except for $PC2_{form}$ vs $PC2_{func}$ in the 35-taxon tree) showed significant but weak correlations (Figs S23-S25). This indicates that major patterns of variation in form and function are only weakly correlated: there is generally no significant correlation between the single most important (most explanatory) PC values of form and function (PC1), and correlations between other sets of PC scores are slight and weak.

6) Primary Determinants of Theropod Skull Shape

Finally, another major question of interest is: does phylogeny or function better explain the range of variation in theropod skull shape? In other words, what is the primary determinant of theropod

cranial form? We addressed this question by using phylogenetic eigenvector regressions (PVR, described above).

PVR has previously been employed to partition the variance in a variable of interest (here, morphometric form metrics) into components related to phenotypic/environmental explanatory variables and phylogeny (Desdevises et al., 2003; Kriloff et al., 2008; Sakamoto et al., 2010). The total amount of variance (here, in form metrics) can be divided into four partitions: a) proportion of variance explained solely by function ($PC1_{func}$ and $PC2_{func}$); b) proportion of variance explained by a combination of function and phylogeny (phylogenetically structured functional variance); c) proportion of variance explained solely by phylogeny (phylogenetic PCO scores); and d) proportion of variance unexplained by this current model. A series of multivariate multiple regressions can be employed to accomplish this task. First, a MMR model was fitted on form PC scores against functional PCs, the multivariate R^2 value of which explains the total proportion of variance explained by function (partition a+b). Second, the form PC score matrix was subjected to a MMR against the PCO axes representing phylogeny (as outlined above). The multivariate R^2 of this corresponds to the total amount of variance explained by phylogeny (partition b+c). Third, a MMR on form PC scores against function + phylogeny was conducted, the R^2 of which represents the overall proportion of variance explained by phenotype and phylogeny combined (partition a+b+c). Fourth, to obtain the individual values of the partitions a, b, and c, R^2 values from the separate MMR analyses were used: $a = R^2_{a+b+c} - R^2_{b+c}$; $b = R^2_{a+b} - a$; and $c = R^2_{b+c} - b$. Fifth, the residual variation (or the unexplained portion of the total variation) was computed as: $d = 1 - R^2_{a+b+c}$, or $d = 1 - (a + b + c)$.

Prior to variance partitioning, the three MMR models (form vs function, form vs phylogeny, and form vs function + phylogeny) were compared using Akaike weights (w_i; Burnham and Anderson 2002) in R to determine which model best explains the variance in form. Akaike weights comparisons reveal that at all sample sizes, the MMR of form PC scores against function PS scores and phylogenetic PCO scores is the best model (Table S10). Therefore, it is meaningful to partition the variance in form between functional and phylogenetic variances.

Partitioning of variance using MPVR reveals that partitions b and c together explain 85%, 77%, 82%, and 71% of total variance of form PCs in the 35-, 30-, 26-, and 24-taxon datasets respectively (Table S11). The phylogeneticaly structured functional variance (partition b) is relatively low (36%, 20%, 22%, and 17% respectively) compared to the proportion of variance solely attributed to phylogeny (49%, 57%, 60%, and 54% respectively). Conversely, the proportion of morphological variance than can be explained by function alone is very low (5%, 12%, 11%, and 14% respectively). Similarly, the proportion of variance unexplained by the current model is very low (10%, 11%, 8%, and 16% respectively). Thus, the majority of morphological variance can be explained by phylogeny with relatively small contributions from functional variance.

7) Sensitivity analyses of biomechanical profiles

Because the functional metrics we employ here (mechanical advantage ratios) rely on anatomical information obtained from both the skull and mandible it inevitably includes extraneous variation stemming from morphofunctional variation of the mandible (which is not incorporated into the geometric morphometric analysis of form). Thus it is necessary to determine the impact of mandible morphological variation in the variation of biomechanical profiles. With our biomechanical profiling, biting levers are taken from the biting positions of the upper tooth row,

so the only mandibular contributions, if any, would be in the muscle levers. Theoretically, differences in mandibular morphology can alter muscle lever lengths even in taxa with very similar skull morphology. This is because muscle levers are taken as the perpendicular distance between the jaw joint and the line of action of the muscle, which is dictated by the cranial origin and mandibular insertion points. Differences in mandibular morphology can potentially drive variation in the insertion points, and thus muscle levers. Here, we employ a simple sensitivity analysis to assess how sensitive the biomechanical metric is to changes in muscle and biting levers.

Sensitivity analyses were conducted on muscle levers and bite levers separately. This allows us to pinpoint variation in biomechanical metrics due to both input parameters. First, we reduced all muscle levers (R_{mAME}, R_{mAMP}, and R_{mPt}) simultaneously by 10% and 20% (MuscAll-90% and MuscAll-80%, respectively). Next, we increased all muscle levers by 10% and 20% (MuscAll-110% and MuscAll-120%). We then increased or decreased each of the muscle levers separately while holding the other two constant (mAME-90%, mAME-80%, mAME-110%, mAME-120%, mAMP-90%, mAMP-80%, mAMP-110%, mAMP-120%, mPt-90%, mPt-80%, mPt-110%, and mPt-120%). For each of these 16 iterations of muscle lever lengths, biomechanical profiles were computed with bite levers fixed.

Similarly for the bite levers, we first increased and decreased all bite levers along the entire tooth row by 10% and 20% consistently across the board (BiteAll-80%, BiteAll-90%, BiteAll-110%, and BiteAll-120%). This simulates the migration of the entire toothrow posteriorly or anteriorly relative to the muscle levers. We further simulated four situations where either: 1), biting levers were progressively increased towards the rostrum while holding the posterior-most biting lever constant; 2), the biting levers were progressively decreased anteriorly while the posterior-most biting lever was held constant; 3), the biting levers were progressively increased towards the posterior-most biting position while the anterior-most lever was held constant; and 4), the biting levers were progressively reduced posteriorly while holding the anterior-most lever constant. The first two simulate situations where the posterior extent of the tooth row remains the same as in the original condition but the tooth rows are either stretched anteriorly or compressed posteriorly. Extension and compression were simulated at 10% and 20% each (BiteAnt-80%, BiteAnt-90%, BiteAnt-110%, and BiteAnt-120%). On the other hand, the latter two simulate situations where the anterior extent of the tooth row remains constant (i.e., same skull length) but the posterior extent of the tooth row is either posteriorly extended or anteriorly compressed. Again, extension and compression were simulated under 10% and 20% changes relative to original lever lengths (BitePost-80%, BitePost-90%, BitePost-110%, BitePost-120%). In these four situations, the anterior-most or posterior-most levers were reduced/increased by 10% or 20% but the remaining teeth were adjusted equally based on the number of levers. For instance, in BitePost-80%, the posterior-most biting lever will be reduced by 20%, but the remaining levers will be evenly reduced according to the number of biting levers, so $R_{B(i)adj} = R_{Bite} \times (1 - 0.2 / (n - 1) \times i)$, where n is the number of biting levers for the ith biting lever moving anteriorly. The nth, or anterior-most, biting lever is not affected. Similarly, for an increase, $R_{B(i)adj} = R_{Bite} \times (1 + 0.2 / (n - 1) \times i)$. These general forms apply for both posterior and anterior extension/reduction. Muscle levers were fixed at original lengths for bite lever simulations. Thus, in total, 12 iterations on bite levers were used to compute biomechanical profiles along the tooth row.

The coefficients of the original profile, 16 profiles of the muscle lever iterations, and 12 profiles of the bite lever iterations were pooled and the effects of the changes to muscle or bite

levers on polynomial coefficients were compared (Fig S26). There is no obvious difference in the range of the intercept β_0 between the changes to muscle lever lengths and changes to bite lever lengths (Fig. S26A). On the other hand, there is considerable difference in the range of values for the slope β_1 and curvature β_2, between muscle lever and bite lever simulations (Fig S26B, C), with changes to bite lever lengths evoking wider ranges of changes to these two coefficients. In order to visualize the multidimensional impact between the lever length simulations, the biomechanical coefficients were subjected to a PCA and the scores along the first two PC axes were plotted as a biplot (Fig. S27). While changes to muscle levers show changes to coefficients, the changes are constrained along a near-linear trajectory. On the other hand, changes to bite levers result in higher variation in the biomechanical coefficients.

A point worthy of note is the way in which alterations to muscle lever lengths result in changes to coefficients that are all along the same trajectory of change, regardless whether all or one muscle levers were adjusted. For instance, MuscAll-120%, mAME-120%, mAMP-120%, and mPt-120% all fall along the same trajectory, although MuscAll-120% is separated considerably from the single-lever examples (Fig. S27). Interestingly, coefficients derived from simulations where bite levers were consistently increased or decreased (BiteAll-80%, BiteAll-90%, BiteAll-110%, and BiteAll-120%) fall along the same trajectory as the coefficients of the muscle simulations. On the other hand, anterior or posterior extension/compression of biting levers result in highly variable coefficients. This implies that changes to muscle levers and uniform changes to bite levers do not alter the shapes of the biomechanical profiles to any great effect, but disproportional changes to the tooth row morphology impact drastically on the shapes and positions of the biomechanical profiles. Thus while biomechanical profiling is still sensitive to variation in muscle lever lengths, it is substantially more sensitive to variation in bite lever lengths. In other words, the morphology of the skull has a much greater affect on mechanical advantage profiles than the morphology of the mandible.

9) Supplementary References

Adams, D.C., Rohlf, F.J., and Slice, D.E. 2004. Geometric morphometrics: ten years of progress following the 'revolution.' Italian Journal of Zoology 71, 5-16.

Benson, R.B.J. 2010. A description of *Megalosaurus bucklandii* (Dinosauria: Theropoda) from the Bathonian of the United Kingdom and the relationships of Middle Jurassic theropods. Zoological Journal of the Linnean Society 158, 882-935.

Benson, R.B.J., Carrano, M.T., and Brusatte, S.L. 2010. A new clade of archaic large-bodied predatory dinosaurs (Theropoda: Allosauroidea) that survived to the latest Mesozoic. Naturwissenschaften 97, 71-78.

Blomberg, S.P., Garland, T., and Ives, A.R. 2003. Testing for phylogenetic signal in comparative data: behavioral traits are more labile. Evolution 57, 717-745.

Brusatte, S.L., Benton, M.J., Ruta, M., and Lloyd, G.T. 2008a. Superiority, competition, and opportunism in the evolutionary radiation of dinosaurs. Science 321, 1485–1488.

Brusatte, S.L., Benton, M.J., Ruta, M., and Lloyd, G.T. 2008b. The first 50 myr of dinosaur evolution: macroevolutionary pattern and morphological disparity. Biology Letters 4, 733–736.

Brusatte, S.L., Montanari, S., Yi, H.-Y., and Norell, M.A. 2011. Phylogenetic corrections for morphological disparity analysis: new methodology and case studies. Paleobiology 37, 1–22.

Brusatte, S.L., Benton, M.J., Lloyd, G.T., Ruta, M., and Wang, S.C. 2011. Macroevolutionary patterns in the evolutionary radiation of archosaurs (Tetrapoda: Diapsida). Earth and Environmental Science Transactions of the Royal Society of Edinburgh, in press.

Brusatte, S.L., Norell, M.A., Carr, T.D., Erickson, G.M., Hutchinson, J.R., Balanoff, A.M., Bever, G.S., Choiniere, J.N., Makovicky, P.J., and Xu, X. 2010a. Tyrannosaur paleobiology: new research on ancient exemplar organisms. Science 329, 1481-1485.

Brusatte, S.L., and Sereno, P.C. 2008. Phylogeny of Allosauroidea (Dinosauria: Theropoda): comparative analysis and resolution. Journal of Systematic Palaeontology 6, 155-182.

Bonnan, M.F. 2004. Morphometric analysis of humerus and femur shape in Morrison sauropods: implications for functional morphology and paleobiology. Paleobiology 30, 444-470.

Bonnan, M.F. 2007. Linear and geometric morphometric analysis of long bone scaling patterns in Jurassic neosauropod dinosaurs: their functional and paleobiological implications. The Anatomical Record 290, 1089-1111.

Bookstein, F.L. 1991. Morphometric Tools for Landmark Data. Cambridge University Press, Cambridge, UK.

Butler, R. J., and Goswami, A. 2008. Body size evolution in Mesozoic birds: little evidence for Cope's rule. Journal of Evolutionary Biology 21, 1673-1682.

Carrano, M.T., and Sampson, S.D. 2008. The phylogeny of Ceratosauria (Dinosauria: Theropoda). Journal of Systematic Palaeontology 6, 183-236.

Chinnery, B. 2004. Morphometric analysis of evolutionary trends in the ceratopsian postcranial skeleton. Journal of Vertebrate Paleontology 24, 591-609.

Ciampaglio, C.N., Kemp, M., and McShea, D.W. 2001. Detecting changes in morphospace occupation patterns in the fossil record: characterization and analysis of measures of disparity. Paleobiology 27, 695–715.

Cisneros, J.C., and Ruta, M. 2010. Morphological diversity and biogeography of procolophonids (Amniota: Parareptilia). Journal of Systematic Palaeontology 8, 607–625.

Csiki, Z., Vremir, M., Brusatte, S.L., and Norell, M.A. 2010. An aberrant island-dwelling theropod dinosaur from the Late Cretaceous of Romania. Proceedings of the National Academy of Sciences (USA) 107, 15357-15361.

Desdevises, Y., Legendre, P., Azouzi, L., and Morand, S. 2003. Quantifying phylogenetically structured environmental variation. Evolution 57, 2647-2652.

Diniz-Filho, J.A.F., De Sant'ana, C.E.R., and Bini, L.M. 1998. An eigenvector method for estimating phylogenetic inertia. Evolution 52, 1247-1262.

Elewa, A.M.T. 2004. Morphometrics—Applications in Biology and Paleontology. Springer-Verlag Publishers, Heidelberg, Germany.

Erwin, D.H. 2007. Disparity: morphological pattern and developmental context. Palaeontology 50, 57–73.

Felsenstein, J. 1985. Phylogenies and the comparative method. Ameican Naturalist 125, 1-15.

Foote, M. 1993. Discordance and concordance between morphological and taxonomic diversity. Paleobiology 20, 185–204.

Garland, T., Harvey, P.H., and Ives, A.R. 1992. Procedures for the analysis of comparative data using phylogenetically independent contrasts. Systematic Biology 41, 18-32.

Kembel, S., Ackerly, D., Blomberg, S., Cowan, P., Helmus, M., Morlan, H., and Webb, C. 2009. Picante: R tools for integrating phylogenies and ecology. R package v. 0.7-2. See http://www.CRAN.R-project.org/package=picante

Klingenberg, C.P. 2011. MorphoJ: an integrated software package for geometric morphometrics.

Molecular Ecology Resources 11, 353-357.
Klingenberg, C.P., and Gidaszewski, N.A. 2010. Testing and quantifying phylogenetic signals and homoplasy in morphometric data. Systematic Biology 59, 245-261.
Kriloff, A., Germain, D., Canoville, A., Vincent, P., Sache, M., and Laurin, M. 2008. Evolution of bone microanatomy of the tetrapod tibia and its use in palaeobiological inference. Journal of Evolutionary Biology 21, 807-826.
MacLeod, N. 2010. PalaeoMath 101: Principal warps, relative warps, and Procrustes PCA. Palaeontological Association Newsletter 75, 22-32.
MacLeod, N., and Forey, P.L. 2002. Morphometrics, Shape and Phylogenetics. Taylor & Francis, London.
Maddison, W.P. 1991. Squared-change parsimony reconstructions of ancestral states for continuous-valued characters on a phylogenetic tree. Systematic Zoology 40, 304-314.
Midford, P.E., Garland, T., and Maddison, W.P. 2005. PDAP Package of Mesquite. Version 1.07.
Nesbitt, S.J., Smith, N.D., Irmis, R.B., Turner, A.H., Downs, A., and Norell, M.A. 2009. A complete skeleton of a Late Triassic saurischian and the early evolution of dinosaurs. Science 326, 1530-1533.
O'Higgins, P. 2000. The study of morphological variation in the hominid fossil record: biology, landmarks and geometry. Journal of Anatomy 197, 103-120.
Pierce, S.E., Angielczyk, K.D., and Rayfield, E.J. 2008. Patterns of morphospace occupation and mechanical performance in extant crocodilian skulls: a combined geometric morphometric and finite element modeling approach. Journal of Morphology 269, 840-864.
Pierce, S.E., Angielczyk, K.D., and Rayfield, E.J. 2009a. Morphospace occupation in thalattosuchian crocodylomorphs: skull shape variation, species delineation and temporal patterns. Palaeontology 52, 1057-1097.
Pierce, S.E., Angielczyk, K.D., and Rayfield, E.J. 2009b. Shape and mechanics in thalattosuchian (Crocodylomorpha) skulls: implications for feeding behaviour and niche partitioning. Journal of Anatomy 215, 555-576.
Purvis, A., and Rambaut, A. 1995. Comparative analysis by independent contrasts (CAIC) - an Apple Macintosh application for analysing comparative data. Computer Applications in the Biosciences 11, 247-251.
Rasband, W.S., 1997-2011. ImageJ, US National Institutes of Health, Bethesda, Maryland, USA, http://imagej.nih.gov/ij/.
Rohlf, F.J. 2000. Statistical power comparisons among alternative morphometric methods. American Journal of Physical Anthropology 111, 463-478.
Rohlf, F.J. 2010. TpsDig 2. Department of Ecology and Evolution, State University of New York, Stony Brook, NY.
Rohlf, F.J., and Marcus, L.F. 1993. A revolution in morphometrics. Trends in Ecology and Evolution 8, 129-132.
Rohlf, F.J., and Slice D.E. 1990. Extensions of the Procrustes method for the optimal superimposition of landmarks. Systematic Zoology 30, 40-59.
Ruta, M. 2009. Patterns of morphological evolution in major groups of Palaeozoic Temnospondyli (Amphibia: Tetrapoda). Special Papers in Palaeontology 81, 91–120.

Ruta, M., Wagner, P.J., Coates, M.I. 2006. Evolutionary patterns in early tetrapods. I. Rapid initial diversification followed by decrease in rates of character change. Proceedings of the Royal Society of London, Series B 273, 2107-2111.

Sakamoto, M. 2010. Jaw biomechanics and the evolution of biting performance in theropod dinosaurs. Proceedings of the Royal Society of London, Series B 277, 3327-3333.

Sakamoto, M., Lloyd, G.T., and Benton, M.J. 2010. Phylogenetically structured variance in felid bite force: the role of phylogeny in the evolution of biting performance. Journal of Evolutionary Biology 23, 463-478.

Souter, T., Cornette, R., Pedraza, J., Hutchinson, J., and Baylac, M. 2010. Two applications of 3D semi-landmark morphometrics implying different template designs: the theropod pelvis and the shrew skull. Comptes Rendus Palevol 9, 411-422.

Stayton, C.T., and Ruta, M. 2006. Geometric morphometrics of the skull roof of stereospondyls (Amphibia: Temnospondyli). Palaeontology 49, 307-337.

Turner, A.H., Pol, D., Clarke, J.A., Erickson, G.M., and Norell, M.A. 2007. A basal dromaeosaurid and size evolution preceding avian flight. Science 317, 1378-1381.

Westneat, M.W. 1994. Transmission of force and velocity in the feeding mechanisms of labrid fishes (Teleostei, Perciformes). Zoomorphology 114, 103-118.

Wills, M.A., Briggs, D.E.G., and Fortey, R.A. 1994. Disparity as an evolutionary index: a comparison of Cambrian and Recent arthropods. Paleobiology 20, 93–130.

Wills, M.A. 1998. Crustacean disparity through the Phanerozoic: comparing morphological and stratigraphic data. Biological Journal of the Linnean Society 65, 455–500.

Xu, X., Clark, J.M., Mo, J., Choiniere, J., Forster, C. A., Erickson, G.M., Hone, D.W.E., Sullivan, C., Eberth, D.A., Nesbitt, S., Zhao, Q., Hernandez, R., Jia, C-K., Han, F., and Guo, Y. 2009. A Jurassic ceratosaur from China helps clarify avian digital homologies Nature 459, 940-944.

Young, M.T., Brusatte, S.L., Ruta, M., Andrade, M.B. 2010. The evolution of Metriorhynchoidea (Mesoeucrocodylia, Thalattosuchia): an integrated approach using geometric morphometrics, analysis of disparity, and biomechanics. Zoological Journal of the Linnean Society 158, 801-859.

Young, M.T. and Larvan, M.D. 2010. Macroevolutionary trends in the skull of sauropodomorph dinosaurs—the largest terrestrial animals to heve ever lived. *In*: Elewa, A.M.T. (ed.), Morphometrics for Nonmorphometricians. Springer-Verlag, Heidelberg, pp. 259-269.

Zelditch, M.L., Sheets, H.D., and Fink, W.L. 2004. Geometric Morphometics for Biologists: A Primer. Elsevier Academic Press, San Diego, CA.